CONTENTS

S.NO	Title of paper	Name of the author/s	Department of the teacher	Page No
Calendar Year 2022				
1	Fault Rectification in Grid-Connected PV System for Maximum Power Point Tracking Using IT-SMC	Dr. G. Anand	EEE	6-19
2	Reliability of Gas Insulated System under Electric Field Stress with Optimal Design of FGM Post Type Spacer	D. Deepak Chowdary	EEE	20-37
3	Unsteady flow analysis using hydrological and hydraulic models for real-time flood forecasting in the Vamasadara River basin	Mrs Arunima Mahapatra	CIVIL	38-64
4	Experimental and numerical modeling of wave transmission over the submerged breakwater and rigid vegetation display	G Giridhar	CIVIL	65-76
5	The selection of clinical orthodontic implant materials by entropy weight methods through hybrid multi-criteria decision-making techniques	M. Amareswari Reddy	CIVIL	77-87
6	Box–Behnken Design: Optimization and Prediction of TI-6AL-7NB	M.Amareswari Reddy	CIVIL	88-99
7	Existence, uniqueness and stability analysis of a tempered fractional order thermistor boundary value problem.	Md. Khuddush	BS&H	100-122
8	Infinitely many positive solutions for an iterative system of singular BVP on time scales	Khuddush Mahammad	BS&H	123-137
9	Global existence and blowup of solutions for a semi-linear Klein-Gordon equation with the product of logarithmic and power-type nonlinearity	Mahammad Khuddush	BS&H	138-152
10	Assessment of Quercetin Content in Selected Vegetables and Fruits by Conventional Extraction and High-Performance Liquid Chromatography	N. Swathi	BS&H	153-158
11	Almost Periodic Positive E Solutions for a Delayed Nonlinear Density-dependent Mortality Nicholson's Blowflies model on time scales.	Khuddush Mahammad	BS&H	159-170
12	Denumerably many positive radial solutions for the iterative system of Minkowski-curvature equations	Khuddush Mahammad	BS&H	171-190

13	Existence theory and stability analysis to the system of infinite point fractional order bps by multivariate best proximity point theorem	Khuddush Mahammad	BS&H	191-211
14	Infinitely many positive solutions for an iterative system of fractional BVPs with multistrip Riemann-Stieltjes integral boundary conditions	Khuddush Mahammad	BS&H	212-228
15	Global existence and blow-up of solutions for a p-Kirchhoff-type parabolic equation with logarithmic nonlinearity	Khuddush Mahammad	BS&H	229-248
16	Existence of infinitely many positive radial solutions for an iterative system of nonlinear elliptic equations on an exterior domain	Khuddush Mahammad	BS&H	249-261
17	Global exponential stability of almost periodic solutions for quaternion-valued RNNs with mixed delays on time scales	Khuddush Mahammad	BS&H	262-289
18	Existence of Solutions to the ∞-point Fractional BVP Posed on Half-Line via a Family of Measure of Noncompactness in the H¨older Space Cℓ,α(R+)	Khuddush Mahammad	BS&H	290-306
19	Denumerably many positive radial solutions for the iterative system of elliptic equations in an Annulus.	Khuddush Mahammad	BS&H	307-317
20	Existence of solutions for n-dimensional fractional order bvp with ∞–point boundary conditions via the concept of measure of noncompactness	Khuddush Mahammad	BS&H	318-336
21	Nonlinear two-point iterative functional boundary value problems on time scales	Khuddush Mahammad	BS&H	337-347
22	Existence and stability analysis to the sequential coupled hybrid system of fractional differential equations with two different fractional derivatives	Mahammad Khuddush	BS&H	348-359
23	Existence theory and stability analysis to the system of fractional order BVP with Riemann-Liouville integral boundary conditions	Khuddush Mahammad	BS&H	360-385
24	Iterative System of Nabla Fractional Difference Equations with Two-Point Boundary Conditions	Khuddush Mahammad	BS&H	386-403
25	Opinion Mining Using Normal Discriminant Piecewise Regressive (NDPR) Sentiment Classification Technique	Dr. K. Anuradha	CSE	404-419
Calendar Year 2021				
1	Automated Smart Billing System Using RFID Technology	Sabbi Surya Kala	ECE	420-426
2	Design of Linear Antenna Array for Smart Antenna using Whale Optimization Algorithm	K Rajesh Kumar	ECE	427-438

3	Electric Field Stress in a Three-Phase Common Enclosure Gas Insulated Busduct with FGM Post Type Spacer and Reduction with Metal Inserts	Deepak Chowdary Duvvada	EEE	439-456
4	SPWM Fed Induction Motor Drive Performance Using SIMULINK	Dr. Anand Gondesi	EEE	457-466
5	SPWM Fed Induction Motor Drive Performance Using SIMULINK	Ch. Ravi Kumar	EEE	457-466
6	SPWM Fed Induction Motor Drive Performance Using SIMULINK	S. Varalakshmi	EEE	457-466
7	SPWM Fed Induction Motor Drive Performance Using SIMULINK	S. Hema	EEE	457-466
8	GIS-Based Flood Hazard Mapping: A Case Study of Tandava River Basin Andhra Pradesh	Mrs Arunima Mahapatra	CIVIL	467-475
9	Development of real-time flood forecast model for Vamsadara River through hydrological approach	Mrs Arunima Mahapatra	CIVIL	476-496
10	Determination of Guaiacol in Presence of monovalent inorganic salt and its assessment in Citrus sinensis leaves and Citrus limon peels	N. Swathi	BS&H	497-501
11	Fuzzy Transportation model using LR flat Trapezoidal approximations.	B. Pardha Saradhi	BS&H	502-512
12	''Hesitant Fuzzy Project Planning and Scheduling using Critical Path Technique''	B. Pardha Saradhi	BS&H	513-527
13	Legal Policies for Sustainable Security and Privacy in Big Data and Information sharing- A managerial perspective	K. Sowjanya Naidu	CSE	528-543
Calendar Year 2020				
1	Particle Swarm Optimization for robot target tracking application	R. Santosh Sai	ECE	544-547
2	Design of Linear and Circular Antenna Array for Side Lobe Reduction Using the Method Moth Flame Optimization Algorithm	K Rajesh Kumar	ECE	548-560
3	" Reduction of PAPR in OFDM Signals Using Hybrid Optimization GWOFA in OFDM Systems".	Dr. R. Sridevi	ECE	561-571
4	Optimization of PAPR in MB-OFDM UWB Signals Using SM-HOA Technique	Dr. R. Sridevi	ECE	572-581
5	Design of Sliding Mode Observer-Based Controller of Single-Phase Induction Motor	Dr Anand Gondesi	EEE	582-587
6	Study of electric field stress on the surface contour and at the triple junction in three-phase GIS with FGM spacer under the depression defect	Deepak Chowdary Duvvada	EEE	588-601

7	Power System Contingency Analysis by using Voltage and Active Power Performance Index	Mr. Ch. Arun Kumar	EEE	602-610
8	Design Of Functional Observer Based Load Frequency Controller for Inter-Connected Power System",	Anand Gondesi	EEE	611-615
9	Use of bottom ash in improving Strength characteristics of black cotton soil	P. Sridevi	CIVIL	616-622
10	Impact of Niobium on Lithium-Titanate Anode Materials of Lithium-ion Batteries	D. Deenabandhu	BS&H	623-633
11	Self-Realization to Search for Identity: A Study on Select Novels of Maya Angelou	Dr V Radha Devi	BS&H	634-641
12	Collaborative Teaching and Learning in ESL Classroom	Dr V Radha Devi	BS&H	642-648
13	Trace element contamination in fruits and vegetables grown in low nutrient availability soil environments by using inductively coupled plasma mass spectrometry	N. Swathi	BS&H	649-654
14	Synthesis and Characterization of Nano-Acetamiprid New Plant Safeguard Nanomaterial	N. Swathi	BS&H	655-662
15	" Q-HeteLearn: A Progressive Learning approach for Classifying Meta-Paths in Heterogeneous Information Networks"	Madhavi Dabbiru	CSE	663-666
16	Efficient Roadside framework placement using vanet for reducing network delays	Dr. G. Vamsi Krishna	CSE	667-674
Calendar Year 2019				
1	· "SLM Technique based on Firefly Algorithm for Reduction of PAPR in OFDM Systems "	Dr. R. Sridevi	ECE	675-681
2	" Performance Improvement of OFDM Systems by Reducing PAPR using SLM-Grasshopper Optimization",	Dr. R. Sridevi	ECE	682-689
3	Analysis Of Indian Natural Chromite Ore and Rocks by Nuclear Analytical Technique	S. Siva Jyothi	BS&H	690-699
4	Nuclear Analytical Technique –PIXE, A Suitable method for Elemental Analysis of Conventional to Advanced Materials	S. Siva Jyothi	BS&H	700-706
5	A Cuisine Based Recommender System Using K-NIN	Madhavi Dabbiru	CSE	707-711
6	A survey Paper Exploring Engineer Exploring Engineer Approaches, Methods & Challenges	Dr. K. Anuradha	CSE	712-722
7	Three Node Tandem Communication Network Model with Duane Arrival Process having Phase Type Service	K. AsishVardhan	CSE	723-732

Calendar Year 2018				
1	Design Of a Novel Sliding mode Functional Observer Based Load Frequency Controller for Interconnected Power System	Anand Gondesi	EEE	733-745
2	A Survey of Data Mining Techniques on Information Networks	Dabbiru Madhavi	CSE	746-754
3	Diagnosis of children with dyslexia using machine learning techniques	Dr. G. Vamsi Krishna	CSE	755-770
4	IoT using Machine learning techniques,	Dr. G. Vamsi Krishna	CSE	771--779
5	Implementation of Smart Home Automation with Enhanced Security	Dr. K. Anuradha	CSE	780-785
6	Implementation of High-Speed Double Tail Comparator	Dr. K. Anuradha	CSE	786-791

Fault Rectification in Grid Connected PV System for Maximum Power Point Tracking Using IT-SMC

Dr. Ch. Varaha Narasimha Raja[*], *K.L.S.S. Sanjay*[#], *R.S.S.S. Rohit*[#], *A.N.S. Jyothi*[#], Dr. G. Anand[&]
[*]Assistant Professor, [#]UG Students
Department of EEE, ANITS(A), Andhra Pradesh, India
[&]Assistant Professor, Department of EEE, Dr. Lankapalli Bullayya College of Engineering

ABSTRACT: ***Photovoltaic (PV) systems are becoming increasingly popular as a source of renewable energy. However, creating control schemes that ensure maximum efficiency is difficult. Extraction of power from grid-connected PV arrays Grid fault mitigation is still a difficult problem to solve. In the community of control an integral is proposed in this study. Grid-based terminal sliding mode control (ITSM) scheme PV arrays linked together the strategy tries to maximize obtaining power while minimizing the consequences of interruptions generated by changes in irradiance and oscillations in the bulk voltage. Voltage drag is effectively eliminated, and Maximum power point tracking is one of the advantages. Characteristics of the proposed method the effectiveness of the A simulation study was used to evaluate the proposed strategy involving a variety of operational situations and malfunctioning components circumstance. In this paper the fault will be mitigated by controller and the maximum power extracted by irradiance fluctuations and oscillations in the voltage. Elimination of fluctuations and disturbances and maximum power can be tracked among the proposed approach. By considering various faulty cases under the concepts of Irradiance and temperature.***

Keywords: Photovoltaic, Integral terminal sliding mode control, electric power quality

I. INTRODUCTION

Solar energy is freely available, plentiful and maintainable in nature throughout the year and this energy is being converted to electricity. Solar panels have photovoltaic cells (PV) which directly converts light into electricity [1]. This PV cells have an efficiency of up to 30% which provides small output power compared to the input it takes. To maximize the efficiency and to reduce installation cost MPP trackers are used with the system. The output power of a solar PV depends upon on solar irradiance level, temperature and load current which lead to nonlinear operation of the system [2, 27]. By using a PV model for testing the performance of PV systems and observing performance of the system by considering three operation points current, voltage and MPP and by comparison it offers a PV model which is fast and accurate which is applicable to all PV cells [3]. By integrating a lower cost highly efficient MPPT tracker to be integrated into a PV cell which can result in 25% energy enhancement compared to standard PV cell while still performing with better voltage regulation. MPPT, an affordable solution for small PV energy systems is used which results in better efficiency and helps in transfer of more energy to the load [4]. The photovoltaic (PV) generation are extensively increasing, since it is considered as an essentially inexhaustible and broadly available energy resource. However, the output power induced in the photovoltaic modules depends on solar radiation and temperature of the solar cells. Hence using MPPT is done by using ITSMC controller which helps in improving energy conversion efficiency of the PV system [5].

The focus is the model of photovoltaic cell for energy harvest application (EHV). This model facilitates to specify the optimal conditions for operating the PV cell and define the maximum power point (MPPT) [6, 27]. Pilot line production by fabricating high efficiency solar cell are used in small high efficiency modules integrated proto type of solar powered portable device like

cell phones , hand held computer etc. The excellent cell characterisation achieved at low illumination density increase the benefit of solar power supply compared to standard solar cell [7].The day to day applications like Water pumping is becoming popular using inverter powered by photovoltaic arrays [8]. A Current-fed parallel resonant push-pull inverter and PV cells are used for residential applications in rural areas such as water pumping system [9].

The operating point (I, V) corresponds to a point on the power-voltage (P-V) curve at maximum point is called the maximum power point tracking PV system can extract maximum power point tracking system to get the best performance from solar PV panels [10]. PI based controllers are most commonly used controllers for the power production. MPPT device is charge control devices which is more efficient that allows a panel array to be of higher voltage than the battery bank .To implement MPPT, sense the voltage and current and implement the MPPT, from that obtained reference voltage as output it is compared with the actual PV voltage to find the error .this error is then fed to the PI controller .The output of PI controller will give the required duty ratio for PWM generator and this value is compared with the carrier signal and given to the MOSFET.A distributed MPPT pattern can be used for PV system, which permits the control of each DC-link voltage [11]. It gives better MPPT tracking performance since it has a closed loop control mechanism. It is a technique used with variable power sources to maximize energy extraction as conditions vary. To enhance the efficiency of the solar device, a maximum power point tracking algorithm is essential. There are methods for MPPT such as fractional open circuit voltage, fractional short circuit current. A DC-DC converter is used between the solar cell and the load as an interface. The duty cycle is varied so that the impedance matching between the cell output and the load is achieved, by tracking the maximum power point of the cell [13].The nonlinear characteristics of PV cells were simulated for MPPT by using a sliding mode control method based on fuzzy exponential approach rate (SMC-FEAR) [14]. The solar PV array is operated at maximum power point through a boost converter. The DC bus voltage of the system is held constant through the DC link voltage proportional-integral (PI) controller. The output of DC link voltage PI controller and the PV array feed forward term are used to generate reference speed command[15].

In this present paper proposes a novel ITSMC control scheme for grid-connected PV arrays subject to uncertainties and irradiance fluctuations. The main contributions of this paper is to design of a new integral terminal sliding mode control (ITSMC) for a grid-connected PV systems, Implementation of a new ITSMC-based MPPT scheme for stand-alone PV power systems. The rest of the paper is organized as follows. The grid connected PV power generation system is discussed in section II. Section III provides the necessary details for the design of the proposed ITSMC approach for the grid connected PV. Section IV, simulation results are provided in sections IV to demonstrate the effectiveness of the proposed control strategy in achieving maximum power under various disturbances.

II. SYSTEM MODEL

A. PV CELL MODELLING

When photons of light strike's a solar cell technically a semiconductor p-n junction. They get absorbed in solar cell thus resulting in breaking the bond of outer electrons in the semiconductor. These electrons are emitted when energy of photon is greater than the band gap energy. Thus a semiconductor device which converts light into electrical energy by photovoltaic effect The process of generation of voltage or electric current in a photovoltaic cell when exposed to sun light is recognized as photovoltaic cell or photo electric cell [18].The whole phenomena involves absorption of solar rays, ejection or generation of electrons and collection of these free charged at the end of a PV system.

The Shockley diode equation of a single diode PV cell [19]

$$I_D = I_o \left[\exp\left(\frac{qV_{PV}}{AKT}\right) - 1\right] \quad (1)$$

The output PV current with output PV voltage Vpv is defined

$$I_{PV} = I_{SC} - I_o \left[\exp\left(\frac{qV_{PV}}{AKT}\right) - 1\right] \quad (2)$$

Here the variation of the reverse saturation current Io of a PV cell is given by 3

$$I_o = I_{or} \left[\frac{T}{T_R}\right]^3 exp\left(\frac{qE_g}{K\alpha}\left[\frac{1}{T_R} - \frac{1}{T}\right]\right) \quad (3)$$

B. Grid Connected PV array

The diagrammatic representation of a grid connected PV array is depicted in the figure 1. The PV array is attached to the DC-DC converter and then to the DC-AC inverter that is ultimately connected to the grid. The two parameters Ipv and Vpv are approximated from the PV array which is given to the Perturb and Observe Algorithm [20].It yields the reference voltage at the maximum power. The ITSMC controller receives the reference voltage so that it can keep the output voltage in track with the reference voltage. It is obtained by controlling and modifying the duty cycle.

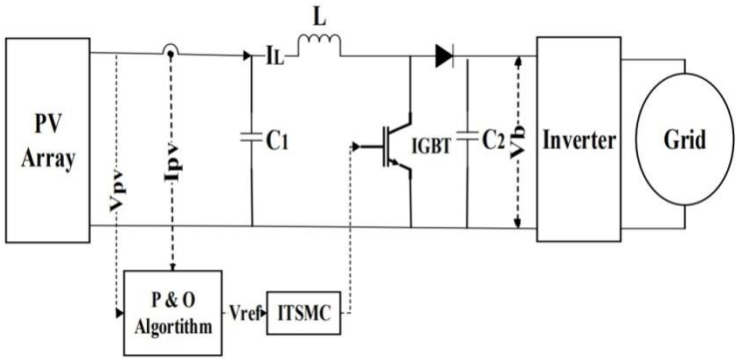


Fig. 1. Topology of a grid connected PV array

In fig 1, a fundamental DC-DC converter circuit is also known as boost converter can be observed. A single-pole double-throw (SPDT) switch is connected to the DC input voltage as shown. IGBT has improved power gain than usual bipolar type transistors mainly because they combine the higher voltage operation of the bipolar type transistor and lower input losses of MOSFET [21]. So, IGBT's are preferred over BJT or MOSFET.

A DC-DC boost converter is to control the output voltage of the PV array (V_{PV}) and achieve maximum solar power generation. The capacitor current is given by[22]:

$$I_{C1} = C_1 \frac{dV_{pv}}{dt} = I_{PV} - I_L \quad (4)$$

Where, I_L is the current through the inductor.

The voltage across the inductor L is found out as:

$$V_L = L\frac{dIL}{dt} = V_{PV} - V_b(1 - t) \quad (5)$$

Where, t is the duty cycle fed to the IGBT switch and V_b is the bulk voltage across the capacitor C_2.

C. MPP searching

The main features of a PV cell are the short circuit current and open circuit voltage. The current obtained from the PV cell at zero load resistance is known as the short circuit current. When the load resistance is infinity, the current is zero and the open circuit voltage becomes maximum. Maximum power is achieved when there is a blend of best voltage and current as shown in fig 2.

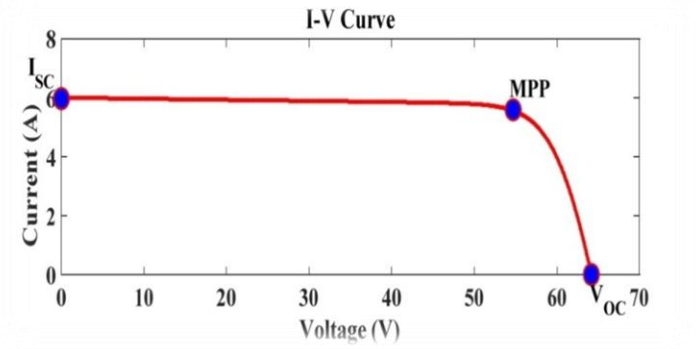


Fig. 2. I-V characteristic curve showing crucial points

Maximum Power Point Tracking algorithm is essential to improve the efficiency of the solar device. There are various methods for MPPT, such as fractional short circuit current, Perturb and observer, fractional open circuit voltage, fuzzy control and neural control [23]. Perturb and Observe Algorithm is opted due to its simplicity and popularity for less implementation cost [24]. Perturb and observe technique has simple implementation, optimum MPP tracking time and is economical.

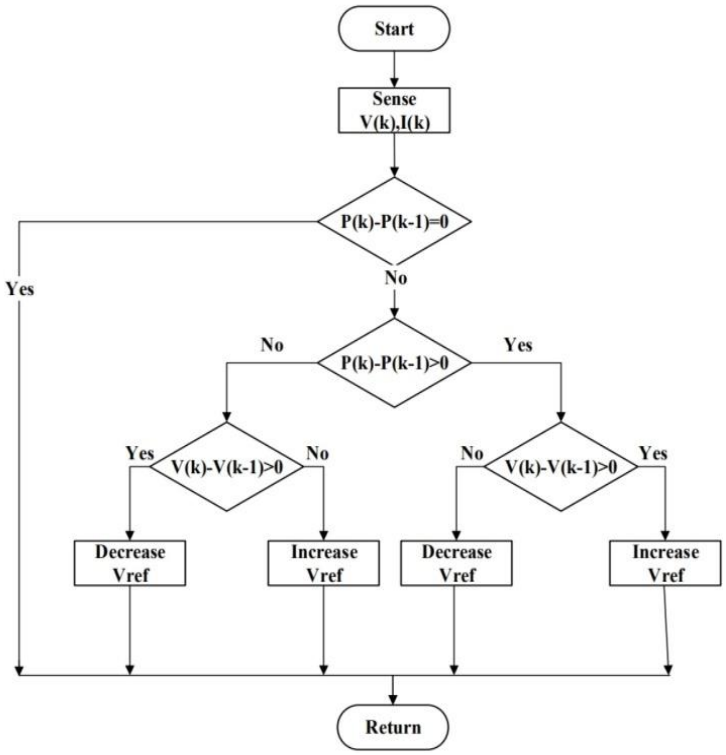


Fig. 3. MPPT flowchart of proposed approach

Fig 3.Depicts general flowchart for perturb and observe algorithm that tracks the maximum power point by altering the PV voltage in line with the reference voltage given by the algorithm. The change in the PV voltage depends on the PV power. The reference voltage is also varied. For Example, during a rise in power, the perturbation should be in the same direction. When power is reduced, the perturbation will progress in the reverse direction. The whole process repeats until the MPP is obtained.

III. CONTROL SCHEME

Due to the unhinged instantaneous dc input and ac output powers, voltage ripples often occur on the dc link voltage at the output of the boost converter in grid connected PV systems. This ripple leads to fluctuations in the PV output voltage, as well as sudden variations in the input voltage of the boost converter [26]. This will lead to power losses due to the resulting improper MPP operations. Hence, the proposed approach ITSMC is designed for the proper MPPT control under uncertain conditions. The aim of the ITSMC is to hold the system error on an integral terminal sliding surface and then unite this error to the origin in finite time [27].

Consider the following switching variable for a grid connected PV device:

$$s=e(t)+\alpha e_i(t), \tag{6}$$

where $e(t) = V_{PV} — V_{ref}$ refers to the error between the output PV voltage V_{PV} and the reference voltage V_{ref} and $e_i(t)$ is the integral term added to the original error ($\ddot{e}_7(t)$ = sign(e(t))). Also, α is a constant coefficient which is greater than zero.

Consider the following sliding manifold σ:

$$\sigma = \dot{e}(t) + \alpha \dot{e}_i(t) \tag{7}$$

The control signal is obtained when $\dot{\sigma}=0$. Thus,

$$\sigma = \dot{e}(t) + \alpha \dot{e}_i(t) \tag{8}$$

Equation (8) leads to:

$$\ddot{V}_{PV} - \ddot{V}_{ref} + \alpha \ddot{e}_i(t) = 0 \tag{9}$$

Equation (4) provides the expression of $\ddot{V}_{PV}$, which when substituted in equation (9) leads to,

$$\frac{1}{C_1}[I_{PV} - \dot{I}_L] - \dot{V}_{ref} + \alpha \ddot{e}_i(t) = 0 \tag{10}$$

Substituting equation(5) in equation (10) yields:

$$u = \frac{1}{V_b}\left[L\dot{I}_{PV} + LC_1\alpha\ddot{e}_i(t) - LC_1\ddot{V}_{ref} - V_{PV} + V_b - ksign(s)\right] \tag{11}$$

Where *k* is a positive constant. Note that $\ddot{V}_{ref}$ is bounded and is within acceptable ranges thus achieving proper performance of the proposed approach.

Consider the following Lyapunov function:

$$V = \frac{1}{2}\sigma^2 \tag{12}$$

$$\dot{V} = \sigma\dot{\sigma} < 0 \tag{13}$$

Substituting equation (8) in equation (13) we get,

$$\dot{V} = \sigma\{\ddot{e}(t) + \alpha\ddot{e}_i(t)\} \tag{14}$$

$$\dot{V} = \sigma\{e(t) + \ddot{\alpha} e_{i(t)}\}$$

$$\dot{V} = \sigma\{\frac{1}{C_1}[I_{PV} - I_L] - V_{ref} + \alpha\ddot{e}_i(t)\}$$

$$= \sigma\{\frac{1}{C_1}I_{PV} - \frac{\dot{1}}{LC1}V_{PV} + \frac{1}{LC_1}V_b(1-u) - \ddot{V}ref + \alpha e_i\ddot{(t)}\}$$

$$= ||\alpha||\{\left|\left|\frac{I_{PV}}{C1}I_{PV}\right|\right| - ||\frac{V_{PV}}{LC_1}|| + \left|\left|\frac{V_b}{LC_1}\right|\right| - \left|\left|\frac{V_B}{LC_1}\right|\right| - \left|\left|\frac{V_b}{LC_1}\right|\right|u - ||\ddot{V}_{ref}|| + \alpha||\ddot{e}_i(t)||\} \tag{15}$$

Substituting *u* in the above equation yields:

$$\dot{V} \leq ||\sigma||\{—||\frac{Vb}{}LC1||k\} \tag{16}$$

$$\dot{V} \leq —||\sigma||\{||V_b/LC_1||k\} \tag{17}$$

It is obvious that if eq. (17) holds then the exponential convergence of *e* to zero is guaranteed.

IV. SIMULATION RESULTS

We conducted a series of computer simulation under various operating conditions to evaluate the performance of the proposed control scheme. The solar panel Sun Power SPR-305E-WHT-D with 96 cells per module is considered in the simulation. The array consists of 66 panel strings and 5 series-connected modules of string. The capacitor C1 value is taken to be 100F and an inductor L with a value of 5 mH is used. A diode with a length of 0.1m is connected to the capacitor C2.which is given as 24mF In ITSMC, k is set to 5,and is 0.5is the voltage source's switching frequency. The frequency converter is 60 hertz, and the frequency of the PWM is 5000 hertz. The initial duty cycle value is assumed to be 0.5. Ideally, the PV array should be capable of delivering a maximum of 100 W/m2.at the number 1000 Irradiance of W/m2 with a total of 330 sun power modules. The scenarios below demonstrate the controller and the performance under varying irradiance conditions were evaluated.

Case-1: The irradiance is considered to be 1000 W/m^2 and at a temperature of 25^{o}C. Fig.4 shows the better SMC model of irradiance and temperature, which is of constant.

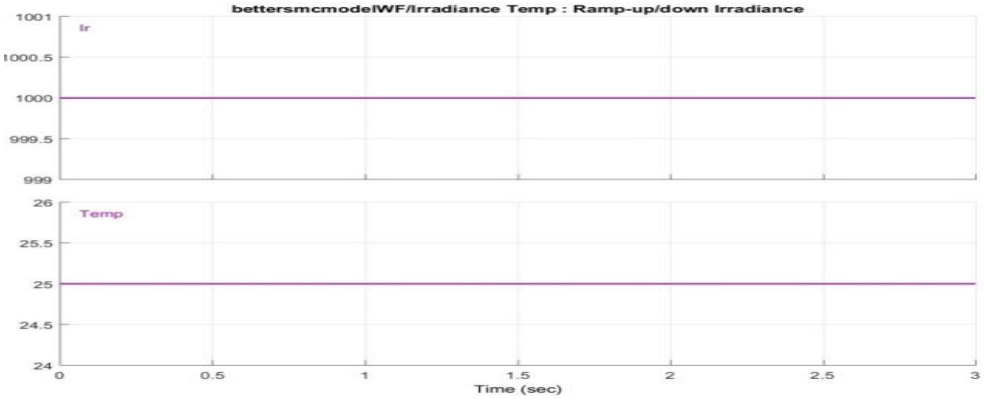


Fig.4. Irradiance and temperature for Case-1

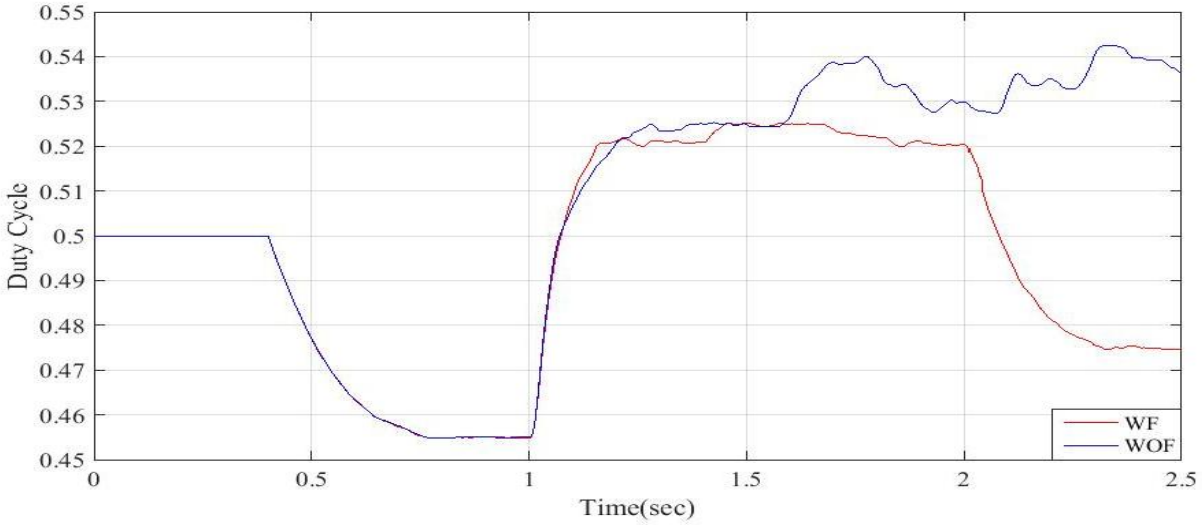


Fig. 5. Duty cycle for Case-1

MPPT controller generates duty cycle in order to create switching signals for the converter. The switching signal allows the boost converter to operate the solar PV system at optimum voltage and current so that the maximum power extraction is possible.

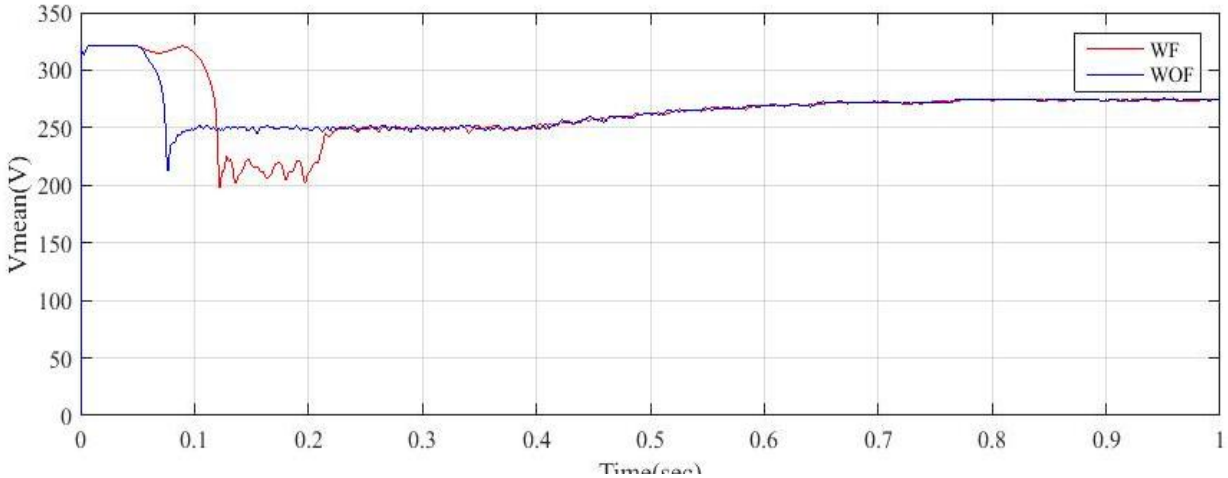


Fig.6. Output voltage of Boost Converter for Case-1

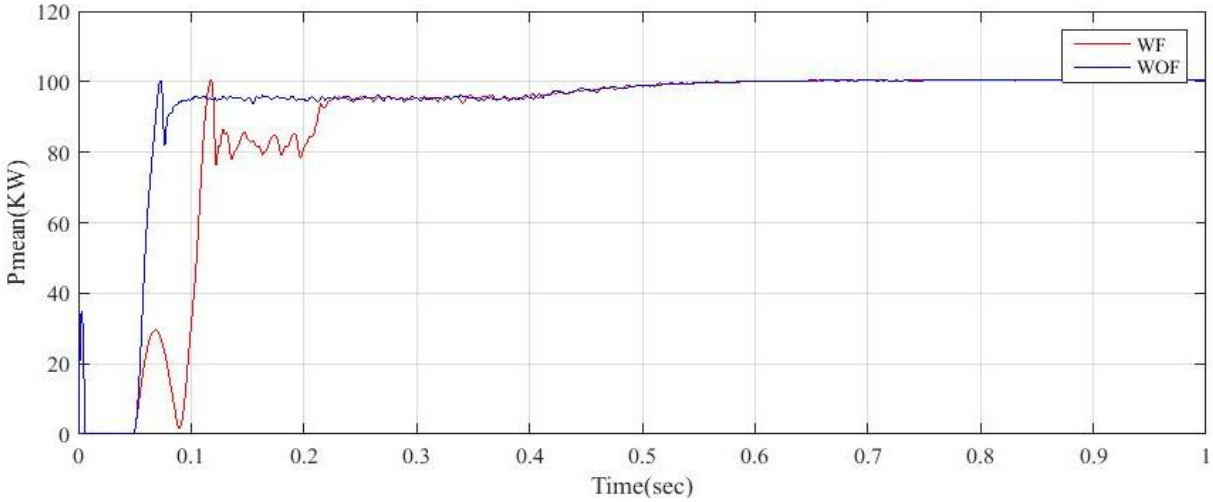


Fig.7. Output power of Boost Converter for Case-1

From fig.7 we obseved that under fault condition controller has taken 0.2 sec of time to attain the maximum stability whereas in the case of without fault it takes less than 0.1 sec to rectify the disturbances occurred and attains the maximum power.Simillarly from fig.8 it is clear that with fault condition voltage gradually decreases from maximum then it encounterd with the disturbances upto 0.2 sec then stabilzes as with the without fault case and gradually increases.This implies the need for a DC-DC converter in the structure of the PV power system. When the single-phase DC-DC converter is replaced by a three-phase one, several advantages appear as faster response,low stresses on active devices,filters components reduction, high-frequency transformer reduction.

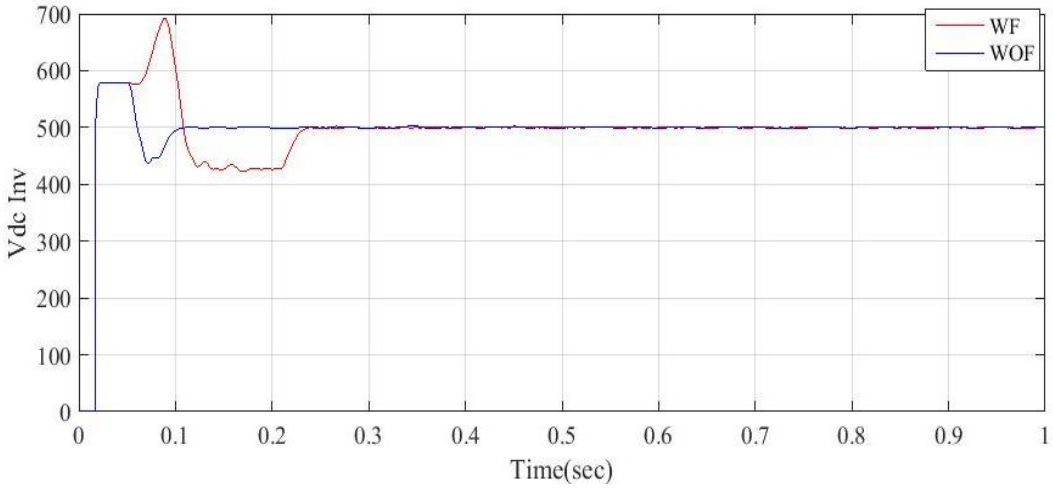


Fig.8. Output voltage of Inverter for Case-1

The high efficiency is one of the most important characteristics of a PV inverter.Thus,whenever possible,these inverters are nonisolated electronic circuits,since a transformer imposes an efficiency drop.The efficiency drop is 2% larger for a low than that for a high-frequency transformer. Hence, when grid isolation is mandatory, the incorporation of a high-frequency transformer.

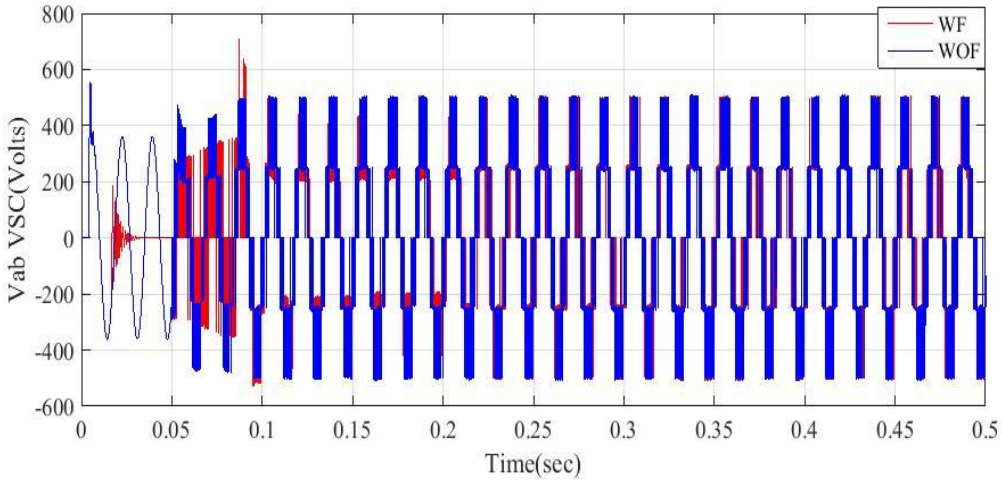


Fig.9.Output Voltage of One of three phases of FITSMC for Case-1

From the above graph of voltage it is seen that it is free from distortions and smooth voltage is obtained.

Case-2**:** The irradiance to be constant and the temperature to be varying as shown in Fig.10. The output voltage and the boost converter's output voltage and power are then impacted and are shown.

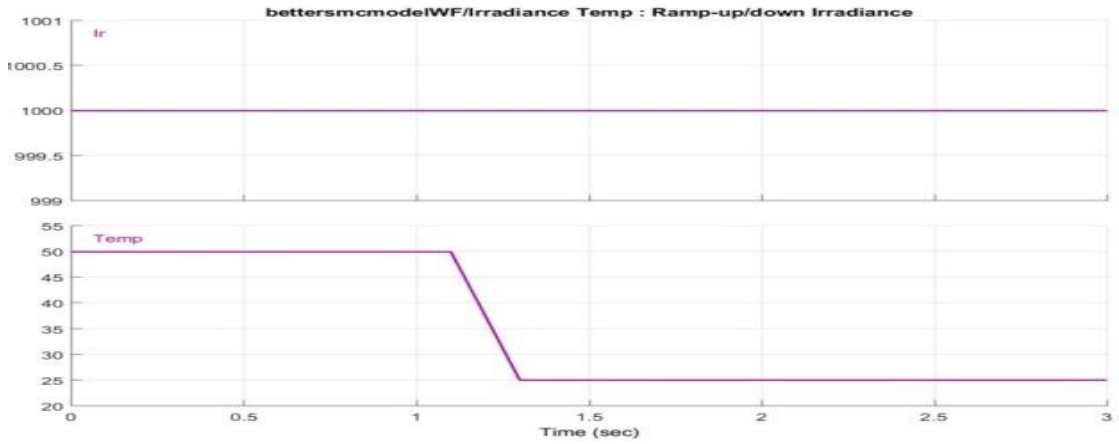


Fig. 10. Irradiance and temperature input to PV module in case-2

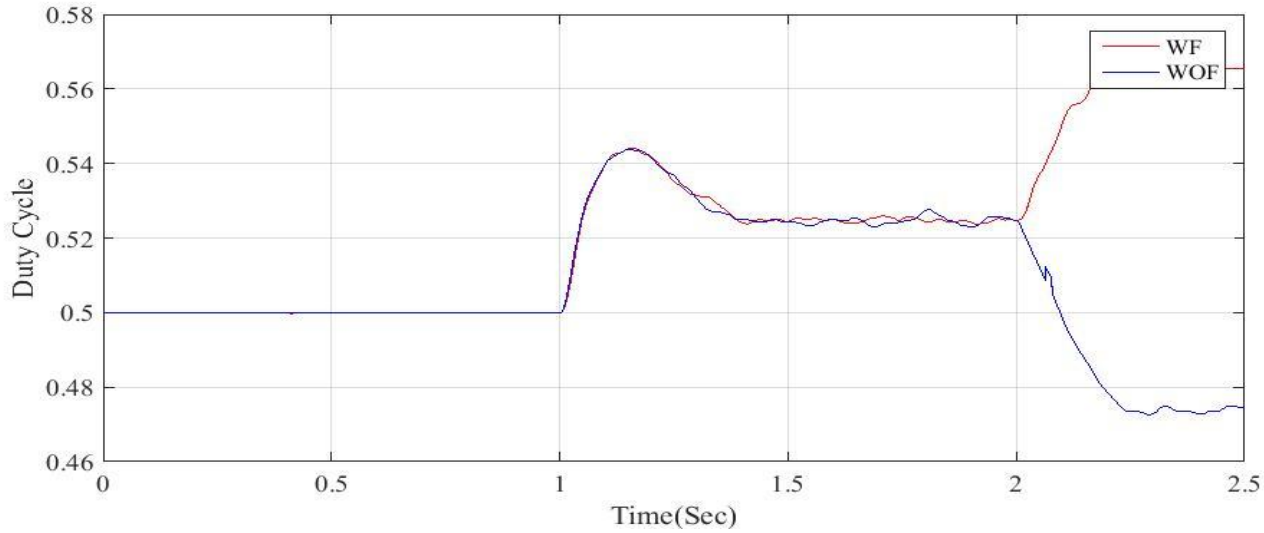


Fig. 11. Scenario 2 duty cycle

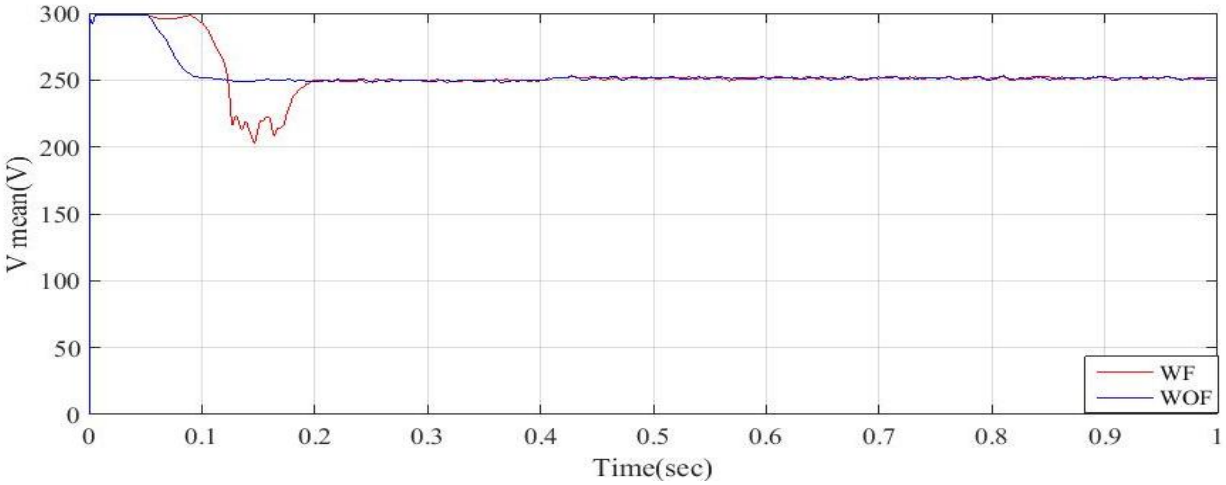


Fig.12. Boost converter output voltage for case-2

Here we can observe that there is a change in voltage with respect to change in temperature, though the voltage falls initially but it settles soon and is on track again. With respect to fault, we can observe a voltage bump but it also falls back on track. From, above figure it is clear that, in spite of the change in temperature, the controller maintains voltage close to the desired value.

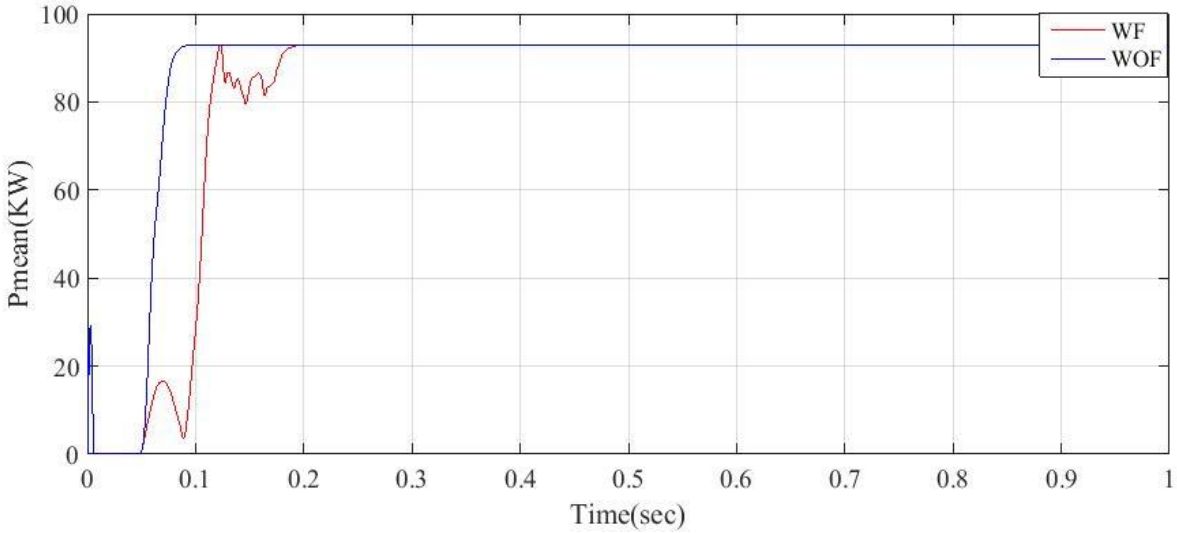


Fig.13. Boost converter output power for case-2

From fig. 13, observe that the power increases slowly irrespective of change in temperature. When a fault occurs we can observe that there is a voltage spike initially and then slowly adjusts itself to the desired value and then remains constant.

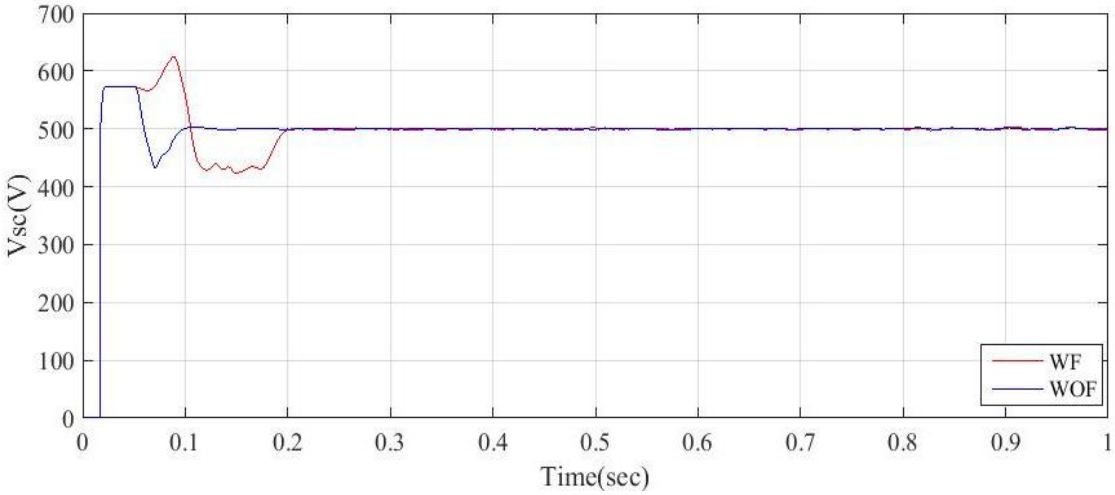


Fig.14. Output Voltage of Transformer for case-2

From the above figure, we can conclude that when the temperature decreases there is also a fall in transformer voltage but it sets back into the desired range. But when there is a fault, before settling back it further drops below the required and thenn settles back. From the above figure we can observe that it is almost ripple-free.

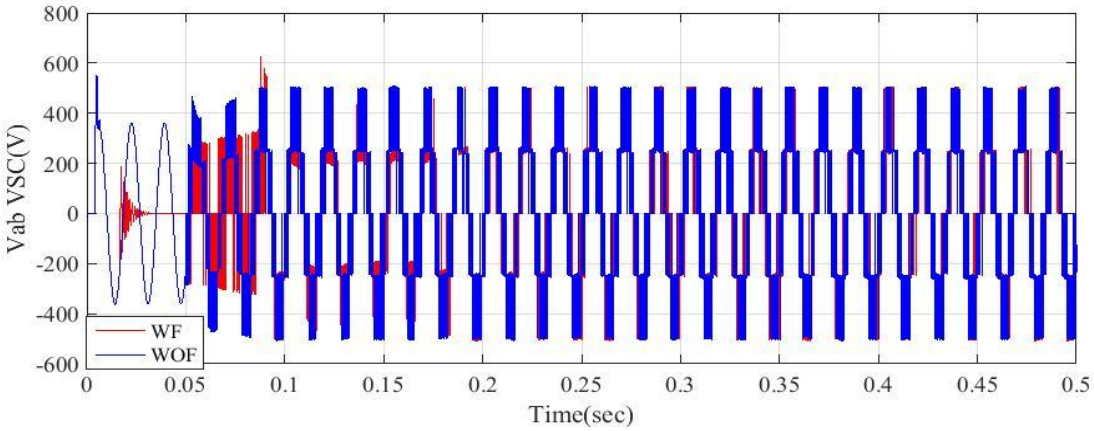


Fig. 15. Output Voltage of One of three phases of FITSMC

From the above figure, we can observe that the output through FITSMC is constant and is distortion free.

V. CONCLUSION

For a grid-connected PV array under varied operating situations, this research developed an integrated terminal sliding mode control mechanism. The concept, which was based on sliding mode, intended to maximize power extraction while minimizing the impacts of irradiance changes and bulk voltage oscillations. The perturb and observe approach was used to establish the reference for maximum power point tracking. In the design, an IGBT switch was employed because it requires low driving power and a simple drive circuit. From Case-1 and Case-2 we can observe that proposed ITSMC controller can effectively reduces the fault under different input conditions. In short, we can conclude that the designed ITSMC has good maximum power point tracking and voltage sag reduction.

VI. REFERENCES

1 G. Prakash and S. Pradeepa, "Design and Modeling of MPPT for Solar Based Power Source," 2018 4th International Conference on Electrical Energy Systems (ICEES), 2018, pp. 624-629.
2 O. Ibrahim, N. Z. Yahaya, N. Saad and M. W. Umar, "Matlab/Simulink model of solar PV array with perturb and observe MPPT for maximising PV array efficiency," 2015 IEEE Conference on Energy Conversion (CENCON), 2015, pp. 254-258.
3 Hyeonah Park and Hyosung Kim, "PV cell modelling on single-diode equivalent circuit," IECON 2013 - 39th Annual Conference of the IEEE Industrial Electronics Society, 2013, pp. 1845-1849..
4 4.J. H. R. Enslin, M. S. Wolf, D. B. Snyman and W. Swiegers, "Integrated photovoltaic maximum power point tracking converter," in IEEE Transactions on Industrial Electronics, vol. 44, no. 6, pp. 769-773, Dec. 1997.
5 T. L. Kottas, Y. S. Boutalis and A. D. Karlis, "New maximum power point tracker for PV arrays using fuzzy controller in close cooperation with fuzzy cognitive networks," in IEEE Transactions on Energy Conversion, vol. 21, no. 3, pp. 793-803, Sept. 2006.

6 R. Aloulou *et al.*, "Improved circuit model of photovoltaic cell for energy harvesting application," *MELECON 2014 - 2014 17th IEEE Mediterranean Electrotechnical Conference*, 2014, pp. 548-552.

7 S. W. Glunz *et al.*, "High-efficiency silicon solar cells for low-illumination applications," *Conference Record of the Twenty-Ninth IEEE Photovoltaic Specialists Conference, 2002.*, 2002, pp. 450-453.

8 M. S. Taha and K. Suresh, "Maximum power point tracking inverter for photovoltaic source pumping applications," *Proceedings of International Conference on Power Electronics, Drives and Energy Systems for Industrial Growth*, 1996, pp. 883-886 vol.2.

9 D. C. Martins, M. Mezaroba, R. Ruther and I. Barbi, "Water pumping from photovoltaic cells using a current-fed parallel resonant push-pull inverter," *Conference Record of the Twenty-Eighth IEEE Photovoltaic Specialists Conference - 2000 (Cat. No.00CH37036)*, 2000, pp. 1529-1532.

10 R. Verma and M. A. Ansari, "Photovoltaic Power Efficient Adjustment using Maximum Power Point Tracking and Boost Converter," 2021 4th International Conference on Recent Developments in Control, Automation & Power Engineering (RDCAPE), 2021, pp. 43-46.

11 M. N. Dehedkar and S. Vitthalrao Murkute, "Optimization of PV System using Distributed MPPT Control," 2018 International Conference on System Modeling & Advancement in Research Trends (SMART), 2018, pp. 216-220.

12 T. Esram and P.L. Chapman,"Comparision of photovoltaic array maximum power point tracking techniques," IEEETrans.Energy Convers., vol.22, no.2, pp.439-449,june.2007.

13 J. W. Zanotti and D. C. Martins, "Input characteristic impedance technique of power converters circuits applied to the maximum power point tracker of photovoltaic panels," 2014 IEEE Asia Pacific Conference on Circuits and Systems (APCCAS), 2014, pp. 292-295.

14 J. Tian, G. Chen and L. Luo, "Sliding Mode MPPT Control Based on Fuzzy Exponential Approach Rate for PV Cells," IEEE 4th Conference on Energy Internet and Energy System Integration (EI2), *2020*, pp. 623-626.

15 M. Kashif, S. Murshid and B. Singh, "Standalone solar PV array fed SMC based PMSM driven water pumping system," 2018 IEEMA Engineer Infinite Conference (eTechNxT), 2018, pp. 1-6.

16 L. R. Shahida and T. M. George, "Implementation of sliding mode control for a buck converter in a photovoltaic system," 2014 International Conference on Advances in Green Energy (ICAGE), 2014, pp. 245-250.

17 S. Pandey, B. Dwivedi and A. Tripathi, "Performance analysis of SMC controlled PV fed boost converter," 2016 7th India International Conference on Power Electronics (IICPE), 2016, pp. 1-4.

18 M. G. Villalva, J. R. Gazoli, E. R. Filho, “Comprehensive Approach to Modeling and Simulation of Photovoltaic Arrays” IEEE transactions on power electronics, vol. 24, no. 5, may 2009.

19 H. S. Rauschenbach, Solar Cell Array Design Handbook. New York: Van Nostrand Reinhold, 1980.

20 X. Liu X., L.A.C. Lopez, “An improved perturbation and observation maximum power point tracking algorithm for PV arrays,”, Proc. of IEEE Power Electronics Specialists Conf., 2004.
21 H-J. Choe, Y-C.Chung, C-H.Sung, J-J.Yun, B. Kang, “Passive Snubber for Reducing Switching-Power Losses of an IGBT in a DC–DC Boost Converter” IEEE transactions on power electronics, vol. 29, no. 12, December 2014.
22 D. G. Montoya, C. A. Ramos-Paja, R. Giral “Improved Design of Sliding-Mode Controllers Based on the Requirements of MPPT Techniques” IEEE transactions on Power Electronics, vol. 31, no. 1, pp. 235-247, Jan. 2016.
23 T. Esram and P. L. Chapman, “Comparison of photovoltaic array maximum power point tracking techniques,” IEEE Trans. Energy Convers., vol. 22, no. 2, pp. 439–449, Jun. 2007.
24 N. Femia, G. Petrone, G. Spagnuolo, and M. Vitelli, “Optimization of perturb and observe maximum power point tracking method,” IEEE Trans. Power Electron., vol. 20, no. 4, pp. 963–973, Jul.2005.
25 M. Salem, Y. Atia” Control scheme towards enhancing power quality and operational efficiency of single-phase two-stage grid-connected photovoltaic systems” J. of Electrical Systems and Information Technology, vol.2, no. 3, pp.314-327, May 2015.
26 C. Chiu., C Shen., "Finite-time control of DC-DC buck convertersvia integral terminal sliding modes," International Journal of Electronics, vol. 99, no. 5, pp .643-655, 2012.
27 Ch. V. N. Raja, P. Sai Vamsi, K. Sowjanya, M. Hari Vardhan, P. Rajeev “Necessity to Design a Controller for PV Module,” International Journal of Innovative Technology and Exploring Engineering (IJITEE), Vol. 9, No. 3, pp. 1932 – 1937, March 2020.

Reliability of Gas Insulated System under Electric Field Stress with Optimal Design of FGM Post Type Spacer

Akanksha Mishra [1], G. V. Nagesh Kumar[2*], D. Deepak Chowdary[3] and B. Sravana Kumar[4]

•

[1]Department of Electrical and Electronics Engineering, Vignan's Institute of Engineering for Women, Visakhapatnam, India; misakanksha@gmail.com
[2]Department of Electrical and Electronics Engineering, JNTUA CE Pulivendula, A.P, India; drgvnk14@gmail.com
[3]Department of Electrical and Electronics Engineering, Dr. L Bullayya College of Engineering, A.P, India; duvvada27@gmail.com
[4]Department of Electrical and Electronics Engineering, GITAM University, Visakhapatnam, A.P, India; sravanbali@gmail.com
*Corresponding Author

Abstract

Gas Insulated Substation (GIS) is essential for the transmission and control of power both in AC and DC electrical systems. Functionally Graded Material (FGM) technology is widely used for the design of the spacer material in the GIS to reduce the electric stress in the system. Optimal designing of the material of the spacer gradings with a particular attention to the number of gradings may prove to be very useful in reduction of the stress in the GIS at an effective cost. This paper deals with the design and development of an optimal dielectric material for the functionally graded material (FGM) spacer in a GIS. A novel optimization method has been proposed which is used for the optimization of the conductor material and the FGM epoxy spacer. The optimal value for each grading of functionally graded material spacer is determined by the proposed method. A dual-objective function is chosen for the optimization problem. The objective of the problem is to minimize the maximum field stress in addition to the standard deviation in the electric field. A post type spacer has been considered for the study. Initially, the optimization of the dielectric material is done only for 4 gradings. Gradually, the number of gradings in the FGM-spacer is increased to determine the optimal number of gradings suitable for the design.

Keywords: HVDC, Gas Insulated Substation, Functionally Graded Material, Optimization

I. Introduction

In the modern industrial world, electric power systems may easily be designated as the backbone of the world economy. A reliable power system is therefore a basic necessity in the present century. The ever-increasing load on the transmission system makes the goal rather difficult to be achieved. The privatization of power industry and rapid industrialization has increased the rapid changes in the power exchanges which may cause further instability in the transmission systems. The need for the electric power systems to become more compact and robust is at a constant rise.

The precedence of HVDC over HVAC transmission system for long distance has been established over time. Hence, the improvement of the performance and reliability of the HVDC systems is a focus of many recent researches. GIS has been associated with a considerable number of power system disturbances and failures. Hence improvement in the performance of the GIS plays an important role in increasing the reliability and stability of the power system. A lot of research is being conducted on the design aspects of HVDC power systems to improve its robustness and reliability. Wang et al [1] have proposed a method for charge dissipation from a GIS without opening the tank. Richard et al [2] have designed an efficient insulated bus pipe for shipboard applications. Sridhar et al [3] have estimated the power loss in a 420KV AC GIB by finite element method in 2-dimension. Riechert [4] has proposed the design of a compact gas Insulated System with reduced footprint on the environment. Volpov et al [5] has analyzed and formulated the SF6 spacer design for both HVAC and DC under time-varying and impulse operating conditions. Kosse et al [6] performed the design and testing for compact DC-GIS at 550 KV. The platform size of the system is expected to reduce by 10% by opting for modular designing method. Electric field stress in the power systems is the crucial factor that determines the consistency and robustness of the GIS. It has been established that the most serious distortion of electric field in a GIS occurs at the triple junction [7].

Sayed et al [8] have calculated electric field stress for different spacer types in the bus duct. An insulation compounding scheme has been proposed to reduce the flashover and stress in the AC and DC systems [9]. Zhang et al [10] have proposed the design of basin type insulators for an HVDC GIS to reduce the stress and flashover at the weak links. Researchers have studied and presented the advantage of an FGM spacer design on the electric field distribution in an GIS [11]. The effectiveness of the design has been evaluated for a multi-particle contamination [12]. Kurimoto et al [13] proposed a U-shaped distribution of ε-FGM spacer for efficient reduction in electric stress. Adari et al [14] proposed an FGM cone type spacer and studied its effectiveness under delaminated condition.

Many researchers have proposed the use of FGM post type spacer as it is effective in reduction of electric filed stress and at the same time its simple design makes it easy to manufacture and cost effective. It is very effective in reducing the field stress at the triple junction even under a protrusion and depression condition [15,16]. Ten gradings of equal dimensions have been used in the spacer and the dielectric coefficient of the material has been designated in an increasing order. Naik et al. [17] have used a di-post FGM spacer which has been found very effective in reduction of the electric field stress. The advantageous position of the spacer due to its simple design has been cited. Metwally [18] has compared the design of disc-type, conical-shaped and the post type spacer. In this work it has been cited that while post type spacer is effective in reducing the electric field stress, inclusion of metal cavities in the design limits the flexibility of the design and limits the manufacturing cost of the spacer.

In all the above methods, it has been proposed to vary the dielectric strength of the FGM-spacer in a specific pattern for various spacer designs. However, the researchers have not concentrated on the optimization aspect of the design. The proposed designs although effective may not be the optimal solution for the problem. Recently, researchers have proposed the use of optimization methods for the optimization of the ε-FGM spacer design. Qasim etal. [19] has proposed the use of PSO for the optimization of the FGM-spacer. Talaat etal. [20] have optimized the dielectric material for a cone shaped spacer using COMSOL-live link. A U-shaped permittivity distribution has been preferred in the design. Although some research has been conducted on the optimization of the FGM-spacer. In the above works, the area of research has been limited to the optimization of the FGM-material only for a fixed number of gradings. Hence, there is a scope for further research in the design of FGM spacer, to be able to qualify the GIS as properly optimized. A detailed study to determine the number of gradings and the appropriate dimensions of the same is

necessary. The number and dimensions of the gradings may vary as per requirement based on the electric field strength in the zone. Also, the determination of the dielectric coefficient for each grading should be done very precisely to be able to provide an optimal solution to the problem.

In this paper, an optimization algorithm has been proposed for the GIS. Dual objectives have been chosen for the optimization, namely, reduction of the maximum electric field and the standard deviation in the field stress with equal weightage. The FGM-spacer material has been optimized for 4 gradings initially. The detailed results are observed. Progressively, the number of gradings is increased in the high stress zones and the optimization process is repeated. The process is continued until an increase in the number of gradings improves the value of the objective function. Since, the gradings have been designed as per requirement; they may not be of equal dimensions. At the same time, since the number of gradings is as per optimization requirements, so the cost of extra gradings is avoided. The results to verify the proposed methodology have been presented and analyzed in detail.

II. Mathematical Modelling of HVDC GIS

The distribution of electric field intensity, E can be determined from the Poisson's Equation [21].

$$E = -\nabla V \tag{1}$$

Where, V is the electric Potential applied in Volt (V)

The electric flux density D in the distributed area is given by

$$D = \varepsilon_0 \varepsilon_r E(C/m^2) \tag{2}$$

where, $\varepsilon_0 = 8.854 \times 10^{-12}(F/m)$ and ε_r = relative dielectric strength of the medium

We know,

$$\nabla . D = \rho_v \tag{3}$$

ρ_v = volume charge density in C/m^3

$$-\nabla.(\varepsilon_0 \varepsilon_r (\nabla V)) = \rho_v \tag{4}$$

Assuming there are no free charges, $\rho_v = 0$, we have

$$\nabla^2 V = 0 \tag{5}$$

The finite element method can be used to analyze different constructions of the GIB. In FEM, the electrostatic energy in the given space can be minimized by the following analysis.

$$W = \frac{1}{2}\int_v \varepsilon E^2 dv \tag{6}$$

In 3-D dimensions the electrostatic energy in terms of electrical potential is given by-

$$W = \frac{1}{2}\int_v \left[\varepsilon_r \left(\frac{\partial V}{\partial r}\right)^2 + \varepsilon_\phi \left(\frac{\partial V}{\partial \phi}\right)^2 + \varepsilon_z \left(\frac{\partial V}{\partial z}\right)^2 \right] ds \tag{7}$$

Where, $\boldsymbol{\varepsilon_r}$, $\boldsymbol{\varepsilon_\emptyset}$ and $\boldsymbol{\varepsilon_z}$ are the r, ϕ, z- components of the dielectric constant.

In this case, $\left(\frac{\partial V}{\partial \emptyset}\right) = \mathbf{0}$. For a 2D simulation,

$$W = \frac{1}{2}\int_v \left[\varepsilon_r \left(\frac{\partial V}{\partial r}\right)^2 + \varepsilon_z \left(\frac{\partial V}{\partial z}\right)^2 \right] ds \tag{8}$$

Where, s is the bounded surface.

After further simplification,

$$\left\lfloor \frac{\partial W'}{\partial V_1} \right\rfloor ---- \left\lfloor \frac{\partial W'}{\partial V_n} \right\rfloor = 0 \tag{9}$$

$\frac{\partial W'}{\partial V}$ should be calculated at every dielectric constant domain.

III. Proposed Objective Function for the Design of the Spacer Material

When the spacer is inserted in the system, the electric field distribution becomes non-uniform. It is maximum at the junctions. A multi-objective function is chosen for optimization of spacer material.

I. Minimization of Electric Field

The electric stress distribution in the bus duct is non-uniform. It is highest at the junction of the spacer, SF6 gas and the outer coating. The objective is to reduce the maximum stress incurred by a GIS in order to reduce the occurrences of localized heating.

$$F_1(\varepsilon_i) = Max\left(E_i(\varepsilon_i)\right)\ V/m \tag{10}$$

Let,

$$Objective\ 1 = Min\ \left(F_1(\varepsilon_i)\right)$$

where, Max(E_i) is the maximum electric field for the material ε_i for each polygon of the spacer. The objective of the optimization is to choose ε of the spacer material such that the peak value electric field in the system is minimized.

Constraints:

The material of the spacer can be varied within upper and lower bounds.

$$\varepsilon_{i\,min} < \varepsilon_i < \varepsilon_{i\,max} \tag{11}$$

II. Uniform Electric Field distribution

The non-uniformity in the distribution of electric stress leads to the creation of local hot spots. To make the field distribution uniform, the standard deviation of the electric field in the system is minimized.

$$F_2(\varepsilon_i) = Min(\sigma(\varepsilon_i)) \tag{12}$$

$$\sigma(\varepsilon_i) = \sqrt{\frac{\sum_{i=1}^{n}(E_j - \mu)^2}{N}}\ V/m \tag{13}$$

E_j is the electric field at the nodes.

where, N = No. of samples

No. of samples is chosen such that the distance between neighboring samples is less than d_{max}

$$N:\ d_{min} < d < d_{max}$$

The multi-objective function is given by-

$$\min(F(\varepsilon_i)) = w_1 \times F_1(\varepsilon_i) + w_2 \times F_2(\varepsilon_i) \tag{14}$$

$$w_1 + w_2 = 1 \tag{15}$$

w_1 and w_2 are chosen such that $w_1 \times F_1(\varepsilon_i) \approx w_2 \times F_2(\varepsilon_i)$. Thus, equal weightage is given to both the objectives.

IV. Optimization of Dielectric Material of FGM Spacer

A reliable algorithm for optimization of the GIB is developed in this research paper. The flowchart for the proposed optimization algorithm is shown in Fig. 1. The flowchart explains the process of optimization of the dielectric material of each polygon of the post type spacer.

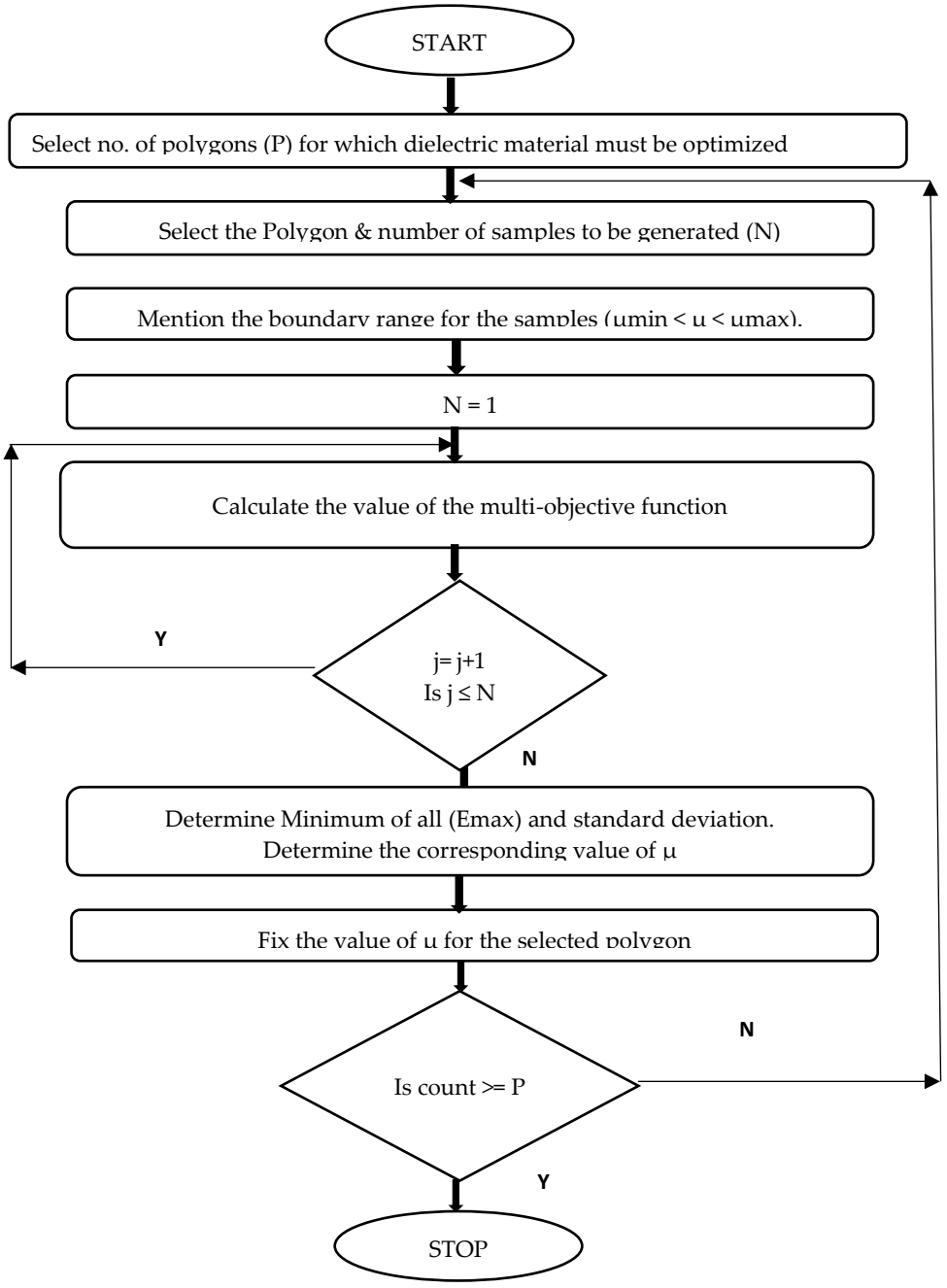


Figure 1: Flowchart depicting the optimization process for GIB post type spacer

The procedure for optimization of the spacer material is mentioned in the steps mentioned below-

Step-1 Install the post-type spacer in the GIS and optimize the dielectric strength of the material for the given multi-objective function (Fig. 1).

Step-2 Provide 4 gradings in the spacer and follow the procedure mentioned in the previous step to optimize the material of each grading.

Step-3 Increase the gradings to 6. Optimize the grading material and compare the value of the parameters and the objective function with the previous case.

Step-4 If a considerable improvement is noticed repeat the step for 8 gradings else GOTO Step-7.

Step-5 The location of the grading is chosen as per the electric field distribution in the various zones of the FGM-spacer. The zone under higher electric stress is graded into smaller zones for further optimization.

Step-6 Compare and analyze the results to obtain the final design of the FGM-Spacer.

Step-7 End Process.

III. Results

A HVDC GIS is considered for the study. The radius of the outer enclosure is 56 mm. The conductor radius is 20.4mm. The insulating medium is SF6 gas with dielectric constant of 1.06. A copper conductor is chosen for the study, with a dielectric constant of 1. The voltage applied to the conductor in this study is 1V. The values for the other voltages can be taken proportionately. The aim of the research is to develop an optimal Post-type FGM spacer for a HVDC GIS. A bi-objective function, consisting of minimization of the electric stress and the stress deviation is chosen for the optimization problem. COMSOL software has been used for the design while MATLAB software has been used for the optimization of the design.

I. Design of 4G- FGM Spacer

After the conductor radius has been optimized, the study focuses on the design of an optimal FGM post-type spacer model. Then, a post-type spacer is designed for the system. Initially, the FGM spacer has been graded into 4 equal layers, each of approximately 9mm as shown in Table 1. The material of each of the gradings of the spacer were optimized. Fig. 2 shows a sample of the optimization result for the 4^{th} grading of the spacer material. It is observed that the objective function has the minimum value at $\varepsilon = 4$. Hence, the value has been chosen for the design. Similarly, the optimization has been performed for each of the gradings of the spacer. The distribution of permittivity in the FGM spacer has been shown in Fig. 3. It is observed that the permittivity in the first grading is 4.4 while the other three gradings have a permittivity of 4 for optimal operation. The surface plots for voltage and the electric field stress distribution are shown in Fig. 4 and 5 respectively. Fig. 6 shows the line plot for the stress distribution in the FGM-spacer.

Table 1: *Permittivity distribution in 4-G FGM Spacer*

Grading No.	Distance from the Outer enclosure (mm)	Permittivity of the FGM gradings
1	0-9	4.4
2	9-18	4
3	18-27	4
4	27-36	4

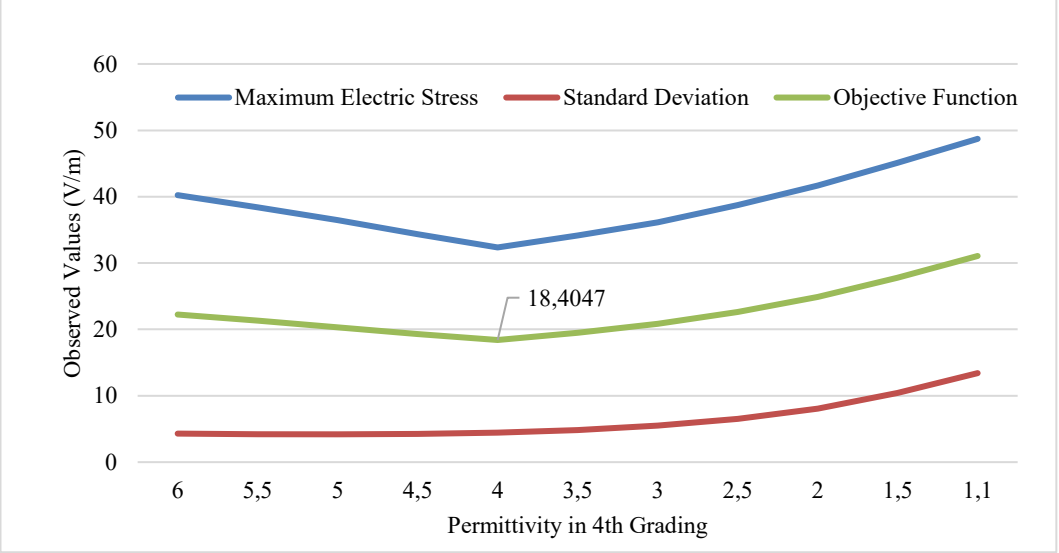


Figure 2: *Distribution of Objective function, Maximum Stress, and Standard Deviation vs permittivity for the 4th Grading of 4G-FGM Spacer*

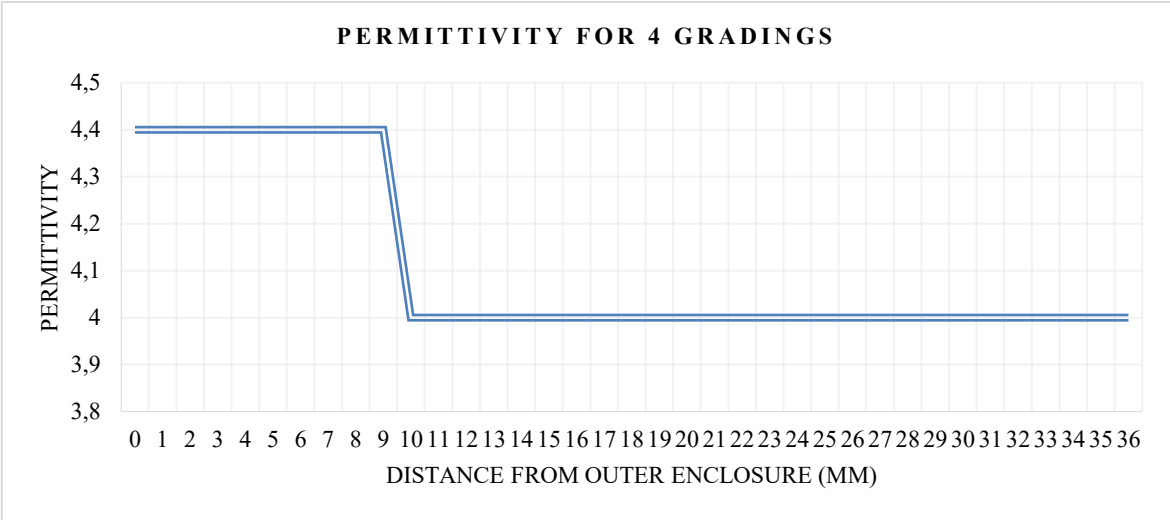


Figure 3: *Distribution of Permittivity in a 4-G FGM Spacer*

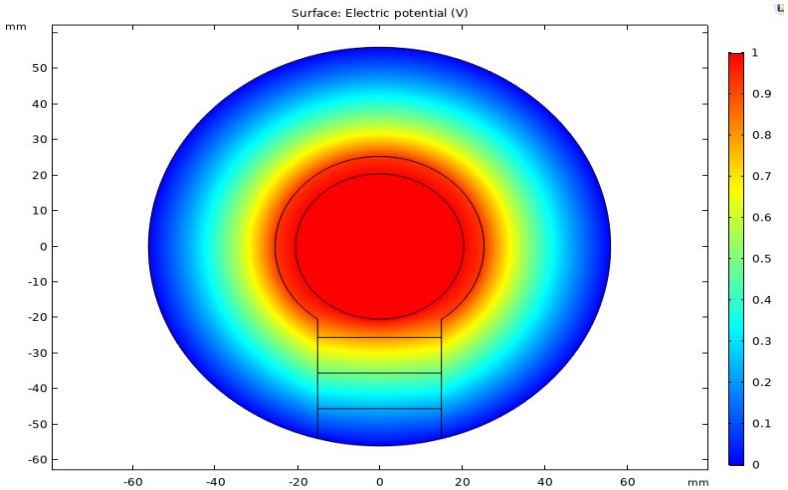


Figure 4: *Electric Potential Distribution for 4-G FGM Post Type Spacer*

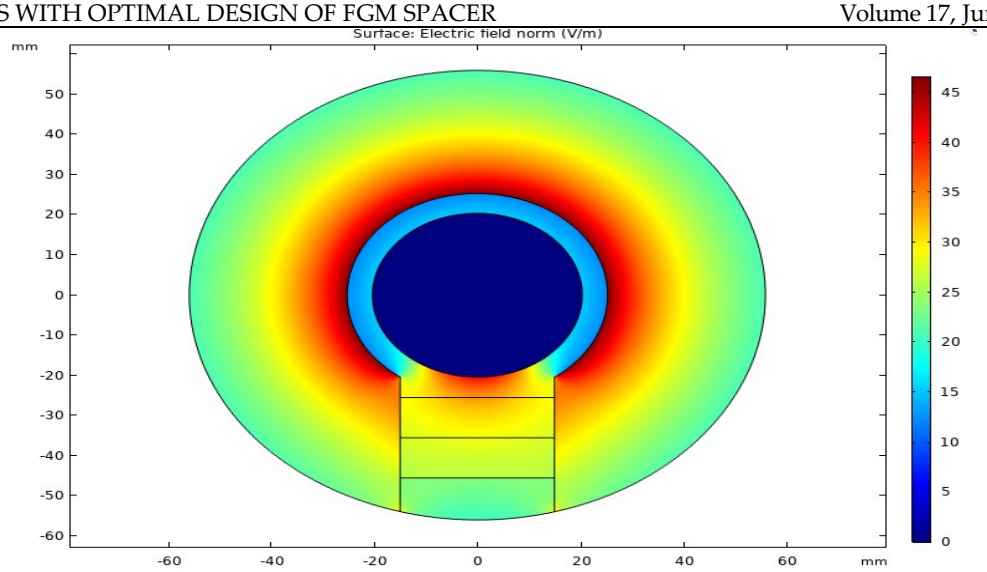


Figure 5: *Electric Field Stress Distribution Surface Plot for 4-G FGM Post Type Spacer*

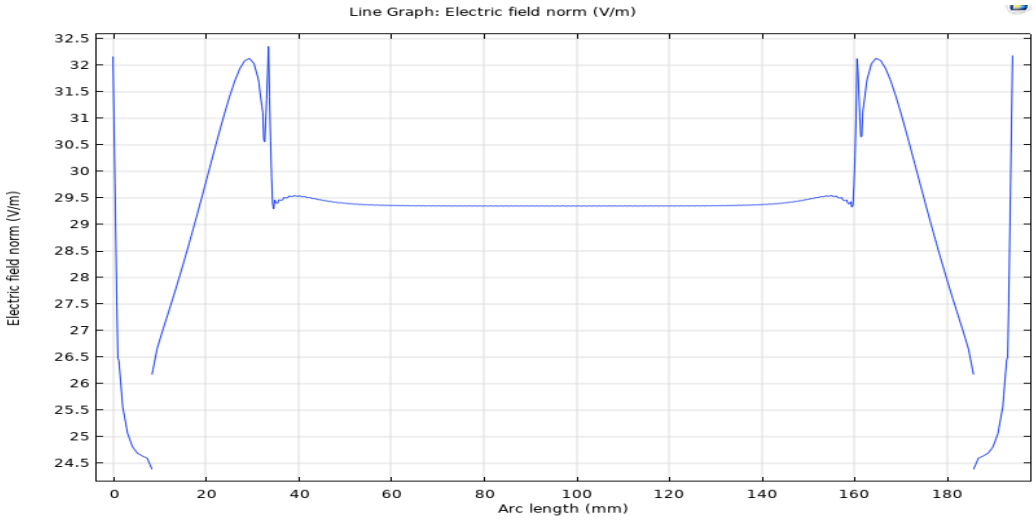


Figure 6: *Electric Field Stress Distribution Line Plot for 4-G FGM Post Type Spacer*

II. Design of 6G FGM Spacer

In a 4G FGM spacer, it is observed that the stress in grading 3 and 4 is much higher in comparison to grading 1 and 2. Hence, the layers 3 and 4 are subdivided into two more layers. The distribution of gradings with respect to distance is shown in Table 2.

Table 2: *Permittivity distribution in 6G FGM Spacer*

Grading No.	Distance from the Outer enclosure (mm)	Permittivity of the FGM gradings
1	0-9	4.8
2	9-18	3.8
3	18-22.5	3.7
4	22.5-27	4.1
5	27-31.5	4.1
6	31.5-36	3.6

The optimization of the permittivity for the 6G spacer material is performed for the chosen objective function. Fig. 7 shows the variation of objective function for various values of permittivity for the 6th grading in the 6G- FGM spacer.

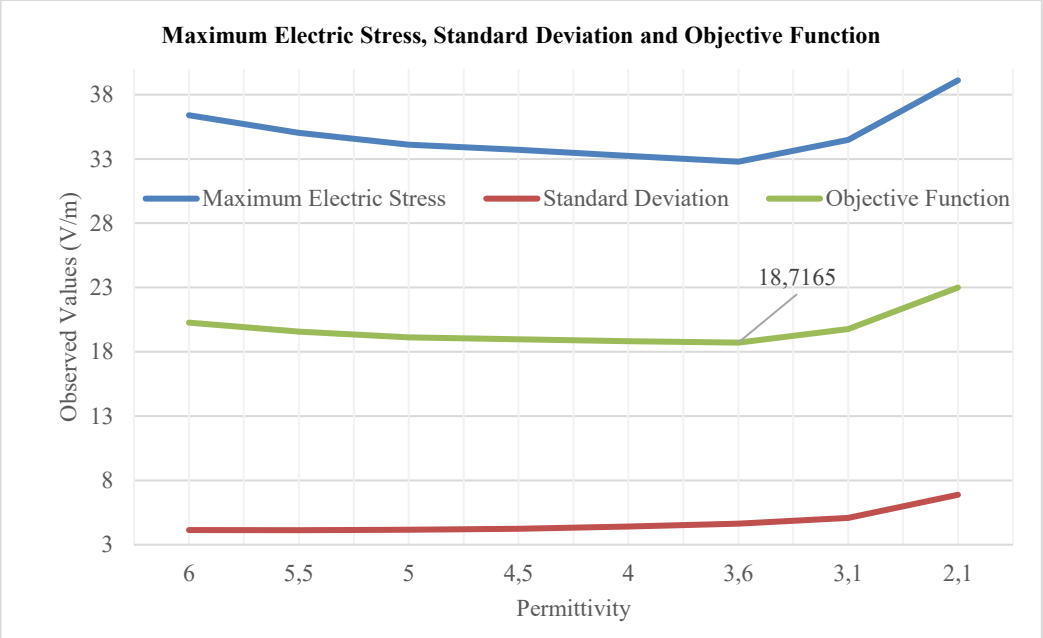


Figure 7: *Distribution of Objective function, Maximum Stress, and Standard Deviation vs permittivity for the 6th Grading of 6G-FGM Spacer*

The optimal permittivity distribution for a 6G-FGM spacer is shown in Fig. 8.

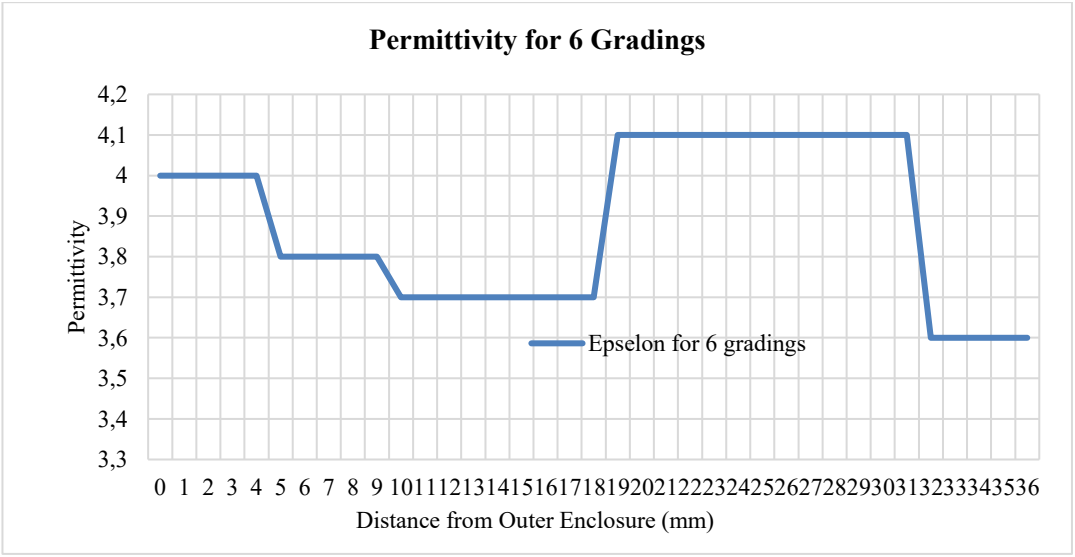


Figure 8: *Distribution of Permittivity in a 6G-FGM Spacer*

The surface plots for electric potential and electric stress for a 6G-FGM post type spacer are shown in Fig. 9 and 10 respectively. Fig. 11 shows the line plot for distribution of stress vs arc length.

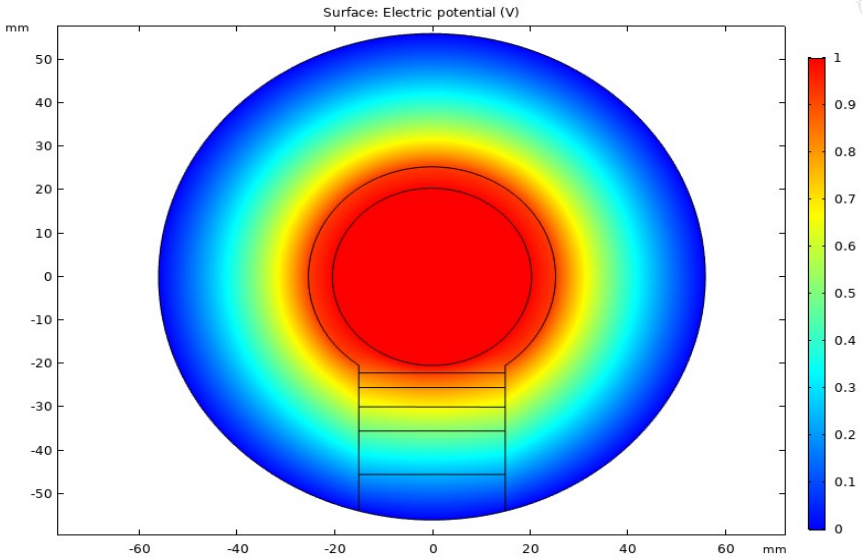


Figure 9: *Electric Potential Distribution for 6-G FGM Post Type Spacer*

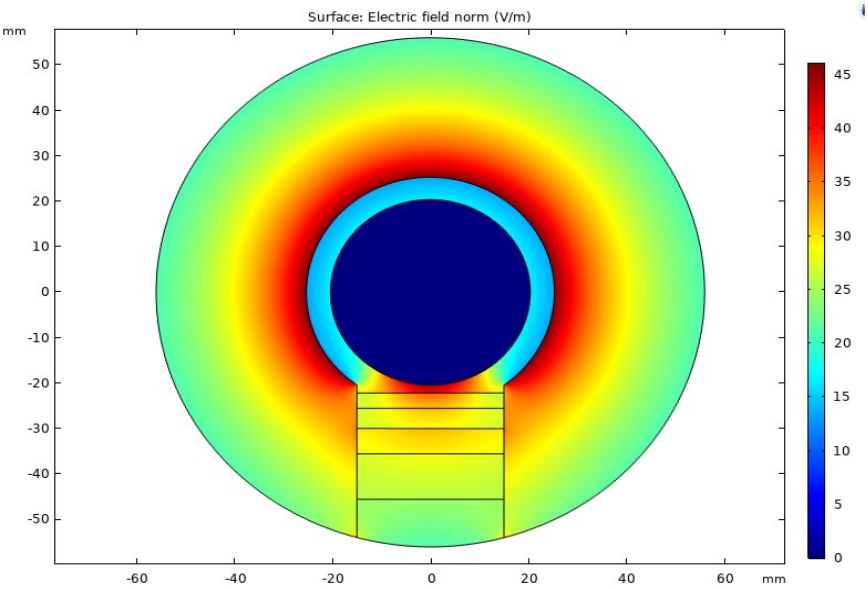


Figure 10: *Electric Field Stress Distribution Surface Plot for 6-G FGM Post Type Spacer*

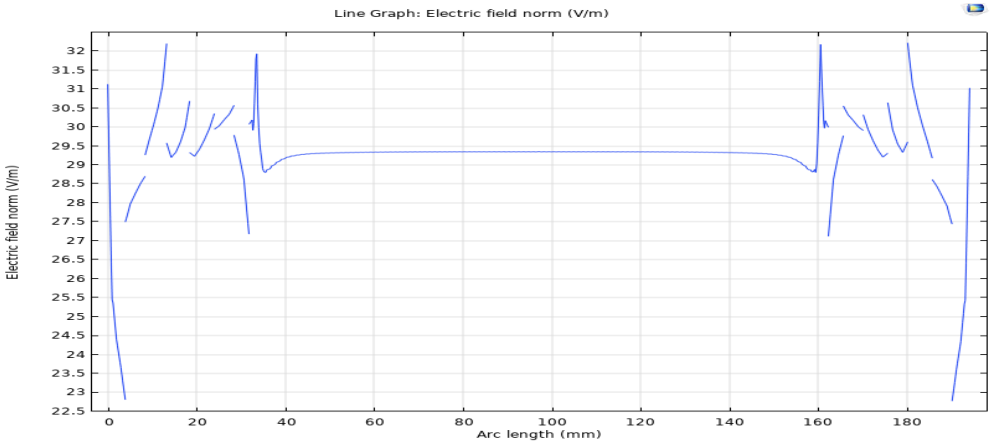


Figure 11: *Electric Field Stress Distribution Line Plot for 6G-FGM Post Type Spacer*

III. Design of 8-G FGM Spacer

The remaining two slots in the 8G-FGM spacer are subdivided to make 8 gradings in the FGM spacer as shown in Table 3. The dielectric strength of the FGM spacer is optimized for the given objective function. A sample of the optimization process is shown in Fig. 12. The optimized distribution of dielectric strength in the spacer is shown in Fig. 13.

Table 3: *Permittivity distribution in 8G-FGM Spacer*

Grading No.	Distance from the Outer enclosure (mm)	Permittivity of the FGM gradings
1	0-4.5	4.7
2	4.5-9	3.7
3	9-13.5	3.6
4	13.5-18	4.1
5	18-22.5	4.4
6	22.5-27	4.5
7	27-31.5	4.7
8	31.5-36	4

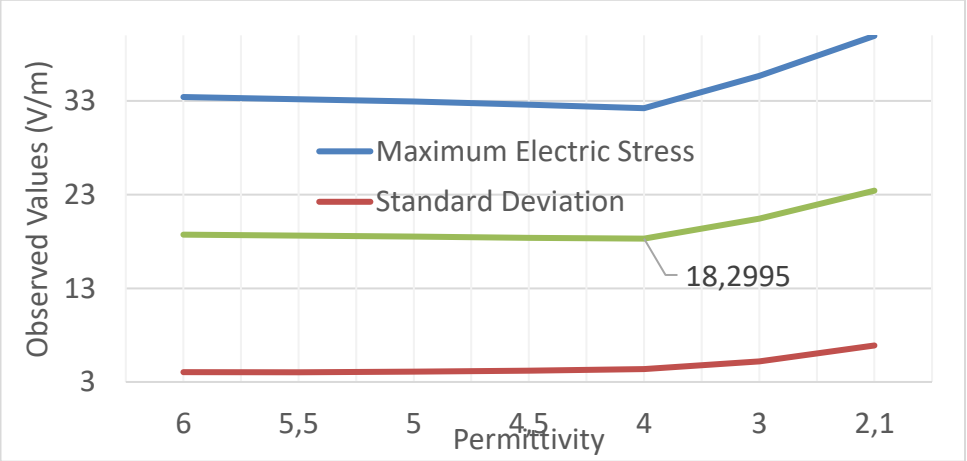


Figure 12: *Distribution of Objective function, Maximum Stress, and Standard Deviation vs permittivity for the 8th Grading of 8G-FGM Spacer*

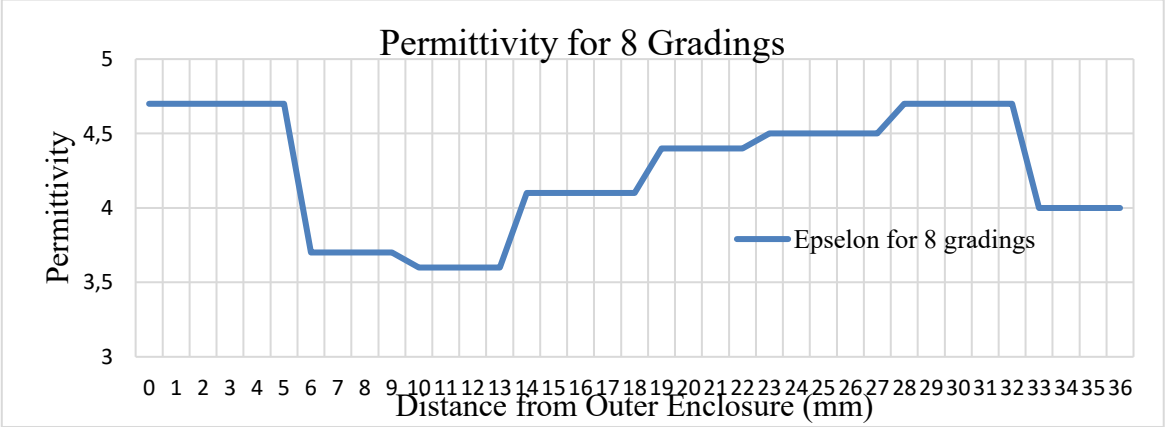


Figure 13: *Distribution of Permittivity in 8G-FGM Spacer*

The performance of the spacer is studied in terms of electric potential distribution and electric stress distribution as shown in the surface plots in Fig. 14 and Fig. 15 respectively. The line plot for electric stress vs arc length and arrow line showing the direction of the stress distribution is shown in Fig. 16 and Fig. 17 respectively. The zoomed contour plot in Fig. 18 focuses on the electric field in the stress zone. The 3D view of the electric stress distribution can be seen in Fig. 19.

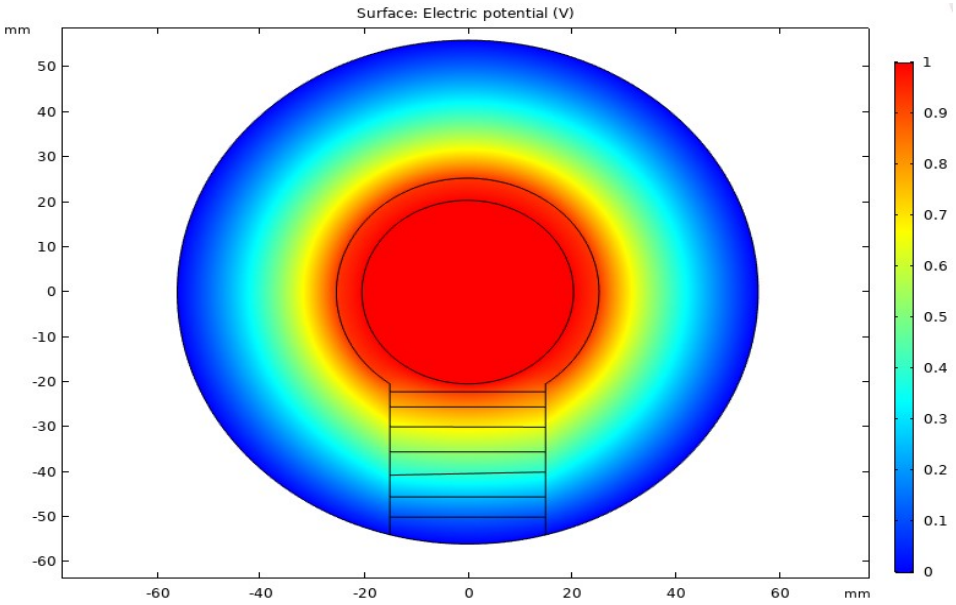


Figure 14: *Electric Field Stress Distribution Surface Plot for 8G- FGM Post Type Spacer*

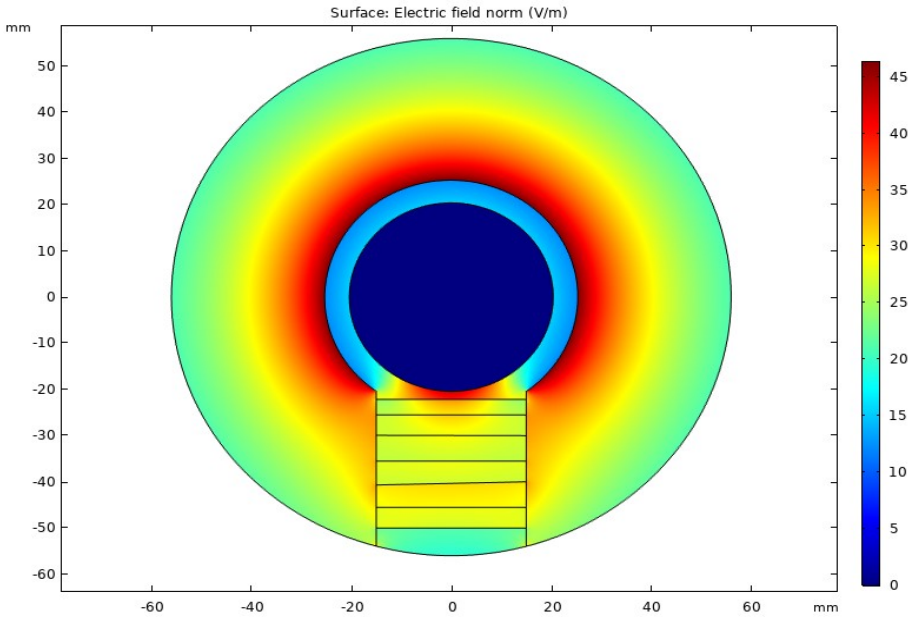


Figure 15: *Electric Potential Distribution for 6-G FGM Post Type Spacer*

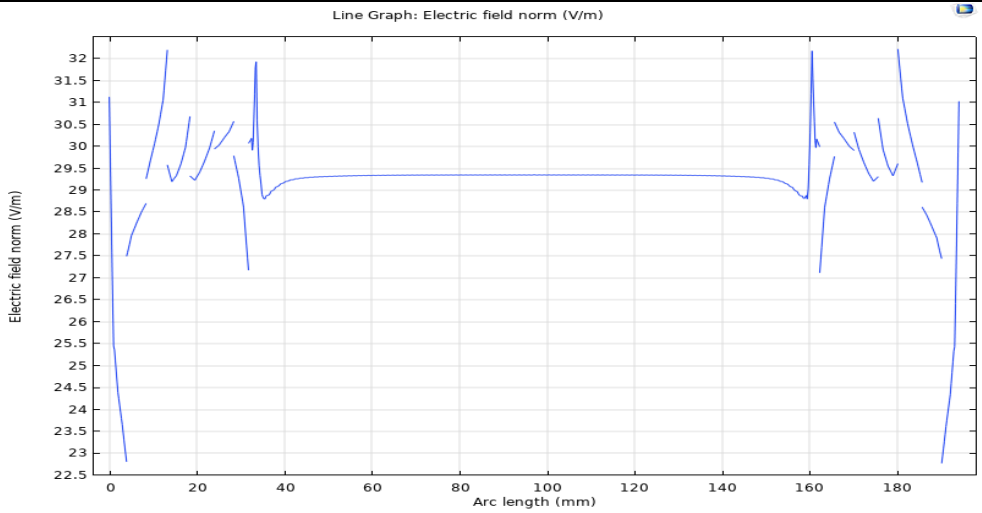


Figure 16: *Electric Field Stress Distribution Line Plot for 6-G FGM Post Type Spacer*

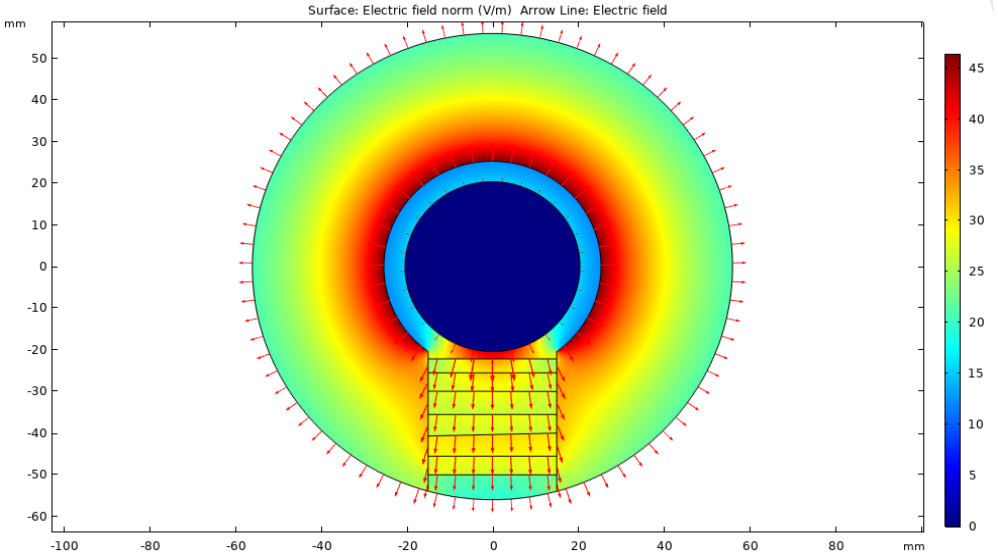


Figure 17: *Arrow line showing direction of field stress*

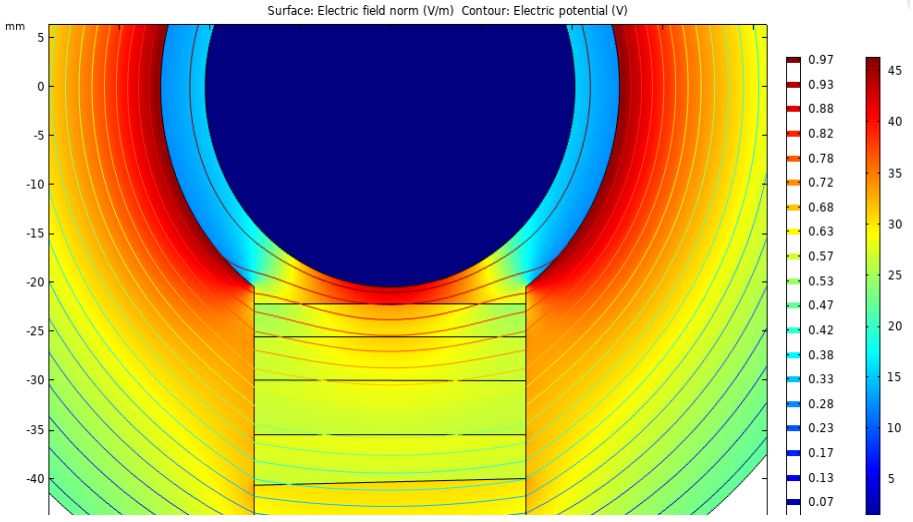
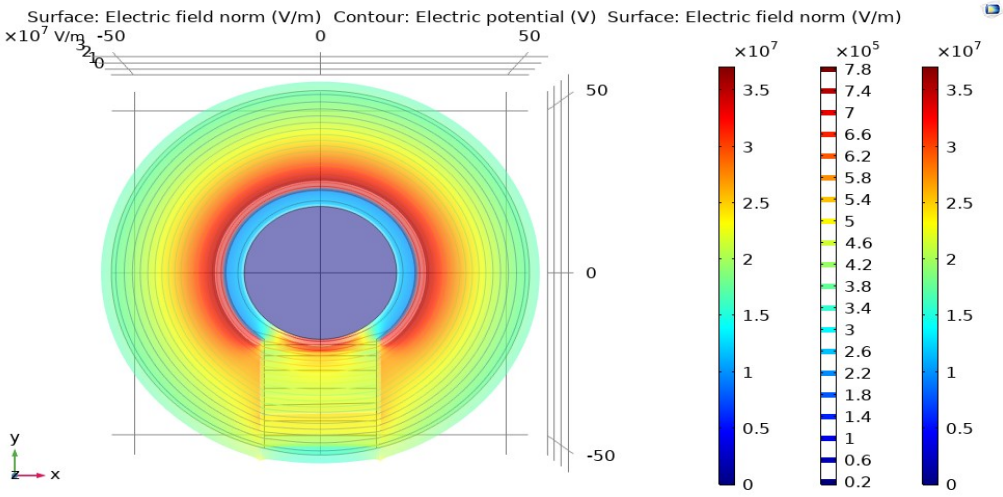
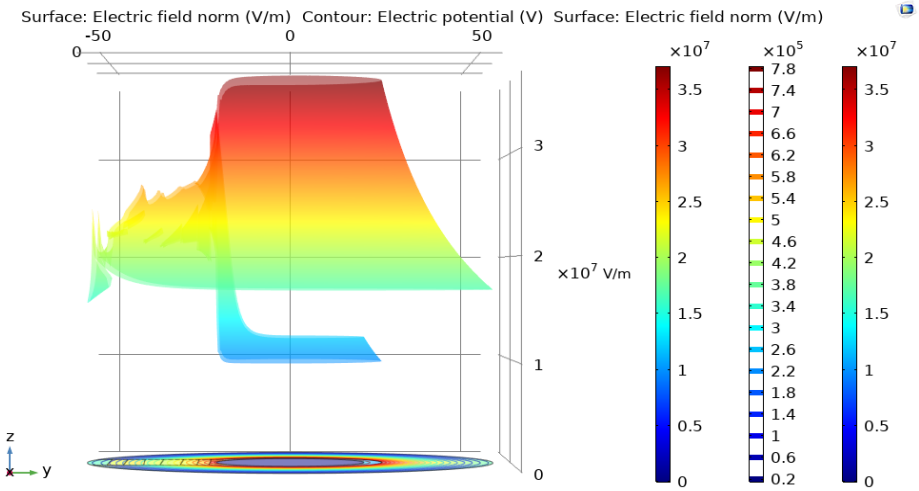


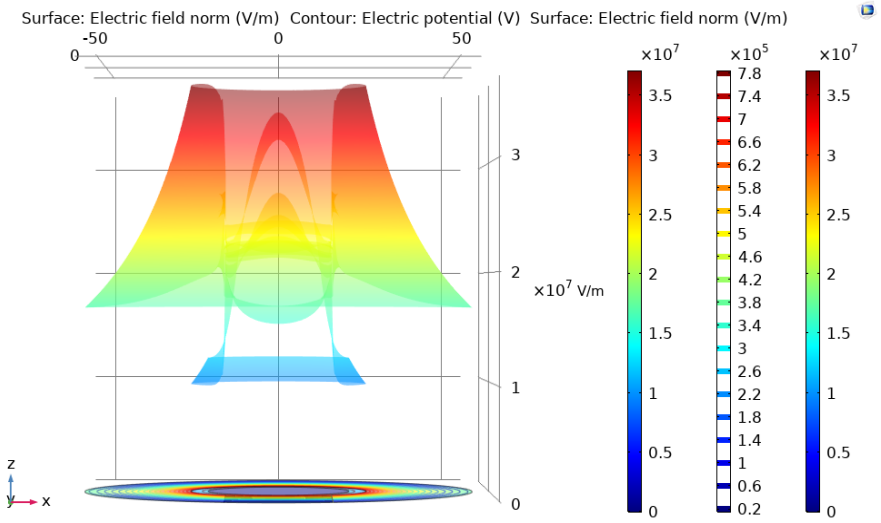
Figure 18: *Zoomed Contour Plot for Electric Stress Distribution*



(a) XY View of electric stress distribution



(b) YZ view of Electric Stress Distribution



© XZ View of Electric Stress Distribution

Figure 19: *3D View of Electric Stress Distribution*

IV. Comparative Analysis of Results

A comprehensive data of the electric field distribution can be observed in Table 4 shown below. Fig. 20 shows the variation of the dielectric strength of the material in different zones for 4G-FGM, 6G-FGM and 8G-FGM respectively.

Table 4: *Distribution of dielectric strength in FGM Spacer*

Type	0 - 4.5 mm	4.5 - 9 mm	9 - 13.5 mm	13.5 – 18 mm	18 – 22.5 mm	22.5 – 27 mm	27 – 31.5 mm	31.5 – 35.5 mm
8 - Grad	4.7	3.7	3.6	4.1	4.4	4.5	4.7	4
6 - Grad	4.8		3.8		3.7	4.1	4.1	3.6
4 - Grad	4.4		4		4		4	
0 - Grad	4.1							

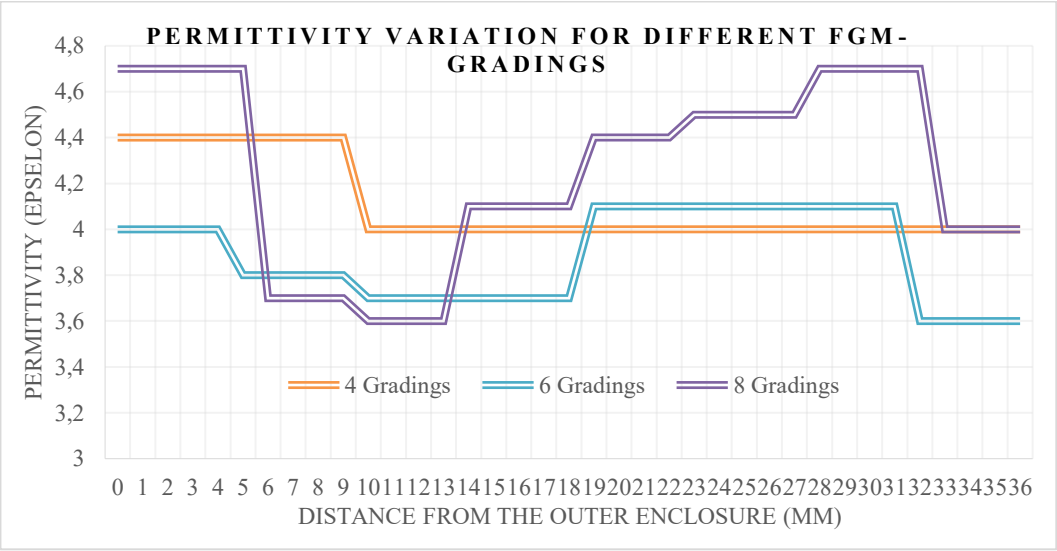


Figure 20: *Distribution of dielectric strength in the FGM-Spacer*

The comparison of the study for different gradings is presented in Table 4. Since, the average of the dielectric strength of the material in each case of FGM spacer is nearly equal to 4.1. The results obtained for different grading types are represented in Table 5. The minimum value for objective function is 18.29 which is obtained in case of 8G FGM spacer.

Table 5: *Comparison of Gradings*

S. No.	Grading Case	Maximum Electric Stress	Standard Deviation	Objective Function
1	0G; Ɛ = 4	34.4184	4.2164	19.3174
2	4G	32.3525	4.4569	18.4047
3	6G	32.7852	4.6477	18.7165
4	8G	32.2214	4.3777	18.2995

Grading high (GH), grading low (GL) and grading U (GU) are the standard methods of distribution of dielectric strength in the spacer material. The performance of the proposed design has been compared with each of the existing methods in Table 6. The distribution of the dielectric material in each of the above methods is shown in Fig. 21.

The average value of the dielectric strength in each of the cases has been maintained nearly equal to maintain uniformity.

Table 6: *Comparison with Existing Methods*

S. No.	Parameter	Proposed 8G FGM	GH-8G FGM	GL-8G FGM	GU-8G FGM
1	Maximum Electric Stress	32.2214	38.6171	35.8664	33.417
2	Standard Deviation	4.3777	4.2556	5.28	4.1066
3	Objective Function	18.2995	21.4363	20.5737	18.76

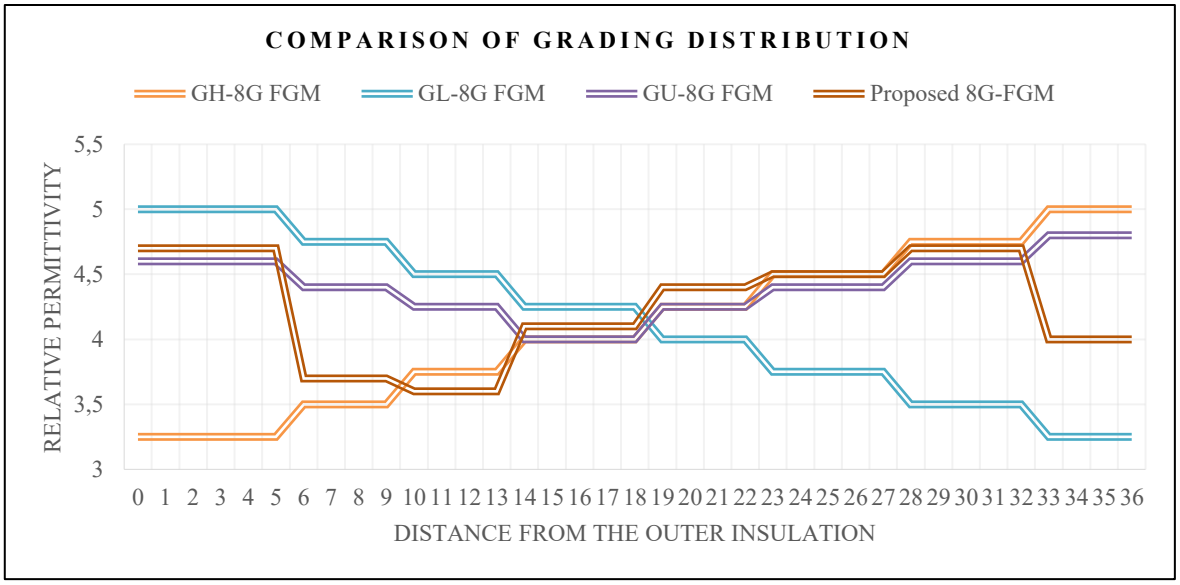


Figure 21: *Distribution of gradings in the FGM spacer for different configurations.*

V. Conclusion

An optimum design of GIS spacer can increase the reliability of the electric transmission system. In this paper, the FGM GIS spacer is designed and the results have been studied. It is observed that

- The FGM method reduces the electric stress in the spacer. There is a marked reduction in the values of the objective in FGM cases.
- The distribution of stress in the post-type spacer has been studied for each of category of FGM grading.
- All the FGM gradings have shown a satisfactory performance in reduction of the maximum electric stress and objective function. However, the 8G- FGM has been most effective in the reduction of the electric stress and the objective function.
- The comparison of the results with existing FGM methods shows that the proposed method helps to achieve a lower objective function value. Thus, the performance of the proposed FGM is better in comparison to the state of art methods.

References

[1] Feng W., Fangwei L., Lipeng Z., She C., Chuanyang L., and Yi X. (2021). Short-time X-ray Irradiation as a Non-contact Charge Dissipation Solution for Insulators in HVDC GIS/GIL, *IEEE Transactions on Dielectrics and Electrical Insulation*, 28(2): 704-709.

[2] Richard W., Moni I., Ruth H. P., Charles S. (2007). Insulated Bus Pipe (IBP) for Shipboard Applications, *IEEE Electric Ship Technologies Symposium*.8:122-129.

[3] Sridhar C., Venkatesh S. (2013). Power Loss Estimation in a 420kV Gas Insulated Busbar (GIB) by Theoretical and Simulation Techniques – A Comparison, *2013 IEEE 1st International Conference on Condition Assessment Techniques in Electrical Systems (CATCON)*, India,213-217.

[4] Uwe R. (2020). Compact High Voltage Direct Current Gas-insulated Systems, *IEEE PES Transmission and Distribution Conference and Exposition*, Chicago,1-4.

[5] Evgeni V. (2004). Dielectric Strength Coordination and Generalized Spacer Design Rules for HVAC & DC SF Gas Insulated Systems, *IEEE Transactions on Dielectrics and Electrical Insulation*, 11(6):949-963.

[6] Maria K., Karsten J., Mark K., Dejun L, (2019). Overview of development, design, testing and application of compact gas-insulated DC systems up to ±550 kV, *Global Energy Interconnection*, 2(6): 567-577.

[7] Boxue D., Jin L. and Hucheng L.(2019). Electrical Field Distribution along HVDC GIL Spacer in SF6/N2 Gaseous Mixture, *Electric Power Conversion*, 1-19.

[8] Sayed A. W., Turky G.M., Shabayek D. M. (2014). Electric Field Stress Calculation for different spacer types in Bus Duct, *International Journal of Scientific Research Engineering & Technology (IJSRET)*, 3(6): 958-963.

[9] C. Li, B. Liu, J. Wang, R. Gong etal(2019). Novel HVDC Spacers in GIS/GIL by Adaptively Controlling Surface Charges – Insulation Compounding Scheme, *2nd International Conference on High Voltage Engineering and Power Systems (ICHVEPS),* Indonesia,38-44.

[10] Zhang B., Zhong J., Han G. (2020). Modification of HVDC GIS/GIL Basin Insulators Based on Electrical and Mechanical Collaborative Design, *2020 IEEE International Conference on High Voltage Engineering and Application (ICHVE)*, China, 1-5.

[11] Syarif H., Fransiskus D., Umar K. (2016). Electric Field Optimization on 150 kV GIS Spacer using Functionally Gradient Material, *2nd International Conference of Industrial, Mechanical, Electrical, Chemical Engineering (ICIMECE),*Indonesia, 254-259.

[12] Abd Allah M. A., Sayed A. W., Youssef A. A. (2013) Effect of Functionally Graded Material of Disc Spacer with Presence of Multi-Contaminating Particles on Electric Field inside Gas Insulated Bus Duct, *International Journal of Electrical and Computer Engineering (IJECE)*, 3(6): 831-848.

[13] Muneaki K., Masahiro H., Hitoshi O. (2010). Application of Functionally Graded Material for Reducing Electric Field on Electrode and Spacer Interface, *IEEE Transactions on Dielectrics and Electrical Insulation*, 17(1):256-263.

[14] Jagadeesh A., Venkata Siva Krishna R. G., Venkata Nagesh Kumar G. (2018). Mitigation of field stress with metal inserts for cone type spacer in a gas insulated busduct under delamination, *Engineering Science and Technology*, 21(5): 850–861.

[15] Janaki P., Karthick N. & Nagesh Kumar G. V., (2020). Study of electrostatic field effect in a three-phase gas-insulated busduct with FGM spacer under the effect of protrusion, *Journal of Electromagnetic Waves and Applications*, 34(16): 2107–2129.

[16] Janaki P., Nagesh Kumar G. V., Deepak Chowdary D., Sravana Kumar B.(2020). Study of electric field stress on the surface contour and at the triple junction in three phase GIS with FGM spacer under the depression defect, *International Journal of Emerging Electric Power Systems*, 21(5):20200080.

[17] Gopichand Naik M., Amarnath J., and Kamakshiah S.,(2012) Computation of Electric Field for FGM Spacer Using Di-Post Insulator in GIS, *International Journal of Electrical Engineering*, 5(4): 465-474.

[18] Metwally I. A., (2012). Reduction of electric-field intensification inside GIS by controlling spacer material and design, *Journal of Electrostatics*, 70(2): 217-224.

[19] Syed Abdullah Q. and Nandini G. (2015). Use of Particle Swarm Optimization in the Computation of an optimal permittivity distribution in Functionally Graded Material insulators, *International Conference on Condition Assessment Techniques in Electrical Systems (CATCON),* India, 184-188.

[20] Talaata M., El-Zein A., Amin M. (2017). Developed optimization technique used for the distribution of U-shaped permittivity for cone type spacer in GIS, *Electric Power Systems Research,* 163:754-766.

[21] William H. Hayt Jr., Engineering Electromagnetics, fifth ed., McGraw-Hill Book Company, 1989.

Corrected Proof

Journal of Hydroinformatics

Check for updates

© 2022 The Authors

Journal of Hydroinformatics Vol 00 No 0, 1 doi: 10.2166/hydro.2022.065

Unsteady flow analysis using hydrological and hydraulic models for real-time flood forecasting in the Vamsadhara river basin

Arunima Mahapatra *, Vazeer Mahammood and K. Venkatesh

Department of Civil Engineering, Andhra University College of Engineering (A), Visakhapatnam, Andhra Pradesh 530003, India
*Corresponding author. E-mail: arunimamahapatra162@gmail.com

AM, 0000-0003-1130-9196; VM, 0000-0003-1667-5232

ABSTRACT

The river Vamsadhara runs through the states of Andhra Pradesh (AP) and Odisha along a stretch of coastline that is prone to cyclonic storms. Riverine flow, along with cyclonic gales, is a crucial issue for most of India's coastal districts. As a result, a developed flood forecasting model is required to mitigate the danger of flooding to a certain level. For evaluating maximum water depth and inundation of flood plains induced by storms under existing and future land use circumstances, hydrological and hydraulic models are more prominently studied. The current work employs hydrological and hydrodynamic models to simulate a real flood inundation model for unsteady flow conditions. The technique involves the processing of the digital elevation models (DEM) to generate flood hydrographs that serve as boundary conditions for the reaches. In the present analysis, Manning's roughness coefficient is used as a sensitive parameter. Calibration and validation of extreme flood events that occurred in 2006, 2010, and 2013 using observed water levels yielded good results, with model performances of 0.79, 0.68, and 0.84, respectively. The findings of the generated depth, velocity, and flood extent maps are presented. These maps can be used to plan for flood disasters and long-term watershed management.

Key words: flood inundation modeling, HEC-HMS, HEC-RAS, river Vamsadhara, unsteady flow

HIGHLIGHTS

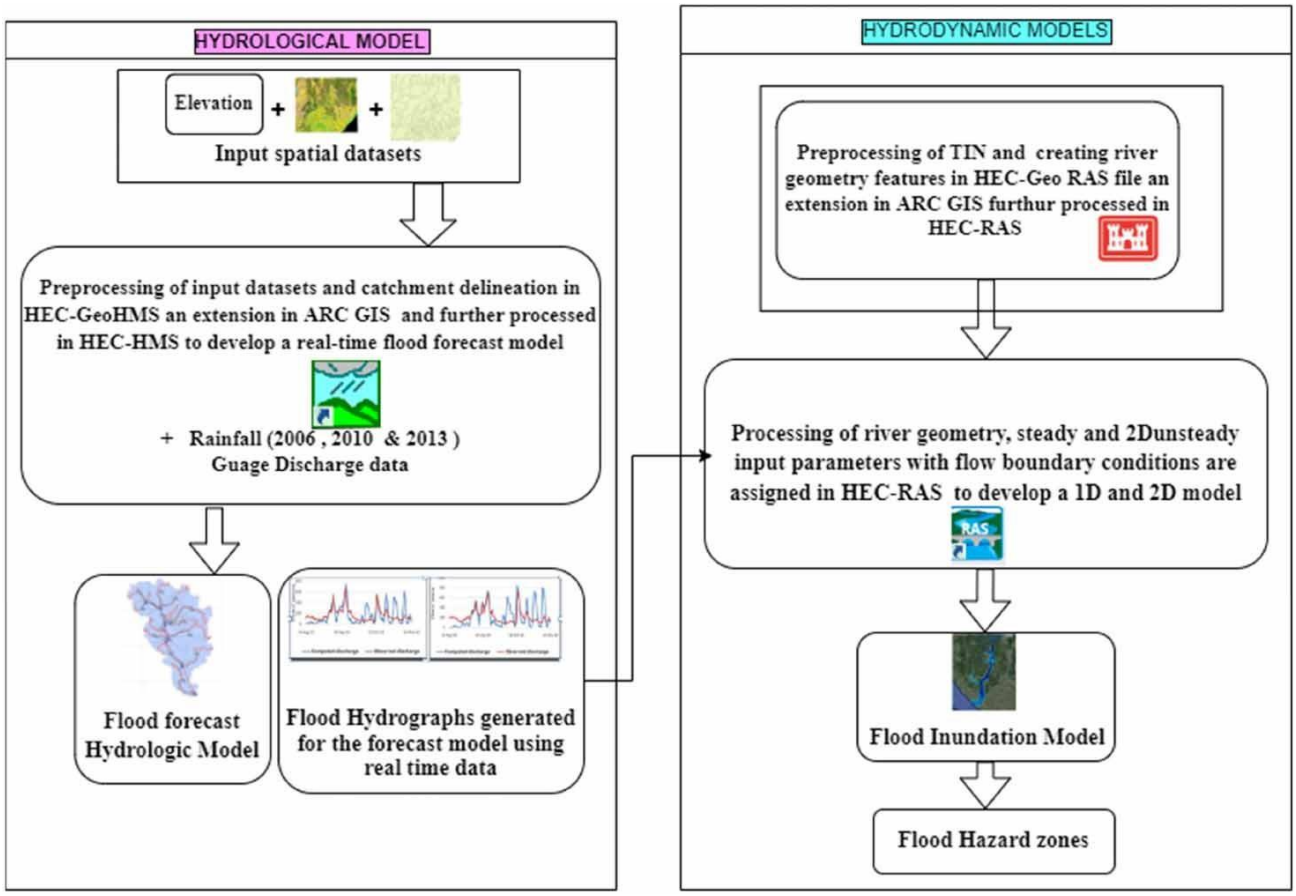
- To develop a calibrated rainfall-runoff model for a large river basin.
- Interactions between hydrologic and hydrodynamic models.
- Simulations of two-dimensional unsteady flow hydrodynamic model.
- The high-risk zones generated by this model may help to plan flood prevention, mitigation, relief, and restoration efforts by related government agencies.

This is an Open Access article distributed under the terms of the Creative Commons Attribution Licence (CC BY 4.0), which permits copying, adaptation and redistribution, provided the original work is properly cited (http://creativecommons.org/licenses/by/4.0/).

Downloaded from http://iwaponline.com/jh/article-pdf/doi/10.2166/hydro.2022.065/1120810/jh2022065.pdf
by guest

Corrected Proof

GRAPHICAL ABSTRACT



NOTATIONS

Abbreviation	Description
1D	One-dimensional
2D	Two-dimensional
CWC	Central Water Commission
DEM	Digital elevation model
DGPS	Differential Geographical Positioning System
DTM	Digital Terrain Model
GCP	Ground Control Points
GD	Gauge discharge
GIS	Geographic Information System
HEC-HMS	Hydrologic Engineering Center's Hydrologic Modeling System
HEC-RAS	Hydrologic Engineering Center's River Analysis System
HFL	High flood level
IMD	Indian Meteorological Department
LISS	Linear Imaging Self-scanning Sensor
LULC	Land Use Land Cover
MIKE-SHE	Generalized River Modeling Package- Systeme Hydroloque Europeen
NRSC	National Remote Sensing Centre
NSE	Nash–Sutcliffe model efficiency coefficient
R^2	Coefficient of determination
SANDRP	South Asia Network on Dams, Rivers, and People
SCS-CN	The Soil Conservation Service Curve Number
SCS-UH	The Soil Conservation Service Unit Hydrograph

Downloaded from http://iwaponline.com/jh/article-pdf/doi/10.2166/hydro.2022.065/1120810/jh2022065.pdf
by guest

Corrected Proof

SRTM	Shuttle Radar Topography Mission
TIN	Triangular Irregular Networks
USACE	United States Army Corps of Engineers
USDA	United States Department Of Agriculture
UTM	Universal Transverse Mercator
VRB	Vamsadhara river basin
WGS 1984	World Geodetic System84
WSEL/WSE	Water surface elevation

1. INTRODUCTION

In a tropical country like India, floods are the most frequent and extensive natural catastrophes (Sahoo & Sreeja 2015). The coastal area surrounding India's east coast is a densely populated stretch that is vulnerable to natural calamities such as tropical cyclones (Sahoo & Bhaskaran 2018). According to a report by the Indian Meteorological Department (IMD), the Andhra Pradesh (AP) coast ranks as the second most cyclone-prone area after Odisha and has the second-largest vulnerable region to floods after Kerala. Tropical cyclones bring heavy rain and strong winds, causing devastation on most of the east-flowing rivers like Vamsadhara and Nagavalli, which record high daily rainfall. While such hydro-meteorological calamities as floods cannot be totally controlled, they may be regulated through the application of advanced geospatial tools and decision support systems to reduce risk and prevent it (Khan *et al.* 2014). The hydrological modeling system (HMS) is vital in analyzing the hydrological components and flood hydrographs by utilizing geospatial data to extract the input parameters essential for modeling from resources such as digital elevation models (DEM) and land use land cover (LULC). Furthermore, these pre-acquired flood hydrographs are integrated into hydraulic models to help in understanding the complexities of flood prediction and analysis. As a result, flood damage may be reduced by establishing an early warning system in advance and delivering a flood forecasting service to the public (Borsch & Simonov 2016). In a conventional flood warning system, the stream water levels are monitored and warnings are issued with maps of the area that correlate to the river water levels (Fang *et al.* 2008; Ostheimer 2012; Krajewski *et al.* 2016).

To construct a fully functioning hydraulic model, it is necessary to choose an acceptable hydrodynamic model as well as the input variables and boundary conditions that will be employed in the model. Researchers have differing perspectives on the choosing and selecting of hydrodynamic models, which include one-dimensional (1D) and two-dimensional (2D) models, which have been a focus of study in recent years. Horritt *et al.* (2007), Anees *et al.* (2016), and Montané *et al.* (2017) demonstrated the benefit of hydraulic modeling in simulating flood events, estimating vulnerable areas, and identifying flood hazard zones, all of which are required components of developing any flood and risk management strategy involving 1D or 2D flow. Earlier studies have shown that a continuously simulated hydrological and hydrodynamic 1D steady-flow model can predict flood hazard zones (Sindhu & Rao 2016; Mahapatra *et al.* 2021). As floods are so unpredictable, an unsteady flow analysis seems to be the best technique to visualize flood hazard zones. The unsteady flow analysis was used for inundation mapping because water can flow in both directions once it reaches the floodplain (Patel *et al.* 2017; Mihu-Pintilie *et al.* 2019; Shustikova *et al.* 2019). The hydrodynamic models solve shallow water equations and provide more accurate estimates of inundation time and duration (Teng *et al.* 2017). They can also anticipate flood velocity, water surface elevation (WSE), and flooded areas, laying the basis for mitigation strategies. Such an unsteady flow simulation can quantify the spatial risk by converting the flood depth and duration to meaningful and perceptible data. The flood depth is a significant factor in determining the extent to which the flood plain gets inundated (Neelz & Pender 2013). Villazon *et al.* (2009) employed Hydrologic Engineering Center's River Analysis System (HEC-RAS) to evaluate the unsteady flow process in the Pirai river during flood events and to quantify the peak discharge.

Two prerequisites for risk evaluation studies are flood mapping and hazard assessment. Previous studies (Bhandari *et al.* 2017; Kayyun & Dagher 2018; Pathan & Agnihotri 2020) assessed the computational approaches to use for flood hazard and stream flow modeling. Mani *et al.* (2014) and Kalimisetty *et al.* (2021) developed a method for estimating floods by combining 1D and 2D flow simulations using MIKE-SHE. Sarchani *et al.* (2020) found that combining 1D/2D hydraulic models gives a more realistic depiction of floodplain area, flow rates, and water depths at high peak discharge. Ongdas *et al.* (2020) discovered submerged regions during flood occurrences with varying return times on the river Yesil in Kazakhstan. Following the flow of inundation mapping, hazard quantification through the generation of flood maps that regulate flood risk management techniques plays a critical role. These flood inundation maps developed in the Geographic Information System (GIS) are regarded to be reliant on the output provided by hydraulic model simulation results used to assess flood hazards. The

Downloaded from http://iwaponline.com/jh/article-pdf/doi/10.2166/hydro.2022.065/1120810/jh2022065.pdf
by guest

Corrected Proof

development of the digital terrain model (DTM) and GIS had a profound influence on the ability to characterize and comprehend the consequences of extremely varied boundary conditions on the hydrologic response (Ramírez 2000). Several previous studies (Dewan *et al.* 2007; Giardino *et al.* 2012) evaluated, verified, and assessed flood extent and damage using remote sensing techniques in combination with auxiliary field measurements in GIS platforms. With improved processing capabilities and meteorological and terrain data, the usage of hydrological and hydrodynamic models for inundation zone identification and hazard assessment has expanded significantly (Andrysiak & Maidment 2000). Talukdar *et al.* (2021) investigated the Baitarani river basin in Odisha using a dynamic wave momentum equation to combine hydrologic and FLOW-2D models. The study found that the Bhadrak district is most susceptible to Baitarani river flooding during major floods, showing that the 2D model mapping was adequately accurate. Surwase *et al.* (2019) utilized HEC-RAS to model flooding along the Mahanadi River in Odisha in 2008. The model's flood extent and flood hazard map were verified using a satellite image, which produced good results. Khattak *et al.*'s (2016) study demonstrates the use of hydraulic models and the GIS to construct flood extent maps for a stretch of Pakistan's Kabul river. GIS approaches, HEC-RAS, and multi-criteria decision analysis are promising for developing realistic flood extent predictions that are more effective in flood risk zonation (Ouma & Tateishi 2014; Rahmati *et al.* 2015; Mishra & Satapathy 2021). Based on literature reviews, it may be stated that combining hydrological and hydrodynamic models enhances flood hazard response and management. This strategy is based on flood predictions to minimize loss of life and property. Flood risk analyses on large scales are rare and suffer from constraints due to a lack of data and methods to accurately reflect hydrodynamic processes (Vorogushyn *et al.* 2018). In this context, acquiring high-resolution elevation data and satellite data during storm occurrences for calibration and validation is a challenging and crucial component of the study.

Floods are frequent in the Vamsadhara river basin (VRB) and have caused havoc in 1999, 2004, 2006, 2009, 2010, 2013, 2014, and 2018 (https://www.cwcvsk.gov.in/strmlist.html). The severity of rains that occurred in 2006, 2010 (Jal), and 2013 (Phallin) was exceptionally high, affecting both the Odisha and AP coasts. According to reports, floods in 2006 affected 18,912 villages, 67.39 lakh people, and 4.90 lakh acres of agricultural land. These floods hit all major rivers, including Vamsadhara, which were flooded, posing a threat to life and property in 27 districts (https://health.odisha.gov.in/PDF/Disaster_Management.pdf). The 2010 Jal cyclone brought heavy rainfall to the region, affecting 2,73,483 people and causing major agricultural damage in AP (https://apsdma.ap.gov.in/common_mns/DM_plans/DDMP_pdf/District%20DM%20plan-Srikakulam%20District%202015.pdf). The extremely violent cyclone storm 'Phailin' that battered Odisha's coast in 2013 severely destroyed houses, agriculture, and communication infrastructure. (https://documents1.worldbank.org/curated/en/168471468257979992/pdf/838860WP0P14880Box0382116B00PUBLIC0.pdf). However, no substantial hydrological studies have been conducted in the majority of the VRB so far. This necessitates the construction of a watershed model and the categorization of flood-inundated areas in the watershed in order to evaluate and forecast flood risk. The significance of this research is to generate the simplest and most reliable model for predicting the affected region of the large flood plain in future emergency scenarios.

To fill this void, the research aims to investigate flood forecasting and analysis approaches by integrating hydrological and hydrodynamic models for stream flow in the VRB and mapping flood-prone areas. The hydrological modeling system (HEC-HMS) was utilized to generate peak flood flow hydrographs at defined sites. These hydrographs were then used to run a hydrodynamic model, notably in the HEC-RAS, to anticipate floods. These two models were computed and verified individually for these three major storm events from 2006, 2010, and 2013, utilizing input datasets, observation data, simulation techniques, and statistical model performances. The integrated applications are being used to simulate floods and determine the degree of flooding. Thus, this method is used in the VRB, which has historical significance when it comes to flooding events.

2. MATERIAL AND METHODS

The research methodology comprises three major stages, which have been discussed. (1) HEC-GeoHMS is a GIS extension that is used to preprocess the drainage networks and basin characteristics before calibrating and validating flood discharges at gauge stations in HEC-HMS in order to generate a calibrated hydrological flood forecasting model using various approaches such as loss, transform, and routing methods. (2) Generating hydrodynamic models in HEC-RAS by creating river geometrics, applying roughness coefficients, and peak discharges as input to steady-flow analysis, and then calibrating and validating with the measured water levels. (3) As floods are so unpredictable, an unsteady flow analysis is carried out to determine the flood-

Downloaded from http://iwaponline.com/jh/article-pdf/doi/10.2166/hydro.2022.065/1120810/jh2022065.pdf
by guest

Corrected Proof

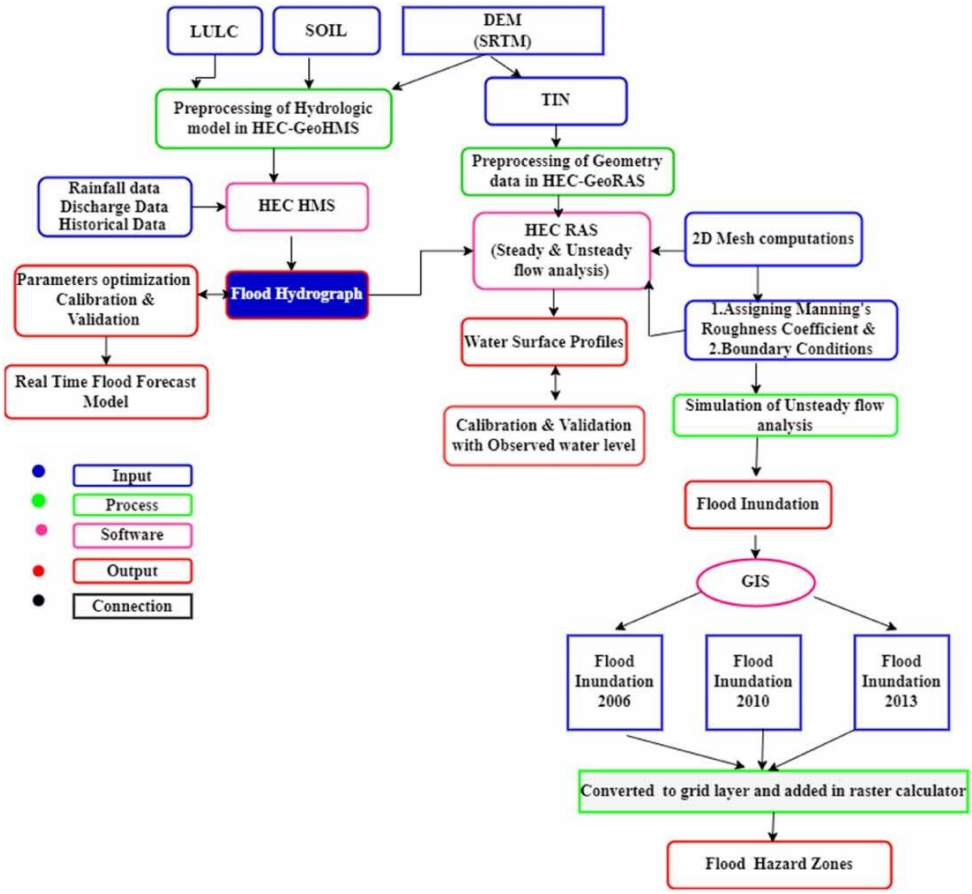


Figure 1 | A schematic representation of the flow chart for the development of the HEC-RAS model.

related hazard zones in the research area. Figure 1 depicts the schematic representation of the flow chart for the development of the flood model.

To calculate the excess rainfall for each basin, it was necessary to use a mathematical equation that represented rainfall loss or to transform the excess rainfall into direct runoff. HEC-HMS has a total of 12 distinct loss models, some of which are intended particularly for event simulation and others for continuous simulation (USACE 2008). Among the methods for simulation investigations, gridded loss methods and soil moisture accounting loss methods are not favored since they need a large number of parameters. The Soil Conservation Service Curve Number (SCS-CN) technique was chosen from the other loss methods for event-based simulation studies. As Sardoii *et al.* (2012) suggest, SCS-CN yields better outcomes than the other loss methods. The watershed coefficient is referred to as the curve number (CN). It is based on the characteristics of a watershed, such as land use and land cover (wasteland, agriculture, forest, and, more recently, urban (USDA-SCS 1986)). It has a range of 0–100, and it is employed to calculate the amount of rain that falls on the catchment. This method is simple to apply because it requires only a few watershed parameters, such as the CN number and initial abstraction (Wagener & Wheater 2006). Less optimized parameters have a key influence in increasing the accuracy of any model. The model performs better because there are fewer parameters that increase accuracy. The risk of uncertainty and the number of predictor variables go up when there are more parameters, which might result in over-parameterization. In Table 1, Equations (1) and (2) provide information on how much rain penetrates the surface and when it flows off.

The transform model replicates the process of excess precipitation into direct runoff from a watershed. This excess precipitation has a uniform geographical distribution and a steady intensity throughout time (USACE 2008). HEC-HMS provides a total of eight distinct transformation models. Among them, the SCS Unit Hydrograph (UH) model was selected since it is extensively used and requires minimal parameters to calculate runoff rates. When compared to other models that are more difficult and need more inputs for most catchments, it simply takes one input, i.e., lag time. Ramly & Tahir (2015)

Downloaded from http://iwaponline.com/jh/article-pdf/doi/10.2166/hydro.2022.065/1120810/jh2022065.pdf
by guest

Corrected Proof

Table 1 | Equations used in the present study

Equation	Formulae	Description
1	$S = \frac{25,400}{CN} - 254$	where Q denotes runoff depth, P represents monthly rainfall, S denotes maximum possible retention, and CN indicates curve number
2	$Q = \frac{(P - 0.2S)^2}{(P + 0.8S)}$	
3	$Q_{peak} = \frac{(C \times A)}{T_{peak}}$	where Q_{peak} denotes peak discharge, C denotes conversion constant, T_{peak} denotes time to peak, D denotes duration, T_{lag} denotes time lag, S denotes slope, CN denotes curve number, A denotes area, and L denotes hydraulic length
4	$T_{peak} = \frac{D}{2} + T_{lag}$	
5	$T_{lag} = \frac{L^{0.8}\left(\frac{1,000}{CN} - 9\right)^{0.7}}{734.45 \times \sqrt{s}}$	
6	$S = K(xI + (1 - x)Q$	where S denotes storage in the river reach, K denotes travel time, and x denotes weighting factor varied between 0 and 0.5.
7	$Z_2 + Y_2 + \frac{a_2 V_2^2}{2g} = Z_1 + Y_1 + \frac{a_1 V_2^2}{2g} + h_e$	where Z_1 and Z_2 refer to the height of the main channel inverts, Y_1 and Y_2 refer to the water level at cross-sections, V_1 and V_2 refer to average velocities, a_1 and a_2 refer to velocity weighing coefficients, g refers to gravity acceleration, and h_e energy head loss
8	$\frac{\partial H}{\partial t} + \frac{\partial (uh)}{\partial x} + \frac{\partial (vh)}{\partial x} + q = 0$	where t denotes time, H denotes the water surface elevation, h denotes the water depth, q denotes a source or sinks term, and u and v denote the X and Y velocity components, respectively
9	$V = -\frac{(RH)^{2/3}}{n}\frac{\nabla H}{(\nabla H)^{1/2}}$	where V denotes velocity equation given by Manning's roughness coefficient (n), R denotes the hydraulic radius, and H denotes the water surface elevation

conclude that this SCS-UH approach requires fewer parameters and can be used to accurately simulate stream flows in different watersheds around the world. Equations (3)–(5) and Table 1 are used to calculate the peak discharge for each basin using the SCS-UH. Khodaparast *et al.* (2010) suggest that SCS-UH is more consistent and yields superior results over other transform models. The Muskingum routing technique is a lumped flow routing methodology derived for eight basin reaches using Equation (6) and (Table 1). Since its debut in 1930, this approach has been mostly used to analyze river engineering in order to determine hydrologic routing variables (Tewolde & Smithers 2006). One of the drawbacks of using the aforementioned approaches to construct a hydrological model is the unavailability of data.

The standard step approach for uniform flow analysis in HEC-RAS is used to construct water surface profiles from one cross-section to the next by resolving the energy equation using an iterative process termed the standard step method, as presented in Equation (7) and Table 1. Most of the flood flows are somewhat diffusive, so they may be modeled using the diffusive-wave method (Ponce 1989). To compute 2D unsteady flow in HEC-RAS, there are two methods, the Diffusive- wave method and the Full momentum method. The 2D diffusive-wave method was chosen over the other method because it enables computations to run faster and steadily. This approach allows for realistic modeling of the majority of 2D modeling scenarios, such as flood modeling, where inertial forces predominate over frictional and other forces. Typically, the diffusive- wave equation may be applied to larger river systems. The use of the diffusive-wave model provides a sufficiently precise answer if the underlying assumptions are met; it mostly computes approximate global estimations (i.e., flood extents). HEC-RAS will employ both continuity and diffusive-wave versions of the momentum equation to compute WSE at a point in time. Equations (8) and (9) and (Table 1) indicate the unsteady differential mass conservation (continuity) form and Manning's formula in the diffusion-wave equation.

Downloaded from http://iwaponline.com/jh/article-pdf/doi/10.2166/hydro.2022.065/1120810/jh2022065.pdf
by guest

Corrected Proof

Efficiency measures of the model are determined by assessing its performance both before and after calibration, as well as its accuracy during validation, using the criteria mentioned below (Moriasi *et al.* 2013). Equation (10) shows the Nash–Sutcliffe model efficiency (NSE), and the coefficient of determination (R^2) in Equation (11) is used in evaluating the model's overall performance.

The NSE is an indicator of the effectiveness of the model in terms of its ability to predict variation (Nash & Sutcliffe 1970). The NSE indicates the degree to which the line fits into 1:1. NSE values vary from —infinity to 1, with 1 being the best fit and values between 0.5 and 1 signifying satisfactory performance (Moriasi *et al.* 2013).

$$\mathrm{NSE}(E) = 1 - \left[\frac{\sum_{i=1}^{n} (m_{\mathrm{obs},i} - m_{\mathrm{sim},i})^2}{\sum_{i=1}^{n} (m_{\mathrm{obs},i} - m_{\mathrm{mean}})^2}\right] \tag{10}$$

The R^2 quantifies the variance ratio and the correlation between simulated and observed values in the model.

$$R^2 = \left[\frac{\sum_{i=1}^{n} (m_{\mathrm{obs},i} - m_{\mathrm{sim},i})^2}{\sum_{i=1}^{n} (m_{\mathrm{obs},i} - m_{\mathrm{mean}})^2}\right] \tag{11}$$

2.1. Study area and data used

The river Vamsadhara flows between the Rushikulya river in Odisha and the river Godavari in AP. It covers 8,015 km² in Odisha and 2,815 km² in AP, with a total aerial extent of 10,830 km² (https://sandrp.in/2017/05/23/rivers-profile-of-andhra-pradesh-and-telangana-states/). The river starts on the border of Kalahandi and Rayagada districts in Odisha. It flows through Odisha's Rayagada and Gajapati districts and into AP's Srikakulam district, where it meets the Bay of Bengal at Kalingapatnam. It is located between latitudes 18°15′N and 19°57′N and longitudes 83°25′E and 84°57′E, as shown in Figure 2. During the southwest monsoon season, the basin gets most of its rain from June to December. An annual rainfall in the basin reaches a high of 2,591 mm and a low of 410 mm. A field survey is carried out using a Differential Geographical Positioning System (DGPS) to determine the Geographical Coordinate Points (GCPs) of gauge stations and high flood levels (HFLs) at diverse locations. The GCPs of the gauge stations (point data) are represented in the GIS as shown in Figure 3.

2.2. Hydrologic model setup and basin delineation

The ArcGIS stream generation tool was used to delineate the VRB and sub-basins using a Digital Elevation Model (DEM) of 30 m resolution projected in Universal Transverse Mercator (i.e., UTM) of zone 44, WGS84. This basin model was divided into 17 sub-basins using a series of trials to enhance the accuracy of the model (Hromadka *et al.* 1988). Parameters like the CN grid derived from a soil land use polygon and hydrological soil groups are categorized as inputs into HEC-GeoHMS. As part of a simulation, a basin is imported into HEC-HMS after it has been set up for basin features, parameters, and hydrologic modeling processes (HMS). HEC-HMS combines basin, meteorological, time-series data, and controls specifications for each model run. The hydrologic components of the basin model comprise 17 sub-basins, 8 junctions, and 8 main reaches. The meteorological model, on the other hand, specifies the daily rainfall supplied as an input. In the control specification for simulation, the beginning date and the ending date are specified for a period of 90 days. Gauge discharge (GD) data at Junction 91 (J91) (Gunupur) and Junction 81 (J81) (Kashinagar) are incorporated into real-time-series data with all meteorological components to calibrate and simulate the created model (Table 2). Thus, the hydrological model is further calibrated and validated in HEC-HMS, as illustrated in Figure 4. The SCS-CN (loss method) approach is used for estimating rainfall excess, while the transform method is used for converting direct runoff to point runoff, and the Muskingum method for hydrologic routing. HMS determined the flood flows at each reach of the river during flood occurrences in 2006, 2010, and 2013. So, the model's performance was checked and found to be good (Mahapatra *et al.* 2021).

Downloaded from http://iwaponline.com/jh/article-pdf/doi/10.2166/hydro.2022.065/1120810/jh2022065.pdf
by guest

Corrected Proof

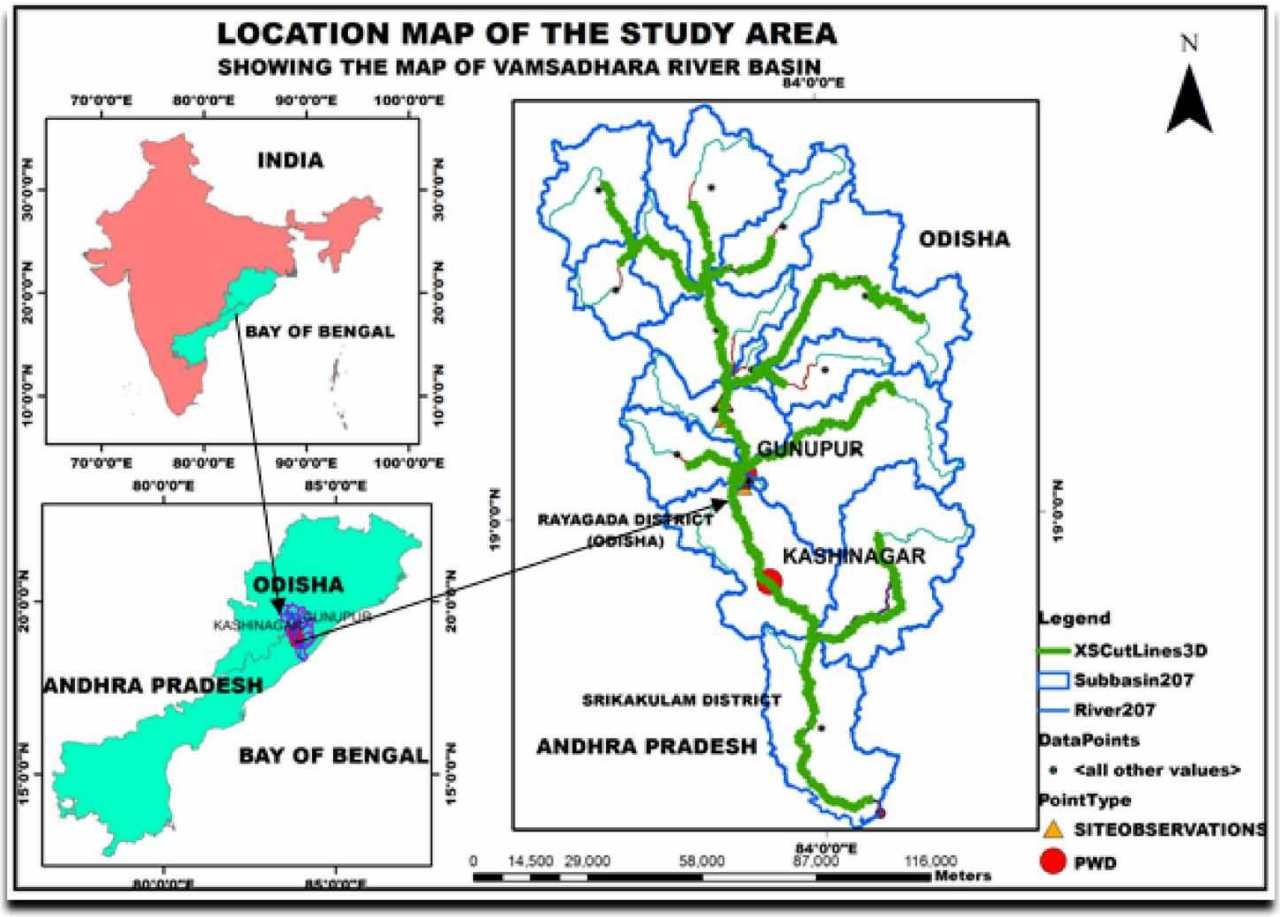


Figure 2 | Geographic position of the VRB.

2.2.1. HEC-HMS simulation and calibration/validation approach

The HEC-HMS modeling system was used to simulate 90 days of daily rainfall over 3 years (2006 for calibration, 2010 and 2013 for validation). The hydrologic parameters in the model were subjected to sensitivity analysis, and three parameters were shown to be the most sensitive. CN, travel time (K), and runoff coefficient (x) were also shown to be the most sensitive parameters in other studies based on the parameter sensitivity analysis (Sardoii *et al.* 2012; Tahmasbinejad *et al.* 2012). During the calibration process, the pre-set values for these parameters were fine-tuned to the measured value by comparing simulated results with real-time data that had acceptable range indicators that were confirmed by the model's statistical performance (Mahapatra *et al.* 2021), while fitting the computed discharge values with historical data at gauge stations in the basin. In Table 3, the calibrated parameters CN, K, and x were computed for the run in 2006. The NSE and R^2 indices were utilized to do statistical analysis. It was determined that the calibration procedure was effective in terms of both visual and statistical comparisons. The model was run using predefined values of the calibrated model in the validation phase, and the corresponding values obtained were evaluated statistically in the same way as the calibration process was done. Thus, the model can be utilized as a real-time flood forecast model because it is calibrated and further evaluated with 2 years of real-time data that corresponded well with the observed data.

2.3. Hydrodynamic model setup

2.3.1. 1D hydrodynamic model

The following are the essential input data for running a hydraulic steady model and simulating water levels in a river: geometry data, boundary conditions, Manning's roughness coefficient (n), and flow hydrograph data for the VRB, with a total

Downloaded from http://iwaponline.com/jh/article-pdf/doi/10.2166/hydro.2022.065/1120810/jh2022065.pdf
by guest

Corrected Proof

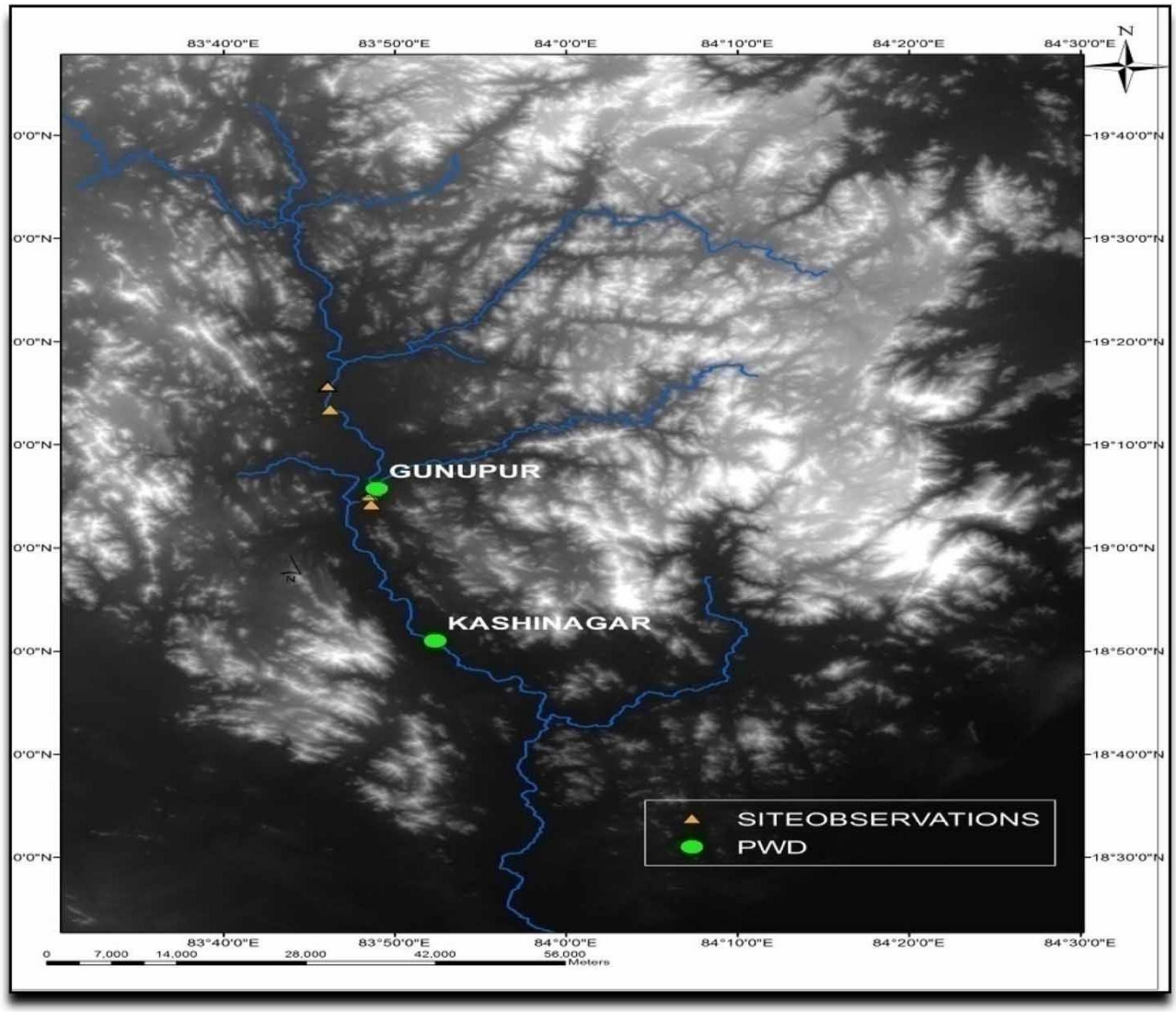


Figure 3 | Location of CWC gauging stations.

Table 2 | Data and their sources used for creating modeling system

S. No.	Data type	Source
1	Shuttle Radar Topography Mission (SRTM) DEM (30 m resolution)	Earth Explorer, http://eros.usgs.gov
2	Annual rainfall data grids from 2001 to 2013, Land use and Land cover map of the study area	National Remote Sensing Centre (NRSC), Hyderabad
3	River discharge and gauge data at Gunupur, Kashinagar	CWC, Bhubaneswar, Odisha
4	Resourcesat-1, Linear Imaging Self-scanning Sensor (LISS) III image	Bhuvan website

of 544 river cross-sections, generated using the Triangular Irregular Network (TIN) in HEC-GeoRAS. Figure 5 depicts the cross-sections of VRB created in HEC-GeoRAS. These pre-processed DTM files containing geometric data are further used in HEC-RAS to input the requisite steady-flow data. Three profiles were evaluated using flow data, and the river station (RS) boundary conditions were inputs for the calculation of steady-flow analysis. The land use information was collected by

Downloaded from http://iwaponline.com/jh/article-pdf/doi/10.2166/hydro.2022.065/1120810/jh2022065.pdf
by guest

Corrected Proof

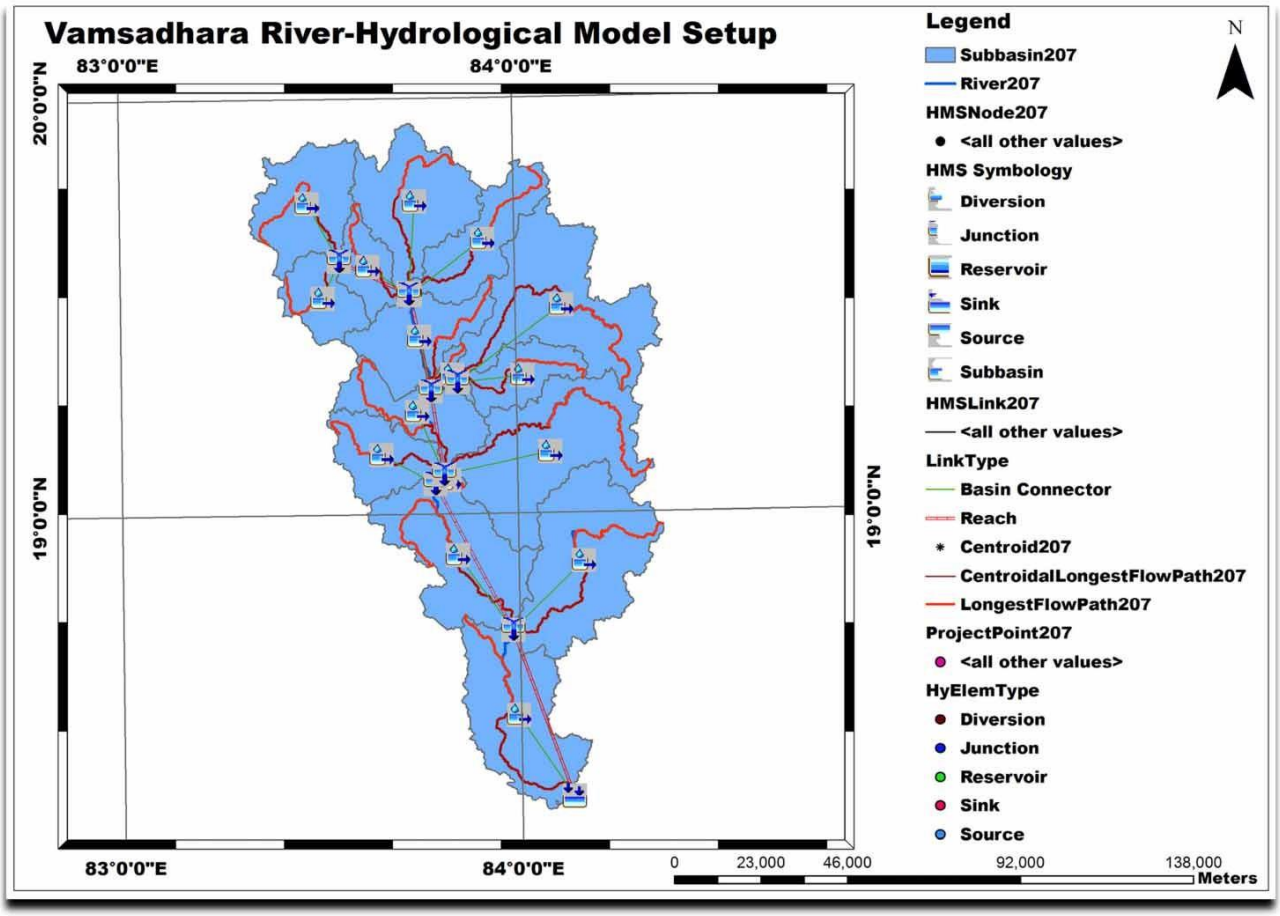


Figure 4 | HEC-HMS hydrological model setup of the VRB.

the NSRC, which is an essential spatial information used in computing roughness coefficient. As seen in Figure 6, the river basin has 75.02 km² of forest area, 45.28 km² of cultivated land, 47.25 km² of wasteland, 9.738 km² of built-up area, and 9.76 km² of maximum water bodies. Manning's roughness coefficient is determined for each of the catchment's river stations. Since the study region is largely covered with dense forest, the roughness coefficient (n) was set to 0.035 in this study. The model was calibrated for 2006 using many trials of Manning's value. It was then checked at the R140 and R150 reaches, where the 2010 and 2013 floods happened, to verify the accuracy of the model.

2.3.2. 2D hydrodynamic model

While for setting the model calculations in 2D unsteady flow analysis that incorporates 2D flow areas (mesh network), the DEM is processed to build a terrain model using the RAS-Mappers tool in HEC-RAS. The DTM improves by taking into account the linear features of the visible soil surface. It includes updated terrain data as well as natural topography features like breaklines and ridges (Hirt 2014). The terrain 2D mesh network was constructed for the study region using the SRTM 30-m DEM as shown in Figure 7. At the beginning of the simulation, the initial flow, storage area conditions, and boundary conditions are assigned to the 2D flow area to perform the unsteady flow analysis. The upstream Boundary Condition (BC) is often a known inflow hydrograph, while the downstream BC is described as a known stage or flow hydrograph, rating curve, or normal depth. For the river of 254 km reach length, the flow hydrograph for a period of 90 days from 15 August 2006 to 15 November 2006, consisting of a flooding event, was routed. The following are the major reaches R10, R60, R90, R100, R110, R140, R150, and R170 with flow hydrographs serving as boundary conditions. In the downstream BC, the normal depth with a friction slope was set at 0.031. Figure 8(a)–8(c) illustrates the inflow hydrographs attributed to the river reaches during the 2006, 2010, and 2013 floods.

Downloaded from http://iwaponline.com/jh/article-pdf/doi/10.2166/hydro.2022.065/1120810/jh2022065.pdf
by guest

Corrected Proof

Table 3 | Computed and calibrated hydrological parameters of the VRB

	Basin details						Calibrated		
S. No.	Sub-basins	A (km^2)	CN	Main reaches	K	x	CN	K	x
1	W340	1,011.0	76.6	R170	10.3	0.2	76.6	10.3	0.20
2	W330	1,016.6	45.3	R150	7.2	0.2	38.5	7.23	0.19
3	W320	1,226.8	47.9				40.7		
4	W310	22.2	55.3	R140	0.44	0.2	47.0	0.46	0.20
5	W300	471.2	45.3				38.5		
6	W290	502.8	99.0	R110	3.95	0.2	91.0	3.96	0.19
7	W280	1,312.0	37.0				34.8		
8	W270	80.3	53.9	R100	1.2	0.2	49.6	2.7	0.20
9	W260	369.3	48.0				44.2		
10	W250	609.2	41.6	R90	4.46	0.2	38.3	5.0	0.19
11	W240	0.59	51	R40	0.05	0.2	46.9	0.05	0.30
12	W230	1,289.5	37				34		
13	W220	363.8	46.3				42.6		
14	W210	584.0	41				37.7		
15	W200	288.9	45.7	R60	4.7	0.2	42.0	7.0	0.19
16	W190	845.8	41.5				38.2		
17	W180	681.8	70.7				65.1		

In HEC-RAS Mapper, a spatially varying land classification data set is created and then connected to the 2D flow area mesh using Manning's n values. Despite the widespread availability of traditional Manning's n values, predicting the value that should be utilized to simulate the flood on a large scale is difficult. This is mostly due to the diversity of roughness levels, which may vary by region (Schumann *et al.* 2007). As a consequence, this model must be simulated against a genuine flood occurrence before producing the necessary results, or an actual survey of the area must be conducted to determine the friction coefficient (Hunter *et al.* 2007), while the latter is unsuitable for large regions. Several studies, however, approximated Manning's roughness coefficient (n) with a respectable degree of precision using a look-up database of land use land cover applied to a hydrodynamic numerical model (Hossain *et al.* 2009; Lumbroso & Gaume 2012). Manning's roughness coefficient (n) is optimized in 10% increments from its base value throughout each simulation to produce calibrated roughness values ranging from 0.030 to 0.050, as mentioned in Table 4.

After providing the model with inputs, including unsteady flow data, it is then made to run for simulation. The theta (θ) parameters are examined, i.e., a weighting factor of 1.0 is selected for the research area, which varies from 0.6 to 1.0. As stated by Pappenberger *et al.* (2005), the probability of obtaining a successful model result is significantly increased when the weighting factor is set to 1.0. Water surface tolerance is set to 0.003 m, and the algorithm is run for 20 iterations with an initial condition ramp-up fraction of 0.1. After simulation, the velocity, depth, and WSE profiles are imported into Arc GIS to generate flood inundation mapping for the three flood events.

3. RESULTS AND DISCUSSIONS

3.1. Hydrological model calibration and validation

The hydrological model for the VRB has been calibrated using historical data from the two CWC GD stations located on J91 and J81 within the river basin (Gunupur and Kashinagar). Each hydrologic model was simulated and calibrated using a set of possible combinations of all parameters CN, K, and x values, as listed in Table 3. Calibration was conducted for the 2006 flood event, and Figure 9(a) and 9(b) illustrates the hydrograph of computed and observed discharge at Gunupur and Kashinagar gauge stations. As indicated in Table 5, the disparity between actual and simulated discharge is within an acceptable range. Sabzevari *et al.* (2009) define the acceptable level for relative % errors between actual and computed values as

Downloaded from http://iwaponline.com/jh/article-pdf/doi/10.2166/hydro.2022.065/1120810/jh2022065.pdf
by guest

Corrected Proof

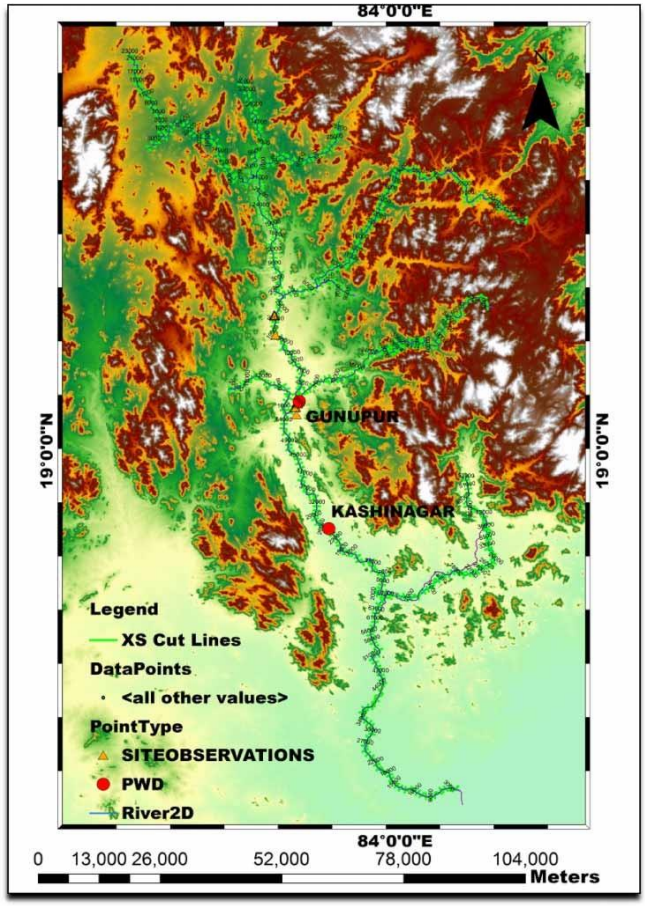


Figure 5 | River cross-sections generated in HEC-GeoRAS.

+20%. The model's efficiency was estimated for the 2006 flood model at two gauge stations with NSE (E) values of 0.78 and 0.77. The R^2 values found for the model were 0.703 and 0.707, which are within the acceptable range according to Moriasi *et al.* (2013).

The model was validated at two GD stations during the 2010 and 2013 floods, as shown in Table 6. Figure 9(c) and 9(d) compare the computed and actual discharge at both the GD stations during the 2010 flood event, which match well at the peak. Similarly, the hydrograph generated between the calculated and observed discharge during the 2013 flood event is shown in Figure 9(e) and 9(f), and it is very similar to historical data at both the Gunupur and Kashinagar gauges. In Table 6, the findings exhibit a low degree of variance within +20% acceptable level (Sabzevari *et al.* 2009) from the observed data, which is acceptable. The validated model performances in 2010 with E were 0.81 and 0.80. However, the 2013 model's performance is E equal to 0.84 and 0.82, which are satisfactory and acceptable. For the 2010 flood, R^2 values of 0.72 and 0.75 were obtained. However, they were 0.70 and 0.73 for the 2013 flood, which is deemed to be acceptable. Furthermore, the HEC-RAS model was fed with peak flow data derived from the standardized model at designated locations within the watershed.

3.2. Hydrodynamic model calibration and validation

The HEC-RAS model created for the VRB was calibrated and verified at two gauging stations on reaches R140 and R150 at cross-sections RS 3000 and RS 24000 for flow by comparing simulated values with observed data. Chow *et al.* (1988) recommended a roughness range of 0.035–0.065 for the river stretch and 0.08–0.15 for the overflow area. In the modeling process, the roughness coefficient (n) value of 0.035 is employed until the final fitted values nearly match the values at gauge stations. Table 7 shows the results of the calibration for the floods on 30 September 2006. The statistical indicators NSE and R^2 show that correlations for both calibration and validation are within an acceptable range of the values listed in Tables 7 and 8. The validation phase was carried out for two peak occurrences: the floods of 19 September 2010 and

Downloaded from http://iwaponline.com/jh/article-pdf/doi/10.2166/hydro.2022.065/1120810/jh2022065.pdf
by guest

Corrected Proof

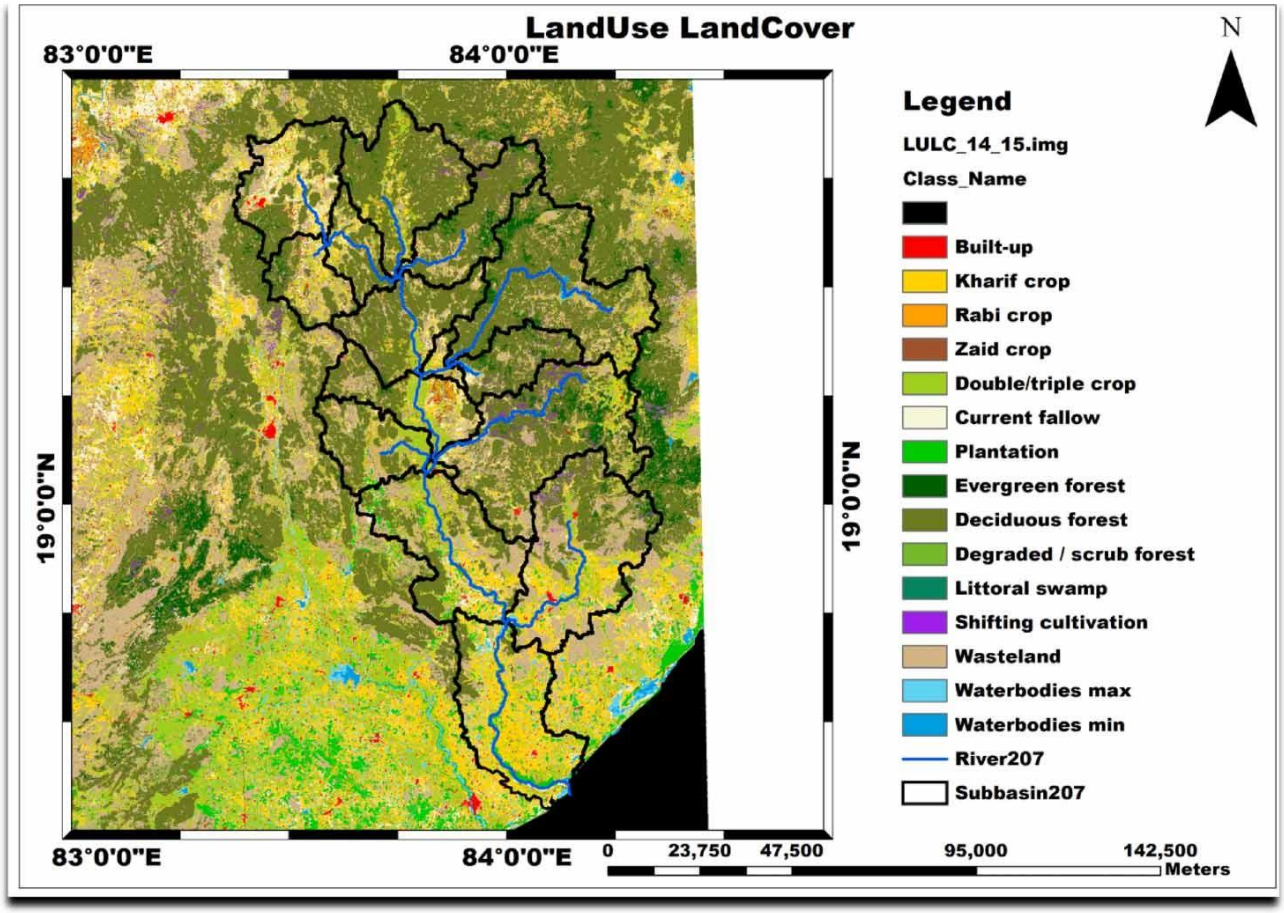


Figure 6 | Land use land cover map of the VRB.

28 October 2013. As shown in Table 8, the discrepancy between actual and simulated water surface levels was slight, so the findings are regarded as good. Thus, it can be said that the RAS model was able to accurately predict stream flow in the Vamsadhara river watershed.

3.3. Flood depth estimation and risk mapping

2D unsteady flood inundation models have been developed for the VRB for main reaches of length 254 km from upstream to downstream ends using the hydrodynamic model approach. The values in Table 4 are calibrated Manning's coefficients that are employed in the modeling process in acquiring the simulation results, i.e., the area of spatial flood inundation, for flood occurrences. Figure 10(a) and 10(b) illustrates the flood inundation region for the flood event that occurred on 30 September 2006, which covered a maximum depth of 22.5 m and a maximum WSE of 273.9 m. The maximum inundation depth and the maximum WSE for the cyclone that occurred on 19 September 2010 are shown in Figure 10(c) and 10(d). They are 21.9 and 190.5 m, respectively. The maximum flood inundation depth and WSE for the cyclone on 28 October 2013 are 20.1 m and 250.78 m as shown in Figure 10(e) and 10(f), respectively.

After examining flood inundation extents in Ras Mapper, flood risk maps are generated for flood occurrences by exporting the raster inundation layers and processing them in Arc GIS. Flood risk maps show the geographical distribution of risk, which is considered as the likelihood of occurrence of an event multiplied by the consequences. These maps of flooding may be created using deterministic or probabilistic approaches (Bates *et al.* 2004; Merz *et al.* 2007; Baldassarre *et al.* 2009a). The VRB, with its braided rivers and frequent flash floods, requires the adoption of a probabilistic depiction of flood extent (Alfonso *et al.* 2016).

Downloaded from http://iwaponline.com/jh/article-pdf/doi/10.2166/hydro.2022.065/1120810/jh2022065.pdf
by guest

Corrected Proof

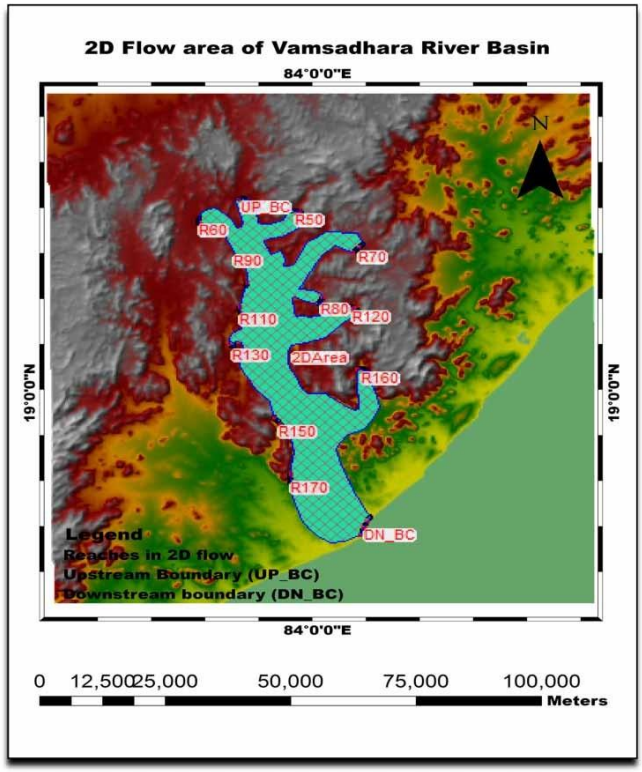


Figure 7 | Boundary condition along with 2D flow area and flow mesh of the VRB.

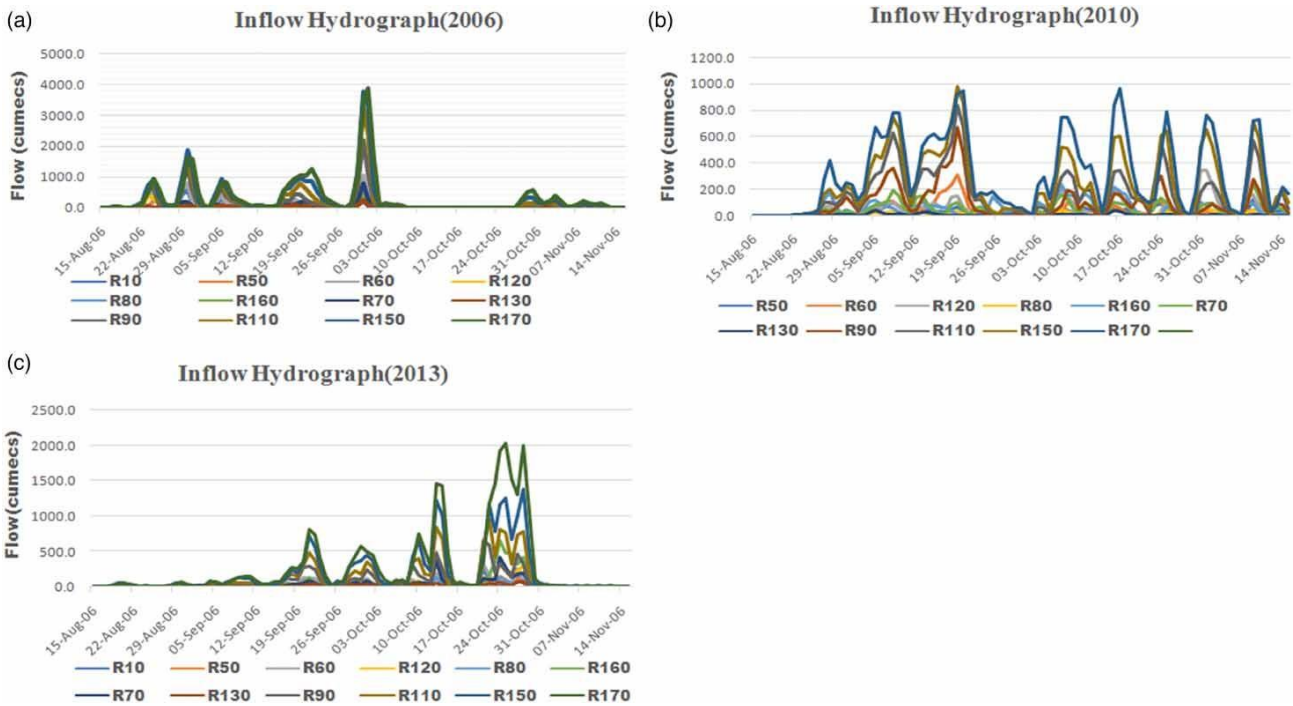


Figure 8 | Inflow hydrograph from HMS for the flood events occurring in (a) 2006; (b) 2010; and (c) 2013.

Downloaded from http://iwaponline.com/jh/article-pdf/doi/10.2166/hydro.2022.065/1120810/jh2022065.pdf
by guest

Corrected Proof

Table 4 | Manning's roughness was calibrated and used in the 2D HEC-RAS model

S. No.	Land use land cover (LULC)	*n*-Value
1	Built-up	0.045
2	Kharif crop	0.05
3	Rabi crop	0.05
4	Zaid crop	0.05
5	Double/triple crop	0.05
6	Current fallow	0.03
7	Plantation	0.05
8	Evergreen forest	0.11
9	Deciduous forest	0.11
10	Degraded/scrub forest	0.11
12	Wasteland	0.04
13	Waterbodies max	0.09
14	Waterbodies min	0.05

The flood inundation areas of the two states of AP (blue) and Odisha (red) caused by the 2006 cyclone are seen in Figure 11. As depicted in Tables 9 and 10, the total area inundated by the storm is 1,322.07 km², comprising 380.56 km² in the upstream river basin (Odisha) and 941.49 km² in the downstream river basin (AP). Table 11 illustrates the basin's flood inundation area and danger level, which have been divided into six categories: H1, H2, H3, H4, H5, and H6. H1, H2, and H3 represent minor flooding that inundates low-lying regions near water bodies. As shown in Tables 9 and 10, H1 covers an inundated area of 11.82 and 44.7 km² during the 2006 flood event in Odisha and AP states, whereas H2 covers an area of 12.93 and 42.23 km², respectively. For the H3 zone, the inundated areas are 15.11 and 47.43 km². H4 flood risk is a moderate zone with an inundated area of 16.47 and 52.23 km², which is more significant. It is likely that major travel routes may be disrupted. Some structures may be impacted above the floor level, which is a concern. Flood-affected areas may necessitate evacuation. H5 and H6 are extreme and major flood hazard zones where single-storey houses may be submerged, and people are not safe even if they make their way to the roof. The inundation areas for both states are shown in Tables 9 and 10. Table 12 shows the areas inundated and the maximum depths obtained during the 2010 and 2013 flood events. A flood extent map of the VRB with flood hazard zones is shown in Figure 12.

Figure 13 depicts a total of 87 villages from 10 mandals impacted by the 2006 flood. These villages include Bramini, Kotturu, Gara, Polaki, Narasannapeta, Jalumuru, Srikakulam, Hiramandalam, Sarubujjili, and Amadalavalasa, which are mostly flood-affected villages along the downstream of the Vamsadhara river, which fall in Srikakulam district (AP). The aforementioned findings have been confirmed in line with Srikakulam Collectorate's disaster management strategy (https://apsdma.ap.gov.in/common_mns/DM_plans/DDMP_pdf/Srikakulam/Srikakulam-DDMP-Volume%20II%20Disaster%20Prevention%20and%20Prepardness%20Plan.pdf). In Odisha, the Gunupur, Gudari, Padmapur, and Ramanguda tehsils/blocks of Rayagada district, as well as the Kashinagar tehsil of Gajapati district, are also impacted. As stated in Table 13, roughly 38 villages are mostly impacted in Odisha's Rayagada and Gajapati districts.

3.4. Model application

The suitability of different models will vary depending on the required degree of precision and the complexities of the region to be depicted. If the goal of the work is to find the inundated area that will be flooded at each cross-section, a 1D model may be enough, like the Vamsadhara river. However, the 1D method's usefulness depends on the modeled region. A 1D model is unlikely to accurately estimate the maximum inundation extent in more complex regions or for large river basins since the inundation extent is determined by how flow propagates along floodplain boundaries. To predict the maximum flood extent, 2D or 1D–2D models can be used. These models will need more time to set up and compute than the 1D model, but they may be essential in more complex regions. When it comes to flooding dynamics and comprehensive information about velocities on the floodplain, a 2D or 1D–2D model is necessary. This is owing to the intrinsic limits of 1D modeling,

Downloaded from http://iwaponline.com/jh/article-pdf/doi/10.2166/hydro.2022.065/1120810/jh2022065.pdf
by guest

Corrected Proof

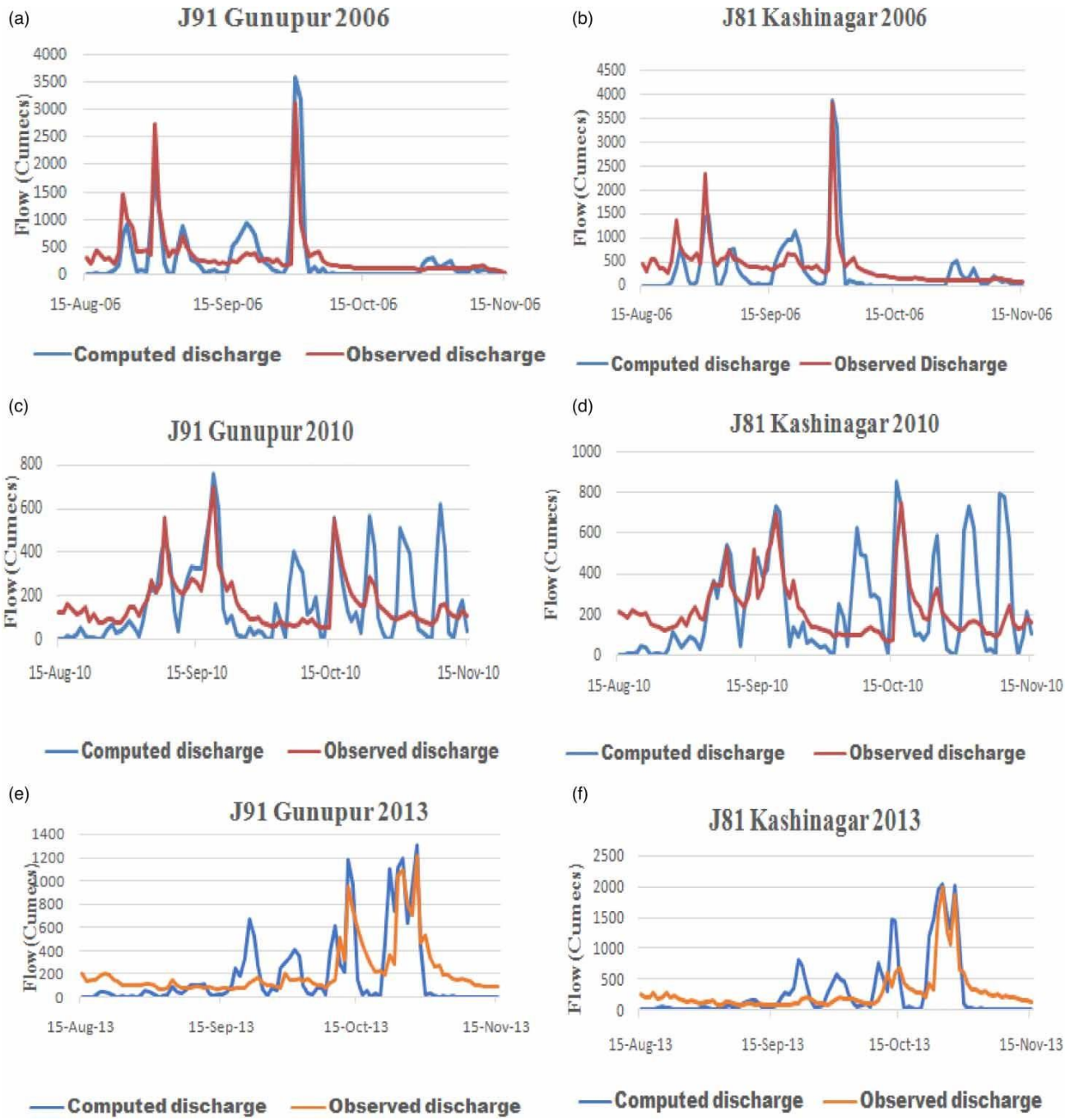


Figure 9 | Observed and simulated discharge of the VRB: (a) and (b) 2006 flood hydrograph at Gunupur and Kashinagar; (c) and (d) 2010 flood hydrograph at Gunupur and Kashinagar; and (e) and (f) 2013 flood hydrograph at Gunupur and Kashinagar.

Table 5 | Model calibration results for the 30 September 2006 flood event in HEC-HMS

Measure	Gauge discharge station	Simulated discharge (cumecs)	Observed discharge (cumecs)	Difference	Percent difference
Volume (MM)	(Gunupur)	325	406	—81	—19.9
	Kashinagar	277	347	—70	—20
Peak flow (m^3/s)	(Gunupur)	3,598.9	3,127.2	471.7	15.1
	Kashinagar	3,883.9	3,830.3	53.6	1.4
Time of peak		30 September 2006, 00:00	30 September 2006, 00:00		

Downloaded from http://iwaponline.com/jh/article-pdf/doi/10.2166/hydro.2022.065/1120810/jh2022065.pdf
by guest

Corrected Proof

Table 6 | Validation results for the 19 September 2010 and 28 October 2013 flood events in HEC-HMS

Measure	Flood event	Gauge discharge station	Simulated discharge (cumecs)	Observed discharge (cumecs)	Difference	Percent difference
Volume (MM)	2010	Gunupur	195.92	197.42	−1.5	−0.76
		Kashinagar	197.39	186.39	11	5.90
	2013	Gunupur	220.62	251.15	−30.53	−12.1
		Kashinagar	231.33	238.91	−7.58	−3.17
Peak flow (m^3/s)	2010	Gunupur	756.8	700	56.8	8.11
		Kashinagar	856.9	750	106.9	14.2
	2013	Gunupur	1,308.8	1,211.4	97.4	8.04
		Kashinagar	2,033.9	1,998.9	35	1.75

Table 7 | Model calibration results for the 30 September 2006 flood event in HEC-RAS

S. No.	Gauge discharge station	Computed discharge (cumecs)	Calculated water depth (m)	Observed water depth (m)	Difference in water depth	NSE	R^2
1	Gunupur	3,598.9	3.76	3.69	−0.07	0.76	0.71
2	Kashinagar	3,883.9	6.25	5.47	−0.78	0.79	0.73

Table 8 | Validation results for the 19 September 2010 and 28 October 2013 flood events in HEC-RAS

S. No.	Gauge discharge station	Flood event	Computed discharge (cumecs)	Calculated water depth (m)	Observed water depth (m)	Difference in water depth	NSE	R^2
1	Gunupur	2010	756.8	2.87	2.42	−0.45	0.65	0.51
2	Gunupur	2013	1,308.8	3.62	3.57	−0.05	0.82	0.84
3	Kashinagar	2010	856.9	5.17	4.90	−0.27	0.68	0.52
4	Kashinagar	2013	2,033.9	5.91	5.38	−0.53	0.79	0.75

such as the stability concerns with the 1D Vamsadhara river model, which were connected to cross-sectional spacing, substantial energy losses within the river channel, and flow being limited between channel banks.

The features of the floodplain, such as the floodplain behind the levee, its shape, and rural and urban floods, will have a significant influence on whatever model is chosen and how this model is developed.

Case I: The 1D model is difficult to use to represent flow in a river if the main channel is constrained by a levee, but both 1D–2D and 2D models may be used to describe the channel–floodplain interaction where the floodplain and river are sep- arated by a levee or other barrier. The results utilizing a purely 2D model will probably be quite sensitive to the breaklines used to capture the barriers. The banks are represented clearly in the 1D–2D case with the lateral structures, and there is no risk of leakage due to 2D cell displacement, as is the case with pure 2D models. However, for this type of case, the model's performance and stability would be significantly impacted by the parameters defining the lateral structures.

Case II: If the landscape around the river is V-shaped and there is no barrier separating the floodplain from the river, it is probable that a less complex model is required. One of the limitations of 1D modeling is that for each cross-section, a single water surface is calculated. This simplification will be more realistic if the floodplain is V-shaped than if it is confined by a levee. Thus, V-shaped floodplains are best represented by a 1D modeling technique. A 2D model may also be used as an alternative. It is not necessary to use breaklines or smaller cell sizes to record the bank elevations if there are no obstructions between the river and the floodplain. In some situations, the sub-grid approach makes it possible to use very large computational mesh sizes. This means that calculation times can be kept under control even at the catchment scale. Using a

Downloaded from http://iwaponline.com/jh/article-pdf/doi/10.2166/hydro.2022.065/1120810/jh2022065.pdf
by guest

Corrected Proof

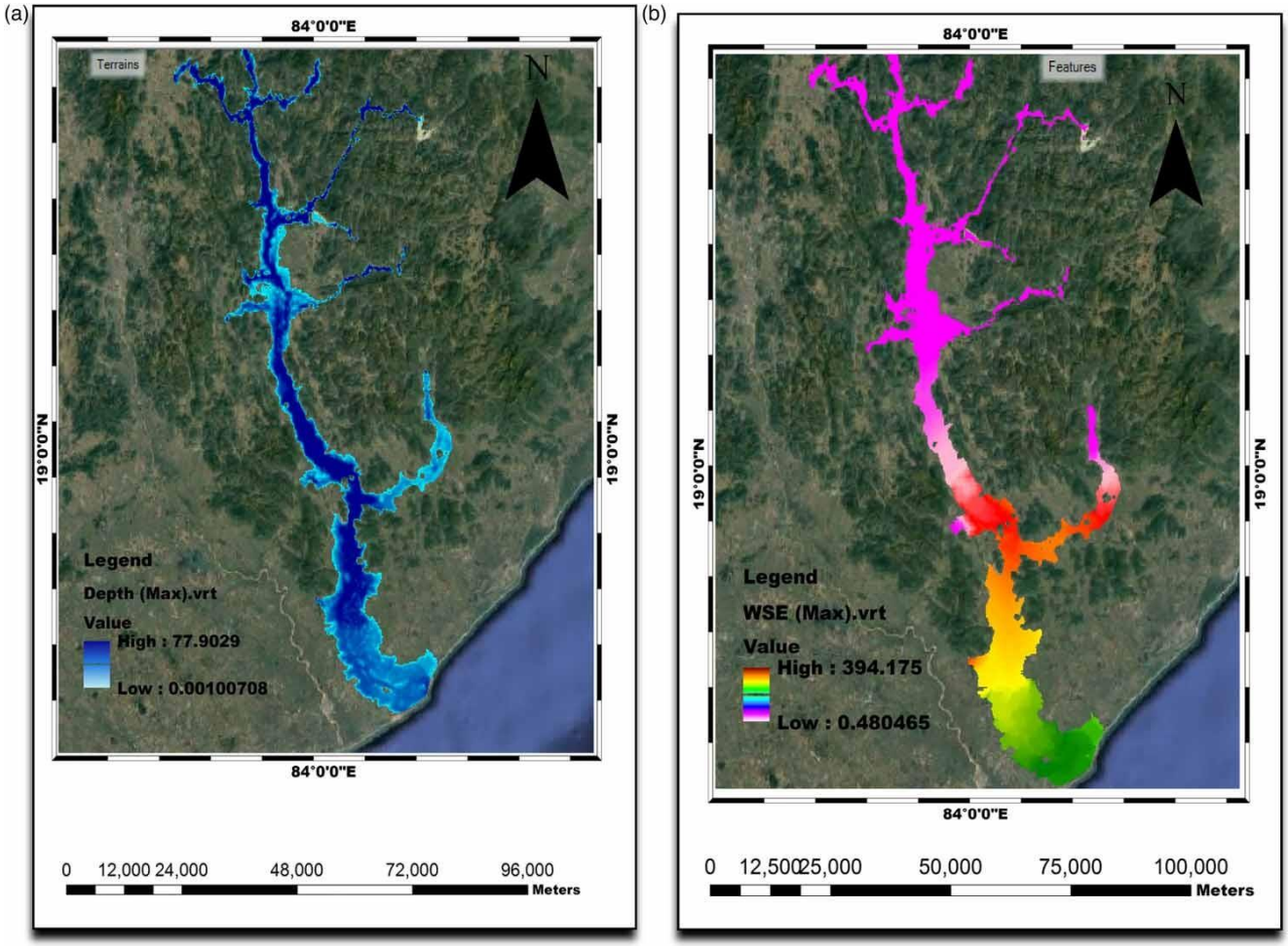


Figure 10 | Flood inundation extent in the VRB generated as a result of the storms. The following are the inundations: In 2006, (a and b) depth (max) and water surface elevation (WSE Max). In 2010, (c and d) depth (max) and water surface elevation (WSE max). In 2013, (e and f) depth (max) and water surface elevation (WSE max). (*continued.*).

1D–2D technique for a V-shaped catchment might be challenging since there is no apparent demarcation between the main channel (which should be represented in 1D) and the floodplain. As a result, locating acceptable places for the lateral structures will be problematic. The flow will likely be predominant in the direction of the stream in a V-shaped valley, so a combined 1D–2D method is not required to represent this sort of terrain.

Case III: In the case of a simple or rural floodplain with few obstructions to the flow of water, it may be modeled using a 2D or 1D–2D model with a large cell size (~ 20 m). Important topographical features may be defined using breaklines. A 1D model may be enough if there are few obstacles to the flow and the friction coefficient can be used to find the obstacles.

Case IV: Multiple barriers slow the flow and influence the flood propagation in urban floodplains. This research does not investigate urban flooding caused by rivers. Literature suggests that 2D models of urban floodplains are sensitive to mesh resolution and that the use of larger cell sizes may reduce model precision because obstacles cannot be accurately modeled (Yu & Lane 2006a). Studies show that using sub-grid terrain representation could make it possible for cells to be bigger (Yu & Lane 2006b, 2011).

This Vamsadhara model may be utilized instantaneously for similar types of basins where rapid forecasting is required in a short time span to prevent losses on the ground. A similar investigation might be performed on different river basins in the future to evaluate river flow modeling using different 2D models. In addition, future studies should focus on 2D models of meandering rivers.

Downloaded from http://iwaponline.com/jh/article-pdf/doi/10.2166/hydro.2022.065/1120810/jh2022065.pdf
by guest

Corrected Proof

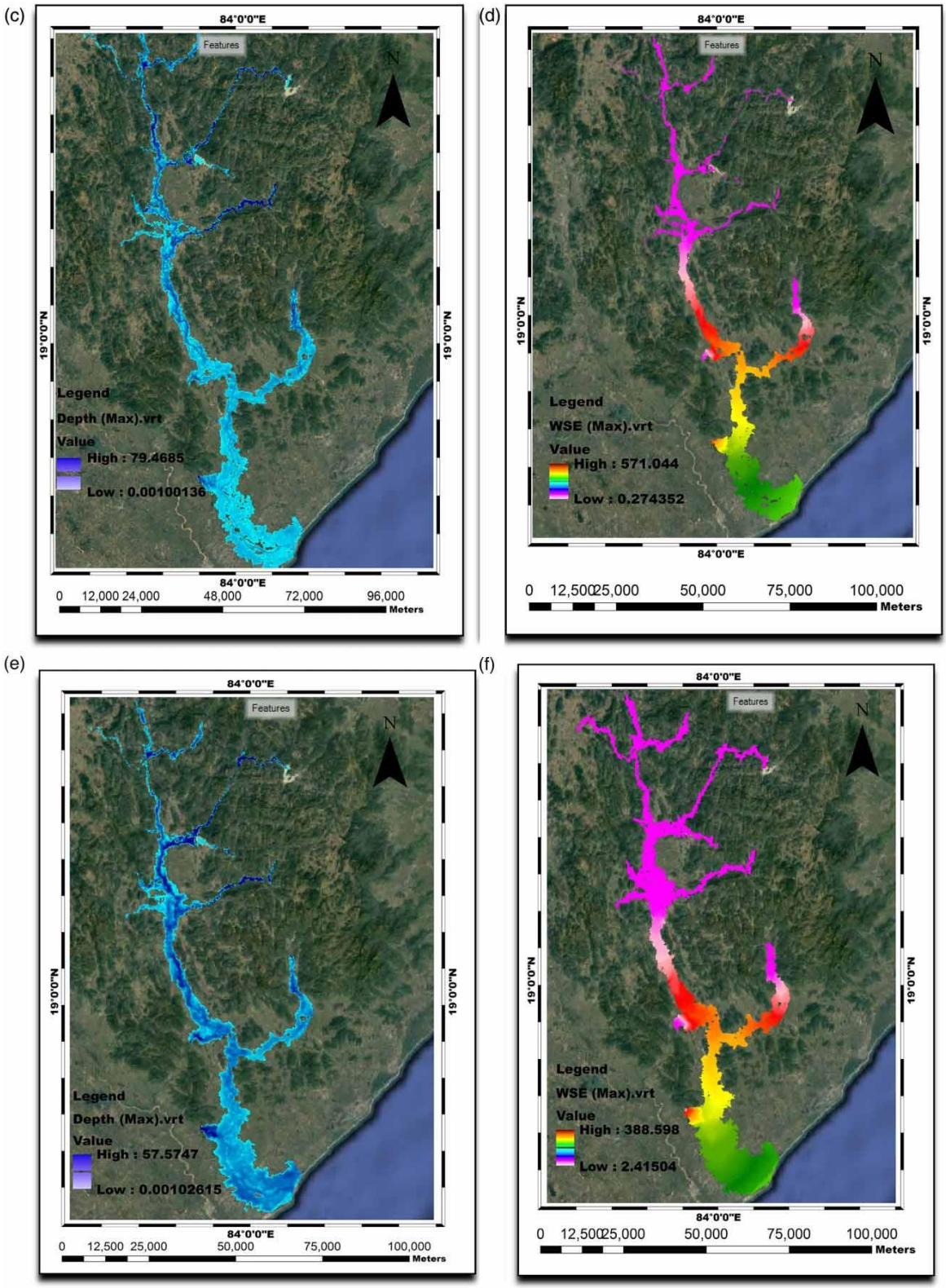


Figure 10 | Continued.

Downloaded from http://iwaponline.com/jh/article-pdf/doi/10.2166/hydro.2022.065/1120810/jh2022065.pdf
by guest

Corrected Proof

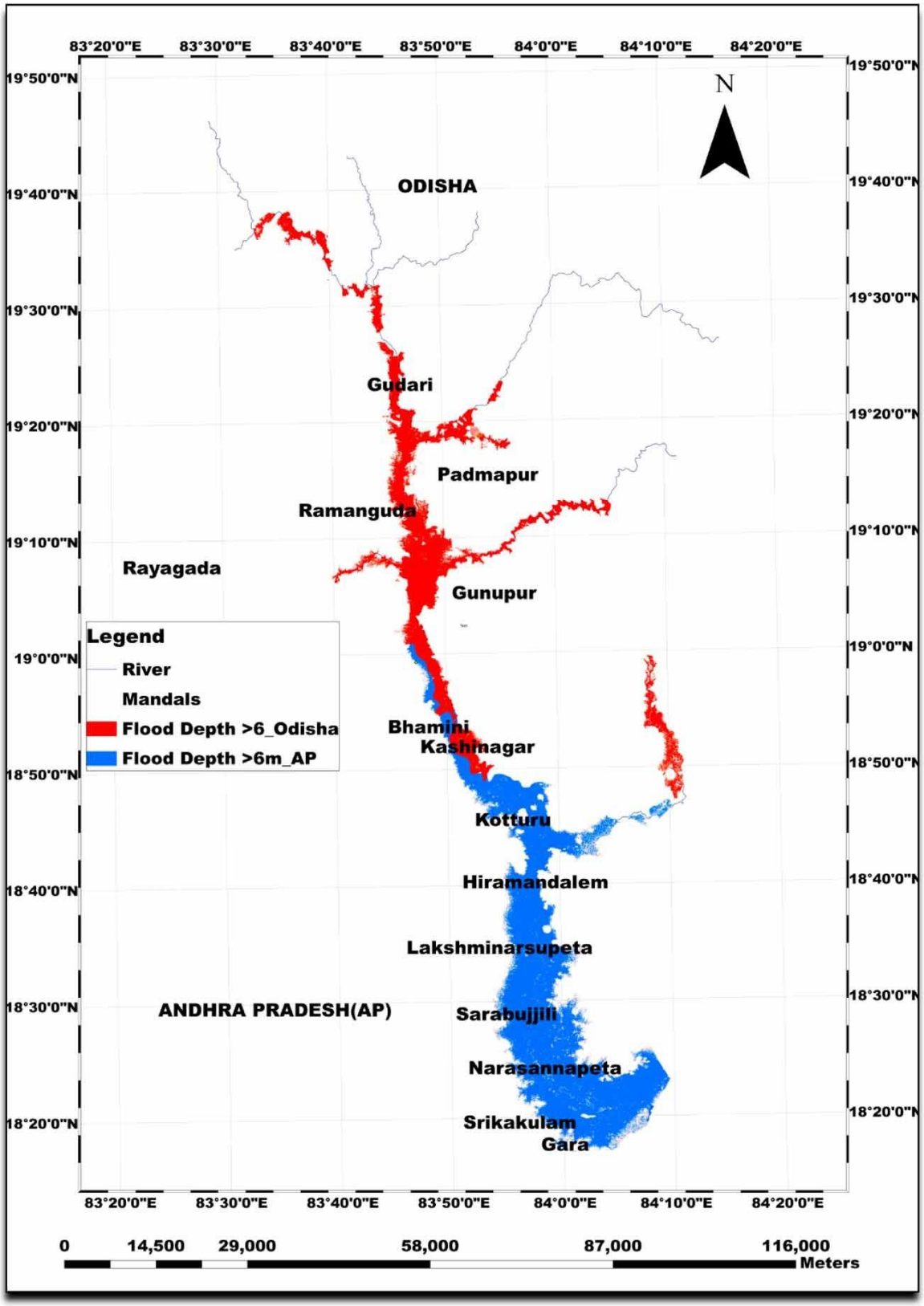


Figure 11 | Flood-inundated extent map of the VRB falls in Odisha and AP states showing the flood-affected mandals.

Downloaded from http://iwaponline.com/jh/article-pdf/doi/10.2166/hydro.2022.065/1120810/jh2022065.pdf
by guest

Corrected Proof

Table 9 | Inundated areas of the VRB (Odisha) during the 2006 flood event

S. No.	Water depth (m)	Total flood area (km²)	
		Area	%
1	,2 m	11.82	3.1
2	2–3 m (below minor)	12.93	3.3
3	3–4 m (minor)	15.11	3.9
4	4–5 m (moderate)	16.47	4.3
5	5–6 m (major)	17.14	4.5
6	-6 m (above major)	307.09	80.56
	Total	380.56	

Table 10 | Inundated areas of the VRB (AP) during the 2006 flood event

S. No.	Water depth (m)	Total flood area (km²)	
		Area	%
1	,2 m	44.70	4.6
2	2–3 m (below minor)	42.23	4.4
3	3–4 m (minor)	47.43	5.0
4	4–5 m (moderate)	52.23	5.5
5	5–6 m (major)	54.53	5.7
6	-6 m (above major)	700.37	74.2
	Total	941.49	

Table 11 | Flood hazard classification (http://www.bom.gov.au/qld/flood/brochures/cooper/cooper.shtml)

S. No.	Flood hazard	Depth (m)	Hazard
1	H1	,2	Very low
2	H2	2–3	Below minor
3	H3	3–4	Minor
4	H4	4–5	Moderate
5	H5	5–6	Major
6	H6	-6	Major

Table 12 | Inundated areas and maximum depths obtained for various flood events

Flood event	Maximum flood depth (m)	Total flood area (km²)					
		H1	H2	H3	H4	H5	H6
2006	22.5	56.522	55.169	62.543	68.70	71.671	1007.46
2010	21.9	58.320	61.840	65.510	70.33	88.490	408.30
2013 (Phallin)	20.1	60.950	95.742	96.511	97.07	93.420	474.05

Downloaded from http://iwaponline.com/jh/article-pdf/doi/10.2166/hydro.2022.065/1120810/jh2022065.pdf
by guest

Corrected Proof

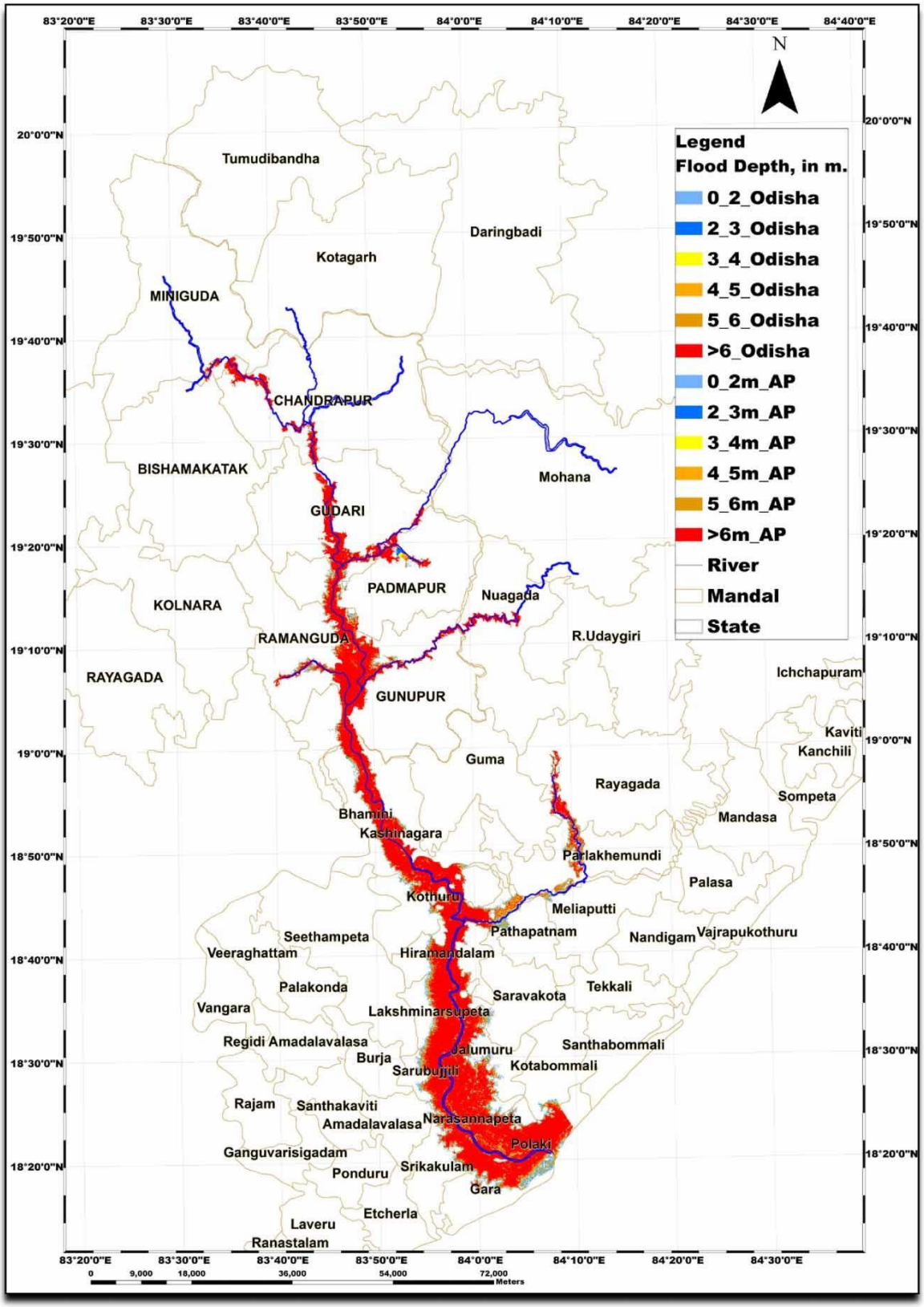


Figure 12 | Flood extent map of the VRB showing flood danger zones.

Downloaded from http://iwaponline.com/jh/article-pdf/doi/10.2166/hydro.2022.065/1120810/jh2022065.pdf
by guest

Corrected Proof

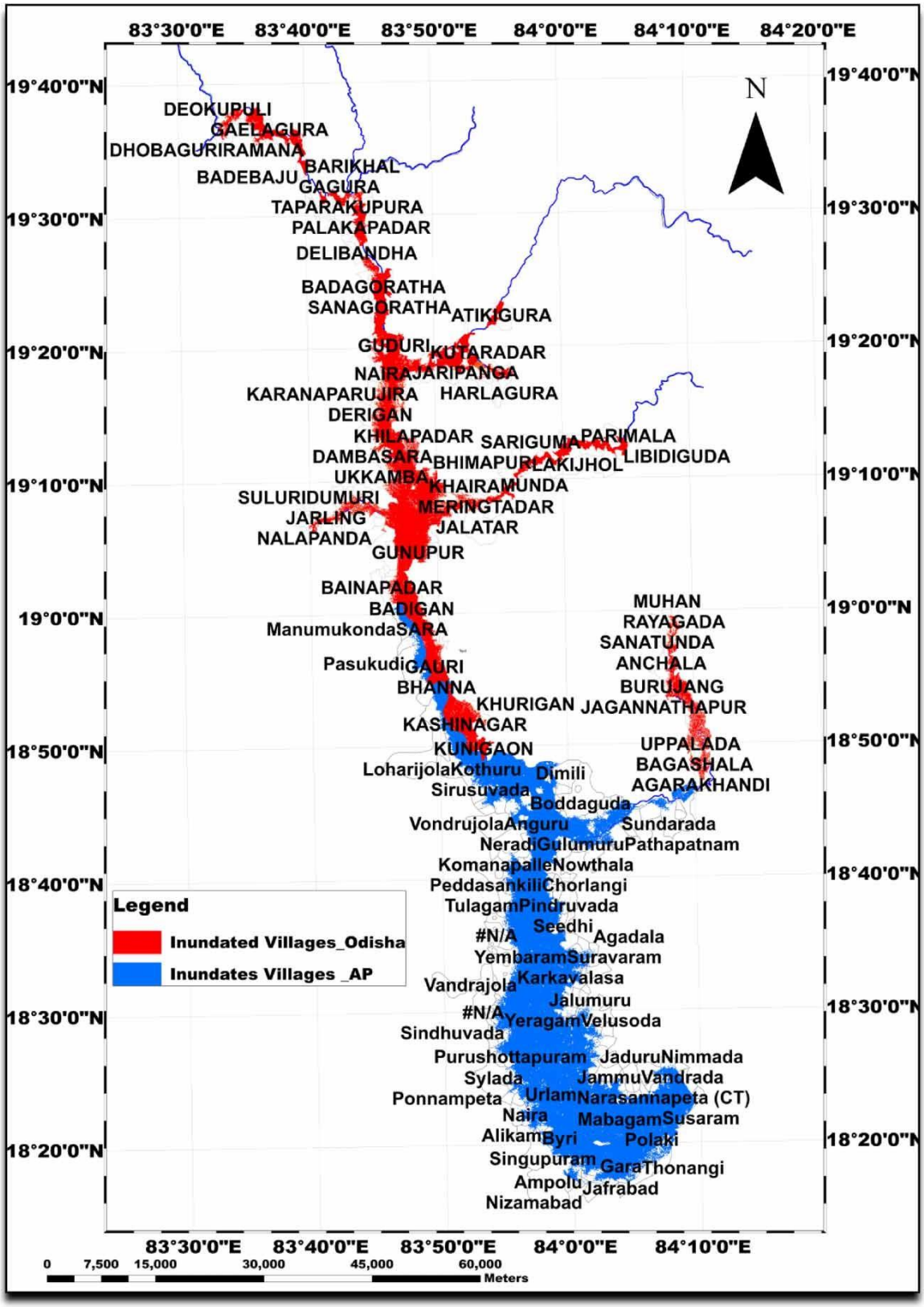


Figure 13 | Villages inundated in AP and Odisha states impacted by the 2006 flood event.

Downloaded from http://iwaponline.com/jh/article-pdf/doi/10.2166/hydro.2022.065/1120810/jh2022065.pdf
by guest

Corrected Proof

Table 13 | List of most affected villages in Odisha's Rayagada and Gajapati districts due to the 2006 flood event

S. No.	Village	S. No.	Village	S. No.	Village	S. No.	Village
1	Palasing	11	Kashinagar	21	Laxmipur	31	Limameda
2	Badigam	12	Kidigam	22	Khalagumuda	32	Dhepo Kalama
3	Sahara	13	Hadubhangi	23	Limapadar	33	Kalama
4	Khandava	14	Bainaguda	24	Serema	34	Kotturu
5	Purtiguda	15	Sanahuma	25	Bhamini	35	Bikrampur
6	Vannal	16	Kareiguda	26	Bhaleri	36	Gadiakhala
7	Kitting	17	Naira	27	Amiti	37	Turkaniguda
8	Bathava	18	Derigam	28	Bharising	38	Pradhaniguda
9	R.K.Pur	19	Radhu	29	Bagasala		
10	Budura	20	Radhuguda	30	Chalakamba		

4. CONCLUSIONS

The work proposes a conceptual method for merging the hydrologic model HEC-HMS with the hydrodynamic model and delineating flood inundation zones in a 2D unsteady flow for the VRB using HEC-RAS. The research also showed that the 2D diffusion-wave approach is extremely effective for determining WSE, depth, and velocity. Its animation capabilities aid in visual comprehension. The HMS and RAS models were calibrated and validated using three flood events from 2006, 2010, and 2013. As a result, based on statistical analyses, the generated models may be considered to have provided an acceptable quantified output. The study also examined the feasibility of using HEC-RAS for flood risk assessments. The expected flood regions for upstream and downstream of the basin allocated to danger zones were computed and found to be reasonable based on visual observation and historical data. Further vulnerability assessments could not be performed owing to a lack of data for the areas. Although it is possible to verify the accuracy of flood risk maps by delineating inundated areas over historical data (e.g., satellite images), this could not be done during flood events due to a lack of available satellite images. The Srikakulam district collectorate's (AP) data were utilized to verify the accuracy of the maps of the villages downstream of the basin, and the findings indicate that the maps are reasonably good. Thus, for flood forecasting in the VRB and for other hydro-meteorologically similar river basins, this calibrated model can be used as a reference model. Using this proposed model, stakeholders may examine various mitigation measures and approaches in response to anticipated flooding situations.

Despite continuous research, flood modeling at high spatial and temporal resolutions remains a substantial difficulty in hydrologic and hydraulic studies. Modeling applications provided for employing hydrologic models have significant drawbacks, including: (a) during flood events, model findings also revealed that simulated values were somewhat higher than observed levels; this discrepancy may be due to input data (DEM, rainfall, soil, and LULC) and a small subset of observation data (stage and discharge). Second, delineating the basin model into more than 17 sub-basins may aid in improving model accuracy (Hromadka *et al.* 1988). (b) Simulated data are exported and used as input in the hydrodynamic model: flow hydrographs derived from the hydrological model can be used as boundary conditions in hydrodynamic modeling. As a result, hydrodynamic modeling has its own set of inherent uncertainties, such as the quality of topographical data and the effect of roughness coefficient on flow levels, velocity, etc. Numerous investigations have proven that even small topographic inaccuracies may significantly affect model findings (Bates *et al.* 1997; Aronica *et al.* 1998; Nicholas & Walling 1998; Wilson 2004). Each model is simply a rough approximation of the actual geometry, which depends on the effective roughness coefficient. Minimizing the uncertainty in surface roughness can considerably improve the calculation of flood extent on landscapes (Aronica *et al.* 1998; Marks & Bates 2000). According to Hunter *et al.* (2007), an actual survey of river cross-sections in the area is required to quantify the friction coefficient and hence increases the model's accuracy relative to the projected value. Large-scale surveys are becoming more difficult and impractical to undertake. (c) Flood-inundated regions' delineation in unsteady flow analysis: simulated hydrographs generated by calibrated models were used as input for hydrodynamic modeling. Uncertainties include the need for a high-resolution DEM to adequately depict the river flood plain, setting up the model, and model parameters such as friction, flow data, and geometry inputs for the model (e.g., flood plain and channel). It is also important to consider how long the computations will take when selecting mesh size and

Downloaded from http://iwaponline.com/jh/article-pdf/doi/10.2166/hydro.2022.065/1120810/jh2022065.pdf
by guest

Corrected Proof

DEM resolution (Shustikova *et al.* 2019). Flood risk assessment is complex owing to the enormous number of variables that must be evaluated, as well as the fact that risk is dynamic, influenced by various factors such as climate change, model setup, and so on (Costabile *et al.* 2015).

Furthermore, as previously stated, the inaccuracies in the simulations from the integrated modeling system of flooding assessment derive from a variety of sources of uncertainty, which most likely spread in an uncertain and quasi-way. The next step of investigation must be focused on the evaluation and measurement of these flaws, as well as how they spread across the modeling system.

ACKNOWLEDGEMENTS

The authors are grateful to the officials and members of the India Meteorological Department, Survey of India (Bhubaneswar), Central Water Commission (Bhubaneswar), NRSC (Hyderabad), Srikakulam Collectorate Office (Disaster Management Plan), and Water Resources Department (Visakhapatnam) for providing data and other pertinent information.

DATA AVAILABILITY STATEMENT

Data cannot be made publicly available; readers should contact the corresponding author for details.

CONFLICT OF INTEREST

The authors declare there is no conflict.

REFERENCES

Alfonso, L., Mukolwe, M. & Baldassarre, G. D. 2016 Probabilistic flood maps to support decision-making: mapping the value of information. *Water Resour. Res.* 52, 1026–1043. http://doi/10.1002/2015WR017378.

Andrysiak Jr., P. B. & Maidment, D. 2000 *Visual Floodplain Modeling with Geographic Information Systems (GIS)*. *PhD Thesis*, Austin Center for Research in Water Resources, the University of Texas.

Anees, M. T., Abdullah, K., Nawawi, M. N. M., Ab Rahman, N. N. N., Piah, A. R. M., Zakaria, N. A., Syakir, M. I. & Mohd. Omar, A. K. 2016 Numerical modeling techniques for flood analysis. *J. Afr. Earth. Sci.* http://doi/10.1016/j.jafrearsci.2016.10.001.

Aronica, G., Hankin, B. & Beven, K. J. 1998 Uncertainty and equifinality in calibrating distributed roughness coefficients in a flood propagation model with limited data. *Adv. Water Resour.* 22 (4), 349–365.

Baldassarre, D., Castellarin, G., Montanari, A. & Brath, A. 2009a Probability weighted hazard maps for comparing different flood risk management strategies: a case study. *Nat. Hazards*. http://doi/10.1007/s11069-009-9355-6.

Bates, P. D., Anderson, M. G., Hervouet, J. M. & Hawkes, J. C. 1997 Investigating the behaviour of two-dimensional finite element models of compound channel flow. *Earth Surf. Process. Landf.* 22 (1), 3–17.

Bates, P. D., Horritt, M. S., Aronica, G. & Beven, K. 2004 Bayesian updating of flood inundation likelihoods conditioned on flood extent data. *Hydrol. Process.* 18, 3347–3370.

Bhandari, M., Nyaupane, N., Mote, S., Kalra, A. & Ahmad, S. 2017 2D unsteady routing and flood inundation mapping for lower region of Brazos river watershed. World Environmental and Water Resources Congress 2017, Sacramento, CA, 292–303. http://doi/10.1061/9780784480625.027

Borsch, S. & Simonov, Y. 2016 Operational hydrologic forecast system in Russia. *Flood Forecast.* 169–181. http://doi/10.1016/b978-0-12-801884-2.00007-4.

Chow, V. T., Maidment, D. R. & Mays, L. W. 1988 *Development of Hydrology*.

Costabile, P., Macchione, F., Natale, L. & Petaccia, G. 2015 Flood mapping using LIDAR DEM. Limitations of the 1-D modeling highlighted by the 2-D approach. *Nat. Hazards* 77, 181–204.

Dewan, A. M., Islam, M. M., Kumamoto, T. & Nishigaki, M. 2007 Evaluating flood hazard for land-use planning in Greater Dhaka of Bangladesh using remote sensing and GIS techniques. *Water Resour. Manage.* 21, 1601–1612.

Fang, Z., Bedient, P. B., Benavides, J. & Zimmer, A. L. 2008 Enhanced radar-based flood alert system and floodplain map library. *J. Hydrol. Eng.* 13 (10), 926–938. http://doi/10.1061/(ASCE)1084-0699(2008)13:10(926).

Giardino, M., Perotti, L., Lanfranco, M. & Perrone, G. 2012 GIS and geomatics for disaster management and emergency relief: a proactive response to natural hazards. *Appl. Geomatics.* 4 (1), 33–46. http://doi/10.1007/s12518-011-0071-z.

Hirt, C. 2014 Digital terrain models. *Encycl. Geod.* 1–6. https://doi/10.1007/978-3-319-02370-0_31-1.

Horritt, M. S., Di Baldassarre, G., Bates, P. D. & Brath, A. 2007 Comparing the performance of a 2-D finite element and a 2-D finite volume model of floodplain inundation using airborne SAR imagery. *Hydrol. Process.* 21 (20), 2745–2759. http://doi/10.1002/hyp.6486.

Hossain, A. K. M. A., Jia, Y. & Chao, X. 2009 Estimation of manning roughness coefficient distribution for the hydrodynamic model using remotely sensed land cover features. *Geoinformatics* 635–638.

Downloaded from http://iwaponline.com/jh/article-pdf/doi/10.2166/hydro.2022.065/1120810/jh2022065.pdf
by guest

Corrected Proof

Hromadka II., T. V., McCuen, R. H. & Yen, C. C. 1988 Effect of watershed subdivision on prediction accuracy of hydrologic models. *Hydrosoft* 1(1), 19–28. http://doi/10.1016/j.apgeog.2017.01.002.

Hunter, N. M., Bates, P. D., Horritt, M. S. & Wilson, M. D. 2007 Simple spatially-distributed models for predicting flood inundation: a review. *Geomorphology* 90 (3–4), 208–225. http://doi/10.1016/j.geomorph.2006.10.02.

Kalimisetty, S., Singh, A., DurgaRao, K. H. V. & Mahammood, V. 2021 1D and 2D model coupling approach for the development of operational spatial flood early warning system. *Geocarto Int.* 1–16. http://doi/10.1080/10106049.2021.1886335.

Kayyun, T. S. & Dagher, D. H. 2018 2D-Unsteady flow within a reach in Tigris River. *Int. J. Sci. Eng. Res.* 9 (5), 2246–2251.

Khan, S. I., Hong, Y., Gourley, J. J., Khattak, M. U. & De Groeve, T. 2014 Multi-sensor imaging and space-ground cross-validation for 2010 flood along Indus River, Pakistan. *Remote Sens.* 6, 2393–2407.

Khattak, M. S., Anwar, F., Saeed, T. U., Sharif, M., Sheraz, K. & Ahmed, A. 2016 Floodplain mapping using HEC-RAS and ArcGIS: a case study of Kabul River, Arab. *J. Sci. Eng.* 41 (4), 1375–1390. http://doi/10.1007/s13369-015-1915-3.

Khodaparast, R., Dastorani, M. T., Vafakhah, M., Talebi, A. & Dashti, J. 2010 The comparison between SCS Unit hydrograph and Snyder Unit hydrograph in runoff rate estimation by HEC-HMS model (Case study: Sadde torogh watershed, Mashhad). In *6th National Conference of Science and Engineering Watershed Management*. University of Tarbiat Modares, pp. 1–8.

Krajewski, W. F., Ceynar, D., Demir, I., Goska, R., Kruger, A., Langel, C., Mantilla, R., Niemeier, J., Quintero, F., Seo, B.-C., Small, S. J., Weber, L. J. & Young, N. C. 2016 Real-time flood forecasting and information system for the state of Iowa. *Bull. Am. Meteorol. Soc.* 98 (3), 539–554. http://doi/10.1175/BAMS-D-15-00243.1.

Lumbroso, D. & Gaume, E. 2012 Reducing the uncertainty in indirect estimates of extreme flash flood discharges. *J. Hydrol.* 414–415, 16–30.

Mahapatra, A., Mahammood, V. & DurgaRao, K. H. V. 2021 Development of real-time flood forecast model for Vamsadhara river through hydrological approach. *Int. J. Adv Technol. Eng. Explor.* 81 (8), 1059–1079. http://doi/10.19101/IJATEE.2021.874272.

Mani, P., Chatterjee, C. & Kumar, R. 2014 Flood hazard assessment with multiparameter approach derived from coupled 1D and 2D hydrodynamic flow model. *Nat. Hazards* 70 (2), 1553–1574. http://doi/10.1007/s11069-013-0891-8.

Marks, K. & Bates, P. 2000 Integration of high-resolution topographic data with floodplain flow models. *Hydrol. Process.* 14 (11–12), 2109.

Merz, B., Thieken, A. H., Gocht, M., 2007 Flood risk mapping at the local scale: concepts and challenges, Ch. 13. In: *Flood Risk Management in Europe: Innovation in Policy and Practice* (Begum, S., Stive, M. J. F. & Hall, J. W., eds). *Advances in Natural and Technological Hazards Research* Series no. 25. Springer, Dordrecht, The Netherlands, pp. 231–251.

Mihu-Pintilie, A., Cîmpianu, C. I., Stoleriu, C. C., Pérez, M. N. & Paveluc, L. E. 2019 Using high-density LiDAR data and 2D streamflow hydraulic modeling to improve urban flood hazard maps: a HEC-RAS multi-scenario approach. *Water* 11, 1832.

Mishra, D. & Satapathy, S. 2021 MCDM approach for mitigation of flooding risks in Odisha (India) based on information retrieval. *Int. J. Cognit. Inf. Nat. Intell.* 14 (2), 77–91. https://doi.org/10.4018/IJCINI.2020040105.

Montané, A., Buffin-Bélanger, T., Vinet, F. & Vento, O. 2017 Mappings extreme floods with numerical floodplain models (NFM) in France. *Appl. Geogr.* 80, 15–22.

Moriasi, D. N., Arnold, J. G., Van Liew, M. W., Bingner, R. L., Harmel, R. D. & Veith, T. L. 2013 Model evaluation guidelines for systematic quantification of accuracy in watershed simulations. *Trans. ASABE* 50 (3), 885–900.

Nash, J. E. & Sutcliffe, J. V. 1970 River flow forecasting through conceptual models part 1 – a discussion of principals. *J. Hydrol.* 10, 282–290.

Neelz, S. & Pender, G. 2013 *Benchmarking of 2D Hydraulic Modelling Packages*. Environmental Agency, Bristol, UK. https://consult.environment-agency.gov.uk/engagement/bostonbarriertwao/results/appendix-6—neelz–s.—pender–g.–2013–benchmarking-the-latest-generation-of-2d-hydraulic-modelling-packages.-bristol_environment-agency.pdf

Nicholas, A. P. & Walling, D. E. 1998 Numerical modelling of floodplain hydraulics and suspended sediment transport and deposition. *Hydrol. Process.* 12 (8), 1339–1355.

Ongdas, N., Akiyanova, F., Karakulov, Y. & Muratbayeva, A. 2020 Application of HEC-RAS (2D) for Flood Hazard Maps. *Water* 12, 2672.

Ostheimer, C. J. 2012 'Development of a flood-warning system and flood-inundation mapping in Licking County, Ohio.' Scientific Investigations Report 2012–5137, U.S. Geological Survey, 13.

Ouma, Y. O. & Tateishi, R. 2014 Urban flood vulnerability and risk mapping using integrated multi-parametric AHP and GIS: methodological overview and case study assessment. *Water* 6, 1515–1545. https://doi.org/10.3390/w6061515.

Pappenberger, F., Beven, K., Horritt, M. & Blazkova, S. 2005 Uncertainty in the calibration of effective roughness parameters in HEC-RAS using inundation and downstream level observations. *J. Hydrol.* 302, 46–69. https://doi.org/10.1016/j.jhydrol.2004.06.036.

Patel, D. P., Ramirez, J. A., Srivastava, P. K., Bray, M. & Han, D. 2017 Assessment of flood inundation mapping of Surat city by coupled 1D/2D hydrodynamic modeling: a case application of the new HEC-RAS 5. *Nat. Hazards* 89, 93–130.

Pathan, A. K. I. & Agnihotri, P. G. 2020 2-D unsteady flow modelling and inundation mapping for lower region of Purna Basin using HEC-RAS. *Nat. Environ. Pollut. Technol.* 19 (1), 277–285.

Ponce, V. M. 1989 *Engineering Hydrology Principles and Practice*. Prentice Hall, Englewood Cliffs, NJ.

Rahmati, O., Zeinivand, H. & Besharat, M. 2015 Flood hazard zoning in Yasooj region, Iran, using GIS and multi-criteria decision analysis. *Geomatics Nat. Hazards Risk* 37–41. https://doi.org/10.1080/19475705.2015.1045043.

Ramírez, J. A. 2000 *Prediction and Modeling of Flood Hydrology and Hydraulics*. Cambridge University Press, Cambridge, UK.

Ramly, S. & Tahir, W. 2015 Application of HEC-GeoHMS and HECHMS as rainfall–runoff model for flood simulation. In: *ISFRAM 2015*. Springer, Singapore, pp. 181–192. https://doi.org/10.1007/ 978-981-10-0500-8_15.

Downloaded from http://iwaponline.com/jh/article-pdf/doi/10.2166/hydro.2022.065/1120810/jh2022065.pdf
by guest

Corrected Proof

Sabzevari, T., Ardakanian, R., Shamsaee, A. & Talebi, A. 2009 Estimation of flood hydrograph in no statistical watersheds using HEC-HMS model and GIS (Case study: Kasilian watershed). *J. Water Eng.* 4, 1–11.

Sahoo, B. & Bhaskaran, P. K. 2018 Multi-hazard risk assessment of coastal vulnerability from tropical cyclones – a GIS-based approach for the Odisha coast. *J. Environ. Manage.* 206, 1166–1178. http://doi/10.1016/j.jenvman.2017.10.075.

Sahoo, S. N. & Sreeja, P. 2015 Development of flood inundation maps and quantification of flood risk in an urban catchment of Brahmaputra river. *J. Risk Uncertainty Eng. Syst. Part A: Civ. Eng.* 3 (1), 1–11. https://doi.org/10.1061/AJRUA6.0000822.

Sarchani, S., Seiradakis, K., Coulibaly, P. & Tsanis, I. 2020 Flood inundation mapping in an ungauged basin. *Water* 12 (6), 1532. http://doi/10.3390/w12061532.

Sardoii, E. R., Rostami, N., Sigaroudi, S. K. & Taheri, S. 2012 Calibration of loss estimation methods in HEC-HMS for simulation of surface runoff (case study: Amirkabir dam watershed, Iran). *Adv. Environ. Biol.* 6 (1), 343–348.

Schumann, G., Matgen, P., Hoffmann, L., Hostache, R., Pappenberger, F. & Pfister, L. 2007 Deriving distributed roughness values from satellite radar data for flood inundation modelling. *J. Hydrol.* 344 (1–2), 96–111.

Shustikova, I., Domeneghetti, A., Neal, J. C., Bates, P. & Castellarin, A. 2019 Comparing 2D capabilities of HEC-RAS and LISFLOOD-FP on complex topography. *Hydrol. Sci. J.* 64, 1769–1782.

Sindhu, K. & Rao, K. H. V. D. 2016 Hydrological and hydrodynamic modeling for flood damage mitigation in Brahmani-Baitarani river basin, India. *Geocarto Int.* 6049 (April). http://doi/10.1080/10106049.2016.1178818.

Surwase, T., Srinivasarao, G., Manjusree, P., Begum, A., Nagamani, P. V. & Jaisankar, G. 2019 *Proceedings of International Conference on Remote Sensing for Disaster Management*. In *Proceedings of International Conference on Remote Sensing for Disaster Management, Springer Series in Geomechanics and Geoengineering*, 2019, no. September 2008, pp. 851–863. Springer. https://doi.org/10.1007/978-3-319-77276-9_77

Tahmasbinejad, F. Z. H., Feyzolahpour, M. & Murnipour, M. 2012 Rainfall-runoff simulation and modeling of Karun river using HEC-RAS and HEC-HMS models, Izeh district, Iran. *J. Appl. Sci.* 12 (18), 1900–1908.

Talukdar, G. J., Swain, B. & Patra, K. C. 2021 Flood inundation mapping and hazard assessment of Baitarani river basin using hydrologic and hydraulic model. *Nat. Hazards* 109 (1), 389–403. http://doi/10.1007/s11069-021-04841-3.

Teng, J., Jakeman, A. J., Vaze, J., Croke, B. F. W., Dutta, D. & Kim, S. 2017 Flood inundation modelling: a review of methods, recent advances and uncertainty analysis. *Environ. Modell. Software* 90, 201–216.

Tewolde, M. H. & Smithers, J. 2006 Flood routing in ungauged catchments using Muskingum methods. *Water SA* 32, 379–388.

USDA-SCS 1986 Urban hydrology for small watersheds. Tech. Release No. 55, USDA-SCS, Washington, DC. https://www.nrcs.usda.gov/Internet/FSE_DOCUMENTS/stelprdb1044171.pdf

U.S. Army Corps of Engineers 2008 *Hydrologic Modeling System User's Manual*, no. September. Hydrologic Engineering Center, Davis, CA.

Villazon, M. F., Aranibar, C. & Willams, P. 2009 Hydrodynamics unsteady flow model applied to river Piraifor flood events estimation in Santa Cruz-Bolivia. In: *Proceedings at 1st International Congress of Hydro-Climatology*, 24–28 August, CD-ROM PP.1-12. SENAMHI, Cochabamba, Bolivia.

Vorogushyn, S., Bates, P. D., de Bruijn, K., Castellarin, A., Kreibich, H., Priest, S. & Merz, B. 2018 Evolutionary leap in large-scale flood risk assessment needed. *Water* 5 (2), e1266. https://doi/10.1002/wat2.1266.

Wagener, T. & Wheater, H. S. 2006 Parameter estimation and regionalization for continuous rainfall-runoff models including uncertainty. *J. Hydrol.* 320 (1–2), 132–154. https://doi. org/ 10. 1016/j. jhydrol. 2005. 07. 015.

Wilson, M. D. 2004 *Evaluating the Effect of Data and Data Uncertainty on Predictions of Flood Inundation*. University of Southampton, Southampton, p. 276. Available from: https://isni.org/isni/0000000135704065.

Yu, D. & Lane, S. N. 2006a Urban fluvial flood modelling using a two-dimensional diffusion-wave treatment, part 1: mesh resolution effects. *Hydrol. Process.* 20 (7), 1541–1565.

Yu, D. & Lane, S. N. 2006b Urban fluvial flood modelling using a two-dimensional diffusion-wave treatment, part 2: Development of a sub-grid-scale treatment. *Hydrological Processes* 20 (7), 1567–1583.

Yu, D. & Lane, S. N. 2011 Interactions between subgrid-scale resolution, feature representation and grid-scale resolution in flood inundation modelling. *Hydrol. Process.* 25 (1), 36–53.

First received 16 May 2022; accepted in revised form 16 September 2022. Available online 28 September 2022

Downloaded from http://iwaponline.com/jh/article-pdf/doi/10.2166/hydro.2022.065/1120810/jh2022065.pdf
by guest

Experimental and Numerical Modeling of Wave Transmission Over Submerged Breakwater and Rigid Vegetation



Munireddy G. Mutukuru, P. Kishorekumar Reddy, and Gorle Giridhar

Abstract The wave–structure interaction besides hydrodynamics over natural and submerged breakwaters is an empirical process due to the complex flow process. A better understanding of the wave transmission through natural and artificial submerged breakwaters is vital in the field of coastal conservation. The studies investigating transmission coefficient (K_T), in general using phase averaging approach, in particular are limited. In this study, numerical simulations are carried out using one-dimensional Boussinesq wave model for submerged (i) broad dykes, (ii) narrow dykes, (iii) semi-circular breakwater and (iv) rigid vegetation. The validation of the model is done with a series of experimental observations carried out in two-dimensional wave flume for each breakwater. K_T decreases with increasing wave steepness, relative crest width, relative water depth, relative crest free board for all kinds of breakwater configurations. In particular, K_T was observed to be more for broad dykes and less for rigid vegetation. Model results were compared using physical model tests, and also with numerical and empirical models. Furthermore, wave transmission coefficients obtained from the laboratory model experimental investigation are in good agreement with the numerical simulations. Phase averaging approach gives more insight into the physical description of the wave–structure interaction over and around submerged breakwaters where limited experimental data is available.

Article highlights: numerical simulation of semi-circular breakwater and rigid vegetation to the laboratory scale was new attempt to understand the wave transformation over these structures. physical and numerical modeling of broad, narrow dykes and semi-circular breakwater and their performance comparison was an additional attempt maintaining their constant volumetric proportions.

M. G. Mutukuru (✉) · G. Giridhar
Department of Civil Engineering, Andhra University, Visakhapatnam, Andhra Pradesh, India
e-mail: mgmreddy@gmail.com

G. Giridhar
e-mail: gorlegiridhar@gmail.com

P. Kishorekumar Reddy
Department of Civil Engineering, KSRM College of Engineering, YSR Kadapa, Andhra Pradesh, India
e-mail: palemkishore@gmail.com

© The Author(s), under exclusive license to Springer Nature Singapore Pte Ltd. 2021

S. Chandrasekaran et al. (eds.), *Recent Advances in Structural Engineering*,
Lecture Notes in Civil Engineering 135, https://doi.org/10.1007/978-981-33-6389-2_25

Keywords Submerged breakwaters · Wave transmission coefficient · Boussinesq wave model · Rigid vegetation

1 Introduction

Submerged breakwater is constructed as a primary defense system along the shoreline or on seaside of any important structure of national importance to overcome the problem of coastal erosion which is a typical problem worldwide. Submerged breakwaters are useful for breaking of waves far away from the shoreline and thereby reducing the force of wave energy. Submerged breakwaters can be of great societal relevance in terms of preserving the culture of historical town sights and landscapes [7, 12, 29]. Design of a submerged breakwater is a sensitive coastal engineering problem, where the reliability of the design depends on the knowledge of relationship between wave transmission and structural parameters like crest width and submergence ratio.

Some of the physical processes have been well understood and widely researched through physical models in the laboratory [1, 3, 5, 6, 8, 11, 16, 20, 24, 25, 30]. Owing to several structural and environmental variables associated with the hydro-morphodynamics around submerged breakwaters, it is practically impossible to realize a complete understanding of hydro-morphodynamics with physical model tests. Numerical modeling is the only feasible technique, which could address this knowledge gap.

More stable breakwaters also developed and one of them is semi-submersible semi-circular porous breakwater that provides high stability against wave action. The semi-submersible semi-circular breakwater that was first installed at the Yangtze River Estuary, China in year 2000 was proven to be effective in attenuating the wave energy. Semi-circular breakwater model was tested by varying front wall porosity at 0 (i.e., no perforations), 9, 18, and 27% and empirical models are proposed to provide design formulas for wave transmission. The overall results indicate that permeable SCB models are good energy dissipaters [9]. Later series of laboratory experiments in a 2D monochromatic wave flume was conducted by Sreenivasa Reddy and Muni Reddy [27] to evaluate the transmission characteristics of scaled down SBW physical models of different radii and different submergence ratios, and reported that transmission coefficient decreases as the incident wave steepness increases for different submergence ratios.

The new concept "Bio-shields" coastal vegetation often being referred to increasingly is considered as a possible alternative for structural coastal protection, since it is one of the most natural eco-friendly systems that are sustainable [2]. The "Bio-shield" is also efficient in the conservation of a beach and acts as buffer zones in reducing the energy from disastrous ocean wave interaction on the beach [23]. The great Indian Ocean tsunami has demonstrated that plantation along a coastal belt plays a significant role in limiting the disaster levels by minimizing the inundation

reach as well as run-up on coastal structures and beaches. However, wave transformations over or around submerged breakwaters, such as wave transmission in particular, through phase averaging approach are still limited and it is important to further enhance the knowledge in this domain.

In numerical modeling of monochromatic waves around submerged breakwaters, there are many complex hydrodynamic characteristics to be dealt with. In order to simulate these complex hydrodynamic characteristics, a time-dependent, nonlinear dispersive wave model is the most straightforward approach. Hence, efforts have been made in this study to discuss the evolution of waves in the vicinity of submerged breakwaters using Boussinesq-type equations [14, 19]. Boussinesq-type equations have made remarkable development over the last couple of decades largely due to the critical steps provided by Johnson [12], Kriezi and Karambas [15], Cruz [4].

MIKE 21 BW model numerically solves the 2D and 1D Boussinesq-type equations. The model has capability to simulate various processes in coastal area such as shoaling, refraction, diffraction, reflection, and breaking [26]. MIKE 21 BW model can be employed using one or two horizontal space coordinates. In the case of two horizontal space coordinates, the model solves the enhanced Boussinesq equations by an implicit finite difference technique, while in one horizontal space coordinates, the equations are solved using a standard Galerkin finite element method. According to these basic information and differences between these modules of MIKE 21 BW, one can conclude that the two horizontal space coordinates may be a better choice to be employed for simulating the wave field around and behind the submerged breakwaters.

In order to study the behavior of natural and artificial submerged vegetation in steady flow conditions and to have a preliminary idea as to how the submerged structural parameters influence the flow behavior, experiments in a hydraulic wave flume have been carried out and compared with 1DH Boussinesq numerical model.

2 Experimental Investigation

In the present study, experimental investigations were carried out to study K_T for natural and artificial submerged breakwaters under the action of monochromatic waves. The artificial submerged breakwaters include: (1) broad dykes, (2) narrow dykes and (3) semi-circular breakwaters, and rigid vegetation is considered as the natural submerged breakwater system.

The design of the experiments starts from the selection of testing facility, selection of instrumentation and data acquisition system, fabrication of physical models. The data collection was followed by analyses of measured physical quantities to understand the phenomenon under investigation. The scheme of experiments is measuring the wave run-up, wave reflection for different water depths (d), wave heights (H) and periods (T) of regular waves. Water depth was varied to simulate the tidal variation.

2.1 Testing Facility

The experiments were carried out in a two-dimensional (2D) wave flume of 45 m long, 1.2 m wide and 1.2 m deep in the Department of Civil Engineering at Andhra University College of Engineering, Visakhapatnam, India. One end of the wave flume is fitted with wave generator and the other end is provided with a rubble absorber to absorb the incident wave energy. The flume is capable of generating regular waves of different amplitudes and frequencies. The water depth can be varied from a minimum of 0.25 m to maximum of 0.80 m. Electromechanical linear actuator system designed for sinusoidal wave generation was installed in the wave flume, with features of servo drive cum controller as the driving mechanism. The wave generating system can generate different kinds of 2D regular wave sequence or sea state within the mechanical, geometrical, and hydraulic limitations of the system. To measure the water surface elevation, capacitance-type wave probe is used. Wave propagation in the flume can be viewed from the digital oscilloscope and the data can be retrieved for further analysis.

2.2 Fabrication of Physical Models

In the present investigation stable rubble mound breakwater, semi-circular breakwater and rigid vegetation models are prepared to a scale keeping the flume facility limitations after the dimensional analysis. Different porosities in terms of percentage openings were provided to simulate the structural porosity for semi-circular breakwater.

2.2.1 Rubble Mound Type Breakwater

Model mound type breakwater is constructed with horizontal crest and slopes of 1V:2H on both sides. Broad and narrow crested breakwaters are considered in the study with two crest widths of 0.4 and 1.2 m. The breakwater model was fixed at a distance of 30 m from the wave paddle. The hydrodynamic parameters involved in the present study are shown in Table 1.

2.2.2 Semi-circular Breakwater

Semi-circular porous breakwaters were also fabricated and used in the present investigation. The perforated semi-circular breakwater is proved to be an effective anti-reflection structure with high-energy dissipation ability. The perforated structures control the height of the waves mainly by transmission, reflection and found to be most effective when used at locations where wave conditions are relatively mild.

Table 1 Ranges of the hydrodynamics parameters considered in the present study

Submerged breakwater	Semicircular breakwater	Vegetation
Crest height, $h = 0.2$ m	Crest height, $h = 0.31, 0.35$ m	Vegetation height, $h = 0.3$ m
Crest width, $B = 0.40, 1.2$ m	Crest radius, $B = 0.31, 0.35$ m	Meadow width, $B = 1.1$ m
Wave period, $T = 1.5$–3.0 s	Wave period, $T = 1.5$–3.0 s	Wave period, $T = 1.5$–3.0 s
Wave height, $H =$ 0.05–0.15 m	Wave height, $H =$ 0.05–0.15 m	Wave height, $H =$ 0.05–0.15 m
Relative submergence depth, $\frac{\mathbf{h_c}}{\mathbf{d}} = 0.67, 0.5, 0.33, 0.2$	Relative submergence depth, $\frac{\mathbf{h_c}}{\mathbf{d}} = 0.67, 0.5, 0.33, 0.2$	Relative submergence depth, $\frac{\mathbf{h_c}}{\mathbf{d}} = 0.67, 0.5, 0.33, 0.2$
Wave steepness, $\frac{H}{L} =$ 0.02–0.15	Wave steepness, $\frac{H}{L} =$ 0.02–0.15	Wave steepness, $\frac{H}{L} =$ 0.02–0.15
Relative crest width, $\frac{B}{L} =$ 0.06–1.0	Relative crest width, $\frac{B}{L} =$ 0.06–0.5	Relative crest width, $\frac{B}{L} =$ 0.06–0.7
Relative crest height, $\frac{\mathbf{h_c}}{\mathbf{H}} = 0.5$ to -10	Relative crest height, $\frac{\mathbf{h_c}}{\mathbf{H}} = 0.5$ to -14	Relative crest height, $\frac{\mathbf{h_c}}{\mathbf{H}} = 0.5$ to -12

Two models of radii 0.31 and 0.35 m were used. These radii were arrived by equivalent volume of 0.40 and 0.6 m. The perforations were provided on both sides of the semi-circular breakwater with circular openings.

In the present investigation seven types of breakwater configurations were studied, such as BDWEBW, BDWET, NDWEBW, NDWET, SCWET31, SCWET35 and VEGWET.

2.2.3 Rigid Vegetation

In the present study rigid vegetation model was prepared by using uPVC pipe of diameter 22 mm, and the height of the stem is 300 mm. The stems are fitted into the wooden plank of 1100 mm × 1000 mm. The center-to-center spacing provided between the stems is 100 mm along the width and length of wooden plank. The physical models are represented in Fig. 1 (panel-I).

2.2.4 Rigid Vegetation

In the present study rigid vegetation model was prepared by using uPVC pipe of diameter 22 mm, and the height of the stem is 300 mm. The stems are fitted into the wooden plank of 1100 mm × 1000 mm. The center-to-center spacing provided between the stems is 100 mm along the width and length of wooden plank. The physical models are represented in Fig. 1 (panel-I).

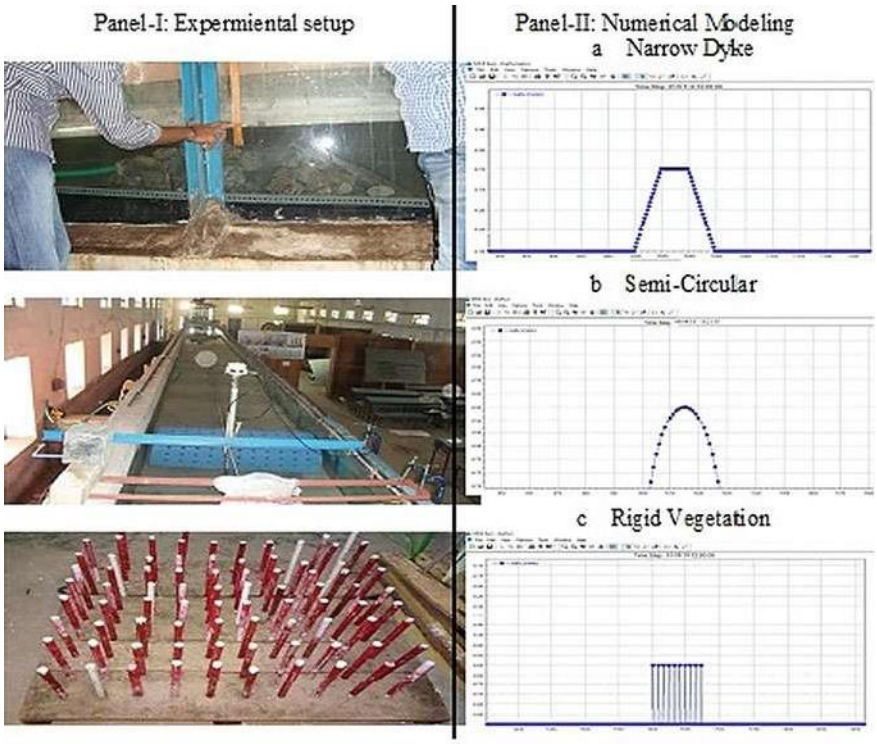


Fig. 1 Cross-sectional views of the breakwaters considered in the study. Panel-1: Fabricated models fixed in the wave flume during the experimental setup. Panel-II: Outline of bathymetry with **a** narrow dyke, **b** semi-circular, **c** rigid vegetation breakwater generated in the numerical modeling

3 Numerical Investigation

To investigate the hydrodynamic processes over and around submerged breakwaters, numerical simulations are carried out to model the physical phenomena of artificial and natural breakwaters (Fig. 1 panel-II).

In recent decades, either phase-averaged or phase-resolving numerical models are widely in use for wave modeling around submerged breakwaters. In a phase-resolving model, the sea surface is resolved, and the model treats the wave field deterministically, while in a phase-averaged model, the statistics of the sea surface are computed, so this model treats the wave field stochastically. Therefore, the accuracy of predictions by these models is to a great extent dependent on input data, such as bathymetry files and wave data, as well as open boundary conditions, model parameters, simplifications, modeling techniques and the numerical scheme. Some of the phase-averaged approaches include spectral wave models, Boussinesq equation, the mild-slope equation, and shallow-water equations. Out of these Boussinesq equation wave models are found to be robust in several coastal applications. However,

as a major limitation, application of the Boussinesq equations is restricted to only intermediate and shallow water depths.

4 Results and Discussion

In the present study, comparison of K_T for different breakwater configurations, tidal level variations with relative crest free board (h_c/H) at particular relative submergence depth (h_c/d = 0.2, 0.33, 0.5 and 0.67) are presented. The comparison was mainly carried out for vegetation (VEWET) with conventional mound type breakwater configurations like NDWET, NDWEBW, BDWET, BDWEBW and SCWET. In the first case a constant water depth was maintained, and the breakwater heights were varied. This simulates the investigation on the site where the tidal fluctuations are insignificant. In the second case, constant breakwater height was maintained, and water depths were varied to simulate the investigation on the site where the tidal variations are significant. Comparison was carried out with numerical modeling using one-dimensional BW module for corresponding breakwater configurations and vegetation. In Figs. 2 and 3 solid symbols indicate results of the experimental investigation and open or hollow symbol indicates results of the numerical modeling. Continuous line indicates the general trend of the variation of the K_T with dimensionless parameters for experimental observations.

4.1 Effect of Wave Steepness (H/L)

Wave steepness is a dimensionless parameter, which gives representation of the wave size. In this study, the effect of wave height is represented in terms of wave steepness parameter (H/L). The higher the wave steepness parameter, the steeper will be the incident waves. When the wave approaches the seaward slope of the breakwater, it shoals and eventually breaks on reaching the wave steepness limit. The K_T takes place as the wave propagates over the crest width of the breakwater. K_T decreases with the wave steepness for submerged breakwaters for relative submergence water depth h_c/d = 0.67, 0.5, 0.33 and 0.20 as shown in Fig. 2. K_T at $h_c/d = 0.2$ is much better than that of the h_c/d = 0.67, 0.5 and 0.33. Waves of mild steepness manage to transmit over the crest of the breakwater with less interaction with the structure due to their limited wave amplitudes. As a result, lower K_T values will be anticipated when exposed to waves of higher steepness. The reason for this could be the increase in the resistance force in the porous media of the submerged breakwater, because the length of the porous media increases when the slope gradient of the structure decreases. Results of measurement and data processing of transmitted waves through the meadow width of rigid vegetation showed that the transmission coefficient (K_T) decreased with increasing wave steepness. It is observed that the wave heights decay exponentially as the wave propagates through the submerged vegetation models and the steeper

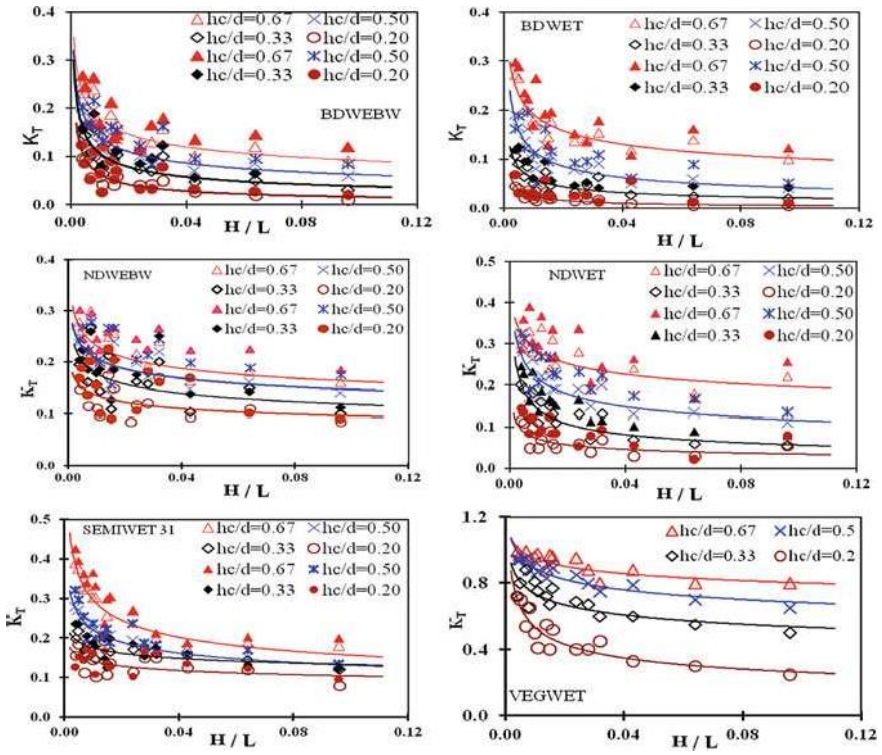


Fig. 2 Comparison of transmission coefficient (K_T) against wave steepness (H/L) for regular waves at different submergence ratios (h_c/d) and for different breakwater configurations

waves, represented by a higher value of H/L, exhibits lower wave attenuation for the simulated submerged models. For submerged breakwaters, the increase in the wave height leads to a lower transmission coefficient. There is more dissipation by the crest of the breakwater for a steeper wave than a lower wave. However, when the crest height is far below the still water level, the breakwater crest has lost its influence and every wave may propagate unhindered. So, an increasing in wave height now leads to an increasing transmission coefficient in the wave flume. In considering the overall spatial distribution of wave heights, it can be noted that the wave damping effect of the submerged breakwater on the incoming wave increases when the slope gradient of the structure becomes steeper and the incident wave height becomes higher.

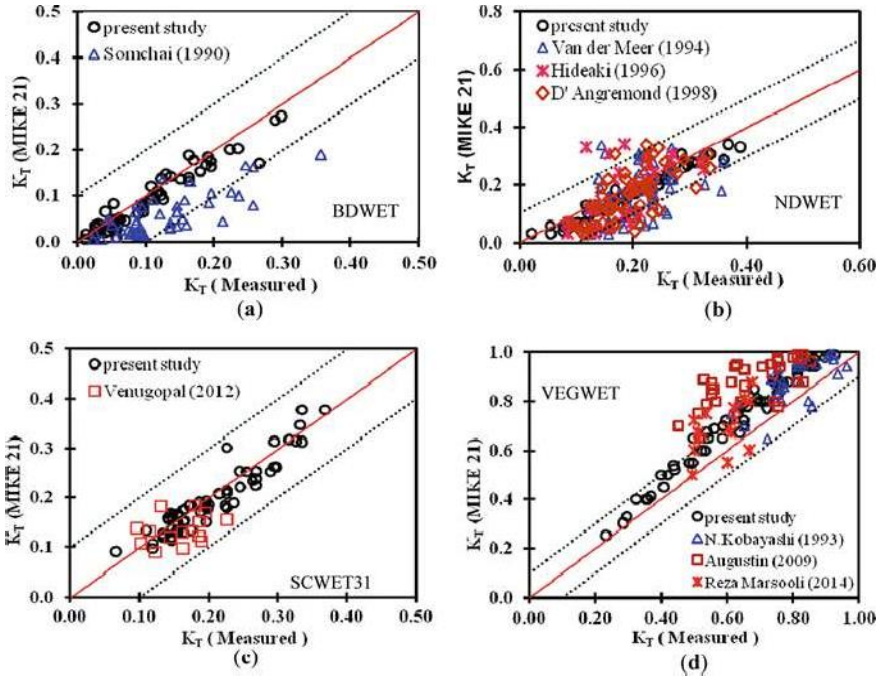


Fig. 3 Validation of numerical model with experimental and literature observations for **a** broad dyke, **b** narrow dyke, **c** semi-circular, **d** rigid vegetation. Dotted lines correspond to 90% confidence intervals

4.2 Reliability of the Numerical Modeling

Measured and numerical model K_T values are compared and shown in Fig. 3a for BDWET. Measured values of van der Meer and Daemen [28] was also incorporated for comparing the K_T values of different relative water depths. In the present study, K_T results show good correlation between measured and modeled values, thereby demonstrating one-dimensional Boussinesq wave model is robust and reliable than linear models. Figure 3b shows the comparison of measured and modeled K_T values of NDWET. Measured values of Okuzono et al. [10], Venugopal et al. [31], d'Angremond et al. [6] were also incorporated in the comparison of K_T values for different relative crest width (B/L). This figure shows a large scatter in the K_T values of the above investigators. In the present study, K_T results show good correlation between measured and modeled values. In this case measured values are on lower side of the line equality. This is because the phenomenon of extreme wave breaking with narrow dykes is highly complex and one-dimensional Boussinesq wave model is able to perform and is reliable than linear models. Figure 3c shows the comparison of measured and modeled K_T values of SCWET31. Venugopal et al. [31] presented the lower range of K_T values. In the present study, experiments and modeling were carried

out over wide range and the K_T results show good correlation between measured and modeled values. Figure 3d shows the comparison of measured and modeled K_T values of VEGWET. Measured values of Kobayashi et al. [14] were also incorporated in comparison to K_T values for a relative meadow width (B/L). Results of the Augustin et al. [2], Marsooli and Weiming [23] show scatter around the line of equality whilst Augustin et al. [2] results are above the line of equality indicating overprediction by the modeling. In the present study, experiments and modeling were carried out over wide range and the K_T results show that all the values are above the line of equality, indicating overprediction by the modeling above the 10% confidence level.

5 Conclusions

In the present study, the wave interaction with submerged breakwaters has been simulated using one-dimensional module and verified against the experimental results. Systematic experimental investigation was carried out for seven submerged barrier configurations.

Transmission coefficient K_T decreases with increase in wave steepness H/L. Measured and numerical model K_T values are validated and compared for different submerged breakwater configurations and rigid vegetation and also compared with the results of the other authors. These comparisons show good agreement between the modeled and measured K_T values. K_T results show good correlation between measured and modeled values.

Acknowledgements The authors acknowledge DHI (India) Water and Environment Pvt Ltd to provide the MIKE license to carry out the Boussinesq wave model studies. The authors also acknowledge the help and guidance received from Department of Marine and Coastal at DHI during the model studies.

Conflict of Interest The authors declare that they have no conflict of interest.

References

1. C.B. Adams, C.J. Sonu, Wave transmission across submerged near-surface breakwaters, in *Proceedings of 20th International Coastal Engineering Conference*, Taipei, ASCE, vol. 2 (1986), pp. 1729–1738
2. L.N. Augustin, J.L. Irish, P. Lynett, Laboratory and numerical studies of wave damping by emergent and near-emergent wetland vegetation. Coast. Eng. **56**, 332–340 (2009)
3. B. Mariano, M. Calabrese, Conceptual approach for prediction of wave transmission at low-crested breakwaters. J. Waterway Port Coast Ocean Eng. **133**, 213–224 (2007)
4. E.C. Cruz, M. Isobe, A. Watanabe, Boussinesq equations for wave transformation on porous beds. Coast. Eng. **30**(1), 125–156 (1997)
5. T.M. Dick, A. Brebner, Solid and permeable submerged breakwaters, in *Proceedings of 11th International Conference on Coastal Engineering*, ASCE (1968), pp. 1141–1158

6. K. d'Angremond, J.W. Van der Meer, R.J. De Jong, Wave transmission at low-crested structures, in *Proceedings of 25th International Conference on Coastal Engineering*, ASCE (1996), pp. 2418–2427
7. Y. Goda, H. Takeda, Y. Moriya, Laboratory investigation on wave transmission over breakwaters. Rep. Port Harbour Res. Inst. **13**, 38 (1967)
8. Y. Goda, J. Ahrens, New formulation for wave transmission over and through low crested structures, in *Proceedings of the International Conference on Coastal Engineering*. ASCE (2008)
9. H.M. Teh, V. Venugopal, T. Bruce, Hydrodynamic performance of a free surface semicircular perforated breakwater. Coast. Eng. **138**(2), 149–163 (2010)
10. H. Okuzono, K. Takahashi, T. Abe, T. Maeda, H. Gahara, A study on environmental submerged breakwaters, in *Proceedings of Civil Engineering in the Ocean*, vol. 12 (1996), pp. 497–502
11. J.W. Johnson, R.A. Fuchs, J.R. Morison, The damping action of submerged breakwaters. Trans. Am. Geophys. Union **32**(5), 704–718 (1951)
12. H.K. Johnson, T.V. Karambas, I. Avgeris, B. Zanuttigh, D. Gonzalez-Marco, I. Caceres, Modelling of waves and currents around submerged breakwaters. J. Coast. Eng. **52**, 949–969 (2005)
13. H.K. Johnson, Wave modeling in the vicinity of submerged breakwaters. J. Coast. Eng. **60**, 940–949 (2006)
14. N. Kobayashi, A.W. Raichle, T. Asano, Wave attenuation by vegetation. J. Waterway Port Coast. Ocean Eng. **119**, 30–48 (1993)
15. E. Kriezi, T. Karambas, Modelling wave deformation due to submerged break-waters. Proc. ICE Marit. Eng. **163–1**, 19–29 (2010)
16. I.J. Losada, R. Silva, M.A. Losada, 3-D non-breaking regular wave interaction with submerged breakwaters. Coast. Eng. 229–248 (1996)
17. MIKE21 User Guide and Reference Manual, Danish Hydraulic Institute, Water and Environment, Denmark. DHI (2017)
18. A. Panizzo, R. Briganti, Analysis of wave transmission behind low-crested break-waters using neural networks. Coast. Eng. **54**, 643–656 (2007)
19. P.A. Madsen, O.R. Sorensen, A new form of the Boussinesq equations with improved linear dispersion characteristics. Part 2. A slowly-varying bathymetry. Coast. Eng. **18**, 183–204 (1992)
20. M. Petti, P. Ruol, Laboratory tests on the interaction between nonlinear long waves and submerged breakwaters, in *Proceedings of 23rd International Conference on Coastal Engineering*. ASCE (1992)
21. F.T. Pinto, A.C.V. Neves, Environmental aspects of using detached breakwaters for coastal protection purposes, situation and perspectives for the European Union, Porto, Portugal (2003)
22. R.S. Ranasinghe, Numerical modelling of wave transformation over submerged breakwaters using Boussinesq-type models. J. Nat. Sci. Found. Sri Lanka **46**(3), 369–379 (2018)
23. R. Marsooli, W. Weiming, Numerical investigation of wave attenuation by vegetation using a 3D RANS model. J. Adv. Water Resour. 245–257 (2014)
24. T. Schlurmann, M. Bleck, H. Oumeraci, Wave transformation at artificial reefs described by the Hilbert-Huang transformation (HHT), in *Proceedings of 28th International Conference on Coastal Engineering*. ASCE (2002)
25. S.R. Seabrook, K.R. Hall, Wave transmission at submerged rubble mound breakwaters, in *Proceedings of 26th International Conference on Coastal Engineering*. ASCE (1998)
26. O.R. Sorensen, H.A. Schaffer, P.A. Madsen, Surf zone dynamics simulated by a Boussinesq type model. III. Wave-induced horizontal nearshore circulations. Coast. Eng. **33**, 155–176 (1998)
27. K. Sreenivasa Reddy, M.G. Muni Reddy, Experimental studies on low crested rubble mound, semicircular breakwaters and vertical wall system. Int. J. Ocean Clim. Syst. **4**(3), 213–216 (2013)
28. J.W. van der Meer, I.F.R. Daemen, Stability and transmission at low-crested rubble mound structures. J. Waterways Port Coast. Ocean Eng. **120**(1), 1–19 (1994)

29. J.W. van der Meer, R. Briganti, B. Wang, B. Zanuttigh, Wave transmission at low crested structures, including oblique wave attack, in *Proceedings of 29th International Conference on Coastal Engineering*. ASCE (2004)
30. J.W. van der Meer, R. Briganti, B. Zanuttigh, B. Wang, Wave transmission at low-crested structures, including oblique wave attack. J. Coast. Eng. **52**, 915–929 (2005)
31. J. Venugopal, H.M. The, T. Bruce, Hydrodynamic characteristics of a free-surface semicircular breakwater exposed to waves. J. Waterway Port Coast. Ocean Eng. **138**, 149–163 (2012)

ISSN: 0974-5823 Vol. 7 No. 1 January, 2022

International Journal of Mechanical Engineering

The Selection of Clinical Orthodontic Implant Materials by Entropy Weight Methods through Hybrid Multi criteria Decision making Techniques

M. Amareswari Reddy

Assistant professor, Dr.L.B.College of Engineering, Visakhapatnam, A.P, INDIA

Prof. K. Venkata Subbaiah

Senior Professor, Mechanical Engineering Department, Andhra University, Visakhapatnam, A.P, INDIA

Dr. Challa. Suresh

Associate professor, Avanthi College of Engineering and technology , Visakhapatnam, A.P, INDIA

Abstract

The purpose of this research is to determine the most appropriate material that can be used in tooth implantation by employing multi-criteria decision-making techniques. The following techniques used in this research paper: Entropy weighting with Combinative Distance-Based Assessment (CODAS), The Technique for Order of Preference by Similarity to Ideal Solution (TOPSIS), Additive Ratio Assessment (ARAS), Titanium grades 1–4 and Ti-6Al-4V, Ti-6al-7Nb, and Ti–29Nb–13Ta–4.6Zr are used as selection criteria. The proposed material selection technique is relatively inexpensive and may be advantageous when numerical selection of material properties or aspects of user interaction are required. The purpose of this paper is to determine which material is the most compatible from a health and transactional standpoint. Ti-6Al-4V is the optimal material for dental implant design, according to proposed techniques, followed by Ti–6al–7nb.

Keywords -- Multi-criteria decision making, weighting estimation by entropy, ARAS, TOPSIS, CODAS, material selection, dental implant

I. INTRODUCTION

The human body is made up of numerous organic and inorganic components. Bones are a critical component of the human body as they provide the body with strength, flexibility, and form via the collagen and hydroxyapatite found in bone [1,2]. Calcium, magnesium, and potassium, as well as electrolytes, are the primary components of bones. Accidents, aging, and illness are the leading causes of bone failure. The use of biomedical implants is necessary to compensate for the limitations imposed by bone fracture [3,4]. Although the human body does not completely absorb foreign substances except those that are edible, it is noted that Titanium is a Benchmark discovery that can be used in a variety of compositions as titanium alloy for medical implants.

The materials used in the development and adoption of a product are critical. Numerous products with a variety of different properties are now available. The design engineer should think multiple times prior selecting the best material for a particular application [5]. Material selection error can wreak havoc on the manufacturing and implementation processes. When selecting materials for a particular product, the engineer must take a number of factors into account. Material selection has become more complicated and difficult in recent years because of material properties such as physical, electric, magnetic, efficiency, mechanical, and chemical [6]. Additionally, the material's performance, availability, cost, and manufacturing shape. Market impact should also be considered. As a result, a more detailed mathematical approach to material collection are expected, with a variety of alternative strategies and influencing parameters [7].

Rigid materials and superalloys play a significant part in the world's most advanced technical areas, including aerospace, marine, chemical, and biomedical applications. Rigid materials and superalloys are essentially materials and alloys with superior chemical, physical, thermal, and biological characteristics [8]. There is a need of research to comprehend and find the most notable materials for their particular functions in the engineering and biological fields. Despite decades of research, selecting the best material with the lowest cost, highest sustainability, and longest life remained as an incomplete challenging problem and seeking new contributions. Additionally, the difficulty increases when selecting materials for objects with smaller dimensions such as dental implants, heart stunts.

This prompted us to develop a method for selecting the optimal material for dental implantation. The purpose of this research paper is to determine the most effective material selection techniques. There is a dearth of research on effective strategies for material selection for small dimensions.

In this paper, we show that the Suitable approaches for selection of material using MCDM techniques. MCDM methods such as TOPIS, ARAS, and CODAS using entropy weight methodology are taken into consideration. From the overall literature review, MCDM can be categorized as below:

1. MCDM approaches can be grouped into two categories – Qualitative and Quantitative measurements
2. Qualitative measurements include TOPSIS, SAW, COPRAS, COPRAS-G methods.
3. Quantitative measurements include AHP and Fuzzy procedures.
4. MCDM problem can be solved using the below steps:

a. Creation of Decision-making Matrix

b. Normalization of Decision-making Matrix

c. Weighted Decision-making Matrix of normalization

d. Assessment Scoring

e. Ranking

II. METHODS

The overall process flow of this research is depicted in Figure 1, along with the stages involved. Six stages comprise the proposed framework. The material is selected in phase 1, and the entropy-based calculation criteria are determined in phase 2. Phase 3 implements the TOPSIS method, while phases 4 and 5 implement the CODAS and ARAS methods, respectively. The final phase represents the rankings of the selected materials and presents the conclusion.

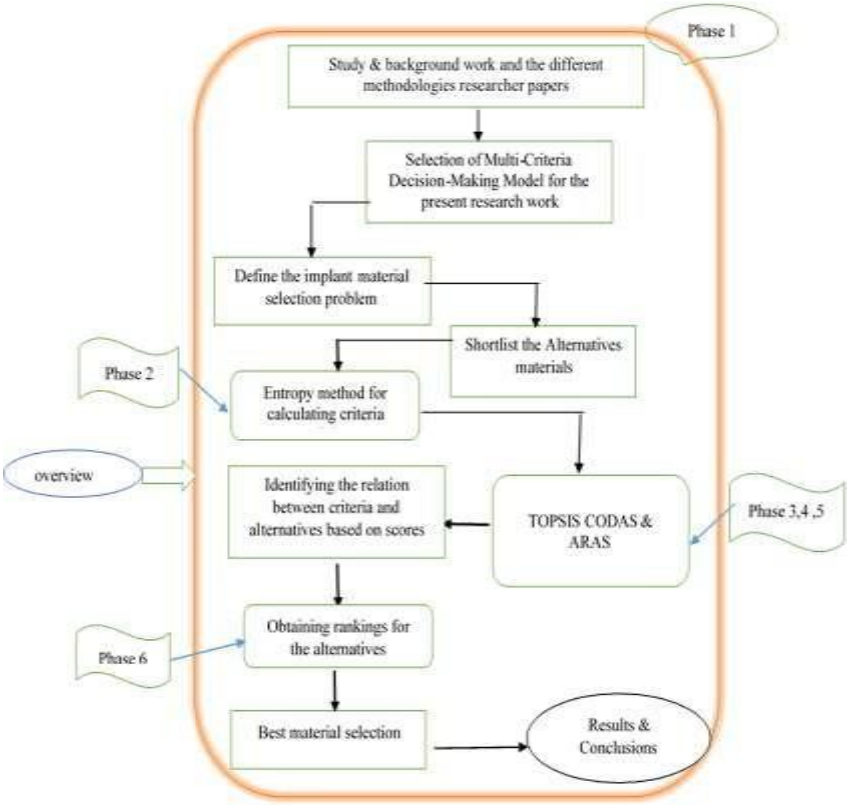


Figure 1: Process Overall Flow

2.1 Entropy weight

Claude E. Shannon invented the idea of "entropy" in the year 1948 to measure the weights of attributes. According to the author [8], entropy is indeed a calculation of its unsafeness related to a probability distribution of the knowledge quality of a particular message and examined the weights incertitude by differential distribution of chance. The following stages represents the calculated attribute weights:

Step 1: Decision-Making Matrix (z_{ij})

$$Z = [z_{ij}]_{n\times m} = \begin{bmatrix} z_{11} & z_{12} & \ldots\ldots & z_{1m} \\ z_{21} & z_{22} & \ldots\ldots & z_{2m} \\ \ldots & \ldots & \ldots & \\ z_{n1} & z_{n2} & \ldots\ldots & z_{nm} \end{bmatrix} \quad (1)$$

Step 2: Determination of Normalized-Decision Matrix (Q_{ij})

$$_{ij}Q = \frac{z_{ij}}{\sum_{i=1}^{m} z_{ij}} \quad (2)$$

Step 3: Entropy Estimation (E_j)

$$E_j = -k \sum_{i=1}^{m} Q_{ij} \ln Q_{ij} \quad (3)$$

Where, $k = \frac{1}{\ln(m)}$; m = number of attributes.

Step 4: Determination of Degree of Diversification (D_j)

$$D_j = 1 - E_j \quad (4)$$

Step 5: Determination of Weights of Criteria (W_j)

$$_{j}W = \frac{D_j}{\sum_{j=1}^{n} D_j} \quad (5)$$

2.2 CODAS Technique:

CODAS technique for problem-solving of material selection is discussed in [9]. The technique utilizes two measures for the determination of the acceptability of alternatives of the materials. The first measure is the negative-ideal outcome of Euclidean distance between the key and principal metric. The second measure is the Taxicab distance between the standard space apathies. CODAS steps are defined as below:

Step 1: Decision-making Matrix of normalisation (k_{ij})

$$k_{ij} = \begin{cases} \frac{z_{ij}}{\max_i z_{ij}}, & \text{if } j = K_b \\ \frac{z_{ij}}{\min_i z_{ij}}, & \text{if } j = K_{nb} \end{cases} \quad (6)$$

Where K_b & K_{nb} are beneficial and non- beneficial values.

Step 2: Weighted Decision-making Matrix of normalisation (r_{ij}) $r_{ij} = w_j n_{ij}$ (7)

Step 3: Solution with a negative-ideal outcome (ks)

$$ks = [ks_j]_{1\times m} \quad (8)$$

Step 4: Euclidean (E_i) and Taxicab (T_i)values

$$E_i = \sqrt{\sum_{j=1}^{m}(r_{ij} - ns_j)^2} \quad (9)$$

$$T_i = \sum_{j=1}^{m}|r_{ij} - ns_j| \quad (10)$$

Step 5: Determination of Relative assessment (h_{ik})

$R_a = [h_{ik}]_{n\times m}$

$$h_{ik} = (E_i - E_k) + (T(E_i - E_k) \times (T_i - T_k)) \quad (11)$$

T Denotes equality of the Euclidean

$$(z) = \{^{1,\ \ if\ |z| \geq r}_{0,\ \ if\ |z| < r}\}$$

Step 6: Score of Assessment (H_i)

$$H_i = \sum_{j=1}^{n} h_{ik} \quad (12)$$

2.3 TOPSIS Technique:

Yoon and Hwang established TOPSIS as a criterion based decision-making technique [10]. TOPIS is a multi-objective optimization approach, to achieve the specific optimal condition by considering all response parameters of a material. TOPSIS execution steps are as below:

Step 1: Decision-making Matrix of normalisation (n_{ij})

$$n_{ij} = \frac{z_{ij}}{\sqrt{\sum_{i=1}^{m} z^2_{ij}}} \quad (13)$$

Step 2: Weighted Decision-making Matrix of normalisation (r_{ij})

$$r_{ij} = w_j n_{ij} \quad (14)$$

Where w_j ($0< w_j< 1$), $\sum_{i=1}^{n} W_i = 1$

Step 3: Solution with a positive & negative-ideal outcome solution (S_p & S_n)

$$S_p = \{ma(r_{ij}), min(r_{ij})\} \quad (15)$$

$$S_n = \{mi(r_{ij}), max(r_{ij})\} \quad (16)$$

Step 4: Euclidean (E_i) values

$$E_{pi} = \sqrt{\sum_{j=1}^{m}(r_{ij} - s_{pj})^2} \quad (17)$$

$$E_{ni} = \sqrt{\sum_{j=1}^{m} (r_{ij} - s_{pj})^2} \quad (18) \qquad (18)$$

Step 5: Relative assessment (h_{ik})

$$h_{ik} = \frac{E_{pi}}{(E_{pi} + E_{ni})} \quad (19)$$

Step 6: Assessment score (H_i)

$$H_i = \sum_{j=1}^{n} h_{ik} \quad (20)$$

2.4 ARAS Technique:

The ARAS approach is based on ratio sums of alternatives with a two-stage linear normalization procedure [12]. In this approach, the optimal parameters are determined using a utility function [13]. Below are the execution steps of ARAS Technique:

Step 1: Determination of Normalization of Decision matrix (n_{ij})

$$n_{ij} = \frac{z_{ij}}{\sum_{i=0}^{m} z_{ij}} \quad \text{For Beneficial attributes} \quad (21)$$

$$n_{ij} = \frac{1/z_{ij}}{\sum_{i=0}^{m} 1/z_{ij}} \quad \text{For Non- Beneficial attributes} \quad (22)$$

Step 2: Determination of Weighted normalized decision matrix (r_{ij})

$$r_{ij} = w_j n_{ij} \quad (23)$$

Step 3: Optimality function (S_i)

$$S_i = \sum_{j=0}^{n} r_{ij} \quad (24)$$

Step 4: Degree of the utility (K_i)

$$K_i = \frac{S_i}{S_o} \quad (25)$$

Step 5: Assessment score (H_i)

$$H_i = \sum_{j=1}^{m} K_i \quad (26)$$

CASE STUDY:

CLINICAL ORTHODONTIC IMPLANT MATERIALS SELECTION

Nowadays, dental implants made of titanium and its components account for a sizable portion of the market [13]. Seven distinct forms of titanium are discussed in this article as implant biomaterials (ASTM). Titanium alloys from Grade 1 to Grade 4 , Ti-6Al-4V (Ti-64), Ti-6Al-7Nb (Ti-6/7) and Ti–29Nb–13Ta–4.6Zr (TNTZ) as listed in Table 1[14,15] along with their mechanical and physical properties are used in this study. Youngs Modulus (Gpa), Ultimate Tensile Strength (MPa), Yield Strength (MPa), Elongation (%), density (g/cc), and Cost ($/kg) are six different parameters that have been taken into consideration for this study. The purpose of this research paper is to compare the above mentioned MCDM approaches (CODAS, TOPSIS & ARAS) for determining the optimal material for dental implantation.

The entropy weights are calculated and evaluated for all selected materials using three multi-criteria decision-making techniques; the results are compared for accuracy using Spearman rank-order correlation coefficients; and finally, the materials are ordered in highest to the lowest according to the rank obtained by the assessment score (H_i). The material with the highest score of assessment would be chosen. Youngs Modulus, Ultimate Tensile Strength, and Yield Strength are considered beneficial criteria when selecting a material, whereas Elongation, density, and cost are considered non-beneficial criteria.

TABLE 1: MECHANICAL CHARACTERISTICS OF SELECTED TITANIUM COMPONENTS

Criteria	EM	UTS	YS	EL	DE	CO
Ti-35A	0.8947	0.2581	0.1932	0.4167	0.9778	0.9231
Ti-50A	0.8947	0.3710	0.3125	0.5000	0.9778	1.0000
Ti-65A	0.8947	0.4839	0.4318	0.5556	0.9778	0.9231
Ti-75A	0.9123	0.5914	0.5489	0.6667	0.9778	0.8571
Ti-64	1.0000	1.0000	0.9875	1.0000	1.0000	0.4138
Ti-6/7	1.0000	0.9677	1.0000	1.0000	1.0000	0.3429
TNTZ	0.7018	0.9796	0.9818	0.7576	1.0000	0.2857

TABLE 2: NORMALIZED DECISION-MAKING MATRIX

Criteria/ Alternatives	Elastic Modulus (GPa) EM	Ultimate Tensile Strength (MPa) UTS	Yield Strength (MPa) YS	Elongation (%) EL	Density (g/cc) DE	Cost ($/kg) CO
Titanium -35A	102	240	170	24	4.5	1.3
Titanium -50A	102	345	275	20	4.5	1.2
Titanium -65A	102	450	380	18	4.5	1.3
Titanium -75A	104	550	483	15	4.5	1.4
Ti-6Al-4V (Ti-64)	114	930	869	10	4.4	2.9
Ti-6Al-7Nb (Ti-6/7)	114	900	880	10	4.4	3.5
Ti–29Nb–13Ta–4.6Zr (TNTZ)	80	911	864	13.2	4.4	4.2

III. RESULTS

3.1 Entropy weight

The normalized decision-making matrix for titanium materials is shown in Table 2. The entropy weight-based properties have been calculated and tabulated using formulas (1-2).

The entropy weight-based calculation would be carried out using formulas (3-5). The entropy, degree of diversification, and attribute weights are calculated and are represented in Table 3.

TABLE 3 ENTROPY WEIGHTS

	EM	UTS	YS	EL	DE	CO
Entropy	0.9972	0.9481	0.9297	0.9758	1.0000	0.9347
Degree of diversification	0.0028	0.0519	0.0703	0.0242	0.0000	0.0653
Weights of Attributes	0.0131	0.2419	0.3275	0.1128	0.0001	0.3045

3.2 CODAS Approach

CODAS techniques calculate weights for each material and property independently using the Entropy values defined in Table 3. Table 4 summarizes the weights calculated using CODAS techniques and equation (7). For the CODAS technique, Euclidean and taxicab distances should be calculated. Distances are calculated using equations (8,9,10). The Euclidean and taxicab distances are calculated and represented in Table 5 using table 4 as an input. The ranking order would be determined using Equations (11,12). The ranking order is determined using data from Table 5, the equations are applied to the data, and the final output is represented in Table 6. According to Table 6, the optimal material for dental implantation is Ti-6Al-4V.

TABLE 4: WEIGHTED MATRIX FROM CODAS

Criteria	EM	UTS	YS	EL	DE	CO
Ti-35A	0.0117	0.0624	0.0633	0.0470	0.0001	0.2811
Ti-50A	0.0117	0.0897	0.1023	0.0564	0.0001	0.3045
Ti-65A	0.0117	0.1170	0.1414	0.0627	0.0001	0.2811
Ti-75A	0.0120	0.1431	0.1798	0.0752	0.0001	0.2610
Ti-64	0.0131	0.2419	0.3234	0.1128	0.0001	0.1260
Ti-6/7	0.0131	0.2341	0.3275	0.1128	0.0001	0.1044
TNTZ	0.0092	0.2369	0.3216	0.0855	0.0001	0.0870
Weights	0.0131	0.2419	0.3275	0.1128	0.0001	0.3045
ns	0.009	0.062	0.063	0.047	0.0001	0.0870

TABLE 5: EUCLIDEAN AND TAXICAB FROM CODAS

Criteria	Ei	Ti
Ti-35A	0.1941	0.1966
Ti-50A	0.2229	0.2958
Ti-65A	0.2168	0.3451
Ti-75A	0.2262	0.4021
Ti-64	0.3252	0.5484
Ti-6/7	0.3224	0.5230
TNTZ	0.3141	0.4713

TABLE 6: RANKING FROM CODAS

Criteria	Hi	Rank
Ti-35A	-0.4639	7
Ti-50A	-0.2624	5
Ti-65A	-0.3050	6
Ti-75A	-0.2396	4
Ti-64	0.4563	1
Ti-6/7	0.4366	2
TNTZ	0.3780	3

3.3 TOPSIS Approach

TOPSIS techniques calculate weights for each material and property independently using the Entropy values defined in Table 3. Table 7 summarizes the weights calculated using TOPSIS techniques and equations (13,14). For the TOPSIS technique, positive & negative-ideal outcomes should be calculated. Outcomes are calculated using equations (15,16). The Euclidean distance is calculated on the outcomes using equations (17-20) and are represented in Table 8. The ranking order would be determined using Equations (19,20). The ranking order is determined using data from Table 8, the equations are applied to the data, and the final output is represented in Table 9. According to Table 9, the optimal material for dental implantation is Ti-6Al-4V.

TABLE 7: MATRIX OF NORMALISATION FROM TOPSIS

Criteria	EM	UTS	YS	EL	DE	CO
Ti-35A	0.374	0.134	0.102	0.551	0.382	0.194
Ti-50A	0.374	0.193	0.166	0.459	0.382	0.179
Ti-65A	0.374	0.252	0.229	0.413	0.382	0.194
Ti-75A	0.381	0.308	0.291	0.344	0.382	0.209
Ti-64	0.418	0.521	0.523	0.229	0.373	0.432
Ti-6/7	0.418	0.504	0.530	0.229	0.373	0.521
TNTZ	0.293	0.510	0.520	0.303	0.373	0.626

TABLE 8: EUCLIDEAN FROM TOPSIS

Criteria	Si+	Si-	(Si+) + (Si-)
Ti-35A	0.172	0.132	0.304
Ti-50A	0.146	0.139	0.284
Ti-65A	0.120	0.142	0.262
Ti-75A	0.095	0.149	0.244
Ti-64	0.077	0.180	0.258
Ti-6/7	0.104	0.173	0.277
TNTZ	0.136	0.167	0.303

TABLE 9: RANKING FROM TOPSIS

Criteria	Ci	Rank
Ti-35A	0.433	7
Ti-50A	0.488	6
Ti-65A	0.541	5
Ti-75A	0.611	3
Ti-64	0.700	1
Ti-6/7	0.624	2
TNTZ	0.5500	4

3.4 ARAS Approach

ARAS techniques calculate weights for each material and property independently using the Entropy values defined in Table 10. Table 11 summarizes the weights calculated using ARAS techniques and equations (21,22,23). For the ARAS optimality function

(Si), utility degree (Ui) should be calculated. Si, Ui are calculated using equations (24,25). The calculated Si, Ui for all the materials are represented in Table 11. The ranking order would be determined using Equations (26). The ranking order is determined using data from Table 11, the equations are applied to the data, and the final output is represented in Table 11. As per Table 11, the optimal material for dental implantation is Ti-6Al-4V.

TABLE 10. WEIGHTED MATRIX FROM ARAS

Criteria	EM	UTS	YS	EL	DE	CO
Ti-35A	0.002	0.011	0.012	0.008	0.000	0.049
Ti-50A	0.002	0.016	0.019	0.010	0.000	0.053
Ti-65A	0.002	0.021	0.026	0.011	0.000	0.049
Ti-75A	0.002	0.025	0.033	0.013	0.000	0.045
Ti-64	0.002	0.043	0.059	0.019	0.000	0.022
Ti-6/7	0.002	0.041	0.060	0.019	0.000	0.018
TNTZ	0.001	0.042	0.059	0.014	0.000	0.015
Weights	0.0131	0.2419	0.3275	0.1128	0.0001	0.3045
optimal value	0.0018	0.0428	0.0600	0.0191	0.0000	0.0530

TABLE 11. RANKING FROM ARAS

Criteria	Si	Ki	Rank
Ti-35A	0.0812	0.4591	7
Ti-50A	0.0988	0.5590	6
Ti-65A	0.1078	0.6099	5
Ti-75A	0.1181	0.6681	4
Ti-64	0.1450	0.8200	1
Ti-6/7	0.1406	0.7952	2
TNTZ	0.1318	0.7455	3
optimal value	0.1768		

III. RESULT AND DISCUSSION

Table 12 shows the rankings of all the alternative materials derived using the three preference ranking methods. Spearman's rank correlation coefficients between the rankings obtained using different methods. It is found that the Spearman's rank correlation coefficients between the rankings are reasonable, and the coefficient between ARAS and CODAS is higher than those of other pairs. Different coefficients have been obtained in the literature depending on the rankings obtained with the methods. The coefficient ARAS and CODAS methods was obtained as 1 in our study. Chatterjee and Chakraborty [22] obtained this value as 1.00 with a perfect correlation. The correlation coefficient value (0.96 in our study) for TOPSIS methods was obtained as 0.83. It can be concluded that the correlations acquired between these methods are generally in acceptable range. Accuracy of calculations is measured according to proposed algorithm; the higher ranking accuracy can be reached when aggregating the both particular methods in comparison with accuracy of Entropy weight.

TABLE 12 RANKINGS

Method	Material Ranks						
	Ti-35A	Ti-50A	Ti-65A	Ti-75A	Ti-64	Ti-6/7	TNTZ
CODAS	7	5	6	4	1	2	3
TOPSIS	7	6	5	3	1	2	4
ARAS	7	6	5	4	1	2	3

In this article the effectiveness of the number of criteria in the ranking performance of CODAS, TOPSIS, and ARAS methods is represented by seven Titanium material selection for dental applications areas. Consequently, the choosing of the best and worst materials depends solely upon the most relevant parameter for the highest priority weight. Dental implant designers will now be able to focus on defining the most relevant criteria dictating the whole selection process rather than designing detailed material selection decision matrices. A significant position can also be given to the methods using which parameters weights are calculated. This statistical approach significantly reduces the difficulty of the decision-making process, as the right material can now be selected on the basis of a single criteria. In all three methods the ranking of the material is found to outperform MCDM approaches.

1. A comprehensive study has been performed on the chosen seven distinct materials, using entropy approaches in conjunction with hybrid multi-criteria procedures and ranking was obtained. Ti-6Al-4V was assessed to be the optimal material for dental implants, Ti-6Al-7Nb was found to be the second most effective material.
2. Finally, the CODAS, TOPSIS, and ARAS approaches were compared using Spearman rank order correlation coefficients, and the results indicate a strong and positive correlation between these three approaches. As a result, MCDM approaches are an effective tool for resolving complex material selection challenges for dental restorations as well as other medical surgical components.

FUTURE SCOPE

It may be the scope for future scholars to explore the validation of the relevant result of this report for other decision-making issues.

REFERENCES

[1] Dammak F, Baccour L, Alimi A M, Nov. 2015, "The impact of criterion weights techniques in TOPSIS method of multi-criteria decision making in crisp and intuitionistic fuzzy domains", in IEEE Int. Conf. Fuzzy Syst., pp. 11-22.

[2] Jee D. H, Kang K J, 2000, "A method for optimal material selection aided with decision making theory", in Mater. Des., vol. 21, pp.199–206.

[3] Jovanovic S, Savic S, Jovicic N, Boskovic G, Djordjevic Z, 2016, "Using multi-criteria decision making for selection of the optimal strategy for municipal solid waste management", in Waste Manag. Res., vol. 34, pp. 884–895.

[4] Maniya K, Bhatt M G, June 2010, "A selection of material using a novel type decision-making method: Preference selection index method", in Mater. Des., vol. 34, pp. 1785–1789.

[5] Ljungberg L Y, Edwards K L, May 2000, "Design, materials selection and marketing of successful products", in Mater. Des., vol.24, pp.519–529.

[6] Ching-Lai Hwang Kwangsun Yoon, Dec.1981. "Multiple attribute decision making methods and applications a state-of-the-art survey", in Springer-Verlag

[7] Parr G R, Gardner L K, Toth, June 1985,"Titanium: The mystery metal of implant dentistry", in Dental materials aspect. J. Prosthet. Dent.,Vol. 54, pp. 410–414

[8] Stojcic M. et.al., 2019, "Application of MCDM methods in sustainability engineering: a literature review 2008", in Mater. Des., vol.11, pp.340- 350.

[9] Branemark PI, Hansson B.O, Ohman A. et.al., 1977, "Osseointegrated implants in the treatment of the edentulous jaw", in Scand. J. Plast. Reconstr. Surg., vol. 16, pp. 125–132.

[10] Smith D C, 1993, "Dental implants: Materials and design considerations" in Int. J. Prosthodont. Vol. 6, pp. 106–117.

[11] Sykaras N, Iacopino A M, Marker V A, Triplett R G, Woody R. D, 2000, "Implant materials, designs, and surface topographies: their effect on osseointegration. A literature review" in Int. J. Oral Maxillofac. Implants vol. 15, pp. 675–690.

[12] Ighravwe D E, Babatunde, D E, 2019, "Evaluation of landfill gas plant siting problem: a multi-criteria approach" in Environ. Heal. Eng. Manag., vol. 6, pp.1–10.

[13] Gonzalez J E G, Mirza-Rosca J C, 1999 " Study of the corrosion behavior of titanium and some of its alloys for biomedical and dental implant applications", in J. Electroanal Chem., pp.109–115.

[14] Rao R V, Patel B K, , 2010 "A subjective and objective integrated multiple attribute decision making method for material selection", in Mater. Des.,vol.31, pp.4738–4747.

[15] Jahan A, Ismail M Y, Sapuan S M, Mustapha F, 2010, "Material screening and choosing methods - A review", in Mater. Des., vol. 31, pp. 696–705.

[16] Osman R B, Swain M V, 2015, "A critical review of dental implant materials with an emphasis on titanium versus zirconia" in Materials (Basel), vol. 8, pp. 932–958.

[17] Dev S, Aherwar A, Patnaik A, 2019 , "Material selection for automotive piston component using entropy-VIKOR method", in Silicon, vol. 1, pp.155–169.

[18] Ecer Fatih, 2021, “A consolidated MCDM framework for performance assessment of battery electric vehicles based on ranking strategies” in Renewable and Sustainable Energy Reviews, pp.143-150.

[19] Almutairi, Khalid. et al., Jan.2021, "Ranking locations for hydrogen production using hybrid wind-solar: A Case Study", in Sustainability, vol. 8, pp.515- 524.

[20] Ersoy Y, March 2021, “Equipment selection for an e-commerce company using Entropy-based TOPSIS, EDAS and CODAS methods during the COVID-19”, in Log Forum, vol. 3, pp. 341-358.

[21] Mi Xiaomei, Huchang Liao, 2020, “Renewable energy investments by a combined compromise solution method with stochastic information”, in Journal of Cleaner Production, vol. 2, pp. 276: 283.

[22] Chatterjee, P. & Chakraborty, (2014), “'Flexible manufacturing system selection using preference ranking methods: A comparative study”. Int. J. Ind. Eng. Comput. 5, 315–338

JOURNAL OF ALGEBRAIC STATISTICS
Volume 13, No. 3, 2022, p. 2464 - 2475
https://publishoa.com
ISSN: 1309-3452

Box–Behnken Design: Optimization and Prediction of TI-6AL-7NB

M. Amareswari Reddy [1], Prof. K. Venkata Subbaiah [2], Dr. Challa. Suresh [3]

[1] *Assistant Professor, Dr. L.B.College of Engineering, Visakhapatnam, Andhra Pradesh, India.*
[2] *Senior Professor, Mechanical Engineering Department, Andhra University, Visakhapatnam, Andhra Pradesh, India.*
[3] *Associate professor, Avanthi College of Engineering and Technology, Visakhapatnam, Andhra Pradesh, India.*

Email : [1] *modem.amareswari@gmail.com,* [2] *kvsubbaiah.mech@auvsp.edu.in,* [3] *drchallasuresh@gmail.com*

ABSTRACT

Titanium's enhanced mechanical properties, corrosion resistance, and biocompatibility have expanded its usage in biomedical applications. Using the response surface approach, the present study optimizes the process parameters during the machining of titanium alloys: Ti-6Al-7Nb utilized in dental implantation by wire electrical discharge machining (WEDM) (RSM). WEDM parameters such as servo voltage, pulse-on time, pulse-off time, and wire feed rate were modified to determine their influence on the cut quality of Ti-6Al-7Nb utilizing surface roughness and material removal rate as response parameters.

I. INTRODUCTION

Titanium alloys are one of the most used materials for biocompatibility. Because of their high mechanical and corrosion resistance, titanium and titanium alloys have been used as implant materials [1]. Commercially in the early stage, pure titanium (CP-Ti) was the most commonly used in dental as biomaterial, despite its low strength, refining issues, and poor abrasion resistance. That's why long-term use of titanium in dental implants and detachable partial dentures is out of the question [4]. Ti-6Al-4V alloy, first designed as an aeronautical material, has been evaluated as a substitute for CP-Ti due to its good mechanical qualities and adequate corrosion resistance [5]; nevertheless, the cytotoxicity of elemental Vanadium remains debatable [6]. Consequently, several studies have demonstrated that the Vanadium and Aluminum ions produced by this ternary alloy might generate cytotoxic effects and neurological problems, respectively [7]. In addition, this alloy has transferred adequate strain to neighboring bones over time, resulting in bone resorption and, ultimately, implant loosening [8]. Vanadium-free β-alloys, particularly Ti-6Al-7Nb alloy [9], were also employed as implants due to their enhanced mechanical properties, corrosion resistance, and biocompatibility. It has been studied as a novel alloy for complete hip prosthesis, designed for orthopedic applications as a wrought material. Niobium was replaced with Vanadiums, as it has similarly sustained the transition in the binary system, which is essential for forming the two-phase structure. As a result, Niobium was chosen as the third component of the titanium, aluminum, and niobium alloy [10] to generate the desired microstructure. WEDM is an unconventional machining technique used to cut any conductive material. Elect thermal machining can generate intricate forms in a single setup while maintaining incredible precision and accuracy. During this process, the material will deteriorate by using successive sparks. Discharges occur between the workpiece and a moving wire electrode immersed in a fluid that acts as dielectric media.

A Computer Numerical Control is used to alter the mobility of the wire (CNC). Because it does not leave a blemish on the workpiece, wire electrical discharge machining (WEDM) is suitable for cutting both thin and thick components. Consequently, WEDM is recognized as a robust machining process and is widely utilized in numerous industries, including the tool and die, aircraft, automobile, and medical sectors [11]. Because WEDM is a complex stochastic process mechanism, even a slight variation in one of the process parameters can affect the responses, including material removal rate, kerf width, surface roughness, and other characteristics. Therefore, it is vital to pick the optimal process parameter combinations. Response Surface Methodology (RSM) [12] predominantly utilizes the statistical regression technique since it is practical, inexpensive, and relatively straightforward. It is required to construct experimental designs for many parameters to represent and evaluate each parameter's influence on the strategy function (or functions). George E. P. Box and Donald Behnken created the box-Behnken design (BBD) in 1990 [13], which requires three levels for each element, and has fewer total runs than Central Composite Design (CCD). Face-centered CCD is the most widely employed RSM in existing research [14]. The benefit of RSM is its ability to minimize prediction error and enhance estimates utilizing polynomial equations. RSM is used to build first and second-order polynomial equations. Typically, this polynomial model is referred to as a regression model. Equations 1 and 2 express the first and second-order models, respectively.

$$z = \beta_o + \sum_{u=i}^{k} \beta_u m_u + \delta \qquad 1$$

$$z = \beta_o + \sum_{u=i}^{k} \beta_u m_u + \sum_{u=1}^{k} \beta_{uu} {m_u}^2 + \sum_u \sum_v^k \beta_{uv} m_u m_v + \delta \qquad 2$$

JOURNAL OF ALGEBRAIC STATISTICS
Volume 13, No. 3, 2022, p. 2464 - 2475
https://publishoa.com
ISSN: 1309-3452

In the above equation, $\beta_u, \beta_{uu}, \beta_{uv}$ are the linear, quadratic, and interaction terms' coefficients, respectively, where z is the response function. The terms m_u and m_v are independent variables. Most research employed quadratic equations to create models [15] because a polynomial or quadratic equation of the second order is adequate for the optimal zone, and the value is near the response region. Many research works are carried out on modeling, and optimization studies in machining have applied the response surface technique and forecasted the chip-tool contact temperature using RSM. Montgome [16] improved power consumption in their study using Taguchi and central composite design (CCD). They used the first-order model to determine the significant factors and the second-order model to illustrate the effect of the interaction between variables. Various studies [17] by scholars have used RSM regression models to predict responses from non-conventional approaches like neural networks. When four components at three levels are studied, they conclude RSM is the superior method for predicting and optimizing the effect of parameters compared to the Taguchi method. The RSM presents statistically planned experiments for concluding data. In RSM, the second-order model is the most commonly employed approximation polynomial model. Common second-order model structures include the 3k factorial, Boehlert, Box-Behnken, and CCD. The survey finds that the second-order model is the most commonly used approximating polynomial model in RSM; hence, the Box-Behnken is the optimal design for data optimization in the manufacture of dental implants. Box and Behnken created and developed the Box-Behnken Design [18]. The Box-Behnken design gives three evenly spaced levels (1, 0, +1) for each variable). The required number of experiments is based on the equation $x = 2l(l_1) + p$, where l is the number of variables and p is the number of points at the center. The design is shown as a cube; all points are located on a 2-radius sphere. In addition, this design has no points at the vertices of the zone formed by the top and lower bounds of each variable [19]. With 13 experimental points, the Box-Behnken design for three variables optimizes through experimentation.
Regarding the number of necessary runs, this design is more inexpensive and efficient than 3k designs with 27 trials. Therefore, this strategy is advantageous for avoiding tests conducted under severe conditions, which may provide undesirable findings. However, it is unhelpful in cases where we want to know the extreme reactions. The Box-Behnken design has been utilized to determine the appropriate experimental settings, optimizing many processes' performance.

II. MATERIALS

The performance characteristics for Ti-6Al-7Nb were evaluated utilizing wire cut EDM with a 10mm thickness and six distinct process settings. Brass wire with a wire diameter of 0.25mm was employed as the electrode. Distilled Water was used as a coolant. Proper selection of machining variables plays a significant role in material removal and surface finish. The RSM methodology was utilized in the present work, an effective technique for designing performance parameters. RSM was used to evaluate the optimum machining settings for minimal surface roughness and maximum material removal rate using six process variables, including peak current, pulse on time, the pulse of time, peak current pulse on time, and servo voltage. The selected three levels as shown in the table 1. According to the RSM quality designing concept for the BBD method, 52 experiments are selected and presented in the table 2. The extents of these process variables were chosen based on reviewing the relevant literature, machine capabilities, and preliminary testing. Experiments utilizing the one variable at a time method. Table 1 lists the stages of several processes of the parameters and their respective labels. Using a scanning probe microscope, the surface roughness was evaluated.

Table 1 Levels of process parameters

S.No	Symbols	Input factors	Level- I	Level - II	Level -III	Units
1	A	Pulse on Time (Ton)	114	118	122	µs
2	B	Pulse on Time (Toff)	42	48	54	µs
3	C	Peak current (IP)	140	180	220	Ampere
4	D	Servo voltage(SV)	45	55	65	Volt
5	E	Wire feed rate (WF)	5	8	12	m/min
6	F	Wire Tension(WT)	550	1000	1350	gram

JOURNAL OF ALGEBRAIC STATISTICS
Volume 13, No. 3, 2022, p. 2464 - 2475
https://publishoa.com
ISSN: 1309-3452

Table 2: BBD with six parameters, as well as experimental MRR and SR

	Factor						Response	
Std	A:Ton	B:Toff	C:IP	D:SV	E:WF	F:WT	MRR	SR
	µs	µs	Ampere	Volt	m/min	gram	mm^3/min	µm
1	118	59	210	55	6	550	0.588	2.98
2	118	47	210	55	12	550	1.024	3.29
3	118	59	210	55	6	1450	0.604	2.99
4	118	59	170	55	12	1000	0.547	2.81
5	118	53	210	55	9	1000	0.707	3.15
6	114	53	170	55	9	1450	0.437	3.01
7	118	53	250	45	9	1450	0.837	3.39
8	122	47	210	65	9	1000	1.012	3.5
9	122	53	170	55	9	550	0.842	3.27
10	114	59	210	65	9	1000	0.407	2.65
11	122	53	210	65	12	1000	0.822	3.32
12	118	59	250	55	12	1000	0.804	3.07
13	118	59	170	55	6	1000	0.553	2.79
14	118	53	250	45	9	550	0.841	3.34
15	118	47	170	55	6	1000	0.971	3.25
16	114	59	210	45	9	1000	0.492	2.82
17	122	59	210	65	9	1000	0.804	3.16
18	118	53	210	55	9	1000	0.668	3.15
19	118	59	210	55	12	550	0.601	3
20	114	53	250	55	9	1450	0.552	3.01
21	122	47	210	45	9	1000	1.292	3.78
22	118	53	210	55	9	1000	0.585	3.11
23	114	53	210	45	12	1000	0.533	2.85
24	118	53	250	65	9	1450	0.79	3.18
25	118	59	250	55	6	1000	0.811	3.06
26	118	53	210	55	9	1000	0.671	3.19
27	122	59	210	45	9	1000	1.007	3.41
28	118	47	250	55	6	1000	1.032	3.38
29	118	53	210	55	9	1000	0.67	3.15
30	122	53	250	55	9	1450	1.064	3.62
31	118	47	210	55	12	1450	0.974	3.32
32	118	53	170	65	9	550	0.556	2.97
33	114	47	210	65	9	1000	0.507	3.1

JOURNAL OF ALGEBRAIC STATISTICS
Volume 13, No. 3, 2022, p. 2464 - 2475
https://publishoa.com
ISSN: 1309-3452

34	114	53	250	55	9	550	0.547	2.98
35	114	53	170	55	9	550	0.418	2.99
36	118	59	210	55	12	1450	0.598	2.98
37	114	47	210	45	9	1000	0.87	3.2
38	118	53	170	45	9	550	0.647	3.28
39	114	53	210	65	12	1000	0.441	2.78
40	122	53	210	45	6	1000	1.087	3.43
41	118	47	250	55	12	1000	1.042	3.48
42	118	47	170	55	12	1000	0.966	3.25
43	122	53	250	55	9	550	1.152	3.72
44	122	53	210	65	6	1000	0.821	3.33
45	114	53	210	65	6	1000	0.432	2.73
46	118	53	210	55	9	1000	0.709	3.18
47	118	47	210	55	6	1450	0.993	3.35
48	122	53	210	45	12	1000	1.087	3.44
49	118	47	210	55	6	550	1.026	3.31
50	118	53	170	45	9	1450	0.637	3.21
51	114	53	210	45	6	1000	0.541	2.83
52	122	53	170	55	9	1450	0.835	3.25
53	118	53	250	65	9	550	0.785	3.19
54	118	53	170	65	9	1450	0.55	2.99

III. RESULTS

The actual observations, predicted values, and various calculated parameters for adequacy, response surface equations, and correlation coefficient values are presented in the proper sequence.
The variance analysis findings for the introduced models are displayed in Table 3. The corresponding P-value for the model is statistically significant.

Table 3: The effect of Process parameters on MRR

Source	Sum of Squares	df	Mean Square	F-value	p-value	
Model	2.57	27	0.0951	30.72	< 0.0001	significant
A-Ton	0.2182	1	0.2182	70.53	< 0.0001	
B-Toff	0.3666	1	0.3666	118.50	< 0.0001	
C-IP	5.217E-06	1	5.217E-06	0.0017	0.9676	
D-SV	0.0774	1	0.0774	25.00	< 0.0001	
E-WF	0.0008	1	0.0008	0.2503	0.6210	
F-WT	0.0008	1	0.0008	0.2640	0.6117	
AB	0.0000	1	0.0000	0.0091	0.9248	
AC	0.0109	1	0.0109	3.52	0.0721	

JOURNAL OF ALGEBRAIC STATISTICS
Volume 13, No. 3, 2022, p. 2464 - 2475
https://publishoa.com
ISSN: 1309-3452

AD	0.0083	1	0.0083	2.69	0.1130	
AE	0.0000	1	0.0000	0.0000	1.0000	
AF	0.0018	1	0.0018	0.5721	0.4562	
BC	0.0179	1	0.0179	5.77	0.0237	
BD	0.0158	1	0.0158	5.09	0.0327	
BE	6.250E-06	1	6.250E-06	0.0020	0.9645	
BF	0.0012	1	0.0012	0.3723	0.5470	
CD	0.0007	1	0.0007	0.2272	0.6376	
CE	0.0000	1	0.0000	0.0079	0.9298	
CF	0.0004	1	0.0004	0.1229	0.7287	
DE	0.0000	1	0.0000	0.0131	0.9098	
DF	0.0000	1	0.0000	0.0068	0.9348	
EF	0.0002	1	0.0002	0.0524	0.8208	
A^2	0.0064	1	0.0064	2.08	0.1616	
B^2	0.1157	1	0.1157	37.40	< 0.0001	
C^2	0.0154	1	0.0154	4.97	0.0347	
D^2	2.716E-06	1	2.716E-06	0.0009	0.9766	
E^2	0.0079	1	0.0079	2.55	0.1224	
F^2	0.0000	1	0.0000	0.0040	0.9500	
Residual	0.0804	26	0.0031			
Lack of Fit	0.0703	21	0.0033	1.66	0.3019	not significant
Pure Error	0.0101	5	0.0020			
Cor Total	2.65	53				

It also displays in table 4, the R^2-statistic value and the corrected R^2-statistic value. R^2-statistic is defined as the proportion of variance.

Table 4: R^2 values on MRR

Source	Std. Dev.	R^2	Adjusted R^2	Predicted R^2	PRESS	
Linear	0.0809	0.8838	0.8689	0.8484	0.4013	
2FI	0.0885	0.9053	0.8432	0.7292	0.7166	
Quadratic	**0.0556**	**0.9696**	**0.9380**	**0.8557**	**0.3821**	**Suggested**
Cubic	0.0454	0.9938	0.9588	0.3798	1.64	Aliased

The variance analysis findings for the introduced models are displayed in Table 5. The corresponding P-value for the model is statistically significant.

Table 5: The effect of Process parameters on SR

JOURNAL OF ALGEBRAIC STATISTICS
Volume 13, No. 3, 2022, p. 2464 - 2475
https://publishoa.com
ISSN: 1309-3452

Source	Sum of Squares	df	Mean Square	F-value	p-value	
Model	3.11	27	0.1152	49.64	< 0.0001	significant
A-Ton	0.1506	1	0.1506	64.88	< 0.0001	
B-Toff	0.1832	1	0.1832	78.95	< 0.0001	
C-IP	0.0073	1	0.0073	3.15	0.0876	
D-SV	0.0482	1	0.0482	20.75	0.0001	
E-WF	0.0036	1	0.0036	1.54	0.2264	
F-WT	4.870E-07	1	4.870E-07	0.0002	0.9886	
AB	0.0018	1	0.0018	0.7756	0.3865	
AC	0.0861	1	0.0861	37.11	< 0.0001	
AD	0.0060	1	0.0060	2.59	0.1197	
AE	0.0006	1	0.0006	0.2639	0.6118	
AF	0.0036	1	0.0036	1.56	0.2233	
BC	0.0036	1	0.0036	1.56	0.2233	
BD	0.0002	1	0.0002	0.0862	0.7714	
BE	6.250E-06	1	6.250E-06	0.0027	0.9590	
BF	0.0008	1	0.0008	0.3447	0.5622	
CD	0.0036	1	0.0036	1.56	0.2233	
CE	0.0010	1	0.0010	0.4363	0.5147	
CF	0.0000	1	0.0000	0.0108	0.9181	
DE	0.0000	1	0.0000	0.0054	0.9421	
DF	0.0001	1	0.0001	0.0485	0.8275	
EF	0.0002	1	0.0002	0.0862	0.7714	
A^2	0.0056	1	0.0056	2.41	0.1324	
B^2	0.0151	1	0.0151	6.51	0.0169	
C^2	0.0035	1	0.0035	1.49	0.2332	
D^2	0.0021	1	0.0021	0.8895	0.3543	
E^2	0.0585	1	0.0585	25.21	< 0.0001	
F^2	0.0123	1	0.0123	5.30	0.0296	
Residual	0.0603	26	0.0023			
Lack of Fit	0.0564	21	0.0027	3.40	0.0893	not significant
Pure Error	0.0040	5	0.0008			
Cor Total	3.17	53				

It also displays in table 6, the R^2-statistic value and the corrected R^2-statistic value. R^2-statistic is defined as the proportion of variance.

Table 6: R^2 values on SR

JOURNAL OF ALGEBRAIC STATISTICS
Volume 13, No. 3, 2022, p. 2464 - 2475
https://publishoa.com
ISSN: 1309-3452

Source	Std. Dev.	R^2	Adjusted R^2	Predicted R^2	PRESS	
Linear	0.0766	0.9130	0.9019	0.8818	0.3747	
2FI	0.0725	0.9469	0.9121	0.8242	0.5575	
Quadratic	**0.0482**	**0.9810**	**0.9612**	**0.9053**	**0.3003**	**Suggested**
Cubic	0.0342	0.9970	0.9804	0.5612	1.39	Aliased

The fact that the Model F-value was calculated to be 30.72 indicates that the model is significant. A noise level of this magnitude would only have a 0.01 percent chance of producing an F-value of this magnitude.
P-values that are lower than 0.0500 denote the significance of the model terms. In this particular scenario, the relevant model terms are A, B, D, BC, BD, B^2, and C^2. When the model terms are insignificant, values greater than 0.1000 show this. Your model could be improved by using model reduction if it has many terms that are not significant (not counting those that are required to support hierarchy). The lack of Fit F-value is 1.66 suggests that it is not statistically significant compared to the pure error. There is a 30.19 percent probability that the F-value for lack of fit might be this high owing to noise. A lack of fit that is not large is considered good because we want the model to be accurate.
The ratio of the variability described by the model to the overall variability of the actual data serves as a measure of model fit. The closer R^2 is to 1, the better a model matches the experimental data. The calculated value of R^2 of 0.9696 for material removal rate indicates that the model explains about 96.9% of the variance. The calculated value of R^2 of 0.9612 for surface roughness indicates that the model explains about 96.1% of the variance. Hence the regression equation for MRR and SR is given in table 7.

Table 7: Equation for MRR &SR

MRR	=	SR	=
+31.84633		+3.29	
-0.314339	Ton	+0.1752	A
-0.416909	Toff	-0.2657	B
-0.046532	IP	+0.0507	C
+0.014606	SV	-0.0991	D
-0.061361	WF	+0.0285	E
+0.000803	WT	-0.0003	F
-0.000078	Ton * Toff	+0.0150	AB
+0.000230	Ton * IP	+0.1038	AC
-0.000570	Ton * SV	-0.0194	AD
+6.78141E-17	Ton * WF	-0.0102	AE
-8.26389E-06	Ton * WT	-0.0189	AF
+0.000197	Toff * IP	+0.0213	BC
+0.000740	Toff * SV	-0.0050	BD
+0.000035	Toff * WF	-0.0007	BE
+4.44444E-06	Toff * WT	-0.0089	BF
+0.000023	IP * SV	+0.0212	CD
+0.000015	IP * WF	+0.0131	CE
-2.70833E-07	IP * WT	+0.0011	CF
+0.000075	SV * WF	+0.0015	DE
+3.61111E-07	SV * WT	+0.0033	DF
-3.33333E-06	WF * WT	-0.0052	EF
+0.001562	Ton^2	+0.0233	A^2
+0.002946	$Toff^2$	+0.0383	B^2
+0.000024	IP^2	+0.0183	C^2
-5.13889E-06	SV^2	-0.0142	D^2
+0.003077	WF^2	-0.1027	E^2
-5.41838E-09	WT^2	+0.0273	F^2

The standard probability curve for the MRR and SR residuals is depicted in Figures 1 a and b respectively. The fact that

JOURNAL OF ALGEBRAIC STATISTICS
Volume 13, No. 3, 2022, p. 2464 - 2475
https://publishoa.com
ISSN: 1309-3452

the residuals are oriented around a straight line provides evidence that the model assumptions are correct and suggests that the errors follow a normal distribution.

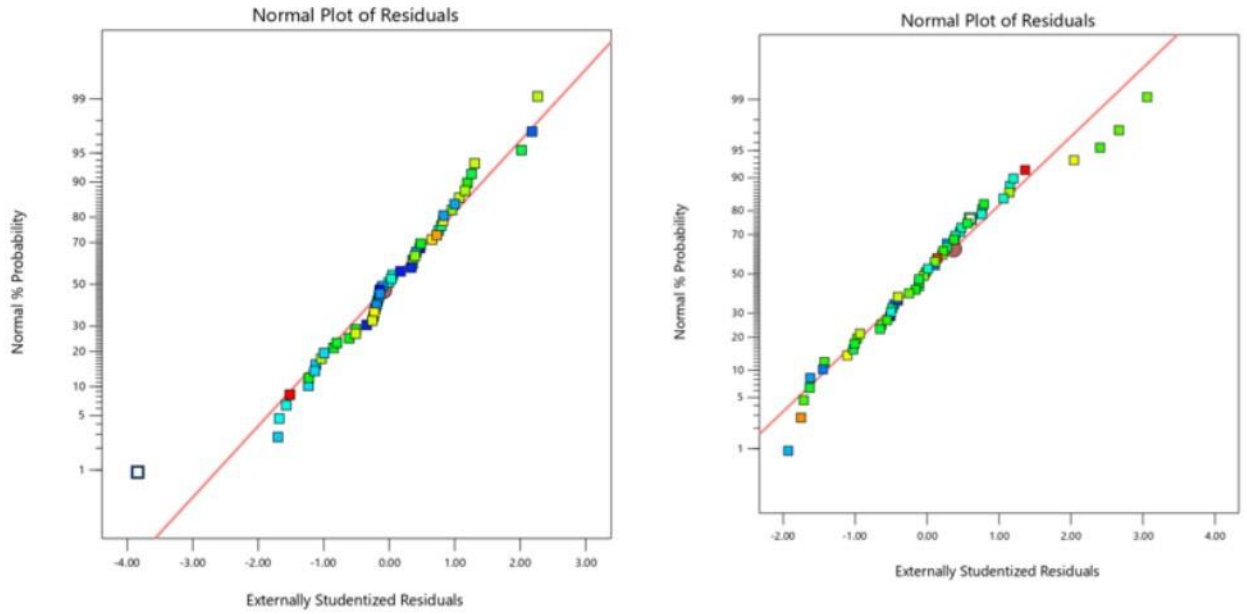


Fig 1: Normal plot of residuals for the MRR and SR

Figure 2 shows the curve that represents the MRR and SR residuals. The fact that the residuals are lower than the red straight line shows that the model assumptions are accurate and that the experimental runs are consistent with the residual.

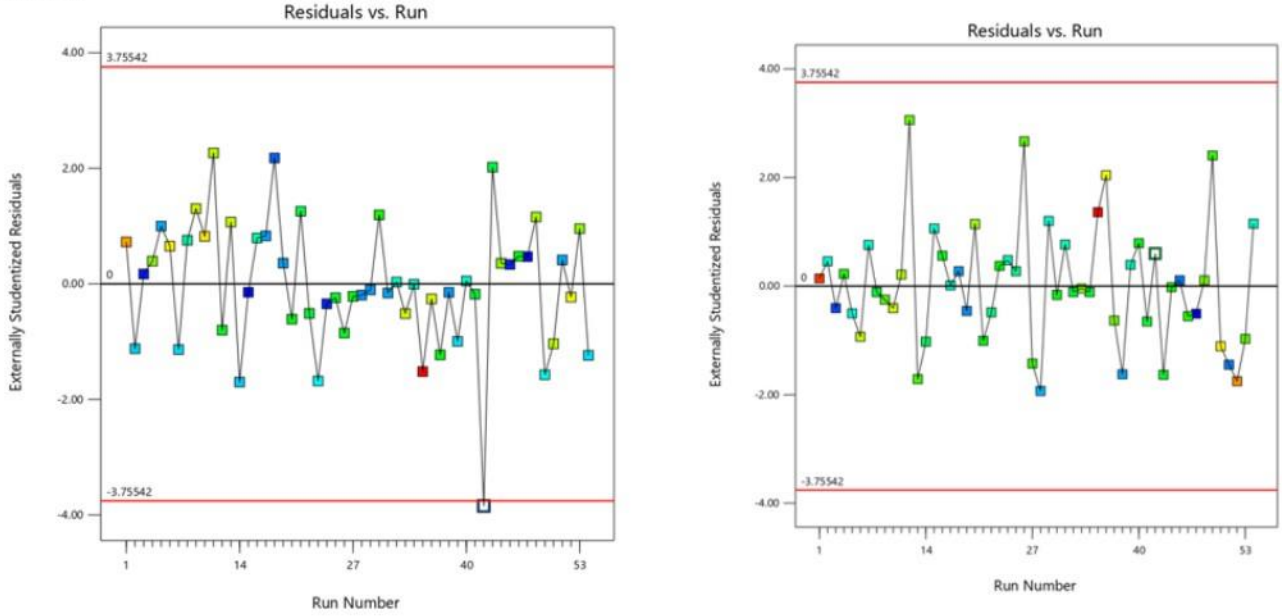


Fig 2: Residuals for the MRR and SR with Run

The response surface plot of the Ton and Toff parameter against surface roughness and material removal rate is displayed in Figure 3. The gradient for pulse-on time and pulse-off time improves from the lowest to the maximum levels when considering material removal rate and surface roughness. This suggests that an increase in either the pulse-on time or the pulse-off time will lead to a rise in both the surface roughness and the material is removal rate.

JOURNAL OF ALGEBRAIC STATISTICS
Volume 13, No. 3, 2022, p. 2464 - 2475
https://publishoa.com
ISSN: 1309-3452

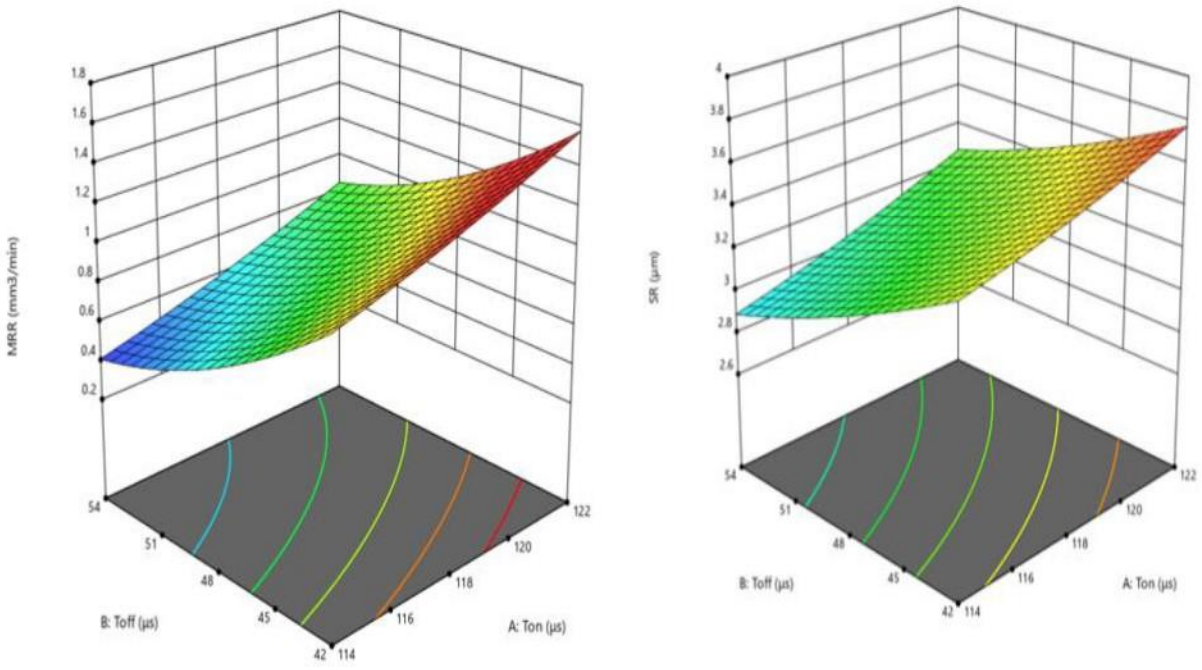


Fig 3: Response surface plot for the MRR and SR with T_{on} and T_{off}

Figure 4 compares the predicted values to the actual values obtained through experimentation. The difference between the predicted and actual values of the experiment is less than 0.1 for both MRR and SR, demonstrating that the model is dependable and can make accurate predictions.

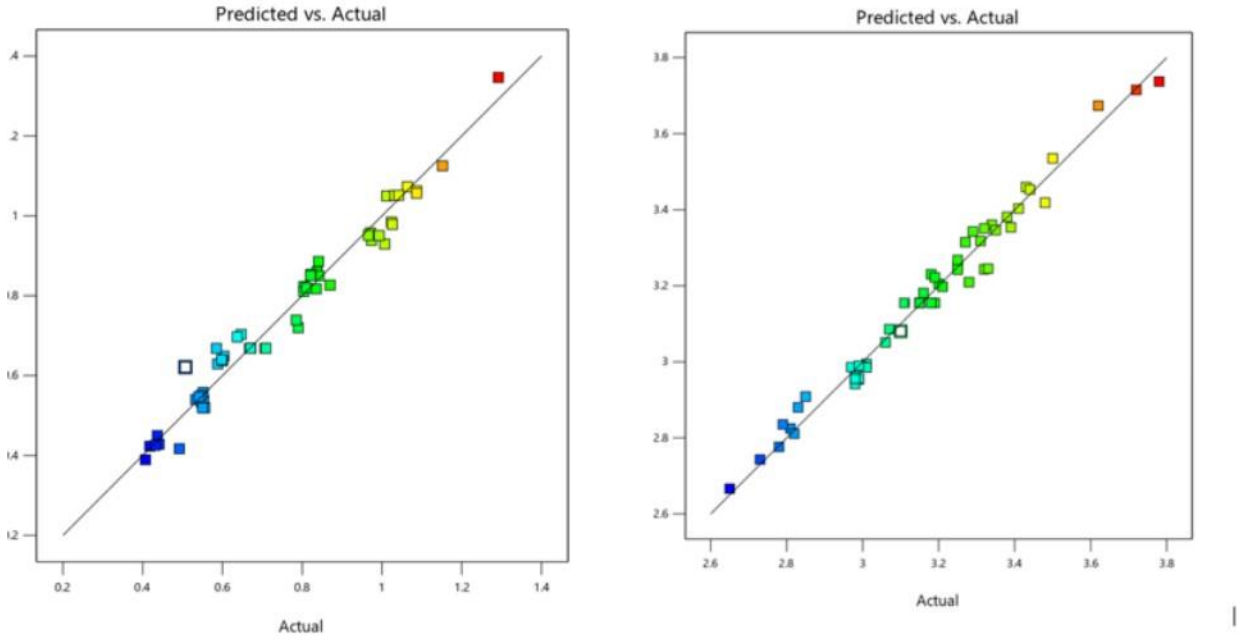


Fig: 4 Normal plot of residuals for material removal rate and Surface roughness

JOURNAL OF ALGEBRAIC STATISTICS
Volume 13, No. 3, 2022, p. 2464 - 2475
https://publishoa.com
ISSN: 1309-3452

Run Order	Material Removal Rate		Surface Roughness	
	Actual Value	Predicted Value	Actual Value	Predicted Value
1	1.15	1.13	3.72	3.72
2	0.5880	0.6290	2.98	2.97
3	0.4320	0.4256	2.73	2.74
4	0.9660	0.9512	3.25	3.24
5	0.5560	0.5192	2.97	2.99
6	1.09	1.06	3.43	3.46
7	0.5980	0.6396	2.98	2.96
8	0.7070	0.6683	3.15	3.16
9	1.03	0.9787	3.31	3.32
10	1.09	1.06	3.44	3.45
11	1.01	0.9296	3.41	3.40
12	0.8210	0.8506	3.33	3.25
13	1.02	0.9847	3.29	3.34
14	0.5850	0.6683	3.11	3.16
15	0.4180	0.4234	2.99	2.96
16	0.7090	0.6683	3.18	3.16
17	0.5500	0.5192	2.99	2.99
18	0.4920	0.4170	2.82	2.81
19	0.5470	0.5336	2.81	2.82
20	0.8370	0.8597	3.39	3.35
21	0.7850	0.7392	3.19	3.22
22	0.8040	0.8231	3.07	3.09
23	0.6370	0.6967	3.21	3.20
24	0.4370	0.4499	3.01	2.99
25	0.8110	0.8200	3.06	3.05
26	0.8220	0.8534	3.32	3.24
27	0.8420	0.8501	3.27	3.31
28	0.5330	0.5403	2.85	2.91
29	0.5470	0.5509	2.98	2.94
30	0.8700	0.8264	3.20	3.21
31	0.5520	0.5579	3.01	2.99
32	0.6700	0.6683	3.15	3.16
33	1.03	1.05	3.38	3.38
34	0.6680	0.6683	3.15	3.16
35	1.29	1.35	3.78	3.74
36	1.04	1.05	3.48	3.42
37	0.8410	0.8857	3.34	3.36
38	0.5410	0.5464	2.83	2.88
39	0.6010	0.6376	3.00	2.99
40	0.6710	0.6683	3.19	3.16
41	0.8040	0.8107	3.16	3.18
42	0.5070	0.6213	*3.10*	*3.08*
43	0.7900	0.7197	3.18	3.23
44	0.9710	0.9577	3.25	3.25
45	0.4410	0.4284	2.78	2.78
46	0.8350	0.8171	3.25	3.27
47	0.4070	0.3894	2.65	2.67
48	0.9930	0.9507	3.35	3.35
49	0.6470	0.7032	3.28	3.21
50	1.01	1.05	3.50	3.54
51	0.5530	0.5375	2.79	2.84
52	1.06	1.07	3.62	3.67
53	0.9740	0.9388	3.32	3.35
54	0.6040	0.6490	2.99	2.95

IV. CONCLUSION

Using BBD of RSM, the influence of WEDM process parameters, namely Ton, Toff, WE, WT, SV, and IP, on MRR and SR responses was empirically examined in the current study. In addition, individual reaction and multi-objective/response optimizations were performed to determine the ideal WEDM process parameter settings for each process. Analysis of variance (ANOVA) was utilized to assess the importance of process parameters. From this investigation, the following inferences may be made:

1. The MRR is significantly impacted by the dynamic interaction between the pulse off time, denoted by Toff, and the peak current, denoted by Ip. In contrast, the SR is significantly impacted by the interactions between Ton and Toff and between Ton and Ip.
2. The duration of effort that the pulse on, pulse off, and the peak current significantly impact the material removal rate (MRR) and surface roughness (SR). Pulse on time is the factor that has the most significant impact on MRR and SR.
3. The MRR and SR rise when Ton and IP are both increased, but the MRR and SR fall when Toff is decreased.
4. The three-dimensional response surface and graphical representations provided by RSM may help observe and analyze the influence that changes in process parameters have on the responses.

REFERENCES

1. P. Dayanand, R. Shrikantha, S. Raviraj. International Journal of Engineering and Management Sciences, 3(1), 1-8 (2012). 11. Landfried, R.; Kern, F.; Gadow,
2. Wasif, M.: Effects of Wire EDM Process Parameters over the Titanium Alloys (Ti6Al-4V), Materials Cloud Archive 2020.X, https://doi.org/10.24435/materialscloud:e7-rf, 2020.
3. Simon, V.: Multi-objective optimization of hypoid gears to improve operating haracteristics, Mech. Mach. Theory, 146, 103727, https://doi.org/10.1016/j.mechmachtheory.2019.103727, 2019.
4. Somashekhar, K. P., Mathew, J., and Ramachandran, N.: A feasibility approach by simulated annealing on optimization of micro-wire electric discharge machining parameters, Int. J. Adv. Manuf. Tech., 61, 1209–1213, 2012.
5. Takayama, Y., Makino, Y., Niu., Y., and Uchida, H.: The Latest Technology of Wire-cut EDM, Proc. CIRP, 42, 623–626, https://doi.org/10.1016/j.procir.2016.02.259, 2016
6. Electrically conductive ZTA–TiC ceramics: influence of TiC particle size on material properties and electrical dischargemachining. Int. J. Refract.Met.HardMater.49, 334–338 (2015)
7. Maher, I.; Ling, L.H.; Sarhan, A.A.; Hamdi, M.: Improve wire EDM performance at differentmachining parameters-ANFIS modeling.IFAC Papers OnLine 48(1), 105–110 (2015)
8. Raksiri, C. and Chatchaikulsiri, P.: CNC Wire-Cut Parameter Optimized Determination of the Stair Shape Workpiece, International Journal of Mechanical and Mechatronics Engineering , 4, 924–929, 2010.
9. Reddy, V. C., Deepthi, N., and Jayakrishna, N.: Multiple Response Optimization of Wire EDM on Aluminium HE30 by using Grey Relational Analysis, Mater. Today-Proc., 2, 2548–2554, https://doi.org/10.1016/j.matpr.2015.07.201, 2015.
10. Saini, P. K. and Verma, M.: Experimental Investigation of Wire-EDM Process Parameters on MRR of Ti-6al-4v Alloy, International Journal of Innovative Technology and Exploring Engineering (IJITEE), 4, 16–20, 2014.
11. Sandeep, K.: Research Trends in Electrical Discharge Machining: A Review, Res. J. Eng. Sci., 2, 56–60, 2013.
12. Anderson, Mark J. and Whitcomb, Patrick J. 2004. Design solutions from concept through manufacture: Response surface methods for process optimization. Desktop Engineering. http://www.deskeng.com/ (accessed May 16, 2006).
13. Bobbili, R.; Madhu, V.; Gogia, A.K.: Modelling and analysis of material removal rate and surface roughness in wire-cut EDM of armour materials. Eng. Sci. Technol. Int. J. 18(4), 664–668 (2015)
14. Nayak, B.B.; Mahapatra, S.S.: Optimization of WEDM processn parameters using deep cryo-treated Inconel

718 as work material.Eng. Sci. Technol. Int. J. 19(1), 161–170 (2016)

15. Minto, Charles. Response Surface Modeling of Drug Interactions.2006 http://eurosiva.org/Archive/Vienna/abstracts (accessed May 16, 2006).
16. Montgomery, Douglas C. Design and Analysis of Experiments: Response surface method and designs. New Jersey: John Wiley and Sons, Inc. 2005.
17. Oehlert, Gary W. . Design and analysis of experiments: Response surface design. New York: W.H. Freeman and Company 2000
18. Singh, V. K., & Singh, S. Multi-objective optimization using taguchi based grey relational analysis for wire edm of inconel 625. J. Mater. Sci. Mech. Eng,2 (2015).(11), 38{42.
19. Tonday, H., & Tigga, A. Analysis of effects of cutting parameters of wire electrical discharge machining on material removal rate and surface integrity. In Iop conference series: Materials science and engineering (2016).(Vol. 115, p. 012013).
20. Sanghani, C., & Acharya, G. (2016). A review of research on improvement and optimization of performance measures for electrical discharge machining.

The Journal of Analysis
https://doi.org/10.1007/s41478-022-00438-6

ORIGINAL RESEARCH PAPER

Existence, uniqueness and stability analysis of a tempered fractional order thermistor boundary value problems

Mahammad Khuddush[1] · K. Rajendra Prasad[2]

Received: 28 November 2021 / Accepted: 4 May 2022
© The Author(s), under exclusive licence to The Forum D'Analystes 2022

Abstract
In this paper, we derive the sufficient conditions for the existence, uniqueness and Hyers–Ulam stability of the tempered fractional order thermistor two-point boundary value problem. Further, we also establish uniqueness of the solution to the addressed problem by using Rus's theorem in a complete metric space.

Keywords Thermistor problem · Tempered Caputo fractional derivative · Boundary value problem · Hyers–Ulam stability · Complete metric space · Rus's theorem

Mathematics Subject Classification 35B15 · 26A33 · 47H08 · 47H10

1 Introduction

The theory of fractional differential equations has gained remarkable popularity and significance during last few years and has become an important field of investigation due to its attractive applications in various branches of chemistry, physics, polymer rheology, aerodynamics, electrodynamics of complex medium, etc. Fractional order differential equations also serve as an excellent tool for the hereditary properties and description of memory in various materials. Fractional differential equations have been used for mathematical modeling in potential fields, signal processing, viscoelastic materials, diffusion problems, heat propagation, control theory and

Communicated by Samy Ponnusamy.

✉ Mahammad Khuddush
khuddush89@gmail.com

[1] Department of Mathematics, Dr. Lankapalli Bullayya College of Engineering , Visakhapatnam, Andhra Pradesh 530013, India

[2] Department of Applied Mathematics, College of Science and Technology, Andhra University, Visakhapatnam 530003, India

Published online: 03 June 2022

many others. In recent years, there are certain papers and monographs dealing with the existence and uniqueness solutions of fractional order nonlinear boundary value problems, see [1–4, 6, 11, 15, 16, 20–22, 29, 30, 35–37] and references therein.

Thermistor is a thermo-electric device constructed from a ceramic material whose electrical conductivity depends strongly on the temperature [31]. They can be used as a switching device in many electronic circuits. An application of thermistor problems in heating processes and current flow can be found in various fields of electronics and its related industries [33]. In General, there are two types of thermistors, the first have an electrical conductivity that increases with the increasing of temperature and the second have an electrical conductivity that decreases with the increasing of temperature [13, 17]. In [32], Sidi et al., studied the global existence of solutions to the following fractional Caputo nonlocal thermistor initial value problem

$$ {}_{0}^{\mathrm{C}}\mathrm{D}_{\mathrm{s}}^{2\ell}\mathrm{z}(\mathrm{s}) = \frac{\mu\, \mathrm{g}(\mathrm{z}(\mathrm{s}))}{\left[\int_0^T \mathrm{g}(\mathrm{z}(\tau))\mathrm{d}\tau\right]^2},\ 0<\ell<\frac{1}{2},\ 0<\mathrm{s}<\infty, \tag{1} $$

$$ \mathrm{z}(0) = \mathrm{z}_0. \tag{2} $$

Recently, Sajediy and Eghbali [28] studied the Hyers–Ulam, Hyers–Ulam–Rassias, Mittag–Leffler–Hyers–Ulam and Mittag–Leffler–Hyers–Ulam–Rassias stability of (1)–(2).

On the otherhand, the tempered fractional derivative is one of the generalized forms of the fractional derivatives. Multiplying classical fractional derivative by an exponential factor leads to the tempered fractional derivative. This new fractional operator depends on a parameter λ, and the classical Riemann–Liouville and Caputo fractional derivatives are obtained in special cases for $\lambda = 0$. Now a days, the tempered fractional derivative has become a popular topic for investigation due to its application in physics, groundwater hydrology, poroelasticity, geophysical flow, finance [7–9, 18, 24]. In [41], Zaky studied the well-posedness of the solution to the following two-point nonlinear tempered fractional boundary value problem

$$ {}_{0}^{\mathrm{C}}\mathrm{D}_{\mathrm{z}}^{\alpha,\ell}\vartheta(\mathrm{z}) = \mathrm{g}(\mathrm{z},\vartheta(\mathrm{z}))\ \mathrm{z}\in[0,\mathrm{T}],\alpha\in(0,1), $$

$$ a\vartheta(0) + be^{\ell \mathrm{T}}\vartheta(\mathrm{T}) = c, $$

and also derived and analyzed a Jacobi spectral-collocation method for the numerical solution. In [38], Yadav et. al discussed the numerical approximation to solve regular tempered fractional Sturm–Liouville problem

$$ {}_{\mathrm{z}}^{\mathrm{C}}\mathrm{D}_{b}^{\alpha,\ell}\left[\mathrm{p}(\mathrm{z}){}_{a}^{\mathrm{C}}\mathrm{D}_{\mathrm{z}}^{\alpha,\ell}\vartheta(\mathrm{z})\right] = \lambda\,\phi(\mathrm{z})\vartheta(\mathrm{z}))\ \mathrm{z}\in[a,b],\alpha\in(0,1), $$

$$ \vartheta(a) = 0,\ \left[\mathrm{p}(\mathrm{z}){}_{a}^{\mathrm{C}}\mathbb{D}_{\mathrm{z}}^{\alpha,\ell}\vartheta(\mathrm{z})\right]\Big|_{\mathrm{z}=b} = 0, $$

by using finite difference method. Recntly, Pandey et al. [19] studied the properties of eigenvalue for the regular temepered fractional Sturm–Liouville problem

$$
\begin{aligned}
&{}_{z}^{C}D_{b}^{\alpha,\ell}\left[p(z){}_{a}^{C}D_{z}^{\alpha,\ell}\vartheta(z)\right]+\phi(z)\vartheta(z)=\lambda\psi_{\lambda}(z)\vartheta(z)\ z\in[a,b],\alpha\in(0,1),\\
&\vartheta(a)=0,\ \vartheta(b)=0,
\end{aligned}
$$

by using fractional variational appraoch. Recently, Khuddush et al. [10] studied the following tempered Riemann–Liouville fractional order boundary value problem

$$
\begin{aligned}
{}_{0}^{RL}D_{s}^{\delta_2,\lambda}\left[p_j(s){}_{0}^{RL}D_{s}^{\delta_1,\lambda}z_j(s)\right]&=\mu_j\varphi\big(s,z(s)\big),\ s\in[0,T],\delta_1,\delta_2\in(1,2),\\
z_j(0)&=\lim_{s\to 0}\left[{}_{0}^{RL}D_{s}^{\delta_1,\lambda}(e^{\lambda s}z_j(s))\right]=0,\\
e^{\lambda T}z_j(T)&=\lim_{s\to T}\left[{}_{0}^{RL}D_{s}^{\delta_1,\lambda}(e^{\lambda s}z_j(s))\right]=0,
\end{aligned}
$$

where $j\in\{1,2,3,\cdots\}$, $\lambda\geq 0$, and derived sufficient conditions for the existence of solutions to the system via the Hausdorff measure of noncompactness and Meir–Keeler fixed point theorem in a tempered sequence spaces.

Motivated by above mentioned works, in this paper we study the thermistor problem with two-point boundary conditions and tempered Caputo type fractional derivative

$$
{}_{0}^{C}D_{s}^{2\ell,\lambda}z(s)=\frac{\mu g(z(s))}{\left[\int_0^T g(z(\tau))d\tau\right]^2},\ 0<\ell<\frac{1}{2},\ 0<s<T, \tag{3}
$$

$$
az(0)+be^{\lambda T}z(T)=c, \tag{4}
$$

where $\lambda\geq 0$, $\mu>0$, ${}^{C}D_{0^+}^{2\ell}$ denotes the tempered Caputo fractional derivative of order 2ℓ and derive sufficient conditions for existence, uniqueness and Hyers–Ulam stability of solutions. Further, we also study uniqueness of solution by using Rus's theorem in a complete metric space.

The rest of the paper is organized in the following fashion. In Sect. 2, we convert the boundary value problem (3)–(4) into equivalent integral equation. In Sect. 3, we develop a criteria for the existence and uniqueness of solutions to the problem (3)–(4). In Sect. 4, we also study uniqueness of solution by Rus's theorem on complete metric space. Finally, we analyse Hyers–Ulam stability of the addressed problem.

2 Preliminaries

In this section, we first give the definitions and some properties of the tempered fractional calculus. Denote $L([a,\ b])$ as the integrable space which includes the Lebesgue measurable functions on the finite interval $[a,\ b]$. Let $AC[a,\ b]$ be the space of real values functions $z(s)$ which are absolutely continuous on $[a,\ b]$. For $n\in\mathbb{N}^{+}$, we denote $AC^{n}[a,b]$ as the space of real values functions $z(\tau)$ which have continuous derivatives up to order $n-1$ on $[a,\ b]$ such that $\frac{d^{n-1}z(s)}{ds^{n-1}}\in AC[a,b]$.

Definition 1 [14, 27] Suppose that the real function $\mathtt{z}(\mathtt{s})$ is piecewise continuous on (a,b) and $\mathtt{z}(\mathtt{s}) \in L([a,b])$, $\theta > 0$, $\lambda \geq 0$. The Riemann–Liouville tempered fractional integral of order θ is defined as

$$ {}_a\mathbb{I}_{\mathtt{s}}^{\theta,\lambda}\mathtt{z}(\mathtt{s}) = e^{-\lambda \mathtt{s}}\, {}_a\mathtt{I}_{\mathtt{s}}^{\theta}\big(e^{\lambda \mathtt{s}}\mathtt{z}(\mathtt{s})\big) = \frac{1}{\Gamma(\theta)}\int_a^{\mathtt{s}} e^{-\lambda(\mathtt{s}-\mathtt{t})}(\mathtt{s}-\mathtt{t})^{\theta-1}\mathtt{z}(\mathtt{t})\mathtt{dt}, $$

where ${}_a\mathtt{I}_{\mathtt{s}}^{\theta}$ denotes the Riemann–Liouville fractional integral [12]

$$ {}_a\mathtt{I}_{\mathtt{t}}^{\theta}\mathtt{z}(\mathtt{s}) = \frac{1}{\Gamma(\theta)}\int_a^{\mathtt{s}} (\mathtt{s}-\mathtt{t})^{\theta-1}\mathtt{z}(\mathtt{s})\mathtt{ds}. $$

Definition 2 [14, 27] For $n-1<\theta<n$, $n \in \mathbb{N}^+$, $\lambda \geq 0$. The Caputo tempered fractional derivative of order θ is defined as

$$ {}_a^{\mathtt{C}}\mathtt{D}_{\mathtt{s}}^{\theta,\lambda}\mathtt{z}(\mathtt{s}) = e^{-\lambda \mathtt{s}}\, {}_a^{\mathtt{C}}\mathtt{D}_{\mathtt{s}}^{\theta}\big(e^{\lambda \mathtt{s}}\mathtt{z}(\mathtt{s})\big) = \frac{e^{-\lambda \mathtt{s}}}{\Gamma(n-\theta)}\int_a^{\mathtt{s}} \frac{1}{(\mathtt{s}-\mathtt{t})^{\theta-n+1}}\frac{\mathtt{d}^n}{\mathtt{dt}^n}\big(e^{\lambda \mathtt{t}}\mathtt{z}(\mathtt{t})\big)\mathtt{dt}, $$

where ${}_a^{\mathtt{C}}\mathtt{D}_{\mathtt{s}}^{\theta}$ denotes the Caputo fractional derivative [12]

$$ {}_a^{\mathtt{C}}\mathtt{D}_{\mathtt{s}}^{\theta}\mathtt{z}(\mathtt{s}) = \frac{1}{\Gamma(n-\theta)}\int_a^{\mathtt{s}} \frac{1}{(\mathtt{s}-\mathtt{t})^{\theta-n+1}}\frac{\mathtt{d}^n}{\mathtt{dt}^n}\big(\mathtt{z}(\mathtt{t})\big)\mathtt{dt}. $$

Lemma 1 (*Composite property* [14]) *Let* $\mathtt{z}(\mathtt{s}) \in AC^n[a,b]$ *and* $n-1<\theta<n$. *Then the Caputo tempered fractional derivative and the Riemann–Liouville tempered fractional integral have the composite property*:

$$ {}_a\mathtt{I}_{\mathtt{s}}^{\theta,\lambda}\big[{}_a^{\mathtt{C}}\mathtt{D}_{\mathtt{s}}^{\alpha,\lambda}\mathtt{z}(\mathtt{s})\big] = \mathtt{z}(\mathtt{s}) - \sum_{k=0}^{n-1} e^{\lambda \mathtt{s}}\frac{(\mathtt{s}-a)^k}{k!}\left[\frac{\mathtt{d}^k}{\mathtt{ds}^k}\big(e^{\lambda \mathtt{s}}\mathtt{z}(\mathtt{s})\big)\right]\Big|_{\mathtt{s}=a} \tag{5} $$

and

$$ {}_a^{\mathtt{C}}\mathtt{D}_{\mathtt{s}}^{\alpha,\lambda}\big[{}_a\mathtt{I}_{\mathtt{s}}^{\theta,\lambda}\mathtt{z}(\mathtt{s})\big] = \mathtt{z}(\mathtt{s}). \tag{6} $$

Lemma 2 *The boundary value problem* (3)–(4) *is equivalent to the integral equation*

$$\left.\begin{aligned} \mathtt{z}(\mathtt{s}) = \frac{c}{a+b}e^{-\lambda \mathtt{s}} &- \frac{b\mu}{a+b}\int_0^T \frac{e^{-\lambda(\mathtt{s}-\mathtt{t})}(\mathtt{T}-\mathtt{t})^{2\ell-1}}{\Gamma(2\ell)} \frac{\mathtt{g}(\mathtt{z}(\mathtt{t}))}{\left[\int_0^T \mathtt{g}(\mathtt{z}(\tau))\mathtt{d}\tau\right]^2}\mathtt{dt} \\ &+ \mu\int_0^{\mathtt{s}} \frac{e^{-\lambda(\mathtt{s}-\mathtt{t})}(\mathtt{s}-\mathtt{t})^{2\ell-1}}{\Gamma(2\ell)} \frac{\mathtt{g}(\mathtt{z}(\mathtt{t}))}{\left[\int_0^T \mathtt{g}(\mathtt{z}(\tau))\mathtt{d}\tau\right]^2}\mathtt{dt}. \end{aligned}\right\} \tag{7}$$

Proof Let $\mathtt{z}(\mathtt{s})$ be a solution of (3)–(4) and applying the operator $\mathtt{I}_{0^+}^{2\ell,\lambda}$ to both sides of (3) and using (5), we get

$$\mathtt{z}(\mathtt{s}) = e^{-\lambda \mathtt{s}}\mathtt{z}(0) + \frac{\mu}{\Gamma(2\ell)}\int_0^{\mathtt{s}} e^{-\lambda(\mathtt{s}-\mathtt{t})}(\mathtt{s}-\mathtt{t})^{2\ell-1} \frac{\mathtt{g}(\mathtt{z}(\mathtt{t}))}{\left[\int_0^T \mathtt{g}(\mathtt{z}(\tau))\mathtt{d}\tau\right]^2}\mathtt{dt}. \tag{8}$$

Taking $\mathtt{s} = \mathtt{T}$ in (8) results

$$\mathtt{z}(\mathtt{T}) = e^{-\lambda \mathtt{T}}\mathtt{z}(0) + \frac{\mu}{\Gamma(2\ell)}\int_0^T e^{-\lambda(\mathtt{T}-\mathtt{t})}(\mathtt{T}-\mathtt{t})^{2\ell-1} \frac{\mathtt{g}(\mathtt{z}(\mathtt{t}))}{\left[\int_0^T \mathtt{g}(\mathtt{z}(\tau))\mathtt{d}\tau\right]^2}\mathtt{dt}.$$

Plugging it into the boundary condition (4) results

$$\mathtt{z}(0) = \frac{c}{a+b} - \frac{b\mu}{a+b}\int_0^T \frac{e^{\lambda \mathtt{t}}(\mathtt{T}-\mathtt{t})^{2\ell-1}}{\Gamma(2\ell)} \frac{\mathtt{g}(\mathtt{z}(\mathtt{t}))}{\left[\int_0^T \mathtt{g}(\mathtt{z}(\tau))\mathtt{d}\tau\right]^2}\mathtt{dt}.$$

Substituting it into (8), we get (7).

Conversely, suppose $\mathtt{z}(\mathtt{s})$ is a solution of the integral equation (7). Then equation (7) can be rewritten as

$$\begin{aligned} \mathtt{z}(\mathtt{s}) = e^{-\lambda \mathtt{s}} &\left\{ \frac{c}{a+b} - \frac{b\mu}{a+b}\int_0^T \frac{e^{\lambda \mathtt{t}}(\mathtt{T}-\mathtt{t})^{2\ell-1}}{\Gamma(2\ell)} \frac{\mathtt{g}(\mathtt{z}(\mathtt{t}))}{\left[\int_0^T \mathtt{g}(\mathtt{z}(\tau))\mathtt{d}\tau\right]^2}\mathtt{dt} \right\} \\ &+ \mathtt{I}_{0^+}^{2\ell,\lambda}\left\{ \frac{\mu \mathtt{g}(\mathtt{z}(\mathtt{t}))}{\left[\int_0^T \mathtt{g}(\mathtt{z}(\tau))\mathtt{d}\tau\right]^2} \right\}. \end{aligned} \tag{9}$$

Applying the operator ${}^{\mathtt{C}}\mathtt{D}_{0^+}^{2\ell,\lambda}$ to both sides of (9) and using (6), we get (3). Next taking $\mathtt{s} = 0$ and $\mathtt{T}$ in (9), implies

$$\mathtt{z}(0)=\frac{c}{a+b}-\frac{b\mu}{a+b}\int_0^T\frac{e^{\lambda \mathtt{t}}(\mathtt{T}-\mathtt{t})^{2\ell-1}}{\Gamma(2\ell)}\frac{\mathtt{g}(\mathtt{z}(\mathtt{t}))}{\left[\int_0^T \mathtt{g}(\mathtt{z}(\tau))\mathtt{d}\tau\right]^2}\mathtt{dt}$$

and

$$\mathtt{z}(\mathtt{T})=\frac{c}{a+b}e^{-\lambda \mathtt{T}}+\frac{a\mu}{a+b}e^{-\lambda \mathtt{T}}\int_0^T\frac{e^{\lambda \mathtt{t}}(\mathtt{T}-\mathtt{t})^{2\ell-1}}{\Gamma(2\ell)}\frac{\mathtt{g}(\mathtt{z}(\mathtt{t}))}{\left[\int_0^T \mathtt{g}(\mathtt{z}(\tau))\mathtt{d}\tau\right]^2}\mathtt{dt},$$

from which we obtain (4). □

3 Main results

In this section, we derive sufficient conditions for the existence and uniqueness of solutions to the thermistor BVP (3)–(4).

Theorem 1 *For some $r_0>0$, let $\mathbb{E}=\left[\frac{c}{a+b}e^{-\lambda \mathtt{T}}-r_0,\frac{c}{a+b}e^{-\lambda \mathtt{T}}+r_0\right]$ and*

- $(\mathtt{G}_1)$ the function $\mathtt{g}:\mathbb{E}\to\mathbb{R}$ is continuous for all $\mathtt{s}\in[0,\mathtt{T}]$.
- $(\mathtt{G}_2)$ the function $\mathtt{g}:\mathbb{E}\to\mathbb{R}$ is a Lipschitz continuous function with Lipschitz constant $\mathtt{L}$ such that $c_1\le \mathtt{g}(\mathtt{z})\le c_2$, where c_1 and c_2 are two positive constants with $\frac{\mu}{\lambda^{2\ell}}\left[\frac{\mathtt{L}}{c_1^2\mathtt{T}^2}+\frac{2c_2^2\mathtt{L}}{c_1^4\mathtt{T}}\right]\left[\frac{be^{\lambda \mathtt{T}}}{a+b}+1\right]<1$.

Then the thermistor BVP (3)–(4) has a unique solution in $\mathrm{C}[0,\mathtt{T}]$.

Proof Let us define $\mathbb{B}_{r_0}=\left\{\mathtt{z}\in \mathrm{C}[0,\mathtt{T}]:\|\mathtt{z}-\frac{\mathtt{c}}{\mathtt{a}+\mathtt{b}}\mathtt{e}^{-\lambda \mathtt{s}}\|\le \mathtt{r}_0\right\}$. Then $\mathbb{B}_{r_0}$ is a closed subset of the Banach space of all continuous functions on $[0,\mathtt{T}]$ equipped with the Chebyshev norm. It is clear that $\mathbb{B}_{r_0}\neq\emptyset$, since $\frac{c}{a+b}e^{-\lambda \mathtt{s}}\in\mathbb{B}_{r_0}$.

Let the operator $\aleph:\mathbb{B}_{r_0}\to \mathrm{C}[0,\mathtt{T}]$ defined as follows

$$\left.\begin{aligned}(\aleph\mathtt{z})(\mathtt{s})=\frac{c}{a+b}e^{-\lambda \mathtt{s}}&-\frac{b\mu}{a+b}\int_0^T\frac{e^{-\lambda(\mathtt{s}-\mathtt{t})}(\mathtt{T}-\mathtt{t})^{2\ell-1}}{\Gamma(2\ell)}\frac{\mathtt{g}(\mathtt{z}(\mathtt{t}))}{\left[\int_0^T \mathtt{g}(\mathtt{z}(\tau))\mathtt{d}\tau\right]^2}\mathtt{dt}\\&+\mu\int_0^{\mathtt{s}}\frac{e^{-\lambda(\mathtt{s}-\mathtt{t})}(\mathtt{s}-\mathtt{t})^{2\ell-1}}{\Gamma(2\ell)}\frac{\mathtt{g}(\mathtt{z}(\mathtt{t}))}{\left[\int_0^T \mathtt{g}(\mathtt{z}(\tau))\mathtt{d}\tau\right]^2}\mathtt{dt}.\end{aligned}\right\}\tag{10}$$

Firstly, we show that the operator $\aleph$ is self-mapping on $\mathtt{B}_{r_0}$. Let $\mathtt{z}\in\mathtt{B}_{r_0}$ and $\mathtt{s}\in[0,\mathtt{T}]$, we have

$$\left|\aleph z(s)-\frac{c}{a+b}e^{-\lambda s}\right|\le\left|\frac{b\mu}{a+b}\int_0^T\frac{e^{-\lambda(s-t)}(T-t)^{2\ell-1}}{\Gamma(2\ell)}\frac{g(z(t))}{\left[\int_0^T g(z(\tau))d\tau\right]^2}dt\right|$$
$$+\mu\left|\int_0^s\frac{e^{-\lambda(s-t)}(s-t)^{2\ell-1}}{\Gamma(2\ell)}\frac{g(z(t))}{\left[\int_0^T g(z(\tau))d\tau\right]^2}dt\right| \tag{11}$$
$$\le\left[\frac{b}{a+b}+1\right]\frac{\mu c_2T^{2\ell-2}e^{\lambda T}}{c_1^2\Gamma(2\ell+1)}:=r_0.$$

Therefore, $\aleph z\in\mathbb{B}_{r_0}$. Next, let $z_1,z_2\in B_{r_0}$ and $s\in[0,T]$, we have

$$\begin{aligned}
&|(\aleph z_1)(s)-(\aleph z_2)(s)|\\
&=\left|\frac{b\mu}{a+b}\int_0^T\frac{e^{-\lambda(s-t)}(T-t)^{2\ell-1}}{\Gamma(2\ell)}\left\{\frac{g(z_1(t))}{\left[\int_0^T g(z_1(\tau))d\tau\right]^2}-\frac{g(z_2(t))}{\left[\int_0^T g(z_2(\tau))d\tau\right]^2}\right\}dt\right|\\
&\quad+\mu\left|\int_0^s\frac{e^{-\lambda(s-t)}(s-t)^{2\ell-1}}{\Gamma(2\ell)}\left\{\frac{g(z_1(t))}{\left[\int_0^T g(z_1(\tau))d\tau\right]^2}-\frac{g(z_2(t))}{\left[\int_0^T g(z_2(\tau))d\tau\right]^2}\right\}dt\right|\\
&=\left|\frac{b\mu}{a+b}\int_0^T\frac{e^{-\lambda(s-t)}(T-t)^{2\ell-1}}{\Gamma(2\ell)}\left\{\frac{1}{\left[\int_0^T g(z_1(\tau))d\tau\right]^2}(g(z_1(t))-g(z_2(t)))\right.\right.\\
&\quad\left.\left.+g(z_2)\left\{\frac{1}{\left[\int_0^T g(z_1(\tau))d\tau\right]^2}-\frac{1}{\left[\int_0^T g(z_2(\tau))d\tau\right]^2}\right\}\right\}dt\right|\\
&\quad+\mu\left|\int_0^s\frac{e^{-\lambda(s-t)}(s-t)^{2\ell-1}}{\Gamma(2\ell)}\left\{\frac{1}{\left[\int_0^T g(z_1(\tau))d\tau\right]^2}(g(z_1(t))-g(z_2(t)))\right\}\right.\\
&\quad\left.+g(z_2)\left\{\frac{1}{\left[\int_0^T g(z_1(\tau))d\tau\right]^2}-\frac{1}{\left[\int_0^T g(z_2(\tau))d\tau\right]^2}\right\}\right\}dt\Bigg|\\
&\le\frac{b\mu}{a+b}\int_0^T\frac{e^{-\lambda(s-t)}(T-t)^{2\ell-1}}{\Gamma(2\ell)}|I_1(t)|dt+\mu\int_0^s\frac{e^{-\lambda(s-t)}(s-t)^{2\ell-1}}{\Gamma(2\ell)}|I_1(t)|dt,
\end{aligned}$$

where

$$
\begin{aligned}
|\mathtt{I}_1(\mathtt{t})| &= \Bigg| \frac{1}{\left[\int_0^T \mathtt{g}(\mathtt{z}_1(\tau))\mathtt{d}\tau\right]^2}(\mathtt{g}(\mathtt{z}_1(\mathtt{t})) - \mathtt{g}(\mathtt{z}_2(\mathtt{t}))) + \mathtt{g}(\mathtt{z}_2) \\
&\qquad \left\{ \frac{1}{\left[\int_0^T \mathtt{g}(\mathtt{z}_1(\tau))\mathtt{d}\tau\right]^2} - \frac{1}{\left[\int_0^T \mathtt{g}(\mathtt{z}_2(\tau))\mathtt{d}\tau\right]^2} \right\} \Bigg| \\
&\leq \frac{1}{\left[\int_0^T \mathtt{g}(\mathtt{z}_1(\tau))\mathtt{d}\tau\right]^2} |\mathtt{g}(\mathtt{z}_1(\mathtt{t})) - \mathtt{g}(\mathtt{z}_2(\mathtt{t}))| \\
&\qquad + \frac{|\mathtt{g}(\mathtt{z}_2(\tau))|}{\left[\int_0^T \mathtt{g}(\mathtt{z}_1(\tau))\mathtt{d}\tau\right]^2 \left[\int_0^T \mathtt{g}(\mathtt{z}_2(\tau))\mathtt{d}\tau\right]^2} \\
&\qquad \times \int_0^T |\mathtt{g}(\mathtt{z}_1(\tau)) - \mathtt{g}(\mathtt{z}_2(\tau))|\mathtt{d}\tau \int_0^T |\mathtt{g}(\mathtt{z}_1(\tau)) + \mathtt{g}(\mathtt{z}_2(\tau))|\mathtt{d}\tau \\
&\leq \frac{\mathtt{L}}{c_1^2\mathtt{T}^2} |\mathtt{z}_1(\mathtt{t}) - \mathtt{z}_2(\mathtt{t})| + \frac{2c_2^2\mathtt{T}^2\mathtt{L}}{c_1^4\mathtt{T}^4} \int_0^T |\mathtt{z}_1(\tau) - \mathtt{z}_2(\tau)|\mathtt{d}\tau \\
&\leq \frac{\mathtt{L}}{c_1^2\mathtt{T}^2} \|\mathtt{z}_1 - \mathtt{z}_2\| + \frac{2c_2^2\mathtt{L}}{c_1^4\mathtt{T}} \|\mathtt{z}_1 - \mathtt{z}_2\| \\
&= c_3 \|\mathtt{z}_1 - \mathtt{z}_2\|,
\end{aligned} \tag{12}
$$

where $c_3 = \frac{\mathtt{L}}{c_1^2\mathtt{T}^2} + \frac{2c_2^2\mathtt{L}}{c_1^4\mathtt{T}}$. So,

$$
\begin{aligned}
&|(\aleph \mathtt{z}_1)(\mathtt{s}) - (\aleph \mathtt{z}_2)(\mathtt{s})| \\
&\quad \leq \frac{bc_3\mu}{a+b}\int_0^T \frac{e^{-\lambda(\mathtt{s}-\mathtt{t})}(\mathtt{T}-\mathtt{t})^{2\ell-1}}{\Gamma(2\ell)}\|\mathtt{z}_1-\mathtt{z}_2\|\mathtt{dt} \\
&\qquad + c_3\mu\int_0^{\mathtt{s}} \frac{e^{-\lambda(\mathtt{s}-\mathtt{t})}(\mathtt{s}-\mathtt{t})^{2\ell-1}}{\Gamma(2\ell)}\|\mathtt{z}_1-\mathtt{z}_2\|\mathtt{dt} \\
&\quad = \frac{bc_3\mu\, e^{-\lambda(\mathtt{s}-\mathtt{T})}}{(a+b)\lambda^{2\ell}}\|\mathtt{z}_1-\mathtt{z}_2\|\int_0^{\lambda\mathtt{T}} \frac{e^{-r}r^{2\ell-1}}{\Gamma(2\ell)}\mathtt{d}r + \frac{c_3\mu}{\lambda^{2\ell}}\|\mathtt{z}_1-\mathtt{z}_2\|\int_0^{\lambda\mathtt{s}} \frac{e^{-r}r^{2\ell-1}}{\Gamma(2\ell)}\mathtt{d}r \\
&\quad \leq \frac{bc_3\mu\, e^{\lambda\mathtt{T}}}{(a+b)\lambda^{2\ell}}\|\mathtt{z}_1-\mathtt{z}_2\|\int_0^{\infty} \frac{e^{-r}r^{2\ell-1}}{\Gamma(2\ell)}\mathtt{d}r + \frac{c_3\mu}{\lambda^{2\ell}}\|\mathtt{z}_1-\mathtt{z}_2\|\int_0^{\infty} \frac{e^{-r}r^{2\ell-1}}{\Gamma(2\ell)}\mathtt{d}r \\
&\quad \leq \frac{bc_3\mu\, e^{\lambda\mathtt{T}}}{(a+b)\lambda^{2\ell}}\|\mathtt{z}_1-\mathtt{z}_2\|\frac{\Gamma(2\ell)}{\Gamma(2\ell)} + \frac{c_3\mu}{\lambda^{2\ell}}\|\mathtt{z}_1-\mathtt{z}_2\|\frac{\Gamma(2\ell)}{\Gamma(2\ell)} \\
&\quad = \frac{c_3\mu}{\lambda^{2\ell}}\left[\frac{be^{\lambda\mathtt{T}}}{a+b}+1\right]\|\mathtt{z}_1-\mathtt{z}_2\|,
\end{aligned}
\tag{13}
$$

which shows that $\aleph$ is a contraction. Hence by Banach fixed point theorem, $\aleph$ has a unique fixed point and is the solution of (3)–(4). □

Example 1 Consider the following fractional order thermistor BVP

$$
{}^{\mathtt{C}}\mathtt{D}_{0^+}^{\frac{2}{3},7}\mathtt{z}(\mathtt{s}) = \frac{2+\sin(\mathtt{z})}{\left[\int_0^1 (2+\sin(\mathtt{z}(\tau)))\mathtt{d}\tau\right]^2},\ 0<\mathtt{s}<1, \tag{14}
$$

$$
15000\mathtt{z}(0) + 5e^7\mathtt{z}(1) = c, \tag{15}
$$

So, $\ell = \frac{1}{3}, \lambda = 7, \mu = \mathtt{T} = 1, a = 15000, b = 5$ and $\mathtt{g}(\mathtt{z}) = 2+\sin(\mathtt{z})$. Then, $c_1 = 2, c_2 = 3$ and

$$|\mathrm{g}(\mathrm{z}_1) - \mathrm{g}(\mathrm{z}_2)| = |\sin(\mathrm{z}_1) - \sin(\mathrm{z}_2)|$$
$$\leq |\mathrm{z}_1 - \mathrm{z}_2|.$$

That is, the Lipschitz constant $\mathrm{L} = 1$. Finally, by simple calculations, we can see that

$$\frac{\mu}{\lambda^{2\ell}}\left[\frac{\mathrm{L}}{c_1^2\mathrm{T}^2} + \frac{2c_2^2\mathrm{L}}{c_1^4\mathrm{T}}\right]\left[\frac{be^{\lambda\mathrm{T}}}{a+b} + 1\right] \approx 0.5130634591 < 1.$$

Hence by Theorem 1, the thermistor problem (14)–(15) has a unique solution in $\mathrm{C}[0,1]$.

Theorem 2 *Assume that*

(G_3) the function $\mathrm{g} : \mathbb{R} \to \mathbb{R}$ is continuous,
(G_4) there exist positive constants d_1 and d_2 such that $d_1 \leq \mathrm{g}(\mathrm{z}) \leq d_2$ for $\mathrm{z} \in \mathbb{R}$.

Then the thermistor BVP (3)–(4) has at least one solution in $\mathrm{C}[0,\mathrm{T}]$.

Proof We divide the proof into four steps. $\aleph$ **is continuous:** Let z_n be a sequence such that $\mathrm{z}_n \to \mathrm{z}$ in $\mathrm{C}[0,\mathrm{T}]$. Then for $\mathrm{s} \in [0,\mathrm{T}]$, we have

$$|\aleph\mathrm{z}_n(\mathrm{s}) - \aleph\mathrm{z}(\mathrm{s})| \leq \frac{\mu}{\lambda^{2\ell}}\left[\frac{1}{d_1^2\mathrm{T}^2} + \frac{2d_2^2}{d_1^4\mathrm{T}}\right]\left[\frac{be^{\lambda\mathrm{T}}}{a+b} + 1\right]\|\mathrm{g}(\mathrm{z}_n) - \mathrm{g}(\mathrm{z})\|_\infty.$$

Since g is continuous, $\|\aleph\mathrm{z}_n(\mathrm{s}) - \aleph\mathrm{z}(\mathrm{s})\| \to 0$ as $n \to \infty$.

$\aleph$ **maps bounded set into bounded sets in** $\mathrm{C}[0,\mathrm{T}]$: Let us define $\mathbb{S}_\delta = \{\mathrm{z} \in \mathrm{C}[0,\mathrm{T}] : \|\mathrm{z}\|_\infty \leq \delta\}$. Now we prove that for any $\mathrm{z} \in \mathbb{S}_\delta$, $\|\aleph\mathrm{z}\|_\infty < \infty$. From (11), we get

$$|\aleph\mathrm{z}| \leq \frac{c}{a+b} + \left[\frac{b}{a+b} + 1\right]\frac{\mu\, c_2\mathrm{T}^{2\ell-2}e^{\lambda\mathrm{T}}}{c_1^2\Gamma(2\ell+1)}.$$

Thus,

$$\|\aleph\mathrm{z}\|_\infty \leq \frac{c}{a+b} + \left[\frac{b}{a+b} + 1\right]\frac{\mu\, c_2\mathrm{T}^{2\ell-2}e^{\lambda\mathrm{T}}}{c_1^2\Gamma(2\ell+1)} < \infty.$$

$\aleph$ **maps bounded sets into equicontinuous sets of** $\mathrm{C}[0,\mathrm{T}]$: Let $\mathrm{s}_1, \mathrm{s}_2 \in [0,\mathrm{T}]$ such that $\mathrm{s}_1 < \mathrm{s}_2$. Let $\mathrm{z} \in \mathbb{S}_\delta$. Then

$$
\begin{aligned}
|(\aleph z)(s_2)-(\aleph z)(s_1)| \leq & \left\{\frac{c}{a+b}+\frac{b\mu}{a+b}\int_0^T \frac{e^{\lambda t}(T-t)^{2\ell-1}}{\Gamma(2\ell)}\frac{g(z(t))}{\left[\int_0^T g(z(\tau))d\tau\right]^2}dt\right\} \\
& |e^{-\lambda s_1}-e^{-\lambda s_2}| \\
& +\mu\left|\int_0^{s_2}\frac{e^{-\lambda(s_2-t)}(s_2-t)^{2\ell-1}}{\Gamma(2\ell)}\frac{g(z(t))}{\left[\int_0^T g(z(\tau))d\tau\right]^2}dt\right. \\
& \left.-\int_0^{s_1}\frac{e^{-\lambda(s_1-t)}(s_1-t)^{2\ell-1}}{\Gamma(2\ell)}\frac{g(z(t))}{\left[\int_0^T g(z(\tau))d\tau\right]^2}dt\right| \\
\leq & \left\{\frac{c}{a+b}+\frac{bc_2\mu}{(a+b)c_1^2T^2}\int_0^T\frac{e^{\lambda t}(T-t)^{2\ell-1}}{\Gamma(2\ell)}dt\right\}\lambda^2 e^{-\lambda s_3}|s_2-s_1| \\
& +\mu\int_0^{s_1}\frac{e^{\lambda t}|e^{-\lambda s_2}(s_2-t)^{2\ell-1}-e^{-\lambda s_1}(s_1-t)^{2\ell-1}|}{\Gamma(2\ell)}\frac{g(z(t))}{\left[\int_0^T g(z(\tau))d\tau\right]^2}dt \\
& +\mu\left|\int_{s_1}^{s_2}\frac{e^{-\lambda(s_2-t)}(s_2-t)^{2\ell-1}}{\Gamma(2\ell)}\frac{g(z(t))}{\left[\int_0^T g(z(\tau))d\tau\right]^2}dt\right| \\
\leq & \left\{\frac{c}{a+b}+\frac{bc_2\mu}{(a+b)c_1^2T^2\lambda^{2\ell}}\int_0^\infty\frac{e^{-r}r^{2\ell-1}}{\Gamma(2\ell)}dr\right\}\lambda^2|s_2-s_1| \\
& +\frac{c_2\mu}{c_1^2T^2}\int_0^{s_1}\frac{e^{\lambda t}e^{-\lambda s_1}|(s_2-t)^{2\ell-1}-(s_1-t)^{2\ell-1}|}{\Gamma(2\ell)}dt \\
& +\frac{c_2\mu}{c_1^2T^2}\int_{s_1}^{s_2}\frac{e^{\lambda t}e^{-\lambda s_1}(s_2-t)^{2\ell-1}}{\Gamma(2\ell)}dt \\
\leq & \lambda^2\left[\frac{c}{a+b}+\frac{bc_2\mu}{(a+b)c_1^2T^2\lambda^{2\ell}}\right]|s_2-s_1| \\
& +\frac{c_2\mu}{c_1^2T^2}\int_0^{s_1}\frac{e^{\lambda t}|(s_2-t)^{2\ell-1}-(s_1-t)^{2\ell-1}|}{\Gamma(2\ell)}dt \\
& +\frac{\mu c_2 e^{\lambda T}}{c_1^2T^2}\frac{(s_2-s_1)^{2\ell}}{\Gamma(2\ell+1)} \\
& \to 0 \quad \text{as} \quad s_1 \to s_2.
\end{aligned}
$$

Next, by above steps along with Arzela-Ascoli theorem, it can be seen that the operator $\aleph : C[0,T] \to C[0,T]$ is completely continuous.

A priori bound: Let $\mathbb{P} = \{z \in C[0,T] : z = \alpha \aleph z \text{ for some } 0<\alpha<1\}$. Let $z \in \mathbb{P}$. Then

$$z(s) = \frac{\alpha c}{a+b}e^{-\lambda s} - \frac{\alpha b\mu}{a+b}\int_0^T \frac{e^{-\lambda(s-t)}(T-t)^{2\ell-1}}{\Gamma(2\ell)} \frac{g(z(t))}{\left[\int_0^T g(z(\tau))d\tau\right]^2} dt + \alpha\mu \int_0^s \frac{e^{-\lambda(s-t)}(s-t)^{2\ell-1}}{\Gamma(2\ell)} \frac{g(z(t))}{\left[\int_0^T g(z(\tau))d\tau\right]^2} dt.$$

From (G_4), we have

$$\begin{aligned} |\aleph z(s)| &= \frac{\alpha c}{a+b}e^{-\lambda s} + \left|\frac{\alpha b\mu}{a+b}\int_0^T \frac{e^{-\lambda(s-t)}(T-t)^{2\ell-1}}{\Gamma(2\ell)} \frac{g(z(t))}{\left[\int_0^T g(z(\tau))d\tau\right]^2} dt\right| \\ &\quad + \left|\alpha\mu \int_0^s \frac{e^{-\lambda(s-t)}(s-t)^{2\ell-1}}{\Gamma(2\ell)} \frac{g(z(t))}{\left[\int_0^T g(z(\tau))d\tau\right]^2} dt\right| \\ &\le \frac{c}{a+b} + \left[\frac{b}{a+b}+1\right]\frac{\mu c_2 T^{2\ell-2}e^{\lambda T}}{c_1^2\Gamma(2\ell+1)} < \infty. \end{aligned}$$

This shows that the $\mathbb{P}$ is bounded. Therefore, by an application of the Schaefer fixed point theorem, $\aleph$ has a fixed point which is a solution of the problem (3)–(4). □

Example 2 Consider the following fractional order thermistor BVP

$${}^{c}D_{0^+}^{2\ell,\lambda} z(s) = \frac{\mu(5+3\cos(z))}{\left[\int_0^T (5+3\cos(z(\tau)))d\tau\right]^2}, \quad 0<\ell<\frac{1}{2}, \ \lambda>0, \ 0<s<T, \tag{16}$$

$$az(0) + be^{\lambda T} z(T) = c, \tag{17}$$

So, $g(z) = 5 + 3\cos(z)$. Then, $d_1 = 5, d_2 = 8$. Hence by Theorem 2, the thermistor problem (16)-(17) has atleast one solution in $C[0,T]$.

4 Uniqueness by Rus's Theorem

In this section, we derive sufficient conditions for the existence of unique solution to the thermistor problem (3)–(4), where we employ two metrics under Rus's theorem (see, [5, 34] for more details).

Consider the set of real valued functions that are defined and continuous on $[0, \mathtt{T}]$ and denote this space by $\mathcal{Y} = \mathrm{C}([0, \mathtt{T}])$. For functions $\mathtt{z}_1, \mathtt{z}_2 \in \mathcal{Y}$, consider the following two metrics on $\mathcal{Y}$:

$$\mathrm{d}(\mathtt{z}_1, \mathtt{z}_2) = \max_{\mathtt{s} \in [0,\mathtt{T}]} |\mathtt{z}_1(\mathtt{s}) - \mathtt{z}_2(\mathtt{s})|, \tag{18}$$

$$\varrho(\mathtt{z}_1, \mathtt{z}_2) = \left[\int_0^{\mathtt{T}} |\mathtt{z}_1(\mathtt{s}) - \mathtt{z}_2(\mathtt{s})|^{\mathtt{p}} \mathtt{ds} \right]^{\frac{1}{\mathtt{p}}}, \quad \mathtt{p} > 1. \tag{19}$$

For d in (18), the pair $(\mathcal{Y}, \mathrm{d})$ forms a complete metric space. For ϱ in (19), the pair $(\mathcal{Y}, \varrho)$ forms a metric space. The relationship between the two metrics on $\mathcal{Y}$ is given by

$$\varrho(\mathtt{z}_1, \mathtt{z}_2) \leq \mathtt{T}^{1/\mathtt{p}} \mathrm{d}(\mathtt{z}_1, \mathtt{z}_2) \quad \text{for all} \quad \mathtt{z}_1, \mathtt{z}_2 \in \mathcal{Y}. \tag{20}$$

Theorem 3 (*Rus* [26]) *Let $\mathcal{Y}$ be a nonempty set and let* d *and ϱ be two metrics on $\mathcal{Y}$ such that $(\mathcal{Y}, \mathrm{d})$ forms a complete metric space. If the mapping $\mathcal{K} : \mathcal{Y} \to \mathcal{Y}$ is continuous with respect to* d *on $\mathcal{Y}$ and*

$$\mathrm{d}(\mathcal{K}\mathtt{z}_1, \mathcal{K}\mathtt{z}_2) \leq \alpha \varrho(\mathtt{z}_1, \mathtt{z}_2), \tag{21}$$

for some $\alpha > 0$ and for all $\mathtt{z}_1, \mathtt{z}_2 \in \mathcal{Y}$,

$$\varrho(\mathcal{K}\mathtt{z}_1, \mathcal{K}\mathtt{z}_2) \leq \beta \varrho(\mathtt{z}_1, \mathtt{z}_2), \tag{22}$$

for some $0 < \beta < 1$ for all $\mathtt{z}_1, \mathtt{z}_2 \in \mathcal{Y}$, then there is a unique $\mathtt{z}^{\star} \in \mathcal{Y}$ such that $\mathcal{K}\mathtt{z}^{\star} = \mathtt{z}^{\star}$.

Theorem 4 *Assume that* $(\mathtt{G}_3)$ *and the following condition hold.*

$(\mathtt{G}_5)$ $$\left| \frac{\mathtt{g}(\mathtt{z}_1(\mathtt{t}))}{\left[\int_0^{T} \mathtt{g}(\mathtt{z}_1(\tau)) \mathtt{d}\tau \right]^2} - \frac{\mathtt{g}(\mathtt{z}_2(\mathtt{t}))}{\left[\int_0^{T} \mathtt{g}(\mathtt{z}_2(\tau)) \mathtt{d}\tau \right]^2} \right| \mathtt{dt} \leq \mathtt{N} |\mathtt{z}_1 - \mathtt{z}_2| \text{ for } \mathtt{z}_1, \mathtt{z}_2 \in \mathcal{Y}.$$

Also, assume that there are constants $\mathtt{p} > 1$ and $\mathtt{q} > 1$ such that $1/\mathtt{p} + 1/\mathtt{q} = 1$ with

$$\mu \mathtt{N} \mathtt{T}^{1/\mathtt{p}} e^{\lambda \mathtt{T}} \left[\int_0^{T} |\aleph(\mathtt{s}, \mathtt{s})|^{\mathtt{q}} \mathtt{ds} \right]^{\frac{1}{\mathtt{q}}} < 1, \tag{23}$$

then the thermistor problem (3)–(4) has a unique (nontrivial) solution in $\mathcal{Y}$.

Proof For any $\mathtt{z} \in \mathcal{Y}$, define an operator $\mathcal{K} : \mathcal{Y} \to \mathbb{R}$ by

$$(\mathcal{K}\mathtt{z})(\mathtt{s}) = \frac{c}{a+b}e^{-\lambda \mathtt{s}} - \frac{b\mu}{a+b}\int_0^T \frac{e^{-\lambda(\mathtt{s}-\mathtt{t})}(\mathtt{T}-\mathtt{t})^{2\ell-1}}{\Gamma(2\ell)} \frac{\mathtt{g}(\mathtt{z}(\mathtt{t}))}{\left[\int_0^T \mathtt{g}(\mathtt{z}(\tau))\mathtt{d}\tau\right]^2}\mathtt{dt}$$
$$+ \mu\int_0^{\mathtt{s}} \frac{e^{-\lambda(\mathtt{s}-\mathtt{t})}(\mathtt{s}-\mathtt{t})^{2\ell-1}}{\Gamma(2\ell)} \frac{\mathtt{g}(\mathtt{z}(\mathtt{t}))}{\left[\int_0^T \mathtt{g}(\mathtt{z}(\tau))\mathtt{d}\tau\right]^2}\mathtt{dt}.$$

Then the operator $\mathcal{K}$ rewritten as

$$(\mathcal{K}\mathtt{z})(\mathtt{s}) = \frac{c}{a+b}e^{-\lambda \mathtt{s}} + \mu\int_0^T \aleph(\mathtt{s},\mathtt{t})e^{-\lambda(\mathtt{s}-\mathtt{t})} \frac{\mathtt{g}(\mathtt{z}(\mathtt{t}))}{\left[\int_0^T \mathtt{g}(\mathtt{z}(\tau))\mathtt{d}\tau\right]^2}\mathtt{dt}, \tag{24}$$

where

$$\aleph(\mathtt{s},\mathtt{t}) = \frac{1}{\Gamma(2\ell)}\begin{cases} -\frac{b}{a+b}(\mathtt{T}-\mathtt{t})^{2\ell-1} + (\mathtt{s}-\mathtt{t})^{2\ell-1}, & \mathtt{t}\le \mathtt{s}, \\ -\frac{b}{a+b}(\mathtt{T}-\mathtt{t})^{2\ell-1}, & \mathtt{s}\le \mathtt{t}. \end{cases}$$

Also, it can be seen that $|\aleph(\mathtt{s},\mathtt{t})| \le |\aleph(\mathtt{t},\mathtt{t})|$ for all $\mathtt{s},\mathtt{t}\in[0,\mathtt{T}]$.

Now, let $\mathtt{z}_1,\mathtt{z}_2 \in \mathcal{Y}$ and $\mathtt{s}\in[0,\mathtt{T}]$. Then by Hölder's inequality [23] and (12), we have

$$\begin{aligned}
&|(\mathcal{K}\mathtt{z}_1)(\tau) - (\mathcal{K}\mathtt{z}_2)(\tau)| \\
&= \mu\left|\int_0^T \aleph(\mathtt{s},\mathtt{t})e^{-\lambda(\mathtt{s}-\mathtt{t})}\left\{\frac{\mathtt{g}(\mathtt{z}_1(\mathtt{t}))}{\left[\int_0^T \mathtt{g}(\mathtt{z}_1(\tau))\mathtt{d}\tau\right]^2} - \frac{\mathtt{g}(\mathtt{z}_2(\mathtt{t}))}{\left[\int_0^T \mathtt{g}(\mathtt{z}_2(\tau))\mathtt{d}\tau\right]^2}\right\}\mathtt{dt}\right| \\
&\le \mu e^{\lambda \mathtt{T}}\int_0^T |\aleph(\mathtt{t},\mathtt{t})|\left|\frac{\mathtt{g}(\mathtt{z}_1(\mathtt{t}))}{\left[\int_0^T \mathtt{g}(\mathtt{z}_1(\tau))\mathtt{d}\tau\right]^2} - \frac{\mathtt{g}(\mathtt{z}_2(\mathtt{t}))}{\left[\int_0^T \mathtt{g}(\mathtt{z}_2(\tau))\mathtt{d}\tau\right]^2}\right|\mathtt{dt} \\
&\le \mu\mathtt{N}e^{\lambda \mathtt{T}}\left[\int_0^T |\aleph(\mathtt{s},\mathtt{s})|^{\mathtt{q}}\mathtt{ds}\right]^{\frac{1}{\mathtt{q}}}\left[\int_0^{\mathtt{T}} |\mathtt{z}_1(\mathtt{s}) - \mathtt{z}_2(\mathtt{s})|^{\mathtt{p}}\mathtt{ds}\right]^{\frac{1}{\mathtt{p}}} \\
&\le \mu\mathtt{N}e^{\lambda \mathtt{T}}\left[\int_0^T |\aleph(\mathtt{s},\mathtt{s})|^{\mathtt{q}}\mathtt{ds}\right]^{\frac{1}{\mathtt{q}}}\varrho(\mathtt{z}_1,\mathtt{z}_2).
\end{aligned} \tag{25}$$

Thus, defining

$$\alpha = \mu N e^{\lambda T}\left[\int_0^T |\aleph(s,s)|^q ds\right]^{\frac{1}{q}},$$

we see that

$$d(\mathcal{K}z_1, \mathcal{K}z_2) \leq \alpha\varrho(z_1, z_2), \tag{26}$$

for some $\alpha > 0$ for all $z_1, z_2 \in \mathcal{Y}$, and so the inequality (10) of Theorem 3 holds. Now, for all $z_1, z_2 \in \mathcal{Y}$, we may apply (20) to (26) to obtain

$$d(\mathcal{K}z_1, \mathcal{K}z_2) \leq \alpha\varrho(z_1, z_2) \leq \alpha T^{1/p} d(z_1, z_2).$$

Thus, given any $\varepsilon > 0$ we can choose $\delta = \varepsilon[\alpha T^{1/p}]^{-1}$ so that $d(\mathcal{K}z_1, \mathcal{K}z_2) < \varepsilon$, whenever $d(z_1, z_2) < \delta$. Hence $\mathcal{K}$ is continuous on $\mathcal{Y}$ with respect to the metric d. Finally, we show that $\mathcal{K}$ is contractive on $\mathcal{Y}$ with respect to the metric ϱ. From (25), for each $z_1, z_2 \in \mathcal{Y}$ consider

$$\left[\int_0^T |(\mathcal{K}z_1)(\tau) - (\mathcal{K}z_2)(\tau)|^p d\tau\right]^{\frac{1}{p}} \leq \left[\int_0^T \left|\mu N e^{\lambda T}\left[\int_0^T |\aleph(s,s)|^q ds\right]^{\frac{1}{q}} \varrho(z_1, z_2)\right|^p d\tau\right]^{\frac{1}{p}}$$

$$\leq \mu N T^{1/p} e^{\lambda T}\left[\int_0^T |\aleph(s,s)|^q ds\right]^{\frac{1}{q}} \varrho(z_1, z_2).$$

That is

$$\varrho(\mathcal{K}z_1, \mathcal{K}z_2) \leq \mu N T^{1/p} e^{\lambda T}\left[\int_0^T |\aleph(s,s)|^q ds\right]^{\frac{1}{q}} \varrho(z_1, z_2).$$

From the assumption (23), we have

$$\varrho(\mathcal{K}z_1, \mathcal{K}z_2) \leq \beta\varrho(z_1, z_2)$$

for some $\beta < 1$ and all $z_1, z_2 \in \mathcal{Y}$. Thus, Theorem 3, the operator $\mathcal{K}$ has a unique fixed point in $\mathcal{Y}$. Therefore, the boundary value problem (3) has a unique (nontrivial) solution. □

For the choices $p = 2$ and $q = 2$ our Theorem 4 becomes the following new result.

Theorem 5 *Assume that* (G_3) *and* (G_5) *hold. Also, assume that*

$$\mu N e^{\lambda T}\sqrt{\left[T\int_0^T |\aleph(s,s)|^2 ds\right]} < 1, \tag{27}$$

then the thermister problem (3)–(4) has a unique (nontrivial) solution in $\mathcal{Y}$.

Example 3 Consider the following fractional order thermistor BVP

$$ {}^{c}\mathtt{D}_{0^+}^{\frac{2}{3},1}\mathtt{z}(\mathtt{s}) = \frac{\frac{1}{2}(1+\cos(\mathtt{z}))}{\left[\int_0^1 (1+\cos(\mathtt{z}(\tau)))\mathtt{d}\tau\right]^2}, \ 0<\mathtt{s}<1, \tag{28} $$

$$ 100\mathtt{z}(0) + 2e^1\,\mathtt{z}(1) = c, \tag{29} $$

So, $\ell = \frac{1}{3}, \mu = \frac{1}{2}, \lambda = \mathtt{T} = 1$ and $\mathtt{g}(\mathtt{z}) = 1+\cos(\mathtt{z})$. Then,

$$
\begin{aligned}
&\left|\frac{\mathtt{g}(\mathtt{z}_1(\mathtt{t}))}{\left[\int_0^T \mathtt{g}(\mathtt{z}_1(\tau))\mathtt{d}\tau\right]^2} - \frac{\mathtt{g}(\mathtt{z}_2(\mathtt{t}))}{\left[\int_0^T \mathtt{g}(\mathtt{z}_2(\tau))\mathtt{d}\tau\right]^2}\right|\mathtt{d}\mathtt{t} = \left|\frac{1+\cos(\mathtt{z}_1)}{\left[\int_0^1 (1+\cos(\mathtt{z}_1(\tau)))\mathtt{d}\tau\right]^2}\right.\\
&\quad\left. - \frac{1+\cos(\mathtt{z}_2)}{\left[\int_0^1 (1+\cos(\mathtt{z}_2(\tau)))\mathtt{d}\tau\right]^2}\right|\\
&\le \frac{\left|[\cos(\mathtt{z}_1)-\cos(\mathtt{z}_2)]\left[\int_0^1(1+\cos(\mathtt{z}_2(\tau)))\mathtt{d}\tau\right]^2\right|}{\left|\int_0^1(1+\cos(\mathtt{z}_1(\tau)))\mathtt{d}\tau\right|^2\left|\int_0^1(1+\cos(\mathtt{z}_2(\tau)))\mathtt{d}\tau\right|^2}\\
&\quad + \frac{\left|(1+\cos(\mathtt{z}_2))\left(\left[\int_0^1(1+\cos(\mathtt{z}_2(\tau)))\mathtt{d}\tau\right]^2 - \left[\int_0^1(1+\cos(\mathtt{z}_1(\tau)))\mathtt{d}\tau\right]^2\right)\right|}{\left|\int_0^1(1+\cos(\mathtt{z}_1(\tau)))\mathtt{d}\tau\right|^2\left|\int_0^1(1+\cos(\mathtt{z}_2(\tau)))\mathtt{d}\tau\right|^2}\\
&\le 4|\cos(\mathtt{z}_1)-\cos(\mathtt{z}_2)| + 8|\cos(\mathtt{z}_2)-\cos(\mathtt{z}_1)|\\
&\le 12|\mathtt{z}_1-\mathtt{z}_2| = \mathtt{N}|\mathtt{z}_1-\mathtt{z}_2|
\end{aligned}
$$

and

$$ \mu\mathtt{N}e^{\lambda\mathtt{T}}\sqrt{\left[\mathtt{T}\int_0^T |\aleph(\mathtt{s},\mathtt{s})|^2\mathtt{d}\mathtt{s}\right]} \approx 0.5539061455 < 1. $$

Hence by Theorem 5, the thermistor problem (28)–(29) has a unique solution in $C[0,1]$.

5 Stability analysis

In this section, we derive necessary conditions for the stability analysis of Hyers–Ulam's type. For some positive $\varepsilon > 0$, consider the inequality given by

$$\left| {}^{c}\mathrm{D}_{0^+}^{2\ell,\lambda} z(s) - \frac{\mu g(z(s))}{\left[\int_0^T g(z(\tau))\mathrm{d}\tau\right]^2} \right| \leq \varepsilon \tag{30}$$

for $s \in [0, T]$. Then the thermistor problem (3)-(4) is Hyers–Ulam stable if there exist constants $Q > 0$ such that for each solution $z \in C[0, T]$ of the inequality (30), there exists a unique solution $y \in C[0, T]$ with

$$|(z(s) - y(s)| \leq Q\left[1 - \frac{\mu}{\lambda^{2\ell}}\left(\frac{L}{c_1^2 T^2} + \frac{2c_2^2 L}{c_1^4 T}\right)\left(\frac{be^{\lambda T}}{a+b} + 1\right)\right]^{-1} \varepsilon. \tag{31}$$

Remark 1 We say that $z \in C[0, T]$ is a solution of the inequality (30) if there exist function $\varphi \in C[0, T]$ which depend upon z such that

(i) $|\varphi(s)| \leq \varepsilon$, $s \in [0, T]$, and
(ii) for $s \in [0, T]$,

$${}^{c}\mathrm{D}_{0^+}^{2\ell,\lambda} z(s) = \frac{\mu g(z(s))}{\left[\int_0^T g(z(\tau))\mathrm{d}\tau\right]^2} + \varphi(s). \tag{32}$$

Lemma 3 *Let $z \in C[0, T]$ be the solution of the inequality (30). Then the following inequality hold*:

$$\left| z(s) - \frac{c}{a+b}e^{-\lambda s} + \frac{b\mu}{a+b}\int_0^T \frac{e^{-\lambda(s-t)}(T-t)^{2\ell-1}}{\Gamma(2\ell)} \frac{g(z(t))}{\left[\int_0^T g(z(\tau))\mathrm{d}\tau\right]^2}\mathrm{d}t \right.$$

$$\left. -\mu\int_0^s \frac{e^{-\lambda(s-t)}(s-t)^{2\ell-1}}{\Gamma(2\ell)} \frac{g(z(t))}{\left[\int_0^T g(z(\tau))\mathrm{d}\tau\right]^2}\mathrm{d}t \right| \leq Q\varepsilon.$$

Proof From the Remark 1 and Lemma 2, the solution of (32) and (4) is given by

$$\begin{cases} \mathtt{z}(\mathtt{s}) = \dfrac{c}{a+b}e^{-\lambda \mathtt{s}} - \dfrac{b}{a+b}\displaystyle\int_0^T \frac{e^{-\lambda(\mathtt{s}-\mathtt{t})}(\mathtt{T}-\mathtt{t})^{2\ell-1}}{\Gamma(2\ell)} \left\{ \frac{\mu \mathtt{g}(\mathtt{z}(\mathtt{t}))}{\left[\displaystyle\int_0^T \mathtt{g}(\mathtt{z}(\tau))\mathtt{d}\tau\right]^2} + \varphi(\mathtt{t}) \right\} \mathtt{d}\mathtt{t} \\ \qquad\qquad + \displaystyle\int_0^{\mathtt{s}} \frac{e^{-\lambda(\mathtt{s}-\mathtt{t})}(\mathtt{s}-\mathtt{t})^{2\ell-1}}{\Gamma(2\ell)} \left\{ \frac{\mu \mathtt{g}(\mathtt{z}(\mathtt{t}))}{\left[\displaystyle\int_0^T \mathtt{g}(\mathtt{z}(\tau))\mathtt{d}\tau\right]^2} + \varphi(\mathtt{t}) \right\} \mathtt{d}\mathtt{t}. \end{cases} \tag{33}$$

Then we have from (33) that

$$\begin{aligned} &\left| \mathtt{z}(\mathtt{s}) - \frac{c}{a+b}e^{-\lambda \mathtt{s}} + \frac{b\mu}{a+b}\int_0^T \frac{e^{-\lambda(\mathtt{s}-\mathtt{t})}(\mathtt{T}-\mathtt{t})^{2\ell-1}}{\Gamma(2\ell)} \frac{\mathtt{g}(\mathtt{z}(\mathtt{t}))}{\left[\displaystyle\int_0^T \mathtt{g}(\mathtt{z}(\tau))\mathtt{d}\tau\right]^2} \mathtt{d}\mathtt{t} \right. \\ &\quad \left. - \mu \int_0^{\mathtt{s}} \frac{e^{-\lambda(\mathtt{s}-\mathtt{t})}(\mathtt{s}-\mathtt{t})^{2\ell-1}}{\Gamma(2\ell)} \frac{\mathtt{g}(\mathtt{z}(\mathtt{t}))}{\left[\displaystyle\int_0^T \mathtt{g}(\mathtt{z}(\tau))\mathtt{d}\tau\right]^2} \mathtt{d}\mathtt{t} \right| \\ &\le \left| \frac{b}{a+b}\int_0^T \frac{e^{-\lambda(\mathtt{s}-\mathtt{t})}(\mathtt{T}-\mathtt{t})^{2\ell-1}}{\Gamma(2\ell)} \varphi(\mathtt{t})\mathtt{d}\mathtt{t} \right| + \left| \int_0^{\mathtt{s}} \frac{e^{-\lambda(\mathtt{s}-\mathtt{t})}(\mathtt{s}-\mathtt{t})^{2\ell-1}}{\Gamma(2\ell)} \varphi(\mathtt{t})\mathtt{d}\mathtt{t} \right| \\ &\le \frac{\varepsilon b e^{\lambda \mathtt{T}}}{(a+b)\lambda^{2\ell}} \int_0^\infty \frac{e^{-r} r^{2\ell-1}}{\Gamma(2\ell)} \mathtt{d}r + \frac{\varepsilon}{\lambda^{2\ell}} \int_0^\infty \frac{e^{-r} r^{2\ell-1}}{\Gamma(2\ell)} \mathtt{d}r \\ &= \frac{1}{\lambda^{2\ell}} \left(\frac{b e^{\lambda \mathtt{T}}}{a+b} + 1 \right) \varepsilon := \mathtt{Q}\varepsilon. \end{aligned}$$

□

Theorem 6 *Suppose* $(\mathtt{G}_1)$–$(\mathtt{G}_2)$ *satisfied. Then the system of boundary value problems* (3)–(4) *is Hyers–Ulam stable, provided*

$$\mathtt{Q}\left[1 - \frac{\mu}{\lambda^{2\ell}} \left(\frac{\mathtt{L}}{c_1^2 \mathtt{T}^2} + \frac{2c_2^2 \mathtt{L}}{c_1^4 \mathtt{T}} \right) \left(\frac{b e^{\lambda \mathtt{T}}}{a+b} + 1 \right) \right]^{-1} < 1.$$

Proof Let $\mathtt{z} \in \mathrm{C}[0, \mathtt{T}]$ be the solution to the inequality (30) and let $\mathtt{y} \in \mathrm{C}[0, \mathtt{T}]$ be the unique solution to the thermistor problem (3)–(4). Then by Lemma 3 and (13), we have

$$
\begin{aligned}
&|z(s)-y(s)| \\
&\leq \left| z(s)-\frac{c}{a+b}e^{-\lambda s}+\frac{b\mu}{a+b}\int_0^T \frac{e^{-\lambda(s-t)}(T-t)^{2\ell-1}}{\Gamma(2\ell)}\frac{g(y(t))}{\left[\int_0^T g(y(\tau))d\tau\right]^2}dt \right. \\
&\quad \left. -\mu\int_0^s \frac{e^{-\lambda(s-t)}(s-t)^{2\ell-1}}{\Gamma(2\ell)}\frac{g(y(t))}{\left[\int_0^T g(y(\tau))d\tau\right]^2}dt \right| \\
&\leq \left| z(s)-\frac{c}{a+b}e^{-\lambda s}+\frac{b\mu}{a+b}\int_0^T \frac{e^{-\lambda(s-t)}(T-t)^{2\ell-1}}{\Gamma(2\ell)}\frac{g(z(t))}{\left[\int_0^T g(z(\tau))d\tau\right]^2}dt \right. \\
&\quad \left. -\mu\int_0^s \frac{e^{-\lambda(s-t)}(s-t)^{2\ell-1}}{\Gamma(2\ell)}\frac{g(z(t))}{\left[\int_0^T g(z(\tau))d\tau\right]^2}dt \right| \\
&\quad + \left| \frac{b\mu}{a+b}\int_0^T \frac{e^{-\lambda(s-t)}(T-t)^{2\ell-1}}{\Gamma(2\ell)}\left\{\frac{g(z(t))}{\left[\int_0^T g(z(\tau))d\tau\right]^2}-\frac{g(y(t))}{\left[\int_0^T g(y(\tau))d\tau\right]^2}\right\}dt \right| \\
&\quad + \left| \mu\int_0^s \frac{e^{-\lambda(s-t)}(s-t)^{2\ell-1}}{\Gamma(2\ell)}\left\{\frac{g(z(t))}{\left[\int_0^T g(z(\tau))d\tau\right]^2}-\frac{g(y(t))}{\left[\int_0^T g(y(\tau))d\tau\right]^2}\right\}dt \right| \\
&\leq Q\varepsilon+\frac{\mu}{\lambda^{2\ell}}\left[\frac{L}{c_1^2T^2}+\frac{2c_2^2L}{c_1^4T}\right]\left[\frac{be^{\lambda T}}{a+b}+1\right]\|z-y\|.
\end{aligned}
$$

Taking supremum on both sides over s, we obtain

$$
\|z-y\| \leq Q\varepsilon+\frac{\mu}{\lambda^{2\ell}}\left[\frac{L}{c_1^2T^2}+\frac{2c_2^2L}{c_1^4T}\right]\left[\frac{be^{\lambda T}}{a+b}+1\right]\|z-y\|.
$$

Therefore,

$$
\|z-y\| \leq Q\left[1-\frac{\mu}{\lambda^{2\ell}}\left(\frac{L}{c_1^2T^2}+\frac{2c_2^2L}{c_1^4T}\right)\left(\frac{be^{\lambda T}}{a+b}+1\right)\right]^{-1}\varepsilon.
$$

This completes the proof. □

Example 4 Consider the following fractional order thermistor BVP

$$ {}^{c}\mathrm{D}_{0^+}^{\frac{2}{5},5}\mathrm{z}(\mathrm{s}) = \frac{2+\frac{1}{2}\sin(\mathrm{z})+\frac{1}{2}\cos(\mathrm{z})}{\left[\int_0^1 (2+\frac{1}{2}\sin(\mathrm{z}(\tau))+\frac{1}{2}\cos(\mathrm{z}))\mathrm{d}\tau\right]^2}, \ 0<\mathrm{s}<1, \tag{34} $$

$$ 85\times 10^4\mathrm{z}(0)+2e^5\mathrm{z}(1)=c, \tag{35} $$

So, $\ell=\frac{1}{5},\lambda=5,\mu=\mathrm{T}=1,a=85\times 10^4,b=2$ and $\mathrm{g}(\mathrm{z})=2+\frac{1}{2}\sin(\mathrm{z})+\frac{1}{2}\cos(\mathrm{z})$. Then, $c_1=2,c_2=3$ and

$$ \begin{aligned} |\mathrm{g}(\mathrm{z}_1)-\mathrm{g}(\mathrm{z}_2)| &= \frac{1}{2}|\sin(\mathrm{z}_1)+\cos(\mathrm{z}_1)-\sin(\mathrm{z}_2)-\cos(\mathrm{z}_2)| \\ &\le \frac{1}{2}|\mathrm{z}_1-\mathrm{z}_2|. \end{aligned} $$

That is, the Lipschitz constant $\mathrm{L}=\frac{1}{2}$. By simple calculations, we obtain $\mathrm{Q}=0.5254890010$,

$$ \frac{\mu}{\lambda^{2\ell}}\left[\frac{\mathrm{L}}{c_1^2\mathrm{T}^2}+\frac{2c_2^2\mathrm{L}}{c_1^4\mathrm{T}}\right]\left[\frac{be^{\lambda\mathrm{T}}}{a+b}+1\right]\approx 0.3612736882<1 $$

and

$$ \mathrm{Q}\left[1-\frac{\mu}{\lambda^{2\ell}}\left(\frac{\mathrm{L}}{c_1^2\mathrm{T}^2}+\frac{2c_2^2\mathrm{L}}{c_1^4\mathrm{T}}\right)\left(\frac{be^{\lambda\mathrm{T}}}{a+b}+1\right)\right]^{-1}\approx 0.8227138781<1. $$

Hence by Theorem 6, the thermistor problem (34)–(35) is Hyers–Ulam stable.

6 Conclusion

In the present paper, we studied tempered fractional order boundary value problem. The fractional derivative used in our problem is the so-called tempered fractional Caputo derivative, which generalizes well-known classical Caputo fractional derivative. By applying our findings, we derived sufficient conditions for the existence, uniqueness of the tempered fractional order thermistor two-point boundary value problem. Further, we also studied Hyers–Ulam stability of the system. Finally numerical example is also provided to illustrate our obtained results. In the future, the following aspects can be explored further:

(1) Further investigation is needed to study system of singular temepered fractional Sturm–Liouville boundary value problem. Here taking singularities over nonlinear term is challenging.
(2) The idea used in this paper can be further developed to study infinite systems of fractional difference equations [42] and dynamic equations on time scales [24, 39, 40] etc.

Acknowledgements The authors would like to thank the referees for their valuable suggestions and comments for the improvement of the paper.

Author Contributions The study was carried out in collaboration of all authors. All authors read and approved the final manuscript.

Funding Not Applicable.

Data availibility statement Data sharing not applicable to this paper as no data sets were generated or analyzed during the current study.

Declarations

Conflict of interest It is declared that authors has no competing interests.

Ethical approval This article does not contain any studies with human participants or animals performed by any of the authors.

References

1. Abdeljawad, T., F. Jarad, and J. Alzabut. 2018. Fractional proportional differences with memory. *The European Physical Journal Special Topics* 226 (16–18): 3333–3354. https://doi.org/10.1140/epjst/e2018-00053-5.
2. Abdeljawad, T., F. Jarad, S.F. Mallak, and J. Alzabut. 2019. Lyapunov type inequalities via fractional proportional derivatives and application on the free zero disc of Kilbas-Saigo generalized Mittag–Leffler functions. *The European Physical Journal Plus* 134 (5): 247.
3. Abu-Shady, M., and M. K. A. Kaabar. 2021. A generalized definition of the fractional derivative with applications. *Mathematical Problems in Engineering*, Article ID 9444803. https://doi.org/10.1155/2021/944803
4. Achar, S.J., C. Baishya, and M.K.A. Kaabar. 2021. Dynamics of the worm transmission in wireless sensor network in the framework of fractional derivatives. *Mathematical Methods in the Applied Sciences*. https://doi.org/10.1002/mma.8039.
5. Almuthaybiria, S.S., and C.C. Tisdell. 2020. Sharper existence and uniqueness results for solutions to third order boundary value problems. *Mathematical Modelling and Analysis* 25 (3): 409–420.
6. Alzabut, J., et al. 2021. Asymptotic stability of nonlinear discrete fractional pantograph equations with nonlocal initial conditions. *Symmetry* 13 (3): 473. https://doi.org/10.3390/sym13030473.
7. Cartea, A., and D. del Castillo-Negrete. 2007. Fractional diffusion models of option prices in markets with jumps. *Physica A: Statistical Mechanics and its Applications* 374 (2): 749–763.
8. Hanyga, A. 2001. Wave propagation in media with singular memory. *Mathematical and computer modelling* 34 (12–13): 1399–1421.
9. He, J.Q., et al. 2015. Study on force distribution of the tempered glass based on laser interference technology. *Optik* 126 (24): 5276–5279.
10. Khuddush, M., K.R. Prasad, and D. Leela. 2022. Existence of solutions for an infinite system of tempered fractional order boundary value problems in the spaces of tempered sequences. *Turkish Journal of Mathematics* 46: 433–452. https://doi.org/10.3906/mat-2106-110.
11. Kaabar, M.K.A., et al. 2021. Investigation of the fractional strongly singular thermostat model via fixed point techniques. *Mathematics* 9 (18): 2298.
12. Kilbas, A.A., H.M. Srivastava, and J.J. Trujillo. 2006. *Theory and applications of fractional differential equations, North-Holland Mathematics Studies 204*. Amsterdam: Elsevier Science B. V.
13. Kwok, K. 1995. *Complete guide to semiconductor devices*. New york: McGraw-Hill.
14. Li, C., W. Can, and L. Zhao. Deng. 2019. Well-posedness and numerical algorithm for the tempered fractional ordinary differential equations. *Discrete and Continuous Dynamical Systems* 24 (4): 1989–2015.
15. Deressa, C.T., S. Etemad, M.K.A. Kaabar, and S. Rezapour. 2022. Qualitative analysis of a hyper-chaotic Lorenz–Stenflo mathematical model via the caputo fractional operator. *Journal of Function Spaces*. https://doi.org/10.1155/2022/4975104.
16. Matar, M.M., et al. 2021. Investigation of the p-Laplacian nonperiodic nonlinear boundary value problem via generalized Caputo fractional derivatives. *Advances in Difference Equations* 1: 1–18.
17. Maclen, E.D. 1979. *Thermistors*. Glasgow: Electrochemical Publication.

18. Meerschaert, M.M., F. Sabzikar, M.S. Phanikumar, and A. Zeleke. 2014. Tempered fractional time series model for turbulence in geophysical flows. *Journal of Statistical Mechanics: Theory and Experiment* 2014 (9): P09023.
19. Pandey, P. K., R. K. Pandey, S. Yadav, and O. P. Agrawal. 2021. Variational approach for tempered fractional Sturm–Liouville problem. *International Journal of Applied and Computational Mathematics* 7 (51). https://doi.org/10.1007/s40819-021-01000-x
20. Prasad, K.R., M. Khuddush, and D. Leela. 2021. Existence of solutions for *n*-dimensional fractional order hybrid BVPs with integral boundary conditions by an application of *n*-fixed point theorem. *Analytical Chemistry* 29: 963–985. https://doi.org/10.1007/s41478-020-00291-5.
21. Prasad, K.R., M. Khuddush, and D. Leela. 2022. Existence theory and stability analysis to the system of fractional order BVP with Riemann-Liouville integral boundary conditions. *The Journal of Analysis*. https://doi.org/10.1007/s41478-021-00371-0.
22. Prasad, K.R., M. Khuddush, and M. Rashmita. 2022. Denumerably many positive solutions for rl-fractional order bvp having denumerably many singularities. *TWMS Journal of Applied and Engineering Mathematics* 12 (1): 302–313.
23. Rogers, L.J. 1888. An extension of a certain theorem in inequalities. *Messenger of Math* 17: 145–150.
24. Rosenau, P. 1992. Tempered diffusion: A transport process with propagating fronts and inertial delay. *Physical Review A* 46 (12): R7371.
25. Rosiak, M.N. 2019. Uncountably many nonoscillatory bounded solutions to second-order nonlinear neutral dynamic equations. *Turkish Journal of Mathematics* 43 (3): 1699–1711.
26. Rus, I.A. 1977. On a fixed point theorem of Maia. *Studia Universitatis Babes–Bolyai Mathematica* 22: 40–42.
27. Sabzikar, F., M.M. Meerschaert, and J. Chen. 2015. Tempered fractional calculus. *Journal of Computational Physics* 293: 14–28.
28. Sajediy, L., and N. Eghbali. 2020. Generalized stability of thermistor problem. *The Applied Mathematics E-Notes* 20: 516–527.
29. Samei, M.E., L. Karimi, and M.K.A. Kaabar. 2022. To investigate a class of multi-singular pointwise defined fractional q-integro-differential equation with applications. *AIMS Mathematics* 7 (5): 7781–7816.
30. Shammakh, W., A.G.M. Selvam, V. Dhakshinamoorthy, and J. Alzabut. 2022. A study of generalized hybrid discrete pantograph equation via Hilfer fractional operator. *Fractal and Fractional* 6 (3): 152. https://doi.org/10.3390/fractalfract6030152.
31. Sidi Ammi, M.R., and D.F.M. Torres. 2008. Numerical analysis of a nonlocal parabolic problem resulting from thermistor problem. *Mathematics and Computers in Simulation* 77: 291–300.
32. Sidi Ammi, M.R., I. Jamiai, and D.F.M. Torres. 2017. global existence of solutions for a fractional caputo nonlocal thermistor problem. *Advances in Difference Equations* 363: 14.
33. Sidi Ammi, M.R., and D.F.M. Torres. 2012. Optimal control of nonlocal thermistor equations. *International Journal of Control* 85: 1789–1801.
34. Stinson, C.P., S.S. Almuthaybiri, and C.C. Tisdell. 2020. A note regarding extensions of fixed point theorems involving two metrics via an analysis of iterated functions. *The ANZIAM Journal* 61 (EMAC2019): C15–C30.
35. Sudsutad, W., J. Alzabut, S. Nontasawatsri, and C. Thaiprayoon. 2020. Stability analysis for a generalized proportional fractional Langevin equation with variable coefficient and mixed integro-differential boundary conditions. *Journal of Nonlinear Functional Analysis* 23: 1–24.
36. Sudsutad, W., J. Alzabut, C. Tearnbucha, and C. Thaiprayoon. 2020. On the oscillation of differential equations in frame of generalized proportional fractional derivatives. *AIMS Mathematics* 5 (2): 856–871. https://doi.org/10.3934/math.2020058.
37. Victor, D.W.J., and M. Khuddush. 2022. Existence of solutions for *n*-dimensional fractional order bvp with ∞-point boundary conditions via the concept of measure of noncompactness. *Advanced Studies: Ero-Tbilisi Mathematical Journal* 15 (1): 19–37.
38. Yadav, S., R.K. Pandey, and P.K. Pande. 2020. Numerical approximation of tempered fractional Sturm-Liouville problem with application in fractional diffusion equation. *International Journal of Numerical Methods in Fluids*. https://doi.org/10.1002/fld.4901.
39. Yantir, A., I. Kubiaczyk, and A. Sikorska-Nowak. 2013. Nonlinear Sturm–Liouville dynamic equation with a measure of noncompactness in Banach spaces. *Bulletin of the Belgian Mathematical Society.* Simon Stevin 20: 587–601.
40. Yantir, A., and I. Kubiaczyk, A. Sikorska-Nowak. 2015. Caratheodory solutions of Sturm-Liouville dynamic equation with a measure of noncompactness in Banach spaces. *Open Mathematics* 13 (1).

41. Zaky, M.A. 2019. Existence, uniqueness and numerical analysis of solutions of tempered fractional boundary value problems. *Applied Numerical Mathods* 145: 429–457.
42. Zhou, W.X., and H.Z. Liu. 2013. Existence solutions for boundary value problem of nonlinear fractional q-difference equations. *Advances in Difference Equations* 2013: 113. https://doi.org/10.1186/1687-1847-2013-113.

Publisher's Note Springer Nature remains neutral with regard to jurisdictional claims in published maps and institutional affiliations.

Cubo
A Mathematical Journal

CUBO, A Mathematical Journal
Vol. 24, no. 01, pp. 21–35, April 2022

Infinitely many positive solutions for an iterative system of singular BVP on time scales

K. Rajendra Prasad[1]
Mahammad Khuddush[2]
K. V. Vidyasagar[3]

[1] *Department of Applied Mathematics, College of Science and Technology, Andhra University, Visakhapatnam, 530003, India.*
rajendra92@rediffmail.com

[2] *Department of Mathematics, Dr. Lankapalli Bullayya College, Resapuvanipalem, Visakhapatnam, 530013, India.*
khuddush89@gmail.com

[3] *Department of Mathematics, S. V. L. N. S. Government Degree College, Bheemunipatnam, Bheemili, 531163, India.*
vidyavijaya08@gmail.com

ABSTRACT

In this paper, we consider an iterative system of singular two-point boundary value problems on time scales. By applying Hölder's inequality and Krasnoselskii's cone fixed point theorem in a Banach space, we derive sufficient conditions for the existence of infinitely many positive solutions. Finally, we provide an example to check the validity of our obtained results.

RESUMEN

En este artículo, consideramos un sistema iterativo de problemas de valor en la frontera singulares de dos puntos en escalas de tiempo. Aplicando la desigualdad de Hölder y el teorema de punto fijo cónico de Krasnoselskii en un espacio de Banach, derivamos condiciones suficientes para la existencia de una cantidad infinita de soluciones positivas. Finalmente, entregamos un ejemplo para verificar la validez de nuestros resultados.

Keywords and Phrases: Iterative system, time scales, singularity, cone, Krasnoselskii's fixed point theorem, positive solutions.

2020 AMS Mathematics Subject Classification: 34B18, 34N05.

Accepted: 15 October, 2021
Received: 18 January, 2021

©2022 K. R. Prasad *et al.* This open access article is licensed under a Creative Commons Attribution-NonCommercial 4.0 International License.

1 Introduction

The theory of time scales was created to unify continuous and discrete analysis. Difference and differential equations can be studied simultaneously by studying dynamic equations on time scales. A time scale is any closed and nonempty subset of the real numbers. So, by this theory, we can extend known results from continuous and discrete analysis to a more general setting. As a matter of fact, this theory allows us to consider time scales which possess hybrid behaviours (both continuous and discrete). These types of time scales play an important role for applications, since most of the phenomena in the environment are neither only discrete nor only continuous, but they possess both behaviours. Moreover, basic results on this issue have been well documented in the articles [1, 2] and the monographs of Bohner and Peterson [6, 7]. There is a great deal of research activity devoted to existence of solutions to the dynamic equations on time scales, see for example [8, 9, 13, 16–19] and references therein.

In [14], Liang and Zhang studied countably many positive solutions for nonlinear singular m–point boundary value problems on time scales,

$$\begin{aligned}\big(\varphi(\upsilon^{\Delta}(t))\big)^{\nabla}+a(t)f\big(\upsilon(t)\big)=0,\ t\in[0,\mathfrak{T}]_{\mathbb{T}},\\ \upsilon(0)=\sum_{i=1}^{m-2}a_i\upsilon(\xi_i),\ \upsilon^{\Delta}(\mathfrak{T})=0,\end{aligned}$$

by using the fixed-point index theory and a new fixed-point theorem in cones.

In [12], Khuddush, Prasad and Vidyasagar considered second order n-point boundary value problem on time scales,

$$\begin{aligned}\upsilon_i^{\Delta\nabla}(t)+\lambda(t)\mathrm{g}_{\ell}\big(\upsilon_{i+1}(t)\big)=0,\ 1\le i\le n,\ t\in(0,\sigma(a)]_{\mathbb{T}},\\ \upsilon_{n+1}(t)=\upsilon_1(t),\ t\in(0,\sigma(a)]_{\mathbb{T}},\\ \upsilon_i^{\Delta}(0)=0,\ \upsilon_i(\sigma(a))=\sum_{k=1}^{n-2}c_k\upsilon_i(\zeta_k),\ 1\le i\le n,\end{aligned}$$

and established existence of positive solutions by applying Krasnoselskii's fixed point theorem.

Inspired by the aforementioned works, in this paper by applying Hölder's inequality and Krasnoselskii's cone fixed point theorem in a Banach space, we establish the existence of infinitely many positive solutions for the iterative system of two-point boundary value problems with n–singularities on time scales,

$$\left.\begin{aligned}\upsilon_{\ell}^{\Delta\Delta}(t)+\lambda(t)\mathrm{g}_{\ell}\big(\upsilon_{\ell+1}(t)\big)=0,\ 1\le\ell\le m,\ t\in(0,\mathfrak{T})_{\mathbb{T}},\\ \upsilon_{m+1}(t)=\upsilon_1(t),\ t\in(0,\mathfrak{T})_{\mathbb{T}},\end{aligned}\right\}\tag{1.1}$$

$$\left.\begin{aligned}\upsilon_{\ell}(0)=\upsilon_{\ell}^{\Delta}(0),\ 1\le\ell\le m,\\ \upsilon_{\ell}(\mathfrak{T})=-\upsilon_{\ell}^{\Delta}(\mathfrak{T}),\ 1\le\ell\le m,\end{aligned}\right\}\tag{1.2}$$

where $m \in \mathbb{N}$, $\lambda(t) = \prod_{i=1}^{k} \lambda_i(t)$ and each $\lambda_i(t) \in L_{\Delta}^{p_i}([0,\mathfrak{T}]_{\mathbb{T}})$ $(p_i \geq 1)$ has n–singularities in the interval $(0,\mathfrak{T})_{\mathbb{T}}$.

We assume the following conditions are true throughout the paper:

(H_1) $\mathrm{g}_\ell : [0,+\infty) \to [0,+\infty)$ is continuous.

(H_2) $\lim\limits_{t \to t_i} \lambda_i(t) = \infty$, where $0 < t_n < t_{n-1} < \cdots < t_1 < \mathfrak{T}$.

2 Preliminaries

In this section, we introduce some basic definitions and lemmas which are useful for our later discussions.

Definition 2.1 ([6]). *A time scale $\mathbb{T}$ is a nonempty closed subset of the real numbers $\mathbb{R}$. $\mathbb{T}$ has the topology that it inherits from the real numbers with the standard topology. It follows that the jump operators $\sigma, \rho : \mathbb{T} \to \mathbb{T}$, and the graininess $\mu : \mathbb{T} \to [0,+\infty)$ are defined by*

$$\sigma(t) = \inf\{\tau \in \mathbb{T} : \tau > t\},$$

$$\rho(t) = \sup\{\tau \in \mathbb{T} : \tau < t\},$$

and

$$\mu(t) = \sigma(t) - t,$$

respectively.

- *The point $t \in \mathbb{T}$ is left-dense, left-scattered, right-dense, right-scattered if $\rho(t) = t$, $\rho(t) < t$, $\sigma(t) = t$, $\sigma(t) > t$, respectively.*
- *If $\mathbb{T}$ has a right-scattered minimum m, then $\mathbb{T}_\kappa = \mathbb{T}\backslash\{m\}$; otherwise $\mathbb{T}_\kappa = \mathbb{T}$.*
- *If $\mathbb{T}$ has a left-scattered maximum m, then $\mathbb{T}^\kappa = \mathbb{T}\backslash\{m\}$; otherwise $\mathbb{T}^\kappa = \mathbb{T}$.*
- *A function $f : \mathbb{T} \to \mathbb{R}$ is called rd-continuous provided it is continuous at right-dense points in $\mathbb{T}$ and its left-sided limits exist (finite) at left-dense points in $\mathbb{T}$. The set of all rd-continuous functions $f : \mathbb{T} \to \mathbb{R}$ is denoted by $C_{rd} = C_{rd}(\mathbb{T}) = C_{rd}(\mathbb{T},\mathbb{R})$.*
- *A function $f : \mathbb{T} \to \mathbb{R}$ is called ld-continuous provided it is continuous at left-dense points in $\mathbb{T}$ and its right-sided limits exist (finite) at right-dense points in $\mathbb{T}$. The set of all ld-continuous functions $f : \mathbb{T} \to \mathbb{R}$ is denoted by $C_{ld} = C_{ld}(\mathbb{T}) = C_{ld}(\mathbb{T},\mathbb{R})$.*
- *By an interval time scale, we mean the intersection of a real interval with a given time scale, i.e., $[a,b]_{\mathbb{T}} = [a,b] \cap \mathbb{T}$. Other intervals can be defined similarly.*

Definition 2.2 ([5,11]). *Let μ_Δ and μ_∇ be the Lebesgue $\Delta-$measure and the Lebesgue $\nabla-$measure on $\mathbb{T}$, respectively. If $A \subset \mathbb{T}$ satisfies $\mu_\Delta(A) = \mu_\nabla(A)$, then we call A measurable on $\mathbb{T}$, denoted $\mu(A)$ and this value is called the Lebesgue measure of A. Let P denote a proposition with respect to $t \in \mathbb{T}$.*

(i) If there exists $\Gamma_1 \subset A$ with $\mu_\Delta(\Gamma_1) = 0$ such that P holds on $A\backslash\Gamma_1$, then P is said to hold Δ–a.e. on A.

(ii) If there exists $\Gamma_2 \subset A$ with $\mu_\nabla(\Gamma_2) = 0$ such that P holds on $A\backslash\Gamma_2$, then P is said to hold ∇–a.e. on A.

Definition 2.3 ([4,5]). *Let $E \subset \mathbb{T}$ be a $\Delta-$measurable set and $p \in \bar{\mathbb{R}} \equiv \mathbb{R} \cup \{-\infty, +\infty\}$ be such that $p \geq 1$ and let $f : E \to \bar{\mathbb{R}}$ be a $\Delta-$measurable function. We say that f belongs to $L^p_\Delta(E)$ provided that either*

$$\int_E |f|^p(s)\Delta s < \infty \quad \text{if} \quad p \in [1, +\infty),$$

or there exists a constant $M \in \mathbb{R}$ such that

$$|f| \leq M, \quad \Delta - a.e. \text{ on } E \quad \text{if} \quad p = +\infty.$$

Lemma 2.4 ([20]). *Let $E \subset \mathbb{T}$ be a $\Delta-$measurable set. If $f : \mathbb{T} \to \mathbb{R}$ is $\Delta-$integrable on E, then*

$$\int_E f(s)\Delta s = \int_E f(s)ds + \sum_{i \in I_E} \big(\sigma(t_i) - t_i\big) f(t_i) + r(f, E),$$

where

$$r(f, E) = \begin{cases} \mu_{\mathtt{N}}(E) f(M), & \text{if } \mathtt{N} \in \mathbb{T}, \\ \\ 0, & \text{if } \mathtt{N} \notin \mathbb{T}, \end{cases}$$

$I_E := \{i \in I : t_i \in E\}$ and $\{t_i\}_{i \in I}$, $I \subset \mathbb{N}$, is the set of all right-scattered points of $\mathbb{T}$.

Lemma 2.5. *For any $\mathrm{y}(t) \in \mathcal{C}_{rd}([0, \mathfrak{T}]_{\mathbb{T}})$, the boundary value problem,*

$$\upsilon_1^{\Delta\Delta}(t) + \mathrm{y}(t) = 0, \ t \in (0, \mathfrak{T})_{\mathbb{T}}, \tag{2.1}$$

$$\upsilon_1(0) = \upsilon_1^{\Delta}(0), \ \upsilon_1(\mathfrak{T}) = -\upsilon_1^{\Delta}(\mathfrak{T}), \tag{2.2}$$

has a unique solution

$$\upsilon_1(t) = \int_0^{\mathfrak{T}} \aleph(t, \tau)\mathrm{y}(\tau)\Delta\tau, \tag{2.3}$$

where

$$\aleph(t, \tau) = \frac{1}{2 + \mathfrak{T}} \begin{cases} (\mathfrak{T} - t + 1)(\sigma(\tau) + 1), & \text{if } \ \sigma(\tau) < t, \\ \\ (\mathfrak{T} - \sigma(\tau) + 1)(t + 1), & \text{if } \ t < \tau. \end{cases} \tag{2.4}$$

Proof. Suppose υ_1 is a solution of (2.1), then

$$\begin{aligned}\upsilon_1(t) &= -\int_0^t \int_0^\tau \mathrm{y}(\tau_1)\Delta\tau_1\Delta\tau + A_1 t + A_2 \\ &= -\int_0^t (t-\sigma(\tau))\mathrm{y}(\tau)\Delta\tau + A_1 t + A_2,\end{aligned}$$

where $A_1 = \upsilon_1^{\Delta}(0)$ and $A_2 = \upsilon_1(0)$. By the conditions (2.2), we get

$$A_1 = A_2 = \frac{1}{2+\mathfrak{T}}\int_0^{\mathfrak{T}} (\mathfrak{T}-\sigma(\tau)+1)\mathrm{y}(\tau)\Delta\tau.$$

So, we have

$$\begin{aligned}\upsilon_1(t) &= \int_0^t (t-\sigma(\tau))\mathrm{y}(\tau)\Delta\tau + \frac{1}{2+\mathfrak{T}}\int_0^{\mathfrak{T}} (\mathfrak{T}-\sigma(\tau)+1)(1+t)\mathrm{y}(\tau)\Delta\tau \\ &= \int_0^{\mathfrak{T}} \aleph(t,\tau)\mathrm{y}(\tau)\Delta\tau.\end{aligned}$$

This completes the proof. □

Lemma 2.6. *Suppose (H_1)–(H_2) hold. For $\varepsilon \in (0, \frac{\mathfrak{T}}{2})_{\mathbb{T}}$, let $\mathcal{G}(\varepsilon) = \dfrac{\varepsilon+1}{\mathfrak{T}+1} < 1$. Then $\aleph(t,\tau)$ has the following properties:*

(i) $0 \le \aleph(t,\tau) \le \aleph(\tau,\tau)$ *for all* $t,\tau \in [0,1]_{\mathbb{T}}$,

(ii) $\mathcal{G}(\varepsilon)\aleph(\tau,\tau) \le \aleph(t,\tau)$ *for all* $t \in [\varepsilon, \mathfrak{T}-\varepsilon]_{\mathbb{T}}$ *and* $\tau \in [0,1]_{\mathbb{T}}$.

Proof. (i) is evident. To prove *(ii)*, let $t \in [\varepsilon, \mathfrak{T}-\varepsilon]_{\mathbb{T}}$ and $t \le \tau$. Then

$$\frac{\aleph(t,\tau)}{\aleph(\tau,\tau)} = \frac{t+1}{\tau+1} \ge \frac{\varepsilon+1}{\mathfrak{T}+1} = \mathcal{G}(\varepsilon).$$

For $\tau \le t$,

$$\frac{\aleph(t,\tau)}{\aleph(\tau,\tau)} = \frac{\mathfrak{T}-t+1}{\mathfrak{T}-\tau+1} \ge \frac{\varepsilon+1}{\mathfrak{T}+1} = \mathcal{G}(\varepsilon).$$

This completes the proof. □

Notice that an $m-$tuple $(\upsilon_1(t), \upsilon_2(t), \upsilon_3(t), \ldots, \upsilon_m(t))$ is a solution of the iterative boundary value problem (1.1)–(1.2) if and only if

$$\begin{aligned}\upsilon_\ell(t) &= \int_0^1 \aleph(t,\tau)\lambda(\tau)\mathrm{g}_\ell(\upsilon_{\ell+1}(\tau))\Delta\tau,\ t \in (0,\mathfrak{T})_{\mathbb{T}},\ 1 \le \ell \le m, \\ \upsilon_{m+1}(t) &= \upsilon_1(t),\ t \in (0,\mathfrak{T})_{\mathbb{T}},\end{aligned}$$

i.e.,

$$\begin{aligned}\upsilon_1(t) = \int_0^1 \aleph(t,\tau_1)\lambda(\tau_1)\mathrm{g}_1\Big(\int_0^1 \aleph(\tau_1,\tau_2)\lambda(\tau_2)\mathrm{g}_2\Big(\int_0^1 \aleph(\tau_2,\tau_3)\cdots \\ \times\, \mathrm{g}_{m-1}\Big(\int_0^1 \aleph(\tau_{m-1},\tau_m)\lambda(\tau_m)\mathrm{g}_m(\upsilon_1(\tau_m))\Delta\tau_m\Big)\cdots\Delta\tau_3\Big)\Delta\tau_2\Big)\Delta\tau_1.\end{aligned}$$

Let $\mathtt{B}$ be the Banach space $C_{rd}((0,\mathfrak{T})_{\mathbb{T}},\mathbb{R})$ with the norm $\|\upsilon\| = \max_{t\in(0,\mathfrak{T})_{\mathbb{T}}} |\upsilon(t)|$. For $\varepsilon \in \left(0,\frac{\mathfrak{T}}{2}\right)_{\mathbb{T}}$, we define the cone $\mathtt{K}_\varepsilon \subset \mathtt{B}$ as

$$\mathtt{K}_\varepsilon = \left\{\upsilon \in \mathtt{B} : \upsilon(t) \text{ is nonnegative and } \min_{t\in[\varepsilon,\,\mathfrak{T}-\varepsilon]_{\mathbb{T}}} \upsilon(t) \geq \mathcal{G}(\varepsilon)\|\upsilon(t)\|\right\}.$$

For any $\upsilon_1 \in \mathtt{K}_\varepsilon$, define an operator $\Omega : \mathtt{K}_\varepsilon \to \mathtt{B}$ by

$$\begin{aligned}(\Omega\upsilon_1)(t) = \int_0^1 \aleph(t,\tau_1)\lambda(\tau_1)\mathrm{g}_1\bigg(\int_0^1 \aleph(\tau_1,\tau_2)\lambda(\tau_2)\mathrm{g}_2\bigg(\int_0^1 \aleph(\tau_2,\tau_3)\cdots \\ \times \mathrm{g}_{m-1}\bigg(\int_0^1 \aleph(\tau_{m-1},\tau_m)\lambda(\tau_m)\mathrm{g}_m(\upsilon_1(\tau_m))\Delta\tau_m\bigg)\cdots\Delta\tau_3\bigg)\Delta\tau_2\bigg)\Delta\tau_1.\end{aligned}$$

Lemma 2.7. *Assume that (H_1)–(H_2) hold. Then for each $\varepsilon \in \left(0,\frac{\mathfrak{T}}{2}\right)_{\mathbb{T}}$, $\Omega(\mathtt{K}_\varepsilon) \subset \mathtt{K}_\varepsilon$ and $\Omega : \mathtt{K}_\varepsilon \to \mathtt{K}_\varepsilon$ are completely continuous.*

Proof. From Lemma 2.6, $\aleph(t,\tau) \geq 0$ for all $t,\tau \in (0,\mathfrak{T})_{\mathbb{T}}$. So, $(\Omega\upsilon_1)(t) \geq 0$. Also, for $\upsilon_1 \in \mathtt{K}_\varepsilon$, we have

$$\begin{aligned}\|\Omega\upsilon_1\| &= \max_{t\in(0,\mathfrak{T})_{\mathbb{T}}} \int_0^1 \aleph(t,\tau_1)\lambda(\tau_1)\mathrm{g}_1\bigg(\int_0^1 \aleph(\tau_1,\tau_2)\lambda(\tau_2)\mathrm{g}_2\bigg(\int_0^1 \aleph(\tau_2,\tau_3)\cdots \\ &\quad\times \mathrm{g}_{m-1}\bigg(\int_0^1 \aleph(\tau_{m-1},\tau_m)\lambda(\tau_m)\mathrm{g}_m(\upsilon_1(\tau_m))\Delta\tau_m\bigg)\cdots\Delta\tau_3\bigg)\Delta\tau_2\bigg)\Delta\tau_1 \\ &\leq \int_0^1 \aleph(\tau_1,\tau_1)\lambda(\tau_1)\mathrm{g}_1\bigg(\int_0^1 \aleph(\tau_1,\tau_2)\lambda(\tau_2)\mathrm{g}_2\bigg(\int_0^1 \aleph(\tau_2,\tau_3)\cdots \\ &\quad\times \mathrm{g}_{m-1}\bigg(\int_0^1 \aleph(\tau_{m-1},\tau_m)\lambda(\tau_m)\mathrm{g}_m(\upsilon_1(\tau_m))\Delta\tau_m\bigg)\cdots\Delta\tau_3\bigg)\Delta\tau_2\bigg)\Delta\tau_1.\end{aligned}$$

Again from Lemma 2.6, we get

$$\begin{aligned}\min_{t\in[\varepsilon,\mathfrak{T}-\varepsilon]_{\mathbb{T}}} \big\{(\Omega\upsilon_1)(t)\big\} \geq \mathcal{G}(\varepsilon)\int_0^1 \aleph(\tau_1,\tau_1)\lambda(\tau_1)\mathrm{g}_1\bigg(\int_0^1 \aleph(\tau_1,\tau_2)\lambda(\tau_2)\mathrm{g}_2\bigg(\int_0^1 \aleph(\tau_2,\tau_3)\cdots \\ \times \mathrm{g}_{m-1}\bigg(\int_0^1 \aleph(\tau_{m-1},\tau_m)\lambda(\tau_m)\mathrm{g}_m(\upsilon_1(\tau_m))\Delta\tau_m\bigg)\cdots\Delta\tau_3\bigg)\Delta\tau_2\bigg)\Delta\tau_1.\end{aligned}$$

It follows from the above two inequalities that

$$\min_{t\in[\varepsilon,\mathfrak{T}-\varepsilon]_{\mathbb{T}}} \big\{(\Omega\upsilon_1)(t)\big\} \geq \mathcal{G}(\varepsilon)\|\Omega\upsilon_1\|.$$

So, $\Omega\upsilon_1 \in \mathtt{K}_\varepsilon$ and thus $\Omega(\mathtt{K}_\varepsilon) \subset \mathtt{K}_\varepsilon$. Next, by standard methods and the Arzela-Ascoli theorem, it can be proved easily that the operator Ω is completely continuous. The proof is complete. □

3 Infinitely many positive solutions

For the existence of infinitely many positive solutions for iterative system of boundary value problem (1.1)–(1.2), we apply following theorems.

Theorem 3.1 ([10]). *Let $\mathcal{E}$ be a cone in a Banach space $\mathcal{X}$ and let $\mathtt{M}_1$, $\mathtt{M}_2$ be open sets with $0 \in \mathtt{M}_1, \overline{\mathtt{M}}_1 \subset \mathtt{M}_2$. Let $\mathcal{A} : \mathcal{E} \cap (\overline{\mathtt{M}}_2 \backslash \mathtt{M}_1) \to \mathcal{E}$ be a completely continuous operator such that*

(a) $\|\mathcal{A}v\| \leq \|v\|$, $v \in \mathcal{E} \cap \partial \mathtt{M}_1$, *and* $\|\mathcal{A}v\| \geq \|v\|$, $v \in \mathcal{E} \cap \partial \mathtt{M}_2$, *or*

(b) $\|\mathcal{A}v\| \geq \|v\|$, $v \in \mathcal{E} \cap \partial \mathtt{M}_1$, *and* $\|\mathcal{A}v\| \leq \|v\|$, $v \in \mathcal{E} \cap \partial \mathtt{M}_2$.

Then $\mathcal{A}$ *has a fixed point in* $\mathcal{E} \cap (\overline{\mathtt{M}}_2 \backslash \mathtt{M}_1)$.

Theorem 3.2 ([7, 15]). *Let* $f \in L^p_\nabla(J)$ *with* $p > 1$, $g \in L^q_\Delta(J)$ *with* $q > 1$, *and* $\frac{1}{p} + \frac{1}{q} = 1$. *Then* $fg \in L^1_\Delta(J)$ *and* $\|fg\|_{L^1_\Delta} \leq \|f\|_{L^p_\Delta} \|g\|_{L^q_\Delta}$, *where*

$$\|f\|_{L^p_\Delta} := \begin{cases} \Big[\int_J |f|^p(s)\Delta s\Big]^{\frac{1}{p}}, & p \in \mathbb{R}, \\ \inf\Big\{M \in \mathbb{R} \,/\, |f| \leq M \ \Delta - a.e. \ on \ J\Big\}, & p = \infty, \end{cases}$$

and $J = [a, b)_{\mathbb{T}}$.

Theorem 3.3 (Hölder's inequality [3, 4, 15]). *Let* $f \in L^{p_i}_\Delta(J)$ *with* $p_i > 1$, *for* $i = 1, 2, \ldots, n$ *and* $\sum_{i=1}^n \frac{1}{p_i} = 1$. *Then* $\prod_{i=1}^k \mathtt{g}_i \in L^1_\Delta(J)$ *and* $\Big\|\prod_{i=1}^k \mathtt{g}_i\Big\|_1 \leq \prod_{i=1}^k \|\mathtt{g}_i\|_{p_i}$. *Further, if* $f \in L^1_\Delta(J)$ *and* $g \in L^\infty_\Delta(J)$, *then* $fg \in L^1_\Delta(J)$ *and* $\|fg\|_1 \leq \|f\|_1 \|g\|_\infty$.

We need the following condition in the sequel:

(H_3) There exists $\delta_i > 0$ such that $\lambda_i(t) > \delta_i$ $(i = 1, 2, \ldots, n)$ for $t \in [0, \mathfrak{T}]_{\mathbb{T}}$.

Consider the following three possible cases for $\lambda_i \in L^{p_i}_\Delta(0, \mathfrak{T})_{\mathbb{T}}$:

$$\sum_{i=1}^n \frac{1}{p_i} < 1, \quad \sum_{i=1}^n \frac{1}{p_i} = 1, \quad \sum_{i=1}^n \frac{1}{p_i} > 1.$$

Firstly, we seek infinitely many positive solutions for the case $\displaystyle\sum_{i=1}^n \frac{1}{p_i} < 1$.

Theorem 3.4. *Suppose* (H_1)*–*(H_3) *hold, let* $\{\varepsilon_r\}_{r=1}^\infty$ *be such that* $0 < \varepsilon_1 < \mathfrak{T}/2$, $\varepsilon \downarrow t^*$ *and* $0 < t^* < t_n$. *Let* $\{\Gamma_r\}_{r=1}^\infty$ *and* $\{\Lambda_r\}_{r=1}^\infty$ *be such that*

$$\Gamma_{r+1} < \mathcal{G}(\varepsilon_r)\Lambda_r < \Lambda_r < \theta\Lambda_r < \Gamma_r, \ r \in \mathbb{N},$$

where

$$\theta = \max\left\{\left[\mathcal{G}(\varepsilon_1)\prod_{i=1}^k \delta_i \int_{\varepsilon_1}^{\mathfrak{T}-\varepsilon_1} \aleph(\tau, \tau)\Delta\tau\right]^{-1}, \ 1\right\}.$$

Assume that $\mathtt{g}_\ell$ *satisfies*

(C_1) $\mathtt{g}_\ell(\upsilon) \leq \mathfrak{N}_1\Gamma_r \ \forall \ t \in (0, \mathfrak{T})_{\mathbb{T}}$, $0 \leq \upsilon \leq \Gamma_r$, *where*

$$\mathfrak{N}_1 < \left[\|\aleph\|_{L^q_\Delta} \prod_{i=1}^k \|\lambda_i\|_{L^{p_i}_\Delta}\right]^{-1},$$

(C_2) $\mathtt{g}_\ell(\upsilon) \geq \theta\Lambda_r \ \forall \ t \in [\varepsilon_r, \mathfrak{T} - \varepsilon_r]_{\mathbb{T}}$, $\mathcal{G}(\varepsilon_r)\Lambda_r \leq \upsilon \leq \Lambda_r$.

Then the iterative boundary value problem (1.1)–(1.2) *has infinitely many solutions* $\{(\mathfrak{v}_1^{[r]}, \mathfrak{v}_2^{[r]}, \dots, \mathfrak{v}_m^{[r]})\}_{r=1}^{\infty}$ *such that* $\mathfrak{v}_\ell^{[r]}(t) \geq 0$ *on* $(0, \mathfrak{T})_{\mathbb{T}}$, $\ell = 1, 2, \dots, m$ *and* $r \in \mathbb{N}$.

Proof. Let

$$\mathtt{M}_{1,r} = \{\mathfrak{v} \in \mathtt{B} : \|\mathfrak{v}\| < \Gamma_r\}, \quad \mathtt{M}_{2,r} = \{\mathfrak{v} \in \mathtt{B} : \|\mathfrak{v}\| < \Lambda_r\},$$

be open subsets of $\mathtt{B}$. Let $\{\varepsilon_r\}_{r=1}^{\infty}$ be given in the hypothesis and we note that

$$t^* < t_{r+1} < \varepsilon_r < t_r < \frac{\mathfrak{T}}{2},$$

for all $r \in \mathbb{N}$. For each $r \in \mathbb{N}$, we define the cone $\mathtt{K}_{\varepsilon_r}$ by

$$\mathtt{K}_{\varepsilon_r} = \Big\{\mathfrak{v} \in \mathtt{B} : \mathfrak{v}(t) \geq 0, \min_{t \in [\varepsilon_r, \mathfrak{T} - \varepsilon_r]_{\mathbb{T}}} \mathfrak{v}(t) \geq \mathcal{G}(\varepsilon_r)\|\mathfrak{v}(t)\|\Big\}.$$

Let $\mathfrak{v}_1 \in \mathtt{K}_{\varepsilon_r} \cap \partial \mathtt{M}_{1,r}$. Then, $\mathfrak{v}_1(\tau) \leq \Gamma_r = \|\mathfrak{v}_1\|$ for all $\tau \in (0, \mathfrak{T})_{\mathbb{T}}$. By (C_1) and for $\tau_{m-1} \in (0, \mathfrak{T})_{\mathbb{T}}$, we have

$$\begin{aligned}\int_0^{\mathfrak{T}} \aleph(\tau_{m-1}, \tau_m)\lambda(\tau_m)\mathtt{g}_m(\mathfrak{v}_1(\tau_m))\Delta\tau_m &\leq \int_0^{\mathfrak{T}} \aleph(\tau_m, \tau_m)\lambda(\tau_m)\mathtt{g}_m(\mathfrak{v}_1(\tau_m))\Delta\tau_m \\ &\leq \mathfrak{N}_1\Gamma_r \int_0^{\mathfrak{T}} \aleph(\tau_m, \tau_m)\prod_{i=1}^{k}\lambda_i(\tau_m)\Delta\tau_m.\end{aligned}$$

There exists a $q > 1$ such that $\dfrac{1}{q} + \displaystyle\sum_{i=1}^{n}\frac{1}{p_i} = 1$. So,

$$\begin{aligned}\int_0^{\mathfrak{T}} \aleph(\tau_{m-1}, \tau_m)\lambda(\tau_m)\mathtt{g}_m(\mathfrak{v}_1(\tau_m))\Delta\tau_m &\leq \mathfrak{N}_1\Gamma_r\big\|\aleph\big\|_{L_\Delta^q}\left\|\prod_{i=1}^{k}\lambda_i\right\|_{L_\Delta^{p_i}} \\ &\leq \mathfrak{N}_1\Gamma_r\|\aleph\|_{L_\Delta^q}\prod_{i=1}^{k}\|\lambda_i\|_{L_\Delta^{p_i}} \leq \Gamma_r.\end{aligned}$$

It follows in similar manner (for $\tau_{m-2} \in (0, \mathfrak{T})_{\mathbb{T}}$), that

$$\begin{aligned}&\int_0^{\mathfrak{T}} \aleph(\tau_{m-2}, \tau_{m-1})\lambda(\tau_{m-1})\mathtt{g}_{m-1}\bigg(\int_0^{\mathfrak{T}} \aleph(\tau_{m-1}, \tau_m)\lambda(\tau_m)\mathtt{g}_m(\mathfrak{v}_1(\tau_m))\Delta\tau_m\bigg)\Delta\tau_{m-1} \\ &\qquad \leq \int_0^{\mathfrak{T}} \aleph(\tau_{m-2}, \tau_{m-1})\lambda(\tau_{m-1})\mathtt{g}_{m-1}(\Gamma_r)\Delta\tau_{m-1} \\ &\qquad \leq \int_0^{\mathfrak{T}} \aleph(\tau_{m-1}, \tau_{m-1})\lambda(\tau_{m-1})\mathtt{g}_{m-1}(\Gamma_r)\Delta\tau_{m-1} \\ &\qquad \leq \mathfrak{N}_1\Gamma_r \int_0^{\mathfrak{T}} \aleph(\tau_{m-1}, \tau_{m-1})\prod_{i=1}^{k}\lambda_i(\tau_{m-1})\Delta\tau_{m-1} \\ &\qquad \leq \mathfrak{N}_1\Gamma_r\|\aleph\|_{L_\Delta^q}\prod_{i=1}^{k}\|\lambda_i\|_{L_\Delta^{p_i}} \leq \Gamma_r.\end{aligned}$$

Continuing with this bootstrapping argument, we get

$$\begin{aligned}(\Omega\upsilon_1)(t) &= \int_0^{\mathfrak{T}} \aleph(t,\tau_1)\lambda(\tau_1)\mathrm{g}_1\bigg(\int_0^{\mathfrak{T}} \aleph(\tau_1,\tau_2)\lambda(\tau_2)\mathrm{g}_2\bigg(\int_0^{\mathfrak{T}} \aleph(\tau_2,\tau_3)\cdots \\ &\quad\times \mathrm{g}_{m-1}\bigg(\int_0^{\mathfrak{T}} \aleph(\tau_{m-1},\tau_m)\lambda(\tau_m)\mathrm{g}_m(\upsilon_1(\tau_m))\Delta\tau_m\bigg)\cdots\Delta\tau_3\bigg)\Delta\tau_2\bigg)\Delta\tau_1 \\ &\leq \Gamma_r.\end{aligned}$$

Since $\Gamma_r = \|\upsilon_1\|$ for $\upsilon_1 \in \mathtt{K}_{\varepsilon_r} \cap \partial\mathtt{M}_{1,r}$, we get

$$\|\Omega\upsilon_1\| \leq \|\upsilon_1\|. \tag{3.1}$$

Let $t \in [\varepsilon_r, \mathfrak{T}-\varepsilon_r]_{\mathbb{T}}$. Then,

$$\Lambda_r = \|\upsilon_1\| \geq \upsilon_1(t) \geq \min_{t\in[\varepsilon_r,\mathfrak{T}-\varepsilon_r]_{\mathbb{T}}} \upsilon_1(t) \geq \mathcal{G}(\varepsilon_r)\,\|\upsilon_1\| \geq \mathcal{G}(\varepsilon_r)\Lambda_r.$$

By (C_2) and for $\tau_{m-1} \in [\varepsilon_r, \mathfrak{T}-\varepsilon_r]_{\mathbb{T}}$, we have

$$\begin{aligned}\int_0^{\mathfrak{T}} \aleph(\tau_{m-1},\tau_m)\lambda(\tau_m)\mathrm{g}_m(\upsilon_1(\tau_m))\Delta\tau_m &\geq \int_{\varepsilon_r}^{\mathfrak{T}-\varepsilon_r} \aleph(\tau_{m-1},\tau_m)\lambda(\tau_m)\mathrm{g}_m(\upsilon_1(\tau_m))\Delta\tau_m \\ &\geq \mathcal{G}(\varepsilon_r)\theta\Lambda_r \int_{\varepsilon_r}^{\mathfrak{T}-\varepsilon_r} \aleph(\tau_m,\tau_m)\lambda(\tau_m)\Delta\tau_m \\ &\geq \mathcal{G}(\varepsilon_r)\theta\Lambda_r \int_{\varepsilon_r}^{\mathfrak{T}-\varepsilon_r} \aleph(\tau_m,\tau_m)\prod_{i=1}^{k}\lambda_i(\tau_m)\Delta\tau_m \\ &\geq \mathcal{G}(\varepsilon_1)\theta\Lambda_r \prod_{i=1}^{k}\delta_i \int_{\varepsilon_1}^{\mathfrak{T}-\varepsilon_1} \aleph(\tau_m,\tau_m)\Delta\tau_m \\ &\geq \Lambda_r.\end{aligned}$$

Continuing with the bootstrapping argument, we get

$$\begin{aligned}(\Omega\upsilon_1)(t) &= \int_0^{\mathfrak{T}} \aleph(t,\tau_1)\lambda(\tau_1)\mathrm{g}_1\bigg(\int_0^{\mathfrak{T}} \aleph(\tau_1,\tau_2)\lambda(\tau_2)\mathrm{g}_2\bigg(\int_0^{\mathfrak{T}} \aleph(\tau_2,\tau_3)\cdots \\ &\quad\times \mathrm{g}_{m-1}\bigg(\int_0^{\mathfrak{T}} \aleph(\tau_{m-1},\tau_m)\lambda(\tau_m)\mathrm{g}_m(\upsilon_1(\tau_m))\Delta\tau_m\bigg)\cdots\Delta\tau_3\bigg)\Delta\tau_2\bigg)\Delta\tau_1 \\ &\geq \Lambda_r.\end{aligned}$$

Thus, if $\upsilon_1 \in \mathtt{K}_{\varepsilon_r} \cap \partial\mathtt{K}_{2,r}$, then

$$\|\Omega\upsilon_1\| \geq \|\upsilon_1\|. \tag{3.2}$$

It is evident that $0 \in \mathtt{M}_{2,k} \subset \overline{\mathtt{M}}_{2,k} \subset \mathtt{M}_{1,k}$. From (3.1)–(3.2), it follows from Theorem 3.1 that the operator Ω has a fixed point $\upsilon_1^{[r]} \in \mathtt{K}_{\varepsilon_r} \cap \big(\overline{\mathtt{M}}_{1,r}\backslash\mathtt{M}_{2,r}\big)$ such that $\upsilon_1^{[r]}(t) \geq 0$ on $(0,\mathfrak{T})_{\mathbb{T}}$, and $r \in \mathbb{N}$. Next setting $\upsilon_{m+1} = \upsilon_1$, we obtain infinitely many positive solutions $\{(\upsilon_1^{[r]}, \upsilon_2^{[r]}, \ldots, \upsilon_m^{[r]})\}_{r=1}^{\infty}$ of (1.1)–(1.2) given iteratively by

$$\upsilon_\ell(t) = \int_0^{\mathfrak{T}} \aleph(t,\tau)\lambda(\tau)\mathrm{g}_\ell(\upsilon_{\ell+1}(\tau))\Delta\tau,\ t \in (0,\mathfrak{T})_{\mathbb{T}},\ \ell = m, m-1, \ldots, 1.$$

The proof is completed. □

For $\sum_{i=1}^{n} \frac{1}{p_i} = 1$, we have the following theorem.

Theorem 3.5. *Suppose* (H_1)–(H_3) *hold, let* $\{\varepsilon_r\}_{r=1}^{\infty}$ *be such that* $0 < \varepsilon_1 < \mathfrak{T}/2$, $\varepsilon \downarrow t^*$ *and* $0 < t^* < t_n$. *Let* $\{\Gamma_r\}_{r=1}^{\infty}$ *and* $\{\Lambda_r\}_{r=1}^{\infty}$ *be such that*

$$\Gamma_{r+1} < \mathcal{G}(\varepsilon_r)\Lambda_r < \Lambda_r < \theta\Lambda_r < \Gamma_r, \ r \in \mathbb{N},$$

where

$$\theta = \max\left\{ \left[\mathcal{G}(\varepsilon_1) \prod_{i=1}^{k} \delta_i \int_{\varepsilon_1}^{\mathfrak{T}-\varepsilon_1} \aleph(\tau,\tau)\Delta\tau \right]^{-1}, \ 1 \right\}.$$

Assume that g_ℓ *satisfies* (C_2) *and*

(C_3) $\mathrm{g}_j(\upsilon) \le \mathfrak{N}_2\Gamma_r \ \forall \ t \in (0,\mathfrak{T})_{\mathbb{T}}$, $0 \le \upsilon \le \Gamma_r$, *where*

$$\mathfrak{N}_2 < \min\left\{ \left[\|\aleph\|_{L_\Delta^\infty} \prod_{i=1}^{k} \|\lambda_i\|_{L_\Delta^{p_i}} \right]^{-1}, \theta \right\}.$$

Then the iterative boundary value problem (1.1)–(1.2) *has infinitely many solutions* $\{(\upsilon_1^{[r]}, \upsilon_2^{[r]}, \ldots, \upsilon_m^{[r]})\}_{r=1}^{\infty}$ *such that* $\upsilon_\ell^{[r]}(t) \ge 0$ *on* $(0,\mathfrak{T})_{\mathbb{T}}$, $\ell = 1, 2, \ldots, m$ *and* $r \in \mathbb{N}$.

Proof. For a fixed r, let $\mathtt{M}_{1,r}$ be as in the proof of Theorem 3.4 and let $\upsilon_1 \in \mathtt{K}_{\varepsilon_r} \cap \partial\mathtt{M}_{2,r}$. Again

$$\upsilon_1(\tau) \le \Gamma_r = \|\upsilon_1\|,$$

for all $\tau \in (0,\mathfrak{T})_{\mathbb{T}}$. By (C_3) and for $\tau_{\ell-1} \in (0,\mathfrak{T})_{\mathbb{T}}$, we have

$$\begin{aligned}
\int_0^{\mathfrak{T}} \aleph(\tau_{m-1},\tau_m)\lambda(\tau_m)\mathrm{g}_m(\upsilon_1(\tau_m))\Delta\tau_m &\le \int_0^{\mathfrak{T}} \aleph(\tau_m,\tau_m)\lambda(\tau_m)\mathrm{g}_m(\upsilon_1(\tau_m))\Delta\tau_m \\
&\le \mathfrak{N}_1\Gamma_r \int_0^{\mathfrak{T}} \aleph(\tau_m,\tau_m) \prod_{i=1}^{k} \lambda_i(\tau_m)\Delta\tau_m \\
&\le \mathfrak{N}_1\Gamma_r \|\aleph\|_{L_\Delta^\infty} \left\| \prod_{i=1}^{k} \lambda_i \right\|_{L_\Delta^{p_i}} \\
&\le \mathfrak{N}_1\Gamma_r \|\aleph\|_{L_\Delta^\infty} \prod_{i=1}^{k} \|\lambda_i\|_{L_\Delta^{p_i}} \le \Gamma_r.
\end{aligned}$$

It follows in similar manner (for $\tau_{m-2} \in [0,1]_{\mathbb{T}}$), that

$$\begin{aligned}\int_0^{\mathfrak{T}} \aleph(\tau_{m-2},\tau_{m-1})\lambda(\tau_{m-1})\mathtt{g}_{m-1}\bigg(\int_0^{\mathfrak{T}} \aleph(\tau_{m-1},\tau_m)\lambda(\tau_m)\mathtt{g}_m(\upsilon_1(\tau_m))\Delta\tau_m\bigg)\Delta\tau_{m-1}&\\ \leq \int_0^{\mathfrak{T}} \aleph(\tau_{m-2},\tau_{m-1})\lambda(\tau_{m-1})\mathtt{g}_{m-1}(\Gamma_r)\Delta\tau_{m-1}&\\ \leq \int_0^{\mathfrak{T}} \aleph(\tau_{m-1},\tau_{m-1})\lambda(\tau_{m-1})\mathtt{g}_{m-1}(\Gamma_r)\Delta\tau_{m-1}&\\ \leq \mathfrak{N}_1\Gamma_r\int_0^{\mathfrak{T}} \aleph(\tau_{m-1},\tau_{m-1})\prod_{i=1}^{k}\lambda_i(\tau_{m-1})\Delta\tau_{m-1}&\\ \leq \mathfrak{N}_1\Gamma_r\|\aleph\|_{L^{\infty}_{\Delta}}\prod_{i=1}^{k}\|\lambda_i\|_{L^{p_i}_{\Delta}} \leq \Gamma_r.&\end{aligned}$$

Continuing with this bootstrapping argument, we get

$$\begin{aligned}(\Omega\upsilon_1)(t) = \int_0^{\mathfrak{T}} \aleph(t,\tau_1)\lambda(\tau_1)\mathtt{g}_1\bigg(\int_0^{\mathfrak{T}} \aleph(\tau_1,\tau_2)\lambda(\tau_2)\mathtt{g}_2\bigg(\int_0^{\mathfrak{T}} \aleph(\tau_2,\tau_3)\cdots&\\ \times \mathtt{g}_{m-1}\bigg(\int_0^{\mathfrak{T}} \aleph(\tau_{m-1},\tau_m)\lambda(\tau_m)\mathtt{g}_m(\upsilon_1(\tau_m))\Delta\tau_m\bigg)\cdots\Delta\tau_3\bigg)\Delta\tau_2\bigg)\Delta\tau_1&\\ \leq \Gamma_r.&\end{aligned}$$

Since $\Gamma_r = \|\upsilon_1\|$ for $\upsilon_1 \in \mathtt{K}_{\varepsilon_r} \cap \partial\mathtt{M}_{1,r}$, we get

$$\|\Omega\upsilon_1\| \leq \|\upsilon_1\|. \tag{3.3}$$

Now define $\mathtt{M}_{2,r} = \{\upsilon_1 \in \mathtt{B} : \|\upsilon_1\| < \Lambda_r\}$. Let $\upsilon_1 \in \mathtt{K}_{\varepsilon_r} \cap \partial\mathtt{M}_{2,r}$ and let $\tau \in [\varepsilon_r,\, \mathfrak{T}-\varepsilon_r]_{\mathbb{T}}$. Then, the argument leading to (3.2) can be done to the present case. Hence, the theorem. □

Lastly, the case $\displaystyle\sum_{i=1}^{n}\frac{1}{p_i} > 1$.

Theorem 3.6. *Suppose (H_1)–(H_3) hold, let $\{\varepsilon_r\}_{r=1}^{\infty}$ be such that $0 < \varepsilon_1 < \mathfrak{T}/2$, $\varepsilon \downarrow t^*$ and $0 < t^* < t_n$. Let $\{\Gamma_r\}_{r=1}^{\infty}$ and $\{\Lambda_r\}_{r=1}^{\infty}$ be such that*

$$\Gamma_{r+1} < \mathcal{G}(\varepsilon_r)\Lambda_r < \Lambda_r < \theta\Lambda_r < \Gamma_r,\ r \in \mathbb{N},$$

where

$$\theta = \max\bigg\{\bigg[\mathcal{G}(\varepsilon_1)\prod_{i=1}^{k}\delta_i\int_{\varepsilon_1}^{\mathfrak{T}-\varepsilon_1}\aleph(\tau,\tau)\Delta\tau\bigg]^{-1},\ 1\bigg\}.$$

Assume that $\mathtt{g}_\ell$ satisfies (C_2) and

(C_4) $\mathtt{g}_j(\upsilon) \leq \mathfrak{N}_3\Gamma_r\ \forall\ t \in (0,\mathfrak{T})_{\mathbb{T}}$, $0 \leq \upsilon \leq \Gamma_r$, *where* $\mathfrak{N}_3 < \min\bigg\{\bigg[\|\aleph\|_{L^{\infty}_{\Delta}}\prod_{i=1}^{k}\|\lambda_i\|_{L^{1}_{\Delta}}\bigg]^{-1}, \theta\bigg\}$.

Then the iterative boundary value problem (1.1)–(1.2) *has infinitely many solutions $\{(\upsilon_1^{[r]},\upsilon_2^{[r]},\ldots,\upsilon_m^{[r]})\}_{r=1}^{\infty}$ such that $\upsilon_\ell^{[r]}(t) \geq 0$ on $(0,\mathfrak{T})_{\mathbb{T}}$, $\ell = 1,2,\ldots,m$ and $r \in \mathbb{N}$.*

Proof. The proof is similar to the proof of Theorem 3.4. So, we omit the details here. □

4 Example

In this section, we present an example to check validity of our main results.

Example 4.1. Consider the following boundary value problem on $\mathbb{T} = \mathbb{R}$.

$$\left.\begin{aligned} \upsilon_\ell''(t) + \lambda(t)\mathrm{g}_\ell(\upsilon_{\ell+1}(t)) = 0,\ \ell = 1,2, \\ \upsilon_3(t) = \upsilon_1(t), \end{aligned}\right\} \tag{4.1}$$

$$\left.\begin{aligned} \upsilon_\ell(0) = \upsilon_\ell'(0), \\ \upsilon_\ell(1) = -\upsilon_\ell'(1), \end{aligned}\right\} \tag{4.2}$$

where

$$\lambda(t) = \lambda_1(t)\lambda_2(t)$$

in which

$$\lambda_1(t) = \frac{1}{|t-\frac{1}{4}|^{\frac{1}{2}}} \quad \text{and} \quad \lambda_2(t) = \frac{1}{|t-\frac{3}{4}|^{\frac{1}{2}}},$$

$$\mathrm{g}_1(\upsilon) = \mathrm{g}_2(\upsilon) = \begin{cases} \frac{1}{5}\times 10^{-4}, & \upsilon \in (10^{-4}, +\infty), \\ \frac{25\times 10^{-(4r+3)} - \frac{1}{5}\times 10^{-4r}}{10^{-(4r+3)} - 10^{-4r}}(\upsilon - 10^{-4r}) + & \\ \frac{1}{5}\times 10^{-8r}, & \upsilon \in \left[10^{-(4r+3)}, 10^{-4r}\right], \\ 25\times 10^{-(4r+3)}, & \upsilon \in \left(\frac{1}{5}\times 10^{-(4r+3)}, 10^{-(4r+3)}\right), \\ \frac{25\times 10^{-(4r+3)} - \frac{1}{5}\times 10^{-8r}}{\frac{1}{5}\times 10^{-(4r+3)} - 10^{-(4r+4)}}(\upsilon - 10^{-(4r+4)}) + & \\ \frac{1}{5}\times 10^{-8r}, & \upsilon \in \left(10^{-(4r+4)}, \frac{1}{5}\times 10^{-(4r+3)}\right], \\ 0, & \upsilon = 0. \end{cases}$$

Let

$$t_r = \frac{31}{64} - \sum_{k=1}^{r} \frac{1}{4(k+1)^4}, \quad \varepsilon_r = \frac{1}{2}(t_r + t_{r+1}), \quad r = 1,2,3,\ldots,$$

then

$$\varepsilon_1 = \frac{15}{32} - \frac{1}{648} < \frac{15}{32},$$

and

$$t_{r+1} < \varepsilon_r < t_r, \quad \varepsilon_r > \frac{1}{5}.$$

Therefore,

$$\mathcal{G}(\varepsilon_r) = \frac{\varepsilon_r + 1}{\mathfrak{T} + 1} = \frac{\varepsilon_r + 1}{2} > \frac{1}{5}, \quad r = 1,2,3,\ldots$$

It is clear that

$$t_1 = \frac{15}{32} < \frac{1}{2}, \quad t_r - t_{r+1} = \frac{1}{4(r+2)^4}, \quad r = 1,2,3,\ldots$$

Since $\sum_{x=1}^{\infty} \frac{1}{x^4} = \frac{\pi^4}{90}$ and $\sum_{x=1}^{\infty} \frac{1}{x^2} = \frac{\pi^2}{6}$, it follows that

$$t^* = \lim_{r\to\infty} t_r = \frac{31}{64} - \sum_{k=1}^{\infty} \frac{1}{4(r+1)^4} = \frac{47}{64} - \frac{\pi^4}{360} = 0.4637941914,$$

$$\lambda_1, \lambda_2 \in L^p[0,1] \text{ for all } 0 < p < 2, \text{ and } \delta_1 = \delta_2 = (4/3)^{1/4},$$

$$\mathcal{G}(\varepsilon_1) = 0.7336033951.$$

$$\int_{\varepsilon_1}^{\mathfrak{T}-\varepsilon_1} \aleph(\tau,\tau)\Delta\tau = \int_{\frac{15}{32}-\frac{1}{648}}^{1-\frac{15}{32}+\frac{1}{648}} \frac{(2-\tau)(1+\tau)}{3} d\tau = 0.04918197801.$$

Thus, we get

$$\begin{aligned}\theta &= \max\left\{\left[\mathcal{G}(\varepsilon_1)\prod_{i=1}^{k}\delta_i\int_{\varepsilon_1}^{\mathfrak{T}-\varepsilon_1}\aleph(\tau,\tau)\nabla\tau\right]^{-1}, 1\right\}\\ &= \max\left\{\frac{1}{0.04166167167}, 1\right\}\\ &= 24.00287746.\end{aligned}$$

Next, let $0 < \mathfrak{a} < 1$ be fixed. Then $\lambda_1, \lambda_2 \in L^{1+\mathfrak{a}}[0,1]$ and $\frac{2}{1+\mathfrak{a}} > 1$ for $0 < \mathfrak{a} < 1$. It follows that

$$\prod_{i=1}^{k} \|\lambda_i\|_{L_\Delta^{p_i}} \approx \pi - \ln(7 - 4\sqrt{3}),$$

and also $\|\aleph\|_\infty = \frac{2}{3}$. So, for $0 < \mathfrak{a} < 1$, we have

$$\mathfrak{N}_1 < \left[\|\aleph\|_\infty \prod_{i=1}^{k} \|\lambda_i\|_{L_\Delta^{p_i}}\right]^{-1} \approx 0.2597173925.$$

Taking $\mathfrak{N}_1 = \frac{1}{4}$. In addition if we take

$$\Gamma_r = 10^{-4r}, \quad \Lambda_r = 10^{-(4r+3)},$$

then

$$\Gamma_{r+1} = 10^{-(4r+4)} < \frac{1}{5} \times 10^{-(4r+3)} < \mathcal{G}(\varepsilon_r)\Lambda_r < \Lambda_r = 10^{-(4r+3)} < \Gamma_r = 10^{-4r},$$

$\theta\Lambda_r = 24.00287746 \times 10^{-(4r+3)} < \frac{1}{4} \times 10^{-4r} = \mathfrak{N}_1\Gamma_r$, $r = 1, 2, 3, \ldots$, and $\mathfrak{g}_1, \mathfrak{g}_2$ satisfy the following growth conditions:

$$\begin{aligned}&\mathfrak{g}_1(\upsilon) = \mathfrak{g}_2(\upsilon) \le \mathfrak{N}_1\Gamma_r = \frac{1}{4} \times 10^{-4r}, \quad \upsilon \in \left[0, 10^{-4r}\right],\\ &\mathfrak{g}_1(\upsilon) = \mathfrak{g}_2(\upsilon) \ge \theta\Lambda_r = 24.00287746 \times 10^{-(4r+3)}, \quad \upsilon \in \left[\frac{1}{5} \times 10^{-(4r+3)}, 10^{-(4r+3)}\right].\end{aligned}$$

Then all the conditions of Theorem 3.4 are satisfied. Therefore, by Theorem 3.4, the iterative boundary value problem (1.1) has infinitely many solutions $\{(\upsilon_1^{[r]}, \upsilon_2^{[r]})\}_{r=1}^{\infty}$ such that $\upsilon_\ell^{[r]}(t) \ge 0$ on $[0,1]$, $\ell = 1, 2$ and $r \in \mathbb{N}$.

Acknowledgements

The authors would like to thank the referees for their valuable suggestions and comments for the improvement of the paper.

References

[1] R. P. Agarwal and M. Bohner, "Basic calculus on time scales and some of its applications", Results Math., vol. 35, no. 1–2, pp. 3–22, 1999.

[2] R. P. Agarwal, M. Bohner, D. O'Regan and A. Peterson, "Dynamic equations on time scales: a survey", J. Comput. Appl. Math., vol. 141, no. 1-2, pp. 1–26, 2002.

[3] R. P. Agarwal, V. Otero-Espinar, K. Perera and D. R. Vivero, "Basic properties of Sobolev's spaces on time scales", Adv. Difference. Equ., Art. ID 38121, 14 pages, 2006.

[4] G. A. Anastassiou, *Intelligent mathematics: computational analysis*, Intelligent Systems Reference Library, vol. 5, Heidelberg: Springer, 2011.

[5] M. Bohner and H. Luo, "Singular second-order multipoint dynamic boundary value problems with mixed derivatives", Adv. Difference Equ., Art. ID 54989, 15 pages, 2006.

[6] M. Bohner and A. Peterson, *Dynamic equations on time scales: An introduction with applications*, Boston: Birkhäuser Boston, Inc., 2001.

[7] M. Bohner and A. Peterson, *Advances in dynamic equations on time scales*, Boston: Birkhäuser Boston, Inc., 2003.

[8] A. Dogan, "Positive solutions of the p-Laplacian dynamic equations on time scales with sign changing nonlinearity", Electron. J. Differential Equations, Paper No. 39, 17 pages, 2018.

[9] A. Dogan, "Positive solutions of a three-point boundary-value problem for p-Laplacian dynamic equation on time scales".‘ Ukraïn. Mat. Zh., vol. 72, no. 6, pp. 790–805, 2020.

[10] D. Guo and V. Lakshmikantham, *Nonlinear problems in abstract cones*, Boston: Academic Press, 1988.

[11] G. S. Guseinov, "Integration on time scales", J. Math. Anal. Appl., vol. 285, no.1, pp. 107–127, 2003.

[12] M. Khuddush, K. R. Prasad and K. V. Vidyasagar, "Infinitely many positive solutions for an iterative system of singular multipoint boundary value problems on time scales", Rend. Circ. Mat. Palermo, ll Ser., 2021. doi: 10.1007/s12215-021-00650-6

[13] C. Kunkel, "Positive solutions to singular second-order boundary value problems on time scales", Adv. Dyn. Syst. Appl., vol. 4, no. 2, pp. 201–211, 2019.

[14] S. Liang and J. Zhang, "The existence of countably many positive solutions for nonlinear singular m-point boundary value problems on time scales", J. Comput. Appl. Math., vol. 223, no. 1, pp. 291–303, 2009.

[15] U. M. Özkan, M. Z. Sarikaya and H. Yildirim, "Extensions of certain integral inequalities on time scales", Appl. Math. Lett., vol. 21, no. 10, pp. 993–1000, 2008.

[16] K. R. Prasad and M. Khuddush, "Countably infinitely many positive solutions for even order boundary value problems with Sturm-Liouville type integral boundary conditions on time scales", Int. J. Anal. Appl., vol. 15, no. 2, pp. 198–210, 2017.

[17] K. R. Prasad and M. Khuddush, "Existence of countably many symmetric positive solutions for system of even order time scale boundary value problems in Banach spaces", Creat. Math. Inform., vol. 28, no. 2, pp. 163–182, 2019.

[18] K. R. Prasad, M. Khuddush and K. V. Vidyasagar, "Denumerably many positive solutions for iterative systems of singular two-point boundary value problems on time scales", Int. J. Difference Equ., vol. 15, no. 1, pp. 153–172, 2020.

[19] S. Tikare and C. C. Tisdell, "Nonlinear dynamic equations on time scales with impulses and nonlocal conditions", J. Class. Anal., vol. 16, no. 2, pp. 125–140, 2020.

[20] P. A. Williams, "Unifying fractional calculus with time scales", Ph.D. thesis, University of Melbourne, Melbourne, Australia, 2012.

ANNALI DELL'UNIVERSITA' DI FERRARA (2022) 68:187–201
https://doi.org/10.1007/s11565-022-00395-9

Global existence and blowup of solutions for a semilinear Klein-Gordon equation with the product of logarithmic and power-type nonlinearity

Mahammad Khuddush[1] · K. Rajendra Prasad[2] · B. Bharathi[3]

Received: 8 June 2021 / Accepted: 17 March 2022 / Published online: 4 April 2022
© The Author(s) under exclusive license to Università degli Studi di Ferrara 2022

Abstract
In this paper we study the initial boundary value problem of a semilinear Klein-Gordon equation with the multiplication of logarithmic and polynomial nonlinearities. By using potential well method and energy method, we obtain the existence of global solutions and finite-time blowup solutions.

Keywords Global existence · Klein-Gordan equation · Blowup · Logarithmic nonlinearity · Potential well

Mathematics Subject Classification 35L05 · 35L10 · 35B40

1 Introduction

In this paper we consider the following initial boundary value problem for a semilinear Klein-Gordan equation with polynomial nonlinearity of the factor of logarithmic term

$$\left.\begin{aligned} &\frac{\partial^2 \mathrm{z}}{\partial t^2} - \Delta \mathrm{z} + \mathrm{z} = |\mathrm{z}|^{\mathrm{p}} \log |\mathrm{z}|, && x \in \Omega,\ t > 0, \\ &\mathrm{z}(x,0) = \mathrm{z}_0(x),\ \frac{\partial \mathrm{z}}{\partial t}(x,0) = \mathrm{z}_1(x), && x \in \Omega, \\ &\mathrm{z}(x,t) = 0, && x \in \partial\Omega,\ t > 0, \end{aligned}\right\} \tag{1}$$

✉ Mahammad Khuddush
khuddush89@gmail.com

[1] Department of Mathematics, Dr. Lankapalli Bullayya College, Visakhapatnam, Andhra Pradesh 530013, India

[2] Department of Applied Mathematics, College of Science and Technology, Andhra University, Visakhapatnam 530003, India

[3] Department of Mathematics, College of Engineering for Women, Gayatri Vidya Parishad, Visakhapatnam 530048, India

where Ω is a bounded domain $\mathbb{R}^n$ and $1 < \mathrm{p} < \infty$ if $n = 1, 2$ and $2 < \mathrm{p} < \frac{4}{n-2} (3 \leq n \leq 5)$ are constants.

The Klein-Gordon equation is the first relativistic equation in quantum mechanics for the wave function of a particle with zero spin. It was proposed as a relativistic generalization of the Schrodinger equation and was investigated in many papers [1, 6–8, 10, 12, 13, 17, 22, 27, 29, 32]. The problem (1) is applied in many branches of physics such as nuclear physics, optics and geophysics [5, 9, 18]. In [31] Yang and Xu studied the following nonlinear Klein-Gordon equations with arbitrarily positive initial energy

$$\begin{aligned} &\frac{\partial^2 \mathrm{z}}{\partial t^2} - \Delta \mathrm{z} + \mathrm{z} = \mathrm{f}(\mathrm{z}), \qquad (x,t) \in \mathbb{R}^n \times (0, +\infty), \\ &\mathrm{z}(x,0) = \mathrm{z}_0(x), \qquad \frac{\partial \mathrm{z}}{\partial t}(x,0) = \mathrm{z}_1(x), \quad x \in \mathbb{R}^n. \end{aligned}$$

By applying concavity method they derived sufficient conditions on initial data such that the solution blows up in finite time. In [26], Liu and Ahmad studied the following Klein-Gordon equations with arbitrarily positive initial energy

$$\begin{aligned} &\frac{\partial^2 \mathrm{z}}{\partial t^2} - \Delta \mathrm{z} + \mathrm{z} = a_1 |\mathrm{z}|^p + \sum_{k=2}^{l} a_k |\mathrm{z}|^{p_k - 1} \mathrm{z} - \sum_{j=1}^{s} b_j |\mathrm{z}|^{q_j - 1} \mathrm{z}, \ x \in \mathbb{R}^n, t > 0, \\ &\mathrm{z}(x,0) = \mathrm{z}_0(x), \ \frac{\partial \mathrm{z}}{\partial t}(x,0) = \mathrm{z}_1(x), \quad x \in \mathbb{R}^n. \end{aligned}$$

and they proved the global existence and finite time blow up of solution with low and critical initial energy levels by applying the potential well and convexity methods.

In the following we quote few works with logarithmic nonlinearity which gives some information to study problem (1). In [23], Lian and Xu studied the following nonlinear wave equation with weak and strong damping terms and logarithmic source term at three different initial energy levels

$$\begin{aligned} &\frac{\partial^2 \mathrm{z}}{\partial t^2} - \Delta \mathrm{z} - \omega \Delta \frac{\partial \mathrm{z}}{\partial t} + \mu \frac{\partial \mathrm{z}}{\partial t} = \mathrm{z} \log |\mathrm{z}|, \qquad (x,t) \in \mathbb{R}^n \times (0, +\infty), \\ &\mathrm{z}(x,0) = \mathrm{z}_0(x), \ \frac{\partial \mathrm{z}}{\partial t}(x,0) = \mathrm{z}_1(x), \qquad x \in \mathbb{R}^n, \\ &\mathrm{z}(x,t) = 0, \qquad x \in \partial\Omega, \ t > 0, \end{aligned}$$

In [14], Gorka studied the following problem

$$\left.\begin{aligned} &\frac{\partial^2 \mathrm{z}}{\partial t^2} - \Delta \mathrm{z} + \mathrm{z} = \varepsilon \mathrm{z} \log |\mathrm{z}|^2, \qquad x \in \mathcal{O}, \ t > 0, \\ &\mathrm{z}(x,0) = \mathrm{z}_0(x), \ \frac{\partial \mathrm{z}}{\partial t}(x,0) = \mathrm{z}_1(x), \qquad x \in \mathcal{O}, \\ &\mathrm{z}(x,t) = 0, \qquad x \in \partial\mathcal{O}, \ t > 0, \end{aligned}\right\} \tag{2}$$

where $\mathcal{O} = [a, b]$, the parameter ε measures the force of the nonlinear interactions. The problem (2) is a relativistic version of logarithmic quantum mechanics introduced by I. Bialynicki-Birula and J. Mycielski [3, 4]. In [16] Hiramatsu et al., introduced the following equation

$$\left.\begin{aligned} &\frac{\partial^2 \mathrm{z}}{\partial t^2} - \Delta \mathrm{z} + \mathrm{z} + \frac{\partial \mathrm{z}}{\partial t} + \mathrm{z}|\mathrm{z}|^2 = \mathrm{z}\log|\mathrm{z}|^2, && x \in \Omega,\ t > 0,\\ &\mathrm{z}(x,0) = \mathrm{z}_0(x),\ \frac{\partial \mathrm{z}}{\partial t}(x,0) = \mathrm{z}_1(x), && x \in \Omega,\\ &\mathrm{z}(x,t) = 0, && x \in \partial\Omega,\ t > 0, \end{aligned}\right\} \tag{3}$$

for studying the dynamics of Q-ball in theoretical physics. The logarithmic nonlinearity appears in inflation cosmology and supersymmetric field theories, quantum mechanics and nuclear physics [2, 11, 24]. By using the same method and technique as the one in [14], Han [15] studied the weak solution of the problem (3). Recently by using potential well method, Lian et al. [21] studied existence of global and blowup of solutions for the semilinear hyperbolic equation

$$\begin{aligned} &\frac{\partial^2 \mathrm{z}}{\partial t^2} - \Delta \mathrm{z} = |\mathrm{z}|^{\mathrm{p}}\log|\mathrm{z}|, && x \in \Omega,\ t > 0,\ k > 1,\\ &\mathrm{z}(x,0) = \mathrm{z}_0(x),\ \frac{\partial \mathrm{z}}{\partial t}(x,0) = \mathrm{z}_1(x), && x \in \Omega,\\ &\mathrm{z}(x,t) = 0, && x \in \partial\Omega,\ t > 0. \end{aligned}$$

In [28], Peng and Zhou studied the initial boundary value problem of a semilinear heat equation with logarithmic nonlinearity

$$\begin{aligned} &\frac{\partial \mathrm{z}}{\partial t} - \Delta \mathrm{z} = |\mathrm{z}|^{\mathrm{p}-2}\mathrm{z}\log|\mathrm{z}|, && x \in \Omega,\ t > 0,\\ &\mathrm{z}(x,0) = \mathrm{z}_0(x), && x \in \Omega,\\ &\mathrm{z}(x,t) = 0, && x \in \partial\Omega,\ t > 0. \end{aligned}$$

and obtained the existence of global solutions and finite-time blowup solutions by using potential well method. Motivated by the works mentioned above, in this paper we studied existence of global solutions and finite-time blowup of solutions for the problem (1) by utilizing potential well method.

2 Preliminaries

Let $\mathcal{H}^1(\Omega)$ denote the Sobolev space with the usual scalar products and norm. $\mathcal{H}_0^1(\Omega)$ denotes the closure in $\mathcal{H}^1(\Omega)$ of $\mathcal{C}_0^\infty(\Omega)$. For simplicity of notations, hereafter we denote by $\|\cdot\|_{\mathrm{p}}$ the Lebesgue space $\mathrm{L}^{\mathrm{p}}(\Omega)$ norm and $\|\cdot\|$ denotes $\mathrm{L}^2(\Omega)$ norm. Now

we endowed the norm for $\mathcal{H}_0^1(\Omega)$:

$$\|\mathtt{z}\|^2_{\mathcal{H}_0^1(\Omega)} = \|\mathtt{z}\|^2 + \|\nabla \mathtt{z}\|^2.$$

Definition 1 The function $\mathtt{z} = \mathtt{z}(x,t)$ is said to be a weak solutions of (1) on $\Omega \times [0,\mathtt{T})$ if $\mathtt{z} \in \mathcal{C}\big([0,\mathtt{T}], \mathcal{H}_0^1(\Omega)\big)$, $\mathtt{z}_t \in \mathcal{C}^1\big([0,\mathtt{T}], \mathtt{L}^2(\Omega)\big)$, $\mathtt{z}_{tt} \in \mathcal{C}\big([0,\mathtt{T}], \mathcal{H}^{-1}(\Omega)\big)$ such that $\mathtt{z}(x,0) = \mathtt{z}_0(x)$ in $\mathcal{H}_0^1(\Omega)$, $\mathtt{z}_t(x,0) = \mathtt{z}_1(x)$ in $\mathtt{L}^2(\Omega)$ and

$$(\mathtt{z}_t, \omega) + \int_\Omega (\nabla \mathtt{z}, \nabla \omega) d\tau + \int_\Omega (\mathtt{z}, \omega) d\tau = \int_\Omega (|\mathtt{z}|^{\mathtt{p}} \log |\mathtt{z}|, \omega) d\tau + (\mathtt{z}_1, \omega)$$

for any $\omega \in \mathcal{H}_0^1(\Omega)$, $t \in [0,\mathtt{T})$ and $\mathtt{z}$ holds the energy inequality $\mathtt{E}(t) \leq \mathtt{E}(0)$ for every $t \in [0,\mathtt{T})$, where

$$\mathtt{E}(t) = \frac{1}{2}\|\mathtt{z}_t\|^2 + \frac{1}{2}\|\mathtt{z}\|^2_{\mathcal{H}_0^1(\Omega)} - \frac{1}{\mathtt{p}+1}\int_\Omega |\mathtt{z}|^{\mathtt{p}+1} \log |\mathtt{z}| dx + \frac{1}{(\mathtt{p}+1)^2}\|\mathtt{z}\|^{\mathtt{p}+1}_{\mathtt{p}+1}$$

and

$$\mathtt{E}(0) = \frac{1}{2}\|\mathtt{z}_1\|^2 + \frac{1}{2}\|\mathtt{z}_0\|^2_{\mathcal{H}_0^1(\Omega)} - \frac{1}{\mathtt{p}+1}\int_\Omega |\mathtt{z}_0|^{\mathtt{p}+1} \log |\mathtt{z}_0| dx + \frac{1}{(\mathtt{p}+1)^2}\|\mathtt{z}_0\|^{\mathtt{p}+1}_{\mathtt{p}+1}.$$

2.1 Potential wells

Define two real-valued $\mathcal{C}^1$ functionals on $\mathcal{H}_0^1(\Omega)$, known as potential energy and Nehari functionals and are

$$\mathtt{J}(\mathtt{z}) = \frac{1}{2}\|\mathtt{z}\|^2_{\mathcal{H}_0^1(\Omega)} - \frac{1}{\mathtt{p}+1}\int_\Omega |\mathtt{z}|^{\mathtt{p}+1} \log |\mathtt{z}| dx + \frac{1}{(\mathtt{p}+1)^2}\|\mathtt{z}\|^{\mathtt{p}+1}_{\mathtt{p}+1}$$

and

$$\mathtt{I}(\mathtt{z}) = \langle \mathtt{J}'(\mathtt{z}), \mathtt{z}\rangle = \|\mathtt{z}\|^2_{\mathcal{H}_0^1(\Omega)} - \int_\Omega |\mathtt{z}|^{\mathtt{p}+1} \log |\mathtt{z}| dx,$$

where $\langle\,,\rangle$ denotes the dual pairing between $\mathcal{H}^{-1}(\Omega)$ and $\mathcal{H}_0^1(\Omega)$. Then it is clear that

$$\mathtt{J}(\mathtt{z}) = \left[\frac{\mathtt{p}-1}{2(\mathtt{p}+1)}\right]\|\mathtt{z}\|^2_{\mathcal{H}_0^1(\Omega)} + \frac{1}{\mathtt{p}+1}\mathtt{I}(\mathtt{z}) + \frac{1}{(\mathtt{p}+1)^2}\|\mathtt{z}\|^{\mathtt{p}+1}_{\mathtt{p}+1} \tag{4}$$

and

$$\mathtt{E}(t) = \frac{1}{2}\|\mathtt{z}_t\|^2 + \mathtt{J}(\mathtt{z}). \tag{5}$$

Next, define Nehari manifold as

$$\mathtt{N}(\mathtt{z}) = \{\mathtt{z} \in \mathcal{H}_0^1(\Omega) \,|\, \mathtt{I}(\mathtt{z}) = 0, \mathtt{z} \neq 0\}.$$

It is easy to show that each half line starting from the origin of $\mathcal{H}_0^1(\Omega)$ intersects exactly once the manifold $\mathtt{N}$ separates the two unbounded sets $\mathtt{N}$ separates the two unbounded sets

$$\mathtt{N}^+ = \{\mathtt{z} \in \mathcal{H}_0^1(\Omega) \,|\, \mathtt{I}(\mathtt{z}) > 0\} \cup \{0\},$$

$$\mathtt{N}^- = \{\mathtt{z} \in \mathcal{H}_0^1(\Omega) \,|\, \mathtt{I}(\mathtt{z}) < 0\}.$$

The mountain pass level of $\mathtt{J}(\mathtt{z})$ (also known as potential well depth) is defined as

$$\mathrm{d} = \inf\{\mathtt{J}(\mathtt{z}) \,|\, \mathtt{z} \in \mathtt{N}\}. \tag{6}$$

Finally, we define the potential well

$$\mathrm{W} = \{\mathtt{z} \in \mathcal{H}_0^1(\Omega) \,|\, \mathtt{I}(\mathtt{z}) > 0, \mathtt{J}(\mathtt{z}) < \mathrm{d}\} \cup \{0\}$$

and the outer of the potential well

$$\mathrm{V} = \{\mathtt{z} \in \mathcal{H}_0^1(\Omega) \,|\, \mathtt{I}(\mathtt{z}) < 0, \mathtt{J}(\mathtt{z}) < \mathrm{d}\}.$$

Let ρ be any fixed positive real number. Now we extend above single potential wells to the family of potential wells as

$$\mathtt{J}_\rho(\mathtt{z}) = \frac{\rho}{2}\|\mathtt{z}\|^2_{\mathcal{H}_0^1(\Omega)} - \frac{1}{\mathtt{p}+1}\int_\Omega |\mathtt{z}|^{\mathtt{p}+1}\log|\mathtt{z}|dx + \frac{1}{(\mathtt{p}+1)^2}\|\mathtt{z}\|^{\mathtt{p}+1}_{\mathtt{p}+1}$$

and

$$\mathtt{I}_\rho(\mathtt{z}) = \langle \mathtt{J}'_\rho(\mathtt{z}), \mathtt{z}\rangle = \rho\|\mathtt{z}\|^2_{\mathcal{H}_0^1(\Omega)} - \int_\Omega |\mathtt{z}|^{\mathtt{p}+1}\log|\mathtt{z}|dx,$$

The Nehari manifold as

$$\mathtt{N}_\rho(\mathtt{z}) = \{\mathtt{z} \in \mathcal{H}_0^1(\Omega) \,|\, \mathtt{I}_\rho(\mathtt{z}) = 0, \mathtt{z} \neq 0\}$$

and the depth of the potential well (or mountain pass level) as

$$\mathrm{d}(\rho) = \inf\left\{\mathtt{J}(\mathtt{z}) \mid \mathtt{z} \in \mathtt{N}_\rho\right\}. \tag{7}$$

Finally, the potential well

$$\mathrm{W}_\rho = \{\mathtt{z} \in \mathcal{H}_0^1(\Omega) \mid \mathtt{I}_\rho(\mathtt{z}) > 0, \mathtt{J}_\rho(\mathtt{z}) < \mathrm{d}(\rho)\} \cup \{0\}$$

and the outer of the potential well

$$\mathrm{V}_\rho = \{\mathtt{z} \in \mathcal{H}_0^1(\Omega) \mid \mathtt{I}_\rho(\mathtt{z}) < 0, \mathtt{J}_\rho(\mathtt{z}) < \mathrm{d}(\rho)\}.$$

In the next lemma we seek unique positive critical point of $\mathtt{J}(\lambda\mathtt{z})$.

Lemma 1 *Let* $\mathtt{z} \in \mathcal{H}_0^1(\Omega)$ *with* $\|\mathtt{z}\| \neq 0$ *and let* $\mathtt{f}(\lambda) = \mathtt{J}(\lambda\mathtt{z})$, *then we have*

(i) $\lim_{\lambda\to 0} \mathtt{f}(\lambda) = 0$ *and* $\lim_{\lambda\to+\infty} \mathtt{f}(\lambda) = -\infty$,

(ii) there exists unique $\lambda^* = \lambda^*(\mathtt{z})$ *in the interval* $(0, +\infty)$ *such that* $\mathtt{f}'(\lambda)|_{\lambda=\lambda^*} = 0$, *and* $\mathtt{f}(\lambda)$ *is increasing on* $0 \le \lambda \le \lambda^*$, *decreasing on* $\lambda^* \le \lambda < +\infty$ *and takes maximum at* $\lambda = \lambda^*$, *i.e., there exists a unique* $\lambda^* \in (0, +\infty)$ *such that* $\mathtt{I}(\lambda^*\mathtt{z}) = 0$ *and* $\mathtt{I}(\lambda\mathtt{z}) = \lambda\mathtt{f}'(\lambda) > 0$ *for* $(0, \lambda^*)$ *and* $\mathtt{I}(\lambda\mathtt{z}) < 0$ *for* $(\lambda^*, +\infty)$.

Proof (i) We have

$$\begin{aligned}
\mathtt{f}(\lambda) &= \mathtt{J}(\lambda\mathtt{z}) \\
&= \frac{\lambda^2}{2}\|\mathtt{z}\|^2_{\mathcal{H}_0^1(\Omega)} - \frac{\lambda^{\mathtt{p}+1}}{\mathtt{p}+1}\int_\Omega |\mathtt{z}|^{\mathtt{p}+1}\log|\lambda\mathtt{z}|dx + \frac{\lambda^{\mathtt{p}+1}}{(\mathtt{p}+1)^2}\|\mathtt{z}\|^{\mathtt{p}+1}_{\mathtt{p}+1} \\
&= \frac{\lambda^2}{2}\|\mathtt{z}\|^2_{\mathcal{H}_0^1(\Omega)} - \frac{\lambda^{\mathtt{p}+1}}{\mathtt{p}+1}\int_\Omega |\mathtt{z}|^{\mathtt{p}+1}\log|\mathtt{z}|dx \\
&\quad - \frac{\lambda^{\mathtt{p}+1}}{\mathtt{p}+1}\log|\lambda|\|\mathtt{z}\|^{\mathtt{p}+1}_{\mathtt{p}+1} + \frac{\lambda^{\mathtt{p}+1}}{(\mathtt{p}+1)^2}\|\mathtt{z}\|^{\mathtt{p}+1}_{\mathtt{p}+1}.
\end{aligned}$$

Since $\|\mathtt{z}\| \neq 0$, it follows that $\lim_{\lambda\to 0} \mathtt{f}(\lambda) = 0$ and $\lim_{\lambda\to+\infty} \mathtt{f}(\lambda) = -\infty$.

$$\begin{aligned}
(ii) \qquad \mathtt{f}'(\lambda) &= \lambda\|\mathtt{z}\|^2_{\mathcal{H}_0^1(\Omega)} - \lambda^{\mathtt{p}}\int_\Omega |\mathtt{z}|^{\mathtt{p}+1}\log|\mathtt{z}|dx - \lambda^{\mathtt{p}}\log|\lambda|\|\mathtt{z}\|^{\mathtt{p}+1}_{\mathtt{p}+1} \\
&= \lambda\left[\|\mathtt{z}\|^2_{\mathcal{H}_0^1(\Omega)} - \lambda^{\mathtt{p}-1}\int_\Omega |\mathtt{z}|^{\mathtt{p}+1}\log|\mathtt{z}|dx - \lambda^{\mathtt{p}-1}\log|\lambda|\|\mathtt{z}\|^{\mathtt{p}+1}_{\mathtt{p}+1}\right].
\end{aligned} \tag{8}$$

Let $\mathtt{h}(\lambda) = \|\mathtt{z}\|^2_{\mathcal{H}^1_0(\Omega)} - \lambda^{\mathtt{p}-1} \int\limits_{\Omega} |\mathtt{z}|^{\mathtt{p}+1} \log|\mathtt{z}| dx - \lambda^{\mathtt{p}-1} \log|\lambda| \|\mathtt{z}\|^{\mathtt{p}+1}_{\mathtt{p}+1}$. Recalling the assumption $\mathtt{p} > 1$, we deduce that

$$\mathtt{h}'(\lambda) = -(\mathtt{p}-1)\lambda^{\mathtt{p}-2} \int\limits_{\Omega} |\mathtt{z}|^{\mathtt{p}+1} \log|\mathtt{z}| dx - (\mathtt{p}-1)\lambda^{\mathtt{p}-2} \log|\lambda| \|\mathtt{z}\|^{\mathtt{p}+1}_{\mathtt{p}+1} < 0. \quad (9)$$

and

$$\lim_{\lambda \to 0^+} \mathtt{h}(\lambda) = \|\nabla \mathtt{z}\|^2 + \|\mathtt{z}\|^2 > 0, \quad \lim_{\lambda \to +\infty} \mathtt{h}(\lambda) = -\infty. \quad (10)$$

Therefore, it is easily seen from (9) and (10) that there exists a unique $\lambda^* = \lambda^*(\mathtt{z}) > 0$ such that $\mathtt{h}(\lambda^*) = 0$. Moreover, it follows from (8) that $\mathtt{f}'(\lambda)|\lambda = \lambda^* = \lambda^* \mathtt{h}(\lambda^*) = 0$. Since $\mathtt{h}(\lambda) > 0$ on $(0, \lambda^*)$ and $\mathtt{h}(\lambda) < 0$ on $(\lambda^*, +\infty)$, we get that $\mathtt{f}(\lambda \mathtt{z})$ is increasing on $0 < \lambda \le \lambda^*$, decreasing on $\lambda^* \le \lambda < +\infty$ and takes the maximum at $\lambda = \lambda^*$. The proof is complete. □

Lemma 2 *Let* ρ *be any fixed positive real number. Then we have following assertions:*

(i) if $0 < \|\mathtt{z}\|_{\mathcal{H}^1_0(\Omega)} \le \delta(\rho)$, *then* $\mathtt{I}_\rho(\mathtt{z}) > 0$.
(ii) if $\mathtt{I}_\rho(\mathtt{z}) < 0$, *then* $\|\mathtt{z}\|_{\mathcal{H}^1_0(\Omega)} > \delta(\rho)$.
(iii) if $\mathtt{I}_\rho(\mathtt{z}) \neq 0$ *and* $\mathtt{I}_\rho(\mathtt{z}) = 0$, *then* $\|\mathtt{z}\|_{\mathcal{H}^1_0(\Omega)} > \delta(\rho)$,

where $\delta(\rho)$ *is the unique real root of equation* $\mathtt{c}^{\mathtt{p}+2}\delta^{\mathtt{p}} = \rho$, *and*

$$\mathtt{c} = \sup \left\{ \frac{\|\mathtt{z}\|_{\mathtt{p}+1}}{\|\mathtt{z}\|_{\mathcal{H}^1_0(\Omega)}} : \mathtt{z} \in \mathcal{H}^1_0(\Omega) \backslash \{0\} \right\}. \quad (11)$$

Proof Let $\Psi(\delta) = \mathtt{c}^{\mathtt{p}+2}\delta^{\mathtt{p}}$.
(i) Suppose $0 < \|\mathtt{z}\|_{\mathcal{H}^1_0(\Omega)} \le \delta(\rho)$. Then, we have

$$\begin{aligned} \int\limits_{\Omega} |\mathtt{z}|^{\mathtt{p}+1} \log|\mathtt{z}| dx &< \|\mathtt{z}\|^{\mathtt{p}+2}_{\mathtt{p}+2} \le \mathtt{c}^{\mathtt{p}+2} \|\mathtt{z}\|^{\mathtt{p}+2}_{\mathcal{H}^1_0(\Omega)} \\ &= \Psi(\|\mathtt{z}\|_{\mathcal{H}^1_0(\Omega)}) \|\mathtt{z}\|^2_{\mathcal{H}^1_0(\Omega)} \le \rho \|\mathtt{z}\|^2_{\mathcal{H}^1_0(\Omega)}. \end{aligned}$$

This proves (i).
(ii) Suppose $\mathtt{I}_\rho(\mathtt{z}) < 0$, then

$$\begin{aligned} \rho \|\mathtt{z}\|^2_{\mathcal{H}^1_0(\Omega)} &< \int\limits_{\Omega} |\mathtt{z}|^{\mathtt{p}+1} \log|\mathtt{z}| dx < \|\mathtt{z}\|^{\mathtt{p}+2}_{\mathtt{p}+2} \le \mathtt{c}^{\mathtt{p}+2} \|\mathtt{z}\|^{\mathtt{p}+2}_{\mathcal{H}^1_0(\Omega)} \\ &= \Psi(\|\mathtt{z}\|_{\mathcal{H}^1_0(\Omega)}) \|\mathtt{z}\|^2_{\mathcal{H}^1_0(\Omega)}, \end{aligned}$$

which implies that $\|\mathtt{z}\|_{\mathcal{H}^1_0(\Omega)} > \delta(\rho)$.

(iii) Suppose $\mathtt{I}_\rho(z) = 0$ and $\|z\|_{\mathcal{H}_0^1(\Omega)} \neq 0$ then from

$$\rho\|z\|^2_{\mathcal{H}_0^1(\Omega)} = \int_\Omega |z|^{p+1} \log |z| dx < \|z\|^{p+2}_{p+2} \leq c^{p+2}\|z\|^{p+2}_{\mathcal{H}_0^1(\Omega)}$$
$$= \Psi(\|z\|_{\mathcal{H}_0^1(\Omega)})\|z\|^2_{\mathcal{H}_0^1(\Omega)},$$

we obtain $\|z\|_{\mathcal{H}_0^1(\Omega)} > \delta(\rho)$. This completes the proof. □

Lemma 3 *Let* $d(\rho)$ *be given in (6) have the following properties:*

(i) $d(\rho) = k(\rho)\delta^2(\rho) > 0$ *for* $0 < \delta < \frac{p+1}{2}$, $k(\rho) = \frac{1}{2} - \frac{\rho}{p+1}$,

(ii) there exists a unique $\rho_0 > \frac{p+1}{2}$ *such that* $d(\rho_0) = 0$ *and* $d(\rho) > 0$ *for* $0 < \rho < \rho_0$,

(iii) $d(\rho)$ *is strictly increasing on* $0 < \rho \leq 1$, *decreasing on* $1 \leq \rho \leq \rho_0$ *and maximum* $d = d(1)$ *at* $\rho = 1$.

Proof The proof of the present lemma is similar to the proof of the Lemma 2.4 of [20] □

2.2 Invariant sets

Theorem 1 *Let* $z_0(x) \in \mathcal{H}_0^1(\Omega)$ *and* $z_1(x) \in L^2(\Omega)$ *and* $0 < e < d$, *then there exits a* $\rho \in (1, \rho_2)$ *such that* $D(\rho) = e$, *where* ρ_2 *is the constant in Lemma 3. Furthermore, if* $w = w(x, t)$ *is a weak solution of the problem (1) with* $E(0) = e$, *then we have*

(i) $z \in W_\rho$ *for any* $1 \leq \rho < \rho_2$, *provided* $I(z_0) > 0$.

(ii) $z \in V_\rho$ *for any* $1 \leq \rho < \rho_2$, *provided* $I(z_0) < 0$.

Proof The proof of the present theorem is similar to the proof of the Proposition 2.6 of [20] □

Theorem 2 *Let* $z_0(x) \in \mathcal{H}_0^1(\Omega)$ *and* $z_1(x) \in L^2(\Omega)$. *Suppose that* $E(0) = d$, $I(z_0) < 0$ *and* $(z_0, z_1) \geq 0$, *then the set* $\mathcal{V}' = \{z \in \mathcal{H}_0^1(\Omega) : I(z) < 0\}$ *is invariant under the flow of (1).*

Proof The proof of the present theorem is similar to the proof of the Lemma 2.7 of [30]. □

Theorem 3 *For some positive constant* $a := c^{-\frac{p+2}{p}}$, *where* c *is given in (11), let*

$$\mathcal{B}_a = \left\{ z \in \mathcal{H}_0^1(\Omega) : \|z\|_{\mathcal{H}_0^1(\Omega)} \geq a \right\}.$$

Then all nontrivial solutions of (1) with $E(0) = 0$ *belong to* $\mathcal{B}_a$.

Proof Let $z(t)$ be any solution of (1) with $E(0) = 0$ and $[0, T)$ be time interval of $z(t)$. Now from the energy inequality $E(t) \leq E(0)$, i.e., $\frac{1}{2}\|z_t\|^2 + J(z) \leq 0$ for $0 \leq t < T$, which implies $J(z) \leq 0$. From (4), we get

$$\left[\frac{p-1}{2(p+1)}\right]\|z\|^2_{\mathcal{H}_0^1(\Omega)} + \frac{1}{p+1}I(z) + \frac{1}{(p+1)^2}\|z\|^{p+1}_{p+1} \leq 0.$$

Since $\mathtt{p} > 1$, it follows that

$$\mathtt{I}(\mathtt{z}) \leq 0.$$

By the definition of $\mathtt{I}(\mathtt{z})$, we get

$$\|\mathtt{z}\|^2_{\mathcal{H}_0^1(\Omega)} \leq \int_\Omega |\mathtt{z}|^{\mathtt{p}+1} \log |\mathtt{z}| dx \leq \|\mathtt{z}\|^{\mathtt{p}+2}_{\mathtt{p}+2} \leq \mathtt{c}^{\mathtt{p}+2} \|\mathtt{z}\|^{\mathtt{p}+2}_{\mathcal{H}_0^1(\Omega)}.$$

Hence,

$$\frac{1}{\mathtt{c}^{\mathtt{p}+2}} \leq \|\mathtt{z}\|^{\mathtt{p}}_{\mathcal{H}_0^1(\Omega)}.$$

This completes the proof. □

Theorem 4 *Let* $\mathtt{z}_0(x) \in \mathcal{H}_0^1(\Omega)$ *and* $\mathtt{z}_1(x) \in \mathtt{L}^2(\Omega)$. *Suppose that* $\mathtt{E}(0) < 0$ *or* $\mathtt{E}(0) = 0$ *with* $\mathtt{z}_0 \neq 0$, *then all solutions of (1) belong to* $\mathtt{V}_\rho$ *for* $0 < \rho < \frac{\mathtt{p}+1}{2}$.

Proof Let $\mathtt{z}(t)$ be any solution of (1) on $[0, \mathtt{T})$ with $\mathtt{E}(0) = 0$. Then by energy inequality, we have

$$\frac{1}{2}\|\mathtt{z}_t\|^2 + \frac{1}{\mathtt{p}+1}\mathtt{I}_\rho(\mathtt{z}) + \mathtt{k}(\rho)\|\mathtt{z}\|^2_{\mathcal{H}_0^1(\Omega)} \leq \frac{1}{2}\|\mathtt{z}_t\|^2 + \mathtt{J}(\mathtt{z}) = \mathtt{E}(0)$$

for $0 \leq t < \mathtt{T}$ and $0 < \rho < (\mathtt{p}+1)/2$. From the above inequality, by Lemma 3 and Theorem 3, we have

(i) $\mathtt{I}_\rho(\mathtt{z}) < 0$ and $\mathtt{I}(\mathtt{z}) < 0 < \mathtt{d}(\rho)$ if $\mathtt{E}(0) < 0$.
(ii) $\|\mathtt{z}_0\|_{\mathcal{H}_0^1(\Omega)} \geq a$ for $0 \leq t < \mathtt{T}$ if $\mathtt{E}(0) = 0$ and $\mathtt{z}_0 \neq 0$.

Thus, from (i) and (ii), we have $\mathtt{z}(t) \in \mathtt{V}_\rho$ for $0 \leq t < \mathtt{T}$, $0 < \rho < \frac{\mathtt{p}+1}{2}$. □

3 Global existence and finite-time blowup of solutions

In this section by using potential wells, we study global existence and finite-time blowup property in finite-time for the solution of (1).

Theorem 5 *Let* $\mathtt{z}_0(x) \in \mathcal{H}_0^1(\Omega)$ *and* $\mathtt{z}_1(x) \in \mathtt{L}^2(\Omega)$. *Suppose that* $0 < \mathtt{E}(0) \leq \mathtt{d}$ *and* $\mathtt{I}(\mathtt{z}_0) \geq 0$ *or* $\|\mathtt{z}_0\|_{\mathcal{H}_0^1(\Omega)} \geq 0$, *then the problem (1) has a global weak solution* $\mathtt{z}(t) \in \mathtt{L}^\infty\big((0, +\infty); \mathcal{H}_0^1(\Omega)\big)$ *with* $\mathtt{z}_t(t) \in \mathtt{L}^\infty\big((0, +\infty); \mathtt{L}^\infty(\Omega)\big)$ *and* $\mathtt{z}(t) \in \mathtt{W}$ *for* $0 \leq t < \infty$.

Proof We divide the proof into two steps.
Step 1: The case $\mathtt{E}(0) < \mathtt{d}$ **and** $\mathtt{I}(\mathtt{z}_0) > 0$ **or** $\|\mathtt{z}_0\|_{\mathcal{H}_0^1(\Omega)} = 0$.

The similar arguments employed in Theorem 3.1 in [20] and Theorem 3.2 in [25], we can construct approximate solutions $\mathtt{z}_{\mathtt{m}}(x,t)$ of (1) such that

$$\frac{1}{2}\|\mathtt{z}_{\mathtt{m}t}\|^2 + \mathtt{J}(\mathtt{z}_{\mathtt{m}}) = \mathtt{E}_{\mathtt{m}}(0) < \mathtt{d},\ 0 \le t < +\infty \tag{12}$$

and $\mathtt{z}_{\mathtt{m}}(t) \in \mathtt{W}$ for sufficiently large $\mathtt{m}$ and $0 \le t < +\infty$. Now by potential energy functional, we get

$$\begin{aligned}\mathtt{J}(\mathtt{z}_{\mathtt{m}}) = &\left[\frac{\mathtt{p}-1}{2(\mathtt{p}+1)}\right]\|\mathtt{z}_{\mathtt{m}}\|^2_{\mathcal{H}^1_0(\Omega)} + \frac{1}{\mathtt{p}+1}\mathtt{I}(\mathtt{z}_{\mathtt{m}})\\ &+\frac{1}{(\mathtt{p}+1)^2}\|\mathtt{z}_{\mathtt{m}}\|^{\mathtt{p}+1}_{\mathtt{p}+1} \ge \left[\frac{\mathtt{p}-1}{2(\mathtt{p}+1)}\right]\|\mathtt{z}_{\mathtt{m}}\|^2_{\mathcal{H}^1_0(\Omega)}.\end{aligned} \tag{13}$$

From (12) and (13), we have

$$\left[\frac{\mathtt{p}-1}{2(\mathtt{p}+1)}\right]\|\mathtt{z}_{\mathtt{m}}\|^2_{\mathcal{H}^1_0(\Omega)} \le \frac{1}{2}\|\mathtt{z}_{\mathtt{m}t}\|^2 + \left[\frac{\mathtt{p}-1}{2(\mathtt{p}+1)}\right]\|\mathtt{z}_{\mathtt{m}}\|^2_{\mathcal{H}^1_0(\Omega)} < \mathtt{d},\ 0 \le t < +\infty,$$

Thus, for $0 \le t < +\infty$, we have

$$\|\mathtt{z}_{\mathtt{m}}\|^2_{\mathcal{H}^1_0(\Omega)} < \frac{2(\mathtt{p}+1)\mathtt{d}}{\mathtt{p}-1}, \tag{14}$$

$$\|\mathtt{z}_{\mathtt{m}}\|^2_{\mathtt{p}+1} \le \mathtt{c}^2\|\mathtt{z}_{\mathtt{m}}\|^2_{\mathcal{H}^1_0(\Omega)} < \frac{2(\mathtt{p}+1)\mathtt{d}}{\mathtt{p}-1}, \tag{15}$$

$$\int_{\Omega}|\mathtt{z}_{\mathtt{m}}|^{\mathtt{p}+1}\log|\mathtt{z}_{\mathtt{m}}|dx < \|\mathtt{z}_{\mathtt{m}}\|^{\mathtt{p}+2}_{\mathtt{p}+2} \le \mathtt{c}^{\mathtt{p}+2}\|\mathtt{z}\|^{\mathtt{p}+2}_{\mathcal{H}^1_0(\Omega)} < \mathtt{c}^{\mathtt{p}+2}\left[\frac{2(\mathtt{p}+1)\mathtt{d}}{\mathtt{p}-1}\right]^{\frac{\mathtt{p}+2}{2}} \tag{16}$$

and

$$\|\mathtt{z}_{\mathtt{m}t}\|^2 < 2\mathtt{d}. \tag{17}$$

Hence, by compactness method and from (14)-(17), the problem (1) has a global weak solution $\mathtt{z}(t) \in \mathtt{L}^{\infty}\big([0,+\infty), \mathcal{H}^1_0(\Omega)\big)$ with $\mathtt{z}_t(t) \in \mathtt{L}^{\infty}\big([0,+\infty), \mathtt{L}^2(\Omega)\big)$ and $\mathtt{z}(t) \in \mathtt{W}$ for $0 \le t < +\infty$.

Step 2: The case $\mathtt{E}(0) = \mathtt{d}$ and $\mathtt{I}(\mathtt{z}_0) \ge 0$ or $\|\mathtt{z}_0\|_{\mathcal{H}^1_0(\Omega)} \ge 0$.

We further divide the proof into two cases.

Case (i) $\|\mathtt{z}_0\|_{\mathcal{H}^1_0(\Omega)} > 0$.

Let $\lambda_{0\mathtt{m}} = 1 - \frac{1}{\mathtt{m}}$ and $\mathtt{z}_{0\mathtt{m}} = \lambda_{\mathtt{m}}\mathtt{z}_0$, $\mathtt{m} = 2, 3, \cdots$. Consider the initial conditions

$$\mathtt{z}(x,0) = \mathtt{z}_{0\mathtt{m}}(x),\ \mathtt{z}_t(x,0) = \mathtt{z}_1(x)$$

and the corresponding problem

$$\left.\begin{aligned} &\frac{\partial^2 \mathtt{z}}{\partial t^2} - \Delta \mathtt{z} + \mathtt{z} = |\mathtt{z}|^{\mathtt{p}} \log |\mathtt{z}|, && x \in \Omega,\ t > 0, \\ &\mathtt{z}(x,0) = \mathtt{z}_{0\mathtt{m}}(x),\ \mathtt{z}_t(x,0) = \mathtt{z}_1(x), && x \in \Omega, \\ &\mathtt{z}(x,t) = 0, && x \in \partial\Omega,\ t > 0. \end{aligned}\right\} \tag{18}$$

By Lemma 1 and $\mathtt{I}(\mathtt{z}_0) \geq 0$, we get $\lambda^* = \lambda^*(\mathtt{z}_0) \geq 1$. Therefore $\mathtt{I}(\mathtt{z}_{0\mathtt{m}}) > 0$ and $\mathtt{J}(\mathtt{z}_{0\mathtt{m}}) = \mathtt{J}(\lambda_{\mathtt{m}} \mathtt{z}_0) < \mathtt{J}(\mathtt{z}_0)$. Further,

$$0 < \mathtt{E}_{\mathtt{m}}(0) \equiv \frac{1}{2}\|\mathtt{z}_1\|^2 + \mathtt{J}(\mathtt{z}_{0\mathtt{m}}) < \frac{1}{2}\|\mathtt{z}_1\|^2 + \mathtt{J}(\mathtt{z}_0) = \mathtt{E}(0) = \mathtt{d}.$$

It follows from the Step 1 that for each $\mathtt{m}$, the problem (18) has a global solution $\mathtt{z}_{\mathtt{m}}(t) \in \mathtt{L}^{\infty}\big([0,+\infty), \mathcal{H}_0^1(\Omega)\big)$ and $\mathtt{z}_{\mathtt{m}}(t) \in \mathtt{W}$ for $0 \leq t < +\infty$ satisfying

$$(\mathtt{z}_{\mathtt{m}t}, \omega) + \int_{\Omega} (\nabla \mathtt{z}_{\mathtt{m}}, \nabla \omega) d\tau + \int_{\Omega} (\mathtt{z}_{\mathtt{m}}, \omega) d\tau = \int_{\Omega} (|\mathtt{z}_{\mathtt{m}}|^{\mathtt{p}} \log |\mathtt{z}_{\mathtt{m}}|, \omega) d\tau + (\mathtt{z}_1, \omega) \tag{19}$$

for every $\omega \in \mathcal{H}_0^1(\Omega)$, $0 \leq t < +\infty$ and

$$\frac{1}{2}\|\mathtt{z}_{\mathtt{m}t}\|^2 + \mathtt{J}(\mathtt{z}_{\mathtt{m}}) = \mathtt{E}_{\mathtt{m}}(0) < \mathtt{d},\ 0 \leq t < +\infty. \tag{20}$$

The remaining proof is similar to Step 1.
Case (ii) $\|\mathtt{z}_0\|_{\mathcal{H}_0^1(\Omega)} = 0$. Then $\mathtt{J}(\mathtt{z}_0) = 0$ and $\frac{1}{2}\|\nabla \mathtt{z}_1\|^2 = \mathtt{E}(0) = \mathtt{d}$. Let $\lambda_{\mathtt{m}} = 1 - \frac{1}{\mathtt{m}}$ and $\mathtt{z}_{1\mathtt{m}} = \lambda_{\mathtt{m}} \mathtt{z}_1$, $\mathtt{m} = 2, 3, \cdots$. Consider the initial conditions

$$\mathtt{z}(x,0) = \mathtt{z}_0(x),\ \mathtt{z}_t(x,0) = \mathtt{z}_{1\mathtt{m}}(x)$$

and the corresponding problem

$$\left.\begin{aligned} &\frac{\partial^2 \mathtt{z}}{\partial t^2} - \Delta \mathtt{z} + \mathtt{z} = |\mathtt{z}|^{\mathtt{p}} \log |\mathtt{z}|, && x \in \Omega,\ t > 0, \\ &\mathtt{z}(x,0) = \mathtt{z}_0(x),\ \mathtt{z}_t(x,0) = \mathtt{z}_{1\mathtt{m}}(x), && x \in \Omega, \\ &\mathtt{z}(x,t) = 0, && x \in \partial\Omega,\ t > 0. \end{aligned}\right\} \tag{21}$$

Also,

$$0 < \mathtt{E}_{\mathtt{m}}(0) \equiv \frac{1}{2}\|\mathtt{z}_{1\mathtt{m}}\|^2 + \mathtt{J}(\mathtt{z}_0) = \frac{1}{2}\|\lambda_{\mathtt{m}} \mathtt{z}_1\|^2 < \mathtt{E}(0) = \mathtt{d},$$

it follows from Step 1 that for each $\mathtt{m}$, the problem (21) has a global solution $\mathtt{z}_{\mathtt{m}}(t) \in \mathtt{L}^{\infty}\big([0,+\infty), \mathcal{H}_0^1(\Omega)\big)$ with $\mathtt{z}_t(t) \in \mathtt{L}^{\infty}\big([0,+\infty), \mathtt{L}^2(\Omega)\big)$ and $\mathtt{z}_{\mathtt{m}}(t) \in \mathrm{W}$ for $0 \leq t < +\infty$ satisfying (19) and (20). The rest of the proof is similar to the Case (i).

□

Theorem 6 *If* $\mathtt{z}_0(x) \in \mathcal{H}_0^1(\Omega)$ *and* $\mathtt{z}_1(x) \in \mathtt{L}^2(\Omega)$. *Suppose that* $0 < \mathtt{E}(0) \leq \mathrm{d}$, $\mathtt{I}(\mathtt{z}_0) < 0$ *and* $(\mathtt{z}_0, \mathtt{z}_1) \geq 0$, *then the weak solution of (1) blows up in finite-time such that* $\lim_{t\to \mathtt{T}^-} \|\mathtt{z}(\cdot,t)\| = +\infty$.

Proof We divide the proof into two steps.

Step 1: The case $\mathtt{E}(0) < \mathrm{d}$ **and** $\mathtt{I}(\mathtt{z}_0) < 0$.

Suppose $\mathtt{z}(x,t)$ be any solution of (1) and define a function $\aleph : [0,+\infty) \to (0,+\infty)$ by $\aleph(t) = \|\mathtt{z}\|^2$. Then $\aleph'(t) = 2(\mathtt{z}, \mathtt{z}_t)$ and

$$\begin{aligned}\aleph''(t) &= 2\|\mathtt{z}_t\|^2 + 2(\mathtt{z}, \mathtt{z}_{tt}) \\ &= 2\|\mathtt{z}_t\|^2 - 2\left[\|\mathtt{z}\|^2_{\mathcal{H}_0^1(\Omega)} - \int_{\Omega} |\mathtt{z}|^{\mathtt{p}+1}\log|\mathtt{z}|dx\right] \\ &= 2\|\mathtt{z}_t\|^2 - 2\mathtt{I}(\mathtt{z}). \end{aligned} \tag{22}$$

Now from the energy inequality, we have

$$\frac{1}{2}\|\mathtt{z}_t\|^2 + \frac{1}{2}\|\mathtt{z}\|^2_{\mathcal{H}_0^1(\Omega)} - \frac{1}{\mathtt{p}+1}\int_{\Omega} |\mathtt{z}|^{\mathtt{p}+1}\log|\mathtt{z}|dx + \frac{1}{(\mathtt{p}+1)^2}\|\mathtt{z}\|^{\mathtt{p}+1}_{\mathtt{p}+1} \leq \mathtt{E}(0).$$

That is

$$\begin{aligned} 2\int_{\Omega} |\mathtt{z}|^{\mathtt{p}+1}\log|\mathtt{z}|dx &\geq (\mathtt{p}+1)\|\mathtt{z}_t\|^2 + (\mathtt{p}+1)\|\mathtt{z}\|^2_{\mathcal{H}_0^1(\Omega)} \\ &\quad + \frac{2}{\mathtt{p}+1}\|\mathtt{z}\|^{\mathtt{p}+1}_{\mathtt{p}+1} - 2(\mathtt{p}+1)\mathtt{E}(0) \\ &\geq (\mathtt{p}+1)\|\mathtt{z}_t\|^2 + (\mathtt{p}+1)\|\mathtt{z}\|^2_{\mathcal{H}_0^1(\Omega)} - 2(\mathtt{p}+1)\mathtt{E}(0). \end{aligned} \tag{23}$$

Substituting (23) into (22), we get

$$\begin{aligned}\aleph''(t) &\geq (\mathtt{p}+3)\|\mathtt{z}_t\|^2 + (\mathtt{p}-1)\|\mathtt{z}\|^2_{\mathcal{H}_0^1(\Omega)} - 2(\mathtt{p}+1)\mathtt{E}(0) \\ &\geq (\mathtt{p}-1)\aleph(t) + (\mathtt{p}+3)\|\mathtt{z}_t\|^2 - 2(\mathtt{p}+1)\mathtt{E}(0). \end{aligned} \tag{24}$$

Suppose $0 < \mathtt{E}(0) \leq \mathrm{d}$, then from Theorem 1, we have $\mathtt{z}(t) \in \mathrm{V}_{\rho}$ for $1 < \rho < \rho_2$ and $t > 0$. So, $\mathtt{I}_{\rho}(\mathtt{z}) < 0$ and by Lemma 2, we get $\|\mathtt{z}\|_{\mathcal{H}_0^1(\Omega)} \geq \delta(\rho)$ for $1 < \rho < \rho_2$ and $t > 0$. That is $\mathtt{I}_{\rho_2}(\mathtt{z}) < 0$ and $\|\mathtt{z}\|_{\mathcal{H}_0^1(\Omega)} \geq \delta(\rho_2)$ for $t > 0$. Since $\aleph'(0) = 2(\mathtt{z}_0, \mathtt{z}_1) \geq 0$ and from (22), it follows that

$$\aleph''(t) \geq 2(\rho_2 - 1)\|\mathtt{z}\|^2_{\mathcal{H}_0^1(\Omega)} - 2\mathtt{I}_{\rho_2}(\mathtt{z}) \geq 2(\rho_2 - 1)\delta^2(\rho_2) > 0,$$
$$\aleph'(t) \geq 2(\rho_2 - 1)\delta^2(\rho_2)t + \aleph'(0) \geq 2(\rho_2 - 1)\delta^2(\rho_2)t,$$

and

$$\aleph(t) \geq (\rho_2 - 1)\delta^2(\rho_2)t^2 + \aleph(0) \geq (\rho_2 - 1)\delta^2(\rho_2)t^2.$$

So, there exists a $\hat{t} > 0$ such that for $t \geq \hat{t}$, we get $(\mathtt{p} - 1)\aleph(t) > 2(\mathtt{p} + 1)\mathtt{E}(0)$. Therefore, from (24) we obtain

$$\aleph(t)\aleph''(t) - \left[\frac{\mathtt{p}+3}{4}\right]\left(\aleph'(t)\right)^2 \geq (\mathtt{p}+3)\Big[\|\mathtt{z}\|^2\|\mathtt{z}_t\|^2 - (\mathtt{z}, \mathtt{z}_t)^2\Big] > 0 \ \text{ for all } \ t \geq \hat{t}. \tag{25}$$

Step 2: The case $\mathtt{E}(0) = \mathrm{d}$ **and** $\mathtt{I}(\mathtt{z}_0) < 0$.

From (24), we have

$$\aleph''(t) \geq (\mathtt{p} - 1)\aleph(t) + (\mathtt{p} + 3)\|\mathtt{z}_t\|^2 - 2(\mathtt{p} + 1)\mathrm{d}. \tag{26}$$

From (22) and by Theorem 2, it follows that $\aleph''(t) > 0$ for $0 \leq t < +\infty$, i.e., $\aleph'(t)$ is strictly increasing for $0 \leq t < +\infty$. Since $\aleph'(0) = 2(\mathtt{z}_0, \mathtt{z}_1) \geq 0$, for any $t^* > 0$ we get

$$\aleph'(t) \geq \aleph'(t^*) > 0, \ t \geq t^*$$

and

$$\aleph(t) \geq \aleph'(t^*)(t - t^*) + \aleph(t^*) > \aleph'(t^*)(t - t^*), \ t \geq t^*.$$

So, there exists a $\hat{t} > 0$ such that for $t \geq \hat{t}$, we obtain

$$(\mathtt{p} - 1)\aleph(t) \geq 2(\mathtt{P} + 1)\mathrm{d}.$$

From (26), we get

$$\aleph''(t) \geq (\mathtt{p} + 3)\|\mathtt{z}_t\|^2.$$

Hence,

$$\aleph(t)\aleph''(t) - \left[\frac{\mathtt{p}+3}{4}\right]\left(\aleph'(t)\right)^2 \geq (\mathtt{p}+3)\Big[\|\mathtt{z}\|^2\|\mathtt{z}_t\|^2 - (\mathtt{z}, \mathtt{z}_t)^2\Big] > 0 \ \text{ for all } \ t \geq \hat{t}.$$

Finally, by Levine's concavity argument [19] that $\aleph(t)$ can not remain finite for all $t \geq \hat{t}$ and therefore reaches a contradiction. This completes proof. □

Acknowledgements The authors would like to thank the referees for their valuable suggestions and comments for the improvement of the paper.

Author Contributions The study was carried out in collaboration of all authors. All authors read and approved the final manuscript.

Funding Not Applicable.

Data availibility statement Data sharing not applicable to this paper as no data sets were generated or analyzed during the current study.

Declarations

Conflict of interest It is declared that authors has no competing interests.

Ethical approval This article does not contain any studies with human participants or animals performed by any of the authors.

References

1. Avrin, J.D.: Convergence properties of the strongly damped nonlinear Klein-Gordon equation. J. Differ. Eq. **67**, 243–255 (1987)
2. Barrow, J.D., Parsons, P.: Inflationary models with logarithmic potentials. Phys. Rev. D **52**, 5576–5587 (1995)
3. Bia lynicki-Birula, I., Mycielski, J.: Wave equations with logarithmic nonlinearities. Bull. Acad. Polon. Sci. Ser. Sci. Math. Astronom. Phys. **23**(4), 461–466 (1975)
4. Bia lynicki-Birula, I., Mycielski, J.: Nonlinear wave mechanics. Ann. Phys. **100**(1–2), 62–93 (1976)
5. Buljan, H., Siber, A., Soljacic, M., Schwartz, T., Segev, M., Christodoulides, D.N.: Incoherent white light solitons in logarithmically saturable noninstantaneous nonlinear media. Phys. Rev. E (3) 68(3), 036607, 6 pp (2003)
6. Cazenave, T.: Uniform estimates for solutions of nonlinear Klein-Gordon equations. J. Func. Anal. **60**, 36–55 (1985)
7. Chen, Y., Qiu, X., Xu, R., et al.: Global existence and blowup of solutions for a class of nonlinear wave equations with linear pseudo-differential operator. Eur. Phys. J. Plus **135**, 573 (2020). https://doi.org/10.1140/epjp/s13360-020-00568-5
8. Cordeiro, S. M., Pereira, D. C., Ferreira, J., Raposo, C. A.: Global solutions and exponential decay to a Klein-Gordon equation of Kirchhoff-Carrier type with strong damping and nonlinear logarithmic source term. Partial Differ. Eq. Appl. Math. **3** (2021). https://doi.org/10.1016/j.padiff.2020.100018
9. De Martino, S., Falanga, M., Godano, C., Lauro, G.: Logarithmic Schrodinger-like equation as a model for magma transport. Europhys. Lett. **63**(3), 472–475 (2003)
10. Ekinci, F., Pişkin, E.: Global existence and growth of solutions to coupled degeneratly damped Klein-Gordon equations. Al-Qadisiyah J. Pure Sci. **27**(1), 29–40 (2022)
11. Enqvist, K., McDonald, J.: Q-balls and baryogenesis in the MSSM. Phys. Lett. B **425**, 309–321 (1998)
12. Ginibre, J., Velo, G.: The global Cauchy problem for the nonlinear Klein Gordon equation. Math. Z. **189**(4), 487–505 (1985)
13. Ginibre, J., Velo, G.: The global Cauchy problem for the nonlinear Klein Gordon equation II. Ann. Inst. H. Poincare Anal. NonLineaire **6**(1), 15–35 (1989)
14. Górka, P.: Logarithmic Klein-Gordon equation. Acta Phys. Polon. B **40**, 59–66 (2009)
15. Han, X.: Global existence of weak solutions for a logarithmic wave equation arising from Q-ball dynamics. Bull. Korean Math. Soc. **50**(1), 275–283 (2013)
16. Hiramatsu, T., Kawasaki, M., Takahashi, F.: Numerical study of Q-ball formation in gravity mediation. J. Cosmol. Astropar. Phys. **2010**(6), 008 (2010)
17. Komech, A.I., Kopylova, E.A.: Weighted energy decay for 3D Klein-Gordon equation. J. Differ. Eq. **248**, 501–520 (2010)

18. Krolikowski, W., Edmundson, D., Bang, O.: Unified model for partially coherent solitons in logarithmically nonlinear media. Phys. Rev. E **61**, 3122–3126 (2000)
19. Levine, H.A.: Some nonexistence and instability theorems for solutions of formally parabolic equation of the form $pu_t = -au + Fu$, Arch. Ration. Mech. Anal. **51**(5), 371–386 (1973)
20. Lian, W., Ahmed, M.S., Xu, R.: Global existence and blow up solution for semilinear hyperbolic equation with logarithmic nonlinearity. Nonlinear Anal. **184**, 239–257 (2019)
21. Lian, W., Ahmed, M.S., Xu, R.: Global existence and blow up of solution for semi-linear hyperbolic equation with the product of logarithmic and power type nonlinearity. Opuscula Math. **40**(1), 111–130 (2020)
22. Lian, W., Xu, R.Z., Radulescu, V.D., Yang, Y.B., Zhao, N.: Global well-posedness for a class of fourth order nonlinear strongly damped wave equations. Adv. Calc. Var. (2019). https://doi.org/10.1515/acv-2019-0039
23. Lian, W., Xu, R.: Global well-posedness of nonlinear wave equation with weak and strong damping terms and logarithmic source term, advances in nonlinear. Analysis **1**, 613–632 (2020)
24. Linde, A.: Strings, textures, inflation and spectrum bending. Phys. Lett. B **284**(3–4), 215–222 (1992)
25. Liu, Y.: On potential wells and vacuum isolating of solutions for semilinear wave equations. J. Differ. Eq. **192**, 155–169 (2003)
26. Luo, Y., Ahmed, M.S.: Cauchy problem of nonlinear Klein-Gordon equations with general nonlinearities. Rend. Circ. Mat. Palermo, II. Ser (2021). https://doi.org/10.1007/s12215-021-00698-4
27. Nakamura, M.: The Cauchy problem for the Klein-Gordon equation under the quartic potential in the de Sitter spacetime. J. Math. Phy., Nakamura M. The Cauchy problem for the Klein-Gordon equation under the quartic potential in the de Sitter spacetime. J. Math. Phy. **62**(12) (2021)
28. Peng, J., Zhou, J.: Global existence and blowup of solutions to a semilinear heat equation with logarithmic nonlinearity. Appl. Anal. (2019). https://doi.org/10.1080/00036811.2019.1698726
29. Polat, N., Taskesen, H.: On the existence of global solutions for a nonlinear Klein-Gordon equation. Filomat **28**(5), 1073–1079 (2014)
30. Xu, R.: Initial boundary value problem for semilinear hyperbolic equations and parabolic equations with critical initial data. Quart. Appl. Math. **68**, 459–468 (2010)
31. Yang, Y., Xu, R.: Finite time blowup for nonlinear Klein-Gordon equations with arbitrarily positive initial energy. Appl. Math. Lett. **77**, 21–26 (2018). https://doi.org/10.1016/j.aml.2017.09.014
32. Ye, Y.: Global solution and blowup of logarithmic Klein-Gordon equation. Bull. Korean Math. Soc. **57**(2), 281–294 (2020)

Publisher's Note Springer Nature remains neutral with regard to jurisdictional claims in published maps and institutional affiliations.

Est. 1984

ORIENTAL JOURNAL OF CHEMISTRY
An International Open Access, Peer Reviewed Research Journal

www.orientjchem.org

ISSN: 0970-020 X
CODEN: OJCHEG
2022, Vol. 38, No.(5):
Pg. 1244-1249

Assessment of Quercetin Content in Selected Vegetables and Fruits by Conventional Extraction and High Performance Liquid Chromatography

N. SWATHI[1] and N. V. S. VENUGOPAL[1]*

Department of Chemistry, GITAM School of Science, GITAM (Deemed to be University), Visakhapatnam-530045, A. P, India.
*Corresponding author E-mail: vnutulap@gitam.edu

http://dx.doi.org/10.13005/ojc/380520

(Received: September 10, 2022; Accepted: October 15, 2022)

ABSTRACT

One of the dietary flavonoids which can be found in a variety of vegetables and fruits is Quercetin (3,3′,4,5,7-pentahydroxyflavone).Quercetin reduce infection risk and also has unique biological property which improves the physical performance. The current research work describes the extraction and characteristic of quercetin present in carrot (Daucus carota sp. sativus) and grapes (genus vitis). A liquid-solid extraction method of quercetin contained in carrot and grapes was developed, in which Quercetin is extracted from a solid mixture using a liquid solvent (methanol). Determination of Quercetin is studied by using High performance liquid chromatography. The separation study was performed on Zodiac C18, 250mmx 4.6mm, 5μm column, detection at 280nm and flow rate applied 1mL/minute. The limits of detection(LOD) and quantification(LOQ) parameters were in the ranges of 0.1–0.3 and 0.3–1.0 μg/mL respectively. The results of carrot and grape meet the specified specification limit. The detection of the active substance in carrot and grapes using the HPLC method has the advantage of being simple, fast, and accurate and the reported method was validated.

Keywords: Quercetin, Extraction, High performance liquid chromatography, Carrot (*Daucus carota sp. sativus*), Grapes (*Genus vitis*), Method validation.

INTRODUCTION

Quercetin (QRN) is a flavonol (plant polyphenol) found in fruits, vegetables, seeds and edible parts. It is also present in medicinal botanicals, plays a key role in developing antioxidants. Phenolic compound play a crucial role in maintaining nutritious substances which help to improve human health from chronic diseases. Fig. 1 shows the chemical structure of QRN. Whose name is derived from the Latin word "quercetum,"which signifies"oak forest," it is a category in the class of flavonoids, and a sub class of flavonol[1]. Flavonoids are phenolic compounds with a three-ring system, composed of 15 carbon atoms in the form of C_6,C_3,C_6. This compound cannot be synthesised by the human body[2]. QRN a yellow crystalline substance which is soluble in alcohol is anticipated that persons with balanced nutrition consume 25–50 mg per day[3]. The optimal effective dose of QRN for decreasing blood

This is an Open Access article licensed under a Creative Commons license: Attribution 4.0 International (CC- BY).
Published by Oriental Scientific Publishing Company © 2018

pressure and inflammation has been determined[4]. QRN is not a carcinogen, and may protect against Genotoxicants[5]. In the food sector, antioxidant supplementation may help to avoid mycotoxin toxicity[6]. The bioctivity and solubility of QRN in the body increase when combined with metal ions to build a complex[7]. Green tea infusions and bitterness are due to poly phenols were investigated8. Deep Eutectic Solvents (DESs) gives high yield for extraction of QRN and its glycosylated form from onion peels[9]. Phenolic compounds have antioxidant, antimutagenic, anticarcinogenic, anti-inflammatory, and antimicrobial activities[10]. QRN play a vital role in the treatment of rheumatoid arthritis[13] and it has been demonstrated to lessen the risk of death in COVID-19 patients due to presence of anti-inflammatory and antioxidant activities.[11]

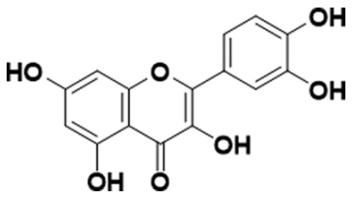


Fig. 1. Structure of QRN

The carrot and grape contains the most important phenolic compound which act as anti-oxidant activities and non–carcenogenic along with other nutritional compounds. The author reported QRN content present in vegetable (carrot) and fruit (grape) extraction and characteristics by using HPLC-UV method.

MATERIALS AND METHODS

Solvents and chemicals

Reference standard of QRN was purchased from Sigma-Aldrich. Methanol, acetonitrile and HPLC-grade water, orthophosphoric acid, acquired from Merck, India

Plant materials

The fresh and healthy vegetable carrot (*Daucus carota sp. sativus*) and fruit grape (*Genus vitis*) were procured by cultivators from local market, Visakhapatnam, Andhra Pradesh, India. The selected vegetable and fruit samples were stored in glass containers and kept at room temperature.

Sample and standard solution preparation

The fruit and vegetable material procured from cultivators were dried and washed with plenty of water after washing/cleaning, the materials were properly cut into small slices or pieces and placed on a clean filter paper for further work. Then the plant material is finely grounded by using a potable grinding machine, Maceration technique was adopted for the extraction procedure in which 100 g of each sample was soaked in small portions with (1:20) methanol and 1:1 aqueous Hydrochloric acid solution in a conical flask with occasional shaking for two hours and using orbital shaking incubator for 60 minutes. The contents are occasionally heated for 1 h at 60°C on water bath and the contents were cooled and subjected to filtration. The process was repeated for 3 times and filtrate was mixed. The filtrate obtained was dried by using a rotary vaccum evaporator at 40°C to get viscous concentrate sample and stored for analysis.

Mobile phase preparation

Prepare a mixture of Methanol and Water in a ratio of 700:300 v/v with 1.0 mL formic acid.

Preparation of Standard Solution

10 mg of QRN standard was taken into a clean and dry 50.0 mL volumetric flask. 5 mL of diluent was added, then dilute to the desired volume with diluent. Transfered 1.0 mL into 10.0 mL volumetric flask and dilute to the volume with diluent. Further 1.0 mL of this solution take into 20.0 mL volumetric flask and dilute to the volume with diluent.

Preparation of test solution

Weighed accurately and transfer about 1000 mg of test sample into a clean and dry 10.0 mL volumetric flask. Add about 5 mL of diluent, sonicate to dissolve the content and dilute to the volume with diluent.

Sample preparation optimization

Various methods have been reported for the extraction and quantification of QRN[12-16]. The procedure was optimized with regard to mobile phase Acetonitrile-Water, Methanol and Water in a ratio of 700:300 v/v with 1.0 mL formic acid.

Chromatographic conditions

Agilent Technologies, 1260 was used for method development, quantification and method

validation. The various chromatographic conditions were given in Table 1.

Table 1: Chromatographic conditions

Instrument	High Performance Liquid Chromatograph, Agilent 1260
Detector	UV
Diluent	Mobile phase
Column	Zodiac C18, 250mmx 4.6mm, 5µm
Wavelength of detection	280nm
Injection volume	10µL
Chromatogram run time	30 min
Column temperature	35ºC
Sampler cooler temperature	10ºC
Flow rate	1.0 mL/min
Pump mode	Isocratic

RESULTS AND DISCUSSION

The most abundant dietary flavonoid is QRN and is used to reduce the blood pressure, inflammation, blood sugar etc. The QRN content in fruits and vegetables is very imperative. QRN maximum wavelength was obtained at 285nm in Methanol. The optimum mobile phase was a mixture of acetonitrile-water and 700:300v/v with 1.0 mL formic acid. The chromatograms show a very good baseline resolution of analytes. Chromatograms of QRN were presented in Fig. 2-5. The QRN content in selected carrot and grape samples were presented in Table 2.

Method validation

Method validation was performed as per AOAC (Association of Official Analytical Chemists) and ICH guidelines. Limit of Detection (LOD), Limit of Quantitation (LOQ), Precision at LOQ level, System suitability, Specificity, Linearity, Accuracy etc were studied.

Table 2: QRN content in grape and carrot

Fruit/vegetable	Sample-1	Sample-2	Sample-3	Sample-4	Sample-5
Grape(mg/100g) white	1.43	1.57	1.29	1.59	1.31
Carrot(mg/100g)	0.84	0.37	0.65	0.49	0.92

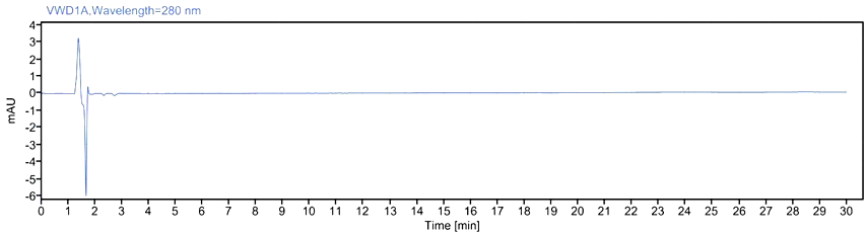


Fig. 2. Blank chromatogram

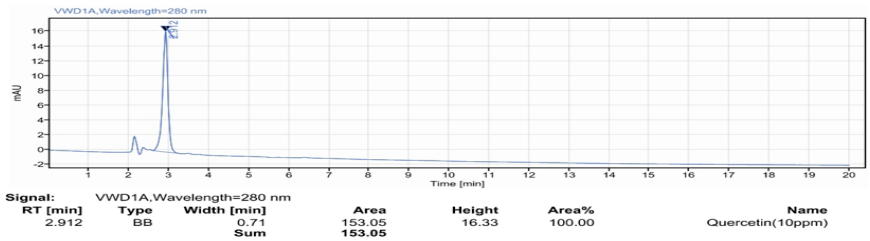


Fig. 3. QRN-HPLC Standard chromatogram

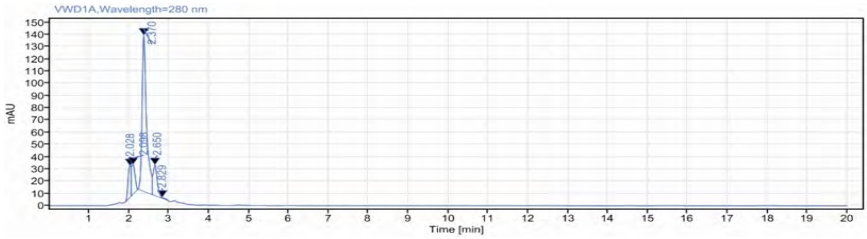


Fig. 4. QRN HPLC chromatogram-Carrot sample

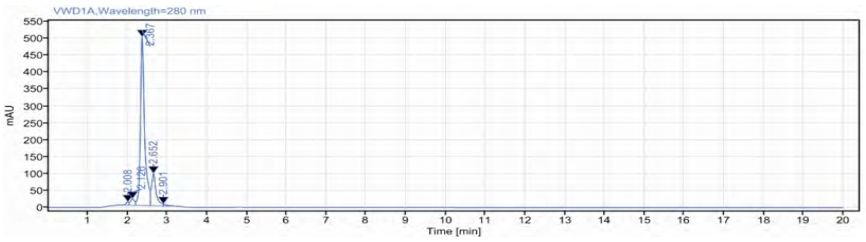


Fig. 5. QRN HPLC chromatogram-Grape sample

Limit of detection and Limit of Quantification

LOQ : Transfer 2.5 mL of standard solution in to 10 mL volumetric flask and make up to mark with diluent. **LOD**: Transfer 3.3 mL of LOQ Solution into 10 mL volumetric flask and dilute to the volume with diluent. Limit of Quantification is considered for this validation is 25% of the specification and Limit of Detection is considered for this validation is 33% of the LOQ Solution. Injected blank followed by six injections of LOQ solution and inject LOD solution in triplicate. The areas of standard, LOQ and LOD were presented in Table 3.

Table 3: Area of Standard LOQ and LOD

					Area of Standard solution					
Sr. No	Name	I-1	I-2	1-3	I-4	1-5	I-6	Average	SD	RSD%
1	Quercetin	88.29	89.06	88.86	90.19	90.38	94.81	90.27	2.37	2.62
					Area of LOQ solution					
		I-1	I-2	1-3	I-4	1-5	I-6	Average	SD	RSD%
2	Quercetin	19.52	19.3	19.35	19.21	19.4	19.35	19.355	0.10	0.53
					Area of LOD solutions					
		I-1	I-2	Injection-3	Average	SD	RSD%			
3	Quercetin	5.94	6.14	6.15	6.08	0.12	1.95			

I:Injection SD: Standard deviation RSD

System suitability

Injected system suitability solution in six replicates. The %RSD values (given in Table 4) of the peak area and Retention time of all analytes were less than 2.0% which satisfy the acceptance criteria.

Table 4: Percentage of RSD

					Area of Standard solutions					
Sr. No	Name	I-1	I-2	1-3	I-4	1-5	I-6	Average	SD	RSD%
1	Quercetin	91.95	90.89	91.16	90.67	92.34	91.12	91.36	0.65	0.71

Specificity

Specificity reveals that the method is proficient of resolving the analyte(s). Accurately weighed and transfer about 10 mg of QRN standard into a clean and dry 50.0 mL volumetric flask. Further dilutions were done and dilute to the volume with diluent.

Preparation of test solution

Weigh accurately and transfer about 1000 mg of test sample into a clean and dry 10.0 mL volumetric flask. Add about 5 mL of diluent, sonicate to dissolve the content and dilute to the volume with diluent.

Preparation of Spiked solution

Weighed accurately and transfer about 1000 mg of test sample into a clean and dry 10.0 mL volumetric flask. Add about 5 mL of diluent, sonicate to dissolve the content and added 0.5 mL of Stock Standard solution and dilute to the volume with diluent.

No significant interference of blank and Impurity peak with analyte peak was observed.

Linearity

The linearity test reveals that the method

of detection has a linear retort to concentration over the range of concentrations of the fastidious product. Linearity to be performed separately by preparing in the range 25%-200% of Impurities concentration. Correlation coefficient of each impurity should be more than 0.99. Areas of standard and linearity were given Table 5 and 6, the linearity graph was shown in Fig. 6. Based on final result the Correlation Coefficient was found with in acceptance criteria.

Table 5: Area of standard solution

	Area of standard solution								
Name	I-1	I-2	I-3	I-4	I-5	I-6	Average	SD	RSD%
Quercetin	91.95	90.89	91.16	90.67	92.34	91.12	91.36	0.65	0.71

I -Injection

Table 6: Linearity

Sr. No	Injection Id	Areas of linearity	
		Percentage	Quercetin
1	Solution-1	25	19.91
2	Solution-2	50	44.35
3	Solution-3	100	93.02
4	Solution-4	150	138.3
5	Solution-5	200	193.36
Correlation Coefficient			0.9985

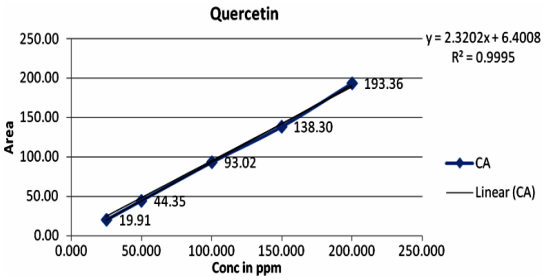


Fig. 6. Linearity graph of QRN

Accuracy

Generally accuracy reveals the potential of the method to recuperate a identified quantity of active or degradant etc. from the placebo matrix. To demonstrate accuracy for Quercetin impurities, revival test was performed using solutions containing 50%, 100% and 200% of the theoretical active concentration in the end product. Every level was performed in triplicate and the mean value for QRN level was calculated and reported. Percentage of RSD, LOQ level not more than 15.0%. The acceptance criteria for impurities in this parameter are that recovery for each of the concentration levels is within the limits 80.0%–120.0%. The accuracy results were given in Table 7 and recovery in Table 8.

Table 7: Accuracy

		Accuracy at LOQ			
I- 1	I-2	I-3	Average	SD	%RSD
9.04	9.10	9.19	9.11	0.08	0.83
		Accuracy at 50%			
22.39	21.84	22.11	22.11	0.28	1.24
		Accuracy at 100%			
61.99	62.3	62.04	62.11	0.17	0.27
		Accuracy at 200%			
163.17	164.00	162.95	163.37	0.55	0.34

I- Injection

Table 8: Percentage recovery

Name	Accuracy at LOQ Result	Accuracy at 50% Result	Accuracy at 100% Result	Accuracy at 200% Result
Quercetin	101.15	104.04	102.14	100.51

CONCLUSION

The QRN content varies between geographical areas, cultivators and plant parts. Methanol was used for the extraction of grape and carrot and the high total phenolic content shows strong antioxidant activities. Determination of quercetin is studied by using High performance liquid chromatography. The chromatographic separation was performed on Zodiac C18, 250mmx 4.6mm, 5μm column, detection at 255nm and flow rate 1mL/minute. The limits of detection(LOD) and quantification(LOQ) parameters were in the ranges of 0.1–0.3 and 0.3–1.0 μg/mL. The detection of the active substance in carrot and grapes using the HPLC method has the advantage of being simple, fast, accurate and the reported method was validated.

ACKNOWLEDGEMENT

We are thankful to the management,

Department of chemistry, School of science, GITAM (Deemed to be University) Visakhapatnam, Andhra Pradesh, India for their support and encouragement given to us.

REFERENCES

1. Tsanova, S.; Ribarova, F.; Petkov, V., *Bulg Chem Commun.*, **2018**, *50*(1), 69-73.
2. David, A.V.; Arulmoli, R.; Parasuraman, S., *Pharmacognosy reviews.*, **2016**, *10*(20), 84-89.
3. Septembre-Malaterre, A.; Boumendjel, A.; Seteyen, A. L. S.; Boina, C.; Gasque, P.; Guiraud, P.; Sélambarom, J., *Phytomedicine Plus.*, **2022**, *2*(1),100220.
4. Dabeek, W. M.;Marra, M. V., *Nutrients.*, **2019**, *11*(10), 2288.
5. Batiha, G.E.S.; Beshbishy, A.M.; Ikram, M.; Mulla, Z.S.; El-Hack, M.E.A.; Taha, A.E.; Algammal, A.M.; Elewa, Y.H.A., **Foods.**, **2020**, *9*, 374.
6. Yang, D.; Wang, T.; Long, M.; Li, P., *Oxidative Medicine and Cellular Longevity.*, **2020**, 8825387.
7. Moodi, Z.; Bagherzade, G.; Peters, J., *Bioinorganic chemistry and applications.*, **2021**, 8818452
8. Chen,Y.H.; Zhang,Y.H.; Chen,G.S.;Yin, J.F.; Chen, J. X.; Wang, F.; Xu,Y.Q., *NPJ science of food.*, **2022**, *6*(1), 1-8.
9. Ciardi, M.; Ianni, F.; Sardella, R;, Di Bona, S.; Cossignani, L.; Germani, R.; Clementi, C., *Materials.*, **2021**, *14*(21), 6465.
10. Sharifi, N.; Mahernia, S.; Amanlou, M., *Pharmaceutical Sciences.*, **2016**, *23*(1), 59-65.
11. Khursheed, R.; Singh, S. K.; Kapoor, B.; Gulati, M.; Wadhwa, S.; Gupta, S.;Kumar, V., *GEN Open.*, **2021**, *1*(1), 43-52.
12. Bhagat, S.; Rathore, M.; Kachhwaha, S.; Sharma, H. K., *Ind. J. Pure App. Biosci.*, **2021**, *9*, 254-261.
13. Berwal, M., *Indian Journal of Arid Horticulture.*, **2018**, *13*(1-2), 107-108.
14. Gull, T.; Sultana, B.; Anwar, F.; Nouman, W.; Mehmood, T.; *Sher, M.*, **2018**, *12*(3), 1539-1547.
15. Olajire, A.;Azeez, L., *African Journal of Food Science Technology.*, **2011**, *2*(2), 22-29.
16. Proestos, C.; Boziaris, I. S.; Nychas, G. J.; Komaitis, M., *Food chemistry.*, **2006**, *95*(4), 664- 671.

TWMS J. App. and Eng. Math. V.12, N.3, 2022, pp. 876-887

ALMOST PERIODIC POSITIVE SOLUTIONS FOR A DELAYED NONLINEAR DENSITY DEPENDENT MORTALITY NICHOLSON'S BLOWFLIES MODEL ON TIME SCALES

K. R. PRASAD[1], M. KHUDDUSH[1], K. V. VIDYASAGAR[1], §

Abstract. In this paper we discuss a nonlinear density dependent mortality Nicholson's blowflies equation with multiple pairs of time varying delays. By contraction mapping theorem, we derived the necessary conditions for the existence of almost periodic positive solutions and by selecting suitable Lyapunov functionnal we study global asymptotic stability of the addressed model. Finally, some numerical simulations are listed to show the validity of our methods.

Keywords: Time scale, Nicholson's blowflies model; almost periodic positive solution, global asymptotic stability.

AMS Subject Classification: 34K14, 39A30, 34N05.

1. Introduction

The delay differential equation

$$\vartheta'(t) = \alpha\vartheta(t) + \beta\vartheta(t-\tau)e^{-\gamma\vartheta(t-\tau)},\ t \in \mathbb{R}$$

describes a population of the Australian sheep blowfly proposed by Gurney [10] in 1980 and is agreed with the experimental data obtained by Nicholson [18] in 1954. Since this equation explains Nicholson blowfly more accurately, the model and it's modifications have been now refereed to as the Nicholson's blowflies model. The theory of Nicholson's blowflies model has made remarkable progress (see[6, 12, 17, 21] and references therein). Recently, Qian and Wang [22], studied a nonlinear density dependent mortality Nicholson's blowflies equation with multiple pairs of time-varying delays

$$\vartheta'(t) = a(t) + b(t)e^{-\vartheta(t)} + \sum_{j=1}^{m} \beta_j(t)\vartheta(t-h_j(t))e^{-\gamma_j(t)\vartheta(t-g_j(t))},\ t \in \mathbb{R}, \tag{1}$$

[1] Department of Applied Mathematics, College of Science and Technology, Andhra University, Visakhapatnam, India - 530003.
e-mail: rajendra92@rediffmail.com; ORCID: https://orcid.org/0000-0001-8162-1391.
e-mail: khuddush89@gmail.com; ORCID: https://orcid.org/0000-0002-1236-8334.
e-mail: vidyavijaya08@gmail.com; ORCID: https://orcid.org/0000-0003-4532-8176.

§ Manuscript received: July 06, 2020; accepted: September 10, 2020.
TWMS Journal of Applied and Engineering Mathematics, Vol.12, No.3 © Işık University, Department of Mathematics, 2022; all rights reserved.

and by utilising differential inequality techniques and the fluctuation lemma, a delay-independent criterion was determined to ensure the global asymptotic stability of the model.

Many authors [1, 9] believe that the discrete time model governed by difference equations are more appropriate than the continuous ones when the populations have non-overlapping generations. Discrete time models can also provide efficient computational models of continuous models for numerical simulations. Recently, Zhu [25] considered the following discrete delayed Ricker model with survival rate,

$$\vartheta(t+1) = \gamma(t)\vartheta(t) + \vartheta(\tau(t))e^{r(t)\left[1-\frac{\vartheta(\tau(t))}{k(t)}\right]},\ t \in \mathbb{Z}^+, \tag{2}$$

and established global attractivity, extreme stability, and the periodicity of the solution of the model.

The differential, difference and dynamic equations on time scales are three theories which play important role for modeling in the environment. Among them, the theory of dynamic equations on time scales is the most recent and was introduced by Stefan Hilger in his PhD thesis in 1988 with three main features: unification, extension and discretization. Since a time scale is any closed and nonempty subset of the real numbers set, so we can extend known results from continuous and discrete analysis to a more general setting. As a matter of fact, this theory allows us to consider time scales which possess hybrid behaviours (both continuous and discrete). These types of time scales play an important role for applications, since most of the phenomena in the environment are neither only discrete nor only continuous, but they possess both behaviors [4, 5, 23]. Moreover, basic results on this issue have been well documented in the articles [2, 3] and monographs of Bohner and Peterson [7, 8]. In the real world phenomena, since the almost periodic variation of the environment plays a crucial role in many biological and ecological dynamical systems and is more frequent and general than the periodic variation of the environment. In this paper we systematically unify the existence of almost periodic solutions for nonlinear density dependent mortality Nicholson's blowflies equation with multiple pairs of time varying delays modelled by ordinary differential equations and their discrete analogues in the form of difference equations and to extend these results to more general time scales. The concept of almost periodic time scales was proposed by Li and Wang [13]. Based on this concept, some works have been done (see [14, 15, 16, 19, 20]).

Motivated by aforementioned works, in this paper we study almost periodic positive solutions of a nonlinear density dependent mortality Nicholson's blowflies equation with multiple pairs of time-varying delays,

$$\vartheta^{\Delta}(t) = -a(t)\vartheta(t) + b(t)e^{-\vartheta(t)} + \sum_{\ell=1}^{n} \beta_\ell(t)\vartheta(t-h_\ell(t))e^{-\gamma_\ell(t)\vartheta(t-g_\ell(t))}, \tag{3}$$

where $t \in \mathbb{T}$ ($\mathbb{T}$ is an arbitrary almost periodic time scale), $a(t)\vartheta(t) - b(t)e^{-\vartheta(t)}$ represents the death rate of the population, $\beta_\ell(t)\vartheta(t-h_\ell(t))\ e^{-\gamma_\ell(t)\vartheta(t-g_\ell(t))}$ describes the time dependent birth function which involves maturation delay $h_\ell(t)$ and incubation delay $g_\ell(t)$ and gains the reproduces at its maximum rate $\frac{1}{\gamma_\ell(t)}$, all parameter functions of (3) are nonnegative, bounded positive almost periodic functions, and $\ell \in \mathfrak{J} := \{1, 2, ..., n\}$. When $\mathbb{T} = \mathbb{Z}^+$, the model (3) is similar to the model (2).

For any bounded function $f(t)$, we denote $f^+ = \sup_{t\in\mathbb{T}} f(t), f^- = \inf_{t\in\mathbb{T}} f(t)$.

We assume the following conditions are true throughout the paper:

(H_1) We assume that the bounded almost periodic functions $a(t)$, $b(t)$, $\beta_\ell(t)$, $g_\ell(t)$, $h_\ell(t)$ satisfy $0 < a^- \leq a(t) \leq a^+$, $0 < b^- \leq b(t) \leq b^+$, $0 < \beta_\ell^- \leq \beta_\ell(t) \leq \beta_\ell^+$, $0 < g_\ell^- \leq g_\ell(t) \leq g_\ell^+$, $0 < h_\ell^- \leq h_\ell(t) \leq h_\ell^+$ for $\ell = 1, 2, 3, \cdots, n$.

(H_2) The initial functions associated with equation (3) is given by

$$\vartheta(t;\varphi) = \varphi(t) \text{ for } t \in [-\varrho^*, 0]_{\mathbb{T}},\ \varrho^* = \max\left\{\max_{\ell\in\mathfrak{J}} g_\ell^+,\ \max_{\ell\in\mathfrak{J}} h_\ell^+\right\}$$

where $\varphi(\cdot)$ denotes a real-valued bounded and continuous functions defined on $[-\varrho^*, 0]_{\mathbb{T}}$.

Due to biological reasons of the model (3), positive solutions are only meaningful. So, we restrict our attention to positive solutions of equation (3).

2. Preliminaries

In this section, we introduce some definitions and state some preliminary results which are useful in the sequel.

Definition 2.1. [7] *A time scale $\mathbb{T}$ is a nonempty closed subset of the real numbers $\mathbb{R}$. $\mathbb{T}$ has the topology that it inherits from the real numbers with the standard topology. It follows that the jump operators $\sigma, \rho : \mathbb{T} \to \mathbb{T}$, and the graininess $\mu : \mathbb{T} \to [0, \infty)$ are defined by $\sigma(t) = \inf\{\tau \in \mathbb{T} : \tau > t\}$, $\rho(t) = \sup\{\tau \in \mathbb{T} : \tau < t\}$ and $\mu(t) = \rho(t) - t$, respectively.*

- *In this definition we put $\inf \emptyset = \sup \mathbb{T}$ and $\sup \emptyset = \inf \mathbb{T}$.*
- *The point $t \in \mathbb{T}$ is left-dense, left-scattered, right-dense, right-scattered if $\rho(t) = t$, $\rho(t) < t$, $\sigma(t) = t$, $\sigma(t) > t$, respectively.*
- *A function $f : \mathbb{T} \to \mathbb{R}$ is called rd-continuous provided it is continuous at right-dense points in $\mathbb{T}$ and its left-sided limits exist (finite) at left-dense points in $\mathbb{T}$. The set of all rd-continuous functions $f : \mathbb{T} \to \mathbb{R}$ is denoted by $C_{rd} = C_{rd}(\mathbb{T}) = C_{rd}(\mathbb{T}, \mathbb{R})$.*
- *A function $f : \mathbb{T} \to \mathbb{R}$ is called ld-continuous provided it is continuous at left-dense points in $\mathbb{T}$ and its right-sided limits exist (finite) at right-dense points in $\mathbb{T}$. The set of all ld-continuous functions $f : \mathbb{T} \to \mathbb{R}$ is denoted by $C_{ld} = C_{ld}(\mathbb{T}) = C_{ld}(\mathbb{T}, \mathbb{R})$.*
- *By an interval time scale, we mean the intersection of a real interval with a given time scale. i.e., $[a, b]_{\mathbb{T}} = [a, b] \cap \mathbb{T}$ other intervals can be defined similarly.*

Definition 2.2. [7] *A function $p : \mathbb{T} \to \mathbb{R}$ is called regressive provided $1 + \mu(t)p(t) \neq 0$ for all $t \in \mathbb{T}^k$; $p : \mathbb{T} \to \mathbb{R}$ is called positively regressive provided $1 + \mu(t)p(t) > 0$ for all $t \in \mathbb{T}^k$ The set of all regressive and rd-continuous functions $p : \mathbb{T} \to \mathbb{R}$ will be denoted by $\mathcal{R} = \mathcal{R}(\mathbb{T}, \mathbb{R})$ and the set of all positively regressive functions and rd-continuous functions will be denoted by $\mathcal{R}^+ = \mathcal{R}^+(\mathbb{T}, \mathbb{R})$.*

Definition 2.3. [7] *If p is regressive function, then the generalized exponential function e_p is defined by*

$$e_p(t, s) = \exp\left\{\int_s^t \xi_{\mu(x)}(p(x))\Delta x\right\}$$

with the cylinder transformation

$$\xi_h(z) = \begin{cases} \dfrac{Log(1 + hz)}{h}, & h \neq 0, \\ z, & h = 0. \end{cases}$$

Lemma 2.1. [7] *Assume that $p, q : \mathbb{T} \to \mathbb{R}$ are two regressive functions; then*

(i) $e_0(t, s) \equiv 1$ *and* $e_p(t, t) \equiv 1$; (*ii*) $e_p(t, s) = 1/e_p(s, t) = e_{\ominus p}(s, t)$;

(iii) $e_p(t, s)e_p(s, r) = e_p(t, r)$; (*iv*) $(e_p(\cdot, s))^\Delta = p(t)e_p(t, s)$.

Lemma 2.2. [7] *Suppose that $p \in \mathcal{R}^+$, then*

(i) $e_p(t,s) > 0$ *for all* $t, s \in \mathbb{T}$;

(ii) *if* $p(t) \leq q(t)$ *for all* $t \geq s$, $t, s \in \mathbb{T}$, *then* $e_p(t,s) \leq e_q(t,s)$ *for all* $t \geq s$.

Lemma 2.3. [7] *If* $p \in \mathcal{R}$ *and* $a, b, c \in \mathbb{T}$, *then* $[e_p(c,\cdot)]^\Delta = -p[e_p(c,\cdot)]^\sigma$, *and*

$$\int_a^b p(t)e_p(c,\sigma(t))\Delta t = e_p(c,a) - e_p(c,b).$$

Lemma 2.4. [7] *Let* $p : \mathbb{T} \to \mathbb{R}$ *be right-dense continuous and regressive,* $a \in \mathbb{T}$ *and* $u_a \in \mathbb{R}$. *Then the unique solution of the initial value problem*

$$u^\Delta(t) = p(t)u(t) + f(t), \quad u(a) = u_a$$

is given by

$$u(t) = e_r(t,a)u_a + \int_a^t e_r(t,\sigma(s))f(s)\Delta s.$$

Lemma 2.5 ([7], Corollary 6.7, pp 257)**.** *Let* $p \in \mathcal{R}^+(\mathbb{T},\mathbb{R})$, $p(t) \geq 0$, $u(t) \in \mathcal{R}$ *and* $\alpha \in \mathbb{R}$. *Then*

$$u(t) \leq \alpha + \int_{t_0}^t u(s)p(s)\Delta(s), \ \forall t \in \mathbb{T},$$

implies

$$u(t) \leq \alpha e_p(t,t_0), \ \forall t \in \mathbb{T}.$$

Definition 2.4. [13] *A time scale* $\mathbb{T}$ *is called an almost periodic time scale if*

$$\Pi := \{\tau \in \mathbb{R} : t + \tau \in \mathbb{T}, \forall t \in \mathbb{T}\} \neq \{0\}.$$

Definition 2.5. [13] *Let* $\mathbb{T}$ *be an almost periodic time scale. A function* $f \in C(\mathbb{T},\mathbb{R})$ *is said to be almost periodic on* $\mathbb{T}$, *if, for any* $\varepsilon > 0$, *the set*

$$E(\varepsilon, f) = \{\tau \in \Pi : |f(t+\tau) - f(t)| < \varepsilon, \forall t \in \mathbb{T}\}$$

is relatively dense in $\mathbb{T}$; *that is, for any* $\varepsilon > 0$, *there exists a constant* $l(\varepsilon) > 0$ *such that each interval of length* $l(\varepsilon)$ *contains at least one* $\tau \in E(\varepsilon, f)$ *such that*

$$|f(t+\tau) - f(t)| < \varepsilon, \ \forall t \in \mathbb{T}.$$

The set $E(\varepsilon, f)$ *is called the* $\varepsilon-$*translation number of* $f(t)$. *We denote the set of all such functions by* $AP(\mathbb{T})$.

Lemma 2.6. [13] *If* $f \in C(\mathbb{T},\mathbb{R})$ *is an almost periodic function, then* f *is bounded on* $\mathbb{T}$.

Lemma 2.7. [13] *If* $f, g \in C(\mathbb{T},\mathbb{R})$ *are almost periodic functions, then* $f+g$, fg *are also almost periodic.*

Definition 2.6. [24] *Let* $\vartheta \in \mathbb{R}^m$ *and* $\mathcal{A}(t)$ *be an* $m \times m$ *rd-continuous matrix on* $\mathbb{T}$; *the linear system*

$$\vartheta^\Delta(t) = \mathcal{A}(t)\vartheta(t), \ t \in \mathbb{T}, \tag{4}$$

is said to admit an exponential dichotomy on $\mathbb{T}$ *if there exist positive constants* k, α, *projection* P, *and the fundamental solution matrix* $\vartheta(t)$ *of* (4) *satisfying*

$$|\vartheta(t)\mathcal{P}\vartheta^{-1}(\sigma(\tau))|_0 \leq ke_{\ominus\alpha}(t,\sigma(\tau)), \ \tau, t \in \mathbb{T}, \ t \geq \tau,$$

$$|\vartheta(t)(\mathcal{I}-\mathcal{P})\vartheta^{-1}(\sigma(s))|_0 \leq ke_{\ominus\alpha}(\sigma(\tau),t), \ \tau, t \in \mathbb{T}, \ t \leq \tau,$$

where $|\cdot|_0$ *is a matrix norm on* $\mathbb{T}$; *that is, if* $\mathcal{A} = (a_{ij})_{m\times m}$, *then we can take* $|\mathcal{A}|_0 = (\sum_{i=1}^m \sum_{j=1}^m |a_{ij}|^2)^{1/2}$.

Lemma 2.8. [13] *If the linear system* (4) *admits an exponential dichotomy, then the following system* $\vartheta^{\Delta}(t) = \mathcal{A}(t)\vartheta(t) + f(t),\ t \in \mathbb{T}$, *has a solution as follows:*

$$\vartheta(t) = \int_{-\infty}^{t} \vartheta(t)\mathcal{P}\vartheta^{-1}(\sigma(\tau))f(\tau)\Delta\tau - \int_{t}^{+\infty} \vartheta(t)(\mathcal{I}-\mathcal{P})\vartheta^{-1}(\sigma(\tau))f(\tau)\Delta\tau,$$

where $\vartheta(t)$ *is the fundamental solution matrix of* (4).

Lemma 2.9. [13] *Let* $\mathcal{A}(t)$ *be a regressive* $n \times n$ *matrix-valued function on* $\mathbb{T}$. *Let* $t_0 \in \mathbb{T}$ *and* $\vartheta_0 \in \mathbb{R}^n$, *then the initial value problem* $\vartheta^{\Delta}(t) = \mathcal{A}(t)\vartheta(t),\ \vartheta(t_0) = \vartheta_0$ *has a unique solution* $\vartheta(t) = e_{\mathcal{A}}(t, t_0)\vartheta_0$.

Lemma 2.10. [13] *Let* $d_i(t) > 0$ *be a function on* $\mathbb{T}$ *such that* $-d_i(t) \in \mathcal{R}^+$ *for all* $t \in \mathbb{T}$ *and* $\min\limits_{1\le i\le m}\Big\{\inf\limits_{t\in\mathbb{T}} d_i(t)\Big\} > 0$. *Then the linear system*

$$\vartheta^{\Delta}(t) = diag\big(-d_1(t), -d_2(t), \cdots, -d_m(t)\big)\vartheta(t)$$

admits an exponential dichotomy on $\mathbb{T}$.

3. Existence of the unique positive almost periodic solution

Let $\mathcal{B} = \{\vartheta(t) : \vartheta \in \mathcal{C}(\mathbb{T}, \mathbb{R}),\ \vartheta(t)$ is almost periodic function$\}$ with norm

$$\|\vartheta\|_{\mathcal{B}} = \sup_{t\in\mathbb{T}} |\vartheta(t)|.$$

Then $\mathcal{B}$ is a Banach space.

Theorem 3.1. *Assume that* (H_1) *and* (H_2) *hold. Let* $\mathfrak{M} > \mathfrak{m}$ *be two positive constants satisfy*

(i) $\mathfrak{M} = (\|\varphi\|_{\mathcal{B}} + b^*)e^{+},\ b^* = \max\limits_{t\in[t_0,+\infty)_{\mathbb{T}}} \int_{t_0}^{t} b(\tau)\Delta\tau,\ e^{+} = \max\limits_{t\in[t_0,+\infty)_{\mathbb{T}}} e^{\int_{t_0}^{t}\sum_{\ell=1}^{n}\beta_\ell(s)\Delta s}$.

(ii) $\dfrac{1}{a^+}\left[b^- e^{-\mathfrak{M}} + \sum\limits_{\ell=1}^{n}\beta_\ell^- e^{-\gamma_\ell^+\mathfrak{M}}\right] \ge \mathfrak{m} \ge \dfrac{1}{a^+}\sum\limits_{\ell=1}^{n}\beta_\ell^- e^{-\gamma_\ell^+\mathfrak{M}}$.

Then the solution $\vartheta(t) = \vartheta(t, t_0, \varphi) \ge 0$ *for all* $t \in [t_0, \eta(\varphi))_{\mathbb{T}}$, *of* (3) *satisfies*

$$\mathfrak{m} \le \vartheta(t) \le \mathfrak{M},\ t \in [t_0, +\infty)_{\mathbb{T}}.$$

Proof. Let $\vartheta(t) = \vartheta(t, t_0, \varphi)$ is a solution of (3) with the initial condition $\vartheta(t_0) = \varphi$, where $\varphi(\cdot)$ denotes a real-valued bounded and continuous functions defined on $[-\varrho^*, 0]_{\mathbb{T}}$. At first, we prove that $\vartheta(t) \le \mathfrak{M},\ t \in [t_0, \eta(\varphi))_{\mathbb{T}}$, where $[t_0, \eta(\varphi))_{\mathbb{T}}$ is the maximal right interval of existence of $\vartheta(t, t_0, \varphi)$. For all $t \in [t_0, \eta(\varphi))_{\mathbb{T}}$, let $\varpi(t) = \max\limits_{t_0-\varrho\le\tau\le t} \vartheta(\tau)$, we get

$$\begin{aligned}\vartheta^{\Delta}(t) =& -a(t)\vartheta(t) + b(t)e^{-\vartheta(t)} + \sum_{\ell=1}^{n}\beta_\ell(t)\vartheta(t-h_\ell(t))e^{-\gamma_\ell(t)\vartheta(t-g_\ell(t))}\\ \le& b(t) + \sum_{\ell=1}^{n}\beta_\ell(t)\vartheta(t-h_\ell(t)) \le b(t) + \sum_{\ell=1}^{n}\beta_\ell(t)\varpi(t).\end{aligned}$$

So,

$$\begin{aligned}\vartheta(t) &\le \vartheta(t_0) + b^* + \int_{t_0}^{t}\left[\sum_{\ell=1}^{n}\beta_\ell(\tau)\varpi(\tau)\right]\Delta\tau\\ &\le \|\varphi\|_{\mathcal{B}} + b^* + \int_{t_0}^{t}\left[\sum_{\ell=1}^{n}\beta_\ell(\tau)\right]\varpi(\tau)\Delta\tau,\ t \in [t_0, \eta(\varphi))_{\mathbb{T}}.\end{aligned} \tag{5}$$

Since (5) is true for every $t \in [t_0, \eta(\varphi))_{\mathbb{T}}$ and $\varpi(t) = \max_{t_0-\varrho\leq\tau\leq t} \vartheta(\tau)$, it follows that

$$\varpi(t) \leq \|\varphi\|_{\mathcal{B}} + b^* + \int_{t_0}^{t} \left[\sum_{\ell=1}^{n} \beta_\ell(\tau)\right] \varpi(\tau)\Delta\tau,\ t \in [t_0, \eta(\varphi))_{\mathbb{T}}.$$

Now by Lemma 2.5, we get

$$\vartheta(t) \leq \varpi(t) \leq (\|\varphi\|_{\mathcal{B}} + b^*) \exp\left\{\int_{t_0}^{t} \left[\sum_{\ell=1}^{n} \beta_\ell(\tau)\right] \Delta\tau\right\},\ t \in [t_0, \eta(\varphi))_{\mathbb{T}}.$$

Thus,

$$\vartheta(t) \leq \mathfrak{M},\ t \in [t_0, \eta(\varphi))_{\mathbb{T}}.$$

Next, we show that

$$\mathfrak{m} \leq \vartheta(t),\ t \in [t_0, \eta(\varphi))_{\mathbb{T}}. \tag{6}$$

To prove this claim, we show that for any $\lambda < 1$, the following inequality holds

$$\vartheta(t) > \lambda\mathfrak{m},\ t \in [t_0, \eta(\varphi))_{\mathbb{T}}. \tag{7}$$

By way of contradiction, assume that (7) does not hold. Then, there exists $t^* \in [t_0, \eta(\varphi))_{\mathbb{T}}$ such that

$$\vartheta(t^*) \leq \lambda\mathfrak{m},\ \vartheta(t) > \lambda,\ t \in [t_0 - \varrho, t^*)_{\mathbb{T}}.$$

Therefore, there must be a positive constant $\mu \leq 1$ such that

$$\vartheta(t^*) = \lambda\mu\mathfrak{m},\ \vartheta(t) > \lambda\mu,\ t \in [t_0 - \varrho, t^*)_{\mathbb{T}}.$$

Since $\lambda\mu < 1$, it follows that

$$\begin{aligned}
0 \geq \vartheta^{\Delta}(t^*) &= -a(t^*)\vartheta(t^*) + b(t^*)e^{-\vartheta(t^*)} + \sum_{\ell=1}^{n} \beta_\ell(t^*)\vartheta(t^* - h_\ell(t^*))e^{-\gamma_\ell(t^*)\vartheta(t^*-g_\ell(t^*))} \\
&\geq -a^+\lambda\mu\mathfrak{m} + b^-e^{-\mathfrak{M}} + \sum_{\ell=1}^{n} \beta_\ell^-\lambda\mu e^{-\gamma_\ell^+\mathfrak{M}} \geq b^-e^{-\mathfrak{M}} - \lambda\mu\left[a^+\mathfrak{m} - \sum_{\ell=1}^{n} \beta_\ell^- e^{-\gamma_\ell^+\mathfrak{M}}\right] \\
&\geq b^-e^{-\mathfrak{M}} - \left[a^+\mathfrak{m} - \sum_{\ell=1}^{n} \beta_\ell^- e^{-\gamma_\ell^+\mathfrak{M}}\right] > 0.
\end{aligned}$$

Which is a contradiction and hence (7) holds. Letting $\lambda \to 1$, we get (6). Similar to the proof of Theorem 2.3.1 in [11], we can obtain that $\eta(\varphi) = +\infty$. Therefore,

$$\mathfrak{m} \leq \vartheta(t) \leq \mathfrak{M},\ t \in [t_0, +\infty)_{\mathbb{T}}.$$

□

For $\varpi \in \mathcal{B}$, consider the equation

$$\vartheta^{\Delta}(t) = -a(t)\vartheta(t) + b(t)e^{-\varpi(t)} + \sum_{\ell=1}^{n} \beta_\ell(t)\varpi(t - h_\ell(t))e^{-\gamma_\ell(t)\varpi(t-g_\ell(t))}. \tag{8}$$

Since $\inf_{t\in\mathbb{T}} a(t) = a^- > 0$, then from Lemma 2.10 the linear equation $\vartheta^{\Delta}(t) = -a(t)\vartheta(t)$ admits exponential dichotomy on $\mathbb{T}$. Hence, by Lemma 2.8, the equation (8) has exactly one almost periodic solution,

$$\vartheta_{\varpi}(t) = \int_{-\infty}^{t} e_{-a}(t, \sigma(\tau))\left[b(\tau)e^{-\varpi(\tau)} + \sum_{\ell=1}^{n} \beta_\ell(\tau)\varpi(\tau - h_\ell(\tau))e^{-\gamma_\ell(\tau)\varpi(\tau-g_\ell(\tau))}\right]\Delta\tau.$$

Define the operator $\aleph : \mathcal{B} \to \mathcal{B}$,

$$(\aleph\varpi)(t) = \int_{-\infty}^{t} e_{-a}(t, \sigma(\tau))\Big[b(\tau)e^{-\varpi(\tau)} + \sum_{\ell=1}^{n} \beta_\ell(\tau)\varpi(\tau - h_\ell(\tau))e^{-\gamma_\ell(\tau)\varpi(\tau-g_\ell(\tau))}\Big]\Delta\tau.$$

It is clear that, $\varpi(t)$ is the almost periodic solution of equation (3) if and only if ϖ is the fixed point of the operator $\aleph$.

For convenience, we take $M = \max\Big\{\sum_{\ell=1}^{n} \beta_\ell^+ \|\varphi\|_{\mathcal{B}} e^+,\ a^+\mathfrak{M}\Big\}$,

Theorem 3.2. *Suppose that the hypothesis of Theorem 3.1 satisfied. Then equation* (3) *has a unique almost periodic positive solution.*

Proof. It is clear from the Theorem 3.1 that $\aleph$ is self mapping on Ξ, where

$$\Xi = \big\{\varpi(t) \in \mathcal{B} : \mathfrak{m} \le \varpi(t) \le \mathfrak{M},\ t \in \mathbb{T}\big\}.$$

Next, we prove that $\aleph$ is a contraction mapping on Ξ. For $\vartheta, \varpi \in \Xi$, consider

$$\begin{aligned}
&\|\aleph\vartheta - \aleph\varpi\|_{\mathcal{B}} = \sup_{t\in\mathbb{T}} |(\aleph\vartheta)(t) - (\aleph\varpi)(t)| \\
&\le \sup_{t\in\mathbb{T}} \Big\{ \int_{-\infty}^{t} e_{-a}(t, \sigma(\tau))\Big[- b(\tau)\Big(e^{-\vartheta(\tau)} - e^{-\varpi(\tau)}\Big) \\
&\quad + \sum_{\ell=1}^{n} \beta_\ell(\tau)\Big(\big[\vartheta(\tau - g_\ell(\tau))e^{-\gamma_\ell(\tau)\vartheta(\tau-g_\ell(\tau))} - \varpi(\tau - g_\ell(\tau))e^{-\gamma_\ell(\tau)\varpi(\tau-g_\ell(\tau))}\big] \\
&\quad + \int_{\tau-g_\ell(\tau)}^{\tau-h_\ell(\tau)} \vartheta^{\Delta}(s)e^{-\gamma_\ell(\tau)\vartheta(\tau-g_\ell(\tau))}\Delta s - \int_{\tau-g_\ell(\tau)}^{\tau-h_\ell(\tau)} \varpi^{\Delta}(s)e^{-\gamma_\ell(\tau)\varpi(\tau-g_\ell(\tau))}\Delta s\Big)\Big]\Delta\tau\Big\}
\end{aligned}$$

From Theorem 3.1, we note that

$$\vartheta^{\Delta}(t) \le \sum_{\ell=1}^{n} \beta_\ell(t)\varpi(t) \le \sum_{\ell=1}^{n} \beta_\ell(t)\|\varphi\|_{\mathcal{B}} \exp\Big\{\int_{t_0}^{t} \sum_{\ell=1}^{n} \beta_\ell(s)\Delta s\Big\} \le \sum_{\ell=1}^{n} \beta_\ell^+ \|\varphi\|_{\mathcal{B}} e^+,$$

and $\varpi^{\Delta}(t) \ge -a(t)\varpi(t) \ge -a^+\mathfrak{M}$. Therefore,

$$\begin{aligned}
&\|\aleph\vartheta - \aleph\varpi\|_{\mathcal{B}} \le \sup_{t\in\mathbb{T}} \int_{-\infty}^{t} e_{-a}(t, \sigma(\tau))\Big[b^+\Big|e^{-\vartheta(\tau)} - e^{-\varpi(\tau)}\Big| \\
&\quad + \sum_{\ell=1}^{n} \beta_\ell^+\Big|\vartheta(\tau - g_\ell(\tau))e^{-\gamma_\ell(\tau)\vartheta(\tau-g_\ell(\tau))} - \varpi(\tau - g_\ell(\tau))e^{-\gamma_\ell(\tau)\varpi(\tau-g_\ell(\tau))}\Big| \\
&+ \sum_{\ell=1}^{n} \beta_\ell^+\big[g_\ell(\tau) - h_\ell(\tau)\big]\Big|\sum_{\ell=1}^{n} \beta_\ell^+\|\varphi\|_{\mathcal{B}}e^+e^{-\gamma_\ell(\tau)\vartheta(\tau-g_\ell(\tau))} - (d^+ + a^+\mathfrak{M})e^{-\gamma_\ell(\tau)\varpi(\tau-g_\ell(\tau))}\Big|\Big]\Delta\tau \\
&\le \sup_{t\in\mathbb{T}} \int_{-\infty}^{t} e_{-a}(t, \sigma(\tau))\Big[b^+\Big|e^{-\vartheta(\tau)} - e^{-\varpi(\tau)}\Big| \\
&\quad + \sum_{\ell=1}^{n} \beta_\ell^+\Big|\vartheta(\tau - g_\ell(\tau))e^{-\gamma_\ell(\tau)\vartheta(\tau-g_\ell(\tau))} - \varpi(\tau - g_\ell(\tau))e^{-\gamma_\ell(\tau)\varpi(\tau-g_\ell(\tau))}\Big| \\
&\quad + \sum_{\ell=1}^{n} \beta_\ell^+\big[g_\ell(\tau) - h_\ell(\tau)\big]M\Big|e^{-\gamma_\ell(\tau)\vartheta(\tau-g_\ell(\tau))} - e^{-\gamma_\ell(\tau)\varpi(\tau-g_\ell(\tau))}\Big|\Big]\Delta\tau.
\end{aligned}$$

By mean value theorem, we have $\left|e^{-\vartheta(\tau)}-e^{-\varpi(\tau)}\right| \le e^{-\xi_1}\left|\vartheta(\tau)-\varpi(\tau)\right|$ where ξ_1 lies between $\vartheta(\tau)$ and $\varpi(\tau)$,

$$\begin{aligned}&\left|\vartheta(\tau-g_\ell(\tau))e^{-\gamma_\ell(\tau)\vartheta(\tau-g_\ell(\tau))}-\varpi(\tau-g_\ell(\tau))e^{-\gamma_\ell(\tau)\varpi(\tau-g_\ell(\tau))}\right|\\&\qquad\le(1-\gamma_\ell\xi_2)e^{-\gamma_\ell^-\xi_2}\left|\vartheta(\tau-g_\ell(\tau))-\varpi(\tau-g_\ell(\tau))\right|,\end{aligned}$$

where ξ_2 lies between $\vartheta(\tau-g_\ell(\tau))$ and $\varpi(\tau-g_\ell(\tau))$, and

$$\left|e^{-\gamma_\ell(\tau)\vartheta(\tau-g_\ell(\tau))}-e^{-\gamma_\ell(\tau)\varpi(\tau-g_\ell(\tau))}\right|\le\gamma_\ell^+e^{-\gamma_\ell^-\xi_3}\left|\vartheta(\tau-g_\ell(\tau))-\varpi(\tau-g_\ell(\tau))\right|,$$

where ξ_3 lies between $\vartheta(\tau-g_\ell(\tau))$ and $\varpi(\tau-g_\ell(\tau))$.
Hence,

$$\begin{aligned}\|\aleph\vartheta-\aleph\varpi\|_{\mathcal{B}}&\le\sup_{t\in\mathbb{T}}\int_{-\infty}^{t}e_{-a}(t,\sigma(\tau))\Big[b^+e^{-\xi_1}\left|\vartheta(\tau)-\varpi(\tau)\right|\\&\quad+\sum_{\ell=1}^{n}\beta_\ell^+(1-\gamma_\ell\xi_2)e^{-\gamma_\ell^-\xi_2}\left|\vartheta(\tau-g_\ell(\tau))-\varpi(\tau-g_\ell(\tau))\right|\\&\quad+M\sum_{\ell=1}^{n}\beta_\ell^+\left[g_\ell(\tau)-h_\ell(\tau)\right]\gamma_\ell^+e^{-\gamma_\ell^-\xi_3}\left|\vartheta(\tau-g_\ell(\tau))-\varpi(\tau-g_\ell(\tau))\right|\Big]\Delta\tau\\&\le\sup_{t\in\mathbb{T}}\int_{-\infty}^{t}e_{-a}(t,\sigma(\tau))\Big[b^+e^{-\xi_1}+\sum_{\ell=1}^{n}\beta_\ell^+(1-\gamma_\ell^-\xi_2)e^{-\gamma_\ell^-\xi_2}\\&\qquad+M\sum_{\ell=1}^{n}\beta_\ell^+g_\ell^+\gamma_\ell^+e^{-\gamma_\ell^-\xi_3}\Big]\Delta\tau\,\|\vartheta-\varpi\|_{\mathcal{B}}\\&\le\frac{1}{a^-}\Big[b^+e^{-\xi_1}+\sum_{\ell=1}^{n}\beta_\ell^+(1-\gamma_\ell^-\xi_2)e^{-\gamma_\ell^-\xi_2}+M\sum_{\ell=1}^{n}\beta_\ell^+g_\ell^+\gamma_\ell^+e^{-\gamma_\ell^-\xi_3}\Big]\|\vartheta-\varpi\|_{\mathcal{B}}\end{aligned}$$

Since $\frac{1}{a^-}\Big[b^+e^{-\xi_1}+\sum_{\ell=1}^{n}\beta_\ell^+(1-\gamma_\ell^-\xi_2)e^{-\gamma_\ell^-\xi_2}+M\sum_{\ell=1}^{n}\beta_\ell^+g_\ell^+\gamma_\ell^+e^{-\gamma_\ell^-\xi_3}\Big]<1$, it follows that $\aleph$ is a contraction mapping. Thus, by the contraction mapping fixed point theorem, the operator $\aleph$ has a unique fixed point ϑ^* in Ξ. This implies that the equation (3) has a unique almost periodic positive solution $\vartheta^*(t)$ and $\mathfrak{m}\le\vartheta^*(t)\le\mathfrak{M}$. □

For convenience, we take

$$\begin{aligned}\Gamma=2\Big[b^--\sum_{\ell=1}^{n}\beta_\ell^+-\mathfrak{M}\sum_{\ell=1}^{n}\beta_\ell^+\gamma_\ell^--M\sum_{\ell=1}^{n}\beta_\ell^+g_\ell^+\gamma_\ell^+\Big]\\\times\Big[b^++\sum_{\ell=1}^{n}\beta_\ell^++\mathfrak{M}\sum_{\ell=1}^{n}\beta_\ell^+\gamma_\ell^-+M\sum_{\ell=1}^{n}\beta_\ell^+g_\ell^+\gamma_\ell^+\Big]^{-2}.\end{aligned}$$

Theorem 3.3. *Suppose that the hypothesis of the Theorem 3.2 is satisfied and for any* $t_0\in[-\varrho^*,+\infty)_{\mathbb{T}}$,

$$\int_{t_0}^{t}(\Gamma-\mu(\tau))\Delta\tau\to+\infty\ \text{as}\ t\to+\infty.$$

Then equation (3) *has unique globally asymptotically stable almost periodic positive solution.*

Proof. By Theorem 3.2, we know that (3) has a unique almost periodic positive solution $\vartheta^*(t)$, and $\mathfrak{m} \leq \vartheta^*(t) \leq \mathfrak{M}$. Suppose $\vartheta(t)$ is any arbitrary solution of (8) with initial function $\varphi(t) > 0$, $t \in [\varrho^*, 0]_{\mathbb{T}}$. Now we prove that $\vartheta^*(t)$ is globally asymptotically stable.

Let $\varpi(t) = \vartheta(t) - \vartheta^*(t)$ and define $\mathcal{V}(\varpi) = \varpi^2$. Then, we have

$$\begin{aligned}
\mathcal{V}^{\Delta}(\varpi) =& 2\varpi(t)\varpi^{\Delta}(t) + \mu(t)(\varpi^{\Delta}(t))^2 \\
=& 2\varpi\Big[- a(t)\big(\vartheta(t) - \vartheta^*(t)\big) + b(t)\left(e^{-\vartheta(t)} - e^{-\vartheta^*(t)}\right) \\
&+ \sum_{\ell=1}^{n} \beta_\ell(t)\left(\vartheta(t-h_\ell(t))e^{-\gamma_\ell(t)\vartheta(t-g_\ell(t))} - \vartheta^*(t-h_\ell(t))e^{-\gamma_\ell(t)\vartheta^*(t-g_\ell(t))}\right)\Big] \\
&+ \mu(t)\Big[- a(t)\big(\vartheta(t) - \vartheta^*(t)\big) + b(t)\left(e^{-\vartheta(t)} - e^{-\vartheta^*(t)}\right) \\
&+ \sum_{\ell=1}^{n} \beta_\ell(t)\left(\vartheta(t-h_\ell(t))e^{-\gamma_\ell(t)\vartheta(t-g_\ell(t))} - \vartheta^*(t-h_\ell(t))e^{-\gamma_\ell(t)\vartheta^*(t-g_\ell(t))}\right)\Big]^2
\end{aligned}$$

Similar argument employed in Theorem 3.2 yields,

$$\begin{aligned}
\mathcal{V}^{\Delta}(\varpi) =& 2\left[-b^- + \sum_{\ell=1}^{n}\beta_\ell^+ + \mathfrak{M}\sum_{\ell=1}^{n}\beta_\ell^+\gamma_\ell^- + M\sum_{\ell=1}^{n}\beta_\ell^+ g_\ell^+\gamma_\ell^+\right]\|\varpi\|_{\mathcal{B}} \\
&+ \mu(t)\left[b^+ + \sum_{\ell=1}^{n}\beta_\ell^+ + \mathfrak{M}\sum_{\ell=1}^{n}\beta_\ell^+\gamma_\ell^- + M\sum_{\ell=1}^{n}\beta_\ell^+ g_\ell^+\gamma_\ell^+\right]^2\|\varpi\|_{\mathcal{B}} \\
=& -\left[b^+ + \sum_{\ell=1}^{n}\beta_\ell^+ + \mathfrak{M}\sum_{\ell=1}^{n}\beta_\ell^+\gamma_\ell^- + M\sum_{\ell=1}^{n}\beta_\ell^+ g_\ell^+\gamma_\ell^+\right]^2\Big[\Gamma - \mu(t)\Big]\|\varpi\|_{\mathcal{B}}.
\end{aligned}$$

Let $\Omega(\vartheta) = \left[b^+ + \sum_{\ell=1}^{n}\beta_\ell^+ + \mathfrak{M}\sum_{\ell=1}^{n}\beta_\ell^+\gamma_\ell^- + M\sum_{\ell=1}^{n}\beta_\ell^+ g_\ell^+\gamma_\ell^+\right]^2\vartheta^2$, then

$$\mathcal{V}^{\Delta}(\varpi(t)) \leq -\Big[\Gamma - \mu(t)\Big]\Omega(\|\vartheta\|_{\mathcal{B}}).$$

Integrating from t_0 to t, we obtain

$$\mathcal{V}(\varpi(t)) \leq \mathcal{V}(\varpi(t_0)) - \int_{t_0}^{t}\Big[\Gamma - \mu(\tau)\Big]\Omega(\|\vartheta\|_{\mathcal{B}})\Delta\tau.$$

So, we get

$$\int_{t_0}^{t}\Big[\Gamma - \mu(\tau)\Big]\Omega(\|\vartheta\|_{\mathcal{B}})\Delta\tau \leq \mathcal{V}(\varpi(t_0)) - \mathcal{V}(\varpi(t)) < \mathcal{V}(\varpi(t_0)) < +\infty.$$

Since

$$\int_{t_0}^{t}(\Gamma - \mu(\tau))\Delta\tau \to +\infty \text{ as } t \to +\infty,$$

it follows that

$$\Omega(\|\vartheta\|_{\mathcal{B}}) \to 0, \ i.e., \ \|\vartheta(t) - \vartheta^*(t)\|_{\mathcal{B}} \to 0.$$

Hence, $\vartheta^*(t)$ is globally asymptotically stable. □

4. Examples

Example 4.1. *Consider following nonlinear density dependent mortality Nicholson's blowflies model for* $\mathbb{T} = \mathbb{R}$.

$$\left.\begin{aligned} \vartheta^{\Delta}(t) =& -(2+\sin(2t))\vartheta(t) + |\cos(t)|e^{-\vartheta(t)} \\ &+ |\sin(t)|\vartheta\left(t - 2e^{\cos(\sqrt{2}t)}\right) e^{-(2+\sin(t))\vartheta\left(t-(4+2e^{\sin(\sqrt{2}t)})\right)}, \\ \vartheta(0) =& 0.1. \end{aligned}\right\} \tag{9}$$

It is clear that (9) satisfies all the assumptions of Theorem 3.3. Therefore, equation (9) has a unique almost periodic positive solution $\vartheta^*(t)$ which is globally asymptotically stable. The numerical simulations in Fig. 1 strongly support the conclusion.

Example 4.2. *Consider following nonlinear density dependent mortality Nicholson's blowflies model for* $\mathbb{T} = \mathbb{Z}^+$.

$$\left.\begin{aligned} \vartheta(t+1) =& \vartheta(t) - (1+\cos t)\vartheta(t) + |\sin(t)|e^{-\vartheta(t)} \\ &+ |\sin(t)|\vartheta\left(t - e^{\sin(\sqrt{2}t)}\right) e^{-(2+\sin(t))\vartheta\left(t-(4+2e^{\cos(\sqrt{2}t)})\right)}, \\ \vartheta(0) =& 0.05. \end{aligned}\right\} \tag{10}$$

It is clear that (10) satisfies all the assumptions of Theorem 3.3. Therefore, equation (10) has a unique almost periodic positive solution $\vartheta^*(t)$ which is globally asymptotically stable. The numerical simulations in Fig. 2 strongly support the conclusion.

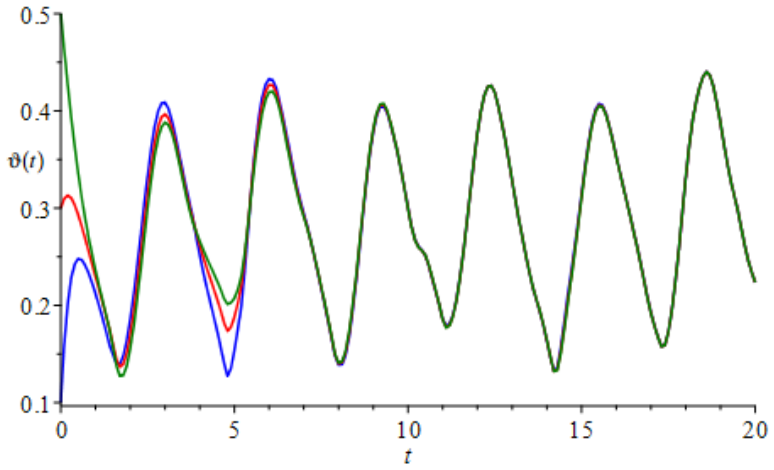


Figure 1. Numerical solution $\vartheta(t)$ of equation (9) for initial value $\varphi(\tau) = 0.1, 0.3, 0.5\,\tau \in [-(4+2e), 0]$.

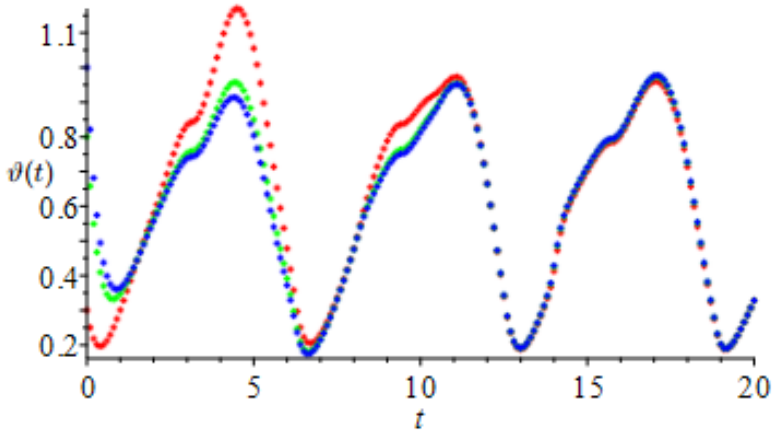


FIGURE 2. Numerical solution $\vartheta(t)$ of equation (9) for initial value $\varphi(\tau) = 0.3, 0.8, 1\,\tau \in [-(4+2e), 0]$.

Acknowledgement. The authors cordially thanks the anonymous referees for their valuable comments which led to the improvement of this paper.

REFERENCES

[1] Agarwal, R. P, (2000), Difference equations and inequalities: theory, methods, and applications, CRC Press.
[2] Agarwal, R. P., and Bohner, M., (1999), Basic calculus on time scales and some of its applications, Results Math., 35(1), 3–22.
[3] Agarwal, R. P., Bohner, M., O'Regan, D., Peterson, A., (2002), Dynamic equations on time scales: a survey, J. Comput. Appl. Math. 141, no. 1-2, 1–26.
[4] Babenko, S.V., Martynyuk, A. A., (2014), Stability of a dynamic graph on time scales. Nonlinear Dynamics and Systems Theory 14(1), 30-–43.
[5] Bartosiewicz, Z., Pawluszewicz, E., (2006), Realizations of linear control systems on time scales. Control & Cybernetics 35(4), 769–786.
[6] Berezansky, L., Braverman, E., Idels, L., (2010), Nicholson's bloflies differential equations revisited: main results and open problems, Appl. Math. Model. 34(6), 1405–1417
[7] Bohner, M., Peterson, A., (2001), Dynamic equations on time scales: An introduction with applications, Birkhauser Boston, Inc., Boston.
[8] Bohner, M., Peterson, A., (2003), Dynamic equations on time scales: An introduction with applications, Birkhauser Boston, Inc., Boston.
[9] Goh, B. S., (2012), Management and analysis of biological populations, Elsevier.
[10] Gurney, W. S. C., Blythe, S. P., Nisbet, R. M., (1980), Nicholson's bloflies revisited, Nature, 287, 17–21.
[11] Hale, J. H., Verduyn Lunel, S. M., (1993), Introduction to Functional Differential Equations, Springer-Verlag, New York, 1993.
[12] Huang, C., Long, X., Huang, L., Fu, S., (2019), Stability of almost periodic Nicholson's blowflies model involving patch structure and mortality terms, Can. Math. Bull., 63(2), 405–422.
[13] Li, Y. K., Wang, C., (2011), Uniformly almost periodic functions and almost periodic solutions to dynamic equations on time scales, Abstr. Appl. Anal., Art. ID 341520, 22 pp.
[14] Liang, T., Yang, Y., Liu, Y., Li, L., (2014), Existence and global exponential stability of almost periodic solutions to Cohen–Grossberg neural networks with distributed delays on time scales, Neurocomputing, 123, 207–215.
[15] Liao, Q., Li, B., Li, Y., (2015), Permanence and almost periodic solutions for an $n-$species Lotka-Volterra food chain system on time scales, Asian-Eur. Jour. of Math., 8(2), 1550027.
[16] Lizama, C., Mesquita, J. G., Ponce, R., (2014), A connection between almost periodic functions defined on time scales and $\mathbb{R}$, Appl. Anal. 93, 2547–2558.

[17] Long, X., Gong, S., (2020) New results on stability of Nicholson's blowflies equation with multiple pairs of time-varying delays, Appl. Math. Lett., 100, 106027. https://doi.org/10.1016/j.aml.2019.106027.
[18] Nicholson, A. J., (1954), An outline of the dynamics of animal population, Aust. J. Zool., 2, 9–65.
[19] Prasad, K. R., and Mahammad. Khuddush, (2020), Existence and uniform asymptotic stability of positive almost periodic solutions for three-species Lotka–Volterra competitive system on time scales, Asian Eur. J. Math., 13(3), 2050058.
[20] Prasad, K. R., and Mahammad. Khuddush, (2019), Existence and global exponential stability of positive almost periodic solutions for a time scales model of Hematopoiesis with multiple time varying variable delays, Int. J. Difference Equ., 14(2), 149–167.
[21] Qian, C., Hu, Y., (2020), Novel stability criteria on nonlinear density dependent mortality Nicholson's blowflies systems in asymptotically almost periodic environments, J. Inequal. Appl., 13(2020). https://doi.org/10.1186/s13660-019-2275-4.
[22] Qian, C., Wang, G., (2020), Dynamic analysis on a delayed nonlinear density-dependent mortality Nicholson's blowflies model, Int. J. Control. https://doi.org/10.1080/00207179.2020.1725134
[23] Yao, Z, (2015), Existence and Global exponential stability of an almost periodic solution for a host-macroparasite equation on time scales. Adv. Differ. Equ. 2015:41. DOI 10.1186/s13662-015-0383-0.
[24] Zhang, J., Fan, M., (2010), Existence and roughness of exponential dichotomies of linear dynamic equations on time scales, Comput. Math. Appl., 59(8), 2658–2675.
[25] Zhu, Z. Q., (2019), Stable analysis for a delayed population model with survival rate, Miskolc Math. Notes, 20(1), 611–624.



Kapula Rajendra Prasad received his M.Sc. and Ph.D. degrees from Andhra University, Visakhapatnam, India. Dr. Prasad did his post doctoral work at Auburn University, Auburn, USA. Currently, he is working as a professor and chairman-board of studies in the Department of Applied Mathematics, Andhra University, Visakhapatnam, India. His major research interest includes ODE, PDE, difference equations, dynamic equations on time scales, fractional order differential equations, mathematical modeling and fixed point theory.



Mahammad Khuddush received his M.Sc., M.Phil. and Ph.D. degrees from Andhra University, Visakhapatnam, India. His major research interest includes ODE, PDE, dynamic equations on time scales, fractional order differential equations, mathematical modeling and fixed point theory.



Kuparala Venkata Vidyasagar received his M.Sc. from Andhra University, Visakhapatnam, India. He is working as a lecturer in the Department of Mathematics, Government Degree College for Women, Marripalem, Narsipatman, India and also pursuing his Ph.D. under the guidance of Prof. K. Rajendra Prasad, Department of Applied Mathematics, Andhra University, Visakhapatnam, India. His research area is dynamic equations on time scales.

Int. J. Nonlinear Anal. Appl. 13 (2022) 1, 3613-3632
ISSN: 2008-6822 (electronic)
http://dx.doi.org/10.22075/ijnaa.2021.23621.2567

Denumerably many positive radial solutions for the iterative system of Minkowski-Curvature equations

Mahammad Khuddush[a,*], Kapula Rajendra Prasad[b], Botta Bharathi[b,c]

[a]Department of Mathematics, Dr. Lankapalli Bullayya College, Resapuvanipalem, Visakhapatnam, 530013, India
[b]Department of Applied Mathematics, College of Science and Technology, Andhra University, Visakhapatnam, 530003, India
[c]Department of Mathematics, College of Engineering for Women, Gayatri Vidya Parishad, Madhurawada, Visakhapatnam, 530048, India

(Communicated by Mohammadbagher Ghaemi)

Abstract

This paper deals with the existence of denumerably many positive radial solutions to the iterative system of Dirichlet problems

$$\begin{gathered}\mathtt{div}\left(\frac{\nabla \mathtt{z}_{\mathtt{j}}}{\sqrt{1-|\nabla \mathtt{z}_{\mathtt{j}}|^2}}\right)+\mathtt{g}_{\mathtt{j}}\left(\mathtt{z}_{\mathtt{j}+1}\right)=0 \quad \text{in} \quad \Omega, \\ \mathtt{z}_{\mathtt{j}}=0 \quad \text{on} \quad \partial\Omega,\end{gathered}$$

where $\mathtt{j} \in \{1,2,\cdots,n\}$, $\mathtt{z}_1=\mathtt{z}_{n+1}$, Ω is a unit ball in $\mathbb{R}^{\mathrm{N}}$ involving the mean curvature operator in Minkowski space by applying Krasnoselskii's fixed point theorem, Avery-Henderson fixed point theorem and a new (Ren-Ge-Ren) fixed point theorem in cones.

Keywords: Positive radial solution, Minkowski-curvature equation, fixed point theorem, cone
2010 MSC: Primary 35A24; Secondary 34B15, 35A20, 35J93.

1. Introduction

The Dirichlet problems involving the mean curvature operator in Minkowski space

$$\mathcal{M}_{\mathcal{C}}(\mathtt{z})=\mathtt{div}\left(\frac{\nabla \mathtt{z}}{\sqrt{1-|\nabla \mathtt{z}|^2}}\right)$$

*Corresponding author
Email addresses: khuddush89@gmail.com (Mahammad Khuddush), rajendra92@rediffmail.com (Kapula Rajendra Prasad), bharathi0401@gmail.com (Botta Bharathi)

Received: June 2021 *Accepted:* August 2021

arise from the study of spacelike submanifolds of codimension in the flat Minkowski space with prescribed mean extrinsic curvature [3, 13]. Due to its important background, the existence of radial solutions for such problems has been studied by many researchers, see [2, 4, 5, 6, 7, 10, 11, 17] and the references therein. However, most of the results in the above mentioned references are concerned with nonsingular problems, there are only a few works on singular problems, see [14] for the weakly singular cases and [15] for the strongly singular cases. Recently, [16] Pei and Wang established the existence and uniqueness of positive radial solutions are obtained for a mean curvature equation in Lorentz–Minkowski space of the form

$$\begin{gathered}\mathcal{M}_{\mathcal{C}}(\mathtt{z})+\mathtt{f}\big(|x|,\mathtt{z}\big)=0 \ \text{ in } \ \Omega,\\ \mathtt{z}=0 \ \text{ on } \ \partial\Omega,\end{gathered}$$

where Ω is a unit ball in $\mathbb{R}^{\mathrm{N}}$, $\mathtt{f}(r,u)$ may be singular at $r=0$ and 1, and strongly singular at $\mathtt{z}=0$, by applying the perturbation technique and Schauder fixed point theorem.

Motivated by the results mentioned above, in this paper, we aim to establish the existence denumerably many positive radial solutions of the following iterative system of Dirichlet problems associated with the Minkowski-curvature equations

$$\left.\begin{gathered}\mathtt{div}\left(\frac{\boldsymbol{\nabla}\mathtt{z}_{\mathtt{j}}}{\sqrt{1-|\boldsymbol{\nabla}\mathtt{z}_{\mathtt{j}}|^2}}\right)+\mathtt{g}_{\mathtt{j}}\left(\mathtt{z}_{\mathtt{j}+1}\right)=0 \ \text{ in } \ \Omega,\\ \mathtt{z}_{\mathtt{j}}=0 \ \text{ on } \ \partial\Omega,\end{gathered}\right\} \tag{1.1}$$

where $\mathtt{j}\in\{1,2,\cdots,n\}$, $\mathtt{z}_1=\mathtt{z}_{n+1}$, Ω is a unit ball in $\mathbb{R}^{\mathrm{N}}$ by applying the Krasnoselskii's fixed point theorem, Avery-Hender fixed point theorem and a new(Ren-Ge-Ren) fixed point theorem in cones.

The study of positive radial solutions to (1.1) reduces to the study of positive solutions to the following boundary value problems:

$$\left.\begin{gathered}\left[r^{\mathtt{N}-1}\phi\big(\mathtt{z}_{\mathtt{j}}'\big)\right]'+r^{\mathtt{N}-1}\mathtt{g}_{\mathtt{j}}(\mathtt{z}_{\mathtt{j}+1})=0,\ \mathtt{N}\geq 1,\\ \mathtt{z}_{\mathtt{j}}'(0)=\mathtt{z}_{\mathtt{j}}(1)=0,\end{gathered}\right\} \tag{1.2}$$

where $\mathtt{j}\in\{1,2,\cdots,n\}$, $\phi(\tau)=\tau/\sqrt{1-\tau^2}$, $\tau\in(-1,1)$, and $\mathtt{z}_1=\mathtt{z}_{n+1}$, by the change of variable $\mathtt{z}_{\mathtt{j}}(x)=\mathtt{z}_{\mathtt{j}}(r)$ with $r=|x|$.

Throughout this paper, we make the following assumptions:

$(\mathcal{H}_1)$ $\mathtt{g}_{\mathtt{j}}:(0,+\infty)\to[0,+\infty)$ is continuous.

$(\mathcal{H}_2)$ there exists a sequence $\{r_k\}_{k=1}^{\infty}$ such that $0<r_{k+1}<r_k<\frac{1}{2}$, $k\in\mathbb{N}$,

$$\lim_{k\to\infty}r_k=r^*<\frac{1}{2}.$$

The rest of the paper is organized in the following fashion. In Section 2, we convert the boundary value problem (1.2) into equivalent integral equation. In Section 3, we establish a criteria for the existence of denumerably many positive solutions for the boundary value problem (1.2) by applying Krasnoselskii's fixed point theorem, Avery-Henderson fixed point theorem and new(Ren-Ge-Ren) fixed point theorem in cones.

2. Preliminaries

In this section we provide some lemmas which are useful in the main results of the paper.

Lemma 2.1 ([14]). *Let* $\phi(\tau) = \dfrac{\tau}{\sqrt{1-\tau^2}}$. *Then* $\phi^{-1}(\tau) = \dfrac{\tau}{\sqrt{1+\tau^2}}$ *and*

$$\phi^{-1}(\tau_1)\phi^{-1}(\tau_2) \leq \phi^{-1}(\tau_1\tau_2) \leq \tau_1\tau_2, \quad \text{for all} \quad \tau_1, \tau_2 \in (0, +\infty).$$

Lemma 2.2 ([12]). *Let* $h \in C[0,1]$. *Then the boundary value problem*

$$\left[r^{\mathtt{N}-1}\phi\left(\mathtt{z}_1'\right)\right]' + h(t) = 0, \ r \in (0,1), \tag{2.1}$$

$$\mathtt{z}_1'(0) = \mathtt{z}_1(1) = 0, \tag{2.2}$$

has a unique solution

$$\mathtt{z}_1(r) = \int_r^1 \phi^{-1}\left(\frac{1}{t^{\mathtt{N}-1}}\int_0^t \tau^{\mathtt{N}-1}h(\tau)d\tau\right)dt. \tag{2.3}$$

From Lemma 2.2, we note that an n-tuple $\left(\mathtt{z}_1, \mathtt{z}_2, \cdots, \mathtt{z}_n\right)$ is a solution of the boundary value problem (1.2) if and only if

$$\mathtt{z}_1(r) = \int_r^1 \phi^{-1}\left[\frac{1}{t_1^{\mathtt{N}-1}}\int_0^{t_1} \tau_1^{\mathtt{N}-1}\mathtt{g}_1\left(\int_{\tau_1}^1 \phi^{-1}\left[\frac{1}{t_2^{\mathtt{N}-1}}\int_0^{t_2} \tau_2^{\mathtt{N}-1}\mathtt{g}_2\left(\int_{\tau_2}^1 \phi^{-1}\left[\cdots\right.\right.\right.\right.$$
$$\left.\left.\left.\left.\mathtt{g}_{n-1}\left(\int_{\tau_{n-1}}^1 \phi^{-1}\left[\frac{1}{t_n^{\mathtt{N}-1}}\int_0^{t_n} \tau_n^{\mathtt{N}-1}\mathtt{g}_n\left(\mathtt{z}_1(\tau_n)\right)d\tau_n\right]dt_n\right)\cdots d\tau_1\right]dt_1.$$

and

$$\mathtt{z}_{\mathtt{j}}(r) = \int_r^1 \phi^{-1}\left(\frac{1}{t^{\mathtt{N}-1}}\int_0^t \tau^{\mathtt{N}-1}\mathtt{g}_{\mathtt{j}}(\mathtt{z}_{\mathtt{j}+1}(\tau))d\tau\right)dt, \ \mathtt{j} = 2, 3, \cdots, n,$$
$$\mathtt{z}_{n+1}(r) = \mathtt{z}_1(r), \ r \in (0,1).$$

We denote the Banach space $\mathcal{C}([0,1], \mathbb{R})$ by $\mathscr{B}$ with the norm $\|\mathtt{z}\| = \max_{r\in[0,1]} |\mathtt{z}(r)|$. For $\delta \in (0, 1/2)$, the cone $\mathtt{P}_\delta \subset \mathscr{B}$ is defined by

$$\mathtt{P}_\delta = \left\{\mathtt{z} \in \mathscr{B} : \mathtt{z}(r) \geq 0, \min_{r\in[\delta,\,1-\delta]} \mathtt{z}(r) \geq \delta\|\mathtt{z}\|\right\},$$

For any $\mathtt{z}_1 \in \mathtt{P}_\delta$, define an operator $\aleph : \mathtt{P}_\delta \to \mathscr{B}$ by

$$(\aleph\mathtt{z}_1)(r) = \int_r^1 \phi^{-1}\left[\frac{1}{t_1^{\mathtt{N}-1}}\int_0^{t_1} \tau_1^{\mathtt{N}-1}\mathtt{g}_1\left(\int_{\tau_1}^1 \phi^{-1}\left[\frac{1}{t_2^{\mathtt{N}-1}}\int_0^{t_2} \tau_2^{\mathtt{N}-1}\mathtt{g}_2\left(\int_{\tau_2}^1 \phi^{-1}\left[\cdots\right.\right.\right.\right.$$
$$\left.\left.\left.\left.\mathtt{g}_{n-1}\left(\int_{\tau_{n-1}}^1 \phi^{-1}\left[\frac{1}{t_n^{\mathtt{N}-1}}\int_0^{t_n} \tau_n^{\mathtt{N}-1}\mathtt{g}_n\left(\mathtt{z}_1(\tau_n)\right)d\tau_n\right]dt_n\right)\cdots d\tau_1\right]dt_1. \tag{2.4}$$

Lemma 2.3 ([9]). *Let* $\mathtt{z} \in \mathcal{C}\left([0,1], [0,+\infty)\right)$ *be such that* $\mathtt{z}'(r)$ *is decreasing in* $[0,1]$. *Then, we have*

$$\min_{r\in[\delta,\,1-\delta]} \mathtt{z}(r) \geq \delta\|\mathtt{z}\|.$$

Lemma 2.4. *Assume that* $(\mathcal{H}_1)$ *holds. Then, for each* $\delta \in (0, 1/2)$, $\aleph(\mathtt{P}_\delta) \subset \mathtt{P}_\delta$ *and* $\aleph : \mathtt{P}_\delta \to \mathtt{P}_\delta$ *is completely continuous.*

Proof . It is easy to see that $\aleph(\mathtt{z}_1(r)) \in \mathscr{B}$ with $\aleph(\mathtt{z}_1(1)) = 0$. Now, for any $\mathtt{z}_1 \in \mathtt{P}_\delta$, we have

$$\begin{aligned}(\aleph\mathtt{z}_1)'(r) = &-\phi^{-1}\left[\frac{1}{r^{\mathtt{N}-1}}\int_0^r \tau_1^{\mathtt{N}-1}\mathtt{g}_1\left(\int_{\tau_1}^1 \phi^{-1}\left[\frac{1}{t_2^{\mathtt{N}-1}}\int_0^{t_2}\tau_2^{\mathtt{N}-1}\mathtt{g}_2\left(\int_{\tau_2}^1\phi^{-1}\left[\cdots\right.\right.\right.\right.\\ &\left.\left.\left.\left.\mathtt{g}_{n-1}\left(\int_{\tau_{n-1}}^1\phi^{-1}\left[\frac{1}{t_n^{\mathtt{N}-1}}\int_0^{t_n}\tau_n^{\mathtt{N}-1}\mathtt{g}_n\big(\mathtt{z}_1(\tau_n)\big)d\tau_n\right]dt_n\right)\cdots d\tau_1\right]\right.\right.\right.\right.\\ \le\ & 0.\end{aligned}$$

It follows that $(\aleph\mathtt{z}_1)(r)$ is decreasing on $[0,1]$, i.e.,

$$(\aleph\mathtt{z}_1)(r) \ge (\aleph\mathtt{z}_1)(1) = 0 \quad \text{for any} \quad r \in [0,1]. \tag{2.5}$$

Since

$$\begin{aligned}r^{\mathtt{N}-1}\phi\big((\aleph\mathtt{z}_1)'(r)\big) = &-\int_0^r \tau_1^{\mathtt{N}-1}\mathtt{g}_1\left(\int_{\tau_1}^1 \phi^{-1}\left[\frac{1}{t_2^{\mathtt{N}-1}}\int_0^{t_2}\tau_2^{\mathtt{N}-1}\mathtt{g}_2\left(\int_{\tau_2}^1\phi^{-1}\left[\cdots\right.\right.\right.\right.\\ &\left.\left.\left.\mathtt{g}_{n-1}\left(\int_{\tau_{n-1}}^1\phi^{-1}\left[\frac{1}{t_n^{\mathtt{N}-1}}\int_0^{t_n}\tau_n^{\mathtt{N}-1}\mathtt{g}_n\big(\mathtt{z}_1(\tau_n)\big)d\tau_n\right]dt_n\right)\cdots d\tau_2\right)d\tau_1,\right.\right.\right.\end{aligned}$$

is decreasing on $[0,1]$, it follows from the fact that ϕ is increasing and $\mathtt{N} \ge 1$ that $(\aleph\mathtt{z}_1)'(r)$ is decreasing on $[0,1]$. Thus, by Lemma 2.3, we have

$$\min_{r\in[\delta,\,1-\delta]} \aleph\mathtt{z}_1(r) \ge \delta\|\aleph\mathtt{z}_1\|. \tag{2.6}$$

From (2.5) and (2.6), we see that $\aleph(\mathtt{P}_\delta) \subset \mathtt{P}_\delta$. Finally by standard methods and the Arzela-Ascoli theorem, the operator $\aleph$ is completely continuous. □

3. Denumerably Many Positive Radial Solutions

For the the existence of denumerably many positive radial solutions for the boundary value problem (1.2), we utilize the following cone fixed point theorems in a Banach space.

Theorem 3.1. *(Krasnoselskii [8]) Let* $\mathscr{B}$ *be Banch space and* $\mathtt{P}$ *be a cone in* $\mathscr{B}$. *Suppose* $\mathtt{E}$ *and* $\mathtt{F}$ *are two open sets with* $0 \in \mathtt{E}, \overline{\mathtt{E}} \subset \mathtt{F}$. *Let* $\aleph : \mathtt{P} \cap (\overline{\mathtt{F}}\backslash\mathtt{E}) \to \mathtt{P}$ *be a completely continuous operator such that*

(a) $\|\aleph\mathtt{z}\| \le \|\mathtt{z}\|$, $\mathtt{z} \in \mathtt{P} \cap \partial\mathtt{E}$, *and* $\|\aleph\mathtt{z}\| \ge \|\mathtt{z}\|$, $\mathtt{z} \in \mathtt{P} \cap \partial\mathtt{F}$, *or*

(b) $\|\aleph\mathtt{z}\| \ge \|\mathtt{z}\|$, $\mathtt{z} \in \mathtt{P} \cap \partial\mathtt{E}$, *and* $\|\aleph\mathtt{z}\| \le \|\mathtt{z}\|$, $\mathtt{z} \in \mathtt{P} \cap \partial\mathtt{F}$.

Then $\aleph$ *has a fixed point in* $\mathtt{P} \cap (\overline{\mathtt{F}}\backslash\mathtt{E})$.

Let ψ be a nonnegative continuous functional on a cone $\mathtt{P}$ of the real Banach space $\mathscr{B}$. Then for any two positive real numbers a' and c', we define the sets

$$\mathtt{P}(\psi, c') = \{\mathtt{z} \in \mathtt{P} : \psi(\mathtt{z}) < c'\}$$

and

$$\mathtt{P}_{a'} = \{\mathtt{z} \in \mathtt{P} : \|\mathtt{z}\| < a'\}.$$

Theorem 3.2. *(Avery-Henderson[1]) Let* $\mathtt{P}$ *be a cone in a real Banach space* $\mathscr{B}$*. Suppose* α *and* γ *are increasing, nonnegative continuous functionals on* $\mathtt{P}$ *and* θ *is nonnegative continuous functional on* $\mathtt{P}$ *with* $\theta(0) = 0$ *such that, for some positive numbers* c' *and* k, $\gamma(\mathtt{z}) \leq \theta(\mathtt{z}) \leq \alpha(\mathtt{z})$ *and* $\|\mathtt{z}\| \leq k\gamma(\mathtt{z})$, *for all* $\mathtt{z} \in \overline{\mathtt{P}(\gamma, c')}$. *Suppose that there exist positive numbers* a' *and* b' *with* $a' < b' < c'$ *such that* $\theta(\mathtt{z}) \leq \lambda\theta(\mathtt{z})$, *for all* $0 \leq \lambda \leq 1$ *and* $\mathtt{z} \in \partial\mathtt{P}(\theta, b')$. *Further, let* $\aleph : \overline{\mathtt{P}(\gamma, c')} \to \mathtt{P}$ *be a completely continuous operator such that*

(a) $\gamma(\aleph\mathtt{z}) > c'$, *for all* $\mathtt{z} \in \partial\mathtt{P}(\gamma, c')$,

(b) $\theta(\aleph\mathtt{z}) < b'$, *for all* $\mathtt{z} \in \partial\mathtt{P}(\theta, b')$,

(c) $\mathtt{P}(\alpha, a') \neq \emptyset$ *and* $\alpha(\aleph\mathtt{z}) > a'$, *for all* $\partial\mathtt{P}(\alpha, a')$.

Then, $\aleph$ *has at least two fixed points* ${}^1\mathtt{z}, {}^2\mathtt{z} \in \mathtt{P}(\gamma, c')$ *such that* $a' < \alpha({}^1\mathtt{z})$ *with* $\theta({}^1\mathtt{z}) < b'$ *and* $b' < \theta({}^2\mathtt{z})$ *with* $\gamma({}^2\mathtt{z}) < c'$.

Theorem 3.3. *(Ren-Ge-Ren[18]) Let* $\mathtt{P}$ *be a cone in a Banach space* $\mathscr{B}$ *Let* α, β *and* γ *be three increasing, nonnegative and continuous functionals on* $\mathtt{P}$, *satisfying for some* $c' > 0$ *and* $M > 0$ *such that* $\gamma(\mathtt{z}) \leq \beta(\mathtt{z}) \leq \alpha(\mathtt{z})$ *and* $\|\mathtt{z}\| \leq M\gamma(\mathtt{z})$, *for all* $\mathtt{z} \in \overline{\mathtt{P}(\gamma, c')}$. *Suppose there exists a completely continuous operator* $\aleph : \overline{\mathtt{P}(\gamma, c')} \to \mathtt{P}$ *and* $0 < a' < b' < c'$ *such that*

(a) $\gamma(\aleph\mathtt{z}) > c'$, *for all* $\mathtt{z} \in \partial\mathtt{P}(\gamma, c')$,

(b) $\beta(\aleph\mathtt{z}) < b'$, *for all* $\mathtt{z} \in \partial\mathtt{P}(\beta, b')$,

(c) $\mathtt{P}(\alpha, a') \neq \emptyset$ *and* $\alpha(\aleph\mathtt{z}) > a'$, *for all* $\partial\mathtt{P}(\alpha, a')$.

Then, $\aleph$ *has at least three fixed points* ${}^1\mathtt{z}, {}^2\mathtt{z}, {}^3\mathtt{z} \in \mathtt{P}(\gamma, c')$ *such that* $\alpha({}^1\mathtt{z}) < a' < \alpha({}^2\mathtt{z})$, $\beta({}^2\mathtt{z}) < b' < \beta({}^3\mathtt{z})$ *and* $\beta({}^3\mathtt{z}) < c'$.

3.1. Existence of (Atleast One) Denumerably Many Positive Radial Solutions

Theorem 3.4. *Assume that* $(\mathcal{H}_1)$–$(\mathcal{H}_2)$ *hold and let* $\{\delta_k\}_{k=1}^{\infty}$ *be a sequence with* $r_{k+1} < \delta_k < r_k$, $k \in \mathbb{N}$. *Let* $\{\mathtt{R}_k\}_{k=1}^{\infty}$ *and* $\{\mathtt{S}_k\}_{k=1}^{\infty}$ *be any two sequences which satisfies the relation*

$$\mathtt{R}_{k+1} < \delta_k\mathtt{S}_k < \mathtt{S}_k < \mathtt{R}_k, \quad \beta_k\phi(\delta_k^{-1}\mathtt{S}_k) < \phi\big(\mathtt{R}_k\big),\ k \in \mathbb{N},$$

Furthermore for each natural number k, *we assume that* $\mathtt{g}_\mathtt{j}(\mathtt{j} = 1, 2, \cdots, n)$ *satisfies*

$(\mathcal{H}_3)$ $\mathtt{g}_\mathtt{j}(\mathtt{z}(r)) \leq \mathtt{N}\phi\big(\mathtt{R}_k\big)$ *for all* $0 \leq \mathtt{z}(r) \leq \mathtt{R}_k$, $r \in [0, 1]$,

$(\mathcal{H}_4)$ $\mathtt{g}_\mathtt{j}(\mathtt{z}(r)) \geq \beta_k\mathtt{N}\phi(\delta_k^{-1}\mathtt{S}_k)$ *for all* $\delta_k\mathtt{S}_k \leq \mathtt{z}(r) \leq \mathtt{S}_k$, $r \in [\delta_k, 1 - \delta_k]$, *where*

$$\beta_k = \frac{(1-\delta_k)^{\mathtt{N}} - \delta_k^{\mathtt{N}}}{(1-\delta_k)^{\mathtt{N}-1}}.$$

The iterative system (1.1) *has denumerably many radial solutions* $\{(\mathtt{z}_1^{[k]}, \mathtt{z}_2^{[k]}, \cdots, \mathtt{z}_n^{[k]})\}_{k=1}^{\infty}$ *such that* $\mathtt{z}_\mathtt{j}^{[k]}(r) \geq 0$ *on* $(0, 1)$, $\mathtt{j} = 1, 2, \cdots, n$ *and* $k \in \mathbb{N}$.

Proof . Consider the sequences $\{\mathtt{E}_k\}_{k=1}^{\infty}$ and $\{\mathtt{F}_k\}_{k=1}^{\infty}$ of open subsets of $\mathscr{B}$ defined by

$$\mathtt{E}_k = \{\mathtt{z} \in \mathscr{B} : \|\mathtt{z}\| < \mathtt{R}_k\},$$

and

$$\mathtt{F}_k = \{\mathtt{z} \in \mathscr{B} : \|\mathtt{z}\| < \mathtt{S}_k\}.$$

Let $\{\delta_k\}_{k=1}^{\infty}$ be as in the hypothesis and note that $r^* < r_{k+1} < \delta_k < r_k < 1/2$, for all $k \in \mathbb{N}$. For each $k \in \mathbb{N}$, define the cone $\mathtt{P}_{\delta_k}$ by

$$\mathtt{P}_{\delta_k} = \left\{ \mathtt{z} \in \mathscr{B} : \mathtt{z}(r) \geq 0 \ \text{ and } \min_{r \in [\delta_k, 1-\delta_k]} \mathtt{z}(r) \geq \delta_k \|\mathtt{z}\| \right\}.$$

Let $\mathtt{z}_1 \in \mathtt{P}_{\delta_k} \cap \partial \mathtt{E}_k$. Then,

$$\mathtt{z}_1(\tau) \leq \mathtt{R}_k = \|\mathtt{z}_1\|$$

for all $\tau \in [0,1]$. Let $0 < \tau_{n-1} < 1$. Then by Lemma 2.1 and $(\mathcal{H}_3)$, we have

$$\begin{aligned}
\int_{\tau_{n-1}}^{1} \phi^{-1}\left[\frac{1}{t_n^{\mathtt{N}-1}} \int_0^{t_n} \tau_n^{\mathtt{N}-1} \mathtt{g}_n\big(\mathtt{z}_1(\tau_n)\big) d\tau_n\right] dt_n &\leq \int_0^1 \phi^{-1}\left[\frac{1}{t_n^{\mathtt{N}-1}} \int_0^{t_n} \tau_n^{\mathtt{N}-1} \mathtt{g}_n\big(\mathtt{z}_1(\tau_n)\big) d\tau_n\right] dt_n \\
&\leq \int_0^1 \phi^{-1}\left[\frac{1}{t_n^{\mathtt{N}-1}} \int_0^{t_n} \tau_n^{\mathtt{N}-1} \mathtt{N}\phi\big(\mathtt{R}_k\big) d\tau_n\right] dt_n \\
&\leq \int_0^1 \phi^{-1}\left(\phi\big(\mathtt{R}_k\big) t_n\right) dt_n \\
&\leq \mathtt{R}_k.
\end{aligned}$$

It follows in similar manner for $0 < \tau_{n-2} < 1$, we have

$$\begin{aligned}
&\int_{\tau_{n-2}}^{1} \phi^{-1}\left[\frac{1}{t_{n-1}^{\mathtt{N}-1}} \int_0^{t_{n-1}} \tau_{n-1}^{\mathtt{N}-1} \mathtt{g}_{n-1}\left(\int_{\tau_{n-1}}^{1} \phi^{-1}\left[\frac{1}{t_n^{\mathtt{N}-1}} \int_0^{t_n} \tau_n^{\mathtt{N}-1} \mathtt{g}_n\big(\mathtt{z}_1(\tau_n)\big) d\tau_n\right] dt_n\right) d\tau_{n-1}\right] dt_{n-1} \\
&\quad \leq \int_0^1 \phi^{-1}\left[\frac{1}{t_{n-1}^{\mathtt{N}-1}} \int_0^{t_{n-1}} \tau_{n-1}^{\mathtt{N}-1} \mathtt{g}_{n-1}\big(\mathtt{R}_k\big) d\tau_{n-1}\right] dt_{n-1} \\
&\quad \leq \int_0^1 \phi^{-1}\left[\frac{1}{t_{n-1}^{\mathtt{N}-1}} \int_0^{t_{n-1}} \tau_{n-1}^{\mathtt{N}-1} \mathtt{N}\phi\big(\mathtt{R}_k\big) d\tau_{n-1}\right] dt_{n-1} \\
&\quad \leq \int_0^1 \phi^{-1}\left(\phi\big(\mathtt{R}_k\big) t_{n-1}\right) dt_{n-1} \\
&\quad \leq \mathtt{R}_k.
\end{aligned}$$

Continuing with this bootstrapping argument, we get

$$\begin{aligned}
(\aleph \mathtt{z}_1)(r) = \int_r^1 \phi^{-1}\Bigg[\frac{1}{t_1^{\mathtt{N}-1}} \int_0^{t_1} \tau_1^{\mathtt{N}-1} \mathtt{g}_1\Bigg(\int_{\tau_1}^{1} \phi^{-1}\Bigg[\frac{1}{t_2^{\mathtt{N}-1}} \int_0^{t_2} \tau_2^{\mathtt{N}-1} \mathtt{g}_2\Bigg(\int_{\tau_2}^{1} \phi^{-1}\Bigg[\cdots \\
\mathtt{g}_{n-1}\Bigg(\int_{\tau_{n-1}}^{1} \phi^{-1}\left[\frac{1}{t_n^{\mathtt{N}-1}} \int_0^{t_n} \tau_n^{\mathtt{N}-1} \mathtt{g}_n\big(\mathtt{z}_1(\tau_n)\big) d\tau_n\right] dt_n\Bigg) \cdots d\tau_1\Bigg] dt_1 \\
\leq \mathtt{R}_k.
\end{aligned}$$

Since $\mathtt{R}_k = \|\mathtt{z}_1\|$ for $\mathtt{z}_1 \in \mathtt{P}_{\delta_k} \cap \partial \mathtt{E}_k$, we get

$$\|\aleph \mathtt{z}_1\| \leq \|\mathtt{z}_1\|. \tag{3.1}$$

Let $r \in [\delta_k, 1-\delta_k]$. Then,

$$\mathtt{S}_k = \|\mathtt{z}_1\| \geq \mathtt{z}_1(r) \geq \min_{r\in[\delta_k,1-\delta_k]} \mathtt{z}_1(r) \geq \delta_k \|\mathtt{z}_1\| \geq \delta_k \mathtt{S}_k.$$

By $(\mathcal{H}_4)$ and for $\tau_{n-1} \in [\delta_k, 1-\delta_k]$, we have

$$\begin{aligned}
\int_{\tau_{n-1}}^{1} \phi^{-1}\left[\frac{1}{t_n^{\mathtt{N}-1}}\int_0^{t_n} \tau_n^{\mathtt{N}-1}\mathtt{g}_n\big(\mathtt{z}_1(\tau_n)\big)d\tau_n\right]dt_n &\geq \int_{1-\delta_k}^{1} \phi^{-1}\left[\frac{1}{t_n^{\mathtt{N}-1}}\int_{\delta_k}^{1-\delta_k} \tau_n^{\mathtt{N}-1}\mathtt{g}_n\big(\mathtt{z}_1(\tau_n)\big)d\tau_n\right]dt_n \\
&\geq \delta_k \phi^{-1}\left[\frac{1}{t_n^{\mathtt{N}-1}}\int_{\delta_k}^{1-\delta_k} \tau_n^{\mathtt{N}-1}\mathtt{g}_n\big(\mathtt{z}_1(\tau_n)\big)d\tau_n\right] \\
&\geq \delta_k \phi^{-1}\left[\frac{1}{(1-\delta_k)^{\mathtt{N}-1}}\int_{\delta_k}^{1-\delta_k} \tau_n^{\mathtt{N}-1}\beta_k \mathtt{N}\phi\left(\frac{\mathtt{S}_k}{\delta_k}\right)d\tau_n\right] \\
&\geq \delta_k \phi^{-1}\left[\frac{(1-\delta_k)^{\mathtt{N}}-\delta_k^{\mathtt{N}}}{(1-\delta_k)^{\mathtt{N}-1}}\beta_k\phi\left(\frac{\mathtt{S}_k}{\delta_k}\right)\right] \\
&\geq \mathtt{S}_k.
\end{aligned}$$

In similar manner (for $\tau_{n-2} \in [\delta_k, 1-\delta_k]$,) that

$$\begin{aligned}
&\int_{\tau_{n-2}}^{1} \phi^{-1}\left[\frac{1}{t_{n-1}^{\mathtt{N}-1}}\int_0^{t_{n-1}} \tau_{n-1}^{\mathtt{N}-1}\mathtt{g}_{n-1}\left(\int_{\tau_{n-1}}^{1} \phi^{-1}\left[\frac{1}{t_n^{\mathtt{N}-1}}\int_0^{t_n} \tau_n^{\mathtt{N}-1}\mathtt{g}_n\big(\mathtt{z}_1(\tau_n)\big)d\tau_n\right]dt_n\right)d\tau_{n-1}\right]dt_{n-1} \\
&\quad\geq \int_{1-\delta_k}^{1} \phi^{-1}\left[\frac{1}{t_{n-1}^{\mathtt{N}-1}}\int_{\delta_k}^{1-\delta_k} \tau_{n-1}^{\mathtt{N}-1}\mathtt{g}_{n-1}\left(\int_{\tau_{n-1}}^{1} \phi^{-1}\left[\frac{1}{t_n^{\mathtt{N}-1}}\int_0^{t_n} \tau_n^{\mathtt{N}-1}\mathtt{g}_n\big(\mathtt{z}_1(\tau_n)\big)d\tau_n\right]dt_n\right)d\tau_{n-1}\right]dt_{n-1} \\
&\quad\geq \int_{1-\delta_k}^{1} \phi^{-1}\left[\frac{1}{t_{n-1}^{\mathtt{N}-1}}\int_{\delta_k}^{1-\delta_k} \tau_{n-1}^{\mathtt{N}-1}\mathtt{g}_{n-1}\big(\mathtt{S}_k\big)d\tau_{n-1}\right]dt_{n-1} \\
&\quad\geq \delta_k \phi^{-1}\left[\frac{1}{(1-\delta_k)^{\mathtt{N}-1}}\int_{\delta_k}^{1-\delta_k} \tau_{n-1}^{\mathtt{N}-1}\beta_k \mathtt{N}\phi\left(\frac{\mathtt{S}_k}{\delta_k}\right)d\tau_{n-1}\right] \\
&\quad\geq \delta_k \phi^{-1}\left[\frac{(1-\delta_k)^{\mathtt{N}}-\delta_k^{\mathtt{N}}}{(1-\delta_k)^{\mathtt{N}-1}}\beta_k\phi\left(\frac{\mathtt{S}_k}{\delta_k}\right)\right] \\
&\quad\geq \mathtt{S}_k.
\end{aligned}$$

Continuing with bootstrapping argument, we get

$$\begin{aligned}
(\aleph \mathtt{z}_1)(r) = \int_r^1 \phi^{-1}\Bigg[\frac{1}{t_1^{\mathtt{N}-1}}\int_0^{t_1} \tau_1^{\mathtt{N}-1}\mathtt{g}_1\Bigg(\int_{\tau_1}^{1} \phi^{-1}\Bigg[\frac{1}{t_2^{\mathtt{N}-1}}\int_0^{t_2} \tau_2^{\mathtt{N}-1}\mathtt{g}_2\Bigg(\int_{\tau_2}^{1} \phi^{-1}\Bigg[\cdots \\
\mathtt{g}_{n-1}\left(\int_{\tau_{n-1}}^{1} \phi^{-1}\left[\frac{1}{t_n^{\mathtt{N}-1}}\int_0^{t_n} \tau_n^{\mathtt{N}-1}\mathtt{g}_n\big(\mathtt{z}_1(\tau_n)\big)d\tau_n\right]dt_n\right)\cdots d\tau_1\Bigg]dt_1 \\
\geq \mathtt{S}_k.
\end{aligned}$$

Thus, if $\mathtt{z}_1 \in \mathtt{P}_{\delta_k} \cap \partial \mathtt{F}_k$, then

$$\|\aleph \mathtt{z}_1\| \geq \|\mathtt{z}_1\|. \tag{3.2}$$

It is evident that $0 \in \mathtt{F}_k \subset \overline{\mathtt{F}}_k \subset \mathtt{E}_k$. From (3.1),(3.2), it follows from Theorem 3.1 that the operator $\aleph$ has a fixed point $\mathtt{z}_1^{[k]} \in \mathtt{P}_{\delta_k} \cap \left(\overline{\mathtt{E}}_k \backslash \mathtt{F}_k\right)$ such that $\mathtt{z}_1^{[k]}(t) \geq 0$ on $(0,1)$, and $k \in \mathbb{N}$. Next setting $\mathtt{z}_{\mathtt{j}+1} = \mathtt{z}_1$, we obtain denumerably many positive solutions $\{(\mathtt{z}_1^{[k]}, \mathtt{z}_2^{[k]}, \cdots, \mathtt{z}_n^{[k]})\}_{k=1}^{\infty}$ of (1.1) given iteratively by

$$\mathtt{z}_{\mathtt{j}}(r) = \int_r^1 \phi^{-1}\left(\frac{1}{t^{\mathtt{N}-1}} \int_0^t \tau^{\mathtt{N}-1} \mathtt{g}_{\mathtt{j}}(\mathtt{z}_{\mathtt{j}+1}(\tau)) d\tau\right) dt, \ \mathtt{j} = n, n-1, \cdots, 2, 1.$$

The proof is completed. □

Example 3.5. *Consider the following iterative system of Dirichlet problems*

$$\left.\begin{array}{ll} \mathcal{M}_C(\mathtt{z}_{\mathtt{j}}) + \mathtt{g}_{\mathtt{j}}(\mathtt{z}_{\mathtt{j}+1}) = 0 & \text{in } \Omega \\ \mathtt{z}_{\mathtt{j}} = 0 & \text{on } \partial\Omega, \end{array}\right\} \tag{3.3}$$

where $\mathtt{j} = 1, 2$, $\mathtt{N} = 1$ and $\mathtt{z}_1 = \mathtt{z}_3$. Let

$$r_k = \frac{31}{64} - \sum_{s=1}^{k} \frac{1}{4(s+1)^4}, \ \delta_k = \frac{1}{2}(r_k + r_{k+1}), \ k = 1, 2, 3, \cdots,$$

then

$$\delta_1 = \frac{15}{32} - \frac{1}{648} < \frac{15}{32}$$

and

$$r_{k+1} < \delta_k < r_k, \ \delta_k > \frac{1}{5}.$$

It is easy to see

$$r_1 = \frac{15}{32} < \frac{1}{2}, \ r_k - r_{k+1} = \frac{1}{4(k+2)^4}, \ k = 1, 2, 3, \cdots.$$

Since $\sum_{k=1}^{\infty} \frac{1}{k^4} = \frac{\pi^4}{90}$ and $\sum_{k=1}^{\infty} \frac{1}{k^2} = \frac{\pi^2}{6}$, it follows that

$$\begin{aligned} r^* = \lim_{k\to\infty} r_k &= \frac{31}{64} - \sum_{j=1}^{\infty} \frac{1}{4(j+1)^4} \\ &= \frac{47}{64} - \frac{\pi^4}{360} > \frac{1}{5}. \end{aligned}$$

In addition if we take

$$\mathtt{R}_k = 10^{-4k}, \ \mathtt{S}_k = 10^{-(4k+2)},$$

then

$$\begin{aligned} \mathtt{R}_{k+1} = 10^{-(4k+4)} &< \frac{1}{5} \times 10^{-(4k+2)} < \delta_k \mathtt{S}_k \\ &< \mathtt{S}_k = 10^{-(4k+2)} < \mathtt{R}_k = 10^{-4k}, \end{aligned}$$

$$\phi(\mathtt{R}_k) = \frac{1}{\sqrt{10^{8k}-1}}, \ \phi(\mathtt{S}_k) = \frac{1}{\sqrt{10^{8k+4}-1}}, \quad \text{and} \quad \phi\left(\frac{\mathtt{S}_k}{\delta_k}\right) = \frac{1}{\sqrt{10^{8k+4} \times \delta_k^2 - 1}}.$$

Since ϕ is increasing and $\delta_k^{-1}S_k \leq 5S_k \leq R_k$, it follows that

$$\beta_k N\phi\left(\frac{S_k}{\delta_k}\right) \leq N\phi(R_k), \quad \beta_k = 1 - 2\delta_k < 1.$$

Let M_1 and M_2 be two positive numbers such that

$$\beta_k N\phi\left(\frac{S_k}{\delta_k}\right) \leq M_1 \times 10^{-8k} \leq M_2 \times 10^{8k} \leq N\phi(R_k),$$

and

$$g_1(z) = g_2(z) = \begin{cases} M_2 \times 10^{-4}, & z \in (10^{-4}, +\infty), \\ \frac{M_1\times 10^{-(4k+2)} - M_2 \times 10^{-4k}}{10^{-(4k+2)} - 10^{-4k}}(z - 10^{-4k}) + M_2 \times 10^{-4k}, & \\ \qquad z \in \left[10^{-(4k+2)}, 10^{-4k}\right], & \\ M_1 \times 10^{-(4k+2)}, \qquad z \in \left(\frac{1}{5} \times 10^{-(4k+2)}, 10^{-(4k+2)}\right), & \\ \frac{M_1\times 10^{-(4k+2)} - M_2 \times 10^{-(4k+4)}}{\frac{1}{5}\times 10^{-(4k+2)} - 10^{-(4k+4)}}(z - 10^{-(4k+4)}) + M_2 \times 10^{-(4k+4)}, & \\ \qquad z \in \left(10^{-(4k+4)}, \frac{1}{5} \times 10^{-(4k+2)}\right], & \\ 0, \qquad z = 0. & \end{cases}$$

Then, g_1 and g_2 satisfies the following growth conditions:

$$g_1(z) = g_2(z) \leq N\phi(R_k), \quad z \in \left[0, 10^{-4k}\right],$$
$$g_1(z) = g_2(z) \geq \beta_k N\phi\left(\frac{S_k}{\delta_k}\right), \quad z \in \left[\frac{1}{5} \times 10^{-(4k+2)}, 10^{-(4k+2)}\right].$$

All the conditions of Theorem 3.4 are satisfied. Therefore, by Theorem 3.4, the boundary value problem (3.3) has denumerably many positive radial solutions $\{(z_1^{[k]}, z_2^{[k]})\}_{k=1}^{\infty}$ such that $10^{-(4k+2)} \leq \|z_j^{[k]}\| \leq 10^{-4k}$ for each $k = 1, 2, 3, \cdots$, $j = 1, 2$.

3.2. Existence of Atleast Two Denumerably Many Families of Positive Radial Solutions

In order to use Theorem 3.2, let $\delta_k < r_k < 1 - \delta_k$ and δ_k of Theorem 3.1, we define the nonnegative, increasing, continuous functional γ_k, β_k, and α_k by

$$\gamma(z) = \min_{r\in[r_k, 1-\delta_k]} z(r) = z(r_k),$$
$$\theta(z) = \max_{r\in[\delta_k, r_k]} z(r) = z(r_k),$$
$$\alpha(z) = \max_{r\in[\delta_k, 1-\delta_k]} z(r) = z(1 - \delta_k).$$

It is obvious that for each $\mathtt{z} \in \mathtt{P}$,

$$\gamma_k(\mathtt{z}) = \theta_k(\mathtt{z}) \leq \alpha_k(\mathtt{z}).$$

In addition, by Lemma 2.3, for each $\mathtt{z} \in \mathtt{P}$,

$$\gamma(\mathtt{z}) = \mathtt{z}(r_k) \geq \delta_k \|\mathtt{z}\|.$$

Thus

$$\|\mathtt{z}\| \leq \delta_k^{-1}\gamma(\mathtt{z}), \quad \text{for all} \quad \mathtt{z} \in \mathtt{P}.$$

Finally, we also note that

$$\theta(\lambda \mathtt{z}) = \lambda\theta(\mathtt{z}), \quad 0 \leq \lambda \leq 1 \quad \text{and} \quad \mathtt{z} \in \mathtt{P}.$$

Theorem 3.6. *Assume that* $(\mathcal{H}_1)$*–*$(\mathcal{H}_2)$ *hold and let* $\{\delta_k\}_{k=1}^{\infty}$ *be a sequence with* $r_{k+1} < \delta_k < r_k$, $k \in \mathbb{N}$. *Let* $\{\mathtt{R}_k\}_{k=1}^{\infty}$, $\{\mathtt{Q}_k\}_{k=1}^{\infty}$ *and* $\{\mathtt{S}_k\}_{k=1}^{\infty}$ *be three sequences which satisfies the relation*

$$\mathtt{R}_{k+1} < \mathtt{Q}_k < \delta_k \mathtt{S}_k < \mathtt{S}_k < \mathtt{R}_k, \quad \beta_k \phi(\delta_k^{-1}\mathtt{S}_k) < \phi(\mathtt{R}_k),\ k \in \mathbb{N}.$$

Furthermore for each natural number k, *we assume that* $\mathtt{g}_\mathtt{j}(\mathtt{j} = 1, 2, \cdots, n)$ *satisfies*

$(\mathcal{H}_5)$ $\mathtt{g}_\mathtt{j}(\mathtt{z}) > \beta_k \mathtt{N}\phi(\delta_k^{-1}\mathtt{S}_k)$, *for all* $\mathtt{S}_k \leq \mathtt{z}(r) \leq \delta_k^{-1}\mathtt{S}_k$,

$(\mathcal{H}_6)$ $\mathtt{g}_\mathtt{j}(\mathtt{z}) < \mathtt{N}\phi(\mathtt{R}_k)$, *for all* $0 \leq \mathtt{z}(r) \leq \delta_k^{-1}\mathtt{R}_k$,

$(\mathcal{H}_7)$ $\mathtt{g}_\mathtt{j}(\mathtt{z}) > \beta_k \mathtt{N}\phi(\delta_k^{-1}\mathtt{Q}_k)$, *for all* $0 \leq \mathtt{z}(r) \leq \mathtt{Q}_k$.

Then the boundary value problem (1.1) *has two denumerably many families of radial solutions* $\{({}^1\mathtt{z}_1^{[k]}, {}^1\mathtt{z}_2^{[k]}, \cdots, {}^1\mathtt{z}_n^{[k]})\}_{k=1}^{\infty}$ *and* $\{({}^2\mathtt{z}_1^{[k]}, {}^2\mathtt{z}_2^{[k]}, \cdots, {}^2\mathtt{z}_n^{[k]})\}_{k=1}^{\infty}$ *satisfying*

$$\mathtt{Q}_k < \alpha_k\left({}^1\mathtt{z}_\mathtt{j}^{[k]}\right) \quad \text{with} \quad \theta_k\left({}^1\mathtt{z}_\mathtt{j}^{[k]}\right) < \mathtt{S}_k, \ \mathtt{j} = 1, 2, \cdots, n,\ k \in \mathbb{N}$$

and

$$\mathtt{S}_k < \theta_k\left({}^2\mathtt{z}_\mathtt{j}^{[k]}\right) \quad \text{with} \quad \gamma_k\left({}^2\mathtt{z}_\mathtt{j}^{[k]}\right) < \mathtt{R}_k, \ \mathtt{j} = 1, 2, \cdots, n,\ k \in \mathbb{N}.$$

Proof . We begin by defining the completely continuous operator $\aleph$ by (2.4). So it is easy to check that $\aleph : \overline{\mathtt{P}(\gamma, \mathtt{S}_k)} \to \mathtt{P}$, for $k \in \mathbb{N}$. Firstly, we shall verify that condition (a) of Theorem 3.2 is satisfied. So, let us choose $\mathtt{z}_1 \in \partial\mathtt{P}(\gamma, \mathtt{S}_k)$. Then $\gamma(\mathtt{z}_1) = \min_{r\in[r_k, 1-\delta_k]} \mathtt{z}_1(r) = \mathtt{z}_1(r_k) = \mathtt{S}_k$ this implies that $\mathtt{S}_k \leq \mathtt{z}_1(r)$ for $r \in [r_k, 1]$. Since $\|\mathtt{z}_1\| \leq \delta_k^{-1}\gamma(\mathtt{z}_1) = \delta_k^{-1}\mathtt{S}_k$. So we have

$$\mathtt{S}_k \leq \mathtt{z}_1(r) \leq \delta_k^{-1}\mathtt{S}_k, \ r \in [r_k, 1 - \delta_k].$$

Let $\tau_{n-1} \in [r_k, 1 - \delta_k]$. Then by $(\mathcal{H}_5)$, we have

$$\begin{aligned}
\int_{\tau_{n-1}}^{1} \phi^{-1}\left[\frac{1}{t_n^{\mathtt{N}-1}}\int_0^{t_n} \tau_n^{\mathtt{N}-1}\mathtt{g}_n\big(\mathtt{z}_1(\tau_n)\big)d\tau_n\right]dt_n &\geq \int_{1-\delta_k}^{1} \phi^{-1}\left[\frac{1}{t_n^{\mathtt{N}-1}}\int_{\delta_k}^{1-\delta_k} \tau_n^{\mathtt{N}-1}\mathtt{g}_n\big(\mathtt{z}_1(\tau_n)\big)d\tau_n\right]dt_n \\
&\geq \delta_k\phi^{-1}\left[\frac{1}{t_n^{\mathtt{N}-1}}\int_{\delta_k}^{1-\delta_k} \tau_n^{\mathtt{N}-1}\mathtt{g}_n\big(\mathtt{z}_1(\tau_n)\big)d\tau_n\right] \\
&\geq \delta_k\phi^{-1}\left[\frac{1}{(1-\delta_k)^{\mathtt{N}-1}}\int_{\delta_k}^{1-\delta_k} \tau_n^{\mathtt{N}-1}\beta_k\mathtt{N}\phi\left(\frac{\mathtt{S}_k}{\delta_k}\right)d\tau_n\right] \\
&\geq \delta_k\phi^{-1}\left[\frac{(1-\delta_k)^{\mathtt{N}} - \delta_k^{\mathtt{N}}}{(1-\delta_k)^{\mathtt{N}-1}}\beta_k\phi\left(\frac{\mathtt{S}_k}{\delta_k}\right)\right] \\
&\geq \mathtt{S}_k.
\end{aligned}$$

In similar manner (for $\tau_{n-2} \in\in [r_k, 1-\delta_k]$,) that

$$\begin{aligned}
&\int_{\tau_{n-2}}^{1} \phi^{-1}\left[\frac{1}{t_{n-1}^{N-1}}\int_0^{t_{n-1}} \tau_{n-1}^{N-1} g_{n-1}\left(\int_{\tau_{n-1}}^{1}\phi^{-1}\left[\frac{1}{t_n^{N-1}}\int_0^{t_n}\tau_n^{N-1} g_n\big(z_1(\tau_n)\big)d\tau_n\right]dt_n\right)d\tau_{n-1}\right]dt_{n-1}\\
&\quad\geq \int_{1-\delta_k}^{1} \phi^{-1}\left[\frac{1}{t_{n-1}^{N-1}}\int_{\delta_k}^{1-\delta_k} \tau_{n-1}^{N-1} g_{n-1}\left(\int_{\tau_{n-1}}^{1}\phi^{-1}\left[\frac{1}{t_n^{N-1}}\int_0^{t_n}\tau_n^{N-1} g_n\big(z_1(\tau_n)\big)d\tau_n\right]dt_n\right)d\tau_{n-1}\right]dt_{n-1}\\
&\quad\geq \int_{1-\delta_k}^{1} \phi^{-1}\left[\frac{1}{t_{n-1}^{N-1}}\int_{\delta_k}^{1-\delta_k} \tau_{n-1}^{N-1} g_{n-1}\big(S_k\big)d\tau_{n-1}\right]dt_{n-1}\\
&\quad\geq \delta_k\phi^{-1}\left[\frac{1}{(1-\delta_k)^{N-1}}\int_{\delta_k}^{1-\delta_k} \tau_{n-1}^{N-1}\beta_k N\phi\left(\frac{S_k}{\delta_k}\right)d\tau_{n-1}\right]\\
&\quad\geq \delta_k\phi^{-1}\left[\frac{(1-\delta_k)^N-\delta_k^N}{(1-\delta_k)^{N-1}}\beta_k\phi\left(\frac{S_k}{\delta_k}\right)\right]\\
&\quad\geq S_k.
\end{aligned}$$

Continuing with bootstrapping argument, we get

$$\begin{aligned}
\gamma(\aleph z_1) &= \min_{r\in[r_k,1-\delta_k]}(\aleph z_1)(r) = (\aleph z_1)(r_k)\\
&= \int_{r_k}^{1}\phi^{-1}\left[\frac{1}{t_1^{N-1}}\int_0^{t_1}\tau_1^{N-1}g_1\left(\int_{\tau_1}^{1}\phi^{-1}\left[\frac{1}{t_2^{N-1}}\int_0^{t_2}\tau_2^{N-1}g_2\left(\int_{\tau_2}^{1}\phi^{-1}\Big[\cdots\right.\right.\right.\right.\\
&\qquad g_{n-1}\left(\int_{\tau_{n-1}}^{1}\phi^{-1}\left[\frac{1}{t_n^{N-1}}\int_0^{t_n}\tau_n^{N-1}g_n\big(z_1(\tau_n)\big)d\tau_n\right]dt_n\right)\cdots d\tau_1\Big]dt_1\\
&\geq \int_{1-\delta_k}^{1}\phi^{-1}\left[\frac{1}{t_1^{N-1}}\int_0^{t_1}\tau_1^{N-1}g_1\left(\int_{\tau_1}^{1}\phi^{-1}\left[\frac{1}{t_2^{N-1}}\int_0^{t_2}\tau_2^{N-1}g_2\left(\int_{\tau_2}^{1}\phi^{-1}\Big[\cdots\right.\right.\right.\right.\\
&\qquad g_{n-1}\left(\int_{\tau_{n-1}}^{1}\phi^{-1}\left[\frac{1}{t_n^{N-1}}\int_0^{t_n}\tau_n^{N-1}g_n\big(z_1(\tau_n)\big)d\tau_n\right]dt_n\right)\cdots d\tau_1\Big]dt_1\\
&\geq S_k.
\end{aligned}$$

This proves (i) of Theorem 3.2. We next address (ii) of Theorem 3.2. So, we choose $z_1 \in \partial P(\theta, R_k)$. Then $\theta(z_1) = \max_{r\in[\delta_k,r_k]} z_1(r) = z_1(r_k) = R_k$ this implies that $0 \leq z_1(r) \leq R_k$ for $r \in [0, r_k]$. Since $\|z_1\| \leq \delta_k^{-1}\gamma(z_1) = \delta_k^{-1}\theta(z_1) = \delta_k^{-1}R_k$. So we have

$$0 \leq z_1(r) \leq \delta_k^{-1}R_k,\ r \in [0,1].$$

Let $0 < \tau_{n-1} < 1$. Then by $(\mathcal{H}_6)$, we have

$$\begin{aligned}
\int_{\tau_{n-1}}^{1}\phi^{-1}\left[\frac{1}{t_n^{N-1}}\int_0^{t_n}\tau_n^{N-1}g_n\big(z_1(\tau_n)\big)d\tau_n\right]dt_n &\leq \int_0^1\phi^{-1}\left[\frac{1}{t_n^{N-1}}\int_0^{t_n}\tau_n^{N-1}g_n\big(z_1(\tau_n)\big)d\tau_n\right]dt_n\\
&\leq \int_0^1\phi^{-1}\left[\frac{1}{t_n^{N-1}}\int_0^{t_n}\tau_n^{N-1}N\phi\big(R_k\big)d\tau_n\right]dt_n\\
&\leq \int_0^1\phi^{-1}\left(\phi\big(R_k\big)t_n\right)dt_n\\
&\leq R_k.
\end{aligned}$$

It follows in similar manner for $0 < \tau_{n-2} < 1$, we have

$$\begin{aligned}
&\int_{\tau_{n-2}}^{1} \phi^{-1}\left[\frac{1}{t_{n-1}^{N-1}}\int_0^{t_{n-1}} \tau_{n-1}^{N-1} g_{n-1}\left(\int_{\tau_{n-1}}^{1} \phi^{-1}\left[\frac{1}{t_n^{N-1}}\int_0^{t_n} \tau_n^{N-1} g_n\big(z_1(\tau_n)\big)d\tau_n\right]dt_n\right)d\tau_{n-1}\right]dt_{n-1}\\
&\qquad \le \int_0^1 \phi^{-1}\left[\frac{1}{t_{n-1}^{N-1}}\int_0^{t_{n-1}} \tau_{n-1}^{N-1} g_{n-1}\big(S_k\big)d\tau_{n-1}\right]dt_{n-1}\\
&\qquad \le \int_0^1 \phi^{-1}\left[\frac{1}{t_{n-1}^{N-1}}\int_0^{t_{n-1}} \tau_{n-1}^{N-1} N\phi\big(R_k\big)d\tau_{n-1}\right]dt_{n-1}\\
&\qquad \le \int_0^1 \phi^{-1}\left(\phi\big(R_k\big)t_{n-1}\right)dt_{n-1}\\
&\qquad \le R_k.
\end{aligned}$$

Continuing with this bootstrapping argument, we get

$$\begin{aligned}
\theta_k(\aleph z_1) &= \max_{r\in[\delta_k, r_k]}(\aleph z_1)(r) = (\aleph z_1)(r_k)\\
&= \int_{r_k}^{1} \phi^{-1}\left[\frac{1}{t_1^{N-1}}\int_0^{t_1} \tau_1^{N-1} g_1\left(\int_{\tau_1}^{1} \phi^{-1}\left[\frac{1}{t_2^{N-1}}\int_0^{t_2} \tau_2^{N-1} g_2\left(\int_{\tau_2}^{1} \phi^{-1}\Big[\cdots\right.\right.\right.\right.\\
&\quad \left.\left.\left.\left. g_{n-1}\left(\int_{\tau_{n-1}}^{1} \phi^{-1}\left[\frac{1}{t_n^{N-1}}\int_0^{t_n} \tau_n^{N-1} g_n\big(z_1(\tau_n)\big)d\tau_n\right]dt_n\right)\cdots d\tau_1\Big]dt_1\right.\right.\right.\right.\\
&\le \int_0^{1} \phi^{-1}\left[\frac{1}{t_1^{N-1}}\int_0^{t_1} \tau_1^{N-1} g_1\left(\int_{\tau_1}^{1} \phi^{-1}\left[\frac{1}{t_2^{N-1}}\int_0^{t_2} \tau_2^{N-1} g_2\left(\int_{\tau_2}^{1} \phi^{-1}\Big[\cdots\right.\right.\right.\right.\\
&\quad \left.\left.\left.\left. g_{n-1}\left(\int_{\tau_{n-1}}^{1} \phi^{-1}\left[\frac{1}{t_n^{N-1}}\int_0^{t_n} \tau_n^{N-1} g_n\big(z_1(\tau_n)\big)d\tau_n\right]dt_n\right)\cdots d\tau_1\Big]dt_1\right.\right.\right.\right.\\
&\le R_k.
\end{aligned}$$

Hence condition (c) is satisfied. Finally we verify that (c) of Theorem 3.2 is also satisfied. We note that $z_1(r) = Q_k/4$, $r \in [0,1]$ is a member of $P(\alpha_k, Q_k)$ and $Q_k/4 < Q_k$. So $P(\alpha_k, Q_k) \neq \emptyset$. Now let $z_1 \in P(\alpha_k, Q_k)$. Then $\alpha_k(z_1) = \max_{r\in[\delta_k, 1-\delta_k]} z_1(r) = z_1(1-\delta_k) = Q_k$, i.e., $0 \le z_1(r) \le Q_k$, for $r \in [\delta_k, 1-\delta_k]$. Let $0 < \tau_{n-1} < 1$. Then by $(\mathcal{H}_7)$, we have

$$\begin{aligned}
\int_{\tau_{n-1}}^{1} \phi^{-1}\left[\frac{1}{t_n^{N-1}}\int_0^{t_n} \tau_n^{N-1} g_n\big(z_1(\tau_n)\big)d\tau_n\right]dt_n &\ge \int_{1-\delta_k}^{1} \phi^{-1}\left[\frac{1}{t_n^{N-1}}\int_{\delta_k}^{1-\delta_k} \tau_n^{N-1} g_n\big(z_1(\tau_n)\big)d\tau_n\right]dt_n\\
&\ge \delta_k \phi^{-1}\left[\frac{1}{t_n^{N-1}}\int_{\delta_k}^{1-\delta_k} \tau_n^{N-1} g_n\big(z_1(\tau_n)\big)d\tau_n\right]\\
&\ge \delta_k \phi^{-1}\left[\frac{1}{(1-\delta_k)^{N-1}}\int_{\delta_k}^{1-\delta_k} \tau_n^{N-1}\beta_k N\phi\left(\frac{Q_k}{\delta_k}\right)d\tau_n\right]\\
&\ge \delta_k \phi^{-1}\left[\frac{(1-\delta_k)^N - \delta_k^N}{(1-\delta_k)^{N-1}}\beta_k \phi\left(\frac{Q_k}{\delta_k}\right)\right]\\
&\ge Q_k.
\end{aligned}$$

Continuing with this bootstrapping argument, we get

$$\begin{aligned}\alpha_k(\aleph \mathtt{z}_1) &= \max_{r\in[\delta_k,1-\delta_k]}(\aleph \mathtt{z}_1)(r) = (\aleph \mathtt{z}_1)(1-\delta_k)\\ &= \int_{1-\delta_k}^{1} \phi^{-1}\left[\frac{1}{t_1^{\mathtt{N}-1}}\int_0^{t_1}\tau_1^{\mathtt{N}-1}\mathtt{g}_1\left(\int_{\tau_1}^{1}\phi^{-1}\left[\frac{1}{t_2^{\mathtt{N}-1}}\int_0^{t_2}\tau_2^{\mathtt{N}-1}\mathtt{g}_2\left(\int_{\tau_2}^{1}\phi^{-1}\left[\cdots\right.\right.\right.\right.\right.\\ &\quad \left.\left.\left.\left.\left.\mathtt{g}_{n-1}\left(\int_{\tau_{n-1}}^{1}\phi^{-1}\left[\frac{1}{t_n^{\mathtt{N}-1}}\int_0^{t_n}\tau_n^{\mathtt{N}-1}\mathtt{g}_n\big(\mathtt{z}_1(\tau_n)\big)d\tau_n\right]dt_n\right)\cdots d\tau_1\right]dt_1\\ &\geq \mathtt{Q}_k.\end{aligned}$$

Thus condition (c) of Theorem 3.2 is satisfied. Since all hypotheses of Theorem 3.2 are satisfied, the assertion follows. □

Example 3.7. *Consider the following iterative system of Dirichlet problems*

$$\left.\begin{aligned}\mathcal{M}_{\mathcal{C}}(\mathtt{z}_{\mathtt{j}}) + \mathtt{g}_{\mathtt{j}}(\mathtt{z}_{\mathtt{j}+1}) = 0 \quad &in \quad \Omega\\ \mathtt{z}_{\mathtt{j}} = 0 \quad &on \quad \partial\Omega,\end{aligned}\right\} \tag{3.4}$$

where $\mathtt{j} = 1, 2$, $\mathtt{N} = 1$ and $\mathtt{z}_1 = \mathtt{z}_3$. Let r_k, δ_k be the same as of Example 3.5. In addition if we take

$$\mathtt{R}_k = 10^{-4k},\ \mathtt{Q}_k = 10^{-(4k+3)} \quad \text{and} \quad \mathtt{S}_k = 10^{-(4k+2)},$$

then

$$\begin{aligned}\mathtt{R}_{k+1} = 10^{-(4k+4)} < \mathtt{Q}_k = 10^{-(4k+3)} &< \frac{1}{5}\times 10^{-(4k+2)} < \delta_k \mathtt{S}_k\\ &< \mathtt{S}_k = 10^{-(4k+2)} < \mathtt{R}_k = 10^{-4k},\end{aligned}$$

$$\phi(\mathtt{R}_k) = \frac{1}{\sqrt{10^{8k}-1}},\ \phi(\mathtt{Q}_k) = \frac{1}{\sqrt{10^{8k+6}-1}},\ \phi(\mathtt{S}_k) = \frac{1}{\sqrt{10^{8k+4}-1}},$$

$$\phi(\delta_k^{-1}\mathtt{R}_k) = \frac{1}{\sqrt{10^{8k}\times\delta_k^2-1}} \quad \text{and} \quad \phi(\delta_k^{-1}\mathtt{Q}_k) = \frac{1}{\sqrt{10^{8k+6}\times\delta_k^2-1}}.$$

Since ϕ is increasing and $\delta_k^{-1}\mathtt{S}_k \leq 5\mathtt{S}_k \leq \mathtt{R}_k$, it follows that

$$\beta_k \mathtt{N}\phi(\delta_k^{-1}\mathtt{S}_k) \leq \mathtt{N}\phi(\mathtt{R}_k), \quad \beta_k = 1-2\delta_k < 1.$$

Let $\mathtt{N}_1$ and $\mathtt{N}_2$ be two positive numbers such that

$$\mathtt{N}_1\times 10^{-8k} \leq \mathtt{N}_2\times 10^{-8k} \leq \beta_k\mathtt{N}\phi(\delta_k^{-1}\mathtt{Q}_k) \leq \beta_k\mathtt{N}\phi(\delta_k^{-1}\mathtt{S}_k) \leq \mathtt{N}_2\times 10^{8k} \leq \mathtt{N}\phi(\mathtt{R}_k),$$

and

$$g_1(z) = g_2(z) = \begin{cases} N_2 \times 10^{-6}, & z \in (5 \times 10^{-4}, +\infty), \\ N_2 \times 10^{-(4k+2)}, & z \in \left(10^{-(4k+2)}, 5 \times 10^{-4k}\right], \\ \frac{N_2 \times 10^{-(4k+3)} - N_2 \times 10^{-(4k+2)}}{5 \times 10^{-(4k+3)} - 10^{-(4k+2)}}(z - 10^{-(4k+2)}) + N_2 \times 10^{-(4k+2)}, & \\ \qquad z \in \left[5 \times 10^{-(4k+3)}, 10^{-(4k+2)}\right], & \\ N_2 \times 10^{-(4k+3)}, & z \in \left(10^{-(4k+3)}, 5 \times 10^{-(4k+3)}\right), \\ \frac{N_1 \times 10^{-(4k+4)} - N_2 \times 10^{-(4k+3)}}{10^{-(4k+4)} - 10^{-(4k+3)}}(z - 10^{-(4k+3)}) + N_2 \times 10^{-(4k+3)}, & \\ \qquad z \in \left(10^{-(4k+4)}, 10^{-(4k+3)}\right], & \\ 0, & z = 0. \end{cases}$$

Then, g_1 and g_2 satisfies the following growth conditions:

$$g_1(z) = g_2(z) \geq \beta_k N \phi(\delta_k^{-1} S_k), \quad z \in \left[10^{-(4k+2)}, 5 \times 10^{-(4k+2)}\right],$$

$$g_1(z) = g_2(z) \leq N \phi(R_k), \quad z \in \left[0, 5 \times 10^{-4k}\right],$$

$$g_1(z) = g_2(z) \geq \beta_k N \phi(\delta_k^{-1} Q_k), \quad z \in \left[0, 10^{-(4k+3)}\right].$$

All the conditions of Theorem 3.6 are satisfied. Therefore, by Theorem 3.6, the boundary value problem (3.4) has two denumerably many families of radial solutions $\{({}^1z_1^{[k]}, {}^1z_2^{[k]})\}_{k=1}^{\infty}$ and $\{({}^2z_1^{[k]}, {}^2z_2^{[k]})\}_{k=1}^{\infty}$ satisfying

$$10^{-(4k+3)} < \max_{r \in [\delta_k, 1-\delta_k]} {}^1z_j^{[k]}(r) \quad \text{with} \quad \max_{r \in [\delta_k, r_k]} {}^1z_j^{[k]}(r) < 10^{-(4k+2)}, \ j = 1, 2, \ k \in \mathbb{N}$$

and

$$10^{-(4k+2)} < \max_{r \in [\delta_k, r_k]} {}^2z_j^{[k]}(r) \quad \text{with} \quad \min_{r \in [r_k, 1-\delta_k]} {}^2z_j^{[k]}(r) < 10^{-4k}, \ j = 1, 2, \ k \in \mathbb{N}.$$

3.3. Existence of Atleast Three Denumerably Many Families of Positive Radial Solutions

In order to use Theorem 3.3, let $\delta_k < r_k < 1 - \delta_k$ and δ_k of Theorem 3.1, we define the nonnegative, increasing, continuous functional γ_k, β_k, and α_k by

$$\gamma(z) = \max_{r \in [\delta_k, r_k]} z(r) = z(r_k),$$

$$\beta(z) = \min_{r \in [r_k, 1-\delta_k]} z(r) = z(r_k),$$

$$\alpha(z) = \max_{r \in [\delta_k, 1-\delta_k]} z(r) = z(1 - \delta_k).$$

It is obvious that for each $\mathtt{z} \in \mathtt{P}$,

$$\gamma_k(\mathtt{z}) \leq \beta_k(\mathtt{z}) \leq \alpha_k(\mathtt{z}).$$

In addition, by Lemma 2.3, for each $\mathtt{z} \in \mathtt{P}$,

$$\gamma(\mathtt{z}) = \mathtt{z}(r_k) \geq \delta_k \|\mathtt{z}\|.$$

Thus

$$\|\mathtt{z}\| \leq \delta_k^{-1}\gamma(\mathtt{z}), \quad \text{for all} \quad \mathtt{z} \in \mathtt{P}.$$

Theorem 3.8. *Assume that* $(\mathcal{H}_1)$*–*$(\mathcal{H}_2)$ *hold and let* $\{\delta_k\}_{k=1}^{\infty}$ *be a sequence with* $r_{k+1} < \delta_k < r_k$, $k \in \mathbb{N}$. *Let* $\{\mathtt{R}_k\}_{k=1}^{\infty}$, $\{\mathtt{Q}_k\}_{k=1}^{\infty}$ *and* $\{\mathtt{S}_k\}_{k=1}^{\infty}$ *be three sequences which satisfies the relation*

$$\mathtt{R}_{k+1} < \mathtt{Q}_k < \delta_k \mathtt{S}_k < \mathtt{S}_k < \mathtt{R}_k, \quad \beta_k \phi(\delta_k^{-1}\mathtt{S}_k) < \phi(\mathtt{R}_k),\ k \in \mathbb{N}.$$

Furthermore for each natural number k, *we assume that* $\mathtt{g}_\mathtt{j}(\mathtt{j} = 1, 2, \cdots, n)$ *satisfies*

$(\mathcal{H}_8)$ $\mathtt{g}_\mathtt{j}(\mathtt{z}) < \mathtt{N}\phi(\mathtt{R}_k)$, *for all* $0 \leq \mathtt{z}(r) \leq \delta_k^{-1}\mathtt{R}_k$,

$(\mathcal{H}_9)$ $\mathtt{g}_\mathtt{j}(\mathtt{z}) > \beta_k \mathtt{N}\phi(\delta_k^{-1}\mathtt{S}_k)$, *for all* $\mathtt{S}_k \leq \mathtt{z}(r) \leq \delta_k^{-1}\mathtt{S}_k$,

$(\mathcal{H}_{10})$ $\mathtt{g}_\mathtt{j}(\mathtt{z}) < \mathtt{N}\phi(\mathtt{Q}_k)$, *for all* $0 \leq \mathtt{z}(r) \leq \delta_k^{-1}\mathtt{Q}_k$.

Then the boundary value problem (1.1) *has three denumerably many families of radial solutions* $\{({}^1\mathtt{z}_1^{[k]}, {}^1\mathtt{z}_2^{[k]}, \cdots, {}^1\mathtt{z}_n^{[k]})\}_{k=1}^{\infty}$, $\{({}^2\mathtt{z}_1^{[k]}, {}^2\mathtt{z}_2^{[k]}, \cdots, {}^2\mathtt{z}_n^{[k]})\}_{k=1}^{\infty}$ *and* $\{({}^3\mathtt{z}_1^{[k]}, {}^3\mathtt{z}_2^{[k]}, \cdots, {}^3\mathtt{z}_n^{[k]})\}_{k=1}^{\infty}$ *satisfying*

$$0 \leq \alpha_k\left({}^1\mathtt{z}_\mathtt{j}^{[k]}\right) < \mathtt{Q}_k < \alpha_k\left({}^2\mathtt{z}_\mathtt{j}^{[k]}\right),\ \mathtt{j} = 1, 2, \cdots, n,\ k \in \mathbb{N},$$

$$\beta_k\left({}^2\mathtt{z}_\mathtt{j}^{[k]}\right) < \mathtt{S}_k < \beta_k\left({}^3\mathtt{z}_\mathtt{j}^{[k]}\right),\ \mathtt{j} = 1, 2, \cdots, n,\ k \in \mathbb{N},$$

and

$$\gamma_k\left({}^3\mathtt{z}_\mathtt{j}^{[k]}\right) < \mathtt{R}_k,\ \mathtt{j} = 1, 2, \cdots, n,\ k \in \mathbb{N}.$$

Proof . We define the completely continuous operator $\aleph$ by (2.4). So it is easy to check that $\aleph : \overline{\mathtt{P}(\gamma, \mathtt{R}_k)} \to \mathtt{P}$, for $k \in \mathbb{N}$. In order to prove that all the conditions of Theorem 3.3 are satisfied, we choose $\mathtt{z}_1 \in \partial\mathtt{P}(\gamma, \mathtt{R}_k)$. Then $\gamma(\mathtt{z}_1) = \max_{r\in[\delta_k, r_k]} \mathtt{z}_1(r) = \mathtt{z}_1(r_k) = \mathtt{R}_k$ this implies that $0 \leq \mathtt{z}_1(r) \leq \mathtt{R}_k$ for $r \in [0, r_k]$. Since $\|\mathtt{z}_1\| \leq \delta_k^{-1}\gamma(\mathtt{z}_1) = \delta_k^{-1}\mathtt{R}_k$. So we have

$$0 \leq \mathtt{z}_1(r) \leq \delta_k^{-1}\mathtt{R}_k,\ r \in [0, 1].$$

Let $0 < \tau_{n-1} < 1$. Then by Lemma 2.1 and $(\mathcal{H}_8)$, we have

$$\begin{aligned}
\int_{\tau_{n-1}}^{1} \phi^{-1}\left[\frac{1}{t_n^{\mathtt{N}-1}}\int_0^{t_n} \tau_n^{\mathtt{N}-1}\mathtt{g}_n\big(\mathtt{z}_1(\tau_n)\big)d\tau_n\right]dt_n &\leq \int_0^{1} \phi^{-1}\left[\frac{1}{t_n^{\mathtt{N}-1}}\int_0^{t_n} \tau_n^{\mathtt{N}-1}\mathtt{g}_n\big(\mathtt{z}_1(\tau_n)\big)d\tau_n\right]dt_n \\
&\leq \int_0^{1} \phi^{-1}\left[\frac{1}{t_n^{\mathtt{N}-1}}\int_0^{t_n} \tau_n^{\mathtt{N}-1}\mathtt{N}\phi\big(\mathtt{R}_k\big)d\tau_n\right]dt_n \\
&\leq \int_0^{1} \phi^{-1}\left(\phi\big(\mathtt{R}_k\big)t_n\right)dt_n \\
&\leq \mathtt{R}_k.
\end{aligned}$$

It follows in similar manner for $0<\tau_{n-2}<1$, we have

$$\begin{aligned}
&\int_{\tau_{n-2}}^{1}\phi^{-1}\left[\frac{1}{t_{n-1}^{N-1}}\int_0^{t_{n-1}}\tau_{n-1}^{N-1}g_{n-1}\left(\int_{\tau_{n-1}}^{1}\phi^{-1}\left[\frac{1}{t_n^{N-1}}\int_0^{t_n}\tau_n^{N-1}g_n\big(z_1(\tau_n)\big)d\tau_n\right]dt_n\right)d\tau_{n-1}\right]dt_{n-1}\\
&\quad\le\int_0^1\phi^{-1}\left[\frac{1}{t_{n-1}^{N-1}}\int_0^{t_{n-1}}\tau_{n-1}^{N-1}g_{n-1}\big(R_k\big)d\tau_{n-1}\right]dt_{n-1}\\
&\quad\le\int_0^1\phi^{-1}\left[\frac{1}{t_{n-1}^{N-1}}\int_0^{t_{n-1}}\tau_{n-1}^{N-1}N\phi\big(R_k\big)d\tau_{n-1}\right]dt_{n-1}\\
&\quad\le\int_0^1\phi^{-1}\left(\phi\big(R_k\big)t_{n-1}\right)dt_{n-1}\\
&\quad\le R_k.
\end{aligned}$$

Continuing with this bootstrapping argument, we get

$$\begin{aligned}
\gamma_k(\aleph z_1)&=\max_{r\in[\delta_k,r_k]}(\aleph z_1)(r)=(\aleph z_1)(r_k)\\
&=\int_{r_k}^{1}\phi^{-1}\left[\frac{1}{t_1^{N-1}}\int_0^{t_1}\tau_1^{N-1}g_1\left(\int_{\tau_1}^{1}\phi^{-1}\left[\frac{1}{t_2^{N-1}}\int_0^{t_2}\tau_2^{N-1}g_2\left(\int_{\tau_2}^{1}\phi^{-1}\Bigg[\cdots\right.\right.\right.\right.\\
&\quad\left.\left.\left.\left.g_{n-1}\left(\int_{\tau_{n-1}}^{1}\phi^{-1}\left[\frac{1}{t_n^{N-1}}\int_0^{t_n}\tau_n^{N-1}g_n\big(z_1(\tau_n)\big)d\tau_n\right]dt_n\right)\cdots d\tau_1\right]dt_1\right.\right.\right.\\
&\le\int_0^{1}\phi^{-1}\left[\frac{1}{t_1^{N-1}}\int_0^{t_1}\tau_1^{N-1}g_1\left(\int_{\tau_1}^{1}\phi^{-1}\left[\frac{1}{t_2^{N-1}}\int_0^{t_2}\tau_2^{N-1}g_2\left(\int_{\tau_2}^{1}\phi^{-1}\Bigg[\cdots\right.\right.\right.\right.\\
&\quad\left.\left.\left.\left.g_{n-1}\left(\int_{\tau_{n-1}}^{1}\phi^{-1}\left[\frac{1}{t_n^{N-1}}\int_0^{t_n}\tau_n^{N-1}g_n\big(z_1(\tau_n)\big)d\tau_n\right]dt_n\right)\cdots d\tau_1\right]dt_1\right.\right.\right.\\
&\le R_k.
\end{aligned}$$

Hence condition (a) is satisfied. Secondly, we show that (b) of Theorem 3.3 is fulled. For this we select $z_1\in\partial P(\beta,S_k)$. Then $\beta(z_1)=\min_{r\in[r_k,1-\delta_k]}z_1(r)=z_1(r_k)=S_k$, i.e. $z_1(r)\ge S_k$, for $r\in[r_k,1-\delta_k]$. So we have $\|z_1\|\ge S_k$, for $r\in[r_k,1-\delta_k]$. Noticing that $\|z_1\|\le\delta_k^{-1}\gamma_k(z_1)\le\delta_k^{-1}\beta_k(z_1)=\delta_k^{-1}S_k$. we have

$$S_k\le z_1(r)\le\delta_k^{-1}S_k,\ \text{ for }\ r\in[r_k,1-\delta_k].$$

Let $0<\tau_{n-1}<1$. The by $(\mathcal{H}_9)$, we have

$$\begin{aligned}
\int_{\tau_{n-1}}^{1}\phi^{-1}\left[\frac{1}{t_n^{N-1}}\int_0^{t_n}\tau_n^{N-1}g_n\big(z_1(\tau_n)\big)d\tau_n\right]dt_n&\ge\int_{1-\delta_k}^{1}\phi^{-1}\left[\frac{1}{t_n^{N-1}}\int_{\delta_k}^{1-\delta_k}\tau_n^{N-1}g_n\big(z_1(\tau_n)\big)d\tau_n\right]dt_n\\
&\ge\delta_k\phi^{-1}\left[\frac{1}{t_n^{N-1}}\int_{\delta_k}^{1-\delta_k}\tau_n^{N-1}g_n\big(z_1(\tau_n)\big)d\tau_n\right]\\
&\ge\delta_1\phi^{-1}\left[\frac{1}{(1-\delta_k)^{N-1}}\int_{\delta_k}^{1-\delta_k}\tau_n^{N-1}\beta_kN\phi\left(\frac{S_k}{\delta_1}\right)d\tau_n\right]\\
&\ge\delta_1\phi^{-1}\left[\frac{(1-\delta_k)^N-\delta_k^N}{(1-\delta_k)^{N-1}}\beta_k\phi\left(\frac{S_k}{\delta_1}\right)\right]\\
&\ge S_k.
\end{aligned}$$

In similar manner (for $\tau_{n-2} \in [\delta_k, 1-\delta_k]$,) that

$$\begin{aligned}
&\int_{\tau_{n-2}}^{1} \phi^{-1}\left[\frac{1}{t_{n-1}^{N-1}}\int_0^{t_{n-1}} \tau_{n-1}^{N-1} g_{n-1}\left(\int_{\tau_{n-1}}^{1}\phi^{-1}\left[\frac{1}{t_n^{N-1}}\int_0^{t_n}\tau_n^{N-1} g_n\big(z_1(\tau_n)\big)d\tau_n\right]dt_n\right)d\tau_{n-1}\right]dt_{n-1}\\
&\quad\geq \int_{1-\delta_k}^{1} \phi^{-1}\left[\frac{1}{t_{n-1}^{N-1}}\int_{\delta_k}^{1-\delta_k} \tau_{n-1}^{N-1} g_{n-1}\left(\int_{\tau_{n-1}}^{1}\phi^{-1}\left[\frac{1}{t_n^{N-1}}\int_0^{t_n}\tau_n^{N-1} g_n\big(z_1(\tau_n)\big)d\tau_n\right]dt_n\right)d\tau_{n-1}\right]dt_{n-1}\\
&\quad\geq \int_{1-\delta_k}^{1} \phi^{-1}\left[\frac{1}{t_{n-1}^{N-1}}\int_{\delta_k}^{1-\delta_k} \tau_{n-1}^{N-1} g_{n-1}\big(S_k\big)d\tau_{n-1}\right]dt_{n-1}\\
&\quad\geq \delta_k\phi^{-1}\left[\frac{1}{(1-\delta_k)^{N-1}}\int_{\delta_k}^{1-\delta_k} \tau_{n-1}^{N-1}\beta_k N\phi\left(\frac{S_k}{\delta_1}\right)d\tau_{n-1}\right]\\
&\quad\geq \delta_1\phi^{-1}\left[\frac{(1-\delta_k)^N-\delta_k^N}{(1-\delta_k)^{N-1}}\beta_k\phi\left(\frac{S_k}{\delta_1}\right)\right]\\
&\quad\geq S_k.
\end{aligned}$$

Continuing with this bootstrapping argument, we get

$$\begin{aligned}
\beta_k(\aleph z_1) &= \min_{r\in[r_k,1-\delta_k]}(\aleph z_1)(r) = (\aleph z_1)(r_k)\\
&= \int_{r_k}^{1}\phi^{-1}\left[\frac{1}{t_1^{N-1}}\int_0^{t_1}\tau_1^{N-1}g_1\left(\int_{\tau_1}^{1}\phi^{-1}\left[\frac{1}{t_2^{N-1}}\int_0^{t_2}\tau_2^{N-1}g_2\left(\int_{\tau_2}^{1}\phi^{-1}\left[\cdots\right.\right.\right.\right.\right.\\
&\quad\left.\left.\left.\left.\left. g_{n-1}\left(\int_{\tau_{n-1}}^{1}\phi^{-1}\left[\frac{1}{t_n^{N-1}}\int_0^{t_n}\tau_n^{N-1}g_n\big(z_1(\tau_n)\big)d\tau_n\right]dt_n\right)\cdots d\tau_1\right]dt_1\right.\right.\right.\right.\right.\\
&\geq \int_{1-\delta_k}^{1}\phi^{-1}\left[\frac{1}{t_1^{N-1}}\int_0^{t_1}\tau_1^{N-1}g_1\left(\int_{\tau_1}^{1}\phi^{-1}\left[\frac{1}{t_2^{N-1}}\int_0^{t_2}\tau_2^{N-1}g_2\left(\int_{\tau_2}^{1}\phi^{-1}\left[\cdots\right.\right.\right.\right.\right.\\
&\quad\left.\left.\left.\left.\left. g_{n-1}\left(\int_{\tau_{n-1}}^{1}\phi^{-1}\left[\frac{1}{t_n^{N-1}}\int_0^{t_n}\tau_n^{N-1}g_n\big(z_1(\tau_n)\big)d\tau_n\right]dt_n\right)\cdots d\tau_1\right]dt_1\right.\right.\right.\right.\right.\\
&\geq S_k.
\end{aligned}$$

Hence condition (b) is satisfied. Finally we verify that (c) of Theorem 3.3 is also satisfied. Since $0 \in P$ and $Q_k > 0$, it follows that $P(\alpha_k, Q_k) \neq \emptyset$. Now let $z_1 \in P(\alpha_k, Q_k)$. Then $\alpha_k(z_1) = \max_{r\in[\delta_k,1-\delta_k]} z_1(r) = z_1(1-\delta_k) = Q_k$, i.e., $0 \leq z_1(r) \leq Q_k$, for $r \in [\delta_k, 1-\delta_k]$. Also, $\|z_1\| \leq \delta_k^{-1}\gamma_k(z_1) \leq \delta_k^{-1}\alpha_k(z_1) = \delta_k^{-1}Q_k$. Then we get

$$0 \leq z_1(r) \leq \delta_k^{-1}Q_k, \quad \text{for} \quad r \in [0,1].$$

Let $0 < \tau_{n-1} < 1$. Then by $(\mathcal{H}_{10})$, we have

$$\begin{aligned}
\int_{\tau_{n-1}}^{1}\phi^{-1}\left[\frac{1}{t_n^{N-1}}\int_0^{t_n}\tau_n^{N-1}g_n\big(z_1(\tau_n)\big)d\tau_n\right]dt_n &\leq \int_0^1\phi^{-1}\left[\frac{1}{t_n^{N-1}}\int_0^{t_n}\tau_n^{N-1}g_n\big(z_1(\tau_n)\big)d\tau_n\right]dt_n\\
&\leq \int_0^1\phi^{-1}\left[\frac{1}{t_n^{N-1}}\int_0^{t_n}\tau_n^{N-1}N\phi\big(Q_k\big)d\tau_n\right]dt_n\\
&\leq \int_0^1\phi^{-1}\left(\phi\big(Q_k\big)t_n\right)dt_n\\
&\leq Q_k.
\end{aligned}$$

Continuing with this bootstrapping argument, we get

$$\begin{aligned}
\alpha_k(\aleph \mathtt{z}_1) &= \max_{r\in[\delta_k,1-\delta_k]}(\aleph \mathtt{z}_1)(r)\\
&= (\aleph \mathtt{z}_1)(1-\delta_k)\\
&= \int_{1-\delta_k}^{1} \phi^{-1}\left[\frac{1}{t_1^{\mathtt{N}-1}}\int_0^{t_1}\tau_1^{\mathtt{N}-1}\mathtt{g}_1\left(\int_{\tau_1}^{1}\phi^{-1}\left[\frac{1}{t_2^{\mathtt{N}-1}}\int_0^{t_2}\tau_2^{\mathtt{N}-1}\mathtt{g}_2\left(\int_{\tau_2}^{1}\phi^{-1}\left[\cdots\right.\right.\right.\right.\right.\\
&\quad \left.\left.\left.\left.\left.\mathtt{g}_{n-1}\left(\int_{\tau_{n-1}}^{1}\phi^{-1}\left[\frac{1}{t_n^{\mathtt{N}-1}}\int_0^{t_n}\tau_n^{\mathtt{N}-1}\mathtt{g}_n\big(\mathtt{z}_1(\tau_n)\big)d\tau_n\right]dt_n\right)\cdots d\tau_1\right]dt_1\\
&\le \int_0^{1} \phi^{-1}\left[\frac{1}{t_1^{\mathtt{N}-1}}\int_0^{t_1}\tau_1^{\mathtt{N}-1}\mathtt{g}_1\left(\int_{\tau_1}^{1}\phi^{-1}\left[\frac{1}{t_2^{\mathtt{N}-1}}\int_0^{t_2}\tau_2^{\mathtt{N}-1}\mathtt{g}_2\left(\int_{\tau_2}^{1}\phi^{-1}\left[\cdots\right.\right.\right.\right.\right.\\
&\quad \left.\left.\left.\left.\left.\mathtt{g}_{n-1}\left(\int_{\tau_{n-1}}^{1}\phi^{-1}\left[\frac{1}{t_n^{\mathtt{N}-1}}\int_0^{t_n}\tau_n^{\mathtt{N}-1}\mathtt{g}_n\big(\mathtt{z}_1(\tau_n)\big)d\tau_n\right]dt_n\right)\cdots d\tau_1\right]dt_1\\
&\le \mathtt{Q}_k.
\end{aligned}$$

Thus condition (c) of Theorem 3.3 is satisfied. Since all hypotheses of Theorem 3.3 are satisfied, the assertion follows. □

Example 3.9. *Consider the following iterative system of Dirichlet problems*

$$\left.\begin{aligned} \mathcal{M}_{\mathcal{C}}(\mathtt{z}_{\mathtt{j}}) + \mathtt{g}_{\mathtt{j}}(\mathtt{z}_{\mathtt{j}+1}) = 0 \quad &in \quad \Omega\\ \mathtt{z}_{\mathtt{j}} = 0 \qquad\qquad\qquad\quad &on \quad \partial\Omega, \end{aligned}\right\} \tag{3.5}$$

where $\mathtt{j} = 1, 2$, $\mathtt{N} = 1$ and $\mathtt{z}_1 = \mathtt{z}_3$. Let Let r_k, δ_k be the same as of Example 3.5. In addition if we take

$$\mathtt{R}_k = 10^{-4k},\ \mathtt{Q}_k = 10^{-(4k+3)} \ \text{ and } \ \mathtt{S}_k = 10^{-(4k+2)},$$

then

$$\begin{aligned}
\mathtt{R}_{k+1} = 10^{-(4k+4)} < \mathtt{Q}_k = 10^{-(4k+3)} &< \frac{1}{5}\times 10^{-(4k+2)} < \delta_k \mathtt{S}_k\\
&< \mathtt{S}_k = 10^{-(4k+2)} < \mathtt{R}_k = 10^{-4k},
\end{aligned}$$

$$\phi(\mathtt{R}_k) = \frac{1}{\sqrt{10^{8k}-1}},\ \phi(\mathtt{Q}_k) = \frac{1}{\sqrt{10^{8k+6}-1}},\ \phi(\mathtt{S}_k) = \frac{1}{\sqrt{10^{8k+4}-1}},$$

$$\phi(\delta_k^{-1}\mathtt{R}_k) = \frac{1}{\sqrt{10^{8k}\times\delta_k^2-1}},\ \phi(\delta_k^{-1}\mathtt{Q}_k) = \frac{1}{\sqrt{10^{8k+6}\times\delta_k^2-1}} \ \text{ and } \ \phi(\delta_k^{-1}\mathtt{S}_k) = \frac{1}{\sqrt{10^{8k+4}\times\delta_k^2-1}}.$$

Since ϕ is increasing and $\delta_k^{-1}\mathtt{S}_k \le 5\mathtt{S}_k \le \mathtt{R}_k$, it follows that

$$\beta_k \mathtt{N}\phi(\delta_k^{-1}\mathtt{S}_k) \le \mathtt{N}\phi(\mathtt{R}_k), \quad \beta_k = 1-2\delta_k < 1.$$

Let $\mathtt{N}_2$ be a positive number such that

$$\mathtt{N}_2\times 10^{-8k} \le \beta_k \mathtt{N}\phi(\delta_k^{-1}\mathtt{S}_k) \le \mathtt{N}_2\times 10^{8k} \le \mathtt{N}\phi(\mathtt{Q}_k) \le \mathtt{N}\phi(\mathtt{R}_k),$$

and

$$\mathtt{g}_1(\mathtt{z})=\mathtt{g}_2(\mathtt{z})=\begin{cases}\mathtt{N}_2\times 10^{-6}, & \mathtt{z}\in(5\times 10^{-4},+\infty),\\ \mathtt{N}_2\times 10^{-(4k+2)}, & \mathtt{z}\in\left(10^{-(4k+2)},5\times 10^{-4k}\right],\\ \frac{\mathtt{N}_2\times 10^{-(4k+3)}-\mathtt{N}_2\times 10^{-(4k+2)}}{5\times 10^{-(4k+3)}-10^{-(4k+2)}}(\mathtt{z}-10^{-(4k+2)})+\mathtt{N}_2\times 10^{-(4k+2)}, & \mathtt{z}\in\left[5\times 10^{-(4k+3)},10^{-(4k+2)}\right],\\ \mathtt{N}_2\times 10^{-(4k+3)}, & \mathtt{z}\in\left(10^{-(4k+3)},5\times 10^{-(4k+3)}\right),\\ 0, & \mathtt{z}=0.\end{cases}$$

Then, $\mathtt{g}_1$ and $\mathtt{g}_2$ satisfies the following growth conditions:

$$\mathtt{g}_1(\mathtt{z})=\mathtt{g}_2(\mathtt{z})\le \mathtt{N}\phi(\mathtt{R}_k),\quad \mathtt{z}\in\left[0,5\times 10^{-4k}\right],$$
$$\mathtt{g}_1(\mathtt{z})=\mathtt{g}_2(\mathtt{z})\ge \beta_k\mathtt{N}\phi(\delta_k^{-1}\mathtt{S}_k),\quad \mathtt{z}\in\left[10^{-(4k+2)},5\times 10^{-(4k+2)}\right],$$
$$\mathtt{g}_1(\mathtt{z})=\mathtt{g}_2(\mathtt{z})\le \mathtt{N}\phi(\mathtt{Q}_k),\quad \mathtt{z}\in\left[0,5\times 10^{-(4k+3)}\right].$$

All the conditions of Theorem 3.8 are satisfied. Therefore, by Theorem 3.8, the boundary value problem (3.5) has three denumerably many families of radial solutions $\{({}^1\mathtt{z}_1^{[k]},{}^1\mathtt{z}_2^{[k]})\}_{k=1}^{\infty}$, $\{({}^2\mathtt{z}_1^{[k]},{}^2\mathtt{z}_2^{[k]})\}_{k=1}^{\infty}$ and $\{({}^3\mathtt{z}_1^{[k]},{}^3\mathtt{z}_2^{[k]})\}_{k=1}^{\infty}$ satisfying

$$0\le\max_{r\in[\delta_k,1-\delta_k]}{}^1\mathtt{z}_{\mathtt{j}}^{[k]}<10^{-(4k+3)}<\max_{r\in[\delta_k,1-\delta_k]}{}^2\mathtt{z}_{\mathtt{j}}^{[k]},\ \mathtt{j}=1,2,\ k\in\mathbb{N},$$

$$\min_{r\in[r_k,1-\delta_k]}{}^2\mathtt{z}_{\mathtt{j}}^{[k]}<10^{-(4k+2)}<\min_{r\in[r_k,1-\delta_k]}{}^3\mathtt{z}_{\mathtt{j}}^{[k]},\ \mathtt{j}=1,2,\ k\in\mathbb{N},$$

and

$$\max_{r\in[\delta_k,r_k]}{}^3\mathtt{z}_{\mathtt{j}}^{[k]}<10^{-4k},\ \mathtt{j}=1,2,\ k\in\mathbb{N}.$$

Acknowledgements

The authors would like to thank the referees for their valuable suggestions and comments for the improvement of the paper.

References

[1] R.I. Avery and J. Henderson, *Two positive fixed points of nonlinear operators on ordered Banach spaces*, Comm. Appl. Nonlinear Anal. 8 (2001) 27–36.

[2] A. Azzollini, *Ground state solution for a problem with mean curvature operator in Minkowski space*, J. Funct. Anal. 266 (2014) 2086–2095.
[3] R. Bartnik and L. Simon, *Spacelike hypersurfaces with prescribed boundary values and mean curvature*, Commun. Math. Phys. 87 (1982) 131–152.
[4] C. Bereanu, P. Jebelean and P.J. Torres, *Multiple positive radial solutions for a Dirichlet problem involving the mean curvature operator in Minkowski space*, J. Funct. Anal. 265 (2013) 644–659.
[5] C. Bereanu and J. Mawhin, *Existence and multiplicity results for some nonlinear problems with singular ϕ-Laplacian*, J. Differ. Equ. 243 (2007) 536–557.
[6] A. Boscaggin, M. Garrione, *Pairs of nodal solutions for a Minkowski-curvature boundary value problem in a ball*, Commun. Contemp. Math. 21 1850006 (2019) 18 pages.
[7] C. Corsato, F. Obersnel, P. Omari and S. Rivetti, *Positive solutions of the Dirichlet problem for the prescribed mean curvature equation in Minkowski space*, J. Math. Anal. Appl. 405 (2013) 227–239.
[8] D. Guo and V. Lakshmikantham, *Nonlinear Problems in Abstract Cones*, Academic Press, San Diego, 1988.
[9] S. Hu and H. Wang, *Convex solutions of boundary value problems aising from Monge-Ampere equations*, Discret. Contin. Dyn. Syst. 16 (2006) 705–720.
[10] M. Khuddush and K.R. Prasad, *Positive solutions for an iterative system of nonlinear elliptic equations*, Bull. Malays. Math. Sci. Soc. 45 (2022) 245–272.
[11] M. Khuddush, K.R. Prasad and B. Bharathi, *Local existence and blow up of solutions for a system of viscoelastic wave equations of Kirchhoff type with delay and logarithmic nonlinearity*, Int. J. Math. Model. Comp. 11(3) (2021) 1–11.
[12] Z.T. Liang, L. Duan and D.D. Ren, *Multiplicity of positive radial solutions of singular Minkowski-curvature equations*, Arch. Math. 113 (2019) 415–422.
[13] J. Mawhin, *Radial solution of Neumann problem for periodic perturbations of the mean extrinsic curvature operator*, Milan J. Math. 79 (2011) 95–112.
[14] M. Pei and L. Wang, *Multiplicity of positive radial solutions of a singular mean curvature equations in Minkowski space*, Appl. Math. Lett. 60 (2016) 50–55.
[15] M. Pei, L. Wang, *Positive radial solutions of a mean curvature equation in Minkowski space with strong singularity*, Proc. Am. Math. Soc. 145 (2017) 4423–4430.
[16] M. Pei and L. Wang, *Positive radial solutions of a mean curvature equation in Lorentz-Minkowski space with strong singularity*, App. Anal. 99(9) (2020) 1631–1637.
[17] K.R. Prasad, M. Khuddush and B. Bharathi, *Denumerably many positive radial solutions for the iterative system of elliptic equations in an annulus*, Palestine J. Math. 11(1) (2022) 549–559.
[18] J.L. Ren, W.G. Ge and B.X. Ren, *Existence of positive solutions for quasi-linear boundary value problems*, Acta Math. Appl. Sinica, English Ser. 21(3) (2005) 353–358.

Int. J. Nonlinear Anal. Appl. 13 (2022) 2, 1713–1733
ISSN: 2008-6822 (electronic)
http://dx.doi.org/10.22075/ijnaa.2022.25945.3167

Existence theory and stability analysis to the system of infinite point fractional order BVPs by multivariate best proximity point theorem

Mahammad Khuddush[a,*], Kapula Rajendra Prasad[b], Doddi Leela[b]

[a]Department of Mathematics, Dr. Lankapalli Bullayya College of Engineering, Resapuvanipalem, Visakhapatnam, 530013, India
[b]Department of Applied Mathematics, College of Science and Technology, Andhra University, Visakhapatnam, 530003, India

(Communicated by Oluwatosin Temitope Mewomo)

Abstract

This paper deals with the existence of solutions to the system of nonlinear infinite-point fractional order boundary value problems by an application of n-best proximity point theorem in a complete metric space. Further, we study Hyers-Ulam stability of the addressed system. An appropriate example is provided to check the validity of obtained results.

Keywords: Fractional derivative, boundary value problem, n-best proximity point theorem, metric space, Hyers-Ulam stability
2020 MSC: Primary 34A08, Secondary 34B15, 47H10, 54H25

1 Introduction

Fractional calculus is one of the useful fields of applied mathematics which has applications in the areas such as engineering, economics, control theory, chemistry, biology, medicine and other fields, see [21, 24, 25, 26, 39, 40]. Fractional differential equations can describe many phenomena in various fields of engineering and scientific disciplines In consequence, the subject of fractional differential equations is gaining much importance and attention. In recent years, there are a large number of papers dealing with the existence, uniqueness and multiple solutions of boundary value problems for nonlinear differential equations of fractional order. For examples and recent development of the topic, see [1, 3, 4, 6, 7, 13, 16, 17, 18, 20, 23, 27, 28, 29, 30, 34, 41] and references therein.

Fixed point theory is an indispensable tool for solving the equation $\aleph \mathtt{z} = \mathtt{z}$ for a mapping $\aleph$ defined on a subset of a metric space, a normed linear space or a topological vector space. As a non-self mapping $\aleph : \mathtt{A} \to \mathtt{B}$ does not necessarily have a fixed point, one often tries to determine an element $\mathtt{z}$ which is in some sense closest to $\aleph\mathtt{z}$. Best approximation theorems and best proximity point theorems are pertinent in this perspective. A classical best approximation theorem, due to Fan [12], asserts that if $\mathtt{A}$ is a non-empty compact convex subset of a Hausdorff locally convex topological vector space $\mathtt{Y}$ with a semi-norm $\mathtt{p}$ and $\aleph : \mathtt{A} \to \mathtt{Y}$ is a continuous mapping, then there is an element $\mathtt{z}$ in $\mathtt{A}$ satisfying the

*Corresponding author
Email addresses: khuddush89@gmail.com (Mahammad Khuddush), krajendra92@rediffmail.com (Kapula Rajendra Prasad), leelaravidadi@gmail.com (Doddi Leela)

Received: January 2022 *Accepted:* May 2022

condition that $\mathtt{d}_{\mathtt{p}}(\mathtt{z}, \aleph\mathtt{z}) = \mathtt{d}_{\mathtt{p}}(\aleph\mathtt{z}, \mathtt{A})$. There have been many subsequent extensions and variants of Fan's Theorem, see [2, 8, 14, 15, 19, 22, 31, 32, 35, 36] and references therein.

Basically the proximity theory is useful tool to find proximity point when the given mapping is non self. Let $\mathtt{A}$ and $\mathtt{B}$ be two non empty subsets of $\mathtt{Y}$ such that $\aleph : \mathtt{A} \to \mathtt{B}$ then a point $\mathtt{z} \in \mathtt{A}$ for which $\mathtt{d}(\mathtt{z}, \aleph\mathtt{z}) = \mathtt{d}(\mathtt{A}, \mathtt{B})$ is called a best proximity point of $\aleph$. It should be noted that best proximity point reduced to fixed point when the mapping $\aleph$ is self mapping that is $\mathtt{A} = \mathtt{B}$.

In [5], Afshari, Jarad and Abdeljawad discussed the admissibility of two multi-valued mappings in the category of complete b-metric spaces to obtain the existence of a common fixed point and by using the triangular admissibility, they proved the uniqueness of the common fixed point. As an application of their finding, the existence and uniqueness of the following fractional order boundary value problem studied,

$$\begin{gathered}
{}^{\mathtt{RL}}\mathtt{D}^{\varrho}_{0+}\mathtt{z}_1(\mathtt{s}) + \mathtt{f}(\mathtt{s}, \mathtt{z}_2(\mathtt{s})),\ 0 < \mathtt{s} < 1,\ 1 < \varrho \leq 2,\\
{}^{\mathtt{RL}}\mathtt{D}^{\xi}_{0+}\mathtt{z}_2(\mathtt{s}) + \mathtt{g}(\mathtt{s}, \mathtt{z}_1(\mathtt{s})),\ 0 < \mathtt{s} < 1,\ 1 < \xi \leq 2,\\
\mathtt{z}_1(0) = \mathtt{z}_2(0) = 0,\ \mathtt{z}_1(1) = \int_0^1 \varphi(\mathtt{t})\mathtt{z}_1(\mathtt{t})\mathrm{d}\mathtt{t},\ \mathtt{z}_2(1) = \int_0^1 \varphi(\mathtt{t})\mathtt{z}_2(\mathtt{t})\mathrm{d}\mathtt{t}.
\end{gathered}$$

Recently, Prasad, Khuddush and Leela [30] established the existence of unique solution for a two-point fractional order boundary value problem,

$$\begin{gathered}
{}^{\mathtt{RL}}\mathtt{D}^{\zeta}\mathtt{z}(\mathtt{s}) + \mathtt{F}\big(\mathtt{s}, \mathtt{z}(\mathtt{s}), \mathtt{z}(\mathtt{s}), \mathtt{z}(\mathtt{s})\big) + \varphi(\mathtt{s})\mathtt{z}(\mathtt{s}) = 0,\ 0 < \mathtt{s} < \mathtt{T},\ 2 < \zeta \leq 3,\\
\mathtt{z}(0) = \mathtt{z}''(0) = 0,\ \mathtt{z}(\mathtt{T}) = \int_0^{\mathtt{T}} \mathtt{z}(\mathtt{t})\mathrm{d}\mathtt{t},
\end{gathered}$$

by proving the existence and the uniqueness of solutions of the operator equation $\mathtt{A}(\mathtt{z}, \mathtt{z}, \mathtt{z}) + \mathtt{B}\mathtt{z} = \mathtt{z}$ in a real Banach space. Motivated by aforementioned works, in this paper we study the concept of n-best proximity point in a complete metric space and establish the existence and uniqueness theorems. Moreover, as an application of our results we study the following system of n-nonlinear infinite-point fractional order boundary value problems

$$\begin{cases}
{}^{\mathtt{RL}}\mathtt{D}^{ß_1}_{0+}\mathtt{z}_1(\mathtt{s}) = \mathtt{g}_1\big(\mathtt{s}, \mathtt{z}_1(\mathtt{s}), \mathtt{z}_2(\mathtt{s}), \cdots, \mathtt{z}_{n-1}(\mathtt{s}), \mathtt{z}_n(\mathtt{s})\big),\\
{}^{\mathtt{RL}}\mathtt{D}^{ß_2}_{0+}\mathtt{z}_2(\mathtt{s}) = \mathtt{g}_2\big(\mathtt{s}, \mathtt{z}_2(\mathtt{s}), \mathtt{z}_1(\mathtt{s}), \cdots, \mathtt{z}_{n-1}(\mathtt{s}), \mathtt{z}_n(\mathtt{s})\big),\\
\qquad\qquad \vdots\\
{}^{\mathtt{RL}}\mathtt{D}^{ß_{n-1}}_{0+}\mathtt{z}_{n-1}(\mathtt{s}) = \mathtt{g}_{n-1}\big(\mathtt{s}, \mathtt{z}_{n-1}(\mathtt{s}), \mathtt{z}_2(\mathtt{s}), \cdots, \mathtt{z}_1(\mathtt{s}), \mathtt{z}_n(\mathtt{s})\big),\\
{}^{\mathtt{RL}}\mathtt{D}^{ß_n}_{0+}\mathtt{z}_n(\mathtt{s}) = \mathtt{g}_n\big(\mathtt{s}, \mathtt{z}_n(\mathtt{s}), \mathtt{z}_2(\mathtt{s}), \cdots, \mathtt{z}_{n-1}(\mathtt{s}), \mathtt{z}_1(\mathtt{s})\big),
\end{cases} \tag{1.1}$$

satisfying

$$\mathtt{z}_i(0) = 0 \ \text{ and } \ {}^{\mathtt{RL}}\mathtt{D}^{\alpha_i}_{0+}\mathtt{z}_i(1) = \sum_{\mathtt{j}=1}^{\infty} \delta_{i\mathtt{j}}\, {}^{\mathtt{RL}}\mathtt{D}^{\alpha_i}_{0+}\mathtt{z}_i\big(\sigma_i(\tau_{i\mathtt{j}})\big),\ i = 1, 2, \cdots, n, \tag{1.2}$$

where $0 < \mathtt{s} < 1$, $1 < ß_i \leq 2$, $0 < \alpha_i < ß_i - 1$, $\delta_{i\mathtt{j}} > 0$, ${}^{\mathtt{RL}}\mathtt{D}^{\star}_{0+}$ denotes the standard Riemann-Liouville fractional derivative of order $\star \in \{ß_i, \alpha_i\}, i = 1, 2, \cdots, n$, $\mathtt{g}_i : [0,1] \times [0, +\infty)^n \to [0, +\infty)$, $\sigma_i : [0,1] \to [0,1]$ are continuous functions. In [30], authors studied the fixed point theorem of mixed monotone ternary operators on Banach spaces, whereas in this paper, we study n-best proximity poin theorem on metric spaces. Therefore, by applying our results we can study different kind differential equations whereas results in [30] can only applicable for certain type of differential equations.

2 Preliminaries

In this section, we construct kernel for the boundary value problem (1.1)–(1.2) and estimate bounds for it, which are useful for our later discussions.

Definition 2.1. [21] The Riemann-Liouville fractional integral of order $\xi > 0$ of a function $\mathtt{g} : (0, +\infty) \to \mathbb{R}$ is defined by

$${}^{\mathtt{RL}}\mathtt{I}^{\xi}_{0+}\mathtt{g}(\mathtt{s}) = \int_0^{\mathtt{s}} \frac{(\mathtt{s} - \mathtt{t})^{\xi - 1}}{\Gamma(\xi)}\mathtt{g}(\mathtt{t})\mathrm{d}\mathtt{t}.$$

Definition 2.2. [21] Let k be a positive integer. The Riemann-Liouville fractional derivative of order $\xi > 0$ of a continuous function $g : (0, +\infty) \to \mathbb{R}$ is defined by

$$^{RL}D^{\xi}_{0+}g(s) = \frac{d^k}{ds^k}\int_0^s \frac{(s-t)^{k-\xi-1}}{\Gamma(k-\xi)}g(t)dt,$$

where $k-1 < \xi \leq k$, provided that the right-hand side exists.

Remark 2.3. ([21]) In this work we need the following composition relations:

(a) $^{RL}D^{\xi}_{0+}\,{}^{RL}I^{\xi}_{0+}g(s) = g(s)$, $\xi > 0, g(s) \in L^1(0, +\infty)$;

(b) $^{RL}D^{\zeta}_{0+}\,{}^{RL}I^{\xi}_{0+}g(s) = {}^{RL}I^{\xi-\zeta}_{0+}g(s)$, $\xi > \zeta > 0, g(s) \in L^1(0, +\infty)$.

Remark 2.4. ([10]) For $\zeta > -1$, we have

$$^{RL}D^{\xi}_{0+}s^{\zeta} = \frac{\Gamma(\zeta+1)}{\Gamma(\zeta-\xi+1)}s^{\zeta-\xi},$$

giving inparticular $^{RL}D^{\xi}_{0+}s^{\xi-m} = 0$, $m = 1, 2, \cdots, N$, where N is the smallest integer greater than or equal to ξ.

Lemma 2.5. [21] Let k be a positive integer. The general solution to $^{RL}D^{\xi}_{0+}g(s) = 0$ with $k-1 < \xi \leq k$ is the function

$$g(s) = \sum_{j=1}^{k} a_j s^{\xi-j},$$

where a_j is a real number.

Lemma 2.6. [21] Let $\zeta > 0$. Then for any function $g : (0, +\infty) \to \mathbb{R}$, we have

$$^{RL}I^{\zeta}_{0+}\,{}^{RL}D^{\zeta}_{0+}g(s) = g(s) + \sum_{j=1}^{k} a_j s^{\zeta-j},$$

where a_j is a real number and k is the smallest integer greater that or equal to ζ, and

$$^{RL}D^{\zeta}_{0+}\,{}^{RL}I^{\zeta}_{0+}g(s) = g(s).$$

In order to study the system of boundary value problems (1.1)–(1.2), we first consider the corresponding linear boundary value problem,

$$^{RL}D^{\beta_i}_{0+}z_i(s) = h_i(s),\ 0 < s < 1, \tag{2.1}$$

$$z_i(0) = 0 \ \text{ and } \ ^{RL}D^{\alpha_i}_{0+}z_i(1) = \sum_{j=1}^{\infty}\delta_{ij}z_i\big(\sigma_i(\tau_{ij})\big),\ i = 1, 2, \cdots, n, \tag{2.2}$$

where $h_i \in C[0, 1]$ is a given function.

Lemma 2.7. Suppose $\sum_{j=1}^{m}\delta_{ij}\big(\sigma_i(\tau_{ij})\big)^{\beta_i-1}$ converges $\frac{2\Gamma(\beta_i)}{\Gamma(\beta_i-\alpha_i)}$. The boundary value problem (2.1)–(2.2) has a unique solution

$$z_i(s) = \int_0^1 G_i(s,t)h_i(t)dt - s^{\beta_i-1}\sum_{j=1}^{\infty}\delta_{ij}\int_0^{\sigma_i(\tau_{ij})}\frac{(\sigma_i(\tau_{ij})-t)^{\beta_i-1}}{\Gamma(\beta_i)}h_i(t)dt, \tag{2.3}$$

where

$$G_i(s,t) = \frac{1}{\Gamma(\beta_i)}\begin{cases} s^{\beta_i-1}(1-t)^{\beta_i-\alpha_i-1} + (s-t)^{\beta_i-1}, & t \leq s, \\ s^{\beta_i-1}(1-t)^{\beta_i-\alpha_i-1}, & s \leq t. \end{cases}$$

Proof . Let $z_i(s)$ be a solution of (2.1). Then, by Lemma 2.6, we have

$$z_i(s) = a_1 s^{ß_i-1} + a_2 s^{ß_i-2} + \int_0^s \frac{(s-t)^{ß_i-1}}{\Gamma(ß_i)} h_i(t)dt, \tag{2.4}$$

where a_1 and a_2 are constants. Using condition $z_i(0) = 0$, we get $a_2 = 0$. So, (2.4) reduces to

$$z_i(s) = a_1 s^{ß_i-1} + \int_0^s \frac{(s-t)^{ß_i-1}}{\Gamma(ß_i)} h_i(t)dt. \tag{2.5}$$

Before applying (2.2), we first take

$${}^{RL}D_{0^+}^{\alpha_i} z_i(1) = \sum_{j=1}^{m} \delta_{ij} z_i\big(\sigma_i(\tau_{ij})\big),$$

and using Remark 2.4 to get

$$\begin{aligned} a_1 = &\frac{1}{\sum_{j=1}^{m} \delta_{ij}\big(\sigma_i(\tau_{ij})\big)^{ß_i-1} - \frac{\Gamma(ß_i)}{\Gamma(ß_i-\alpha_i)}} \Bigg[\int_0^1 \frac{(1-t)^{ß_i-\alpha_i-1}}{\Gamma(ß_i-\alpha_i)} h_i(t)dt \\ &- \sum_{j=1}^{m} \delta_{ij} \int_0^{\sigma_i(\tau_{ij})} \frac{(\sigma_i(\tau_{ij})-t)^{ß_i-1}}{\Gamma(ß_i)} h_i(t)dt \Bigg]. \end{aligned}$$

Plugging a_2 value into (2.5), we obtain

$$\begin{aligned} z_i(s) = &\frac{1}{\sum_{j=1}^{m} \delta_{ij}\big(\sigma_i(\tau_{ij})\big)^{ß_i-1} - \frac{\Gamma(ß_i)}{\Gamma(ß_i-\alpha_i)}} \Bigg[\int_0^1 \frac{s^{ß_i-1}(1-t)^{ß_i-\alpha_i-1}}{\Gamma(ß_i-\alpha_i)} h_i(t)dt \\ &- s^{ß_i-1} \sum_{j=1}^{m} \delta_{ij} \int_0^{\sigma_i(\tau_{ij})} \frac{(\sigma_i(\tau_{ij})-t)^{ß_i-1}}{\Gamma(ß_i)} h_i(t)dt \Bigg] + \int_0^s \frac{(s-t)^{ß_i-1}}{\Gamma(ß_i)} h_i(t)dt \Bigg\} \end{aligned} \tag{2.6}$$

Since

$$\big|\delta_{ij} z_i\big(\sigma_i(\tau_{ij})\big)\big| \le \delta_{ij} \|z_i\|,$$

and

$$\begin{aligned} \left| \delta_{ij} \int_0^{\sigma_i(\tau_{ij})} \frac{(\sigma_i(\tau_{ij})-t)^{ß_i-1}}{\Gamma(ß_i)} h_i(t)dt \right| &\le \frac{\delta_{ij}}{\Gamma(ß_i)} \left| \int_0^{\sigma_i(\tau_{ij})} v(t) h_i(t)dt \right| \\ &\le \frac{\delta_{ij}}{\Gamma(ß_i)} \left| \int_0^{\tau_{ij}} v(t) h_i(t)dt \right| \\ &\le \frac{\delta_{ij}}{\Gamma(ß_i)} \|v\|_{L_1} \|h_i\|_{L_1}, \end{aligned}$$

where $v(t) = (\sigma_i(\tau_{ij}) - t)^{ß_i-1}$. Then, by comparison test, the series in (2.2) and

$$\sum_{j=1}^{\infty} \delta_{ij} \int_0^{\sigma_i(\tau_{ij})} \frac{(\sigma_i(\tau_{ij})-t)^{ß_i-1}}{\Gamma(ß_i)} h_i(t)dt$$

are convergent. So, by taking the limit as $m \to \infty$ in (2.6), we obtain

$$\begin{aligned} z_i(s) &= \int_0^1 \frac{s^{ß_i-1}(1-t)^{ß_i-\alpha_i-1}}{\Gamma(ß_i)} h_i(t)dt - s^{ß_i-1} \sum_{j=1}^{\infty} \delta_{ij} \int_0^{\sigma_i(\tau_{ij})} \frac{\Gamma(ß_i-\alpha_i)(\sigma_i(\tau_{ij})-t)^{ß_i-1}}{\Gamma(ß_i)^2} h_i(t)dt \\ &\quad + \int_0^s \frac{(s-t)^{ß_i-1}}{\Gamma(ß_i)} h_i(t)dt \\ &= \int_0^1 G_i(s,t) h_i(t)dt - s^{ß_i-1} \sum_{j=1}^{\infty} \delta_{ij} \int_0^{\sigma_i(\tau_{ij})} \frac{\Gamma(ß_i-\alpha_i)(\sigma_i(\tau_{ij})-t)^{ß_i-1}}{\Gamma(ß_i)^2} h_i(t)dt. \end{aligned} \tag{2.7}$$

Conversely, it is clear that (2.7) satisfies $\mathtt{z}_i(0)=0$. Next applying the operator $\mathtt{D}_{0^+}^{ß_i}$ and $\mathtt{D}_{0^+}^{\alpha_i}$ to the two sides of (2.7) respectively and using Remark 2.3 and Remark 2.4, we obtain $\mathtt{D}_{0^+}^{ß_i}\mathtt{z}_i(\mathtt{s})=\mathtt{h}_i(\mathtt{s})$ and

$$\begin{aligned}\mathtt{D}_{0^+}^{\alpha_i}\mathtt{z}_i(\mathtt{s})=&\int_0^1\frac{\mathtt{s}^{ß_i-\alpha_i-1}(1-\mathtt{t})^{ß_i-\alpha_i-1}}{\Gamma(ß_i-\alpha_i)}\mathtt{h}_i(\mathtt{t})\mathtt{d}\mathtt{t}-\mathtt{s}^{ß_i-\alpha_i-1}\sum_{\mathtt{j}=1}^{\infty}\delta_{i\mathtt{j}}\int_0^{\sigma_i(\tau_{i\mathtt{j}})}\frac{(\sigma_i(\tau_{i\mathtt{j}})-\mathtt{t})^{ß_i-1}}{\Gamma(ß_i)}\mathtt{h}_i(\mathtt{t})\mathtt{d}\mathtt{t}\\&+\int_0^{\mathtt{s}}\frac{(\mathtt{s}-\mathtt{t})^{ß_i-\alpha_i-1}}{\Gamma(ß_i-\alpha_i)}\mathtt{h}_i(\mathtt{t})\mathtt{d}\mathtt{t}.\end{aligned}$$

Substituting $\mathtt{s}=1$, we get

$$\mathtt{D}_{0^+}^{\alpha_i}\mathtt{z}_i(1)=2\int_0^1\frac{(1-\mathtt{t})^{ß_i-\alpha_i-1}}{\Gamma(ß_i-\alpha_i)}\mathtt{h}_i(\mathtt{t})\mathtt{d}\mathtt{t}-\sum_{\mathtt{j}=1}^{\infty}\delta_{i\mathtt{j}}\int_0^{\sigma_i(\tau_{i\mathtt{j}})}\frac{(\sigma_i(\tau_{i\mathtt{j}})-\mathtt{t})^{ß_i-1}}{\Gamma(ß_i)}\mathtt{h}_i(\mathtt{t})\mathtt{d}\mathtt{t}.\tag{2.8}$$

But,

$$\begin{aligned}\sum_{\mathtt{j}=1}^{m}\delta_{i\mathtt{j}}\mathtt{z}_i\big(\sigma_i(\tau_{i\mathtt{j}})\big)=&\sum_{\mathtt{j}=1}^{m}\delta_{i\mathtt{j}}\left(\sigma_i(\tau_{i\mathtt{j}})\right)^{ß_i-1}\int_0^1\frac{(1-\mathtt{t})^{ß_i-\alpha_i-1}}{\Gamma(ß_i)}\mathtt{h}_i(\mathtt{t})\mathtt{d}\mathtt{t}\\&-\sum_{\mathtt{j}=1}^{m}\delta_{i\mathtt{j}}\left(\sigma_i(\tau_{i\mathtt{j}})\right)^{ß_i-1}\sum_{\mathtt{j}=1}^{\infty}\delta_{i\mathtt{j}}\int_0^{\sigma_i(\tau_{i\mathtt{j}})}\frac{\Gamma(ß_i-\alpha_i)(\sigma_i(\tau_{i\mathtt{j}})-\mathtt{t})^{ß_i-1}}{\Gamma(ß_i)^2}\mathtt{h}_i(\mathtt{t})\mathtt{d}\mathtt{t}\\&+\sum_{\mathtt{j}=1}^{m}\delta_{i\mathtt{j}}\int_0^{\sigma_i(\tau_{i\mathtt{j}})}\frac{(\sigma_i(\tau_{i\mathtt{j}})-\mathtt{t})^{ß_i-1}}{\Gamma(ß_i)}\mathtt{h}_i(\mathtt{t})\mathtt{d}\mathtt{t}.\end{aligned}$$

Since $\sum_{\mathtt{j}=1}^{m}\delta_{i\mathtt{j}}\left(\sigma_i(\tau_{i\mathtt{j}})\right)^{ß_i-1}$ converges to $\frac{2\Gamma(ß_i)}{\Gamma(ß_i-\alpha_i)}$, it follows by taking limit $m\to+\infty$ that

$$\begin{aligned}\sum_{\mathtt{j}=1}^{\infty}\delta_{i\mathtt{j}}\mathtt{z}_i\big(\sigma_i(\tau_{i\mathtt{j}})\big)=&2\int_0^1\frac{(1-\mathtt{t})^{ß_i-\alpha_i-1}}{\Gamma(ß_i-\alpha_i)}\mathtt{h}_i(\mathtt{t})\mathtt{d}\mathtt{t}\\&-2\sum_{\mathtt{j}=1}^{\infty}\delta_{i\mathtt{j}}\int_0^{\sigma_i(\tau_{i\mathtt{j}})}\frac{(\sigma_i(\tau_{i\mathtt{j}})-\mathtt{t})^{ß_i-1}}{\Gamma(ß_i)}\mathtt{h}_i(\mathtt{t})\mathtt{d}\mathtt{t}\\&+\sum_{\mathtt{j}=1}^{m}\delta_{i\mathtt{j}}\int_0^{\sigma_i(\tau_{i\mathtt{j}})}\frac{(\sigma_i(\tau_{i\mathtt{j}})-\mathtt{t})^{ß_i-1}}{\Gamma(ß_i)}\mathtt{h}_i(\mathtt{t})\mathtt{d}\mathtt{t}\\=&2\int_0^1\frac{(1-\mathtt{t})^{ß_i-\alpha_i-1}}{\Gamma(ß_i-\alpha_i)}\mathtt{h}_i(\mathtt{t})\mathtt{d}\mathtt{t}-\sum_{\mathtt{j}=1}^{\infty}\delta_{i\mathtt{j}}\int_0^{\sigma_i(\tau_{i\mathtt{j}})}\frac{(\sigma_i(\tau_{i\mathtt{j}})-\mathtt{t})^{ß_i-1}}{\Gamma(ß_i)}\mathtt{h}_i(\mathtt{t})\mathtt{d}\mathtt{t}.\end{aligned}\tag{2.9}$$

By (2.8) and (2.9), we get (2.2). Which shows that the solution of the integral equation (2.3) satisfies the differential equation (2.1) under infinite-point boundary conditions (2.2). □

Remark 2.8. The supposition $\sum_{\mathtt{j}=1}^{m}\delta_{\mathtt{j}}\big(\sigma(\tau_{\mathtt{j}})\big)^{ß-1}$ converges to $\frac{2\Gamma(ß)}{\Gamma(ß-\alpha)}$ in the Lemma 2.7 is valid. For example: Let $ß=\frac{3}{2},\alpha=\frac{1}{3}$, $\delta_{\mathtt{j}}=\frac{18\Gamma(5/6)}{\pi^{5/2}\mathtt{j}}$, $\tau_{\mathtt{j}}=\frac{1}{\mathtt{j}^3}$ and $\sigma(\mathtt{s})=\mathtt{s}^{2/3}$. Then

$$\sum_{\mathtt{j}=1}^{m}\delta_{\mathtt{j}}\big(\sigma(\tau_{\mathtt{j}})\big)^{ß-1}=\sum_{\mathtt{j}=1}^{m}\frac{18\Gamma(5/6)}{\pi^{5/2}\mathtt{j}^2}\to\frac{3\Gamma(5/6)}{\sqrt{\pi}}=\frac{2\Gamma(ß)}{\Gamma(ß-\alpha)}\quad\text{as}\quad m\to+\infty.$$

The following properties are evident from the definition of $\mathtt{G}_i(\mathtt{s},\mathtt{t})$.

Lemma 2.9. The kernel $\mathtt{G}_i(\mathtt{s},\mathtt{t})$ has the following properties:

(*i*) $\mathtt{G}_i(\mathtt{s},\mathtt{t})$ is nonnegative and continuous on $[0,1]\times[0,1]$.

(*ii*) $\mathtt{G}_i(\mathtt{s},\mathtt{t})\le\mathtt{G}_i(1,\mathtt{t})$ for $\mathtt{s},\mathtt{t}\in[0,1]\times[0,1]$.

3 Main Results

To establish our main results, it is fundamental to recall some notions, definitions amd lemmas which will be useful in the sequel.

Let $\mathtt{A}$ and $\mathtt{B}$ be any two nonempty subset of a metric space $(\mathtt{Y},\mathtt{d})$. Define

$$\begin{aligned}\mathcal{P}_{\mathtt{A}} &= \{\mathtt{z}_2 \in \mathtt{Y} : \mathtt{d}(\mathtt{z}_1,\mathtt{z}_2) = \mathtt{d}(\mathtt{z}_1,\mathtt{A})\},\\ \mathtt{d}(\mathtt{A},\mathtt{B}) &:= \inf\{\mathtt{d}(\mathtt{z}_1,\mathtt{z}_2) : \mathtt{z}_1 \in \mathtt{A}, \mathtt{z}_2 \in \mathtt{B}\},\\ \mathtt{A}_0 &= \{\mathtt{z}_1 \in \mathtt{A} : \mathtt{d}(\mathtt{z}_1,\mathtt{z}_2) = \mathtt{d}(\mathtt{A},\mathtt{B}),\ \text{for some } \mathtt{z}_2 \in \mathtt{B}\},\end{aligned}$$

and

$$\mathtt{B}_0 = \{\mathtt{z}_2 \in \mathtt{B} : \mathtt{d}(\mathtt{z}_1,\mathtt{z}_2) = \mathtt{d}(\mathtt{A},\mathtt{B}),\ \text{for some } \mathtt{z}_1 \in \mathtt{A}\}.$$

Definition 3.1. [37] Let $\mathtt{A}$ and $\mathtt{B}$ be two nonempty subsets of a metric space $(\mathtt{Y},\mathtt{d})$. An element $\mathtt{z} \in \mathtt{A}$ is said to be a best proximity point of the nonself mapping $\aleph : \mathtt{A} \to \mathtt{B}$ iff it satisfies the condition

$$\mathtt{d}(\mathtt{z},\aleph\mathtt{z}) = \mathtt{d}(\mathtt{A},\mathtt{B}).$$

Definition 3.2. [33] Let $(\mathtt{A},\mathtt{B})$ be a pair of nonempty subsets of a metric space $(\mathtt{Y},\mathtt{d})$ with $\mathtt{A}_0 \neq \emptyset$. Then the pair $(\mathtt{A},\mathtt{B})$ has $\mathcal{P}$-property if and only if

$$\begin{pmatrix}\mathtt{d}(\mathtt{z}_1,\mathtt{y}_1) &= \mathtt{d}(\mathtt{A},\mathtt{B})\\ \mathtt{d}(\mathtt{z}_2,\mathtt{y}_2) &= \mathtt{d}(\mathtt{A},\mathtt{B})\end{pmatrix} \implies \mathtt{d}(\mathtt{z}_1,\mathtt{z}_2) = \mathtt{d}(\mathtt{y}_1,\mathtt{y}_2),$$

where $\mathtt{z}_1,\mathtt{z}_2 \in \mathtt{A}$ and $\mathtt{y}_1,\mathtt{y}_2 \in \mathtt{B}$.

Definition 3.3. [11] A map $\varphi : [0,+\infty) \to [0,+\infty)$ is called a $\mathtt{c}$-comparison function if it satisfies:

(*i*) φ is a monotone increasing,

(*ii*) $\sum_{n=0}^{\infty} \varphi^n(t)$ converges for all $t \in [0,+\infty)$.

If we replace the second condition by $\lim_{n\to\infty} \varphi^n(\mathtt{t}) = 0$ for all $\mathtt{t} \in [0,+\infty)$, we obtain the notion of comparison function, which is more general than the one of $\mathtt{c}$-comparison function. It is known that if φ is a comparison function, then $\varphi(\mathtt{t}) < \mathtt{t}$ for all $t > 0$ and $\varphi(0) = 0$.

Let Θ be the set of all continuous functions $\theta : [0,+\infty)^{n+3} \to [0,+\infty)$ such that for every $\mathtt{t},\mathtt{s},\mathtt{z}_1,\mathtt{z}_2,\cdots,\mathtt{z}_n \in [0,+\infty)$,

$$\begin{aligned}&\theta(0,\mathtt{t},\mathtt{s},\mathtt{z}_1,\mathtt{z}_2,\cdots,\mathtt{z}_{n-3},\mathtt{z}_{n-2},\mathtt{z}_{n-1},\mathtt{z}_n) = 0,\\ &\theta(\mathtt{t},\mathtt{s},0,\mathtt{z}_1,\mathtt{z}_2,\cdots,\mathtt{z}_{n-3},\mathtt{z}_{n-2},\mathtt{z}_{n-1},\mathtt{z}_n) = 0,\\ &\theta(\mathtt{t},\mathtt{s},\mathtt{z}_1,\mathtt{z}_2,0,\cdots,\mathtt{z}_{n-3},\mathtt{z}_{n-2},\mathtt{z}_{n-1},\mathtt{z}_n) = 0,\\ &\qquad\qquad\vdots\\ &\theta(\mathtt{t},\mathtt{s},\mathtt{z}_1,\mathtt{z}_2,\mathtt{z}_3,\cdots,0,\mathtt{z}_{n-2},\mathtt{z}_{n-1},\mathtt{z}_n) = 0,\\ &\theta(\mathtt{t},\mathtt{s},\mathtt{z}_1,\mathtt{z}_2,\mathtt{z}_3,\cdots,\mathtt{z}_{n-2},\mathtt{z}_{n-1},0,\mathtt{z}_n) = 0,\end{aligned}$$

if n is odd and

$$\begin{aligned}&\theta(0,\mathtt{t},\mathtt{s},\mathtt{z}_1,\mathtt{z}_2,\cdots,\mathtt{z}_{n-3},\mathtt{z}_{n-2},\mathtt{z}_{n-1},\mathtt{z}_n) = 0,\\ &\theta(\mathtt{t},\mathtt{s},0,\mathtt{z}_1,\mathtt{z}_2,\cdots,\mathtt{z}_{n-3},\mathtt{z}_{n-2},\mathtt{z}_{n-1},\mathtt{z}_n) = 0,\\ &\theta(\mathtt{t},\mathtt{s},\mathtt{z}_1,\mathtt{z}_2,0,\cdots,\mathtt{z}_{n-3},\mathtt{z}_{n-2},\mathtt{z}_{n-1},\mathtt{z}_n) = 0,\\ &\qquad\qquad\vdots\\ &\theta(\mathtt{t},\mathtt{s},\mathtt{z}_1,\mathtt{z}_2,\mathtt{z}_3,\cdots,\mathtt{z}_{n-2},0,\mathtt{z}_{n-1},\mathtt{z}_n) = 0,\\ &\theta(\mathtt{t},\mathtt{s},\mathtt{z}_1,\mathtt{z}_2,\mathtt{z}_3,\cdots,\mathtt{z}_{n-2},\mathtt{z}_{n-1},\mathtt{z}_n,0) = 0,\end{aligned}$$

if n is even.

Definition 3.4. [37] Let θ be a continuous function in Θ and φ be a comparison function. A mapping $\aleph : \mathtt{A} \to \mathtt{B}$ is said to be a generalized almost (φ, θ)-contraction if

$$\mathtt{d}(\aleph \mathtt{z}_1, \aleph \mathtt{z}_2) = \varphi\big(\mathtt{d}(\mathtt{z}_1, \mathtt{z}_2)\big) + \theta\big(\mathtt{d}(\mathtt{z}_2, \aleph \mathtt{z}_1) - \mathtt{d}(\mathtt{A}, \mathtt{B}), \mathtt{d}(\mathtt{z}_1, \aleph \mathtt{z}_2) - \mathtt{d}(\mathtt{A}, \mathtt{B}), \mathtt{d}(\mathtt{z}_1, \aleph \mathtt{z}_1) - \mathtt{d}(\mathtt{A}, \mathtt{B}), \mathtt{d}(\mathtt{z}_2, \aleph \mathtt{z}_2) - \mathtt{d}(\mathtt{A}, \mathtt{B})\big)$$

for all $\mathtt{z}_1, \mathtt{z}_2 \in \mathtt{A}$.

Definition 3.5. [38] Let $(\mathtt{Y}, \mathtt{d})$ be a metric space with $\mathtt{A} \neq \emptyset$ and $\mathtt{B} \neq \emptyset$ are closed subsets. Let $\aleph : \mathtt{Y}^2 \to \mathtt{Y}$ be a mapping such that $\mathtt{d}\big(\mathtt{z}_1, \aleph(\mathtt{z}_1, \mathtt{z}_2)\big) = \mathtt{d}\big(\mathtt{A}, \mathtt{B}\big)$ and $\mathtt{d}\big(\mathtt{z}_2, \aleph(\mathtt{z}_2, \mathtt{z}_1)\big) = \mathtt{d}\big(\mathtt{A}, \mathtt{B}\big)$. Then $\aleph$ has a coupled best proximity point $(\mathtt{z}_1, \mathtt{z}_2)$.

Definition 3.6. [27] An element $(\mathtt{z}_1, \mathtt{z}_2, \mathtt{z}_3, \cdots, \mathtt{z}_{n-1}, \mathtt{z}_n) \in \mathtt{Y}^n$ is called an n-fixed point of a mapping $\aleph : \mathtt{Y}^n \to \mathtt{Y}$ if

$$\begin{aligned}
&\aleph(\mathtt{z}_1, \mathtt{z}_2, \mathtt{z}_3, \mathtt{z}_4, \cdots, \mathtt{z}_{n-1}, \mathtt{z}_n) = \mathtt{z}_1,\ \aleph(\mathtt{z}_2, \mathtt{z}_1, \mathtt{z}_3, \mathtt{z}_4, \cdots, \mathtt{z}_{n-1}, \mathtt{z}_n) = \mathtt{z}_2,\\
&\aleph(\mathtt{z}_3, \mathtt{z}_2, \mathtt{z}_1, \mathtt{z}_4, \cdots, \mathtt{z}_{n-1}, \mathtt{z}_n) = \mathtt{z}_3,\ \aleph(\mathtt{z}_4, \mathtt{z}_1, \mathtt{z}_3, \mathtt{z}_1, \cdots, \mathtt{z}_{n-1}, \mathtt{z}_n) = \mathtt{z}_4,\\
&\qquad\qquad\qquad\qquad \vdots\\
&\aleph(\mathtt{z}_{n-1}, \mathtt{z}_2, \mathtt{z}_3, \mathtt{z}_4, \cdots, \mathtt{z}_1, \mathtt{z}_n) = \mathtt{z}_{n-1},\ \aleph(\mathtt{z}_n, \mathtt{z}_2, \mathtt{z}_3, \mathtt{z}_4, \cdots, \mathtt{z}_{n-1}, \mathtt{z}_1) = \mathtt{z}_n.
\end{aligned}$$

Now we define n-best proximity point as follows:

Definition 3.7. Let $(\mathtt{Y}, \mathtt{d})$ be a metric space with $\mathtt{A} \neq \emptyset$ and $\mathtt{B} \neq \emptyset$ are closed subsets. Let $\aleph : \mathtt{Y}^n \to \mathtt{Y}$ be a mapping such that

$$\begin{aligned}
&\mathtt{d}\big(\mathtt{z}_1, \aleph(\mathtt{z}_1, \mathtt{z}_2, \mathtt{z}_3, \cdots, \mathtt{z}_{n-1}, \mathtt{z}_n)\big) = \mathtt{d}\big(\mathtt{A}, \mathtt{B}\big),\ \mathtt{d}\big(\mathtt{z}_2, \aleph(\mathtt{z}_2, \mathtt{z}_1, \mathtt{z}_3, \cdots, \mathtt{z}_{n-1}, \mathtt{z}_n)\big) = \mathtt{d}\big(\mathtt{A}, \mathtt{B}\big),\\
&\mathtt{d}\big(\mathtt{z}_3, \aleph(\mathtt{z}_3, \mathtt{z}_2, \mathtt{z}_1, \cdots, \mathtt{z}_{n-1}, \mathtt{z}_n)\big) = \mathtt{d}\big(\mathtt{A}, \mathtt{B}\big),\ \mathtt{d}\big(\mathtt{z}_4, \aleph(\mathtt{z}_4, \mathtt{z}_2, \mathtt{z}_3, \mathtt{z}_1, \cdots, \mathtt{z}_{n-1}, \mathtt{z}_n)\big) = \mathtt{d}\big(\mathtt{A}, \mathtt{B}\big),\\
&\qquad\qquad\qquad\qquad \vdots\\
&\mathtt{d}\big(\mathtt{z}_{n-1}, \aleph(\mathtt{z}_{n-1}, \mathtt{z}_2, \mathtt{z}_3, \cdots, \mathtt{z}_1, \mathtt{z}_n)\big) = \mathtt{d}\big(\mathtt{A}, \mathtt{B}\big),\ \mathtt{d}\big(\mathtt{z}_n, \aleph(\mathtt{z}_n, \mathtt{z}_2, \mathtt{z}_3, \cdots, \mathtt{z}_{n-1}, \mathtt{z}_1)\big) = \mathtt{d}\big(\mathtt{A}, \mathtt{B}\big).
\end{aligned}$$

Then $\aleph$ has an n-best proximity point $(\mathtt{z}_1, \mathtt{z}_2, \mathtt{z}_3, \cdots, \mathtt{z}_{n-1}, \mathtt{z}_n)$.

If $\mathtt{A} = \mathtt{B}$, then n-best proximity point $(\mathtt{z}_1, \mathtt{z}_2, \mathtt{z}_3, \cdots, \mathtt{z}_{n-1}, \mathtt{z}_n)$ of $\aleph$ is an n-fixed pooint of $\aleph$.

Theorem 3.8. Let $(\mathtt{Y}, \mathtt{d})$ be a complete metric space. Let $\mathtt{A} \neq \emptyset, \mathtt{B} \neq \emptyset$ are closed subsets with $\mathtt{A}_0$ and $\mathtt{B}_0$ are nonempty. Let $\aleph : \mathtt{Y}^n \to \mathtt{Y}$ be a continuous mapping which satisfies

(*i*) $\aleph(\mathtt{A}_0 \times \mathtt{B}_0 \times \mathtt{A}_0 \times \cdots \times \mathtt{B}_0 \times \mathtt{A}_0 (n \text{ products})) \subseteq \mathtt{B}_0$,

(*ii*) $\aleph(\mathtt{B}_0 \times \mathtt{A}_0 \times \mathtt{B}_0 \times \cdots \times \mathtt{A}_0 \times \mathtt{B}_0 (n \text{ products})) \subseteq \mathtt{A}_0$,

(*iii*) Pair $(\mathtt{A}, \mathtt{B})$ has the $(\mathcal{P})$-property.

Let θ be a continuous function in Θ and φ be a comparison function satisfying

$$\mathtt{d}\big(\aleph(\mathtt{z}_1, \mathtt{z}_2, \mathtt{z}_3, \cdots, \mathtt{z}_{n-1}, \mathtt{z}_n), \aleph(\mathtt{y}_1, \mathtt{y}_2, \mathtt{y}_3, \cdots, \mathtt{y}_{n-1}, \mathtt{y}_n)\big) \leq \varphi(\eta_1) + \theta(\eta_2), \tag{3.1}$$

where $\eta_1 = \max\limits_{1 \leq i \leq n} \mathtt{d}(\mathtt{z}_i, \mathtt{y}_i)$ and

$$\begin{aligned}
\eta_2 = \Big(&\mathtt{d}\big(\mathtt{y}_1, \aleph(\mathtt{z}_1, \mathtt{z}_2, \mathtt{z}_3, \cdots, \mathtt{z}_{n-1}, \mathtt{z}_n)\big) - \mathtt{d}\big(\mathtt{A}, \mathtt{B}\big), \mathtt{d}\big(\mathtt{y}_2, \aleph(\mathtt{z}_2, \mathtt{z}_1, \mathtt{z}_3, \cdots, \mathtt{z}_{n-1}, \mathtt{z}_n)\big) - \mathtt{d}\big(\mathtt{A}, \mathtt{B}\big),\\
&\mathtt{d}\big(\mathtt{y}_3, \aleph(\mathtt{z}_3, \mathtt{z}_2, \mathtt{z}_1, \cdots, \mathtt{z}_{n-1}, \mathtt{z}_n)\big) - \mathtt{d}\big(\mathtt{A}, \mathtt{B}\big), \cdots, \mathtt{d}\big(\mathtt{y}_n, \aleph(\mathtt{z}_n, \mathtt{z}_2, \mathtt{z}_3, \cdots, \mathtt{z}_{n-1}, \mathtt{z}_1)\big) - \mathtt{d}\big(\mathtt{A}, \mathtt{B}\big),\\
&\mathtt{d}\big(\mathtt{z}_1, \aleph(\mathtt{z}_1, \mathtt{z}_2, \mathtt{z}_3, \cdots, \mathtt{z}_{n-1}, \mathtt{z}_n)\big) - \mathtt{d}\big(\mathtt{A}, \mathtt{B}\big), \mathtt{d}\big(\mathtt{z}_2, \aleph(\mathtt{z}_2, \mathtt{z}_1, \mathtt{z}_3, \cdots, \mathtt{z}_{n-1}, \mathtt{z}_n)\big) - \mathtt{d}\big(\mathtt{A}, \mathtt{B}\big),\\
&\mathtt{d}\big(\mathtt{z}_3, \aleph(\mathtt{z}_3, \mathtt{z}_2, \mathtt{z}_1, \cdots, \mathtt{z}_{n-1}, \mathtt{z}_n)\big) - \mathtt{d}\big(\mathtt{A}, \mathtt{B}\big), \cdots, \mathtt{d}\big(\mathtt{z}_n, \aleph(\mathtt{z}_n, \mathtt{z}_2, \mathtt{z}_3, \cdots, \mathtt{z}_{n-1}, \mathtt{z}_1)\big) - \mathtt{d}\big(\mathtt{A}, \mathtt{B}\big)\Big)
\end{aligned}$$

for all $\mathtt{z}_i, \mathtt{y}_i \in \mathtt{Y}$. Then $(\mathtt{y}_1, \mathtt{y}_1, \mathtt{y}_1, \cdots, \mathtt{y}_1, \mathtt{y}_1)$ is the unique n-best proximity point of $\aleph$.

Proof . Choose $\mathtt{z}_{0,2i} \in \mathtt{A}_0$ and $\mathtt{z}_{0,2i-1} \in \mathtt{B}_0$. Then, $\aleph(\mathtt{z}_{0,2}, \mathtt{z}_{0,1}, \mathtt{z}_{0,3}, \cdots, \mathtt{z}_{0,n-1}, \mathtt{z}_{0,n})$, $\aleph(\mathtt{z}_{0,4}, \mathtt{z}_{0,1}, \mathtt{z}_{0,2}, \cdots, \mathtt{z}_{0,n-1}, \mathtt{z}_{0,n})$, $\aleph(\mathtt{z}_{0,6}, \mathtt{z}_{0,1}, \mathtt{z}_{0,2}, \cdots, \mathtt{z}_{0,n-1}, \mathtt{z}_{0,n}), \cdots \in \mathtt{B}_0$ and $\aleph(\mathtt{z}_{0,1}, \mathtt{z}_{0,2}, \mathtt{z}_{0,3}, \cdots, \mathtt{z}_{0,n-1}, \mathtt{z}_{0,n})$, $\aleph(\mathtt{z}_{0,3}, \mathtt{z}_{0,2}, \mathtt{z}_{0,3}, \cdots, \mathtt{z}_{0,n-1}, \mathtt{z}_{0,n})$, $\aleph(\mathtt{z}_{0,5}, \mathtt{z}_{0,2}, \mathtt{z}_{0,3}, \cdots, \mathtt{z}_{0,n-1}, \mathtt{z}_{0,n}), \cdots \in \mathtt{A}_0$. So, there exists $\mathtt{z}_{1,2i} \in \mathtt{A}_0$ and $\mathtt{z}_{1,2i-1} \in \mathtt{B}_0$ such that

$$\begin{aligned}
&\mathtt{d}\big(\mathtt{z}_{1,1}, \aleph(\mathtt{z}_{0,1}, \mathtt{z}_{0,2}, \mathtt{z}_{0,3}, \cdots, \mathtt{z}_{0,n-1}, \mathtt{z}_{0,n})\big) = \mathtt{d}\big(\mathtt{z}_{1,2}, \aleph(\mathtt{z}_{0,2}, \mathtt{z}_{0,1}, \mathtt{z}_{0,3}, \cdots, \mathtt{z}_{0,n-1}, \mathtt{z}_{0,n})\big)\\
&\mathtt{d}\big(\mathtt{z}_{1,3}, \aleph(\mathtt{z}_{0,3}, \mathtt{z}_{0,2}, \mathtt{z}_{0,1}, \cdots, \mathtt{z}_{0,n-1}, \mathtt{z}_{0,n})\big) = \cdots = \mathtt{d}\big(\mathtt{z}_{1,n}, \aleph(\mathtt{z}_{0,n}, \mathtt{z}_{0,2}, \mathtt{z}_{0,3}, \cdots, \mathtt{z}_{0,n-1}, \mathtt{z}_{0,1})\big)\\
&= \mathtt{d}(\mathtt{A}, \mathtt{B}).
\end{aligned}$$

Continuing this process, we construct n-sequences $(\mathtt{z}_{k,2i})$ in $\mathtt{A}$ and $(\mathtt{z}_{k,2i-1})$ in $\mathtt{B}$ for $i = 1, 2 \cdots, n$ such that

$$\begin{aligned}
&\mathtt{d}\big(\mathtt{z}_{k+1,1}, \aleph(\mathtt{z}_{k,1}, \mathtt{z}_{k,2}, \mathtt{z}_{k,3}, \cdots, \mathtt{z}_{k,n-1}, \mathtt{z}_{k,n})\big) = \mathtt{d}(\mathtt{A}, \mathtt{B}),\\
&\mathtt{d}\big(\mathtt{z}_{k+1,2}, \aleph(\mathtt{z}_{k,2}, \mathtt{z}_{k,1}, \mathtt{z}_{k,3}, \cdots, \mathtt{z}_{k,n-1}, \mathtt{z}_{k,n})\big) = \mathtt{d}(\mathtt{A}, \mathtt{B}),\\
&\mathtt{d}\big(\mathtt{z}_{k+1,3}, \aleph(\mathtt{z}_{k,3}, \mathtt{z}_{k,2}, \mathtt{z}_{k,1}, \cdots, \mathtt{z}_{k,n-1}, \mathtt{z}_{k,n})\big) = \mathtt{d}(\mathtt{A}, \mathtt{B}),\\
&\qquad\qquad\vdots\\
&\mathtt{d}\big(\mathtt{z}_{k+1,n-1}, \aleph(\mathtt{z}_{k,n-1}, \mathtt{z}_{k,2}, \mathtt{z}_{k,3}, \cdots, \mathtt{z}_{k,1}, \mathtt{z}_{k,n})\big) = \mathtt{d}(\mathtt{A}, \mathtt{B}),\\
&\mathtt{d}\big(\mathtt{z}_{k+1,n}, \aleph(\mathtt{z}_{k,n}, \mathtt{z}_{k,2}, \mathtt{z}_{k,3}, \cdots, \mathtt{z}_{k,n-1}, \mathtt{z}_{k,1})\big) = \mathtt{d}(\mathtt{A}, \mathtt{B})
\end{aligned}$$

for $k = 0, 1, 2, \cdots$.

Case (i) Suppose there exists $k \in \mathbb{N}$ such that $\mathtt{d}(\mathtt{z}_{k,1}, \mathtt{z}_{k+1,1}) = \mathtt{d}(\mathtt{z}_{k,2}, \mathtt{z}_{k+1,2}) = \cdots = \mathtt{d}(\mathtt{z}_{k,n}, \mathtt{z}_{k+1,n}) = 0$. Thus,

$$\begin{aligned}
\mathtt{d}(\mathtt{A}, \mathtt{B}) &\le \mathtt{d}\big(\mathtt{z}_{k,1}, \aleph(\mathtt{z}_{k,1}, \mathtt{z}_{k,2}, \mathtt{z}_{k,3}, \cdots, \mathtt{z}_{k,n-1}, \mathtt{z}_{k,n})\big)\\
&\le \mathtt{d}(\mathtt{z}_{k,1}, \mathtt{z}_{k+1,1}) + \mathtt{d}\big(\mathtt{z}_{k+1,1}, \aleph(\mathtt{z}_{k,1}, \mathtt{z}_{k,2}, \mathtt{z}_{k,3}, \cdots, \mathtt{z}_{k,n-1}, \mathtt{z}_{k,n})\big)\\
&= \mathtt{d}(\mathtt{A}, \mathtt{B}).
\end{aligned}$$

Thus we have $\mathtt{d}(\mathtt{A}, \mathtt{B}) = \mathtt{d}\big(\mathtt{z}_{k,1}, \aleph(\mathtt{z}_{k,1}, \mathtt{z}_{k,2}, \mathtt{z}_{k,3}, \cdots, \mathtt{z}_{k,n-1}, \mathtt{z}_{k,n})\big)$. Similarly, we obtain

$$\begin{aligned}
&\mathtt{d}(\mathtt{A}, \mathtt{B}) = \mathtt{d}\big(\mathtt{z}_{k,2}, \aleph(\mathtt{z}_{k,2}, \mathtt{z}_{k,1}, \mathtt{z}_{k,3}, \cdots, \mathtt{z}_{k,n-1}, \mathtt{z}_{k,n})\big),\\
&\mathtt{d}(\mathtt{A}, \mathtt{B}) = \mathtt{d}\big(\mathtt{z}_{k,3}, \aleph(\mathtt{z}_{k,3}, \mathtt{z}_{k,2}, \mathtt{z}_{k,1}, \cdots, \mathtt{z}_{k,n-1}, \mathtt{z}_{k,n})\big),\\
&\qquad\vdots\\
&\mathtt{d}(\mathtt{A}, \mathtt{B}) = \mathtt{d}\big(\mathtt{z}_{k,n}, \aleph(\mathtt{z}_{k,n}, \mathtt{z}_{k,2}, \mathtt{z}_{k,3}, \cdots, \mathtt{z}_{k,n-1}, \mathtt{z}_{k,1})\big).
\end{aligned}$$

Therefore, $(\mathtt{z}_{k,1}, \mathtt{z}_{k,2}, \mathtt{z}_{k,3}, \cdots, \mathtt{z}_{k,n-1}, \mathtt{z}_{k,n})$ is an n-best proximity point of $\aleph$.

Case (ii) Suppose that $\mathtt{d}(\mathtt{z}_{k,i}, \mathtt{z}_{k+1,i}) > 0$ for some i. Since pair $(\mathtt{A}, \mathtt{B})$ has the $\mathcal{P}$-property, $\mathtt{d}\big(\mathtt{z}_{k,1}, \aleph(\mathtt{z}_{k-1,1}, \mathtt{z}_{k-1,2}, \mathtt{z}_{k-1,3}, \cdots, \mathtt{z}_{k-1,n-1}, \mathtt{z}_{k-1,n})\big) = \mathtt{d}(\mathtt{A}, \mathtt{B})$ and $\mathtt{d}\big(\mathtt{z}_{k+1,1}, \aleph(\mathtt{z}_{k,1}, \mathtt{z}_{k,2}, \mathtt{z}_{k,3}, \cdots, \mathtt{z}_{k,n-1}, \mathtt{z}_{k,n})\big) = \mathtt{d}(\mathtt{A}, \mathtt{B})$ and using (3.1), we have

$$\begin{aligned}
\mathtt{d}(\mathtt{z}_{k,1}, \mathtt{z}_{k+1,1}) &= \mathtt{d}\big(\aleph(\mathtt{z}_{k-1,1}, \mathtt{z}_{k-1,2}, \mathtt{z}_{k-1,3}, \cdots, \mathtt{z}_{k-1,n-1}, \mathtt{z}_{k-1,n}), \aleph(\mathtt{z}_{k,1}, \mathtt{z}_{k,2}, \mathtt{z}_{k,3}, \cdots, \mathtt{z}_{k,n-1}, \mathtt{z}_{k,n})\big)\\
&\le \varphi\big(\max_{1\le i\le n} \mathtt{d}(\mathtt{z}_{k-1,i}, \mathtt{z}_{k,i})\big) + \theta(\eta_3),\\
&= \varphi\big(\max_{1\le i\le n} \mathtt{d}(\mathtt{z}_{k-1,i}, \mathtt{z}_{k,i})\big),
\end{aligned}$$

where

$$\begin{aligned}
\eta_3 = \Big(&\mathtt{d}\big(\mathtt{z}_{k,1}, \aleph(\mathtt{z}_{k-1,1}, \mathtt{z}_{k-1,2}, \mathtt{z}_{k-1,3}, \cdots, \mathtt{z}_{k-1,n-1}, \mathtt{z}_{k-1,n})\big) - \mathtt{d}\big(\mathtt{A}, \mathtt{B}\big),\\
&\mathtt{d}\big(2_{k,2}, \aleph(\mathtt{z}_{k-1,2}, \mathtt{z}_{k-1,1}, \mathtt{z}_{k-1,3}, \cdots, \mathtt{z}_{k-1,n-1}, \mathtt{z}_{k-1,n})\big) - \mathtt{d}\big(\mathtt{A}, \mathtt{B}\big),\\
&\mathtt{d}\big(\mathtt{z}_{k,3}, \aleph(\mathtt{z}_{k-1,3}, \mathtt{z}_{2}, \mathtt{z}_{k-1,1}, \cdots, \mathtt{z}_{k-1,n-1}, \mathtt{z}_{k-1,n})\big) - \mathtt{d}\big(\mathtt{A}, \mathtt{B}\big),\\
&\qquad\vdots\\
&\mathtt{d}\big(\mathtt{z}_{k,n}, \aleph(\mathtt{z}_{k-1,n}, \mathtt{z}_{k-1,2}, \mathtt{z}_{k-1,3}, \cdots, \mathtt{z}_{k-1,n-1}, \mathtt{z}_{k-1,1})\big) - \mathtt{d}\big(\mathtt{A}, \mathtt{B}\big),\\
&\mathtt{d}\big(\mathtt{z}_{k-1,1}, \aleph(\mathtt{z}_{k-1,1}, \mathtt{z}_{k-1,2}, \mathtt{z}_{k-1,3}, \cdots, \mathtt{z}_{k-1,n-1}, \mathtt{z}_{k-1,n})\big) - \mathtt{d}\big(\mathtt{A}, \mathtt{B}\big),\\
&\mathtt{d}\big(2_{k-1,2}, \aleph(\mathtt{z}_{k-1,2}, \mathtt{z}_{k-1,1}, \mathtt{z}_{k-1,3}, \cdots, \mathtt{z}_{k-1,n-1}, \mathtt{z}_{k-1,n})\big) - \mathtt{d}\big(\mathtt{A}, \mathtt{B}\big),\\
&\mathtt{d}\big(\mathtt{z}_{k-1,3}, \aleph(\mathtt{z}_{k-1,3}, \mathtt{z}_{2}, \mathtt{z}_{k-1,1}, \cdots, \mathtt{z}_{k-1,n-1}, \mathtt{z}_{k-1,n})\big) - \mathtt{d}\big(\mathtt{A}, \mathtt{B}\big),\\
&\qquad\vdots\\
&\mathtt{d}\big(\mathtt{z}_{k-1,n}, \aleph(\mathtt{z}_{k-1,n}, \mathtt{z}_{k-1,2}, \mathtt{z}_{k-1,3}, \cdots, \mathtt{z}_{k-1,n-1}, \mathtt{z}_{k-1,1})\big) - \mathtt{d}\big(\mathtt{A}, \mathtt{B}\big)\Big).
\end{aligned}$$

Since $\mathtt{d}\big(\mathtt{z}_{k,1}, \aleph(\mathtt{z}_{k-1,1}, \mathtt{z}_{k-1,2}, \mathtt{z}_{k-1,3}, \cdots, \mathtt{z}_{k-1,n-1}, \mathtt{z}_{k-1,n})\big) = \mathtt{d}\big(\mathtt{A}, \mathtt{B}\big)$, it follows from the property of θ that $\theta(\eta_3) = 0$. Similarly, we can prove that

$$\mathtt{d}(\mathtt{z}_{k,\mathtt{j}}, \mathtt{z}_{k+1,\mathtt{j}}) \leq \varphi\big(\max_{1\leq i\leq n} \mathtt{d}(\mathtt{z}_{k-1,i}, \mathtt{z}_{k,i})\big), \ \mathtt{j} = 2, 3, \cdots, n.$$

Combining above all, we get

$$\max_{1\leq \mathtt{j}\leq n} \mathtt{d}(\mathtt{z}_{k,\mathtt{j}}, \mathtt{z}_{k+1,\mathtt{j}}) \leq \varphi\big(\max_{1\leq i\leq n} \mathtt{d}(\mathtt{z}_{k-1,i}, \mathtt{z}_{k,i})\big). \tag{3.2}$$

Repeating (3.2) k-times, we obtain

$$\begin{aligned}\max_{1\leq \mathtt{j}\leq n} \mathtt{d}(\mathtt{z}_{k,\mathtt{j}}, \mathtt{z}_{k+1,\mathtt{j}}) &\leq \varphi\big(\max_{1\leq i\leq n} \mathtt{d}(\mathtt{z}_{k-1,i}, \mathtt{z}_{k,i})\big)\\ &\leq \varphi^2\big(\max_{1\leq i\leq n} \mathtt{d}(\mathtt{z}_{k-2,i}, \mathtt{z}_{k-1,i})\big)\\ &\vdots\\ &\leq \varphi^k\big(\max_{1\leq i\leq n} \mathtt{d}(\mathtt{z}_{0,i}, \mathtt{z}_{1,i})\big).\end{aligned}$$

Thus,

$$\lim_{k\to+\infty} \mathtt{d}(\mathtt{z}_{k,\mathtt{j}}, \mathtt{z}_{k+1,\mathtt{j}}) = 0, \ \mathtt{j} = 1, 2, \cdots, n.$$

On other hand,

$$\begin{aligned}\mathtt{d}(\mathtt{A}, \mathtt{B}) &\leq \mathtt{d}\big(\mathtt{z}_{k,1}, \aleph(\mathtt{z}_{k,1}, \mathtt{z}_{k,2}, \mathtt{z}_{k,3}, \cdots, \mathtt{z}_{k,n-1}, \mathtt{z}_{k,n})\big)\\ &\leq \mathtt{d}(\mathtt{z}_{k,1}, \mathtt{z}_{k+1,1}) + \mathtt{d}\big(\mathtt{z}_{k+1,1}, \aleph(\mathtt{z}_{k,1}, \mathtt{z}_{k,2}, \mathtt{z}_{k,3}, \cdots, \mathtt{z}_{k,n-1}, \mathtt{z}_{k,n})\big)\\ &\leq \mathtt{d}(\mathtt{z}_{k,1}, \mathtt{z}_{k+1,1}) + \mathtt{d}(\mathtt{A}, \mathtt{B}).\end{aligned}$$

Letting $k \to +\infty$ in the above inequalities, we get

$$\mathtt{d}\big(\mathtt{z}_{k,1}, \aleph(\mathtt{z}_{k,1}, \mathtt{z}_{k,2}, \mathtt{z}_{k,3}, \cdots, \mathtt{z}_{k,n-1}, \mathtt{z}_{k,n})\big) = \mathtt{d}(\mathtt{A}, \mathtt{B}).$$

Similary, we can prove

$$\mathtt{d}\big(\mathtt{z}_{k,\mathtt{j}}, \aleph(\mathtt{z}_{k,1}, \mathtt{z}_{k,2}, \mathtt{z}_{k,3}, \cdots, \mathtt{z}_{k,n-1}, \mathtt{z}_{k,n})\big) = \mathtt{d}(\mathtt{A}, \mathtt{B}), \ \mathtt{j} = 2, 3, \cdots, n.$$

Consider $\varepsilon > 0$. Since $\varphi^k\big(\max_{1\leq i\leq n} \mathtt{d}(\mathtt{z}_{0,i}, \mathtt{z}_{1,i})\big)$ as $k \to +\infty$, there exists $k_0 \in \mathbb{N}$ such that

$$\mathtt{d}(\mathtt{z}_{k,i}, \mathtt{z}_{k+1,i}) < \frac{1}{2}(\varepsilon - \varphi(\varepsilon))$$

hold for all $k \geq k_0$ and $i = 1, 2, \cdots, n$.

Claim: $\max_{1\leq i\leq n} \mathtt{d}(\mathtt{z}_{k,i}, \mathtt{z}_{m,i}) < \varepsilon$ for all $m > k \geq k_0$. (3.3)

We use the induction on m to prove above claim. Assume inequality (3.3) holds for $m = p$. Now, we prove relation (3.3) for $m = p + 1$. By using the triangular inequality, we have

$$\mathtt{d}(\mathtt{z}_{k,1}, \mathtt{z}_{p+1,1}) \leq \mathtt{d}(\mathtt{z}_{k,1}, \mathtt{z}_{k+1,1}) + \mathtt{d}(\mathtt{z}_{k+1,1}, \mathtt{z}_{p+1,1}). \tag{3.4}$$

Since pair $(\mathtt{A}, \mathtt{B})$ has the $\mathcal{P}$-property, $\mathtt{d}\big(\mathtt{z}_{k+1,1}, \aleph(\mathtt{z}_{k,1}, \mathtt{z}_{k,2}, \mathtt{z}_{k,3}, \cdots, \mathtt{z}_{k,n-1}, \mathtt{z}_{k,n})\big) = \mathtt{d}\big(\mathtt{z}_{p+1,1}, \aleph(\mathtt{z}_{p,1}, \mathtt{z}_{p,2}, \mathtt{z}_{p,3}, \cdots, \mathtt{z}_{p,n-1}, \mathtt{z}_{p,n})\big) = \mathtt{d}(\mathtt{A}, \mathtt{B})$ and using (3.1), we have

$$\begin{aligned}\mathtt{d}(\mathtt{z}_{k+1,1}, \mathtt{z}_{p+1,1}) &= \mathtt{d}\big(\aleph(\mathtt{z}_{k,1}, \mathtt{z}_{k,2}, \mathtt{z}_{k,3}, \cdots, \mathtt{z}_{k,n-1}, \mathtt{z}_{k,n}), \aleph(\mathtt{z}_{p,1}, \mathtt{z}_{p,2}, \mathtt{z}_{p,3}, \cdots, \mathtt{z}_{p,n-1}, \mathtt{z}_{p,n})\big)\\ &\leq \varphi\big(\max_{1\leq i\leq n} \mathtt{d}(\mathtt{z}_{k,i}, \mathtt{z}_{p,i})\big) + \theta(\ell_1),\end{aligned} \tag{3.5}$$

where

$$\begin{aligned}\ell_1 = \Big(& \mathtt{d}\big(\mathtt{z}_{p,1}, \aleph(\mathtt{z}_{k,1}, \mathtt{z}_{k,2}, \mathtt{z}_{k,3}, \cdots, \mathtt{z}_{k,n-1}, \mathtt{z}_{k,n})\big) - \mathtt{d}\big(\mathtt{A}, \mathtt{B}\big),\\ & \mathtt{d}\big(\mathtt{z}_{p,2}, \aleph(\mathtt{z}_{k,2}, \mathtt{z}_{k,1}, \mathtt{z}_{k,3}, \cdots, \mathtt{z}_{k,n-1}, \mathtt{z}_{k,n})\big) - \mathtt{d}\big(\mathtt{A}, \mathtt{B}\big),\\ & \qquad \vdots \\ & \mathtt{d}\big(\mathtt{z}_{p,n}, \aleph(\mathtt{z}_{k,n}, \mathtt{z}_{k,2}, \mathtt{z}_{k,3}, \cdots, \mathtt{z}_{k,n-1}, \mathtt{z}_{k,1})\big) - \mathtt{d}\big(\mathtt{A}, \mathtt{B}\big),\\ & \mathtt{d}\big(\mathtt{z}_{k,1}, \aleph(\mathtt{z}_{k,1}, \mathtt{z}_{k,2}, \mathtt{z}_{k,3}, \cdots, \mathtt{z}_{k,n-1}, \mathtt{z}_{k,n})\big) - \mathtt{d}\big(\mathtt{A}, \mathtt{B}\big),\\ & \mathtt{d}\big(\mathtt{z}_{k,2}, \aleph(\mathtt{z}_{k,2}, \mathtt{z}_{k,1}, \mathtt{z}_{k,3}, \cdots, \mathtt{z}_{k,n-1}, \mathtt{z}_{k,n})\big) - \mathtt{d}\big(\mathtt{A}, \mathtt{B}\big),\\ & \qquad \vdots \\ & \mathtt{d}\big(\mathtt{z}_{k,n}, \aleph(\mathtt{z}_{k,n}, \mathtt{z}_{k,2}, \mathtt{z}_{k,3}, \cdots, \mathtt{z}_{k,n-1}, \mathtt{z}_{k,1})\big) - \mathtt{d}\big(\mathtt{A}, \mathtt{B}\big)\Big).\end{aligned}$$

By using the properties of θ and $\lim_{k\to+\infty} \mathtt{d}\big(\mathtt{z}_{k,1}, \aleph(\mathtt{z}_{k,1}, \mathtt{z}_{k,2}, \mathtt{z}_{k,3}, \cdots, \mathtt{z}_{k,n-1}, \mathtt{z}_{k,n})\big) = \mathtt{d}\big(\mathtt{A}, \mathtt{B}\big)$, we get

$$\limsup_{k\to+\infty} \theta(\ell_1) = 0.$$

Similarly, we can have

$$\begin{aligned}\mathtt{d}(\mathtt{z}_{k+1,i}, \mathtt{z}_{p+1,i}) &= \mathtt{d}\big(\aleph(\mathtt{z}_{k,1}, \mathtt{z}_{k,2}, \mathtt{z}_{k,3}, \cdots, \mathtt{z}_{k,n-1}, \mathtt{z}_{k,n}), \aleph(\mathtt{z}_{p,1}, \mathtt{z}_{p,2}, \mathtt{z}_{p,3}, \cdots, \mathtt{z}_{p,n-1}, \mathtt{z}_{p,n})\big)\\ &\leq \varphi\big(\max_{1\leq i\leq n} \mathtt{d}(\mathtt{z}_{k,i}, \mathtt{z}_{p,i})\big) + \theta(\ell_i),\ i = 2, 3, \cdots, n \end{aligned} \tag{3.6}$$

and

$$\limsup_{k\to+\infty} \theta(\ell_i) = 0, \quad i = 2, 3, \cdots, n.$$

Thus for k_0 large enough, we have

$$\theta(\ell_i) < \frac{1}{2}(\varepsilon - \varphi(\varepsilon)),\ i = 1, 2, \cdots, n.$$

Combining all the relations, from $i = 1$ to n, we obtain

$$\max_{1\leq i\leq n} \mathtt{d}(\mathtt{z}_{k,i}, \mathtt{z}_{p+1,i}) < \varepsilon.$$

Hence, the claim. Thus $(\mathtt{z}_{k,2i})$ and $(\mathtt{z}_{k,2i-1})$ are Cauchy sequences in $\mathtt{A}$ and $\mathtt{B}$ respectively. Since $(\mathtt{Y}, \mathtt{d})$ is complete, there exist $\mathtt{y}_i \in \mathtt{Y}$, $i = 1, 2, \cdots, n$ such that

$$\lim_{k\to+\infty} \mathtt{z}_{k,i} = \mathtt{y}_i,\ i = 1, 2, \cdots, n.$$

Since $\mathtt{A}$ and $\mathtt{B}$ are closed, we get $\mathtt{y}_{2i} \in \mathtt{A}$ and $\mathtt{y}_{2i-1} \in \mathtt{B}$. Since $\aleph$ is continuous,

$$\lim_{k\to+\infty} \mathtt{d}\big(\mathtt{z}_{k,1}, \aleph(\mathtt{z}_{k,1}, \mathtt{z}_{k,2}, \mathtt{z}_{k,3}, \cdots, \mathtt{z}_{k,n-1}, \mathtt{z}_{k,n})\big) = \mathtt{d}\big(\mathtt{A}, \mathtt{B}\big),$$

implies

$$\mathtt{d}\big(\mathtt{y}_1, \aleph(\mathtt{y}_1, \mathtt{y}_2, \mathtt{y}_3, \cdots, \mathtt{y}_{n-1}, \mathtt{y}_n)\big) = \mathtt{d}\big(\mathtt{A}, \mathtt{B}\big).$$

Similarly, we can prove

$$\begin{aligned}&\mathtt{d}\big(\mathtt{y}_2, \aleph(\mathtt{y}_2, \mathtt{y}_1, \mathtt{y}_3, \cdots, \mathtt{y}_{n-1}, \mathtt{y}_n)\big) = \mathtt{d}\big(\mathtt{A}, \mathtt{B}\big),\\ &\mathtt{d}\big(\mathtt{y}_3, \aleph(\mathtt{y}_3, \mathtt{y}_2, \mathtt{y}_1, \cdots, \mathtt{y}_{n-1}, \mathtt{y}_n)\big) = \mathtt{d}\big(\mathtt{A}, \mathtt{B}\big),\\ &\qquad \vdots \\ &\mathtt{d}\big(\mathtt{y}_n, \aleph(\mathtt{y}_n, \mathtt{y}_2, \mathtt{y}_3, \cdots, \mathtt{y}_{n-1}, \mathtt{y}_1)\big) = \mathtt{d}\big(\mathtt{A}, \mathtt{B}\big).\end{aligned}$$

Thus, $(\mathtt{y}_1, \mathtt{y}_2, \mathtt{y}_3, \cdots, \mathtt{y}_{n-1}, \mathtt{y}_n)$ is an n-best proximity point of $\aleph$. Now, we show that $\mathtt{y}_1 = \mathtt{y}_2 = \mathtt{y}_3 = \cdots = \mathtt{y}_{n-1} = \mathtt{y}_n$. Using the $\mathcal{P}$-property of pair $(\mathtt{A}, \mathtt{B})$, we get

$$\mathtt{d}(\mathtt{y}_1, \mathtt{y}_2) = \mathtt{d}\big(\aleph(\mathtt{y}_1, \mathtt{y}_2, \mathtt{y}_3, \cdots, \mathtt{y}_{n-1}, \mathtt{y}_n), \aleph(\mathtt{y}_2, \mathtt{y}_1, \mathtt{y}_3, \cdots, \mathtt{y}_{n-1}, \mathtt{y}_n)\big).$$

Using inequality (3.1), we get

$$\begin{aligned}\mathtt{d}(\mathtt{y}_1,\mathtt{y}_2) &= \mathtt{d}\big(\aleph(\mathtt{y}_1,\mathtt{y}_2,\mathtt{y}_3,\cdots,\mathtt{y}_{n-1},\mathtt{y}_n),\aleph(\mathtt{y}_2,\mathtt{y}_1,\mathtt{y}_3,\cdots,\mathtt{y}_{n-1},\mathtt{y}_n)\big)\\ &\le \varphi\big(\max\{\mathtt{d}(\mathtt{y}_1,\mathtt{y}_2),\mathtt{d}(\mathtt{y}_2,\mathtt{y}_1)\}\big)+\theta(\ell)\\ &\le \varphi\big(\mathtt{d}(\mathtt{y}_1,\mathtt{y}_2)\big),\end{aligned}\tag{3.7}$$

since

$$\begin{aligned}\ell = \Big(&\mathtt{d}\big(\mathtt{y}_2,\aleph(\mathtt{y}_2,\mathtt{y}_1,\mathtt{y}_3,\cdots,\mathtt{y}_{n-1},\mathtt{y}_n)\big)-\mathtt{d}(\mathtt{A},\mathtt{B}),\mathtt{d}\big(\mathtt{y}_1,\aleph(\mathtt{y}_2,\mathtt{y}_1,\mathtt{y}_3,\cdots,\mathtt{y}_{n-1},\mathtt{y}_n)\big)-\mathtt{d}(\mathtt{A},\mathtt{B}),\\ &\mathtt{d}\big(\mathtt{y}_3,\aleph(\mathtt{y}_2,\mathtt{y}_1,\mathtt{y}_3,\cdots,\mathtt{y}_{n-1},\mathtt{y}_n)\big)-\mathtt{d}(\mathtt{A},\mathtt{B}),\cdots,\mathtt{d}\big(\mathtt{y}_n,\aleph(\mathtt{y}_2,\mathtt{y}_1,\mathtt{y}_3,\cdots,\mathtt{y}_{n-1},\mathtt{y}_n)\big)-\mathtt{d}(\mathtt{A},\mathtt{B}),\\ &\mathtt{d}\big(\mathtt{y}_1,\aleph(\mathtt{y}_2,\mathtt{y}_1,\mathtt{y}_3,\cdots,\mathtt{y}_{n-1},\mathtt{y}_n)\big)-\mathtt{d}(\mathtt{A},\mathtt{B}),\mathtt{d}\big(\mathtt{y}_2,\aleph(\mathtt{y}_2,\mathtt{y}_1,\mathtt{y}_3,\cdots,\mathtt{y}_{n-1},\mathtt{y}_n)\big)-\mathtt{d}(\mathtt{A},\mathtt{B}),\\ &\mathtt{d}\big(\mathtt{y}_3,\aleph(\mathtt{y}_2,\mathtt{y}_1,\mathtt{y}_3,\cdots,\mathtt{y}_{n-1},\mathtt{y}_n)\big)-\mathtt{d}(\mathtt{A},\mathtt{B}),\cdots,\mathtt{d}\big(\mathtt{y}_n,\aleph(\mathtt{y}_2,\mathtt{y}_1,\mathtt{y}_3,\cdots,\mathtt{y}_{n-1},\mathtt{y}_n)\big)-\mathtt{d}(\mathtt{A},\mathtt{B})\Big)\\ = \Big(&0,\mathtt{d}\big(\mathtt{y}_1,\aleph(\mathtt{y}_2,\mathtt{y}_1,\mathtt{y}_3,\cdots,\mathtt{y}_{n-1},\mathtt{y}_n)\big)-\mathtt{d}(\mathtt{A},\mathtt{B}),\mathtt{d}\big(\mathtt{y}_3,\aleph(\mathtt{y}_2,\mathtt{y}_1,\mathtt{y}_3,\cdots,\mathtt{y}_{n-1},\mathtt{y}_n)\big)-\mathtt{d}(\mathtt{A},\mathtt{B}),\\ &\cdots,\mathtt{d}\big(\mathtt{y}_n,\aleph(\mathtt{y}_2,\mathtt{y}_1,\mathtt{y}_3,\cdots,\mathtt{y}_{n-1},\mathtt{y}_n)\big)-\mathtt{d}(\mathtt{A},\mathtt{B}),\mathtt{d}\big(\mathtt{y}_1,\aleph(\mathtt{y}_2,\mathtt{y}_1,\mathtt{y}_3,\cdots,\mathtt{y}_{n-1},\mathtt{y}_n)\big)-\mathtt{d}(\mathtt{A},\mathtt{B}),\\ &0,\mathtt{d}\big(\mathtt{y}_3,\aleph(\mathtt{y}_2,\mathtt{y}_1,\mathtt{y}_3,\cdots,\mathtt{y}_{n-1},\mathtt{y}_n)\big)-\mathtt{d}(\mathtt{A},\mathtt{B}),\cdots,\mathtt{d}\big(\mathtt{y}_n,\aleph(\mathtt{y}_2,\mathtt{y}_1,\mathtt{y}_3,\cdots,\mathtt{y}_{n-1},\mathtt{y}_n)\big)-\mathtt{d}(\mathtt{A},\mathtt{B})\Big).\end{aligned}$$

So, $\theta(\ell)=0$. Since $\varphi(\mathtt{t})<\mathtt{t}$ for all $\mathtt{t}>0$, we have from (3.7) that

$$\mathtt{d}(\mathtt{y}_1,\mathtt{y}_2)\le\varphi\big(\mathtt{d}(\mathtt{y}_1,\mathtt{y}_2)\big)<\mathtt{d}(\mathtt{y}_1,\mathtt{y}_2)\implies \mathtt{y}_1=\mathtt{y}_2.$$

Similarly, we can prove $\mathtt{y}_1=\mathtt{y}_2=\mathtt{y}_3=\cdots=\mathtt{y}_n$. To prove the uniqueness, let ζ be another n-best proximity point. Then,

$$\begin{aligned}\mathtt{d}(\mathtt{y}_1,\zeta) &= \mathtt{d}\big(\aleph(\mathtt{y}_1,\mathtt{y}_1,\mathtt{y}_1,\cdots,\mathtt{y}_1,\mathtt{y}_1),\aleph(\zeta,\zeta,\zeta,\cdots,\zeta,\zeta)\big)\\ &\le \varphi\big(\mathtt{d}(\mathtt{y}_1,\zeta)\big).\end{aligned}$$

Again, since $\varphi(\mathtt{t})<\mathtt{t}$ for all $\mathtt{t}>0$, we conclude that $\mathtt{d}(\mathtt{y}_1,\zeta)=0$. Thus, $\mathtt{y}_1=\zeta$. The proof is completed. □

Corollary 3.9. Let $(\mathtt{Y},\mathtt{d})$ be a complete metric space. Let $\mathtt{A}\neq\emptyset,\mathtt{B}\neq\emptyset$ are closed subsets with $\mathtt{A}_0$ and $\mathtt{B}_0$ are nonempty. Let $\aleph:\mathtt{Y}^n\to\mathtt{Y}$ be a continuous mapping which satisfies

(*i*) $\aleph(\mathtt{A}_0\times\mathtt{A}_0\times\cdots\times\mathtt{A}_0(n\text{ products}))\subseteq\mathtt{B}_0$ (or) $\aleph(\mathtt{B}_0\times\mathtt{B}_0\times\cdots\times\mathtt{B}_0(n\text{ products}))\subseteq\mathtt{A}_0$,

(*ii*) Pair $(\mathtt{A},\mathtt{B})$ has the $\mathcal{P}$-property.

Let θ be a continuous function in Θ and φ be a comparison function satisfying

$$\mathtt{d}\big(\aleph(\mathtt{z}_1,\mathtt{z}_2,\mathtt{z}_3,\cdots,\mathtt{z}_{n-1},\mathtt{z}_n),\aleph(\mathtt{y}_1,\mathtt{y}_2,\mathtt{y}_3,\cdots,\mathtt{y}_{n-1},\mathtt{y}_n)\big)\le\varphi(\eta_1)+\theta(\eta_2),\quad\text{for all }\ \mathtt{z}_i,\mathtt{y}_i\in\mathtt{Y}.$$

where η_1 and η_2 are defined in Theorem 3.8. Then $(\mathtt{y}_1,\mathtt{y}_1,\mathtt{y}_1,\cdots,\mathtt{y}_1,\mathtt{y}_1)$ is the unique n-best proximity point of $\aleph$.

Proof . Choose $\mathtt{z}_{0,i}\in\mathtt{A}_0$. Since $\aleph(\mathtt{A}_0\times\mathtt{A}_0\times\cdots\times\mathtt{A}_0)\subseteq\mathtt{B}_0$, we get, $\aleph(\mathtt{z}_{0,1},\mathtt{z}_{0,2},\mathtt{z}_{0,3},\cdots,\mathtt{z}_{0,n-1},\mathtt{z}_{0,n})$, $\aleph(\mathtt{z}_{0,2},\mathtt{z}_{0,1},\mathtt{z}_{0,3},\cdots,\mathtt{z}_{0,n-1},\mathtt{z}_{0,n})$, $\cdots$ $\aleph(\mathtt{z}_{0,n},\mathtt{z}_{0,2},\mathtt{z}_{0,3},\cdots,\mathtt{z}_{0,n-1},\mathtt{z}_{0,1})\in\mathtt{B}_0$. Then by following Theorem 3.8, we get that $(\mathtt{y}_1,\mathtt{y}_2,\mathtt{y}_3,\cdots,\mathtt{y}_{n-1},\mathtt{y}_n)$ is the unique n-best proximity point of $\aleph$. □

Take $\mathtt{B}=\mathtt{A}$ in Theorem 3.8, we have the following result.

Corollary 3.10. Let $\mathtt{A}$ a closed subsets of a complete metric space $(\mathtt{Y},\mathtt{d})$. Let $\aleph:\mathtt{Y}^n\to\mathtt{Y}$ be a continuous mapping with $\aleph(\mathtt{A}\times\mathtt{A}\times\cdots\times\mathtt{A}(n\,\text{times}))\subseteq\mathtt{A}$. Suppose there exists a comparison function φ and $\theta\in\Theta$ such that

$$\mathtt{d}\big(\aleph(\mathtt{z}_1,\mathtt{z}_2,\mathtt{z}_3,\cdots,\mathtt{z}_{n-1},\mathtt{z}_n),\aleph(\mathtt{y}_1,\mathtt{y}_2,\mathtt{y}_3,\cdots,\mathtt{y}_{n-1},\mathtt{y}_n)\big)\le\varphi(\eta_1)+\theta(\eta_3),\quad\text{for all }\ \mathtt{z}_i,\mathtt{y}_i\in\mathtt{Y}.$$

where η_1 is defined in Theorem 3.8 and

$$\begin{aligned}\eta_3 = \Big(&\mathtt{d}\big(\mathtt{y}_1,\aleph(\mathtt{z}_1,\mathtt{z}_2,\mathtt{z}_3,\cdots,\mathtt{z}_{n-1},\mathtt{z}_n)\big),\mathtt{d}\big(\mathtt{y}_2,\aleph(\mathtt{z}_2,\mathtt{z}_1,\mathtt{z}_3,\cdots,\mathtt{z}_{n-1},\mathtt{z}_n)\big),\\ &\mathtt{d}\big(\mathtt{y}_3,\aleph(\mathtt{z}_3,\mathtt{z}_2,\mathtt{z}_1,\cdots,\mathtt{z}_{n-1},\mathtt{z}_n)\big),\cdots,\mathtt{d}\big(\mathtt{y}_n,\aleph(\mathtt{z}_n,\mathtt{z}_2,\mathtt{z}_3,\cdots,\mathtt{z}_{n-1},\mathtt{z}_1)\big),\\ &\mathtt{d}\big(\mathtt{z}_1,\aleph(\mathtt{z}_1,\mathtt{z}_2,\mathtt{z}_3,\cdots,\mathtt{z}_{n-1},\mathtt{z}_n)\big),\mathtt{d}\big(\mathtt{z}_2,\aleph(\mathtt{z}_2,\mathtt{z}_1,\mathtt{z}_3,\cdots,\mathtt{z}_{n-1},\mathtt{z}_n)\big),\\ &\mathtt{d}\big(\mathtt{z}_3,\aleph(\mathtt{z}_3,\mathtt{z}_2,\mathtt{z}_1,\cdots,\mathtt{z}_{n-1},\mathtt{z}_n)\big),\cdots,\mathtt{d}\big(\mathtt{z}_n,\aleph(\mathtt{z}_n,\mathtt{z}_2,\mathtt{z}_3,\cdots,\mathtt{z}_{n-1},\mathtt{z}_1)\big)\Big).\end{aligned}$$

Then there exists a unique n-fixed point of $\aleph$.

4 Existence of Solutions for System of Fractional Order BVPs (1.1)–(1.2)

In this section, we derive necessary conditions for the existence of solutions for the problem (1.1)–(1.2). On the set $\mathtt{Y} = C([0,1],\mathbb{R})$ of all continuous real-valued functions defined on $[0,1]$, we take the metric $\mathtt{d}$ on $\mathtt{Y}$ defined by

$$\mathtt{d}(\mathtt{z},\mathtt{y}) = \sup_{\mathtt{s}\in[0,1]} |\mathtt{z}(\mathtt{s}) - \mathtt{y}(\mathtt{s})|$$

for all $\mathtt{z},\mathtt{y} \in \mathtt{Y}$.

Define an operator $\aleph : \mathtt{Y}^n \to \mathtt{Y}$ by

$$\aleph(\mathtt{z}_1,\mathtt{z}_2,\cdots,\mathtt{z}_{n-1},\mathtt{z}_n) = \sum_{i=1}^{n} \aleph_i \mathtt{z}_i,$$

where

$$\begin{aligned}
\aleph_1\mathtt{z}_1(\mathtt{s}) &= \int_0^1 \mathtt{G}_1(\mathtt{s},\mathtt{t})\mathtt{g}_1(\mathtt{t},\mathtt{z}_1(\mathtt{t}),\mathtt{z}_2(\mathtt{t}),\cdots,\mathtt{z}_n(\mathtt{t}))\mathtt{dt} \\
&\quad - \mathtt{s}^{ß_1-1}\sum_{\mathtt{j}=1}^{\infty}\delta_{1\mathtt{j}}\int_0^{\sigma_1(\tau_{1\mathtt{j}})}\frac{(\sigma_1(\tau_{1\mathtt{j}})-\mathtt{t})^{ß_1-1}}{\Gamma(ß_1)}\mathtt{g}_1(\mathtt{t},\mathtt{z}_1(\mathtt{t}),\mathtt{z}_2(\mathtt{t}),\cdots,\mathtt{z}_n(\mathtt{t}))\mathtt{dt}, \\
\aleph_2\mathtt{z}_2(\mathtt{s}) &= \int_0^1 \mathtt{G}_2(\mathtt{s},\mathtt{t})\mathtt{g}_2(\mathtt{t},\mathtt{z}_2(\mathtt{t}),\mathtt{z}_1(\mathtt{t}),\cdots,\mathtt{z}_n(\mathtt{t}))\mathtt{dt} \\
&\quad - \mathtt{s}^{ß_2-1}\sum_{\mathtt{j}=1}^{\infty}\delta_{2\mathtt{j}}\int_0^{\sigma_2(\tau_{2\mathtt{j}})}\frac{(\sigma_2(\tau_{2\mathtt{j}})-\mathtt{t})^{ß_2-1}}{\Gamma(ß_2)}\mathtt{g}_2(\mathtt{t},\mathtt{z}_2(\mathtt{t}),\mathtt{z}_1(\mathtt{t}),\cdots,\mathtt{z}_n(\mathtt{t}))\mathtt{dt}, \\
&\vdots \\
\aleph_n\mathtt{z}_n(\mathtt{s}) &= \int_0^1 \mathtt{G}_n(\mathtt{s},\mathtt{t})\mathtt{g}_n(\mathtt{t},\mathtt{z}_n(\mathtt{t}),\mathtt{z}_2(\mathtt{t}),\cdots,\mathtt{z}_1(\mathtt{t}))\mathtt{dt} \\
&\quad - \mathtt{s}^{ß_n-1}\sum_{\mathtt{j}=1}^{\infty}\delta_{n\mathtt{j}}\int_0^{\sigma_n(\tau_{n\mathtt{j}})}\frac{(\sigma_n(\tau_{n\mathtt{j}})-\mathtt{t})^{ß_n-1}}{\Gamma(ß_n)}\mathtt{g}_n(\mathtt{t},\mathtt{z}_n(\mathtt{t}),\mathtt{z}_2(\mathtt{t}),\cdots,\mathtt{z}_1(\mathtt{t}))\mathtt{dt}.
\end{aligned}$$

Then from Lemma 2.7, it is clear that $(\mathtt{z}_1,\mathtt{z}_2,\cdots,\mathtt{z}_n)$ is a solution of the system (1.1)–(1.2) if and only if it is a fixed point of $\aleph$.

Theorem 4.1. Suppose there exists $\mathtt{M} > 0$ such that

$$|\mathtt{g}_i(\mathtt{s},\mathtt{z}_i,\mathtt{z}_2,\cdots,\mathtt{z}_1,\cdots,\mathtt{z}_n) - \mathtt{g}_i(\mathtt{s},\mathtt{y}_i,\mathtt{y}_2,\cdots,\mathtt{y}_1,\cdots,\mathtt{y}_n)| \le \mathtt{M}\sum_{i=1}^{n}|\mathtt{z}_i - \mathtt{y}_i| \quad \text{for all} \quad \mathtt{z}_i,\mathtt{y}_i \in \mathtt{Y} \tag{4.1}$$

and $i = 1,2,\cdots,n$. Further, there exist $\wp_1 > 0$ and $0 < \wp_2 < 1$ such that

$$|\mathtt{g}_i(\mathtt{t},0,0,\cdots,0,0)| \le \wp_1$$

and

$$\sum_{i=1}^{n}\left[\mathtt{G}_i^{\star} + \frac{2\Gamma(ß_i)}{\Gamma(ß_i+1)\Gamma(ß_i-\alpha_i)}\right] \le \wp_2,$$

where $\mathtt{G}_i^{\star} = \max_{\mathtt{s}\in[0,1]}\int_0^1 \mathtt{G}_i(\mathtt{s},\mathtt{t})\mathtt{dt}$. Then there exists a unique solution to the boundary value problem (1.1)–(1.2).

Proof . Define a set $\mathtt{A}$ by $\mathtt{A} = \{\mathtt{z} \in \mathtt{Y} : |\mathtt{z}(s)| \le \wp_3 \text{ for } s \in [0,1]\}$, where $\wp_3 > \dfrac{\wp_1\wp_2}{1-n\wp_2}$. Then it is clear that $\mathtt{A}$ is a

closed subset of $\mathtt{Y}$. Now, we prove $\aleph\big(\mathtt{A}\times\mathtt{A}\times\cdots\times\mathtt{A}(n\,\text{times})\big)\subseteq\mathtt{A}$. Let $(\mathtt{z}_1,\mathtt{z}_2,\cdots,\mathtt{z}_n)\in\mathtt{A}^n$. Then,

$$
\begin{aligned}
|\aleph(\mathtt{z}_1,\mathtt{z}_2,\cdots,\mathtt{z}_n)| &\le \sum_{i=1}^{n}|\aleph_i\mathtt{z}_i(\mathtt{s})| = \sum_{i=1}^{n}\Big|\int_0^1 \mathtt{G}_i(\mathtt{s},\mathtt{t})\mathtt{g}_i(\mathtt{t},\mathtt{z}_i(\mathtt{t}),\mathtt{z}_2(\mathtt{t}),\cdots,\mathtt{z}_n(\mathtt{t}))\mathtt{dt}\\
&\quad - \mathtt{s}^{ß_i-1}\sum_{\mathtt{j}=1}^{\infty}\delta_{i\mathtt{j}}\int_0^{\sigma_i(\tau_{i\mathtt{j}})}\frac{(\sigma_i(\tau_{i\mathtt{j}})-\mathtt{t})^{ß_i-1}}{\Gamma(ß_i)}\mathtt{g}_i(\mathtt{t},\mathtt{z}_i(\mathtt{t}),\mathtt{z}_2(\mathtt{t}),\cdots,\mathtt{z}_n(\mathtt{t}))\mathtt{dt}\Big|\\
&\le \sum_{i=1}^{n}\Bigg[\int_0^1|\mathtt{G}_i(\mathtt{s},\mathtt{t})|\big[|\mathtt{g}_i(\mathtt{t},\mathtt{z}_i(\mathtt{t}),\mathtt{z}_2(\mathtt{t}),\cdots,\mathtt{z}_n(\mathtt{t}))-\mathtt{g}_i(\mathtt{t},0,0,\cdots,0)|+|\mathtt{g}_i(\mathtt{t},0,0,\cdots,0)|\big]\mathtt{dt}\\
&\quad + |\mathtt{s}|^{ß_i-1}\sum_{\mathtt{j}=1}^{\infty}\delta_{i\mathtt{j}}\int_0^{\sigma_i(\tau_{i\mathtt{j}})}\frac{(\sigma_i(\tau_{i\mathtt{j}})-\mathtt{t})^{ß_i-1}}{\Gamma(ß_i)}\big[|\mathtt{g}_i(\mathtt{t},\mathtt{z}_i(\mathtt{t}),\mathtt{z}_2(\mathtt{t}),\cdots,\mathtt{z}_n(\mathtt{t}))-\mathtt{g}_i(\mathtt{t},0,0,\cdots,0)|\\
&\qquad + |\mathtt{g}_i(\mathtt{t},0,0,\cdots,0)|\big]\mathtt{dt}\Bigg]\\
&\le \sum_{i=1}^{n}\Bigg[\int_0^1|\mathtt{G}_i(\mathtt{s},\mathtt{t})|\big[\sum_{\mathtt{j}=1}^{n}|\mathtt{z}_\mathtt{j}(\mathtt{t})|+|\mathtt{g}_i(\mathtt{t},0,0,\cdots,0)|\big]\mathtt{dt} + |\mathtt{s}|^{ß_i-1}\sum_{\mathtt{j}=1}^{\infty}\delta_{i\mathtt{j}}\int_0^{\sigma_i(\tau_{i\mathtt{j}})}\frac{(\sigma_i(\tau_{i\mathtt{j}})-\mathtt{t})^{ß_i-1}}{\Gamma(ß_i)}\\
&\qquad \times\big[\sum_{\mathtt{j}=1}^{n}|\mathtt{z}_\mathtt{j}(\mathtt{t})|+|\mathtt{g}_i(\mathtt{t},0,0,\cdots,0)|\big]\mathtt{dt}\Bigg]\\
&\le \sum_{i=1}^{n}\Bigg[\int_0^1|\mathtt{G}_i(\mathtt{s},\mathtt{t})|(n\wp_3+\wp_1)\mathtt{dt}+\sum_{\mathtt{j}=1}^{\infty}\delta_{i\mathtt{j}}\int_0^{\sigma_i(\tau_{i\mathtt{j}})}\frac{(\sigma_i(\tau_{i\mathtt{j}})-\mathtt{t})^{ß_i-1}}{\Gamma(ß_i)}(n\wp_3+\wp_1)\mathtt{dt}\Bigg]\\
&\le (n\wp_3+\wp_1)\sum_{i=1}^{n}\Bigg[\mathtt{G}_i^{\star}+\frac{1}{\Gamma(ß_i+1)}\sum_{\mathtt{j}=1}^{\infty}\delta_{i\mathtt{j}}(\sigma_i(\tau_{i\mathtt{j}}))^{ß_i-1}\Bigg]\\
&= (n\wp_3+\wp_1)\sum_{i=1}^{n}\Bigg[\mathtt{G}_i^{\star}+\frac{2\Gamma(ß_i)}{\Gamma(ß_i+1)\Gamma(ß_i-\alpha_i)}\Bigg] = (n\wp_3+\wp_1)\wp_2\le\wp_3.
\end{aligned}
$$

That is, $\aleph(\mathtt{z}_1,\mathtt{z}_2,\cdots,\mathtt{z}_n)\in\mathtt{A}$. Therefore, $\aleph(\mathtt{A}^n)\subseteq\mathtt{A}$. Next, let $(\mathtt{z}_1,\mathtt{z}_2,\cdots,\mathtt{z}_n),(\mathtt{y}_1,\mathtt{y}_2,\cdots,\mathtt{y}_n)\in\mathtt{Y}^n$. Then

$$
\begin{aligned}
\mathtt{d}\big(\aleph(\mathtt{z}_1,\mathtt{z}_2,\cdots,\mathtt{z}_n),\aleph(\mathtt{y}_1,\mathtt{y}_2,\cdots,\mathtt{y}_n)\big) &= \sup_{\mathtt{s}\in[0,1]}|\aleph(\mathtt{z}_1,\mathtt{z}_2,\cdots,\mathtt{z}_n)-\aleph(\mathtt{y}_1,\mathtt{y}_2,\cdots,\mathtt{y}_n)|\\
&\le \sup_{\mathtt{s}\in[0,1]}\sum_{i=1}^{n}|\aleph_i(\mathtt{z}_i(\mathtt{s})-\mathtt{y}_i(\mathtt{s}))|\\
&\le \sup_{\mathtt{s}\in[0,1]}\sum_{i=1}^{n}\Bigg[\int_0^1|\mathtt{G}_i(\mathtt{s},\mathtt{t})|\big[|\mathtt{g}_i(\mathtt{t},\mathtt{z}_i(\mathtt{t}),\mathtt{z}_2(\mathtt{t}),\cdots,\mathtt{z}_1(\mathtt{t}),\cdots,\mathtt{z}_n(\mathtt{t}))\\
&\qquad - \mathtt{g}_i(\mathtt{t},\mathtt{y}_i(\mathtt{t}),\mathtt{y}_2(\mathtt{t}),\cdots,\mathtt{y}_1(\mathtt{t}),\cdots,\mathtt{y}_n(\mathtt{t}))\big]\mathtt{dt}\\
&\quad + |\mathtt{s}|^{ß_i-1}\sum_{\mathtt{j}=1}^{\infty}\delta_{i\mathtt{j}}\int_0^{\sigma_i(\tau_{i\mathtt{j}})}\frac{(\sigma_i(\tau_{i\mathtt{j}})-\mathtt{t})^{ß_i-1}}{\Gamma(ß_i)}\big[|\mathtt{g}_i(\mathtt{t},\mathtt{z}_i(\mathtt{t}),\mathtt{z}_2(\mathtt{t}),\cdots,\mathtt{z}_1(\mathtt{t}),\cdots,\mathtt{z}_n(\mathtt{t}))\\
&\qquad - \mathtt{g}_i(\mathtt{t},\mathtt{y}_i(\mathtt{t}),\mathtt{y}_2(\mathtt{t}),\cdots,\mathtt{y}_1(\mathtt{t}),\cdots,\mathtt{y}_n(\mathtt{t}))\big]\mathtt{dt}\Bigg]
\end{aligned}
$$

$$
\begin{aligned}
&\leq \sum_{i=1}^{n}\Bigg[\int_0^1 |\mathtt{G}_i(\mathtt{s},\mathtt{t})|\sum_{\mathtt{k}=1}^{n}|\mathtt{z}_{\mathtt{k}}(\mathtt{t})-\mathtt{y}_{\mathtt{k}}(\mathtt{t})|\mathtt{dt}\\
&\qquad\qquad+\sum_{\mathtt{j}=1}^{\infty}\delta_{i\mathtt{j}}\int_0^{\sigma_i(\tau_{i\mathtt{j}})}\frac{(\sigma_i(\tau_{i\mathtt{j}})-\mathtt{t})^{ß_i-1}}{\Gamma(ß_i)}\sum_{\mathtt{k}=1}^{n}|\mathtt{z}_{\mathtt{k}}(\mathtt{t})-\mathtt{y}_{\mathtt{k}}(\mathtt{t})|\mathtt{dt}\Bigg]\\
&\leq \sum_{i=1}^{n}\Bigg[\int_0^1 |\mathtt{G}_i(\mathtt{s},\mathtt{t})|\, n\max_{1\leq i\leq n}|\mathtt{z}_i(\mathtt{s})-\mathtt{y}_i(\mathtt{s})|\mathtt{dt}\\
&\qquad\qquad+\sum_{\mathtt{j}=1}^{\infty}\delta_{i\mathtt{j}}\int_0^{\sigma_i(\tau_{i\mathtt{j}})}\frac{(\sigma_i(\tau_{i\mathtt{j}})-\mathtt{t})^{ß_i-1}}{\Gamma(ß_i)}\, n\max_{1\leq i\leq n}|\mathtt{z}_i(\mathtt{s})-\mathtt{y}_i(\mathtt{s})|\mathtt{dt}\Bigg]\\
&\leq n\sum_{i=1}^{n}\Bigg[\int_0^1 |\mathtt{G}_i(\mathtt{s},\mathtt{t})|\max_{1\leq i\leq n}\Big\{\sup_{\mathtt{s}\in[0,1]}|\mathtt{z}_i(\mathtt{s})-\mathtt{y}_i(\mathtt{s})|\Big\}\mathtt{dt}\\
&\qquad\qquad+n\sum_{\mathtt{j}=1}^{\infty}\delta_{i\mathtt{j}}\int_0^{\sigma_i(\tau_{i\mathtt{j}})}\frac{(\sigma_i(\tau_{i\mathtt{j}})-\mathtt{t})^{ß_i-1}}{\Gamma(ß_i)}\max_{1\leq i\leq n}\Big\{\sup_{\mathtt{s}\in[0,1]}|\mathtt{z}_i(\mathtt{s})-\mathtt{y}_i(\mathtt{s})|\Big\}\mathtt{dt}\Bigg]\\
&\leq n\sum_{i=1}^{n}\Bigg[\int_0^1 |\mathtt{G}_i(\mathtt{s},\mathtt{t})|\mathtt{dt}+\sum_{\mathtt{j}=1}^{\infty}\delta_{i\mathtt{j}}\int_0^{\sigma_i(\tau_{i\mathtt{j}})}\frac{(\sigma_i(\tau_{i\mathtt{j}})-\mathtt{t})^{ß_i-1}}{\Gamma(ß_i)}\mathtt{dt}\Bigg]\max_{1\leq i\leq n}\mathtt{d}(\mathtt{z}_i,\mathtt{y}_i)\\
&\leq n\sum_{i=1}^{n}\Bigg[\mathtt{G}_i^{\star}+\frac{2\Gamma(ß_i)}{\Gamma(ß_i+1)\Gamma(ß_i-\alpha_i)}\Bigg]\max_{1\leq i\leq n}\mathtt{d}(\mathtt{z}_i,\mathtt{y}_i)\\
&\leq n\wp_2\max_{1\leq i\leq n}\mathtt{d}(\mathtt{z}_i,\mathtt{y}_i).
\end{aligned}
$$

Define $\varphi:[0,+\infty)\to[0,+\infty)$ by $\varphi(\mathtt{s})=n\wp_2\mathtt{s}$ and $\theta:[0,+\infty)^{2n}\to[0,+\infty)$ by $\theta(\mathtt{t}_1,\mathtt{t}_2,\cdots,\mathtt{t}_n,\mathtt{s}_1,\mathtt{s}_2,\cdots,\mathtt{s}_n)=\inf\{\mathtt{t}_1,\mathtt{t}_2,\cdots,\mathtt{t}_n,\mathtt{s}_1,\mathtt{s}_2,\cdots,\mathtt{s}_n\}$. Then

$$
\begin{aligned}
\mathtt{d}\big(\aleph(\mathtt{z}_1,\mathtt{z}_2,\cdots,\mathtt{z}_n),\aleph(\mathtt{y}_1,\mathtt{y}_2,\cdots,\mathtt{y}_n)\big)&\leq\wp_2\max_{1\leq i\leq n}\mathtt{d}(\mathtt{z}_i,\mathtt{y}_i)\\
&\leq\varphi(\max_{1\leq i\leq n}\mathtt{d}(\mathtt{z}_i,\mathtt{y}_i))\\
&\leq\varphi(\max_{1\leq i\leq n}\mathtt{d}(\mathtt{z}_i,\mathtt{y}_i))+\theta(\ell_4),
\end{aligned}
$$

where

$$
\begin{aligned}
\ell_4=\Big(&\mathtt{d}\big(\mathtt{y}_1,\aleph(\mathtt{z}_1,\mathtt{z}_2,\mathtt{z}_3,\cdots,\mathtt{z}_{n-1},\mathtt{z}_n)\big),\mathtt{d}\big(\mathtt{y}_2,\aleph(\mathtt{z}_2,\mathtt{z}_1,\mathtt{z}_3,\cdots,\mathtt{z}_{n-1},\mathtt{z}_n)\big),\\
&\mathtt{d}\big(\mathtt{y}_3,\aleph(\mathtt{z}_3,\mathtt{z}_2,\mathtt{z}_1,\cdots,\mathtt{z}_{n-1},\mathtt{z}_n)\big),\cdots,\mathtt{d}\big(\mathtt{y}_n,\aleph(\mathtt{z}_n,\mathtt{z}_2,\mathtt{z}_3,\cdots,\mathtt{z}_{n-1},\mathtt{z}_1)\big),\\
&\mathtt{d}\big(\mathtt{z}_1,\aleph(\mathtt{z}_1,\mathtt{z}_2,\mathtt{z}_3,\cdots,\mathtt{z}_{n-1},\mathtt{z}_n)\big),\mathtt{d}\big(\mathtt{z}_2,\aleph(\mathtt{z}_2,\mathtt{z}_1,\mathtt{z}_3,\cdots,\mathtt{z}_{n-1},\mathtt{z}_n)\big),\\
&\mathtt{d}\big(\mathtt{z}_3,\aleph(\mathtt{z}_3,\mathtt{z}_2,\mathtt{z}_1,\cdots,\mathtt{z}_{n-1},\mathtt{z}_n)\big),\cdots,\mathtt{d}\big(\mathtt{z}_n,\aleph(\mathtt{z}_n,\mathtt{z}_2,\mathtt{z}_3,\cdots,\mathtt{z}_{n-1},\mathtt{z}_1)\big)\Big)
\end{aligned}
$$

□

5 Hyers-Ulam Stability Analysis

In this section, we derive necessary conditions for the stability analysis of Hyers-Ulam's type. For some positive $\varepsilon_i>0$, $i=1,2,\cdots,n$, consider the system of inequalities given by

$$
\begin{cases}
\Big|{}^{\mathtt{RL}}\mathtt{D}_{0+}^{ß_1}\mathtt{z}_1(\mathtt{s})-\mathtt{g}_1\big(\mathtt{s},\mathtt{z}_1(\mathtt{s}),\mathtt{z}_2(\mathtt{s}),\cdots,\mathtt{z}_{n-1}(\mathtt{s}),\mathtt{z}_n(\mathtt{s})\big)\Big|\leq\varepsilon_1,\\
\Big|{}^{\mathtt{RL}}\mathtt{D}_{0+}^{ß_2}\mathtt{z}_2(\mathtt{s})-\mathtt{g}_2\big(\mathtt{s},\mathtt{z}_2(\mathtt{s}),\mathtt{z}_1(\mathtt{s}),\cdots,\mathtt{z}_{n-1}(\mathtt{s}),\mathtt{z}_n(\mathtt{s})\big)\Big|\leq\varepsilon_2,\\
\qquad\qquad\vdots\\
\Big|{}^{\mathtt{RL}}\mathtt{D}_{0+}^{ß_{n-1}}\mathtt{z}_{n-1}(\mathtt{s})-\mathtt{g}_{n-1}\big(\mathtt{s},\mathtt{z}_{n-1}(\mathtt{s}),\mathtt{z}_2(\mathtt{s}),\cdots,\mathtt{z}_1(\mathtt{s}),\mathtt{z}_n(\mathtt{s})\big)\Big|\leq\varepsilon_{n-1},\\
\Big|{}^{\mathtt{RL}}\mathtt{D}_{0+}^{ß_n}\mathtt{z}_n(\mathtt{s})-\mathtt{g}_n\big(\mathtt{s},\mathtt{z}_n(\mathtt{s}),\mathtt{z}_2(\mathtt{s}),\cdots,\mathtt{z}_{n-1}(\mathtt{s}),\mathtt{z}_1(\mathtt{s})\big)\Big|\leq\varepsilon_n,
\end{cases}
\tag{5.1}
$$

for $\mathtt{s} \in [0,1] := \mathtt{I}$. Then the system of boundary value problems (1.1)-(1.2) is Hyers–Ulam stable if there exist constants $\mathtt{L}_i > 0$, $i = 1, 2, \cdots, n$ such that for each solution $(\mathtt{z}_1, \mathtt{z}_2, \cdots, \mathtt{z}_n) \in \mathrm{C}^n(\mathtt{I}, \mathbb{R})$ of the system of inequalities (5.1), there exists a unique solution $(\mathtt{y}_1, \mathtt{y}_2, \cdots, \mathtt{y}_n) \in \mathrm{C}^n(\mathtt{I}, \mathbb{R})$ with

$$|(\mathtt{z}_1, \mathtt{z}_2, \cdots, \mathtt{z}_n)(\mathtt{s}) - (\mathtt{y}_1, \mathtt{y}_2, \cdots, \mathtt{y}_n)(\mathtt{s})| \leq \left(\sum_{i=1}^{n} \mathtt{L}_i + \mathtt{M}\wp_2 \right) \varepsilon. \tag{5.2}$$

Remark 5.1. We say that $(\mathtt{z}_1, \mathtt{z}_2, \cdots, \mathtt{z}_n) \in \mathrm{C}^n(\mathtt{I}, \mathbb{R})$ is a solution of the system of inequalities (5.1) if there exist functions $\psi_i \in \mathrm{C}^n(\mathtt{I}, \mathbb{R})$ which depend upon $\mathtt{z}_i$ respectively such that

(*i*) $|\psi_i| \leq \varepsilon_i$, $\mathtt{s} \in \mathtt{I}$, and

(*ii*) for $\mathtt{s} \in \mathtt{I}$,

$$\begin{cases} {}^{\mathtt{RL}}\mathtt{D}_{0^+}^{ß_1} \mathtt{z}_1(\mathtt{s}) = \mathtt{g}_1\big(\mathtt{s}, \mathtt{z}_1(\mathtt{s}), \mathtt{z}_2(\mathtt{s}), \cdots, \mathtt{z}_{n-1}(\mathtt{s}), \mathtt{z}_n(\mathtt{s})\big) + \psi_1(\mathtt{s}), \\ {}^{\mathtt{RL}}\mathtt{D}_{0^+}^{ß_2} \mathtt{z}_2(\mathtt{s}) = \mathtt{g}_2\big(\mathtt{s}, \mathtt{z}_2(\mathtt{s}), \mathtt{z}_1(\mathtt{s}), \cdots, \mathtt{z}_{n-1}(\mathtt{s}), \mathtt{z}_n(\mathtt{s})\big) + \psi_2(\mathtt{s}), \\ \qquad\qquad \vdots \\ {}^{\mathtt{RL}}\mathtt{D}_{0^+}^{ß_{n-1}} \mathtt{z}_{n-1}(\mathtt{s}) = \mathtt{g}_{n-1}\big(\mathtt{s}, \mathtt{z}_{n-1}(\mathtt{s}), \mathtt{z}_2(\mathtt{s}), \cdots, \mathtt{z}_1(\mathtt{s}), \mathtt{z}_n(\mathtt{s})\big) + \psi_{n-1}(\mathtt{s}), \\ {}^{\mathtt{RL}}\mathtt{D}_{0^+}^{ß_n} \mathtt{z}_n(\mathtt{s}) = \mathtt{g}_n\big(\mathtt{s}, \mathtt{z}_n(\mathtt{s}), \mathtt{z}_2(\mathtt{s}), \cdots, \mathtt{z}_{n-1}(\mathtt{s}), \mathtt{z}_1(\mathtt{s})\big) + \psi_n(\mathtt{s}), \end{cases} \tag{5.3}$$

Lemma 5.2. Let $(\mathtt{z}_1, \mathtt{z}_2, \cdots, \mathtt{z}_n) \in \mathrm{C}^n(\mathtt{I}, \mathbb{R})$ be the solution of the system of inequalities (5.1). Then the following inequalities hold:

$$\begin{cases} \Big| \mathtt{z}_1(\mathtt{s}) - \displaystyle\int_0^1 \mathtt{G}_1(\mathtt{s}, \mathtt{t}) \mathtt{g}_1(\mathtt{t}, \mathtt{z}_1(\mathtt{t}), \mathtt{z}_2(\mathtt{t}), \cdots, \mathtt{z}_n(\mathtt{t})) \mathrm{d}\mathtt{t} \\ + \mathtt{s}^{ß_1 - 1} \displaystyle\sum_{\mathtt{j}=1}^{\infty} \delta_{1\mathtt{j}} \int_0^{\sigma_1(\tau_{1\mathtt{j}})} \frac{(\sigma_1(\tau_{1\mathtt{j}}) - \mathtt{t})^{ß_1 - 1}}{\Gamma(ß_1)} \mathtt{g}_1(\mathtt{t}, \mathtt{z}_1(\mathtt{t}), \mathtt{z}_2(\mathtt{t}), \cdots, \mathtt{z}_n(\mathtt{t})) \mathrm{d}\mathtt{t} \Big| \leq \mathtt{L}_1 \varepsilon_1, \\ \Big| \mathtt{z}_2(\mathtt{s}) - \displaystyle\int_0^1 \mathtt{G}_2(\mathtt{s}, \mathtt{t}) \mathtt{g}_2(\mathtt{t}, \mathtt{z}_2(\mathtt{t}), \mathtt{z}_1(\mathtt{t}), \cdots, \mathtt{z}_n(\mathtt{t})) \mathrm{d}\mathtt{t} \\ + \mathtt{s}^{ß_2 - 1} \displaystyle\sum_{\mathtt{j}=1}^{\infty} \delta_{2\mathtt{j}} \int_0^{\sigma_2(\tau_{2\mathtt{j}})} \frac{(\sigma_2(\tau_{2\mathtt{j}}) - \mathtt{t})^{ß_2 - 1}}{\Gamma(ß_2)} \mathtt{g}_2(\mathtt{t}, \mathtt{z}_2(\mathtt{t}), \mathtt{z}_1(\mathtt{t}), \cdots, \mathtt{z}_n(\mathtt{t})) \mathrm{d}\mathtt{t} \Big| \leq \mathtt{L}_2 \varepsilon_2, \\ \qquad\qquad \vdots \\ \Big| \mathtt{z}_n(\mathtt{s}) - \displaystyle\int_0^1 \mathtt{G}_n(\mathtt{s}, \mathtt{t}) \mathtt{g}_n(\mathtt{t}, \mathtt{z}_n(\mathtt{t}), \mathtt{z}_2(\mathtt{t}), \cdots, \mathtt{z}_1(\mathtt{t})) \mathrm{d}\mathtt{t} \\ + \mathtt{s}^{ß_n - 1} \displaystyle\sum_{\mathtt{j}=1}^{\infty} \delta_{n\mathtt{j}} \int_0^{\sigma_n(\tau_{n\mathtt{j}})} \frac{(\sigma_n(\tau_{n\mathtt{j}}) - \mathtt{t})^{ß_n - 1}}{\Gamma(ß_n)} \mathtt{g}_n(\mathtt{t}, \mathtt{z}_n(\mathtt{t}), \mathtt{z}_2(\mathtt{t}), \cdots, \mathtt{z}_1(\mathtt{t})) \mathrm{d}\mathtt{t} \Big| \leq \mathtt{L}_n \varepsilon_n. \end{cases}$$

Proof . From the Remark 5.1 and Lemma 2.7, the solution of (5.3) and (1.2) is given by

$$\begin{cases} z_1(s) = \int_0^1 G_1(s,t)[g_1(t,z_1(t),z_2(t),\cdots,z_n(t)) + \psi_1(t)]dt \\ - s^{\beta_1-1}\sum_{j=1}^{\infty}\delta_{1j}\int_0^{\sigma_1(\tau_{1j})}\frac{(\sigma_1(\tau_{1j})-t)^{\beta_1-1}}{\Gamma(\beta_1)}[g_1(t,z_1(t),z_2(t),\cdots,z_n(t)) + \psi_1(t)]dt \\ z_2(s) = \int_0^1 G_2(s,t)[g_2(t,z_2(t),z_1(t),\cdots,z_n(t)) + \psi_2(t)]dt \\ - s^{\beta_2-1}\sum_{j=1}^{\infty}\delta_{2j}\int_0^{\sigma_2(\tau_{2j})}\frac{(\sigma_2(\tau_{2j})-t)^{\beta_2-1}}{\Gamma(\beta_2)}[g_2(t,z_2(t),z_2(t),\cdots,z_n(t)) + \psi_2(t)]dt \\ \qquad\qquad\qquad\qquad \vdots \\ z_n(s) = \int_0^1 G_n(s,t)[g_n(t,z_n(t),z_2(t),\cdots,z_1(t)) + \psi_n(t)]dt \\ - s^{\beta_n-1}\sum_{j=1}^{\infty}\delta_{nj}\int_0^{\sigma_n(\tau_{nj})}\frac{(\sigma_n(\tau_{nj})-t)^{\beta_n-1}}{\Gamma(\beta_n)}[g_n(t,z_n(t),z_2(t),\cdots,z_1(t)) + \psi_n(t)]dt \end{cases} \tag{5.4}$$

From first equation of the system (5.4), we have

$$\begin{aligned} &\Big|z_1(s) - \int_0^1 G_1(s,t)g_1(t,z_1(t),z_2(t),\cdots,z_n(t))dt \\ &\quad + s^{\beta_1-1}\sum_{j=1}^{\infty}\delta_{1j}\int_0^{\sigma_1(\tau_{1j})}\frac{(\sigma_1(\tau_{1j})-t)^{\beta_1-1}}{\Gamma(\beta_1)}g_1(t,z_1(t),z_2(t),\cdots,z_n(t))dt\Big| \\ &\quad \le \int_0^1 |G_1(s,t)||\psi_1(t)|dt + |s|^{\beta_1-1}\sum_{j=1}^{\infty}\delta_{1j}\int_0^{\sigma_1(\tau_{1j})}\frac{(\sigma_1(\tau_{1j})-t)^{\beta_1-1}}{\Gamma(\beta_1)}|\psi_1(t)|dt \\ &\quad \le \left[G_1^{\star} + \frac{2\Gamma(\beta_1)}{\Gamma(\beta_1+1)\Gamma(\beta_1-\alpha_1)}\right]\varepsilon_1 := L_1\varepsilon_1. \end{aligned}$$

Similarly we can prove other inequalities. □

Theorem 5.3. Suppose (4.1) holds. Then the system of boundary value problems (1.1)–(1.2) is Hyers-Ulam stabile, if

$$\sum_{i=1}^{n} L_i + M\wp_2 < 1,$$

where $\wp_2$ is defined in Theorem 4.1.

Proof . Let $(z_1, z_1, \cdots, z_n) \in C^n(I,\mathbb{R})$ be the solution to the system of inequalities (5.1) and let $(y_1, y_1, \cdots, y_n) \in$

$C^n(I,\mathbb{R})$ be the unique solution to the system of boundary value problems (1.1)–(1.2). Then by Lemma 5.2, we have

$$\begin{aligned}
|z_1(s)-y_1(s)| &\le \Big| z_1(s)-\int_0^1 G_1(s,t)g_1(t,y_1(t),y_2(t),\cdots,y_n(t))dt \\
&\quad + s^{ß_1-1}\sum_{j=1}^{\infty}\delta_{1j}\int_0^{\sigma_1(\tau_{1j})}\frac{(\sigma_1(\tau_{1j})-t)^{ß_1-1}}{\Gamma(ß_1)}g_1(t,y_1(t),y_2(t),\cdots,y_n(t))dt\Big| \\
&\le \Big| z_1(s)-\int_0^1 G_1(s,t)g_1(t,z_1(t),z_2(t),\cdots,z_n(t))dt \\
&\quad + s^{ß_1-1}\sum_{j=1}^{\infty}\delta_{1j}\int_0^{\sigma_1(\tau_{1j})}\frac{(\sigma_1(\tau_{1j})-t)^{ß_1-1}}{\Gamma(ß_1)}g_1(t,z_1(t),z_2(t),\cdots,z_n(t))dt\Big| \\
&\quad + \int_0^1 |G_1(s,t)||g_1(t,z_1(t),z_2(t),\cdots,z_n(t))-g_1(t,y_1(t),y_2(t),\cdots,y_n(t))|dt \\
&\quad + |s|^{ß_1-1}\sum_{j=1}^{\infty}\delta_{1j}\int_0^{\sigma_1(\tau_{1j})}\frac{(\sigma_1(\tau_{1j})-t)^{ß_1-1}}{\Gamma(ß_1)} \\
&\qquad \times |g_1(t,z_1(t),z_2(t),\cdots,z_n(t))-g_1(t,y_1(t),y_2(t),\cdots,y_n(t))|dt \\
&\le L_1\varepsilon_1 + M\int_0^1 |G_1(s,t)\sum_{j=1}^{n}|z_j(t)-y_j(t)|dt \\
&\quad + M\sum_{j=1}^{\infty}\delta_{1j}\int_0^{\sigma_1(\tau_{1j})}\frac{(\sigma_1(\tau_{1j})-t)^{ß_1-1}}{\Gamma(ß_1)}\sum_{j=1}^{n}|z_j(t)-y_j(t)|dt \\
&\le L_1\varepsilon_1 + M\int_0^1 |G_1(s,t)|dt\sum_{j=1}^{n}\|z_j-y_j\| \\
&\quad + M\sum_{j=1}^{\infty}\delta_{1j}\int_0^{\sigma_1(\tau_{1j})}\frac{(\sigma_1(\tau_{1j})-t)^{ß_1-1}}{\Gamma(ß_1)}dt\sum_{j=1}^{n}\|z_j-y_j\|.
\end{aligned}$$

Taking supremum on both sides over s, we obtain

$$\|z_1-y_1\| \le L_1\varepsilon_1 + M\left[G_i^{\star}+\frac{2\Gamma(ß_1)}{\Gamma(ß_1+1)\Gamma(ß_1-\alpha_1)}\right]\sum_{j=1}^{n}\|z_j-y_j\|.$$

Similarly, we can have

$$\|z_i-y_i\| \le L_i\varepsilon_i + M\left[G_i^{\star}+\frac{2\Gamma(ß_i)}{\Gamma(ß_i+1)\Gamma(ß_i-\alpha_i)}\right]\sum_{j=1}^{n}\|z_j-y_j\|,\ i=2,3,\cdots,n.$$

Adding all the above inequalities from $i=1$ to n, we obtain

$$\begin{aligned}
\sum_{i=1}^{n}\|z_i-y_i\| &\le \sum_{i=1}^{n}L_i\varepsilon_i + M\sum_{i=1}^{n}\left[G_i^{\star}+\frac{2\Gamma(ß_i)}{\Gamma(ß_i+1)\Gamma(ß_i-\alpha_i)}\right]\sum_{j=1}^{n}\|z_j-y_j\| \\
&\le \sum_{i=1}^{n}L_i\varepsilon_i + M\wp_2\sum_{j=1}^{n}\|z_j-y_j\|.
\end{aligned}$$

That is

$$\sum_{i=1}^{n}\|z_i-y_i\| \le \frac{1}{1-M\wp_2}\sum_{i=1}^{n}L_i\varepsilon_i.$$

Let $\varepsilon=\max\{\varepsilon_i : i=1,2,\cdots,n\}$. Then, we have

$$\begin{aligned}
\|(z_1,z_2,\cdots,z_n)-(y_1,y_2,\cdots,y_n)\| &\le \sum_{j=1}^{n}\|z_j-y_j\| \\
&\le \frac{\sum_{i=1}^{n}L_i}{1-M\wp_2}\varepsilon.
\end{aligned}$$

□

Example 5.4.

$$\begin{cases} {}^{\mathrm{RL}}\mathtt{D}_{0+}^{3/2}\mathtt{z}_1(\mathtt{s}) = 1+\mathtt{s}+\dfrac{1}{3}\sin\big(\mathtt{z}_1(\mathtt{s})-\mathtt{z}_2(\mathtt{s})\big), \\ {}^{\mathrm{RL}}\mathtt{D}_{0+}^{5/4}\mathtt{z}_2(\mathtt{s}) = 2\sin(\mathtt{s})+\dfrac{1}{3}\cos\big(\mathtt{z}_2(\mathtt{s})-\mathtt{z}_1(\mathtt{s})\big), \end{cases} \tag{5.5}$$

for $0 < \mathtt{s} < 1$, satisfying

$$\mathtt{z}_i(0) = 0 \quad \text{and} \quad {}^{\mathrm{RL}}\mathtt{D}_{0+}^{\alpha_i}\mathtt{z}_i(1) = \sum_{\mathtt{j}=1}^{\infty}\delta_{i\mathtt{j}}\,{}^{\mathrm{RL}}\mathtt{D}_{0+}^{\alpha_i}\mathtt{z}_i\big(\sigma_i(\tau_{i\mathtt{j}})\big),\ i=1,2. \tag{5.6}$$

So, we have $n=2$, $ß_1=\frac{3}{2}$, $ß_2=\frac{5}{4}$. Let $\alpha_1=\frac{1}{3}$, $\alpha_2=\frac{1}{5}$, $\delta_{1\mathtt{j}}=\frac{18\Gamma(5/6)}{\pi^{5/2}\mathtt{j}}$, $\delta_{2\mathtt{j}}=\frac{60\sqrt{2}\Gamma(19/20)\sin(\pi/20)}{\pi^2\Gamma(3/4)\mathtt{j}}$, $\tau_{1\mathtt{j}}=\frac{1}{\mathtt{j}^3}$, $\tau_{2\mathtt{j}}=\frac{1}{\mathtt{j}}$, $\sigma_1(\mathtt{s})=\mathtt{s}^{2/3}$ and $\sigma_2(\mathtt{s})=\mathtt{s}^4$. Then

$$\sum_{\mathtt{j}=1}^{m}\delta_{1\mathtt{j}}\big(\sigma_1(\tau_{1\mathtt{j}})\big)^{ß_1-1} = \sum_{\mathtt{j}=1}^{m}\frac{18\Gamma(5/6)}{\pi^{5/2}\mathtt{j}^2} \to \frac{3\Gamma(5/6)}{\sqrt{\pi}} = \frac{2\Gamma(ß_1)}{\Gamma(ß_1-\alpha_1)} \quad \text{as} \quad m\to+\infty$$

and

$$\begin{aligned}\sum_{\mathtt{j}=1}^{m}\delta_{2\mathtt{j}}\big(\sigma_2(\tau_{2\mathtt{j}})\big)^{ß_2-1} &= \sum_{\mathtt{j}=1}^{m}\frac{60\sqrt{2}\Gamma(19/20)\sin(\pi/20)}{\pi^2\Gamma(3/4)\mathtt{j}^2} \\ &\to \frac{10\sqrt{2}\Gamma(19/20)\sin(\pi/20)}{\Gamma(3/4)} = \frac{2\Gamma(ß_2)}{\Gamma(ß_2-\alpha_2)} \quad \text{as} \quad m\to+\infty.\end{aligned}$$

Let $\mathtt{z}_i, \mathtt{y}_i \in \mathtt{Y}$. Then

$$\begin{aligned}|\mathtt{g}_1(\mathtt{s},\mathtt{z}_1,\mathtt{z}_2)-\mathtt{g}_1(\mathtt{s},\mathtt{y}_1,\mathtt{y}_2)| &\le \frac{1}{3}|\sin\big(\mathtt{z}_1(\mathtt{s})-\mathtt{z}_2(\mathtt{s})\big)-\sin\big(\mathtt{y}_1(\mathtt{s})-\mathtt{y}_2(\mathtt{s})\big)| \\ &\le \frac{1}{3}|\big(\mathtt{z}_1(\mathtt{s})-\mathtt{z}_2(\mathtt{s})\big)-\big(\mathtt{y}_1(\mathtt{s})-\mathtt{y}_2(\mathtt{s})\big)| \\ &\le \frac{1}{3}\sum_{i=1}^{2}|\mathtt{z}_i-\mathtt{y}_i|,\end{aligned}$$

$$\begin{aligned}|\mathtt{g}_2(\mathtt{s},\mathtt{z}_1,\mathtt{z}_2)-\mathtt{g}_2(\mathtt{s},\mathtt{y}_1,\mathtt{y}_2)| &\le \frac{1}{3}|\cos\big(\mathtt{z}_1(\mathtt{s})-\mathtt{z}_2(\mathtt{s})\big)-\cos\big(\mathtt{y}_1(\mathtt{s})-\mathtt{y}_2(\mathtt{s})\big)| \\ &\le \frac{1}{3}|\big(\mathtt{z}_1(\mathtt{s})-\mathtt{z}_2(\mathtt{s})\big)-\big(\mathtt{y}_1(\mathtt{s})-\mathtt{y}_2(\mathtt{s})\big)| \\ &\le \frac{1}{3}\sum_{i=1}^{2}|\mathtt{z}_i-\mathtt{y}_i|,\end{aligned}$$

$|\mathtt{g}_2(\mathtt{s},\mathtt{z}_1,\mathtt{z}_2)| = |1+\mathtt{s}| \le 2$, $|\mathtt{g}_2(\mathtt{s},\mathtt{z}_1,\mathtt{z}_2)| = |2\sin(\mathtt{s})| \le 2$. So, $\mathtt{M}=\frac{1}{3}$, $\wp_1=2$ and

$$\sum_{i=1}^{2}\mathtt{L}_i = \sum_{i=1}^{2}\left[\mathtt{G}_i^{\star}+\frac{2\Gamma(ß_i)}{\Gamma(ß_i+1)\Gamma(ß_i-\alpha_i)}\right] \approx 0.5571212542 = \wp_2.$$

$$\sum_{i=1}^{n}\mathtt{L}_i + \mathtt{M}\wp_2 \approx 0..7428283389 < 1,$$

Therefore, all the conditions of of Theorem 4.1 are satisfied, so there exists a solution for the system (5.5)–(5.6). Also, in view of Theorem 5.3, the condition of Hyers–Ulam stabilities are also satisfied. Therefore, the solution of system (5.5)–(5.6) is Hyers–Ulam stable.

6 Conclusion

The proximity theory is useful tool to find proximity point when the given mapping is non-self. We established the existence of solutions to the system of nonlinear infinite-point fractional order boundary value problems by an application of n-best proximity point theorem in a complete metric space. By applying our results we can study different kind differential equations whereas results in [28, 30, 33] can only applicable for certain type of differential equations. Therefore, our findings are extended and more general. In the future, the following aspects can be explored further: (1) we study best proximity points of cyclic mappings. (2) we try to apply our obtained results for fractional difference equations, dynamical equations on time scales, fractional differential equations on time scales, etc.

Acknowledgements

The authors would like to thank the referees for their valuable suggestions and comments for the improvement of the paper.

References

[1] T. Abdeljawad, J. Alzabut, A. Mukheimer and Y. Zaidan, *Banach contraction principle for cyclical mappings on partial metric spaces*, Fixed Point Theory Appl. **2012** (2012), no. 1, 1–7.

[2] T. Abdeljawad, J. Alzabut, A. Mukheimer and Y. Zaidan, *Best proximity points for cyclical contraction mappings with θ-boundedly compact decompositions*, J. Comput. Anal. Appl. **15** (2013), no. 4, 678–85.

[3] M. Abu-Shady and M.K.A. Kaabar, *A generalized definition of the fractional derivative with applications*, Math. Prob. Engin. **2021** (2021).

[4] S. J. Achar, C. Baishya and M.K.A. Kaabar, *Dynamics of the worm transmission in wireless sensor network in the framework of fractional derivatives*, Math. Meth. Appl. Sci. **45** (2022), no. 8, 4278–4294.

[5] H. Afshari, F. Jarad and T. Abdeljawad, *On a new fixed point theorem with an application on a coupled system of fractional differential equations*, Adv. Differ. Equ., **461** (2020).

[6] J. Alzabut, R.P. Agarwal, S.R. Grace, J.M. Jonnalagadda, A.G. Selvam and C. Wang, *A survey on the oscillation of solutions for fractional difference equations*, Math. **10** (2022), no. 6.

[7] J. Alzabut, A. G. Selvam, D. Vignesh and Y. Gholami, *Solvability and stability of nonlinear hybrid Δ-difference equations of fractional order*, Int. J. Nonlinear Sci. Num. Simul. **2021** (2021).

[8] M. Aslantas H. Sahin and I. Altun, *Best proximity point theorems for cyclic p-contractions with some consequences and applications*, Nonlinear Anal. Model. Control **26** (2021), no. 1, 113–129.

[9] M.I. Ayari, *A best proximity point theorem for α-proximal Geraghty non-self mappings*, *Fixed Point Theory Appl.* **2019**(2019).

[10] Z. Bai and H. Lu, *Positive solutions for a boundary value problem of nonlinear fractional differential equations*, J. Math. Anal. Appl. **311** (2005), 495–505.

[11] V. Berinde, *Approximating fixed points of weak φ-contractions using the Picard iteration*, *Fixed Point Theory Appl.* **4**(2) (2003), 131–142.

[12] K. Fan, *Extensions of two fixed point theorems of F.E. Browder*, Math. Z. **112** (1969), 234–240.

[13] M.Q. Feng, X.M. Zhang and W.G. Ge, *New existence results for higher-order nonlinear fractional differential equation with integral boundary conditions*, Bound. Value Prob. **2011** (2011), Art. ID 720702, 1–20.

[14] N. Goswami, R. Roy, V.N. Mishra and L.M.S. Ruiz, *Common best proximity point results for T-GKT cyclic φ-contraction mappings in partial metric spaces with some applications*, Symmetry, **13** (2021), no. 6, 1098.

[15] M. Hristov, A. Ilchev and B. Zlatanov, *On the best proximity points for p-cyclic summing contractions*, Math. **8** (2020), no. 7, 1060.

[16] S. Jabeen, Z. Zheng, M. U. Rehman, W. Wei and J. Alzabut, *Some fixed point results of weak-fuzzy graphical contraction mappings with application to integral equations*, Math. **9** (2021), no. 5.

[17] M.K.A. Kaabar, A. Refice, M.S. Souid, F. Martínez, S. Etemad, Z. Siri and S. Rezapour, *Existence and UHR stability of solutions to the implicit nonlinear FBVP in the variable order settings*, Math. **9** (2021), no. 14, 1693.

[18] M. K. A. Kaabar, M. Shabibi, J. Alzabut, S. Etemad, W. Sudsutad, F. Martinez, S. Rezapour, *Investigation of the fractional strongly singular thermostat model via fixed point techniques*, Math. 9 (2021), no. 18, 2298.

[19] A. Khemphet, *Best proximity coincidence point theorem for G-proximal generalized geraghty mapping in a metric space with graph G*, Thai J. Math. **18** (2020), no. 3, 1161–1171.

[20] M. Khuddush and K. R. Prasad, *Infinitely many positive solutions for an iterative system of conformable fractional order dynamic boundary value problems on time scales*, Turk. J. Math. **46** (2022), no. 2, 338–359.

[21] A.A. Kilbas, H.M. Srivastava and J.J. Trujillo, *Theory and applications of fractional differential equations*, North-Holland Mathematics Studies, 204, Elsevier, North Holland, 2006.

[22] S. Komal, P. Kumam, K. Khammahawong and K. Sitthithakerngkiet, *Best proximity coincidence point theorems for generalized non-linear contraction mappings*, Filomat **32** (2018), no. 19, 6753–6768.

[23] M. M. Matar, M. I. Abbas, J. Alzabut, M. K. Kaabar, S. Etemad, S. Rezapour, *Investigation of the p-Laplacian nonperiodic nonlinear boundary value problem via generalized Caputo fractional derivatives*, Adv. Differ. Equ. **2021** (2021), no. 1, 1–8.

[24] K. S. Miller, B. Ross, *An introduction to the fractional calculus and fractional differential equation*, John Wiley, New York, (1993).

[25] H. Mohammadi, M.K.A. Kaabar, J. Alzabut, A.G.M. Selvam and S. Rezapour, *Complete model of Crimean-Congo hemorrhagic fever (CCHF) transmission cycle with nonlocal fractional derivative*, J. Funct. Spaces **2021** (2021), 1–12.

[26] I. Podlubny, *Fractional differential equations*, Academic Press, San Diego, 1999.

[27] K. R. Prasad, M. Khuddush, D. Leela, *Existence of solutions for n-dimensional fractional order hybrid BVPs with integral boundary conditions by an application of n-fixed point theorem*, J. Anal. **29** (2021), no. 3, 963–985.

[28] K. R. Prasad, M. Khuddush and D. Leela, *Existence, uniqueness and Hyers–Ulam stability of a fractional order iterative two-point boundary value problems*, Afr. Mat. **32** (2021)no. 7, 1227–1237.

[29] K. R. Prasad, D. Leela and M. Khuddush, *Existence and uniqueness of positive solutions for system of (p, q, r)-Laplacian fractional order boundary value problems*, Adv. Theory Nonlinear Anal. Appl. **5** (2021), 138–157.

[30] K. R. Prasad, M. Khuddush, D. Leela, *Existence of solutions for fractional order BVPs by mixed monotone ternary operator with perturbation on Banach spaces*, J. Adv. Math. Stud. **14** (2021), no. 1, 109–125.

[31] J.B. Prolla, *Fixed point theorems for set valued mappings and existence of best approximations*, Numer. Funct. Anal. Optim. **5** (1982-1983), 449–455.

[32] S. Reich, *Approximate selections, best approximations, fixed points and invariant sets*, J. Math. Anal. Appl. **62** (1978), 104–113.

[33] V.S. Raj, *A best proximity point theorem for weakly contractive non-self mappings*, Nonlinear Anal. **74** (2011), no. 14, 4804–4808.

[34] S. Rezapour, A. Imran, A. Hussain, F. Martínez, S. Etemad and M.K.A. Kaabar, *Condensing functions and approximate endpoint criterion for the existence analysis of quantum integro-difference FBVPs*, Symmetry **13** (2021), no. 3, 469.

[35] Y. Rohen and N. Mlaiki, *Tripled best proximity point in complete metric spaces*, Open Math., **18** (2020), 204–210.

[36] H. Sahin, *Best proximity point theory on vector metric spaces*, Commun. Fac. Sci. Univ. Ank. Ser. A1 Math. Stat. **70** (2021), no. 1, 130–142.

[37] B. Samet, *Some results on best proximity points*, J. Optim. Theory Appl. **159** (2013), no. 1, 281–291.

[38] W. Shatanawi and A. Pitea, *Best proximity point and best proximity coupled point in a complete metric space with (P)-property*, Filomat **29** (2015), no. 1, 63–74.

[39] H.M. Srivastava, *Diabetes and its resulting complications: Mathematical modeling via fractional calculus*, Public

Health Open Access **4** (2020), no. 3, 1–5.

[40] H.M. Srivastava, K.M. Saad and M.M. Khader, *An efficient spectral collocation method for the dynamic simulation of the fractional epidemiological model of the Ebola virus*, Chaos, Solitons and Fractals **140** (2020), 1–7.

[41] S. Muthaiah, J. Alzabut, D. Baleanu, M.E. Samei and A. Zada, *Existence, uniqueness and stability analysis of a coupled fractional-order differential systems involving Hadamard derivatives and associated with multi-point boundary conditions*, Adv. Diff. Equ. **2021** (2021), no. 1, 1–46.

Afrika Matematika (2022) 33:91
https://doi.org/10.1007/s13370-022-01026-4

Infinitely many positive solutions for an iterative system of fractional BVPs with multistrip Riemann–Stieltjes integral boundary conditions

Mahammad Khuddush[1] · **K. Rajendra Prasad**[2] · **P. Veeraiah**[2]

Received: 11 August 2021 / Accepted: 13 August 2022 / Published online: 7 September 2022
© African Mathematical Union and Springer-Verlag GmbH Deutschland, ein Teil von Springer Nature 2022

Abstract
In this paper, the existence of infinitely many positive solutions for an iterative system of singular fractional order boundary value problems having increasing homeomorphism and positive homomorphism operator (IHPHO) with Rieman–Stieltjes integral boundary conditions are discussed. The arguments are discussed via Hölder's inequality and Krasnoselskii's cone fixed point theorem in a Banach space. Finally, some examples are included to ensure the abstract results.

Keywords Iterative system · Boundary value problem · Riemann–Liouville fractional derivative · Fixed point theorem · Positive solutions · Multi-strip

Mathematics Subject Classification 26A33 · 34A08 · 34B16

1 Introduction

Fractional calculus is one of the useful fields of applied mathematics which has applications in the areas such as engineering, economics, control theory, chemistry, biology, medicine and other fields, see Refs. [14, 17, 18, 25, 26, 32]. Fractional differential equations can describe many phenomena in various fields of engineering and scientific disciplines In consequence, the subject of frac-tional differential equations is gaining much importance and attention. In recent years,there are a large number of papers dealing with the existence, uniqueness and multiple solutions of boundary value problems for nonlinear differential equations of fractional order. For examples and recent development of the topic, see Refs. [1, 2, 4, 10–13, 19–23, 27–31] and references therein.

✉ Mahammad Khuddush
khuddush89@gmail.com

[1] Department of Mathematics, Dr. Lankapalli Bullayya College of Engineering, Visakhapatnam, Andhra Pradesh 530013, India

[2] Department of Applied Mathematics, College of Science and Technology, Andhra University, Visakhapatnam 530003, India

The study of turbulent flow through porous media is important for a wide range of scientific and engineering applications such as fluidized bed combustion, compact heat exchangers, combustion in an inert porous matrix, high temperature gas-cooled reactors, chemical catalytic reactors [7] and drying of different products such as iron ore [16]. To study this type of problems, Leibenson [15] introduced the p-Laplacian equation,

$$\big(\phi_{\mathtt{p}}(\mathtt{z}'(\mathtt{t}))\big)' = \mathtt{g}\big(\mathtt{t}, \mathtt{z}(\mathtt{t}), \mathtt{z}'(\mathtt{t})\big),$$

where $\phi_{\mathtt{p}}(\mathtt{z}) = |\mathtt{z}|^{\mathtt{p}-2}\mathtt{z}$, $\mathtt{p} > 1$. The operator $\phi_{\mathtt{p}}$ is invertible and its inverse operator is defined by $\phi_{\mathtt{q}}$, where $\mathtt{q} > 1$ is a constant such that $\mathtt{q} = \mathtt{p}/(\mathtt{p}-1)$.

The fractional order p-Laplacian operator arises in many applied fields such as turbulant filtration in porous media, blood flow problems, rheology, modelling of viscoplasticity, material science, and it is worth developing the theory to fractional differential equations with p-Laplacian operator. In this paper we use a new operator called increasing homeomorphism and positive homomorphism operator, which improves and generalizes the p-Laplacian operator for some $\mathtt{p} > 1$, and ϕ is not necessarily odd. Moreover research on increasing homeomorphism and positive homomorphism operators has gained momentum recently. In Ref. [8], Ege and topal considered the fractional boundary value problem with IHPHO,

$$\begin{aligned} {}^{\mathtt{C}}\mathtt{D}^{q}\big(\phi({}^{\mathtt{C}}\mathtt{D}^{r}\mathtt{z}(\mathtt{t}))\big) + \mathtt{g}\big(\mathtt{t}, \mathtt{z}(\mathtt{t})\big) &= 0, 0 < \mathtt{t} < 1 \\ \alpha_1\mathtt{z}(0) - \beta_1\mathtt{z}'(0) &= -\gamma_1\mathtt{z}(\xi_1), \\ \alpha_2\mathtt{z}(1) + \beta_2\mathtt{z}'(1) &= -\gamma_2\mathtt{z}(\xi_2), \\ {}^{\mathtt{C}}\mathtt{D}^{r}\mathtt{z}(0) &= 0, \end{aligned}$$

where ${}^{\mathtt{C}}\mathtt{D}^{q}$ and ${}^{\mathtt{C}}\mathtt{D}^{r}$ are Caputo fractional derivatives of orders $0 < q \leq 1 < r \leq 2$ and established existence of positive solutions by utilizing Krasnoselskii's and Legget–Williams cone fixed point theorems on a Banach space.

In Ref. [24], Song and Cui studied the following fractional differential equation with the Riemann–Stieltjes integral boundary conditions,

$$\begin{aligned} {}^{\mathtt{C}}\mathtt{D}_{1^-}^{\alpha}\mathtt{D}_{0^+}^{\beta}\mathtt{z}(\mathtt{t}) &= \mathtt{g}(\mathtt{t}, \mathtt{z}(\mathtt{t}), \mathtt{D}_{0^+}^{\beta+1}\mathtt{z}(\mathtt{t}), \mathtt{D}_{0^+}^{\beta}\mathtt{z}(\mathtt{t})), 0 < \mathtt{t} < 1, \\ \mathtt{z}(0) = \mathtt{z}'(0) = 0, \quad \mathtt{z}(1) &= \int_0^1 \mathtt{z}(\mathtt{t})\mathrm{d}\mho(\mathtt{t}), \end{aligned}$$

where ${}^{\mathtt{C}}\mathtt{D}_{1^-}^{\alpha}$ is the left Caputo fractional derivative of order $1 < \alpha \leq 2$ and $\mathtt{D}_{0^+}^{\beta}$ is the right Riemann–Liouville fractional derivative of order $0 < \beta \leq 1$, $\int_0^1 \mathtt{z}(\mathtt{t})\mathrm{d}\mho(\mathtt{t})$ is the Riemann–Stieltjes integral of z with respect to $\mho$, $\mho : [0, 1] \to \mathbb{R}$ is a function of bounded variation and $\mathrm{d}\mho$ is a signed measure and established existence of solutions by the method of coincidence degree theory. Recently, Bashirahmad et al. [3] established existence and uniqueness results to the following Riemann–Stieltjes integro-multipoint boundary value problem of Caputo–Riemann–Liouville type integro-differential equations,

$$\begin{aligned} {}^{\mathtt{C}}\mathtt{D}^{\mathtt{p}_2}[({}^{\mathtt{C}}\mathtt{D}^{\mathtt{p}_1} + \kappa)\mathtt{z}(\mathtt{t}) + \mu\mathtt{I}^{\alpha}\mathtt{h}(\mathtt{t}, \mathtt{z}(\mathtt{t}))] &= \mathtt{g}(\mathtt{t}, \mathtt{z}(\mathtt{t})), \ a < \mathtt{t} < b, \ 1 < \mathtt{p}_1, \mathtt{p}_2 \leq 2, \\ \mathtt{z}'(a) = \mathtt{z}(b) &= \mathtt{z}'(b) = 0, \\ \mathtt{z}(a) = \sum_{i=1}^{m-2} \lambda_i \mathtt{z}(\xi_i) &+ \int_a^b \mathtt{z}(\mathtt{t})\mathrm{d}\mho(\mathtt{t}), \end{aligned}$$

by an application of Leray-Schauder alternative criterian, Leray-Schauder degree theory and Shaefer like fixed point theorems.

Inspired by aforementioned works, in this paper we consider the following fractional differential equation,

$$\left.\begin{aligned} \frac{\mathrm{d}}{\mathrm{d}t}\left[\phi\left({}^{\mathrm{RL}}\mathrm{D}_{0^+}^{\ell_1} z_i(t)\right)\right] + \lambda(t) g_i\left(z_{i+1}(t)\right) = 0,\ t \in (0,1),\ \ell_1 \in (2,3], \\ z_{n+1}(t) = z_1(t),\ t \in (0,1),\ i = 1,2,3,\cdots,n, \end{aligned}\right\} \tag{1}$$

satisfying multistrip Riemann–Stieltjes integral boundary conditions,

$$\left.\begin{aligned} z_i(0) = {}^{\mathrm{RL}}\mathrm{D}_{0^+}^{\ell_2}(z_i(0)) = {}^{\mathrm{RL}}\mathrm{D}_{0^+}^{\ell_1}(z_i(0)) = 0,\ \ell_2 \in (0,1], \\ z_i(1) = \sum_{j=1}^{m} \delta_j \int_{\mathcal{J}_j} z_i(\tau)\mathrm{d}\mho(\tau),\ i = 1,2,3,\cdots,n, \end{aligned}\right\} \tag{2}$$

where ${}^{\mathrm{RL}}\mathrm{D}_{0^+}^{\star}$ is a Riemann–Liouville fractional derivative of order $\star \in \{\ell_1, \ell_2\}$, $\int_{\mathcal{J}_j} z_i(\tau)\mathrm{d}\mho(\tau)$ denotes Riemann–Stieltjes integral of $z_i(\tau)$ with respect to $\mho$, $\Omega : [0,1] \to \mathbb{R}$ is a function of bounded variation and $\mathrm{d}\mho$ is a signed measure, $\phi : \mathbb{R} \to \mathbb{R}$ is an IHPHO with $\phi(0) = 0$ and each $\lambda(t) \in L^p[0,1](p > 0)$ has a singularity in the interval $(0, 1/2)$. The multistrip integral boundary conditions in (2) state that the value of unknown function at the right end point $t = 1$ of the given interval is equal to the linear combination of the Riemann–Stieltjes integral values of the unknown function on the subinterval $\mathcal{J}_j$, for $j = 1, 2, \cdots, m$. Equation (1) in integer derivative describes diffusion phenomena with a source or a reaction term. For instance, in thermal conduction, it can be interpreted as the one-dimensional heat conduction equation which models the steady-states of a heated bar of length a with a controller at $z = 0$ that adds or removes heat according to a sensor, while the left endpoint is maintained at $0°C$ and g is the distributed temperature source function depending on delayed temperatures. We refer the interested reader to Refs. [5, 6] and the references therein for more details

The space of all Lebesgue integrable functions is denoted by $L^p[0,1]$ with the norm, $\|\cdot\|_p$ defined by

$$\|g\|_p = \left[\int_0^1 |g(\zeta)|^p \mathrm{d}\zeta\right]^{\frac{1}{p}}, \quad \text{for } 1 \le p < \infty$$

and

$$\|g\|_\infty = \underset{0\le\zeta\le1}{ess.sup}|g(\zeta)|, \quad \text{for } p = \infty.$$

A projection $\phi : \mathbb{R} \to \mathbb{R}$ is called a IHPHO, if the following three conditions are fulfilled,

(a) $\phi(\tau_1) \le \phi(\tau_2)$ whenever $\tau_1 \le \tau_2$, for any real numbers τ_1, τ_2.
(b) ϕ is a continuous bijection and its inverse ϕ^{-1} is continuous.
(c) $\phi(\tau_1\tau_2) = \phi(\tau_1)\phi(\tau_2)$ for any real numbers τ_1, τ_2.

The following conditions are hold throughout the paper:

($\mathcal{H}_1$) $g_i : [0, +\infty) \to [0, +\infty)$ are continuous,
($\mathcal{H}_2$) there exists a sequence $\{t_j\}_{j=1}^{\infty}$ such that $0 < t_{j+1} < t_j < \frac{1}{2}$,

$$\lim_{j\to\infty} t_j = t^* < \frac{1}{2}, \ \lim_{t\to t_j} \lambda(t) = +\infty, \ j = 1,2,3,\cdots,$$

and $\lambda(\mathtt{t})$ does not vanish identically on any subinterval of $[0, 1]$. Moreover, $0 < \psi(\tau) < \infty$ for $0 < \tau < 1$, where

$$\psi(\tau) = \phi^{-1}\left(\int_0^{\tau} \lambda(\mathtt{t})\mathrm{d}\mathtt{t}\right).$$

$(\mathcal{H}_3)$ $\mho$ be nondecreasing and of bounded variation function such that $0 < \Delta < 1$, where

$$\Delta = \sum_{\mathtt{j}=1}^{m} \delta_{\mathtt{j}} \int_{\mathcal{J}_{\mathtt{j}}} \tau^{\ell_1 - 1}\mathrm{d}\mho(\tau).$$

2 Kernel and its bounds

In this section, we construct kernel for the boundary value problem (1)–(2) and estimate bounds for it, which are useful for our later discussions.

Definition 1 [14] The Riemann–Liouville (RL) fractional integral of order δ of a function $\mathtt{g} : (0, \infty) \to \mathbb{R}$ is defined by

$$\mathcal{I}_{0^+}^{\delta}\mathtt{g}(\mathtt{s}) = \int_0^s \frac{(\mathtt{s} - x)^{\delta - 1}}{\Gamma(\delta)}\mathtt{g}(x)dx,\ \delta > 0.$$

Lemma 1 [14, 18] *The general solution to* $\mathrm{D}_{0^+}^{\gamma}\mathtt{g}(\mathtt{t}) = 0$ *with* $\gamma \in (m - 1, m]$ *and* $m > 1$ *is the function*

$$\mathtt{g}(\mathtt{t}) = \sum_{\ell_1=1}^{m} d_{\ell_1}\mathtt{t}^{\gamma - \ell_1},$$

where d_{ℓ_1} *is a real number.*

Lemma 2 [14, 18] *Let* $\gamma > 0$. *Then for any function* $\mathtt{g} : (0, \infty) \to \mathbb{R}$, *we have*

$$\mathrm{D}_{0^+}^{-\gamma}\mathrm{D}_{0^+}^{\gamma}\mathtt{g}(\mathtt{t}) = \mathtt{g}(\mathtt{t}) + \sum_{\ell_1=1}^{m} d_{\ell_1}\mathtt{t}^{\gamma - \ell_1},$$

where d_{ℓ_1} *is a real number and* $m \in \mathbb{Z}$ *is the smallest integer greater that or equal to* γ.

Lemma 3 *Suppose that* $(\mathcal{H}_3)$ *holds. Let* $\mathtt{h} \in \mathrm{C}[0, 1]$. *Then the boundary value problem*

$$^{\mathrm{RL}}\mathrm{D}_{0^+}^{\ell_1}\left(\mathtt{z}_1(\mathtt{t})\right) + \mathtt{h}(\mathtt{t}) = 0,\ \mathtt{t} \in (0, 1),\ \ell_1 \in (2, 3], \tag{3}$$

satisfying multistrip Riemann–Stieltjes integral boundary conditions,

$$\left.\begin{aligned} \mathtt{z}_1(0) = {}^{\mathrm{RL}}\mathrm{D}_{0^+}^{\ell_2}(\mathtt{z}_1(0)) = 0,\ \ell_2 \in (0, 1], \\ \mathtt{z}_1(1) = \sum_{\mathtt{j}=1}^{m} \delta_{\mathtt{j}} \int_{\mathcal{J}_{\mathtt{j}}} \mathtt{z}_1(\tau)\mathrm{d}\mho(\tau), \end{aligned}\right\} \tag{4}$$

has a unique solution

$$\mathtt{z}_1(\mathtt{t}) = \int_0^1 \aleph(\mathtt{t}, \tau)\mathtt{h}(\tau)\mathrm{d}\tau,$$

where

$$\aleph(\mathtt{t},\tau)=\aleph_1(\mathtt{t},\tau)+\aleph_2(\mathtt{t},\tau)$$

in which

$$\aleph_1(\mathtt{t},\tau)=\frac{1}{\Gamma(\ell_1)}\begin{cases}\mathtt{t}^{\ell_1-1}(1-\tau)^{\ell_1-1}-(\mathtt{t}-\tau)^{\ell_1-1}, & \tau<\mathtt{t},\\ \mathtt{t}^{\ell_1-1}(1-\tau)^{\ell_1-1}, & \mathtt{t}<\tau,\end{cases}$$

and $\aleph_2(\mathtt{t},\tau)=\dfrac{\mathtt{t}^{\ell_1-1}}{1-\Delta}\displaystyle\sum_{\mathtt{j}=1}^{m}\delta_{\mathtt{j}}\int_{\mathcal{J}_{\mathtt{j}}}\aleph_1(\mathtt{s},\tau)\mathrm{d}\mho(\mathtt{s})$.

Proof The equivalent inegral equation of (3) is given by

$$\mathtt{z}_1(\mathtt{t})=-\frac{1}{\Gamma(\ell_1)}\int_0^t(\mathtt{t}-\tau)^{\ell_1-1}\mathtt{h}(\tau)\mathrm{d}\tau+c_1\mathtt{t}^{\ell_1-1}+c_2\mathtt{t}^{\ell_1-2}+c_3\mathtt{t}^{\ell_1-3},\tag{5}$$

where c_1, c_2, c_3 are arbitrary constants. Using boundary conditions (4), we get $c_2=c_3=0$ and

$$c_1=\frac{1}{\Gamma(\ell_1)}\int_0^t(\mathtt{t}-\tau)^{\ell_1-1}\mathtt{h}(\tau)\mathrm{d}\tau+\sum_{\mathtt{j}=1}^{m}\delta_{\mathtt{j}}\int_{\mathcal{J}_{\mathtt{j}}}\mathtt{z}_1(\tau)\mathrm{d}\mho(\tau).$$

So, the Eq. (3) takes place

$$\mathtt{z}_1(\mathtt{t})=\int_0^1\aleph_1(\mathtt{t},\tau)\mathtt{h}(\tau)\mathrm{d}\tau+\mathtt{t}^{\ell_1-1}\sum_{\mathtt{j}=1}^{m}\delta_{\mathtt{j}}\int_{\mathcal{J}_{\mathtt{j}}}\mathtt{z}_1(\tau)\mathrm{d}\mho(\tau).\tag{6}$$

By simple calculations, we obtain

$$\sum_{\mathtt{j}=1}^{m}\delta_{\mathtt{j}}\int_{\mathcal{J}_{\mathtt{j}}}\mathtt{z}_1(\tau)\mathrm{d}\mho(\tau)=\frac{1}{1-\Delta}\sum_{\mathtt{j}=1}^{m}\delta_{\mathtt{j}}\int_{\mathcal{J}_{\mathtt{j}}}\int_0^1\aleph_1(\mathtt{s},\tau)\mathrm{d}\tau\mathrm{d}\mho(\mathtt{s}).$$

Substituting above identity into (6), we obtain

$$\mathtt{z}_1(\mathtt{t})=\int_0^1\left(\aleph_1(\mathtt{t},\tau)+\frac{\mathtt{t}^{\ell_1-1}}{1-\Delta}\sum_{\mathtt{j}=1}^{m}\delta_{\mathtt{j}}\int_{\mathcal{J}_{\mathtt{j}}}\aleph_1(\mathtt{s},\tau)\mathrm{d}\mho(\mathtt{s})\right)\mathtt{h}(\tau)\mathrm{d}\tau=\int_0^1\aleph(\mathtt{t},\tau)\mathtt{h}(\tau)\mathrm{d}\tau.$$

□

Lemma 4 *Let* $\varepsilon\in(0,1/2)$. *The function* $\aleph_1(\mathtt{t},\tau)$ *has the following properties*

(i) $\aleph_1(\mathtt{t},\tau)\le(\ell_1-1)\aleph(\tau)$ *for* $t,\tau\in[0,1]$.
(ii) $\aleph_1(\mathtt{t},\tau)\ge\varepsilon^{2\ell_1-1}\aleph(\tau)$ *for* $\mathtt{t}\in[\varepsilon,1-\varepsilon]$, $\tau\in[0,1]$.

Proof For $\tau\le t$, we have

$$\begin{aligned}\aleph_1(\mathtt{t},\tau)&=\frac{1}{\Gamma(\ell_1)}\left[(\ell_1-1)\int_{t-\tau}^{t-t\tau}\mathtt{y}^{\ell_1-2}\mathrm{d}\mathtt{y}\right]\le\frac{\ell_1-1}{\Gamma(\ell_1)}(\mathtt{t}-t\tau)^{\ell_1-2}[(\mathtt{t}-t\tau)-(\mathtt{t}-\tau)]\\&\le\frac{\ell_1-1}{\Gamma(\ell_1)}\mathtt{t}^{\ell_1-2}(1-\tau)^{\ell_1-2}(1-\mathtt{t})\tau\le\frac{\ell_1-1}{\Gamma(\ell_1)}\tau(1-\tau)^{\ell_1-1}:=(\ell_1-1)\aleph(\tau),\end{aligned}$$

and for $\mathtt{t} \in [\varepsilon, 1-\varepsilon]$, we have

$$\begin{aligned}\aleph_1(\mathtt{t},\tau) &= \frac{1}{\Gamma(\ell_1)}\left[\mathtt{t}^{\ell_1-2}(1-\tau)^{\ell_1-2}\mathtt{t}(1-\tau) - (\mathtt{t}-\tau)^{\ell_1-2}(\mathtt{t}-\tau)\right]\\ &\geq \frac{1}{\Gamma(\ell_1)}\left[\mathtt{t}^{\ell_1-2}(1-\tau)^{\ell_1-2}\mathtt{t}(1-\tau) - (\mathtt{t}-t\tau)^{\ell_1-2}(\mathtt{t}-\tau)\right]\\ &\geq \frac{1}{\Gamma(\ell_1)}\left[\mathtt{t}^{\ell_1-2}(1-\tau)^{\ell_1-2}(1-\mathtt{t})\tau\right] \geq \frac{1}{\Gamma(\ell_1)}\mathtt{t}^{\ell_1-1}(1-\mathtt{t})\tau(1-\tau)^{\ell_1-1}\\ &\geq \frac{\varepsilon^{2\ell_1-1}}{\Gamma(\ell_1)}\tau(1-\tau)^{\ell_1-1} := \varepsilon^{2\ell_1-1}\aleph(\tau).\end{aligned}$$

Since other case is trivial, this completes the proof. □

Lemma 5 *Let $\varepsilon \in (0, 1/2)$ and $\delta = \sum_{\mathtt{j}=1}^{m}\delta_{\mathtt{j}}\int_{\mathcal{J}_{\mathtt{j}}}\mathrm{d}\mho(\mathtt{s})$. The kernel $\aleph(\mathtt{t},\tau)$ has the following properties*

(i) $\aleph(\mathtt{t},\tau) \leq \dfrac{(\ell_1-1)(1-\Delta+\delta)}{1-\Delta}\aleph(\tau)$ *for* $t, \tau \in [0,1]$.

(ii) $\aleph(\mathtt{t},\tau) \geq \dfrac{\varepsilon^{3\ell_1-2}(1-\Delta+\delta)}{1-\Delta}\aleph(\tau)$ *for* $\mathtt{t} \in [\varepsilon, 1-\varepsilon]$, $\tau \in [0,1]$.

Proof From Lemma 4, we have

$$\begin{aligned}\aleph(\mathtt{t},\tau) &= \aleph_1(\mathtt{t},\tau) + \frac{\mathtt{t}^{\ell_1-1}}{1-\Delta}\sum_{\mathtt{j}=1}^{m}\delta_{\mathtt{j}}\int_{\mathcal{J}_{\mathtt{j}}}\aleph_1(\mathtt{s},\tau)\mathrm{d}\mho(\mathtt{s})\\ &\leq (\ell_1-1)\aleph(\tau) + \frac{1}{1-\Delta}\sum_{\mathtt{j}=1}^{m}\delta_{\mathtt{j}}\int_{\mathcal{J}_{\mathtt{j}}}(\ell_1-1)\aleph(\tau)\mathrm{d}\mho(\mathtt{s}) \leq \frac{(\ell_1-1)(1-\Delta+\delta)}{1-\Delta}\aleph(\tau),\end{aligned}$$

and for $\mathtt{t} \in [\varepsilon, 1-\varepsilon]$, we have

$$\begin{aligned}\aleph(\mathtt{t},\tau) &= \aleph_1(\mathtt{t},\tau) + \frac{\mathtt{t}^{\ell_1-1}}{1-\Delta}\sum_{\mathtt{j}=1}^{m}\delta_{\mathtt{j}}\int_{\mathcal{J}_{\mathtt{j}}}\aleph_1(\mathtt{s},\tau)\mathrm{d}\mho(\mathtt{s})\\ &\geq \varepsilon^{2\ell_1-1}\aleph(\tau) + \frac{\varepsilon^{\ell_1-1}}{1-\Delta}\sum_{\mathtt{j}=1}^{m}\delta_{\mathtt{j}}\int_{\mathcal{J}_{\mathtt{j}}}\varepsilon^{2\ell_1-1}\aleph(\tau)\mathrm{d}\mho(\mathtt{s})\\ &\geq \varepsilon^{3\ell_1-2}\aleph(\tau) + \frac{\varepsilon^{3\ell_1-2}\delta}{1-\Delta}\aleph(\tau) \geq \frac{\varepsilon^{3\ell_1-2}(1-\Delta+\delta)}{1-\Delta}\aleph(\tau).\end{aligned}$$

This completes the proof. □

Lemma 6 *Let $\mathtt{f} \in \mathcal{C}[0,1]$. The boundary value problem*

$$\frac{\mathrm{d}}{\mathrm{d}\mathtt{t}}\left[\phi\left({}^{\mathrm{RL}}\mathrm{D}_{0^+}^{\ell_1}\mathrm{z}_{\mathtt{i}}(\mathtt{t})\right)\right] + \mathtt{f}(\mathtt{t}) = 0,\ \mathtt{t} \in (0,1), \tag{7}$$

$$\mathrm{z}_1(0) = {}^{\mathrm{RL}}\mathrm{D}_{0^+}^{\ell_2}(\mathrm{z}_1(0)) = {}^{\mathrm{RL}}\mathrm{D}_{0^+}^{\ell_1}(\mathrm{z}_1(0)) = 0,\ \mathrm{z}_1(1) = \sum_{\mathtt{j}=1}^{m}\delta_{\mathtt{j}}\int_{\mathcal{J}_{\mathtt{j}}}\mathrm{z}_1(\tau)\mathrm{d}\mho(\tau) \tag{8}$$

has a unique solution

$$\mathrm{z}_1(\mathtt{t}) = \int_0^1 \aleph(\mathtt{t},\tau)\phi^{-1}\left[\int_0^{\tau}\mathtt{f}(\mathtt{s})\mathrm{d}\mathtt{s}\right]\mathrm{d}\tau.$$

Proof Integrating Eq. (7), we get $\phi\left({}^{RL}D_{0^+}^{\ell_1}(z_1(t))\right) = -\int_0^t f(\tau)d\tau + C_1$, Since ϕ is IHPHO, $\phi(0) = 0$ and using boundary condition ${}^{RL}D_{0^+}^{\ell_1}(z_1(0)) = 0$, we get $C_1 = 0$. So we left with

$$ {}^{RL}D_{0^+}^{\ell_1}(z_1(t)) + \phi^{-1}\left[\int_0^t f(\tau)d\tau\right] = 0, $$

and

$$ z_1(0) = {}^{RL}D_{0^+}^{\ell_2}(z_1(0)) = 0,\ z_1(1) = \sum_{j=1}^{m}\delta_j\int_{\mathcal{J}_j} z_1(\tau)d\vartheta(\tau), $$

which has a unique solution

$$ z_1(t) = \int_0^1 \aleph(t,\tau)\phi^{-1}\left[\int_0^\tau f(s)ds\right]d\tau. $$

□

We note that an n-tuple $(z_1, z_2, \cdots, z_n)$ is a solution of (1)–(2) if and only if

$$ z_1(t) = \int_0^1 \aleph(t,\tau_1)\phi^{-1}\Big[\int_0^{\tau_1}\lambda(s_1)g_1\Big[\int_0^1 \aleph(s_1,\tau_2)\phi^{-1}\Big[\int_0^{\tau_2}\lambda(s_2)g_2\cdots $$
$$ g_{n-1}\Big[\int_0^1 \aleph(s_{n-1},\tau_n)\phi^{-1}\Big[\int_0^{\tau_n}\lambda(s_n)g_n(z_1(s_n))ds_n\Big]d\tau_n\cdots ds_1\Big]d\tau_1 $$

and

$$ z_i(t) = \int_0^1 \aleph(t,\tau)\phi^{-1}\left[\int_0^\tau \lambda(s)g_i(z_{i+1}(s))ds\right]d\tau,\ i = 2,3,\cdots,n, $$
$$ z_{n+1}(t) = z_1(t),\ 0 < t < 1. $$

We denote the Banach space $C([0,1],\mathbb{R})$ by $\mathcal{B}$ with the norm $\|z\| = \max_{t\in[0,1]}|z(t)|$. For $\varepsilon \in (0, 1/2)$, the cone $\mathcal{P}_\varepsilon \subset \mathcal{B}$ is defined by

$$ \mathcal{P}_\varepsilon = \left\{z \in \mathcal{B} : z(t) \geq 0,\ \min_{t\in[\varepsilon,1-\varepsilon]} z(t) \geq \frac{\varepsilon^{3\ell_1-2}}{\ell_1 - 1}\|z(t)\|\right\}, $$

For any $z_1 \in \mathcal{P}_\varepsilon$, define an operator $\mathscr{Y} : \mathcal{P}_\varepsilon \to \mathcal{B}$ by

$$ (\mathscr{Y}z_1)(t) = \int_0^1 \aleph(t,\tau_1)\phi^{-1}\Big[\int_0^{\tau_1}\lambda(s_1)g_1\Big[\int_0^1 \aleph(s_1,\tau_2)\phi^{-1}\Big[\int_0^{\tau_2}\lambda(s_2)g_2\cdots $$
$$ g_{n-1}\Big[\int_0^1 \aleph(s_{n-1},\tau_n)\phi^{-1}\Big[\int_0^{\tau_n}\lambda(s_n)g_n(z_1(s_n))ds_n\Big]d\tau_n\cdots ds_1\Big]d\tau_1. $$

Lemma 7 *For each $\varepsilon \in (0, 1/2)$, $\mathscr{Y}(\mathcal{P}_\varepsilon) \subset \mathcal{P}_\varepsilon$ and $\mathscr{Y} : \mathcal{P}_\varepsilon \to \mathcal{P}_\varepsilon$ is completely continuous.*

Proof Let $\varepsilon \in (0, 1/2)$. Since $g_i(z(\tau))$ is nonnegative for $\tau \in [0,1]$, $z \in \mathcal{P}_\varepsilon$. Since $\aleph(t,\tau)$ is nonnegative for all $t, \tau \in [0,1]$, it follows that $\mathscr{Y}(z(t)) \geq 0$ for all $t \in [0,1]$, $z \in \mathcal{P}_\varepsilon$. Now, by Lemma 5, we have

$$
\begin{aligned}
&\min_{t\in[\varepsilon,1-\varepsilon]}(\mathscr{Y}z_1)(t)\\
&\quad=\min_{t\in[\varepsilon,1-\varepsilon]}\Big\{\int_0^1\aleph(t,\tau_1)\phi^{-1}\Big[\int_0^{\tau_1}\lambda(s_1)g_1\Big[\int_0^1\aleph(s_1,\tau_2)\phi^{-1}\Big[\int_0^{\tau_2}\lambda(s_2)g_2\cdots\\
&\qquad g_{n-1}\Big[\int_0^1\aleph(s_{n-1},\tau_n)\phi^{-1}\Big[\int_0^{\tau_n}\lambda(s_n)g_n(z_1(s_n))ds_n\Big]d\tau_n\cdots ds_1\Big]d\tau_1\Big\}\\
&\quad\geq\frac{\varepsilon^{3\ell_1-2}(1-\Delta+\delta)}{1-\Delta}\int_0^1\aleph(\tau_1)\phi^{-1}\Big[\int_0^{\tau_1}\lambda(s_1)f_1\Big[\int_0^1\aleph(s_1,\tau_2)\phi^{-1}\Big[\int_0^{\tau_2}\lambda(s_2)f_2\cdots\\
&\qquad f_{n-1}\Big[\int_0^1\aleph(s_{n-1},\tau_n)\phi^{-1}\Big[\int_0^{\tau_n}\lambda(s_n)f_n(z_1(s_n))ds_n\Big]d\tau_n\cdots ds_1\Big]d\tau_1\\
&\quad\geq\frac{\varepsilon^{3\ell_1-2}}{\ell_1-1}\max_{t\in[0,1]}\Big\{\int_0^1\aleph(t,\tau_1)\phi^{-1}\Big[\int_0^{\tau_1}\lambda(s_1)g_1\Big[\int_0^1\aleph(s_1,\tau_2)\phi^{-1}\Big[\int_0^{\tau_2}\lambda(s_2)g_2\cdots\\
&\qquad g_{n-1}\Big[\int_0^1\aleph(s_{n-1},\tau_n)\phi^{-1}\Big[\int_0^{\tau_n}\lambda(s_n)g_n(z_1(s_n))ds_n\Big]d\tau_n\cdots ds_1\Big]d\tau_1\Big\}\\
&\quad\geq\frac{\varepsilon^{3\ell_1-2}}{\ell_1-1}\max_{t\in[0,1]}|\mathscr{Y}z_1(t)|.
\end{aligned}
$$

Thus $\mathscr{Y}(\mathcal{P}_\varepsilon)\subset\mathcal{P}_\varepsilon$. Therefore, the operator $\mathscr{Y}$ is completely continuous by standard methods and by the Arzela-Ascoli theorem. □

3 Infinitely many positive solutions

For the the existence of infinitely many positive solutions for bvp (1)–(2), we utilize the following theorems.

Theorem 1 (Krasnoselskii's) [9] *Let $\mathcal{E}$ be a cone in a Banach space $\mathcal{X}$ and $\Lambda_1,\ \Lambda_2$ are open sets with $0\in\Lambda_1$, $\overline{\Lambda}_1\subset\Lambda_2$. Let $\mathscr{Y}:\mathcal{E}\cap(\overline{\Lambda}_2\backslash\Lambda_1)\to\mathcal{E}$ be a completely continuous operator such that*

(a) $\|\mathscr{Y}z\|\leq\|z\|,\ z\in\mathcal{E}\cap\partial\Lambda_1$, and $\|\mathscr{Y}z\|\geq\|z\|,\ z\in\mathcal{E}\cap\partial\Lambda_2$, or
(b) $\|\mathscr{Y}z\|\geq\|z\|,\ z\in\mathcal{E}\cap\partial\Lambda_1$, and $\|\mathscr{Y}z\|\leq\|z\|,\ z\in\mathcal{E}\cap\partial\Lambda_2$.

Then $\mathscr{Y}$ has a fixed point in $\mathcal{E}\cap(\overline{\Lambda}_2\backslash\Lambda_1)$.

Theorem 2 (Hölder's) *Let $f\in L^p[0,1]$ and $g\in L^q[0,1]$, where $p>1$, $q>1$, with $\frac{1}{p}+\frac{1}{q}=1$. Then $fg\in L^1[0,1]$ and $\|fg\|_1\leq\|f\|_p\|g\|_q$.*

Further, if $f\in L^1[0,1]$ and $g\in L^\infty[0,1]$. Then $fg\in L^1[0,1]$ and $\|fg\|_1\leq\|f\|_1\|g\|_\infty$.

Consider the following three possible cases for $\lambda\in L^p[0,1]:0<p<1, p=1, p=\infty$.

Firstly, we seek infinitely many positive solutions for the case $p>1$.

Theorem 3 *Assume that $(\mathcal{H}_1)$–$(\mathcal{H}_3)$ hold, let $\{\varepsilon_k\}_{k=1}^\infty$ be such that $t_{k+1}<\varepsilon_k<t_k$, $k=1,2,3,\cdots$. Let $\{R_k\}_{k=1}^\infty$ and $\{r_k\}_{k=1}^\infty$ be such that*

$$R_{k+1}<\frac{\varepsilon_k^{3\ell_1-2}}{\ell_1-1}r_k<\eta r_k<R_k,\ k\in\mathbb{N},$$

where

$$\eta=\max\left\{\left[\frac{\varepsilon_1^{3\ell_1-2}(1-\Delta+\delta)}{1-\Delta}\int_{\varepsilon_1}^{1-\varepsilon_1}\aleph(\tau)\phi^{-1}\Big[\int_{\varepsilon_1}^{\tau}\lambda(s)ds\Big]d\tau\right]^{-1},\ 1\right\}.$$

Assume that $\mathtt{g}_\mathtt{i}$ *satisfies*

$$(\mathcal{A}_1)\ \ \mathtt{g}_\mathtt{i}(\mathtt{z}(\mathtt{t})) \le \phi(\mathtt{M}_1 R_k) \text{ for all } 0 \le \mathtt{z}(\mathtt{t}) \le R_k,\ \mathtt{t} \in [0,1],$$
$$\text{where } \mathtt{M}_1 < \frac{1-\Delta}{(\ell_1-1)(1-\Delta+\delta)\|\aleph\|_\mathtt{q}\left\|\phi^{-1}(\lambda(\cdot))\right\|_\mathtt{p}}.$$
$$(\mathcal{A}_2)\ \ \mathtt{g}_\mathtt{i}(\mathtt{z}(\mathtt{t})) \ge \phi(\eta r_k) \text{ for all } \frac{\varepsilon_k^{3\ell_1-2}}{\ell_1-1} r_k \le \mathtt{z}(\mathtt{t}) \le r_k,\ \mathtt{t} \in [\varepsilon_k, 1-\varepsilon_k].$$

The iterative system (1)–(2) *has infinitely many solutions* $\{(\mathtt{z}_1^{[k]}, \mathtt{z}_2^{[k]}, \cdots, \mathtt{z}_n^{[k]})\}_{k=1}^\infty$ *such that* $\mathtt{z}_\mathtt{i}^{[k]}(\mathtt{t}) \ge 0$ *on* $(0,1)$, $\mathtt{i} = 1, 2, \cdots, n$ *and* $k \in \mathbb{N}$.

Proof Consider the sequences $\{\Lambda_{1,k}\}_{k=1}^\infty$ and $\{\Lambda_{2,k}\}_{k=1}^\infty$ of open subsets of $\mathcal{B}$ defined by

$$\Lambda_{1,k} = \{\mathtt{z} \in \mathcal{B} : \|\mathtt{z}\| < R_k\},\ \Lambda_{2,k} = \{\mathtt{z} \in \mathcal{B} : \|\mathtt{z}\| < r_k\}.$$

Let $\{\varepsilon_k\}_{k=1}^\infty$ be as in the hypothesis and note that $\mathtt{t}^* < \mathtt{t}_{k+1} < \varepsilon_k < \mathtt{t}_k < \frac{1}{2}$, for all $k \in \mathbb{N}$. For each $k \in \mathbb{N}$, define the cone $\mathcal{P}_{\varepsilon_k}$ by

$$\mathcal{P}_{\varepsilon_k} = \left\{ \mathtt{z} \in \mathcal{B} : \mathtt{z}(\mathtt{t}) \ge 0 \ \text{ and } \min_{\mathtt{t} \in [\varepsilon_k, 1-\varepsilon_k]} \mathtt{z}(\mathtt{t}) \ge \frac{\varepsilon_k^{3\ell_1-2}}{\ell_1-1} \|\mathtt{z}(\mathtt{t})\| \right\}.$$

Let $\mathtt{z}_1 \in \mathcal{P}_{\varepsilon_k} \cap \partial\Lambda_{1,k}$. Then, $\mathtt{z}_1(\tau) \le R_k = \|\mathtt{z}_1\|$ for all $\tau \in [0,1]$. By $(\mathcal{A}_1)$ and $0 < \tau_{n-1} < 1$, we have

$$\begin{aligned}
&\int_0^1 \aleph(\tau_{n-1}, \tau_n)\phi^{-1}\Big[\int_0^{\tau_n} \lambda(\mathtt{s}_n)\mathtt{g}_n(\mathtt{z}_1(\mathtt{s}_n))\mathrm{d}\mathtt{s}_n\Big]\mathrm{d}\tau_n \\
&\quad\le \frac{(\ell_1-1)(1-\Delta+\delta)}{1-\Delta}\int_0^1 \aleph(\tau_n)\phi^{-1}\Big[\int_0^{\tau_n} \lambda(\mathtt{s}_n)\mathtt{g}_n(\mathtt{z}_1(\mathtt{s}_n))\mathrm{d}\mathtt{s}_n\Big]\mathrm{d}\tau_n \\
&\quad\le \frac{(\ell_1-1)(1-\Delta+\delta)}{1-\Delta}\mathtt{M}_1 R_k \int_0^1 \aleph(\tau_n)\phi^{-1}\Big[\int_0^{\tau_n} \lambda(\mathtt{s}_n)\mathrm{d}\mathtt{s}_n\Big]\mathrm{d}\tau_n \\
&\quad\le \frac{(\ell_1-1)(1-\Delta+\delta)}{1-\Delta}\mathtt{M}_1 R_k \int_0^1 \aleph(\tau_n)\psi(\tau_n)\mathrm{d}\tau_n.
\end{aligned}$$

There exists a $\mathtt{q} > 1$ such that $\frac{1}{\mathtt{q}} + \frac{1}{\mathtt{p}} = 1$. So,

$$\begin{aligned}
\int_0^1 \aleph(\tau_{n-1}, \tau_n)\phi^{-1}\Big[\int_0^{\tau_n} \lambda(\mathtt{s}_n)\mathtt{g}_n(\mathtt{z}_1(\mathtt{s}_n))\mathrm{d}\mathtt{s}_n\Big]\mathrm{d}\tau_n &\le \frac{(\ell_1-1)(1-\Delta+\delta)}{1-\Delta}\mathtt{M}_1 R_k \|\aleph\|_\mathtt{q}\|\psi\|_\mathtt{p} \\
&\le R_k.
\end{aligned}$$

It follows in similar manner (for $0 < \tau_{n-2} < 1$) that

$$\begin{aligned}
&\int_0^1 \aleph(\tau_{n-2},\tau_{n-1})\phi^{-1}\Big[\int_0^{\tau_{n-1}} \lambda(s_{n-1})g_{n-1}\Big[\int_0^1 \aleph(s_{n-1},\tau_n)\\
&\quad\times \phi^{-1}\Big[\int_0^{\tau_n} \lambda(s_n)g_n(z_1(s_n))ds_n\Big]d\tau_n\Big]ds_{n-1}\Big]d\tau_{n-1}\\
&\le \frac{(\ell_1-1)(1-\Delta+\delta)}{1-\Delta}\int_0^1 \aleph(\tau_{n-1})\phi^{-1}\Big[\int_0^{\tau_{n-1}} \lambda(s_{n-1})g_{n-1}(R_k)ds_{n-1}\Big]d\tau_{n-1}\\
&\le \frac{(\ell_1-1)(1-\Delta+\delta)}{1-\Delta}\mathbb{M}_1 R_k\int_0^1 \aleph(\tau_{n-1})\psi(\tau_{n-1})d\tau_{n-1}\\
&\le \frac{(\ell_1-1)(1-\Delta+\delta)}{1-\Delta}\mathbb{M}_1 R_k\|\aleph\|_{\mathfrak{q}}\|\psi\|_{\mathfrak{p}}\\
&\le R_k.
\end{aligned}$$

Continuing with this bootstrapping argument, we get

$$\begin{aligned}
(\mathscr{Y}z_1)(t) = &\int_0^1 \aleph(t,\tau_1)\phi^{-1}\Big[\int_0^{\tau_1}\lambda(s_1)g_1\Big[\int_0^1 \aleph(s_1,\tau_2)\phi^{-1}\Big[\int_0^{\tau_2}\lambda(s_2)g_2\cdots\\
&g_{n-1}\Big[\int_0^1 \aleph(s_{n-1},\tau_n)\phi^{-1}\Big[\int_0^{\tau_n}\lambda(s_n)g_n(z_1(s_n))ds_n\Big]d\tau_n\cdots ds_1\Big]d\tau_1\\
&\le R_k.
\end{aligned}$$

Since $R_k = \|z_1\|$ for $z_1 \in \mathcal{P}_{\varepsilon_k}\cap\partial\Lambda_{1,k}$, we get

$$\|\mathscr{Y}z_1\| \le \|z_1\|. \tag{9}$$

Let $t \in [\varepsilon_k, 1-\varepsilon_k]$. Then, $r_k = \|z_1\| \ge z_1(t) \ge \min_{t\in[\varepsilon_k,1-\varepsilon_k]} z_1(t) \ge \dfrac{\varepsilon_k^{3\ell_1-2}}{\ell_1-1}\|z_1\| \ge \dfrac{\varepsilon_k^{3\ell_1-2}}{\ell_1-1}r_k$. By $(\mathcal{A}_2)$ and for $\tau_{n-1}\in[\varepsilon_k,1-\varepsilon_k]$, we have

$$\begin{aligned}
&\int_0^1 \aleph(\tau_{n-1},\tau_n)\phi^{-1}\Big[\int_0^{\tau_n}\lambda(s_n)g_n(z_1(s_n))ds_n\Big]d\tau_n\\
&\quad\ge \frac{\varepsilon_k^{3\ell_1-2}(1-\Delta+\delta)}{1-\Delta}\int_0^1 \aleph(\tau_n)\phi^{-1}\Big[\int_0^{\tau_n}\lambda(s_n)g_n(z_1(s_n))ds_n\Big]d\tau_n\\
&\quad\ge \frac{\varepsilon_k^{3\ell_1-2}(1-\Delta+\delta)}{1-\Delta}\int_{\varepsilon_k}^{1-\varepsilon_k} \aleph(\tau_n)\phi^{-1}\Big[\int_0^{\tau_n}\lambda(s_n)g_n(z_1(s_n))ds_n\Big]d\tau_n\\
&\quad\ge \frac{\varepsilon_k^{3\ell_1-2}(1-\Delta+\delta)}{1-\Delta}\int_{\varepsilon_k}^{1-\varepsilon_k} \aleph(\tau_n)\phi^{-1}\Big[\int_{\varepsilon_k}^{\tau_n}\lambda(s_n)g_n(z_1(s_n))ds_n\Big]d\tau_n\\
&\quad\ge \frac{\varepsilon_k^{3\ell_1-2}(1-\Delta+\delta)}{1-\Delta}\eta r_k\int_{\varepsilon_k}^{1-\varepsilon_k} \aleph(\tau_n)\phi^{-1}\Big[\int_{\varepsilon_k}^{\tau_n}\lambda(s_n)ds_n\Big]d\tau_n\\
&\quad\ge \frac{\varepsilon_k^{3\ell_1-2}(1-\Delta+\delta)}{1-\Delta}\eta r_k\int_{\varepsilon_1}^{1-\varepsilon_1} \aleph(\tau_n)\phi^{-1}\Big[\int_{\varepsilon_1}^{\tau_n}\lambda(s_n)ds_n\Big]d\tau_n\\
&\quad\ge r_k.
\end{aligned}$$

Continuing with bootstrapping argument, we get

$$(\mathscr{Y}z_1)(t) = \int_0^1 \aleph(t,\tau_1)\phi^{-1}\Big[\int_0^{\tau_1}\lambda(s_1)g_1\Big[\int_0^1 \aleph(s_1,\tau_2)\phi^{-1}\Big[\int_0^{\tau_2}\lambda(s_2)g_2\cdots$$
$$g_{n-1}\Big[\int_0^1 \aleph(s_{n-1},\tau_n)\phi^{-1}\Big[\int_0^{\tau_n}\lambda(s_n)g_n(z_1(s_n))ds_n\Big]d\tau_n\cdots ds_1\Big]d\tau_1$$
$$\geq r_k.$$

Thus, if $z_1 \in \mathcal{P}_{\varepsilon_k}\cap\partial\Lambda_{2,k}$, then

$$\|\mathscr{Y}z_1\| \geq \|z_1\|. \tag{10}$$

It is evident that $0 \in \Lambda_{2,k} \subset \overline{\Lambda}_{2,k} \subset \Lambda_{1,k}$. From (9),(10), it follows from Theorem 1 that the operator $\mathscr{Y}$ has a fixed point $z_1^{[k]} \in \mathcal{P}_{\varepsilon_k}\cap\left(\overline{\Lambda}_{1,k}\backslash\Lambda_{2,k}\right)$ such that $z_1^{[k]}(t) \geq 0$ on $(0,1)$, and $k \in \mathbb{N}$. Next setting $z_{n+1} = z_1$, we obtain infinitely many positive solutions $\{(z_1^{[k]}, z_2^{[k]}, \cdots, z_n^{[k]})\}_{k=1}^{\infty}$ of (1)–(2) given iteratively by

$$z_i(t) = \int_0^1 \aleph(t,\tau)\phi^{-1}\left[\int_0^{\tau}\lambda(s)g_i(z_{i+1}(s))ds\right]d\tau,\ i = 1,2,\cdots,n-1,n,$$
$$z_{n+1} = z_1.$$

The proof is completed. □

For $p = 1$, we have the following theorem.

Theorem 4 *Assume that* $(\mathcal{H}_1)$–$(\mathcal{H}_3)$ *hold, let* $\{\varepsilon_k\}_{k=1}^{\infty}$ *be such that* $t_{k+1} < \varepsilon_k < t_k$, $k = 1,2,3,\cdots$. *Let* $\{R_k\}_{k=1}^{\infty}$ *and* $\{r_k\}_{k=1}^{\infty}$ *be such that*

$$R_{k+1} < \frac{\varepsilon_k^{3\ell_1-2}}{\ell_1-1}r_k < \eta r_k < R_k,\ k \in \mathbb{N},$$

Assume that g_i *satisfies* $(\mathcal{A}_2)$
$(\mathcal{A}_3)$ $g_i(z(t)) \leq \phi(M_2R_k)$ *for all* $0 \leq z(t) \leq R_k$, $t \in [0,1]$, *where*

$$M_2 < \min\left\{\frac{1-\Delta}{(\ell_1-1)(1-\Delta+\delta)\|\aleph\|_{\infty}\|\psi\|_1},\ \eta\right\}.$$

The iterative system (1)–(2) *has infinitely many solutions* $\{(z_1^{[k]}, z_2^{[k]}, \cdots, z_n^{[k]})\}_{k=1}^{\infty}$ *such that* $z_i^{[k]}(t) \geq 0$ *on* $(0,1)$, $i = 1,2,\cdots,n$ *and* $k \in \mathbb{N}$.

Proof Let $\Lambda_{1,k}$ be as in the proof of Theorem 3 and let $z_1 \in \mathcal{P}_{\varepsilon_k}\cap\partial\Lambda_{2,k}$. Again $z(\tau) \leq R_k = \|z_1\|$, for all $\tau \in [0,1]$. By $(\mathcal{A}_3)$ and $0 < \tau_{n-1} < 1$, we have

$$\int_0^1 \aleph(\tau_{n-1},\tau_n)\phi^{-1}\Big[\int_0^{\tau_n}\lambda(s_n)g_n(z_1(s_n))ds_n\Big]d\tau_n$$
$$\leq \frac{(\ell_1-1)(1-\Delta+\delta)}{1-\Delta}\int_0^1 \aleph(\tau_n)\phi^{-1}\Big[\int_0^{\tau_n}\lambda(s_n)g_n(z_1(s_n))ds_n\Big]d\tau_n$$
$$\leq \frac{(\ell_1-1)(1-\Delta+\delta)}{1-\Delta}M_1R_k\int_0^1 \aleph(\tau_n)\psi(\tau_n)d\tau_n$$
$$\leq \frac{(\ell_1-1)(1-\Delta+\delta)}{1-\Delta}M_1R_k\|\aleph\|_{\infty}\|\psi\|_1 \leq R_k.$$

Continuing with this bootstrapping argument, we get

$$(\mathscr{Y}\mathrm{z}_1)(\mathrm{t}) = \int_0^1 \aleph(\mathrm{t},\tau_1)\phi^{-1}\Big[\int_0^{\tau_1}\lambda(\mathrm{s}_1)\mathrm{g}_1\Big[\int_0^1 \aleph(\mathrm{s}_1,\tau_2)\phi^{-1}\Big[\int_0^{\tau_2}\lambda(\mathrm{s}_2)\mathrm{g}_2\cdots$$
$$\mathrm{g}_{n-1}\Big[\int_0^1 \aleph(\mathrm{s}_{n-1},\tau_n)\phi^{-1}\Big[\int_0^{\tau_n}\lambda(\mathrm{s}_n)\mathrm{g}_n(\mathrm{z}_1(\mathrm{s}_n))\mathrm{d}\mathrm{s}_n\Big]\mathrm{d}\tau_n\cdots\mathrm{d}\mathrm{s}_1\Big]\mathrm{d}\tau_1$$
$$\leq R_k.$$

Thus, $\|\mathscr{Y}\mathrm{z}_1\| \leq \|\mathrm{z}_1\|$, for $\mathrm{z}_1 \in \mathcal{P}_{\varepsilon_k}\cap\partial\Lambda_{1,k}$. Now define $\Lambda_{2,k} = \{\mathrm{z}\in\mathcal{B} : \|\mathrm{z}\| < r_k\}$. Let $\mathrm{z}_1 \in \mathcal{P}_{\varepsilon_k}\cap\partial\Lambda_{2,k}$ and let $\tau\in[\varepsilon_k,\ 1-\varepsilon_k]$. Then, the argument leading to (10) can be done to the present case. Hence, the theorem. □

Lastly, the case $\mathrm{p} = \infty$.

Theorem 5 *Assume that* $(\mathcal{H}_1)$–$(\mathcal{H}_3)$ *holds, let* $\{\varepsilon_k\}_{k=1}^{\infty}$ *be such that* $t_{k+1} < \varepsilon_k < \mathrm{t}_k$, $k = 1, 2, 3, \cdots$. *Let* $\{R_k\}_{k=1}^{\infty}$ *and* $\{r_k\}_{k=1}^{\infty}$ *be such that*

$$R_{k+1} < \frac{\varepsilon_k^{3\ell_1-2}}{\ell_1-1}r_k < \eta r_k < R_k,\ k\in\mathbb{N},$$

Assume that g_i *satisfies* $(\mathcal{A}_2)$
$(\mathcal{A}_4)$ $\mathrm{g}_\mathrm{i}(\mathrm{z}(\mathrm{t})) \leq \phi(\mathtt{M}_3 R_k)$ *for all* $0\leq \mathrm{z}(\mathrm{t})\leq R_k,\ \mathrm{t}\in[0,1]$, *where*

$$\mathtt{M}_3 < \min\left\{\frac{1-\Delta}{(\ell_1-1)(1-\Delta+\delta)\|\aleph\|_1\,\|\psi\|_\infty},\ \eta\right\}.$$

The iterative system (1)–(2) *has infinitely many solutions* $\{(\mathrm{z}_1^{[k]}, \mathrm{z}_2^{[k]},\cdots,\mathrm{z}_n^{[k]})\}_{k=1}^{\infty}$ *such that* $\mathrm{z}_\mathrm{i}^{[k]}(\mathrm{t}) \geq 0$ *on* $(0,1)$, $\mathrm{i} = 1, 2, \cdots, n$ *and* $k\in\mathbb{N}$.

Proof The proof is similar to the proof of Theorem 3. So, we omit details here. □

4 Example

In this section, we present two examples to check validity of our obtained results.

Example 1 Consider the following fractional order boundary value problem,

$$\left.\begin{aligned}\frac{d}{dt}\Big[\phi(\mathrm{D}_{0^+}^{7/3}\mathrm{z}_\mathrm{i}(\mathrm{t}))\Big] + \lambda(\mathrm{t})\mathrm{g}_\mathrm{i}(\mathrm{z}_{\mathrm{i}+1}(\mathrm{t})) = 0,\ 0<\mathrm{t}<1,\ \mathrm{i}=1,2,\\ \mathrm{z}_3(\mathrm{t}) = \mathrm{z}_1(\mathrm{t}),\ 0<\mathrm{t}<1,\end{aligned}\right\} \tag{11}$$

$$\mathrm{z}_\mathrm{i}(0) = \mathrm{D}_{0^+}^{1/2}\mathrm{z}_\mathrm{i}(0) = \mathrm{D}_{0^+}^{7/3}(\mathrm{z}_\mathrm{i}(0)) = 0,\ \mathrm{z}_\mathrm{i}(1) = \sum_{\mathrm{j}=1}^{2}\delta_\mathrm{j}\int_{\mathcal{J}_\mathrm{j}}\mathrm{z}_\mathrm{i}(\tau)\mathrm{d}\mho(\tau),\ \mathrm{i}=1,2, \tag{12}$$

where $\delta_1 = \delta_2 = \frac{1}{2}$, $\mathcal{J}_1 = [1/2, 5/6]$, $\mathcal{J}_2 = [2/3, 4/5]$, $\lambda(\mathrm{t}) = \dfrac{1}{|t-\frac{1}{4}|^{1/2}}$,

$$\phi(\mathrm{z}) = \begin{cases}\mathrm{z}^2, & \mathrm{z}>0,\\ \dfrac{\mathrm{z}^3}{1+\mathrm{z}^2}, & \mathrm{z}\leq 0,\end{cases}$$

and

$$\mathtt{g}_{\mathtt{i}}(\mathtt{z})=\begin{cases}6\times 10^{-16}, & \mathtt{z}\in(10^{-16},+\infty),\\ \frac{48754292\times 10^{-(16k+8)}-6\times 10^{-16k}}{10^{-(16k+8)}-10^{-16k}}(\mathtt{z}-10^{-16k})+105\times 10^{-16k}, & \\ & \mathtt{z}\in\left[10^{-(16k+8)},10^{-16k}\right],\\ 48754292\times 10^{-(16k+8)}, & \mathtt{z}\in\left(\frac{3}{12500}\times 10^{-(16k+8)},10^{-(16k+8)}\right),\\ \frac{48754292\times 10^{-(16k+8)}-6\times 10^{-(16k+16)}}{\frac{3}{12500}\times 10^{-(16k+8)}-10^{-(16k+16)}}(\mathtt{z}-10^{-(16k+16)})+6\times 10^{-(16k+16)}, & \\ & \mathtt{z}\in\left(10^{-(16k+16)},\frac{3}{12500}\times 10^{-(16k+8)}\right],\end{cases}$$

for $\mathtt{i}=1,2$, and

$$\mho(\mathtt{t})=\begin{cases}\mathtt{t}, & \mathtt{t}\in[0,1/2)\cup[2/3,5/6),\\ \frac{1}{2}, & \mathtt{t}\in[1/2,2/3),\\ \frac{5}{6}, & \mathtt{t}\in[5/6,1].\end{cases}$$

Let

$$t_k=\frac{31}{64}-\sum_{r=1}^{k}\frac{1}{4(r+1)^4},\ \varepsilon_k=\frac{1}{2}(t_k+t_{k+1}),\ k=1,2,3,\cdots,$$

then $\varepsilon_1=\frac{15}{32}-\frac{1}{648}<\frac{15}{32}$ and $t_{k+1}<\varepsilon_k<\mathtt{t}_k$, $\varepsilon_k>\frac{1}{5}$. Therefore, $\frac{\varepsilon_k^{3\ell_1-2}}{\ell_1-1}>\frac{3}{12500}$, $k=1,2,3,\cdots$. It is easy to see

$$t_1=\frac{15}{32}<\frac{1}{2},\ \mathtt{t}_k-t_{k+1}=\frac{1}{4(k+2)^4},\ k=1,2,3,\cdots.$$

Since $\sum_{j=1}^{\infty}\frac{1}{j^4}=\frac{\pi^4}{90}$ and $\sum_{j=1}^{\infty}\frac{1}{j^2}=\frac{\pi^2}{6}$, it follows that

$$\mathtt{t}^*=\lim_{j\to\infty}\mathtt{t}_j=\frac{31}{64}-\sum_{i=1}^{\infty}\frac{1}{4(i+1)^4}=\frac{47}{64}-\frac{\pi^4}{360}>\frac{1}{5},$$

$$\Delta=\sum_{\mathtt{j}=1}^{m}\delta_{\mathtt{j}}\int_{\mathcal{J}_{\mathtt{j}}}\tau^{\ell_1-1}\mathrm{d}\mho(\tau)=0.14948324,\ \delta=\sum_{\mathtt{j}=1}^{m}\delta_{\mathtt{j}}\int_{\mathcal{J}_{\mathtt{j}}}\mathrm{d}\mho(\mathtt{s})=\frac{3}{20},$$

$$\int_{\varepsilon_1}^{1-\varepsilon_1}\aleph(\tau)\phi^{-1}\Big[\int_{\varepsilon_1}^{\tau}\lambda(\mathtt{s})\mathrm{d}\mathtt{s}\Big]\mathrm{d}\tau\approx 0.003168742754,$$

$$\frac{\varepsilon_1^{3\ell_1-2}(1-\Delta+\delta)}{1-\Delta}\int_{\varepsilon_1}^{1-\varepsilon_1}\aleph(\tau)\phi^{-1}\Big[\int_{\varepsilon_1}^{\tau}\lambda(\mathtt{s})\mathrm{d}\mathtt{s}\Big]\mathrm{d}\tau\approx 0.0001432166715.$$

So, $\eta=\max\left\{\frac{1}{0.0001432166715},1\right\}=6982.427322$. Next, let $\mathtt{p}=\mathtt{q}=2$. Then

$$\|\aleph\|_{\mathtt{q}}=\left[\int_0^1|\aleph(\tau)|^2\mathrm{d}\tau\right]^{\frac{1}{2}}\approx 0.143619053,\ \|\psi\|_{\mathtt{p}}=\left[\int_0^1|\phi^{-1}(\lambda(\tau))|^2\mathrm{d}\tau\right]^{\frac{1}{2}}\approx 1.652891650.$$

So, $\mathtt{M}_1 < \dfrac{1-\Delta}{(\ell_1-1)(1-\Delta+\delta)\|\aleph\|_{\mathtt{q}}\left\|\phi^{-1}(\lambda(\cdot))\right\|_{\mathtt{p}}} \approx 2.685736039$. Taking $\mathtt{M}_1 = 2.5$. In addition, if we take $R_k = 10^{-8k}$, $r_k = 10^{-(8k+4)}$, then

$$R_{k+1} = 10^{-(8k+8)} < \frac{3}{12500} \times 10^{-(8k+4)} < \frac{\varepsilon_k^{3\ell_1-2}}{\ell_1-1} r_k < r_k = 10^{-(8k+4)} < R_k = 10^{-8k},$$

$\eta r_k = 6982.427322 \times 10^{-(8k+4)} < 2.5 \times 10^{-8k} = \mathtt{M}_1 R_k$, $k = 1, 2, 3, \cdots$, and $\mathtt{g}_{\mathtt{i}}$ satisfies the following growth conditions:

$$\mathtt{g}_{\mathtt{i}}(\mathtt{z}) \le \phi(\mathtt{K}_1 R_k) = \mathtt{M}_1^2 R_k^2 = 6.25 \times 10^{-16k}, \quad \mathtt{z} \in \left[0, 10^{-16k}\right]$$

$$\mathtt{g}_{\mathtt{i}}(\mathtt{z}) \ge \phi(\eta r_k) = \eta^2 r_k^2 = 48754291.31 \times 10^{-(16k+8)}, \quad \mathtt{z} \in \left[\frac{3}{12500} \times 10^{-(16k+8)}, 10^{-(16k+8)}\right].$$

Then all the conditions of Theorem 3 are satisfied. Therefore, by Theorem 3, the boundary value problem (11)–(12) has infinitely many positive solutions $\{\mathtt{z}_{\mathtt{i}}^{[k]}\}_{k=1}^{\infty}$ such that $10^{-(8k+4)} \le \|\mathtt{z}_{\mathtt{i}}^{[k]}\| \le 10^{-8k}$ for each $\mathtt{i} = 1, 2, 3, \cdots, n$, $k = 1, 2, 3, \cdots$.

Example 2 Consider the following fractional order boundary value problem,

$$\left.\begin{gathered} \frac{d}{dt}\left[\phi(\mathtt{D}_{0^+}^{5/2}\mathtt{z}_{\mathtt{i}}(\mathtt{t}))\right] + \lambda(\mathtt{t})\mathtt{g}_{\mathtt{i}}(\mathtt{z}_{\mathtt{i}+1}(\mathtt{t})) = 0,\ 0 < \mathtt{t} < 1,\ \mathtt{i} = 1, 2, \\ \mathtt{z}_3(\mathtt{t}) = \mathtt{z}_1(\mathtt{t}),\ 0 < \mathtt{t} < 1, \end{gathered}\right\} \tag{13}$$

$$\mathtt{z}_{\mathtt{i}}(0) = \mathtt{D}_{0^+}^{1/2}\mathtt{z}_{\mathtt{i}}(0) = \mathtt{D}_{0^+}^{5/2}(\mathtt{z}_{\mathtt{i}}(0)) = 0,\ \mathtt{z}_{\mathtt{i}}(1) = \sum_{\mathtt{j}=1}^{2} \delta_{\mathtt{j}} \int_{\mathcal{J}_{\mathtt{j}}} \mathtt{z}_{\mathtt{i}}(\tau)\mathrm{d}\mho(\tau),\ \mathtt{i} = 1, 2, \tag{14}$$

where $\delta_1 = 0.1$, $\delta_2 = 0.2$, $\mathcal{J}_1 = [0.5, 0.9]$, $\mathcal{J}_2 = [0.6, 0.8]$, $\lambda(\mathtt{t}) = \dfrac{1}{|t - \frac{1}{3}|^{1/2}}$,

$$\phi(\mathtt{z}) = \begin{cases} \dfrac{\mathtt{z}^3}{1+\mathtt{z}^2}, & \mathtt{z} \le 0, \\ \mathtt{z}^2, & \mathtt{z} > 0, \end{cases}$$

and

$$\mathtt{g}_{\mathtt{i}}(\mathtt{z}) = \begin{cases} 25 \times 10^{-16}, & \mathtt{z} \in (10^{-16}, +\infty), \\ \frac{26930632\times10^{-(16k+8)} - 25\times10^{-16k}}{10^{-(16k+8)} - 10^{-16k}}(\mathtt{z} - 10^{-16k}) + 105 \times 10^{-16k}, & \\ \qquad \mathtt{z} \in \left[10^{-(16k+8)}, 10^{-16k}\right], & \\ 26930632 \times 10^{-(16k+8)}, & \mathtt{z} \in \left(\frac{1}{10504} \times 10^{-(16k+8)}, 10^{-(16k+8)}\right), \\ \frac{26930632\times10^{-(16k+8)} - 25\times10^{-(16k+16)}}{\frac{1}{10504}\times10^{-(16k+8)} - 10^{-(16k+16)}}(\mathtt{z} - 10^{-(16k+16)}) + 25 \times 10^{-(16k+16)}, & \\ \qquad \mathtt{z} \in \left(10^{-(16k+16)}, \frac{1}{10504} \times 10^{-(16k+8)}\right], & \end{cases}$$

for $\mathtt{i} = 1, 2$, and

$$\mho(\mathtt{t}) = \begin{cases} \mathtt{t}, & \mathtt{t} \in [0, 2/5) \cup [3/5, 4/5), \\ \frac{2}{5}, & \mathtt{t} \in [2/5, 3/5), \\ \frac{4}{5}, & \mathtt{t} \in [4/5, 1]. \end{cases}$$

Let t_k and ε_k be as in Example 1. Then $\varepsilon_1 = \frac{15}{32} - \frac{1}{648} < \frac{15}{32}$, $t_{k+1} < \varepsilon_k < \mathtt{t}_k$, $\varepsilon_k > \frac{1}{5}$. Also, $\frac{\varepsilon_k^{3\ell_1-2}}{\ell_1-1} > \frac{1}{10504}$, $k = 1, 2, 3, \cdots$, and

$$\mathtt{t}^* = \lim_{j\to\infty} \mathtt{t}_j = \frac{31}{64} - \sum_{i=1}^{\infty} \frac{1}{4(i+1)^4} = \frac{47}{64} - \frac{\pi^4}{360} > \frac{1}{5},$$

$$\Delta = \sum_{\mathtt{j}=1}^{m} \delta_{\mathtt{j}} \int_{\mathcal{J}_{\mathtt{j}}} \tau^{\ell_1-1} \mathrm{d}\mho(\tau) = 0.127464, \ \delta = \sum_{\mathtt{j}=1}^{m} \delta_{\mathtt{j}} \int_{\mathcal{J}_{\mathtt{j}}} \mathrm{d}\mho(\mathtt{s}) \approx 0.12,$$

$$\int_{\varepsilon_1}^{1-\varepsilon_1} \aleph(\tau)\phi^{-1}\Big[\int_{\varepsilon_1}^{\tau} \lambda(\mathtt{s})\mathrm{d}\mathtt{s}\Big]\mathrm{d}\tau \approx 0.0048436344,$$

$$\frac{\varepsilon_1^{3\ell_1-2}(1-\Delta+\delta)}{1-\Delta} \int_{\varepsilon_1}^{1-\varepsilon_1} \aleph(\tau)\phi^{-1}\Big[\int_{\varepsilon_1}^{\tau} \lambda(\mathtt{s})\mathrm{d}\mathtt{s}\Big]\mathrm{d}\tau \approx 0.000135327645.$$

So, $\eta = \max\left\{\frac{1}{0.000135327645}, 1\right\} = 5189.47316$. Next, let $\mathtt{p} = \mathtt{q} = 2$. Then

$$\|\aleph\|_{\mathtt{q}} = \left[\int_0^1 |\aleph(\tau)|^2 \mathrm{d}\tau\right]^{\frac{1}{2}} \approx 0.143619053, \ \|\psi\|_{\mathtt{p}} = \left[\int_0^1 |\phi^{-1}(\lambda(\tau))|^2 \mathrm{d}\tau\right]^{\frac{1}{2}} \approx 1.326356.$$

So, $\mathtt{M}_1 < \dfrac{1-\Delta}{(\ell_1-1)(1-\Delta+\delta)\|\aleph\|_{\mathtt{q}} \left\|\phi^{-1}(\lambda(\cdot))\right\|_{\mathtt{p}}} \approx 5.63436346$. Taking $\mathtt{M}_1 = 5.2$. In addition, if we take $R_k = 10^{-8k}$, $r_k = 10^{-(8k+4)}$, then

$$R_{k+1} = 10^{-(8k+8)} < \frac{1}{10504} \times 10^{-(8k+4)} \le \frac{\varepsilon_k^{3\ell_1-2}}{\ell_1-1} r_k < r_k = 10^{-(8k+4)} < R_k = 10^{-8k},$$

$\eta r_k = 5189.47316 \times 10^{-(8k+4)} < 5.2 \times 10^{-8k} = \mathtt{M}_1 R_k$, $k = 1, 2, 3, \cdots$, and $\mathtt{g}_{\mathtt{i}}$ satisfies the following growth conditions:

$$\mathtt{g}_{\mathtt{i}}(\mathtt{z}) \le \phi(\mathtt{M}_1 R_k) = \mathtt{M}_1^2 R_k^2 = 27.04 \times 10^{-16k}, \ \ \mathtt{z} \in \left[0, 10^{-16k}\right]$$

$$\mathtt{g}_{\mathtt{i}}(\mathtt{z}) \ge \phi(\eta r_k) = \eta^2 r_k^2 = 26930631.68 \times 10^{-(16k+8)}, \ \ \mathtt{z} \in \left[\frac{1}{10504} \times 10^{-(16k+8)}, 10^{-(16k+8)}\right].$$

Then all the conditions of Theorem 3 are satisfied. Therefore, by Theorem 3, the boundary value problem (11)–(12) has infinitely many positive solutions $\{\mathtt{z}_{\mathtt{i}}^{[k]}\}_{k=1}^{\infty}$ such that $10^{-(8k+4)} \le \|\mathtt{z}_{\mathtt{i}}^{[k]}\| \le 10^{-8k}$ for each $\mathtt{i} = 1, 2, 3, \cdots, n$, $k = 1, 2, 3, \cdots$.

5 Conclusion

The research of fractional order differential equations with multistrip Riemann–Stieltjes integral boundary conditions has become a new area of investigation. Moreover, in this paper we considered iterative system with singularities. By the use of Krasnoselskii's cone fixed point theorem in a Banach space, sufficient conditions are derived for the existence of infinitely many positive solutions for the problem. An example is presented to illustrate the main results. The conclusion obtained in this paper will be useful in the application point of view. Also, we expect to find some applications in more nonlinear problems.

Acknowledgements The authors would like to thank the referees for their valuable suggestions and comments for the improvement of the paper.

Author Contributions The study was carried out in collaboration of all authors. All authors read and approved the final manuscript.

Funding Not applicable.

Data availibility statement Data sharing not applicable to this paper as no data sets were generated or analyzed during the current study.

Declarations

Conflict of interest It is declared that authors has no competing interests.

Ethical approval This article does not contain any studies with human participants or animals performed by any of the authors.

References

1. Abdeljawad, T., Jarad, F., Alzabut, J.: Fractional proportional differences with memory. Eur. Phys. J. Spec. Top. **226**(16–18), 3333–3354 (2018). https://doi.org/10.1140/epjst/e2018-00053-5
2. Abdeljawad, T., Jarad, F., Mallak, S.F., Alzabut, J.: Lyapunov type inequalities via fractional proportional derivatives and application on the free zero disc of Kilbas-Saigo generalized Mittag-Leffler functions. Eur. Phys. J. Plus **134**(5), 247 (2019)
3. Ahmad, B., Alsaedi, A., Alruwaily, Y.: On Riemann-Stieltjes integral boundary value problems of Caputo-Riemann-Liouville type fractional integro-differential equations. Filomat **34**(8), 2723–2738 (2020)
4. Alsaedi, A., Alghamdi, N., Ahmad, Bashir, Ntouyas, S.K.: Nonlinear three-point multi-term multivalued fractional order boundary value problems. Matematički Vesnik **72**(1), 66–80 (2020)
5. Cannon, J.: The solution of the heat equation subject to the specification of energy. Q. Appl. Math. **21**, 155–160 (1963)
6. Chegis, R.: Numerical solution of a heat conduction problem with an integral boundary condition. Litovsk. Mat. Sb **24**, 209–215 (1984)
7. de Lemos, M. J. S.: Turbulence in Porous Media. Modeling and Applications, 2nd edn., Elsevier, Oxford, UK (2012)
8. Ege, S.M., Topal, F.S.: Existence of positive solutions for fractional order boundary value problems. J. Appl. Anal. Comp. **7**(2), 702–712 (2017)
9. Guo, D., Lakshmikantham, V.: Nonlinear Problems in Abstract Cones. Academic Press, San Diego (1988)
10. Khuddush, M., Prasad, K.R.: Infinitely many positive solutions for an iterative system of conformable fractional order dynamic boundary value problems on time scales. Turk. J. Math. (2021). https://doi.org/10.3906/mat-2103-117
11. Khuddush, M., Prasad, K.R.: Existence, uniqueness and stability analysis of a tempered fractional order thermistor boundary value problems. J. Anal. (2022). https://doi.org/10.1007/s41478-022-00438-6
12. Khuddush, M., Prasad, K.R.: Iterative system of nabla fractional difference equations with two-point boundary conditions. Math. Appl. **11**(1), 57–74 (2022)
13. Khuddush, M., Prasad, K.R., Leela, D.: Existence of solutions for an infinite system of tempered fractional order boundary value problems in the spaces of tempered sequences. Turk. J. Math. **46**, 433–452 (2022). https://doi.org/10.3906/mat-2106-110
14. Kilbas, A.A., Srivastava, H.M., Trujillo, J.J.: Theory and applications of fractional differential equations, North-Holland Mathematics Studies 204. Elsevier Science B. V., Amsterdam (2006)
15. Leibenson, L.S.: General problem of the movement of a compressible fluid in a porous medium. Izvestiia Akademii Nauk Kirgizskoi SSR **9**, 7–10 (1983)
16. Ljung, A.L., Frishfelds, V., Lundström, T.S., Marjavaara, B.D.: Discrete and continuous modeling of heat and mass transport in drying of a bed of iron ore pellets. Dry. Technol. **30**(7), 760–773 (2012)
17. Miller, K.S., Ross, B.: An Introduction to the Fractional Calculus and Fractional Differential Equation. Wiley, New York (1993)
18. Podlubny, I.: Fractional Differential Equations. Academic Press, San Diego (1999)

19. Prasad, K.R., Khuddush, M., Leela, D.: Existence of solutions for n-dimensional fractional order hybrid BVPs with integral boundary conditions by an application of n-fixed point theorem. J. Anal. (2021). https://doi.org/10.1007/s41478-020-00291-5
20. Prasad, K.R., Khuddush, M., Leela, D.: Existence, uniqueness and Hyers-Ulam stability of a fractional order iterative two-point boundary value Problems. Afr. Mat. (2021). https://doi.org/10.1007/s13370-021-00895-5
21. Prasad, K.R., Leela, D., Khuddush, M.: Existence and uniqueness of positive solutions for system of (p, q, r)-Laplacian fractional order boundary value problems. Adv. Theory Nonlinear Anal. Appl. **5**(1), 138–157 (2021). https://doi.org/10.31197/atnaa.703304
22. Prasad, K.R., Khuddush, M., Veeraiah, P.: Countably infinitely many positive solutions for iterative system of singular RL fractional order bvp with RS integral boundary conditions. J. Interdiscipl. Math. (2022). https://doi.org/10.1080/09720502.2021.1936636
23. Saadi, A., Benbachir, M.: Positive solutions for three-point nonlinear fractional boundary value problems. Electron. J. Qual. Theory Diff. Equ. **3**, 1–19 (2011)
24. Song, S., Cui, Y.: Existence of solutions for integral boundary value problems of mixed fractional differential equations under resonance. Bound. Value Probl. **1**, 1–12 (2020)
25. Srivastava, H.M.: Diabetes and its resulting complications: mathematical modeling via fractional calculus. Public Health Open Access **4**(3), 1–5 (2020)
26. Srivastava, H.M., Saad, K.M., Khader, M.M.: An efficient spectral collocation method for the dynamic simulation of the fractional epidemiological model of the Ebola virus. Chaos, Solitons Fractals **140**, 1–7 (2020)
27. Sudsutad, W., Alzabut, J., Nontasawatsri, S., Thaiprayoon, C.: *Stability analysis for a generalized proportional fractional Langevin equation with variable coefficient and mixed integro-differential boundary conditions*. J. Nonlinear Funct. Anal. Article ID 23, 1–24 (2020)
28. Sudsutad, W., Alzabut, J., Tearnbucha, C., Thaiprayoon, C.: On the oscillation of differential equations in frame of generalized proportional fractional derivatives. AIMS Math. **5**(2), 856–871 (2020). https://doi.org/10.3934/math.2020058
29. Torres, F.J.: Existence of a positive solution for a boundary value problem of a nonlinear fractional differential equation. BIMS **39**(2), 307–323 (2013)
30. Victor, D.W.J., Khuddush, M.: Existence of solutions for n-dimensional fractional order bvp with ∞-point boundary conditions via the concept of measure of noncompactness. Adv. Stud.: Euro-Tbilisi Math. J. **15**(1), 19–37 (2022). https://doi.org/10.32513/asetmj/19322008202
31. Zhang, S.Q.: Existence results of positive solutions to fractional differential equation with integral boundary conditions. Math. Bohem. **135**(2), 299–317 (2010)
32. Zhou, Y.: Basic Theory of Fractional Differential Equations. World Scientific, Singapore (2014)

Publisher's Note Springer Nature remains neutral with regard to jurisdictional claims in published maps and institutional affiliations.

Springer Nature or its licensor holds exclusive rights to this article under a publishing agreement with the author(s) or other rightsholder(s); author self-archiving of the accepted manuscript version of this article is solely governed by the terms of such publishing agreement and applicable law.

Journal of Elliptic and Parabolic Equations (2022) 8:919–938
https://doi.org/10.1007/s41808-022-00181-w

Global existence and blow-up of solutions for a p-Kirchhoff type parabolic equation with logarithmic nonlinearity

Mahammad Khuddush[1] · **Rajendra Prasad Kapula**[2] · **Sa-Botta Bharathi**[3]

Received: 8 June 2022 / Accepted: 10 August 2022 / Published online: 25 August 2022
© Orthogonal Publisher and Springer Nature Switzerland AG 2022

Abstract
In this paper a class of p-Kirchhoff type parabolic equation with logarithmic nonlinearity is considered. By applying Galerkin's approximation and the modified potential well method, some sufficient conditions are obtained for the existence of global and finite blow up of solutions.

Keywords p-Kirchhoff · Potential well · Global existence · Blow up · Logarithmic nonlinearity

Mathematics Subject Classification 35K20 · 35K92

1 Introduction

In recent years researchers are shown much attention to study Kirchhoff type problems for their applications to the modeling of various physical and biological phenomena. More specifically, Kirchhoff [11] proposed the following Kirchhoff model

$$\varrho\frac{\partial^2\varpi}{\partial t^2}-\left(\frac{P_0}{h}-\frac{E}{2L}\int_0^L\left|\frac{\partial\varpi}{\partial x}\right|dx\right)\frac{\partial^2\varpi}{\partial x^2}=0,$$

and is a generalization of the D'Alembert wave equation for free vibrations of elastic strings, here L is the length of the string, h is the area of the cross section, E is the

✉ Mahammad Khuddush
khuddush89@gmail.com

[1] Department of Mathematics, Dr. Lankapalli Bullayya College of Engineering, Visakhapatnam, Andhra Pradesh 530013, India

[2] Department of Applied Mathematics, College of Science and Technology, Andhra University, Visakhapatnam 530003, India

[3] Department of Mathematics, College of Engineering for Women Gayatri Vidya Parishad, Visakhapatnam 530048, India

Young modulus of the material, ϱ is the mass density and P_0 is the initial tension. For the existence, uniqueness and regularities of solutions to Kirchhoff type equations were well studied by various authors, see [2, 3, 7–10, 16, 18] and the references therein. When the length changes of the string produced by transverse vibrations is taken into account, the classical D'Alembert wave equation for free vibrations of elastic strings is given by (see [5])

$$\epsilon\varpi_{tt}^{\epsilon} + \varpi_{t}^{\epsilon} - \mathtt{M}\left(\int_{\Omega} |\nabla\varpi^{\epsilon}|^{\mathtt{p}} dx\right)\Delta_{\mathtt{p}}\varpi^{\epsilon} = \mathtt{f}(t, x, \varpi^{\epsilon})$$

where $\mathtt{M}(\tau) = \alpha + \beta\tau$, $\alpha, \beta > 0$ and $\mathtt{p} > 1$. Fu and Xian [4] studied the following Kirchhoff type parabolic equation

$$\varpi_{t} - \mathtt{M}\left(\int_{\Omega} |\nabla\varpi|^{\mathtt{p}} dx\right)\Delta_{\mathtt{p}}\varpi = \mathtt{f}(t, x, \varpi)$$

which describes the motion of a nonstationary fluid in a nonhomogeneous and anisotropic medium. Chipot and Savitska [1] studied the following class of nonlinear nonlocal diffusion problems associated with a p-Laplace type operator

$$\varpi_{t} - \nabla \cdot \left(\alpha\|\nabla\varpi\|_{\mathtt{p}}^{\mathtt{p}}\right)|\nabla\varpi|^{\mathtt{p}-2}\nabla\varpi = \mathtt{f}(x)$$

with the same boundary conditions of (1) and established the existence, uniqueness and asymptotic behavior of solutions to the problem. Based on mountain pass theorem and the Nehari manifold, Sattinger [17] first to study the following nonlinear hyperbolic equation

$$\varpi_{tt} - \nabla^2\varpi + f(x, \varpi) = 0$$

by introducing potential well method. Leter Liu [14] and Liu and Zhao[15] modified the standard potential well method by introducing a family of potential wells which include the known one as a special case. By using this modified potential well method they derived a threshold result for global existence and nonexistence of solutions when the initial energy is subcritical.

Recently, Han and Li [6] by applying the modified potential well method and variational method to study the long time behaviors of solutions, i.e., global existence and blow up in finite time of solutions are obtained for arbitrary initial energy to a class of parabolic equation of Kirchhoff type

$$\varpi_{t} - \left(\alpha + \beta\int_{\Omega} |\nabla\varpi|^{2} dx\right)\Delta\varpi = |\varpi|^{\mathtt{q}-1}\varpi.$$

More recently, Li and Han [13] studied the following p-Kirchhoff equation,

$$\varpi_{t} - \left(\alpha + \beta\int_{\Omega} |\nabla\varpi|^{\mathtt{p}} dx\right)\Delta_{\mathtt{p}}\varpi = |\varpi|^{\mathtt{q}-1}\varpi$$

and by applying Galerkin's approximation and the modified potential well method, they obtained a threshold result for the solutions to exist globally or to blow up in finite time for subcritical and critical initial energy. Motivated by aforementioned works in this paper, we study p-Kirchhoff type parabolic equation with logarithmic nonlinearity

$$\begin{cases} \varpi_t - \left(\alpha + \beta \int_\Omega |\nabla \varpi|^{\mathrm{p}} dx\right) \Delta_{\mathrm{p}} \varpi = |\varpi|^{\mathrm{q}-2} \varpi \ln |\varpi|^k, \quad (x,t) \in \Omega \times (0,T), \\ \varpi(x,t) = 0, \quad (x,t) \in \partial\Omega \times (0,T), \\ \varpi(x,0) = \varpi_0(x), \quad x \in \Omega, \end{cases} \tag{1}$$

where $k(>1), \alpha, \beta$ are positive real numbers, $\Delta_{\mathrm{p}} \varpi = \mathrm{div}\left(|\nabla \varpi|^{\mathrm{p}-2} |\nabla \varpi|\right)$ is a p-Laplacian operator with $\mathrm{p} > \max\{2n/(n+2), 1\}, 2\mathrm{p} < \mathrm{q} < \mathrm{p}^* - 1$, p^* is the Sobolev conjugate of p. i.e., $\mathrm{p}^* = +\infty$ for $n \le \mathrm{p}$ and $\mathrm{p}^* = n\mathrm{p}/(n-\mathrm{p})$ for $n > \mathrm{p}$, $\Omega \subset \mathbb{R}^n, n \ge 1$ is a bounded smooth domain with the boundary $\partial\Omega$ and $\varpi_0 \in \mathbb{W}_0^{1,\mathrm{p}}(\Omega)$.

2 Preliminaries

In this paper, we use $\mathbb{W}_0^{1,\mathrm{p}}(\Omega)$ to denote the Sobolev space equipped with the norm $\|\varpi\|_{\mathbb{W}_0^{1,\mathrm{p}}(\Omega)} = \|\nabla \varpi\|_{\mathrm{p}}$. We denote by $\|\cdot\|_{\mathrm{q}}$ the Lebesgue space $L^{\mathrm{q}}(\Omega), (1 \le \mathrm{q} \le \infty)$ norm and by $(\cdot,\cdot)$ the inner product in $L^2(\Omega)$. To establish main results of the paper, we required the following definitions and lemmas.

2.1 Potential wells

Define two real-valued $\mathcal{C}^1$ functionals on $\mathbb{W}_0^{1,\mathrm{p}}(\Omega)$, known as potential energy and Nehari functionals and are

$$\mathtt{J}(\varpi) = \frac{\alpha}{\mathrm{p}} \|\nabla \varpi\|_{\mathrm{p}}^{\mathrm{p}} + \frac{\beta}{2\mathrm{p}} \|\nabla \varpi\|_{\mathrm{p}}^{2\mathrm{p}} - \frac{k}{\mathrm{q}} \int_\Omega |\varpi|^{\mathrm{q}} \log |\varpi| dx + \frac{k}{\mathrm{q}^2} \|\varpi\|_{\mathrm{q}}^{\mathrm{q}},$$

and

$$\mathtt{I}(\varpi) = \alpha \|\nabla \varpi\|_{\mathrm{p}}^{\mathrm{p}} + \beta \|\nabla \varpi\|_{\mathrm{p}}^{2\mathrm{p}} - k \int_\Omega |\varpi|^{\mathrm{q}} \log |\varpi| dx.$$

Next, define Nehari's manifolds as

$$\mathcal{N} = \left\{ \varpi \in \mathbb{W}_0^{1,\mathtt{p}}(\Omega) \mid \mathtt{I}(\varpi) = 0, \|\nabla \varpi\|_{\mathtt{p}} \neq 0 \right\},$$
$$\mathcal{N}^+ = \left\{ \varpi \in \mathbb{W}_0^{1,\mathtt{p}}(\Omega) \mid \mathtt{I}(\varpi) > 0 \right\},$$
$$\mathcal{N}^- = \left\{ \varpi \in \mathbb{W}_0^{1,\mathtt{p}}(\Omega) \mid \mathtt{I}(\varpi) < 0 \right\},$$

and the depth of the potential well (or mountain pass level) as

$$\mathtt{d} = \inf_{\varpi \in \mathbb{W}_0^{1,\mathtt{p}}(\Omega)\setminus\{0\}} \sup_{\lambda \geq 0} \mathtt{J}(\lambda \varpi) = \inf_{\varpi \in \mathcal{N}} \mathtt{J}(\varpi).$$

Finally, we define the potential well

$$\mathcal{W} = \left\{ \varpi \in \mathbb{W}_0^{1,\mathtt{p}}(\Omega) \mid \mathtt{I}(\varpi) > 0, \mathtt{J}(\varpi) < \mathtt{d} \right\} \cup \{0\},$$

and the outer of the potential well

$$\mathcal{V} = \left\{ \varpi \in \mathbb{W}_0^{1,\mathtt{p}}(\Omega) \mid \mathtt{I}(\varpi) < 0, \mathtt{J}(\varpi) < \mathtt{d} \right\}.$$

Definition 1 The function $\varpi = \varpi(x,t)$ is said to be a weak solutions of (1) on $\Omega \times [0,T)$ if $\varpi \in L^{\infty}\left(0,T;\mathbb{W}_0^{1,\mathtt{p}}(\Omega)\right)$ with $\varpi_t \in L^2\left(0,T;L^2(\Omega)\right)$ such that $\varpi(x,0) = \varpi_0(x) \in \mathbb{W}_0^{1,\mathtt{p}}(\Omega)$ and

$$\begin{cases} (\varpi_t, \omega) + \left(\left[\alpha + \beta \displaystyle\int_\Omega |\nabla \varpi|^{\mathtt{p}} dx \right] |\nabla \varpi|^{\mathtt{p}-2} |\nabla \varpi|, \nabla \omega \right) \\ \qquad = \left(|\varpi|^{\mathtt{q}-2} \varpi \log |\varpi|^k, \omega \right), \ \text{ a.e. } t \in (0,T), \end{cases} \tag{2}$$

for any $\omega \in \mathbb{W}_0^{1,p}(\Omega)$ and $\varpi(x,t)$ satisfies

$$\int_0^t \|\varpi_\tau\|_2^2 d\tau + \mathtt{J}(\varpi(x,t)) = \mathtt{J}(\varpi_0), \ \text{ a.e. } t \in (0,T). \tag{3}$$

Lemma 1 $\mathtt{d}$ *is positive*.

Proof Since $\mathtt{q}+1 < \mathtt{p}^*$, it follows that $\mathbb{W}_0^{1,p}(\Omega)$ can be embedded in $L^{\mathtt{q}+1}(\Omega)$. Let $\mathtt{C}$ be an embedded constant. Then $\|\varpi\|_{\mathtt{q}+1} \leq \mathtt{C}\|\nabla \varpi\|_{\mathtt{p}}$ for $\varpi \in \mathbb{W}_0^{1,p}(\Omega)$. So for any $\varpi \in \mathcal{N}$, we have

$$\begin{aligned} \alpha \|\nabla \varpi\|_{\mathtt{p}}^{\mathtt{p}} \leq \alpha \|\nabla \varpi\|_{\mathtt{p}}^{\mathtt{p}} + \beta \|\nabla \varpi\|_{\mathtt{p}}^{2\mathtt{p}} &= k \int_\Omega |\varpi|^{\mathtt{q}} \log |\varpi| dx \leq k \|\varpi\|_{\mathtt{q}+1}^{\mathtt{q}+1} \\ &\leq k \mathtt{C}^{\mathtt{q}+1} \|\nabla \varpi\|_{\mathtt{p}}^{\mathtt{q}+1}. \end{aligned}$$

From the above inequality, we get

$$\|\nabla \varpi\|_{\mathtt{p}} \geq \left(\frac{\alpha}{k \mathtt{C}^{\mathtt{q}+1}} \right)^{1/(\mathtt{q}+1-\mathtt{p})}.$$

Since $q > 2p$, we have

$$\begin{aligned} J(\varpi) &= \frac{\alpha}{p}\|\nabla\varpi\|_p^p + \frac{\beta}{2p}\|\nabla\varpi\|_p^{2p} - \frac{k}{q}\int_\Omega |\varpi|^q \log|\varpi| dx + \frac{k}{q^2}\|\varpi\|_q^q \\ &= \frac{\alpha}{p}\|\nabla\varpi\|_p^p + \frac{\beta}{2p}\|\nabla\varpi\|_p^{2p} - \frac{1}{q}\left[\alpha\|\nabla\varpi\|_p^p + \beta\|\nabla\varpi\|_p^{2p}\right] + \frac{k}{q^2}\|\varpi\|_q^q \\ &\geq \frac{\alpha(q-p)}{pq}\|\nabla\varpi\|_p^p + \frac{\beta(q-2p)}{2pq}\|\nabla\varpi\|_p^{2p} \\ &\geq \frac{\alpha(q-p)}{pq}\left(\frac{\alpha}{kC^{q+1}}\right)^{p/(q+1-p)} + \frac{\beta(q-2p)}{2pq}\left(\frac{\alpha}{kC^{q+1}}\right)^{2p/(q+1-p)}. \end{aligned}$$

Thus,

$$d \geq \frac{\alpha(q-p)}{pq}\left(\frac{\alpha}{kC^{q+1}}\right)^{p/(q+1-p)} + \frac{\beta(q-2p)}{2pq}\left(\frac{\alpha}{kC^{q+1}}\right)^{2p/(q+1-p)}.$$

This completes the proof. □

Next, for any $\delta > 0$, define the modified Nehari's functional and Nehari's manifold as follows:

$$\begin{aligned} I_\delta(\varpi) &= \delta\Big(\alpha + \beta\|\nabla\varpi\|_p^p\Big)\|\nabla\varpi\|_p^p - k\int_\Omega |\varpi|^q \log|\varpi| dx, \\ \mathcal{N}_\delta &= \Big\{\varpi \in \mathbb{W}_0^{1,p}(\Omega) \mid I_\delta(\varpi) = 0, \|\nabla\varpi\|_p \neq 0\Big\}. \end{aligned}$$

The depth of the modified potential well (or mountain pass level) is given by

$$d(\delta) = \inf_{\varpi\in\mathcal{N}_\delta} J(\varpi).$$

Then the modified potential well and outer of the modified potential well are given respectively by

$$\begin{aligned} \mathcal{W}_\delta &= \Big\{\varpi \in \mathbb{W}_0^{1,p}(\Omega) \mid I_\delta(\varpi) > 0, J(\varpi) < d(\delta)\Big\} \cup \{0\}, \\ \mathcal{V}_\delta &= \Big\{\varpi \in \mathbb{W}_0^{1,p}(\Omega) \mid I_\delta(\varpi) < 0, J(\varpi) < d(\delta)\Big\}. \end{aligned}$$

Lemma 2 *Let $\varpi \in \mathbb{W}_0^{1,p}(\Omega)$ with $\|\varpi\| \neq 0$ and let $f(\lambda) = J(\lambda\varpi)$, then we have*

(i) $\lim_{\lambda\to 0} f(\lambda) = 0$ *and* $\lim_{\lambda\to+\infty} f(\lambda) = -\infty$.
(ii) *there exists unique $\lambda^* = \lambda^*(\varpi)$ in the interval $(0, +\infty)$ such that $f'(\lambda)|_{\lambda=\lambda^*} = 0$, $f(\lambda) \nearrow$ on $[0, \lambda^*]$. $f(\lambda) \searrow$ on $[\lambda^*, +\infty)$ and takes maximum at $\lambda = \lambda^*$.*
(iii) $I(\lambda\varpi) > 0$ *on* $(0, \lambda^*)$, $I(\lambda\varpi) < 0$ *on* $(\lambda^*, +\infty)$ *and* $I(\lambda^*\varpi) = 0$.

Proof (*i*) We have

$$\begin{aligned}\mathtt{f}(\lambda) &= \mathtt{J}(\lambda\varpi)\\ &= \lambda^{\mathtt{p}}\frac{\alpha}{\mathtt{p}}\|\nabla\varpi\|_{\mathtt{p}}^{\mathtt{p}} + \lambda^{2\mathtt{p}}\frac{\beta}{2\mathtt{p}}\|\nabla\varpi\|_{\mathtt{p}}^{2\mathtt{p}} - \lambda^{\mathtt{q}}\frac{k}{\mathtt{q}}\int_\Omega |\varpi|^{\mathtt{q}}\log|\lambda\varpi|dx + \lambda^{\mathtt{q}}\frac{k}{\mathtt{q}^2}\|\varpi\|_{\mathtt{q}}^{\mathtt{q}}\\ &= \lambda^{\mathtt{p}}\frac{\alpha}{\mathtt{p}}\|\nabla\varpi\|_{\mathtt{p}}^{\mathtt{p}} + \lambda^{2\mathtt{p}}\frac{\beta}{2\mathtt{p}}\|\nabla\varpi\|_{\mathtt{p}}^{2\mathtt{p}} - \lambda^{\mathtt{q}}\frac{k}{\mathtt{q}}\int_\Omega |\varpi|^{\mathtt{q}}\log|\varpi|dx + \lambda^{\mathtt{q}}\frac{k}{\mathtt{q}^2}\|\varpi\|_{\mathtt{q}}^{\mathtt{q}}\\ &\quad - \lambda^{\mathtt{q}}\frac{k}{\mathtt{q}}\log\lambda\|\varpi\|_{\mathtt{q}}^{\mathtt{q}}.\end{aligned}$$

Since $\|\varpi\| \neq 0$, it follows that $\lim_{\lambda\to 0}\mathtt{f}(\lambda) = 0$ and $\lim_{\lambda\to+\infty}\mathtt{f}(\lambda) = -\infty$.

(*ii*) For any $\lambda > 0$, we have

$$\begin{aligned}\mathtt{f}'(\lambda) &= \alpha\lambda^{\mathtt{p}-1}\|\nabla\varpi\|_{\mathtt{p}}^{\mathtt{p}} + \beta\lambda^{2\mathtt{p}-1}\|\nabla\varpi\|_{\mathtt{p}}^{2\mathtt{p}}\\ &\quad - k\lambda^{\mathtt{q}-1}\int_\Omega |\varpi|^{\mathtt{q}}\log|\varpi|dx - k\lambda^{\mathtt{q}-1}\log\lambda\|\varpi\|_{\mathtt{q}}^{\mathtt{q}}\\ &= \lambda^{\mathtt{q}-1}\Big[\alpha\lambda^{\mathtt{p}-\mathtt{q}}\|\nabla\varpi\|_{\mathtt{p}}^{\mathtt{p}}\\ &\quad + \beta\lambda^{2\mathtt{p}-\mathtt{q}}\|\nabla\varpi\|_{\mathtt{p}}^{2\mathtt{p}} - k\int_\Omega |\varpi|^{\mathtt{q}}\log|\varpi|dx - k\log\lambda\|\varpi\|_{\mathtt{q}}^{\mathtt{q}}\Big].\end{aligned}$$

Let

$$\varphi(\lambda) = \alpha\lambda^{\mathtt{p}-\mathtt{q}}\|\nabla\varpi\|_{\mathtt{p}}^{\mathtt{p}} + \beta\lambda^{2\mathtt{p}-\mathtt{q}}\|\nabla\varpi\|_{\mathtt{p}}^{2\mathtt{p}} - k\int_\Omega |\varpi|^{\mathtt{q}}\log|\varpi|dx - k\log\lambda\|\varpi\|_{\mathtt{q}}^{\mathtt{q}}.$$

Since $2\mathtt{p} < \mathtt{q}$, we deduce that

$$\begin{aligned}\varphi'(\lambda) &= \alpha(\mathtt{p}-\mathtt{q})\lambda^{\mathtt{p}-\mathtt{q}-1}\|\nabla\varpi\|_{\mathtt{p}}^{\mathtt{p}} + \beta(2\mathtt{p}-\mathtt{q})\lambda^{2\mathtt{p}-\mathtt{q}-1}\|\nabla\varpi\|_{\mathtt{p}}^{2\mathtt{p}} - \frac{k}{\lambda}\|\varpi\|_{\mathtt{q}}^{\mathtt{q}}\\ &\leq \alpha(\mathtt{p}-\mathtt{q})\lambda^{\mathtt{p}-\mathtt{q}-1}\|\nabla\varpi\|_{\mathtt{p}}^{\mathtt{p}} + \beta(2\mathtt{p}-\mathtt{q})\lambda^{2\mathtt{p}-\mathtt{q}-1}\|\nabla\varpi\|_{\mathtt{p}}^{2\mathtt{p}}\\ &< 0\end{aligned} \tag{4}$$

and

$$\lim_{\lambda\to 0^+}\varphi(\lambda) = +\infty \qquad \lim_{\lambda\to+\infty}\varphi(\lambda) = -\infty. \tag{5}$$

Therefore, from (4) and (5) it is known that there exists a unique $\lambda^* = \lambda^*(\varpi) > 0$ such that $\varphi(\lambda^*) = 0$. Moreover, it follows from (4) that $\mathtt{f}'(\lambda)|_{\lambda=\lambda^*} = (\lambda^*)^{\mathtt{q}-1}\varphi(\lambda^*) = 0$. Since $\varphi(\lambda) > 0$ on $(0, \lambda^*)$ and $\varphi(\lambda) < 0$ on $(\lambda^*, +\infty)$, we get that $\mathtt{f}'(\lambda)$ is increasing on $0 < \lambda \leq \lambda^*$, decreasing on $\lambda^* \leq \lambda < +\infty$ and takes its maximum at $\lambda = \lambda^*$.

(*iii*) For any $\lambda > 0$, we have

$$\begin{aligned}\mathtt{I}(\lambda\varpi) &= \lambda^{\mathtt{p}}\alpha\|\nabla\varpi\|_{\mathtt{p}}^{\mathtt{p}} + \lambda^{2\mathtt{p}}\beta\|\nabla\varpi\|_{\mathtt{p}}^{2\mathtt{p}} - \lambda^{\mathtt{q}}k\int_\Omega |\varpi|^{\mathtt{q}}\log|\lambda\varpi|dx\\ &= \lambda\mathtt{f}'(\lambda).\end{aligned} \tag{6}$$

Then the results of (*iii*) follow from (*ii*) and the above equality (6). This completes proof. □

Lemma 3 *Let* $\mathtt{C}$ *be constant given in Lemma* 1 *and let*

$$\ell(\delta) = \left(\frac{\beta}{k\mathtt{C}^{q+1}}\right)^{1/(q+1-2p)}.$$

Then, we have

(i) $\mathtt{I}_\delta(\varpi) \geq 0$ *if* $0 < \|\nabla\varpi\|_p \leq \ell(\delta)$,
(ii) $\|\nabla\varpi\|_p > \ell(\delta)$ *if* $\mathtt{I}_\delta(\varpi) < 0$,
(iii) $\|\nabla\varpi\|_p > \ell(\delta)$ (or) $\|\nabla\varpi\|_p = 0$ *if* $\mathtt{I}_\delta(\varpi) = 0$.

Proof (*i*) Suppose $0 < \|\nabla\varpi\|_p \leq \ell(\delta)$. Then by Sobolev's inequality, we obtain

$$\begin{aligned} k\int_\Omega |\varpi|^q \log|\varpi| dx &\leq k\|\varpi\|_{q+1}^{q+1} \leq k\mathtt{C}^{q+1}\|\nabla\varpi\|_p^{q+1} \\ &= k\mathtt{C}^{q+1}\|\nabla\varpi\|_p^{q+1-2p}\|\nabla\varpi\|_p^{2p} \\ &\leq \beta\|\nabla\varpi\|_p^{2p} + \alpha\|\nabla\varpi\|_p^p. \end{aligned}$$

This proves (*i*). The proofs of (*ii*) and (*iii*) are very similar to (*i*), we omit details here. This completes proof. □

Lemma 4 *The function* $\mathtt{d}(\delta)$ *satisfies the following properties*:

(i) $\lim_{\lambda\to 0^+}\mathtt{d}(\delta) = 0$, $\lim_{\lambda\to+\infty}\mathtt{d}(\delta) = -\infty$.
(ii) $\mathtt{d}(\delta)$ *is increasing on* $0 < \delta \leq 1$, *decreasing on* $\delta \geq 1$, *and takes its maximum* $\delta = \delta(1)$ *at* $\delta = 1$.

Proof (*i*) For any $\varpi \in \mathbb{W}_0^{1,p}(\Omega)$, $\|\varpi\|_p \neq 0$ and for any $\delta > 0$, there exists a unique $\lambda = \lambda(\delta) > 0$ such that $\mathtt{I}_\delta(\lambda\varpi) = 0$. That is,

$$\lambda^p\delta\Big(\alpha + \lambda^p\beta\|\nabla\varpi\|_p^p\Big)\|\nabla\varpi\|_p^p - \lambda^q k\int_\Omega |\varpi|^q \log|\lambda\varpi| dx = 0. \tag{7}$$

From (7), we derive

$$\delta = \frac{\lambda^{q-p}k\int_\Omega |\varpi|^q \log|\lambda\varpi| dx}{\big(\alpha + \lambda^p\beta\|\nabla\varpi\|_p^p\big)\|\nabla\varpi\|_p^p}$$

Since $q > p$ and by above expression it can seen that δ is increasing with respect to λ on $(0, +\infty)$, which implies that the inverse function $\lambda(\delta)$ is also increasing on $\delta > 0$.

Furthermore, we can deduce from (7) that $\lim_{\delta\to 0}\lambda(\delta)=0$ and $\lim_{\delta\to+\infty}\lambda(\delta)=+\infty$. Since $\lambda\varpi\in\mathcal{N}_\delta$, $\mathtt{d}(\delta)\le \mathtt{J}(\lambda\varpi)$. It follows that

$$0\le\lim_{\delta\to 0}\mathtt{d}(\delta)\le\lim_{\delta\to 0}\mathtt{J}(\lambda\varpi)=\lim_{\lambda\to 0}\mathtt{J}(\lambda\varpi)=0.$$

That is

$$\lim_{\delta\to 0}\mathtt{d}(\delta)=0.$$

On the other hand,

$$\lim_{\delta\to+\infty}\mathtt{d}(\delta)\le\lim_{\delta\to+\infty}\mathtt{J}(\lambda\varpi)=\lim_{\lambda\to+\infty}\mathtt{J}(\lambda\varpi)=-\infty.$$

That is

$$\lim_{\delta\to 0}\mathtt{d}(\delta)=-\infty.$$

(*ii*) Clearly, we only need to prove that for any $0<\delta^*<\delta^{**}<1$ or $\delta^*>\delta^{**}>1$ and any $\varpi\in\mathcal{N}_{\delta^{**}}$ there exist a $\omega\in\mathcal{N}_{\delta^*}$ and a constant $\varepsilon(\delta^*,\delta^{**})>0$ such that $\mathtt{J}(\varpi)-\mathtt{J}(\omega)>\varepsilon(\delta^*,\delta^{**})$. In fact, for any $\varpi\in\mathcal{N}_{\delta^{**}}$, we have $\lambda(\delta^{**})=1$ and $\|\nabla\varpi\|_{\mathtt{p}}>r(\delta^{**})$. Take $\omega=\lambda(\delta^*)\varpi$, then $\omega\in\mathcal{N}_{\delta^*}$. Let $\mathtt{h}(\lambda)=\mathtt{J}(\lambda(\delta)\varpi)$,

$$\begin{aligned}\frac{d}{dt}\mathtt{h}(\lambda)&=\alpha(1-\delta)\lambda^{\mathtt{p}-1}\|\nabla\varpi\|_{\mathtt{p}}^{\mathtt{p}}+\beta(1-\delta)\lambda^{2\mathtt{p}-1}\|\nabla\varpi\|_{\mathtt{p}}^{2\mathtt{p}}+\frac{1}{\lambda}\mathtt{I}_\delta(\lambda\varpi)\\&=\alpha(1-\delta)\lambda^{\mathtt{p}-1}\|\nabla\varpi\|_{\mathtt{p}}^{\mathtt{p}}+\beta(1-\delta)\lambda^{2\mathtt{p}-1}\|\nabla\varpi\|_{\mathtt{p}}^{2\mathtt{p}}.\end{aligned}$$

If $0<\delta^*<\delta^{**}<1$, since $\lambda(\delta)$ is increasing in δ and $\lambda(\delta^{**})=1$, then

$$\begin{aligned}\mathtt{J}(\varpi)-\mathtt{J}(\omega)&=\mathtt{h}(1)-\mathtt{h}\big(\lambda(\delta^*)\big)\\&=\int_{\lambda(\delta^*)}^1\frac{d}{dt}\mathtt{h}(\lambda)d\lambda\\&=\int_{\lambda(\delta^*)}^1\Big[\alpha(1-\delta)\lambda^{\mathtt{p}-1}\|\nabla\varpi\|_{\mathtt{p}}^{\mathtt{p}}+\beta(1-\delta)\lambda^{2\mathtt{p}-1}\|\nabla\varpi\|_{\mathtt{p}}^{2\mathtt{p}}\Big]d\lambda\\&\ge\big[\alpha(1-\delta^{**})\lambda^{\mathtt{p}-1}(\delta^*)r^{\mathtt{p}}(\delta^{**})\\&\quad+\beta(1-\delta^{**})\lambda^{2\mathtt{p}-1}(\delta^*)r^{2\mathtt{p}}(\delta^{**})\big](1-\lambda(\delta^*))\\&=\varepsilon(\delta^*,\delta^{**})>0.\end{aligned}$$

If $\delta^*>\delta^{**}>1$, then

$$\begin{aligned}
\mathtt{J}(\varpi) - \mathtt{J}(\omega) &= \mathtt{h}(1) - \mathtt{h}\big(\lambda(\delta^*)\big) \\
&= \int_{\lambda(\delta^*)}^{1} \frac{d}{dt}\mathtt{h}(\lambda)d\lambda \\
&= \int_{1}^{\lambda(\delta^*)} \Big[\alpha(\delta-1)\lambda^{\mathtt{p}-1}\|\nabla\varpi\|_{\mathtt{p}}^{\mathtt{p}} + \beta(\delta-1)\lambda^{2\mathtt{p}-1}\|\nabla\varpi\|_{\mathtt{p}}^{2\mathtt{p}}\Big]d\lambda \\
&\geq \big[\alpha(\delta^{**}-1)\lambda^{\mathtt{p}-1}(\delta^{**})r^{\mathtt{p}}(\delta^{**}) \\
&\quad + \beta(\delta^{**}-1)\lambda^{2\mathtt{p}-1}(\delta^{**})r^{2\mathtt{p}}(\delta^{**})\big](\lambda(\delta^*)-1) \\
&= \varepsilon(\delta^*, \delta^{**}) > 0.
\end{aligned}$$

Furthermore, since $\mathtt{d}(\delta)$ is continuous with respect to δ and from the results obtained in (*i*), we see that there exists a $\widetilde{\delta} > 1$ such that $\mathtt{d}(\widetilde{\delta}) = 0$. This completes proof. □

Lemma 5 *Assume* $\varpi \in \mathbb{W}_0^{1,\mathtt{p}}(\Omega)$, $0 < \mathtt{J}(\varpi) < \mathtt{d}$, *and* $\delta_1 < 1 < \delta_2$ *are the two roots of the equation* $\mathtt{d}(\delta) = \mathtt{J}(\varpi)$. *Then the sign of* $\mathtt{I}_\delta(\varpi)$ *does not change for* $\delta_1 < \delta < \delta_2$.

Proof First $\mathtt{J}(\varpi) > 0$ implies $\|\varpi\|_{\mathtt{p}} \neq 0$. If the sign of $\mathtt{I}_\delta(\varpi)$ changes for $\delta_1 < \delta < \delta_2$, then there exists a $\hat{\delta} \in (\delta_1, \delta_2)$ such that $\mathtt{I}_{\hat{\delta}}(\varpi) = 0$. Thus by the definition of $\mathtt{d}(\delta)$ we have $\mathtt{J}(\varpi) \geq \mathtt{d}(\hat{\delta})$, which is contradictive with $\mathtt{J}(\varpi) = \mathtt{d}(\delta_1) = \mathtt{d}(\delta_2) < \mathtt{d}(\hat{\delta})$. □

Lemma 6 *Assume that* $\varpi(x,t)$ *is a weak solution to problem* (1) *with* $0 < \mathtt{J}(\varpi_0) < \mathtt{d}$ *and* T *is the maximal existence time. Let* $\delta_1 < 1 < \delta_2$ *be the two roots of the equation* $\mathtt{d}(\delta) = \mathtt{J}(\varpi_0)$.

(i) *If* $\mathtt{I}(\varpi_0) > 0$, *then* $\varpi(x,t) \in \mathscr{W}_\delta$ *for* $\delta_1 < \delta < \delta_2$ *and* $0 < t < T$.
(ii) *If* $\mathtt{I}(\varpi_0) < 0$, *then* $\varpi(x,t) \in \mathscr{V}_\delta$ *for* $\delta_1 < \delta < \delta_2$ *and* $0 < t < T$.

Proof Proof of the present theorem is standard, see Lemma 2.6. of [6]. So, we omit details here.

3 The main results

In this section we consider the behaviors of the solution of Problem (1) under the condition $\mathtt{J}(\varpi_0) < \mathtt{d}$ and give the threshold result for the solutions to exist globally or to blow up in finite time.

Consider the following functional:

$$\mathtt{E}(\varpi) = \left(\frac{\alpha}{\mathtt{p}} + \frac{\beta}{2\mathtt{p}}\int_\Omega |\nabla\varpi|^{\mathtt{p}}dx\right)\int_\Omega |\nabla\varpi|^{\mathtt{p}}dx, \quad \varpi \in \mathbb{W}_0^{1,\mathtt{p}}(\Omega).$$

It is easy to see that $\mathtt{E} \in \mathtt{C}^1(\mathbb{W}_0^{1,\mathtt{p}}(\Omega), \mathbb{R})$, and the nonlocal operator is the Fréchet derivative operator of $\mathtt{E}$ in the weak sense.

Denote $\mathtt{L} = \mathtt{E}' : \mathbb{W}_0^{1,\mathtt{p}}(\Omega) \to \mathbb{W}^{-1,\mathtt{q}}(\Omega)$, then $\varpi, \omega \in \mathbb{W}_0^{1,\mathtt{p}}(\Omega)$, we have

$$\begin{aligned}\langle \mathtt{L}\varpi, \omega\rangle &= \left(\alpha + \beta\|\nabla\varpi\|_{\mathtt{p}}^{\mathtt{p}}\right)\int_\Omega |\nabla\varpi|^{\mathtt{p}-2}\nabla\varpi\cdot\nabla\omega\, dx\\ &= \mathtt{M}\left(\|\nabla\varpi\|_{\mathtt{p}}^{\mathtt{p}}\right)\int_\Omega |\nabla\varpi|^{\mathtt{p}-2}\nabla\varpi\cdot\nabla\omega\, dx.\end{aligned}$$

where $\mathtt{q}$ is the Hölder's conjugate of $\mathtt{p}$ and $\langle , \rangle$ denotes the pairing between $\mathbb{W}^{-1,\mathtt{q}}(\Omega)$ and $\mathbb{W}_0^{1,\mathtt{p}}(\Omega)$.

Lemma 7 [6, 13] *The nonlocal* $\mathtt{p}$*-Laplacian* $\mathtt{L}$ *has the following properties*:

(i) $\mathtt{L}$ *is continuous, bounded and satisfies following inequalities*

$$\begin{aligned}&\langle \mathtt{L}\varpi - \mathtt{L}\omega, \varpi\\ &\quad - \omega\rangle \geq \left[\mathtt{M}\left(\|\nabla\varpi\|_{\mathtt{p}}^{\mathtt{p}}\right)\|\nabla\varpi\|_{\mathtt{p}}^{\mathtt{p}-1}\right.\\ &\quad \left.-\mathtt{M}\left(\|\nabla\omega\|_{\mathtt{p}}^{\mathtt{p}}\right)\|\nabla\omega\|_{\mathtt{p}}^{\mathtt{p}-1}\right]\left(\|\nabla\varpi\|_{\mathtt{p}} - \|\nabla\omega\|_{\mathtt{p}}\right)\end{aligned} \tag{8}$$

(ii) $\mathtt{L}$ *is a mapping of type* $\mathtt{S}_+$, *i.e. if* $\varpi_n \rightharpoonup u$ *weakly in* $\mathbb{W}_0^{1,\mathtt{p}}(\Omega)$ *and* $\overline{\lim}_{n\to\infty}\langle \mathtt{L}\varpi_n, \varpi_n - \varpi\rangle \leq 0$, *then* $\varpi_n \to \varpi$ *strongly in* $\mathbb{W}_0^{1,\mathtt{p}}(\Omega)$.

Theorem 1 (*Global existence for* $\mathtt{J}(\varpi_0) < \mathtt{d}$). *If* $\varpi_0(x) \in \mathbb{W}_0^{1,\mathtt{p}}(\Omega)$. *Suppose that* $\mathtt{J}(\varpi_0) \leq \mathtt{d}$ *and* $\mathtt{I}(\varpi_0) > 0$, *then the problem* (1) *has a global weak solution* $\varpi(t) \in \mathtt{L}^\infty\left(0, +\infty; \mathbb{W}_0^{1,\mathtt{p}}(\Omega)\right)$ *with* $\varpi_t \in \mathtt{L}^2\left(0, +\infty; \mathtt{L}^2(\Omega)\right)$ *and* $\varpi(t) \in \mathscr{W}$ *for* $0 \leq t < \infty$. *Moreover*, $\|\varpi\|_2^2 \leq \left[\|\varpi_0\|_2^{2(1-\mathtt{p})} + \mathcal{K}(\mathtt{p}-1)t\right]^{-1/(1-\mathtt{p})}$, *where* $\mathcal{K}$ *is a positive constant. In addition, if the weak solution is bounded, then it is unique*.

Proof We divide the proof into three steps.

Step 1: Global existence.

Global existence of weak solutions will be proved by combining Galerkin's approximation with a priori estimates. Let $\{\psi_{\mathtt{j}}(x)\}$ be a system of orthogonal basis of $\mathbb{W}_0^{1,\mathtt{p}}(\Omega)$ and construct the approximate solutions $\varpi^m(x,t)$ to Problem (1).

$$\varpi^m(x,t) = \sum_{\mathtt{j}=1}^{m} b_{\mathtt{j}}^m(t)\psi_{\mathtt{j}}(x), \quad \mathtt{j} = 1, 2, \ldots,$$

satisfying for $\mathtt{j} = 1, 2, \ldots, m$

$$\begin{aligned}&(\varpi_t^m, \psi_{\mathtt{j}}) + \mathtt{M}\left(\|\nabla\varpi^m\|_{\mathtt{p}}^{\mathtt{p}}\right)\left(|\nabla\varpi^m|^{\mathtt{p}-2}\nabla\varpi^m, \nabla\psi_{\mathtt{j}}\right)\\ &\quad = \left(|\varpi^m|^{\mathtt{q}-2}\varpi^m \log|\varpi^m|^k, \psi_{\mathtt{j}}\right),\end{aligned} \tag{9}$$

$$\varpi^m(x,0)=\sum_{j=1}^{m} a_j^m \psi_j(x) \to \varpi_0(x) \ \text{ in } \ \mathbb{W}_0^{1,p}(\Omega). \tag{10}$$

Multiplying (9) by $\frac{d}{dt}b_j^m(t)$, summing for j from 1 to m, and integrating with respect to t from 0 to t, we obtain

$$\int_0^t \|\varpi_\tau^m\|_2^2 d\tau + J(\varpi^m(x,t)) = J(\varpi^m(x,0)), \quad 0 \le t < \infty. \tag{11}$$

Since $\varpi^m(x,0) \to \varpi_0(x)$ in $\mathbb{W}_0^{1,p}(\Omega)$, we have

$$J(\varpi^m(x,0)) \to J(\varpi_0(x)) < d \ \text{ and } \ I(\varpi^m(x,0)) \to I(\varpi_0(x)) > 0.$$

Then for sufficiently large m and for any $0 \le t < \infty$, we obtain

$$\int_0^t \|\varpi_\tau^m\|_2^2 d\tau + J(\varpi^m(x,t)) = J(\varpi^m(x,0)) < d \ \text{ and } \ I(\varpi^m(x,0)) > 0. \tag{12}$$

Similarly to the proof of Lemma 6 we can show from (12) that $\varpi^m(x,t)$ for sufficiently large m and $0 \le t < \infty$. Thus $I(\varpi^m(x,t)) > 0$ for all $t \ge 0$. Then from the following equality

$$J(\varpi^m) = \frac{\alpha(q-p)}{pq}\|\nabla\varpi^m\|_p^p + \frac{\beta(q-2p)}{2pq}\|\nabla\varpi^m\|_p^{2p} + \frac{k}{q^2}\|\varpi^m\|_q^q + \frac{1}{q}I(\varpi^m)$$

and (12), we get

$$\int_0^t \|\varpi_\tau^m\|_2^2 d\tau + \frac{\alpha(q-p)}{pq}\|\nabla\varpi^m\|_p^p + \frac{\beta(q-2p)}{2pq}\|\nabla\varpi^m\|_p^{2p} + \frac{k}{q^2}\|\varpi^m\|_q^q < d,$$

for sufficiently large m and for any $0 \le t < \infty$, which then yields

$$\|\varpi^m\|_{\mathbb{W}_0^{1,p}(\Omega)}^p \le \frac{dpq}{\alpha(q-p)}, \quad 0 \le t < \infty, \tag{13}$$

$$\int_0^t \|\varpi_\tau^m\|_2^2 d\tau < d, \quad 0 \le t < \infty. \tag{14}$$

$$\|\varpi^m\|_q^q < \frac{dq^2}{k}. \tag{15}$$

By (13) we also see that there exists a constant $C > 0$, independent of m and t such that

$$\begin{aligned}\left\| M\big(\|\nabla\varpi^m\|_p^p\big)|\nabla\varpi^m|^{p-2}\nabla\varpi^m \right\|_{p/(p-1)} &\le \left\| \big(\alpha+\beta\|\nabla\varpi^m\|_p^p\big)|\nabla\varpi^m|^{p-2}\nabla\varpi^m \right\|_{p/(p-1)} \\ &\le C.\end{aligned} \tag{16}$$

Then by (13)–(16), the standard diagonal method and Aubin-Lions' compactness embedding theorem, there exist $\varpi \in \mathbb{W}_0^{1,\mathtt{p}}(\Omega)$ and a subsequence of $\{\varpi^m\}$, still denoted as $\{\varpi^m\}$, such that for each $T > 0$, as $m \to +\infty$,

$$\begin{cases} \varpi_t^m \rightharpoonup \varpi_t, \ \text{ weakly in } \ \mathtt{L}^2\big(0,T;\mathtt{L}^2(\Omega)\big), \\ \varpi^m \rightharpoonup \varpi, \ \text{ weakly* in } \ \mathtt{L}^\infty\big(0,T;\mathbb{W}_0^{1,\mathtt{p}}(\Omega)\big), \\ \varpi^m \to \varpi, \ \text{ strongly* in } \ \mathtt{L}^\infty(\Omega\times(0,T)) \ \text{ a.e. in } \ \Omega\times(0,T), \\ \mathtt{M}\big(\|\nabla\varpi^m\|_{\mathtt{p}}^{\mathtt{p}}\big)|\nabla\varpi^m|^{\mathtt{p}-2}\nabla\varpi^m \rightharpoonup \xi \ \text{ weakly* in } \ \mathtt{L}^\infty\big(0,T;\mathtt{L}^{\mathtt{p}/(\mathtt{p}-1)}(\Omega)\big) \end{cases} \tag{17}$$

Clearly, (17) implies that

$$|\varpi^m|^{\mathtt{q}-2}\varpi^m \log|\varpi^m| \to |\varpi|^{\mathtt{q}-2}\varpi \log|\varpi| \ \text{ a.e. in } \ \Omega\times(0,T). \tag{18}$$

On the other hand, since

$$\inf_{y\in(0,1)} y^{\mathtt{q}-1}\log y = -\frac{1}{e(\mathtt{q}-1)},$$

and

$$\log y = 2\log\left(y^{\frac{1}{2}}\right) \le 2y^{\frac{1}{2}} \ \text{ for } \ y > 0.$$

Let

$$\mu = \frac{2\mathtt{q}}{2\mathtt{q}-1} > 1,$$

by (15), we know that

$$\begin{aligned} \int_\Omega \big(|\varpi^m|^{\mathtt{q}-1}\log|\varpi^m|\big)^\mu dx &= \int_{\{x\in\Omega:\,\varpi^m(x)\le 1\}} \big(|\varpi^m|^{\mathtt{q}-1}\log|\varpi^m|\big)^\mu dx \\ &\quad + \int_{\{x\in\Omega:\,\varpi^m(x)>1\}} \big(|\varpi^m|^{\mathtt{q}-1}\log|\varpi^m|\big)^\mu dx \\ &\le \frac{|\Omega|}{[e(\mathtt{q}-1)]^\mu} + 2^\mu \int_\Omega |\varpi^m|^{\mu\left(\mathtt{q}-1+\frac{1}{2}\right)} dx \\ &= \frac{|\Omega|}{[e(\mathtt{q}-1)]^\mu} + 2^\mu \|\varpi^m\|_{\mathtt{q}}^{\mathtt{q}} \\ &\le \frac{|\Omega|}{[e(\mathtt{q}-1)]^\mu} + \frac{2^\mu \mathtt{d}\mathtt{q}^2}{k}. \end{aligned} \tag{19}$$

Hence, it follows from (18) and (19) that

$$|\varpi^m|^{\mathtt{q}-2}\varpi^m \log|\varpi^m| \rightharpoonup |\varpi|^{\mathtt{q}-2}\varpi\log|\varpi| \ \text{ weakly* in } \ \mathtt{L}^\infty\big(0,T;\mathtt{L}^\mu(\Omega)\big) \tag{20}$$

We will show that ϖ is a weak solution to problem (1) for any $T > 0$. For this, fix $T > 0$ and denote $\Omega_T = \Omega\times(0,T)$. We see from (13) that $\int_\Omega |\varpi^m(x,T)|^2 dx \le \mathtt{C}$.

Therefore, there exists a subsequence of $\{\varpi(x,T)\}$ (which we still denote by $\{\varpi(x,T)\}$ and a function $u \in \mathrm{L}^2(\Omega)$ such that $\{\varpi(x,T)\} \to u$ weakly in $\mathrm{L}^2(\Omega)$. Then for any $\eta(x) \in \mathrm{C}_0^\infty(\Omega)$ and $\theta(t) \in \mathrm{C}^1[0,T]$, it follows that

$$\begin{aligned}&\int\int_{\Omega_T} \varpi_t^m \eta\theta dxdt\\ &= \int_\Omega \left[\varpi^m(x,T)\theta(T) - \varpi^m(x,0)\theta(0)\right]\eta dx - \int\int_{\Omega_T} \varpi^m \eta\theta_t dxdt.\end{aligned}$$

Taking limit $m \to \infty$ in the above identity, we obtain

$$\int_\Omega (u - \varpi(x,T))\theta(T)\eta dx - \int_\Omega (\varpi_0(x) - \varpi(x,0))\theta(0)\eta dx = 0.$$

Putting $\theta(T) = 0, \theta(0) = 1$ and by the density of $\mathrm{C}_0^\infty(\Omega)$ in $\mathrm{L}^2(\Omega)$, we have $u = \varpi(x,T)$ and $\varpi(x,0) = \varpi_0(x)$ for almost every $x \in \Omega$. By the weakly lower semi-continuity of the $\mathrm{L}^2(\Omega)$ norm, we get

$$\int_\Omega \varpi^2(x,T)dx \le \liminf_{m\to\infty} \int_\Omega |\varpi^m(x,T)|^2 dx. \tag{21}$$

From (17) and (20), it can be seen that

$$\lim_{m\to\infty} \int\int_{\Omega_T} |\varpi^m|^{\mathrm{q}} \log|\varpi^m| dxdt = \int\int_{\Omega_T} |\varpi|^{\mathrm{q}} \log|\varpi| dxdt. \tag{22}$$

Let $V_k = \mathrm{span}\{\psi_1, \psi_2, \dots, \psi_k\}$. Then for any $\omega \in \mathrm{C}(0,T;V_k)(k \le m)$, it follows from (9) that

$$\begin{aligned}\int\int_{\Omega_T} \left[\varpi_t^m \omega + \mathrm{M}\left(\|\nabla\varpi^m\|_{\mathrm{p}}^{\mathrm{p}}\right)|\nabla\varpi^m|^{\mathrm{p}-2}\nabla\varpi^m\nabla\omega\right]dxdt\\ = k\int\int_{\Omega_T} |\varpi^m|^{\mathrm{q}-2}\varpi^m \log|\varpi^m|\omega dxdt,\end{aligned} \tag{23}$$

In particular, we have

$$\int\int_{\Omega_T} \left[\varpi_t^m \varpi^m + \mathrm{M}\left(\|\nabla\varpi^m\|_{\mathrm{p}}^{\mathrm{p}}\right)|\nabla\varpi^m|^{\mathrm{p}}\right]dxdt = k\int\int_{\Omega_T} |\varpi^m|^{\mathrm{q}} \log|\varpi^m| dxdt, \tag{24}$$

Letting $m \to \infty$ in (23) and using (17), (20) we obtain

$$\int\int_{\Omega_T} \left[\varpi_t \omega + \xi\nabla\omega\right]dxdt = k\int\int_{\Omega_T} |\varpi|^{\mathrm{q}-2}\varpi \log|\varpi|\omega dxdt, \tag{25}$$

Choosing $\omega = \varpi^m$ in (25), letting $m \to \infty$ and uing ((20), we get

$$\frac{1}{2}\int_{\Omega}(\varpi^2(x,T)-\varpi_0^2(x))dx+\int\int_{\Omega_T}\xi\nabla\varpi dxdt=k\int\int_{\Omega_T}|\varpi|^{\mathtt{q}}\log|\varpi|dxdt \tag{26}$$

Our next goal is to show that $\xi=\mathtt{M}\big(\|\nabla\varpi\|_{\mathtt{p}}^{\mathtt{p}}\big)|\nabla\varpi|^{\mathtt{p}-2}\nabla\varpi$. For this, let

$$\mathtt{S}_m=\int\int_{\Omega_T}\mathtt{M}\big(\|\nabla\varpi^m\|_{\mathtt{p}}^{\mathtt{p}}\big)\big(|\nabla\varpi^m|^{\mathtt{p}-2}\nabla\varpi^m-|\nabla\varpi|^{\mathtt{p}-2}\nabla\varpi\big)(\nabla\varpi^m-\nabla\varpi)dxdt.$$

Then it is clear that $\mathtt{S}_m\geq 0$. Then from [13], it can be proved easily that

$$\mathtt{M}\big(\|\nabla\varpi\|_{\mathtt{p}}^{\mathtt{p}}\big)|\nabla\varpi|^{\mathtt{p}-2}\nabla\varpi\to m(t)|\nabla\varpi|^{\mathtt{p}-2}\nabla\varpi\ \text{ strongly in }\ \big(\mathtt{L}^{\mathtt{p}/(\mathtt{p}-1)}(\Omega_T)\big)^n. \tag{27}$$

Therefore, by (21), (22) (26) and (27), we obtain

$$\begin{aligned}0\leq\limsup_{m\to\infty}\mathtt{S}_m&\leq\int\int_{\Omega_T}\big[k|\varpi|^{\mathtt{p}}\log|\varpi|-\xi\nabla\varpi\big]dxdt\\&\quad+\frac{1}{2}\int_{\omega}\varpi_0^2(x)dx-\frac{1}{2}\int_{\omega}\varpi^2(x,T)dx\\&=0.\end{aligned}$$

That is $\mathtt{S}_m\to 0$ as $m\to\infty$, which in turn implies that $\nabla\varpi^m\to\nabla\varpi$ strongly in $(\mathtt{L}^{\mathtt{p}}(\Omega_T))^n$. Which implies that

$$\int_{\Omega}|\nabla\varpi^m-\nabla\varpi|^{\mathtt{p}}dx\to 0,\ \int_{\Omega}|\nabla\varpi^m|^{\mathtt{p}}dx\to\int_{\Omega}|\nabla\varpi|^{\mathtt{p}}dx\ \text{ a.e. in }\ (0,T), \tag{28}$$

$$\nabla\varpi^m\to\nabla\varpi\ \text{ a.e. in }\ \Omega_T. \tag{29}$$

From (28), it is clear that $m(t)=\mathtt{M}\big(\|\nabla\varpi\|_{\mathtt{p}}^{\mathtt{p}}\big)$ and from (29), we get

$$\mathtt{M}\big(\|\nabla\varpi^m\|_{\mathtt{p}}^{\mathtt{p}}\big)|\nabla\varpi^m|^{\mathtt{p}-2}\nabla\varpi^m\to\mathtt{M}\big(\|\nabla\varpi\|_{\mathtt{p}}^{\mathtt{p}}\big)|\nabla\varpi|^{\mathtt{p}-2}\nabla\varpi\ \text{ a.e. in }\ \Omega_T$$

which further implies $\xi=\mathtt{M}\big(\|\nabla\varpi\|_{\mathtt{p}}^{\mathtt{p}}\big)|\nabla\varpi|^{\mathtt{p}-2}\nabla\varpi$. Therefore, from (25), we have

$$\int\int_{\Omega_T}\Big[\varpi_t\omega+\mathtt{M}\big(\|\nabla\varpi\|_{\mathtt{p}}^{\mathtt{p}}\big)|\nabla\varpi|^{\mathtt{p}-2}\nabla\varpi\nabla\omega\Big]dxdt=k\int\int_{\Omega_T}|\varpi|^{\mathtt{q}-2}\varpi\log|\varpi|\omega dxdt.$$

Since $\omega\in\mathtt{C}^1(0,T;\mathtt{C}_0^\infty(\Omega))$ is arbitrary and by the density of $\mathtt{C}_0^\infty(\Omega)$ in $\mathtt{W}_0^{1,\mathtt{p}}(\Omega)$ to $\mathtt{L}^2(\Omega)$, we get

$$\begin{aligned}(\varpi_t,\omega)+\Big(\big[\alpha+\beta\int_{\Omega}|\nabla\varpi|^{\mathtt{p}}dx\big]|\nabla\varpi|^{\mathtt{p}-2}|\nabla\varpi|,\nabla\omega\Big)\\=\big(|\varpi|^{\mathtt{q}-2}\varpi\log|\varpi|^k,\omega\big)\ \text{ a.e. }\ t\in(0,T),\end{aligned}$$

for any $\omega \in \mathbb{W}_0^{1,\mathtt{p}}(\Omega)$. Finally, to prove (3) we first assume that $\varpi(x,t)$ is smooth enough such that $\varpi_t \in \mathbb{L}^2\big(0,T;\mathbb{W}_0^{1,\mathtt{p}}(\Omega)\big)$. Choosing $\omega = \varpi_t$ as a test function and integrating (2) over $[0,\ t]$ we get (3). By the density of $\mathbb{L}^2\big(0,T;\mathbb{W}_0^{1,\mathtt{p}}(\Omega)\big)$ in $\mathbb{L}^2(\Omega\times(0,T))$, it is known that (3) also holds for weak solutions of (1). Hence, ϖ is a global weak solution of problem (1).

Step 2: Decay rate. Let $\omega = \varpi$ in (2), we obtain

$$\frac{1}{2}\frac{d}{dt}\|\varpi\|_2^2 = (\varpi_t,\varpi) = -\alpha\|\nabla\varpi\|_{\mathtt{p}}^{\mathtt{p}} - \beta\|\nabla\varpi\|_{\mathtt{p}}^{2\mathtt{p}} + k\int_\Omega |\varpi|^{\mathtt{q}}\log|\varpi|dx = -\mathtt{I}(\varpi).$$

From Lemma 6 it follows that $\varpi(x,t)\in\mathscr{W}_\delta$ for $\delta_1<\delta<\delta_2$ and $0<t<\infty$ under the condition $\mathtt{J}(\varpi_0)<\mathtt{d}$ and $\mathtt{I}(\varpi_0)>0$. Thus we have $\mathtt{I}_{\delta_1}(\varpi)\geq 0$ for $0<t<\infty$. Thus,

$$\begin{aligned}\frac{1}{2}\frac{d}{dt}\|\varpi\|_2^2 &= -\mathtt{I}(\varpi) = \alpha(\delta_1-1)\|\nabla\varpi\|_{\mathtt{p}}^{\mathtt{p}} + \beta(\delta_1-1)\|\nabla\varpi\|_{\mathtt{p}}^{2\mathtt{p}} - \mathtt{I}_{\delta_1}(\varpi)\\ &\leq \frac{\beta(\delta_1-1)}{\mathtt{C}_1^{2\mathtt{p}}}\|\varpi\|_2^{2\mathtt{p}},\end{aligned}$$

where $\mathtt{C}_1>0$ is the best embedding constant from $\mathbb{W}_0^{1,\mathtt{p}}(\Omega)$ to $\mathbb{L}^2(\Omega)$. Consequently,

$$\|\varpi\|_2^2 \leq \Big[\|\varpi_0\|_2^{2(1-\mathtt{p})} + \mathcal{K}(\mathtt{p}-1)t\Big]^{-1/(\mathtt{p}-1)},$$

where $\mathcal{K} = \frac{2\beta(1-\delta_1)}{\mathtt{C}_1^{2\mathtt{p}}} > 0$.

Step 3: Uniqueness of bounded solution. To prove the uniqueness of bounded weak solution, we assume that both ϖ and ω are bounded weak solutions of Problem (1). Then, for any $\psi\in\mathbb{W}_0^{1,\mathtt{p}}(\Omega)$, we have

$$\begin{aligned}&(\varpi_t,\psi) + \mathtt{M}\big(\|\nabla\varpi\|_{\mathtt{p}}^{\mathtt{p}}\big)\big(|\nabla\varpi|^{\mathtt{p}-2}\nabla\varpi,\nabla\psi\big) = \big(|\varpi|^{\mathtt{q}-2}\varpi\log|\varpi|^k,\psi\big),\\ &(\omega_t,\psi) + \mathtt{M}\big(\|\nabla\omega\|_{\mathtt{p}}^{\mathtt{p}}\big)\big(|\nabla\omega|^{\mathtt{p}-2}\nabla\omega,\nabla\psi\big) = \big(|\omega|^{\mathtt{q}-2}\omega\log|\omega|^k,\psi\big).\end{aligned}$$

Subtracting the above two equalities, taking $\psi = \varpi-\omega\in\mathbb{W}_0^{1,\mathtt{p}}(\Omega)$ and integrating over $(0,\ t)$ for any $t>0$, we obtain

$$\begin{aligned}&\int_0^t\int_\Omega(\varpi-\omega)_\tau^2 dxd\tau + \int_0^t\Big[\mathtt{M}\big(\|\nabla\varpi\|_{\mathtt{p}}^{\mathtt{p}}\big)\|\nabla\varpi\|_{\mathtt{p}}^{\mathtt{p}-1} - \mathtt{M}\big(\|\nabla\omega\|_{\mathtt{p}}^{\mathtt{p}}\big)\|\nabla\omega\|_{\mathtt{p}}^{\mathtt{p}-1}\Big]\\ &\quad\times\big(\|\nabla\varpi\|_{\mathtt{p}} - \|\nabla\omega\|_{\mathtt{p}}\big)d\tau\\ &\leq k\int_0^t\int_\Omega\Big[|\varpi|^{\mathtt{q}-2}\varpi\log|\varpi| - |\omega|^{\mathtt{q}-2}\omega\log|\omega|\Big](\varpi-\omega)dxd\tau\end{aligned}\tag{30}$$

Since $(\varpi-\omega)(x,0)=0$ and the second part of the left hand side of (30) is nonnegative, we obtain, with the help of the boundedness of ϖ and ω, that

$$\int_\Omega (\varpi-\omega)^2(x,t)dx \le \mathtt{C}^* \int_0^t \int_\Omega (\varpi-\omega)^2(x,t)dxdt,$$

where $\mathtt{C}^* > 0$ is a constant depending only on $\mathtt{q}, k$ and the bound of ϖ, ω. It then follows from Gronwall's inequality that

$$\int_\Omega (\varpi-\omega)^2(x,t)dx = 0.$$

Thus $\varpi = \omega$ a.e. in $\Omega \times (0,\infty)$ and this completes whole proof. □

Theorem 2 (*Blow-up for* $\mathtt{J}(\varpi_0) < \mathtt{d}$). *Let* ϖ *be a weak solution of problem* (1) *with* $\varpi_0(x) \in \mathbb{W}_0^{1,\mathtt{p}}(\Omega)$. *If* $\mathtt{J}(\varpi_0) \le \mathtt{d}$ *and* $\mathtt{I}(\varpi_0) < 0$, *then there exists a finite time* $\mathtt{T}$ *such that* ϖ *blows up at* $\mathtt{T}$ *in the sense that*

$$\lim_{t\to\mathtt{T}} \int_0^t \|\varpi\|_2^2 d\tau = +\infty.$$

Proof Suppose that ϖ is a global weak solution of problem (1) with $\mathtt{J}(\varpi_0) \le \mathtt{d}, \mathtt{I}(\varpi_0) < 0$ and define

$$\mathcal{A}(t) = \int_0^t \|\varpi\|_2^2 d\tau,$$

then

$$\mathcal{A}'(t) = \|\varpi\|_2^2 \tag{31}$$

and

$$\begin{aligned}\mathcal{A}''(t) &= 2(\varpi_t, \varpi)\\ &= -2\left[\alpha\|\nabla\varpi\|_{\mathtt{p}}^{\mathtt{p}} + \beta\|\nabla\varpi\|_{\mathtt{p}}^{2\mathtt{p}} - k\int_\Omega |\varpi|^{\mathtt{q}} \log|\varpi| dx\right]\\ &= -2\mathtt{I}(\varpi).\end{aligned} \tag{32}$$

On the other hand,

$$\mathtt{J}(\varpi) = \frac{\alpha(\mathtt{q}-\mathtt{p})}{\mathtt{pq}}\|\nabla\varpi\|_{\mathtt{p}}^{\mathtt{p}} + \frac{\beta(\mathtt{q}-2\mathtt{p})}{2\mathtt{pq}}\|\nabla\varpi\|_{\mathtt{p}}^{2\mathtt{p}} + \frac{k}{\mathtt{q}^2}\|\varpi\|_{\mathtt{q}}^{\mathtt{q}} + \frac{1}{\mathtt{q}}\mathtt{I}(\varpi).$$

By (3), (31) and (32), we get

$$\begin{aligned}
\mathcal{A}''(t) &= \frac{2\alpha(q-p)}{p}\|\nabla\varpi\|_p^p + \frac{\beta(q-2p)}{p}\|\nabla\varpi\|_p^{2p} + \frac{k}{q}\|\varpi\|_q^q - 2qJ(\varpi) \\
&= \frac{2\alpha(q-p)}{p}\|\nabla\varpi\|_p^p + \frac{\beta(q-2p)}{p}\|\nabla\varpi\|_p^{2p} + \frac{k}{q}\|\varpi\|_q^q \\
&\quad + 2q\int_0^t \|\varpi_\tau\|_2^2 d\tau - 2J(\varpi_0) \\
&\geq \frac{\beta(q-2p)}{p}\|\nabla\varpi\|_p^{2p} + 2q\int_0^t \|\varpi_\tau\|_2^2 d\tau - 2J(\varpi_0) \\
&\geq \frac{\beta(q-2p)}{p}\left[\|\nabla\varpi\|_p^2 - 1\right] + 2q\int_0^t \|\varpi_\tau\|_2^2 d\tau - 2J(\varpi_0) \\
&\geq \frac{\beta(q-2p)}{p}\left[\frac{1}{C_1^2}\|\varpi\|_2^2 - 1\right] + 2q\int_0^t \|\varpi_\tau\|_2^2 d\tau - 2J(\varpi_0) \\
&= \frac{\beta(q-2p)}{pC_1^2}\mathcal{A}'(t) + 2q\int_0^t \|\varpi_\tau\|_2^2 d\tau - \left[2J(\varpi_0) + \frac{\beta(q-2p)}{p}\right].
\end{aligned}$$

Note that

$$\left(\mathcal{A}'(t)\right)^2 = 4\left[\int_0^t\int_\Omega \varpi_t\cdot\varpi dx d\tau\right]^2 + 2\|\varpi_0\|_2^2\mathcal{A}'(t) - \|\varpi_0\|_2^4.$$

Hence, by combining the above two inequalities and applying Cauchy-Schwartz inequality we have

$$\begin{aligned}
&\mathcal{A}''(t)\mathcal{A}(t) - \frac{q+1}{2}\left(\mathcal{A}'(t)\right)^2 \\
&\quad\geq 2q\int_0^t \|\varpi_\tau\|_2^2 d\tau\int_0^t \|\varpi\|_2^2 d\tau - \left[2J(\varpi_0) + \frac{\beta(q-2p)}{p}\right]\mathcal{A}(t) \\
&\qquad + \frac{\beta(q-2p)}{pC_1^2}\mathcal{A}'(t)\mathcal{A}(t) - 2(q+1)\left[\int_0^t\int_\Omega \varpi_t\varpi dx d\tau\right]^2 \\
&\qquad - (q+1)\|\varpi_0\|_2^2\mathcal{A}'(t) + \frac{q+1}{2}\|\varpi_0\|_2^4 \\
&\quad\geq \frac{\beta(q-2p)}{pC_1^2}\mathcal{A}'(t)\mathcal{A}(t) \\
&\qquad - \left[2J(\varpi_0) + \frac{\beta(q-2p)}{p}\right]\mathcal{A}(t) - (q+1)\|\varpi_0\|_2^2\mathcal{A}'(t).
\end{aligned} \tag{33}$$

Next, we discuss the following two cases:

(*i*) If $\mathtt{J}(\varpi_0) < \mathtt{d}$. By Lemma 5 we know that $\varpi(t) \in \mathscr{V}_\delta$ for $t \geq 0$ and $\delta_1 < \delta < \delta_2$, where $\delta_1 < 1 < \delta_2$ are the two roots of $\mathtt{d}(\delta) = \mathtt{J}(\varpi_0)$. Hence $\mathtt{I}_{\delta_2} \leq 0$ and $\|\nabla\varpi\|_{\mathtt{p}} \geq \ell(\delta_2)$ for $t \geq 0$. Then it follows from (32) that for $t \geq 0$.

$$\begin{aligned}\mathcal{A}''(t) &= -2\mathtt{I}(\varpi) = 2\alpha(\delta_2 - 1)\|\nabla\varpi\|_{\mathtt{p}}^{\mathtt{p}} + 2\beta(\delta_2 - 1)\|\nabla\varpi\|_{\mathtt{p}}^{2\mathtt{p}} - 2\mathtt{I}_{\delta_2}(\varpi)\\ &\geq 2\alpha(\delta_2 - 1)\ell^{\mathtt{p}}(\delta_2),\end{aligned}$$

it follows that

$$\mathcal{A}'(t) \geq 2\alpha(\delta_2 - 1)\ell^{\mathtt{p}}(\delta_2)t,$$

and

$$\mathcal{A}(t) \geq \alpha(\delta_2 - 1)\ell^{\mathtt{p}}(\delta_2)t^2.$$

So, there exists a $t^* > 0$ such that for $t \geq t^*$, we have

$$\begin{aligned}\frac{\beta(\mathtt{q} - 2\mathtt{p})}{2\mathtt{p}\mathtt{C}_1^2}\mathcal{A}(t) &\geq (\mathtt{q} + 1)\|\varpi_0\|_2^2\\ \frac{\beta(\mathtt{q} - 2\mathtt{p})}{2\mathtt{p}\mathtt{C}_1^2}\mathcal{A}'(t) &\geq 2\mathtt{J}(\varpi_0) + \frac{\beta(\mathtt{q} - 2\mathtt{p})}{\mathtt{p}}.\end{aligned}$$

Thus, from (33), we get

$$\mathcal{A}''(t)\mathcal{A}(t) - \frac{\mathtt{q} + 1}{2}\big(\mathcal{A}'(t)\big)^2 > 0 \quad \text{for all} \quad t \geq t^*. \tag{34}$$

(*ii*) If $\mathtt{J}(\varpi_0) \leq 0$. Let T be a maximum existence time and $0 < \delta < \frac{\mathtt{q}}{2\mathtt{p}}$. Then

$$\begin{aligned}&\frac{\|\nabla\varpi\|_{\mathtt{p}}^{\mathtt{p}}}{\mathtt{q}}\left\{\frac{\alpha(\mathtt{q} - \mathtt{p}\delta)}{\mathtt{p}} + \frac{\beta(\mathtt{q} - 2\mathtt{p}\delta)}{2\mathtt{p}}\|\nabla\varpi\|_{\mathtt{p}}^{\mathtt{p}}\right\}\\ &\quad + \frac{1}{\mathtt{q}}\mathtt{I}_\delta(\varpi)\\ &\leq \frac{\|\nabla\varpi\|_{\mathtt{p}}^{\mathtt{p}}}{\mathtt{q}}\left\{\frac{\alpha(\mathtt{q} - \mathtt{p}\delta)}{\mathtt{p}} + \frac{\beta(\mathtt{q} - 2\mathtt{p}\delta)}{2\mathtt{p}}\|\nabla\varpi\|_{\mathtt{p}}^{\mathtt{p}}\right\}\\ &\quad + \frac{k}{\mathtt{q}^2}\|\varpi\|_{\mathtt{q}}^{\mathtt{q}} + \frac{1}{\mathtt{q}}\mathtt{I}_\delta(\varpi)\\ &= \mathtt{J}(\varpi) \leq \mathtt{J}(\varpi_0).\end{aligned}$$

If $\mathtt{J}(\varpi_0) < 0$, then $\mathtt{J}(\varpi(x,t)) < 0 < \mathtt{d}(\delta)$ and $\mathtt{I}(\varpi(x,t)) < 0$ for all $0 \leq t < T$, which implies that $\varpi(x,t) \in \mathscr{V}_\delta$. If $\mathtt{J}(\varpi_0) = 0$ and $\|\nabla\varpi_0\|_{\mathtt{p}} \neq 0$, then $\mathtt{J}(\varpi(x,t)) \leq 0$ for all $0 \leq t < T$, which also implies that there exists a constant $\mathtt{c} > 0$ such that $\|\nabla\varpi(x,t)\|_{\mathtt{p}} \geq \mathtt{c}$. So again we get that $\mathtt{I}(\varpi(x,t)) < 0$ and $\mathtt{J}(\varpi(x,t)) \leq 0 < \mathtt{d}(\delta)$, i.e. $\varpi(x,t) \in \mathscr{V}_\delta$. Therefore, with δ_2 replaced by δ, we can proceed similarly to case (*i*) to show that (34) still holds for sufficiently large t.

Finally, by Levine's concavity argument [12] that $\mathcal{A}(t)$ can not remain finite for all $t \geq t^*$ and therefore reaches a contradiction. The proof is complete □

The results for other critical cases $\mathtt{J}(\varpi_0) = \mathtt{d}$ and $\mathtt{J}(\varpi_0) > \mathtt{d}$ are equivalent ideas in [6]. So, we omitted results for other cases.

Acknowledgements The authors would like to thank the referees for their valuable suggestions and comments for the improvement of the paper.

Author contributions The study was carried out in collaboration of all authors. All authors read and approved the final manuscript.

Funding Not applicable.

Data availability statement Data sharing not applicable to this paper as no data sets were generated or analyzed during the current study.

Declarations

Conflict of interest It is declared that authors has no competing interests.

Ethical approval This article does not contain any studies with human participants or animals performed by any of the authors.

References

1. Chipot, M., Savitska, T.: Nonlocal p-Laplace equations depending on the L^p norm of the gradient. Adv. Differ. Equ. **19**(11–12), 997–1020 (2014)
2. D'Ancona, P., Shibata, Y.: on global solvability of non-linear viscoelastic equation in the analytic category. Math. Methods Appl. Sci. **17**, 477–489 (1994)
3. D'Ancona, P., Spagnolo, S.: Global solvability for the degenerate Kirchhoff equation with real analytic data. Invent. Math. **108**, 247–262 (1992)
4. Fu, Y.Q., Xiang, M.Q.: Existence of solutions for parabolic equations of Kirchhoff type involving variable exponent. Appl. Anal. **95**(3), 524–544 (2016). https://doi.org/10.1080/00036811.2015.1022153
5. Ghisi, M., Gobbino, M.: Hyperbolic-parabolic singular perturbation for mildly degenerate Kirchhoff equations: time-decay estimates. J. Differ. Equ. **245**(10), 2979–3007 (2008). https://doi.org/10.1016/j.jde.2008.04.017
6. Han, Y.Z., Li, Q.W.: Threshold results for the existence of global and blow-up solutions to Kirchhoff equations with arbitrary initial energy. Comput. Math. Appl. **75**(9), 3283–3297 (2018). https://doi.org/10.1016/j.camwa.2018.01.047
7. Hou, A.J., Liao, J.F.: Existence of positive solution for a class of nonlocal problem with strong singularity and linear term. Differ. Equ. Appl. **12**(3), 277–290 (2020)
8. Khuddush, M., Prasad, K.R., Botta, B.: Local existence and blow up of solutions for a system of viscoelastic wave equations of Kirchhoff type with delay and logarithmic nonlinearity. Int. J. Math. Model. Comput. **11**(3), 1–11 (2021)
9. Khuddush, M., Prasad, K.R.: Positive solutions for an iterative system of nonlinear elliptic equations. Bull. Malays. Math. Sci. Soc. **45**, 245–272 (2022). https://doi.org/10.1007/s40840-021-01183-y
10. Khuddush, M., Prasad, K.R., Bharathi, B.: Global existence and blowup of solutions for a semilinear Klein–Gordon equation with the product of logarithmic and power-type nonlinearity. Ann. Univ. Ferrara **68**, 187–201 (2022). https://doi.org/10.1007/s11565-022-00395-9

11. Kirchhoff, G.: Mechanik. Teubner, Leipzig (1883)
12. Levine, H.A.: Some nonexistence and instability theorems for solutions of formally parabolic equation of the form $pu_t = -au + Fu$. Arch. Ration. Mech. Anal. **51**(5), 371–386 (1973). https://doi.org/10.1007/BF00263041
13. Li, J., Han, Y.: Global existence and finite time blow-up of solutions to a nonlocal pLaplace equation. Math. Model. Anal. **24**(2), 195–217 (2019). https://doi.org/10.3846/mma.2019.014
14. Liu, Y.C.: On potential wells and vacuum isolating of solutions for semilinear wave equations. J. Differ. Equ. **192**(1), 155–169 (2003)
15. Liu, Y.C., Zhao, J.S.: On potential wells and applications to semilinear hyperbolic equations and parabolic equations. Nonlinear Anal. **64**, 2665–2687 (2006)
16. Nishihara, K.: On a global solution of some quasilinear hyperbolic equation. Tokyo J. Math. **7**, 437–459 (1984)
17. Sattinger, D.H.: On global solution of nonlinear hyperbolic equations. Arch. Ration. Mech. Anal. **30**(2), 148–172 (1968). https://doi.org/10.1007/BF00250942
18. Sun, Y.J., Tan, Y.X.: Kirchhoff type equations with strong singularities. Commun. Pure Appl. Anal. **18**(1), 181–193 (2019)

Publisher's Note Springer Nature remains neutral with regard to jurisdictional claims in published maps and institutional affiliations.

Springer Nature or its licensor holds exclusive rights to this article under a publishing agreement with the author(s) or other rightsholder(s); author self-archiving of the accepted manuscript version of this article is solely governed by the terms of such publishing agreement and applicable law.

Afrika Matematika (2022) 33:93
https://doi.org/10.1007/s13370-022-01027-3

Existence of infinitely many positive radial solutions for an iterative system of nonlinear elliptic equations on an exterior domain

Mahammad Khuddush[1] · **K. Rajendra Prasad**[2]

Received: 31 October 2021 / Accepted: 16 August 2022 / Published online: 13 September 2022
© African Mathematical Union and Springer-Verlag GmbH Deutschland, ein Teil von Springer Nature 2022

Abstract
In this paper by an application of Krasnoselskii's fixed point theorem, we establish the existence of infinitely many positive radial solutions to the iterative system of nonlinear elliptic equations of the form

$$\Delta v_{\mathtt{j}} + \frac{(N-2)^2 r_0^{2N-2}}{|\mathtt{x}|^{2N-2}} v_{\mathtt{j}} + \mathtt{Q}(|\mathtt{x}|)\mathtt{g}_{\mathtt{j}}(v_{\mathtt{j}+1}) = 0, \quad \mathtt{x} \in \Omega,$$
$$v_{\mathtt{j}}|_{\partial\Omega} = 0, \quad \lim_{|\mathtt{x}|\to\infty} v_{\mathtt{j}}(\mathtt{x}) = 0,$$

where $\mathtt{j} \in \{1, 2, 3, \ldots, m\}$, $v_1 = v_{m+1}$, $\Delta v = \mathtt{div}(\nabla v)$, $N > 2$, $0 < r_0 < \pi/2$, $\Omega = \{v \in \mathbb{R}^N | \ |v| > r_0\}$, $\mathtt{Q} = \prod_{i=1}^{n} \mathtt{Q}_i$, each $\mathtt{Q}_i : (r_0, +\infty) \to (0, +\infty)$ is continuous, $r^{N-1}\mathtt{Q}$ is integrable, may have singularities, and $\mathtt{g}_{\mathtt{j}} : [0, +\infty) \to \mathbb{R}$ is continuous.

Keywords Nonlinear elliptic systems · Exterior domain · Positive radial solution · Krasnoselskii's fixed point theorem

Mathematics Subject Classification 35J66 · 35J60 · 34B18 · 47H10

1 Introduction

The semilinear elliptic equation of the form

$$\Delta v + \mathtt{g}(|\mathtt{x}|)v + \mathtt{h}(|\mathtt{x}|)v^p = 0 \tag{1}$$

arise in various fields of pure and applied mathematics such as Riemannian geometry, nuclear physics, astrophysics and so on. For more details of the background of (1), see [22, 28]. Study

✉ Mahammad Khuddush
khuddush89@gmail.com

[1] Department of Mathematics, Dr. Lankapalli Bullayya College of Engineering, Visakhapatnam, Andhra Pradesh 530013, India

[2] Department of Applied Mathematics, College of Science and Technology Andhra University, Visakhapatnam 530003, India

of nonlinear elliptic system of equations,

$$\left.\begin{aligned} \Delta v_{\mathtt{j}} + \mathtt{g}_{\mathtt{j}}(v_{\mathtt{j}+1}) = 0 \ \text{ in } \ \Omega, \\ v_{\mathtt{j}} = 0 \ \text{ on } \ \partial\Omega, \end{aligned}\right\} \tag{2}$$

where $\mathtt{j} \in \{1, 2, 3, \ldots, m\}$, $v_1 = v_{m+1}$, and Ω is a bounded domain in $\mathbb{R}^N$, has an important applications in population dynamics, combustion theory and chemical reactor theory. The recent literature for the existence, multiplicity and uniqueness of positive solutions, see [2–6, 8, 10–26, 29] and references therein.

In [1], Aberqi, Bennouna and Elmassoudi established an existence results for the following nonlinear elliptic equations with some measure data in Musielak–Orlicz spaces,

$$\mathtt{A}v + \mathtt{K}(\mathtt{x}, v, \nabla v) = \mu.$$

In [7], Dong and Wei established the existence of radial solutions for the following nonlinear elliptic equations with gradient terms in annular domains,

$$\begin{aligned} &\Delta v + \mathtt{g}\big(|\mathtt{x}|, v, \frac{\mathtt{x}}{|\mathtt{x}|} \cdot \nabla v\big) = 0 \ \text{ in } \ \Omega_a^b, \\ &v = 0 \ \text{ on } \ \partial\Omega_a^b, \end{aligned}$$

by using Schauder's fixed point theorem and contraction mapping theorem. In [15], Kajikiya and Ko established the existence of positive radial solutions for a semipositone elliptic equation of the form,

$$\begin{aligned} &\Delta v + \lambda \mathtt{g}(v) = 0 \ \text{ in } \ \Omega, \\ &v = 0 \ \text{ on } \ \partial\Omega, \end{aligned}$$

where Ω is a ball or an annulus in $\mathbb{R}^N$. Recently, Son and Wang [27] established positive radial solutions to the nonlinear elliptic systems,

$$\left.\begin{aligned} \Delta v_{\mathtt{j}} + \lambda \mathtt{K}_{\mathtt{j}}(|\mathtt{x}|)\mathtt{g}_{\mathtt{j}}(v_{\mathtt{j}+1}) = 0 \ \text{in} \ \Omega_{\mathtt{E}}, \\ v_{\mathtt{j}} = 0 \ \text{on} \ |\mathtt{x}| = r_0, \\ v_{\mathtt{j}} \to 0 \ \text{as} \ |\mathtt{x}| \to +\infty, \end{aligned}\right\} \tag{3}$$

where $\mathtt{j} \in \{1, 2, 3, \ldots, m\}$, $v_1 = v_{m+1}$, $\lambda > 0$, $N > 2$, $r_0 > 0$, and $\Omega_{\mathtt{E}}$ is an exterior of a ball. Motivated by the above works, in this paper we study the existence of infinitely many positive radial solutions for the following iterative system of nonlinear elliptic equations in an exterior domain,

$$\left.\begin{aligned} \Delta v_{\mathtt{j}} + \frac{(N-2)^2 r_0^{2N-2}}{|\mathtt{x}|^{2N-2}} v_{\mathtt{j}} + \mathtt{Q}(|\mathtt{x}|)\mathtt{g}_{\mathtt{j}}(v_{\mathtt{j}+1}) = 0, \ \ \mathtt{x} \in \Omega, \\ v_{\mathtt{j}}|_{\partial\Omega} = 0, \ \lim_{|\mathtt{x}|\to\infty} v_{\mathtt{j}}(\mathtt{x}) = 0, \end{aligned}\right\} \tag{4}$$

where $\mathtt{j} \in \{1, 2, 3, \ldots, m\}$, $v_1 = v_{m+1}$, $\Delta v = \mathtt{div}(\nabla v)$, $N > 2$, $0 < r_0 < \pi/2$, $\Omega = \{v \in \mathbb{R}^N | \ |v| > r_0\}$, $\mathtt{Q} = \prod_{i=1}^n \mathtt{Q}_i$, each $\mathtt{Q}_i : (r_0, +\infty) \to (0, +\infty)$ is continuous, $r^{N-1}\mathtt{Q}$ is integrable, may have singularities, and $\mathtt{g}_{\mathtt{j}} : [0, +\infty) \to \mathbb{R}$ is continuous, by an application of Krasnoselskii's fixed point theorem. As far as we know there is no known results for considered iterative sytem (4) in the literature and (3) is a particular case of (4).

The study of positive radial solutions to (4) reduces to the study of positive solutions to the following iterative system of two-point boundary value problems,

$$\left.\begin{aligned} v_{\jmath}''(\tau) + r_0^2 v_{\jmath}(\tau) + \varphi(\tau) g_{\jmath}\left(v_{\jmath+1}(\tau)\right) = 0,\ 0 < \tau < 1, \\ v_{\jmath}(0) = 0,\ v_{\jmath}(1) = 0, \end{aligned}\right\} \tag{5}$$

where $\jmath \in \{1, 2, 3, \ldots, m\}$, $v_1 = v_{m+1}$, $0 < r_0 < \pi/2$, and $\varphi(\tau) = \frac{r_0^2}{(N-2)^2} \tau^{\frac{2(N-1)}{2-N}} \prod_{i=1}^{n} \varphi_i(\tau)$, $\varphi_i(\tau) = \mathrm{Q}_i(r_0 \tau^{\frac{1}{2-N}})$ by a Kelvin type transformation through the change of variables $r = |\mathrm{x}|$ and $\tau = \left(\frac{r}{r_0}\right)^{2-N}$. Here φ_i may have singularities on $[0, 1]$. Thus for each $i \in \{1, 2, 3, \ldots, n\}$, we assume that the following conditions hold throughout the paper:

($\mathcal{H}_1$) $\varphi_i \in L^{p_i}[0, 1]$, $(p_i \geq 1)$ and may have infinitely many singularities on $(0, 1/2)$.

($\mathcal{H}_2$) There exists a sequence $\{\tau_k\}_{k=1}^{\infty}$ such that $0 < \tau_{k+1} < \tau_k < \frac{1}{2}$, $k \in \mathbb{N}$,

$$\lim_{k\to\infty} \tau_k = \tau^* < \frac{1}{2}, \quad \lim_{\tau\to\tau_k} \varphi_i(\tau) = +\infty,\ k \in \mathbb{N},\ i = 1, 2, 3, \ldots, n.$$

Moreover, there exists $\varphi_i^* > 0$ such that

$$\varphi_i^* < \varphi_i(\tau) < \infty \ \text{ a.e. on } [0, 1].$$

The rest of the paper is organized in the following fashion. In Sect. 2, we convert the boundary value problem (5) into equivalent integral equation which involves the kernel. Also, we estimate bounds for the kernel which are useful in our main results. In Sect. 3, we develop a criteria for the existence of infinitely many positive radial solutions for (4) by applying Krasnoselskii's cone fixed point theorem in a Banach space. Finally, as an application, an example to demonstrate our results is given.

2 Kernel and its bounds

In order to study BVP (5), we first consider the corresponding linear boundary value problem,

$$\left.\begin{aligned} -\left(v_1''(\tau) + r_0^2 v_1(\tau)\right) = \varphi(\tau) y(\tau),\ 0 < \tau < 1, \\ v_1(0) = v_1(1) = 0, \end{aligned}\right\} \tag{6}$$

where $y \in \mathcal{C}[0, 1]$ is a given function.

Lemma 1 *For every $y \in \mathcal{C}[0, 1]$, the linear boundary value problem (6) has a unique solution*

$$v_1(\tau) = \int_0^1 \aleph_{r_0}(\tau, s) \varphi(s) y(s) ds, \tag{7}$$

where

$$\aleph_{r_0}(\tau, s) = \frac{1}{r_0 \sin(r_0)} \begin{cases} \sin(r_0 s) \sin(r_0(1-\tau)), & 0 \leq s \leq \tau \leq 1, \\ \sin(r_0 \tau) \sin(r_0(1-s)), & 0 \leq \tau \leq s \leq 1. \end{cases}$$

Lemma 2 *The kernel $\aleph_{r_0}(\tau, s)$ has the following properties:*

(i) *$\aleph_{r_0}(\tau, s)$ is nonnegative and continuous on $[0, 1] \times [0, 1]$,*

(ii) *$\aleph_{r_0}(\tau, s) \leq \aleph_{r_0}(s, s)$ for $t, \tau \in [0, 1]$,*

(iii) *there exists $\varepsilon \in (0, \frac{1}{2})$ such that $\delta(\varepsilon)\aleph_{r_0}(s, s) \leq \aleph_{r_0}(\tau, s)$ for $\tau \in [\varepsilon, 1-\varepsilon]$, $s \in [0, 1]$.*

Proof From the definition of kernel $\aleph_{r_0}(\tau, s)$, it is clear that (i) and (ii) hold. To prove (iii), let $\tau \in [\varepsilon, 1-\varepsilon]$ and $s \le \tau$, then

$$\frac{\aleph_{r_0}(\tau, s)}{\aleph_{r_0}(s, s)} = \frac{\sin(r_0(1-\tau))}{\sin(r_0(1-s))} \ge \frac{\sin(r_0\varepsilon)}{\sin(r_0)} := \delta(\varepsilon),$$

and for $\tau \le s$, we have

$$\frac{\aleph_{r_0}(\tau, s)}{\aleph_{r_0}(s, s)} = \frac{\sin(r_0\tau)}{\sin(r_0 s)} \ge \frac{\sin(r_0\varepsilon)}{\sin(r_0)}.$$

This completes the proof. □

From Lemma 1, we note that an m-tuple $(v_1, v_2, \cdots, v_m)$ is solution of the boundary value problem (5) if and only, if

$$v_1(\tau) = \int_0^1 \aleph_{r_0}(\tau, s_1)\varphi(s_1)\mathrm{g}_1\Big[\int_0^1 \aleph_{r_0}(s_1, s_2)\varphi(s_2)\mathrm{g}_2\Big[\int_0^1 \aleph_{r_0}(s_2, s_3)\varphi(s_3)\mathrm{g}_4 \cdots$$
$$\mathrm{g}_{m-1}\Big[\int_0^1 \aleph_{r_0}(s_{m-1}, s_m)\varphi(s_m)\mathrm{g}_m\big(v_1(s_m)\big)ds_m\Big]\cdots\Big]ds_3\Big]ds_2\Big]ds_1.$$

In general,

$$v_{\mathrm{j}}(\tau) = \int_0^1 \aleph_{r_0}(\tau, s)\varphi(s)\mathrm{g}_{\mathrm{j}}\big(v_{\mathrm{j}+1}(s)\big)ds, \ \mathrm{j} = 1, 2, 3, \cdots, m,$$
$$v_1(\tau) = v_{m+1}(\tau).$$

We denote the Banach space $\mathcal{C}((0,1), \mathbb{R})$ by $\mathscr{B}$ with the norm $\|v\| = \max_{\tau\in[0,1]} |v(\tau)|$. For $\varepsilon \in (0, 1/2)$, the cone $\mathcal{P}_\varepsilon \subset \mathscr{B}$ is defined by

$$\mathcal{P}_\varepsilon = \Big\{v \in \mathscr{B} : v(\tau) \ge 0, \min_{\tau\in[\varepsilon,\,1-\varepsilon]} v(\tau) \ge \delta(\varepsilon)\|v\|\Big\}.$$

For any $v_1 \in \mathcal{P}_\varepsilon$, define an operator $\Omega : \mathcal{P}_\varepsilon \to \mathscr{B}$ by

$$(\mathcal{T}v_1)(\tau) = \int_0^1 \aleph_{r_0}(\tau, s_1)\varphi(s_1)\mathrm{g}_1\Big[\int_0^1 \aleph_{r_0}(s_1, s_2)\varphi(s_2)\mathrm{g}_2\Big[\int_0^1 \aleph_{r_0}(s_2, s_3)\varphi(s_3)\mathrm{g}_4 \cdots$$
$$\mathrm{g}_{m-1}\Big[\int_0^1 \aleph_{r_0}(s_{m-1}, s_m)\varphi(s_m)\mathrm{g}_m\big(v_1(s_m)\big)ds_m\Big]\cdots\Big]ds_3\Big]ds_2\Big]ds_1.$$

Lemma 3 *For each $\varepsilon \in (0, 1/2)$, $\mathcal{T}(\mathcal{P}_\varepsilon) \subset \mathcal{P}_\varepsilon$ and $\mathcal{T} : \mathcal{P}_\varepsilon \to \mathcal{P}_\varepsilon$ is completely continuous.*

Proof Let $\varepsilon \in (0, 1/2)$. Since $\mathrm{g}_{\mathrm{j}}(v_{\mathrm{j}+1}(\tau))$ is nonnegative for $\tau \in [0, 1]$, $v_1 \in \mathcal{P}_\varepsilon$. Since $\aleph_{r_0}(\tau, s)$, is nonnegative for all $\tau, s \in [0, 1]$, it follows that $\mathcal{T}(v_1(\tau)) \ge 0$ for all $\tau \in [0, 1]$, $v_1 \in \mathcal{P}_\varepsilon$ Now, by Lemmas 1 and 2, we have

$$
\begin{aligned}
&\min_{\tau\in[\varepsilon,1-\varepsilon]}(\mathcal{T}v_1)(\tau)\\
&= \min_{\tau\in[\varepsilon,1-\varepsilon]}\Bigg\{\int_0^1 \aleph_{r_0}(\tau,s_1)\varphi(s_1)\mathfrak{g}_1\Bigg[\int_0^1 \aleph_{r_0}(s_1,s_2)\varphi(s_2)\mathfrak{g}_2\Bigg[\int_0^1 \aleph_{r_0}(s_2,s_3)\varphi(s_3)\mathfrak{g}_4\ldots\\
&\qquad \mathfrak{g}_{m-1}\Bigg[\int_0^1 \aleph_{r_0}(s_{m-1},s_m)\varphi(s_m)\mathfrak{g}_m\big(v_1(s_m)\big)ds_m\Bigg]\cdots\Bigg]ds_3\Bigg]ds_2\Bigg]ds_1\Bigg\}\\
&\geq \delta(\varepsilon)\int_0^1 \aleph_{r_0}(s_1,s_1)\varphi(s_1)\mathfrak{g}_1\Bigg[\int_0^1 \aleph_{r_0}(s_1,s_2)\varphi(s_2)\mathfrak{g}_2\Bigg[\int_0^1 \aleph_{r_0}(s_2,s_3)\varphi(s_3)\mathfrak{g}_4\ldots\\
&\qquad \mathfrak{g}_{m-1}\Bigg[\int_0^1 \aleph_{r_0}(s_{m-1},s_m)\varphi(s_m)\mathfrak{g}_m\big(v_1(s_m)\big)ds_m\Bigg]\cdots\Bigg]ds_3\Bigg]ds_2\Bigg]ds_1\\
&\geq \delta(\varepsilon)\Bigg\{\int_0^1 \aleph_{r_0}(\tau,s_1)\varphi(s_1)\mathfrak{g}_1\Bigg[\int_0^1 \aleph_{r_0}(s_1,s_2)\varphi(s_2)\mathfrak{g}_2\Bigg[\int_0^1 \aleph_{r_0}(s_2,s_3)\varphi(s_3)\mathfrak{g}_4\cdots\\
&\qquad \mathfrak{g}_{m-1}\Bigg[\int_0^1 \aleph_{r_0}(s_{m-1},s_m)\varphi(s_m)\mathfrak{g}_m\big(v_1(s_m)\big)ds_m\Bigg]\cdots\Bigg]ds_3\Bigg]ds_2\Bigg]ds_1\Bigg\}\\
&\geq \delta(\varepsilon)\max_{\tau\in[0,1]}|\mathcal{T}v_1(\tau)|.
\end{aligned}
$$

Thus $\mathcal{T}(\mathcal{P}_\varepsilon)\subset\mathcal{P}_\varepsilon$. Therefore, the operator $\mathcal{T}$ is completely continuous by standard methods and by the Arzela–Ascoli theorem. □

3 Infinitely many positive radial solutions

In this section, we establish the existence of infinitely many positive radial solutions for the system (4) by utilizing following theorems.

Theorem 1 [9] *Let $\mathcal{E}$ be a cone in a Banach space $\mathcal{X}$ and Λ_1, Λ_2 are open sets with $0\in\Lambda_1$, $\overline{\Lambda_1}\subset\Lambda_2$. Let $\mathcal{T}:\mathcal{E}\cap(\overline{\Lambda_2}\backslash\Lambda_1)\to\mathcal{E}$ be a completely continuous operator such that*

(i) $\|\mathcal{T}v\|\geq\|v\|$, $v\in\mathcal{E}\cap\partial\Lambda_1$, *and* $\|\mathcal{T}v\|\leq\|v\|$, $v\in\mathcal{E}\cap\partial\Lambda_2$, *or*
(ii) $\|\mathcal{T}v\|\leq\|v\|$, $v\in\mathcal{E}\cap\partial\Lambda_1$, *and* $\|\mathcal{T}v\|\geq\|v\|$, $v\in\mathcal{E}\cap\partial\Lambda_2$.

Then $\mathcal{T}$ has a fixed point in $\mathcal{E}\cap(\overline{\Lambda_2}\backslash\Lambda_1)$.

Theorem 2 (Hölder's) *Let $f\in L^{p_i}[0,1]$ with $p_i>1$, for $i=1,2,\cdots,n$ and $\sum_{i=1}^{n}\frac{1}{p_i}=1$. Then $\prod_{i=1}^{n}f_i\in L^1[0,1]$ and $\left\|\prod_{i=1}^{n}f_i\right\|_1\leq\prod_{i=1}^{n}\|f_i\|_{p_i}$. Further, if $f\in L^1[0,1]$ and $g\in L^\infty[0,1]$. Then $fg\in L^1[0,1]$ and $\|fg\|_1\leq\|f\|_1\|g\|_\infty$.*

Consider the following three possible cases for $\varphi_i\in L^{p_i}[0,1]$:

$$\sum_{i=1}^{n}\frac{1}{p_i}<1,\quad \sum_{i=1}^{n}\frac{1}{p_i}=1,\quad \sum_{i=1}^{n}\frac{1}{p_i}>1.$$

Firstly, we seek infinitely many positive radial solutions for the case $\sum_{i=1}^{n}\frac{1}{p_i}<1$.

Theorem 3 *Suppose* $(\mathcal{H}_1)-(\mathcal{H}_2)$ *hold, let* $\{\varepsilon_k\}_{k=1}^{\infty}$ *be a sequence with* $\tau_{k+1}<\varepsilon_k<\tau_k$. *Let* $\{\mathtt{E}_k\}_{k=1}^{\infty}$ *and* $\{\mathtt{D}_k\}_{k=1}^{\infty}$ *be such that*

$$\mathtt{E}_{k+1}<\delta(\varepsilon_k)\mathtt{D}_k<\mathtt{D}_k<\theta\mathtt{D}_k<\mathtt{E}_k,\ k\in\mathbb{N},$$

where

$$\theta=\max\left\{\left[\delta(\varepsilon_1)\frac{r_0^2}{(N-2)^2}\prod_{i=1}^{n}\varphi_i^*\int_{\varepsilon_1}^{1-\varepsilon_1}\aleph_{r_0}(s,s)s^{\frac{2(N-1)}{2-N}}ds\right]^{-1},\ 1\right\}.$$

Further, assume that $\mathtt{g}_{\mathtt{j}}$ *satisfies*

$(\mathcal{C}_1)$ $\mathtt{g}_{\mathtt{j}}(v(\tau))\le\mathtt{M}_1\mathtt{E}_k$ *for all* $\tau\in[0,1],\ 0\le v\le\mathtt{E}_k$, *where*

$$\mathtt{M}_1<\left[\frac{r_0^2}{(N-2)^2}\|\aleph_{r_0}\|_q\prod_{i=1}^{n}\|\varphi_i\|_{p_i}\right]^{-1},\quad \aleph_{r_0}(s)=\aleph_{r_0}(s,s)s^{\frac{2(N-1)}{2-N}},$$

$(\mathcal{C}_2)$ $\mathtt{g}_{\mathtt{j}}(v(\tau))\ge\theta\mathtt{D}_k$ *for all* $\tau\in[\varepsilon_k,1-\varepsilon_k],\ \varepsilon_k\mathtt{D}_k\le v\le\mathtt{D}_k$.

The iterative system (4) *has infinitely many radial solutions* $\{(v_1^{[k]},v_2^{[k]},\dots,v_m^{[k]})\}_{k=1}^{\infty}$ *such that* $v_{\mathtt{j}}^{[k]}(\tau)\ge0$ *on* $(0,1)$, $\mathtt{j}=1,2,\dots,m$ *and* $k\in\mathbb{N}$.

Proof Consider the sequences $\{\Lambda_{1,k}\}_{k=1}^{\infty}$ and $\{\Lambda_{2,k}\}_{k=1}^{\infty}$ of open subsets of $\mathscr{B}$ defined by

$$\Lambda_{1,k}=\{v\in\mathscr{B}:\|v\|<\mathtt{E}_k\},\ \Lambda_{2,k}=\{v\in\mathscr{B}:\|v\|<\mathtt{D}_k\}.$$

Let $\{\varepsilon_k\}_{k=1}^{\infty}$ be as in the hypothesis and note that $\tau^*<\tau_{k+1}<\varepsilon_k<\tau_k<\frac{1}{2}$, for all $k\in\mathbb{N}$. For each $k\in\mathbb{N}$, define the cone $\mathcal{P}_{\varepsilon_k}$ by

$$\mathcal{P}_{\varepsilon_k}=\left\{v\in\mathscr{B}:v(\tau)\ge0\ \text{ and }\min_{\tau\in[\varepsilon_k,\,1-\varepsilon_k]}v(t)\ge\delta(\varepsilon_k)\|v(\tau)\|\right\}.$$

Let $v_1\in\mathcal{P}_{\varepsilon_k}\cap\partial\Lambda_{1,k}$. Then, $v_1(s)\le\mathtt{E}_k=\|v_1\|$ for all $s\in[0,1]$. By $(\mathcal{C}_1)$ and $0<s_{m-1}<1$, we have

$$\begin{aligned}
&\int_0^1\aleph_{r_0}(s_{m-1},s_m)\varphi(s_m)\mathtt{g}_m\big(v_1(s_m)\big)ds_m\\
&\le\int_0^1\aleph_{r_0}(s_m,s_m)\varphi(s_m)\mathtt{g}_m\big(v_1(s_m)\big)ds_m\\
&\le\mathtt{M}_1\mathtt{E}_k\int_0^1\aleph_{r_0}(s_m,s_m)\varphi(s_m)ds_m\\
&\le\mathtt{M}_1\mathtt{E}_k\frac{r_0^2}{(N-2)^2}\int_0^1\aleph_{r_0}(s_m,s_m)s_m^{\frac{2(N-1)}{2-N}}\prod_{i=1}^{n}\varphi_i(s_m)ds_m.
\end{aligned}$$

There exists a $q>1$ such that $\sum_{i=1}^{n}\frac{1}{p_i}+\frac{1}{q}=1$. By the first part of Theorem 2, we have

$$\begin{aligned}
\int_0^1\aleph_{r_0}(s_{m-1},s_m)\varphi(s_m)\mathtt{g}_m\big(v_1(s_m)\big)ds_m&\le\mathtt{M}_1\mathtt{E}_k\frac{r_0^2}{(N-2)^2}\|\aleph_{r_0}\|_q\prod_{i=1}^{n}\|\varphi_i\|_{p_i}\\
&\le\mathtt{E}_k.
\end{aligned}$$

It follows in similar manner for $0 < s_{m-2} < 1$,

$$\begin{aligned}
&\int_0^1 \aleph_{r_0}(s_{m-2}, s_{m-1})\varphi(s_{m-1})\mathrm{g}_{m-1}\bigg[\int_0^1 \aleph_{r_0}(s_{m-1}, s_m)\varphi(s_m)\mathrm{g}_m\big(v_1(s_m)\big)ds_m\bigg]ds_{m-1}\\
&\quad\le \int_0^1 \aleph_{r_0}(s_{m-1}, s_{m-1})\varphi(s_{m-1})\mathrm{g}_{m-1}(\mathrm{E}_k)ds_{m-1}\\
&\quad\le \mathrm{M}_1\mathrm{E}_k\int_0^1 \aleph_{r_0}(s_{m-1}, s_{m-1})\varphi(s_{m-1})ds_{m-1}\\
&\quad\le \mathrm{M}_1\mathrm{E}_k\frac{r_0^2}{(N-2)^2}\|\aleph_{r_0}\|_q\prod_{i=1}^n\|\varphi_i\|_{p_i}\\
&\quad\le \mathrm{E}_k.
\end{aligned}$$

Continuing with this bootstrapping argument, we get

$$\begin{aligned}
(\mathcal{T}v_1)(t) &= \int_0^1 \aleph_{r_0}(\tau, s_1)\varphi(s_1)\mathrm{g}_1\bigg[\int_0^1 \aleph_{r_0}(s_1, s_2)\varphi(s_2)\mathrm{g}_2\bigg[\int_0^1 \aleph_{r_0}(s_2, s_3)\varphi(s_3)\mathrm{g}_4\cdots\\
&\qquad \mathrm{g}_{m-1}\bigg[\int_0^1 \aleph_{r_0}(s_{m-1}, s_m)\varphi(s_m)\mathrm{g}_m\big(v_1(s_m)\big)ds_m\bigg]\cdots\bigg]ds_3\bigg]ds_2\bigg]ds_1\\
&\le R_k.
\end{aligned}$$

Since $\mathrm{E}_k = \|v_1\|$ for $v_1 \in \mathcal{P}_{\varepsilon_k}\cap\partial\Lambda_{1,k}$, we get

$$\|\mathcal{T}v_1\| \le \|v_1\|. \tag{8}$$

Let $\tau \in [\varepsilon_k, 1-\varepsilon_k]$. Then, $\mathrm{D}_k = \|v_1\| \ge v_1(\tau) \ge \min_{\tau\in[\varepsilon_k,1-\varepsilon_k]} v_1(t) \ge \varepsilon_k\|v_1\| \ge \varepsilon_k\mathrm{D}_k$. By $(\mathcal{C}_2)$ and for $s_{m-1} \in [\varepsilon_k, 1-\varepsilon_k]$, we have

$$\begin{aligned}
&\int_0^1 \aleph_{r_0}(s_{m-1}, s_m)\varphi(s_m)\mathrm{g}_m\big(v_1(s_m)\big)ds_m\\
&\quad\ge \int_{\varepsilon_k}^{1-\varepsilon_k} \aleph_{r_0}(s_{m-1}, s_m)\varphi(s_m)\mathrm{g}_m\big(v_1(s_m)\big)ds_m\\
&\quad\ge \theta\mathrm{D}_k\int_{\varepsilon_k}^{1-\varepsilon_k} \aleph_{r_0}(s_{m-1}, s_m)\varphi(s_m)ds_m\\
&\quad\ge \theta\mathrm{D}_k\delta(\varepsilon_1)\int_{\varepsilon_1}^{1-\varepsilon_1} \aleph_{r_0}(s_m, s_m)\varphi(s_m)ds_m\\
&\quad\ge \theta\mathrm{D}_k\delta(\varepsilon_1)\frac{r_0^2}{(N-2)^2}\int_{\varepsilon_1}^{1-\varepsilon_1} \aleph_{r_0}(s_m, s_m)s_m^{\frac{2(N-1)}{2-N}}\prod_{i=1}^n\varphi_i(s_m)ds_m\\
&\quad\ge \theta\mathrm{D}_k\delta(\varepsilon_1)\frac{r_0^2}{(N-2)^2}\prod_{i=1}^n\varphi_i^*\int_{\varepsilon_1}^{1-\varepsilon_1} \aleph_{r_0}(s_m, s_m)s_m^{\frac{2(N-1)}{2-N}}ds_m\\
&\quad\ge \mathrm{D}_k.
\end{aligned}$$

Continuing with bootstrapping argument, we get

$$(\mathcal{T}v_1)(\tau) = \int_0^1 \aleph_{r_0}(\tau, s_1)\varphi(s_1)\mathrm{g}_1\Bigg[\int_0^1 \aleph_{r_0}(s_1, s_2)\varphi(s_2)\mathrm{g}_2\Bigg[\int_0^1 \aleph_{r_0}(s_2, s_3)\varphi(s_3)\mathrm{g}_4\cdots$$
$$\mathrm{g}_{m-1}\Bigg[\int_0^1 \aleph_{r_0}(s_{m-1}, s_m)\varphi(s_m)\mathrm{g}_m\big(v_1(s_m)\big)ds_m\Bigg]\cdots\Bigg]ds_3\Bigg]ds_2\Bigg]ds_1$$
$$\geq \mathtt{D}_k.$$

Thus, if $v_1 \in \mathcal{P}_{\varepsilon_k} \cap \partial\Lambda_{2,k}$, then

$$\|\mathcal{T}v_1\| \geq \|v_1\|. \tag{9}$$

It is evident that $0 \in \Lambda_{2,k} \subset \overline{\Lambda}_{2,k} \subset \Lambda_{1,k}$. From (8), (9), it follows from Theorem 1 that the operator $\mathcal{T}$ has a fixed point $v_1^{[k]} \in \mathcal{P}_{\varepsilon_k} \cap \big(\overline{\Lambda}_{1,k}\backslash\Lambda_{2,k}\big)$ such that $v_1^{[k]}(t) \geq 0$ on $(0, 1)$, and $k \in \mathbb{N}$. Next setting $v_{m+1} = v_1$, we obtain infinitely many positive solutions $\{(v_1^{[k]}, v_2^{[k]}, \cdots, v_m^{[k]})\}_{k=1}^{\infty}$ of (5) given iteratively by

$$v_{\mathtt{j}}(\tau) = \int_0^1 \aleph_{r_0}(\tau, s)\varphi(s)\mathrm{g}_{\mathtt{j}}(v_{\mathtt{j}+1}(s))ds,\ \mathtt{j} = 1, 2, \cdots, m-1, m,$$
$$v_{m+1}(\tau) = v_1(\tau).$$

The proof is completed. □

For $\sum_{i=1}^{n} p_i = 1$, we have the following theorem.

Theorem 4 *Suppose $(\mathcal{H}_1)-(\mathcal{H}_2)$ hold, let $\{\varepsilon_k\}_{k=1}^{\infty}$ be a sequence with $\tau_{k+1} < \varepsilon_k < \tau_k$. Let $\{\mathtt{E}_k\}_{k=1}^{\infty}$ and $\{\mathtt{D}_k\}_{k=1}^{\infty}$ be such that*

$$\mathtt{E}_{k+1} < \delta(\varepsilon_k)\mathtt{D}_k < \mathtt{D}_k < \theta\mathtt{D}_k < \mathtt{E}_k,\ k \in \mathbb{N}.$$

Further, assume that $\mathrm{g}_{\mathtt{j}}$ satisfies $(\mathcal{C}_2)$ and $(\mathcal{C}_3)$ $\mathrm{g}_{\mathtt{j}}(v(\tau)) \leq \mathtt{M}_2\mathtt{E}_k$ for all $0 \leq v(\tau) \leq \mathtt{E}_k$, $\tau \in [0, 1]$, where

$$\mathtt{M}_2 < \min\left\{\left[\frac{r_0^2}{(N-2)^2}\|\aleph_{r_0}\|_{\infty}\prod_{i=1}^{n}\|\varphi_i\|_{p_i}\right]^{-1},\ \theta\right\}.$$

The iterative system (4) has infinitely many radial solutions $\{(v_1^{[k]}, v_2^{[k]}, \ldots, v_m^{[k]})\}_{k=1}^{\infty}$ such that $v_{\mathtt{j}}^{[k]}(\tau) \geq 0$ on $(0, 1)$, $\mathtt{j} = 1, 2, \ldots, m$ and $k \in \mathbb{N}$.

Proof Let $\Lambda_{1,k}$ be as in the proof of Theorem 3 and let $v_1 \in \mathcal{P}_{\varepsilon_k} \cap \partial\Lambda_{2,k}$. Again $v_1(\tau) \leq \mathtt{E}_k = \|v_1\|$, for all $\tau_1 \in [0, 1]$. By $(\mathcal{C}_3)$ and $0 < \tau_{m-1} < 1$, we have

$$\begin{aligned}
&\int_0^1 \aleph_{r_0}(s_{m-1}, s_m)\varphi(s_m)\mathtt{g}_m\big(v_1(s_m)\big)ds_m \\
&\leq \int_0^1 \aleph_{r_0}(s_m, s_m)\varphi(s_m)\mathtt{g}_m\big(v_1(s_m)\big)ds_m \\
&\leq \mathtt{M}_1\mathtt{E}_k \int_0^1 \aleph_{r_0}(s_m, s_m)\varphi(s_m)ds_m \\
&\leq \mathtt{M}_1\mathtt{E}_k \frac{r_0^2}{(N-2)^2}\int_0^1 \aleph_{r_0}(s_m, s_m)s_m^{\frac{2(N-1)}{2-N}}\prod_{i=1}^n \varphi_i(s_m)ds_m \\
&\leq \mathtt{M}_1\mathtt{E}_k \frac{r_0^2}{(N-2)^2}\|\aleph_{r_0}\|_\infty \prod_{i=1}^n \|\varphi_i\|_{p_i} \\
&\leq \mathtt{E}_k.
\end{aligned}$$

Continuing with this bootstrapping argument, we get

$$\begin{aligned}
(\mathcal{T}v_1)(t) = &\int_0^1 \aleph_{r_0}(\tau, s_1)\varphi(s_1)\mathtt{g}_1\bigg[\int_0^1 \aleph_{r_0}(s_1, s_2)\varphi(s_2)\mathtt{g}_2\bigg[\int_0^1 \aleph_{r_0}(s_2, s_3)\varphi(s_3)\mathtt{g}_4\cdots \\
&\mathtt{g}_{m-1}\bigg[\int_0^1 \aleph_{r_0}(s_{m-1}, s_m)\varphi(s_m)\mathtt{g}_m\big(v_1(s_m)\big)ds_m\bigg]\cdots\bigg]ds_3\bigg]ds_2\bigg]ds_1 \\
&\leq R_k.
\end{aligned}$$

Thus, $\|\mathcal{T}v_1\| \leq \|v_1\|$, for $v_1 \in \mathcal{P}_{\varepsilon_k} \cap \partial\Lambda_{1,k}$. Now define $\Lambda_{2,k} = \{v \in \mathscr{B} : \|v\| < \mathtt{D}_k\}$. Let $v_1 \in \mathcal{P}_{\mathcal{T}_k} \cap \partial\Lambda_{2,k}$ and let $s_{m-1} \in [\varepsilon_k,\ 1-\varepsilon_k]$. Then, the argument leading to (9) can be done to the present case. Hence, the theorem. □

Finally, we deal with the case $\sum_{i=1}^n p_i > 1$.

Theorem 5 *Suppose* $(\mathcal{H}_1)-(\mathcal{H}_2)$ *hold, let* $\{\varepsilon_k\}_{k=1}^\infty$ *be a sequence with* $\tau_{k+1} < \varepsilon_k < \tau_k$. *Let* $\{\mathtt{E}_k\}_{k=1}^\infty$ *and* $\{\mathtt{D}_k\}_{k=1}^\infty$ *be such that*

$$\mathtt{E}_{k+1} < \delta(\varepsilon_k)\mathtt{D}_k < \mathtt{D}_k < \theta\mathtt{D}_k < \mathtt{E}_k,\ k \in \mathbb{N}.$$

Further, assume that $\mathtt{g}_\mathtt{j}$ *satisfies* $(\mathcal{C}_2)$ *and* $(\mathcal{C}_4)$ $\mathtt{g}_\mathtt{j}(v(\tau)) \leq \mathtt{M}_3\mathtt{E}_k$ *for all* $0 \leq v(\tau) \leq \mathtt{E}_k$, $\tau \in [0,1]$, *where*

$$\mathtt{M}_3 < \min\left\{\left[\frac{r_0^2}{(N-2)^2}\|\aleph_{r_0}\|_\infty \prod_{i=1}^n \|\varphi_i\|_1\right]^{-1},\ \theta\right\}.$$

The iterative system (4) *has infinitely many radial solutions* $\{(v_1^{[k]}, v_2^{[k]}, \ldots, v_m^{[k]})\}_{k=1}^\infty$ *such that* $v_\mathtt{j}^{[k]}(\tau) \geq 0$ *on* $(0,1)$, $\mathtt{j} = 1, 2, \ldots, m$ *and* $k \in \mathbb{N}$.

Proof The proof is similar to the proof of Theorem 3. □

4 Application

Example 1 Consider the following fractional order boundary value problem,

$$\left.\begin{aligned} &\Delta v_{\mathtt{j}} + \frac{(N-2)^2 r_0^{2N-2}}{|\mathtt{x}|^{2N-2}} v_{\mathtt{j}} + \mathtt{Q}(|\mathtt{x}|)\mathtt{g}_{\mathtt{j}}(v_{\mathtt{j}+1}) = 0, \quad \mathtt{x} \in \Omega, \\ &v_{\mathtt{j}}|_{\partial\Omega} = 0, \quad \lim_{|\mathtt{x}|\to\infty} v_{\mathtt{j}}(\mathtt{x}) = 0, \end{aligned}\right\} \tag{10}$$

where $\Omega = \{\mathtt{x} \in \mathbb{R}^3; |\mathtt{x}| > 1\}$, $r_0 = 1$, $N = 3$, $\mathtt{j} \in \{1, 2\}$, $v_3 = v_1$, $\varphi(\tau) = \frac{1}{\tau^4}\prod_{i=1}^{2}\varphi_i(\tau)$, $\varphi_i(\tau) = \mathtt{Q}_i(\frac{1}{\tau})$, in which

$$\mathtt{Q}_1(t) = \frac{1}{|t - 1/4|} \quad \text{and} \quad \mathtt{Q}_2(t) = \frac{1}{|t - 1/3|},$$

$$\mathtt{g}_{\mathtt{j}}(v) = \begin{cases} 290 \times 10^{-4}, \quad v \in (10^{-4}, +\infty), \\ \frac{30\times10^{-(4k+2)} - 290\times10^{-4k}}{10^{-(4k+2)} - 10^{-4k}}(v - 10^{-4k}) + 290 \times 10^{-4k}, \\ \quad v \in \left[10^{-(4k+2)}, 10^{-4k}\right], \\ 30 \times 10^{-(4k+2)}, \quad v \in \left(\frac{1}{5} \times 10^{-(4k+2)}, 10^{-(4k+2)}\right), \\ \frac{30\times10^{-(4k+2)} - 290\times10^{-(4k+4)}}{\frac{1}{5}\times10^{-(4k+2)} - 10^{-(4k+4)}}(v - 10^{-(4k+4)}) + 290 \times 10^{-(4k+4)}, \\ \quad v \in \left(10^{-(4k+4)}, \frac{1}{5} \times 10^{-(4k+2)}\right], \end{cases}$$

$\mathtt{j} = 1, 2$. Let

$$\tau_k = \frac{31}{64} - \sum_{r=1}^{k} \frac{1}{4(r+1)^4}, \ \varepsilon_k = \frac{1}{2}(\tau_k + \tau_{k+1}), \ k = 1, 2, 3, \ldots,$$

then

$$\varepsilon_1 = \frac{15}{32} - \frac{1}{648} < \frac{15}{32}, \ \text{and} \ \tau_{k+1} < \varepsilon_k < \tau_k, \ \varepsilon_k > \frac{1}{5}.$$

It is easy to see

$$\tau_1 = \frac{15}{32} < \frac{1}{2}, \ \tau_k - \tau_{k+1} = \frac{1}{4(k+2)^4}, \ k = 1, 2, 3, \ldots,$$

$$\aleph_{r_0}(\tau, s) = \frac{1}{\sin(1)} \begin{cases} \sin(s)\sin(1-\tau), & 0 \le s \le \tau \le 1, \\ \sin(\tau)\sin(1-s), & 0 \le \tau \le s \le 1. \end{cases}$$

Since $\sum_{k=1}^{\infty} \frac{1}{k^4} = \frac{\pi^4}{90}$ and $\sum_{k=1}^{\infty} \frac{1}{k^2} = \frac{\pi^2}{6}$, it follows that

$$\tau^* = \lim_{k\to\infty} \tau_k = \frac{31}{64} - \sum_{i=1}^{\infty} \frac{1}{4(i+1)^4} = \frac{47}{64} - \frac{\pi^4}{360} > \frac{1}{5},$$

Also,

$$\mathrm{Q}_1, \mathrm{Q}_2 \in L^p[0,1] \quad \text{and} \quad \prod_{i=1}^{2} \varphi_i^* = \frac{1}{\sqrt{12}}.$$

$$\int_{\varepsilon_1}^{1-\varepsilon_1} \aleph_{r_0}(s,s) s^{\frac{2(N-1)}{2-N}} ds = \frac{1}{\sin(1)} \int_{\varepsilon_1}^{1-\varepsilon_1} \frac{\sin(s)\sin(1-s)}{s^4} ds = 0.2903290174,$$

$$\delta(\varepsilon_1) \frac{r_0^2}{(N-2)^2} \prod_{i=1}^{n} \varphi_i^* \int_{\varepsilon_1}^{1-\varepsilon_1} \aleph_{r_0}(s,s) s^{\frac{2(N-1)}{2-N}} ds = 0.04485939891.$$

$$\theta = \max\left\{ \left[\delta(\varepsilon_1) \frac{r_0^2}{(N-2)^2} \prod_{i=1}^{n} \varphi_i^* \int_{\varepsilon_1}^{1-\varepsilon_1} \aleph_{r_0}(s,s) s^{\frac{2(N-1)}{2-N}} ds \right]^{-1}, 1 \right\} \approx 22.29187248.$$

and let $q = 2$, $p_1 = p_2 = 1/4$, then $\prod_{i=1}^{n} \|\varphi_i\|_{p_i} = 0.01733273706$, $\|\aleph_{r_0}\|_q = 0.1970313855$ and

$$\mathtt{M}_1 < \left[\frac{r_0^2}{(N-2)^2} \|\aleph_{r_0}\|_q \prod_{i=1}^{n} \|\varphi_i\|_{p_i} \right]^{-1} \approx 292.8177775.$$

So, let $\mathtt{M}_1 = 291$. In addition, if we take

$$\mathtt{E}_k = 10^{-4k}, \ \mathtt{D}_k = 10^{-(4k+2)},$$

then

$$\begin{aligned} \mathtt{E}_{k+1} = 10^{-(4k+4)} &< \frac{1}{5} \times 10^{-(4k+2)} < \delta(\varepsilon_k)\mathtt{D}_k \\ &< \mathtt{D}_k = 10^{-(4k+2)} < \mathtt{E}_k = 10^{-4k}, \end{aligned}$$

and $\mathtt{g}_1, \mathtt{g}_2$ satisfies the following growth conditions:

$$\mathtt{g}_{\mathtt{j}}(v) \le \mathtt{M}_1 \mathtt{E}_k = 291 \times 10^{-4k}, \quad v \in \left[0, 10^{-4k}\right]$$

$$\mathtt{g}_{\mathtt{j}}(v) \ge \theta \mathtt{D}_k = 22.29187248 \times 10^{-(4k+2)}, \quad v \in \left[\frac{1}{5} \times 10^{-(4k+2)}, 10^{-(4k+2)}\right].$$

Then all the conditions of Theorem 3 are satisfied. Therefore, by Theorem 3, the boundary value problem (10) has infinitely many positive solutions $\{(v_1^{[k]}, v_2^{[k]})\}_{k=1}^{\infty}$ such that $10^{-(4k+2)} \le \|v_{\mathtt{j}}^{[k]}\| \le 10^{-4k}$ for each $k = 1, 2, 3, \cdots$, and $\mathtt{j} = 1, 2$.

5 Conclusion

In this paper, we developed a theory to study existence of infinitely many positive radial solutions for certain type of iterative system of nonlinear elliptic equations by applying Krasnoselskii's cone fixed point theorem in a Banach spaces. In the future, we study the existence of positive radial solutions for an iterative system of elliptic equations with logarithmic nonlinear term. Also, we study global existence and ground state solutions to the addressed problem.

Acknowledgements The authors would like to thank the referees for their valuable suggestions and comments for the improvement of the paper.

Author Contributions The study was carried out in collaboration of all authors. All authors read and approved the final manuscript.

Funding Not Applicable.

Data Availability Data sharing not applicable to this paper as no data sets were generated or analyzed during the current study.

Declarations

Conflict of interest It is declared that authors has no competing interests.

Ethical approval This article does not contain any studies with human participants or animals performed by any of the authors.

References

1. Aberqi, A., Bennouna, J., Elmassoudi, M.: Nonlinear elliptic equations with some measure data in Musielak–Orlicz spaces. Nonlinrear Dyn. Syst. Theory **19**(2), 227–242 (2019)
2. Ali, J., Padhi, S.: Existence of multiple positive radial solutions to elliptic equations in an annulus. Com. App. Anal. **22**(4), 695710 (2018)
3. Ali, J., Shivaji, R., Ramaswamy, M.: Multiple positive solutions for classes of elliptic systems with combined nonlinear effects. Differ. Integral Equ. **19**(6), 669–680 (2006)
4. Ali, J., Brown, K., Shivaji, R.: Positive solutions for $n \times n$ elliptic systems with combined nonlinear effects. Differ. Integral Equ. **24**(3–4), 307–324 (2011)
5. Bouguetof, K., Foukrach, D.: On local existence and blow-up solutions for a time-space fractional variable order superdiffusion equation with exponential nonlinearity. Pan. Am. Math. J. **30**(3), 21–34 (2020)
6. Dalmasso, R.: Existence and uniqueness of positive solutions of semilinear elliptic systems. Nonlinear Anal. **39**(5), 559–568 (2000)
7. Dong, X., Wei, Y.: Existence of radial solutions for nonlinear elliptic equations with gradient terms in annular domains. Nonlinear Anal. **187**, 93–109 (2019)
8. Foukrach, D.: On nonexistence of solutions to a nonlinear Cauchy problem for a higher order hyperbolic equation. Gen. Math. **25**(1–2), 45–52 (2017)
9. Guo, D., Lakshmikantham, V.: Nonlinear Problems in Abstract Cones. Academic Press, San Diego (1988)
10. Hai, D.D.: Uniqueness of positive solutions for semilinear elliptic systems. J. Math. Anal. Appl. **313**(2), 761–767 (2006)
11. Hai, D.D., Shivaji, R.: An existence result on positive solutions for a class of semilinear elliptic systems. Proc. R. Soc. Edinb. Sect. A **134**(1), 137–141 (2004)
12. Hai, D.D., Shivaji, R.: Uniqueness of positive solutions for a class of semipositone elliptic systems. Nonlinear Anal. **66**(2), 396–402 (2007)
13. Kaabar, M.K.A., Shabibi, M., Alzabut, J., Etemad, S., Sudsutad, W., Martínez, F., Rezapour, S.: Investigation of the fractional strongly singular thermostat model via fixed point techniques. Mathematics **9**(18), 2298 (2021)
14. Kaabar, M.K.A., Refice, A., Souid, M.S., Martínez, F., Etemad, S., Siri, Z., Rezapour, S.: Existence and UHR stability of solutions to the implicit nonlinear FBVP in the variable order settings. Mathematics **9**(14), 1693 (2021)
15. Kajikiya, R., Ko, E.: Existence of positive radial solutions for a semipositone elliptic equation. J. Math. Anal. Appl. **484**, 123735 (2020)
16. Khuddush, M., Prasad, K.R.: Positive solutions for an iterative system of nonlinear elliptic equations. Bull. Malays. Math. Sci. Soc. **45**, 245–272 (2022). https://doi.org/10.1007/s40840-021-01183-y
17. Khuddush, M., Prasad, K.R., Bharathi, B.: Denumerably many positive radial solutions for the iterative system of Minkowski–Curvature equations. Int. J. Nonlinear Anal. Appl. **13**(1), 3613–32 (2022)

18. Khuddush, M., Prasad, K.R., Bharathi, B.: Global existence and blowup of solutions for a semilinear Klein–Gordon equation with the product of logarithmic and power-type nonlinearity. Ann. Univ. Ferrara **68**, 187–201 (2022). https://doi.org/10.1007/s11565-022-00395-9
19. Lan, K., Webb, J.R.L.: Positive solutions of semilinear differential equations with singularities. J. Differ. Equ. **148**, 407421 (1998)
20. Matar, N.M., Abbas, M.I., Alzabut, J., Kaabar, M.K.A., Etemad, S., Rezapour, S.: Investigation of the p-Laplacian nonperiodic nonlinear boundary value problem via generalized Caputo fractional derivatives. Adv. Differ. Equ. **2021**(1), 1–18 (2021)
21. Mei, L.: Structure of positive radial solutions of a quasilinear elliptic problem with singular nonlinearity. Complex Var. Elliptic Equ. **63**(11), 1595–603 (2018). https://doi.org/10.1080/17476933.2017.1399367
22. Ni, W.M.: Some aspects of semilinear elliptic equations on $\mathbb{R}^n$, in nonlinear diffusion equations and their equilibrium states II (Ed. by W. M. Ni, L. A. Peletier, J. Serrin). Springer-Verlag, New York, 171–205 (1988)
23. Pandey, P., Gomez-Aguilar, J.F., Kaabar, M.K.A., Siri, Z., Abd Allah, A.M.: Mathematical modeling of COVID-19 pandemic in India using Caputo–Fabrizio fractional derivative. Comput. Biol. Med. **145**, 105518 (2022)
24. Prasad, K. R., Khuddush, M., Bharathi, B.: Local existence and blow up of solutions for a system of viscoelastic wave equations of Kirchhoff type with delay and logarithmic nonlinearity. Int. J. Math. Model. Comput. **11**(3), 1–11. https://doi.org/10.30495/ijm2c.2021.684816
25. Prasad, K.R., Khuddush, M., Bharathi, B.: Denumerably many positive radial solutions for the iterative system of elliptic equations in an annulus. Palestine J. Math. **11**(1), 549–559 (2022)
26. Rezapour, S., Imran, A., Hussain, A., Martinez, F., Etemad, S., Kaabar, M.K.A.: Condensing functions and approximate endpoint criterion for the existence analysis of quantum integro-difference FBVPs. Symmetry **13**(3), 469 (2021)
27. Son, B., Wang, P.: Positive radial solutions to classes of nonlinear elliptic systems on the exterior of a ball. J. Math. Anal. Appl. **488**, 124069 (2020)
28. Yanagida, E.: Uniqueness of positive radial solutions of $\Delta u + texttttg(|texttttx|)u + texttttg(|texttttx|)u^p = 0$ in $\mathbb{R}^n$. Arch. Ratl. Mech. Anal. **115**, 257–274 (1991)
29. Yue, X.-G., Samei, M.E., Fathipour, A., Kaabar, M.K.A., Kashuri, A.: Using Krasnoselskii's theorem to investigate the Cauchy and neutral fractional q-integro-differential equation via numerical technique. Nonlinear Eng. **11**(1), 186–206 (2022). https://doi.org/10.1515/nleng-2022-0023

Publisher's Note Springer Nature remains neutral with regard to jurisdictional claims in published maps and institutional affiliations.

Springer Nature or its licensor holds exclusive rights to this article under a publishing agreement with the author(s) or other rightsholder(s); author self-archiving of the accepted manuscript version of this article is solely governed by the terms of such publishing agreement and applicable law.

Bol. Soc. Mat. Mex. (2022)28:75
https://doi.org/10.1007/s40590-022-00467-y

Sociedad Matemática Mexicana

ORIGINAL ARTICLE

Global exponential stability of almost periodic solutions for quaternion-valued RNNs with mixed delays on time scales

Mahammad Khuddush[1] · **K. Rajendra Prasad**[2]

Received: 20 September 2021 / Accepted: 20 September 2022
© Sociedad Matemática Mexicana 2022

Abstract
This paper deals with the time scale model of time-delayed quaternion-valued recurrent neural networks (QVRNNs). Using contraction mapping principle and exponential dichotomy of linear dynamic equations, we derive sufficient conditions for the existence, uniqueness and the global exponential stability of almost periodic solutions to the addressed QVRNNs. Finally, an appropriate example is given to check the feasibility of our obtained results.

Keywords Quaternion-valued recurrent neural networks · Time scale · Mixed delays · Almost periodic solutions

Mathematics Subject Classification Primary 34N05 · Secondary 34K14

1 Introduction

Many neural network models have been investigated and extensively utilised in domains such as nonlinear dynamics, signal processing, and other areas [9, 12, 17, 22, 24, 27, 28, 34, 36, 45, 47]. Neural networks often need to meet the requirement of stability to be used in these real life applications, see Refs. [1, 4, 8, 11, 13, 14, 37, 49]. For recent works on real valued neural networks

✉ Mahammad Khuddush
khuddush89@gmail.com

K. Rajendra Prasad
rajendra92@rediffmail.com

[1] Department of Mathematics, Dr. Lankapalli Bullayya College of Engineering, Resapuvanipalem, Visakhapatnam, Andhra Pradesh 530013, India

[2] Department of Applied Mathematics, College of Science and Technology, Andhra University, Visakhapatnam 530003, India

Published online: 11 October 2022

(RVNNs), complex valued neural networks (CVNNs) and quaternion valued neural networks (QVNNs), see Refs. [7, 10, 18, 20, 22, 24–27, 33–38, 40–47].

Li et al. [23] derived necessary conditions for the existence and global exponential stability of pseudo-almost periodic solutions of QVRNNs

$$\mathtt{z}_{\mathtt{s}}'(\mathtt{r}) = -\mathtt{A}_{\mathtt{s}}(\mathtt{r})\mathtt{z}_{\mathtt{s}}(\mathtt{r}) + \sum_{\mathfrak{d}=1}^{\mathfrak{p}} \mathtt{A}_{\mathtt{s}\mathfrak{d}}(\mathtt{r})\mathtt{h}_{\mathfrak{d}}\big(\mathtt{z}_{\mathfrak{d}}(\mathtt{r})\big) + \sum_{\mathfrak{d}=1}^{\mathfrak{p}} \mathtt{C}_{\mathtt{s}\mathfrak{d}}(\mathtt{r})\mathtt{K}_{\mathfrak{d}}\big(\mathtt{z}_{\mathfrak{d}}(\mathtt{r}-\tau_{\mathtt{s}\mathfrak{d}}(\mathtt{r}))\big)$$
$$+ \sum_{\mathfrak{d}=1}^{\mathfrak{p}} \mathtt{D}_{\mathtt{s}\mathfrak{d}}(\mathtt{r}) \int_{-\infty}^{\mathtt{r}} \chi_{\mathtt{s}\mathfrak{d}}(\mathtt{r}-\omega)\mathtt{g}_{\mathfrak{d}}(\mathtt{z}_{\mathfrak{d}}(\omega))\mathtt{d}\omega + \mathfrak{P}_{\mathtt{s}}(\mathtt{r}), \ \ \mathtt{r} \in \mathbb{R},$$

by an application of well-known fixed point theorems. Recently, You et al. [45] developed a criteria for the existence, uniqueness and exponential stability of discrete QVNNs

$$\mathtt{z}_{\mathtt{s}}(\kappa+1) = -\mathtt{A}_{\mathtt{s}}\mathtt{z}_{\mathtt{s}}(\kappa-\vartheta) + \sum_{\mathfrak{d}=1}^{\mathfrak{p}} \mathtt{B}_{\mathtt{s}\mathfrak{d}}\mathtt{h}_{\mathfrak{d}}(\mathtt{z}_{\mathfrak{d}}(\kappa)) + \sum_{\mathfrak{d}=1}^{\mathfrak{p}} \mathtt{C}_{\mathtt{s}\mathfrak{d}}\mathtt{g}_{\mathfrak{d}}(\mathtt{z}_{\mathfrak{d}}(\kappa-\tau(\kappa))) + \mathtt{Q}_{\mathtt{s}}.$$

On the other hand, recently, researchers have shown considerable interest in studying dynamic equations on time scales, which puts both disciplines into one frame, in contemplation of merging the study of difference and differential equations. Furthermore, the fundamental findings on this topic are highly supported by Bohner and Peterson's works [5, 6] and articles [2, 3, 15, 16, 19, 39]. Since the environment changes on an almost periodic basis in real-world occurrences. In real life, the almost periodic fluctuation of the ecosystem is more common and pervasive than the periodic fluctuation, so it is a key factor in numerous natural and environmental dynamical frameworks. Some of the good contributions in this field can be found in Refs. [29–32] and references therein.

The works mentioned above inspired us to investigate the following QVRNNs with mixed delays on time scales in this article:

$$\left.\begin{aligned} \mathtt{z}_q^{\Delta}(t) = &-\alpha_q(t)\mathtt{z}_q(t) + \sum_{r=1}^{n} \beta_{qr}(t) f_r\big(\mathtt{z}_r(t)\big) + \sum_{r=1}^{n} \gamma_{qr}(t) g_r\big(\mathtt{z}_r(t-\tau_{qr}(t))\big) \\ &+ \sum_{r=1}^{n} \delta_{qr}(t) \int_{-\infty}^{t} G_{qr}(t-u) h_r(\mathtt{z}_r(u))\Delta u + \mathcal{J}_q(t), \quad t \in \mathbb{T}, \end{aligned}\right\} \tag{1}$$

where $q \in \Omega := \{1, 2, \cdots, n\}$, $\mathtt{z}_q(t) \in \mathbb{H} \otimes \mathbb{T}$ corresponds to the state of the qth unit at time $t, f_r, g_r, h_r \in \mathbb{H} \otimes \mathbb{T}$ denote the activation functions, $\beta_{qr}(t), \gamma_{qr}(t), \delta_{qr}(t) \in \mathbb{H} \otimes \mathbb{T}$ represent the connection weights, the discretely delayed connection weights and the distributively delayed connection weights between the *rth* neuron and the *qth* neuron at time t, respectively; $\mathcal{J}_q(t) \in \mathbb{H} \otimes \mathbb{T}$ is the external input on the *qth* neuron at time $t, \tau_{qr}(t) \geq 0$ denotes the transmission delay, $\alpha_q : \mathbb{T} \to \mathbb{T}^+$ represents the rate with which the *qth* unit will reset its potential to the resting state when disconnected from the network and external inputs. The kernel $G_{qr} : \mathbb{T} \to \mathbb{T}^+$ satisfies that $\int_0^{+\infty} G_{qr}(s)\Delta s \leq 1$, $t \in \mathbb{T}$, $q, r \in \Omega$.

We consider the initial value for system (1) is

$$\mathrm{z}_q(u) = \varphi_q(u),\ u \in (-\infty, 0]_{\mathbb{T}},\ q \in \Omega,$$

where $\varphi_q = \varphi_q^{\mathrm{R}} + \mathbf{i}\varphi_q^{\mathrm{I}} + \mathbf{j}\varphi_q^{\mathrm{J}} + \mathbf{k}\varphi_q^{\mathrm{K}}$ is the quaternion-valued bounded continuous function defined on $(-\infty, 0]_{\mathbb{T}}$. Using contraction mapping principle and exponential dichotomy of linear dynamic equations, we derive sufficient conditions for the existence, uniqueness and the global exponential stability of almost periodic solutions to the QVRNNs (1). Finally, an appropriate example is given to check the feasibility of our obtained results.

2 Preliminaries

In this section, we introduce some definitions and state some preliminary results which are useful in the sequel. For convenience, for any almost periodic function $f(t)$ defined on $\mathbb{T}$, we denote

$$^{+}f = \sup_{t\in\mathbb{T}} |f(t)| \quad \text{and} \quad ^{-}f = \inf_{t\in\mathbb{T}} |f(t)|.$$

We denote the field of quaternion by $\mathbb{H} := \{\mathrm{z}_q : \mathrm{z}_q = \mathrm{z}_q^{\mathrm{R}} + \mathbf{i}\mathrm{z}_q^{\mathrm{I}} + \mathbf{j}\mathrm{z}_q^{\mathrm{J}} + \mathbf{k}\mathrm{z}_q^{\mathrm{K}}\}$, where $\mathrm{z}_q^{\mathrm{R}}, \mathrm{z}_q^{\mathrm{I}}, \mathrm{z}_q^{\mathrm{J}}$ and $\mathrm{z}_q^{\mathrm{K}}$ are all real coefficients. $\mathrm{z}_q^{\mathrm{R}} = \mathcal{R}e(y)$ is the real part of z_q and $\mathcal{I}m(y) = \mathbf{i}\mathrm{z}_q^{\mathrm{I}} + \mathbf{j}\mathrm{z}_q^{\mathrm{J}} + \mathbf{k}\mathrm{z}_q^{\mathrm{K}}$ denotes the imaginary part of z_q. The imaginary units $\mathbf{i}, \mathbf{j}$ and $\mathbf{k}$ satisfy the following multiplication rules

$$\mathbf{i}^2 = \mathbf{j}^2 = \mathbf{k}^2 = \mathbf{ijk} = -1,\ \mathbf{ij} = -\mathbf{ji} = \mathbf{k},\ \mathbf{jk} = -\mathbf{kj} = \mathbf{i},\ \mathbf{ki} = -\mathbf{ik} = \mathbf{j}.$$

From this, it can be concluded that the multiplication of quaternion does not satisfy commutative law. This is the main reason why quaternion are more complicated than the real-valued and complex-valued. Furthermore, $\overline{y}_q = \mathrm{z}_q^{\mathrm{R}} - \mathbf{i}\mathrm{z}_q^{\mathrm{I}} - \mathbf{j}\mathrm{z}_q^{\mathrm{J}} - \mathbf{k}\mathrm{z}_q^{\mathrm{K}} \in \mathbb{H}$ denotes the conjugate of z_q, and the module of quaternion z_q is given by

$$|\mathrm{z}_q| = \sqrt{\mathrm{z}_q\overline{y}_q} = \sqrt{\left(\mathrm{z}_q^{\mathrm{R}}\right)^2 + \left(\mathrm{z}_q^{\mathrm{I}}\right)^2 + \left(\mathrm{z}_q^{\mathrm{J}}\right)^2 + \left(\mathrm{z}_q^{\mathrm{K}}\right)^2}.$$

For a quaternion vector $y = (\mathrm{z}_1, \mathrm{z}_2, \cdots, \mathrm{z}_n)^T \in \mathbb{H}^n$, the norm of y is

$$\|y\| = \sqrt{\sum_{q=1}^{n} |\mathrm{z}_q|^2}.$$

Definition 2.1 [5] A time scale $\mathbb{T}$ is a nonempty closed subset of the real numbers $\mathbb{R}$. $\mathbb{T}$ has the topology that it inherits from the real numbers with the standard topology. It follows that the jump operators $\sigma, \rho : \mathbb{T} \to \mathbb{T}$, and the graininess $\mu : \mathbb{T} \to [0, \infty)$ are defined by $\sigma(t) = \inf\{\tau \in \mathbb{T} : \tau > t\}$, $\rho(t) = \sup\{\tau \in \mathbb{T} : \tau < t\}$ and $\mu(t) = \rho(t) - t$, respectively.

- In this definition, we put $\inf \emptyset = \sup \mathbb{T}$ and $\sup \emptyset = \inf \mathbb{T}$.

- The point $t \in \mathbb{T}$ is left-dense, left-scattered, right-dense, right-scattered if $\rho(t) = t$, $\rho(t) < t$, $\sigma(t) = t$, $\sigma(t) > t$, respectively.
- A function $f : \mathbb{T} \to \mathbb{R}$ is called rd-continuous provided it is continuous at right-dense points in $\mathbb{T}$ and its left-sided limits exist (finite) at left-dense points in $\mathbb{T}$. The set of all rd-continuous functions $f : \mathbb{T} \to \mathbb{R}$ is denoted by $C_{rd} = C_{rd}(\mathbb{T}) = C_{rd}(\mathbb{T}, \mathbb{R})$.
- A function $f : \mathbb{T} \to \mathbb{R}$ is called ld-continuous provided it is continuous at left-dense points in $\mathbb{T}$ and its right-sided limits exist (finite) at right-dense points in $\mathbb{T}$. The set of all ld-continuous functions $f : \mathbb{T} \to \mathbb{R}$ is denoted by $C_{ld} = C_{ld}(\mathbb{T}) = C_{ld}(\mathbb{T}, \mathbb{R})$.
- By an interval time scale, we mean the intersection of a real interval with a given time scale. i.e., $[a, b]_{\mathbb{T}} = [a, b] \cap \mathbb{T}$ other intervals can be defined similarly.

Definition 2.2 [5] A function $p : \mathbb{T} \to \mathbb{R}$ is called regressive provided $1 + \mu(t)p(t) \neq 0$ for all $t \in \mathbb{T}^k$; $p : \mathbb{T} \to \mathbb{R}$ is called positively regressive provided $1 + \mu(t)p(t) > 0$ for all $t \in \mathbb{T}^k$ The set of all regressive and rd-continuous functions $p : \mathbb{T} \to \mathbb{R}$ will be denoted by $\mathcal{R} = \mathcal{R}(\mathbb{T}, \mathbb{R})$ and the set of all positively regressive functions and rd-continuous functions will be denoted by $\mathcal{R}^+ = \mathcal{R}^+(\mathbb{T}, \mathbb{R})$.

Definition 2.3 [5] If p is regressive function, then the generalized exponential function e_p is defined by

$$e_p(t, s) = \exp\left\{ \int_s^t \xi_{\mu(x)}(p(x))\Delta x \right\}$$

with the cylinder transformation

$$\xi_h(w) = \begin{cases} \dfrac{Log(1 + hw)}{h}, & h \neq 0, \\ w, & h = 0. \end{cases}$$

Lemma 2.4 [5] *Let $p : \mathbb{T} \to \mathbb{R}$ be right-dense continuous and regressive, $b \in \mathbb{T}$ and $c \in \mathbb{R}$. Then the unique solution of the initial value problem*

$$\mathrm{z}^{\Delta}(t) = p(t)\mathrm{z}(t) + f(t), \quad \mathrm{z}(b) = c$$

is given by

$$\mathrm{z}(t) = e_r(t, b)c + \int_a^t e_r(t, \sigma(u))f(u)\Delta u.$$

Lemma 2.5 [5] *If $f(t, \cdot)$ and $f^{\Delta}(t, \cdot)$ are continuous, then*

$$\left(\int_a^t f(t,u)\Delta u\right)^{\Delta} = f(\sigma(t),t) + \int_a^t f^{\Delta}(t,u)\Delta u.$$

Definition 2.6 [21] A time scale $\mathbb{T}$ is called an almost periodic time scale if

$$\mho = \{\tau \in \mathbb{R} : t + \tau \in \mathbb{T}, \forall\, t \in \mathbb{T}\} \neq \{0\}.$$

Definition 2.7 [21] Let $\mathbb{T}$ be an almost periodic time scale. A function $\mathtt{z} \in C(\mathbb{T}, \mathbb{R}^n)$ is called an almost periodic function if the ε-translation set of $\mathtt{z}$ i.e.,

$$E\{\varepsilon, \mathtt{z}\} = \left\{\tau \in \mho : |\mathtt{z}(t+\tau) - \mathtt{z}(t)| < \varepsilon, \forall\, t \in \mathbb{T}\right\}$$

is a relatively dense set in $\mathbb{T}$ for all $\varepsilon > 0$, that is, for any given $\varepsilon > 0$, there exists a constant $l(\varepsilon) > 0$ such that each interval of length $l(\varepsilon) > 0$ contains a $\tau(\varepsilon) \in E\{\varepsilon, \mathtt{z}\}$ such that

$$|\mathtt{z}(t+\tau) - \mathtt{z}(t)| < \varepsilon,\ \forall\, t \in \mathbb{T}.$$

τ is called the ε-translation number of $\mathtt{z}(t)$ and $l(\varepsilon)$ is called the inclusion length of $E\{\varepsilon, \mathtt{z}\}$.

Definition 2.8 The solution $\mathtt{z}^*(t) = (\mathtt{z}_1^*(t), \mathtt{z}_2^*(t), \cdots, \mathtt{z}_n^*(t))^T$ be an almost periodic solution of system (1) with initial value $\varphi^*(u) = (\varphi_1^*(u), \varphi_2^*(u), \cdots, \varphi_n^*(u))^T$, $u \in (-\infty, 0]_{\mathbb{T}}$. If there exist positive constants ξ with $\ominus\xi \in \mathcal{R}^+$ and $\mathtt{N} > 1$ such that for an arbitrary solution $\mathtt{z}(t) = (\mathtt{z}_1(t), \mathtt{z}_2(t), \cdots, \mathtt{z}_n(t))^T$ of system (1) with initial value $\varphi(u) = (\varphi_1(u), \varphi_2(u), \cdots, \varphi_n(u))^T$, $u \in (-\infty, 0]_{\mathbb{T}}$ satisfies

$$\|\mathtt{z}(t) - \mathtt{z}^*(t)\| \leq \mathtt{N}\|\varphi - \varphi^*\|_{\widehat{\Upsilon}} \mathtt{e}_{\ominus\xi}(\mathtt{t}, 0),\ \mathtt{t} \in [0, +\infty)_{\mathbb{T}},$$

where

$$\|\varphi - \varphi^*\|_{\widehat{\Upsilon}} = \max_{q\in\Omega}\left\{\sup_{u\in[0,\infty)_{\mathbb{T}}} |\varphi_q^m(u) - \varphi_q^{*m}(u)| : m \in \Lambda\right\}.$$

Then, the solution $\mathtt{z}^*(t)$ is said to be globally exponentially stable.

Definition 2.9 [48] Let $\mathtt{z} \in \mathbb{R}^n$ and $\mathtt{A}(\mathtt{t})$ be an $n \times n$ rd-continuous matrix on $\mathbb{T}$; the linear system

$$\mathtt{z}^{\Delta}(t) = \mathtt{A}(\mathtt{t})\mathtt{z}(\mathtt{t}), \quad \mathtt{t} \in \mathbb{T}, \tag{2}$$

is said to admit an exponential dichotomy on $\mathbb{T}$ if there exist positive constants k, α, projection P, and the fundamental solution matrix $\mathtt{z}(t)$ of (2) satisfying

$$|\mathtt{z}(t)\mathcal{P}\mathtt{z}^{-1}(\sigma(\tau))|_0 \le k e_{\ominus\alpha}(t,\sigma(\tau)), \quad \tau, t \in \mathbb{T},\ t \ge \tau,$$

$$|\mathtt{z}(t)(\mathcal{I}-\mathcal{P})\mathtt{z}^{-1}(\sigma(s))|_0 \le k e_{\ominus\alpha}(\sigma(\tau),t), \quad \tau, t \in \mathbb{T},\ t \le \tau,$$

where $|\cdot|_0$ is a matrix norm on $\mathbb{T}$; that is, if $\mathtt{A} = (\mathtt{a}_{\mathtt{ij}})_{\mathtt{n}\times\mathtt{n}}$, then we can take $|\mathtt{A}|_0 = \big(\sum_{\mathtt{i}=1}^{\mathtt{n}} \sum_{\mathtt{j}=1}^{\mathtt{n}} |\mathtt{a}_{\mathtt{ij}}|^2\big)^{1/2}$.

Lemma 2.10 [21] *If the linear system* (2) *admits an exponential dichotomy, then the following system* $\mathtt{z}^{\Delta}(t) = \mathtt{A}(\mathtt{t})\mathtt{z}(\mathtt{t}) + \mathtt{f}(\mathtt{t}), \quad \mathtt{t} \in \mathbb{T}$, *has a solution as follows*:

$$\mathtt{z}(t) = \int_{-\infty}^{t} \mathtt{z}(t)\mathcal{P}\mathtt{z}^{-1}(\sigma(\tau))f(\tau)\Delta\tau - \int_{t}^{+\infty} \mathtt{z}(t)(\mathcal{I}-\mathcal{P})\mathtt{z}^{-1}(\sigma(\tau))f(\tau)\Delta\tau,$$

where $\mathtt{z}(t)$ is the fundamental solution matrix of (2).

Lemma 2.11 [21] *Let* $\mathtt{A}(\mathtt{t})$ *be a regressive* $n \times n$ *matrix-valued function on* $\mathbb{T}$. *Let* $t_0 \in \mathbb{T}$ *and* $\mathtt{z}_0 \in \mathbb{R}^n$, *then the initial value problem* $\mathtt{z}^{\Delta}(t) = \mathtt{A}(\mathtt{t})\mathtt{z}(\mathtt{t})$, $\mathtt{z}(t_0) = \mathtt{z}_0$ *has a unique solution* $\mathtt{z}(t) = e_{\mathtt{A}}(t, t_0)\mathtt{z}_0$.

Lemma 2.12 [21] *Let* $d_i(t) > 0$ *be a function on* $\mathbb{T}$ *such that* $-d_i(t) \in \mathcal{R}^+$ *for all* $t \in \mathbb{T}$ *and* $\min\limits_{1 \le i \le n} \Big\{ \inf\limits_{t\in\mathbb{T}} d_i(t) \Big\} > 0$. *Then, the linear system*

$$\mathtt{z}^{\Delta}(t) = \mathrm{diag}\big(-d_1(t), -d_2(t), \cdots, -d_m(t)\big)\mathtt{z}(t)$$

admits an exponential dichotomy on $\mathbb{T}$.

Lemma 2.13 [27] *A quaternion-valued function* $y = \mathtt{z}^{\mathtt{R}} + \mathbf{i}\mathtt{z}^{\mathtt{I}} + \mathbf{j}\mathtt{z}^{\mathtt{J}} + \mathbf{k}\mathtt{z}^{\mathtt{K}}$, $\mathtt{z} \in BC(\mathbb{H}\otimes\mathbb{T}, \mathbb{H}\otimes\mathbb{T})$ *is called an almost periodic function if for* $m \in \Lambda := \{\mathtt{R}, \mathtt{I}, \mathtt{J}, \mathtt{K}\}$, $\mathtt{z}^m \in AA(\mathbb{H}\otimes\mathbb{T}, \mathbb{H}\otimes\mathbb{T})$.

To decompose the QVRNN (1) into four real value systems, we need the following assumption:

$(\mathcal{S})$ Let $\mathtt{z}_q = \mathtt{z}_q^{\mathtt{R}} + \mathbf{i}\mathtt{z}_q^{\mathtt{I}} + \mathbf{j}\mathtt{z}_q^{\mathtt{J}} + \mathbf{k}\mathtt{z}_q^{\mathtt{K}}$. Then the activation functions $f_r(\mathtt{z}_r)$, $g_r(\mathtt{z}_r)$ and $h_r(\mathtt{z}_r)$ of (1) can be expressed as

$$\begin{aligned}
f_r(\mathtt{z}_r) =& f_r^{\mathtt{R}}(\mathtt{z}_r^{\mathtt{R}}, \mathtt{z}_r^{\mathtt{I}}, \mathtt{z}_r^{\mathtt{J}}, \mathtt{z}_r^{\mathtt{K}}) + \mathbf{i} f_r^{\mathtt{I}}(\mathtt{z}_r^{\mathtt{R}}, \mathtt{z}_r^{\mathtt{I}}, \mathtt{z}_r^{\mathtt{J}}, \mathtt{z}_r^{\mathtt{K}}) \\
&+ \mathbf{j} f_r^{\mathtt{J}}(\mathtt{z}_r^{\mathtt{R}}, \mathtt{z}_r^{\mathtt{I}}, \mathtt{z}_r^{\mathtt{J}}, \mathtt{z}_r^{\mathtt{K}}) + \mathbf{k} f_r^{\mathtt{K}}(\mathtt{z}_r^{\mathtt{R}}, \mathtt{z}_r^{\mathtt{I}}, \mathtt{z}_r^{\mathtt{J}}, \mathtt{z}_r^{\mathtt{K}}), \\
g_r(\mathtt{z}_r) =& g_r^{\mathtt{R}}(\mathtt{z}_r^{\mathtt{R}}, \mathtt{z}_r^{\mathtt{I}}, \mathtt{z}_r^{\mathtt{J}}, \mathtt{z}_r^{\mathtt{K}}) + \mathbf{i}\, g_r^{\mathtt{I}}(\mathtt{z}_r^{\mathtt{R}}, \mathtt{z}_r^{\mathtt{I}}, \mathtt{z}_r^{\mathtt{J}}, \mathtt{z}_r^{\mathtt{K}}) \\
&+ \mathbf{j}\, g_r^{\mathtt{J}}(\mathtt{z}_r^{\mathtt{R}}, \mathtt{z}_r^{\mathtt{I}}, \mathtt{z}_r^{\mathtt{J}}, \mathtt{z}_r^{\mathtt{K}}) + \mathbf{k}\, g_r^{\mathtt{K}}(\mathtt{z}_r^{\mathtt{R}}, \mathtt{z}_r^{\mathtt{I}}, \mathtt{z}_r^{\mathtt{J}}, \mathtt{z}_r^{\mathtt{K}}), \\
h_r(\mathtt{z}_r) =& h_r^{\mathtt{R}}(\mathtt{z}_r^{\mathtt{R}}, \mathtt{z}_r^{\mathtt{I}}, \mathtt{z}_r^{\mathtt{J}}, \mathtt{z}_r^{\mathtt{K}}) + \mathbf{i}\, h_r^{\mathtt{I}}(\mathtt{z}_r^{\mathtt{R}}, \mathtt{z}_r^{\mathtt{I}}, \mathtt{z}_r^{\mathtt{J}}, \mathtt{z}_r^{\mathtt{K}}) \\
&+ \mathbf{j} h_r^{\mathtt{J}}(\mathtt{z}_r^{\mathtt{R}}, \mathtt{z}_r^{\mathtt{I}}, \mathtt{z}_r^{\mathtt{J}}, \mathtt{z}_r^{\mathtt{K}}) + \mathbf{k}\, h_r^{\mathtt{K}}(\mathtt{z}_r^{\mathtt{R}}, \mathtt{z}_r^{\mathtt{I}}, \mathtt{z}_r^{\mathtt{J}}, \mathtt{z}_r^{\mathtt{K}}).
\end{aligned}$$

Then, by Hamiltons multiplication rules and $(\mathcal{S})$, we can transform system (1) into the following four real-valued systems

$$
\begin{aligned}
&\left(\mathtt{z}\mathtt{R}_{\mathtt{q}}(\mathtt{t})\right)^{\Delta} = -\alpha_{\mathtt{q}}(\mathtt{t})\mathtt{z}_{\mathtt{q}}\mathtt{R}(\mathtt{t}) + \sum_{\mathtt{r}=1}^{\mathtt{n}}\Big[\beta_{\mathtt{qr}}\mathtt{R}(\mathtt{t})\mathtt{f}_{\mathtt{r}}\mathtt{R}\big(\mathtt{z}_{\mathtt{r}}\mathtt{R}(\mathtt{t})\big) - \beta_{\mathtt{qr}}\mathtt{I}(\mathtt{t})\mathtt{f}_{\mathtt{r}}\mathtt{I}\big(\mathtt{z}_{\mathtt{r}}\mathtt{I}(\mathtt{t})\big)\\
&\quad - \beta_{qr}J(t)f_rJ\big(\mathtt{z}_{\mathtt{r}}\mathtt{J}(\mathtt{t})\big) - \beta_{\mathtt{qr}}\mathtt{K}(\mathtt{t})\mathtt{f}_{\mathtt{r}}\mathtt{K}\big(\mathtt{z}_{\mathtt{r}}\mathtt{K}(\mathtt{t})\big)\Big]\\
&\quad + \sum_{r=1}^{n}\Big[\gamma_{qr}R(t)g_rR\big(\mathtt{z}_{\mathtt{r}}\mathtt{R}(\mathtt{t}-\tau_{\mathtt{qr}})\big) - \gamma_{\mathtt{qr}}\mathtt{I}(\mathtt{t})\mathtt{g}_{\mathtt{r}}\mathtt{I}\big(\mathtt{z}_{\mathtt{r}}\mathtt{I}(\mathtt{t}-\tau_{\mathtt{qr}})\big)\\
&\quad - \gamma_{qr}J(t)g_rJ\big(\mathtt{z}_{\mathtt{r}}\mathtt{J}(\mathtt{t}-\tau_{\mathtt{qr}})\big) - \gamma_{\mathtt{qr}}\mathtt{K}(\mathtt{t})\mathtt{g}_{\mathtt{r}}\mathtt{K}\big(\mathtt{z}_{\mathtt{r}}\mathtt{K}(\mathtt{t}-\tau_{\mathtt{qr}})\big)\Big]\\
&\quad + \sum_{r=1}^{n}\Big[\delta_{qr}R(t)\int_{-\infty}^{t}G_{qr}(t-u)h_rR(\mathtt{z}_{\mathtt{r}}\mathtt{R}(\mathtt{u}))\Delta\mathtt{u} - \delta_{\mathtt{qr}}\mathtt{I}(\mathtt{t})\int_{-\infty}^{\mathtt{t}}\mathtt{G}_{\mathtt{qr}}(\mathtt{t}-\mathtt{u})\mathtt{h}_{\mathtt{r}}\mathtt{I}(\mathtt{z}_{\mathtt{r}}\mathtt{I}(\mathtt{u}))\Delta\mathtt{u}\\
&\quad - \delta_{qr}J(t)\int_{-\infty}^{t}G_{qr}(t-u)h_rJ(\mathtt{z}_{\mathtt{r}}\mathtt{J}(\mathtt{u}))\Delta\mathtt{u} - \delta_{\mathtt{qr}}\mathtt{K}(\mathtt{t})\int_{-\infty}^{\mathtt{t}}\mathtt{G}_{\mathtt{qr}}(\mathtt{t}-\mathtt{u})\mathtt{h}_{\mathtt{r}}\mathtt{K}(\mathtt{z}_{\mathtt{r}}\mathtt{K}(\mathtt{u}))\Delta\mathtt{u}\Big] + \mathcal{J}_{\mathtt{q}}\mathtt{R}(\mathtt{t})\\
&= -\alpha_q(t)\mathtt{z}_{\mathtt{q}}\mathtt{R}(\mathtt{t}) + \mathtt{K}_{\mathtt{q}}\mathtt{R}(\mathtt{t},\mathtt{z}(\mathtt{t})) + \mathcal{J}_{\mathtt{q}}\mathtt{R}(\mathtt{t}),\ \mathtt{q}\in\Omega,\\
&\left(\mathtt{z}\mathtt{I}_{\mathtt{q}}(\mathtt{t})\right)^{\Delta} = -\alpha_{\mathtt{q}}(\mathtt{t})\mathtt{z}_{\mathtt{q}}\mathtt{I}(\mathtt{t}) + \sum_{\mathtt{r}=1}^{\mathtt{n}}\Big[\beta_{\mathtt{qr}}\mathtt{R}(\mathtt{t})\mathtt{f}_{\mathtt{r}}\mathtt{I}\big(\mathtt{z}_{\mathtt{r}}\mathtt{I}(\mathtt{t})\big) + \beta_{\mathtt{qr}}\mathtt{I}(\mathtt{t})\mathtt{f}_{\mathtt{r}}\mathtt{R}\big(\mathtt{z}_{\mathtt{r}}\mathtt{R}(\mathtt{t})\big)\\
&\quad + \beta_{qr}J(t)f_rK\big(\mathtt{z}_{\mathtt{r}}\mathtt{K}(\mathtt{t})\big) - \beta_{\mathtt{qr}}\mathtt{K}(\mathtt{t})\mathtt{f}_{\mathtt{r}}\mathtt{J}\big(\mathtt{z}_{\mathtt{r}}\mathtt{J}(\mathtt{t})\big)\Big]\\
&\quad + \sum_{r=1}^{n}\Big[\gamma_{qr}R(t)g_rI\big(\mathtt{z}_{\mathtt{r}}\mathtt{I}(\mathtt{t}-\tau_{\mathtt{qr}})\big) + \gamma_{\mathtt{qr}}\mathtt{I}(\mathtt{t})\mathtt{g}_{\mathtt{r}}\mathtt{R}\big(\mathtt{z}_{\mathtt{r}}\mathtt{R}(\mathtt{t}-\tau_{\mathtt{qr}})\big)\\
&\quad + \gamma_{qr}J(t)g_rK\big(\mathtt{z}_{\mathtt{r}}\mathtt{K}(\mathtt{t}-\tau_{\mathtt{qr}})\big) - \gamma_{\mathtt{qr}}\mathtt{K}(\mathtt{t})\mathtt{g}_{\mathtt{r}}\mathtt{J}\big(\mathtt{z}_{\mathtt{r}}\mathtt{J}(\mathtt{t}-\tau_{\mathtt{qr}})\big)\Big]\\
&\quad + \sum_{r=1}^{n}\Big[\delta_{qr}R(t)\int_{-\infty}^{t}G_{qr}(t-u)h_rI(\mathtt{z}_{\mathtt{r}}\mathtt{I}(\mathtt{u}))\Delta\mathtt{u} + \delta_{\mathtt{qr}}\mathtt{I}(\mathtt{t})\int_{-\infty}^{\mathtt{t}}\mathtt{G}_{\mathtt{qr}}(\mathtt{t}-\mathtt{u})\mathtt{h}_{\mathtt{r}}\mathtt{R}(\mathtt{z}_{\mathtt{r}}\mathtt{R}(\mathtt{u}))\Delta\mathtt{u}\\
&\quad + \delta_{qr}J(t)\int_{-\infty}^{t}G_{qr}(t-u)h_rK(\mathtt{z}_{\mathtt{r}}\mathtt{K}(\mathtt{u}))\Delta\mathtt{u} - \delta_{\mathtt{qr}}\mathtt{K}(\mathtt{t})\int_{-\infty}^{\mathtt{t}}\mathtt{G}_{\mathtt{qr}}(\mathtt{t}-\mathtt{u})\mathtt{h}_{\mathtt{r}}\mathtt{J}(\mathtt{z}_{\mathtt{r}}\mathtt{J}(\mathtt{u}))\Delta\mathtt{u}\Big] + \mathcal{J}_{\mathtt{q}}\mathtt{I}(\mathtt{t})\\
&= -\alpha_q(t)\mathtt{z}_{\mathtt{q}}\mathtt{I}(\mathtt{t}) + \mathtt{K}_{\mathtt{q}}\mathtt{I}(\mathtt{t},\mathtt{z}(\mathtt{t})) + \mathcal{J}_{\mathtt{q}}\mathtt{I}(\mathtt{t}),\ \mathtt{q}\in\Omega,\\
&\left(\mathtt{z}\mathtt{J}_{\mathtt{q}}(\mathtt{t})\right)^{\Delta} = -\alpha_{\mathtt{q}}(\mathtt{t})\mathtt{z}_{\mathtt{q}}\mathtt{J}(\mathtt{t}) + \sum_{\mathtt{r}=1}^{\mathtt{n}}\Big[\beta_{\mathtt{qr}}\mathtt{R}(\mathtt{t})\mathtt{f}_{\mathtt{r}}\mathtt{J}\big(\mathtt{z}_{\mathtt{r}}\mathtt{J}(\mathtt{t})\big) + \beta_{\mathtt{qr}}\mathtt{J}(\mathtt{t})\mathtt{f}_{\mathtt{r}}\mathtt{R}\big(\mathtt{z}_{\mathtt{r}}\mathtt{R}(\mathtt{t})\big)\\
&\quad - \beta_{qr}I(t)f_rK\big(\mathtt{z}_{\mathtt{r}}\mathtt{K}(\mathtt{t})\big) + \beta_{\mathtt{qr}}\mathtt{K}(\mathtt{t})\mathtt{f}_{\mathtt{r}}\mathtt{I}\big(\mathtt{z}_{\mathtt{r}}\mathtt{I}(\mathtt{t})\big)\Big]\\
&\quad + \sum_{r=1}^{n}\Big[\gamma_{qr}R(t)g_rJ\big(\mathtt{z}_{\mathtt{r}}\mathtt{J}(\mathtt{t}-\tau_{\mathtt{qr}})\big) + \gamma_{\mathtt{qr}}\mathtt{J}(\mathtt{t})\mathtt{g}_{\mathtt{r}}\mathtt{R}\big(\mathtt{z}_{\mathtt{r}}\mathtt{R}(\mathtt{t}-\tau_{\mathtt{qr}})\big)\\
&\quad - \gamma_{qr}I(t)g_rK\big(\mathtt{z}_{\mathtt{r}}\mathtt{K}(\mathtt{t}-\tau_{\mathtt{qr}})\big) + \gamma_{\mathtt{qr}}\mathtt{K}(\mathtt{t})\mathtt{g}_{\mathtt{r}}\mathtt{I}\big(\mathtt{z}_{\mathtt{r}}\mathtt{I}(\mathtt{t}-\tau_{\mathtt{qr}})\big)\Big]\\
&\quad + \sum_{r=1}^{n}\Big[\delta_{qr}R(t)\int_{-\infty}^{t}G_{qr}(t-u)h_rJ(\mathtt{z}_{\mathtt{r}}\mathtt{J}(\mathtt{u}))\Delta\mathtt{u} + \delta_{\mathtt{qr}}\mathtt{J}(\mathtt{t})\int_{-\infty}^{\mathtt{t}}\mathtt{G}_{\mathtt{qr}}(\mathtt{t}-\mathtt{u})\mathtt{h}_{\mathtt{r}}\mathtt{R}(\mathtt{z}_{\mathtt{r}}\mathtt{R}(\mathtt{u}))\Delta\mathtt{u}\\
&\quad - \delta_{qr}I(t)\int_{-\infty}^{t}G_{qr}(t-u)h_rK(\mathtt{z}_{\mathtt{r}}\mathtt{K}(\mathtt{u}))\Delta\mathtt{u} + \delta_{\mathtt{qr}}\mathtt{K}(\mathtt{t})\int_{-\infty}^{\mathtt{t}}\mathtt{G}_{\mathtt{qr}}(\mathtt{t}-\mathtt{u})\mathtt{h}_{\mathtt{r}}\mathtt{I}(\mathtt{z}_{\mathtt{r}}\mathtt{I}(\mathtt{u}))\Delta\mathtt{u}\Big] + \mathcal{J}_{\mathtt{q}}\mathtt{J}(\mathtt{t})\\
&= -\alpha_q(t)\mathtt{z}_{\mathtt{q}}\mathtt{J}(\mathtt{t}) + \mathtt{K}_{\mathtt{q}}\mathtt{J}(\mathtt{t},\mathtt{z}(\mathtt{t})) + \mathcal{J}_{\mathtt{q}}\mathtt{J}(\mathtt{t}),\ \mathtt{q}\in\Omega,
\end{aligned}
$$

and

$$
\begin{aligned}
\left(\mathrm{z}_q^{\mathrm{K}}(t)\right)^{\Delta} &= -\alpha_q(t)\mathrm{z}_q^{\mathrm{K}}(t) + \sum_{r=1}^{n}\Big[\beta_{qr}^{\mathrm{R}}(t)f_r^{\mathrm{K}}\left(\mathrm{z}_r^{\mathrm{K}}(t)\right) + \beta_{qr}^{\mathrm{K}}(t)f_r^{\mathrm{R}}\left(\mathrm{z}_r^{\mathrm{R}}(t)\right) \\
&+ \beta_{qr}^{\mathrm{I}}(t)f_r^{\mathrm{J}}\left(\mathrm{z}_r^{\mathrm{J}}(t)\right) - \beta_{qr}^{\mathrm{J}}(t)f_r^{\mathrm{I}}\left(\mathrm{z}_r^{\mathrm{I}}(t)\right)\Big] \\
&+ \sum_{r=1}^{n}\Big[\gamma_{qr}^{\mathrm{R}}(t)g_r^{\mathrm{K}}\left(\mathrm{z}_r^{\mathrm{K}}(t-\tau_{qr})\right) + \gamma_{qr}^{\mathrm{K}}(t)g_r^{\mathrm{R}}\left(\mathrm{z}_r^{\mathrm{R}}(t-\tau_{qr})\right) \\
&+ \gamma_{qr}^{\mathrm{I}}(t)g_r^{\mathrm{J}}\left(\mathrm{z}_r^{\mathrm{J}}(t-\tau_{qr})\right) - \gamma_{qr}^{\mathrm{J}}(t)g_r^{\mathrm{I}}\left(\mathrm{z}_r^{\mathrm{I}}(t-\tau_{qr})\right)\Big] \\
&+ \sum_{r=1}^{n}\Big[\delta_{qr}^{\mathrm{R}}(t)\int_{-\infty}^{t}G_{qr}(t-u)h_r^{\mathrm{K}}(\mathrm{z}_r^{\mathrm{K}}(u))\Delta u + \delta_{qr}^{\mathrm{K}}(t)\int_{-\infty}^{t}G_{qr}(t-u)h_r^{\mathrm{R}}(\mathrm{z}_r^{\mathrm{R}}(u))\Delta u \\
&+ \delta_{qr}^{\mathrm{I}}(t)\int_{-\infty}^{t}G_{qr}(t-u)h_r^{\mathrm{J}}(\mathrm{z}_r^{\mathrm{J}}(u))\Delta u - \delta_{qr}^{\mathrm{J}}(t)\int_{-\infty}^{t}G_{qr}(t-u)h_r^{\mathrm{I}}(\mathrm{z}_r^{\mathrm{I}}(u))\Delta u\Big] \\
&+ \mathcal{J}_q^{\mathrm{K}}(t) \\
&= -\alpha_q(t)\mathrm{z}_q^{\mathrm{K}}(t) + K_q^{\mathrm{K}}(t,\mathrm{z}(t)) + \mathcal{J}_q^{\mathrm{K}}(t),\ q\in\Omega,
\end{aligned}
$$

where

$$
\begin{aligned}
f_r^m\left(\mathrm{z}_r^m(t)\right) &:= f_r^m\left(\mathrm{z}_r^{\mathrm{R}}(t),\mathrm{z}_r^{\mathrm{I}}(t),\mathrm{z}_r^{\mathrm{J}}(t),\mathrm{z}_r^{\mathrm{K}}(t)\right), \\
g_r^m\left(\mathrm{z}_r^m(t-\tau_{qr})\right) &:= g_r^m\left(\mathrm{z}_r^{\mathrm{R}}(t-\tau_{qr}),\mathrm{z}_r^{\mathrm{I}}(t-\tau_{qr}),\mathrm{z}_r^{\mathrm{J}}(t-\tau_{qr}),\mathrm{z}_r^{\mathrm{K}}(t-\tau_{qr})\right)
\end{aligned}
$$

and

$$
h_r^m\left(\mathrm{z}_r^m(u)\right) := h_r^m\left(\mathrm{z}_r^{\mathrm{R}}(u),\mathrm{z}_r^{\mathrm{I}}(u),\mathrm{z}_r^{\mathrm{J}}(u),\mathrm{z}_r^{\mathrm{K}}(u)\right),
$$

$m\in\Lambda,\ r\in\Omega$. Therefore, the system (1) can be decomposed into the following equivalent real system

$$
\left(\mathrm{z}_q^m(t)\right)^{\Delta} = -\alpha_q(t)\mathrm{z}_q^m(t) + K_q^m(t,\mathrm{z}(t)) + \mathcal{J}_q^m(t),\ q\in\Omega, m\in\Lambda.
$$

3 Existence and uniqueness of almost periodic solutions

In this section, we derive sufficient conditions for the existence and uniqueness of almost periodic solutions for the system (1). In this regard, define

$$
\begin{aligned}
\Upsilon = \Big\{ y = \big(&\mathrm{z}_1^{\mathrm{R}},\mathrm{z}_2^{\mathrm{R}},\cdots,\mathrm{z}_n^{\mathrm{R}},\mathrm{z}_1^{\mathrm{I}},\mathrm{z}_2^{\mathrm{I}},\cdots,\mathrm{z}_n^{\mathrm{I}},\mathrm{z}_1^{\mathrm{J}},\mathrm{z}_2^{\mathrm{J}},\cdots,\mathrm{z}_n^{\mathrm{J}},\mathrm{z}_1^{\mathrm{K}},\mathrm{z}_2^{\mathrm{K}},\cdots,\mathrm{z}_n^{\mathrm{K}}\big) \in C(\mathbb{H}\otimes\mathbb{T}) \\
&/\mathrm{z}_q^m \text{ is an almost periodic function, } m\in\Lambda \text{ and } q\in\Omega\Big\}.
\end{aligned}
$$

Then, Υ is a Banach space equipped with norm $\|y\| = \max_{q\in\Omega}\left\{\sup_{t\in\mathbb{T}}|\mathrm{z}_q^m(t)| : m\in\Lambda\right\}$.

We assume that the following conditions hold throughout the paper:

$(\mathcal{S}_1)$ $\alpha_q(t) > 0$ is almost periodic, $-\alpha_q(t) \in \mathcal{R}^+, f_q, g_q, h_q, \beta_{qr}, \gamma_{qr}, \tau_{qr}$ are all almost periodic functions and $t - \tau_{qr} \in \mathbb{T}, q, r \in \Omega$.

$(\mathcal{S}_2)$ There exists a positive constants ${}^+G_{qr}$ such that

$$ {}^+G_{qr} = \int_0^\infty G_{qr}(u)\Delta u. $$

$(\mathcal{S}_3)$ For $r \in \Omega, m \in \Lambda, f_r(0,0,0,0) = g_r(0,0,0,0) = h_r(0,0,0,0) = 0$ and there exist positive constants a_r^m, b_r^m, c_r^m such that

$$\begin{aligned}
|f_r^m(\mathtt{z}_r^{\mathtt{R}}, \mathtt{z}_r^{\mathtt{I}}, \mathtt{z}_r^{\mathtt{J}}, \mathtt{z}_r^{\mathtt{K}}) - f_r^m(u_r^{\mathtt{R}}, u_r^{\mathtt{I}}, u_r^{\mathtt{J}}, u_r^{\mathtt{K}})| &\le a_r^{\mathtt{R}}|\mathtt{z}_r^{\mathtt{R}} - u_r^{\mathtt{R}}| + a_r^{\mathtt{I}}|\mathtt{z}_r^{\mathtt{I}} - u_r^{\mathtt{I}}| \\
&\quad + a_r^{\mathtt{J}}|\mathtt{z}_r^{\mathtt{J}} - u_r^{\mathtt{J}}| + a_r^{\mathtt{K}}|\mathtt{z}_r^{\mathtt{K}} - u_r^{\mathtt{K}}|, \\
|g_r^m(\mathtt{z}_r^{\mathtt{R}}, \mathtt{z}_r^{\mathtt{I}}, \mathtt{z}_r^{\mathtt{J}}, \mathtt{z}_r^{\mathtt{K}}) - g_r^m(u_r^{\mathtt{R}}, u_r^{\mathtt{I}}, u_r^{\mathtt{J}}, u_r^{\mathtt{K}})| &\le b_r^{\mathtt{R}}|\mathtt{z}_r^{\mathtt{R}} - u_r^{\mathtt{R}}| + b_r^{\mathtt{I}}|\mathtt{z}_r^{\mathtt{I}} - u_r^{\mathtt{I}}| \\
&\quad + b_r^{\mathtt{J}}|\mathtt{z}_r^{\mathtt{J}} - u_r^{\mathtt{J}}| + b_r^{\mathtt{K}}|\mathtt{z}_r^{\mathtt{K}} - u_r^{\mathtt{K}}|, \\
|h_r^m(\mathtt{z}_r^{\mathtt{R}}, \mathtt{z}_r^{\mathtt{I}}, \mathtt{z}_r^{\mathtt{J}}, \mathtt{z}_r^{\mathtt{K}}) - h_r^m(u_r^{\mathtt{R}}, u_r^{\mathtt{I}}, u_r^{\mathtt{J}}, u_r^{\mathtt{K}})| &\le c_r^{\mathtt{R}}|\mathtt{z}_r^{\mathtt{R}} - u_r^{\mathtt{R}}| + c_r^{\mathtt{I}}|\mathtt{z}_r^{\mathtt{I}} - u_r^{\mathtt{I}}| \\
&\quad + c_r^{\mathtt{J}}|\mathtt{z}_r^{\mathtt{J}} - u_r^{\mathtt{J}}| + c_r^{\mathtt{K}}|\mathtt{z}_r^{\mathtt{K}} - u_r^{\mathtt{K}}|.
\end{aligned}$$

$(\mathcal{S}_4)$ Let $M_q = \sum_{r=1}^n \left({}^+\beta_{qr}^{\mathtt{R}} + {}^+\beta_{qr}^{\mathtt{I}} + {}^+\beta_{qr}^{\mathtt{J}} + {}^+\beta_{qr}^{\mathtt{K}}\right)\left(a_r^{\mathtt{R}} + a_r^{\mathtt{I}} + a_r^{\mathtt{J}} + a_r^{\mathtt{K}}\right)$, $N_q = \sum_{r=1}^n \left({}^+\gamma_{qr}^{\mathtt{R}} + {}^+\gamma_{qr}^{\mathtt{I}} + {}^+\gamma_{qr}^{\mathtt{J}} + {}^+\gamma_{qr}^{\mathtt{K}}\right)\left(b_r^{\mathtt{R}} + b_r^{\mathtt{I}} + b_r^{\mathtt{J}} + b_r^{\mathtt{K}}\right)$, and $O_q = \sum_{r=1}^n \left({}^+\delta_{qr}^{\mathtt{R}} + {}^+\delta_{qr}^{\mathtt{I}} + {}^+\delta_{qr}^{\mathtt{J}} + {}^+\delta_{qr}^{\mathtt{K}}\right)\left(c_r^{\mathtt{R}} + c_r^{\mathtt{I}} + c_r^{\mathtt{J}} + c_r^{\mathtt{K}}\right)$. Then, there exists a positive constant ℓ such that

$$ \max_{q\in\Omega}\left\{\max_{m\in\Lambda}\left\{\frac{(M_q + N_q + O_q)\ell + {}^+\mathcal{J}_q^m}{{}^-\alpha_q}\right\}\right\} \le \ell, $$

and

$$ \lambda := \max_{q\in\Omega}\left\{\frac{M_q + N_q + O_q}{{}^-\alpha_q}\right\} < 1. $$

Theorem 3.1 *Assume that* $(\mathcal{S})$ *and* $(\mathcal{S}_1)$-$(\mathcal{S}_4)$ *hold. Then, QVRNN* (1) *has a unique almost periodic solution in the region* $\widehat{\Upsilon} = \{\psi \in \Upsilon : \|\psi\| \le \ell\}$.

Proof For any given $\psi = (\psi_1(t), \psi_2(t), \cdots, \psi(t))^T \in \widehat{\Upsilon}$, we first consider the following almost periodic system

$$ \left(\mathtt{z}_q^m(t)\right)^\Delta = -\alpha_q(t)\mathtt{z}_q^m(t) + K_q^m(t, \psi(t)) + \mathcal{J}_q^m(t). \tag{3} $$

From $(\mathcal{S}_1)$ and Lemma 2.12, we see that the linear system $\left(\mathtt{z}_q^m(t)\right)^\Delta = -\alpha_q(t)\mathtt{z}_q^m(t)$

admits an exponential dichotomy. Then, by Lemma 2.10, we can deduce that system (3) has a unique almost periodic solution.

$$\mathtt{z}^{\psi} = \Big((\mathtt{z}^{\psi})_1^{\mathtt{R}}, (\mathtt{z}^{\psi})_2^{\mathtt{R}}, \cdots, (\mathtt{z}^{\psi})_n^{\mathtt{R}}, (\mathtt{z}^{\psi})_1^{\mathtt{I}}, (\mathtt{z}^{\psi})_2^{\mathtt{I}}, \cdots, (\mathtt{z}^{\psi})_n^{\mathtt{I}}, (\mathtt{z}^{\psi})_1^{\mathtt{J}}, (\mathtt{z}^{\psi})_2^{\mathtt{J}}, \cdots, (\mathtt{z}^{\psi})_n^{\mathtt{J}}, (\mathtt{z}^{\psi})_1^{\mathtt{K}}, (\mathtt{z}^{\psi})_2^{\mathtt{K}}, \cdots, (\mathtt{z}^{\psi})_n^{\mathtt{K}}\Big),$$

where

$$(\mathtt{z}^{\psi})_q^m(t) = \int_{-\infty}^{t} e_{-\alpha_q}\big(t, \sigma(u)\big)\big(K_q^m(u, \psi(u)) + \mathcal{J}_q^m(u)\big)\Delta u,\ q \in \Omega, m \in \Lambda. \tag{4}$$

Next, define a function $\mathcal{F} : \Upsilon \to \Upsilon$ by $\mathcal{F}\psi = \mathtt{z}^{\psi}$, $\psi \in \Upsilon$, $\|\psi\| \le \ell$. First, we show that, for any $\psi \in \widehat{\Upsilon}$, we have $\mathcal{F}\psi \in \widehat{\Upsilon}$. But, we have

$$\begin{aligned}
|K_q^{\mathtt{R}}(u, \psi(u))| = \Bigg| & \sum_{r=1}^{n} \Big[\beta_{qr}^{\mathtt{R}}(u) f_r^{\mathtt{R}}\big(\psi_r^{\mathtt{R}}(u)\big) - \beta_{qr}^{\mathtt{I}}(u) f_r^{\mathtt{I}}\big(\psi_r^{\mathtt{I}}(u)\big) \\
& - \beta_{qr}^{\mathtt{J}}(u) f_r^{\mathtt{J}}\big(\psi_r^{\mathtt{J}}(u)\big) - \beta_{qr}^{\mathtt{K}}(u) f_r^{\mathtt{K}}\big(\psi_r^{\mathtt{K}}(u)\big)\Big] \\
& + \sum_{r=1}^{n} \Big[\gamma_{qr}^{\mathtt{R}}(u) g_r^{\mathtt{R}}\big(\psi_r^{\mathtt{R}}(u - \tau_{qr})\big) - \gamma_{qr}^{\mathtt{I}}(u) g_r^{\mathtt{I}}\big(\psi_r^{\mathtt{I}}(u - \tau_{qr})\big) \\
& - \gamma_{qr}^{\mathtt{J}}(u) g_r^{\mathtt{J}}\big(\psi_r^{\mathtt{J}}(u - \tau_{qr})\big) - \gamma_{qr}^{\mathtt{K}}(u) g_r^{\mathtt{K}}\big(\psi_r^{\mathtt{K}}(u - \tau_{qr})\big)\Big] \\
& + \sum_{r=1}^{n} \Big[\delta_{qr}^{\mathtt{R}}(u) \int_{-\infty}^{u} G_{qr}(u - v) h_r^{\mathtt{R}}(\psi_r^{\mathtt{R}}(v))\Delta v \\
& - \delta_{qr}^{\mathtt{I}}(u) \int_{-\infty}^{u} G_{qr}(u - v) h_r^{\mathtt{I}}(\psi_r^{\mathtt{I}}(v))\Delta v \\
& - \delta_{qr}^{\mathtt{J}}(u) \int_{-\infty}^{u} G_{qr}(u - v) h_r^{\mathtt{J}}(\psi_r^{\mathtt{J}}(v))\Delta v \\
& - \delta_{qr}^{\mathtt{K}}(u) \int_{-\infty}^{u} G_{qr}(u - v) h_r^{\mathtt{K}}(\psi_r^{\mathtt{K}}(v))\Delta v\Big]\Bigg| \\
\le & \sum_{r=1}^{n} \Big[|\beta_{qr}^{\mathtt{R}}(u)||f_r^{\mathtt{R}}\big(\psi_r^{\mathtt{R}}(u)\big)| + |\beta_{qr}^{\mathtt{I}}(u)||f_r^{\mathtt{I}}\big(\psi_r^{\mathtt{I}}(u)\big)| \\
& + |\beta_{qr}^{\mathtt{J}}(u)||f_r^{\mathtt{J}}\big(\psi_r^{\mathtt{J}}(u)\big)| + |\beta_{qr}^{\mathtt{K}}(u)||f_r^{\mathtt{K}}\big(\psi_r^{\mathtt{K}}(u)\big)|\Big] \\
& + \sum_{r=1}^{n} \Big[|\gamma_{qr}^{\mathtt{R}}(u)||g_r^{\mathtt{R}}\big(\psi_r^{\mathtt{R}}(u - \tau_{qr})\big)| + |\gamma_{qr}^{\mathtt{I}}(u)||g_r^{\mathtt{I}}\big(\psi_r^{\mathtt{I}}(u - \tau_{qr})\big)|
\end{aligned}$$

$$
\begin{aligned}
&+ |\gamma_{qr}^{\mathrm{J}}(u)||g_r^{\mathrm{J}}\big(\psi_r^{\mathrm{J}}(u-\tau_{qr})\big)| + |\gamma_{qr}^{\mathrm{K}}(u)||g_r^{\mathrm{K}}\big(\psi_r^{\mathrm{K}}(u-\tau_{qr})\big)|\Big] \\
&+ \sum_{r=1}^{n}\Big[|\delta_{qr}^{\mathrm{R}}(u)|\int_{-\infty}^{u}|G_{qr}(u-v)||h_r^{\mathrm{R}}(\psi_r^{\mathrm{R}}(v))|\Delta v \\
&+ |\delta_{qr}^{\mathrm{I}}(u)|\int_{-\infty}^{u}|G_{qr}(u-v)||h_r^{\mathrm{I}}(\psi_r^{\mathrm{I}}(v))|\Delta v \\
&+ |\delta_{qr}^{\mathrm{J}}(u)|\int_{-\infty}^{u}|G_{qr}(u-v)||h_r^{\mathrm{J}}(\psi_r^{\mathrm{J}}(v))|\Delta v \\
&+ |\delta_{qr}^{\mathrm{K}}(u)|\int_{-\infty}^{u}|G_{qr}(u-v)||h_r^{\mathrm{K}}(\psi_r^{\mathrm{K}}(v))|\Delta v\Big] \\
\le{}& \sum_{r=1}^{n}\Big({}^{+}\beta_{qr}^{\mathrm{R}} + {}^{+}\beta_{qr}^{\mathrm{I}} + {}^{+}\beta_{qr}^{\mathrm{J}} + {}^{+}\beta_{qr}^{\mathrm{K}}\Big)\Big(a_r^{\mathrm{R}}|\psi_r^{\mathrm{R}}(u)| + a_r^{\mathrm{I}}|\psi_r^{\mathrm{I}}(u)| + a_r^{\mathrm{J}}|\psi_r^{\mathrm{J}}(u)| + a_r^{\mathrm{K}}|\psi_r^{\mathrm{K}}(u)|\Big) \\
&+ \sum_{r=1}^{n}\Big({}^{+}\gamma_{qr}^{\mathrm{R}} + {}^{+}\gamma_{qr}^{\mathrm{I}} + {}^{+}\gamma_{qr}^{\mathrm{J}} + {}^{+}\gamma_{qr}^{\mathrm{K}}\Big)\Big(b_r^{\mathrm{R}}|\psi_r^{\mathrm{R}}(u-\tau_{qr}(u))| + b_r^{\mathrm{I}}|\psi_r^{\mathrm{I}}(u-\tau_{qr}(u))| \\
&+ b_r^{\mathrm{J}}|\psi_r^{\mathrm{J}}(u-\tau_{qr}(u))| + b_r^{\mathrm{K}}|\psi_r^{\mathrm{K}}(u-\tau_{qr}(u))|\Big) \\
&+ \sum_{r=1}^{n}\int_{-\infty}^{u}|G_{qr}(u-v)|\Big({}^{+}\delta_{qr}^{\mathrm{R}} + {}^{+}\delta_{qr}^{\mathrm{I}} + {}^{+}\delta_{qr}^{\mathrm{J}} + {}^{+}\delta_{qr}^{\mathrm{K}}\Big) \\
&\times \Big(c_r^{\mathrm{R}}|\psi_r^{\mathrm{R}}(v)| + c_r^{\mathrm{I}}|\psi_r^{\mathrm{I}}(v)| + c_r^{\mathrm{J}}|\psi_r^{\mathrm{J}}(v)| + c_r^{\mathrm{K}}|\psi_r^{\mathrm{K}}(v)|\Big)\Delta v \\
\le{}& \sum_{r=1}^{n}\Big({}^{+}\beta_{qr}^{\mathrm{R}} + {}^{+}\beta_{qr}^{\mathrm{I}} + {}^{+}\beta_{qr}^{\mathrm{J}} + {}^{+}\beta_{qr}^{\mathrm{K}}\Big)\Big(a_r^{\mathrm{R}} + a_r^{\mathrm{I}} + a_r^{\mathrm{J}} + a_r^{\mathrm{K}}\Big)\|\psi\|_{\Upsilon^*} \\
&+ \sum_{r=1}^{n}\Big({}^{+}\gamma_{qr}^{\mathrm{R}} + {}^{+}\gamma_{qr}^{\mathrm{I}} + {}^{+}\gamma_{qr}^{\mathrm{J}} + {}^{+}\gamma_{qr}^{\mathrm{K}}\Big)\Big(b_r^{\mathrm{R}} + b_r^{\mathrm{I}} + b_r^{\mathrm{J}} + b_r^{\mathrm{K}}\Big)\|\psi\|_{\Upsilon^*} \\
&+ \sum_{r=1}^{n}{}^{+}G_{qr}\Big({}^{+}\delta_{qr}^{\mathrm{R}} + {}^{+}\delta_{qr}^{\mathrm{I}} + {}^{+}\delta_{qr}^{\mathrm{J}} + {}^{+}\delta_{qr}^{\mathrm{K}}\Big)\Big(c_r^{\mathrm{R}} + c_r^{\mathrm{I}} + c_r^{\mathrm{J}} + c_r^{\mathrm{K}}\Big)\|\psi\|_{\Upsilon^*} \\
\le{}& M_q\ell + N_q\ell + O_q\ell.
\end{aligned}
$$

So, we have

$$
\begin{aligned}
|(\mathcal{F}\psi)_q^{\mathrm{R}}(t)| &= \Big|\int_{-\infty}^{t} e_{-\alpha_q}(t,\sigma(u))\big(K_q^{\mathrm{R}}(u,\psi(u)) + \mathcal{J}_q^{\mathrm{R}}(u)\big)\Delta u\Big| \\
&\le \int_{-\infty}^{t} e_{-\alpha_q}(t,\sigma(u))\big(M_q\ell + N_q\ell + O_q\ell + {}^{+}\mathcal{J}_q^{\mathrm{R}}\big)\Delta u \\
&\le \frac{M_q\ell + N_q\ell + O_q\ell + {}^{+}\mathcal{J}_q^{\mathrm{R}}}{{}^{-}\alpha_q} \\
&\le \ell,\ q \in \Omega.
\end{aligned}
$$

Similar to the above calculations, we can write in general

$$|(\mathcal{F}\psi)_q^m(t)| \leq \frac{M_q\ell + N_q\ell + O_q\ell + {}^{+}\mathcal{J}_q^m}{{}^{-}\alpha_q}$$
$$\leq \ell,\ q \in \Omega, m \in \Lambda,$$

which means that $\mathcal{F}\psi \in \widehat{\Upsilon}$. Hence the mapping $\mathcal{F}$ is a self-mapping from $\widehat{\Upsilon}$ to $\widehat{\Upsilon}$.

Finally, we prove that $\mathcal{F}$ is a contraction mapping. In fact, for any $\psi, \phi \in \Upsilon$, we have

$$\begin{aligned}
&|K_qR(u,\psi(u),\phi(u))|\\
&= \Big|\sum_{r=1}^{n}\Big[\beta_{qr}R(u)\big[f_rR\big(\psi_rR(u)\big) - f_rR\big(\phi_rR(u)\big)\big] - \beta_{qr}I(u)\big[f_rI\big(\psi_rI(u)\big) - f_rI\big(\phi_rI(u)\big)\big]\\
&- \beta_{qr}J(u)\big[f_rJ\big(\psi_rJ(u)\big) - f_rJ\big(\phi_rJ(u)\big)\big] - \beta_{qr}K(u)\big[f_rK\big(\psi_rK(u)\big) - f_rK\big(\phi_rK(u)\big)\big]\Big]\\
&+ \sum_{r=1}^{n}\Big[\gamma_{qr}R(u)\big[g_rK\big(\psi_rK(u-\tau_{qr}(u))\big) - g_rK\big(\phi_rK(u-\tau_{qr}(u))\big)\big]\\
&+ \gamma_{qr}K(t)\big[g_rR\big(\psi_rR(u-\tau_{qr}(u)\big) - g_rR\big(\phi_rR(u-\tau_{qr}(u))\big)\big]\\
&+ \gamma_{qr}I(u)\big[g_rJ\big(\psi_rJ(u-\tau_{qr}(u))\big) - g_rJ\big(\phi_rJ(u-\tau_{qr}(u))\big)\big]\\
&+ \gamma_{qr}J(u)\big[g_rI\big(\psi_rI(u-\tau_{qr}(u)\big) - g_rI\big(\phi_rI(u-\tau_{qr}(u))\big)\big]\Big]\\
&+ \sum_{r=1}^{n}\Big[\delta_{qr}R(u)\int_{-\infty}^{u}G_{qr}(u-v)\big[h_rR(\psi_rR(v)) - h_rR(\phi_rR(v))\big]\Delta v\\
&+ \delta_{qr}I(u)\int_{-\infty}^{u}G_{qr}(u-v)\big[h_rI(\psi_rI(v)) - h_rI(\phi_rI(v))\big]\Delta v\\
&+ \delta_{qr}J(u)\int_{-\infty}^{u}G_{qr}(u-v)\big[h_rJ(\psi_rJ(v)) - h_rJ(\phi_rJ(v))\big]\Delta v\\
&+ \delta_{qr}K(u)\int_{-\infty}^{u}G_{qr}(u-v)\big[h_rK(\psi_rK(v)) - h_rK(\phi_rK(v))\big]\Delta v\Big]\Big|\\
&+ |\beta_{qr}J(u)||f_rJ\big(\psi_rJ(u)\big) - f_rJ\big(\phi_rJ(u)\big)| + |\beta_{qr}K(u)||f_rK\big(\psi_rK(u)\big) - f_rK\big(\phi_rK(u)\big)|\Big]\\
&+ \sum_{r=1}^{n}\Big[|\gamma_{qr}R(u)||g_rK\big(\psi_rK(u-\tau_{qr}(u))\big) - g_rK\big(\phi_rK(u-\tau_{qr}(u))\big)|\\
&+ |\gamma_{qr}K(t)||g_rR\big(\psi_rR(u-\tau_{qr}(u)\big) - g_rR\big(\phi_rR(u-\tau_{qr}(u))\big)|\\
&+ |\gamma_{qr}I(u)||g_rJ\big(\psi_rJ(u-\tau_{qr}(u))\big) - g_rJ\big(\phi_rJ(u-\tau_{qr}(u))\big)|\\
&+ |\gamma_{qr}J(u)||g_rI\big(\psi_rI(u-\tau_{qr}(u)\big) - g_rI\big(\phi_rI(u-\tau_{qr}(u))\big)|\Big]
\end{aligned}$$

$$
\begin{aligned}
&+\sum_{r=1}^{n}\Big[|\delta_{qr}R(u)|\int_{-\infty}^{u}|G_{qr}(u-v)||h_rR(\psi_rR(v))-h_rR(\phi_rR(v))|\Delta v\\
&+|\delta_{qr}I(u)|\int_{-\infty}^{u}|G_{qr}(u-v)||h_rI(\psi_rI(v))-h_rI(\phi_rI(v))|\Delta v\\
&+|\delta_{qr}J(u)|\int_{-\infty}^{u}|G_{qr}(u-v)||h_rJ(\psi_rJ(v))-h_rJ(\phi_rJ(v))|\Delta v\\
&+|\delta_{qr}K(u)|\int_{-\infty}^{u}|G_{qr}(u-v)||h_rK(\psi_rK(v))-h_rK(\phi_rK(v))|\Delta v
\end{aligned}
$$

$$
\begin{aligned}
&\le\sum_{r=1}^{n}\Big({}^{+}\beta_{qr}^{\mathrm{R}}+{}^{+}\beta_{qr}^{\mathrm{I}}+{}^{+}\beta_{qr}^{\mathrm{J}}+{}^{+}\beta_{qr}^{\mathrm{K}}\Big)\Big(a_r^{\mathrm{R}}|\psi_r^{\mathrm{R}}(u)-\phi_r^{\mathrm{R}}(u)|+a_r^{\mathrm{I}}|\psi_r^{\mathrm{I}}(u)-\phi_r^{\mathrm{I}}(u)|\\
&\quad+a_r^{\mathrm{J}}|\psi_r^{\mathrm{J}}(u)-\phi_r^{\mathrm{J}}(u)|+a_r^{\mathrm{K}}|\psi_r^{\mathrm{K}}(u)-\phi_r^{\mathrm{K}}(u)|\Big)\\
&+\sum_{r=1}^{n}\Big({}^{+}\gamma_{qr}^{\mathrm{R}}+{}^{+}\gamma_{qr}^{\mathrm{I}}+{}^{+}\gamma_{qr}^{\mathrm{J}}+{}^{+}\gamma_{qr}^{\mathrm{K}}\Big)\Big(b_r^{\mathrm{R}}|\psi_r^{\mathrm{R}}(u-\tau_{qr}(u))-\phi_r^{\mathrm{R}}(u-\tau_{qr}(u))|\\
&+b_r^{\mathrm{I}}|\psi_r^{\mathrm{I}}(u-\tau_{qr}(u))-\phi_r^{\mathrm{I}}(u-\tau_{qr}(u))|+b_r^{\mathrm{J}}|\psi_r^{\mathrm{J}}(u-\tau_{qr}(u))-\phi_r^{\mathrm{J}}(u-\tau_{qr}(u))|\\
&+b_r^{\mathrm{K}}|\psi_r^{\mathrm{K}}(u-\tau_{qr}(u))-\phi_r^{\mathrm{K}}(u-\tau_{qr}(u))|\Big)\\
&+\sum_{r=1}^{n}\int_{-\infty}^{u}|G_{qr}(u-v)|\Big({}^{+}\delta_{qr}^{\mathrm{R}}+{}^{+}\delta_{qr}^{\mathrm{I}}+{}^{+}\delta_{qr}^{\mathrm{J}}+{}^{+}\delta_{qr}^{\mathrm{K}}\Big)\Big(c_r^{\mathrm{R}}|\psi_r^{\mathrm{R}}(v)-\phi_r^{\mathrm{R}}(v)|\\
&+c_r^{\mathrm{I}}|\psi_r^{\mathrm{I}}(v)-\phi_r^{\mathrm{I}}(v)|+c_r^{\mathrm{J}}|\psi_r^{\mathrm{J}}(v)-\phi_r^{\mathrm{J}}(v)|+c_r^{\mathrm{K}}|\psi_r^{\mathrm{K}}(v)-\phi_r^{\mathrm{K}}(v)|\Big)\Delta v\\
&\le\sum_{r=1}^{n}\Big({}^{+}\beta_{qr}^{\mathrm{R}}+{}^{+}\beta_{qr}^{\mathrm{I}}+{}^{+}\beta_{qr}^{\mathrm{J}}+{}^{+}\beta_{qr}^{\mathrm{K}}\Big)\Big(a_r^{\mathrm{R}}+a_r^{\mathrm{I}}+a_r^{\mathrm{J}}+a_r^{\mathrm{K}}\Big)\|\psi-\phi\|_{\widehat{\Upsilon}}\\
&+\sum_{r=1}^{n}\Big({}^{+}\gamma_{qr}^{\mathrm{R}}+{}^{+}\gamma_{qr}^{\mathrm{I}}+{}^{+}\gamma_{qr}^{\mathrm{J}}+{}^{+}\gamma_{qr}^{\mathrm{K}}\Big)\Big(b_r^{\mathrm{R}}+b_r^{\mathrm{I}}+b_r^{\mathrm{J}}+b_r^{\mathrm{K}}\Big)\|\psi-\phi\|_{\widehat{\Upsilon}}\\
&+\sum_{r=1}^{n}{}^{+}G_{qr}\Big({}^{+}\delta_{qr}^{\mathrm{R}}+{}^{+}\delta_{qr}^{\mathrm{I}}+{}^{+}\delta_{qr}^{\mathrm{J}}+{}^{+}\delta_{qr}^{\mathrm{K}}\Big)\Big(c_r^{\mathrm{R}}+c_r^{\mathrm{I}}+c_r^{\mathrm{J}}+c_r^{\mathrm{K}}\Big)\|\psi-\phi\|_{\widehat{\Upsilon}}\\
&\le(M_q+N_q+O_q)\|\psi-\phi\|_{\widehat{\Upsilon}}
\end{aligned}
$$

So, we have

$$
\begin{aligned}
|(\mathcal{F}\psi - \mathcal{F}\phi)_q^{\mathtt{R}}(t)| &= \Big| \int_{-\infty}^{t} e_{-\alpha_q}(t,\sigma(u))\big(K_q^{\mathtt{R}}(u,\psi(u),\phi(u))\big)\Delta u \Big| \\
&\leq \int_{-\infty}^{t} e_{-\alpha_q}(t,\sigma(u))\big(M_q + N_q + O_q\big)\|\psi - \phi\|_{\widehat{\Upsilon}}\Delta u \\
&\leq \left[\frac{M_q + N_q + O_q}{{}^{-}\alpha_q}\right]\|\psi - \phi\|_{\widehat{\Upsilon}},\ q \in \Omega.
\end{aligned}
$$

Similarly, we can have $|(\mathcal{F}\psi - \mathcal{F}\phi)_q^m(t)| \leq \lambda\|\psi - \phi\|_{\widehat{\Upsilon}},\ q \in \Omega,\ m \in \Lambda$. Hence, from $(\mathcal{S}_4)$ that $\lambda < 1$ so we have $\mathcal{F}$ is a contraction mapping. By the Banach fixed theorem, we have that $\mathcal{F}$ has a fixed point in $\widehat{\Upsilon}$. This completes proof. □

4 Global exponential stability

Theorem 4.1 *If $(\mathcal{S})$ and $(\mathcal{S}_1)$–$(\mathcal{S}_4)$ hold, then the almost periodic solution of system (1) is globally exponentially stable.*

Proof From Theorem 3.1, system (1) has an almost periodic solution $\mathtt{z}^*(t) = (\mathtt{z}_1^*(t), \mathtt{z}_2^*(t), \cdots, \mathtt{z}_n^*(t))^T$ in the region $\widehat{\Upsilon} = \{\mathtt{z} \in \Upsilon : \|y\| \leq \ell\}$ with initial condition $\mathtt{z}^*(u) = \varphi^*(u),\ u \in (-\infty, 0]_{\mathbb{T}}$. Suppose that $\mathtt{z}(t) = (\mathtt{z}_1(t), \mathtt{z}_2(t), \cdots, \mathtt{z}_n(t))^T$ be an arbitrary solution of system (1) with initial value $\mathtt{z}(u) = \varphi(u),\ u \in (-\infty, 0]_{\mathbb{T}}$ and let $X(t) = \mathtt{z}(t) - \mathtt{z}^*(t)$, then we have

$$
\big(X_q^m(t)\big)^{\Delta} = -\alpha_q(t)\big(\mathtt{z}^m(t) - \mathtt{z}^{*m}(t)\big) + K_q^m\big(t, \mathtt{z}(t) - \mathtt{z}^*(t)\big),\ q \in \Omega, m \in \Lambda
$$

with initial condition $X_q^m(t)(u) = \varphi^m(u) - \varphi^{*m}(u),\ u \in (-\infty, 0]_{\mathbb{T}}$. But,

$$
\begin{aligned}
\big(X_q^m(t)\big)^{\Delta} = &-\alpha_q(t)X_q^m(t) + \sum_{r=1}^{n}\Big[\beta_{qr}^{\mathtt{R}}(t)\big[f_r^{\mathtt{R}}\big(\mathtt{z}_r^{\mathtt{R}}(t)\big) - f_r^{\mathtt{R}}\big(\mathtt{z}_r^{*\mathtt{R}}(t)\big)\big] \\
&- \beta_{qr}^{\mathtt{I}}(t)\big[f_r^{\mathtt{I}}\big(\mathtt{z}_r^{\mathtt{I}}(t)\big) - f_r^{\mathtt{I}}\big(\mathtt{z}_r^{*\mathtt{I}}(t)\big)\big] \\
&- \beta_{qr}^{\mathtt{J}}(t)\big[f_r^{\mathtt{J}}\big(\mathtt{z}_r^{\mathtt{J}}(t)\big) - f_r^{\mathtt{J}}\big(\mathtt{z}_r^{*\mathtt{J}}(t)\big)\big] \\
&- \beta_{qr}^{\mathtt{K}}(t)\big[f_r^{\mathtt{K}}\big(\mathtt{z}_r^{\mathtt{K}}(t)\big) - f_r^{\mathtt{K}}\big(\mathtt{z}_r^{*\mathtt{K}}(t)\big)\big]\Big] \\
&+ \sum_{r=1}^{n}\Big[\gamma_{qr}^{\mathtt{R}}(t)\big[g_r^{\mathtt{R}}\big(\mathtt{z}_r^{\mathtt{R}}(t-\tau_{qr}(t))\big) - g_r^{\mathtt{R}}\big(\mathtt{z}_r^{*\mathtt{R}}(t-\tau_{qr}(t))\big)\big] \\
&- \gamma_{qr}^{\mathtt{I}}(t)\big[g_r^{\mathtt{I}}\big(\mathtt{z}_r^{\mathtt{I}}(t-\tau_{qr})\big) - g_r^{\mathtt{I}}\big(\mathtt{z}_r^{*\mathtt{I}}(t-\tau_{qr}(t))\big)\big] \\
&- \gamma_{qr}^{\mathtt{J}}(t)\big[g_r^{\mathtt{J}}\big(\mathtt{z}_r^{\mathtt{J}}(t-\tau_{qr})\big) - g_r^{\mathtt{J}}\big(\mathtt{z}_r^{*\mathtt{J}}(t-\tau_{qr}(t))\big)\big]
\end{aligned}
$$

$$
\begin{aligned}
&- \gamma_{qr}^{\mathtt{K}}(t)\big[g_r^{\mathtt{K}}\big(\mathtt{z}_r^{\mathtt{K}}(t-\tau_{qr})\big) - g_r^{\mathtt{K}}\big(\mathtt{z}_r^{*\mathtt{K}}(t-\tau_{qr}(t))\big)\big]\Big] \\
&+ \sum_{r=1}^{n}\Big[\delta_{qr}^{\mathtt{R}}(t)\int_{-\infty}^{t} G_{qr}(t-u)\big[h_r^{\mathtt{R}}(\mathtt{z}_r^{\mathtt{R}}(u)) - h_r^{\mathtt{R}}(\mathtt{z}_r^{*\mathtt{R}}(u))\big]\Delta u \\
&- \delta_{qr}^{\mathtt{I}}(t)\int_{-\infty}^{t} G_{qr}(t-u)\big[h_r^{\mathtt{I}}(\mathtt{z}_r^{\mathtt{I}}(u)) - h_r^{\mathtt{I}}(\mathtt{z}_r^{*\mathtt{I}}(u))\big]\Delta u \\
&- \delta_{qr}^{\mathtt{J}}(t)\int_{-\infty}^{t} G_{qr}(t-u)\big[h_r^{\mathtt{J}}(\mathtt{z}_r^{\mathtt{J}}(u)) - h_r^{\mathtt{J}}(\mathtt{z}_r^{*\mathtt{J}}(u))\big]\Delta u \\
&- \delta_{qr}^{\mathtt{K}}(t)\int_{-\infty}^{t} G_{qr}(t-u)\big[h_r^{\mathtt{K}}(\mathtt{z}_r^{\mathtt{K}}(u)) - h_r^{\mathtt{K}}(\mathtt{z}_r^{*\mathtt{K}}(u))\big]\Delta u\Big]
\end{aligned}
$$

where

$$
\begin{aligned}
X_q^m(t) &= \mathtt{z}_q^m(t) - \mathtt{z}_q^{*m}(t) \\
&= \big(\mathtt{z}_q^m(0) - \mathtt{z}_q^{*m}(0)\big)e_{-\alpha_q}(t,0) + \int_0^t e_{-\alpha_q}(t,\sigma(v)) \\
&\quad\times\Big[\sum_{r=1}^{n}\Big[\beta_{qr}^{\mathtt{R}}(v)\big[f_r^{\mathtt{R}}\big(\mathtt{z}_r^{\mathtt{R}}(v)\big) - f_r^{\mathtt{R}}\big(\mathtt{z}_r^{*\mathtt{R}}(v)\big)\big] - \beta_{qr}^{\mathtt{I}}(v)\big[f_r^{\mathtt{I}}\big(\mathtt{z}_r^{\mathtt{I}}(v)\big) - f_r^{\mathtt{I}}\big(\mathtt{z}_r^{*\mathtt{I}}(v)\big)\big] \\
&\qquad - \beta_{qr}^{\mathtt{J}}(v)\big[f_r^{\mathtt{J}}\big(\mathtt{z}_r^{\mathtt{J}}(v)\big) - f_r^{\mathtt{J}}\big(\mathtt{z}_r^{*\mathtt{J}}(v)\big)\big] - \beta_{qr}^{\mathtt{K}}(v)\big[f_r^{\mathtt{K}}\big(\mathtt{z}_r^{\mathtt{K}}(v)\big) - f_r^{\mathtt{K}}\big(\mathtt{z}_r^{*\mathtt{K}}(v)\big)\big]\Big] \\
&\quad+\sum_{r=1}^{n}\Big[\gamma_{qr}^{\mathtt{R}}(v)\big[g_r^{\mathtt{R}}\big(\mathtt{z}_r^{\mathtt{R}}(v-\tau_{qr}(v))\big) - g_r^{\mathtt{R}}\big(\mathtt{z}_r^{*\mathtt{R}}(v-\tau_{qr}(v))\big)\big] \\
&\qquad - \gamma_{qr}^{\mathtt{I}}(t)\big[g_r^{\mathtt{I}}\big(\mathtt{z}_r^{\mathtt{I}}(t-\tau_{qr})\big) - g_r^{\mathtt{I}}\big(\mathtt{z}_r^{*\mathtt{I}}(v-\tau_{qr}(v))\big)\big] \\
&\qquad - \gamma_{qr}^{\mathtt{J}}(v)\big[g_r^{\mathtt{J}}\big(\mathtt{z}_r^{\mathtt{J}}(v-\tau_{qr}(v))\big) - g_r^{\mathtt{J}}\big(\mathtt{z}_r^{*\mathtt{J}}(v-\tau_{qr}(v))\big)\big] \\
&\qquad - \gamma_{qr}^{\mathtt{K}}(v)\big[g_r^{\mathtt{K}}\big(\mathtt{z}_r^{\mathtt{K}}(v-\tau_{qr}(v))\big) - g_r^{\mathtt{K}}\big(\mathtt{z}_r^{*\mathtt{K}}(v-\tau_{qr}(v))\big)\big]\Big] \\
&\quad+\sum_{r=1}^{n}\Big[\delta_{qr}^{\mathtt{R}}(v)\int_{-\infty}^{v} G_{qr}(v-u)\big[h_r^{\mathtt{R}}(\mathtt{z}_r^{\mathtt{R}}(u)) - h_r^{\mathtt{R}}(\mathtt{z}_r^{*\mathtt{R}}(u))\big]\Delta u \\
&\qquad - \delta_{qr}^{\mathtt{I}}(v)\int_{-\infty}^{v} G_{qr}(v-u)\big[h_r^{\mathtt{I}}(\mathtt{z}_r^{\mathtt{I}}(u)) - h_r^{\mathtt{I}}(\mathtt{z}_r^{*\mathtt{I}}(u))\big]\Delta u \\
&\qquad - \delta_{qr}^{\mathtt{J}}(v)\int_{-\infty}^{v} G_{qr}(v-u)\big[h_r^{\mathtt{J}}(\mathtt{z}_r^{\mathtt{J}}(u)) - h_r^{\mathtt{J}}(\mathtt{z}_r^{*\mathtt{J}}(u))\big]\Delta u \\
&\qquad - \delta_{qr}^{\mathtt{K}}(v)\int_{-\infty}^{v} G_{qr}(v-u)\big[h_r^{\mathtt{K}}(\mathtt{z}_r^{\mathtt{K}}(u)) - h_r^{\mathtt{K}}(\mathtt{z}_r^{*\mathtt{K}}(u))\big]\Delta u\Big]\Big]\Delta v.
\end{aligned}
$$

For $\vartheta \in \mathbb{R}$, let $W_q^m(\vartheta)$ be defined as

$$W_q^m(\vartheta) = {}^{-}\alpha_q - \vartheta - \exp\{\vartheta \sup_{x\in\mathbb{T}} \mu(x)\}\Big(M_{q_0} + \exp\{\vartheta\, {}^{+}\tau_{qr}\}N_q + O_q\Big).$$

Then, from $(\mathcal{S}_3)$ it is clear that

$$W_q^m(0) = {}^{-}\alpha_q - \Big(M_q + N_q + O_q\Big) > 0.$$

Since $W_q^m(\vartheta)$ is continuous on $[0,+\infty)$ and $W_q^m(\vartheta) \to -\infty$ as $\vartheta \to +\infty$, so there exist ϑ_q^m such that $W_q^m(\vartheta_q^m)$ and $W_q^m(\vartheta) > 0$ for $\vartheta \in (0,\vartheta_q^m)$. So, we can choose a positive constant $\theta = \min_{m\in\Omega} \vartheta_q^m$ and have $W_q^m(\theta) > 0, q \in \Omega, m \in \Lambda$. Therefore, we can chose a positive $0<\xi<\min\{\theta, \min_{q\in\Omega} {}^{-}\alpha_q\}$, then $\xi > 0$ and $\ominus\xi \in \mathcal{R}^+$ and such that $W_q^m(\xi) > 0, q \in \Omega$, i.e.,

$$\frac{\exp\{\xi \sup_{v\in\mathbb{T}} \mu(v)\}}{{}^{-}\alpha_q - \xi}\Big(M_q + \exp\{\xi\, {}^{+}\tau_{qr}\}N_q + O_q\Big) < 1.$$

Let $\mathtt{N} = \frac{\mathtt{M_q}+\mathtt{N_q}+\mathtt{O_q}}{{}^{-}\alpha_q-\xi}$, from $(\mathcal{S}_4)$ we have $\mathtt{N} > 1$. For $\exp\{\xi \sup_{x\in\mathbb{T}} \mu(x)\} > 1$ and $0<{}^{-}\alpha_q - \xi<{}^{-}\alpha_q$, we have

$$\frac{1}{\mathtt{N}} = \frac{M_q + N_q + O_q}{{}^{-}\alpha_q} < \frac{\exp\{\xi \sup_{x\in\mathbb{T}} \mu(x)\}}{{}^{-}\alpha_q - \xi}\Big(M_q + \exp\{\xi\, {}^{+}\tau_{qr}\}N_q + O_q\Big) < 1.$$

Furthermore, for $\xi > 0$, when $t \in (-\infty, 0]_{\mathbb{T}}$, we have $e_{\ominus\xi}(t,0) > 1$,. Therefore, we have

$$\|X_q^m(t)\|_{\widehat{\Upsilon}} \le \mathtt{N} e_{\ominus\xi}(\mathtt{t},0)\|\varphi - \varphi^*\|_{\widehat{\Upsilon}},\ \mathtt{t} \in (-\infty,0]_{\mathbb{T}}, \mathtt{m} \in \Lambda, \mathtt{q} \in \Omega.$$

Claim: $\|X_q^m(t)\|_{\widehat{\Upsilon}} \le \mathtt{N} e_{\ominus\xi}(\mathtt{t},0)\|\varphi - \varphi^*\|_{\widehat{\Upsilon}},\ \mathtt{t} \in (0,\infty)_{\mathbb{T}}, \mathtt{m} \in \Lambda, \mathtt{q} \in \Omega.$

To prove above claim, we prove that for any $\varepsilon > 0$,

$$\|X_q^m(t)\|_{\widehat{\Upsilon}} < (\mathtt{N}+\varepsilon) e_{\ominus\xi}(\mathtt{t},0)\|\varphi - \varphi^*\|_{\widehat{\Upsilon}},\ \mathtt{t} \in (0,\infty)_{\mathbb{T}}, \mathtt{m} \in \Lambda, \mathtt{q} \in \Omega. \tag{5}$$

To prove (5), by contradiction, we assume (5) is not true, then there exists $t \in (0,\infty)_{\mathbb{T}}$ and $q_0 \in \Omega, m_0 \in \Lambda$ such that

$$\begin{aligned}
&\|X_{q_0}^{m_0}(t_1)\|_{\widehat{\Upsilon}} \ge (\mathtt{N}+\varepsilon) e_{\ominus\xi}(\mathtt{t_1},0)\|\varphi - \varphi^*\|_{\widehat{\Upsilon}},\\
&\|X_{q_0}^{m_0}(t)\|_{\widehat{\Upsilon}} \ge (\mathtt{N}+\varepsilon) e_{\ominus\xi}(\mathtt{t},0)\|\varphi - \varphi^*\|_{\widehat{\Upsilon}},\ \mathtt{t} \in (0,\mathtt{t_1})_{\mathbb{T}},\\
&\|X_q^m(t)\|_{\widehat{\Upsilon}} \ge (\mathtt{N}+\varepsilon) e_{\ominus\xi}(\mathtt{t},0)\|\varphi - \varphi^*\|_{\widehat{\Upsilon}},\ \mathtt{t} \in (0,\mathtt{t_1}]_{\mathbb{T}},\ \mathtt{for\ q} \neq_0 \ \mathtt{or\ m} \neq \mathtt{m}_0.
\end{aligned} \tag{6}$$

Therefore, there must exist a constant $q^* \ge 1$ such that

$$\left.\begin{aligned} |X_{q_0}^{m_0}(t_1)|_{\widehat{\Upsilon}} &= q^*(\mathtt{N}+\varepsilon)\mathtt{e}_{\ominus\xi}(\mathtt{t}_1,0)\|\varphi-\varphi^*\|_{\widehat{\Upsilon}},\ \mathtt{m}_0\in\Lambda,\\ |X_{q_0}^{m_0}(t)|_{\widehat{\Upsilon}} &< q^*(\mathtt{N}+\varepsilon)\mathtt{e}_{\ominus\xi}(\mathtt{t},0)\|\varphi-\varphi^*\|_{\widehat{\Upsilon}},\ \mathtt{t}\in(0,\mathtt{t}_1),\\ |X_{q_0}^{m_0}(t)|_{\widehat{\Upsilon}} &< q^*(\mathtt{N}+\varepsilon)\mathtt{e}_{\ominus\xi}(\mathtt{t},0)\|\varphi-\varphi^*\|_{\widehat{\Upsilon}},\ \mathtt{t}\in(0,\mathtt{t}_1]_{\mathbb{T}}, \end{aligned}\right\} \tag{7}$$

for $q\neq 0$ or $m\neq m_0$. So,

$$\begin{aligned} X_{q_0}^{m}(t_1) &= \mathtt{z}_{q_0}^{m}(t_1)-\mathtt{z}^{*m}_{q_0}(t_1)\\ &= \big(\mathtt{z}_{q_0}^{m}(0)-\mathtt{z}^{*m}_{q_0}(0)\big)e_{-\alpha_{q_0}}(t_1,0)+\int_0^{t_1}e_{-\alpha_{q_0}}(t_1,\sigma(v))\\ &\times\Bigg[\sum_{r=1}^{n}\Big[\beta^{\mathtt{R}}_{q_0r}(v)\big[f_r^{\mathtt{R}}\big(\mathtt{z}_r^{\mathtt{R}}(v)\big)-f_r^{\mathtt{R}}\big(\mathtt{z}_r^{*\mathtt{R}}(v)\big)\big]-\beta^{\mathtt{I}}_{q_0r}(v)\big[f_r^{\mathtt{I}}\big(\mathtt{z}_r^{\mathtt{I}}(v)\big)-f_r^{\mathtt{I}}\big(\mathtt{z}_r^{*\mathtt{I}}(v)\big)\big]\\ &\quad-\beta^{\mathtt{J}}_{q_0r}(v)\big[f_r^{\mathtt{J}}\big(\mathtt{z}_r^{\mathtt{J}}(v)\big)-f_r^{\mathtt{J}}\big(\mathtt{z}_r^{*\mathtt{J}}(v)\big)\big]-\beta^{\mathtt{K}}_{q_0r}(v)\big[f_r^{\mathtt{K}}\big(\mathtt{z}_r^{\mathtt{K}}(v)\big)-f_r^{\mathtt{K}}\big(\mathtt{z}_r^{*\mathtt{K}}(v)\big)\big]\Big]\\ &+\sum_{r=1}^{n}\Big[\gamma^{\mathtt{R}}_{q_0r}(v)\big[g_r^{\mathtt{R}}\big(\mathtt{z}_r^{\mathtt{R}}(v-\tau_{q_0r}(v))\big)-g_r^{\mathtt{R}}\big(\mathtt{z}_r^{*\mathtt{R}}(v-\tau_{q_0r}(v))\big)\big]\\ &\quad-\gamma^{\mathtt{I}}_{q_0r}(t)\big[g_r^{\mathtt{I}}\big(\mathtt{z}_r^{\mathtt{I}}(t-\tau_{q_0r})\big)-g_r^{\mathtt{I}}\big(\mathtt{z}_r^{*\mathtt{I}}(v-\tau_{q_0r}(v))\big)\big]\\ &\quad-\gamma^{\mathtt{J}}_{q_0r}(v)\big[g_r^{\mathtt{J}}\big(\mathtt{z}_r^{\mathtt{J}}(v-\tau_{q_0r}(v))\big)-g_r^{\mathtt{J}}\big(\mathtt{z}_r^{*\mathtt{J}}(v-\tau_{q_0r}(v))\big)\big]\\ &\quad-\gamma^{\mathtt{K}}_{q_0r}(v)\big[g_r^{\mathtt{K}}\big(\mathtt{z}_r^{\mathtt{K}}(v-\tau_{q_0r}(v))\big)-g_r^{\mathtt{K}}\big(\mathtt{z}_r^{*\mathtt{K}}(v-\tau_{q_0r}(v))\big)\big]\Big]\\ &+\sum_{r=1}^{n}\Big[\delta^{\mathtt{R}}_{q_0r}(v)\int_{-\infty}^{v}G_{q_0r}(v-u)\big[h_r^{\mathtt{R}}(\mathtt{z}_r^{\mathtt{R}}(u))-h_r^{\mathtt{R}}(\mathtt{z}_r^{*\mathtt{R}}(u))\big]\Delta u\\ &\quad-\delta^{\mathtt{I}}_{q_0r}(v)\int_{-\infty}^{v}G_{q_0r}(v-u)\big[h_r^{\mathtt{I}}(\mathtt{z}_r^{\mathtt{I}}(u))-h_r^{\mathtt{I}}(\mathtt{z}_r^{*\mathtt{I}}(u))\big]\Delta u\\ &-\delta^{\mathtt{J}}_{q_0r}(v)\int_{-\infty}^{v}G_{q_0r}(v-u)\big[h_r^{\mathtt{J}}(\mathtt{z}_r^{\mathtt{J}}(u))-h_r^{\mathtt{J}}(\mathtt{z}_r^{*\mathtt{J}}(u))\big]\Delta u\\ &\quad-\delta^{\mathtt{K}}_{q_0r}(v)\int_{-\infty}^{v}G_{q_0r}(v-u)\big[h_r^{\mathtt{K}}(\mathtt{z}_r^{\mathtt{K}}(u))-h_r^{\mathtt{K}}(\mathtt{z}_r^{*\mathtt{K}}(u))\big]\Delta u\Big]\Bigg]\Delta v. \end{aligned}$$

$$
\begin{aligned}
&\le e_{-(^{-}\alpha_{q_0})}(t_1,0)\|\varphi-\varphi^*\|_{\widehat{\Upsilon}}+\Big[q^*(\mathtt{N}+\varepsilon)\mathtt{e}_{\ominus\xi}(\mathtt{t}_1,0)\|\varphi-\varphi^*\|_{\widehat{\Upsilon}}\Big]\\
&\quad\times\int_0^{t_1}e_{-(^{-}\alpha_{q_0})}(t_1,\sigma(v))e_{\xi}(t_1,\sigma(v))\\
&\quad\times\Bigg[\sum_{r=1}^{n}\big({}^{+}\beta_{q_0r}^{\mathtt{R}}+{}^{+}\beta_{q_0r}^{\mathtt{I}}+{}^{+}\beta_{q_0r}^{\mathtt{J}}+{}^{+}\beta_{q_0r}^{\mathtt{K}}\big)\big(a_r^{\mathtt{R}}+a_r^{\mathtt{I}}+a_r^{\mathtt{J}}+a_r^{\mathtt{K}}\big)e_{\xi}(\sigma(v),v)\\
&\quad+\sum_{r=1}^{n}\big({}^{+}\gamma_{q_0r}^{\mathtt{R}}+{}^{+}\gamma_{q_0r}^{\mathtt{I}}+{}^{+}\gamma_{q_0r}^{\mathtt{J}}+{}^{+}\gamma_{q_0r}^{\mathtt{K}}\big)\big(b_r^{\mathtt{R}}+b_r^{\mathtt{I}}+b_r^{\mathtt{J}}+b_r^{\mathtt{K}}\big)e_{\xi}(\sigma(v),v-\tau_{q_0r}(v))\\
&\quad+\sum_{r=1}^{n}\int_0^{\infty}|G_{q_0r}(u)|\big({}^{+}\delta_{q_0r}^{\mathtt{R}}+{}^{+}\delta_{q_0r}^{\mathtt{I}}+{}^{+}\delta_{q_0r}^{\mathtt{J}}+{}^{+}\delta_{q_0r}^{\mathtt{K}}\big)\\
&\quad\times\big(c_r^{\mathtt{R}}+c_r^{\mathtt{I}}+c_r^{\mathtt{J}}+c_r^{\mathtt{K}}\big)\exp\{-\xi v\}e_{\xi}(\sigma(v),v-u)\Delta u\Bigg]\Delta v\\
&\le e_{-(^{-}\alpha_{q_0})}(t_1,0)\|\varphi-\varphi^*\|_{\widehat{\Upsilon}}+q^*(\mathtt{N}+\varepsilon)\mathtt{e}_{\ominus\xi}(\mathtt{t}_1,0)\|\varphi-\varphi^*\|_{\widehat{\Upsilon}}\int_0^{\mathtt{t}_1}\mathtt{e}_{-(^{-}\alpha_{q_0})\oplus\xi}(\mathtt{t}_1,\sigma(\mathtt{v}))\\
&\quad\times\Bigg[\sum_{r=1}^{n}\big({}^{+}\beta_{q_0r}^{\mathtt{R}}+{}^{+}\beta_{q_0r}^{\mathtt{I}}+{}^{+}\beta_{q_0r}^{\mathtt{J}}+{}^{+}\beta_{q_0r}^{\mathtt{K}}\big)\big(a_r^{\mathtt{R}}+a_r^{\mathtt{I}}+a_r^{\mathtt{J}}+a_r^{\mathtt{K}}\big)e_{\xi}(\sigma(v),v)\\
&\quad+\sum_{r=1}^{n}\big({}^{+}\gamma_{q_0r}^{\mathtt{R}}+{}^{+}\gamma_{q_0r}^{\mathtt{I}}+{}^{+}\gamma_{q_0r}^{\mathtt{J}}+{}^{+}\gamma_{q_0r}^{\mathtt{K}}\big)\big(b_r^{\mathtt{R}}+b_r^{\mathtt{I}}+b_r^{\mathtt{J}}+b_r^{\mathtt{K}}\big)e_{\xi}(\sigma(v),v-\tau_{q_0r}(v))\\
&\quad+\sum_{r=1}^{n}\int_0^{\infty}|G_{q_0r}(u)|\big({}^{+}\delta_{q_0r}^{\mathtt{R}}+{}^{+}\delta_{q_0r}^{\mathtt{I}}+{}^{+}\delta_{q_0r}^{\mathtt{J}}+{}^{+}\delta_{q_0r}^{\mathtt{K}}\big)\\
&\quad\times\big(c_r^{\mathtt{R}}+c_r^{\mathtt{I}}+c_r^{\mathtt{J}}+c_r^{\mathtt{K}}\big)\exp\{-\xi v\}e_{\xi}(\sigma(v),v-u)\Delta u\Bigg]\Delta v\\
&\le e_{-(^{-}\alpha_{q_0})}(t_1,0)\|\varphi-\varphi^*\|_{\widehat{\Upsilon}}+q^*(\mathtt{N}+\varepsilon)\mathtt{e}_{\ominus\xi}(\mathtt{t}_1,0)\|\varphi-\varphi^*\|_{\widehat{\Upsilon}}\int_0^{\mathtt{t}_1}\mathtt{e}_{-(^{-}\alpha_{q_0})\oplus\xi}(\mathtt{t}_1,\sigma(\mathtt{v}))\\
&\quad\times\Bigg[\sum_{r=1}^{n}\big({}^{+}\beta_{q_0r}^{\mathtt{R}}+{}^{+}\beta_{q_0r}^{\mathtt{I}}+{}^{+}\beta_{q_0r}^{\mathtt{J}}+{}^{+}\beta_{q_0r}^{\mathtt{K}}\big)\big(a_r^{\mathtt{R}}+a_r^{\mathtt{I}}+a_r^{\mathtt{J}}+a_r^{\mathtt{K}}\big)\exp\{\xi\sup_{v\in\mathbb{T}}\mu(v)\}\\
&\quad+\sum_{r=1}^{n}\big({}^{+}\gamma_{q_0r}^{\mathtt{R}}+{}^{+}\gamma_{q_0r}^{\mathtt{I}}+{}^{+}\gamma_{q_0r}^{\mathtt{J}}+{}^{+}\gamma_{q_0r}^{\mathtt{K}}\big)\big(b_r^{\mathtt{R}}+b_r^{\mathtt{I}}+b_r^{\mathtt{J}}+b_r^{\mathtt{K}}\big)\exp\{\xi({}^{+}\tau_{q_0r}+\sup_{v\in\mathbb{T}}\mu(v))\}\\
&\quad+\sum_{r=1}^{n}\int_0^{\infty}|G_{q_0r}(u)|\big({}^{+}\delta_{q_0r}^{\mathtt{R}}+{}^{+}\delta_{q_0r}^{\mathtt{I}}+{}^{+}\delta_{q_0r}^{\mathtt{J}}+{}^{+}\delta_{q_0r}^{\mathtt{K}}\big)\\
&\quad\times\big(c_r^{\mathtt{R}}+c_r^{\mathtt{I}}+c_r^{\mathtt{J}}+c_r^{\mathtt{K}}\big)\exp\{-\xi v\}\exp\{\xi(u+\sup_{v\in\mathbb{T}}\mu(v))\}\Delta u\Bigg]\Delta v
\end{aligned}
$$

$$
\begin{aligned}
&\leq q^*(\mathtt{N}+\varepsilon)\mathtt{e}_{\ominus\xi}(\mathtt{t}_1,0)\|\varphi-\varphi^*\|_{\widehat{\Upsilon}}\Bigg\{\frac{1}{\mathtt{q}^*(\mathtt{N}+\varepsilon)}\mathtt{e}_{-(^-\alpha_{\mathtt{q}_0})\oplus\xi}(\mathtt{t}_1,0)+\exp\{\xi\sup_{\mathtt{v}\in\mathbb{T}}\mu(\mathtt{v})\}\\
&\quad\times\Bigg[\sum_{r=1}^{n}\left({}^+\beta^{\mathtt{R}}_{q_0r}+{}^+\beta^{\mathtt{I}}_{q_0r}+{}^+\beta^{\mathtt{J}}_{q_0r}+{}^+\beta^{\mathtt{K}}_{q_0r}\right)\left(a^{\mathtt{R}}_r+a^{\mathtt{I}}_r+a^{\mathtt{J}}_r+a^{\mathtt{K}}_r\right)\\
&\quad+\sum_{r=1}^{n}\left({}^+\gamma^{\mathtt{R}}_{q_0r}+{}^+\gamma^{\mathtt{I}}_{q_0r}+{}^+\gamma^{\mathtt{J}}_{q_0r}+{}^+\gamma^{\mathtt{K}}_{q_0r}\right)\left(b^{\mathtt{R}}_r+b^{\mathtt{I}}_r+b^{\mathtt{J}}_r+b^{\mathtt{K}}_r\right)\exp\{\xi\,{}^+\tau_{q_0r}\}\\
&\quad+\sum_{r=1}^{n}{}^+G_{q_0r}\left({}^+\delta^{\mathtt{R}}_{q_0r}+{}^+\delta^{\mathtt{I}}_{q_0r}+{}^+\delta^{\mathtt{J}}_{q_0r}+{}^+\delta^{\mathtt{K}}_{q_0r}\right)\left(c^{\mathtt{R}}_r+c^{\mathtt{I}}_r+c^{\mathtt{J}}_r+c^{\mathtt{K}}_r\right)\Bigg]\\
&\quad\times\int_0^{t_1}e_{-(^-\alpha_{q_0})\oplus\xi}(t_1,\sigma(v))\Delta v\Bigg\}\\
&\leq q^*(\mathtt{N}+\varepsilon)\mathtt{e}_{\ominus\xi}(\mathtt{t}_1,0)\|\varphi-\varphi^*\|_{\widehat{\Upsilon}}\Bigg\{\frac{1}{(\mathtt{N}+\varepsilon)}\mathtt{e}_{-(^-\alpha_{\mathtt{q}_0})\oplus\xi}(\mathtt{t}_1,0)\\
&\quad+\exp\{\xi\sup_{v\in\mathbb{T}}\mu(v)\}\left(M_{q_0}+\exp\{\xi\,{}^+\tau_{q_0r}\}N_{q_0}+O_{q_0}\right)\int_0^{t_1}e_{-(^-\alpha_{q_0})\oplus\xi}(t_1,\sigma(v))\Delta v\Bigg\}\\
&\leq q^*(\mathtt{N}+\varepsilon)\mathtt{e}_{\ominus\xi}(\mathtt{t}_1,0)\|\varphi-\varphi^*\|_{\widehat{\Upsilon}}\Bigg\{\frac{1}{(\mathtt{N}+\varepsilon)}\mathtt{e}_{-(^-\alpha_{\mathtt{q}_0}-\xi)}(\mathtt{t}_1,0)\\
&\quad+\exp\{\xi\sup_{v\in\mathbb{T}}\mu(v)\}\left(M_{q_0}+\exp\{\xi\,{}^+\tau_{q_0r}\}N_{q_0}+O_{q_0}\right)\left[\frac{1-e_{-(^-\alpha_{q_0}-\xi)}(t_1,0)}{^-\alpha_{q_0}-\xi}\right]\Bigg\}\\
&=q^*(\mathtt{N}+\varepsilon)\mathtt{e}_{\ominus\xi}(\mathtt{t}_1,0)\|\varphi-\varphi^*\|_{\widehat{\Upsilon}}\Bigg\{\left[\frac{1}{(\mathtt{N}+\varepsilon)}-\frac{\exp\{\xi\sup_{\mathtt{v}\in\mathbb{T}}\mu(\mathtt{v})\}}{^-\alpha_{\mathtt{q}_0}-\xi}\left(\mathtt{M}_{\mathtt{q}_0}+\exp\{\xi\,{}^+\tau_{\mathtt{q}_0\mathtt{r}}\}\right.\right.\\
&\quad\left.\left.N_{q_0}+O_{q_0}\right)\right]e_{-(^-\alpha_{q_0}-\xi)}(t_1,0)+\frac{\exp\{\xi\sup_{v\in\mathbb{T}}\mu(v)\}}{^-\alpha_{q_0}-\xi}\left(M_{q_0}+\exp\{\xi\,{}^+\tau_{q_0r}\}N_{q_0}+O_{q_0}\right)\Bigg\}\\
&<q^*(\mathtt{N}+\varepsilon)\mathtt{e}_{\ominus\xi}(\mathtt{t}_1,0)\|\varphi-\varphi^*\|_{\widehat{\Upsilon}}.
\end{aligned}
$$

In general, we can have

$$
X^m_{q_0}(t_1)<q^*\mathtt{N}\mathtt{e}_{\ominus\xi}(\mathtt{t}_1,0)\|\varphi-\varphi^*\|_{\widehat{\Upsilon}},\ \mathtt{m}\in\Lambda. \tag{8}
$$

But, (8) contradicts the first equation of (7). Therefore, (5) holds. This proves the claim. Hence,

$$
\|X^m_q(t)\|_{\widehat{\Upsilon}}<q^*\mathtt{N}\mathtt{e}_{\ominus\xi}(\mathtt{t},0)\|\varphi-\varphi^*\|_{\widehat{\Upsilon}},\quad \mathtt{for\ all\ \ t}\in\mathbb{R}_{\mathbb{T}}.
$$

Hence, the almost periodic solution of system (1) is globally exponentially stable. The proof is complete. □

5 Example

In this section, we provide an example to demonstrate the feasibility of the obtained results. QVRNNs (1) are stimulated by choosing $n=2$ and the following parameters setting:

$$q, r = 1, 2,\ \alpha_1(t) = 1.2 + 0.5|\cos(t)|,\ \alpha_2(t) = 1.5 + 0.2|\sin(4t)|,$$
$$\beta_{11}(t) = \beta_{12}(t) = 0.2|\sin(2t)| + 0.1|\cos(\sqrt{3}t)|\mathbf{i} + 0.3|\sin(\sqrt{3}t)|\mathbf{j} + 0.3|\cos(2t)|\mathbf{k},$$
$$\beta_{21}(t) = \beta_{22}(t) = 0.1|\cos(\sqrt{2}t)| + 0.3|\cos(t)|\mathbf{i} + 0.2|\sin(\sqrt{5}t)|\mathbf{j} + 0.2|\sin(t)|\mathbf{k},$$
$$\gamma_{11}(t) = \gamma_{12}(t) = 0.2|\sin(3t)| + 0.1|\sin(\sqrt{0.5}t)|\mathbf{i} + 0.3|\sin(\sqrt{5}t)|\mathbf{j} + 0.2|\cos(\sqrt{2}t)|\mathbf{k},$$
$$\gamma_{21}(t) = \gamma_{22}(t) = 0.1|\sin(3t)| + 0.2|\cos(t)|\mathbf{i} + 0.1|\cos(t)|\mathbf{j} + 0.1|\sin(t)|\mathbf{k},$$
$$\delta_{11}(t) = \delta_{12}(t) = 0.2|\sin(\sqrt{5}t)| + 0.2|\sin(6t)|\mathbf{i} + 0.1|\sin(t)|\mathbf{j} + 0.1|\cos(t)|\mathbf{k},$$
$$\delta_{21}(t) = \delta_{22}(t) = 0.2|\sin(\sqrt{3}t)| + 0.2|\cos(7t)|\mathbf{i} + 0.2|\sin(\sqrt{5}t)|\mathbf{j} + 0.1|\sin(t)|\mathbf{k},$$
$$f_r(\mathrm{z}_r) = \frac{1}{8}|\mathrm{z}_r^{\mathrm{R}}| + \frac{1}{7}|\sin(\mathrm{z}_r^{\mathrm{I}})|\mathbf{i} + \frac{2}{15}|\sin^2(\mathrm{z}_r^{\mathrm{J}})|\mathbf{j} + \frac{1}{6}\tanh(\mathrm{z}_r^{\mathrm{K}})\mathbf{k},$$
$$g_r(\mathrm{z}_r) = \frac{1}{7}|\mathrm{z}_r^{\mathrm{R}}| + \frac{1}{8}|\sin(\mathrm{z}_r^{\mathrm{I}})|\mathbf{i} + \frac{1}{6}|\sin^2(\mathrm{z}_r^{\mathrm{J}})|\mathbf{j} + \frac{2}{15}\tanh(\mathrm{z}_r^{\mathrm{K}})\mathbf{k},$$
$$h_r(\mathrm{z}_r) = \frac{2}{15}|\mathrm{z}_r^{\mathrm{R}}| + \frac{1}{7}|\sin(\mathrm{z}_r^{\mathrm{I}})|\mathbf{i} + \frac{1}{6}|\sin^2(\mathrm{z}_r^{\mathrm{J}})|\mathbf{j} + \frac{1}{8}\tanh(\mathrm{z}_r^{\mathrm{K}})\mathbf{k},$$
$$\mathcal{J}_1(t) = 0.2|\sin(\sqrt{2}t)| + 0.3|1 + \sin(5t)|\mathbf{i} + 0.5|\cos(\sqrt{2}t)|\mathbf{j} + 0.1|1 + \cos(\sqrt{2}t)|\mathbf{k},$$
$$\mathcal{J}_2(t) = 0.3|1 + \cos(\sqrt{3}t)| + 0.2|1 + \cos(t)|\mathbf{i} + 0.1|1 + \cos(\sqrt{2}t)|\mathbf{j} + 0.4|\sin(\sqrt{2}t)|\mathbf{k},$$

$\tau_{11} = \tau_{12}(t) = \tau_{21}(t) = \tau_{22}(t) = 0.5$, $G_{qr}(u) = e^{-2u}(1 - \cos(u))$. After certain simple calculations, we obtain ${}^{-}\alpha_1 = 1.2, {}^{-}\alpha_2 = 1.5, \int_0^\infty G_{qr}(u)du = 1/10 < 1$,

$$M_1 = \sum_{r=1}^{2}\left({}^{+}\beta_{1r}^{\mathrm{R}} + {}^{+}\beta_{1r}^{\mathrm{I}} + {}^{+}\beta_{1r}^{\mathrm{J}} + {}^{+}\beta_{1r}^{\mathrm{K}}\right)\left(a_r^{\mathrm{R}} + a_r^{\mathrm{I}} + a_r^{\mathrm{J}} + a_r^{\mathrm{K}}\right) \approx 0.2555357143,$$
$$M_2 = \sum_{r=1}^{2}\left({}^{+}\beta_{2r}^{\mathrm{R}} + {}^{+}\beta_{2r}^{\mathrm{I}} + {}^{+}\beta_{2r}^{\mathrm{J}} + {}^{+}\beta_{2r}^{\mathrm{K}}\right)\left(a_r^{\mathrm{R}} + a_r^{\mathrm{I}} + a_r^{\mathrm{J}} + a_r^{\mathrm{K}}\right) \approx 0.2271428571,$$
$$N_1 = \sum_{r=1}^{2}\left({}^{+}\gamma_{1r}^{\mathrm{R}} + {}^{+}\gamma_{1r}^{\mathrm{I}} + {}^{+}\gamma_{1r}^{\mathrm{J}} + {}^{+}\gamma_{1r}^{\mathrm{K}}\right)\left(b_r^{\mathrm{R}} + b_r^{\mathrm{I}} + b_r^{\mathrm{J}} + b_r^{\mathrm{K}}\right) \approx 0.2271428571,$$
$$N_2 = \sum_{r=1}^{2}\left({}^{+}\gamma_{2r}^{\mathrm{R}} + {}^{+}\gamma_{2r}^{\mathrm{I}} + {}^{+}\gamma_{2r}^{\mathrm{J}} + {}^{+}\gamma_{2r}^{\mathrm{K}}\right)\left(b_r^{\mathrm{R}} + b_r^{\mathrm{I}} + b_r^{\mathrm{J}} + b_r^{\mathrm{K}}\right) \approx 0.1419642857,$$
$$O_1 = \sum_{r=1}^{2}\left({}^{+}\delta_{1r}^{\mathrm{R}} + {}^{+}\delta_{1r}^{\mathrm{I}} + {}^{+}\delta_{1r}^{\mathrm{J}} + {}^{+}\delta_{1r}^{\mathrm{K}}\right)\left(c_r^{\mathrm{R}} + c_r^{\mathrm{I}} + c_r^{\mathrm{J}} + c_r^{\mathrm{K}}\right) \approx 0.1703571429,$$
$$O_2 = \sum_{r=1}^{2}\left({}^{+}\delta_{2r}^{\mathrm{R}} + {}^{+}\delta_{2r}^{\mathrm{I}} + {}^{+}\delta_{2r}^{\mathrm{J}} + {}^{+}\delta_{1r}^{\mathrm{K}}\right)\left(c_r^{\mathrm{R}} + c_r^{\mathrm{I}} + c_r^{\mathrm{J}} + c_r^{\mathrm{K}}\right) \approx 0.1987500000.$$

Let $\ell = 5$. Then

$$\max_{q\in\Omega}\left\{\max_{m\in\Lambda}\left\{\frac{(M_q + N_q + O_q)\ell + {}^{+}\mathcal{J}_q^m}{{}^{-}\alpha_q}\right\}\right\} = \max\{3.637648810, 2.559523809\}$$
$$= 3.637648810 < \ell,$$

and

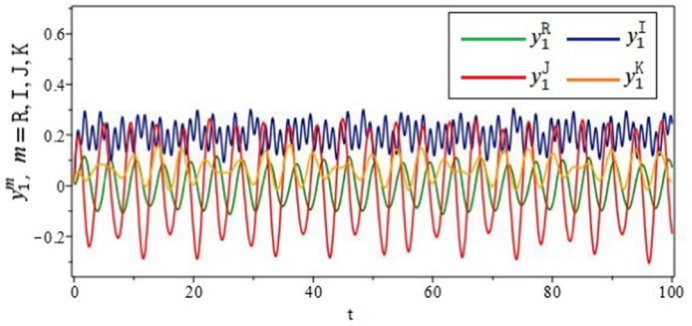


Fig. 1 Continuous situation of $z_1^R, z_1^I, z_1^J, z_1^K$ for system (1) with the initial values $(z_1^R, z_1^I, z_1^J, z_1^K)^T = (0.01, 0.01, 0.01, 0.01)^T$ when $t \in [0, 100]$

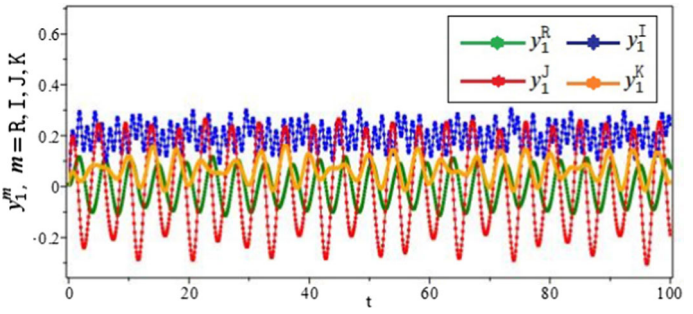


Fig. 2 Discrete situation of $z_1^R, z_1^I, z_1^J, z_1^K$ for system (1) with the initial values $(z_1^R, z_1^I, z_1^J, z_1^K)^T = (0.01, 0.01, 0.01, 0.01)^T$ when $t \in [0, 100]$

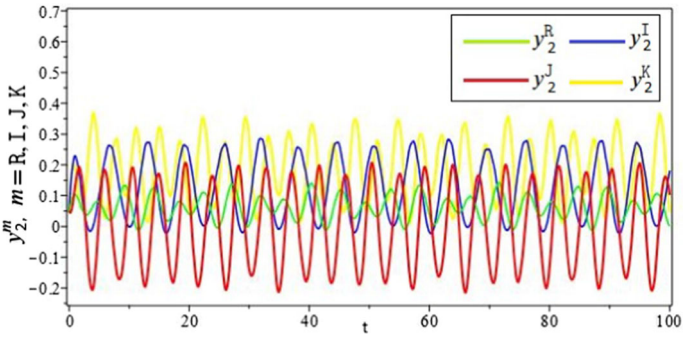


Fig. 3 Continuous situation of $z_2^R, z_2^I, z_2^J, z_2^K$ for system (1) with the initial values $(z_2^R, z_2^I, z_2^J, z_2^K)^T = (0.05, 0.05, 0.05, 0.05)^T$ when $t \in [0, 100]$

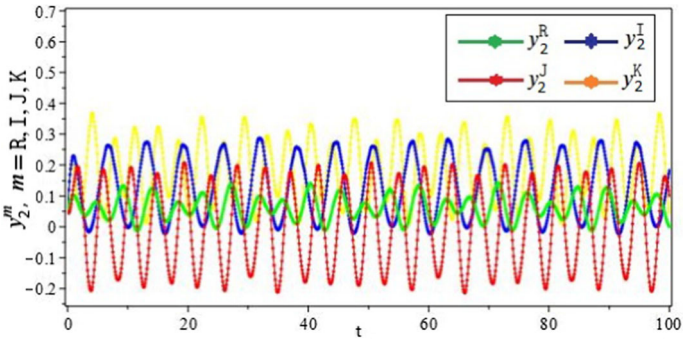


Fig. 4 Discrete situation of $z_1^R, z_2^I, z_2^J, z_2^K$ for system (1) with the initial values $(z_2^R, z_2^I, z_2^J, z_2^K)^T = (0.05, 0.05, 0.05, 0.05)^T$ when $t \in [0, 100]$

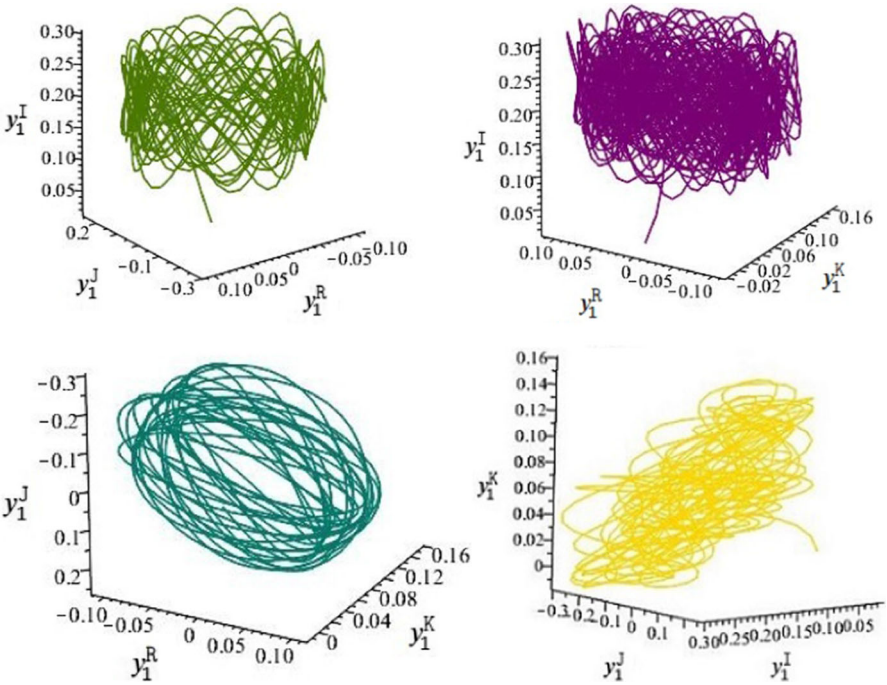


Fig. 5 Continuous situation of three of $z_1^R, z_1^I, z_1^J, z_1^K$ for system (1) with the initial values $(z_1^R, z_1^I, z_1^J, z_1^K)^T = (0.01, 0.01, 0.01, 0.01)^T$ when $t \in [0, 100]$

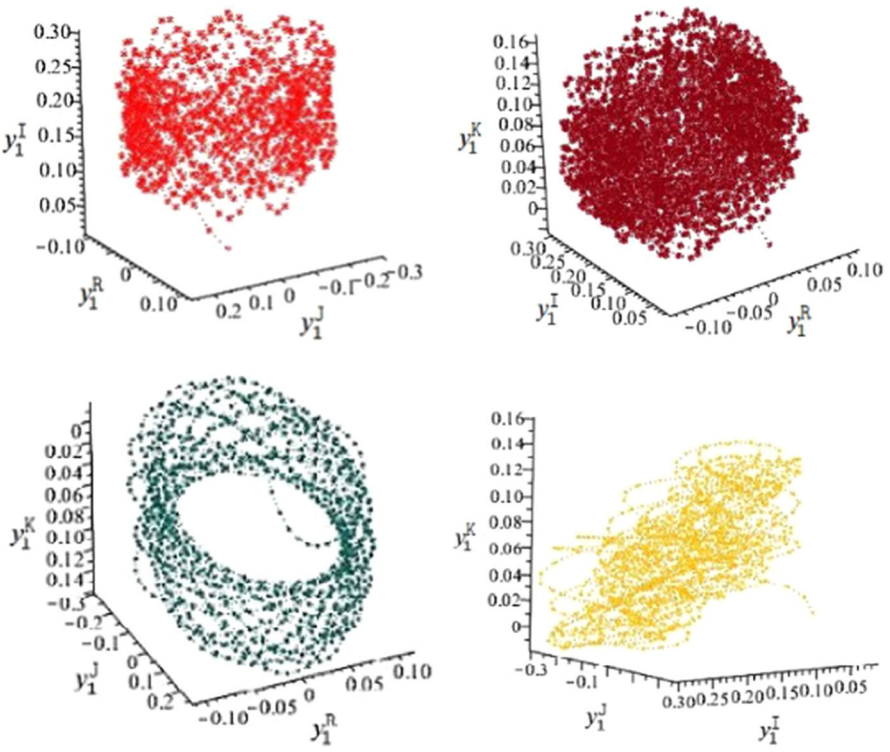


Fig. 6 Discrete situation of three of $z_1^R, z_1^I, z_1^J, z_1^K$ for system (1) with the initial values $(z_1^R, z_1^I, z_1^J, z_1^K)^T = (0.01, 0.01, 0.01, 0.01)^T$ when $t \in [0, 100]$

$$\lambda = \max_{q\in\Omega}\left\{\frac{M_q + N_q + O_q}{^{-}\alpha_q}\right\} = \max\{0.5441964286, 0.3785714285\}$$
$$= 0.5441964286 < 1.$$

All conditions of Theorem 3.1 are satisfied, therefore, the system (1) has a unique almost periodic solution in the region $\widehat{\Upsilon} = \{\psi \in \Upsilon : \|\psi\| \leq 5\}$ and is globally exponentially stable. In particular, the continuous-time neural network and the discrete-time analogue described by (1) have the similar dynamical behaviors. Figures 1, 2, 3 and 4 of system (1) illustrate the numerical simulations of state variables of $z_q^m, q = 1, 2, m \in \Lambda$ and show the existence, uniqueness and the stability of almost periodic solutions of system (1). In Figures 5, 6, 7 and 8 of system (1) depict the curves of neurons $z_q^m, q = 1, 2, m \in \Lambda$ in 3-dimension space.

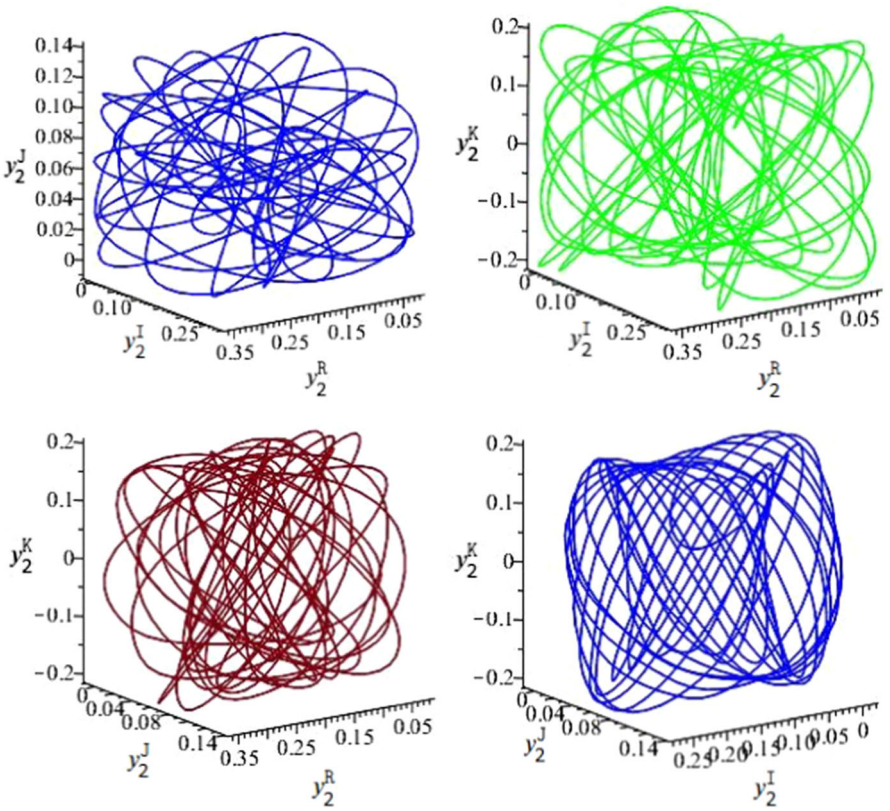


Fig. 7 Continuous situation of three of $z_2^R, z_2^I, z_2^J, z_2^K$ for system (1) with the initial values $(z_2^R, z_2^I, z_2^J, z_2^K)^T = (0.05, 0.05, 0.05, 0.05)^T$ when $t \in [0, 100]$

6 Conclusion

In this paper, we considered a class of quaternion-valued recurrent neural networks with mixed delays on time scales. Based on the exponential dichotomy of linear dynamic equations on time scales, Banach's fixed point theorem and the theory of calculus on time scales, we obtain some sufficient conditions on the existence and global exponential stability of almost periodic solutions to the quaternion-valued recurrent neural networks. To demonstrate the usefulness of the presented results, numerical examples and computer simulations are given. Furthermore, the method of this paper can be used to study other types of quaternion-valued neural networks such as Hopfield neural networks, BAM neural networks, Cohen-Grossberg neural networks and so on.

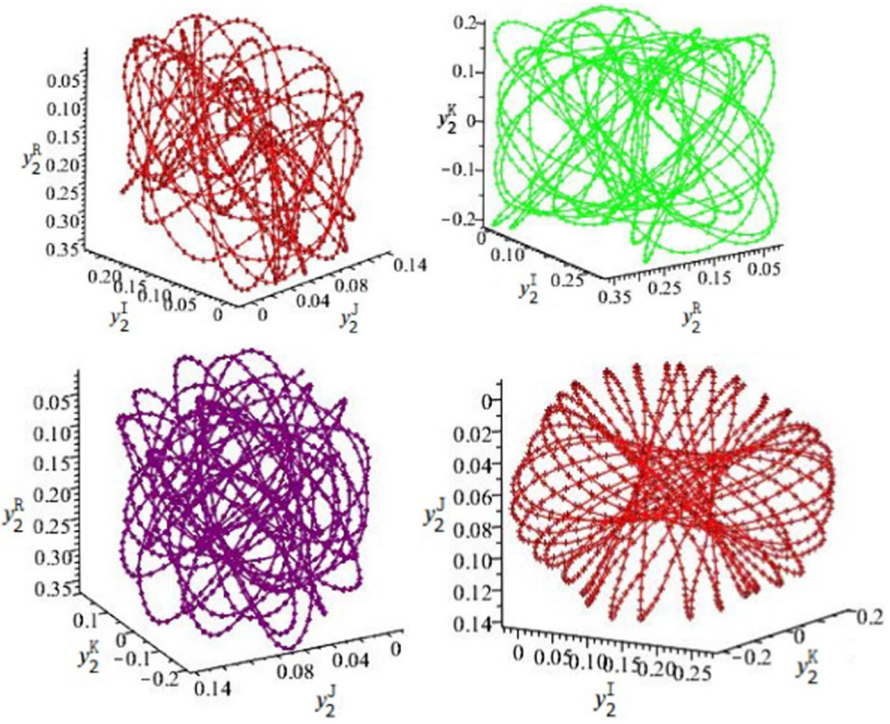


Fig. 8 Discrete situation of three of $z_2^R, z_2^I, z_2^J, z_2^K$ for system (1) with the initial values $(z_2^R, z_2^I, z_2^J, z_2^K)^T = (0.05, 0.05, 0.05, 0.05)^T$ when $t \in [0, 100]$

Acknowledgements The authors would like to thank the referees and editor for their valuable suggestions and comments for the improvement of the paper.

Author Contributions The study was carried out in collaboration of all authors. All authors read and approved the final manuscript.

Funding Not applicable.

Data Availability Data sharing not applicable to this paper as no data sets were generated or analyzed during the current study.

Declarations

Conflict of interest It is declared that authors has no competing interests.

Ethical approval This article does not contain any studies with human participants or animals performed by any of the authors.

References

1. Abu-Shady, M., Kaabar, M.K.A.: A generalized definition of the fractional derivative with applications. Math. Probl. Eng. (2021). https://doi.org/10.1155/2021/9444803
2. Agarwal, R.P., Bohner, M.: Basic calculus on time scales and some of its applications. Results Math. **35**(1–2), 3–22 (1999)
3. Agarwal, R.P., Bohner, M., O'Regan, D., Peterson, A.: Dynamic equations on time scales: a survey. J. Comput. Appl. Math. **141**(1–2), 1–26 (2002)
4. Achar, S.J., Baishya, C., Kaabar, M.K.A.: Dynamics of the worm transmission in wireless sensor network in the framework of fractional derivatives. Math. Methods Appl. Sci. (2021). https://doi.org/10.1002/mma.8039
5. Bohner, M., Peterson, A.: Dynamic Equations on Time Scales: An Introduction with Applications. Birkhäuser Boston Inc, Boston (2001)
6. Bohner, M., Peterson, A.: Advances in Dynamic Equations on Time Scales. Birkhäuser Boston Inc, Boston (2003)
7. Chen, H., Zhong, S., Shao, J.: Exponential stability criterion for interval neural networks with discrete and distributed delays. Appl. Math. Comput. **250**, 121–130 (2015)
8. Chen, X., Song, Q., Li, Z.: Design and analysis of quaternion-valued neural networks for associative memories. IEEE Trans. Syst. Man Cybern. Syst. **49**, 2305–2314 (2018)
9. Debbouche, N., Ouannas, A., Batiha, I.M., Grassi, G., Kaabar, M.K.A., Jahanshahi, H., Ali, A.A., Aljuaid, A.M.: Chaotic behavior analysis of a new incommensurate fractional-order Hopfield neural network system. Complexity (2021). https://doi.org/10.1155/2021/3394666
10. Dong, T., Liao, X., Wang, A.: Stability and hopf bifurcation of a complex-valued neural network with two time delays. Nonlinear Dyn. **82**, 173–184 (2015)
11. Hirose, A.: Complex-valued and quaternion neural networks to deal with complex amplitude and polarization: their strength in electronics. In: Proceedings of APSIPA Annual Summit and Conference, pp. 566–571 (2018)
12. Hu, B., Song, Q., Li, K., Zhao, Z., Liu, Y., Alsaadi, F.: Global μ-synchronization of impulsive complex-valued neural networks with leakage delay and mixed time-varying delays. Neurocomputing **307**, 106–116 (2018)
13. Kaabar, M.K.A., Martinez, F., Gomez-Aguilar, J.F., Ghanbari, B., Kaplan, M., Günerhan, H.: New approximate analytical solutions for the nonlinear fractional Schrödinger equation with second-order spatio-temporal dispersion via double Laplace transform method. Math. Methods Appl. Sci. **44**(14), 11138–11156 (2021)
14. Kaabar, M.K.A., Shabibi, M., Alzabut, J., Etemad, S., Sudsutad, W., Martinez, F., Rezapour, S.: Investigation of the fractional strongly singular thermostat model via fixed point techniques. Mathematics **9**(18), 2298 (2021)
15. Khuddush, M., Prasad, K.R.: Infinitely many positive solutions for an iterative system of conformable fractional order dynamic boundary value problems on time scales. Turk. J. Math. **46**(2), 338–359 (2022)
16. Khuddush, M., Prasad, K.R.: Nonlinear two-point iterative functional boundary value problems on time scales. J. Appl. Math. Comput. (2022). https://doi.org/10.1007/s12190-022-01703-4
17. Kravchenko, V.V.: Applied quaternionic analysis: Maxwell's system and Dirac's equation. In: Functional-Analytic and Complex Methods, Their Interactions and Applications to Partial Differential Equations, Proceedings of the International Graz Workshop, pp. 143–160 (2001)
18. Li, Y., Li, B., Yao, S., Xiong, L.: The global exponential pseudo almost periodic synchronization of quaternion-valued cellular neural networks with time-varying delays. Neurocomputing **303**, 75–87 (2018)
19. Li, Y., Shen, S.: Pseudo almost periodic synchronization of Clifford-valued fuzzy cellular neural networks with time-varying delays on time scales. Adv. Differ. Equ. **2020**, 593 (2020). https://doi.org/10.1186/s13662-020-03041-w
20. Li, Y., Qin, J., Li, B.: Existence and global exponential stability of anti-periodic solutions for delayed quaternion-valued cellular neural networks with impulsive effects. Math. Methods Appl. Sci. **42**(1), 5–23 (2019)
21. Li, Y.K., Wang, C.: Uniformly almost periodic functions and almost periodic solutions to dynamic equations on time scales. Abstr. Appl. Anal. Art. ID 341520, 22 pp (2011)

22. Li, Y., Wang, H., Meng, X.: Almost automorphic synchronization of quaternion-valued high-order hopfield neural networks with time-varying and distributed delays. IMA J. Math. Control I **36**(3), 983–1013 (2019)
23. Li, Y.K., Xiang, J.L., Li, B.: Pseudo-almost-periodic solutions of quaternion-valued RNNs with mixed delays via a direct method. J. Ineq. Appl. **88**, 1–17 (2020)
24. Liu, Y., Zhang, D., Lu, J., Cao, J.: Global μ-stability criteria for quaternion-valued neural networks with unbounded time-varying delays. Inf. Sci. (NY) **360**, 273–288 (2016)
25. Liu, Y., Zheng, Y., Lu, J., Cao, J., Rutkowski, L.: Constrained quaternion-variable convex optimization: a quaternion-valued recurrent neural network approach. IEEE Trans. Neural Netw. Learn. Syst. (2019). https://doi.org/10.1109/TNNLS.2019.2916597
26. Liu, X., Li, Z.: Global μ-stability of quaternion-valued neural networks with unbounded and asynchronous time-varying delays. IEEE Access **7**, 9128–9141 (2019)
27. Meng, X., Li, Y.: Pseudo almost periodic solutions for quaternion-valued cellular neural networks with discrete and distributed delays. J. Inequal. Appl. **2018**, 245 (2018)
28. Morais, J. P., Georgiev, S., Spröβig, W.: Real Quaternionic Calculus Handbook. Birkhuser. Springer, Basel (2014)
29. Prasad, K.R., Khuddush, M.: Existence and global exponential stability of positive almost periodic solutions for a time scales model of Hematopoiesis with multiple time varying variable delays. Int. J. Differ. Equ. **14**(2), 149–167 (2019)
30. Prasad, K.R., Khuddush, M.: Existence and uniform asymptotic stability of positive almost periodic solutions for three-species LotkaVolterra competitive system on time scales. Asian Eur. J. Math. **13**(03), 2050058 (2020)
31. Prasad, K.R., Khuddush, M., Vidyasagar, K.V.: Almost periodic positive solutions for a time-delayed SIR epidemic model with saturated treatment on time scales. J. Math. Model. **9**(1), 45–60 (2021)
32. Prasad, K.R., Khuddush, M., Vidyasagar, K.V.: Almost periodic positive solutions for a delayed nonlinear density dependent mortality Nicholson's blowflies model on time scales. TWMS J. App. Eng. Math. **12**(3), 876–887 (2022)
33. Samidurai, R., Sriraman, R., Zhu, S.: Leakage delay-dependent stability analysis for complex-valued neural networks with discrete and distributed time-varying delays. Neurocomputing **338**, 262–273 (2019)
34. Tan, M., Liu, Y., Xu, D.: Multistability analysis of delayed quaternion-valued neural networks with nonmonotonic piecewise nonlinear activation functions. Appl. Math. Comput. **341**, 229–255 (2019)
35. Tu, Z., Zhao, Y., Ding, N., Feng, N., Wei, Z.: Stability analysis of quaternion-valued neural networks with both discrete and distributed delays. Appl. Math. Comput. **343**, 342–353 (2019)
36. Wang, P., Zou, W., Su, H.: Stability of complex-valued impulsive stochastic functional differential equations on networks with Markovian switching. Appl. Math. Comput. **348**, 338–354 (2019)
37. Wu, R., Huang, H., Qian, X., Huang, T.: A *L*-BFGS based learning algorithm for complex-valued feed forward neural networks. Neural Process Lett. **47**, 1271–1284 (2018)
38. Xiang, J., Li, Y.: Pseudo almost automorphic solutions of quaternion-valued neural networks with infinitely distributed delays via a non-decomposing method. Adv. Differ. Equ. **2019**(1), 356 (2019)
39. Xiao, Q., Huang, T.: Stability of delayed inertial neural networks on time scales: a unified matrix-measure approach. Neural Netw. **130**, 33–38 (2020)
40. Xu, Q., Zhuang, S., Xu, X., Che, C., Xia, Y.: Stabilization of a class of fractional-order nonautonomous systems using quadratic Lyapunov functions. Adv. Differ. Equ. **2018**, Ariticle ID 14 (2018)
41. Xu, Q., Xu, X., Zhuang, S., Xiao, J., Song, C., Che, C.: New complex projective synchronization strategies for drive-response networks with fractional complex-variable dynamics. Appl. Math. Comput. **338**, 552–566 (2018)
42. Xu, X., Yang, J., Xu, Y.: Mean square exponential stability of stochastic complex–valued neural networks with mixed delays. Complexity **20**, Article ID 34293, 26 pp (2019)
43. Xu, X., Zhang, J., Shi, J.: Dynamical behaviour analysis of delayed complex-valued neural networks with impulsive effect. Int. J. Syst. Sci. **48**, 686–694 (2017)
44. Xue, H., Xu, X., Zhang, J., Yang, X.: Robust stability of impulsive switched neural networks with multiple time delays. Appl. Math. Comput. **359**, 456–475 (2019)
45. You, X., Dian, S., Guo, R., Li, S.: Exponential stability analysis for discrete-time quaternion-valued neural networks with leakage delay and discrete time-varying delays. Neurocomputing **430**, 71–81 (2021)
46. Yu, T., Cao, D., Liu, S., Chen, H.: Stability analysis of neural networks with periodic coefficients and piecewise constant arguments. J. Frankl. Inst. **353**, 409–425 (2016)

47. Yuan, Y., Song, Q., Liu, Y., Alsaadi, F.: Synchronization of complex-valued neural networks with mixed two additive time-varying delays. Neurocomputing **332**, 149–158 (2019)
48. Zhang, J., Fan, M.: Existence and roughness of exponential dichotomies of linear dynamic equations on time scales. Comput. Math. Appl. **59**(8), 2658–2675 (2010)
49. Zhang, Z., Wang, H., Xu, F., Jin, Y.: Complex-valued convolutional neural network and its application in polarimetric SAR image classification. IEEE Trans. Geosci. Remote Sens. **55**, 7177–7188 (2017)

Publisher's Note Springer Nature remains neutral with regard to jurisdictional claims in published maps and institutional affiliations.

Springer Nature or its licensor holds exclusive rights to this article under a publishing agreement with the author(s) or other rightsholder(s); author self-archiving of the accepted manuscript version of this article is solely governed by the terms of such publishing agreement and applicable law.

Filomat 36:10 (2022), 3527–3543
https://doi.org/10.2298/FIL2210527K



Published by Faculty of Sciences and Mathematics,
University of Niš, Serbia
Available at: http://www.pmf.ni.ac.rs/filomat

Existence of Solutions to the ∞-point Fractional BVP Posed on Half-Line via a Family of Measure of Noncompactness in the Hölder Space $\mathbb{C}^{\ell,\alpha}(\mathbb{R}_+)$

Mahammad Khuddush[a], K. Rajendra Prasad[b], D. Leela[b]

[a]*Department of Mathematics, Dr. Lankapalli Bullayya College of Engineering, Resupuvanipalem, Visakhapatnam, 530013, India*
[b]*Department of Applied Mathematics, College of Science and Technology, Andhra University, Visakhapatnam, 530003, India*

Abstract. This paper deals with the existence of solutions for the Riemann-Liouville fractional order boundary value problem with infinite-point boundary conditions posed on half-line via the concept of a family of measures of noncompactness in the space of functions $\mathbb{C}^{\ell,\alpha}(\mathbb{R}_+)$ satisfying the Hölder condition and a generalized Darbo fixed point theorem.

1. Introduction

Fractional differential equations with boundary conditions have occupied an important role in the fractional calculus domain, since these problems appear in various applications of sciences and engineering: electricity, mechanics, finance, control theory, biology, chemistry, chemistry, economics [12, 15, 19, 38–41]. In recent years, there are certain papers and monographs dealing with the existence, uniqueness and stability analysis of fractional order nonlinear boundary value problems, see ([5, 17, 23–25, 31, 33, 34, 43, 44, 46]) and references therein.

Measures of noncompactness play an important area in fixed point theory and have many applications in various branches of nonlinear analysis, including differential equations, integral and integro-differential equations, optimization, etc. Roughly speaking, a measure of noncompactness is a function defined on the family of all nonempty and bounded subsets of a certain metric space such that it is equal to zero on the whole family of relatively compact sets. The concept of measure of noncompactness was first introduced by Kuratowski [26]. Later, the Italian mathematician Darbo [14] used the Kuratowski measure in order to investigate a class of operators (condensing operators) whose properties can be characterized as being intermediate between those of contraction and compact mappings. Darbo's fixed point theorem is useful in establishing existence results for different classes of operator equations. For details on various measures of noncompactness see [7].

Existence of solutions for differential and integral equations has been investigated by many authors in various types of measure of noncompactness. Benchohra et al. [8] investigated a class of boundary value

2020 *Mathematics Subject Classification*. Primary 47H08, 47H10; Secondary 45E10
Keywords. Fractional derivative, boundary value problem, Family of measure of noncompactness, Darbo fixed point theorem, Hölder space $\mathbb{C}^{\ell,\alpha}(\mathbb{R}_+)$
Received: 27 June 2021; Revised: 27 December 2021; Accepted: 30 December 2021
Communicated by Hari M. Srivastava
Email addresses: khuddush89@gmail.com (Mahammad Khuddush), krajendra92@rediffmail.com (K. Rajendra Prasad), leelaravidadi@gmail.com (D. Leela)

problems for fractional differential equations involving nonlinear integral conditions using the technique associated with measures of weak noncompactness. Aghajani et al. [3] proved the solvability of a large class of nonlinear fractional integro-differential equations by establishing some fractional integral inequalities and using the nonlinear alternative of Leray-Schauder type. Li et al. [28] studied on the existence of mild solutions for fractional semilinear differential equations with nonlocal conditions. In [30], Mohiuddine et al. studied the existence of solutions of infinite systems of second-order differential equations in the Banach sequence space ℓ_p by using technique based upon measures of noncompactness in conjunction with a Darbo-type fixed point theorem. In [37], Sriviastava et al. obtained existence results for an infinite system of differential equations of order n with boundary conditions in the Banach spaces c_0 and ℓ_1 with the help of a technique associated with measures of noncompactness. B. Hazarika et al. [21] established existence of solution for infinite system of nonlinear integral equations in the Banach spaces ℓ_p, $p > 1$ with help of measure of noncompactness and generalized Meir-Keeler fixed point theorem later in [22], they studied nonlinear functional integral equation with help of measure of noncompactness, simulation function and generalized Darbo fixed point theorem. Wang et al. [45] applied a new variant flxed point theorem to investigate some fractional differential equations in Banach spaces. Liang et al. [29] studied the solvability for a coupled system of nonlinear fractional difierential equations in a Banach space using the measures of noncompactness and the well known fixed point theorem of Monch type. Borisut et al [10] studied fractional order boundary value problem based on Kransnoselskii's fixed point theorem and Darbo's fixed point theorem together and the idea of the measure of noncompactness.

In [16], Derbazi et al. established the existence of weak solutions for the following fractional boundary value problem

$$\begin{gathered}
\mathtt{D}_{0^+}^{\alpha}\mathtt{z}(\mathtt{t}) = \mathtt{g}(\mathtt{t}, x(\mathtt{t})),\ 0 \le \mathtt{t} \le \mathtt{T},\ 1 < \alpha \le 2,\\
a_1\mathtt{z}(0) + b_1\mathtt{z}(\mathtt{T}) = \lambda_1 \mathtt{I}^{\beta_1}\mathtt{z}(\eta),\ \beta_1 > 0\\
a_2\,\mathtt{D}_{0^+}^{\beta_2}\mathtt{z}(\xi) + b_2\,\mathtt{D}_{0^+}^{\beta_3}\mathtt{z}(\eta) = \lambda_2,\ 0 < \beta_2, \beta_3 \le 1,
\end{gathered}$$

by using the Monch's fixed point theorem combined with the technique of measures of weak noncompactness. In [35], Prasad et al. investigated the existence of solutions for infinite systems of regular fractional Sturm-Liouville problems

$$\begin{gathered}
\mathtt{D}_{\mathtt{T}^-}^{\gamma}\Big[\mathtt{p}_\mathtt{j}(\mathtt{t})\mathtt{D}_{0^+}^{\gamma}(\mathtt{z}_\mathtt{j}(\mathtt{t}))\Big] = \lambda_\mathtt{j}\mathtt{g}_\mathtt{j}(\mathtt{t}, \mathtt{z}(\mathtt{t})),\ 0 < \mathtt{t} < \mathtt{T},\ \gamma \in (0,1),\\
\mathtt{z}_\mathtt{j}(0) = 0,\ \mathtt{D}_{0^+}^{\gamma}\mathtt{z}_\mathtt{j}(\mathtt{T}) = 0,\ \mathtt{j} \in \mathbb{N},
\end{gathered}$$

by an application of Meir-Keeler fixed point theorem in the tempered sequence spaces. Recently, Salem et al. [36] investigated the existence of solutions for the infinite system

$$\begin{gathered}
{}^{\rho_\mathtt{j}}\mathtt{D}^{\lambda_\mathtt{j}}\Big({}^{\rho_\mathtt{j}}\mathtt{D}^{\mu_\mathtt{j}} + \xi\Big)\mathtt{z}_\mathtt{j}(\mathtt{t}) = \mathtt{g}_\mathtt{j}(\mathtt{t}, \mathtt{z}_\mathtt{j}(\mathtt{t}), \varphi({}^{\rho}\mathtt{D}^{\nu}\mathtt{z}(\mathtt{t}))),\ 0 < \mathtt{t} < 1,\ 0 < \rho_\mathtt{j}, \mu_\mathtt{j}, \nu < 1 < \lambda_\mathtt{j} \le 2,\\
\mathtt{z}_\mathtt{j}(0) = {}^{\rho_i}\mathtt{D}^{\mu_i}\mathtt{z}_\mathtt{j}(0) = 0,\ \mathtt{z}_\mathtt{j}(1) = a_\mathtt{j}\mathtt{z}_\mathtt{j}(\eta_i),\ 0 < \eta_\mathtt{j} < 1,\ \mathtt{j} \in \mathbb{N},
\end{gathered}$$

by using the measure of noncompactness technique and applying the Darbo's fixed point theorem in the Banach spaces $\ell_\mathtt{p}$, $\mathtt{p} \ge 1$. Motivated by aforementioned works, in this paper we study fractional order differential equation with infinite-point boundary conditions

$$\left.\begin{aligned}
\mathtt{D}_{0^+}^{\delta}\mathtt{z}(\mathtt{t}) = \mathtt{g}\Big(\mathtt{t}, \mathtt{z}(\mathtt{t})\Big),\ \ell < \delta < \ell + 1,\ \mathtt{t} \in \mathbb{R}_+ := [0, \infty),\\
\mathtt{z}(0) = \mathtt{z}''(0) = \cdots = \mathtt{z}^{(\ell)}(0) = 0,\\
\lim_{\mathtt{t}\to+\infty} \mathtt{D}_{0^+}^{\delta-1}\mathtt{z}(\mathtt{t}) + \sum_{\mathtt{j}=1}^{\infty} \mathtt{c}_\mathtt{j}\mathtt{z}\Big(\varphi(\tau_\mathtt{j})\Big) = 0,
\end{aligned}\right\} \tag{1}$$

where $\mathtt{c}_\mathtt{j}$ is a positive real number, $\mathtt{g} : \mathbb{R}_+ \times \mathbb{R} \to \mathbb{R}$, $\varphi : \mathbb{R}_+ \to \mathbb{R}$ are continuous functions and $\mathtt{D}_{0^+}^{\delta}$ is the Riemann-Liouville fractional derivative of order δ.

The rest of the paper is organized in the following fashion. In Section 2, we provide some definitions and lemmas which will be useful in our main results. In Section 3, we study existence of at least one fixed point theorems for class of operators. In Section 4, we study existence of solution for fractional order boundary value problem (1) as an application fixed point theorem. Finally, we provide an example to check feasibility of our results.

2. Preliminaries

In this section, we present some definitions and lemmas on fractional calculus and the concept of measure of noncompactness. Throughout the paper we assume that X is a Banach space. For a subset E of X, the closure and convex hull of E in X are denoted by $\overline{E}$ and $conv(E)$, respectively. Further, we denote the family of nonempty bounded subsets of X by $\mathfrak{M}_X$ and $\mathfrak{N}_X$ is the subfamily consisting of all relatively compact subsets of X. Let $\mathbb{C}(I)$ be the space of continuous functions defined on I with the norm given by

$$\|z\| = \sup_{t\in I} |z(t)|.$$

In addition, $L_1(I)$ denotes the class of the Lebesgue integrable functions on the interval I with the norm given by

$$\|z\|_{L_1} = \int_I z(s)ds.$$

Definition 2.1. *[25] The Riemann-Liouville fractional integral of order $\beta > 0$ for a function $f : (0,\infty) \to \mathbb{R}$ is defined as*

$$I_{0^+}^{\beta} f(t) = \frac{1}{\Gamma(\beta)} \int_0^t (t-s)^{\beta-1} f(s)ds,$$

provided that the right side is pointwise defined on $(0,\infty)$.

Definition 2.2. *[25] The Riemann-Liouville fractional derivative of order $\beta > 0$ for a continuous function $f : (0,\infty) \to \mathbb{R}$ is defined as*

$$D_{0^+}^{\beta} f(t) = \frac{1}{\Gamma(m-\beta)} \left(\frac{d}{dt}\right)^m \int_0^t \frac{f(s)}{(t-s)^{\gamma-m-1}} ds,$$

where $m = [\beta] + 1$, provided that the right side is pointwise defined on $(0,\infty)$.

Remark 2.3. *([25]) In this work we need the following composition relations:*

(*a*) $D_{0^+}^{\beta} I_{0^+}^{\beta} f(t) = f(t)$, $\beta > 0, f(t) \in L^1(0,+\infty)$;

(*b*) $D_{0^+}^{\gamma} I_{0^+}^{\beta} f(t) = I_{0^+}^{\beta-\gamma} f(t)$, $\beta > \gamma > 0, f(t) \in L^1(0,+\infty)$.

Remark 2.4. *([5]) For $\eta > -1$, we have*

$$D_{0^+}^{\beta} t^{\eta} = \frac{\Gamma(\eta+1)}{\Gamma(\eta-\beta+1)} t^{\eta-\beta},$$

giving inparticular $D_{0^+}^{\beta} t^{\beta-m} = 0$, $m = 1,2,\cdots,N$, where N is the smallest integer greater than or equal to β.

Lemma 2.5. *[25] The general solution to $D_{0^+}^{\beta} y(t) = 0$ with $\beta \in (m-1,m]$ and $m > 1$ is the function*

$$y(t) = a_1 t^{\beta-1} + a_2 t^{\beta-2} + \cdots + a_m t^{\beta-m},\ a_i \in \mathbb{R},\ i = 1,2,\cdots,m.$$

Lemma 2.6. *[25] Let $\beta > 0$. Then the following equality holds for $\mathtt{y}(\mathtt{t})$:*

$$\mathtt{I}_{0^+}^{\beta}\mathtt{D}_{0^+}^{\beta}\mathtt{y}(t) = \mathtt{y}(t) + a_1\mathtt{t}^{\beta-1} + a_2\mathtt{t}^{\beta-2} + \cdots + a_m\mathtt{t}^{\beta-m},\ a_{\mathtt{i}} \in \mathbb{R},\ \mathtt{i} = 1, 2, \cdots, m$$

and m is the smallest integer greater than or equal to γ.

Lemma 2.7. *Suppose $\sum_{\mathtt{j}=1}^{m} \mathtt{c}_{\mathtt{j}}\varphi(\tau_{\mathtt{j}})^{\delta-1}$ converges to $\Gamma(\delta)$ and let $\varpi \in L^1(\mathbb{R}_+)$. Then the fractional order boundary value problem*

$$\mathtt{D}_{0^+}^{\delta}\mathtt{z}(\mathtt{t}) = \varpi(\mathtt{t}),\ \ell < \delta < \ell + 1,\ \mathtt{t} \in \mathbb{R}_+ \tag{2}$$

satisfying infinite-point boundary conditions

$$\mathtt{z}(0) = 0, \mathtt{z}'(0) = \mathtt{z}''(0) = \cdots = \mathtt{z}^{(\ell-1)}(0) = 0, \tag{3}$$

$$\lim_{\mathtt{t}\to+\infty} \mathtt{D}_{0^+}^{\delta-1}\mathtt{z}(\mathtt{t}) + \sum_{\mathtt{j}=1}^{\infty} \mathtt{c}_{\mathtt{j}}\mathtt{z}\Big(\varphi(\tau_{\mathtt{j}})\Big) = 0, \tag{4}$$

has a unique solution

$$\left.\begin{aligned}\mathtt{z}(\mathtt{t}) = \int_0^{\mathtt{t}} \frac{(\mathtt{t}-\mathtt{s})^{\delta-1}}{\Gamma(\delta)}\varpi(\mathtt{s})\mathtt{ds} - \frac{\mathtt{t}^{\delta-1}}{2\Gamma(\delta)}\int_0^{\infty} \varpi(\mathtt{s})\mathtt{ds} \\ - \frac{\mathtt{t}^{\delta-1}}{2\Gamma(\delta)}\sum_{\mathtt{j}=1}^{\infty} \mathtt{c}_{\mathtt{j}}\int_0^{\varphi(\tau_{\mathtt{j}})} \frac{(\varphi(\tau_{\mathtt{j}})-\mathtt{s})^{\delta-1}}{\Gamma(\delta)}\varpi(\mathtt{s})\mathtt{ds}.\end{aligned}\right\} \tag{5}$$

Proof. Let $\mathtt{z}(\mathtt{t})$ be a solution of (2). Then, by Lemma 2.6, we have

$$\mathtt{z}(\mathtt{t}) = a_1\mathtt{t}^{\delta-1} + a_2\mathtt{t}^{\delta-2} + \cdots + a_{\ell+1}\mathtt{t}^{\delta-\ell-1} + \int_0^{\mathtt{t}} \frac{(\mathtt{t}-\mathtt{s})^{\delta-1}}{\Gamma(\delta)}\varpi(\mathtt{s})\mathtt{ds} \tag{6}$$

for some $a_m \in \mathbb{R}$, $m = 1, 2, \cdots, \ell + 1$. Using conditions (3), we get $a_2 = a_3 = \cdots = a_{\ell+1} = 0$. So, (6) reduces to

$$\mathtt{z}(\mathtt{t}) = a_1\mathtt{t}^{\delta-1} + \int_0^{\mathtt{t}} \frac{(\mathtt{t}-\mathtt{s})^{\delta-1}}{\Gamma(\delta)}\varpi(\mathtt{s})\mathtt{ds}. \tag{7}$$

Before applying (4), we first take

$$\lim_{\mathtt{t}\to+\infty} \mathtt{D}_{0^+}^{\delta-1}\mathtt{z}(\mathtt{t}) = -\sum_{\mathtt{j}=1}^{m} \mathtt{c}_{\mathtt{j}}\mathtt{z}\Big(\varphi(\tau_{\mathtt{j}})\Big)$$

and using Remark 2.4 to get

$$a_1 = \frac{-1}{\sum_{\mathtt{j}=1}^{m} \mathtt{c}_{\mathtt{j}}\varphi(\tau_{\mathtt{j}})^{\delta-1} + \Gamma(\delta)}\left[\int_0^{\infty} \varpi(\mathtt{s})\mathtt{ds} + \sum_{\mathtt{j}=1}^{m} \mathtt{c}_{\mathtt{j}}\int_0^{\varphi(\tau_{\mathtt{j}})} \frac{(\varphi(\tau_{\mathtt{j}})-\mathtt{s})^{\delta-1}}{\Gamma(\delta)}\varpi(\mathtt{s})\mathtt{ds}\right].$$

Plugging a_2 value into (7), we obtain

$$\left.\begin{aligned}\mathtt{z}(\mathtt{t}) = &\frac{-\mathtt{t}^{\delta-1}}{\sum_{\mathtt{j}=1}^{m} \mathtt{c}_{\mathtt{j}}\varphi(\tau_{\mathtt{j}})^{\delta-1} - \Gamma(\delta)}\left[\int_0^{\infty} \varpi(\mathtt{s})\mathtt{ds} + \sum_{\mathtt{j}=1}^{m} \mathtt{c}_{\mathtt{j}}\int_0^{\varphi(\tau_{\mathtt{j}})} \frac{(\varphi(\tau_{\mathtt{j}})-\mathtt{s})^{\delta-1}}{\Gamma(\delta)}\varpi(\mathtt{s})\mathtt{ds}\right] \\ &+ \int_0^{\mathtt{t}} \frac{(\mathtt{t}-\mathtt{s})^{\delta-1}}{\Gamma(\delta)}\varpi(\mathtt{s})\mathtt{ds}\end{aligned}\right\} \tag{8}$$

Since

$$\left|c_j \omega\Big(\varphi(\tau_j)\Big)\right| \le c_j \|\omega\|$$

and

$$\begin{aligned}\left|c_j \int_0^{\varphi(\tau_j)} \frac{(\varphi(\tau_j)-s)^{\delta-1}}{\Gamma(\delta)}\omega(s)ds\right| &\le \frac{c_j}{\Gamma(\delta)}\left|\int_0^{\varphi(\tau_j)} u(s)\omega(s)ds\right| \\ &\le \frac{c_j}{\Gamma(\delta)}\left|\int_0^{\tau_j} u(s)\omega(s)ds\right| \\ &\le \frac{c_j}{\Gamma(\delta)}\|u\|_{L_1}\|z\|_{L_1},\end{aligned}$$

where $u(s) = (\varphi(\tau_j) - s)^{\delta-1}$. Then, by comparison test, the series in (4) and

$$\sum_{j=1}^{\infty} c_j \int_0^{\varphi(\tau_j)} \frac{(\varphi(\tau_j)-s)^{\delta-1}}{\Gamma(\delta)}\omega(s)ds$$

are convergent. So, by taking the limit as $m \to \infty$ in (8), we obtain (5).

Conversely, it is clear that (3) satisfies (6). Next applying the operator $D_{0^+}^{\delta-1}$ and $D_{0^+}^{\delta}$ to the two sides of (5) respectively and using Remark 2.3 and Remark 2.4, we obtain

$$\lim_{t\to+\infty} D_{0^+}^{\delta-1} z(t) = \frac{1}{2}\int_0^{\infty} \omega(s)ds - \frac{1}{2}\sum_{j=1}^{\infty} c_j \int_0^{\varphi(\tau_j)} \frac{(\varphi(\tau_j)-s)^{\delta-1}}{\Gamma(\delta)}\omega(s)ds \tag{9}$$

and

$$D_{0^+}^{\delta} z(t) = \omega(s).$$

Also note that

$$\begin{aligned}\sum_{j=1}^{m} c_j z\Big(\varphi(\tau_j)\Big) = \sum_{j=1}^{m} c_j \int_0^{\varphi(\tau_j)} \frac{(\varphi(\tau_j)-s)^{\delta-1}}{\Gamma(\delta)}\omega(s)ds - \frac{1}{2\Gamma(\delta)}\sum_{j=1}^{m} c_j \varphi(\tau_j)^{\delta-1}\int_0^{\infty}\omega(s)ds \\ - \frac{1}{2\Gamma(\delta)}\sum_{i=1}^{m} c_i\varphi(\tau_i)^{\delta-1}\sum_{j=1}^{\infty} c_j \int_0^{\varphi(\tau_j)} \frac{(\varphi(\tau_j)-s)^{\delta-1}}{\Gamma(\delta)}\omega(s)ds.\end{aligned}$$

Since $\sum_{i=1}^{m} c_i\varphi(\tau_i)^{\delta-1}$ converges to $\Gamma(\delta)$, it follows by taking limit $t \to +\infty$ that

$$\sum_{j=1}^{\infty} c_j z\Big(\varphi(\tau_j)\Big) = -\frac{1}{2}\int_0^{\infty}\omega(s)ds + \frac{1}{2}\sum_{j=1}^{\infty} c_j \int_0^{\varphi(\tau_j)} \frac{(\varphi(\tau_j)-s)^{\delta-1}}{\Gamma(\delta)}\omega(s)ds. \tag{10}$$

By adding (9) and (10), we get (4). Which shows that the solution of the integral equation (5) satisfies the differential equation (2) under infinite-point boundary conditions (3) and (4). □

Remark 2.8. *The supposition* $\sum_{j=1}^{m} c_j\varphi(\tau_j)^{\delta-1}$ *converges to* $\Gamma(\delta)$ *in the Lemma 2.7 is valid. For example: Let* $\delta = \frac{9}{2}$, $c_j = \frac{99225}{16\pi^{11/2}j^4}$, $\tau_j = \frac{1}{j}$ *and* $\varphi(t) = t^{4/7}$. *Then*

$$\sum_{j=1}^{m} c_j\varphi(\tau_j)^{\delta-1} = \sum_{j=1}^{m} \frac{99225}{16\pi^{11/2}j^6} \to \frac{105}{16}\sqrt{\pi} = \Gamma(\delta) \text{ as } m \to +\infty.$$

For $\ell \in \mathbb{N}$, $\mathbb{C}^{\ell}(\mathbb{R}_+)$ denotes the space of all real functions which are ℓ-times continuously differentiable on $\mathbb{R}_+$ with the family of seminorms

$$|\mathtt{z}|^{\mathtt{T}} = \sup\{\mathtt{z}^{(i)}(\mathtt{t}) : 0 \le i \le \ell,\ \mathtt{t} \in [0,\mathtt{T}]\}$$

for all $\mathtt{T} \ge 1$. Then the space $\mathbb{C}^{\ell}(\mathbb{R}_+)$ is a Fréchet space with respect to the distance

$$d(u,v) = \sup\left\{\frac{1}{2^{\mathtt{T}}}\min\left\{1, |u-v|^{\mathtt{T}}_{\mathbb{C}^{\ell}}\right\} : \mathtt{T} \in \mathbb{N}\right\}.$$

For $\alpha \in (0,1]$, the space α-Hölder continuous functions $\mathcal{H}_{\alpha}(\mathbb{R}_+)$ is the family of all continuous functions $\mathtt{z} = \mathtt{z}(\mathtt{t})$ on $\mathbb{R}_+$ such that, for every $\mathtt{T} > 0$, there exists $N_{\mathtt{T}} > 0$,

$$\sup\left\{\frac{|\mathtt{z}(\mathtt{t}_1) - \mathtt{z}(\mathtt{t}_2)|}{|\mathtt{t}_1 - \mathtt{t}_2|^{\alpha}} : \mathtt{t}_1, \mathtt{t}_2 \in [0,\mathtt{T}], \mathtt{t}_1 \ne \mathtt{t}_2\right\} < N_{\mathtt{T}}.$$

The space $\mathcal{H}_{\alpha}(\mathbb{R}_+)$ is equipped with the family of seminorms

$$|\mathtt{z}|^{\mathtt{T}}_{\mathcal{H}_{\alpha}} = |\mathtt{z}(0)| + \sup\left\{\frac{|\mathtt{z}(\mathtt{t}_1) - \mathtt{z}(\mathtt{t}_2)|}{|\mathtt{t}_1 - \mathtt{t}_2|^{\alpha}} : \mathtt{t}_1, \mathtt{t}_2 \in [0,\mathtt{T}], \mathtt{t}_1 \ne \mathtt{t}_2\right\}.$$

Then, $\mathcal{H}_{\alpha}(\mathbb{R}_+)$ is a Fréchet space with respect to the distance

$$d(u,v) = \sup\left\{\frac{1}{2^{\mathtt{T}}}\min\left\{1, |u-v|^{\mathtt{T}}_{\mathcal{H}_{\alpha}}\right\} : \mathtt{T} \in \mathbb{N}\right\}.$$

For fixed $\alpha \in (0,1]$, the space $\mathbb{C}^{\ell,\alpha}(\mathbb{R}_+)$ denotes the space of all functions $\mathtt{z} \in \mathbb{C}^{\ell}(\mathbb{R}_+)$ whose ℓth-derivative is Hölder continuous with exponent α. Then $\mathbb{C}^{\ell,\alpha}(\mathbb{R}_+)$ equipped with the family of seminorms

$$|\mathtt{z}|^{\mathtt{T}}_{\alpha} = |\mathtt{z}|^{\mathtt{T}}_{\mathbb{C}^k} + |\mathtt{z}^{(\ell)}|^{\mathtt{T}}_{\mathcal{H}_{\alpha}}$$

for all $\mathtt{T} \in \mathbb{N}$. Then the space $\mathbb{C}^{\ell,\alpha}(\mathbb{R}_+)$ is a Fréchet space with respect to the distance

$$d(u,v) = \sup\left\{\frac{1}{2^{\mathtt{T}}}\min\left\{1, |u-v|^{\mathtt{T}}_{\alpha}\right\} : \mathtt{T} \in \mathbb{N}\right\}.$$

It can be seen that $\mathbb{C}^{\ell,\alpha}(\mathbb{R}_+)$ is a linear subspace of $\mathbb{C}^{\ell}(\mathbb{R}_+)$. Further, let $\mathfrak{M}_{\mathbb{C}^{\ell,\alpha}}$ be the family of all nonempty and bounded subsets of $\mathbb{C}^{\ell,\alpha}(\mathbb{R}_+)$, and let $\mathfrak{N}_{\mathbb{C}^{\ell,\alpha}}$ be the family of all nonempty and relatively compact subsets of $\mathbb{C}^{\ell,\alpha}(\mathbb{R}_+)$,

Definition 2.9. *[20] A family of mapping $\left\{\aleph^{\mathtt{T}}_{\alpha,\ell}\right\}_{\mathtt{T}\in\mathbb{N}}$, where $\alpha \in (0,1]$ and $\aleph^{\mathtt{T}}_{\alpha,\ell} : \mathfrak{M}_{\mathbb{C}^{\ell,\alpha}} \to \mathbb{R}_+$ is said to be a measure of noncompactness in $\mathbb{C}^{\ell,\alpha}(\mathbb{R}_+)$ if it satisfies the following conditions,*

($\mathtt{C}_1$) *The family Ker* $\left\{\aleph^{\mathtt{T}}_{\alpha,\ell}\right\} = \{\mathtt{S} \in \mathfrak{M}_{\mathbb{C}^{\ell,\alpha}} : \aleph^{\mathtt{T}}_{\alpha,\ell}(\mathtt{S}) = 0\ \forall\ \mathtt{T} \in \mathbb{N}\} \ne \emptyset$ *and Ker* $\left\{\aleph^{\mathtt{T}}_{\alpha,\ell}\right\} \subseteq \mathfrak{N}_{\mathbb{C}^{\ell,\alpha}}$.

($\mathtt{C}_2$) $\mathtt{S} \subseteq \mathcal{T} \implies \aleph^{\mathtt{T}}_{\alpha,\ell}(\mathtt{S}) \le \aleph^{\mathtt{T}}_{\alpha,\ell}(\mathcal{T})$ *for* $\mathtt{T} \in \mathbb{N}$.

($\mathtt{C}_3$) $\aleph^{\mathtt{T}}_{\alpha,\ell}(\overline{\mathtt{S}}) = \aleph^{\mathtt{T}}_{\alpha,\ell}(\mathtt{S})$ *for* $\mathtt{T} \in \mathbb{N}$.

($\mathtt{C}_4$) $\aleph^{\mathtt{T}}_{\alpha,\ell}(conv(\mathtt{S})) = \aleph^{\mathtt{T}}_{\alpha,\ell}(\mathtt{S})$ *for* $\mathtt{T} \in \mathbb{N}$.

($\mathtt{C}_5$) $\aleph^{\mathtt{T}}_{\alpha,\ell}(c\mathtt{S} + (1-c)\mathcal{T}) \le c\aleph^{\mathtt{T}}_{\alpha,\ell}(\mathtt{S}) + (1-c)\aleph^{\mathtt{T}}_{\alpha,\ell}(\mathcal{T})$ *for* $c \in [0,1]$ *and* $\mathtt{T} \in \mathbb{N}$.

($\mathtt{C}_6$) *If* $\{\mathtt{S}_n\}_{n=1}^{\infty}$ *be a nonincreasing sequence of closed chains from* $\mathfrak{M}_{\mathbb{C}^{\ell,\alpha}}$ *such that* $\lim_{n\to\infty} \aleph^{\mathtt{T}}_{\alpha,\ell}(\mathtt{S}_n) = 0$ *for each* $\mathtt{T} \in \mathbb{N}$, *then* $\mathtt{S}_{\infty} = \bigcap_{n=1}^{\infty} \mathtt{S}_n \ne \emptyset$.

Suppose $\mathtt{T} \in \mathbb{N}$, *and* $\mathtt{S}$ *is a bounded subset of the space* $\mathbb{C}^{\ell,\alpha}(\mathbb{R}_+)$. *For* $\mathtt{z} \in \mathtt{S}$ *and* $\varepsilon > 0$ *we denote*

$$\begin{aligned}
\mu^{\mathtt{T}}(\mathtt{z},\varepsilon) &= \sup\left\{|\mathtt{z}^{(l)}(\mathtt{t}_1) - \mathtt{z}^{(l)}(\mathtt{t}_2)| : \mathtt{t}_1,\mathtt{t}_2 \in [0,\mathtt{T}], |\mathtt{t}_1 - \mathtt{t}_2| \le \varepsilon, l = 1,2,\cdots,k\right\},\\
\mu^{\mathtt{T}}_{\alpha}(\mathtt{z},\varepsilon) &= \sup\left\{\frac{|\mathtt{z}^{(\ell)}(\mathtt{t}_1) - \mathtt{z}^{(\ell)}(\mathtt{t}_2)|}{|\mathtt{t}_1 - \mathtt{t}_2|^{\alpha}} : \mathtt{t}_1,\mathtt{t}_2 \in [0,\mathtt{T}], \mathtt{t}_1 \neq \mathtt{t}_2, |\mathtt{t}_1 - \mathtt{t}_2| \le \varepsilon\right\},\\
\mu^{\mathtt{T}}(\mathtt{S},\varepsilon) &= \sup_{\mathtt{z}\in\mathtt{S}} \mu^{\mathtt{T}}(\mathtt{z},\varepsilon),\\
\mu^{\mathtt{T}}_{\alpha}(\mathtt{S},\varepsilon) &= \sup_{\mathtt{z}\in\mathtt{S}} \mu^{\mathtt{T}}_{\alpha}(\mathtt{z},\varepsilon),\\
\aleph^{\mathtt{T}}_{\alpha,\ell}(\mathtt{S},\varepsilon) &= \mu^{\mathtt{T}}(\mathtt{S},\varepsilon) + \mu^{\mathtt{T}}_{\alpha}(\mathtt{S},\varepsilon).
\end{aligned}$$

Theorem 2.10. *(Darbo [20]) Let* $\mathtt{C}$ *be a nonempty, closed and convex subset of the Fréchet space* $\mathbb{C}^{\alpha,\ell}(\mathbb{R}_+)$ *and* $\mathcal{F} : \mathtt{C} \to \mathtt{C}$ *be a continuous operator such that, for each* $\mathtt{T} \in \mathbb{N}$, *there exists* $\mathcal{L}_{\mathtt{T}} \in [0,1)$ *so that*

$$\aleph^{\mathtt{T}}_{\alpha,\ell}(\mathcal{F}(\mathtt{S})) \le \mathcal{L}_{\mathtt{T}}\aleph^{\mathtt{T}}_{\alpha,\ell}(\mathtt{S})$$

for each $\mathtt{S} \in \mathtt{C}$. *Then* $\mathcal{F}$ *has at least one fixed point in the set* $\mathtt{C}$.

3. Main Results

In this section, we present an extension of Darbo's fixed point theorem 2.10 and consequence results.

Definition 3.1. *[18] Let* $\mathcal{R}$ *denotes the class of functions* $\pi : \mathbb{R}_+ \to [0,1)$ *such that*

$$\pi(\xi_n) \to 1 \implies \xi_n \to 0.$$

Theorem 3.2. *[1] Let* $\mathcal{E}$ *be a Hausdorff locally convex linear topological space,* $\mathtt{C}$ *be a nonempty convex subset of* $\mathcal{E}$ *and* $\mathcal{F} : \mathtt{C} \to \mathcal{E}$ *be a continuous mapping such that*

$$\mathcal{F}(\mathtt{C}) \subset \mathcal{A} \subset \mathtt{C},$$

with $\mathcal{A}$ *compact. Then* $\mathcal{F}$ *has at least one fixed point.*

Theorem 3.3. *Let* $\mathtt{C}$ *be a nonempty, bounded, closed and convex subset of the Fréchet space* $\mathtt{C}^{\alpha,\ell}(\mathbb{R}_+)$ *and* $\mathcal{F} : \mathtt{C} \to \mathtt{C}$ *be a continuous operator such that, for each* $\mathtt{T} \in \mathbb{N}$,

$$\aleph^{\mathtt{T}}_{\alpha,\ell}(\mathcal{F}(\mathtt{S})) \le \pi\left(\aleph^{\mathtt{T}}_{\alpha,\ell}(\mathtt{S})\right)\aleph^{\mathtt{T}}_{\alpha,\ell}(\mathtt{S}) \tag{11}$$

for any subset $\mathtt{S} \in \mathtt{C}$ *and* $\pi \in \mathcal{R}$. *Then* $\mathcal{F}$ *has at least one fixed point in* $\mathtt{C}$.

Proof. By induction, we define a sequence $\{\mathtt{C}_{\mathtt{p}}\}$ by taking $\mathtt{C}_0 = \mathtt{C}$ and $\mathtt{C}_{\mathtt{p}} = conv(\mathcal{F}\mathtt{C}_{\mathtt{p}-1})$, $p \ge 1$. We have $\mathtt{C}_1 = conv(\mathcal{F}\mathtt{C}_0) \subseteq \mathtt{C}_0$, so continuing this process we get

$$\mathtt{C}_0 \supseteq \mathtt{C}_1 \supseteq \mathtt{C}_2 \supseteq \cdots.$$

If $\aleph^{\mathtt{T}}_{\alpha,\ell}(\mathtt{C}_N) = 0$ for some positive integer N and for all $\mathtt{T}$, then $\mathtt{C}_N$ is relatively compact. Thus, Theorem 3.2 gives that $\mathcal{F}$ has a fixed point. Otherwise, let $\mathtt{T} \ge 0$ be a number such that $\aleph^{\mathtt{T}}_{\alpha,\ell}(\mathtt{C}_{\mathtt{p}}) \neq 0$ for any $\mathtt{p} \ge 0$. From (11), we have

$$\begin{aligned}
\aleph^{\mathtt{T}}_{\alpha,\ell}(\mathtt{C}_{\mathtt{p}+1}) &= \aleph^{\mathtt{T}}_{\alpha,\ell}(conv(\mathcal{F}\mathtt{C}_{\mathtt{p}}))\\
&= \aleph^{\mathtt{T}}_{\alpha,\ell}(\mathcal{F}\mathtt{C}_{\mathtt{p}}) \le \pi\left(\aleph^{\mathtt{T}}_{\alpha,\ell}(\mathtt{C}_{\mathtt{p}})\right)\aleph^{\mathtt{T}}_{\alpha,\ell}(\mathtt{C}_{\mathtt{p}}) \le \aleph^{\mathtt{T}}_{\alpha,\ell}(\mathtt{C}_{\mathtt{p}}),
\end{aligned} \tag{12}$$

which implies that $\aleph^{\mathtt{T}}_{\alpha,\ell}(\mathtt{C_p})$ is a positive decreasing sequence of real numbers, so, there exists a $\zeta \geq 0$ such that $\aleph^{\mathtt{T}}_{\alpha,\ell}(\mathtt{C_p}) \to \zeta$ as $\mathtt{p} \to \infty$. Now we show that $\zeta = 0$. Suppose by contrary $\zeta \neq 0$. Then, from (12), we have

$$\frac{\aleph^{\mathtt{T}}_{\alpha,\ell}(\mathtt{C_{p+1}})}{\aleph^{\mathtt{T}}_{\alpha,\ell}(\mathtt{C_p})} \leq \pi\Big(\aleph^{\mathtt{T}}_{\alpha,\ell}(\mathtt{C_p})\Big) < 1 \implies \pi\Big(\aleph^{\mathtt{T}}_{\alpha,\ell}(\mathtt{C_p})\Big) \to 1 \text{ as } n \to \infty.$$

Since $\pi \in \mathcal{R}$, we obtain $\zeta = 0$ and hence $\aleph^{\mathtt{T}}_{\alpha,\ell}(\mathtt{C_p}) \to 0$ as $\mathtt{p} \to \infty$. In view of $(\mathtt{C}_6)$, $\mathtt{C}_\infty = \bigcap_{\mathtt{p}=1}^{\infty} \mathtt{C_p}$ is nonempty, closed, convex and $\mathtt{C}_\infty \subset \mathtt{C}$. Also, the set $\mathtt{C}_\infty$ is invariant under the operator $\mathcal{F}$ and $\mathtt{C}_\infty \in Ker\left\{\aleph^{\mathtt{T}}_{\alpha,\ell}\right\}$. Therefore, by Theorem 3.2 the operator $\mathcal{F}$ has a fixed point. □

Corollary 3.4. *Let* $\mathtt{C}$ *be a nonempty, bounded, closed and convex subset of the Fréchet space* $\mathtt{C}^{\alpha,\ell}(\mathbb{R}_+)$ *and* $\mathcal{F} : \mathtt{C} \to \mathtt{C}$ *be a continuous operator such that, for each* $\mathtt{T} \in \mathbb{N}$,

$$\aleph^{\mathtt{T}}_{\alpha,\ell}(\mathcal{F}(\mathtt{S})) \leq \phi\left(\aleph^{\mathtt{T}}_{\alpha,\ell}(\mathtt{S})\right)$$

for any subset $\mathtt{S} \in \mathtt{C}$ *and* $\phi : \mathbb{R}_+ \to \mathbb{R}_+$ *is a nondecreasing and upper semicontinuous function such that* $\phi(\mathtt{t}) < \mathtt{t}$ *for all* $\mathtt{t} > 0$. *Then* $\mathcal{F}$ *has at least one fixed point.*

Proof. The proof is similar to the proof of Corollary 2.2. in [2]. □

Corollary 3.5 (Darbo [20]). *Let* $\mathtt{C}$ *be a nonempty, bounded, closed and convex subset of the Fréchet space* $\mathtt{C}^{\alpha,\ell}(\mathbb{R}_+)$ *and* $\mathcal{F} : \mathtt{C} \to \mathtt{C}$ *be a continuous operator such that, for each* $\mathtt{T} \in \mathbb{N}$, *there exists* $\mathfrak{L}_{\mathtt{T}} \in [0, 1)$,

$$\aleph^{\mathtt{T}}_{\alpha,\ell}(\mathcal{F}(\mathtt{S})) \leq \mathfrak{L}_{\mathtt{T}} \aleph^{\mathtt{T}}_{\alpha,\ell}(\mathtt{S})$$

for any subset $\mathtt{S} \in \mathtt{C}$. *Then* $\mathcal{F}$ *has at least one fixed point in* $\mathtt{C}$.

Proof. Put $\pi(\mathtt{t}) = \mathfrak{L}_{\mathtt{T}}$ in Theorem 3.3, we get desired result. □

Theorem 3.6. *Suppose* $\left\{\aleph^{\mathtt{T}}_{\alpha,\ell,1}\right\}_{\mathtt{T}\in\mathbb{N}}, \left\{\aleph^{\mathtt{T}}_{\alpha,\ell,2}\right\}_{\mathtt{T}\in\mathbb{N}}, \cdots, \left\{\aleph^{\mathtt{T}}_{\alpha,\ell,n}\right\}_{\mathtt{T}\in\mathbb{N}}$, *are n families of measures of noncompactness in Fréchet spaces* $\mathbb{C}^{\ell,\alpha}_1(\mathbb{R}_+), \mathbb{C}^{\ell,\alpha}_2(\mathbb{R}_+), \cdots, \mathbb{C}^{\ell,\alpha}_n(\mathbb{R}_+)$ *respectively. Moreover, assume that the function* $\mathcal{F} : [0,\infty)^n \to [0,\infty)$ *is convex and* $\mathcal{F}(\omega_1, \omega_2, \cdots, \omega_n) = 0$ *if and only if* $\omega_i = 0$ *for* $i = 1, 2, \cdots, n$. *Then*

$$\aleph^{\mathtt{T}}_{\alpha,\ell}(E) = \mathcal{F}\Big(\aleph^{\mathtt{T}}_{\alpha,\ell,1}(E_1), \aleph^{\mathtt{T}}_{\alpha,\ell,2}(E_2), \cdots, \aleph^{\mathtt{T}}_{\alpha,\ell,n}(E_n)\Big)$$

defines a measure of noncompactness in $\mathbb{C}^{\ell,\alpha}_1(\mathbb{R}_+) \times \mathbb{C}^{\ell,\alpha}_2(\mathbb{R}_+) \times \cdots \times \mathbb{C}^{\ell,\alpha}_n(\mathbb{R}_+)$ *where* E_i *denotes the natural projection of* E *into* $\mathbb{C}^{\ell,\alpha}_i(\mathbb{R}_+)$ *for* $i = 1, 2, \cdots, n$.

Proof. The proof is similar to the proof of Theorem 3.3.1. in [7]. □

Definition 3.7. *[13] An element* $(\mathtt{z}_1, \mathtt{z}_2) \in E \times E$ *is called a coupled fixed point of a mapping* $\mathcal{F} : E \times E \to E$ *if*

$$\mathcal{F}(\mathtt{z}_1, \mathtt{z}_2) = \mathtt{z}_1, \ \mathcal{F}(\mathtt{z}_2, \mathtt{z}_1) = \mathtt{z}_2.$$

Theorem 3.8. *Let* Λ *be a nonempty, bounded, closed and convex subset of a Fréchet space* $\mathbb{C}^{\ell,\alpha}(\mathbb{R}_+)$ *and* $\psi : \mathbb{R}_+ \to \mathbb{R}_+$ *be a nondecreasing and upper semicontinuous function such that* $\psi(\mathtt{t}) < \mathtt{t}$ *for all* $\mathtt{t} > 0$. *Suppose that* $\mathcal{F} : \Lambda \times \Lambda \to \Lambda$ *is a continuous operator satisfying*

$$\aleph^{\mathtt{T}}_{\alpha,\ell}\left(\mathcal{F}(E_1 \times E_2)\right) \leq \psi\left[\frac{1}{2}\left(\aleph^{\mathtt{T}}_{\alpha,\ell}(E_1) + \aleph^{\mathtt{T}}_{\alpha,\ell}(E_2)\right)\right] \tag{13}$$

for all $E_1, E_2 \subset \Lambda$. *Then* $\mathcal{F}\mathcal{G}$ *has at least a coupled fixed point.*

Proof. From Theorem 3.6, it can be seen that $\widetilde{\aleph}^{\mathrm{T}}_{\alpha,\ell}(E) = \aleph^{\mathrm{T}}_{\alpha,\ell}(E_1) + \aleph^{\mathrm{T}}_{\alpha,\ell}(E_2)$ is a measure of noncompactness in the space $\mathbb{C}^{\ell,\alpha}(\mathbb{R}_+) \times \mathbb{C}^{\ell,\alpha}(\mathbb{R}_+)$, where E_1, E_2 denote the natural projections of E. Next, consider the map $\widetilde{\mathcal{F}} : \Lambda \times \Lambda \to \Lambda \times \Lambda$ defined by

$$\widetilde{\mathcal{F}}(\omega_1, \omega_2) = (\mathcal{F}(\omega_1, \omega_2), \mathcal{F}(\omega_2, \omega_1)).$$

Since $\mathcal{F}$ is continuous on $\Lambda \times \Lambda$, $\mathcal{F}$ is continuous on $\Lambda \times \Lambda$. Let $E \subset \Lambda \times \Lambda$ be a nonempty subset. Then, from C_2 and (13), we get

$$\begin{aligned}
\widetilde{\aleph}^{\mathrm{T}}_{\alpha,\ell}(\widetilde{\mathcal{F}}(E)) &\le \widetilde{\aleph}^{\mathrm{T}}_{\alpha,\ell}(\mathcal{F}(E_1 \times E_2) \times \mathcal{F}(E_2 \times E_1)) \\
&\le \widetilde{\aleph}^{\mathrm{T}}_{\alpha,\ell}(\mathcal{F}(E_1 \times E_2)) + \widetilde{\aleph}^{\mathrm{T}}_{\alpha,\ell}(\mathcal{F}(E_2 \times E_1)) \\
&\le \psi\left[\frac{1}{2}\left(\aleph^{\mathrm{T}}_{\alpha,\ell}(E_1) + \aleph^{\mathrm{T}}_{\alpha,\ell}(E_2)\right)\right] + \psi\left[\frac{1}{2}\left(\aleph^{\mathrm{T}}_{\alpha,\ell}(E_2) + \aleph^{\mathrm{T}}_{\alpha,\ell}(E_1)\right)\right] \\
&\le 2\psi\left[\frac{1}{2}\left(\aleph^{\mathrm{T}}_{\alpha,\ell}(E_1) + \aleph^{\mathrm{T}}_{\alpha,\ell}(E_2)\right)\right].
\end{aligned}$$

Taking $\vartheta^{\mathrm{T}}_{\alpha,\ell} = \frac{1}{2}\widetilde{\aleph}^{\mathrm{T}}_{\alpha,\ell}$, we obtain

$$\vartheta^{\mathrm{T}}_{\alpha,\ell}(\widetilde{\mathcal{F}}(E)) \le \psi(\vartheta^{\mathrm{T}}_{\alpha,\ell}(E)).$$

Since $\widetilde{\aleph}^{\mathrm{T}}_{\alpha,\ell}$ is a measure of noncompactness, $\vartheta^{\mathrm{T}}_{\alpha,\ell}$ is too. Therefore, all the conditions of Corollary 3.4 are satisfied and hence, $\mathcal{F}$ has a coupled fixed point. □

Definition 3.9. *[9] Denote $E^3 := E \times E \times E$. Then an element $(\mathtt{z}_1, \mathtt{z}_2, \mathtt{z}_3) \in E^3$ is called a tripled fixed point of a mapping $\mathcal{F} : E^3 \to E$ if*

$$\mathcal{F}(\mathtt{z}_1, \mathtt{z}_2, \mathtt{z}_3) = \mathtt{z}_1,\ \mathcal{F}(\mathtt{z}_2, \mathtt{z}_1, \mathtt{z}_3) = \mathtt{z}_2,\ \mathcal{F}(\mathtt{z}_3, \mathtt{z}_2, \mathtt{z}_1) = \mathtt{z}_3.$$

Theorem 3.10. *Let Λ be a nonempty, bounded, closed and convex subset of a Fréchet space $\mathbb{C}^{\ell,\alpha}(\mathbb{R}_+)$ and $\psi : \mathbb{R}_+ \to \mathbb{R}_+$ be a nondecreasing and upper semicontinuous function such that $\psi(\mathtt{t}) < \mathtt{t}$ for all $\mathtt{t} > 0$. Suppose that $\mathcal{F} : \Lambda \times \Lambda \times \Lambda \to \Lambda$ is a continuous operator satisfying*

$$\aleph^{\mathrm{T}}_{\alpha,\ell}(\mathcal{F}(E_1 \times E_2 \times E_3)) \le \psi\left[\frac{1}{3}\left(\aleph^{\mathrm{T}}_{\alpha,\ell}(E_1) + \aleph^{\mathrm{T}}_{\alpha,\ell}(E_2) + \aleph^{\mathrm{T}}_{\alpha,\ell}(E_3)\right)\right] \tag{14}$$

for all $E_1, E_2, E_3 \subset \Lambda$. Then $\mathcal{F}\mathcal{G}$ has a tripled fixed point.

Proof. From Theorem 3.6, it can be seen that $\widetilde{\aleph}^{\mathrm{T}}_{\alpha,\ell}(E) = \aleph^{\mathrm{T}}_{\alpha,\ell}(E_1) + \aleph^{\mathrm{T}}_{\alpha,\ell}(E_2) + \aleph^{\mathrm{T}}_{\alpha,\ell}(E_3)$ is a measure of noncompactness in the space $\mathbb{C}^{\ell,\alpha}(\mathbb{R}_+) \times \mathbb{C}^{\ell,\alpha}(\mathbb{R}_+) \times \mathbb{C}^{\ell,\alpha}(\mathbb{R}_+)$, where E_1, E_2, E_3 denote the natural projections of E. Next, consider the map $\widetilde{\mathcal{F}} : \Lambda \times \Lambda \times \Lambda \to \Lambda \times \Lambda \times \Lambda$ defined by

$$\widetilde{\mathcal{F}}(\omega_1, \omega_2, \omega_3) = (\mathcal{F}(\omega_1, \omega_2, \omega_3), \mathcal{F}(\omega_2, \omega_1, \omega_3), \mathcal{F}(\omega_3, \omega_2, \omega_1)).$$

Since $\mathcal{F}$ is continuous on $\Lambda \times \Lambda \times \Lambda$, $\mathcal{F}$ is continuous on $\Lambda \times \Lambda \times \Lambda$. Let $E \subset \Lambda \times \Lambda \times \Lambda$ be a nonempty subset. Then, from C_2 and (14), we get

$$\begin{aligned}
\widetilde{\aleph}^{\mathrm{T}}_{\alpha,\ell}(\widetilde{\mathcal{F}}(E)) &\le \widetilde{\aleph}^{\mathrm{T}}_{\alpha,\ell}(\mathcal{F}(E_1 \times E_2 \times E_3) \times \mathcal{F}(E_2 \times E_1 \times E_3) \times \mathcal{F}(E_3 \times E_2 \times E_1)) \\
&\le \widetilde{\aleph}^{\mathrm{T}}_{\alpha,\ell}(\mathcal{F}(E_1 \times E_2 \times E_3)) + \widetilde{\aleph}^{\mathrm{T}}_{\alpha,\ell}(\mathcal{F}(E_2 \times E_1 \times E_3)) + \widetilde{\aleph}^{\mathrm{T}}_{\alpha,\ell}(\mathcal{F}(E_3 \times E_2 \times E_1)) \\
&\le \psi\left[\frac{1}{3}\left(\aleph^{\mathrm{T}}_{\alpha,\ell}(E_1) + \aleph^{\mathrm{T}}_{\alpha,\ell}(E_2) + \aleph^{\mathrm{T}}_{\alpha,\ell}(E_3)\right)\right] + \psi\left[\frac{1}{3}\left(\aleph^{\mathrm{T}}_{\alpha,\ell}(E_2) + \aleph^{\mathrm{T}}_{\alpha,\ell}(E_1) + \aleph^{\mathrm{T}}_{\alpha,\ell}(E_3)\right)\right] \\
&\qquad + \psi\left[\frac{1}{3}\left(\aleph^{\mathrm{T}}_{\alpha,\ell}(E_3) + \aleph^{\mathrm{T}}_{\alpha,\ell}(E_2) + \aleph^{\mathrm{T}}_{\alpha,\ell}(E_1)\right)\right] \\
&\le 3\psi\left[\frac{1}{3}\left(\aleph^{\mathrm{T}}_{\alpha,\ell}(E_1) + \aleph^{\mathrm{T}}_{\alpha,\ell}(E_2) + \aleph^{\mathrm{T}}_{\alpha,\ell}(E_3)\right)\right].
\end{aligned}$$

Taking $\vartheta^{\mathtt{T}}_{\alpha,\ell} = \frac{1}{3}\widetilde{\aleph}^{\mathtt{T}}_{\alpha,\ell}$, we obtain

$$\vartheta^{\mathtt{T}}_{\alpha,\ell}(\widetilde{\mathcal{F}}(E)) \leq \psi(\vartheta^{\mathtt{T}}_{\alpha,\ell}(E)).$$

Since $\widetilde{\aleph}^{\mathtt{T}}_{\alpha,\ell}$ is a measure of noncompactness, $\vartheta^{\mathtt{T}}_{\alpha,\ell}$ is too. Therefore, all the conditions of Corollary 3.4 are satisfied and hence, $\mathcal{F}$ has a tripled fixed point. □

Definition 3.11. *[32] Denote $E^n := \prod_{\mathtt{j}=1}^{n} E_{\mathtt{j}}$. Then an element $(\mathtt{z}_1, \mathtt{z}_2, \cdots, \mathtt{z}_{n-1}, \mathtt{z}_n) \in E^n$ is called an n-fixed point of a mapping $\mathcal{F} : E^n \to E$ if*

$$\begin{aligned}
\mathcal{F}(\mathtt{z}_1, \mathtt{z}_2, \mathtt{z}_3, \cdots, \mathtt{z}_{n-1}, \mathtt{z}_n) &= \mathtt{z}_1,\\
\mathcal{F}(\mathtt{z}_2, \mathtt{z}_1, \mathtt{z}_3, \cdots, \mathtt{z}_{n-1}, \mathtt{z}_n) &= \mathtt{z}_2,\\
\mathcal{F}(\mathtt{z}_3, \mathtt{z}_2, \mathtt{z}_1, \cdots, \mathtt{z}_{n-1}, \mathtt{z}_n) &= \mathtt{z}_3,\\
&\vdots\\
\mathcal{F}(\mathtt{z}_{n-1}, \mathtt{z}_2, \mathtt{z}_3, \cdots, \mathtt{z}_1, \mathtt{z}_n) &= \mathtt{z}_{n-1}\\
\mathcal{F}(\mathtt{z}_n, \mathtt{z}_2, \mathtt{z}_3, \cdots, \mathtt{z}_{n-1}, \mathtt{z}_1) &= \mathtt{z}_n
\end{aligned}$$

Theorem 3.12. *Let Λ be a nonempty, bounded, closed and convex subset of a Fréchet space $\mathbb{C}^{\ell,\alpha}(\mathbb{R}_+)$ and $\psi : \mathbb{R}_+ \to \mathbb{R}_+$ be a nondecreasing and upper semicontinuous function such that $\psi(\mathtt{t}) < \mathtt{t}$ for all $\mathtt{t} > 0$. Suppose that $\mathcal{F} : \Lambda^n \to \Lambda$ is a continuous operator satisfying*

$$\aleph^{\mathtt{T}}_{\alpha,\ell}(\mathcal{F}(E^n)) \leq \psi\left[\frac{1}{n}\sum_{\mathtt{j}=1}^{n} \aleph^{\mathtt{T}}_{\alpha,\ell}(E_{\mathtt{j}})\right] \tag{15}$$

for all $E_{\mathtt{j}} \subset \Lambda$, $\mathtt{j} = 1, 2, \cdots, n$. Then $\mathcal{F}\mathcal{G}$ has an n-fixed point.

Proof. From Theorem 3.6, it can be seen that $\widetilde{\aleph}^{\mathtt{T}}_{\alpha,\ell}(E) = \sum_{\mathtt{j}=1}^{n} \aleph^{\mathtt{T}}_{\alpha,\ell}(E_{\mathtt{j}})$ is a measure of noncompactness in the space $\mathbb{C}^{\ell,\alpha}(\mathbb{R}_+)^n$, where $E_{\mathtt{j}}$ $(\mathtt{j} = 1, 2, \cdots, n)$ denote the natural projections of E. Next, consider the map $\widetilde{\mathcal{F}} : \Lambda^n \to \Lambda^n$ defined by

$$\widetilde{\mathcal{F}}(\omega_1, \omega_2, \cdots, \omega_{n-1}, \omega_n) = \begin{bmatrix}
\mathcal{F}(\omega_1, \omega_2, \omega_3, \cdots, \omega_{n-1}, \omega_n)\\
\mathcal{F}(\omega_2, \omega_1, \omega_3, \cdots, \omega_{n-1}, \omega_n)\\
\mathcal{F}(\omega_3, \omega_2, \omega_1, \cdots, \omega_{n-1}, \omega_n)\\
\vdots\\
\mathcal{F}(\omega_{n-1}, \omega_2, \omega_3, \cdots, \omega_1, \omega_n)\\
\mathcal{F}(\omega_n, \omega_2, \omega_1, \cdots, \omega_{n-1}, \omega_1)
\end{bmatrix}$$

Since $\mathcal{F}$ is continuous on Λ^n, $\mathcal{F}$ is continuous on Λ^n. Let $E \subset \Lambda^n$ be a nonempty subset. Then, from $\mathtt{C}_2$, (15) and proceeding similar to the Theorem 3.10, we arrive

$$\widetilde{\aleph}^{\mathtt{T}}_{\alpha,\ell}(\widetilde{\mathcal{F}}(E)) \leq n\psi\left[\frac{1}{n}\sum_{\mathtt{j}=1}^{n} \aleph^{\mathtt{T}}_{\alpha,\ell}(E_{\mathtt{j}})\right].$$

Taking $\vartheta^{\mathtt{T}}_{\alpha,\ell} = \frac{1}{n}\widetilde{\aleph}^{\mathtt{T}}_{\alpha,\ell}$, we obtain

$$\vartheta^{\mathtt{T}}_{\alpha,\ell}(\widetilde{\mathcal{F}}(E)) \leq \psi(\vartheta^{\mathtt{T}}_{\alpha,\ell}(E)).$$

Since $\widetilde{\aleph}^{\mathtt{T}}_{\alpha,\ell}$ is a measure of noncompactness, $\vartheta^{\mathtt{T}}_{\alpha,\ell}$ is too. Therefore, all the conditions of Corollary 3.4 are satisfied and hence, $\mathcal{F}$ has an n-fixed point. □

4. Existence of Solutions for Fractional Order Boundary Value Problem

In this section we present an existence result for the nonlinear fractional order infinite point boundary value problem (1) in the Fréchet space $\mathbb{C}^{\ell,\alpha}(\mathbb{R}_+)$ where $\alpha \in (0,1]$ and $\delta - \ell - \alpha > 0$. We also provide en example to check feasibility of our results.

We assume the following conditions are true in the sequel:

(H_1) $g : \mathbb{R}_+ \times \mathbb{R}_+ \to \mathbb{R}$ is a continuous function and there exist increasing functions $a, b : \mathbb{R}_+ \to \mathbb{R}_+$ satisfying $\lim_{t\to 0} a(t) = \lim_{t\to 0} b(t) = 0, a \in L^1(\mathbb{R}_+)$ and there exits $\lambda > 0$ such that

$$(i)\ |g(s,z_1) - g(s,z_2)| \le a(|z_1 - z_2|),$$
$$(ii)\ \int_0^\infty |g(s,z_1) - g(s,z_2)|ds \le \lambda b(|z_1 - z_2|)$$

for all $s \in \mathbb{R}_+$ and $z_1, z_2 \in \mathbb{R}$. Also assume that

$$g^S = \sup\{|g(s,0)| : s \in \mathbb{R}_+\} < \infty, \quad g^I = \int_0^\infty |g(s,0)|ds < \infty.$$

(H_2) for each $T \in \mathbb{N}$, the exits a positive number R_T such that

$$\Big[a(R_T) + g^S\Big]\Big[M_T + N_T \sum_{j=1}^{\infty} c_j \varphi(\tau_j)^\delta + \frac{2T^{\delta-\ell-\alpha}}{\Gamma(\delta-\ell+1)}\Big] + \Big[\lambda b(R_T) + g^I\Big]N_T \le R_T,$$

where

$$M_T = \sup_{0\le p\le \ell}\left\{\frac{T^{\delta-p}}{\Gamma(\delta-p+1)}\right\}, N_T = \sup_{0\le p\le \ell}\left\{\frac{T^{\delta-p-1}}{2\Gamma(\delta-p)}\right\}.$$

Theorem 4.1. *Assume that the conditions* (H_1)-(H_2) *are satisfied. The the fractional order infinite point boundary value problem* (1) *has at least one solution in the Fréchet space* $\mathbb{C}^{\ell,\alpha}(\mathbb{R}_+)$.

Proof. Define the operator $\mathcal{F} : \mathbb{C}^{\ell,\alpha}(\mathbb{R}_+) \to \mathbb{C}^{\ell,\alpha}(\mathbb{R}_+)$ by

$$\mathcal{F}(z)(t) = \int_0^t \frac{(t-s)^{\delta-1}}{\Gamma(\delta)}\omega(s)ds - \frac{t^{\delta-1}}{2\Gamma(\delta)}\int_0^\infty \omega(s)ds - \frac{t^{\delta-1}}{2\Gamma(\delta)}\sum_{j=1}^{\infty} c_j \int_0^{\varphi(\tau_j)} \frac{(\varphi(\tau_j)-s)^{\delta-1}}{\Gamma(\delta)}\omega(s)ds.$$

Then Lemma 2.7 shows that the fixed points of the operator $\mathcal{F}$ coincides with the solutions of the problem

(1). Let $z \in \mathbb{C}^{\ell,\alpha}(\mathbb{R}_+)$, then by (H_1)–(H_2), we have

$$\begin{aligned}
|\mathcal{F}(z)(t)| =& \Big| \int_0^t \frac{(t-s)^{\delta-1}}{\Gamma(\delta)} g(s,z(s))ds - \frac{t^{\delta-1}}{2\Gamma(\delta)} \int_0^\infty g(s,z(s))ds \\
&- \frac{t^{\delta-1}}{2\Gamma(\delta)} \sum_{j=1}^{\infty} c_j \int_0^{\varphi(\tau_j)} \frac{(\varphi(\tau_j)-s)^{\delta-1}}{\Gamma(\delta)} g(s,z(s))ds \Big| \\
\leq& \int_0^t \frac{(t-s)^{\delta-1}}{\Gamma(\delta)} \Big[|g(s,z(s)) - g(s,0)| + |g(s,0)| \Big] ds \\
&+ \frac{t^{\delta-1}}{2\Gamma(\delta)} \int_0^\infty \Big[|g(s,z(s)) - g(s,0)| + |g(s,0)| \Big] ds \\
&+ \frac{t^{\delta-1}}{2\Gamma(\delta)} \sum_{j=1}^{\infty} c_j \int_0^{\varphi(\tau_j)} \frac{(\varphi(\tau_j)-s)^{\delta-1}}{\Gamma(\delta)} \Big[|g(s,z(s)) - g(s,0)| + |g(s,0)| \Big] ds \\
\leq& \Big[a(|z|_\alpha^T) + g^S \Big] \left[\int_0^t \frac{(t-s)^{\delta-1}}{\Gamma(\delta)} ds + \frac{t^{\delta-1}}{2\Gamma(\delta)} \sum_{j=1}^{\infty} c_j \int_0^{\varphi(\tau_j)} \frac{(\varphi(\tau_j)-s)^{\delta-1}}{\Gamma(\delta)} ds \right] \\
&+ \Big[\lambda b(|z|_\alpha^T) + g^I \Big] \frac{t^{\delta-1}}{2\Gamma(\delta)}.
\end{aligned}$$

Thus,

$$|\mathcal{F}(z)(t)| \leq \Big[\frac{a(|z|_\alpha^T) + g^S}{\Gamma(\delta+1)} \Big] \Big[T^\delta + \frac{T^{\delta-1}}{2\Gamma(\delta)} \sum_{j=1}^{\infty} c_j \varphi(\tau_j)^\delta \Big] + \Big[\lambda b(|z|_\alpha^T) + g^I \Big] \frac{T^{\delta-1}}{2\Gamma(\delta)}. \tag{16}$$

The similar argument gives that

$$|\mathcal{F}'(z)(t)| \leq \Big[a(|z|_\alpha^T) + g^S \Big] \Big[\frac{T^{\delta-1}}{\Gamma(\delta)} + \frac{T^{\delta-2}}{2\Gamma(\delta-1)} \sum_{j=1}^{\infty} c_j \varphi(\tau_j)^\delta \Big] + \Big[\lambda b(|z|_\alpha^T) + g^I \Big] \frac{T^{\delta-2}}{2\Gamma(\delta-1)}. \tag{17}$$

and

$$\begin{aligned}
|\mathcal{F}^{(p)}(z)(t)| =& \Big| \int_0^t \frac{(t-s)^{\delta-p-1}}{\Gamma(\delta-p)} g(s,z(s))ds - \frac{t^{\delta-p-1}}{2\Gamma(\delta-p)} \int_0^\infty g(s,z(s))ds \\
&- \frac{t^{\delta-p-1}}{2\Gamma(\delta-p)} \sum_{j=1}^{\infty} c_j \int_0^{\varphi(\tau_j)} \frac{(\varphi(\tau_j)-s)^{\delta-1}}{\Gamma(\delta)} g(s,z(s))ds \Big| \\
\leq& \Big[a(|z|_\alpha^T) + g^S \Big] \Big[\frac{T^{\delta-p}}{\Gamma(\delta-p+1)} + \frac{T^{\delta-p-1}}{2\Gamma(\delta-p)} \sum_{j=1}^{\infty} c_j \varphi(\tau_j)^\delta \Big] + \Big[\lambda b(|z|_\alpha^T) + g^I \Big] \frac{T^{\delta-p-1}}{2\Gamma(\delta-p)},
\end{aligned} \tag{18}$$

for any $t \in \mathbb{R}_+$ and $p = 2, 3, \cdots, \ell - 1$. From (16)-(18), we get

$$\left.\begin{aligned}
|\mathcal{F}^{(p)}(z)(t)| \leq& \Big[a(|z|_\alpha^T) + g^S \Big] \Big[\sup_{0\leq p\leq \ell} \left\{ \frac{T^{\delta-p}}{\Gamma(\delta-p+1)} \right\} + \sup_{0\leq p\leq \ell} \left\{ \frac{T^{\delta-p-1}}{2\Gamma(\delta-p)} \right\} \sum_{j=1}^{\infty} c_j \varphi(\tau_j)^\delta \Big] \\
&+ \Big[\lambda b(|z|_\alpha^T) + g^I \Big] \sup_{0\leq p\leq \ell} \left\{ \frac{T^{\delta-p-1}}{2\Gamma(\delta-p)} \right\}.
\end{aligned}\right\} \tag{19}$$

Further, let $t_1, t_2 \in [0, T]$ with $t_2 > t_1$. Similar to the above process, we arrive

$$\begin{aligned}\frac{|\mathcal{F}^{(\ell)}(z)(t_2) - \mathcal{F}^{(\ell)}(z)(t_1)|}{|t_2 - t_1|^{\alpha}} &\leq \frac{1}{|t_2 - t_1|^{\alpha}}\Big|\int_0^{t_2} \frac{(t_2 - s)^{\delta-\ell-1}}{\Gamma(\delta-\ell)} g(s, z(s))ds \\ &\quad - \int_0^{t_1} \frac{(t_1 - s)^{\delta-\ell-1}}{\Gamma(\delta-\ell)} g(s, z(s))ds - \frac{[t_2^{\delta-\ell-1} - t_1^{\delta-\ell-1}]}{2\Gamma(\delta-\ell)} \int_0^{\infty} g(s, z(s))ds \\ &\quad - \frac{[t_2^{\delta-\ell-1} - t_1^{\delta-\ell-1}]}{2\Gamma(\delta-\ell)} \sum_{j=1}^{\infty} c_j \int_0^{\varphi(\tau_j)} \frac{(\varphi(\tau_j) - s)^{\delta-1}}{\Gamma(\delta)} g(s, z(s))ds\Big| \\ &\leq \frac{1}{|t_2 - t_1|^{\alpha}}\left[\frac{a(|z|_{\alpha}^{T}) + g^{S}}{\Gamma(\delta-\ell)}\right]\left[\frac{2(t_2 - t_1)^{\delta-\ell}}{\delta-\ell} + \Big(\frac{t_1^{\delta-\ell}}{\delta-\ell} - \frac{t_2^{\delta-\ell}}{\delta-\ell}\Big)\right. \\ &\quad \left. + \frac{1}{2}\Big(\frac{t_1^{\delta-\ell-1}}{\Gamma(\delta-\ell)} - \frac{t_2^{\delta-\ell-1}}{\Gamma(\delta-\ell)}\Big)\sum_{j=1}^{\infty} c_j \varphi(\tau_j)^{\delta}\right] + \frac{1}{2}\Big[\frac{\lambda b(|z|_{\alpha}^{T}) + g^{I}}{|t_2 - t_1|^{\alpha}}\Big]\Big[\frac{t_1^{\delta-\ell-1}}{\Gamma(\delta-\ell)} - \frac{t_2^{\delta-\ell-1}}{\Gamma(\delta-\ell)}\Big].\end{aligned}$$

Since $t_2 > t_1$, $\frac{t_1^{\delta-\ell}}{\delta-\ell} - \frac{t_2^{\delta-\ell}}{\delta-\ell} \leq 0$, $\frac{t_1^{\delta-\ell-1}}{\Gamma(\delta-\ell)} - \frac{t_2^{\delta-\ell-1}}{\Gamma(\delta-\ell)} \leq 0$ and so we get

$$\begin{aligned}\frac{|\mathcal{F}^{(\ell)}(z)(t_2) - \mathcal{F}^{(\ell)}(z)(t_1)|}{|t_2 - t_1|^{\alpha}} &\leq \frac{2\Big[a(|z|_{\alpha}^{T}) + g^{S}\Big]|t_2 - t_1|^{\delta-\ell}}{(\delta-\ell)\Gamma(\delta-\ell)|t_2 - t_1|^{\alpha}} \\ &\leq \frac{2\Big[a(|z|_{\alpha}^{T}) + g^{S}\Big]}{\Gamma(\delta-\ell+1)} T^{\delta-\ell-\alpha}. \end{aligned} \tag{20}$$

From (19) and the above inequality, we deduce that

$$|\mathcal{F}z|_{\alpha}^{T} \leq \Big[a(|z|_{\alpha}^{T}) + g^{S}\Big]\Big[M_T + N_T \sum_{j=1}^{\infty} c_j \varphi(\tau_j)^{\delta} + \frac{2T^{\delta-\ell-\alpha}}{\Gamma(\delta-\ell+1)}\Big] + \Big[\lambda b(|z|_{\alpha}^{T}) + g^{I}\Big]N_T.$$

Therefore, $\mathcal{F}(z) \in \mathbb{C}^{\ell,\alpha}(\mathbb{R}_+)$. Next, let

$$z = \Big\{z \in \mathbb{C}^{\ell,\alpha}(\mathbb{R}_+) : |z|_{\alpha}^{T} \leq R_T \ \text{ for } \ T > 0\Big\}.$$

Then z is nonempty, bounded, closed and convex subset of $\mathbb{C}^{\ell,\alpha}(\mathbb{R}_+)$ and from (H_2) it is clear that $\mathcal{F}$ is self mapping on z. Now, we show that $\mathcal{F}$ is continuous on z. for this, let $z_1, z_2 \in z$ and ε be any positive number such that $|z_1 - z_2|_{\alpha}^{T} \leq \varepsilon$. Let $t \in [0, T]$. Then

$$|(\mathcal{F}z_1)(t) - (\mathcal{F}z_2)(t)| \leq \frac{a\Big(|z_1 - z_2|_{\alpha}^{T}\Big)}{\Gamma(\delta+1)}\left[t^{\delta} + \frac{t^{\delta-1}}{2\Gamma(\delta)}\sum_{j=1}^{\infty} c_j \varphi(\tau_j)^{\delta}\right] + \lambda b\Big(|z_1 - z_2|_{\alpha}^{T}\Big)\frac{t^{\delta-1}}{2\Gamma(\delta)}. \tag{21}$$

Similar to the above argument, we have

$$\begin{aligned}|(\mathcal{F}z_1)'(t) - (\mathcal{F}z_2)'(t)| &\leq a\Big(|z_1 - z_2|_{\alpha}^{T}\Big)\left[\frac{t^{\delta-1}}{\Gamma(\delta)} + \frac{T^{\delta-2}}{2\Gamma(\delta-1)}\sum_{j=1}^{\infty} c_j \varphi(\tau_j)^{\delta}\right] \\ &\quad + \lambda b\Big(|z_1 - z_2|_{\alpha}^{T}\Big)\frac{T^{\delta-2}}{2\Gamma(\delta-1)}\end{aligned} \tag{22}$$

and

$$\begin{aligned}|(\mathcal{F}z_1)^{(p)}(t) - (\mathcal{F}z_2)^{(p)}(t)| &\leq a\Big(|z_1 - z_2|_{\alpha}^{T}\Big)\left[\frac{t^{\delta-p}}{\Gamma(\delta-p+1)} + \frac{T^{\delta-p-1}}{2\Gamma(\delta-p)}\sum_{j=1}^{\infty} c_j \varphi(\tau_j)^{\delta}\right] \\ &\quad + \lambda b\Big(|z_1 - z_2|_{\alpha}^{T}\Big)\frac{T^{\delta-p-1}}{2\Gamma(\delta-p)}\end{aligned} \tag{23}$$

for $\mathtt{p} = 2, 3 \cdots, \ell$. From (21)-(23), we obtain

$$\begin{aligned}
&|(\mathcal{F}\mathtt{z}_1)^{(\mathtt{p})}(\mathtt{t}) - (\mathcal{F}\mathtt{z}_2)^{(\mathtt{p})}(\mathtt{t})| \\
&\quad \le a\Big(|\mathtt{z}_1 - \mathtt{z}_2|_\alpha^{\mathtt{T}}\Big)\left[\sup_{0\le p\le \ell}\left\{\frac{\mathtt{T}^{\delta-\mathtt{p}}}{\Gamma(\delta-\mathtt{p}+1)}\right\} + \sup_{0\le p\le \ell}\left\{\frac{\mathtt{T}^{\delta-\mathtt{p}-1}}{2\Gamma(\delta-\mathtt{p})}\right\}\sum_{\mathtt{j}=1}^{\infty}\mathtt{c}_\mathtt{j}\varphi(\tau_\mathtt{j})^\delta\right] \\
&\qquad + \lambda b\Big(|\mathtt{z}_1 - \mathtt{z}_2|_\alpha^{\mathtt{T}}\Big)\sup_{0\le p\le \ell}\left\{\frac{\mathtt{T}^{\delta-\mathtt{p}-1}}{2\Gamma(\delta-\mathtt{p})}\right\}. \qquad (24)
\end{aligned}$$

for $\mathtt{p} = 0, 1, \cdots, \ell$. Similar to the above process, for $\mathtt{t}_1, \mathtt{t}_2 \in [0, \mathtt{T}]$ with $\mathtt{t}_2 > \mathtt{t}_1$, we obtain

$$\frac{\Big|[(\mathcal{F}\mathtt{z}_1)^{(\ell)}(\mathtt{t}_2) - (\mathcal{F}\mathtt{z}_2)^{(\ell)}(\mathtt{t}_2)] - [(\mathcal{F}\mathtt{z}_1)^{(\ell)}(\mathtt{t}_1) - (\mathcal{F}\mathtt{z}_2)^{(\ell)}(\mathtt{t}_1)]\Big|}{|\mathtt{t}_2 - \mathtt{t}_1|^\alpha} \le \frac{2\mathtt{T}^{\delta-\ell-\alpha}}{\Gamma(\delta-\ell+1)}a\Big(|\mathtt{z}_1 - \mathtt{z}_2|_\alpha^{\mathtt{T}}\Big).$$

Combining above inequality and (24), we get

$$|\mathcal{F}\mathtt{z}_1 - \mathcal{F}\mathtt{z}_2|_\alpha^{\mathtt{T}} \le a\Big(|\mathtt{z}_1 - \mathtt{z}_2|_\alpha^{\mathtt{T}}\Big)\Big[\mathtt{M}_\mathtt{T} + \mathtt{N}_\mathtt{T}\sum_{\mathtt{j}=1}^{\infty}\mathtt{c}_\mathtt{j}\varphi(\tau_\mathtt{j})^\delta + \frac{2\mathtt{T}^{\delta-\ell-\alpha}}{\Gamma(\delta-\ell+1)}\Big] + \lambda b\Big(|\mathtt{z}_1 - \mathtt{z}_2|_\alpha^{\mathtt{T}}\Big)\mathtt{N}_\mathtt{T}.$$

From which we conclude that $\mathcal{F}$ is continuous on $\mathtt{z}$. Finally, we verify the condition (11). Let B be any bounded subset of $\mathbb{C}^{\ell,\alpha}(\mathbb{R}_+)$, ε be any positive number and $\mathtt{T} \in \mathbb{N}$. Let us select $\mathtt{z} \in B$ and $\mathtt{t}_1, \mathtt{t}_2 \in [0, \mathtt{T}]$ with $|\mathtt{t}_1 - \mathtt{t}_2| \le \varepsilon$, we have

$$\begin{aligned}
&|(\mathcal{F}\mathtt{z})(\mathtt{t}_2) - (\mathcal{F}\mathtt{z})(\mathtt{t}_1)| \\
&\quad \le \left[\frac{a(\mathtt{z}(\mathtt{s})) + \mathtt{g}^{\mathtt{S}}}{\Gamma(\delta)}\right]\left[\frac{2(\mathtt{t}_2 - \mathtt{t}_1)^\delta}{\delta} + \frac{\mathtt{t}_1^\delta}{\delta} - \frac{\mathtt{t}_2^\delta}{\delta} + \frac{1}{2}\left(\frac{\mathtt{t}_1^{\delta-1}}{\Gamma(\delta)} - \frac{\mathtt{t}_2^{\delta-1}}{\Gamma(\delta)}\right)\sum_{\mathtt{j}=1}^{\infty}\mathtt{c}_\mathtt{j}\varphi(\tau_\mathtt{j})^\delta\right] \\
&\qquad + \frac{1}{2}\Big[\lambda b\Big(|\mathtt{z}(\mathtt{s})|\Big) + \mathtt{g}^{\mathtt{I}}\Big]\left(\frac{\mathtt{t}_1^{\delta-1}}{\Gamma(\delta)} - \frac{\mathtt{t}_2^{\delta-1}}{\Gamma(\delta)}\right).
\end{aligned}$$

Since $\dfrac{\mathtt{t}_1^\delta}{\delta} - \dfrac{\mathtt{t}_2^\delta}{\delta} \le 0$, $\dfrac{\mathtt{t}_1^{\delta-1}}{\Gamma(\delta)} - \dfrac{\mathtt{t}_2^{\delta-1}}{\Gamma(\delta)} \le 0$, $|\mathtt{t}_2 - \mathtt{t}_1| \le \varepsilon$ and $\varepsilon > 0$ was arbitrary, we have

$$|(\mathcal{F}\mathtt{z})(\mathtt{t}_2) - (\mathcal{F}\mathtt{z})(\mathtt{t}_1)| \to 0 \text{ as } \varepsilon \to 0. \qquad (25)$$

Similar to the above arguments, it can be shown that

$$|(\mathcal{F}\mathtt{z})'(\mathtt{t}_2) - (\mathcal{F}\mathtt{z})'(\mathtt{t}_1)| \to 0 \text{ as } \varepsilon \to 0. \qquad (26)$$

$$|(\mathcal{F}\mathtt{z})^{(\mathtt{p})}(\mathtt{t}_2) - (\mathcal{F}\mathtt{z})^{(\mathtt{p})}(\mathtt{t}_1)| \to 0 \text{ as } \varepsilon \to 0. \qquad (27)$$

From (25)-(27), we obtain

$$\begin{aligned}
\mu^{\mathtt{T}}(\mathcal{F}\mathtt{z}, \varepsilon) &= \sup\Big\{|\mathtt{z}^{(\mathtt{p})}(\mathtt{t}_2) - \mathtt{z}^{(\mathtt{p})}(\mathtt{t}_1)| : \mathtt{t}_1, \mathtt{t}_2 \in [0, \mathtt{T}], |\mathtt{t}_1 - \mathtt{t}_2| \le \varepsilon, \mathtt{p} = 0, 1, \cdots, \ell\Big\} \\
&\to 0 \text{ as } \varepsilon \to 0. \\
\mu^{\mathtt{T}}(\mathcal{F}B, \varepsilon) &= \sup_{\mathtt{z}\in B}\mu^{\mathtt{T}}(\mathcal{F}\mathtt{z}, \varepsilon) \to 0 \text{ as } \varepsilon \to 0. \qquad (28)
\end{aligned}$$

In view of (20), we deduce that

$$\begin{aligned}
\mu_\alpha^{\mathtt{T}}(\mathcal{F}\mathtt{z}, \varepsilon) &= \sup\left\{\frac{|\mathtt{z}^{(\ell)}(\mathtt{t}_1) - \mathtt{z}^{(\ell)}(\mathtt{t}_2)|}{|\mathtt{t}_1 - \mathtt{t}_2|^\alpha} : \mathtt{t}_1, \mathtt{t}_2 \in [0, \mathtt{T}], \mathtt{t}_1 \ne \mathtt{t}_2, |\mathtt{t}_1 - \mathtt{t}_2| \le \varepsilon\right\} \\
&\le \frac{2\Big[a(|\mathtt{z}|_\alpha^{\mathtt{T}}) + \mathtt{g}^{\mathtt{S}}\Big]}{\Gamma(\delta-\ell+1)}\varepsilon^{\delta-\ell-\alpha} \\
&\to 0 \text{ as } \varepsilon \to 0.
\end{aligned}$$

Which gives that

$$\mu^{\mathtt{T}}_{\alpha}(\mathcal{F}B,\varepsilon)=\sup_{\mathtt{z}\in B}\mu^{\mathtt{T}}_{\alpha}(\mathcal{F}\mathtt{z},\varepsilon)\to 0 \ \text{ as } \ \varepsilon\to 0. \tag{29}$$

From (28)-(29), we get

$$\aleph^{\mathtt{T}}_{\alpha,\ell}(\mathcal{F}B)=\lim_{\varepsilon\to 0}\aleph^{\mathtt{T}}_{\alpha,\ell}(\mathcal{F}B,\varepsilon)=\lim_{\varepsilon\to 0}\Big[\mu^{\mathtt{T}}(\mathcal{F}B,\varepsilon)+\mu^{\mathtt{T}}_{\alpha}(\mathcal{F}B,\varepsilon)\Big].$$

Thus,

$$\aleph^{\mathtt{T}}_{\alpha,\ell}(\mathcal{F}B)\le\pi\Big(\aleph^{\mathtt{T}}_{\alpha,\ell}(B)\Big)\aleph^{\mathtt{T}}_{\alpha,\ell}(B),$$

where $\pi\Big(\aleph^{\mathtt{T}}_{\alpha,\ell}(B)\Big)=0$. Therefore, from Theorem 3.3, $\mathcal{F}$ has a fixed point $\mathtt{z}$ in the Fréchet space $\mathbb{C}^{\ell,\alpha}(\mathbb{R}_+)$ which belongs to the set $\mathtt{z}$ and hence the fractional order infinite point boundary value problem (1) has at least one solution in $\mathbb{C}^{\ell,\alpha}(\mathbb{R}_+)$. This completes the proof. □

Example 4.2. *Consider the following fractional order infinite-point boundary value problem*

$$\left.\begin{aligned}&\mathtt{D}^{\frac{5}{2}}_{0^+}\mathtt{z}(\mathtt{t})=\frac{e^{-2t}\sin(\mathtt{z}(\mathtt{t})+1)}{\sqrt{\mathtt{t}+3}},\ \mathtt{t}\in\mathbb{R}_+,\\ &\mathtt{z}(0)=\mathtt{z}'(0)=\mathtt{z}''(0)=0,\ \lim_{t\to+\infty}\mathtt{D}^{\frac{3}{2}}_{0^+}\mathtt{z}(\mathtt{t})=\sum_{\mathtt{j}=1}^{\infty}\frac{135}{2\pi^{7/2}\mathtt{j}}\mathtt{z}\left(\frac{1}{\mathtt{j}^2}\right).\end{aligned}\right\} \tag{30}$$

Comparing (30) with (1), we have $\delta=\frac{5}{2},\ell=2,\mathtt{c}_{\mathtt{j}}=\frac{135}{2\pi^{7/2}\mathtt{j}},\tau_{\mathtt{j}}=\frac{1}{\mathtt{j}},\varphi(\tau_{\mathtt{j}})=\tau_{\mathtt{j}}^2$ and

$$\mathtt{g}(\mathtt{t},\mathtt{z})=\frac{e^{-2\mathtt{t}}\sin(\mathtt{z}(\mathtt{t})+1)}{\sqrt{\mathtt{t}+3}}.$$

Let $\alpha=\frac{1}{3}$. Then, $\delta-\ell-\alpha=\frac{1}{6}>0$. Taking $a(\mathtt{t})=b(\mathtt{t})=\mathtt{t}$ and $\lambda=\frac{1}{2\sqrt{3}}$. Now, we check the conditions of Theorem 4.1. For this, let $\mathtt{s}\in\mathbb{R}_+$ and $\mathtt{z}_1,\mathtt{z}_2\in\mathbb{R}$. Then

$$\begin{aligned}|\mathtt{g}(\mathtt{s},\mathtt{z}_1)-\mathtt{g}(\mathtt{s},\mathtt{z}_2)|&=\left|\frac{e^{-2\mathtt{s}}}{\sqrt{\mathtt{s}+3}}\Big[\sin(\mathtt{z}_1(\mathtt{s})+1)-\sin(\mathtt{z}_2(\mathtt{s})+1)\Big]\right|\\&\le\frac{1}{\sqrt{3}}|(\mathtt{z}_1+1)-(\mathtt{z}_2+1)|\\&\le|\mathtt{z}_1-\mathtt{z}_2|,\end{aligned}$$

$$\begin{aligned}\int_0^{\infty}|\mathtt{g}(\mathtt{s},\mathtt{z}_1)-\mathtt{g}(\mathtt{s},\mathtt{z}_2)|\mathtt{ds}&=\int_0^{\infty}\left|\frac{e^{-2\mathtt{s}}}{\sqrt{s+3}}\Big[\sin(\mathtt{z}_1(\mathtt{s})+1)-\sin(\mathtt{z}_2(\mathtt{s})+1)\Big]\right|\mathtt{ds}\\&\le|(\mathtt{z}_1+1)-(\mathtt{z}_2+1)|\int_0^{\infty}\frac{e^{-2\mathtt{s}}}{\sqrt{3}}\mathtt{ds}\\&\le\frac{1}{2\sqrt{3}}|\mathtt{z}_1-\mathtt{z}_2|=\lambda b\Big(|\mathtt{z}_1-\mathtt{z}_2|\Big),\end{aligned}$$

$$\mathtt{g}^{\mathtt{S}}=\sup\left\{\left|\frac{e^{-2\mathtt{s}}}{\sqrt{s+3}}\sin(1)\right|:\mathtt{s}\in\mathbb{R}_+\right\}=\frac{1}{\sqrt{3}}\quad\text{and}\quad\mathtt{g}^{\mathtt{I}}=\int_0^{\infty}\frac{e^{-2\mathtt{s}}}{\sqrt{\mathtt{s}+3}}\sin(1)\mathtt{ds}\le\frac{1}{\sqrt{3}}.$$

Thus, (H_1) satisfied. Also,

$$\sum_{\mathtt{j}=1}^{m}\mathtt{c}_{\mathtt{j}}\varphi(\tau_{\mathtt{j}})^{\delta-1}=\sum_{\mathtt{j}=1}^{m}\frac{135}{2\pi^{7/2}\mathtt{j}^4}\to\frac{3}{4}\sqrt{\pi}=\Gamma(\delta)\ \text{ as }\ m\to+\infty,$$

$$\sum_{j=1}^{\infty} c_j \varphi(\tau_j)^{\delta} = \sum_{j=1}^{m} \frac{135}{2\pi^{7/2} j^6} \to \frac{1}{14}\pi^{5/2} \text{ as } m \to +\infty,$$

and the relation

$$\Big[a(R_T) + g^S\Big]\Big[M_T + N_T \sum_{j=1}^{\infty} c_j \varphi(\tau_j)^{\delta} + \frac{2T^{\delta-\ell-\alpha}}{\Gamma(\delta-\ell+1)}\Big] + \Big[\lambda b(R_T) + g^I\Big]N_T \le R_T$$

gives

$$\Big[R_T + \frac{1}{\sqrt{3}}\Big]\Big[M_T + N_T\frac{\pi^{5/2}}{14} + \frac{2T^{1/6}}{\sqrt{\pi}}\Big] + \Big[\frac{1}{2\sqrt{3}}R_T + g^I\Big]N_T \le R_T,$$

which is equivalent to

$$R_T \ge \frac{\frac{1}{\sqrt{3}}\Big(M_T + N_T\frac{\pi^{5/2}}{14} + \frac{2T^{1/6}}{\sqrt{\pi}}\Big) + g^I N_T}{1 - \Big(M_T + N_T\frac{\pi^{5/2}}{14} + \frac{2T^{1/6}}{\sqrt{\pi}} + N_T\frac{1}{2\sqrt{3}}\Big)},$$

and the right hand side value of the above inequality is finite, so for each $T \in \mathbb{N}$, $R_T > 0$ exists, which is the solution of the inequality in (H_2). Hence from the Theorem 4.1, the fractional order infinite point boundary value problem (30) has at least one solution in the Fréchet space $\mathbb{C}^{2,\frac{1}{3}}(\mathbb{R}_+)$.

Acknowledgement

The authors express their sincere thanks to the unanimous reviewer for the careful reading of the article and the valuable constructive comments those improved the presentation of the article.

References

[1] R.P. Agarwal, M. Meehan, D. O'regan, Fixed point theory and applications, Cambridge University Press, Cambridge, 2001.
[2] A. Aghajani, R. Allahyari, M. Mursaleen, A generalization of Darbo's theorem with application to the solvability of systems of integral equations, J. Comput. Appl. Math., Vol. 260, 68–77, 2014.
[3] A. Aghajani, Y. Jalilian, J.J. Trujillo, On the existence of solutions of fractional integro-difierential equations, Fract. Calc. Appl. Anal., 15(1), 44–69, 2012.
[4] A. Aghajani, N. Sabzali, Existence of coupled fixed points via measure of noncompactness and applications, J. Nonl. Conv. Anal., 15(5), 941–952, 2014.
[5] Z. Bai, H. Lu, Positive solutions for a boundary value problem of nonlinear fractional differential equations, J. Math. Anal. Appl., 311, 495–505, 2005.
[6] J. Banas, On measures of noncompactness in Banach spaces, Comment. Math. Univ. Carolinae, Vol. 21, 131–143, 1980.
[7] J. Banas, K. Goebel, Measure of Noncompactness in Banach Spaces, Lecture Notes in Pure and Applied Mathematics, Vol. 60, Marcel Dekker, New York, 1980.
[8] M. Benchohra, J.R. Graef, F.Z. Mostafai, Weak solutions for nonlinear fractional difierential equations on reflexive Banach spaces, Electron. J. Qual. Theory., Vol. 54, 1–10, 2010.
[9] M. Borcut, Tripled fixed point theorems for monotone mappings in partially ordered metric spaces, Carpathian J. of Math., 28(2), 215–222, 2012.
[10] P. Borisut, P. Kumam, I. Ahmed K. Sitthithakerngkiet, Nonlinear Caputo Fractional Derivative with Nonlocal Riemann-Liouville Fractional Integral Condition Via Fixed Point Theorems, Symmetry, 11(6), 829, 2019.
[11] L. Cadariu, L. GavruţaL and P. Gavruça, Weighted space method for the stability of some nonlinear equations, Appl. Anal. Discrete Math., 6(1), 126–139, 2012.
[12] K. Cao, Y.Q. Chen, D. Stuart, A Fractional Micro-Macro Model for Crowds of Pedestrians Based on Fractional Mean Field Games, IEEE/CAA J. Automatica Sinica, 3(3), 261–270, 2016.
[13] S. S. Chang, Y. J. Cho, N. J. Huang, Coupled fixed point theorems with applications, J. Korean Math. Soc., Vol. 33, 575–585, 1996.
[14] G. Darbo, Punti uniti in trasformazioni a codominio non compatto. Rend. Sem. Mat. Un. Padova., Vol. 24, 84–92, 1955.
[15] L. Debanath, Recent Applications of Fractional Calculus to Science and Engineering, 3413–3442, 2003.
[16] C. Derbazi, H. Hammouche, M. Benchohra, Weak solutions for some nonlinear fractional differential equations with fractional integral boundary conditions in Banach space, J. Nonlinear funct. Anal., Vol. 2019, Article ID 7, 2019.
[17] M. Q. Feng, X. M. Zhang, W. G. Ge, New existence results for higher-order nonlinear fractional differential equation with integral boundary conditions, Bound. Value Probl., Vol. 2011, Art. ID 720702, 20 pp.

[18] M. Geraghty, On contractive mappings, Proc. Amer. Math. Soc., Vol. 40, 604–608, 1955.
[19] M. Izadi, H. M. Srivastava, A novel matrix technique for multi-order pantograph differential equations of fractional order, Proc. Roy. Soc. London Ser. A: Math. Phys. Engrg. Sci., 477, Article ID 2021031, 1–21, 2021.
[20] H. A. Kayvanloo, M. Khanehgir, and R. Allahyari, A family of measures of noncompactness in the Hölder space $C^{n,\gamma}(\mathbb{R}_+)$ and its application to some fractional differential equations and numerical methods, J. Comp. Appl. Math., Vol. 363, 256–272, 2020.
[21] B. Hazarika, H. M. Srivastava, R. Arab, and M. Rabbani, Existence of solution for an infinite system of nonlinear integral equations via measure of noncompactness and homotopy perturbation method to solve it, J. Comput. Appl. Math. 343, 341–352, 2018.
[22] B. Hazarika, H. M. Srivastava, R. Arab, and M. Rabbani, Application of simulation function and measure of noncompactness for solvability of nonlinear functional integral equations and introduction to an iteration algorithm to find solution, Appl. Math. Comput., 360, 131–146, 2019.
[23] M. Khuddush, K. R. Prasad, Infinitely many positive solutions for an iterative system of conformable fractional order dynamic boundary value problems on time scales, Turk. J. Math., (2021). DOI: 10.3906/mat-2103-117
[24] M. Khuddush, K. R. Prasad, Existence, uniqueness and stability analysis of a tempered fractional order thermistor boundary value problems, J. Anal (2022). https://doi.org/10.1007/s41478-022-00438-6
[25] A. A. Kilbas, H. M. Srivastava, J. J. Trujillo, Theory and applications of fractional differential equations, North-Holland Mathematics Studies 204, Elsevier Science B. V., Amsterdam 2006.
[26] K. Kuratowski, Sur les espaces complets, Fund. Math., Vol. 15, 301–309, 1930.
[27] H. Lee, S. Kim, Multivariate coupled fixed point theorems on ordered partial metric spaces, J. Korean Math. Soc., 51, 1189–1207, 2014.
[28] K. Li, J. Peng, J. Gao, Nonlocal fractional semilinear Differential equations in separable Banach spaces, E. J. Differential Equations, (2013)(7), 1–7, 2013.
[29] J. Liang, Z. Liu, X. Wang, Solvability for a couple system of nonlinear fractional differential equations in a Banach space, Fract. Calc. Appl. Anal., 6(1), 51–63, 2013.
[30] S. A. Mohiuddine, H. M. Srivastava, and A. Alotaibi, Application of measures of noncompactness to the infinite system of second-order differential equations in ℓ_p spaces, Adv. Difference Equations 2016, Article ID 317, 1–13, 2016.
[31] I. Podlubny, Fractional differential equations, Academic Press, San Diego, 1999.
[32] K. R. Prasad, M. Khuddush, D. Leela, Existence of solutions for n-dimensional fractional order hybrid BVPs with integral boundary conditions by an application of n-fixed point theorem, J. Anal., (2021). https://doi.org/10.1007/s41478-020-00291-5
[33] K. R. Prasad, D. Leela, M. Khuddush, Existence and uniqueness of positive solutions for system of (p, q, r)-Laplacian fractional order boundary value problems, Adv. Theory Nonlinear Anal. Appl., 5(1), 138–157, 2021. https://doi.org/10.31197/atnaa.703304
[34] K. R. Prasad, M. Khuddush, D. Leela, Existence, uniqueness and Hyers–Ulam stability of a fractional order iterative two-point boundary value Problems, Afr. Mat., (2021). https://doi.org/10.1007/s13370-021-00895-5
[35] K. R. Prasad, M. Khuddush, D. Leela, Existence of solutions for infinite systems of regular fractional Sturm-Liouville problems in the spaces of tempered sequences, Tbilisi Math. J., 13 (4), 193–209, 2020. DOI: 10.32513/tbilisi/1608606058
[36] A. Salem, H. M. Alshehri, L. Almaghamsi, Measure of noncompactness for an infinite system of fractional Langevin equation in a sequence space, Adv. Differ. Equ. 2021(132), 2021. https://doi.org/10.1186/s13662-021-03302-2
[37] H. M. Srivastava, A. Das, B. Hazarika, and S. A. Mohiuddine, Existence of solutions of infinite systems of differential equations of general order with boundary conditions in the spaces c0 and l1 via the measure of noncompactness, Math. Methods Appl. Sci., 41, 3558–3569, 2018.
[38] H. M. Srivastava, Diabetes and its resulting complications: Mathematical modeling via fractional calculus, Public Health Open Access, 4 (3), 1–5, 2020.
[39] H. M. Srivastava, K. M. Saad, M. M. Khader, An efficient spectral collocation method for the dynamic simulation of the fractional epidemiological model of the Ebola virus, Chaos, Solitons and Fractals, 140, 1–7, 2020.
[40] H. M. Srivastava, Fractional-order derivatives and integrals: Introductory overview and recent developments, Kyungpook Math. J., 60, 73–116, 2020.
[41] V. E. Tarasov, V. V. Tarasova, Time dependent fractional dynamics with memory in quantum and economic physics, Annals of Physics, 383, 579–599, 2017.
[42] C. C. Tisdell, A. Zaidi, Basic qualitative and quantitative results for solutions to nonlinear, dynamic equations on time scales with an application to economic modelling, Nonlinear Anal., Vol. 68, 3504–3524, 2008.
[43] F. J. Torres, Existence of a positive solution for a boundary value problem of a nonlinear fractional differential equation, Bull. Iran. Math. Soc., 39(2), 307–323, 2013.
[44] D. W. J. Victor, M. Khuddush, Existence of solutions for n-dimensional fractional order bvp with ∞-point boundary conditions via the concept of measure of noncompactness, Advanced Studies: Euro-Tbilisi Mathematical Journal, 15(1), 19–37, 2022.
[45] J.R. Wang, Y. Zhou, M. Feckan, Abstract Cauchy problem for fractional differential equations, Nonlinear Dyn., 71:685 (2013) DOI 10.1007/s11071-012-0452-9.
[46] S. Q. Zhang, Existence results of positive solutions to fractional differential equation with integral boundary conditions, Math. Bohem., 135(2), 299–317, 2010.

Palestine Journal of Mathematics

Vol. 11(1)(2022) , 549–559 © Palestine Polytechnic University-PPU 2022

DENUMERABLY MANY POSITIVE RADIAL SOLUTIONS FOR THE ITERATIVE SYSTEM OF ELLIPTIC EQUATIONS IN AN ANNULUS

K. Rajendra Prasad, Mahammad Khuddush and B. Bharathi

Communicated by Martin Bohner

MSC 2010 Classifications: Primary 35J66, 35J60; Secondary 34B18, 47H10.

Keywords and phrases: Nonlinear elliptic system, annulus, positive radial solution, Krasnoselskii's fixed point theorem.

Abstract Sufficient conditions are derived for the existence of denumerably many positive radial solutions to the iterative system of elliptic equations

$$\Delta u_j + P(|x|)g_j(u_{j+1}) = 0,\ R_1 < |x| < R_2,$$
$$u_{\ell+1} = u_1,\ j = 1, 2 \cdots, \ell,$$

$x \in \mathbb{R}^N$, $N > 2$, subject to a linear mixed boundary conditions at R_1 and R_2, by an application of Krasnoselskii's fixed point theorem.

1 Introduction

The system of nonlinear elliptic equations of the form

$$\left.\begin{aligned} \Delta u_j + g_j(u_{j+1}) = 0 \ \text{ in } \ \Omega, \\ u_j = 0 \ \text{ on } \ \partial\Omega, \end{aligned}\right\} \tag{1.1}$$

where $j \in \{1, 2, 3, \cdots, \ell\}$, $u_{\ell+1} = u_1$, and Ω is a bounded domain in $\mathbb{R}^N$, has an important applications in population dynamics, combustion theory and chemical reactor theory. The recent literature for the existence, multiplicity and uniqueness of positive solutions for (1.1), see [5, 3, 6, 9, 10, 11] and references therein.

In [7], Dong and Wei established the existence of radial solutions for the following nonlinear elliptic equations with gradient terms in annular domains,

$$-\Delta u = g\big(|x|, u, \frac{x}{|x|} \cdot \nabla u\big) \ \text{ in } \ \Omega_a^b,$$
$$u = 0 \ \text{ on } \ \partial\Omega_a^b,$$

by using Schauder's fixed point theorem and contraction mapping theorem. In [15], Padhi, Graef and Kanaujiya considered the following elliptic boundary value problem in an annulus,

$$\Delta u + \lambda h(|x|, u) = 0 \ \text{ in } \ \Omega,$$
$$u = 0 \ \text{ on } \ \partial\Omega,$$

and established the existence of positive radial solutions by the revised version of Gustaf-son and Schmitt fixed point theorems. In [12], R. Kajikiya and E. Ko established the existence of positive radial solutions for a semipositone elliptic equation of the form,

$$-\Delta u = \lambda g(u) \ \text{ in } \ \Omega,$$
$$u = 0 \ \text{ on } \ \partial\Omega,$$

where Ω is a ball or an annulus in $\mathbb{R}^N$. Recently, Son and Wang [16] studied positive radial solutions for nonlinear elliptic systems of the form,

$$\Delta u_j + \lambda K_j(|x|) g_j(u_{j+1}) = 0 \text{ in } \Omega,$$
$$u_j = 0 \text{ on } |x| = r_0,$$
$$u_j \to 0 \text{ as } |x| \to +\infty,$$

where $j \in \{1, 2, 3, \cdots, \ell\}$, $u_{\ell+1} = u_1$, $\lambda > 0$, $N > 2$, $r_0 > 0$, and Ω is an exterior of a ball and established existence, multiplicity and uniqueness results for various nonlinearities in g_j. Motivated by the aforementioned works, in this paper we establish the existence of denumerably many positive radial solutions of the iterative system of nonlinear elliptic equation in an annulus,

$$\Delta u_j + P(|x|) g_j(u_{j+1}) = 0, \ R_1 < |x| < R_2, \tag{1.2}$$

with one of the following sets of boundary conditions:

$$\left.\begin{aligned} u_j = 0 \ \text{ on } \ |x| = R_1 \text{ and } |x| = R_2, \\ u_j = 0 \ \text{ on } \ |x| = R_1 \text{ and } \frac{\partial u_j}{\partial r} = 0 \text{ on } |x| = R_2, \\ \frac{\partial u_j}{\partial r} = 0 \ \text{ on } \ |x| = R_1 \text{ and } u_j = 0 \text{ on } |x| = R_2, \end{aligned}\right\} \tag{1.3}$$

where $j \in \{1, 2, 3, \cdots, \ell\}$, $u_{\ell+1} = u_1$, $\Delta u = \operatorname{div}(\nabla u)$, $x \in \mathbb{R}^N$, $N > 2$, $P = \prod_{i=1}^{n} P_i$, each $P_i : (R_1, R_2) \to (0, +\infty)$ is continuous, $r^{2(N-1)}P$ is integrable, may have singularities, by an application of Krasnoselskii's cone fixed point theorem on a Banach space.

The study of positive radial solutions, writing $r = |x|$, the iterative system (1.2) reduces to the study of positive solutions to the following iterative system of ordinary differential equations,

$$u_j''(r) + \frac{N-1}{r} u_j' + P(r) g_j\big(u_{j+1}(r)\big) = 0, \ R_1 \le r \le R_2. \tag{1.4}$$

By the change of variables $v_j(y) = u_j\big(r(y)\big)$ and the transformation $y = -\int_r^{R_2} \tau^{1-N} d\tau$ turns the system (1.4) into

$$v_j''(y) + r^{2(N-1)}(y) P(r(y)) g_j\big(v_{j+1}(y)\big) = 0, \ a < y < 0, \tag{1.5}$$

where $v_1 = v_{\ell+1}$ and $a = -\int_{R_1}^{R_2} \tau^{1-N} d\tau$. Further, it can still transform system (1.5) into

$$\varpi_j''(\tau) + Q(\tau) g_j\big(\varpi_{j+1}(\tau)\big) = 0, \ 0 < \tau < 1, \tag{1.6}$$

where $Q(\tau) = a^2 r^{2(N-1)}\big(a(1-\tau)\big) \prod_{i=1}^{n} Q_i(\tau)$, $Q_i(\tau) = P_i\big(r(a(1-\tau))\big)$, by the change of variables $\varpi_j(\tau) = v_j(y)$ and $\tau = (a-y)/a$. The detailed explanation of the transformation from the equation (1.4) to (1.6) see [4, 13, 14]. By suitable choices of nonnegative real numbers α, β, γ and δ with $d = \alpha\gamma + \alpha\delta + \beta\gamma > 0$, the set of boundary conditions (1.3) reduces to

$$\left.\begin{aligned} \alpha\varpi_j(0) - \beta\varpi_j'(0) = 0, \\ \gamma\varpi_j(1) + \delta\varpi_j'(1) = 0, \end{aligned}\right\} \tag{1.7}$$

where $j \in \{1, 2, 3, \cdots, \ell\}$ and $\varpi_1 = \varpi_{\ell+1}$. We note that Q_i may have singularities on $[0, 1]$. Thus for each $i \in \{1, 2, 3, \cdots, n\}$, we assume that the following conditions hold throughout the paper:

$(\mathcal{H}_1)$ $g_j : [0, +\infty) \to [0, +\infty)$ is continuous.

$(\mathcal{H}_2)$ $Q_i \in L^{p_i}[0, 1], (p_i \ge 1)$ and may have denumerably many singularities on $(0, 1/2)$.

$(\mathcal{H}_3)$ There exists a sequence $\{\tau_k\}_{k=1}^{\infty}$ such that $0 < \tau_{k+1} < \tau_k < \dfrac{1}{2}$, $k \in \mathbb{N}$,

$$\lim_{k\to\infty} \tau_k = \tau^* < \frac{1}{2}, \ \lim_{\tau\to\tau_k} Q_i(\tau) = +\infty, \ k \in \mathbb{N}, \ i = 1, 2, 3, \cdots, n$$

and each $Q_i(\tau)$ does not vanish identically on any subinterval of $[0, 1]$. Moreover, there exists $Q_i^* > 0$ such that

$$Q_i^* < Q_i(\tau) < \infty \ \text{ a.e. on } \ [0, 1].$$

The rest of the paper is organized in the following fashion. In Section 2, we convert the boundary value problem (1.6)–(1.7) into equivalent integral equation which involves the kernel. Also, we estimate bounds for the kernel which are useful in our main results. In Section 3, we establish a criteria for the existence of denumerably many positive radial solutions for (1.2) by applying Krasnoselskii's cone fixed point theorem in a Banach space. Finally, as an application, an example to demonstrate our results is given.

2 Kernel and Its Bounds

In this section, we constructed kernel to the homogeneous boundary value problem corresponding to (1.6)–(1.7) and established certain lemmas for the bounds of the kernel.

Lemma 2.1. *Let* $\mathtt{V} \in \mathcal{C}[0,1]$. *Then the boundary value problem*

$$\varpi_1''(\tau) + \mathtt{V}(\tau) = 0,\ 0 < \tau < 1, \tag{2.1}$$

$$\left.\begin{aligned} \alpha\varpi_1(0) - \beta\varpi_1'(0) &= 0,\\ \gamma\varpi_1(1) + \delta\varpi_1'(1) &= 0, \end{aligned}\right\} \tag{2.2}$$

has a unique solution

$$\varpi_1(\tau) = \int_0^1 \aleph(\tau, s)\mathtt{V}(s)ds, \tag{2.3}$$

where

$$\aleph(\tau,s) = \frac{1}{d}\begin{cases} (\beta+\alpha\tau)(\gamma+\delta-\gamma s), & 0 \le \tau \le s \le 1,\\ (\beta+\alpha s)(\gamma+\delta-\gamma\tau), & 0 \le s \le \tau \le 1. \end{cases}$$

Lemma 2.2. *For* $\mathtt{c} \in (0,1/2)$, *let* $\pi(\mathtt{c}) = \min\left\{\dfrac{\beta+\alpha\mathtt{c}}{\beta+\alpha}, \dfrac{\delta+\gamma\mathtt{c}}{\delta+\gamma}\right\}$. *The kernel* $\aleph(\tau,s)$ *has the following properties:*

(i) $\aleph(\tau,s)$ *is nonnegative and continuous on* $[0,1]\times[0,1]$,

(ii) $\aleph(\tau,s) \le \aleph(s,s)$ *for* $t,\tau \in [0,1]$,

(iii) there exists $\mathtt{c} \in (0,1/2)$ *such that* $\pi(\mathtt{c})\aleph(s,s) \le \aleph(\tau,s)$ *for* $\tau \in [\mathtt{c}, 1-\mathtt{c}]$, $s \in [0,1]$.

Proof. From the definition of kernel $\aleph(\tau,s)$, it is clear that (i) and (ii) hold. To prove (iii), let $\tau \in [\mathtt{c}, 1-\mathtt{c}]$ and $s \le \tau$, then

$$\frac{\aleph(\tau,s)}{\aleph(s,s)} = \frac{\gamma+\delta-\gamma\tau}{\gamma+\delta-\gamma s} \ge \frac{\delta+\gamma\mathtt{c}}{\delta+\gamma} \ge \pi(\mathtt{c}),$$

and for $\tau \le s$, we have

$$\frac{\aleph(\tau,s)}{\aleph(s,s)} = \frac{\beta+\alpha\tau}{\beta+\alpha s} \ge \frac{\beta+\alpha\mathtt{c}}{\beta+\alpha} \ge \pi(\mathtt{c}).$$

This completes the proof. □

From Lemma 2.1, we note that an ℓ-tuple $(\varpi_1, \varpi_2, \cdots, \varpi_\ell)$ is solution of the boundary value problem (1.6)–(1.7) if and only, if

$$\varpi_1(\tau) = \int_0^1 \aleph(\tau,s_1)\mathtt{Q}(s_1)\mathtt{g}_1\left[\int_0^1 \aleph(s_1,s_2)\mathtt{Q}(s_2)\mathtt{g}_2\left[\int_0^1 \aleph(s_2,s_3)\mathtt{Q}(s_3)\mathtt{g}_4\cdots\right.\right.$$
$$\left.\left.\mathtt{g}_{\ell-1}\left[\int_0^1 \aleph(s_{\ell-1},s_\ell)\mathtt{Q}(s_\ell)\mathtt{g}_\ell\big(\varpi_1(s_\ell)\big)ds_\ell\right]\cdots\right]ds_3\right]ds_2\right]ds_1.$$

In general,

$$\varpi_{\mathtt{j}}(\tau) = \int_0^1 \aleph(\tau,s)\mathtt{Q}(s)\mathtt{g}_{\mathtt{j}}\big(\varpi_{\mathtt{j}+1}(s)\big)ds,\ \mathtt{j}=1,2,3,\cdots,\ell,$$
$$\varpi_1(\tau) = \varpi_{\ell+1}(\tau),\ 0<\tau<1.$$

Denote the Banach space $\mathcal{C}([0,1],\mathbb{R})$ by $\mathscr{B}$ with the norm $\|\varpi\| = \max_{\tau\in[0,1]}|\varpi(\tau)|$. For $\mathtt{c}\in(0,1/2)$, the cone $\mathcal{P}_{\mathtt{c}}\subset\mathscr{B}$ is defined by

$$\mathcal{P}_{\mathtt{c}} = \Big\{\varpi\in\mathscr{B} : \varpi(\tau)\geq 0, \min_{\varpi\in[\mathtt{c},\,1-\mathtt{c}]}\varpi(\tau)\geq\pi(\mathtt{c})\|\varpi\|\Big\}.$$

For any $\varpi_1\in\mathcal{P}_{\mathtt{c}}$, define an operator $\mathcal{T}:\mathcal{P}_{\mathtt{c}}\to\mathscr{B}$ by

$$(\mathcal{T}\varpi_1)(\tau) = \int_0^1 \aleph(\tau,s_1)\mathtt{Q}(s_1)\mathtt{g}_1\Bigg[\int_0^1 \aleph(s_1,s_2)\mathtt{Q}(s_2)\mathtt{g}_2\Bigg[\int_0^1 \aleph(s_2,s_3)\mathtt{Q}(s_3)\mathtt{g}_4\cdots$$
$$\mathtt{g}_{\ell-1}\Bigg[\int_0^1 \aleph(s_{\ell-1},s_\ell)\mathtt{Q}(s_\ell)\mathtt{g}_\ell\big(\varpi_1(s_\ell)\big)ds_\ell\Bigg]\cdots\Bigg]ds_3\Bigg]ds_2\Bigg]ds_1.$$

Lemma 2.3. *For each $\mathtt{c}\in(0,1/2)$, $\mathcal{T}(\mathcal{P}_{\mathtt{c}})\subset\mathcal{P}_{\mathtt{c}}$ and $\mathcal{T}:\mathcal{P}_{\mathtt{c}}\to\mathcal{P}_{\mathtt{c}}$ is completely continuous.*

Proof. Let $\mathtt{c}\in(0,1/2)$. Since $\mathtt{g}_{\mathtt{j}}(\varpi_{\mathtt{j}+1}(\tau))$ is nonnegative for $\tau\in[0,1]$, $\varpi_1\in\mathcal{P}_{\mathtt{c}}$. Since $\aleph(\tau,s)$, is nonnegative for all $\tau,s\in[0,1]$, it follows that $\mathcal{T}(\varpi_1(\tau))\geq 0$ for all $\tau\in[0,1]$, $\varpi_1\in\mathcal{P}_{\mathtt{c}}$ Now, by Lemma 2.1 and 2.2, we have

$$\min_{\tau\in[\mathtt{c},1-\mathtt{c}]}(\mathcal{T}\varpi_1)(\tau)$$
$$= \min_{\tau\in[\mathtt{c},1-\mathtt{c}]}\Bigg\{\int_0^1 \aleph(\tau,s_1)\mathtt{Q}(s_1)\mathtt{g}_1\Bigg[\int_0^1 \aleph(s_1,s_2)\mathtt{Q}(s_2)\mathtt{g}_2\Bigg[\int_0^1 \aleph(s_2,s_3)\mathtt{Q}(s_3)\mathtt{g}_4\cdots$$
$$\mathtt{g}_{\ell-1}\Bigg[\int_0^1 \aleph(s_{\ell-1},s_\ell)\mathtt{Q}(s_\ell)\mathtt{g}_\ell\big(\varpi_1(s_\ell)\big)ds_\ell\Bigg]\cdots\Bigg]ds_3\Bigg]ds_2\Bigg]ds_1\Bigg\}$$
$$\geq \pi(\mathtt{c})\int_0^1 \aleph(s_1,s_1)\mathtt{Q}(s_1)\mathtt{g}_1\Bigg[\int_0^1 \aleph(s_1,s_2)\mathtt{Q}(s_2)\mathtt{g}_2\Bigg[\int_0^1 \aleph(s_2,s_3)\mathtt{Q}(s_3)\mathtt{g}_4\cdots$$
$$\mathtt{g}_{\ell-1}\Bigg[\int_0^1 \aleph(s_{\ell-1},s_\ell)\mathtt{Q}(s_\ell)\mathtt{g}_\ell\big(\varpi_1(s_\ell)\big)ds_\ell\Bigg]\cdots\Bigg]ds_3\Bigg]ds_2\Bigg]ds_1$$
$$\geq \pi(\mathtt{c})\Bigg\{\int_0^1 \aleph(\tau,s_1)\mathtt{Q}(s_1)\mathtt{g}_1\Bigg[\int_0^1 \aleph(s_1,s_2)\mathtt{Q}(s_2)\mathtt{g}_2\Bigg[\int_0^1 \aleph(s_2,s_3)\mathtt{Q}(s_3)\mathtt{g}_4\cdots$$
$$\mathtt{g}_{\ell-1}\Bigg[\int_0^1 \aleph(s_{\ell-1},s_\ell)\mathtt{Q}(s_\ell)\mathtt{g}_\ell\big(\varpi_1(s_\ell)\big)ds_\ell\Bigg]\cdots\Bigg]ds_3\Bigg]ds_2\Bigg]ds_1\Bigg\}$$
$$\geq \pi(\mathtt{c})\max_{\tau\in[0,1]}|\mathcal{T}\varpi_1(\tau)|.$$

Thus $\mathcal{T}(\mathcal{P}_{\mathtt{c}})\subset\mathcal{P}_{\mathtt{c}}$. Therefore, the operator $\mathcal{T}$ is completely continuous by standard methods and by the Arzela-Ascoli theorem. □

3 Denumerably Many Positive Radial Solutions

In this section, for the existence of denumerably many positive radial solutions of (1.2), we apply the following theorems.

Theorem 3.1. *[8] Let $\mathcal{E}$ be a cone in a Banach space $\mathcal{X}$ and Λ_1, Λ_2 are open sets with $0\in\Lambda_1,\overline{\Lambda}_1\subset\Lambda_2$. Let $\mathcal{T}:\mathcal{E}\cap(\overline{\Lambda}_2\backslash\Lambda_1)\to\mathcal{E}$ be a completely continuous operator such that*

(a) $\|\mathcal{T}\mathtt{u}\| \le \|\mathtt{u}\|$, $\mathtt{u} \in \mathcal{E} \cap \partial\Lambda_1$, *and* $\|\mathcal{T}\mathtt{u}\| \ge \|\mathtt{u}\|$, $\mathtt{u} \in \mathcal{E} \cap \partial\Lambda_2$, *or*

(b) $\|\mathcal{T}\mathtt{u}\| \ge \|\mathtt{u}\|$, $\mathtt{u} \in \mathcal{E} \cap \partial\Lambda_1$, *and* $\|\mathcal{T}\mathtt{u}\| \le \|\mathtt{u}\|$, $\mathtt{u} \in \mathcal{E} \cap \partial\Lambda_2$.

Then $\mathcal{T}$ *has a fixed point in* $\mathcal{E} \cap (\overline{\Lambda}_2 \backslash \Lambda_1)$.

Theorem 3.2. *(Hölder's) Let* $f \in L^{\mathtt{p}_i}[0,1]$ *with* $\mathtt{p}_i > 1$, *for* $i = 1, 2, \cdots, n$ *and* $\sum_{i=1}^{n} \frac{1}{\mathtt{p}_i} = 1$. *Then* $\prod_{i=1}^{n} f_i \in L^1[0,1]$ *and* $\|\prod_{i=1}^{n} f_i\|_1 \le \prod_{i=1}^{n} \|f_i\|_{\mathtt{p}_i}$. *Further, if* $f \in L^1[0,1]$ *and* $g \in L^\infty[0,1]$. *Then* $fg \in L^1[0,1]$ *and* $\|fg\|_1 \le \|f\|_1 \|g\|_\infty$.

Consider the following three possible cases for $\mathtt{P}_\mathtt{j} \in L^{\mathtt{p}_i}[0,1]$:

$$\sum_{i=1}^{n} \frac{1}{\mathtt{p}_i} < 1, \ \sum_{i=1}^{n} \frac{1}{\mathtt{p}_i} = 1, \ \sum_{i=1}^{n} \frac{1}{\mathtt{p}_i} > 1.$$

Firstly, we seek denumerably many positive radial solutions for the case $\sum_{i=1}^{n} \frac{1}{\mathtt{p}_i} < 1$.

Theorem 3.3. *Suppose* $(\mathcal{H}_1) - (\mathcal{H}_3)$ *hold, let* $\{\mathtt{c}_k\}_{k=1}^{\infty}$ *be a sequence with* $\tau_{k+1} < \mathtt{c}_k < \tau_k$. *Let* $\{\mathtt{A}_k\}_{k=1}^{\infty}$ *and* $\{\mathtt{B}_k\}_{k=1}^{\infty}$ *be such that*

$$\mathtt{A}_{k+1} < \pi(\mathtt{c}_k)\mathtt{B}_k < \mathtt{S}_k < \eta\mathtt{B}_k < \mathtt{A}_k, \ k \in \mathbb{N},$$

where

$$\eta = \max\left\{ \left[\pi(\mathtt{c}_1) a^2 \prod_{i=1}^{n} \mathtt{Q}_i^* \int_{\mathtt{c}_1}^{1-\mathtt{c}_1} \aleph(s,s) \mathtt{r}^{2(N-1)}\big(a(1-s)\big) ds \right]^{-1}, \ 1 \right\}.$$

Further, assume that $\mathtt{g}_\mathtt{j}$ *satisfies*

$(\mathcal{J}_1)$ $\mathtt{g}_\mathtt{j}(\varpi(\tau)) \le \mathtt{N}_1 \mathtt{A}_k$ *for all* $\tau \in [0,1]$, $0 \le \varpi \le \mathtt{A}_k$, *where*

$$\mathtt{N}_1 < \left[a^2 \|\aleph\|_q \prod_{i=1}^{n} \|\mathtt{Q}_i\|_{p_i} \right]^{-1}, \ \aleph(s) = \aleph(s,s)\mathtt{r}^{2(N-1)}\big(a(1-s_\ell)\big),$$

$(\mathcal{J}_2)$ $\mathtt{g}_\mathtt{j}(\varpi(\tau)) \ge \eta\mathtt{B}_k$ *for all* $\tau \in [\mathtt{c}_k, 1-\mathtt{c}_k]$, $\pi(\mathtt{c}_k)\mathtt{B}_k \le \varpi \le \mathtt{B}_k$.

The iterative system (1.2) *has denumerably many positive radial solutions* $\{(\varpi_1^{[k]}, \varpi_2^{[k]}, \cdots, \varpi_\ell^{[k]})\}_{k=1}^{\infty}$ *such that* $\varpi_\mathtt{j}^{[k]}(\tau) \ge 0$ *on* $(0,1)$, $\mathtt{j} = 1, 2, \cdots, \ell$ *and* $k \in \mathbb{N}$.

Proof. Consider the sequences $\{\Lambda_{1,k}\}_{k=1}^{\infty}$ and $\{\Lambda_{2,k}\}_{k=1}^{\infty}$ of open subsets of $\mathscr{B}$ defined by

$$\Lambda_{1,k} = \{\varpi \in \mathscr{B} : \|\varpi\| < \mathtt{A}_k\}, \ \Lambda_{2,k} = \{\varpi \in \mathscr{B} : \|\varpi\| < \mathtt{B}_k\}.$$

Let $\{\mathtt{c}_k\}_{k=1}^{\infty}$ be as in the hypothesis and note that $\tau^* < \tau_{k+1} < \mathtt{c}_k < \tau_k < \frac{1}{2}$, for all $k \in \mathbb{N}$. For each $k \in \mathbb{N}$, define the cone $\mathcal{P}_{\mathtt{c}_k}$ by

$$\mathcal{P}_{\mathtt{c}_k} = \left\{ \varpi \in \mathscr{B} : \varpi(\tau) \ge 0 \ \text{ and } \min_{\tau \in [\mathtt{c}_k, \, 1-\mathtt{c}_k]} \varpi(t) \ge \pi(\mathtt{c}_k)\|\varpi\| \right\}.$$

Let $\varpi_1 \in \mathcal{P}_{\mathtt{c}_k} \cap \partial\Lambda_{1,k}$. Then, $\varpi_1(s) \le \mathtt{A}_k = \|\varpi_1\|$ for all $s \in [0,1]$. By $(\mathcal{J}_1)$ and $0 < s_{\ell-1} < 1$, we have

$$\begin{aligned}
\int_0^1 \aleph(s_{\ell-1}, s_\ell)\mathtt{Q}(s_\ell)\mathtt{g}_\ell\big(\varpi_1(s_\ell)\big) ds_\ell &\le \int_0^1 \aleph(s_\ell, s_\ell)\mathtt{Q}(s_\ell)\mathtt{g}_\ell\big(\varpi_1(s_\ell)\big) ds_\ell \\
&\le \mathtt{N}_1\mathtt{A}_k \int_0^1 \aleph(s_\ell, s_\ell)\mathtt{Q}(s_\ell) ds_\ell \\
&\le \mathtt{N}_1\mathtt{A}_k \int_0^1 \aleph(s_\ell, s_\ell) a^2 \mathtt{r}^{2(n-1)}\big(a(1-s_\ell)\big) \prod_{i=1}^{n} \mathtt{Q}_i(s_\ell) ds_\ell.
\end{aligned}$$

There exists a $\mathtt{q} > 1$ such that $\sum_{i=1}^{n} \frac{1}{\mathtt{p}_i} + \frac{1}{\mathtt{q}} = 1$. By the first part of Theorem 3.2, we have

$$\begin{aligned}\int_0^1 \aleph(s_{\ell-1}, s_\ell)\mathtt{Q}(s_\ell)\mathtt{g}_\ell\big(\varpi_1(s_\ell)\big)ds_\ell &\leq \mathtt{N}_1\mathtt{A}_k a^2\|\aleph\|_q \prod_{i=1}^{n}\|\mathtt{Q}_i\|_{p_i}\\ &\leq \mathtt{A}_k.\end{aligned}$$

It follows in similar manner for $0 < s_{\ell-2} < 1$,

$$\begin{aligned}\int_0^1 \aleph(s_{\ell-2}, s_{\ell-1})\mathtt{Q}(s_{\ell-1})\mathtt{g}_{\ell-1}\left[\int_0^1 \aleph(s_{\ell-1}, s_\ell)\mathtt{Q}(s_\ell)\mathtt{g}_\ell\big(\varpi_1(s_\ell)\big)ds_\ell\right]ds_{\ell-1}&\\ \leq \int_0^1 \aleph(s_{\ell-1}, s_{\ell-1})\mathtt{Q}(s_{\ell-1})\mathtt{g}_{\ell-1}(\mathtt{R}_k)ds_{\ell-1}&\\ \leq \mathtt{M}_1\mathtt{R}_k\int_0^1 \aleph(s_{\ell-1}, s_{\ell-1})\mathtt{Q}(s_{\ell-1})ds_{\ell-1}&\\ \leq \mathtt{N}_1\mathtt{A}_k a^2\|\aleph\|_q\prod_{i=1}^{n}\|\mathtt{Q}_i\|_{p_i}&\\ \leq \mathtt{A}_k.&\end{aligned}$$

Continuing with this bootstrapping argument, we get

$$\begin{aligned}(\Omega\varpi_1)(\tau) = \int_0^1 \aleph(\tau, s_1)\mathtt{Q}(s_1)\mathtt{g}_1\Bigg[\int_0^1 \aleph(s_1, s_2)\mathtt{Q}(s_2)\mathtt{g}_2\Bigg[\int_0^1 \aleph(s_2, s_3)\mathtt{Q}(s_3)\mathtt{g}_4\cdots&\\ \mathtt{g}_{\ell-1}\left[\int_0^1 \aleph(s_{\ell-1}, s_\ell)\mathtt{Q}(s_\ell)\mathtt{g}_\ell\big(\varpi_1(s_\ell)\big)ds_\ell\right]\cdots\Bigg]ds_3\Bigg]ds_2\Bigg]ds_1&\\ \leq \mathtt{A}_k.&\end{aligned}$$

Since $\mathtt{A}_k = \|\varpi_1\|$ for $\varpi_1 \in \mathcal{P}_{\beta_k} \cap \partial\Lambda_{1,k}$, we get

$$\|\Omega\varpi_1\| \leq \|\varpi_1\|. \tag{3.1}$$

Let $\tau \in [\mathtt{c}_k, 1-\mathtt{c}_k]$. Then, $\mathtt{B}_k = \|\varpi_1\| \geq \varpi_1(t) \geq \min_{\tau\in[\mathtt{c}_k, 1-\mathtt{c}_k]} \varpi_1(t) \geq \pi(\mathtt{c}_k)\|\varpi_1\| \geq \mathtt{c}_k\mathtt{B}_k$. By $(\mathcal{J}_2)$ and for $s_{\ell-1} \in [\mathtt{c}_k, 1-\mathtt{c}_k]$, we have

$$\begin{aligned}\int_0^1 \aleph(s_{\ell-1}, s_\ell)\mathtt{Q}(s_\ell)\mathtt{g}_\ell\big(\mathtt{u}_1(s_\ell)\big)ds_\ell&\\ \geq \int_{\mathtt{c}_k}^{1-\mathtt{c}_k} \aleph(s_{\ell-1}, s_\ell)\mathtt{Q}(s_\ell)\mathtt{g}_\ell\big(\mathtt{u}_1(s_\ell)\big)ds_\ell&\\ \geq \eta\mathtt{B}_k\int_{\mathtt{c}_k}^{1-\mathtt{c}_k} \aleph(s_{\ell-1}, s_\ell)\mathtt{Q}(s_\ell)ds_\ell&\\ \geq \eta\mathtt{B}_k\pi(\mathtt{c}_1)\int_{\mathtt{c}_1}^{1-\mathtt{c}_1} \aleph(s_\ell, s_\ell)\mathtt{Q}(s_\ell)ds_\ell&\\ \geq \eta\mathtt{B}_k\pi(\mathtt{c}_1)a^2\int_{\mathtt{c}_1}^{1-\mathtt{c}_1} \aleph(s_\ell, s_\ell)\mathtt{r}^{2(n-1)}\big(a(1-s_\ell)\big)\prod_{i=1}^{n}\mathtt{Q}_i(s_\ell)ds_\ell&\\ \geq \eta\mathtt{B}_k\pi(\mathtt{c}_1)a^2\prod_{i=1}^{n}\mathtt{Q}_i^*\int_{\mathtt{c}_1}^{1-\mathtt{c}_1} \aleph(s_\ell, s_\ell)\mathtt{r}^{2(n-1)}\big(a(1-s_\ell)\big)ds_\ell&\\ \geq \mathtt{B}_k.&\end{aligned}$$

Continuing with bootstrapping argument, we get

$$(\Omega\varpi_1)(\tau) = \int_0^1 \aleph(\tau,s_1)\mathtt{Q}(s_1)\mathtt{g}_1\left[\int_0^1 \aleph(s_1,s_2)\mathtt{Q}(s_2)\mathtt{g}_2\left[\int_0^1 \aleph(s_2,s_3)\mathtt{Q}(s_3)\mathtt{g}_4\cdots\right.\right.$$
$$\left.\left.\mathtt{g}_{\ell-1}\left[\int_0^1 \aleph(s_{\ell-1},s_\ell)\mathtt{Q}(s_\ell)\mathtt{g}_\ell\big(\varpi_1(s_\ell)\big)ds_\ell\right]\cdots\right]ds_3\right]ds_2\Bigg]ds_1$$
$$\geq \mathtt{B}_k.$$

Thus, if $\varpi_1 \in \mathcal{P}_{\mathtt{c}_k}\cap\partial\Lambda_{2,k}$, then

$$\|\Omega\varpi_1\| \geq \|\varpi_1\|. \tag{3.2}$$

It is evident that $0\in\Lambda_{2,k}\subset\overline{\Lambda}_{2,k}\subset\Lambda_{1,k}$. From (3.1),(3.2), it follows from Theorem 3.1 that the operator Ω has a fixed point $\varpi_1^{[k]}\in\mathcal{P}_{\mathtt{c}_k}\cap\big(\overline{\Lambda}_{1,k}\backslash\Lambda_{2,k}\big)$ such that $\varpi_1^{[k]}(\tau)\geq 0$ on $(0,1)$, and $k\in\mathbb{N}$. Next setting $\varpi_{\ell+1}=\varpi_1$, we obtain denumerably many positive radius solutions $\{(\varpi_1^{[k]},\varpi_2^{[k]},\cdots,\varpi_\ell^{[k]})\}_{k=1}^{\infty}$ of (1.3) given iteratively by

$$\varpi_{\mathtt{j}}(\tau) = \int_0^1 \aleph(\tau,s)\mathtt{Q}(s)\mathtt{g}_{\mathtt{j}}(\varpi_{\mathtt{j}+1}(s))ds,\ \mathtt{j}=1,2,\cdots,\ell-1,\ell,$$
$$\varpi_{\ell+1}(\tau)=\varpi_1(\tau).$$

The proof is completed. □

For $\sum_{i=1}^n \mathtt{p}_i = 1$, we have the following theorem.

Theorem 3.4. *Suppose* $(\mathcal{H}_1)-(\mathcal{H}_3)$ *hold, let* $\{\mathtt{c}_k\}_{k=1}^{\infty}$ *be a sequence with* $\tau_{k+1}<\mathtt{c}_k<\tau_k$. *Let* $\{\mathtt{A}_k\}_{k=1}^{\infty}$ *and* $\{\mathtt{B}_k\}_{k=1}^{\infty}$ *be such that*

$$\mathtt{A}_{k+1}<\pi(\mathtt{c}_k)\mathtt{B}_k<\mathtt{S}_k<\eta\mathtt{B}_k<\mathtt{A}_k,\ k\in\mathbb{N},$$

Further, assume that $\mathtt{g}_{\mathtt{j}}$ *satisfies* $(\mathcal{J}_2)$ *and*
$(\mathcal{J}_3)$ $\mathtt{g}_{\iota}(\varpi(\tau))\leq \mathtt{N}_2\mathtt{A}_k$ *for all* $0\leq\varpi(\tau)\leq\mathtt{A}_k$, $\tau\in[0,1]$, *where*

$$\mathtt{N}_2<\min\left\{\left[a^2\|\aleph\|_\infty\prod_{i=1}^n\|\mathtt{Q}_i\|_{\mathtt{p}_i}\right]^{-1},\ \eta\right\}.$$

The iterative system (1.2) *has denumerably many positive radial solutions* $\{(\varpi_1^{[k]},\varpi_2^{[k]},\cdots,\varpi_\ell^{[k]})\}_{k=1}^{\infty}$ *such that* $\varpi_{\mathtt{j}}^{[k]}(\tau)\geq 0$ *on* $(0,1)$, $\mathtt{j}=1,2,\cdots,\ell$ *and* $k\in\mathbb{N}$.

Proof. Let $\Lambda_{1,k}$ be as in the proof of Theorem 3.3 and let $\varpi_1\in\mathcal{P}_{\mathtt{c}_k}\cap\partial\Lambda_{2,k}$. Again $\varpi_1(\tau)\leq\mathtt{A}_k=\|\varpi_1\|$, for all $\tau_1\in[0,1]$. By $(\mathcal{J}_3)$ and $0<\tau_{\ell-1}<1$, we have

$$\int_0^1 \aleph(s_{\ell-1},s_\ell)\mathtt{Q}(s_\ell)\mathtt{g}_\ell\big(\mathtt{u}_1(s_\ell)\big)ds_\ell$$
$$\leq\int_0^1\aleph(s_\ell,s_\ell)\mathtt{Q}(s_\ell)\mathtt{g}_\ell\big(\mathtt{u}_1(s_\ell)\big)ds_\ell$$
$$\leq\mathtt{N}_2\mathtt{A}_k\int_0^1\aleph(s_\ell,s_\ell)\mathtt{Q}(s_\ell)ds_\ell$$
$$\leq\mathtt{N}_2\mathtt{A}_k a^2\int_0^1\aleph(s_\ell,s_\ell)\mathtt{r}^{2(n-1)}\big(a(1-s_\ell)\big)\prod_{i=1}^n\mathtt{Q}_i(s_\ell)ds_\ell$$
$$\leq\mathtt{N}_2\mathtt{A}_k a^2\|\aleph\|_\infty\prod_{i=1}^n\|\mathtt{Q}_i\|_{\mathtt{p}_i}$$
$$\leq\mathtt{A}_k.$$

Continuing with this bootstrapping argument, we get

$$(\Omega\varpi_1)(\tau) = \int_0^1 \aleph(\tau,s_1)\mathtt{Q}(s_1)\mathtt{g}_1\left[\int_0^1 \aleph(s_1,s_2)\mathtt{Q}(s_2)\mathtt{g}_2\left[\int_0^1 \aleph(s_2,s_3)\mathtt{Q}(s_3)\mathtt{g}_4\cdots \right.\right.$$
$$\left.\left.\mathtt{g}_{\ell-1}\left[\int_0^1 \aleph(s_{\ell-1},s_\ell)\mathtt{Q}(s_\ell)\mathtt{g}_\ell\big(\varpi_1(s_\ell)\big)ds_\ell\right]\cdots\right]ds_3\right]ds_2\Big]ds_1$$
$$\leq \mathtt{A}_k.$$

Thus, $\|\Omega\varpi_1\| \leq \|\varpi_1\|$, for $\varpi_1 \in \mathcal{P}_{\mathtt{c}_k}\cap\partial\Lambda_{1,k}$. Rest of the proof is similar to the proof of Theorem 3.3. Hence, the theorem. □

Finally, we deal with the case $\sum_{i=1}^n \mathtt{p}_i > 1$.

Theorem 3.5. *Suppose* $(\mathcal{H}_1)-(\mathcal{H}_3)$ *hold, let* $\{\mathtt{c}_k\}_{k=1}^\infty$ *be a sequence with* $\tau_{k+1} < \mathtt{c}_k < \tau_k$. *Let* $\{\mathtt{A}_k\}_{k=1}^\infty$ *and* $\{\mathtt{B}_k\}_{k=1}^\infty$ *be such that*

$$\mathtt{A}_{k+1} < \pi(\mathtt{c}_k)\mathtt{B}_k < \mathtt{S}_k < \eta\mathtt{B}_k < \mathtt{A}_k,\ k\in\mathbb{N},$$

Further, assume that $\mathtt{g}_\mathtt{j}$ *satisfies* $(\mathcal{J}_2)$ *and*
$(\mathcal{J}_4)$ $\mathtt{g}_\mathtt{j}(\varpi(\tau)) \leq \mathtt{N}_3\mathtt{A}_k$ *for all* $0\leq \mathtt{u}(\tau)\leq \mathtt{A}_k$, $\tau\in[0,1]$, *where*

$$\mathtt{N}_3 < \min\left\{\left[a^2\|\aleph\|_\infty\prod_{i=1}^n\|\mathtt{Q}_i\|_1\right]^{-1},\ \eta\right\}.$$

The iterative system (1.2) *has denumerably many positive radial solutions* $\{(\varpi_1^{[k]},\varpi_2^{[k]},\cdots,\varpi_\ell^{[k]})\}_{k=1}^\infty$ *such that* $\varpi_\mathtt{j}^{[k]}(\tau)\geq 0$ *on* $(0,1)$, $\mathtt{j}=1,2,\cdots,\ell$ *and* $k\in\mathbb{N}$.

Proof. The proof of the present theorem is similar to the proofs of Theorem 3.3 and Theorem 3.4. So, we omit details here. □

4 Application

In this section, we provide an example to illustrate the applicability of main results.

Example 4.1. Consider the following fractional order boundary value problem,

$$\left.\begin{aligned} \Delta\mathtt{u}_\mathtt{j} + \mathtt{P}(|\mathtt{x}|)\mathtt{g}_\mathtt{j}(\mathtt{u}_{\mathtt{j}+1}) = 0,\ 1<|\mathtt{x}|<2,\\ \mathtt{u}_\mathtt{j} = 0 \ \text{ on } \ |\mathtt{x}|=1 \text{ and } |\mathtt{x}|=2,\\ \mathtt{u}_\mathtt{j} = 0 \ \text{ on } \ |\mathtt{x}|=1 \text{ and } \frac{\partial\mathtt{u}_\mathtt{j}}{\partial\mathtt{r}} = 0 \text{ on } |\mathtt{x}|=2,\\ \frac{\partial\mathtt{u}_\mathtt{j}}{\partial\mathtt{r}} = 0 \ \text{ on } \ |\mathtt{x}|=1 \text{ and } \mathtt{u}_\mathtt{j} = 0 \text{ on } |\mathtt{x}|=2, \end{aligned}\right\} \tag{4.1}$$

where $\mathtt{j}\in\{1,2\}$, $\mathtt{u}_3=\mathtt{u}_1$. Let $N=3$ and $\alpha=\beta=\gamma=\delta=1$. Then $d=3$. Now by simple calculations, we get $a=-\frac{1}{2}$ and $r(\tau)=\frac{2}{1-2\tau}$,

$$\mathtt{Q}(\tau) = \frac{1}{4}\left[\frac{2}{2-\tau}\right]^4\prod_{i=1}^2\mathtt{Q}_i(\tau),\ \ \mathtt{Q}_i(\tau) = \mathtt{P}_i\left(\frac{2}{2-\tau}\right),$$

in which

$$\mathtt{P}_1(t) = \frac{1}{|t-1|} \quad \text{and} \quad \mathtt{P}_2(t) = \frac{1}{|t-\frac{1}{2}|},$$

$$\mathtt{g}_{\mathtt{j}}(\varpi)=\begin{cases}0.1\times10^{-4}, & \varpi\in(10^{-4},+\infty),\\ \frac{28\times10^{-(4k+2)}-0.1\times10^{-4k-10}}{10^{-(4k+2)}-10^{-4k}}(\mathtt{u}-10^{-4k})+0.1\times10^{-4k-10}, & \\ \qquad\qquad \varpi\in\left[10^{-(4k+2)},10^{-4k}\right], & \\ 28\times10^{-(4k+2)}, & \varpi\in\left(\frac{1}{5}\times10^{-(4k+2)},10^{-(4k+2)}\right),\\ \frac{28\times10^{-(4k+2)}-0.1\times10^{-(4k+4)}}{\frac{1}{5}\times10^{-(4k+2)}-10^{-(4k+4)}}(\varpi-10^{-(4k+4)})+0.1\times10^{-(4k+4)}, & \\ \qquad\qquad \varpi\in\left(10^{-(4k+4)},\frac{1}{5}\times10^{-(4k+2)}\right], & \\ 0, & \varpi=0,\end{cases}$$

$\mathtt{j}=1,2$. Let

$$\tau_k=\frac{31}{64}-\sum_{r=1}^{k}\frac{1}{4(r+1)^4},\ \mathtt{c}_k=\frac{1}{2}(\tau_k+\tau_{k+1}),\ k=1,2,3,\cdots,$$

then

$$\mathtt{c}_1=\frac{15}{32}-\frac{1}{648}<\frac{15}{32}$$

and

$$\tau_{k+1}<\mathtt{c}_k<\tau_k,\ \pi(\mathtt{c}_k)=\frac{1+\mathtt{c}_k}{2}>\frac{1}{5}.$$

It is easy to see

$$\tau_1=\frac{15}{32}<\frac{1}{2},\ \tau_k-\tau_{k+1}=\frac{1}{4(k+2)^4},\ k=1,2,3,\cdots.$$

Since $\sum_{k=1}^{\infty}\frac{1}{k^4}=\frac{\pi^4}{90}$ and $\sum_{k=1}^{\infty}\frac{1}{k^2}=\frac{\pi^2}{6}$, it follows that

$$\tau^*=\lim_{k\to\infty}\tau_k=\frac{31}{64}-\sum_{i=1}^{\infty}\frac{1}{4(i+1)^4}=\frac{47}{64}-\frac{\pi^4}{360}>\frac{1}{5},$$

Also, $\mathtt{P}_1,\mathtt{P}_2\in L^{\mathtt{p}}[0,1]$, $\prod_{i=1}^{2}\mathtt{Q}_i^*=2$, and

$$\pi(\mathtt{c}_1)a^2\prod_{i=1}^{n}\mathtt{Q}_i^*\int_{\mathtt{c}_1}^{1-\mathtt{c}_1}\aleph(s,s)\mathtt{r}^{2(N-1)}\big(a(1-s)\big)ds\approx0.03636905790.$$

$$\eta=\max\left\{\left[\pi(\mathtt{c}_1)a^2\prod_{i=1}^{n}\mathtt{Q}_i^*\int_{\mathtt{c}_1}^{1-\mathtt{c}_1}\aleph(s,s)\mathtt{r}^{2(N-1)}\big(a(1-s)\big)ds\right]^{-1},\ 1\right\}\approx27.49590057.$$

and let $\mathtt{q}=2,\mathtt{p}_1=\mathtt{p}_2=1/4$, then $\|\aleph\|_q=4.230401435$, $\|\mathtt{Q}_1\|_{p_1}=4.895788358$, $\|\mathtt{Q}_2\|_{p_2}=1.199795099$, and

$$\mathtt{N}_1<\left[a^2\|\aleph\|_q\prod_{i=1}^{n}\|\mathtt{Q}_i\|_{p_i}\right]^{-1}\approx0.1609713891.$$

So, let $\mathtt{N}_1=0.15$. In addition if we take

$$\mathtt{A}_k=10^{-4k},\ \mathtt{B}_k=10^{-(4k+2)},$$

then

$$\begin{aligned}\mathtt{A}_{k+1} = 10^{-(4k+4)} &< \frac{1}{5} \times 10^{-(4k+2)} < \mathtt{c}_k \mathtt{B}_k \\ &< \mathtt{B}_k = 10^{-(4k+2)} < \mathtt{A}_k = 10^{-4k},\end{aligned}$$

and $\mathtt{g}_1, \mathtt{g}_2$ satisfies the following growth conditions:

$$\mathtt{g}_{\mathtt{j}}(\varpi) \leq \mathtt{N}_1 \mathtt{A}_k = 0.15 \times 10^{-4k}, \quad \varpi \in \left[0, 10^{-4k}\right],$$

$$\mathtt{g}_{\mathtt{j}}(\varpi) \geq \eta \mathtt{B}_k = 27.49590057 \times 10^{-(4k+2)}, \quad \varpi \in \left[\frac{1}{5} \times 10^{-(4k+2)}, 10^{-(4k+2)}\right].$$

Then all the conditions of Theorem 3.3 are satisfied. Therefore, by Theorem 3.3, the boundary value problem (4.1) has denumerably many positive radial solutions $\{(\varpi_1^{[k]}, \varpi_2^{[k]})\}_{k=1}^{\infty}$ such that $10^{-(4k+2)} \leq \|\varpi_{\mathtt{j}}^{[k]}\| \leq 10^{-4k}$ for each $k = 1, 2, 3, \cdots$, and $\mathtt{j} = 1, 2$.

References

[1] A. Aberqi, J. Bennouna and M. Elmassoudi, Nonlinear elliptic equations with some measure data in Musielak-Orlicz spaces, *Nonlinrear Dyn. Syst. Theory* **19**(2), 227–242 (2019).

[2] Y. Akdim, M. Rhoudaf and A. Salmani, Existence of solution for nonlinear anisotropic degenerated elliptic unilateral problems, *Nonlinrear Dyn. Syst. Theory* **18**(3), 213–224 (2018).

[3] J. Ali, K. Brown and R. Shivaji, Positive solutions for $n \times n$ elliptic systems with combined nonlinear effects, *Differ. Integral Equ.* **24**(3-4), 307–324 (2011).

[4] J. Ali and S. Padhi, Existence of multiple positive radial solutions to elliptic equations in an annulus, *Com. App. Anal.* **22**(4), 695–710 (2018).

[5] J. Ali, R. Shivaji and M. Ramaswamy, Multiple positive solutions for classes of elliptic systems with combined nonlinear effects, *Differ. Integral Equ.* **19**(6), 669–680 (2006).

[6] R. Dalmasso, Existence and uniqueness of positive solutions of semilinear elliptic systems, *Nonlinear Anal.* **39**(5), 559–568 (2000).

[7] X. Dong and Y. Wei, Existence of radial solutions for nonlinear elliptic equations with gradient terms in annular domains, *Nonlinear Anal.* **187**, 93–109 (2019).

[8] D. Guo and V. Lakshmikantham, *Nonlinear Problems in Abstract Cones*, Academic Press, San Diego, (1988).

[9] D. D. Hai, Uniqueness of positive solutions for semilinear elliptic systems, *J. Math. Anal. Appl.* **313**(2), 761–767 (2006).

[10] D. D. Hai, R. Shivaji, An existence result on positive solutions for a class of semilinear elliptic systems, *Proc. R. Soc. Edinb.*, Sect. A **134**(1), 137–141 (2004).

[11] D. D. Hai and R. Shivaji, Uniqueness of positive solutions for a class of semipositone elliptic systems, *Nonlinear Anal.* **66**(2), 396–402 (2007).

[12] R. Kajikiya and E. Ko, Existence of positive radial solutions for a semipositone elliptic equation, *J. Math. Anal. Appl.* **484**, 123735 (2020).

[13] K. Lan and J. R. L. Webb, Positive solutions of semilinear differential equations with singularities, *J. Differ. Equ.* **148**, 407–421 (1998).

[14] Y. H. Lee, Multiplicity of positive radial solutions for multiparameter semilinear elliptic systems on an annulus. *J. of Differ. Equ.* **174**(2), 420–441 (2001).

[15] S. Padhi, J. R. Graef and A. Kanaujiya, Positive solutions to nonlinear elliptic equations depending on a parameter with Dirichlet boundary conditions. Differ. Equ. Dyn. Syst. (2019). https://doi.org/10.1007/s12591-019-00481-z.

[16] B. Son and P. Wang, Positive radial solutions to classes of nonlinear elliptic systems on the exterior of a ball, *J. Math. Anal. Appl.* **488**, 124069 (2020).

Author information

K. Rajendra Prasad, Department of Applied Mathematics, College of Science and Technology, Andhra University, Visakhapatnam, 530003, India.
E-mail: rajendra92@rediffmail.com

Mahammad Khuddush, Department of Mathematics, Dr. Lankapalli Bullayya College, Resapuvanipalem, Visakhapatnam, 530013, Andhra Pradesh, India.
E-mail: khuddush89@gmail.com

B. Bharathi, Department of Mathematics, College of Engineering for Women, Gayatri Vidya Parishad, Visakhapatnam, 530048, India.
E-mail: bharathi0401@gmail.com

Received: August 23, 2020.
Accepted: November 8, 2020.

Existence of solutions for n-dimensional fractional order bvp with ∞–point boundary conditions via the concept of measure of noncompactness

D. William John Victor[1] and Mahammad Khuddush[2]

[1]Department of Mathematics, A. M. A. L. College, Anakapalle, Kotturu Junction, Visakhapatnam, 531001, India
[2]Department of Mathematics, Dr. Lankapalli Bullayya College, Visakhapatnam, 530013, India

E-mail: dwjvictor69@gmail.com[1], khuddush89@gmail.com[2]

Communicating editor - Managing editors' group

Abstract

In this paper, using the concept of measure of noncompactness we present some results on the existence of n-fixed points for a class of operators. Also as an application, we derive the sufficient conditions for the existence of solutions for n-dimensional fractional order functional boundary value problems.

2010 Mathematics Subject Classification. **47H10**. 34A08, 47H09, 18B40, 34B15.
Keywords. measure of noncompactness, functional differential equation, Caputo fractional derivative, n-fixed point, fixed point theorem.

1 Introduction

Measures of noncompactness play an important role in fixed point theory and have many applications in various branches of nonlinear analysis, including differential equations, integral and integro-differential equations, optimization, etc. Roughly speaking, a measure of noncompactness is a function defined on the family of all nonempty and bounded subsets of a certain metric space such that it is equal to zero on the whole family of relatively compact sets. The concept of measure of noncompactness was first introduced by Kuratowski [14] in 1930. In 1955, the Italian mathematician Darbo [11] used the Kuratowski measure in order to investigate a class of operators (condensing operators) whose properties can be characterized as being intermediate between those of contraction and compact mappings. Darbo's fixed point theorem is useful in establishing existence results for different classes of operator equations. For details on various measures of noncompactness see [6].

The theory of fractional differential equations has gained remarkable popularity and significance during last few years and has become an important field of investigation due to its attractive applications in various branches of chemistry, physics, polymer rheology, aerodynamics, electrodynamics of complex medium, etc. Fractional order differential equations also serve as an excellent tool for the hereditary properties and description of memory in various materials. Fractional differential equations have been used for mathematical modeling in potential fields, signal processing, viscoelastic materials, diffusion problems, heat propagation, control theory and many others. In recent years, there are certain papers and monographs dealing with the existence and uniqueness solutions of fractional order nonlinear boundary value problems, see ([4, 12, 13, 18–21, 23]).

Existence of solutions for fractional differential equations has been investigated by many authors in various types. Recently, Borisut et al [9] studied fractional order boundary value problem based on Kransnoselskiis fixed point theorem and Darbos fixed point theorem together and the idea of the

Advanced Studies: Euro-Tbilisi Mathematical Journal 14(4) (2021), pp. 19–37.
DOI: 10.3251/asetmj/19322008202
Tbilisi Centre for Mathematical Sciences.
Received by the editors: 15 October 2020.
Accepted for publication: 30 October 2021.

measure of noncompactness. Aghajani et al. [2] proved the solvability of a large class of nonlinear fractional integro-differential equations by establishing some fractional integral inequalities and using the nonlinear alternative of Leray-Schauder type. Benchohra et al. [7] investigated a class of boundary value problems for fractional differential equations involving nonlinear integral conditions using the technique associated with measures of weak noncompactness. Lie et al. [16] studied on the existence of mild solutions for fractional semilinear differential equations with nonlocal conditions. Wang et al. [22] applied a new variant flxed point theorem to investigate some fractional differential equations in Banach spaces. Liang et al. [17] studied the solvability for a coupled system of nonlinear fractional difierential equations in a Banach space using the measures of noncompactness and the well known fixed point theorem of Monch type.

Motivated by aforementioned works, in this paper we study n-dimensional Riemann-Liouville fractional order functional differential equation with infinite-point boundary conditions

$$\left.\begin{aligned}
&\mathfrak{D}^a_{0+}\big[\mathrm{z}_1-\varphi\big(t,\mathrm{z}_1(\zeta(t)),\mathrm{z}_2\big(\zeta(t)\big),\cdots,\mathrm{z}_n\big(\zeta(t)\big)\big)\big]\\
&\qquad=\Upsilon\Big(t,\mathrm{z}_1\big(\vartheta(t)\big),\mathrm{z}_2\big(\vartheta(t)\big),\cdots,\mathrm{z}_n\big(\vartheta(t)\big)\Big)\\
&\mathfrak{D}^a_{0+}\big[\mathrm{z}_2-\varphi\big(t,\mathrm{z}_2(\zeta(t)),\mathrm{z}_1\big(\zeta(t)\big),\cdots,\mathrm{z}_n\big(\zeta(t)\big)\big)\big]\\
&\qquad=\Upsilon\Big(t,\mathrm{z}_2\big(\vartheta(t)\big),\mathrm{z}_1\big(\vartheta(t)\big),\cdots,\mathrm{z}_n\big(\vartheta(t)\big)\Big)\\
&\qquad\vdots\\
&\mathfrak{D}^a_{0+}\big[\mathrm{z}_n-\varphi\big(t,\mathrm{z}_n,(\zeta(t)),\mathrm{z}_2\big(\zeta(t)\big),\cdots,\mathrm{z}_1\big(\zeta(t)\big)\big)\big]\\
&\qquad=\Upsilon\Big(t,\mathrm{z}_n\big(\vartheta(t)\big),\mathrm{z}_2\big(\vartheta(t)\big),\cdots,\mathrm{z}_1\big(\vartheta(t)\big)\Big)
\end{aligned}\right\}\tag{1.1}$$

$$\sum_{k=1}^{\infty}\xi_k\mathrm{z}_i\big(\sigma(\tau_k)\big)=\delta,\quad 1\le i\le n,\tag{1.2}$$

where $\xi_k>0,\ \tau_k\in(0,1),\ \sigma(\tau_k)\le\tau_k$ for $k\in\mathbb{N},\ \delta\in\mathbb{R}$ and $\mathfrak{D}^a_{0+}$ is Caputo fractional derivative of order $1<a\le 2$.

The rest of the paper is organized in the following fashion. In Section 2, we provide some definitions and lemmas which will be useful in our main results. Later, we construct Green's function for the homogeneous boundary value problem corresponding to (1.1)-(1.2). In Section 3, we study existence and uniqueness of n-fixed point theorems for contractive type mappings in partially ordered complete metric spaces. In Section 4, we study existence and uniqueness of solution of the hybrid boundary value problem (1.1)-(1.2) as an application n-fixed point theorem.

2 Preliminaries

In this section, we present some definitions and lemmas on fractional calculus and the concept of measure of noncompactness, which will be useful in the sequel.

Let $C(I)$ be the space of continuous functions defined on I with the norm given by

$$\|\mathrm{z}\|=\sup_{t\in I}|\mathrm{z}(t)|.$$

In addition, let $L_1(I)$ denote the class of the Lebesgue integrable functions on the interval $I=[0,1]$

with the norm given by

$$\|\mathrm{z}\|_{L_1} = \int_0^1 \mathrm{z}(s)ds.$$

Throughout the paper we assume that X is a Banach space. For a subset E of X, the closure and convex hull of E in X are denoted by $\overline{E}$ and $conv(E)$, respectively. Let $\overline{\mathscr{B}}_r$ denote the closed ball in X centered at zero and with radius r and $\mathscr{B}(\mathrm{z}_0, r)$ denotes the closed ball centered at z_0 with radius r. Further, we denote the family of nonempty bounded subsets of X by $\mathfrak{M}_X$ and $\mathfrak{N}_X$ is the subfamily consisting of all relatively compact subsets of X.

Definition 2.1. [13] The Riemann-Liouville fractional integral of order γ for a function f is defined as

$$I_{0^+}^{\gamma} f(t) = \frac{1}{\Gamma(\gamma)} \int_0^t (t-s)^{\gamma-1} f(s)ds, \ \gamma > 0.$$

Definition 2.2. [13] The standard RiemannLiouville fractional derivative of order $\gamma > 0$ for a function f is defined as

$$\mathfrak{D}_{0^+}^{\gamma} f(t) = \frac{1}{\Gamma(m-\gamma)} \Big(\frac{d}{dt}\Big)^m \int_0^t (t-s)^{m-\gamma-1} f(s)ds, \ m = [\gamma] + 1,$$

where $[\gamma]$ denotes the integer part of γ.

Lemma 2.3. [13] The general solution to $\mathbb{D}_{0^+}^{\gamma} y(t) = 0$ with $\gamma \in (m-1, m]$ and $m > 1$ is the function

$$y(t) = c_1 t^{\gamma-1} + c_2 t^{\gamma-2} + \cdots + c_m t^{\gamma-m}, \ c_i \in \mathbb{R}, \ i = 1, 2, \cdots, m.$$

Lemma 2.4. [13] Let $\gamma > 0$. Then the following equality holds for $y(t)$:

$$\mathfrak{D}_{0^+}^{-\gamma} \mathfrak{D}_{0^+}^{\gamma} y(t) = y(t) + c_1 t^{\gamma-1} + c_2 t^{\gamma-2} + \cdots + c_m t^{\gamma-m}, \ c_i \in \mathbb{R}, \ i = 1, 2, \cdots, m$$

and m is the smallest integer greater than or equal to γ.

Lemma 2.5. Let $\theta(t) \in C([0,1], \mathbb{R})$ and $\sum_{k=1}^{m} \xi_k \sigma(\tau_k) = \mathfrak{Z}_m^{-1}$. Suppose the series $\sum_{k=1}^{\infty} \xi_k \sigma(\tau_k) = \mathfrak{Z}_{\infty}^{-1}$ is convergent. Then fractional order boundary value problem

$$\mathfrak{D}_{0^+}^{a} \big(\mathrm{z} - \varphi(t, \mathrm{z}(\zeta(t))\big) = \theta(t), \quad 1 < a \leq 2, \tag{2.1}$$

satisfying infinite-point boundary conditions

$$\mathrm{z}_k(0) = 0, \quad \sum_{k=1}^{\infty} \xi_k \mathrm{z}\big(\sigma(\tau_k)\big) = \delta, \tag{2.2}$$

where $\xi_k > 0,\ \tau_k \in (0,1),\ \sigma(\tau_k) \le \tau_k$ for $k \in \mathbb{N},\ \delta \in \mathbb{R}$ has a unique solution

$$\left.\begin{aligned} \mathrm{z}(t) =& \varphi\big(t, \mathrm{z}(\zeta(t))\big) + \int_0^t \frac{(t-s)^{a-1}}{\Gamma(a)}\theta(s)ds - \varphi\big(0, \mathrm{z}(\zeta(0))\big) \\ &- \mathfrak{Z}_\infty t \sum_{k=1}^{\infty} \xi_k \varphi\big(\sigma(\tau_k), \mathrm{z}(\zeta(\sigma(\tau_k)))\big) \\ &- \mathfrak{Z}_\infty t \sum_{k=1}^{\infty} \xi_k \int_0^{\sigma(\tau_k)} \frac{(\sigma(\tau_k)-s)^{a-1}}{\Gamma(a)}\theta(s)ds \\ &+ \mathfrak{Z}_\infty t \sum_{k=1}^{\infty} \xi_k \varphi\big(0, \mathrm{z}(\zeta(0))\big) + \mathfrak{Z}_\infty \delta t. \end{aligned}\right\} \tag{2.3}$$

Proof. Let $\mathrm{z}(t)$ be a solution of (2.1). Then by Lemmas 2.3 and 2.4, we get

$$\mathrm{z}(t) = \varphi\big(t, \mathrm{z}(\zeta(t))\big) + \int_0^t \frac{(t-s)^{a-1}}{\Gamma(a)}\theta(s)ds - A - Bt. \tag{2.4}$$

From the first boundary condition, we obtain $A = \varphi\big(0, \mathrm{z}(\zeta(0))\big)$. Before applying second boundary condition, we first apply

$$\sum_{k=1}^{m} \xi_k \mathrm{z}\big(\sigma(\tau_k)\big) = \delta,$$

to get

$$\begin{aligned} B =& \mathfrak{Z}_m \sum_{k=1}^{m} \xi_k \varphi\big(\sigma(\tau_k), \mathrm{z}(\zeta(\sigma(\tau_k)))\big) + \mathfrak{Z}_m \sum_{k=1}^{m} \xi_k \int_0^{\sigma(\tau_k)} \frac{(\sigma(\tau_k)-s)^{a-1}}{\Gamma(a)}\theta(s)ds \\ &- \mathfrak{Z}_m \sum_{k=1}^{m} \xi_k \varphi\big(0, \mathrm{z}(\zeta(0))\big) - \mathfrak{Z}_m \delta. \end{aligned}$$

Substituting A and B values into (2.4), we get

$$\left.\begin{aligned} \mathrm{z}(t) =& \varphi\big(t, \mathrm{z}(\zeta(t))\big) + \int_0^t \frac{(t-s)^{a-1}}{\Gamma(a)}\theta(s)ds - \varphi\big(0, \mathrm{z}(\zeta(0))\big) \\ &- \mathfrak{Z}_m t \sum_{k=1}^{m} \xi_k \varphi\big(\sigma(\tau_k), \mathrm{z}(\zeta(\sigma(\tau_k)))\big) \\ &- \mathfrak{Z}_m t \sum_{k=1}^{m} \xi_k \int_0^{\sigma(\tau_k)} \frac{(\sigma(\tau_k)-s)^{a-1}}{\Gamma(a)}\theta(s)ds \\ &+ \mathfrak{Z}_m t \sum_{k=1}^{m} \xi_k \varphi\big(0, \mathrm{z}(\zeta(0))\big) + \mathfrak{Z}_m \delta t. \end{aligned}\right\} \tag{2.5}$$

Since

$$\big|\xi_k \mathrm{z}\big(\sigma(\tau_k)\big)\big| \le \xi_k \|\mathrm{z}\|$$

and

$$\left|\xi_k \int_0^{\sigma(\tau_k)} \frac{(\sigma(\tau_k)-s)^{a-1}}{\Gamma(a)}\theta(s)ds\right| \leq \frac{\xi_k}{\Gamma(a)}\left|\int_0^1 \theta(s)ds\right| \leq \frac{\xi_k}{\Gamma(a)}\|\theta\|_{L_1},$$

by the comparison test, the series in (2.2),

$$\sum_{k=1}^{\infty} \xi_k \varphi\big(\sigma(\tau_k), \mathrm{z}(\zeta(\sigma(\tau_k)))\big)$$

and

$$\sum_{k=1}^{\infty} \varepsilon_k \int_0^{\sigma(\tau_k)} \frac{(\sigma(\tau_k)-s)^{a-1}}{\Gamma(a)}\theta(s)ds$$

are convergent. So, by taking the limit as $m \to \infty$ in (2.5), we obtain (2.3).

Conversely, from (2.3), we have $\mathrm{z}(0) = 0$ and

$$\begin{aligned}
\sum_{k=1}^{\infty} \xi_k \mathrm{z}\big(\sigma(\tau_k)\big) &= \sum_{k=1}^{\infty} \xi_k \varphi\big(\sigma(\tau_k), \mathrm{z}(\zeta(\sigma(\tau_k)))\big) + \sum_{k=1}^{\infty} \xi_k \int_0^{\sigma(\tau_k)} \frac{(\sigma(\tau_k)-s)^{a-1}}{\Gamma(a)}\theta(s)ds \\
&\quad - \sum_{k=1}^{\infty} \xi_k \varphi\big(0, \mathrm{z}(\zeta(0))\big) - \mathfrak{Z}_\infty \mathfrak{Z}_\infty^{-1} \sum_{k=1}^{\infty} \xi_k \varphi\big(\sigma(\tau_k), \mathrm{z}(\zeta(\sigma(\tau_k)))\big) \\
&\quad - \mathfrak{Z}_\infty \mathfrak{Z}_\infty^{-1} \sum_{k=1}^{\infty} \xi_k \int_0^{\sigma(\tau_k)} \frac{(\sigma(\tau_k)-s)^{a-1}}{\Gamma(a)}\theta(s)ds \\
&\quad + \mathfrak{Z}_\infty \mathfrak{Z}_\infty^{-1} \sum_{k=1}^{\infty} \xi_k \varphi\big(0, \mathrm{z}(\zeta(0))\big) + \mathfrak{Z}_\infty \delta \mathfrak{Z}_\infty^{-1} \\
&= \delta
\end{aligned}$$

Which shows that the solution of the integral equation (2.3) satisfies the differential equation (2.1) under infinite-point boundary conditions (2.2). Q.E.D.

Definition 2.6. [5] A mapping $\mu : \mathfrak{M}_X \to [0, \infty)$ is said to be a measure of noncompactness in X if it satisfies the following conditions,

(C_1) The family $Ker\mu = \{E \in \mathfrak{M}_X : \mu(E) = 0\} \neq \varnothing$ and $Ker\mu \subseteq \mathfrak{N}_X$.

(C_2) $E \subseteq F \implies \mu(E) \leq \mu(F)$.

(C_3) $\mu(\overline{E}) = \mu(E)$.

(C_4) $\mu(conv(E)) = \mu(E)$.

(C_5) $\mu(cE + (1-c)F) \leq c\mu(E) + (1-c)\mu(F)$ for $0 \leq c < 1$.

(C_6) If $\{E_n\}_{n=1}^{\infty}$ be a nonincreasing sequence of closed sets from $\mathfrak{M}_X$ such that $\lim_{n\to\infty} \mu(E_n) = 0$, then $E_\infty = \bigcap_{n=1}^{\infty} E_n \neq \varnothing$.

The subfamily $Ker\mu$ defined in (C_1) represents kernel of the measure of noncompactness μ and since

$$\mu(E_\infty) = \mu\Big(\bigcap_{n=1}^{\infty} E_n\Big) \leq \mu(E_n),$$

it follows that

$$\bigcap_{n=1}^{\infty} E_n = 0.$$

Hence,

$$E_\infty \in Ker\mu.$$

Theorem 2.7. [6] Suppose $\mu_1, \mu_2, \cdots, \mu_n$ are measures of noncompactness in E_1, $E_2, \cdots, E_n$ respectively. Moreover, assume that the function $T : [0,\infty)^n \to [0,\infty)$ is convex and $T(\mathrm{z}_1, \mathrm{z}_2, \cdots, \mathrm{z}_n) = 0$ if and only if $\mathrm{z}_i = 0$ for $i = 1, 2, \cdots, n$. Then

$$\mu(X) = T\big(\mu_1(X_1), \mu_2(X_2), \cdots, \mu_n(X_n)\big)$$

defines a measure of noncompactness in $E_1 \times E_2 \times \cdots \times E_n$ where X_i denotes the natural projection of X into E_i for $i = 1, 2, \cdots, n$.

Theorem 2.8 (Darbo [5])**.** Let E be a nonempty, bounded, closed and convex subset of a Banach space X and let $T : E \to E$ be a continuous mapping. Further, assume that there is a constant $\lambda \in [0, 1)$ such that

$$\mu(T(F)) \leq \lambda\mu(F)$$

for any nonempty set $F \subset E$. Then T has a fixed point.

Theorem 2.9 (Schauder [1])**.** Let E be a closed, convex subset of a normed linear space X. Then every compact, continuous map $T : E \to E$ has at least one fixed point.

3 Multivariate fixed point theorems

In this section, by using the technique of measure of noncompactness we present some results on the existence of n-fixed point theorems for a class of operators.

Let $\mathcal{BC}(\mathbb{R}^+)$ be the set of all real valued bounded continuous functions defined on $\mathbb{R}^+$. We will assume that the space $\mathcal{BC}(\mathbb{R}^+)$ is equipped with the standard supremum norm

$$\|\mathrm{z}\|_{\mathcal{BC}(\mathbb{R}^+)} = \sup\big\{|\mathrm{z}(t)| : t \geq 0\big\}.$$

Let E be nonempty subset of $\mathcal{BC}(\mathbb{R}^+)$ and $\mathfrak{T} > 0$. For $\mathrm{z} \in E$ and $\varepsilon > 0$, define

$$\omega^{\mathfrak{T}}(\mathrm{z}, \varepsilon) = \sup\big\{|\mathrm{z}(t) - \mathrm{z}(s) : t, s \in [0, \mathfrak{T}],\ |t - s| \leq \varepsilon|\big\},$$
$$\omega^{\mathfrak{T}}(E, \varepsilon) = \sup\big\{\omega^{\mathfrak{T}}(\mathrm{z}, \varepsilon) : \mathrm{z} \in E\big\},$$

Taking into account the fact that the function $\varepsilon \to \omega^{\mathfrak{T}}(E, \varepsilon)$ is nondecreasing, we infer that there exists a finite limit $\lim_{\varepsilon\to 0} \omega^{\mathfrak{T}}(E, \varepsilon)$. Thus, we can put

$$\omega_0^{\mathfrak{T}}(E, \varepsilon) = \lim_{\varepsilon\to 0} \omega^{\mathfrak{T}}(E, \varepsilon),$$

we also define the quantity $\omega_0(E)$ in the following way:

$$\omega_0(E) = \lim_{\mathfrak{T}\to\infty} \omega_0^{\mathfrak{T}}(E, \varepsilon).$$

For a fixed $t \in \mathbb{R}^+$, denote

$$E(t) = \{\mathrm{z}(t) : \mathrm{z} \in E\}.$$

Now, consider the function μ defined on $\mathfrak{M}_{\mathcal{BC}(\mathbb{R}^+)}$ by

$$\mu(E) = \omega_0(E) + \limsup_{t\to\infty} diam(E(t)), \tag{3.1}$$

where

$$diam(E(t)) = \sup\{|\mathrm{y}(t) - \mathrm{z}(t)| : \mathrm{y}, \mathrm{z} \in E\}.$$

It can be seen from [5,6] that the function $\mu(E)$ defines a measure of noncompactness. The $ker\mu$ of this measure contains nonempty and bounded sets E such that functions belonging to E are locally equicontinuous on $\mathbb{R}^+$ and the thickness of the bundle formed by functions from E tends to zero at infinity [3].

Before presenting our first result, we assume throughout this section that Λ is a nonempty, bounded, closed and convex subset of X and

$$\Omega = \{\varrho : [0,\infty) \to [0,\infty)/\varrho \ \text{ is increasing and } \lim_{k\to\infty} \varrho^k(t) = 0 \ \text{ for each } \ t > 0\}.$$

Theorem 3.1. Let $\mathcal{F} : \Lambda^n \to \Lambda$ be a continuous function such that

$$\mu\left(\mathcal{F}\left(\prod_{k=1}^{n} E_k\right)\right) \leq \alpha \max_{1\leq k\leq n} \mu(E_k) \tag{3.2}$$

for any $E_k \subset \Lambda (1 \leq k \leq n)$, where μ is an arbitrary measure of noncompactness and α is a constant with $0 \leq \alpha < 1$. Then $\mathcal{F}$ has an n-fixed point.

Proof. Let us first consider $F(\mathrm{z}_1, \mathrm{z}_2, \cdots, \mathrm{z}_n) = \max\{\mathrm{z}_k : 1 \leq k \leq n\}$ for any $(\mathrm{z}_1, \mathrm{z}_2, \cdots, \mathrm{z}_n) \in [0,\infty)^n$. Then it can be easily verified that all conditions of Theorem 2.7 satisfies. Therefore, $\widetilde{\mu}(E) = \max\{\mu(E_k) : 1 \leq k \leq n\}$ is a measure of noncompactness in the space X^n where E_k $(1 \leq k \leq n)$ denote the natural projections of E. Next, define the map $\widetilde{\mathcal{F}} : \Lambda^n \to \Lambda^n$ by

$$\widetilde{\mathcal{F}}(\mathrm{z}_1, \mathrm{z}_2, \cdots, \mathrm{z}_n) = \begin{pmatrix} \mathcal{F}(\mathrm{z}_1, \mathrm{z}_2, \mathrm{z}_3, \cdots, \mathrm{z}_n) \\ \mathcal{F}(\mathrm{z}_2, \mathrm{z}_1, \mathrm{z}_3, \cdots, \mathrm{z}_n) \\ \mathcal{F}(\mathrm{z}_3, \mathrm{z}_2, \mathrm{z}_1, \cdots, \mathrm{z}_n) \\ \vdots \\ \mathcal{F}(\mathrm{z}_n, \mathrm{z}_2, \mathrm{z}_3, \cdots, \mathrm{z}_1) \end{pmatrix}^T.$$

Since $\mathcal{F}$ is continuous on Λ^n, it follows that $\widetilde{\mathcal{F}}$ is continuous on Λ^n. Let E be a nonempty subset

of Λ^n. Then, by (C_2) and (3.2), we have

$$\begin{aligned}
\widetilde{\mu}\big(\widetilde{\mathcal{F}}(E)\big) &\leq \widetilde{\mu}\begin{pmatrix}\mathcal{F}(E_1\times E_2\times E_3\times\cdots\times E_n)\\ \mathcal{F}(E_2\times E_1\times E_3\times\cdots\times E_n)\\ \mathcal{F}(E_3\times E_2\times E_1\times\cdots\times E_n)\\ \vdots\\ \mathcal{F}(E_n\times E_2\times E_3\times\cdots\times E_1)\end{pmatrix}^T\\
&\leq \max\Big\{\mu\big(\mathcal{F}(E_1\times E_2\times E_3\times\cdots\times E_n)\big),\mu\big(\mathcal{F}(E_2\times E_1\times E_3\times\cdots\times E_n)\big),\\
&\quad \mu\big(\mathcal{F}(E_3\times E_2\times E_1\times\cdots\times E_n)\big),\cdots,\mu\big(\mathcal{F}(E_n\times E_2\times E_3\times\cdots\times E_1)\big)\Big\}\\
&\leq \max\Big\{\alpha\max\{\mu(E_1),\mu(E_2),\mu(E_3),\cdots,\mu(E_n)\},\alpha\max\{\mu(E_2),\mu(E_1),\mu(E_3),\cdots,\mu(E_n)\},\\
&\quad \alpha\max\{\mu(E_3),\mu(E_2),\mu(E_1),\cdots,\mu(E_n)\},\cdots,\alpha\max\{\mu(E_n),\mu(E_2),\mu(E_3),\cdots,\mu(E_1)\}\Big\}\\
&= \alpha\max\{\mu(E_1),\mu(E_2),\mu(E_3),\cdots,\mu(E_n)\}\\
&= \alpha\widetilde{\mu}(E).
\end{aligned}$$

Hence from Darbo fixed point theorem 2.8, $\mathcal{F}$ has n-fixed point. Q.E.D.

Corollary 3.2. Let $\mathcal{F}:\Lambda^n\to\Lambda$ be a continuous function such that

$$\|\mathcal{F}(\mathrm{z}_1,\mathrm{z}_2,\mathrm{z}_3,\cdots,\mathrm{z}_n)-\mathcal{F}(\mathrm{y}_1,\mathrm{y}_2,\mathrm{y}_3,\cdots,\mathrm{y}_n)\|\leq\alpha\max\big\{\|\mathrm{z}_k-\mathrm{y}_k\|:1\leq k\leq n\big\}$$

for any $(\mathrm{z}_1,\mathrm{z}_2,\mathrm{z}_3,\cdots,\mathrm{z}_n),(\mathrm{y}_1,\mathrm{y}_2,\mathrm{y}_3,\cdots,\mathrm{y}_n)\in\Lambda^n$ where $0\leq\alpha<1$ be a constant. Then $\mathcal{F}$ has an n-fixed point.

Proof. We note that the mapping $\mu:\mathfrak{M}_X\to[0,\infty)$ defined by $\mu(E)=diam(E)$ is a measure of noncompactness. Next, let $E_k\subset\Lambda\,(1\leq k\leq n)$ and $(\mathrm{z}_1,\mathrm{z}_2,\mathrm{z}_3,\cdots,\mathrm{z}_n)$, $(\mathrm{y}_1,\mathrm{y}_2,\mathrm{y}_3,\cdots,\mathrm{y}_n)\in\prod_{k=1}^n E_k$. Then

$$\begin{aligned}
\|\mathcal{F}(\mathrm{z}_1,\mathrm{z}_2,\mathrm{z}_3,\cdots,\mathrm{z}_n)-\mathcal{F}(\mathrm{y}_1,\mathrm{y}_2,\mathrm{y}_3,\cdots,\mathrm{y}_n)\| &\leq\alpha\max\big\{\|\mathrm{z}_k-\mathrm{y}_k\|:1\leq k\leq n\big\}\\
&\leq\alpha\max\big\{diam(E_k):1\leq k\leq n\big\}.
\end{aligned}$$

So,

$$diam\left[\mathcal{F}\left(\prod_{k=1}^n E_k\right)\right]\leq\alpha\max\big\{diam(E_k):1\leq k\leq n\big\}.$$

Therefore, by Theorem 3.1, $\mathcal{F}$ has an n-fixed point. Q.E.D.

Lemma 3.3. [3] Let $\varrho\in\Omega$ and $\mathcal{F}:\Lambda\to\Lambda$ be a continuous function satisfying

$$\mu\big(\mathcal{F}(E)\big)\leq\varrho\big(\mu(E)\big)$$

for each $E\subset\Lambda$ where μ is a measure of noncompactness. Then $\mathcal{F}$ has a fixed point.

Theorem 3.4. Let μ be a measure of noncompactness and $\varrho \in \Omega$. Suppose that $\mathcal{F} : \Lambda^n \to \Lambda$ is continuous function such that

$$\mu\left[\mathcal{F}\left(\prod_{k=1}^{n} E_k\right)\right] \leq \varrho\left[\frac{1}{n}\sum_{k=1}^{n}\mu(E_k)\right] \tag{3.3}$$

for all $E_k \subset \Lambda\,(1 \leq k \leq n)$. Then $\mathcal{F}$ has an n-fixed point.

Proof. Define a mapping $\widetilde{\mathcal{F}} : \Lambda^n \to \Lambda^n$ by

$$\widetilde{\mathcal{F}}(\mathrm{z}_1, \mathrm{z}_2, \cdots, \mathrm{z}_n) = \begin{pmatrix} \mathcal{F}(\mathrm{z}_1, \mathrm{z}_2, \mathrm{z}_3, \cdots, \mathrm{z}_n) \\ \mathcal{F}(\mathrm{z}_2, \mathrm{z}_1, \mathrm{z}_3, \cdots, \mathrm{z}_n) \\ \mathcal{F}(\mathrm{z}_3, \mathrm{z}_2, \mathrm{z}_1, \cdots, \mathrm{z}_n) \\ \vdots \\ \mathcal{F}(\mathrm{z}_n, \mathrm{z}_2, \mathrm{z}_3, \cdots, \mathrm{z}_1) \end{pmatrix}^T.$$

Since $\mathcal{F}$ is continuous on Λ^n, it follows that $\widetilde{\mathcal{F}}$ is continuous on Λ^n. Next, consider

$$F(\mathrm{z}_1, \mathrm{z}_2, \cdots, \mathrm{z}_n) = \sum_{k=1}^{n} \mathrm{z}_k$$

for any $(\mathrm{z}_1, \mathrm{z}_2, \cdots, \mathrm{z}_n) \in [0, \infty)^n$. Then it can be easily verified that all conditions of Theorem 2.7 satisfies. Therefore,

$$\widetilde{\mu}(E) = \sum_{k=1}^{n} \mu(E_k)$$

is a measure of noncompactness in the space X^n where $E_k\,(1 \leq k \leq n)$ denote the natural projections of E.

Claim: For any nonempty subset E of Λ^n, $\lambda\big(\mathcal{F}(E)\big) \leq \varrho\big(\lambda(E)\big)$, where $\lambda = \frac{1}{n}\widetilde{\mu}$.

From (C_2) and (3.2), we have

$$\begin{aligned}
\widetilde{\mu}\big(\widetilde{\mathcal{F}}(E)\big) &\leq \widetilde{\mu}\begin{pmatrix}\mathcal{F}(E_1\times E_2\times E_3\times\cdots\times E_n)\\ \mathcal{F}(E_2\times E_1\times E_3\times\cdots\times E_n)\\ \mathcal{F}(E_3\times E_2\times E_1\times\cdots\times E_n)\\ \vdots\\ \mathcal{F}(E_n\times E_2\times E_3\times\cdots\times E_1)\end{pmatrix}^T\\
&\leq \mu\big(\mathcal{F}(E_1\times E_2\times E_3\times\cdots\times E_n)\big)+\mu\big(\mathcal{F}(E_2\times E_1\times E_3\times\cdots\times E_n)\big)\\
&\quad+\mu\big(\mathcal{F}(E_3\times E_2\times E_1\times\cdots\times E_n)\big)\cdots+\mu\big(\mathcal{F}(E_n\times E_2\times E_3\times\cdots\times E_1)\big)\\
&\leq \varrho\left[\frac{\mu(E_1)+\mu(E_2)+\mu(E_3)\cdots+\mu(E_n)}{n}\right]+\varrho\left[\frac{\mu(E_2)+\mu(E_1)+\mu(E_3)\cdots+\mu(E_n)}{n}\right]\\
&+\varrho\left[\frac{\mu(E_3)+\mu(E_2)+\mu(E_1)\cdots+\mu(E_n)}{n}\right]+\cdots+\varrho\left[\frac{\mu(E_n)+\mu(E_2)+\mu(E_3)\cdots+\mu(E_1)}{n}\right]\\
&= n\,\varrho\left[\frac{\mu(E_1)+\mu(E_2)+\mu(E_3)\cdots+\mu(E_n)}{n}\right]\\
&= n\,\varrho\left[\frac{\mu(E)}{n}\right].
\end{aligned}$$

Thus,

$$\frac{1}{n}\widetilde{\mu}\big(\widetilde{\mathcal{F}}(E)\big)\leq\varrho\left[\frac{1}{n}\widetilde{\mu}(E)\right]$$

Hence the claim. Since $\widetilde{\mu}$ is a measure of noncompactness, λ is a measure of noncompactness. Therefore, all the conditions of Lemma 3.3 are satisfied. Hence, $\mathcal{F}$ has an n-fixed point. Q.E.D.

Corollary 3.5. Assume that $\mathcal{F}:\Lambda^n\to\Lambda$ is continuous function such that

$$\mu\left[\mathcal{F}\left(\prod_{k=1}^{n}E_k\right)\right]\leq\frac{\alpha}{n}\left[\sum_{k=1}^{n}\mu(E_k)\right]\tag{3.4}$$

for all $E_k\subset\Lambda\,(1\leq k\leq n)$ and $0\leq\alpha<1$. Then $\mathcal{F}$ has an n-fixed point.

Proof. Let $0\leq\alpha<1$. Define $\varrho(t)=\alpha t$ for each $t\in[0,\infty)$. Then by Theorem 3.4, $\mathcal{F}$ has an n-fixed point. Q.E.D.

Corollary 3.6. Let $\mathcal{F}:\Lambda^n\to\Lambda$ be a continuous function such that

$$\|\mathcal{F}(\mathrm{z}_1,\mathrm{z}_2,\mathrm{z}_3,\cdots,\mathrm{z}_n)-\mathcal{F}(\mathrm{y}_1,\mathrm{y}_2,\mathrm{y}_3,\cdots,\mathrm{y}_n)\|\leq\varrho\left[\sum_{k=1}^{n}\frac{\|\mathrm{z}_k-\mathrm{y}_k\|}{n}\right]$$

for any $(\mathrm{z}_1,\mathrm{z}_2,\mathrm{z}_3,\cdots,\mathrm{z}_n),(\mathrm{y}_1,\mathrm{y}_2,\mathrm{y}_3,\cdots,\mathrm{y}_n)\in\Lambda^n$ and $\varrho\in\Omega$. Then $\mathcal{F}$ has an n-fixed point.

Proof. As discussed in the Corollary 3.2, $\mu : \mathfrak{M}_X \to [0, \infty)$ defined by $\mu(E) = diam(E)$ is a measure of noncompactness. Next, let $E_k \subset \Lambda\,(1 \leq k \leq n)$ and $(\mathrm{z}_1, \mathrm{z}_2, \mathrm{z}_3, \cdots, \mathrm{z}_n)$, $(\mathrm{y}_1, \mathrm{y}_2, \mathrm{y}_3, \cdots, \mathrm{y}_n) \in \prod_{k=1}^{n} E_k$. Then

$$\begin{aligned}\|\mathcal{F}(\mathrm{z}_1, \mathrm{z}_2, \mathrm{z}_3, \cdots, \mathrm{z}_n) - \mathcal{F}(\mathrm{y}_1, \mathrm{y}_2, \mathrm{y}_3, \cdots, \mathrm{y}_n)\| &\leq \varrho\left[\sum_{k=1}^{n} \frac{\|\mathrm{z}_k - \mathrm{y}_k\|}{n}\right] \\ &\leq \varrho\left[\sum_{k=1}^{n} \frac{diam(E_k)}{n}\right].\end{aligned}$$

So,

$$diam\left(\mathcal{F}\left(E\right)\right) \leq \varrho\left[\sum_{k=1}^{n} \frac{diam(E_k)}{n}\right].$$

Hence, by Theorem 3.4, $\mathcal{F}$ has an n-fixed point. Q.E.D.

Corollary 3.7. Let $\mathcal{F} : \Lambda^n \to \Lambda$ be a continuous function such that

$$\|\mathcal{F}(\mathrm{z}_1, \mathrm{z}_2, \mathrm{z}_3, \cdots, \mathrm{z}_n) - \mathcal{F}(\mathrm{y}_1, \mathrm{y}_2, \mathrm{y}_3, \cdots, \mathrm{y}_n)\| \leq \frac{\alpha}{n}\left[\sum_{k=1}^{n} \|\mathrm{z}_k - \mathrm{y}_k\|\right]$$

for any $(\mathrm{z}_1, \mathrm{z}_2, \mathrm{z}_3, \cdots, \mathrm{z}_n), (\mathrm{y}_1, \mathrm{y}_2, \mathrm{y}_3, \cdots, \mathrm{y}_n) \in \Lambda^n$. Then $\mathcal{F}$ has an n-fixed point.

Proof. Let $0 \leq \alpha < 1$ and put $\varrho(t) = \frac{\alpha}{n}$ in Corollary 3.6. Then by Corollary 3.6, $\mathcal{F}$ has an n-fixed point. Q.E.D.

4 Existence of solutions for n-dimensional fractional functional differential equations with ∞-point boundary conditions

In this section, we study the existence of solutions for n-dimensional fractional functional differential equations with ∞-point boundary conditions as an application of earlier results.

From Lemma 2.5, it can be seen that $\mathrm{z} = (\mathrm{z}_1, \mathrm{z}_2, \cdots, \mathrm{z}_n) \in X^n$ is a solution of (1.1)-(1.2) if and only if it is a solution of the integral equations

$$\begin{aligned}\mathrm{z}_1(t) = {} & \varphi\big(t, \mathrm{z}_1(\zeta(t)), \mathrm{z}_2\big(\zeta(t)\big), \cdots, \mathrm{z}_n\big(\zeta(t)\big)\big) \\ & + \int_0^t \frac{(t-s)^{a-1}}{\Gamma(a)} \Upsilon\left(s, \mathrm{z}_1\big(\vartheta(s)\big), \mathrm{z}_2\big(\vartheta(s)\big), \cdots, \mathrm{z}_n\big(\vartheta(s)\big)\right) ds \\ & - \varphi\big(0, \mathrm{z}_1(\zeta(0)), \mathrm{z}_2\big(\zeta(0)\big), \cdots, \mathrm{z}_n\big(\zeta(0)\big)\big) \\ & - \mathfrak{Z}_\infty t \sum_{k=1}^{\infty} \xi_k \varphi\big(\sigma(\tau_k), \mathrm{z}_1(\zeta(\sigma(\tau_k))), \mathrm{z}_2(\zeta(\sigma(\tau_k))), \cdots, \mathrm{z}_n(\zeta(\sigma(\tau_k)))\big) \\ & - \mathfrak{Z}_\infty t \sum_{k=1}^{\infty} \xi_k \int_0^{\sigma(\tau_k)} \frac{(\sigma(\tau_k)-s)^{a-1}}{\Gamma(a)} \Upsilon\left(s, \mathrm{z}_1\big(\vartheta(s)\big), \mathrm{z}_2\big(\vartheta(s)\big), \cdots, \mathrm{z}_n\big(\vartheta(s)\big)\right) ds \\ & + \mathfrak{Z}_\infty t \sum_{k=1}^{\infty} \xi_k \varphi\big(0, \mathrm{z}_1(\zeta(0)), \mathrm{z}_2\big(\zeta(0)\big), \cdots, \mathrm{z}_n\big(\zeta(0)\big)\big) + \mathfrak{Z}_\infty \delta t\end{aligned}$$

$$
\begin{aligned}
\mathrm{z}_2(t) &= \varphi\big(t, \mathrm{z}_2(\zeta(t)), \mathrm{z}_1\big(\zeta(t)\big), \cdots, \mathrm{z}_n\big(\zeta(t)\big)\big) \\
&\quad + \int_0^t \frac{(t-s)^{a-1}}{\Gamma(a)} \Upsilon\left(s, \mathrm{z}_2\big(\vartheta(s)\big), \mathrm{z}_1\big(\vartheta(s)\big), \cdots, \mathrm{z}_n\big(\vartheta(s)\big)\right) ds \\
&\quad - \varphi\big(0, \mathrm{z}_2(\zeta(0)), \mathrm{z}_1\big(\zeta(0)\big), \cdots, \mathrm{z}_n\big(\zeta(0)\big)\big) \\
&\quad - \mathfrak{Z}_\infty t \sum_{k=1}^{\infty} \xi_k \varphi\big(\sigma(\tau_k), \mathrm{z}_2(\zeta(\sigma(\tau_k))), \mathrm{z}_1(\zeta(\sigma(\tau_k))), \cdots, \mathrm{z}_n(\zeta(\sigma(\tau_k)))\big) \\
&\quad - \mathfrak{Z}_\infty t \sum_{k=1}^{\infty} \xi_k \int_0^{\sigma(\tau_k)} \frac{(\sigma(\tau_k)-s)^{a-1}}{\Gamma(a)} \Upsilon\left(s, \mathrm{z}_2\big(\vartheta(s)\big), \mathrm{z}_1\big(\vartheta(s)\big), \cdots, \mathrm{z}_n\big(\vartheta(s)\big)\right) ds \\
&\quad + \mathfrak{Z}_\infty t \sum_{k=1}^{\infty} \xi_k \varphi\big(0, \mathrm{z}_2(\zeta(0)), \mathrm{z}_1\big(\zeta(0)\big), \cdots, \mathrm{z}_n\big(\zeta(0)\big)\big) + \mathfrak{Z}_\infty \delta t \\
&\quad \vdots \\
\mathrm{z}_n(t) &= \varphi\big(t, \mathrm{z}_n(\zeta(t)), \mathrm{z}_2\big(\zeta(t)\big), \cdots, \mathrm{z}_1\big(\zeta(t)\big)\big) \\
&\quad + \int_0^t \frac{(t-s)^{a-1}}{\Gamma(a)} \Upsilon\left(s, \mathrm{z}_n\big(\vartheta(s)\big), \mathrm{z}_2\big(\vartheta(s)\big), \cdots, \mathrm{z}_1\big(\vartheta(s)\big)\right) ds \\
&\quad - \varphi\big(0, \mathrm{z}_n(\zeta(0)), \mathrm{z}_2\big(\zeta(0)\big), \cdots, \mathrm{z}_1\big(\zeta(0)\big)\big) \\
&\quad - \mathfrak{Z}_\infty t \sum_{k=1}^{\infty} \xi_k \varphi\big(\sigma(\tau_k), \mathrm{z}_n(\zeta(\sigma(\tau_k))), \mathrm{z}_2(\zeta(\sigma(\tau_k))), \cdots, \mathrm{z}_1(\zeta(\sigma(\tau_k)))\big) \\
&\quad - \mathfrak{Z}_\infty t \sum_{k=1}^{\infty} \xi_k \int_0^{\sigma(\tau_k)} \frac{(\sigma(\tau_k)-s)^{a-1}}{\Gamma(a)} \Upsilon\left(s, \mathrm{z}_n\big(\vartheta(s)\big), \mathrm{z}_2\big(\vartheta(s)\big), \cdots, \mathrm{z}_1\big(\vartheta(s)\big)\right) ds \\
&\quad + \mathfrak{Z}_\infty t \sum_{k=1}^{\infty} \xi_k \varphi\big(0, \mathrm{z}_n(\zeta(0)), \mathrm{z}_2\big(\zeta(0)\big), \cdots, \mathrm{z}_1\big(\zeta(0)\big)\big) + \mathfrak{Z}_\infty \delta t.
\end{aligned}
$$

Assume that the following assumptions hold throughout the section.

(C_1) $\varphi : \mathbb{R}^+ \times \mathbb{R}^n \to \mathbb{R}$ is continuous and the function $t \to \varphi(t, 0, 0, \cdots, 0)$ is a member of the space $\mathcal{BC}(\mathbb{R}^+)$.

(C_2) there exists $\alpha \in [0, 1)$ such that

$$
|\varphi(t, \mathrm{z}_1, \mathrm{z}_2, \cdots, \mathrm{z}_n) - \varphi(t, \mathrm{y}_1, \mathrm{y}_2, \cdots, \mathrm{y}_n)| \leq \frac{\alpha}{n} \left[\sum_{k=1}^{n} |\mathrm{z}_k - \mathrm{y}_k| \right],
$$

for any $t \geq 0$ and for all $(\mathrm{z}_1, \mathrm{z}_2, \cdots, \mathrm{z}_n), (\mathrm{y}_1, \mathrm{y}_2, \cdots, \mathrm{y}_n) \in \mathbb{R}^n$.

(C_3) the functions $\zeta, \vartheta : \mathbb{R}^+ \to \mathbb{R}^+$ are continuous and $\zeta \to \infty$ as $t \to \infty$.

(C_4) $\Upsilon : \mathbb{R}^+ \times \mathbb{R}^n \to \mathbb{R}$ is a continuous and there exist $\mathrm{z}_{10}, \mathrm{z}_{20}, \cdots, \mathrm{z}_{n0} \in \mathbb{R}$ and a positive constant M such that

$$
\int_0^t \frac{(t-s)^{a-1}}{\Gamma(a)} \Big| \Upsilon\left(s, \mathrm{z}_{10}, \mathrm{z}_{20}, \cdots, \mathrm{z}_{n0}\right) \Big| ds \leq M
$$

for all $t \in \mathbb{R}^+$. Also, assume that

$$(t-s)^{a-1}\Upsilon\left(s, \mathrm{z}_1\big(\vartheta(s)\big), \mathrm{z}_2\big(\vartheta(s)\big), \cdots, \mathrm{z}_n\big(\vartheta(s)\big)\right)$$

is continuous and

$$\lim_{t\to\infty}\int_0^t \frac{(t-s)^{a-1}}{\Gamma(a)}\Upsilon\left(s, \mathrm{z}_1\big(\vartheta(s)\big), \mathrm{z}_2\big(\vartheta(s)\big), \cdots, \mathrm{z}_n\big(\vartheta(s)\big)\right) ds = 0.$$

Theorem 4.1. Assume that the conditions (C_1)-(C_4) hold. Then the fractional boundary value problem (1.1)–(1.2) has at least one solution in the space $\mathscr{C}^n$ where $\mathscr{C} = \mathcal{BC}(\mathbb{R}^+)$.

Proof. Consider the mapping $\mathcal{F} : \mathscr{C}^n \to \mathscr{C}$ defined by

$$\left.\begin{aligned}
\mathcal{F}(\mathrm{z}_1, \mathrm{z}_2, \cdots, \mathrm{z}_n)(t) &= \varphi\big(t, \mathrm{z}_1(\zeta(t)), \mathrm{z}_2\big(\zeta(t)\big), \cdots, \mathrm{z}_n\big(\zeta(t)\big)\big)\\
&+ \int_0^t \frac{(t-s)^{a-1}}{\Gamma(a)}\Upsilon\left(s, \mathrm{z}_1\big(\vartheta(s)\big), \mathrm{z}_2\big(\vartheta(s)\big), \cdots, \mathrm{z}_n\big(\vartheta(s)\big)\right) ds\\
&- \varphi\big(0, \mathrm{z}_1(\zeta(0)), \mathrm{z}_2\big(\zeta(0)\big), \cdots, \mathrm{z}_n\big(\zeta(0)\big)\big)\\
&- \mathfrak{Z}_\infty t\sum_{k=1}^{\infty}\xi_k\varphi\big(\sigma(\tau_k), \mathrm{z}_1(\zeta(\sigma(\tau_k))), \mathrm{z}_2(\zeta(\sigma(\tau_k))), \cdots, \mathrm{z}_n(\zeta(\sigma(\tau_k)))\big)\\
&- \mathfrak{Z}_\infty t\sum_{k=1}^{\infty}\xi_k\int_0^{\sigma(\tau_k)}\frac{(\sigma(\tau_k)-s)^{a-1}}{\Gamma(a)}\Upsilon\left(s, \mathrm{z}_1\big(\vartheta(s)\big), \mathrm{z}_2\big(\vartheta(s)\big), \cdots, \mathrm{z}_n\big(\vartheta(s)\big)\right) ds\\
&+ \mathfrak{Z}_\infty t\sum_{k=1}^{\infty}\xi_k\varphi\big(0, \mathrm{z}_1(\zeta(0)), \mathrm{z}_2\big(\zeta(0)\big), \cdots, \mathrm{z}_n\big(\zeta(0)\big)\big) + \mathfrak{Z}_\infty\delta t
\end{aligned}\right\} \tag{4.1}$$

Define the norm on $\mathscr{C}^n$ by

$$\|(\mathrm{z}_1, \mathrm{z}_2, \cdots, \mathrm{z}_n)\| = \|\mathrm{z}_1\|_{\mathscr{C}} + \|\mathrm{z}_2\|_{\mathscr{C}} + \cdots + \|\mathrm{z}_n\|_{\mathscr{C}}$$

for any $(\mathrm{z}_1, \mathrm{z}_2, \cdots, \mathrm{z}_n) \in \mathscr{C}^n$. It is clear that $\mathcal{F}(\mathrm{z}_1, \mathrm{z}_2, \cdots, \mathrm{z}_n)$ is continuous on $\mathbb{R}^+$ for all $(\mathrm{z}_1, \mathrm{z}_2, \cdots, \mathrm{z}_n) \in \mathscr{C}^n$. Also, from (4.1) and (C_2), we have

$$\begin{aligned}
|\mathcal{F}(\mathrm{z}_1, \mathrm{z}_2, \cdots, \mathrm{z}_n)(t)| &\le \left|\varphi\big(t, \mathrm{z}_1(\zeta(t)), \mathrm{z}_2\big(\zeta(t)\big), \cdots, \mathrm{z}_n\big(\zeta(t)\big)\big) - \varphi(t, 0, 0, \cdots, 0)\right|\\
&+ |\varphi(t, 0, 0, \cdots, 0)| + \int_0^t \frac{(t-s)^{a-1}}{\Gamma(a)}\Big|\Upsilon\left(s, \mathrm{z}_1\big(\vartheta(s)\big), \mathrm{z}_2\big(\vartheta(s)\big), \cdots, \mathrm{z}_n\big(\vartheta(s)\big)\right)\\
&- \Upsilon\left(s, \mathrm{z}_{10}, \mathrm{z}_{20}, \cdots, \mathrm{z}_{n0}\right)\Big| ds + \int_0^t \frac{(t-s)^{a-1}}{\Gamma(a)}\Big|\Upsilon\left(s, \mathrm{z}_{10}, \mathrm{z}_{20}, \cdots, \mathrm{z}_{n0}\right)\Big| ds\\
&+ |\varphi\big(0, \mathrm{z}_1(\zeta(0)), \mathrm{z}_2\big(\zeta(0)\big), \cdots, \mathrm{z}_n\big(\zeta(0)\big)\big)|\\
&+ \mathfrak{Z}_\infty|t|\sum_{k=1}^{\infty}\xi_k|\varphi\big(\sigma(\tau_k), \mathrm{z}_1(\zeta(\sigma(\tau_k))), \mathrm{z}_2(\zeta(\sigma(\tau_k))), \cdots, \mathrm{z}_n(\zeta(\sigma(\tau_k)))\big)|\\
&+ \mathfrak{Z}_\infty|t|\sum_{k=1}^{\infty}\xi_k\int_0^{\sigma(\tau_k)}\frac{(\sigma(\tau_k)-s)^{a-1}}{\Gamma(a)}\Big|\Upsilon\left(s, \mathrm{z}_1\big(\vartheta(s)\big), \mathrm{z}_2\big(\vartheta(s)\big), \cdots, \mathrm{z}_n\big(\vartheta(s)\big)\right)\Big| ds\\
&+ \mathfrak{Z}_\infty|t|\sum_{k=1}^{\infty}\xi_k|\varphi\big(0, \mathrm{z}_1(\zeta(0)), \mathrm{z}_2\big(\zeta(0)\big), \cdots, \mathrm{z}_n\big(\zeta(0)\big)\big)| + \mathfrak{Z}_\infty|\delta||t|.
\end{aligned}$$

Thus,

$$|\mathcal{F}(\mathrm{z}_1,\mathrm{z}_2,\cdots,\mathrm{z}_n)(t)| \leq \frac{\alpha}{n}\left[\sum_{k=1}^{n}\left|\mathrm{z}_k(\zeta(t))\right|\right] + M_0, \tag{4.2}$$

where

$$\begin{aligned}
M_0 = {} & \sup_{t\in\mathbb{R}^+}|\varphi(t,0,0,\cdots,0)| + |\varphi\big(0,\mathrm{z}_1(\zeta(0)),\mathrm{z}_2\big(\zeta(0)\big),\cdots,\mathrm{z}_n\big(\zeta(0)\big)\big)| \\
& + \sup_{t\in\mathbb{R}^+}\int_0^t \frac{(t-s)^{a-1}}{\Gamma(a)}\Big|\Upsilon\left(s,\mathrm{z}_1\big(\vartheta(s)\big),\mathrm{z}_2\big(\vartheta(s)\big),\cdots,\mathrm{z}_n\big(\vartheta(s)\big)\right) \\
& \qquad\qquad - \Upsilon\left(s,\mathrm{z}_{10},\mathrm{z}_{20},\cdots,\mathrm{z}_{n0}\right)\Big|ds \\
& + \mathfrak{Z}_\infty\sum_{k=1}^{\infty}\xi_k\Big|\varphi\big(\sigma(\tau_k),\mathrm{z}_1(\zeta(\sigma(\tau_k))),\mathrm{z}_2(\zeta(\sigma(\tau_k))),\cdots,\mathrm{z}_n(\zeta(\sigma(\tau_k)))\big)\Big| \\
& + \mathfrak{Z}_\infty\sum_{k=1}^{\infty}\xi_k\int_0^{\sigma(\tau_k)}\frac{(\sigma(\tau_k)-s)^{a-1}}{\Gamma(a)}\Big|\Upsilon\left(s,\mathrm{z}_1\big(\vartheta(s)\big),\mathrm{z}_2\big(\vartheta(s)\big),\cdots,\mathrm{z}_n\big(\vartheta(s)\big)\right)\Big|ds \\
& + \mathfrak{Z}_\infty\sum_{k=1}^{\infty}\xi_k|\varphi\big(0,\mathrm{z}_1(\zeta(0)),\mathrm{z}_2\big(\zeta(0)\big),\cdots,\mathrm{z}_n\big(\zeta(0)\big)\big)| + \mathfrak{Z}_\infty|\delta| + M.
\end{aligned}$$

Hence $\mathcal{F}$ maps $\mathscr{C}^n$ into $\mathscr{C}$. Further, from the inequality (4.2), we get

$$\|\mathcal{F}(\mathrm{z}_1,\mathrm{z}_2,\cdots,\mathrm{z}_n)\|_{\mathscr{C}} \leq \frac{\alpha}{n}\left[\sum_{k=1}^{n}\|\mathrm{z}_k\|_{\mathscr{C}}\right] + M_0 \tag{4.3}$$

From (4.3), we have

$$\mathcal{F}\big(\overline{\mathscr{B}}_r^n\big) \subset \overline{\mathscr{B}}_r$$

for $r = \frac{M_0}{1-\alpha}$.

Claim: $\mathcal{F}:\overline{\mathscr{B}}_r^n \to \overline{\mathscr{B}}_r$ is continuous.

Let $\varepsilon > 0, (\mathrm{z}_1,\mathrm{z}_2,\cdots,\mathrm{z}_n) \in \overline{\mathscr{B}}_r^n$ and $(\mathrm{y}_1,\mathrm{y}_2,\cdots,\mathrm{y}_n) \in \overline{\mathscr{B}}_r^n$ with

$$\|(\mathrm{z}_1,\mathrm{z}_2,\cdots,\mathrm{z}_n) - (\mathrm{y}_1,\mathrm{y}_2,\cdots,\mathrm{y}_n)\| \leq \varepsilon,$$

we have

$$\begin{aligned}
\big|\mathcal{F}(\mathrm{z}_1,\mathrm{z}_2,\cdots,\mathrm{z}_n)(t) - \mathcal{F}(\mathrm{y}_1,\mathrm{y}_2,\cdots,\mathrm{y}_n)(t)\big| \leq {} & \frac{\alpha}{n}\left[\sum_{k=1}^{n}\left|\mathrm{z}_k(\zeta(t)) - \mathrm{y}_k(\zeta(t))\right|\right] \\
+ \int_0^t \frac{(t-s)^{a-1}}{\Gamma(a)}\Big|\Upsilon\left(s,\mathrm{z}_1\big(\vartheta(s)\big),\mathrm{z}_2\big(\vartheta(s)\big),\cdots,\mathrm{z}_n\big(\vartheta(s)\big)\right) & \\
- \Upsilon\left(s,\mathrm{y}_1\big(\vartheta(s)\big),\mathrm{y}_2\big(\vartheta(s)\big),\cdots,\mathrm{y}_n\big(\vartheta(s)\big)\right)\Big|ds &
\end{aligned}$$

$$
\begin{aligned}
&+\sum_{k=1}^{n}\left|\mathrm{z}_k(\zeta(0))-\mathrm{y}_k(\zeta(0))\right|+\mathfrak{Z}_\infty\sum_{k=1}^{\infty}\xi_k\left[\sum_{j=1}^{n}\left|\mathrm{z}_j(\zeta(\sigma(\tau_k)))-\mathrm{y}_j(\sigma(\zeta(\tau_k)))\right|\right]\\
&+\mathfrak{Z}_\infty\sum_{k=1}^{\infty}\xi_k\int_0^{\sigma(\tau_k)}\frac{(\sigma(\tau_k)-s)^{a-1}}{\Gamma(a)}\Big|\Upsilon\left(s,\mathrm{z}_1\big(\vartheta(s)\big),\mathrm{z}_2\big(\vartheta(s)\big),\cdots,\mathrm{z}_n\big(\vartheta(s)\big)\right)\\
&\qquad\qquad-\Upsilon\left(s,\mathrm{y}_1\big(\vartheta(s)\big),\mathrm{y}_2\big(\vartheta(s)\big),\cdots,\mathrm{y}_n\big(\vartheta(s)\big)\right)\Big|ds\\
&+\mathfrak{Z}_\infty\sum_{k=1}^{\infty}\xi_k\left[\sum_{j=1}^{n}\left|\mathrm{z}_j(\zeta(0))-\mathrm{y}_j(\zeta(0))\right|\right]
\end{aligned}
$$

On the other hand by condition (C_4), there exists a positive condition $\mathfrak{T}$ such that

$$
\begin{aligned}
&\int_0^t\frac{(t-s)^{a-1}}{\Gamma(a)}\Big|\Upsilon\left(s,\mathrm{z}_1\big(\vartheta(s)\big),\mathrm{z}_2\big(\vartheta(s)\big),\cdots,\mathrm{z}_n\big(\vartheta(s)\big)\right)\\
&\qquad\qquad-\Upsilon\left(s,\mathrm{y}_1\big(\vartheta(s)\big),\mathrm{y}_2\big(\vartheta(s)\big),\cdots,\mathrm{y}_n\big(\vartheta(s)\big)\right)\Big|ds\\
&\qquad\le 2\int_0^t\frac{(t-s)^{a-1}}{\Gamma(a)}\Big|\Upsilon\left(s,\mathrm{z}_1\big(\vartheta(s)\big),\mathrm{z}_2\big(\vartheta(s)\big),\cdots,\mathrm{z}_n\big(\vartheta(s)\big)\right)\Big|ds\\
&\qquad\le\varepsilon
\end{aligned}
$$

for all $t\ge\mathfrak{T}$. Also, from the continuity of Υ on $\mathbb{R}^+\times\mathbb{R}^n$, it follows that

$$
\begin{aligned}
&\left|\mathcal{F}(\mathrm{z}_1,\mathrm{z}_2,\cdots,\mathrm{z}_n)(t)-\mathcal{F}(\mathrm{y}_1,\mathrm{y}_2,\cdots,\mathrm{y}_n)(t)\right|\\
&\le\frac{\alpha}{n}\left[\sum_{k=1}^{n}\left|\mathrm{z}_k(\zeta(t))-\mathrm{y}_k(\zeta(t))\right|\right]+\varepsilon+\sum_{k=1}^{n}\left|\mathrm{z}_k(\zeta(0))-\mathrm{y}_k(\zeta(0))\right|\\
&+\mathfrak{Z}_\infty\sum_{k=1}^{\infty}\xi_k\left[\sum_{j=1}^{n}\left|\mathrm{z}_j(\zeta(\sigma(\tau_k)))-\mathrm{y}_j(\sigma(\zeta(\tau_k)))\right|\right]\\
&+\mathfrak{Z}_\infty\sum_{k=1}^{\infty}\xi_k\int_0^{\sigma(\tau_k)}\frac{(\sigma(\tau_k)-s)^{a-1}}{\Gamma(a)}\,\varepsilon\,ds+\mathfrak{Z}_\infty\sum_{k=1}^{\infty}\xi_k\left[\sum_{j=1}^{n}\left|\mathrm{z}_j(\zeta(0))-\mathrm{y}_j(\zeta(0))\right|\right]\\
&\le\frac{\alpha}{n}\varepsilon+\varepsilon+\varepsilon+\mathfrak{Z}_\infty\sum_{k=1}^{\infty}\xi_k\varepsilon+\mathfrak{Z}_\infty\sum_{k=1}^{\infty}\xi_k\frac{[\sigma(\tau_k)]^a}{\Gamma(a+1)}\varepsilon+\mathfrak{Z}_\infty\sum_{k=1}^{\infty}\xi_k\varepsilon\\
&\le\left[\frac{\alpha}{n}+2\mathfrak{Z}_\infty\sum_{k=1}^{\infty}\xi_k+\mathfrak{Z}_\infty\sum_{k=1}^{\infty}\xi_k\frac{1}{\Gamma(a+1)}+2\right]\varepsilon\\
&\le\left[\frac{\alpha}{n}+\mathfrak{Z}_\infty\sum_{k=1}^{\infty}\xi_k\left[2+\frac{1}{\Gamma(a+1)}\right]+2\right]\varepsilon
\end{aligned}
$$

for all $t \geq \mathfrak{T}$. Now, in case that $t \in [0, \mathfrak{T}]$, we have

$$\begin{aligned}
&\Big|\mathcal{F}(\mathrm{z}_1, \mathrm{z}_2, \cdots, \mathrm{z}_n)(t) - \mathcal{F}(\mathrm{y}_1, \mathrm{y}_2, \cdots, \mathrm{y}_n)(t)\Big| \\
&\qquad \leq \frac{\alpha}{n}\varepsilon + \int_0^t \frac{(t-s)^{a-1}}{\Gamma(a)}\omega^{\mathfrak{T}}(\Upsilon, \varepsilon)ds \\
&\qquad\qquad + \varepsilon + \mathfrak{Z}_\infty \sum_{k=1}^{\infty} \xi_k \varepsilon + \frac{\varepsilon}{\Gamma(a+1)} + \mathfrak{Z}_\infty \sum_{k=1}^{\infty} \xi_k \varepsilon \\
&\qquad \leq \frac{\alpha}{n}\varepsilon + \mathfrak{T}^a \frac{\omega^{\mathfrak{T}}(\Upsilon, \varepsilon)}{\Gamma(a+1)} + \frac{\varepsilon}{\Gamma(a+1)} + 2\mathfrak{Z}_\infty \sum_{k=1}^{\infty} \xi_k \varepsilon + \varepsilon
\end{aligned}$$

where

$$\begin{aligned}
\omega^{\mathfrak{T}}(\Upsilon, \varepsilon) = \sup \Bigg\{ &\Big| \Upsilon\left(s, \mathrm{z}_1\big(\vartheta(s)\big), \mathrm{z}_2\big(\vartheta(s)\big), \cdots, \mathrm{z}_n\big(\vartheta(s)\big)\right) \\
&- \Upsilon\left(s, \mathrm{y}_1\big(\vartheta(s)\big), \mathrm{y}_2\big(\vartheta(s)\big), \cdots, \mathrm{y}_n\big(\vartheta(s)\big)\right) \Big| : s \in [0, \mathfrak{T}],\ \mathrm{z}_i, \mathrm{y}_i \in [-r, r] \\
&\text{for } \ i = 1, 2, \cdots, n, \text{ and } \ \|(\mathrm{z}_1, \mathrm{z}_2, \cdots, \mathrm{z}_n) - (\mathrm{y}_1, \mathrm{y}_2, \cdots, \mathrm{y}_n)\| \leq \varepsilon \Bigg\}.
\end{aligned}$$

From the uniform continuity of Υ on $[0, \mathfrak{T}] \times [-r, r]^n$, we obtain $\omega^{\mathfrak{T}}(\Upsilon, \varepsilon) \to 0$ as $\varepsilon \to 0$. Hence the claim.

Next, fix $\mathfrak{T}, \varepsilon \in \mathbb{R}^+$ and let $E_k\ (1 \leq k \leq n)$ be nonempty subsets of $\overline{\mathscr{B}}_r$ and $t, t' \in [0, \mathfrak{T}]$ with $|t - t'| < \varepsilon$. Now, let $(\mathrm{z}_1, \mathrm{z}_2, \cdots, \mathrm{z}_n) \in \prod_{k=1}^n E_k$. Then, we get

$$\begin{aligned}
&\big|\mathcal{F}(\mathrm{z}_1, \mathrm{z}_2, \cdots, \mathrm{z}_n)(t) - \mathcal{F}(\mathrm{z}_1, \mathrm{z}_2, \cdots, \mathrm{z}_n)(t')\big| \\
&\leq \frac{\alpha}{n}\left[\sum_{k=1}^{n} \omega^{\mathfrak{T}}\big(\mathrm{z}_k, \omega^{\mathfrak{T}}(\vartheta, \varepsilon)\big)\right] + \omega_r^{\mathfrak{T}}(\varphi, \varepsilon) \\
&\quad + \int_0^t \left| \frac{(t-s)^{a-1}}{\Gamma(a)} \Upsilon\left(s, \mathrm{z}_1\big(\vartheta(s)\big), \mathrm{z}_2\big(\vartheta(s)\big), \cdots, \mathrm{z}_n\big(\vartheta(s)\big)\right) \right. \\
&\qquad \left. - \frac{(t'-s)^{a-1}}{\Gamma(a)} \Upsilon\left(s, \mathrm{z}_1\big(\vartheta(s)\big), \mathrm{z}_2\big(\vartheta(s)\big), \cdots, \mathrm{z}_n\big(\vartheta(s)\big)\right) \right| ds \\
&\quad + \int_t^{t'} \left| \frac{(t-s)^{a-1}}{\Gamma(a)} \Upsilon\left(s, \mathrm{z}_1\big(\vartheta(s)\big), \mathrm{z}_2\big(\vartheta(s)\big), \cdots, \mathrm{z}_n\big(\vartheta(s)\big)\right) \right| ds \\
&+ \mathfrak{Z}_\infty \sum_{k=1}^{\infty} \xi_k |\varphi\big(\sigma(\tau_k), \mathrm{z}_1(\zeta(\sigma(\tau_k))), \mathrm{z}_2(\zeta(\sigma(\tau_k))), \cdots, \mathrm{z}_n(\zeta(\sigma(\tau_k)))\big)||t - t'|
\end{aligned}$$

$$
\begin{aligned}
&+ \mathfrak{Z}_\infty \sum_{k=1}^{\infty} \xi_k \int_0^{\sigma(\tau_k)} \frac{(\sigma(\tau_k)-s)^{a-1}}{\Gamma(a)} \big|\Upsilon\left(s, \mathrm{z}_1\big(\vartheta(s)\big), \mathrm{z}_2\big(\vartheta(s)\big), \cdots, \mathrm{z}_n\big(\vartheta(s)\big)\right)\big| ds|t-t'| \\
&+ \mathfrak{Z}_\infty \sum_{k=1}^{\infty} \xi_k |\varphi\big(0, \mathrm{z}_1(\zeta(0)), \mathrm{z}_2\big(\zeta(0)\big), \cdots, \mathrm{z}_n\big(\zeta(0)\big)\big)||t-t'| + \mathfrak{Z}_\infty|\delta||t-t'| \\
&\leq \frac{\alpha}{n}\left[\sum_{k=1}^{n} \omega^{\mathfrak{T}}\big(\mathrm{z}_k, \omega^{\mathfrak{T}}(\vartheta, \varepsilon)\big)\right] + \omega_r^{\mathfrak{T}}(\varphi, \varepsilon) + \int_0^{\mathfrak{T}} \omega_r^{\mathfrak{T}}(f, \varepsilon) ds + Y_r^{\mathfrak{T}}|t-t'| + \eta|t-t'|.
\end{aligned}
$$

Thus,

$$
\begin{aligned}
&\big|\mathcal{F}(\mathrm{z}_1, \mathrm{z}_2, \cdots, \mathrm{z}_n)(t) - \mathcal{F}(\mathrm{z}_1, \mathrm{z}_2, \cdots, \mathrm{z}_n)(t')\big| \\
&\quad \leq \frac{\alpha}{n}\left[\sum_{k=1}^{n} \omega^{\mathfrak{T}}\big(\mathrm{z}_k, \omega^{\mathfrak{T}}(\vartheta, \varepsilon)\big)\right] + \omega_r^{\mathfrak{T}}(\varphi, \varepsilon) + \int_0^{\mathfrak{T}} \omega_r^{\mathfrak{T}}(f, \varepsilon) ds + Y_r^{\mathfrak{T}}\varepsilon + \eta\varepsilon,
\end{aligned} \tag{4.4}
$$

where

$$
\begin{aligned}
&\omega^{\mathfrak{T}}(\vartheta, \varepsilon) = \sup\Big\{|\vartheta(t) - \vartheta(t')| : t, t' \in [0, \mathfrak{T}], |t-t'| \leq \varepsilon\Big\} \\
&\omega^{\mathfrak{T}}\big(\mathrm{z}_k, \omega^{\mathfrak{T}}(\vartheta, \varepsilon)\big) = \sup\Big\{|\mathrm{z}_k(t) - \mathrm{z}_k(t')| : t, t' \in [0, \mathfrak{T}], |t-t'| \leq \omega^{\mathfrak{T}}(\vartheta, \varepsilon)\Big\}, \\
&\omega_r^{\mathfrak{T}}(\varphi, \varepsilon) = \sup\Big\{|\varphi(t, \mathrm{z}_1, \mathrm{z}_2, \cdots, \mathrm{z}_n) - \varphi(t', \mathrm{z}_1, \mathrm{z}_2, \cdots, \mathrm{z}_n)| : t, t' \in [0, \mathfrak{T}], \\
&\qquad\qquad |t-t'| \leq \varepsilon, \sum_{k=1}^{n} |\mathrm{z}_k| \leq r\Big\} \\
&\omega_r^{\mathfrak{T}}(f, \varepsilon) = \sup\Big\{|f(t, s, \mathrm{z}_1, \mathrm{z}_2, \cdots, \mathrm{z}_n) - f(t', s, \mathrm{z}_1, \mathrm{z}_2, \cdots, \mathrm{z}_n)| : \\
&\qquad\qquad t, t', s \in [0, \mathfrak{T}], |t-t'| \leq \varepsilon, \sum_{k=1}^{n} |\mathrm{z}_k| \leq r\Big\} \\
&Y_r^{\mathfrak{T}} = \sup\Big\{|\Upsilon(t, s, \mathrm{z}_1, \mathrm{z}_2, \cdots, \mathrm{z}_n)| : t, s \in [0, \mathfrak{T}], \sum_{k=1}^{n} |\mathrm{z}_k| \leq r\Big\}
\end{aligned}
$$

and

$$
f(t, s, \mathrm{z}_1, \mathrm{z}_2, \cdots, \mathrm{z}_n) = \frac{(t-s)^{a-1}}{\Gamma(a)} \Upsilon\left(s, \mathrm{z}_1\big(\vartheta(s)\big), \mathrm{z}_2\big(\vartheta(s)\big), \cdots, \mathrm{z}_n\big(\vartheta(s)\big)\right)
$$

$$
\begin{aligned}
\eta &= \mathfrak{Z}_\infty \sum_{k=1}^{\infty} \xi_k |\varphi\big(\sigma(\tau_k), \mathrm{z}_1(\zeta(\sigma(\tau_k))), \mathrm{z}_2(\zeta(\sigma(\tau_k))), \cdots, \mathrm{z}_n(\zeta(\sigma(\tau_k)))\big)| \\
&+ \mathfrak{Z}_\infty \sum_{k=1}^{\infty} \xi_k \int_0^{\sigma(\tau_k)} \frac{(\sigma(\tau_k)-s)^{a-1}}{\Gamma(a)} \big|\Upsilon\left(s, \mathrm{z}_1\big(\vartheta(s)\big), \mathrm{z}_2\big(\vartheta(s)\big), \cdots, \mathrm{z}_n\big(\vartheta(s)\big)\right)\big| ds \\
&+ \mathfrak{Z}_\infty \sum_{k=1}^{\infty} \xi_k |\varphi\big(0, \mathrm{z}_1(\zeta(0)), \mathrm{z}_2\big(\zeta(0)\big), \cdots, \mathrm{z}_n\big(\zeta(0)\big)\big)| + \mathfrak{Z}_\infty|\delta|
\end{aligned}
$$

Since $(\mathrm{z}_1, \mathrm{z}_2, \cdots, \mathrm{z}_n)$ is an arbitrary element of $\prod_{k=1}^{n} E_k$, it follows from the inequality (4.4) that

$$\left.\begin{aligned}\omega^{\mathfrak{T}}\left(\mathcal{F}\left(\prod_{k=1}^{n} E_k\right), \varepsilon\right) \leq \frac{\alpha}{n}\left[\sum_{k=1}^{n} \omega^{\mathfrak{T}}\big(E_k, \omega^{\mathfrak{T}}(\vartheta, \varepsilon)\big)\right] + \omega_r^{\mathfrak{T}}(\varphi, \varepsilon) \\ + \int_0^{\mathfrak{T}} \omega_r^{\mathfrak{T}}(f, \varepsilon) ds + Y_r^{\mathfrak{T}} \varepsilon + \eta\varepsilon\end{aligned}\right\} \tag{4.5}$$

Since Υ are uniformly continuous on $[0, \mathfrak{T}] \times [-r, r]^n$, it follows that f is uniformly continuous on $[0, \mathfrak{T}] \times [0, \mathfrak{T}] \times [-r, r]^n$. Also, from uniform continuity of φ, ϑ on $[0, \mathfrak{T}] \times [-r, r]^n$ and $[0, \mathfrak{T}]$ respectively, we have $\omega^{\mathfrak{T}}(\vartheta, \varepsilon) \to 0$, $\omega_r^{\mathfrak{T}}(\varphi, \varepsilon) \to 0$, $\omega_r^{\mathfrak{T}}(f, \varepsilon) \to 0$ as $\varepsilon \to 0$. So, (4.5) becomes

$$\omega_0^{\mathfrak{T}}\left(\mathcal{F}\left(\prod_{k=1}^{n} E_k\right)\right) \leq \frac{\alpha}{n}\left[\sum_{k=1}^{n} \omega_0^{\mathfrak{T}}\big(E_k\big)\right],$$

taking $\mathfrak{T} \to \infty$ on both sides, we obtain

$$\omega_0\left(\mathcal{F}\left(\prod_{k=1}^{n} E_k\right)\right) \leq \frac{\alpha}{n}\left[\sum_{k=1}^{n} \omega_0\big(E_k\big)\right]. \tag{4.6}$$

Hence, from the Corollary 3.5, the fractional boundary value problem (1.1)–(1.2) has a solution in the space $\mathscr{C}^n$. Q.E.D.

Acknowledgements

The authors would like to thank the referees for their valuable suggestions and comments for the improvement of the paper.

References

[1] R. P. Agarwal, M. Meehan, and D. O'Regan, *Fixed point theory and applications*, Cambridge University Press, Cambridge, 2001.

[2] A. Aghajani, Y. Jalilian, and J. J. Trujillo, *On the existence of solutions of fractional integro-difierential equations*, Fract. Calc. Appl. Anal. **15**(1), (2012), 44–69.

[3] A. Aghajani, and N. Sabzali, *Existence of coupled fixed points via measure of noncompactness and applications*, J. Nonl. Conv. Anal. **15**(5), (2014), 941–952.

[4] Z. Bai, and H. Lu, *Positive solutions for a boundary value problem of nonlinear fractional differential equations*, J. Math. Anal. Appl. **311**(2), (2005) 495–505.

[5] J. Banas, *On measures of noncompactness in Banach spaces*, Comment. Math. Univ. Carolinae **21** (1980), 131-143.

[6] J. Banas, and K. Goebel, *Measure of Noncompactness in Banach Spaces*, Lecture Notes in Pure and Applied Mathematics, Vol. 60, Marcel Dekker, New York, 1980.

[7] M. Benchohra, J. R. Graef, and F. Z. Mostafai, *Weak solutions for nonlinear fractional difierential equations on reflexive Banach spaces*, Electron. J. Qual. Theory. **54** (2010), 1–10.

[8] M. Borcut, *Tripled fixed point theorems for monotone mappings in partially ordered metric spaces*, Carpathian J. of Math. **28**(2), (2012), 215–222.

[9] P. Borisut, P. Kumam, I. Ahmed, and K. Sitthithakerngkiet, *Nonlinear Caputo Fractional Derivative with Nonlocal Riemann-Liouville Fractional Integral Condition Via Fixed Point Theorems*, Symmetry, **11**(6), (2019), 829.

[10] L. Cadariu, L. Gavruta, and P. Gavruta, *Weighted space method for the stability of some nonlinear equations*. Appl Anal Discrete Math. **6**(1), (2012), 126–139.

[11] G. Darbo, *Punti uniti in trasformazioni a codominio non compatto. Rend. Sem. Mat. Un.* Padova. **24** (1955), 84–92.

[12] M. Feng, X. Zhang, and W. Ge, *New existence results for higher-order nonlinear fractional differential equation with integral boundary conditions*, Bound. Value Probl. 2011, Art. ID 720702, 20 pp.

[13] A. A. Kilbas, H. M. Srivastava, and J. J. Trujillo, *Theory and applications of fractional differential equations*, North-Holland Mathematics Studies 204, Elsevier Science B. V., Amsterdam 2006.

[14] K. Kuratowski, *Sur les espaces complets*, Fund. Math. 15(1930) 301–309.

[15] H. Lee, and S. Kim, *Multivariate coupled fixed point theorems on ordered partial metric spaces*, J. Korean Math. Soc. *51*(2014), 1189–1207.

[16] K. Li, J. Peng, and J. Gao, Nonlocal fractional semilinear Differential equations in separable Banach spaces, Electron. J. Differential Equations, **2013**(7) (2013), 1–7.

[17] J. Liang, Z. Liu, and X. Wang, *Solvability for a couple system of nonlinear fractional differential equations in a Banach space*, Fract. Calc. Appl. Anal. **16**(1) (2013), 51–63.

[18] I. Podlubny, *Fractional differential equations*, Academic Press, San Diego, 1999.

[19] A. Saadi, and M. Benbachir, *Positive solutions for three-point nonlinear fractional boundary value problems*, E. J. Qualitative Theory of Diff. Equ. **3** (2011), 1–19.

[20] J. Sabatier, O. P. Agarwal, and J. A. T. Machado, *Advances in fractional calculus: Theoretical developments and applications in physics and engineering*, Springer, Dordrecht, 2007.

[21] F. J. Torres, *Existence of a positive solution for a boundary value problem of a nonlinear fractional differential equation*, BIMS **39**(2), (2013), 307–323.

[22] J. Wang, Y. Zhou, and M. Feckan, *Abstract Cauchy problem for fractional differential equations*, Nonlinear Dynam. DOI 10.1007/s11071-012-0452-9.

[23] S. Zhang, *Existence results of positive solutions to fractional differential equation with integral boundary conditions*, Math. Bohem. **135**(2), (2010), 299–317.

Journal of Applied Mathematics and Computing (2022) 68:4241–4251
https://doi.org/10.1007/s12190-022-01703-4

ORIGINAL RESEARCH

Nonlinear two-point iterative functional boundary value problems on time scales

Mahammad Khuddush[1] · **K. Rajendra Prasad**[2]

Received: 7 November 2021 / Revised: 25 December 2021 / Accepted: 28 December 2021 /
Published online: 24 January 2022
© The Author(s) under exclusive licence to Korean Society for Informatics and Computational Applied Mathematics 2022

Abstract
This paper is concerned with second order iterative functional boundary value problem with two-point boundary conditions on time scales. By utilizing Schauder fixed point theorem and contraction mapping principle, we establish some sufficient conditions for the existence, uniqueness and continuous dependence of bounded solutions. Finally, we provide an example to support our main results.

Keywords Time scale · Iterative BVP · Functional differential equation · Continuous dependence

Mathematics Subject Classification 34K42 · 39B12 · 39B82

1 Introduction and preliminaries

Iterative differential equation, as a special type of functional differential equations, in which the deviating argument depends on the state [19]. Many researchers have concentrated on studying first order iterative functional differential equations by different approaches such as Picard's successive approximation, fixed point theory and the technique of nonexpansive operators, see [2,8,13,21]. But the literature related to the second and higher order is very less since the presence of the iterates increases the difficulty of studying them, see [5–7,11,12,15–18,20]. This motivates us to study the following second order iterative functional boundary value problem on time scales

✉ Mahammad Khuddush
khuddush89@gmail.com

1 Department of Mathematics, Dr. Lankapalli Bullayya College, Visakhapatnam, Andhra Pradesh 530013, India

2 Department of Applied Mathematics, College of Science and Technology, Andhra University, Visakhapatnam 530003, India

$$\mathtt{z}^{\Delta\Delta}(\mathtt{s}) + \mathtt{g}\big(\mathtt{s}, \mathtt{z}(\mathtt{s}), \mathtt{z}^{[2]}(\mathtt{s}), \mathtt{z}^{[3]}(\mathtt{s}), \cdots, \mathtt{z}^{[n]}(\mathtt{s})\big) = 0, \ \mathtt{s} \in [a, b]_{\mathbb{T}}, \tag{1}$$

subject to the two-point boundary conditions

$$\mathtt{z}(a) = \mathtt{z}_a, \ \mathtt{z}(\sigma^2(b)) = \mathtt{z}_b, \tag{2}$$

where $\mathbb{T}$ is a time scale, $\mathtt{g} : [a, b]_{\mathbb{T}} \times \mathbb{R}^n \to \mathbb{R}$ is a continuous function and $\mathtt{z}^{[2]}(\mathtt{s}) = \mathtt{z}(\mathtt{z}(\mathtt{s}))$, $\cdots$, $\mathtt{z}^{[n]}(\mathtt{s}) = \mathtt{z}^{[n-1]}(\mathtt{z}(\mathtt{s}))$. For more details about the theory of time scales, refer to [1,3]. By applying Schauder fixed point theorem and contraction mapping principle, we establish the existence and uniqueness of solutions to the BVP (1)–(2). Equation (1) in real continuous time scales describes diffusion phenomena with a source or a reaction term [12]. We refer the interested reader to [9,10,14] and the references therein for more details.

The commonly used technique in the theory of BVPs on time scales involving transforming the BVP (1)–(2) as an equivalent integral equation (see, Chapter 7 of [4])

$$\mathtt{z}(\mathtt{s}) = \mathtt{z}_a + \frac{\mathtt{z}_b - \mathtt{z}_a}{\sigma^2(b) - a}(\mathtt{s} - a) + \int_a^{\sigma(b)} \mathtt{G}(\mathtt{s}, \mathtt{t})\mathtt{g}\big(\mathtt{t}, \mathtt{z}(\mathtt{t}), \mathtt{z}^{[2]}(\mathtt{t}), \mathtt{z}^{[3]}(\mathtt{t}), \cdots, \mathtt{z}^{[n]}(\mathtt{t})\big)\Delta\mathtt{t}, \ \mathtt{s} \in [a, \sigma^2(b)]_{\mathbb{T}}, \tag{3}$$

where

$$\mathtt{G}(\mathtt{s}, \mathtt{t}) = \frac{1}{\sigma^2(b) - a} \begin{cases} (\mathtt{s} - a)(\sigma^2(b) - \sigma(t)), & if \ \ \mathtt{s} \le \mathtt{t}, \\ (\sigma(t) - a)(\sigma^2(b) - \mathtt{s}), & if \ \ \sigma(\mathtt{t}) \le \mathtt{s}. \end{cases} \tag{4}$$

Moreover, we note that $\mathtt{G}(\mathtt{s}, \mathtt{t})$ is nonnegative on $[a, \sigma^2(b)]_{\mathbb{T}} \times [a, b]_{\mathbb{T}}$ and

$$\mathtt{G}(\mathtt{s}, \mathtt{t}) \le \mathtt{G}(\sigma(\mathtt{t}), \mathtt{t}), \ (\mathtt{s}, \mathtt{t}) \in [a, \sigma^2(b)]_{\mathbb{T}} \times [a, b]_{\mathbb{T}}. \tag{5}$$

We difine

$$\mathtt{M} = \max_{\mathtt{s} \in [a, \sigma^2(b)]_{\mathbb{T}}} \int_a^{\sigma(b)} \mathtt{G}(\mathtt{s}, \mathtt{t})\Delta\mathtt{t}. \tag{6}$$

Lemma 1 *For any* $\mathtt{s}_1, \mathtt{s}_2 \in [a, \sigma^2(b)]_{\mathbb{T}}$, *the Green's function* (4) *satisfies*

$$\int_a^{\sigma^2(b)} |\mathtt{G}(\mathtt{s}_1, \mathtt{t}) - \mathtt{G}(\mathtt{s}_2, \mathtt{t})|\Delta\mathtt{t} \le \mathtt{N}|\mathtt{s}_1 - \mathtt{s}_2|,$$

where $\mathtt{N} = 4(\sigma^2(b) - a)$.

Proof Set $\mathtt{G}_1(\mathtt{s},\mathtt{t}) = \frac{(\mathtt{s}-a)(\sigma^2(b)-\sigma(t))}{\sigma^2(b)-a}$ and $\mathtt{G}_2(\mathtt{s},\mathtt{t}) = \frac{(\sigma(t)-a)(\sigma^2(b)-\mathtt{s})}{\sigma^2(b)-a}$. Let $\mathtt{s}_1, \mathtt{s}_2 \in [a, \sigma^2(b)]_{\mathbb{T}}$ with $\mathtt{s}_2 \le \mathtt{s}_1$. Then

$$\begin{aligned}
\int_a^{\mathtt{s}_2} |\mathtt{G}_1(\mathtt{s}_1,\mathtt{t}) - \mathtt{G}_1(\mathtt{s}_2,\mathtt{t})|\Delta\mathtt{t} &= \frac{1}{\sigma^2(b)-a}\int_a^{\mathtt{s}_2} |(\mathtt{s}_1 - a)(\sigma^2(b)-\sigma(t)) \\
&\quad - (\mathtt{s}_2 - a)(\sigma^2(b)-\sigma(t))|\Delta\mathtt{t} \\
&\le \frac{1}{\sigma^2(b)-a}|\mathtt{s}_1 - \mathtt{s}_2|\int_a^{\mathtt{s}_2} |(\sigma^2(b)-\sigma(t))|\Delta\mathtt{t} \\
&\le \frac{1}{\sigma^2(b)-a}|\mathtt{s}_1 - \mathtt{s}_2|\int_a^{\mathtt{s}_2} |(\sigma^2(b)-a)|\Delta\mathtt{t} \\
&\le (\sigma^2(b)-a)|\mathtt{s}_1 - \mathtt{s}_2|, \\
\int_{\mathtt{s}_2}^{\mathtt{s}_1} |\mathtt{G}_1(\mathtt{s}_1,\mathtt{t}) - \mathtt{G}_2(\mathtt{s}_2,\mathtt{t})|\Delta\mathtt{t} &= \frac{1}{\sigma^2(b)-a}\int_{\mathtt{s}_2}^{\mathtt{s}_1} |(\mathtt{s}_1 - a)(\sigma^2(b)-\sigma(t)) \\
&\quad - (\sigma(t) - a)(\sigma^2(b)-\mathtt{s}_2)|\Delta\mathtt{t} \\
&\le \frac{1}{\sigma^2(b)-a}\int_{\mathtt{s}_2}^{\mathtt{s}_1} (\mathtt{s}_1 - a)(\sigma^2(b)-\sigma(t))\Delta\mathtt{t} \\
&\quad + \frac{1}{\sigma^2(b)-a}\int_{\mathtt{s}_2}^{\mathtt{s}_1} (\sigma(t) - a)(\sigma^2(b)-\mathtt{s}_2)\Delta\mathtt{t} \\
&\le \int_{\mathtt{s}_2}^{\mathtt{s}_1} (\mathtt{s}_1 - a)\Delta\mathtt{t} + \int_{\mathtt{s}_2}^{\mathtt{s}_1} (\sigma(t) - a)\Delta\mathtt{t} \\
&\le 2(\sigma^2(b)-a)|\mathtt{s}_1 - \mathtt{s}_2|
\end{aligned}$$

and

$$\begin{aligned}
\int_{\mathtt{s}_1}^{\sigma^2(b)} |\mathtt{G}_2(\mathtt{s}_1,\mathtt{t}) - \mathtt{G}_2(\mathtt{s}_2,\mathtt{t})|\Delta\mathtt{t} &= \frac{1}{\sigma^2(b)-a}\int_a^{\mathtt{s}_2} |(\sigma(t) - a)(\sigma^2(b)-\mathtt{s}_1) \\
&\quad - (\sigma(t) - a)(\sigma^2(b)-\mathtt{s}_2)|\Delta\mathtt{t} \\
&\le \frac{1}{\sigma^2(b)-a}(\sigma(t) - a)\int_a^{\mathtt{s}_2} |\mathtt{s}_1 - \mathtt{s}_2|\Delta\mathtt{t} \\
&\le (\sigma^2(b)-a)|\mathtt{s}_1 - \mathtt{s}_2|.
\end{aligned}$$

Thus,

$$\begin{aligned}
&\int_a^{\sigma^2(b)} |\mathtt{G}(\mathtt{s}_1,\mathtt{t}) - \mathtt{G}(\mathtt{s}_2,\mathtt{t})|\Delta\mathtt{t} \\
&= \int_a^{\mathtt{s}_2} |\mathtt{G}_1(\mathtt{s}_1,\mathtt{t}) - \mathtt{G}_1(\mathtt{s}_2,\mathtt{t})|\Delta\mathtt{t} + \int_{\mathtt{s}_2}^{\mathtt{s}_1} |\mathtt{G}_1(\mathtt{s}_1,\mathtt{t}) - \mathtt{G}_2(\mathtt{s}_2,\mathtt{t})|\Delta\mathtt{t} \\
&\quad + \int_{\mathtt{s}_1}^{\sigma^2(b)} |\mathtt{G}_2(\mathtt{s}_1,\mathtt{t}) - \mathtt{G}_2(\mathtt{s}_2,\mathtt{t})|\Delta\mathtt{t} \le 4(\sigma^2(b)-a)|\mathtt{s}_1 - \mathtt{s}_2|.
\end{aligned}$$

□

Consider the function space

$$\mathtt{C}[a, \sigma^2(b)] = \{\mathtt{z} \mid \mathtt{z} : [a, \sigma^2(b)]_{\mathbb{T}} \to \mathbb{R} \text{ is continuous}\}$$

and for $\mathtt{L} > 0$, define

$$\mathscr{B}(\mathtt{L}) = \{\mathtt{z} \in \mathtt{C}[a, \sigma^2(b)] \mid \|\mathtt{z}\| \leq \mathtt{L},\ \forall\, \mathtt{s} \in [a, \sigma^2(b)]_{\mathbb{T}}\}.$$

Then $\mathscr{B}(\mathtt{L})$ is a Banach space with the norm

$$\|\mathtt{z}\| = \max_{\mathtt{s} \in [a, \sigma^2(b)]_{\mathbb{T}}} |\mathtt{z}(\mathtt{s})|.$$

For $\mathtt{L} > 0$ and $\Bbbk > 0$, define the set

$$\begin{aligned}\mathscr{B}(\mathtt{L}, \Bbbk) = \{\mathtt{z} \in \mathscr{B}(\mathtt{L}) \mid \|\mathtt{z}\| \leq \mathtt{L} \text{ and } |\mathtt{z}(\mathtt{s}_1)\\ -\mathtt{z}(\mathtt{s}_2)| \leq \Bbbk|\mathtt{s}_1 - \mathtt{s}_2|,\ \forall\, \mathtt{s}_1, \mathtt{s}_2 \in [a, \sigma^2(b)]_{\mathbb{T}}\}.\end{aligned}$$

Then $\mathscr{B}(\mathtt{L}, \Bbbk)$ is a closed convex and bounded subset of $\mathscr{B}(\mathtt{L})$. Also, it can be seen from the definition of $\mathscr{B}(\mathtt{L}, \Bbbk)$ that for every $\psi, \phi \in \mathscr{B}(\mathtt{L}, \Bbbk)$,

$$\|\psi^{[i]} - \phi^{[i]}\| \leq \sum_{\mathtt{j}=0}^{i-1} \Bbbk^{\mathtt{j}} \|\psi - \phi\|, \quad i = 1, 2, \cdots \tag{7}$$

Now define an operator $\aleph : \mathscr{B}(\mathtt{L}, \Bbbk) \to \mathscr{B}(\mathtt{L})$ as

$$\begin{aligned}(\aleph \mathtt{z})(\mathtt{s}) &= \mathtt{z}_a + \frac{\mathtt{z}_b - \mathtt{z}_a}{\sigma^2(b) - a}(\mathtt{s} - a)\\ &\quad + \int_a^{\sigma(b)} \mathtt{G}(\mathtt{s}, \mathtt{t})\mathtt{g}\big(\mathtt{t}, \mathtt{z}(\mathtt{t}), \mathtt{z}^{[2]}(\mathtt{t}), \mathtt{z}^{[3]}(\mathtt{t}), \cdots, \mathtt{z}^{[n]}(\mathtt{t})\big)\Delta \mathtt{t},\ \mathtt{s} \in [a, \sigma^2(b)]_{\mathbb{T}}.\end{aligned} \tag{8}$$

Then $\mathtt{z}$ is a solution of (1)–(2) if and only if $\mathtt{z}$ is a fixed point of $\aleph$.

2 Existence and uniqueness of solutions

This section deals with existence and uniqueness of solutions for (1)–(2). In order to reach our goal, we assume the following condition hold:

($\mathcal{H}_1$) Let $\alpha_1, \alpha_2, \cdots, \alpha_n$ be positive constants such that

$$|\mathtt{g}(\mathtt{t}, \mathtt{z}_1, \mathtt{z}_2, \cdots, \mathtt{z}_n) - \mathtt{g}(\mathtt{t}, \widehat{\mathtt{z}}_1, \widehat{\mathtt{z}}_2, \cdots, \widehat{\mathtt{z}}_n)| \leq \sum_{\mathtt{j}=1}^{n} \alpha_{\mathtt{j}} \|\mathtt{z}_{\mathtt{j}} - \widehat{\mathtt{z}}_{\mathtt{j}}\|$$

Lemma 2 *Suppose* $(\mathcal{H}_1)$ *holds. Then operator* $\aleph$ *is continuous and compact on* $\mathscr{B}(\mathtt{L}, \Bbbk)$.

Proof Let $\mathtt{z}, \widehat{\mathtt{z}} \in \mathscr{B}(\mathtt{L}, \Bbbk)$ and $\mathtt{s} \in [a, \sigma^2(b)]_{\mathbb{T}}$. Then by $(\mathcal{H}_1)$, (6) and (7),

$$\begin{aligned}
\|(\aleph\mathtt{z})(\mathtt{s}) - (\aleph\widehat{\mathtt{z}})(\mathtt{s})\| &\leq \int_a^{\sigma(b)} |\mathtt{G}(\mathtt{s}, \mathtt{t})| \Big| \mathtt{g}\big(\mathtt{t}, \mathtt{z}(\mathtt{t}), \mathtt{z}^{[2]}(\mathtt{t}), \mathtt{z}^{[3]}(\mathtt{t}), \cdots, \mathtt{z}^{[n]}(\mathtt{t})\big) \\
&\quad - \mathtt{g}\big(\mathtt{t}, \widehat{\mathtt{z}}(\mathtt{t}), \widehat{\mathtt{z}}^{[2]}(\mathtt{t}), \widehat{\mathtt{z}}^{[3]}(\mathtt{t}), \cdots, \widehat{\mathtt{z}}^{[n]}(\mathtt{t})\big) \Big| \Delta\mathtt{t} \\
&\leq \int_a^{\sigma(b)} |\mathtt{G}(\mathtt{s}, \mathtt{t})| \sum_{\mathtt{j}=1}^{n} \alpha_{\mathtt{j}} \|\mathtt{z}^{[\mathtt{j}]} - \widehat{\mathtt{z}}^{[\mathtt{j}]}\| \Delta\mathtt{t} \\
&\leq \mathtt{M} \sum_{\mathtt{j}=1}^{n} \alpha_{\mathtt{j}} \sum_{i=0}^{\mathtt{j}-1} \Bbbk^i \|\mathtt{z} - \widehat{\mathtt{z}}\|.
\end{aligned}$$

Thus, $\aleph$ is continuous. It can be seen by Arzela-Ascoli theorem that $\aleph$ is compact. □

Lemma 3 *Suppose* $(\mathcal{H}_1)$ *and the following hold.*

$(\mathcal{H}_2)$ $2|\mathtt{z}_a| + |\mathtt{z}_b| + \mathtt{M}\Big[\mathtt{g}^\star + \mathtt{L}\sum_{\mathtt{j}=1}^{n} \alpha_{\mathtt{j}} \sum_{i=0}^{\mathtt{j}-1} \Bbbk^i\Big] \leq \mathtt{L}$, *where* $\mathtt{g}^\star = \max_{\mathtt{t}\in[a,\sigma^2(b)]_{\mathbb{T}}} |\mathtt{g}(\mathtt{t}, 0, 0, \cdots, 0)|$.

Then $|(\aleph\mathtt{z})(\mathtt{s})| \leq \mathtt{L}$ *for all* $\mathtt{s} \in [a, \sigma^2(b)]_{\mathbb{T}}$ *and* $\mathtt{z} \in \mathscr{B}(\mathtt{L}, \Bbbk)$.

Proof Let $\mathtt{z} \in \mathscr{B}(\mathtt{L}, \Bbbk)$ and $\mathtt{s} \in [a, \sigma^2(b)]_{\mathbb{T}}$. Then

$$\begin{aligned}
|(\aleph\mathtt{z})(\mathtt{s})| &= \Big| \mathtt{z}_a + \frac{\mathtt{z}_b - \mathtt{z}_a}{\sigma^2(b) - a}(\mathtt{s} - a) \\
&\quad + \int_a^{\sigma(b)} \mathtt{G}(\mathtt{s}, \mathtt{t}) \mathtt{g}\big(\mathtt{t}, \mathtt{z}(\mathtt{t}), \mathtt{z}^{[2]}(\mathtt{t}), \mathtt{z}^{[3]}(\mathtt{t}), \cdots, \mathtt{z}^{[n]}(\mathtt{t})\big) \Delta\mathtt{t} \Big| \\
&\leq 2\mathtt{z}_a + \mathtt{z}_b + \int_a^{\sigma(b)} |\mathtt{G}(\mathtt{s}, \mathtt{t})| |\mathtt{g}\big(\mathtt{t}, \mathtt{z}(\mathtt{t}), \mathtt{z}^{[2]}(\mathtt{t}), \mathtt{z}^{[3]}(\mathtt{t}), \cdots, \mathtt{z}^{[n]}(\mathtt{t})\big) \\
&\quad - \mathtt{g}(\mathtt{t}, 0, 0, \cdots, 0)| \Delta\mathtt{t} \\
&\quad + \int_a^{\sigma(b)} |\mathtt{G}(\mathtt{s}, \mathtt{t})| |\mathtt{g}(\mathtt{t}, 0, 0, \cdots, 0)| \Delta\mathtt{t} \\
&\leq 2\mathtt{z}_a + \mathtt{z}_b + \mathtt{M} \sum_{\mathtt{j}=1}^{n} \alpha_{\mathtt{j}} \sum_{i=0}^{\mathtt{j}-1} \Bbbk^i \|\mathtt{z}\| + \mathtt{M}\mathtt{g}^\star \\
&\leq 2\mathtt{z}_a + \mathtt{z}_b + \mathtt{M}\left[\mathtt{L} \sum_{\mathtt{j}=1}^{n} \alpha_{\mathtt{j}} \sum_{i=0}^{\mathtt{j}-1} \Bbbk^i + \mathtt{g}^\star \right] \\
&\leq \mathtt{L}.
\end{aligned}$$

□

Lemma 4 *Suppose* $(\mathcal{H}_1)$ *and the following hold.*

$(\mathcal{H}_3)$ $\frac{|z_b - z_a|}{\sigma^2(b)-a} + \mathtt{N}\left[\mathtt{g}^\star + \mathtt{L}\sum_{\mathtt{j}=1}^{n} \alpha_{\mathtt{j}} \sum_{i=0}^{\mathtt{j}-1} \Bbbk^i\right] \leq \Bbbk.$

Then $|(\aleph \mathtt{z})(\mathtt{s}_1) - (\aleph \mathtt{z})(\mathtt{s}_2)| \leq \Bbbk|\mathtt{s}_1 - \mathtt{s}_2|$ *for all* $\mathtt{s}_1, \mathtt{s}_2 \in [a, \sigma^2(b)]_{\mathbb{T}}$ *and* $\mathtt{z} \in \mathscr{B}(\mathtt{L}, \Bbbk)$.

Proof Let $\mathtt{s}_1, \mathtt{s}_2 \in [a, \sigma^2(b)]_{\mathbb{T}}$ and $\mathtt{z} \in \mathscr{B}(\mathtt{L}, \Bbbk)$ with $\mathtt{s}_1 \leq \mathtt{s}_2$. Then

$$
\begin{aligned}
|(\aleph \mathtt{z})(\mathtt{s}_1) - (\aleph \mathtt{z})(\mathtt{s}_2)| \leq{}& \frac{|z_b - z_a|}{\sigma^2(b)-a}|\mathtt{s}_1 - \mathtt{s}_2| + \int_a^{\sigma(b)} |\mathtt{G}(\mathtt{s}_1, \mathtt{t}) \\
&- \mathtt{G}(\mathtt{s}_2, \mathtt{t})||\mathtt{g}\big(\mathtt{t}, \mathtt{z}(\mathtt{t}), \mathtt{z}^{[2]}(\mathtt{t}), \mathtt{z}^{[3]}(\mathtt{t}), \cdots, \mathtt{z}^{[n]}(\mathtt{t})\big)|\Delta \mathtt{t} \\
\leq{}& \frac{|z_b - z_a|}{\sigma^2(b)-a}|\mathtt{s}_1 - \mathtt{s}_2| + \int_a^{\sigma(b)} |\mathtt{G}(\mathtt{s}_1, \mathtt{t}) \\
&- \mathtt{G}(\mathtt{s}_2, \mathtt{t})|\Big|\mathtt{g}\big(\mathtt{t}, \mathtt{z}(\mathtt{t}), \mathtt{z}^{[2]}(\mathtt{t}), \mathtt{z}^{[3]}(\mathtt{t}), \cdots, \mathtt{z}^{[n]}(\mathtt{t})\big)|\Delta \mathtt{t} \\
&- \mathtt{g}(\mathtt{t}, 0, 0, \cdots, 0)\Big|\Delta \mathtt{t} + \int_a^{\sigma(b)} |\mathtt{G}(\mathtt{s}_1, \mathtt{t}) \\
&- \mathtt{G}(\mathtt{s}_2, \mathtt{t})||\mathtt{g}(\mathtt{t}, 0, 0, \cdots, 0)\Big|\Delta \mathtt{t} \\
\leq{}& \frac{|z_b - z_a|}{\sigma^2(b)-a}|\mathtt{s}_1 - \mathtt{s}_2| \\
&+ \mathtt{N}\sum_{\mathtt{j}=1}^{n} \alpha_{\mathtt{j}} \sum_{i=0}^{\mathtt{j}-1} \Bbbk^i \|\mathtt{z}\||\mathtt{s}_1 - \mathtt{s}_2| + \mathtt{N}\mathtt{g}^\star|\mathtt{s}_1 - \mathtt{s}_2| \\
\leq{}& \frac{|z_b - z_a|}{\sigma^2(b)-a}|\mathtt{s}_1 - \mathtt{s}_2| \\
&+ \mathtt{N}\left[\mathtt{L}\sum_{\mathtt{j}=1}^{n} \alpha_{\mathtt{j}} \sum_{i=0}^{\mathtt{j}-1} \Bbbk^i + \mathtt{g}^\star\right]|\mathtt{s}_1 - \mathtt{s}_2| \\
\leq{}& \Bbbk|\mathtt{s}_1 - \mathtt{s}_2|.
\end{aligned}
$$

□

Lemma 5 *Suppose* $(\mathcal{H}_1)$–$(\mathcal{H}_3)$ *hold. Then* $\aleph(\mathscr{B}(\mathtt{L}, \Bbbk)) \subset \mathscr{B}(\mathtt{L}, \Bbbk)$.

Proof It is clear from Lemmas 3 and 4 that $\aleph$ maps $\mathscr{B}(\mathtt{L}, \Bbbk)$ into itself. □

Theorem 1 *Suppose* $(\mathcal{H}_1)$–$(\mathcal{H}_3)$ *hold. Then BPV* (1)–(2) *has a solution in* $\mathscr{B}(\mathtt{L}, \Bbbk)$.

Proof From Lemmas 2 to 5, we see that all the conditions of Schauder's fixed point theorem are satisfied on $\mathscr{B}(\mathtt{L}, \Bbbk)$. thus there exists a fixed point $\mathtt{z}^\star$ in $\mathscr{B}(\mathtt{L}, \Bbbk)$ such that $\aleph \mathtt{z}^\star = \mathtt{z}^\star$. Therefore, $\mathtt{z}^\star$ is a solution of (1)–(2). This completes the proof. □

Theorem 2 *Suppose* $(\mathcal{H}_1)$-$(\mathcal{H}_3)$ *and the following hold.*

$(\mathcal{H}_4)$ $\mathtt{M}\sum_{\mathtt{j}=1}^{n} \alpha_{\mathtt{j}} \sum_{i=0}^{\mathtt{j}-1} \Bbbk^i < 1.$

Then BPV (1)–(2) *has a unique solution in* $\mathscr{B}(\mathtt{L}, \mathbb{k})$.

Proof Let $\mathtt{z}, \widehat{\mathtt{z}} \in \mathscr{B}(\mathtt{L}, \mathbb{k})$ and $\mathtt{s} \in [a, \sigma^2(b)]_{\mathbb{T}}$. Then by Lemma 2,

$$\|(\aleph \mathtt{z})(\mathtt{s}) - (\aleph \widehat{\mathtt{z}})(\mathtt{s})\| \leq \mathtt{M} \sum_{\mathtt{j}=1}^{n} \alpha_{\mathtt{j}} \sum_{i=0}^{\mathtt{j}-1} \mathbb{k}^i \|\mathtt{z} - \widehat{\mathtt{z}}\|$$

Therefore, by the contraction mapping principle $\aleph$ has a unique fixed point in $\mathscr{B}(\mathtt{L}, \mathbb{k})$. This completes the proof.

3 Continuous dependence

In this section, we establish continuous dependence of the unique solution on $\mathtt{g}$.

Theorem 3 *Suppose* $(\mathcal{H}_1)$–$(\mathcal{H}_4)$ *hold. Then unique solution of* (1)–(2) *obtained in Theorem 2 depends continuously on* $\mathtt{g}$.

Proof Let $\mathtt{g}$ and $\widehat{\mathtt{g}}$ be two given functions and consider the corresponding operators $\aleph$ and $\widehat{\aleph}$ defined by (8). Next by Theorem 2, there exist two unique functions $\mathtt{z}(\mathtt{s})$ and $\widehat{\mathtt{z}}(\mathtt{s})$ in $\mathscr{B}(\mathtt{L}, \mathbb{k})$ such that $\mathtt{z} = \aleph \mathtt{z}$ and $\widehat{\mathtt{z}} = \widehat{\aleph}\widehat{\mathtt{z}}$. Then,

$$\begin{aligned}
\|\aleph \widehat{\mathtt{z}} - \widehat{\aleph}\widehat{\mathtt{z}}\| &\leq \int_a^{\sigma(b)} |\mathtt{G}(\mathtt{s}, \mathtt{t})| \Big| \mathtt{g}\big(\mathtt{t}, \widehat{\mathtt{z}}(\mathtt{t}), \widehat{\mathtt{z}}^{[2]}(\mathtt{t}), \widehat{\mathtt{z}}^{[3]}(\mathtt{t}), \cdots, \widehat{\mathtt{z}}^{[n]}(\mathtt{t})\big) \\
&\quad - \widehat{\mathtt{g}}\big(\mathtt{t}, \widehat{\mathtt{z}}(\mathtt{t}), \widehat{\mathtt{z}}^{[2]}(\mathtt{t}), \widehat{\mathtt{z}}^{[3]}(\mathtt{t}), \cdots, \widehat{\mathtt{z}}^{[n]}(\mathtt{t})\big) \Big| \Delta \mathtt{t} \\
&\leq \int_a^{\sigma(b)} |\mathtt{G}(\mathtt{s}, \mathtt{t})| \Big[\Big| \mathtt{g}\big(\mathtt{t}, \widehat{\mathtt{z}}(\mathtt{t}), \widehat{\mathtt{z}}^{[2]}(\mathtt{t}), \widehat{\mathtt{z}}^{[3]}(\mathtt{t}), \cdots, \widehat{\mathtt{z}}^{[n]}(\mathtt{t})\big) \\
&\quad - \widehat{\mathtt{g}}\big(\mathtt{t}, \mathtt{z}(\mathtt{t}), \mathtt{z}^{[2]}(\mathtt{t}), \mathtt{z}^{[3]}(\mathtt{t}), \cdots, \mathtt{z}^{[n]}(\mathtt{t})\big) \Big| \\
&\quad + \Big| \widehat{\mathtt{g}}\big(\mathtt{t}, \mathtt{z}(\mathtt{t}), \mathtt{z}^{[2]}(\mathtt{t}), \mathtt{z}^{[3]}(\mathtt{t}), \cdots, \mathtt{z}^{[n]}(\mathtt{t})\big) \\
&\quad - \widehat{\mathtt{g}}\big(\mathtt{t}, \widehat{\mathtt{z}}(\mathtt{t}), \widehat{\mathtt{z}}^{[2]}(\mathtt{t}), \widehat{\mathtt{z}}^{[3]}(\mathtt{t}), \cdots, \widehat{\mathtt{z}}^{[n]}(\mathtt{t})\big) \Big| \Big] \Delta \mathtt{t} \\
&\leq \int_a^{\sigma(b)} |\mathtt{G}(\mathtt{s}, \mathtt{t})| \Big[\|\mathtt{g} \\
&\quad - \widehat{\mathtt{g}}\| + \sum_{\mathtt{j}=1}^{n} \alpha_{\mathtt{j}} \sum_{i=0}^{\mathtt{j}-1} \mathbb{k}^i \|\mathtt{z} - \widehat{\mathtt{z}}\| \Big] \Delta \mathtt{t} \\
&= \mathtt{M} \Big[\|\mathtt{g} - \widehat{\mathtt{g}}\| + \sum_{\mathtt{j}=1}^{n} \alpha_{\mathtt{j}} \sum_{i=0}^{\mathtt{j}-1} \mathbb{k}^i \|\mathtt{z} - \widehat{\mathtt{z}}\| \Big].
\end{aligned}$$

Therefore,

$$\begin{aligned}\|\mathtt{z}-\widehat{\mathtt{z}}\| &\le \|\aleph\mathtt{z}-\aleph\widehat{\mathtt{z}}\|+\|\aleph\widehat{\mathtt{z}}-\widehat{\aleph}\widehat{\mathtt{z}}\|\\ &\le \mathtt{M}\sum_{\mathtt{j}=1}^{n}\alpha_{\mathtt{j}}\sum_{i=0}^{\mathtt{j}-1}\Bbbk^{i}\|\mathtt{z}-\widehat{\mathtt{z}}\|+\mathtt{M}\Big[\|\mathtt{g}-\widehat{\mathtt{g}}\|+\sum_{\mathtt{j}=1}^{n}\alpha_{\mathtt{j}}\sum_{i=0}^{\mathtt{j}-1}\Bbbk^{i}\|\mathtt{z}-\widehat{\mathtt{z}}\|\Big].\end{aligned}$$

That is

$$\|\mathtt{z}-\widehat{\mathtt{z}}\|\le \mathtt{M}\left[1-2\mathtt{M}\sum_{\mathtt{j}=1}^{n}\alpha_{\mathtt{j}}\sum_{i=0}^{\mathtt{j}-1}\Bbbk^{i}\right]^{-1}\|\mathtt{g}-\widehat{\mathtt{g}}\|.$$

This completes the proof. □

Example 1 Consider the time scale $\mathbb{T}=\{10^m|m\in\mathbb{Z}\}\cup\{0\}$ and $\mathtt{z}_a=1$, $\mathtt{z}_b=2$, $a=0$, $b=1$ in the (1)–(2). It follows from (6) that, for $\mathtt{s}=\frac{1}{10^m}$, $m=-1,0,1,\cdots$,

$$\begin{aligned}\max_{\mathtt{s}\in[0,100]_{\mathbb{T}}}\int_0^{10}\mathtt{G}(\mathtt{s},\mathtt{t})\Delta\mathtt{t} &= \max_m\left[\lim_{k\to+\infty}\int_{\frac{1}{10^k}}^{\frac{1}{10^m}}10\mathtt{t}(10^2-\frac{1}{10^m})\Delta\mathtt{t}\right.\\ &\quad\left.+\int_{\frac{1}{10^m}}^{10}\frac{1}{10^m}(10^2-10\mathtt{t})\Delta\mathtt{t}\right]\\ &= \frac{10}{11}\max_m\left[101\times10^{-2m}-10^{-3m}-10^{-2}\right]\\ &= 8181.818182.\end{aligned}$$

So, $\mathtt{M}=8181.818182$ and $\mathtt{N}=400$. Next, consider the function

$$\begin{aligned}\mathtt{g}(\mathtt{t},\mathtt{z}(\mathtt{t}),\mathtt{z}^{[2]}(\mathtt{t}),\mathtt{z}^{[3]}(\mathtt{t})) &= \cos(\mathtt{t})+\frac{\pi}{154\times10^3}\mathtt{z}(\mathtt{t})\\ &\quad+\frac{\pi}{256\times10^3}\sin(\mathtt{z}^{[2]}(\mathtt{t}))+\frac{\pi}{323\times10^3}\cos(\mathtt{z}^{[3]}(\mathtt{t})).\end{aligned}$$

Then

$$\begin{aligned}&|\mathtt{g}(\mathtt{t},\mathtt{z}_1,\mathtt{z}_2,\mathtt{z}_3)-\mathtt{g}(\mathtt{t},\widehat{\mathtt{z}}_1,\widehat{\mathtt{z}}_2,\widehat{\mathtt{z}}_3)|\le\alpha_1\|\mathtt{z}_1-\widehat{\mathtt{z}}_1\|\\ &\quad+\alpha_2\|\mathtt{z}_2-\widehat{\mathtt{z}}_2\|+\alpha_3\|\mathtt{z}_3-\widehat{\mathtt{z}}_3\|,\end{aligned}$$

where $\alpha_1=\frac{\pi}{154\times10^3}$, $\alpha_2=\frac{\pi}{256\times10^3}$, $\alpha_3=\frac{\pi}{323\times10^3}$ and

$$\mathtt{g}(\mathtt{t},0,0,0)=\cos(\mathtt{t})+\frac{\pi}{323\times10^3}\le1.000009726:=\mathtt{g}^{\star}.$$

Further, let $\mathtt{L} = \frac{\pi}{2.42\times 10^{-4}}$ and $\mathbb{k} = \frac{\pi}{4.95\times 10^{-3}}$. Then

$$2|\mathtt{z}_a| + |\mathtt{z}_b| + \mathtt{M}\left[\mathtt{g}^\star + \mathtt{L}\sum_{\mathtt{j}=1}^{n}\alpha_{\mathtt{j}}\sum_{i=0}^{\mathtt{j}-1}\mathbb{k}^i\right] = 12692.87935 \leq \mathtt{L},$$

$$\frac{|\mathtt{z}_b - \mathtt{z}_a|}{\sigma^2(b) - a} + \mathtt{N}\left[\mathtt{g}^\star + \mathtt{L}\sum_{\mathtt{j}=1}^{n}\alpha_{\mathtt{j}}\sum_{i=0}^{\mathtt{j}-1}\mathbb{k}^i\right] = 620.3552127 \leq \mathbb{k}$$

and

$$\mathtt{M}\sum_{\mathtt{j}=1}^{n}\alpha_{\mathtt{j}}\sum_{i=0}^{\mathtt{j}-1}\mathbb{k}^i = 0.3471772648 < 1.$$

Thus, all assumptions $(\mathcal{H}_1)$–$(\mathcal{H}_4)$ hold. Therefore, the BVP

$$\begin{cases} \mathtt{z}^{\Delta\Delta}(\mathtt{s}) + \cos(\mathtt{s}) + \dfrac{\pi}{154\times 10^3}\mathtt{z}(\mathtt{s}) \\ \quad + \dfrac{\pi}{256\times 10^3}\sin(\mathtt{z}^{[2]}(\mathtt{s})) + \dfrac{\pi}{323\times 10^3}\cos(\mathtt{z}^{[3]}(\mathtt{s})) = 0,\ \mathtt{s}\in[0,1]_{\mathbb{T}}, \\ \mathtt{z}(0) = 1,\ \mathtt{z}(\sigma^2(1)) = 2, \end{cases}$$

has a unique solution in $\mathscr{B}\left(\frac{\pi}{2.42\times 10^{-4}}, \frac{\pi}{4.95\times 10^{-3}}\right)$ and depends continuously on the function $\mathtt{g}$.

4 Conclusion

Iterative differential equation, as a special type of functional differential equations, in which the deviating arguments depend on the state. Many researchers have concentrated on studying first order iterative functional differential equations by different approaches such as Picard's successive approximation, fixed point theory and the technique of nonexpansive operators. But the literature related to the second and higher order is very less since the presence of the iterates increases the difficulty of studying them. This work gives a criteria for the existence, uniqueness and continuous dependence of solutions for nonlinear second order iterative functional boundary values with two-point boundary conditions on time scales. In the future, we study higher order iterative functional boundary value problems on time scales and fractional order iterative boundary value problems on time scales.

Acknowledgements The authors would like to thank the referees for their valuable suggestions and comments for the improvement of the paper.

Author Contributions The study was carried out in collaboration of all authors. All authors read and approved the final manuscript.

Data availibility Data sharing not applicable to this paper as no data sets were generated or analyzed during the current study.

Declarations

Conflict of interest It is declared that authors has no competing interests.

Human and animal right This article does not contain any studies with human participants or animals performed by any of the authors.

References

1. Agarwal, R.P., Bohner, M.: Basic calculus on time scales and some of its applications. Res. Math. **35**, 3–22 (1999)
2. Berinde, V.: Existence and approximation of solutions of some first order iterative differential equations. Miskolc Math. Notes **11**, 13–26 (2010)
3. Bohner, M., Peterson, A.: Dynamic equations on time scales: An introduction with applications. Birkh*ä*user Boston, Inc., Boston, (2001)
4. Bohner, M., Peterson, A.: Advances in dynamic equations on time scales. Birkh*ä*user Boston, Inc., Boston, (2003)
5. Bouakkaz, A., Ardjouni, A., Khemis, R., Djoudi, A.: Periodic solutions of a class of third-order functional differential equations with iterative source terms. Bol. Soc. Mat. Mex. **26**, 443–458 (2020)
6. Bouakkaz, A., Ardjouni, A., Djoudi, A.: Periodic solutions for a second order nonlinear functional differential equation with iterrative terms by Schauder's fixed point theorem. Acta Math. Univ. Comen. **87**(2), 223–235 (2018)
7. Bouakkaz, A., Khemis, R.: Positive periodic solutions for a class of second-order differential equations with state23 dependent delays. Turkish J. Math. **44**(4), 1412–1426 (2020)
8. Bouakkaz, A., Khemis, R.: Positive periodic solutions for revisited Nicholson's blowflies equation with iterative harvesting term. J. Math. Anal. Appl. **494**(2), 124663 (2021)
9. Cannon, J.: The solution of the heat equation subject to the specification of energy. Quart. Appl. Math. **21**, 155–160 (1963)
10. Chegis, R.: Numerical solution of a heat conduction problem with an integral boundary condition. Litovsk. Mat. Sb. **24**, 209–215 (1984)
11. Cheraiet, S., Bouakkaz, A., Khemis, R.: Bounded positive solutions of an iterative three-point boundary-value problem with integral boundary conditions. J. Appl. Math. Comp. **65**, 597–610 (2021)
12. Chouaf, S., Khemis, R., Bouakkaz, A.: Some existence results on positive solutions for an iterative second order boundary value problem with integral boundary conditions. Bol. Soc. Paran. Mat. (2020). https://doi.org/10.5269/bspm.52461
13. Feckan, M.: On a certain type of functional differential equations. Math. Slovaca **43**, 39–43 (1993)
14. Ionkin, N.I.: Solution of a boundary-value problem in heat conduction with a non-classical boundary condition. Differ. Equ. **13**, 204–211 (1977)
15. Kaufmann, E.R.: Existence and uniqueness of solutions for a second-order iterative boundary value problem functional differential equation. Electron. J. Differ. Equ. **150**, 1–6 (2018)
16. Khemis, R., Ardjouni, A., Bouakkaz, A., Djoudi, A.: Periodic solutions of a class of third-order differential equations with two delays depending on time and state. Comment. Math. Univ. Carolinae. **60**, 379–399 (2019)
17. Khuddush, M., Prasad, K.R., Vidyasagar, K.V.: Infinitely many positive solutions for an iterative system of singular multipoint boundary value problems on time scales. Rend. Circ. Mat. Palermo, II. Ser (2021).https://doi.org/10.1007/s12215-021-00650-6
18. Khuddush, M., Prasad, K.R.: Infinitely many positive solutions for an iterative system of conformable fractional order dynamic boundary value problems on time scales. Turk. J. Math. (2021). https://doi.org/10.3906/mat-2103-117
19. Si, J.G., Wang, X.P.: Analytic solutions of a second order iterative functional differential equation. J. Comp. Appl. Math. **126**, 277–285 (2000)

20. Turab, A.: A unique solution of the iterative boundary value problem for a second-order differential equation approached by fixed point results. Alex. Eng. J. **60**(6), 5797–5802 (2021)
21. Zhao, H.Y., Liu, J.: Periodic solutions of an iterative functional differential equation with variable coefficients. Math. Methods Appl. Sci. **40**(1), 286–292 (2017)

Publisher's Note Springer Nature remains neutral with regard to jurisdictional claims in published maps and institutional affiliations.

An International Journal of Optimization and Control: Theories & Applications
ISSN:2146-0957 eISSN:2146-5703
Vol.13, No.2, pp.224-235 (2023)
http://doi.org/10.11121/ijocta.2023.1278

RESEARCH ARTICLE

Existence and stability analysis to the sequential coupled hybrid system of fractional differential equations with two different fractional derivatives

Mohamed Houas,[a] Jehad Alzabut,[b,c] Mahammad Khuddush[d*]

[a] *Laboratory FIMA, UDBKM, Khemis Miliana University, Algeria*
[b] *Department of Mathematics and Sciences, Prince Sultan University, 11586 Riyadh, Saudi Arabia*
[c] *Department of Industrial Engineering, OSTİM Technical University, Ankara 06374, Türkiye*
[d] *Department of Mathematics, Dr. Lankapalli Bullayya College of Engineering, Resapuvanipalem, Visakhapatnam, 530013, Andhra Pradesh, India*
m.houas.st@univ-dbkm.dz, jalzabut@psu.edu.sa, jehad.alzabut@ostimteknik.edu.tr, khuddush89@gmail.com

ARTICLE INFO

Article History:
Received 12 June 2022
Accepted 8 February 2023
Available 29 July 2023

Keywords:
Coupled systems
Hybrid differential equations
Boundary value problem
Fractional derivative
Ulam-Hyers stability

AMS Classification 2010:
26A33; 34A08; 47H10

ABSTRACT

In this paper, we discussed the existence, uniqueness and Ulam-type stability of solutions for sequential coupled hybrid fractional differential equations with two derivatives. The uniqueness of solutions is established by means of Banach's contraction mapping principle, while the existence of solutions is derived from Leray-Schauder's alternative fixed point theorem. Further, the Ulam-type stability of the addressed problem is studied. Finally, an example is provided to check the validity of our obtained results.

CC BY

1. Introduction

Differential equations are essential for a mathematical description of Nature. Many of the general laws of Nature–in physics, chemistry, biology, economics, and engineering find their most natural expression in the language of differential equation. Differential equation (DE) allows us to study all kinds of evolutionary processes with the properties of finite-dimensionality and differentiability. Derivative of arbitrary order arises from many physical processes, such as a charge transport in amorphous semiconductors, electrochemistry and material science, where they are described by differential equations of arbitrary order, see [1–4]. Recently, many researchers have exposed attention in the field of fractional differential equations theory, which will be used to describe phenomena of real-world problems. For more details; we refer the reader to the papers [5–18]. On the other hand, hybrid differential equations have gained extensive attention from many scholars; see for example [19–21]. Hybrid differential equations and coupled hybrid systems involving fractional derivatives have also been investigated by scientific researchers; see for instance [22–28] and the references cited therein. In recent years, sequential fractional hybrid differential equations have been studied by several researchers [29–34]. On the other hand, the stability of solutions of differential equations is important in physical problems because if slight deviations from the mathematical model caused by unavoidable errors in measurement do not have a correspondingly slight effect on the solution, the mathematical equations describing the problem will not accurately predict the future outcome.

*Corresponding Author

For example, one of the difficulties in predicting population growth is the fact that it is governed by the equation $w(t) = ce^{at}$, which is an unstable solution of the equation $w'(t) = aw(t)$. Even if there are no unfavourable factors, very few inaccuracies in the initial population count (c) or breeding rate (a) will result in fairly significant errors in prediction. One of the interesting subjects in this area, is the investigation of the existence and stability of solutions, because the study of the existence of solution of the fractional differential equation(FDE) became important due to the lack of a general formula for solving nonlinear FDEs, see [29,30,32,33]. Recently, Some scholars have discussed the existence, uniqueness, and different types of Ulam stability of solutions of fractional sequential hybrid differential equations [29,32,33] and the references cited therein. The classical form of hybrid differential equation [35] is given by the following differential equation

$$\begin{cases} \dfrac{d}{dt}\left[\dfrac{w(t)}{\psi(t,w(t))}\right] = \varphi(t,w(t)),\ 0 \le t \le T, \\ w(t_0) = \quad w_0,\ w_0 \in \mathbb{R}, \end{cases}$$

where $\psi \in C([0,T]\times\mathbb{R},\mathbb{R}-\{0\})$ and $\varphi \in C([0,T]\times\mathbb{R}\to\mathbb{R})$. Many scientific researchers have studied different fractional types of the above hybrid differential equation. For example in [36], the authors have discussed the fractional hybrid differential equations involving Riemann-Liouville differential operators

$$\begin{cases} {}^{\mathtt{RL}}\mathtt{D}\left[\dfrac{w(t)}{\psi(t,w(t))}\right] = \varphi(t,w(t)),\ 0 \le t \le T, \\ w(0) = \quad 0, \end{cases}$$

where $0 << 1$, $\psi \in C([0,T]\times\mathbb{R},\mathbb{R}-\{0\})$ and $\varphi \in C([0,T]\times\mathbb{R},\mathbb{R})$.

In [37], the authors studied the existence and uniqueness of solutions of coupled hybrid fractional differential equations described by

$$\begin{cases} {}^{\mathtt{C}}\mathtt{D}\left[\dfrac{w(t)}{\psi_1(t,w(t),z(t))}\right] = \varphi(t,w(t),z(t)), \\ {}^{\mathtt{C}}\mathtt{D}\left[\dfrac{z(t)}{\psi_2(t,w(t),z(t))}\right] = \phi(t,w(t),z(t)), \\ w(0) = w(1) = 0, \quad z(0) = z(1) = 0, \end{cases}$$

where $t \in [0,1]$, $1 <\le 2$, $1 <\le 2$, $\psi_j \in C([0,1]\times\mathbb{R},\mathbb{R}-\{0\}), j = 1,2$ and $\varphi,\phi \in C([0,1]\times\mathbb{R},\mathbb{R})$. The existence and uniqueness results were obtained by applying Leray-Schauder's alternative criterion and Banach's contraction mapping principle.

Motivated by above-mentioned works, in this paper, we discuss the existence, uniqueness and Ulam-Hyers-Rassias stability of solution for sequential coupled fractional hybrid system of the following form

$$\begin{cases} {}^{\mathtt{RL}}\mathtt{D}\left[{}^{\mathtt{C}}\mathtt{D}\left[\dfrac{w(t)}{\psi_1(t,w(t),z(t))}\right]\right] \\ \qquad = \displaystyle\sum_{i=1}^{k} \varphi_i(t,w(t),z(t)), \\ {}^{\mathtt{RL}}\mathtt{D}\left[{}^{\mathtt{C}}\mathtt{D}\left[\dfrac{z(t)}{\psi_2(t,w(t),z(t))}\right]\right] \\ \qquad = \displaystyle\sum_{i=1}^{k} \phi_i(t,w(t),z(t)), \\ w(0) = w(1) = 0,\ z(0) = z(1) = 0, \end{cases} \tag{1}$$

where $0 \le t \le 1, 0 <, < 1, + > 1, 0 <, < 1, + > 1$, ${}^{\mathtt{RL}}\mathtt{D}, \in \{,\}$ and ${}^{\mathtt{C}}\mathtt{D}, \in \{,\}$ are the Riemann-Liouville and Caputo fractional derivatives respectively, $\psi_j : [0,1]\times\mathbb{R}^2 \to \mathbb{R}-\{0\}, j = 1,2$ and $\varphi_i, \phi_i : [0,1]\times\mathbb{R}^2 \to \mathbb{R}, 1 \le i \le k$, are continuous functions.

We impose the following hypotheses throughout the paper:

- (H_1) For each $i = 1,2,...,k$, the functions $\varphi_i, \phi_i : [0,1]\times\mathbb{R}^2 \to \mathbb{R}$ are continuous and there exist constants $\pi_i > 0, \vartheta_i > 0$ such that for all $t \in [0,1]$ and $(w_1,z_1),(w_2,z_2) \in \mathbb{R}^2 \to \mathbb{R}$ are continuous and there exist constants $\pi_i > 0, \vartheta_i > 0$ such that for all $t \in [0,1]$ and $(w_1,z_1),(w_2,z_2) \in \mathbb{R}^2$,
  $$|\varphi_i(t,w_1,z_1) - \varphi_i(t,w_2,z_2)| \le \pi_i(|w_1 - z_1| + |w_2 - z_2|),$$
  and
  $$|\phi_i(t,w_1,z_1) - \phi_i(t,w_2,z_2)| \le \vartheta_i(|w_1 - z_1| + |w_2 - z_2|)$$
  for $i = 1,2,\cdots,k$,
- (H_2) For all $j = 1,2$, the functions $\psi_j : [0,1]\times\mathbb{R}^2 \to \mathbb{R}-\{0\}$ are continuous and there exist constants $\Pi_j > 0$ such that
  $$\psi_1(t,w,z) \le \Pi_1 \text{ and } \psi_2(t,w,z) \le \Pi_2,$$
  for each $t \in [0,1]$ and $(w,z) \in \mathbb{R}^2$.
- (H_3) For each $i = 1,2,...,k$, the functions $\varphi_i, \phi_i : [0,1]\times\mathbb{R}^2 \to \mathbb{R}$ are continuous and

there exist constants $\gamma_i, \omega_i, \gamma_i^{'}, \omega_i^{'} \geq 0$ and $\lambda_i > 0, \lambda_i^{'} > 0$ such that for all $t \in J$ and $w, z \in \mathbb{R}$, we have

$$\varphi_i(t,w,z) \leq \lambda_i + \gamma_i |w| + \omega_i |z|,$$

and

$$\phi_i(t,w,z) \leq \lambda_i^{'} + \gamma_i^{'} |w| + \omega_i^{'} |z|.$$

The rest of the paper is organized in the following fashion. In Section 2, we introduce some basic definitions and lemmas which are useful in our main results. In Section 3, we establish a criteria for the existence and uniqueness of solutions to the boundary value problem (1) by applying the Leray-Schauder's alternative fixed point theorem and the Banach's contraction mapping principle in a Banach space. In section 4, we study Ulam-Hyers-Rassias stability of solutions to the problem (1). Finally, as an application, we demonstrate our results with example.

2. Preliminaries

In this section, we introduce some basic definitions and lemmas which are useful for our later discussions.

Definition 1. *[38] The Riemann-Liouville fractional integral of order > 0 for a function $f : (0,\infty) \to \mathbb{R}$ is defined as*

$$\mathtt{I}^{f}(t) = \frac{1}{\Gamma()} \int_0^t (t-s)^{-1} f(s) ds,$$

provided that the right side is pointwise defined on $(0,\infty)$.

Definition 2. *[38] The Riemann-Liouville fractional derivative of order > 0 for a continuous function $f : (0,\infty) \to \mathbb{R}$ is defined as*

$$\mathtt{D}^{f}(t) = \frac{1}{\Gamma(m-)} \left(\frac{d}{dt}\right)^m \int_0^t \frac{f(s)}{(t-s)^{-m-1}} ds,$$

where $m = [] + 1$, provided that the right side is pointwise defined on $(0,\infty)$.

Definition 3. *[38] For a function f given on the interval $[0,\infty)$, The Caputo derivative of fractional order γ for the function f continuous on $[0,\infty)$ is defined as*

$$^{\mathtt{C}}\mathtt{D}^{f}(t) = \frac{1}{\Gamma(m-)} \int_0^t (t-s)^{m--1} f^{(m)}(s) ds,$$

$m = [] + 1$.

Lemma 1. *[12] Let $, > 0$ and $h \in L^1([0,1])$. Then $\mathtt{II}h(t) = \mathtt{I}^{+}h(t)$ and $^{\mathtt{RL}}\mathtt{DI}h(t) = h(t)$.*

Lemma 2. *[12] Let $>> 0$ and $h \in L^1([0,1])$. Then $^{\mathtt{RL}}\mathtt{DI}h(t) = \mathtt{I}^{-}h(t)$.*

Lemma 3. *[12] Let > 0. Then for $w \in C(0,1) \cap L^1(0,1)$ and $^{\mathtt{RL}}\mathtt{D}w \in C(0,1) \cap L^1(0,1)$, we have*

$$\mathtt{I}^{\mathtt{RL}}\mathtt{D}w(t) = w(t) + c_1 t^{-1} + c_2 t^{-2} + \cdots + c_n t^{-n},$$

where $c_i \in \mathbb{R}, i = 1,2,...,n$, $n = [] + 1$.

Lemma 4. *[12] Let > 0. Then*

$$\mathtt{I}\left[^{\mathtt{C}}\mathtt{D}w(t)\right] = w(t) + c_0 + c_1 t, + c_2 t^2 + ... + c_{n-1} t^{n-1},$$

for some $c_i \in \mathbb{R}, i = 0,1,2,...,n-1, n-1 << n$.

Lemma 5. *For $g, h \in C([0,1],\mathbb{R})$ and $\psi_j \in C(([0,1] \times \mathbb{R}^2, \mathbb{R} - \{0\}), j = 1,2$, the boundary value problem*

$$\begin{cases} ^{\mathtt{RL}}\mathtt{D}\left[^{\mathtt{C}}\mathtt{D}\left[\dfrac{w(t)}{\psi_1(t,w(t),z(t))}\right]\right] = g(t), \\ ^{\mathtt{RL}}\mathtt{D}\left[^{\mathtt{C}}\mathtt{D}\left[\dfrac{z(t)}{\psi_2(t,w(t),z(t))}\right]\right] = h(t), \\ w(0) = w(1) = 0, \quad z(0) = z(1) = 0, \end{cases} \tag{2}$$

where $0 \leq t \leq 1$, $0 <, < 1$, $+ > 1$, $0 <, < 1$, $+ > 1$, has a unique solution

$$w(t) = \psi_1(t,w(t),z(t))\left[\int_0^t \frac{(t-s)^{+-1}}{\Gamma(+)} g(s) ds - t^{+-1} \int_0^1 \frac{(1-s)^{+-1}}{\Gamma(+)} g(s) ds\right], \tag{3}$$

and

$$z(t) = \psi_2(t,w(t),z(t))\left[\int_0^t \frac{(t-s)^{+-1}}{\Gamma(+)} g(s) ds - t^{+-1} \int_0^1 \frac{(1-s)^{+-1}}{\Gamma(+)} g(s) ds\right]. \tag{4}$$

Proof. Using Lemma 3, we can write

$$\begin{aligned} \frac{w(t)}{\psi_1(t,w(t),z(t))} &= \mathtt{I}g(t) + a_1 t^{-1}, \\ \frac{z(t)}{\psi_2(t,w(t),z(t))} &= \mathtt{I}h(t) + b_1 t^{-1}, \end{aligned}$$

where $a_1, b_1 \in \mathbb{R}$. Now by Lemma 4, we have

$$w(t)=\psi_1(t,w(t),z(t))\Big[\mathtt{I}^{+}g(t)+\frac{a_1\Gamma()}{\Gamma(+)}t^{+-1}+a_2\Big], \tag{5}$$

$$z(t)=\psi_2(t,w(t),z(t))\Big[\mathtt{I}^{+}h(t)+\frac{b_1\Gamma()}{\Gamma(+)}t^{+-1}+b_2\Big], \tag{6}$$

where $a_2,b_2\in\mathbb{R}$. Using boundary conditions $w(0)=w(1)=z(0)=z(1)=0$, we obtain $a_2=b_2=0$,

$$a_1=-\frac{\Gamma(+)}{\Gamma()}\int_0^1(1-s)^{+-1}g(s)\,ds,$$

and

$$b_1=-\frac{\Gamma(+)}{\Gamma()}\int_0^1(1-s)^{+-1}h(s)\,ds.$$

Substituting the values of $a_j,b_j,j=1,2$ in (5) and (6), we get (3) and (4). □

3. Existence and uniqueness of solutions to the sequential coupled hybrid system

We will use the standard fixed point theorems, to study the fractional hybrid system (1). In this regard, we define the space

$$\mathtt{W}\times\mathtt{Z}=\{(w,z):w,z\in C([0,1],\mathbb{R})\},$$

endowed with the norm $\|(w,z)\|_{\mathtt{W}\times\mathtt{Z}}=\|w\|+\|z\|$, where $\|w\|=\sup\{|w(t)|:t\in[0,1]\}$. It is clear that $(\mathtt{W}\times\mathtt{Z},\|.\|_{\mathtt{W}\times\mathtt{Z}})$ is a Banach space. Define an operator $\mathtt{O}:\mathtt{W}\times\mathtt{Z}\to\mathtt{W}\times\mathtt{Z}$ by

$$\mathtt{O}(w,z)(t)=(\mathtt{O}_1(w,z)(t),\ \mathtt{O}_2(w,z)(t)),\ t\in[0,1],$$

where

$$\mathtt{O}_1(w,z)(t)=\psi_1(t,w(t),z(t))\,\mathfrak{N}_1(t), \tag{7}$$

in which

$$\mathfrak{N}_1(t)=\sum_{i=1}^{k}\int_0^t\frac{(t-s)^{+-1}}{\Gamma(+)}\varphi_i(s,w(s),z(s))\,ds-\sum_{i=1}^{k}\int_0^1\frac{[t(1-s)]^{+-1}}{\Gamma(+)}\varphi_i(s,w(s),z(s))\,ds,$$

and

$$\mathtt{O}_2(w,z)(t)=\psi_2(t,w(t),z(t))\,\mathfrak{N}_2(t), \tag{8}$$

in which

$$\mathfrak{N}_2(t)=\sum_{i=1}^{k}\int_0^t\frac{(t-s)^{+-1}}{\Gamma(+)}\phi_i(s,w(s),z(s))\,ds-\sum_{i=1}^{k}\int_0^1\frac{[t(1-s)]^{+-1}}{\Gamma(+)}\phi_i(s,w(s),z(s))\,ds\Big].$$

Now, we prove the existence of solutions of the fractional hybrid system (1) by applying Leray-Schauder nonlinear alternative [39].

Lemma 6. *(Leray-Schauder alternative). Let $F:E\to E$ be a completely continuous operator (i.e.,a map that restricted to any bounded set in E is compact). Let*

$$(F)=\{u\in E:u=\lambda F(u)\ \text{for some}\ 0<\lambda<1\}.$$

Then either the set (F) is unbounded, or F has at least one fixed point.

Theorem 1. *Assume that hypotheses $(H_j)_{j=2,3}$ are satisfied. Furthermore, assume that*

$$\sum_{i=1}^{k}\left(\frac{\Pi_1\gamma_i}{\Gamma(++1)}+\frac{\Pi_2\gamma_i'}{\Gamma(++1)}\right)<\frac{1}{2},$$

and

$$\sum_{i=1}^{k}\left(\frac{\Pi_1\omega_i}{\Gamma(++1)}+\frac{\Pi_2\omega_i'}{\Gamma(++1)}\right)<\frac{1}{2}.$$

Then the system (1) has at least one solution on $[0,1]$.

Proof. In the first step, we show that the operator $\mathtt{O}:\mathtt{W}\times\mathtt{Z}\to\mathtt{W}\times\mathtt{Z}$ is completely continuous. By continuity of the functions $\psi_j,\varphi_i,\phi_i,j=1,2,i=1,2,...,k$, it follows that the operator $\mathtt{O}$ is continuous.

Let $\Sigma\subset\mathtt{W}\times\mathtt{Z}$ be bounded. Then we can find positive constants $A_i,B_i,i=1,2,...,k$ such that

$$|\varphi_i(t,w(t),z(t))|\le A_i,|\varphi_i(t,w(t),z(t))|\le B_i$$

for all $(w,z)\in\Sigma$. Then for any $(w,z)\in\Sigma$ we have

$$\begin{aligned}&\|\mathtt{O}_1(w,z)\|\\&\le\Pi_1\Big[\frac{1}{\Gamma(+)}\sum_{i=1}^{k}\int_0^t(t-s)^{+-1}|\varphi_i(s,w(s),z(s))|\,ds\\&\quad+\frac{t^{+-1}}{\Gamma(+)}\sum_{i=1}^{k}\int_0^1(1-s)^{+-1}|\varphi_i(s,w(s),z(s))|\,ds\Big]\\&\le\sum_{i=1}^{k}\frac{2\Pi_1A_i}{\Gamma(++1)},\end{aligned}$$

which yields

$$\|\mathtt{O}_1(w,z)\| \leq \sum_{i=1}^{k} \frac{2\Pi_1 A_i}{\Gamma(++1)} < +\infty. \tag{9}$$

Also,

$$\|\mathtt{O}_2(w,z)\| \leq \sum_{i=1}^{k} \frac{2\Pi_2 B_i}{\Gamma(++1)} < +\infty. \tag{10}$$

Hence, by (9) and (10), we deduce that the operator $\mathtt{O}$ is uniformly bounded.

Next, we show that $\mathtt{O}$ is equicontinuous. For all $0 \leq t_2 < t_1 \leq 1$, we have

$$\begin{aligned}
&\left|\mathtt{O}_1(w,z)(t_1) - \mathtt{O}_1(w,z)(t_2)\right| \\
&\leq \sum_{i=1}^{k} \frac{\Pi_1 A_i}{\Gamma(++1)} \Big(\left[(t_1-t_2)^+ + \left|t_1^+ - t_2^+\right|\right] \\
&\quad + \left|t_1^{+-1} - t_2^{+-1}\right| \Big),
\end{aligned} \tag{11}$$

and

$$\begin{aligned}
&\left|\mathtt{O}_2(w,z)(t_1) - \mathtt{O}_2(w,z)(t_2)\right| \\
&\leq \sum_{i=1}^{k} \frac{\Pi_2 B_i}{\Gamma(++1)} \Big(\Big[(t_1-t_2)^+ + \left|t_1^+ - t_2^+\right| \Big] \\
&\quad + |t_1^{+-1} - t_2^{+-1}| \Big).
\end{aligned} \tag{12}$$

From (11) and (12), $\|\mathtt{O}(w,z)(t_1) - \mathtt{O}(w,z)(t_2)\|_{\mathtt{W}\times\mathtt{Z}} \to 0$ as $t_2 \to t_1$. Thus, by using the Arzela-Ascoli theorem one can conclude that the operator $\mathtt{O} : \mathtt{W}\times\mathtt{Z} \to \mathtt{W}\times\mathtt{Z}$ is completely continuous.

Finally, it will be verified that the set

$$\Psi = \Big\{ (w,z) \in \mathtt{W}\times\mathtt{Z}, (w,z) = \mathtt{O}(w,z), 0 \leq\leq 1 \Big\}$$

is bounded. Let $(w,z) \in \Psi$. Then, for each $t \in [0,1]$, we can write

$$w(t) = \mathtt{O}_1(w,z)(t) \quad \text{and} \quad z(t) = \mathtt{O}_2(w,z)(t).$$

Then, we have

$$|w(t)| \leq \Pi_1 |\mathfrak{N}_1(t)|,$$

and

$$|z(t)| \leq \Pi_2 |\mathfrak{N}_2(t)|.$$

From (H_3), we obtain

$$|w(t)| \leq \frac{2\Pi_1}{\Gamma(++1)} \left(\lambda_0 + \lambda_1 |w(t)| + \lambda_2 |z(t)|\right),$$

and

$$|z(t)| \leq \frac{2\Pi_2}{\Gamma(++1)} \left(\gamma_0 + \gamma_1 |w(t)| + \gamma_2 |z(t)|\right).$$

Hence, we have

$$\|w\| \leq \sum_{i=1}^{k} \frac{2\Pi_1}{\Gamma(++1)} \left(\lambda_i + \gamma_i \|w\| + \omega_i \|z\|\right),$$

and

$$\|z\| \leq \sum_{i=1}^{k} \frac{2\Pi_2}{\Gamma(++1)} \left(\lambda_i' + \gamma_i' \|w\| + \omega_i' \|z\|\right),$$

which imply that

$$\begin{aligned}
&\|w\| + \|z\| \\
&\leq \sum_{i=1}^{k} \frac{2\Pi_1}{\Gamma(++1)}\lambda_i + \sum_{i=1}^{k} \frac{2\Pi_2}{\Gamma(++1)}\lambda_i' \\
&+ \left(\sum_{i=1}^{k} \frac{2\Pi_1}{\Gamma(++1)}\gamma_i + \sum_{i=1}^{k} \frac{2\Pi_2}{\Gamma(++1)}\gamma_i' \right) \|w\| \\
&+ \left(\sum_{i=1}^{k} \frac{2\Pi_1}{\Gamma(++1)}\omega_i + \sum_{i=1}^{k} \frac{2\Pi_2}{\Gamma(++1)}\omega_i' \right) \|z\|.
\end{aligned}$$

Consequently,

$$\begin{aligned}
\|(w,z)\|_{\mathtt{W}\times\mathtt{Z}} \leq \frac{1}{G} \Big[&\sum_{i=1}^{k} \frac{2\Pi_1}{\Gamma(++1)}\lambda_i \\
&+ \sum_{i=1}^{k} \frac{2\Pi_2}{\Gamma(++1)}\lambda_i' \Big],
\end{aligned}$$

for all $t \in [0,1]$, where $G = \min\{\mathfrak{d}_1, \mathfrak{d}_2\}$, in which

$$\mathfrak{d}_1 = 1 - \left(\sum_{i=1}^{k} \frac{2\Pi_1}{\Gamma(++1)}\gamma_i + \sum_{i=1}^{k} \frac{2\Pi_2}{\Gamma(++1)}\gamma_i' \right),$$

and

$$\mathfrak{d}_2 = 1 - \left(\sum_{i=1}^{k} \frac{2\Pi_1}{\Gamma(++1)}\omega_i + \sum_{i=1}^{k} \frac{2\Pi_2}{\Gamma(++1)}\omega_i' \right).$$

This shows that the set Ψ is bounded. Hence all the conditions of Lemma 6 are satisfied and consequently the operator $\mathtt{O}$ has at least one fixed point, which corresponds to a solution of the system (1). This completes the proof. □

In the next result, we establish the existence of uniqueness solutions to the fractional hybrid system (1) by using Banach's fixed point theorem.

Theorem 2. *Assume that* $(H_j)_{j=1,2}$ *hold and that*

$$\begin{aligned}
&\sum_{i=1}^{k} \frac{\pi_i}{\Gamma(++1)} < \frac{1}{4\Pi_1}, i = 1,2,\cdots,k, \\
&\sum_{i=1}^{k} \frac{\vartheta_i}{\Gamma(++1)} < \frac{1}{4\Pi_2}, i = 1,2,\cdots,k.
\end{aligned} \tag{13}$$

Then the problem (1) *has a unique solution on* $[0,1]$.

Proof. Define $\sup_{t\in[0,1]} |\varphi_i(t,0,0)| = \Lambda_i < \infty$ and $\sup_{t\in[0,1]} |\phi_i(t,0,0)| = \nabla_i < \infty$, $i = 1,2,...,k$ such that $\max\{\wp_1, \wp_2\} \leq, i = 1,2,...,k$, where

$$\wp_1 = \sum_{i=1}^{k} \frac{\Pi_1 \Lambda_i}{\Gamma(++1)} \left[\frac{1}{4} - \sum_{i=1}^{k} \frac{\Pi_1 \pi_i}{\Gamma(++1)} \right]^{-1},$$

and

$$\wp_2 = \sum_{i=1}^{k} \frac{\Pi_2 \nabla_i}{\Gamma(++1)} \left[\frac{1}{4} - \sum_{i=1}^{k} \frac{\Pi_2 \vartheta_i}{\Gamma(++1)} \right]^{-1}.$$

Firstly, we show that $\mathtt{OB} \subset \mathtt{B}$, where $\mathtt{B} = \left\{(w,z) \in \mathtt{W} \times \mathtt{Z} : \|(w,z)\|_{\mathtt{W}\times\mathtt{Z}} \leq \right\}$. For all $(w,z) \in \mathtt{B}$ and $t \in [0,1]$, we have

$$\begin{aligned}
&|\varphi_i(t, w(t), z(t))| \\
&\leq |\varphi_i(t, w(t), z(t)) - \varphi_i(t,0,0)| + |\varphi_i(t,0,0)| \\
&\leq \pi_i(|w(t)| + |z(t)|) + \Lambda_i \leq \pi_i(\|w\| + \|z\|) + \Lambda_i \\
&\leq \pi_i \|(w,z)\| + \Lambda_i \leq \pi_i + \Lambda_i, \ i = 1,2,...,k.
\end{aligned}$$

Similarly, we have

$$\begin{aligned}
&|\phi_i(t, w(t), z(t))| \\
&\leq |\phi_i(t, w(t), z(t)) - \phi_i(t,0,0)| + |\phi_i(t,0,0)| \\
&\leq \vartheta_i(|w(t)| + |z(t)|) + \nabla_i \leq \vartheta_i(\|w\| + \|z\|) + \nabla_i \\
&\leq \vartheta_i \|(w,z)\| + \nabla_i \leq \vartheta_i + \nabla_i, \ i = 1,2,...,k,
\end{aligned}$$

Using (3), we can write

$$\begin{aligned}
|\mathtt{O}_1(w,z)(t)| &\leq \Pi_1 \sup_{t\in[0,1]} \left\{\mathfrak{N}_1(t)\right\} \\
&\leq \frac{\sum_{i=1}^{k} 2\Pi_1 \pi_i}{\Gamma(++1)} + \frac{\sum_{i=1}^{k} 2\Pi_1 \nabla_i}{\Gamma(++1)},
\end{aligned}$$

which implies that

$$\begin{aligned}
&\|\mathtt{O}_1(w,z)\| \\
&\leq \sum_{i=1}^{k} \frac{\Pi_1 \pi_i}{\Gamma(++1)} + \sum_{i=1}^{k} \frac{\Pi_1 \Lambda_i}{\Gamma(++1)} \\
&\leq \frac{-}{4}.
\end{aligned}$$

Also, by (3), we have

$$\begin{aligned}
&\|\mathtt{O}_2(w,z)\| \\
&\leq \sum_{i=1}^{k} \frac{\Pi_2 \vartheta_i}{\Gamma(++1)} + \sum_{i=1}^{k} \frac{\Pi_2 \nabla_i}{\Gamma(++1)} \\
&\leq \frac{-}{4}.
\end{aligned}$$

From the definition of $\|\cdot\|_{\mathtt{W}\times\mathtt{Z}}$, we have

$$\begin{aligned}
&\|O(w,z)\|_{\mathtt{W}\times\mathtt{Z}} \\
&\leq \sum_{i=1}^{k} \left(\frac{\Pi_1 \pi_i}{\Gamma(++1)} + \frac{\Pi_1 \vartheta_i}{\Gamma(++1)} \right) \\
&\quad + \sum_{i=1}^{k} \left(\frac{\Pi_2 \Lambda_i}{\Gamma(++1)} + \frac{\Pi_2 \nabla_i}{\Gamma(++1)} \right) \\
&\leq \frac{-}{2},
\end{aligned}$$

which implies that $OB \subset B$. Next, for $(w_1,z_1),(w_2,z_2) \in B$ and for each $t \in [0,1]$, we have

$$\begin{aligned}
&\left|\mathtt{O}_1(w_1,z_1)(t) - \mathtt{O}_1(w_2,z_2)(t)\right| \\
&\leq \Pi_1 \sup_{t\in[0,1]} \left\{ \sum_{i=1}^{k} \int_0^t \frac{(t-s)^{+-1}}{\Gamma(+)} \Upsilon(s) ds \right. \\
&\quad \left. + t^{+-1} \sum_{i=1}^{k} \int_0^1 \frac{(1-s)^{+-1}}{\Gamma(+)} \Upsilon_2(s) ds \right\}.
\end{aligned}$$

where

$$\begin{aligned}
\Upsilon_2(s) &= |\varphi_i(s, w_1(s), z_1(s)) - \varphi_i(s, w_2(s), z_2(s))|, \\
\Upsilon_2(s) &= |\varphi_i(s, w_1(s), z_1(s)) - \varphi_i(s, w_2(s), z_2(s))|.
\end{aligned}$$

From (H_1), we can write

$$\begin{aligned}
&\|\mathtt{O}_1(w_1,z_1) - \mathtt{O}_1(w_2,z_2)\| \\
&\leq \sum_{i=1}^{k} \frac{2\Pi_1 \pi_i}{\Gamma(++1)} \|(w_1 - w_2, z_1 - z_2)\|_{\mathtt{W}\times\mathtt{Z}}.
\end{aligned}$$

Similarly, we obtain

$$\begin{aligned}
&\|\mathtt{O}_2(w_1,z_1) - \mathtt{O}_2(w_2,z_2)\| \\
&\leq \sum_{i=1}^{k} \frac{2\Pi_2 \vartheta_i}{\Gamma(++1)} \|(w_1 - w_2, z_1 - z_2)\|_{\mathtt{W}\times\mathtt{Z}}.
\end{aligned}$$

Consequently, we obtain

$$\begin{aligned}
&\|\mathtt{O}(w_1,z_1) - \mathtt{O}(w_2,z_2)\|_{\mathtt{W}\times\mathtt{Z}} \\
&= \|\mathtt{O}_1(w_1,z_1) - \mathtt{O}_1(w_2,z_2)\| \\
&\quad + \|\mathtt{O}_2(w_1,z_1) - \mathtt{O}_2(w_2,z_2)\| \\
&\leq \left[\sum_{i=1}^{k} \left(\frac{2\Pi_1 \pi_i}{\Gamma(++1)} + \frac{2\Pi_2 \vartheta_i}{\Gamma(++1)} \right) \right] \\
&\quad \times \left\|(w_1 - w_2, z_1 - z_2)\right\|_{\mathtt{W}\times\mathtt{Z}}.
\end{aligned}$$

Thanks to (13), we conclude that $\mathtt{O}$ is a contraction mapping. Hence, by the Banach fixed point

theorem, there exists a unique fixed point which is a solution of system (1). This completes the proof. □

4. Stability in Ulam-Hyers-Rassias sense

In the following section, we consider the Ulam's type stability of the fractional hybrid system (1). For $t \in [0,1]$, we give the following inequalities:

$$\begin{cases} \left| {}^{\mathrm{RL}}\mathrm{D}\left[{}^{\mathrm{C}}\mathrm{D}\left[\dfrac{w_1(t)}{\psi_1(t,w_1(t),z_1(t))}\right]\right] - \displaystyle\sum_{i=1}^{k}\varphi_i(t,w_1(t),z_1(t)) \right| \le d_1, \\ \left| {}^{\mathrm{RL}}\mathrm{D}\left[{}^{\mathrm{C}}\mathrm{D}\left[\dfrac{z_1(t)}{\psi_2(t,w_1(t),z_1(t))}\right]\right] - \displaystyle\sum_{i=1}^{k}\phi_i(t,w_1(t),z_1(t)) \right| \le d_2, \end{cases} \tag{14}$$

and

$$\begin{cases} \left| {}^{\mathrm{RL}}\mathrm{D}\left[{}^{\mathrm{C}}\mathrm{D}\left[\dfrac{w_1(t)}{\psi_1(t,w_1(t),z_1(t))}\right]\right] - \displaystyle\sum_{i=1}^{k}\varphi_i(t,w_1(t),z_1(t)) \right| \le d_1 u(t), \\ \left| {}^{\mathrm{RL}}\mathrm{D}\left[{}^{\mathrm{C}}\mathrm{D}\left[\dfrac{z_1(t)}{\psi_2(t,w_1(t),z_1(t))}\right]\right] - \displaystyle\sum_{i=1}^{k}\phi_i(t,w_1(t),z_1(t)) \right| \le d_2 u(t), \end{cases} \tag{15}$$

where $d_j, j = 1,2$ are positive reals numbers and $u : [0,1] \to \mathbb{R}^+$, is continuous function.

Definition 4. *[40] System (1) is Ulam-Hyers stable if there exists a real number $\rho_{\varphi_i,\phi_i} = (\rho_{\varphi_i}, \rho_{\phi_i}) > 0, i = 1,2,...,k$ such that for each $d = \max(d_1,d_2) > 0$ and for each solution $(w_1,z_1) \in \mathtt{W}\times\mathtt{Z}$ of the inequality (14) there exists a solution $(w,z) \in \mathtt{W}\times\mathtt{Z}$ of the system (1) with*

$$|(w_1(t)-w(t), z_1(t)-z(t))| \le \rho_{\varphi_i,\phi_i} d,$$

for $t \in [0,1]$, $i = 1,2,\cdot,k$.

Definition 5. *[40] System (1) is Ulam-Hyers-Rassias stable with respect to $u \in C([0,1],\mathbb{R})$ if there exists a real number $\varsigma_{\varphi_i,\phi_i,u} = (\varsigma_{\varphi_i,u}, \varsigma_{\phi_i,u}) > 0$ such that for each $d = \max(d_1,d_2) > 0$ and for each solution $(w_1,z_1) \in \mathtt{W}\times\mathtt{Z}$ of the inequality (15) there exists a solution $(w,z) \in \mathtt{W}\times\mathtt{Z}$ of the system (1) with*

$$|(w_1(t)-w(t), z_1(t)-z(t))| \le \varsigma_{\varphi_i,\phi_i,u} d u(t),$$

for $t \in [0,1]$, $i = 1,2,\cdot,k$.

Theorem 3. *Assume that $(H_j)_{j=1,2}$ hold. If*

$$\begin{cases} \displaystyle\sum_{i=1}^{k}\frac{\pi_i}{\Gamma(+1)} < \frac{1}{\Pi_1}, \\ \displaystyle\sum_{i=1}^{k}\frac{\vartheta_i}{\Gamma(+1)} < \frac{1}{\Pi_2}, \end{cases} \tag{16}$$

then the problem (1) is Ulam-Hyers stable.

Proof. Let $(w_1,z_1) \in \mathtt{W}\times\mathtt{Z}$ be a solution of the inequality (14) and let $(w,z) \in \mathtt{W}\times\mathtt{Z}$ be the unique solution of the system

$$\begin{cases} {}^{\mathrm{RL}}\mathrm{D}\left[{}^{\mathrm{C}}\mathrm{D}\left[\dfrac{w(t)}{\psi_1(t,w(t),z(t))}\right]\right] = \displaystyle\sum_{i=1}^{k}\varphi_i(t,w(t),z(t)), \\ {}^{\mathrm{RL}}\mathrm{D}\left[{}^{\mathrm{C}}\mathrm{D}\left[\dfrac{z(t)}{\psi_2(t,w(t),z(t))}\right]\right] = \displaystyle\sum_{i=1}^{k}\phi_i(t,w(t),z(t)), \\ w(0) = w_1(0), w(1) = w_1(1), \\ z(0) = z_1(0), z(1) = z_1(1). \end{cases}$$

By Lemma 5, we have

$$w(t) = \psi_1(t,w(t),z(t))\left[\sum_{i=1}^{k}\mathtt{I}^{+}g_i^{w}(t) + \frac{a_1\Gamma()}{\Gamma(+)}t^{+-1} + a_2\right],$$

and

$$z(t) = \psi_2(t,w(t),z(t))\left[\sum_{i=1}^{k}\mathtt{I}^{+}h_i^{z}(t) + \frac{b_1\Gamma()}{\Gamma(+)}t^{+-1} + b_2\right],$$

such that

$$g_i^{w}(t) = \varphi_i(t,w(t),z(t)),\ i = 1,2,\cdots,k,$$
$$h_i^{z}(t) = \phi_i(t,w(t),z(t)),\ i = 1,2,\cdots,k.$$

Integrating (14), we obtain

$$\left|w_1(t) - \psi_1(t,w(t),z(t))\left[\sum_{i=1}^{k}\mathtt{I}^{+}g_i^{w}(t) + \frac{a_3\Gamma()}{\Gamma(+)}t^{+-1} + a_4\right]\right| \le \frac{d_1 t^{+}}{\Gamma(++1)} \le \frac{d_1}{\Gamma(++1)},$$

and

$$\left|z_1(t)-\psi_2(t,w(t),z(t))\left[\sum_{i=1}^{k}\mathtt{I}^{+}h_i^{z}(t)+\frac{b_3\Gamma()}{\Gamma(+)}t^{+-1}+b_4\right]\right| \leq \frac{d_2 t^{+}}{\Gamma(++1)} \leq \frac{d_2}{\Gamma(++1)}.$$

From $(H_j)_{j=1,2}$, we have

$$\begin{aligned}
&|w_1(t)-w(t)| \\
&\leq \left|w_1(t)-\psi_1(t,w(t),z(t))\left[\sum_{i=1}^{k}\mathtt{I}^{+}g_i^{w}(t)+\frac{a_3\Gamma()}{\Gamma(+)}t^{+-1}+a_4\right]\right| \\
&\quad+|\psi_1(t,w(t),z(t))|\sum_{i=1}^{k}\mathtt{I}^{+}|g_i^{w_1}(t)-g_i^{w}(t)| \\
&\leq \frac{d_1}{\Gamma(++1)}+\sum_{i=1}^{k}\Pi_1\mathtt{I}^{+}|g_i^{w_1}(t)-g_i^{w}(t)|,
\end{aligned}$$

this implies that

$$\begin{aligned}
&|w_1(t)-w(t)| \\
&\leq \frac{d_1}{\Gamma(++1)}+\sum_{i=1}^{k}\frac{\Pi_1\pi_i}{\Gamma(++1)}\Big[|w_1(t)-w(t)| \\
&\quad+|z_1(t)-z(t)|\Big].
\end{aligned}$$

Similarly, we get

$$\begin{aligned}
&|z_1(t)-z(t)| \\
&\leq \frac{d_2}{\Gamma(++1)}+\sum_{i=1}^{k}\frac{\Pi_2\vartheta_i}{\Gamma(++1)}\Big[|w_1(t)-w(t)| \\
&\quad+|z_1(t)-z(t)|\Big].
\end{aligned}$$

Thus,

$$\begin{aligned}
&|(w_1(t),z_1(t))-(w(t),z(t))| \\
&\leq \frac{1}{\Gamma(++1)}+\frac{1}{\Gamma(++1)}d := \rho_{\varphi_i,\phi_i}d,
\end{aligned}$$

where

$$\mathfrak{r}_1=\frac{1}{\Pi_1}-\sum_{i=1}^{k}\frac{\pi_i}{\Gamma(++1)},$$

$$\mathfrak{r}_2=\frac{1}{\Pi_2}-\sum_{i=1}^{k}\frac{\vartheta_i}{\Gamma(++1)}.$$

Hence the system (1) is Ulam-Hyers stable. □

Theorem 4. *Assume that* $(H_j)_{j=1,2}$ *and* (16) *hold. Suppose there exist* $\upsilon_{1u}>0,\upsilon_{2u}>0$ *such that*

$$\mathtt{I}^{+}u(t)\leq \upsilon_{1u}u(t),\mathtt{I}^{+}u(t)\leq \upsilon_{2u}u(t),t\in[0,1], \tag{17}$$

where $u\in C([0,1],\mathbb{R}_{+})$ *is nondecreasing. Then the system* (1) *is Ulam-Hyers-Rassias stable.*

Proof. Let $(w_1,z_1)\in \mathtt{W}\times\mathtt{Z}$ is a solution of the inequality (15) and let us assume that $(w,z)\in \mathtt{W}\times\mathtt{Z}$ is a solution of system (1). Thus, we have

$$\begin{aligned}
w(t)=&\psi_1(t,w(t),z(t))\left[\sum_{i=1}^{k}\mathtt{I}^{+}g_i^{w}(t)+\frac{a_1\Gamma()}{\Gamma(+)}t^{+-1}+a_2\right], \\
z(t)=&\psi_2(t,w(t),z(t))\left[\sum_{i=1}^{k}\mathtt{I}^{+}h_i^{z}(t)+\frac{b_1\Gamma()}{\Gamma(+)}t^{+-1}+b_2\right],
\end{aligned}$$

From inequality (15), we have

$$\left|w_1(t)-\psi_1(t,w(t),z(t))\left[\sum_{i=1}^{k}\mathtt{I}^{+}g_i^{w}(t)+\frac{a_3\Gamma()}{\Gamma(+)}t^{+-1}+a_4\right]\right|\leq d_1\mathtt{I}^{+}u(t),$$

and

$$\left|z_1(t)-\psi_2(t,w(t),z(t))\left[\sum_{i=1}^{k}\mathtt{I}^{+}h_i^{z}(t)+\frac{b_3\Gamma()}{\Gamma(+)}t^{+-1}+b_4\right]\right|\leq d_2\mathtt{I}^{+}u(t).$$

Now, using $(H_j)_{j=1,2}$ and (17), we get

$$\begin{aligned}
&|w_1(t)-w(t)| \\
&\leq d_1\upsilon_{1u}u(t)+\sum_{i=1}^{k}\frac{\Pi_1\pi_i}{\Gamma(++1)}(|w_1(t)-w(t)| \\
&\quad+|z_1(t)-z(t)|),
\end{aligned}$$

and

$$\begin{aligned}
&|z_1(t)-z(t)| \\
&\leq d_2\upsilon_{2u}u(t)+\sum_{i=1}^{k}\frac{\Pi_2\vartheta_i}{\Gamma(++1)}(|w_1(t)-w(t)| \\
&\quad+|z_1(t)-z(t)|).
\end{aligned}$$

Consequently,

$$|(w_1(t),z_1(t))-(w(t),z(t))| \leq \frac{\upsilon_{1u}+\upsilon_{2u}}{\min\{\mathbb{k}_1,\mathbb{k}_2\}}du(t) := \varsigma_{\varphi_i,\phi_i,u}du(t),$$

where

$$\mathbb{k}_1 = 1-\sum_{i=1}^{k}\frac{\Pi_1\pi_i}{\Gamma(++1)},$$

and

$$\mathbb{k}_2 = 1-\sum_{i=1}^{k}\frac{\Pi_2\vartheta_i}{\Gamma(++1)}.$$

Hence the system (1) is stable in Ulam-Hyers-Rassias sense. □

5. Application

To illustrate our main results, we treat the following example.

Example 1. *Consider the following fractional hybrid system:*

$$\begin{cases} {}^{RL}\mathrm{D}^{\frac{4}{5}}\left[{}^{C}\mathrm{D}^{\frac{2}{3}}\left[\frac{w(t)}{\frac{\sin w(t)+1}{15}+1+\frac{1}{13}e^{-t^2}\cos z(t)}\right]\right] \\ =\frac{\cos(2\pi w(t))}{60\pi}+\frac{|z(t)|}{30(1+|z(t)|)}+\arctan\left(t^2+2t+1\right) \\ +\frac{|w(t)|}{32(e^t+3\sqrt{\pi})(1+|w(t)|)}+\frac{\sin^2 z(t)}{16(5t^2+2(1+3\sqrt{\pi}))} \\ +\frac{\ln(1+t)}{3}, \\ {}^{RL}\mathrm{D}^{\frac{5}{6}}\left[{}^{C}\mathrm{D}^{\frac{3}{4}}\left[\frac{z(t)}{\frac{3}{7}t\cos w(t)+\frac{1}{7+z(t)}}\right]\right] \\ =\frac{\cos(w(t)+z(t))}{19(\ln(1+t)+2\sqrt{\pi})}+\frac{(1+2e^{1+t})}{2} \\ +\frac{|w(t)|}{3(\pi t+3)^2(1+|w(t)|)}+\frac{\tan^{-1}z(t)}{27}+\sinh\left(1+13e^t\right), \\ w(0)=w(1)=0,\ z(0)=z(1)=0, \end{cases} \tag{18}$$

and the following inequalities

$$\begin{cases} {}^{RL}\mathrm{D}^{\frac{4}{5}}\left[{}^{C}\mathrm{D}^{\frac{2}{3}}\left[\frac{w(t)}{\psi_1(t,w(t),z(t))}\right]\right] \\ \quad -\sum_{i=1}^{2}\varphi_i(t,w(t),z(t))\leq d_1, \\ {}^{RL}\mathrm{D}^{\frac{5}{6}}\left[{}^{C}\mathrm{D}^{\frac{3}{4}}\left[\frac{z(t)}{\psi_2(t,w(t),z(t))}\right]\right] \\ \quad -\sum_{i=1}^{2}\phi_i(t,w(t),z(t))\leq d_2, \end{cases}$$

and

$$\begin{cases} {}^{RL}\mathrm{D}^{\frac{4}{5}}\left[{}^{C}\mathrm{D}^{\frac{2}{3}}\left[\frac{w(t)}{\psi_1(t,w(t),z(t))}\right]\right] \\ \quad -\sum_{i=1}^{2}\varphi_i(t,w(t),z(t))\leq d_1u(t), \\ {}^{RL}\mathrm{D}^{\frac{5}{6}}\left[{}^{C}\mathrm{D}^{\frac{3}{4}}\left[\frac{z(t)}{\psi_2(t,w(t),z(t))}\right]\right] \\ \quad -\sum_{i=1}^{2}\phi_i(t,w(t),z(t))\leq d_2u(t), \end{cases}$$

where

$$\varphi_1(t,w,z)=\frac{\cos(2\pi w)}{60\pi}+\frac{|z|}{30(1+|z|)}+\arctan\left(t^2+2t+1\right),$$

$$\varphi_2(t,w,z)=\frac{|w|}{32(e^t+3\sqrt{\pi})(1+|w|)}+\frac{\ln(1+t)}{3}+\frac{\sin^2 z}{16(5t^2+2(1+3\sqrt{\pi}))},$$

$$\phi_1(t,w,z)=\frac{\cos(w+z)}{19(\ln(1+t)+2\sqrt{\pi})}+\frac{(1+2e^{1+t})}{2},$$

$$\phi_2(t,w,z)=\frac{|w|}{3(\pi t+3)^2(1+|w|)}+\frac{\tan^{-1}z}{27}+\sinh\left(1+13e^t\right),$$

and

$$\psi_1(t,w,z)=\frac{1}{5}(\sin w+1)+1+\frac{1}{13}e^{-t^2}\cos z,$$

$$\psi_2(t,w,z)=\frac{2}{7}t\cos w+\frac{1}{7+z}.$$

For $(w_i,z_i)\in\mathbb{R}^2, i=1,2$ *and* $t\in[0,1]$, *we have*

$$|\varphi_1(t,w_1,z_1)-\varphi_1(t,w_2,z_2)| \leq \frac{1}{30}(|w_1-w_2|+|z_1-z_2|),$$

$$|\varphi_2(t,w_1,z_1)-\varphi_2(t,w_2,z_2)| \leq \frac{1}{32(1+3\sqrt{\pi})}(|w_1-w_2|+|z_1-z_2|),$$

$$|\phi_2(t,w_1,z_1)-\phi_2(t,w_2,z_2)| \leq \frac{1}{38\sqrt{\pi}}(|w_1-w_2|+|z_1-z_2|),$$

$$|\phi_1(t,w_1,z_1)-\phi_2(t,w_2,z_2)| \leq \frac{1}{27}(|w_1-w_2|+|z_1-z_2|),$$

and

$$|\psi_1(t,w,z)|\leq\frac{27}{65},\quad |\psi_2(t,w,z)|\leq\frac{3}{7}.$$

So, we take $\pi_1=\frac{1}{30},\pi_2=\frac{1}{32},\ \vartheta_1=\frac{1}{32(1+3\sqrt{\pi})},\ \vartheta_2=\frac{1}{38\sqrt{\pi}},\ \Pi_1=\frac{27}{65}$ *and* $\Pi_2=\frac{3}{7}$.

Hence, we obtain

$$\sum_{i=1}^{2}\frac{\pi_i}{\Gamma(++1)}=4.972\,2\times10^{-2}<\frac{1}{4\Pi_1}=0.103\,85,$$

and

$$\sum_{i=1}^{2}\frac{\vartheta_i}{\Gamma(++1)}=1.401\,9\times10^{-2}<\frac{1}{4\Pi_2}=0.107\,14.$$

By Theorem 1, we conclude that the system (18) has a unique solution. And from Theorem 3 we deduce that (18) is Ulam-Hyers stable with

$$|(w_2(t),z_2(t))-(w_1(t),z_1(t))|\leq 0.365\,68d,$$

for $t\in[0,1]$, $d>0$. *Let* $u(t)=t^{\frac{\sqrt{5}}{2}}$, *then*

$$\mathrm{I}^{\frac{4}{5}+\frac{2}{3}}u_1(t)=\mathrm{I}^{\frac{4}{5}+\frac{2}{3}}t^{\frac{\sqrt{5}}{2}}\leq\frac{\Gamma\left(\frac{\sqrt{5}+2}{2}\right)}{\Gamma\left(\frac{\sqrt{5}}{2}+\frac{37}{15}\right)}t^{\frac{\sqrt{5}}{2}}=\upsilon_{1u}u(t),$$

and

$$\mathrm{I}^{\frac{5}{6}+\frac{3}{4}}u_2(t)=\mathrm{I}^{\frac{5}{6}+\frac{3}{4}}t^{\frac{\sqrt{5}}{2}}\leq\frac{\Gamma\left(\frac{\sqrt{5}+2}{2}\right)}{\Gamma\left(\frac{\sqrt{5}}{2}+\frac{31}{12}\right)}t^{\frac{\sqrt{5}}{2}}=\upsilon_{2u}u(t).$$

Thus, the condition (17) of Theorem 4 is satisfied with $u(t)=t^{\frac{\sqrt{5}}{2}}$ *and* $\upsilon_{1u}=0.289\,01$, $\upsilon_{2u}=0.252\,74$. *Hence from Theorem 4, the system (18) is Ulam-Hyers-Rassias stable with*

$$|(w_1(t),z_1(t))-(w(t),z(t))|\leq 0.948\,04dt^{\frac{\sqrt{5}}{2}},$$

for $t\in[0,1]$, $d>0$.

Remark 1. *One can easily figure out that problem (18) is not commented by any of the relevant existing results in the literature.*

Acknowledgments

M. Houas is thankful to Khemis Miliana University, J. Alzabut is thankful to Prince Sultan University and OSTİM Technical University, and M. Khuddush is thankful to Dr. Lankapalli Bullayya College of Engineering for their endless support during the achievement of this paper.

References

[1] Gaul, L., Klein, P. & Kemple, S. (1991). Damping description involving fractional operators. *Mechanical Systems and Signal Processing*, 5, 81-88.

[2] Glockle, W. G., Nonnenmacher, T. F. (1995). A fractional calculus approach to self-semilar protein dynamics. *Biophysical Journal*, 68(1), 46-53.

[3] Metzler, R., Schick, W., Kilian, H. G., & Nonnenmacher, T. F. (1995). Relaxation in filled polymers: a fractional calculus approach. *The Journal of Chemical Physics*, 103, 7180-7186.

[4] Scher, H., Montroll, E. W. (1975). Anomalous transit-time dispersion in amorphous solids. *Physical Review B*, 12, 2455-2477.

[5] Anbalagan, P., Ramachandran, R., Alzabut, J., Hincal, E. & Niezabitowski, M. (2022). Improved results on finite-time passivity and synchronization problem for fractional-order memristor-based competitive neural networks: interval matrix approach. *Fractal and Fractional*, 6(1), 1-36.

[6] Diethelm, K., Ford, N. J. (2002). Analysis of fractional differential equations. *Journal of Mathematical Analysis and Applications,* 265, 229-248.

[7] Joseph, D., Raja, R., Alzabut, J., Niezabitowski, M., Selvam, A. G. M. & Bagdasar, O. O. (2021). An LMI approach based mathematical model to control Aedes Aegypti mosquitoes population via biological control. *Mathematical Problems in Engineering*, 2021, Article ID 5565949, 1-18. https://doi.org/10.1155/2021/556599

[8] Khuddush, M., Prasad, K. R. (2023). Existence, uniqueness and stability analysis of a tempered fractional order thermistor boundary value problems. *Journal of Analysis,* 31, 85-107. https://doi.org/10.1007/s41478-022-00438-6

[9] Khuddush, M., Prasad, K. R. & Leela. D. (2022). Existence of solutions to the ∞-point Fractional BVP posed on half-line via a family of measure of noncompactness in the H$\acute{o}$lder Space $\mathbb{C}^{\ell,}(\mathbb{R}^+)$. *Filomat*, 36(10), 3527-3543. https://doi.org/10.2298/FIL2210527K

[10] Khuddush, M., Prasad, K. R. & Veeraiah, P. (2022). Infinitely many positive solutions for an iterative system of fractional BVPs with multistrip Riemann–Stieltjes integral boundary conditions. *Afrika Matematika*, 33, 91. https://doi.org/10.1007/s13370-022-01026-4

[11] Khuddush, M., Kathun, S. (2023). Infinitely many positive solutions and Ulam–Hyers stability of fractional order two-point boundary value problems. *Journal of Analysis*. https://doi.org/10.1007/s41478-023-00549-8

[12] Kilbas, A. A., Marzan, S. A. (2005). Nonlinear differential equation with the Caputo fraction derivative in the space of continuously differentiable functions. *Differential Equations*, 41, 84-89.

[13] Podlubny, L. (1999). *Fractional differential equations*, Academic Press, New York.

[14] Pratap, A., Raja, R., Cao, C., Alzabut, J. & Huang, C. (2020). Finite-time synchronization criterion of graph theory perspective fractional order coupled discontinuous neural networks. *Advances in Difference Equations* 2020, 97. https://doi.org/10.1186/s13662-020-02551-x

[15] Seemab, S., Feckan, M., Alzabut, J. & Abbas, S. (2021). On the existence and Ulam-Hyers stability of a new class of partial (ϕ,χ)-fractional differential equations with impulses. *Filomat*, 35(6), 1977-1991.

[16] Shah, K., Abdeljawad1, T., Abdalla, B. & Abualrub, M. (2022). Utilizing fixed point approach to investigate piecewise equations with nonsingular type derivative. *AIMS Mathematics*, 7(8), 14614–14630.

[17] Shah, K., Arfan, M., Ullah, A., Al-Mdallal, Q., Ansari, K. J. & Abdeljawad, T. (2022).

Computational study on the dynamics of fractional order differential equations with applications. *Chaos, Solitons & Fractals,*, 157, 111955. https://doi.org/10.1016/j.chaos.2022.111955

[18] Victor, D. W. J., Khuddush, M. (2022). Existence of solutions for n-dimensional fractional order BVP with ∞–point boundary conditions via the concept of measure of noncompactness. *Advanced Studies: Euro-Tbilisi Mathematical Journal*, 15(1), 19–37. https://doi.org/10.32513/asetmj/19322008202

[19] Dhage, B. C. (2004). A nonlinear alternative in Banach algebras with applications to functional differential equations. *Nonlinear Functional Analysis and Applications*, 8, 563-575.

[20] Dhage, B. C. (2005). On a fixed point theorem in Banach algebras with applications. *Applied Mathematics Letters*, 18(3), 273-280.

[21] Dhage, B. C., Jadhav, N. (2013). Basic results in the theory of hybrid differential equations with linear perturbations of second type. *Tamkang Journal of Mathematics*, 44(2), 171-186.

[22] Ali, A., Shah, K. & Khan, R. A. (2017). Existence of solution to a coupled system of hybrid fractional differential equations, *Bulletin of Mathematical Analysis and Applications*, 9(1), 9-18.

[23] Alzabut, J., Selvam, A. G. M., Vignesh, D. & Gholami, Y. (2021). Solvability and stability of nonlinear hybrid Δ-difference equations of fractional-order. *International Journal of Nonlinear Sciences and Numerical Simulation*, 2021. https://doi.org/10.1515/ijnsns-2021-0005

[24] Baleanu, D., Etemad, S., Pourrazi, S. & Rezapour, S. (2019). On the new fractional hybrid boundary value problems with three-point integral hybrid conditions. *Advances in Difference Equations*, 473, 1-21.

[25] Buvaneswari, K., Karthikeyan, P. & Baleanu, D. (2020). On a system of fractional coupled hybrid Hadamard differential equations with terminal conditions. *Advances in Difference Equations*, 419, 1-12.

[26] Herzallah, M. A. E., Baleanu, D. (2014). On fractional order hybrid differential equations. *Abstract and Applied Analysis*, 2014, 1-8.

[27] Houas, M. (2021). Existence and stability results for hybrid fractional $q-$ differential pantograph equations. *Asia Mathematika*, 5(2), 20-35.

[28] Houas, M. (2018). Solvability of a system of fractional hybrid differential equations. *Communications in Optimization Theory*, Article ID 12, 1-9. https://doi.org/10.23952/cot.2018.12

[29] Nazir, G., Shah, K., Abdeljawad, T., Khalil, H. & and Khan, R. A. (2020). A prior estimate method to investigate sequential hybrid fractional differential equations. *Fractals*, 28(8), 1-12.

[30] Baitiche, Z., Guerbati, K., Benchohra, M. & Henderson, J. (2020). Boundary value problems for hybrid caputo sequential fractional differential equations. *Communications on Applied Nonlinear Analysis*, 4, 1-16.

[31] Jamil, M., Khan, R. A. & Shah, K. (2019). Existence theory to a class of boundary value problems of hybrid fractional sequential integro-differential equations. *Boundary Value Problems*, 2019: 77, 1-12.

[32] Khan, H., Alshehri, H. M. & Khan, Z. A. (2021). A fractional-order sequential hybrid system with an application to a biological system. *Complexity*, 2021, Article ID 2018307, 1-9.

[33] Khan, R. A., Gul, S., Jarad, F. & Khan, H. (2021). Existence results for a general class of sequential hybrid fractional differential equations. *Advances in Difference Equations*, 2021, 284, 1-14.

[34] Prasad, K. R., Khuddush, M. & Leela, D. (2021). Existence of solutions for $n-$ dimensional fractional order hybrid BVPs with integral boundary conditions by an application of $n-$fixed point theorem. *The Journal of Analysis*, 29(3), 963-985.

[35] Dhage, B. C., Lakshmikantham, V. (2010). Basic results on hybrid differential equations. *Nonlinear Analysis: Hybrid Systems*, 4(3), 414-424.

[36] Zhao, Y, Sun, S., Hana, Z. & Li, Q. (2011). Theory of fractional hybrid differential equations. *Computers & Mathematics with Applications*. 62(3), 1312-1324.

[37] Ahmad, B., Ntouyas, S. K. & Alsaedi, A. (2014). Existence results for a system of coupled hybrid fractional differential equations. *The Scientific World Journal*, 2014. Article ID 426438, 1-7.

[38] Kilbas, A. A., Srivastava, H. M. & Trujillo, J. J. (2006). *Theory and applications of fractional differential equations*. North-Holland Mathematics Studies, 204, Elsevier Science B. V., Amsterdam.

[39] Granas, A., Dugundji, J. (2003). *Fixed Point Theory*. Springer, New York, NY, USA.

[40] Ahmad, B., Ntouyas, S. K. (2015). Existence results for a coupled system of Caputo type sequential fractional differential equations with nonlocal integral boundary conditions. *Applied Mathematics and Computation*, 266, 615-622.

Mohamed Houas *is working as an assistant professor at Universite Djilali BOUNAAMA Khemis Miliana, Algeria and his research interest are fractional differential equations and fractional integral inequalities.*

https://orcid.org/0000-0001-6256-0511

Jehad Alzabut *is working as a professor at Prince Sultan University, Saudi Arabia and his research interest are fractional differential equations, and dynamic equations on time scales.*

https://orcid.org/0000-0002-5262-1138

Mahammad Khuddush *is working as an assistant professor at Dr. Lankapalli Bullayya College of Engineering, India and his research interest are fractional differential equations, dynamic equations on time scales, fixed point theory, neural networks, global existence and blow-up solutions of PDE.*

https://orcid.org/0000-0002-1236-8334

An International Journal of Optimization and Control: Theories & Applications (http://www.ijocta.org)



This work is licensed under a Creative Commons Attribution 4.0 International License. The authors retain ownership of the copyright for their article, but they allow anyone to download, reuse, reprint, modify, distribute, and/or copy articles in IJOCTA, so long as the original authors and source are credited. To see the complete license contents, please visit http://creativecommons.org/licenses/by/4.0/.

The Journal of Analysis
https://doi.org/10.1007/s41478-021-00371-0

ORIGINAL RESEARCH PAPER

Existence theory and stability analysis to the system of fractional order BVP with Riemann-Liouville integral boundary conditions

K. Rajendra Prasad[1] · Mahammad Khuddush[2] · D. Leela[1]

Received: 27 June 2021 / Accepted: 7 November 2021
© The Author(s), under exclusive licence to The Forum D'Analystes 2021

Abstract
In this paper we generalize the fixed point theorem of Krasnoselskii, due to Burton (Appl Math Lett 11:85–88, 1998) to multivariate fixed point theorems of n-variables and then we study existence of solutions to the system of nonlinear fractional order differential equations with Riemann-Liouville type integral boundary conditions. Further, we also study Hyers-Ulam stability of the addressed system.

Keywords Riemann-Liouville fractional derivative and integral · System of equations · Boundary value problem · n-fixed point theorem · Banach space

Mathematics Subject Classification 34A08 · 34B15 · 34K10

1 Introduction

In the qualitative and quantitative theory of fractional differential equations, various theorems have been employed by many researchers in establishing the existence and uniqueness of solutions to the boundary value problems. For a detailed study on the existence and uniqueness of solutions of fractional differential equations, see [7, 8, 11, 14, 16, 19, 22, 31] and references therein.

Communicated by Samy Ponnusamy.

✉ Mahammad Khuddush
khuddush89@gmail.com

[1] Department of Applied Mathematics, College of Science and Technology, Andhra University, Visakhapatnam 530003, India

[2] Department of Mathematics, Dr. Lankapalli Bullayya College, Visakhapatnam 530013, Andhra Pradesh, India

Published online: 17 January 2022

Recently, the coupled and tripled fixed point theorems have been studied by many researchers in different metric spaces, see [2, 3, 13, 17, 21, 26, 28] and reference therein. However, the literature on multivariate fixed point theorems of n-variables contains only a few papers, see [18, 20, 23, 24, 27, 29].

In [1], Ashrafi, Jarad and Abdeljawad studied the existence and uniqueness of the following fractional order boundary value problem studied,

$$
\begin{aligned}
&{}^{RL}\mathrm{D}^{\varrho}_{0^+}\mathrm{z}_1(\mathrm{s}) + \mathrm{f}(\mathrm{s},\mathrm{z}_2(\mathrm{s})), 0<\mathrm{s}<1, 1<\varrho\leq 2,\\
&{}^{RL}\mathrm{D}^{\xi}_{0^+}\mathrm{z}_2(\mathrm{s}) + \mathrm{g}(\mathrm{s},\mathrm{z}_1(\mathrm{s})), 0<\mathrm{s}<1, 1<\xi\leq 2,\\
&\mathrm{z}_1(0) = \mathrm{z}_2(0) = 0,\ \mathrm{z}_1(1) = \int_0^1 \varphi(\mathrm{t})\mathrm{z}_1(\mathrm{t})\mathrm{dt},\ \mathrm{z}_2(1) = \int_0^1 \varphi(\mathrm{t})\mathrm{z}_2(\mathrm{t})\mathrm{dt}.
\end{aligned}
$$

by applying the common fixed point on complete b-metric space. Recently, Prasad, Khuddush and Leela [21] established the existence and unique of solution to the fractional order boundary value problem,

$$
\begin{aligned}
&{}^{C}\mathrm{D}^{\zeta}\mathrm{z}(\mathrm{s}) + \mathrm{F}\big(\mathrm{s},\mathrm{z}(\mathrm{s}),\mathrm{z}(\mathrm{s}),\mathrm{z}(\mathrm{s})\big) + \varphi(\mathrm{s})\mathrm{z}(\mathrm{s}) = 0, 0<\mathrm{s}<\mathrm{T}, 2<\zeta\leq 3,\\
&\mathrm{z}(0) = \mathrm{z}''(0) = 0, \mathrm{z}(\mathrm{T}) = \int_0^{\mathrm{T}} \mathrm{z}(\mathrm{t})\mathrm{dt},
\end{aligned}
$$

by proving the existence and the uniqueness of solutions of the operator equation $\mathrm{A}(\mathrm{z},\mathrm{z},\mathrm{z}) + \mathrm{Bz} = \mathrm{z}$ in a Banach space. Inspired by the works mentioned above, in this paper we study the concept of n-fixed point for nonlinear mappings in a Banach space and establish the existence theorem for contractive type mappings. Moreover, as an application of our results we study the following system of nonlinear two-point fractional order boundary value problems,

$$
\begin{cases}
{}^{RL}\mathrm{D}^{\zeta}_{0^+}\big[\mathrm{z}_1(\mathrm{s}) - \mathrm{F}(\mathrm{s},\mathrm{z}_1(\mathrm{s}))\big] + \mathrm{g}(\mathrm{s},\mathrm{z}_2(\mathrm{s}),\mathrm{z}_3(\mathrm{s}),\ldots,\mathrm{z}_{n-1}(\mathrm{s}),\mathrm{z}_n(\mathrm{s})) = 0,\\
{}^{RL}\mathrm{D}^{\zeta}_{0^+}\big[\mathrm{z}_2(\mathrm{s}) - \mathrm{F}(\mathrm{s},\mathrm{z}_2(\mathrm{s}))\big] + \mathrm{g}(\mathrm{s},\mathrm{z}_1(\mathrm{s}),\mathrm{z}_3(\mathrm{s}),\ldots,\mathrm{z}_{n-1}(\mathrm{s}),\mathrm{z}_n(\mathrm{s})) = 0,\\
\vdots\\
{}^{RL}\mathrm{D}^{\zeta}_{0^+}\big[\mathrm{z}_{n-1}(\mathrm{s}) - \mathrm{F}(\mathrm{s},\mathrm{z}_{n-1}(\mathrm{s}))\big] + \mathrm{g}(\mathrm{s},\mathrm{z}_1(\mathrm{s}),\mathrm{z}_2(\mathrm{s}),\ldots,\mathrm{z}_{n-2}(\mathrm{s}),\mathrm{z}_n(\mathrm{s})) = 0,\\
{}^{RL}\mathrm{D}^{\zeta}_{0^+}\big[\mathrm{z}_n(\mathrm{s}) - \mathrm{F}(\mathrm{s},\mathrm{z}_n(\mathrm{s}))\big] + \mathrm{g}(\mathrm{s},\mathrm{z}_1(\mathrm{s}),\mathrm{z}_2(\mathrm{s}),\ldots,\mathrm{z}_{n-2}(\mathrm{s}),\mathrm{z}_{n-1}(\mathrm{s})) = 0,
\end{cases}
\tag{1}
$$

satisfying

$$
\mathrm{z}_{\mathrm{j}}(0) = 0 \tag{2}
$$

and

$$\begin{cases} z_1(1) = \displaystyle\int_0^1 \frac{(1-t)^{\xi-1}}{\Gamma(\xi)} h(t, z_2(t), z_3(t), z_3(t), \ldots, z_{n-1}(t), z_n(t))dt, \\ z_2(1) = \displaystyle\int_0^1 \frac{(1-t)^{\xi-1}}{\Gamma(\xi)} h(t, z_1(t), z_3(t), z_3(t), \ldots, z_{n-1}(t), z_n(t))dt, \\ \vdots \\ z_{n-1}(1) = \displaystyle\int_0^1 \frac{(1-t)^{\xi-1}}{\Gamma(\xi)} h(t, z_1(t), z_2(t), z_3(t), \ldots, z_{n-2}(t), z_n(t))dt, \\ z_n(1) = \displaystyle\int_0^1 \frac{(1-t)^{\xi-1}}{\Gamma(\xi)} h(t, z_1(t), z_2(t), z_3(t), \ldots, z_{n-2}(t), z_{n-1}(t))dt, \end{cases} \tag{3}$$

where $0 < s < 1$, $0 < \xi \leq 1 < \zeta \leq 2$, ${}^{RL}D_{0^+}^{\zeta}$ denotes the standard Riemann-Liouville fractional derivative of order ζ, $g, h : [0,1] \times [0,+\infty)^{n-1} \to [0,+\infty)$, $F : [0,1] \times [0,+\infty) \to [0,+\infty)$ are continuous functions with $F(0, z_j(0)) = F(1, z_j(1)) = 0$ for $j \in \{1, 2, 3, \ldots, n\}$.

2 Preliminaries

In this section, we construct kernel for the boundary value problem (1)–(3) and estimate bounds for it, which are useful for our later discussions.

Definition 1 [15] The Riemann-Liouville fractional integral of order $\xi > 0$ of a function $g : (0,+\infty) \to \mathbb{R}$ is defined by

$${}^{RL}I_{0^+}^{\xi} g(s) = \int_0^s \frac{(s-t)^{\xi-1}}{\Gamma(\xi)} g(t)dt.$$

Definition 2 [15] Let k be a positive integer. The Riemann-Liouville fractional derivative of order $\xi > 0$ of a continuous function $g : (0,+\infty) \to \mathbb{R}$ is defined by

$${}^{RL}D_{0^+}^{\xi} g(s) = \frac{d^k}{ds^k} \int_0^s \frac{(s-t)^{k-\xi-1}}{\Gamma(k-\xi)} g(t)dt$$

where $k - 1 < \xi \leq k$, provided that the right-hand side exists.

Lemma 1 [15] *Let k be a positive integer. The general solution to ${}^{RL}D_{0^+}^{\xi} g(s) = 0$ with $k - 1 < \xi \leq k$ is the function*

$$g(s) = \sum_{j=1}^{k} a_j s^{\xi - j},$$

where a_j is a real number.

Lemma 2 [15] *Let $\zeta > 0$. Then for any function $g : (0, +\infty) \to \mathbb{R}$, we have*

$$^{RL}I_{0^+}^{\zeta}\, {}^{RL}D_{0^+}^{\zeta} g(s) = g(s) + \sum_{j=1}^{k} a_j s^{\zeta - j},$$

where a_j is a real number and k is the smallest integer greater than or equal to ζ, and

$$^{RL}D_{0^+}^{\zeta}\, {}^{RL}I_{0^+}^{\zeta} g(s) = g(s).$$

In order to study the system of boundary value problems (1)–(3), we first consider the corresponding linear boundary value problem,

$$\begin{cases} -{}^{RL}D_0^{\zeta} + [z(s) - F(s)] = G(s), \ 0 < s < 1, 1 < \zeta \le 2, \\ z(0) = 0, z(1) = \int\limits_0^1 \dfrac{(1-T)^{\xi_j - 1}}{\Gamma(\xi)} V(t)dt, 0 < \xi \le 1, \end{cases} \tag{4}$$

where $F, G, V \in C[0, 1]$ are given functions with $F(0) = F(1) = 0$.

Lemma 3 *The boundary value problem (4) has a unique solution*

$$z(s) = F(s) + \int_0^1 \chi(s,t) G(t)dt + s^{\zeta - 1} \int_0^1 \frac{(1-t)^{\xi - 1}}{\Gamma(\xi)} V(t)dt, \tag{5}$$

where

$$\chi(s,t) = \begin{cases} \dfrac{s^{\zeta-1}(1-t)^{\zeta-1}}{\Gamma(\zeta)} - \dfrac{(s-t)^{\zeta-1}}{\Gamma(\zeta)}, & t \le s, \\ \dfrac{s^{\zeta-1}(1-t)^{\zeta-1}}{\Gamma(\zeta)}, & s \le t. \end{cases}$$

Proof Applying the Rieman-Liouville fractional integral operator $^{RL}I_{0^+}^{\zeta}$ on both sides of the first equation of (4) and applying Lemma 2, we get

$$z(s) = a_1 s^{\zeta - 1} + a_2 s^{\zeta - 2} + F(s) - \int_0^s \frac{(s-t)^{\zeta-1}}{\Gamma(\zeta)} G(t)dt, \tag{6}$$

where $a_1, a_2 \in \mathbb{R}$. Applying boundary conditions (4), we obtain $a_2 = 0$ and

$$a_1 = \int_0^1 \frac{(1-t)^{\xi-1}}{\Gamma(\xi)} V(t)dt + \int_0^1 \frac{(1-t)^{\zeta-1}}{\Gamma(\zeta)} G(t)dt.$$

Substituting a_1 and a_2 values into (6), we get

$$\begin{aligned} z(s) &= F(s) + \int_0^1 \frac{s^{\zeta-1}(1-t)^{\zeta-1}}{\Gamma(\zeta)} G(t)dt - \int_0^s \frac{(s-t)^{\zeta-1}}{\Gamma(\zeta)} G(t)dt \\ &\quad + s^{\zeta-1} \int_0^1 \frac{(1-t)^{\xi-1}}{\Gamma(\xi)} V(t)dt \\ &= F(s) + \int_0^1 \chi(s,t)G(t)dt + s^{\zeta-1} \int_0^1 \frac{(1-t)^{\xi-1}}{\Gamma(\xi)} V(t)dt. \end{aligned}$$

Conversely, applying Riemann-Liouville fractional differential operator ${}^{RL}D_{0^+}^{\zeta}$ on both sides of (5) and using second part of Lemma 2, we get

$$\begin{aligned} {}^{RL}D_{0^+}^{\zeta} z(s) &= {}^{RL}D_{0^+}^{\zeta} F(s) - {}^{RL}D_{0^+}^{\zeta} {}^{RL}I_{0^+}^{\zeta} G(s) \\ &= {}^{RL}D_{0^+}^{\zeta} F(s) - G(s), \end{aligned}$$

where we use the fact ${}^{RL}D_{0^+}^{\zeta} s^{\zeta-1} = 0$. Also it is clear that the integral equation (5) satisfies boundary conditions, i.e.

$$z(0) = 0 \text{ and } z(1) = \int_0^1 \frac{(1-t)^{\xi-1}}{\Gamma(\xi)} V(t)dt.$$

This completes the proof. □

Theorem 1 $(z_1, z_2, \ldots, z_n)$ *is a solution of the system of boundary value problems* (1)–(3) *if and only if it is a solution of the following system of integral equations*

$$
\begin{cases}
\mathtt{z}_1(\mathtt{s}) = \mathtt{F}(\mathtt{s}, \mathtt{z}_1(\mathtt{s})) + \displaystyle\int_0^1 \chi(\mathtt{s},\mathtt{t})\mathtt{g}(\mathtt{t}, \mathtt{z}_2(\mathtt{t}), \mathtt{z}_3(\mathtt{t}), \mathtt{z}_4(\mathtt{t}), \ldots, \mathtt{z}_n(\mathtt{t}))\mathtt{dt} \\
\qquad\qquad + \mathtt{s}^{\zeta-1} \displaystyle\int_0^1 \frac{(1-\mathtt{t})^{\xi-1}}{\Gamma(\xi)} \mathtt{h}(\mathtt{t}, \mathtt{z}_2(\mathtt{t}), \mathtt{z}_3(\mathtt{t}), \mathtt{z}_4(\mathtt{t}), \ldots, \mathtt{z}_n(\mathtt{t}))\mathtt{dt} \\
\mathtt{z}_2(\mathtt{s}) = \mathtt{F}(\mathtt{s}, \mathtt{z}_2(\mathtt{s})) + \displaystyle\int_0^1 \chi(\mathtt{s},\mathtt{t})\mathtt{g}(\mathtt{t}, \mathtt{z}_1(\mathtt{t}), \mathtt{z}_3(\mathtt{t}), \mathtt{z}_4(\mathtt{t}), \ldots, \mathtt{z}_n(\mathtt{t}))\mathtt{dt} \\
\qquad\qquad + \mathtt{s}^{\zeta-1} \displaystyle\int_0^1 \frac{(1-\mathtt{t})^{\xi-1}}{\Gamma(\xi)} \mathtt{h}(\mathtt{t}, \mathtt{z}_1(\mathtt{t}), \mathtt{z}_3(\mathtt{t}), \mathtt{z}_4(\mathtt{t}), \ldots, \mathtt{z}_n(\mathtt{t}))\mathtt{dt} \\
\qquad\qquad \vdots \\
\mathtt{z}_{n-1}(\mathtt{s}) = \mathtt{F}(\mathtt{s}, \mathtt{z}_{n-1}(\mathtt{s})) + \displaystyle\int_0^1 \chi(\mathtt{s},\mathtt{t})\mathtt{g}(\mathtt{t}, \mathtt{z}_1(\mathtt{t}), \mathtt{z}_2(\mathtt{t}), \ldots, \mathtt{z}_{n-2}(\mathtt{t}), \mathtt{z}_n(\mathtt{t}))\mathtt{dt} \\
\qquad\qquad + \mathtt{s}^{\zeta-1} \displaystyle\int_0^1 \frac{(1-\mathtt{t})^{\xi-1}}{\Gamma(\xi)} \mathtt{h}(\mathtt{t}, \mathtt{z}_1(\mathtt{t}), \mathtt{z}_2(\mathtt{t}), \mathtt{z}_3(\mathtt{t}), \ldots, \mathtt{z}_1(\mathtt{t}), \mathtt{z}_{n-2}(\mathtt{t}), \mathtt{z}_n(\mathtt{t}))\mathtt{dt} \\
\mathtt{z}_n(\mathtt{s}) = \mathtt{F}(\mathtt{s}, \mathtt{z}_n(\mathtt{s})) + \displaystyle\int_0^1 \chi(\mathtt{s},\mathtt{t})\mathtt{g}(\mathtt{t}, \mathtt{z}_1(\mathtt{t}), \mathtt{z}_2(\mathtt{t}), \mathtt{z}_3(\mathtt{t}), \ldots, \mathtt{z}_{n-2}(\mathtt{t}), \mathtt{z}_{n-1}(\mathtt{t}))\mathtt{dt} \\
\qquad\qquad + \mathtt{s}^{\zeta-1} \displaystyle\int_0^1 \frac{(1-\mathtt{t})^{\xi-1}}{\Gamma(\xi)} \mathtt{h}(\mathtt{t}, \mathtt{z}_1(\mathtt{t}), \mathtt{z}_2(\mathtt{t}), \mathtt{z}_3(\mathtt{t}), \ldots, \mathtt{z}_{n-2}(\mathtt{t}), \mathtt{z}_{n-1}(\mathtt{t}))\mathtt{dt}
\end{cases}
\tag{7}
$$

Proof The proof follows from Lemma 3. □

Lemma 4 *The kernel* $\chi(\mathtt{s},\mathtt{t})$ *has the following properties*:

(i) $\chi(\mathtt{s},\mathtt{t})$ is nonnegative and continuous on $[0,1] \times [0,1]$.
(ii) $\chi(\mathtt{s},\mathtt{t}) \leq \chi(\mathtt{t},\mathtt{t})$ for $\mathtt{s},\mathtt{t} \in [0,1] \times [0,1]$.
(iii) $\max\limits_{\mathtt{s}\in[0,1]} \displaystyle\int_0^1 \chi(\mathtt{s},\mathtt{t})\mathtt{dt} = \frac{\Gamma(\zeta)}{\Gamma(2\zeta)}$.

Proof From the definition of $\chi(\mathtt{s},\mathtt{t})$, it is clear that $\chi(\mathtt{s},\mathtt{t})$ is continuous on $[0,1] \times [0,1]$. For $\mathtt{t} \leq \mathtt{s}$, we have

$$\begin{aligned}\chi(\mathtt{s},\mathtt{t}) &= \frac{1}{\Gamma(\zeta)}\left[\mathtt{s}^{\zeta-1}(1-\mathtt{t})^{\zeta-1} - (\mathtt{s}-\mathtt{t})^{\zeta-1}\right]\\ &\geq \frac{1}{\Gamma(\zeta)}\left[\mathtt{s}^{\zeta-1}(1-\mathtt{t})^{\zeta-1} - (\mathtt{s}-\mathtt{s}\mathtt{t})^{\zeta-1}\right]\\ &\geq \frac{1}{\Gamma(\zeta)}\left[\mathtt{s}^{\zeta-1}(1-\mathtt{t})^{\zeta-1} - \mathtt{s}^{\zeta-1}(1-\mathtt{t})^{\zeta-1}\right]\\ &= 0\end{aligned}$$

For $\mathtt{s}\leq\mathtt{t}$, it is obvious that $\chi(\mathtt{s},\mathtt{t})\geq 0$. Thus, $\chi(\mathtt{s},\mathtt{t})\geq 0$ for all $\mathtt{s},\mathtt{t}\in[0,1]$. Since, for $\mathtt{t}\leq\mathtt{s}$,

$$\begin{aligned}\frac{\partial\chi(\mathtt{s},\mathtt{t})}{\partial\mathtt{s}} &= \frac{1}{\Gamma(\zeta-1)}\left[\mathtt{s}^{\zeta-2}(1-\mathtt{t})^{\zeta-1} - (\mathtt{s}-\mathtt{t})^{\zeta-2}\right]\\ &= \frac{\mathtt{s}^{\zeta-2}}{\Gamma(\zeta-1)}\left[(1-\mathtt{t})^{\zeta-1} - \left(1-\frac{\mathtt{t}}{\mathtt{s}}\right)^{\zeta-2}\right]\\ &\leq \frac{\mathtt{s}^{\zeta-2}}{\Gamma(\zeta-1)}\left[(1-\mathtt{t})^{\zeta-1} - \left(1-\frac{\mathtt{t}}{\mathtt{s}}\right)^{\zeta-1}\right]\\ &\leq \frac{\mathtt{s}^{\zeta-2}}{\Gamma(\zeta-1)}\left[\left(1-\frac{\mathtt{t}}{\mathtt{s}}\right)^{\zeta-1} - \left(1-\frac{\mathtt{t}}{\mathtt{s}}\right)^{\zeta-1}\right]\\ &= 0,\end{aligned}$$

$\chi(\mathtt{s},\mathtt{t})$ is decreasing with respect to $\mathtt{s}$ on $[\mathtt{t},1]$. It follows that

$$\chi(s,\ t)\leq\ \chi(t,\ t)\ \text{for}\ t\leq\ s.$$

Similarly it can be seen that $\chi(\mathtt{s},\mathtt{t})$ is increasing with respect to $\mathtt{s}$ on $[0,\mathtt{t}]$. It follows that

$$\chi(s,t)\leq\ \chi(t,t)\ \text{for}\ s\leq\ t.$$

Hence,

$$\chi(s,t)\leq\ \chi(t,\ t)\ \text{for all}\ t,\ s\in[0,1].$$

By direct integration of $\chi(s,\ t)$, (*iii*) can be obtain. This completes the proof. □

3 Main results

In this section, we generalize the following fixed point Theorem 2 by Burton [4] to n-fixed point theorem.

Theorem 2 ([4]) *Let* $\mathtt{M}$ *be a closed, convex and nonempty subset of a Banach space* $\mathscr{B}$. *Suppose that* $\mathtt{A}:\mathtt{M}\to\mathscr{B}$ *and* $\mathtt{B}:\mathscr{B}\to\mathscr{B}$ *such that*

(i) $\mathtt{B}$ is a contraction with constant $\alpha<1$,

(ii) the completely continuous property hold for the operators $\mathtt{A}$,
(iii) $\mathtt{z}_0 = \mathtt{B}\mathtt{z}_0 + \mathtt{A}\mathtt{z}_1$, $\mathtt{z}_1 \in \mathtt{M}$, then $\mathtt{z}_0 \in \mathtt{M}$.

Then there is a $\mathtt{z} \in \mathtt{M}$ with $\mathtt{A}\mathtt{z} + \mathtt{B}\mathtt{z} = \mathtt{z}$.

Definition 3 ([18]) An element $(\mathtt{z}_1, \mathtt{z}_2, \ldots, \mathtt{z}_n) \in \mathtt{X}^n$ is called an n-fixed point of a mapping $\aleph : \mathtt{X}^n \to \mathtt{X}$ if

$$\aleph(\mathtt{z}_1, \mathtt{z}_2, \ldots, \mathtt{z}_n) = \mathtt{z}_1, \aleph(\mathtt{z}_2, \mathtt{z}_1, \ldots, \mathtt{z}_n) = \mathtt{z}_2, \ldots \aleph(\mathtt{z}_n, \mathtt{z}_2, \ldots, \mathtt{z}_1) = \mathtt{z}_n.$$

Definition 4 ([30]) Let Φ be the family of all functions $\varphi : [1, +\infty) \to [1, +\infty)$ such that

(i) φ is increasing,
(ii) for each $\mathtt{s} \in [1, +\infty)$, $\lim_{n \to +\infty} \varphi^n(\mathtt{s}) = 1$,
(iii) φ is continuous.

Lemma 5 ([30]) *If $\varphi \in \Phi$, then $\varphi(1) = 1$ and $\varphi(\mathtt{s}) < \mathtt{s}$ for all $\mathtt{s} \in [1, +\infty)$.*

Theorem 3 *Let $\mathscr{B}$ be a Banach space and $\aleph_0 : \mathscr{B} \to \mathscr{B}$. Let $\mathtt{E}$ be a convex, closed and bounded subset of $\mathscr{B}$ and for each $\mathtt{j} \in \{1, 2, \ldots, n-1\}$, $\aleph_\mathtt{j} : \mathtt{E} \to \mathscr{B}$ be completely continuous operators such that*

$(\mathtt{H}_1)$ there exists $\varphi \in \Phi$ and for some $0 < \delta < 1$ such that

$$\|\aleph_0 \mathtt{z} - \aleph_0 \mathtt{y}\| \leq \delta \varphi\left(\frac{\|\mathtt{z} - \mathtt{y}\|}{1 + \|\mathtt{z} - \mathtt{y}\|}\right).$$

$(\mathtt{H}_2)$ $\mathtt{z}_0 = \sum_{\mathtt{j}=0}^{n-1} \aleph_\mathtt{j} \mathtt{z}_\mathtt{j}$ implies $\mathtt{z}_0 \in \mathtt{E}$ for all $\mathtt{z}_\mathtt{j} \in \mathtt{E}$ where $\mathtt{j} = 1, 2, \ldots, n-1$.

Then there exists an n-fixed point of the operator $\aleph(\mathtt{z}_0, \mathtt{z}_1, \ldots, \mathtt{z}_{n-1}) = \sum_{\mathtt{j}=0}^{n-1} \aleph_\mathtt{j} \mathtt{z}_\mathtt{j}$ in $\mathtt{E}^n$.

Proof Since $\mathtt{E}$ is convex, closed and bounded subset of $\mathscr{B}$, follows that $\mathtt{E}^n$ too. Next define operators $\aleph_0^n : \mathscr{B}^n \to \mathscr{B}^n$ and $\aleph_\mathtt{j}^n : \mathtt{E}^n \to \mathscr{B}^n (\mathtt{j} = 1, 2, \ldots, n-1)$ by

$$\begin{aligned}
\aleph_0^n(z_0, z_1, z_2, \ldots, z_{n-2}, z_{n-1}); &= (\aleph_0 z_0, \aleph_0 z_1, \aleph_0 z_2, \ldots, \aleph_0 z_{n-2}, \aleph_0 z_{n-1}) \\
\aleph_1^n(z_0, z_1, z_3, \ldots, z_{n-2}, z_{n-1}); &= (\aleph_1 z_1, \aleph_1 z_0, \aleph_1 z_2, \ldots, \aleph_1 z_{n-2}, \aleph_1 z_{n-1}) \\
\aleph_2^n(z_0, z_1, z_3, \ldots, z_{n-2}, z_{n-1}); &= (\aleph_2 z_3, \aleph_2 z_1, \aleph_1 z_0, \ldots, \aleph_2 z_{n-2}, \aleph_1 z_{n-1}) \\
&\vdots; \\
\aleph_{n-2}^n(z_0, z_1, z_3, \ldots, z_{n-2}, z_{n-1}); &= (\aleph_{n-2} z_{n-2}, \aleph_{n-2} z_1, \aleph_{n-2} z_2, \cdots, \aleph_{n-2} z_0, \aleph_{n-2} z_{n-1}) \\
\aleph_{n-1}^n(z_0, z_1, z_3, \ldots, z_{n-2}, z_{n-1}); &= (\aleph_{n-1} z_{n-1}, \aleph_{n-1} z_1, \aleph_{n-1} z_2, \ldots, \aleph_{n-1} z_{n-2}, \aleph_{n-1} z_0).
\end{aligned}$$

The proof follows if $\sum_{j=0}^{n-1} \aleph_j^n(z_0, z_1, \ldots, z_{n-1}) = (z_0, z_1, \ldots, z_{n-1})$ has atleast one solution. Since

$$\begin{aligned}
&(\aleph(z_0, z_1, \ldots, z_{n-1}), \aleph(z_1, z_0, \ldots, z_{n-1}), \ldots, \aleph(z_{n-1}, z_1, \ldots, z_0)) \\
&\quad = \big(\aleph_0 z_0 + \aleph_1 z_1 + \ldots + \aleph_{n-1} z_{n-1}, \aleph_0 z_1 + \aleph_1 z_0 + \ldots + \aleph_{n-1} z_{n-1}, \\
&\quad \ldots, \aleph_0 z_{n-1} + \aleph_1 z_1 + \ldots + \aleph_{n-1} z_0\big) \\
&\quad = (\aleph_0 z_0, \aleph_0 z_1, \ldots, \aleph_0 z_{n-1}) + (\aleph_1 z_1, \aleph_1 z_0, \ldots, \aleph_1 z_{n-1}) + \\
&\quad \ldots + (\aleph_{n-1} z_{n-1}, \aleph_{n-1} z_1, \ldots, \aleph_{n-1} z_0) \\
&\quad = \sum_{j=0}^{n-1} \aleph_j^n z_j = (z_0, z_1, \ldots, z_{n-1}),
\end{aligned}$$

it follows that the operator $\aleph(z_0, z_1, \ldots, z_{n-1})$ has at least one n-fixed point. Now we prove that the operator $\aleph_j^n$ satisfy the conditions of Theorem 2. Let $z_j = (z_j^1, z_j^2 \ldots, z_j^n) \in E^n$. Then by Lemma 5, we have

$$\begin{aligned}
\|\aleph_0^n z_0 - \aleph_0^n z_1\| &= \|(\aleph_0 z_0^1, \aleph_0 z_0^2, \ldots, \aleph_0 z_0^n) - (\aleph_0 z_1^1, \aleph_0 z_1^2, \ldots, \aleph_0 z_1^n)\| \\
&= \|(\aleph_0 z_0^1 - \aleph_0 z_1^1, \aleph_0 z_0^2 - \aleph_0 z_1^2, \ldots, \aleph_0 z_0^n - \aleph_0 z_1^n)\| \\
&= \sum_{i=1}^{n} \|\aleph_0 z_0^i - \aleph_0 z_1^i\| \le \delta \sum_{i=1}^{n} \varphi\left(\frac{\|z_0^i - z_1^i\|}{1 + \|z_0^i - z_1^i\|}\right) \\
&\le \delta \sum_{i=1}^{n} \frac{\|z_0^i - z_1^i\|}{1 + \|z_0^i - z_1^i\|} \le \delta \sum_{i=1}^{n} \|z_0^i - z_1^i\| \\
&= \delta \|(z_0^1 - z_1^1, z_0^2 - z_1^2, \ldots, z_0^n - z_1^n)\| \\
&= \delta \|z_0 - z_1\|.
\end{aligned}$$

Thus, $\aleph_0^n$ satisfies first condtion. Next, we shat the operators $\aleph_j^n (j = 1, 2, \ldots, n-1)$ compact and continuous on E^n. Let $(y_k)_{k=1}^{\infty} := (y_{1k}, y_{2k}, \ldots, y_{nk}) \in E^n$ converging to $y := (y_1, y_2, \ldots, y_n) \in E^n$. By continuity of $\aleph_j (j = 1, 2 \ldots, n-1)$, we have

$$\begin{aligned}
\lim_{k\to\infty} \aleph_0^n \mathtt{y}_k &= (\lim_{k\to\infty} \aleph_0 \mathtt{y}_k, \lim_{k\to\infty} \aleph_0 \mathtt{y}_{2k}, \ldots, \lim_{k\to\infty} \aleph_0 \mathtt{y}_{nk}) \\
&= (\aleph_0 \mathtt{y}_1, \aleph_0 \mathtt{y}_2, \ldots, \aleph_0 \mathtt{y}_n) \\
&= \aleph_0^n (\mathtt{y}_1, \mathtt{y}_2, \ldots, \mathtt{y}_n) \\
&= \aleph_0^n \mathtt{y}, \\
\lim_{k\to\infty} \aleph_1^n \mathtt{y}_k &= (\lim_{k\to\infty} \aleph_1 \mathtt{y}_{2k}, \lim_{k\to\infty} \aleph_1 \mathtt{y}_{1k}, \ldots, \lim_{k\to\infty} \aleph_0 \mathtt{y}_{nk}) \\
&= (\aleph_1 \mathtt{y}_2, \aleph_1 \mathtt{y}_1, \ldots, \aleph_1 \mathtt{y}_n) \\
&= \aleph_1^n (\mathtt{y}_1, \mathtt{y}_2, \ldots, \mathtt{y}_n), \\
&= \aleph_1^n \mathtt{y}, \\
&\vdots \\
&\vdots \\
\lim_{k\to\infty} \aleph_{n-1}^n \mathtt{y}_k &= (\lim_{k\to\infty} \aleph_{n-1} \mathtt{y}_{(n-1)k}, \lim_{k\to\infty} \aleph_{n-1} \mathtt{y}_{2k}, \ldots, \lim_{k\to\infty} \aleph_{n-1} \mathtt{y}_{1k}) \\
&= (\aleph_{n-1} \mathtt{y}_{n-1}, \aleph_{n-1} \mathtt{y}_2, \ldots, \aleph_0 \mathtt{y}_n) \\
&= \aleph_{n-1}^n (\mathtt{y}_1, \mathtt{y}_2, \ldots, \mathtt{y}_n) \\
&= \aleph_{n-1}^n \mathtt{y},
\end{aligned}$$

So, $\aleph_{\mathtt{j}}^n$ are continuous. Similarly, we can show that $\aleph_{\mathtt{j}}^n$ are uniformly bounded. Next, we show that $\aleph_{\mathtt{j}}^n(\mathtt{E}^n)$ are equi-continuous on $\mathscr{B}^n$. Since $\aleph_{\mathtt{j}}(\mathtt{E})$ are equi-continuous on $\mathscr{B}$, for every $\varepsilon > 0$, there exists $\eta > 0$ such that

$$|\aleph_{\mathtt{j}} \mathtt{z}(u) - \aleph_{\mathtt{j}} \mathtt{z}(v)| \leq \varepsilon \text{whenever} |u - v| < \eta, \text{for} u, v \in \mathtt{I}, \mathtt{z} \in \mathtt{E},$$

where $\mathtt{I}$ is some bounded interval of $\mathbb{R}$. Thus, for any $\mathtt{z} = (\mathtt{z}_1, \mathtt{z}_2, \ldots, \mathtt{z}_n) \in \mathtt{E}^n$, we have

$$
\begin{aligned}
|\aleph_0^n \mathtt{z}(u) - \aleph_0^n \mathtt{z}(v)| &= |(\aleph_0 \mathtt{z}_1(u), \aleph_0 \mathtt{z}_2(u), \ldots, \aleph_0 \mathtt{z}_n(u)) - (\aleph_0 \mathtt{z}_1(v), \aleph_0 \mathtt{z}_2(v), \ldots, \aleph_0 \mathtt{z}_n(v))| \\
&= |(\aleph_0 \mathtt{z}_1(u) - \aleph_0 \mathtt{z}_1(v), \aleph_0 \mathtt{z}_2(u) - \aleph_0 \mathtt{z}_2(v), \ldots, \aleph_0 \mathtt{z}_n(u) - \aleph_0 \mathtt{z}_n(v))| \\
&= \left[\sum_{\mathtt{j}=1}^{n} (\aleph_0 \mathtt{z}_\mathtt{j}(u) - \aleph_0 \mathtt{z}_\mathtt{j}(v))\right]^{1/2} \\
&\leq \sqrt{n\varepsilon}, \\
|\aleph_1^n \mathtt{z}(u) - \aleph_1^n \mathtt{z}(v)| &= |(\aleph_1 \mathtt{z}_2(u), \aleph_1 \mathtt{z}_1(u), \ldots, \aleph_1 \mathtt{z}_n(u)) - (\aleph_1 \mathtt{z}_2(v), \aleph_1 \mathtt{z}_1(v), \ldots, \aleph_1 \mathtt{z}_n(v))| \\
&= |(\aleph_1 \mathtt{z}_2(u) - \aleph_1 \mathtt{z}_2(v), \aleph_1 \mathtt{z}_1(u) - \aleph_1 \mathtt{z}_1(v), \ldots, \aleph_1 \mathtt{z}_n(u) - \aleph_1 \mathtt{z}_n(v))| \\
&= \left[\sum_{\mathtt{j}=1}^{n} (\aleph_1 \mathtt{z}_\mathtt{j}(u) - \aleph_1 \mathtt{z}_\mathtt{j}(v))\right]^{1/2} \\
&\leq \sqrt{n\varepsilon}, \\
&\vdots \\
&\vdots \\
|\aleph_{n-1}^n \mathtt{z}(u) - \aleph_{n-1}^n \mathtt{z}(v)| &= |(\aleph_{n-1} \mathtt{z}_n(u), \aleph_{n-1} \mathtt{z}_2(u), \ldots, \aleph_{n-1} \mathtt{z}_1(u)) \\
&\quad - (\aleph_{n-1} \mathtt{z}_1(v), \aleph_{n-1} \mathtt{z}_2(v), \ldots, \aleph_{n-1} \mathtt{z}_n(v))| \\
&= |(\aleph_{n-1} \mathtt{z}_n(u) - \aleph_{n-1} \mathtt{z}_n(v), \aleph_{n-1} \mathtt{z}_2(u) - \aleph_{n-1} \mathtt{z}_2(v), \\
&\quad \ldots, \aleph_{n-1} \mathtt{z}_1(u) - \aleph_{n-1} \mathtt{z}_1(v))| \\
&= \left[\sum_{\mathtt{j}=1}^{n} (\aleph_0 \mathtt{z}_\mathtt{j}(u) - \aleph_0 \mathtt{z}_\mathtt{j}(v))\right]^{1/2} \\
&\leq \sqrt{n\varepsilon},
\end{aligned}
$$

By Arzela-Ascoli theorem, $\aleph_\mathtt{j}^n(\mathtt{E}^\mathtt{n})$ are compact. Hence, $\aleph_\mathtt{j}^n$ are completely continuous on $\mathtt{E}^\mathtt{n}$. This shows condition (*ii*) of Theorem 2. Finally, let $\mathtt{z}_\mathtt{j} = (\mathtt{z}_\mathtt{j}^1, \mathtt{z}_\mathtt{j}^2 \ldots, \mathtt{z}_\mathtt{j}^n) \in \mathtt{E}^n$ such that $\mathtt{z}_0 = \sum_{\mathtt{j}=0}^{n-1} \aleph_\mathtt{j} \mathtt{z}_\mathtt{j}$, then by hypothesis (*iii*) we can write

$$
\begin{aligned}
(\mathtt{z}_0^1, \mathtt{z}_0^2, \ldots, \mathtt{z}_0^n) &= \sum_{\mathtt{j}=0}^{n-1} \aleph_{\mathtt{j}}^n(\mathtt{z}_{\mathtt{j}}^1, \mathtt{z}_{\mathtt{j}}^2, \ldots, \mathtt{z}_{\mathtt{j}}^n) \\
&= (\aleph_0 \mathtt{z}_0^1, \aleph_0 \mathtt{z}_0^2, \ldots, \aleph_0 \mathtt{z}_0^n) + (\aleph_1 \mathtt{z}_1^2, \aleph_1 \mathtt{z}_1^1, \ldots, \aleph_1 \mathtt{z}_1^n) \\
&+ (\aleph_2 \mathtt{z}_2^3, \aleph_2 \mathtt{z}_2^2, \aleph_2 \mathtt{z}_2^1, \ldots, \aleph_2 \mathtt{z}_2^n) \\
&\ldots + (\aleph_{n-1} \mathtt{z}_{n-1}^n, \aleph_{n-1} \mathtt{z}_{n-1}^2, \ldots, \aleph_{n-1} \mathtt{z}_{n-1}^1) \\
&= \left(\sum_{\mathtt{j}=0}^{n-1} \aleph_{\mathtt{j}} \mathtt{z}_{\mathtt{j}}^{\mathtt{j}+1}, \sum_{\mathtt{j}=0, \mathtt{j}\neq 1}^{n-1} \aleph_{\mathtt{j}} \mathtt{z}_{\mathtt{j}}^2 + \aleph_1 \mathtt{z}_1^1, \sum_{\mathtt{j}=0, \mathtt{j}\neq 2}^{n-1} \aleph_{\mathtt{j}} \mathtt{z}_{\mathtt{j}}^3 + \aleph_2 \mathtt{z}_2^1, \ldots, \right. \\
&\left. \sum_{\mathtt{j}=0}^{n-2} \aleph_{\mathtt{j}} \mathtt{z}_{\mathtt{j}}^n + \aleph_{n-1} \mathtt{z}_{n-1}^1 \right).
\end{aligned}
$$

That is,

$$
\begin{aligned}
\mathtt{z}_0^1 &= \sum_{\mathtt{j}=0}^{n-1} \aleph_{\mathtt{j}} \mathtt{z}_{\mathtt{j}}^{\mathtt{j}+1}, \\
\mathtt{z}_0^2 &= \sum_{\mathtt{j}=0, \mathtt{j}\neq 1}^{n-1} \aleph_{\mathtt{j}} \mathtt{z}_{\mathtt{j}}^2 + \aleph_1 \mathtt{z}_1^1, \\
\mathtt{z}_0^3 &= \sum_{\mathtt{j}=0, \mathtt{j}\neq 2}^{n-1} \aleph_{\mathtt{j}} \mathtt{z}_{\mathtt{j}}^3 + \aleph_2 \mathtt{z}_2^1, \\
&\vdots \\
\mathtt{z}_0^n &= \sum_{\mathtt{j}=0}^{n-2} \aleph_{\mathtt{j}} \mathtt{z}_{\mathtt{j}}^n + \aleph_{n-1} \mathtt{z}_{n-1}^1.
\end{aligned}
$$

From (*iii*), we get $\mathtt{z}_0^1, \mathtt{z}_0^2, \ldots, \mathtt{z}_0^n \in \mathtt{E}$, i.e., $\mathtt{z}_0 = (\mathtt{z}_0^1, \mathtt{z}_0^2, \ldots, \mathtt{z}_0^n) \in \mathtt{E}^n$. Thus, all conditions of Theorem 2 satisfied. Therefore, the equation $\mathtt{z}_0 = \aleph_0^n \mathtt{z}_0 + \aleph_1^n \mathtt{z}_1 + \ldots + \aleph_{n-1}^n \mathtt{z}_{n-1}$ has at least one solution on $\mathtt{E}^n$. Hence, the operator $\aleph(\mathtt{z}_0, \mathtt{z}_1, \ldots, \mathtt{z}_{n-1})$ has at least one n-fixed point. This completes the proof. □

3.1 Existence of solution for the system (1)–(3)

In this section, we derive necessary conditions for the existence of solutions to the system of boundary value problems (1)–(3). Assume that the following conditions hold in the sequel:

$(\mathcal{J}_1)$ there exist $\mathtt{M} > 0$ such that $|\mathtt{F}(\mathtt{s}, \mathtt{z}) - \mathtt{F}(\mathtt{s}, \mathtt{y})| \leq \frac{\mathtt{M}|\mathtt{z}-\mathtt{y}|}{2+2|\mathtt{z}-\mathtt{y}|}$ for $\mathtt{z}, \mathtt{y} \in \mathscr{B}$,

$(\mathcal{J}_2)$ $\mathtt{g}(\mathtt{s},\mathtt{y}_1(\mathtt{s}),\mathtt{y}_2(\mathtt{s}),\ldots,\mathtt{y}_{n-1}(\mathtt{s}))=\sum_{\mathtt{i}=1}^{n-1}\mathtt{g}(\mathtt{s},\mathtt{y}_\mathtt{i}(\mathtt{s}))$ is an increasing function of $\mathtt{y}$, and there is a continuous function $\mathtt{g}^\star(s)$ such that $\sum_{\mathtt{i}=1}^{n-1}\mathtt{g}(\mathtt{s},\mathtt{y}_\mathtt{i}(\mathtt{s}))=\mathtt{g}^\star(s)$ for $\mathtt{s}\in[0,1]$,

$(\mathcal{J}_3)$ $\mathtt{h}(\mathtt{s},\mathtt{y}_1(\mathtt{s}),\mathtt{y}_2(\mathtt{s}),\ldots,\mathtt{y}_{n-1}(\mathtt{s}))=\sum_{\mathtt{i}=1}^{n-1}\mathtt{h}(\mathtt{s},\mathtt{y}_\mathtt{i}(\mathtt{s}))$ is an increasing function of $\mathtt{y}$, and there is a continuous function $\mathtt{h}^\star(s)$ such that $\sum_{\mathtt{i}=1}^{n-1}\mathtt{h}(\mathtt{s},\mathtt{y}_\mathtt{i}(\mathtt{s}))=\mathtt{h}^\star(s)$ for $\mathtt{s}\in[0,1]$.

Theorem 4 *Suppose $(\mathcal{J}_1)$–$(\mathcal{J}_3)$ hold. Then the system of boundary value problems (1)–(3) has a solution.*

Proof Let $\mathtt{E}=\{\mathtt{z}\in\mathscr{B}:\|\mathtt{z}\|\leq\Xi\}$, where $\frac{\mathtt{M}}{2}+\mathtt{F}^\star+\frac{(n-1)\Gamma(\zeta)\|\mathtt{g}^\star\|_{L^1}}{\Gamma(2\zeta)}+\frac{(n-1)\|\mathtt{h}^\star\|_{L^1}}{\Gamma(\xi+1)}\leq\Xi$. It is clear that $\mathtt{E}$ is convex, closed and bounded subset of the Banach space $\mathscr{B}$. Next, define operators $\mathtt{T}_0:\mathscr{B}\to\mathscr{B}$, and $\mathtt{T}_\mathtt{j}:\mathtt{E}\to\mathscr{B}$ by

$$\mathtt{T}_0\mathtt{z}(\mathtt{s})=\ \mathtt{F}(\mathtt{s},\mathtt{z}(\mathtt{s})),$$

$$\mathtt{T}_\mathtt{j}\mathtt{z}_\mathtt{j}(\mathtt{s})=\int_0^1\chi(\mathtt{s},\mathtt{t})\mathtt{g}\big(\mathtt{t},\mathtt{z}_\mathtt{j}(\mathtt{t})\big)\mathtt{dt}+\mathtt{s}^{\zeta-1}\int_0^1\frac{(1-\mathtt{t})^{\xi-1}}{\Gamma(\xi)}\mathtt{h}\big(\mathtt{t},\mathtt{z}_\mathtt{j}(\mathtt{t})\big)\mathtt{dt},\ \mathtt{j}=1,2,\ldots,n.$$

Then, the system (7) can be written in an operator form

$$\begin{cases}\mathtt{z}_1(\mathtt{s})=\mathtt{T}_0\mathtt{z}_1(\mathtt{s})+\mathtt{T}_2\mathtt{z}_2(\mathtt{s})+\mathtt{T}_3\mathtt{z}_3(\mathtt{s})+\ldots+\mathtt{T}_{n-1}\mathtt{z}_{n-1}(\mathtt{s})+\mathtt{T}_n\mathtt{z}_n(\mathtt{s}),\\ \mathtt{z}_2(\mathtt{s})=\mathtt{T}_0\mathtt{z}_2(\mathtt{s})+\mathtt{T}_1\mathtt{z}_1(\mathtt{s})+\mathtt{T}_3\mathtt{z}_3(\mathtt{s})+\ldots+\mathtt{T}_{n-1}\mathtt{z}_{n-1}(\mathtt{s})+\mathtt{T}_n\mathtt{z}_n(\mathtt{s}),\\ \qquad\vdots\\ \mathtt{z}_{n-1}(\mathtt{s})=\mathtt{T}_0\mathtt{z}_{n-1}(\mathtt{s})+\mathtt{T}_1\mathtt{z}_1(\mathtt{s})+\mathtt{T}_2\mathtt{z}_2(\mathtt{s})+\ldots+\mathtt{T}_{n-2}\mathtt{z}_{n-2}(\mathtt{s})+\mathtt{T}_n\mathtt{z}_n(\mathtt{s}),\\ \mathtt{z}_n(\mathtt{s})=\mathtt{T}_0\mathtt{z}_n(\mathtt{s})+\mathtt{T}_1\mathtt{z}_1(\mathtt{s})+\mathtt{T}_2\mathtt{z}_2(\mathtt{s})+\ldots+\mathtt{T}_{n-2}\mathtt{z}_{n-2}(\mathtt{s})+\mathtt{T}_{n-1}\mathtt{z}_{n-1}(\mathtt{s}).\end{cases}\tag{8}$$

Now, we show that the operators $\mathtt{T}_\mathtt{j}'\mathtt{s}$ satisfies all conditions of Theorem 3. For $\mathtt{z},\mathtt{y}\in\mathscr{B}$, we have

$$\begin{aligned}|\mathtt{T}_0\mathtt{z}(\mathtt{s})-\mathtt{T}_0\mathtt{y}(\mathtt{s})|&=|\mathtt{F}(\mathtt{s},\mathtt{z}(\mathtt{s}))-\mathtt{F}(\mathtt{s},\mathtt{y}(\mathtt{s}))|\\&\leq\frac{\mathtt{M}|\mathtt{z}(\mathtt{s})-\mathtt{y}(\mathtt{s})|}{2(1+|\mathtt{z}(\mathtt{s})-\mathtt{y}(\mathtt{s})|)}\\&\leq\frac{\mathtt{M}\|\mathtt{z}(\mathtt{s})-\mathtt{y}(\mathtt{s})\|}{2(1+\|\mathtt{z}(\mathtt{s})-\mathtt{y}(\mathtt{s})\|)}.\end{aligned}$$

Taking supremum on both sides over $\mathtt{s}$, we get

$$\|\mathtt{T}_0\mathtt{z}-\mathtt{T}_0\mathtt{y}\|\leq\delta\varphi\left(\frac{\|\mathtt{z}-\mathtt{y}\|}{1+\|\mathtt{z}-\mathtt{y}\|}\right),$$

where $\delta=\mathtt{M}/2<1$. Next, to prove that $\mathtt{T}_\mathtt{j}'\mathtt{s}$ are compact and continuous on $\mathtt{E}$, we assume the sequence $\{\mathtt{x}_\ell\}_{\ell=1}^{\infty}$ of $\mathtt{E}$ converges to the point $\mathtt{x}\in\mathtt{E}$. Now by Lebesgue dominated convergence theorem, we get

$$\begin{aligned}\lim_{\ell\to\infty}\mathtt{T}_\mathtt{j}\mathtt{x}_\ell(\mathtt{s})&=\int_0^1\chi(\mathtt{s},\mathtt{t})\lim_{\ell\to\infty}\mathtt{g}(\mathtt{t},\mathtt{x}_\ell(\mathtt{t}))\mathtt{dt}+\mathtt{s}^{\zeta-1}\int_0^1\frac{(1-\mathtt{t})^{\xi-1}}{\Gamma(\xi)}\lim_{\ell\to\infty}\mathtt{h}(\mathtt{t},\mathtt{x}_\ell(\mathtt{t}))\mathtt{dt}\\&=\int_0^1\chi(\mathtt{s},\mathtt{t})\mathtt{g}(\mathtt{t},\mathtt{x}(\mathtt{t}))\mathtt{dt}+\mathtt{s}^{\zeta-1}\int_0^1\frac{(1-\mathtt{t})^{\xi-1}}{\Gamma(\xi)}\mathtt{h}(\mathtt{t},\mathtt{x}(\mathtt{t}))\mathtt{dt}\\&=\mathtt{T}_\mathtt{j}\mathtt{x}(\mathtt{s}).\end{aligned}$$

Thus, $\mathtt{T}_\mathtt{j}'\mathtt{s}$ are continuous. Next for $\mathtt{x}\in\mathtt{E}$, we have

$$\begin{aligned}|\mathtt{T}_\mathtt{j}\mathtt{x}(\mathtt{s})|=&\left|\int_0^1\chi(\mathtt{s},\mathtt{t})\mathtt{g}(\mathtt{t},\mathtt{x}(\mathtt{t}))\mathtt{dt}+\mathtt{s}^{\zeta-1}\int_0^1\frac{(1-\mathtt{t})^{\xi-1}}{\Gamma(\xi)}\mathtt{h}(\mathtt{t},\mathtt{x}(\mathtt{t}))\mathtt{dt}\right|\\\leq&\int_0^1|\chi(\mathtt{s},\mathtt{t})||\mathtt{g}(\mathtt{t},\mathtt{x}(\mathtt{t}))|\mathtt{dt}+|\mathtt{s}|^{\zeta-1}\int_0^1\frac{|1-\mathtt{t}|^{\xi-1}}{\Gamma(\xi)}|\mathtt{h}(\mathtt{t},\mathtt{x}(\mathtt{t}))|\mathtt{dt}\\\leq&\int_0^1|\chi(\mathtt{s},\mathtt{t})||\mathtt{g}(\mathtt{t},\mathtt{x}(\mathtt{t}))|\mathtt{dt}+|\mathtt{s}|^{\zeta-1}\int_0^1\frac{|1-\mathtt{t}|^{\xi-1}}{\Gamma(\xi)}|\mathtt{h}(\mathtt{t},\mathtt{x}(\mathtt{t}))|\mathtt{dt}\\\leq&\int_0^1\chi(\mathtt{t},\mathtt{t})|\mathtt{g}^\star(\mathtt{t})|\mathtt{dt}+\int_0^1\frac{|1-\mathtt{t}|^{\xi-1}}{\Gamma(\xi)}|\mathtt{h}^\star(\mathtt{t})|\mathtt{dt}\\=&\frac{\Gamma(\zeta)}{\Gamma(2\zeta)}\|\mathtt{g}^\star\|_{L^1}+\frac{1}{\Gamma(\xi+1)}\|\mathtt{h}^\star\|_{L^1},\end{aligned}$$

which proves that $\mathtt{T}_\mathtt{j}'\mathtt{s}$ are uniformly bounded on $\mathtt{E}$. Let $\mathtt{s}_1,\mathtt{s}_2\in[0,1]$ with $\mathtt{s}_2<\mathtt{s}_1$, we have

$$
\begin{aligned}
|T_j x(s_1) - T_j x(s_2)| = & \left| \int_0^1 \chi(s_1,t) g(t,x(t)) dt + s_1^{\zeta-1} \int_0^1 \frac{(1-t)^{\xi-1}}{\Gamma(\xi)} h(t,x(t)) dt \right. \\
& \left. - \int_0^1 \chi(s_2,t) g(t,x(t)) dt - s_2^{\zeta-1} \int_0^1 \frac{(1-t)^{\xi-1}}{\Gamma(\xi)} h(t,x(t)) dt \right| \\
\leq & \int_0^1 |\chi(s_1,t) - \chi(s_2,t)||g(t,x(t))| dt \\
& + |s_1^{\zeta-1} - s_2^{\zeta-1}| \int_0^1 \frac{|1-t|^{\xi-1}}{\Gamma(\xi)} |h(t,x(t))| dt \\
\leq & \int_0^{s_2} |\chi(s_1,t) - \chi(s_2,t)||g(t,x(t))| dt + \int_{s_2}^{s_1} |\chi(s_1,t) \\
& - \chi(s_2,t)||g(t,x(t))| dt \\
& + \int_{s_1}^1 |\chi(s_1,t) - \chi(s_2,t)||g(t,x(t))| dt + \frac{\|h^\star\|_{L^1}}{\Gamma(\xi+1)} |s_1^{\zeta-1} - s_2^{\zeta-1}|.
\end{aligned}
$$

Since $g(t,x(t))$ is bounded and by the definition of $\chi(s,t)$, it follows that

$$
|T_j x(s_1) - T_j x(s_2)| \to 0 \text{as } s_2 \to s_1.
$$

That is T_j's are equicontinuous and hence T_j's are completely continuous on E. Finally, from the first equation of (8), we have

$$
\begin{aligned}
|z_1(s)| = & |T_0 z_1(s) + T_2 z_2(s) + T_3 z_3(s) + \ldots + T_{n-1} z_{n-1}(s) + T_n z_n(s)| \\
\leq & |T_0 z_1(s)| + \sum_{j=2}^n |T_j z_j(s)| \\
\leq & |F(s,z_1(s))| + \sum_{j=2}^n \left| \int_0^1 \chi(s,t) g\big(t,z_j\big) dt + s^{\zeta-1} \int_0^1 \frac{(1-t)^{\xi-1}}{\Gamma(\xi)} h\big(t,z_j(t)\big) dt \right| \\
\leq & |F(s,z_1(s)) - F(s,0)| + |F(s,0)| + \sum_{j=2}^n \int_0^1 |\chi(s,t)||g\big(t,z_j\big)| dt \\
& + |s|^{\zeta-1} \sum_{j=2}^n \int_0^1 \frac{|1-t|^{\xi-1}}{\Gamma(\xi)} |h\big(t,z_j(t)\big)| dt \\
\leq & \frac{M|z_1|}{2+2|z_1|} + F^\star + \frac{(n-1)\Gamma(\zeta)\|g^\star\|_{L^1}}{\Gamma(2\zeta)} + \frac{(n-1)\|h^\star\|_{L^1}}{\Gamma(\xi+1)} \\
\leq & \frac{M}{2} + F^\star + \frac{(n-1)\Gamma(\zeta)\|g^\star\|_{L^1}}{\Gamma(2\zeta)} + \frac{(n-1)\|h^\star\|_{L^1}}{\Gamma(\xi+1)}.
\end{aligned}
$$

Taking supremum on both sides, we obtain

$$\|z_1\| \leq \frac{M}{2} + F^{\star} + \frac{(n-1)\Gamma(\zeta)\|g^{\star}\|_{L^1}}{\Gamma(2\zeta)} + \frac{(n-1)\|h^{\star}\|_{L^1}}{\Gamma(\xi+1)} \leq \Xi.$$

It follows that $z_1 \in E$. Similarly, we can prove for remaining equations of (8). Thus, all conditions of Theorem 3 are satisfied. Hence, by the Theorem 3, the system (1)–(3) has a solution on [0, 1]. □

4 Hyers-Ulam stability analysis

In this section, we derive necessary conditions for the stability analysis of Hyers-Ulam's type. For some positive $\varepsilon_j > 0$, $j = 1, 2, \ldots, n$, consider the system of inequalities given by

$$\begin{cases} \left|{}^{RL}D^{\zeta}_{0^+}\left[z_1(s) - F(s, z_1(s))\right] + g(s, z_2(s), z_3(s), \ldots, z_{n-1}(s), z_n(s))\right| \leq \varepsilon_1, \\ \left|{}^{RL}D^{\zeta}_{0^+}\left[z_2(s) - F(s, z_2(s))\right] + g(s, z_1(s), z_3(s), \ldots, z_{n-1}(s), z_n(s))\right| \leq \varepsilon_2, \\ \vdots \\ \left|{}^{RL}D^{\zeta}_{0^+}\left[z_{n-1}(s) - F(s, z_{n-1}(s))\right] + g(s, z_1(s), z_2(s), \ldots, z_{n-2}(s), z_n(s))\right| \leq \varepsilon_{n-1}, \\ \left|{}^{RL}D^{\zeta}_{0^+}\left[z_n(s) - F(s, z_n(s))\right] + g(s, z_1(s), z_2(s), \ldots, z_{n-2}(s), z_{n-1}(s))\right| \leq \varepsilon_n, \end{cases} \tag{9}$$

for $s \in (0, 1) := I$. Then the system of boundary value problems (1)-(3) is Hyers-Ulam stable if there exist constants $L_1 > 0, L_2 > 0$ such that for each solution $(z_1, z_2, \ldots, z_n) \in C^n(I, \mathbb{R})$ of the system of inequalities (9), there exists a unique solution $(y_1, y_2, \ldots, y_n) \in C^n(I, \mathbb{R})$ with

$$|(z_1, z_2, \ldots, z_n)(s) - (y_1, y_2, \ldots, y_n)(s)| \leq nL\left[1 - \frac{M}{2} - \frac{(n-1)\widehat{g}\Gamma(\zeta)}{\Gamma(2\zeta)} - \frac{(n-1)\widehat{h}}{\Gamma(\xi+1)}\right]^{-1}\varepsilon. \tag{10}$$

Remark 1 We say that $(z_1, z_2, \ldots, z_n) \in C^n(I, \mathbb{R})$ is a solution of the system of inequalities (9) if there exist functions $\varphi_j \in C^n(I, \mathbb{R})$ which depend upon z_j respectively such that

(i) $|\varphi_j| \leq \varepsilon_j, s \in I$, and
(ii) for $s \in I$,

$$\begin{cases} {}^{RL}D_{0^+}^{\zeta}\left[z_1(s) - F(s, z_1(s))\right] + g(s, z_2(s), z_3(s), \ldots, z_{n-1}(s), z_n(s)) = \varphi_1(s), \\ {}^{RL}D_{0^+}^{\zeta}\left[z_2(s) - F(s, z_2(s))\right] + g(s, z_1(s), z_3(s), \ldots, z_{n-1}(s), z_n(s)) = \varphi_2(s), \\ \vdots \\ {}^{RL}D_{0^+}^{\zeta}\left[z_{n-1}(s) - F(s, z_{n-1}(s))\right] + g(s, z_1(s), z_2(s), \ldots, z_{n-2}(s), z_n(s)) = \varphi_{n-1}(s), \\ {}^{RL}D_{0^+}^{\zeta}\left[z_n(s) - F(s, z_n(s))\right] + g(s, z_1(s), z_2(s), \ldots, z_{n-2}(s), z_{n-1}(s)) = \varphi_n(s), \end{cases} \tag{11}$$

Lemma 6 *Let* $(z_1, z_2, \ldots, z_n) \in C^n(I, \mathbb{R})$ *be the solution of the system of inequalities* (9)*. Then the following inequalities hold*:

$$\begin{cases} \left| z_1(s) - F(s, z_1(s)) - \int_0^1 \chi(s,t) g(t, z_2(t), z_3(t), z_4(t), \ldots, z_n(t)) dt \right. \\ \left. - s^{\zeta-1} \int_0^1 \frac{(1-t)^{\xi-1}}{\Gamma(\xi)} h(t, z_2(t), z_3(t), z_4(t), \ldots, z_n(t)) dt \right| \le L\varepsilon_1, \\ \left| z_2(s) - F(s, z_2(s)) - \int_0^1 \chi(s,t) g(t, z_1(t), z_3(t), z_4(t), \ldots, z_n(t)) dt \right. \\ \left. + s^{\zeta-1} \int_0^1 \frac{(1-t)^{\xi-1}}{\Gamma(\xi)} h(t, z_1(t), z_3(t), z_4(t), \ldots, z_n(t)) dt \right| \le L\varepsilon_2 \\ \vdots \\ \left| z_{n-1}(s) - F(s, z_{n-1}(s)) - \int_0^1 \chi(s,t) g(t, z_1(t), z_2(t), \ldots, z_{n-2}(t), z_n(t)) dt \right. \\ \left. - s^{\zeta-1} \int_0^1 \frac{(1-t)^{\xi-1}}{\Gamma(\xi)} h(t, z_1(t), z_2(t), z_3(t), \ldots, z_1(t), z_{n-2}(t), z_n(t)) dt \right| \le L\varepsilon_{n-1} \\ \left| z_n(s) - F(s, z_n(s)) - \int_0^1 \chi(s,t) g(t, z_1(t), z_2(t), z_3(t), \ldots, z_{n-2}(t), z_{n-1}(t)) dt \right. \\ \left. - s^{\zeta-1} \int_0^1 \frac{(1-t)^{\xi-1}}{\Gamma(\xi)} h(t, z_1(t), z_2(t), z_3(t), \ldots, z_{n-2}(t), z_{n-1}(t)) dt \right| \le L\varepsilon_n \end{cases}$$

Proof From the Remark 1 and Theorem 1, the solution of (11), (2) and (3) is given by

$$
\begin{cases}
z_1(s) = F(s, z_1(s)) + \displaystyle\int_0^1 \chi(s,t) g(t, z_2(t), z_3(t), z_4(t), \ldots, z_n(t)) dt \\
\quad - \displaystyle\int_0^1 \chi(s,t)\varphi_1(t)dt + s^{\zeta-1} \int_0^1 \frac{(1-t)^{\xi-1}}{\Gamma(\xi)} h(t, z_2(t), z_3(t), z_4(t), \ldots, z_n(t)) dt \\
z_2(s) = F(s, z_2(s)) + \displaystyle\int_0^1 \chi(s,t) g(t, z_1(t), z_3(t), z_4(t), \ldots, z_n(t)) dt \\
\quad - \displaystyle\int_0^1 \chi(s,t)\varphi_2(t)dt + s^{\zeta-1} \int_0^1 \frac{(1-t)^{\xi-1}}{\Gamma(\xi)} h(t, z_1(t), z_3(t), z_4(t), \ldots, z_n(t)) dt \\
\vdots \\
z_{n-1}(s) = F(s, z_{n-1}(s)) + \displaystyle\int_0^1 \chi(s,t) g(t, z_1(t), z_2(t), \ldots, z_{n-2}(t), z_n(t)) dt \\
\quad - \displaystyle\int_0^1 \chi(s,t)\varphi_{n-1}(t)dt + s^{\zeta-1} \\
\quad \displaystyle\int_0^1 \frac{(1-t)^{\xi-1}}{\Gamma(\xi)} h(t, z_1(t), z_2(t), z_3(t), \ldots, z_1(t), z_{n-2}(t), z_n(t)) dt \\
z_n(s) = F(s, z_n(s)) + \displaystyle\int_0^1 \chi(s,t) g(t, z_1(t), z_2(t), z_3(t), \ldots, z_{n-2}(t), z_{n-1}(t)) dt \\
\quad - \displaystyle\int_0^1 \chi(s,t)\varphi_n(t)dt + s^{\zeta-1} \\
\quad \displaystyle\int_0^1 \frac{(1-t)^{\xi-1}}{\Gamma(\xi)} h(t, z_1(t), z_2(t), z_3(t), \ldots, z_{n-2}(t), z_{n-1}(t)) dt
\end{cases}
\tag{12}
$$

From first equation of the system (12), we have

$$
\begin{aligned}
&\Big| z_1(s) - F(s, z_1(s)) - \int_0^1 \chi(s,t) g(t, z_2(t), z_3(t), z_4(t), \cdots, z_n(t)) dt \\
&- s^{\zeta-1} \int_0^1 \frac{(1-t)^{\xi-1}}{\Gamma(\xi)} h(t, z_2(t), z_3(t), z_4(t), \ldots, z_n(t)) dt \Big| \le \left| \int_0^1 \chi(s,t)\varphi_1(t)dt \right| \\
&\le \frac{\Gamma(\zeta)}{\Gamma(2\zeta)} \varepsilon_1 := L\varepsilon_1.
\end{aligned}
$$

Similarly we can prove other inequalities. □

Theorem 5 *Suppose* $(\mathcal{J}_1)$ *and for every* $(y_1, y_2, \ldots, y_{n-1}), (x_1, x_2, \ldots, x_{n-1}) \in C^{n-1}(I, \mathbb{R})$, *the following hold*:

$(\mathcal{J}_4)$ there exists $\widehat{\mathtt{g}} > 0$ such that

$$|\mathtt{g}(\mathtt{s}, \mathtt{y}_1(\mathtt{s}), \mathtt{y}_2(\mathtt{s}), \ldots, \mathtt{y}_{n-1}(\mathtt{s})) - \mathtt{g}(\mathtt{s}, \mathtt{x}_1(\mathtt{s}), \mathtt{x}_2(\mathtt{s}), \ldots, \mathtt{x}_{n-1}(\mathtt{s}))| \leq \widehat{\mathtt{g}} \sum_{\mathtt{j}=1}^{n-1} |\mathtt{y}_\mathtt{j} - \mathtt{x}_\mathtt{j}|.$$

$(\mathcal{J}_5)$ there exists $\widehat{\mathtt{h}} > 0$ such that

$$|\mathtt{h}(\mathtt{s}, \mathtt{y}_1(\mathtt{s}), \mathtt{y}_2(\mathtt{s}), \ldots, \mathtt{y}_{n-1}(\mathtt{s})) - \mathtt{h}(\mathtt{s}, \mathtt{x}_1(\mathtt{s}), \mathtt{x}_2(\mathtt{s}), \ldots, \mathtt{x}_{n-1}(\mathtt{s}))| \leq \widehat{\mathtt{h}} \sum_{\mathtt{j}=1}^{n-1} |\mathtt{y}_\mathtt{j} - \mathtt{x}_\mathtt{j}|.$$

Then the system of boundary value problems (1)–(3) is Hyers-Ulam stabile, if

$$n\mathtt{L}\left[1 - \frac{\mathtt{M}}{2} - \frac{(n-1)\widehat{\mathtt{g}}\Gamma(\zeta)}{\Gamma(2\zeta)} - \frac{(n-1)\widehat{\mathtt{h}}}{\Gamma(\xi+1)}\right]^{-1} < 1.$$

Proof Let $(\mathtt{z}_1, \mathtt{z}_1, \ldots, \mathtt{z}_n) \in \mathrm{C}^n(\mathtt{I}, \mathbb{R})$ be the solution to the system of inequalities (9) and let $(\mathtt{y}_1, \mathtt{y}_1, \ldots, \mathtt{y}_n) \in \mathrm{C}^n(\mathtt{I}, \mathbb{R})$ be the unique solution to the system of boundary value problems (1)–(3). Then by Lemma 6, we have

$$
\begin{aligned}
|z_1(s)-y_1(s)| \le & \Big| z_1(s)-F(s,y_1(s)) \\
& -\int_0^1 \chi(s,t)g(t,y_2(t),y_3(t),y_4(t),\ldots,y_n(t))dt \\
& -s^{\zeta-1}\int_0^1 \frac{(1-t)^{\xi-1}}{\Gamma(\xi)}h(t,y_2(t),y_3(t),y_4(t),\ldots,y_n(t))dt\Big| \\
\le & \Big| z_1(s)-F(s,z_1(s)) \\
& -\int_0^1 \chi(s,t)g(t,z_2(t),z_3(t),z_4(t),\ldots,z_n(t))dt \\
& -s^{\zeta-1}\int_0^1 \frac{(1-t)^{\xi-1}}{\Gamma(\xi)}h(t,z_2(t),z_3(t),z_4(t),\ldots,z_n(t))dt\Big| \\
& +|F(s,z_1(s))-F(s,y_1(s))| \\
& +\int_0^1 |\chi(s,t)|g(t,z_2(t),z_3(t),\ldots,z_n(t)) \\
& \quad -g(t,y_2(t),y_3(t),\ldots,y_n(t))|dt \\
& +|s|^{\zeta-1}\int_0^1 \frac{|1-t|^{\xi-1}}{\Gamma(\xi)}|h(t,z_2(t),z_3(t),\ldots,z_n(t)) \\
& \quad -h(t,y_2(t),y_3(t),\ldots,y_n(t))|dt \\
\le & L\varepsilon_1+\frac{M|z_1(s)-y_1(s)|}{2+2|z_1(s)-y_1(s)|}+\widehat{g}\int_0^1 |\chi(s,t)|\sum_{j=2}^{n}|z_j(t)-y_j(t)|dt \\
& +\widehat{h}\int_0^1 \frac{|1-t|^{\xi-1}}{\Gamma(\xi)}\sum_{j=2}^{n}|z_j(t)-y_j(t)|dt \\
\le & L\varepsilon_1+\frac{M|z_1(s)-y_1(s)|}{2+2|z_1(s)-y_1(s)|}+\widehat{g}\int_0^1 |\chi(t,t)|\sum_{j=2}^{n}\|z_j-y_j\|dt \\
& +\widehat{h}\int_0^1 \frac{|1-t|^{\xi-1}}{\Gamma(\xi)}\sum_{j=2}^{n}\|z_j-y_j\|dt \\
\le & L\varepsilon_1+\frac{M}{2}|z_1(s)-y_1(s)|+\frac{\widehat{g}\Gamma(\zeta)}{\Gamma(2\zeta)}\sum_{j=2}^{n}\|z_j-y_j\| \\
& +\frac{\widehat{h}}{\Gamma(\xi+1)}\sum_{j=2}^{n}\|z_j-y_j\|.
\end{aligned}
$$

Taking supremum on both sides over s, we obtain

$$\|z_1 - y_1\| \le L\varepsilon_1 + \frac{M}{2}\|z_1 - y_1\| + \frac{\widehat{g}\Gamma(\zeta)}{\Gamma(2\zeta)}\sum_{j=2}^{n}\|z_j - y_j\| + \frac{\widehat{h}}{\Gamma(\xi+1)}\sum_{j=2}^{n}\|z_j - y_j\|.$$

Similarly, we can have

$$\|z_j - y_j\| \le L\varepsilon_j + \frac{M}{2}\|z_j - y_j\| + \frac{\widehat{g}\Gamma(\zeta)}{\Gamma(2\zeta)} \sum_{i=1,i\neq j}^{n}\|z_i - y_i\| + \frac{\widehat{h}}{\Gamma(\xi+1)}\sum_{i=1,i\neq j}^{n}\|z_i - y_i\|,$$
$$j = 2, 3, \ldots, n.$$

Adding all the above inequalities from $j = 1$ to n, we get

$$\sum_{j=1}^{n}\|z_j - y_j\| \le L\sum_{j=1}^{n}\varepsilon_j + \frac{M}{2}\sum_{j=1}^{n}\|z_j - y_j\| + \frac{(n-1)\widehat{g}\Gamma(\zeta)}{\Gamma(2\zeta)}\sum_{j=1}^{n}\|z_j - y_j\| + \frac{(n-1)\widehat{h}}{\Gamma(\xi+1)}\sum_{j=1}^{n}\|z_j - y_j\|.$$

That is

$$\sum_{j=1}^{n}\|z_j - y_j\| \le L\left[1 - \frac{M}{2} - \frac{(n-1)\widehat{g}\Gamma(\zeta)}{\Gamma(2\zeta)} - \frac{(n-1)\widehat{h}}{\Gamma(\xi+1)}\right]^{-1}\sum_{j=1}^{n}\varepsilon_j$$

Let $\varepsilon = \max\{\varepsilon_j : j = 1, 2, \ldots, n\}$. Then, we have

$$\|(z_1, z_2, \ldots, z_n) - (y_1, y_2, \ldots, y_n)\| \le \sum_{j=1}^{n}\|z_j - y_j\| \le nL\left[1 - \frac{M}{2} - \frac{(n-1)\widehat{g}\Gamma(\zeta)}{\Gamma(2\zeta)} - \frac{(n-1)\widehat{h}}{\Gamma(\xi+1)}\right]^{-1}\varepsilon.$$

□

Example 1

$$\begin{cases} {}^{RL}D_{0^+}^{3/2}\left[z_1(s) - \dfrac{se^{2s}z_1(s)}{4(2+2z_1(s))}\right] + \dfrac{(1+s)z_2(s)}{1+z_2(s)} + \dfrac{(1+s)z_3(s)}{1+z_3(s)} = 0, \\ {}^{RL}D_{0^+}^{3/2}\left[z_2(s) - \dfrac{se^{2s}z_2(s)}{4(2+2z_2(s))}\right] + \dfrac{(1+s)z_1(s)}{1+z_1(s)} + \dfrac{(1+s)z_3(s)}{1+z_3(s)} = 0, \\ {}^{RL}D_{0^+}^{3/2}\left[z_3(s) - \dfrac{se^{2s}z_3(s)}{4(2+2z_3(s))}\right] + \dfrac{(1+s)z_1(s)}{1+z_1(s)} + \dfrac{(1+s)z_2(s)}{1+z_2(s)} = 0, \end{cases} \tag{13}$$

for $0 < s < 1$, satisfying

$$z_1(0) = z_2(0) = z_3(0) = 0 \tag{14}$$

and

$$\begin{cases} z_1(1) = \displaystyle\int_0^1 \frac{(1-t)^{-1/2}}{\Gamma(1/2)} \left[\frac{2tz_2(t)}{3+3z_2(t)} + \frac{2tz_3(t)}{3+3z_3(t)}\right] dt, \\ z_2(1) = \displaystyle\int_0^1 \frac{(1-t)^{-1/2}}{\Gamma(1/2)} \left[\frac{2tz_1(t)}{3+3z_1(t)} + \frac{2tz_3(t)}{3+3z_3(t)}\right] dt, \\ z_3(1) = \displaystyle\int_0^1 \frac{(1-t)^{-1/2}}{\Gamma(1/2)} \left[\frac{2tz_1(t)}{3+3z_1(t)} + \frac{2tz_2(t)}{3+3z_2(t)}\right] dt. \end{cases} \tag{15}$$

So, we have $n = 3, \zeta = \frac{3}{2}, \xi = \frac{1}{2}$, $F(s, x(s)) = \frac{se^{2s}x(s))}{4(2+2x(s))}$, $g(s, x(s)) = \frac{(1+s)x(s)}{1+x(s)}$ and $h(s, x(s)) = \frac{2sx(s)}{3+3x(s)}$. Since $|z_1| \leq |z_1 - z_2| + |z_2|$, it follows that

$$\frac{|z_1|}{1+|z_1|} \leq \frac{|z_1 - z_2| + |z_2|}{1 + |z_1 - z_2| + |z_2|} \text{ and } \frac{1}{1+|z_2 - z_1| + |z_2|} \leq \frac{1}{1+|z_2|}.$$

Thus,

$$\begin{aligned} |F(s, z_1(s)) - F(s, z_2(s))| &= \left|\frac{se^{2s}z_1(s)}{4(2+2z_1(s))} - \frac{se^{2s}z_2(s)}{4(2+2z_2(s))}\right| \\ &\leq \frac{e^2}{8}\left|\frac{z_1(s)}{1+z_1(s)} - \frac{z_2(s)}{1+z_2(s)}\right| \\ &\leq \frac{e^2}{8}\left[\frac{|z_1(s) - z_2(s)| + |z_2(s)|}{1 + |z_1(s) - z_2(s)| + |z_2(s)|}\right. \\ &\quad \left.; -\frac{z_2(s)}{1 + |z_1(s) - z_2(s)| + |z_2(s)|}\right] \\ &\leq \frac{e^2}{8}\left[\frac{|z_1(s) - z_2(s)|}{1 + |z_1(s) - z_2(s)| + |z_2(s)|}\right] \\ &\leq \frac{e^2}{8}\left[\frac{|z_1(s) - z_2(s)|}{1 + |z_1(s) - z_2(s)|}\right], \end{aligned} \tag{16}$$

$\delta = \frac{M}{2} = \frac{e^2}{8} < 1$ and $F^\star = F(0, z_j(0)) = 0$, $j = 1, 2, 3$. Also, for $j = 1, 2, 3$, we have

$$g(s, z_j(s)) = \frac{(1+s)z_j(s)}{1+z_j(s)} \leq 1 + s = g^\star(s),$$

it follows that $\|g^\star(s)\|_{L^1} = \frac{3}{2}$ and

$$\mathtt{h}(\mathtt{s},\mathtt{z}_{\mathtt{j}}(\mathtt{s}))=\frac{2\mathtt{s}\mathtt{z}_{\mathtt{j}}(\mathtt{s})}{3+3\mathtt{z}_{\mathtt{j}}(\mathtt{s})}\leq\frac{2\mathtt{s}}{3}=\mathtt{h}^{\bigstar}(\mathtt{s}),$$

it follows that $\|\mathtt{h}^{\bigstar}(\mathtt{s})\|_{L^1}=\frac{1}{3}$. Finally, let $\Xi=3$. Then

$$\frac{\mathtt{M}}{2}+\mathtt{F}^{\bigstar}+\frac{(n-1)\Gamma(\zeta)\|\mathtt{g}^{\bigstar}\|_{L^1}}{\Gamma(2\zeta)}+\frac{(n-1)\|\mathtt{h}^{\bigstar}\|_{L^1}}{\Gamma(\xi+1)}=2.421378394\leq\Xi.$$

Therefore, all the conditions of Theorem 4 are satisfied, so there exists a solution for the system (13)–(15).

Example 2

$$\begin{cases}{}^{\mathtt{RL}}\mathtt{D}_{0^+}^{5/3}\left[\mathtt{z}_1(\mathtt{s})-\dfrac{\cos(\mathtt{s})\mathtt{z}_1(\mathtt{s})}{40+40\mathtt{z}_1(\mathtt{s})}\right]+e^{-4s}\dfrac{\sin(\mathtt{z}_2(\mathtt{s}))}{5+5\mathtt{s}}=0,\\ {}^{\mathtt{RL}}\mathtt{D}_{0^+}^{5/3}\left[\mathtt{z}_2(\mathtt{s})-\dfrac{\cos(\mathtt{s})\mathtt{z}_2(\mathtt{s})}{40+40\mathtt{z}_2(\mathtt{s})}\right]+e^{-4s}\dfrac{\sin(\mathtt{z}_1(\mathtt{s})|)}{5+5\mathtt{s}}=0,\end{cases}\tag{17}$$

for $0<\mathtt{s}<1$, satisfying

$$\mathtt{z}_1(0)=\mathtt{z}_2(0)=0\tag{18}$$

and

$$\begin{cases}\mathtt{z}_1(1)=\displaystyle\int_0^1\frac{(1-\mathtt{t})^{-3/4}}{\Gamma(1/4)}\frac{e^{-2\mathtt{t}}\sin(\mathtt{z}_2(\mathtt{t}))}{2}\mathtt{dt},\\ \mathtt{z}_2(1)=\displaystyle\int_0^1\frac{(1-\mathtt{t})^{-3/4}}{\Gamma(1/4)}\frac{e^{-2\mathtt{t}}\sin(\mathtt{z}_1(\mathtt{t}))}{2}\mathtt{dt}.\end{cases}\tag{19}$$

So, we have $n=2,\zeta=\frac{5}{3},\xi=\frac{1}{4}$, $\mathtt{F}(\mathtt{s},\mathtt{x}(\mathtt{s}))=\frac{\cos(\mathtt{s})\mathtt{x}(\mathtt{s})}{40+40\mathtt{x}(\mathtt{s})}$, $\mathtt{g}(\mathtt{s},\mathtt{x}(\mathtt{s}))=e^{-4s}\frac{\sin(\mathtt{x}(\mathtt{s})|)}{5+5\mathtt{s}}$ and $\mathtt{h}(\mathtt{s},\mathtt{x}(\mathtt{s}))=\frac{1}{2}e^{-2\mathtt{s}}\sin(\mathtt{x}(\mathtt{s}))$. Then,

$$\begin{aligned}|\mathtt{F}(\mathtt{s},\mathtt{y}(\mathtt{s}))-\mathtt{F}(\mathtt{s},\mathtt{x}(\mathtt{s}))|&\leq\frac{|\mathtt{y}(\mathtt{s})-\mathtt{x}(\mathtt{s})|}{40+40|\mathtt{y}(\mathtt{s})-\mathtt{x}(\mathtt{s})|},(\text{from}(16)),\\ |\mathtt{g}(\mathtt{s},\mathtt{y}(\mathtt{s}))-\mathtt{g}(\mathtt{s},\mathtt{x}(\mathtt{s}))|&\leq|e^{-4\mathtt{s}}|\frac{|\sin(\mathtt{y}(\mathtt{s}))-\sin(\mathtt{x}(\mathtt{s}))|}{|5+5\mathtt{s}|}\\ &\leq\frac{1}{5}|\mathtt{y}(\mathtt{s})-\mathtt{x}(\mathtt{s})|,\end{aligned}$$

and

$$|\mathtt{h}(\mathtt{s},\mathtt{y}(\mathtt{s}))-\mathtt{g}(\mathtt{s},\mathtt{x}(\mathtt{s}))|\leq\frac{1}{2}|e^{-2\mathtt{s}}||\sin(\mathtt{y}(\mathtt{s}))-\sin(\mathtt{x}(\mathtt{s}))|$$
$$\leq\frac{1}{2}|\mathtt{y}(\mathtt{s})-\mathtt{x}(\mathtt{s})|,$$

it follows $\mathtt{M}=\frac{1}{20},\widehat{\mathtt{g}}=\frac{1}{5},\widehat{\mathtt{h}}=\frac{1}{2}$ and $\mathtt{L}=\Gamma(\zeta)/\Gamma(2\zeta)=0.3249437711$. Further,

$$n\mathtt{L}\left[1-\frac{\mathtt{M}}{2}-\frac{(n-1)\widehat{\mathtt{g}}\Gamma(\zeta)}{\Gamma(2\zeta)}-\frac{(n-1)\widehat{\mathtt{h}}}{\Gamma(\xi+1)}\right]^{-1}=0.8417104886<1,$$

so in view of Theorem 5, the condition of Hyers-Ulam stabilities are also satisfied. Therefore, the solution of system (17)–(19) is Hyers–Ulam stable.

5 Conclusion

In the present paper, we studied the concept of *n*-fixed point for nonlinear mappings in a Banach space and establish the existence theorem for contractive type mappings, which generalizes well-known fixed point theorem of Krasnoselskii, due to Burton [4] to multivariate fixed point theorems of *n*-variables. By applying our findings, we studied the existence of solutions to the system of nonlinear two-point fractional order boundary value problems satisfying Riemann-Liouville integral boundary conditions. Further, we also studied Hyers-Ulam stability of the system.

Acknowledgements The authors would like to thank editor and anonymous referees for their valuable suggesions and comments for the improvement of the paper. Third author D. Leela is thankful to DST-INSPIRE, Government of India, New Delhi for awarding SRF No.2017/IF170318.

Author contributions The study was carried out in collaboration of all authors. All authors read and approved the final manuscript.**Data availability statement** Data sharing not applicable to this paper as no data sets were generated or analyzed during the current study.

Declarations

Conflict of interest It is declared that authors has no competing interests.

Ethical approval This article does not contain any studies with human participants or animals performed by any of the authors.

References

1. Afshari, H., F. Jarad, and T. Abdeljawad. 2020. On a new fixed point theorem with an application on a coupled system of fractional differential equations. *Advances in Difference Equations* 2020: 461.
2. Aydi, H., E. Karapinar, and W. Shatanawi. 2011. Coupled fixed point results for (ψ,ϕ)-weakly contractive condition in ordered partial metric spaces. *Computers and Mathematics with Applications* 62: 4449–4460.
3. Berinde, V., and M. Borcut. 2011. Tripled fixed point theorems for contractive type mappings in partially ordered metric spaces. *Nonlinear Analysis: Theory, Methods and Applications* 74 (15): 4889–4897.
4. Burton, T.A. 1998. A fixed point theorem of Krasnoselskii. *Applied Mathematics Letters* 11: 85–88.

5. Cao, K., Y.Q. Chen, and D. Stuart. 2016. A fractional micro-macro model for crowds of pedestrians based on fractional mean field games. *IEEE/CAA Journal of Automatica sinica* 3 (3): 261–270.
6. Cartea, A., and D. del Castillo-Negrete. 2007. Fractional diffusion models of option prices in markets with jumps. *Physica A: Statistical Mechanics and its Applications* 374 (2): 749–763.
7. Cui, Y. 2016. Uniqueness of solution for boundary value problems for fractional differential equations. *Applied Mathematics Letters* 51: 48–54.
8. Dad, E.H.A., M. Benyoub, and M. Ziane. 2021. Existence results for Riemann-Liouville fractional evolution inclusions in Banach spaces. *Afrika Matematika* 32: 317–331. https://doi.org/10.1007/s13370-020-00828-8.
9. Debanath, L. 2003. Recent applications of fractional calculus to science and engineering. *International Journal of Mathematics and Mathematical Sciences* 2003:753601. https://doi.org/10.1155/S0161171203301486
10. Guo, D., and V. Lakshmikantham. 1988. *Nonlinear problems in abstract cones*. San Diego: Academic Press.
11. Hammad, H.A., and M.D. La Sen. 2020. Tripled fixed point techniques for solving system of tripled-fractional differential equations. *AIMS Mathematics* 6 (3): 2330–2343.
12. Hanyga, A. 2001. Wave propagation in media with singular memory. *Mathematical and Computer Modelling* 34 (12–13): 1399–1421.
13. Hassen, S., Aydi, et al. 2012. Tripled fixed point results in generalized metric spaces. *Journal of Applied Mathematics* 2012:314279. https://doi.org/10.1155/2012/314279
14. Khuddush, M., K.R. Prasad, and D. Leela. 2021. Existence of solutions for an infinite system of tempered fractional order boundary value problems in the spaces of tempered sequences. *Turkish Journal of Mathematics*. https://doi.org/10.3906/mat-2106-110.
15. Kilbas, A.A., H.M. Srivastava, and J.J. Trujillo. 2006. *Theory and applications of fractional differential equations, north-holland mathematics studies, 204*. North Holland: Elsevier.
16. Matar, M.M. 2019. Qualitative properties of solution for hybrid nonlinear fractional differential equations. *Afrika Matematika* 30: 1169–1179. https://doi.org/10.1007/s13370-019-00710-2.
17. Prasad, K.R., M. Khuddush, and D. Leela. 2020. Existence of positive solutions for half-linear fractional order BVPs by application of mixed monotone operators. *Creative Mathematics and Informatics* 29: 65–80.
18. Prasad, K.R., M. Khuddush, and D. Leela. 2021. Existence of solutions for n-dimensional fractional order hybrid BVPs with integral boundary conditions by an application of n-fixed point theorem. *The Journal of Analysis*. https://doi.org/10.1007/s41478-020-00291-5.
19. Prasad, K.R., M. Khuddush, and D. Leela. 2021. Existence, uniqueness and Hyers-Ulam stability of a fractional order iterative two-point boundary value Problems. *Afrika Matematika*. https://doi.org/10.1007/s13370-021-00895-5.
20. Prasad, K.R., D. Leela, and M. Khuddush. 2021. Existence and uniqueness of positive solutions for system of (p, q, r)-Laplacian fractional order boundary value problems. *Advances in the Theory of Nonlinear Analysis and its Applications* 5 (1): 138–157. https://doi.org/10.31197/atnaa.703304.
21. Prasad, K.R., M. Khuddush, and D. Leela. 2021. Existence of solutions for fractional order BVPs by mixed monotone ternary operator with perturbation on Banach spaces. *Journal of Advanced Mathematical Studies* 14 (1): 109–125.
22. Srivastava, H.M., K.M. Saad, and M.M. Khader. 2020. An efficient spectral collocation method for the dynamic simulation of the fractional epidemiological model of the Ebola virus. *Chaos, Solitons and Fractals* 140: 1–7.
23. Su, Y., A. Petrusel, and J. Yao. 2016. Multivariate fixed point theorems for contractions and non expansive mappings with applications. *Fixed Point Theory and Applications* 9: 2016.
24. Tang, Y., J. Guan, Y. Xu, and Y. Su. 2017. A kind of system of multivariate variational inequalities and the existence theorem of solutions. *Journal of Inequalities and Applications* 208: 2017.
25. Tarasov, V.E., and V.V. Tarasova. 2017. Time dependent fractional dynamics with memory in quantum and economic physics. *Annals of Physics* 383: 579–599.
26. Tu, Q., et al. 2016. Some new coupled fixed point theorems in partially ordered complete probabilistic metric spaces. *Journal of Nonlinear Sciences and Applications* 9: 1116–1128.
27. Xu, X., et al. 2017. Multivariate contraction mapping principlewith the error estimate formulas in locally convex topological vector spaces and application. *Journal of Nonlinear Sciences and Applications* 10: 1064–1074.
28. Zhang, S.Q. 2010. Existence results of positive solutions to fractional differential equation with integral boundary conditions. *Mathematica Bohemica* 135 (2): 299–317.

29. Zhang, J., R.P. Agarwal, and N. Jiang. 2018. *N*-fixed point theorems and *N*-best proximity point theorems for generalized contraction in partially ordered metric spaces. *Journal of Fixed Point Theory and Applications* 20 (1): 2018.
30. Zheng, D., Z. Cai, and P. Wang. 2017. New fixed point theorems for θ-φ contraction in complete metric spaces. *Journal of Nonlinear Sciences and Applications* 10 (5): 2670.
31. Zou, Y., and G. He. 2017. On the uniqueness of solutions for a class of fractional differential equations. *Applied Mathematics Letter* 74: 68–73.

Publisher's Note Springer Nature remains neutral with regard to jurisdictional claims in published maps and institutional affiliations.

Math. Appl. **11** (2022), 57–74
DOI: 10.13164/ma.2022.06

ITERATIVE SYSTEM OF NABLA FRACTIONAL DIFFERENCE EQUATIONS WITH TWO-POINT BOUNDARY CONDITIONS

MAHAMMAD KHUDDUSH AND K. RAJENDRA PRASAD

Abstract. In this paper, we consider the nabla fractional order boundary value problem

$$\begin{aligned} \nabla_{n_0}^{ß-1}[\nabla z_j(t)] + \varphi(t) g_j(z_{j+1}(t)) &= 0, \quad t \in \mathbb{N}_{n_0+2}^{n},\ 1 < ß < 2, \\ a z_j(n_0+1) - b\nabla z_j(n_0+1) &= 0, \\ c z_j(n) + d\nabla z_j(n) &= 0, \end{aligned}$$

where $j = 1, 2, \ldots, N$, $z_{N+1} = z_1$, $N \in \mathbb{N}$, $n_0, n \in \mathbb{R}$ with $n - n_0 \in \mathbb{N}$ and derive sufficient conditions for the existence of positive solutions by an application of Krasnoselskii's fixed point theorem on a Banach space. Later, we derive sufficient conditions for the existence of a unique solution by applying Rus's contraction mapping theorem in a metric space, where two metrics are employed.

1. Introduction

Fractional calculus is a generalization of classical integer order calculus and has been studied for more than three decades. Unlike integer order derivatives, the fractional derivative is a non local operator, which implies that the future states depend on the current state as well as the history of all the previous states. From this point of view, fractional differential equations provide a powerful tool for mathematical modeling of complex phenomena in science and engineering practices, see [5, 10, 12, 18, 30, 39] and references therein. In the qualitative theory of classical and fractional order differential equations, various theorems have been extensively deployed by researchers in establishing the existence, uniqueness and multiple solutions of boundary value problems, see [29,32–34,41] and the references therein.

Fractional difference equations have been of great interest recently. Díaz and Osler [13] introduced a fractional difference defined as an infinite series, a generalization of the binomial formula for the N^{th} order difference $\Delta^N f$. Gray and Zhang [22] developed a special case for one composition rule and Leibniz formula. They worked exclusively with the nabla operator. For the recent works in discrete fractional calculus, see [2–4, 19–21] and references therein.

On the other hand, differential equations with state-dependent delays have attracted a great deal of interest to the researchers since they widely arise from application models, such as population models [6], mechanical models [26], the

MSC (2020): primary 34A08; secondary 39A12, 34B15.
Keywords: nabla fractional derivative, iterative sysytem, boundary value problem, cone, fixed point theorem, Rus's theorem.

dynamics of economical systems [7], position control [9], two-body problem of classical electrodynamics [14], etc. As a special type of state-dependent delay-differential equations, iterative differential equations have distinctive characteristics and have been investigated in recent years, e.g., equivariance [38], analyticity [40], convexity [36], monotonicity [15], smoothness [11]. In [17], Fečkan, Wang and Zhao established the maximal and minimal nondecreasing bounded solutions of the following iterative functional differential equations

$$z'(t) = g(t, z^{[1]}(t), z^{[2]}(t), \dots, z^{[n]}(t)),$$

where $z^{[j]}(t) := z(z^{[j-1]})(t)$ indicates the j-th iterate of z, where $j = 1, 2, \dots, n$, by the method of lower and upper solutions. Recently, Prasad, Khuddush and Leela [33] derived sufficient conditions for the existence and uniqueness of solutions by applying Schauder fixed point theorem and contraction mapping theorem in a Banach space to the following Caputo type fractional order boundary value problem

$$\begin{aligned} D^{\alpha} z(t) &= g(t, z(t), z^{[2]}(t)), \quad t \in [0, 1], \\ z(0) &= A,\ z(1) = B, \end{aligned}$$

where $1 < \alpha \le 2$ and $0 \le A \le B \le 1$. In [27], Jonnalagadda derived sufficient conditions for the existence of positive solutions for the following Riemann–Liouville nabla fractional order two-point boundary value problem,

$$\begin{aligned} \nabla^{\alpha}_{\rho(a)} z(t) + g(t, z(t)) &= 0, \quad t \in \mathbb{N}^{b}_{a+2},\ 1 < \alpha < 2, \\ z(a) &= 0,\ z(b) = 0 \end{aligned}$$

where $\mathbb{N}^{n}_{n_0} := \{n_0, n_0+1, n_0+2, \dots, n\}$ by applying Krasnoselskii's fixed point theorem. Recently, Eralp and Topal [16] studied the following Caputo nabla fractional order two-point boundary value problem,

$$\begin{aligned} \nabla^{\mu}_{a^*} z(t) + g(t, z(t - (N-1))) &= 0, \quad t \in \mathbb{N}^{b-1}_{a+1},\ 1 < \mu < 2, \\ \alpha z(a - j) - \beta \nabla z(a - (j-1)) &= 0, \quad j = 1, 2, \dots, N-1, \\ \gamma z(b) + \delta \nabla z(b) &= 0, \end{aligned}$$

and obtained the existence of positive solutions by using the Schauder and Banach fixed point theorems. Inspired by the above literature, in this paper, we derive sufficient conditions for the existence of positive solutions for the following iterative system of Riemann–Liouville nabla fractional order difference equations

$$\begin{aligned} \nabla^{ß-1}_{n_0} [\nabla z_j(t)] + \varphi(t) g_j(z_{j+1}(t)) &= 0, \quad t \in \mathbb{N}^{n}_{n_0+2},\ 1 < ß < 2,\ j = 1, 2, \dots, N, \\ z_{N+1}(t) &= z_1(t), \quad t \in \mathbb{N}^{n}_{n_0+2}, \end{aligned} \tag{1.1}$$

satisfying two-point general boundary conditions

$$\begin{aligned} a z_j(n_0 + 1) - b \nabla z_j(n_0 + 1) &= 0, \quad j = 1, 2, \dots, N, \\ c z_j(n) + d \nabla z_j(n) &= 0, \quad j = 1, 2, \dots, N, \end{aligned} \tag{1.2}$$

where $N \in \mathbb{N}$, $n_0, n \in \mathbb{R}$ with $n - n_0 \in \mathbb{N}$, $\varphi(t) \in \ell^p(\mathbb{N}^{n}_{n_0+2})$, $g_j : [0, +\infty) \to [0, +\infty)$ is continuous for each $1 \le j \le n$, by an application of Krasnoselskii's fixed point theorem on a Banach space.

The rest of the paper is organized in the following fashion. In Section 2, we estimate bounds for the kernel and provide some lemmas which are needed in establishing our main results. In Section 3, we establish criteria for the existence of positive solutions for the boundary value problem (1.1)–(1.2) by applying Hölder's inequality and Krasnoselskii's cone fixed point theorem in a Banach space. Also, we derive sufficient conditions for the existence of a unique positive solution to the problem by an application of a fixed point theorem in a complete metric space. Finally, we provide an example to illustrate the main results of the paper.

2. Preliminaries, kernel and bounds

In this section, we present some definitions, lemmas and kernel for the homogeneous boundary value problem corresponding to the problem (1.1)–(1.2), which is useful in the later sections. Throughout the paper, we shall use the following notations. Denote the set of all positive integers, nonpositive integers, real numbers and positive real numbers by $\mathbb{N}$, $\mathbb{N}^-$, $\mathbb{R}$ and $\mathbb{R}^+$, respectively. The generalized rising function is defined by

$$t^{\overline{ß}} = \frac{\Gamma(t+ß)}{\Gamma(t)}$$

for $t \in \mathbb{R}\backslash\mathbb{N}^-$, $ß \in \mathbb{R}$ and $t+ß \in \mathbb{R}\backslash\mathbb{N}^-$. Also, if $t \in \mathbb{N}^-$ and $t+ß \in \mathbb{R}\backslash\mathbb{N}^-$, then we use the convention that $t^{\overline{ß}} = 0$.

For $ß \in \mathbb{R}\backslash\mathbb{N}^-$, define the $ß^{th}$ order nabla fractional Taylor monomial by

$$\mathcal{H}_ß(t, n_0) = \frac{(t-n_0)^{\overline{ß}}}{\Gamma(ß+1)},$$

provided the right hand side exists. Also, $\mathcal{H}_ß(t, n_0) = 0$ for $t \in \mathbb{N}_{n_0}$ and $ß \in \mathbb{N}^-\backslash\{0\}$. Also, we denote

$$\begin{aligned}
\mathbb{N}_{n_0} &= \{n_0, n_0+1, n_0+2, \dots\},\\
\lambda &= (b-a)c + ac\mathcal{H}_{ß-1}(n, n_0) + ad\mathcal{H}_{ß-2}(n, n_0) \neq 0,\\
\widehat{\aleph} &= \frac{1}{\lambda}\Big[ad\mathcal{H}_{ß-1}(n_0+1, n_0)\mathcal{H}_{ß-2}(n, n_0) + (b-a)d\mathcal{H}_{ß-2}(n, n_0)\Big],\\
\aleph^* &= \frac{1}{\lambda}\Big[ac(\mathcal{H}_{ß-1}(n, n_0))^2 + ad\mathcal{H}_{ß-1}(n, n_0) + (b-a)c\mathcal{H}_{ß-1}(n, n_0) + (b-a)d\Big],\\
\varkappa &= \frac{1}{\lambda}\Big[ac\mathcal{H}_{ß-1}(n, n_0)\mathcal{H}_ß(n, n_0) + ad\left[\mathcal{H}_{ß-1}(n, n_0)\right]^2\\
&\qquad + (b-a)c\mathcal{H}_ß(n, n_0) + (b-a)d\mathcal{H}_{ß-1}(n, n_0)\Big].
\end{aligned}$$

Definition 2.1. [21] The operator $\varrho : \mathbb{N}_{n_0+1} \to \mathbb{N}_{n_0}$ for the nabla transformation defined by $\varrho(t) = t-1$ is called the *backward jump operator*.

Definition 2.2. [21] Let $z : N_{n_0+1} \to \mathbb{R}$ and $N \in \mathbb{N}$. The N^{th} order nabla sum of z based at n_0 is given by

$$\nabla_{n_0}^{-N} z(t) = \sum_{\tau=n_0+1}^{t} \mathcal{H}_{N-1}(t, \varrho(\tau))z(\tau),\ t \in \mathbb{N}_{n_0},$$

where, by convention, $\nabla_{n_0}^{-N} z(n_0) = 0$.

Definition 2.3. [21] Let $z : N_{n_0+1} \to \mathbb{R}$ and $ß \in \mathbb{R}^+$. The $ß^{th}$ order nabla sum of z based at n_0 is given by

$$\nabla_{n_0}^{-ß} z(t) = \sum_{\tau=n_0+1}^{t} \mathcal{H}_{ß-1}(t, \varrho(\tau)) z(\tau), \ t \in \mathbb{N}_{n_0},$$

where, by convention, $\nabla_{n_0}^{-ß} z(n_0) = 0$.

Definition 2.4. [21] Let $z : N_{n_0+1} \to \mathbb{R}$, $ß \in \mathbb{R}^+$ and choose $N \in \mathbb{N}_1$ such that $ß \in (N-1, N]$. The $ß^{th}$ order Riemann–Liouville nabla fractional difference of z is given by

$$\nabla_{n_0}^{ß} z(t) = \nabla^N \nabla_{n_0}^{-(N-ß)} z(t), \ t \in N_{n_0+N}.$$

Lemma 2.5. [25] *Let $ß > -1$ and $\tau \in \mathbb{N}_{n_0}$. Then, we have the following properties:*

(i) *If $t \in \mathbb{N}_{\varrho(\tau)}$, then $\mathcal{H}_{ß-1}(t, \varrho(\tau)) \geq 0$, and if $t \in \mathbb{N}_\tau$, then $\mathbb{N}_{\varrho(\tau)} > 0$.*
(ii) *If $t \in \mathbb{N}_{\varrho(\tau)}$ and $ß > 0$, then $\mathcal{H}_ß(t, \varrho(\tau))$ is a decreasing function of τ.*
(iii) *If $t \in \mathbb{N}_\tau$ and $-1 < ß < 0$, then $\mathcal{H}_ß(t, \varrho(\tau))$ is an increasing function of τ.*
(iv) *If $t \in \mathbb{N}_{\varrho(\tau)}$ and $ß \geq 0$, then $\mathcal{H}_ß(t, \varrho(\tau))$ is a nondecreasing function of t.*
(v) *If $t \in \mathbb{N}_\tau$ and $ß > 0$, then $\mathcal{H}_ß(t, \varrho(\tau))$ is an increasing function of t.*
(vi) *If $t \in \mathbb{N}_{\tau+1}$ and $-1 < ß < 0$, then $\mathcal{H}_ß(t, \varrho(\tau))$ is a decreasing function of τ.*

Definition 2.6. [24] Let $0 < p < \infty$ be a finite real number. A sequence of scalars $z = (z_k)_{k\in\mathbb{N}}$ is p-summable if $\sum_{k=1}^{\infty} |z_k|^p < \infty$. A sequence of scalars $z = (z_k)_{k\in\mathbb{N}}$ is bounded if $\sup_{k\in\mathbb{N}} |z_k| < \infty$.

Definition 2.7. [24] If $0 < p < \infty$, then the space ℓ^p consists of all p-summable sequences of scalars. That is, a sequence $z = (z_k)_{k\in\mathbb{N}}$ belongs to ℓ^p if and only if

$$\|z\|_p = \|(z_k)_{k\in\mathbb{N}}\|_p = \left[\sum_{k=1}^{\infty} |z_k|^p\right]^{1/p} < \infty.$$

For $p = \infty$, the space ℓ^p consists of all bounded sequences of scalars. That is, a sequence $z = (z_k)_{k\in\mathbb{N}}$ belongs to ℓ^p if and only if

$$\|z\|_p = \|(z_k)_{k\in\mathbb{N}}\|_p = \sup_{k\in\mathbb{N}} |z_k| < \infty.$$

Remark 2.8. [24] By making appropriate changes in the preceeding definitions, we can consider spaces of sequences that are indexed by sets other than the natural numbers N. For example, if I is a countable index set, then we say that a sequence $z = (z_k)_{k\in I}$ is p-summable if and only if $\sum_{k=1}^{\infty} |z_k|^p < \infty$. For finite p, we let $\ell^p(I)$ be the space of all p-summable sequences indexed by I, and we define $\ell^\infty(I)$ to be the space of all bounded sequences indexed by I.

Lemma 2.9. [8] *Let $b \geq a$ and $f : N_{n_0+1} \to \mathbb{R}$. Then, the boundary value problem*

$$\begin{aligned} \nabla_{n_0}^{ß-1} [\nabla z_1(t)] + f(t) = 0, \quad t \in \mathbb{N}_{n_0+2}^n, \ 1 < ß < 2, \\ a z_1(n_0+1) - b \nabla z_1(n_0+1) = 0, \\ c z_1(n) + d \nabla z_1(n) = 0 \end{aligned}$$

has a unique solution

$$z_1(t) = \sum_{\tau=n_0+1}^{n} \aleph(t,\tau) f(\tau),$$

where

$$\aleph(t,\tau) = \begin{cases} \aleph_1(t,\tau), & t < \varrho(\tau), \\ \aleph_2(t,\tau), & \tau < t, \end{cases}$$

in which

$$\aleph_1(t,\tau) = \frac{1}{\lambda}\Big[ac\mathcal{H}_{\mathfrak{B}-1}(t,n_0)\mathcal{H}_{\mathfrak{B}-1}(n,\varrho(\tau)) + ad\mathcal{H}_{\mathfrak{B}-1}(t,n_0)\mathcal{H}_{\mathfrak{B}-2}(n,\varrho(\tau)) + (b-a)c\mathcal{H}_{\mathfrak{B}-1}(n,\varrho(\tau)) + (b-a)d\mathcal{H}_{\mathfrak{B}-2}(n,\varrho(\tau))\Big]$$

and

$$\aleph_2(t,\tau) = \aleph_1(t,\tau) - \mathcal{H}_{\mathfrak{B}-1}(t,\varrho(\tau)).$$

Lemma 2.10. [28] *Let $b \geq a$. Then*

(i) $\aleph_1(t,\tau)$ *is an increasing function of t for all $(t,\tau) \in \mathbb{N}_{n_0}^n \times \mathbb{N}_{n_0+1}^n$ and $t \leq \varrho(\tau)$.*
(ii) $\aleph_2(t,\tau)$ *is a decreasing function of t for all $(t,\tau) \in \mathbb{N}_{n_0}^n \times \mathbb{N}_{n_0+1}^n$ and $\tau < t$.*

Lemma 2.11. *Suppose that $\widehat{\aleph} > \mathcal{H}_{\mathfrak{B}-1}(n,n_0)$ and let $\eta = (\widehat{\aleph} - \mathcal{H}_{\mathfrak{B}-1}(n,n_0))/\aleph^*$. Then, kernel function $\aleph(t,\tau)$ has the following properties:*

(i) $\aleph(t,\tau) \geq 0$ *for* $(t,\tau) \in \mathbb{N}_{n_0}^n \times \mathbb{N}_{n_0+1}^n$.
(ii) $\aleph(t,\tau) \leq \aleph(\varrho(\tau),\tau)$ *for* $(t,\tau) \in \mathbb{N}_{n_0}^n \times \mathbb{N}_{n_0+1}^n$.
(iii) $\aleph(t,\tau) \geq \eta\aleph(\varrho(\tau),\tau)$ *for* $(t,\tau) \in \mathbb{N}_{n_0}^n \times \mathbb{N}_{n_0+1}^n$.
(iv) $\sum_{\tau=n_0+1}^{n} \aleph(t,\tau) \leq \varkappa$ *for* $t \in \mathbb{N}_{n_0}^n$.

Proof. The results (i) and (iv) are established in [28]. To prove (ii), we let $t < \varrho(\tau)$, then, we have from (i) of Lemma 2.10 that

$$\aleph(t,\tau) = \aleph_1(t,\tau) \leq \aleph_1(\varrho(\tau),\tau).$$

Now, for $\tau < t$, we have from (ii) of Lemma 2.10 that

$$\aleph(t,\tau) = \aleph_2(t,\tau) \leq \aleph_2(\tau,\tau) \leq \aleph_2(\varrho(\tau),\tau) \text{ as } \varrho(\tau) < \tau.$$

From the above two inequalities, we obtain $\aleph(t,\tau) \leq \aleph(\varrho(\tau),\tau)$. Next, we prove (iii). We note from Lemma 2.5 that

$$\begin{gathered} \mathcal{H}_{\mathfrak{B}-1}(n_0+1,n_0) \leq \mathcal{H}_{\mathfrak{B}-1}(t,n_0) \text{ for } t \in N_{n_0+1}, \\ 0 = \mathcal{H}_{\mathfrak{B}-1}(n,n) \leq \mathcal{H}_{\mathfrak{B}-1}(n,\varrho(\tau)) \leq \mathcal{H}_{\mathfrak{B}-1}(n,n_0), \\ \mathcal{H}_{\mathfrak{B}-2}(n,n_0) \leq \mathcal{H}_{\mathfrak{B}-2}(n,\varrho(\tau)) \leq 1, \\ \mathcal{H}_{\mathfrak{B}-1}(\varrho(\tau),n_0) \leq \mathcal{H}_{\mathfrak{B}-1}(\tau,n_0) \leq \mathcal{H}_{\mathfrak{B}-1}(n,n_0), \\ \mathcal{H}_{\mathfrak{B}-1}(t,\varrho(\tau)) \leq \mathcal{H}_{\mathfrak{B}-1}(t,n_0) \leq \mathcal{H}_{\mathfrak{B}-1}(n,n_0). \end{gathered}$$

So,

$$\begin{aligned}\aleph_1(t,\tau) &= \frac{1}{\lambda}\Big[ac\mathcal{H}_{\beta-1}(t,n_0)\mathcal{H}_{\beta-1}(n,\varrho(\tau)) + ad\mathcal{H}_{\beta-1}(t,n_0)\mathcal{H}_{\beta-2}(n,\varrho(\tau))\\ &\qquad + (b-a)c\mathcal{H}_{\beta-1}(n,\varrho(\tau)) + (b-a)d\mathcal{H}_{\beta-2}(n,\varrho(\tau))\Big]\\ &\geq \frac{1}{\lambda}\Big[ad\mathcal{H}_{\beta-1}(n_0+1,n_0)\mathcal{H}_{\beta-2}(n,n_0) + (b-a)d\mathcal{H}_{\beta-2}(n,n_0)\Big] = \widehat{\aleph}\end{aligned}$$

and

$$\begin{aligned}\aleph_1(\varrho(\tau),\tau) &= \frac{1}{\lambda}\Big[ac\mathcal{H}_{\beta-1}(\varrho(\tau),n_0)\mathcal{H}_{\beta-1}(n,\varrho(\tau)) + ad\mathcal{H}_{\beta-1}(\varrho(\tau),n_0)\mathcal{H}_{\beta-2}(n,\varrho(\tau))\\ &\qquad + (b-a)c\mathcal{H}_{\beta-1}(n,\varrho(\tau)) + (b-a)d\mathcal{H}_{\beta-2}(n,\varrho(\tau))\Big]\\ &\leq \frac{1}{\lambda}\Big[ac(\mathcal{H}_{\beta-1}(n,n_0))^2 + ad\mathcal{H}_{\beta-1}(n,n_0)\\ &\qquad + (b-a)c\mathcal{H}_{\beta-1}(n,n_0) + (b-a)d\Big] = \aleph^*.\end{aligned}$$

Therefore, for $t < \varrho(\tau)$, we have

$$\frac{\aleph(t,\tau)}{\aleph(\varrho(\tau),\tau)} = \frac{\aleph_1(t,\tau)}{\aleph_1(\varrho(\tau),\tau)} \geq \frac{\widehat{\aleph}}{\aleph^*} \geq \frac{\widehat{\aleph} - \mathcal{H}_{\beta-1}(n,n_0)}{\aleph^*}$$

and, for $\tau < t$, we get from (i) that

$$\frac{\aleph(t,\tau)}{\aleph(\varrho(\tau),\tau)} = \frac{\aleph_2(t,\tau)}{\aleph_1(\varrho(\tau),\tau)} = \frac{\aleph_1(t,\tau) - \mathcal{H}_{\beta-1}(t,\varrho(\tau))}{\aleph_1(\varrho(\tau),\tau)} \geq \frac{\widehat{\aleph} - \mathcal{H}_{\beta-1}(n,n_0)}{\aleph^*}.$$

This completes the proof. □

We note that an N-tuple $(z_1, z_2, \ldots, z_N)$ is a solution of (1.1)–(1.2) if and only if

$$\begin{aligned}z_1(t) = \sum_{\tau_1=n_0+1}^{n} \aleph(t,\tau_1)\phi(\tau_1)g_1\Bigg[\sum_{\tau_2=n_0+1}^{n} \aleph(\tau_1,\tau_2)\phi(\tau_2)g_2\Bigg[\sum_{\tau_3=n_0+1}^{n} \aleph(\tau_2,\tau_3)\phi(\tau_3)\\ \vdots\\ \times g_{N-2}\Bigg[\sum_{\tau_{N-1}=n_0+1}^{n} \aleph(\tau_{N-2},\tau_{N-1})\phi(\tau_{N-1})\\ \times g_{N-1}\Bigg[\sum_{\tau_N=n_0+1}^{n} \aleph(\tau_{N-1},\tau_N)\phi(\tau_N)g_N(z_1(\tau_N))\Bigg]\Bigg]\end{aligned}$$

and

$$\begin{aligned}z_j(t) &= \sum_{\tau=n_0+1}^{n} \aleph(t,\tau)\phi(\tau)g_j(z_{j+1}(\tau)), \quad j = 2,3,\ldots,N,\\ z_{N+1}(t) &= z_1(t), \quad t \in \mathbb{N}_{n_0}^{n}.\end{aligned}$$

Denote the set of all real-valued functions z defined on $\mathbb{N}_{n_0}^{n}$ by $\mathcal{B}$. Then, $\mathcal{B}$ is a Banach space equipped with the norm $\|z\| = \max_{t\in\mathbb{N}_{n_0}^{n}} |z(t)|$. Next, we take the

cone $\mathcal{D} \subset \mathcal{B}$ defined by

$$\mathcal{D} = \Big\{ z \in \mathcal{B} : z(t) \geq 0 \text{ for } t \in \mathbb{N}_{n_0}^{n} \text{ and } \min_{t \in \mathbb{N}_{n_0+1}^{n-1}} z(t) \geq \eta \|z\| \Big\}.$$

For any $z_1 \in \mathcal{D}$, define an operator $\mathscr{F} : \mathcal{D} \to \mathcal{B}$ by

$$\begin{aligned}(\mathscr{F} z_1)(t) = \sum_{\tau_1=n_0+1}^{n} \aleph(t,\tau_1)\phi(\tau_1) g_1 \Bigg[\sum_{\tau_2=n_0+1}^{n} \aleph(\tau_1,\tau_2)\phi(\tau_2) g_2 \Bigg[\sum_{\tau_3=n_0+1}^{n} \aleph(\tau_2,\tau_3) \\ \vdots \\ \times g_{N-2} \Bigg[\sum_{\tau_{N-1}=n_0+1}^{n} \aleph(\tau_{N-2},\tau_{N-1})\phi(\tau_{N-1}) \\ \times g_{N-1} \Bigg[\sum_{\tau_N=n_0+1}^{n} \aleph(\tau_{N-1},\tau_N)\phi(\tau_N) g_N(z_1(\tau_N)) \Bigg] \Bigg] \Bigg] \Bigg].\end{aligned}$$

Lemma 2.12. *The operator $\mathscr{F}$ is self mapping and completely continuous on $\mathcal{D}$.*

Proof. Since $g_j(z_{j+1}(\tau))$ is nonnegative for $\tau \in \mathbb{N}_{n_0}^{n}$, $z_1 \in \mathcal{D}$ and $\aleph(t,\tau)$ is nonnegative for all $(t,\tau) \in \mathbb{N}_{n_0}^{n} \times \mathbb{N}_{n_0+1}^{n}$, it follows that $\mathscr{F}(z_1(t)) \geq 0$ for all $t \in \mathbb{N}_{n_0}^{n}$, $z_1 \in \mathcal{D}$. Now, by Lemma 2.11, we have

$$\begin{aligned}&\min_{t \in \mathbb{N}_{n_0+1}^{n-1}} (\mathscr{F} z_1)(t) \\ &= \min_{t \in \mathbb{N}_{n_0+1}^{n-1}} \Bigg\{ \sum_{\tau_1=n_0+1}^{n} \aleph(t,\tau_1)\phi(\tau_1) g_1 \Bigg[\sum_{\tau_2=n_0+1}^{n} \aleph(\tau_1,\tau_2)\phi(\tau_2) g_2 \Bigg[\sum_{\tau_3=n_0+1}^{n} \aleph(\tau_2,\tau_3) \\ &\qquad \vdots \\ &\qquad \times g_{N-2} \Bigg[\sum_{\tau_{N-1}=n_0+1}^{n} \aleph(\tau_{N-2},\tau_{N-1})\phi(\tau_{N-1}) \\ &\qquad \times g_{N-1} \Bigg[\sum_{\tau_N=n_0+1}^{n} \aleph(\tau_{N-1},\tau_N)\phi(\tau_N) g_N(z_1(\tau_N)) \Bigg] \Bigg] \Bigg] \Bigg\} \\ &= \eta \sum_{\tau_1=n_0+1}^{n} \aleph(\varrho(\tau_1),\tau_1)\phi(\tau_1) g_1 \Bigg[\sum_{\tau_2=n_0+1}^{n} \aleph(\tau_1,\tau_2)\phi(\tau_2) g_2 \Bigg[\sum_{\tau_3=n_0+1}^{n} \aleph(\tau_2,\tau_3) \\ &\qquad \vdots \\ &\qquad \times g_{N-2} \Bigg[\sum_{\tau_{N-1}=n_0+1}^{n} \aleph(\tau_{N-2},\tau_{N-1})\phi(\tau_{N-1}) \\ &\qquad \times g_{N-1} \Bigg[\sum_{\tau_N=n_0+1}^{n} \aleph(\tau_{N-1},\tau_N)\phi(\tau_N) g_N(z_1(\tau_N)) \Bigg] \Bigg] \Bigg]\end{aligned}$$

$$\geq \eta \max_{t\in\mathbb{N}_{n_0}^n} \Bigg\{ \sum_{\tau_1=n_0+1}^{n} \aleph(t,\tau_1)\phi(\tau_1) g_1 \Bigg[\sum_{\tau_2=n_0+1}^{n} \aleph(\tau_1,\tau_2)\phi(\tau_2) g_2 \Bigg[\sum_{\tau_3=n_0+1}^{n} \aleph(\tau_2,\tau_3)$$

$$\vdots$$

$$\times g_{N-2} \Bigg[\sum_{\tau_{N-1}=n_0+1}^{n} \aleph(\tau_{N-2},\tau_{N-1})\phi(\tau_{N-1})$$

$$\times g_{N-1} \Bigg[\sum_{\tau_N=n_0+1}^{n} \aleph(\tau_{N-1},\tau_N)\phi(\tau_N) g_N(z_1(\tau_N)) \Bigg] \Bigg] \geq \eta \max_{t\in\mathbb{N}_{n_0}^n} |\mathscr{F} z_1(t)|.$$

Thus, $\mathscr{F}(\mathcal{D}) \subset \mathcal{D}$. Therefore, the operator $\mathscr{F}$ is completely continuous by standard methods and by the Arzelà–Ascoli theorem. □

3. Existence of positive solutions

By an application of the following theorems, we derive the sufficient conditions for the existence of positive solutions to the problem (1.1)–(1.2).

Theorem 3.1. (Krasnoselskii's [23]) *Let $\mathcal{D}$ be a cone in a Banach space $\mathcal{B}$ and E_1, E_2 are open sets with $0 \in E_1, \overline{E}_1 \subset E_2$. Let $\mathscr{F} : \mathcal{D} \cap (\overline{E}_2 \backslash E_1) \to \mathcal{D}$ be a completely continuous operator such that*

(a) $\|\mathscr{F} z\| \leq \|z\|$, $z \in \mathcal{D} \cap \partial E_1$, *and* $\|\mathscr{F} z\| \geq \|z\|$, $z \in \mathcal{D} \cap \partial E_2$, *or*
(b) $\|\mathscr{F} z\| \geq \|z\|$, $z \in \mathcal{D} \cap \partial E_1$, *and* $\|\mathscr{F} z\| \leq \|z\|$, $z \in \mathcal{D} \cap \partial E_2$.

Then, $\mathscr{F}$ has a fixed point in $\mathcal{D} \cap (\overline{E}_2 \backslash E_1)$.

Theorem 3.2. (Hölder's inequality [31]) *Fix $1 \leq p \leq \infty$ and let q be the dual index to p, i.e., $1/p + 1/q = 1$. Let $z = (z_k)_{k=1}^n \in \ell^p$ and $\vartheta = (\vartheta_k)_{k=1}^n \in \ell^q$, then the sequence $z\vartheta = (z\vartheta_k)_{k=1}^n \in \ell^1$, and*

$$\|z\vartheta\|_1 \leq \|z\|_p \|\vartheta\|_q.$$

Moreover, if $z \in \ell^1$ and $\vartheta \in \ell^\infty$, then $z\vartheta = (z\vartheta_k)_{k=1}^n \in \ell^1$, and

$$\|z\vartheta\|_1 \leq \|z\|_1 \|\vartheta\|_\infty.$$

We consider the follwoing three possible cases for $\varphi \in \ell^p(N_{n_0}^n) : p > 1$, $p = 1$ and $p = \infty$. The case $p > 1$ is treated in the following theorem.

Theorem 3.3. *Let φ be bounded below by a positive real number $\widehat{\varphi}$ and there exist positive numbers R, r such that $\eta r < r < \theta r < R$, where*

$$\theta > \left[\eta \widehat{\varphi} \sum_{\tau_N=n_0+1}^{n} \aleph(\varrho(\tau_N), \tau_N) \right]^{-1}$$

and g_j, $j = 1, 2, \ldots, N$, satisfies the following conditions

($\mathcal{J}_1$) $g_j(z) \leq M_1 R$ *for* $0 \leq z \leq R$, *where*

$$M_1 < \frac{1}{\|\aleph\|_q \|\varphi\|_p},$$

($\mathcal{J}_2$) $g_j(z) \geq \theta r$ *for* $\eta r \leq z \leq r$.

Then, the problem (1.1)–(1.2) *has at least one positive solution.*

Proof. Consider the open subsets E_1 and E_2 of $\mathcal{B}$ defined by

$$E_1 = \{z \in \mathcal{B} : \|z\| < R\},\ E_2 = \{z \in \mathcal{B} : \|z\| < r\}.$$

Let $z_1 \in \mathcal{D} \cap \partial E_1$. Then, $z_1(\tau) \leq R = \|z_1\|$ for all $\tau \in N_{n_0+1}^n$. By $(\mathcal{J}_1)$ and $\tau_{N-1} \in N_{n_0+1}^n$, we have

$$\begin{aligned}\sum_{\tau_N=n_0+1}^{n} \aleph(\tau_{N-1},\tau_N)\phi(\tau_N)g_N(z_1(\tau_N)) &\leq \sum_{\tau_N=n_0+1}^{n} \aleph(\varrho(\tau_N),\tau_N)\phi(\tau_N)g_N(z_1(\tau_N))\\ &\leq M_1 R \sum_{\tau_N=n_0+1}^{n} \aleph(\varrho(\tau_N),\tau_N)\phi(\tau_N).\end{aligned}$$

There exists a $q > 1$ such that $1/p + 1/q = 1$. By the first part of Theorem 3.2 and for $\aleph := \aleph(\varrho(\tau_N),\tau_N)$, we get

$$\sum_{\tau_N=n_0+1}^{n} \aleph(\tau_{N-1},\tau_N)\phi(\tau_N)g_N(z_1(\tau_N)) \leq M_1 R\|\aleph\|_q\|\varphi\|_p \leq R.$$

It follows in similar manner for $\tau_{N-2} \in N_{n_0+1}^n$,

$$\begin{aligned}\sum_{\tau_{N-1}=n_0+1}^{n} \aleph(\tau_{N-2},\tau_{N-1})\phi(\tau_{N-1})g_{N-1}&\left[\sum_{\tau_N=n_0+1}^{n} \aleph(\tau_{N-1},\tau_N)\phi(\tau_N)g_N(z_1(\tau_N))\right]\\ &\leq \sum_{\tau_{N-1}=n_0+1}^{n} \aleph(\varrho(\tau_{N-1}),\tau_{N-1})\phi(\tau_{N-1})g_{N-1}(R)\\ &\leq M_1 R \sum_{\tau_N=n_0+1}^{n} \aleph(\varrho(\tau_{N-1}),\tau_{N-1})\phi(\tau_{N-1})\\ &\leq M_1 R\|\aleph\|_q\|\varphi\|_p \leq R.\end{aligned}$$

Continuing with this bootstrapping argument, we get

$$\begin{aligned}(\mathscr{F}z_1)(t) = \sum_{\tau_1=n_0+1}^{n} \aleph(t,\tau_1)\phi(\tau_1)g_1&\left[\sum_{\tau_2=n_0+1}^{n} \aleph(\tau_1,\tau_2)\phi(\tau_2)g_2\left[\sum_{\tau_3=n_0+1}^{n} \aleph(\tau_2,\tau_3)\right.\right.\\ &\qquad\qquad\vdots\\ &\times g_{N-2}\left[\sum_{\tau_{N-1}=n_0+1}^{n} \aleph(\tau_{N-2},\tau_{N-1})\phi(\tau_{N-1})\right.\\ &\left.\left.\times g_{N-1}\left[\sum_{\tau_N=n_0+1}^{n} \aleph(\tau_{N-1},\tau_N)\phi(\tau_N)g_N(z_1(\tau_N))\right]\right]\right] \leq R, \quad t \in \mathbb{N}_{n_0}^n.\end{aligned}$$

Since $R = \|z_1\|$ for $z_1 \in \mathcal{D} \cap \partial E_1$, we get

$$\|\mathscr{F}z_1\| \leq \|z_1\|. \tag{3.1}$$

Let $\tau \in \mathbb{N}_{n_0+1}^n$. Then, $r = \|z_1\| \geq z_1(\tau) \geq \min_{\tau \in \mathbb{N}_{n_0+1}^{n-1}} z_1(t) \geq \eta \|z_1\| \geq \theta r$. By $(\mathcal{J}_2)$ and for $\tau_{N-1} \in \mathbb{N}_{n_0+1}^n$, we have

$$\begin{aligned}\sum_{\tau_N=n_0+1}^{n} \aleph(\tau_{N-1},\tau_N)\phi(\tau_N)g_N(z_1(\tau_N)) &\geq \eta \sum_{\tau_N=n_0+1}^{n} \aleph(\varrho(\tau_N),\tau_N)\phi(\tau_N)g_N(z_1(\tau_N))\\ &\geq \eta\theta r \sum_{\tau_N=n_0+1}^{n} \aleph(\varrho(\tau_N),\tau_N)\phi(\tau_N)\\ &\geq \eta\theta r\widehat{\varphi} \sum_{\tau_N=n_0+1}^{n} \aleph(\varrho(\tau_N),\tau_N) \geq r.\end{aligned}$$

Continuing with the bootstrapping argument, we get

$$\begin{aligned}(\mathscr{F}z_1)(t) = \sum_{\tau_1=n_0+1}^{n} \aleph(t,\tau_1)\phi(\tau_1)g_1\Bigg[\sum_{\tau_2=n_0+1}^{n} \aleph(\tau_1,\tau_2)\phi(\tau_2)g_2\Bigg[\sum_{\tau_3=n_0+1}^{n} \aleph(\tau_2,\tau_3)\\ \vdots\\ \times g_{N-2}\Bigg[\sum_{\tau_{N-1}=n_0+1}^{n} \aleph(\tau_{N-2},\tau_{N-1})\phi(\tau_{N-1})\\ \times g_{N-1}\Bigg[\sum_{\tau_N=n_0+1}^{n} \aleph(\tau_{N-1},\tau_N)\phi(\tau_N)g_N(z_1(\tau_N))\Bigg]\Bigg] \geq r, \quad t \in \mathbb{N}_{n_0}^n.\end{aligned}$$

Thus, if $z_1 \in \mathcal{D} \cap \partial E_2$, then

$$\|\mathscr{F}z_1\| \geq \|z_1\|. \tag{3.2}$$

It is evident that $0 \in E_2 \subset \overline{E}_2 \subset E_1$. From (3.1), (3.2), it follows from Theorem 3.1 that the operator $\mathscr{F}$ has a fixed point $z_1 \in \mathcal{D} \cap \left(\overline{E}_1 \backslash E_2\right)$ such that $z_1^{(\tau)} \geq 0$ on $N_{n_0+2}^n$. Next, setting $z_{N+1} = z_1$, we obtain a positive solution $(z_1, z_2, \ldots, z_\ell)$ of (1.1)–(1.2) given iteratively by

$$\begin{aligned}z_j(t) &= \sum_{\tau=n_0+1}^{n} \aleph(t,\tau)\phi(\tau)g_j(z_{j+1}(\tau)), \quad j = 2,3,\ldots,N,\\ z_{N+1}(t) &= z_1(t), \quad t \in \mathbb{N}_{n_0}^n.\end{aligned}$$

The proof is completed. □

For $p = 1$, we have the following theorem.

Theorem 3.4. *Let φ be bounded below by a positive real number $\widehat{\varphi}$ and there exist positive numbers R, r such that $\eta r < r < \theta r < R$, where*

$$\theta > \left[\eta\widehat{\varphi} \sum_{\tau_N=n_0+1}^{n} \aleph(\varrho(\tau_N),\tau_N)\right]^{-1}$$

and g_j, $j = 1,2,\ldots,N$, satisfies $(\mathcal{J}_2)$ and

$(\mathcal{J}_3)$ $g_j(z) \le M_2 R$ *for* $0 \le z \le R$, *where*

$$M_2 < \frac{1}{\|\aleph\|_\infty \|\varphi\|_1}.$$

Then, the problem (1.1)–(1.2) *has at least one positive solution.*

Proof. Consider the open subsets E_1 and E_2 of $\mathcal{B}$ defined by

$$E_1 = \{z \in \mathcal{B} : \|z\| < R\},\ E_2 = \{z \in \mathcal{B} : \|z\| < r\}.$$

Let $z_1 \in \mathcal{D} \cap \partial E_1$. Then, $z_1(\tau) \le R = \|z_1\|$ for all $\tau \in N^n_{n_0+1}$. By $(\mathcal{J}_3)$ and $\tau_{N-1} \in N^n_{n_0+1}$, we have

$$\begin{aligned}\sum_{\tau_N=n_0+1}^{n} \aleph(\tau_{N-1},\tau_N)\phi(\tau_N) g_N(z_1(\tau_N)) &\le \sum_{\tau_N=n_0+1}^{n} \aleph(\varrho(\tau_N),\tau_N)\phi(\tau_N) g_N(z_1(\tau_N)) \\ &\le M_2 R \sum_{\tau_N=n_0+1}^{n} \aleph(\varrho(\tau_N),\tau_N)\phi(\tau_N) \\ &\le M_2 R \|\aleph\|_\infty \|\varphi\|_1 \le R.\end{aligned}$$

It follows in similar manner for $\tau_{N-2} \in N^n_{n_0+1}$,

$$\begin{aligned}&\sum_{\tau_{N-1}=n_0+1}^{n} \aleph(\tau_{N-2},\tau_{N-1})\phi(\tau_{N-1}) g_{N-1}\left[\sum_{\tau_N=n_0+1}^{n} \aleph(\tau_{N-1},\tau_N)\phi(\tau_N) g_N(z_1(\tau_N))\right] \\ &\le \sum_{\tau_{N-1}=n_0+1}^{n} \aleph(\varrho(\tau_{N-1}),\tau_{N-1})\phi(\tau_{N-1}) g_{N-1}(R) \\ &\le M_2 R \sum_{\tau_N=n_0+1}^{n} \aleph(\varrho(\tau_{N-1}),\tau_{N-1})\phi(\tau_{N-1}) \le M_2 R \|\aleph\|_\infty \|\varphi\|_1 \le R.\end{aligned}$$

Continuing with this bootstrapping argument, we get

$$\begin{aligned}(\mathscr{F} z_1)(t) = \sum_{\tau_1=n_0+1}^{n} \aleph(t,\tau_1)\phi(\tau_1) g_1\Bigg[\sum_{\tau_2=n_0+1}^{n} \aleph(\tau_1,\tau_2)\phi(\tau_2) g_2\Bigg[\sum_{\tau_3=n_0+1}^{n} \aleph(\tau_2,\tau_3)\\ \vdots \\ \times g_{N-2}\Bigg[\sum_{\tau_{N-1}=n_0+1}^{n} \aleph(\tau_{N-2},\tau_{N-1})\phi(\tau_{N-1}) \\ \times g_{N-1}\Bigg[\sum_{\tau_N=n_0+1}^{n} \aleph(\tau_{N-1},\tau_N)\phi(\tau_N) g_N(z_1(\tau_N))\Bigg]\Bigg]\Bigg] \le R, \quad t \in \mathbb{N}^n_{n_0}.\end{aligned}$$

Since $R = \|z_1\|$ for $z_1 \in \mathcal{D} \cap \partial E_1$, we get

$$\|\mathscr{F} z_1\| \le \|z_1\|.$$

The rest of the proof is similar to the proof of Theorem 3.3. This completes the proof. □

Theorem 3.5. *Let φ be bounded below by a positive real number $\widehat{\varphi}$ and there exist positive real numbers R, r such that $\eta r < r < \theta r < R$, where*

$$\theta > \left[\eta\widehat{\varphi} \sum_{\tau_N=n_0+1}^{n} \aleph(\varrho(\tau_N), \tau_N)\right]^{-1}$$

and g_j, $j = 1, 2, \ldots, N$, satisfies $(\mathcal{J}_2)$ and

$(\mathcal{J}_4)$ $g_j(z) \leq M_3 R$ for $0 \leq z \leq R$, where

$$M_3 < \frac{1}{\|\aleph\|_1 \|\varphi\|_\infty}.$$

Then, the problem (1.1)–(1.2) has at least one positive solution.

Proof. Proof of the present theorem is similar to the proofs of Therems 3.3 and 3.4. So, we omit the deltails here. □

4. Uniqueness and stability analysis

In this section, we derive sufficient conditions for the existence of a unique solution of the boundary value problem (1.1)–(1.2), where we employ two metrics under Rus's theorem (see [1,37] for more details). In this regard, let $z, \vartheta \in \mathcal{B}$ and consider the following two metrics on $\mathcal{B}$:

$$d_1(z, \vartheta) = \max_{t \in \mathbb{N}_{n_0+1}^{n}} |z(t) - \vartheta(t)|, \tag{4.1}$$

$$d_2(z, \vartheta) = \left[\sum_{t=n_0+1}^{n} |z(t) - \vartheta(t)|^p\right]^{\frac{1}{p}}, \ p > 1. \tag{4.2}$$

For d_1 in (4.1), the pair $(\mathcal{B}, d_1)$ forms a complete metric space. For d_2 in (4.2), the pair $(\mathcal{B}, d_2)$ forms a metric space. The relationship between the two metrics on $\mathcal{B}$ is given by

$$d_2(z, \vartheta) \leq (n - n_0)^{1/p} d_1(z, \vartheta) \text{ for all } z, \vartheta \in \mathcal{B}. \tag{4.3}$$

Theorem 4.1. (Rus [35]) *Let $\mathcal{B}$ be a nonempty set and let d_1 and d_2 be two metrics on $\mathcal{B}$ such that $(\mathcal{B}, d_1)$ forms a complete metric space. If the mapping $\mathscr{F} : \mathcal{B} \to \mathcal{B}$ is continuous with respect to d_1 on $\mathcal{B}$ and*

$$d_1(\mathscr{F}z, \mathscr{F}\vartheta) \leq \alpha d_2(z, \vartheta), \tag{4.4}$$

for some $\alpha > 0$ and for all $z, \vartheta \in \mathcal{B}$,

$$d_2(\mathscr{F}z, \mathscr{F}\vartheta) \leq \beta d_2(z, \vartheta),$$

for some $0 < \beta < 1$ for all $z, \vartheta \in \mathcal{B}$, then there is a unique $z^* \in \mathcal{B}$ such that $\mathscr{F}z^* = z^*$.

Theorem 4.2. *Let φ be bounded above by φ^* and there is some $K > 0$ such that*

$$|g_j(z) - g_j(\vartheta)| \leq K|z - \vartheta| \quad \text{for} \quad z, \vartheta \in \mathcal{B}.$$

Also, assume that there are constants $p > 1$ and $q > 1$ such that $1/p + 1/p = 1$ with

$$(n - n_0)^{1/p} (\varphi^*)^N \varkappa^{N-1} K^{N-1} \|\aleph\|_q < 1, \tag{4.5}$$

then the boundary value problem (1.1)–(1.2) *has a unique solution.*

Proof. Let $z_1, \vartheta_1 \in \mathcal{B}$ be any two solutions of (1.1)–(1.2) and $\tau_{N-1} \in N_{n_0+1}^n$. Then, by Hölder's inequality 3.2, we have

$$\begin{aligned}
&\left| \sum_{\tau_N=n_0+1}^{n} \aleph(\tau_{N-1},\tau_N)\phi(\tau_N)g_N(z_1(\tau_N)) - \sum_{\tau_N=n_0+1}^{n} \aleph(\tau_{N-1},\tau_N)\phi(\tau_N)g_N(\vartheta_1(\tau_N)) \right| \\
&\qquad \le \sum_{\tau_N=n_0+1}^{n} |\aleph(\tau_{N-1},\tau_N)|\,|\phi(\tau_N)|\,|g_N(z_1(\tau_N)) - g_N(\vartheta_1(\tau_N))| \\
&\qquad \le \varphi^* K \sum_{\tau_N=n_0+1}^{n} |\aleph(\varrho(\tau_N),\tau_N)|\,|z_1(\tau_N) - \vartheta_1(\tau_N)| \\
&\qquad \le \varphi^* K \left[\sum_{\tau_N=n_0+1}^{n} |\aleph(\varrho(\tau_N),\tau_N)|^q \right]^{\frac{1}{q}} \left[\sum_{\tau_N=n_0+2}^{n} |z_1(\tau_N) - \vartheta_1(\tau_N)|^p \right]^{\frac{1}{p}} \\
&\qquad \le \varphi^* K \|\aleph\|_q d_2(z_1,\vartheta_1).
\end{aligned}$$

Similarly, for $\tau_{N-2} \in N_{n_0+1}^n$, we have

$$\begin{aligned}
&\left| \sum_{\tau_{N-1}=n_0+1}^{n} \aleph(\tau_{N-2},\tau_{N-1})\phi(\tau_{N-1})g_{N-1}\left[\sum_{\tau_N=n_0+1}^{n} \aleph(\tau_{N-1},\tau_N)\phi(\tau_N)g_N(z_1(\tau_N)) \right] \right. \\
&\left. - \sum_{\tau_{N-1}=n_0+1}^{n} \aleph(\tau_{N-2},\tau_{N-1})\phi(\tau_{N-1})g_{N-1}\left[\sum_{\tau_N=n_0+1}^{n} \aleph(\tau_{N-1},\tau_N)\phi(\tau_N)g_N(\vartheta_1(\tau_N)) \right] \right| \\
&\le \sum_{\tau_{N-1}=n_0+1}^{n} |\aleph(\tau_{N-2},\tau_{N-1})||\phi(\tau_{N-1})| \\
&\times \left| \sum_{\tau_N=n_0+1}^{n} \aleph(\tau_{N-1},\tau_N)\phi(\tau_N)g_N(z_1(\tau_N)) - \sum_{\tau_N=n_0+1}^{n} \aleph(\tau_{N-1},\tau_N)\phi(\tau_N)g_N(\vartheta_1(\tau_N)) \right| \\
&\le \varphi^* \sum_{\tau_{N-1}=n_0+1}^{n} |\aleph(\tau_{N-2},\tau_{N-1})|[\varphi^* K\|\aleph\|_q d_2(z_1,\vartheta_1)] \le (\varphi^*)^2 \varkappa K \|\aleph\|_q d_2(z_1,\vartheta_1).
\end{aligned}$$

Continuing with this bootstrapping argument, we get

$$|(\mathscr{F}z_1)(t) - (\mathscr{F}\vartheta_1)(t)| \le (\varphi^*)^N \varkappa^{N-1} K^{N-1} \|\aleph\|_q d_2(z_1,\vartheta_1). \tag{4.6}$$

Thus, defining

$$\alpha = (\varphi^*)^N \varkappa^{N-1} K^{N-1} \|\aleph\|_q,$$

we see that

$$d(\mathscr{F}z_1, \mathscr{F}\vartheta_1) \le \alpha d_2(z_1,\vartheta_1), \tag{4.7}$$

for some $\alpha > 0$ for all $z_1, \vartheta_1 \in \mathcal{B}$, and so the inequality (4.4) of Theorem 4.1 holds. Now, for all $z_1, \vartheta_1 \in \mathcal{B}$, we may apply (4.3) to (4.7) to obtain

$$d_1(\mathscr{F}z_1, \mathscr{F}\vartheta_1) \le \alpha d_2(z_1,\vartheta_1) \le \alpha (n-n_0)^{1/p} d_1(z_1,\vartheta_1).$$

Thus, given any $ß > 0$, we can choose $\delta = ß/[\alpha(n-n_0)^{1/p}]$ so that $d_1(\mathscr{F}z_1, \mathscr{F}\vartheta_1) < ß$ whenever $d(z_1,\vartheta_1) < \delta$. Hence, $\mathscr{F}$ is continuous on $\mathcal{B}$ with respect to the metric

d_1. Finally, we show that $\mathscr{F}$ is contractive on $\mathcal{B}$ with respect to the metric d_2. From (4.6), for each $z_1, \vartheta_1 \in \mathcal{B}$, consider

$$\begin{aligned}
&\left[\sum_{t=n_0+1}^{n} |(\mathscr{F}z_1)(t) - (\mathscr{F}\vartheta_2)(t)|^p\right]^{\frac{1}{p}} \\
&\leq \left[\sum_{t=n_0+1}^{n} \left|(\varphi^*)^N \varkappa^{N-1} K^{N-1} \|\aleph\|_q d_2(z_1, \vartheta_1)\right|^p\right]^{\frac{1}{p}} \\
&\leq (n-n_0)^{1/p} (\varphi^*)^N \varkappa^{N-1} K^{N-1} \|\aleph\|_q d_2(z_1, \vartheta_1).
\end{aligned}$$

That is,

$$d_2(\mathscr{F}z_1, \mathscr{F}\vartheta_1) \leq (n-n_0)^{1/p} (\varphi^*)^N \varkappa^{N-1} K^{N-1} \|\aleph\|_q d_2(z_1, \vartheta_1).$$

From the assumption (4.5), we have

$$d_2(\mathscr{F}z_1, \mathscr{F}\vartheta_1) \leq \beta d_2(z_1, \vartheta_1)$$

for some $\beta < 1$ and all $z_1, \vartheta_1 \in \mathcal{B}$. Thus, by Theorem 4.1, the operator $\mathscr{F}$ has a unique fixed point in $\mathcal{B}$. Therefore, the boundary value problem (1.1)–(1.2) has a unique solution. □

5. Examples

In this section, we present two examples to check the validity of our main results.

Example 5.1. Consider the following boundary value problem:

$$\begin{aligned}
\nabla_1^{1/2} [\nabla z_j(t)] + \varphi(t) g_j(z_{j+1}(t)) = 0, \quad t \in \mathbb{N}_3^{100}, \ j = 1, 2, \\
z_3(t) = z_1(t), \quad t \in \mathbb{N}_3^{100},
\end{aligned} \tag{5.1}$$

satisfying two-point general boundary conditions

$$\begin{aligned}
z_j(1) - 20\nabla z_j(1) = 0, \quad j = 1, 2, \\
\frac{1}{900} z_j(100) + 4\nabla z_j(100) = 0, \quad j = 1, 2,
\end{aligned} \tag{5.2}$$

where $\varphi(t) = \frac{\pi}{12(t+1)^4}$ and

$$g_j(z) = \begin{cases}
0.2 \times 10^{10}, & z \in (10^4, +\infty), \\
\frac{6.3\times10^8 - 0.2\times10^{10}}{10^2 - 10^4}(z - 10^4) + 0.2 \times 10^{10}, & z \in [10^2, 10^4], \\
6.3 \times 10^8, & z \in (0.0132 \times 10^2, 10^2), \\
\frac{6.3\times10^8 - 0.2\times10^{10}}{0.0132\times10^2 - 0.012\times10^2}(z - 0.012 \times 10^2) + 0.2 \times 10^{10}, & \\
& z \in (0.012 \times 10^2, 0.0132 \times 10^2], \\
0.2 \times 10^{10}, & z \in [0, 0.012 \times 10^2],
\end{cases}$$

Here, $n_0 = 0$, $n = 100$, $a = 1$, $b = 20$, $c = \frac{1}{900}$, $d = 4$. Let $p = q = 2$, $M_1 = 0.3$, $\theta = 6.2 \times 10^6$. By using Maple, we calculated $\lambda = 0.2601595441, \widehat{\aleph} = 17.41443310$, $\aleph^* = 466.8589700$, $\widehat{\varphi} = 2.515840659 \times 10^{-9}$,

$$\sum_{\tau=2}^{100} \aleph(\varrho(\tau), \tau) = 4879.295601, \quad \eta = \frac{\widehat{\aleph} - \mathcal{H}_{\beta-1}(n, n_0)}{\aleph^*} = 0.01316187049,$$

$$\|\aleph\|_2 = \left[\sum_{\tau=2}^{100} |\aleph(\varrho(\tau),\tau)|^2\right]^{1/2} = 723.2219121,$$
$$\|\varphi\|_2 = \left[\sum_{\tau=2}^{100} |\varphi(\tau)|^2\right]^{1/2} = 0.003424534117.$$

Then,

$$M_1 < \frac{1}{\|\aleph\|_2\|\varphi\|_2} = 0.4037633796,$$
$$\theta > \left[\eta\widehat{\varphi}\sum_{\tau=2}^{100} \aleph(\varrho(\tau),\tau)\right]^{-1} = 6.189308432 \times 10^6.$$

Taking $R = 10^{10}$, $r = 10^2$,

$$\eta r = 0.01316187 \times 10^2 < 10^2 = r < \theta r = 6.2 \times 10^8 < 10^{10} = R,$$

and g_j satisfies the following growth conditions:

$$g_j(z) \le M_1 R = 0.3 \times 10^{10}, \quad z \in [0, 10^{10}]$$
$$g_j(z) \ge \theta r = 6.2 \times 10^8, \qquad z \in [0.0132 \times 10^2, 10^2].$$

All the conditions of Theorem 3.3 are satisfied. Therefore, by Theorem 3.3, the boundary value problem (5.1)–(5.2) has at least one positive solution.

Example 5.2. Consider the following boundary value problem:

$$\begin{aligned} \nabla_1^{1/2}[\nabla z_j(t)] + \varphi(t) g_j(z_{j+1}(t)) = 0, \quad t \in \mathbb{N}_3^{100},\ j = 1,2, \\ z_3(t) = z_1(t), \quad t \in \mathbb{N}_3^{100}, \end{aligned} \tag{5.3}$$

satisfying two-point general boundary conditions

$$\begin{aligned} z_j(1) - 20\nabla z_j(1) = 0, \quad j = 1,2, \\ \frac{1}{900} z_j(100) + 4\nabla z_j(100) = 0, \quad j = 1,2, \end{aligned} \tag{5.4}$$

where $n_0 = 0$, $n = 100$, $a = 1$, $b = 20$, $c = \frac{1}{900}$, $d = 4$, $\varphi(t) = \frac{\pi}{6}(t-94)^2$, $g_j(z) = 10^{-11}\sin z$ for $j = 1,2$. Then, it is clear that $N = 2$, $\varphi(t) \le 6\pi = \varphi^*$ and

$$|g_j(z) - g_j(\vartheta)| \le 10^{-11}|z - \vartheta| = K|z - \vartheta|$$

for $z, \vartheta \in \mathcal{B}$. Letting $p = q = \frac{1}{2}$. Then,

$$\|\aleph\|_2 = \left[\sum_{\tau=2}^{100} |\aleph(\varrho(\tau),\tau)|^2\right]^{1/2} = 723.2219121$$

and

$$\begin{aligned} \varkappa = \frac{1}{\lambda}\big[ac\mathcal{H}_{\mathfrak{B}-1}(n,n_0)\mathcal{H}_{\mathfrak{B}}(n,n_0) + ad\left[\mathcal{H}_{\mathfrak{B}-1}(n,n_0)\right]^2 \\ + (b-a)c\mathcal{H}_{\mathfrak{B}}(n,n_0) + (b-a)d\mathcal{H}_{\mathfrak{B}-1}(n,n_0)\big] \\ = 5342.553597. \end{aligned}$$

From the above values, we get

$$(n-n_0)^{1/p}(\varphi^*)^N \varkappa^{N-1} K^{N-1} \|\aleph\|_q = 0.1365967313 < 1.$$

Thus, all the conditions of Theorem 4.2 are satisfied. Therefore, by Theorem 4.2, the problem (5.3)–(5.4) has a unique solution.

6. Conclusion

In this paper, we developed a theory to study the existence and uniqueness of positive solutions of a certain type of a nabla fractional order difference equation by applying Krasnoselskii's cone fixed point theorem in a Banach space and Rus's fixed point theorem in a complete metric space, respectively. To tackle the growth conditions $(\mathcal{J}_i)$, $i = 1, 2, 3, 4$, we chose a particular form of a nonlinear term g_j in Example 5.1 and in Example 5.2 for simplicity. We feel that there are many other nice forms for g_j satisfying growth conditions. In the future, we will study the existence of multiple positive solutions of (1.1)–(1.2) and also study the problem with both Δ operators and mixed Δ and ∇ operators.

Acknowledgement. The authors would like to thank anonymous referees for their valuable suggesions and comments for the improvement of the paper.

References

[1] S. S. Almuthaybiria and C. C. Tisdell, *Sharper existence and uniqueness results for solutions to third order boundary value problems*, Math. Model. Anal. **25** (2020), 409–420.

[2] F. M. Atici and P. W. Eloe, *A transform method in discrete fractional calculus*, Int. J. Difference Equ. **2** (2007), 165–176.

[3] F. M. Atici and P. W. Eloe, *Initial value problems in discrete fractional calculus*, Proc. Am. Math. Soc. **137** (2009), 981–989.

[4] F. M. Atici and P. W. Eloe, *Two-point boundary value problems for finite fractional difference equations*, J. Difference Equ. Appl. **17** (2011), 445–456.

[5] D. Baleanu, K. Diethelm, E. Scalas and J. J. Trujillo, *Fractional Calculus. Models and Numerical Methods*, 2nd ed., Series on Complexity, Nonlinearity and Chaos **5**, World Scientific, Hackensack, NJ, USA, 2017.

[6] J. Bélair, *Population models with state-dependent delays*, Mathematical population dynamics, Proc. 2nd Int. Conf., New Brunswick/NJ (USA) 1989, Lecture Notes in Pure and Applied Mathematics **131**, 1991, pp. 165–176.

[7] J. Bélair and C. Mackey, *Consumer memory and price fluctuations on commodity markets: An integrodifferential model*, J. Dyn. Differ Equations **1** (1989), 299–325.

[8] A. Brackins, *Boundary Value Problems of Nabla Fractional Difference Equations*, Ph.D. Thesis, The University of Nebraska-Lincoln, 2014.

[9] M. Buger and M. R. W. Martin, *The escaping disaster: A problem related to state-dependent delays*, Z. Angew. Math. Phys. **55** (2004), 547–574.

[10] M. Caputo, J. M. Carcione and M. A. B. Botelho, *Modeling extreme event precursors with the fractional diffusion equation*, Fract. Calc. Appl. Anal. **18** (2015), 208–222.

[11] S. Cheng, J. Si and X. Wang, *An existence theorem for iterative functional differential equations*, Acta Math. Hungar. **94** (2002), 1–17.

[12] S. K. Das, S. A. Edalatpanah and T. Mandal, *Application of linear fractional programming problem with fuzzy nature in industry sector*, Filomat **34** (2020), 5073–5084.

[13] J. B. Díaz and T. J. Osler, *Differences of fractional order*, Math. Comput. **28** (1974), 185–202.

[14] R. Driver, *A two-body problem of classical electrodynamics: The one-dimensional case*, Ann. Phys. **21** (1963), 122–142.

[15] E. Eder, *The functional differential equation* $x'(t) = x(x(t))$,, J. Differ. Equations **54** (1984), 390–400.
[16] B. Eralp and F. S. Topal, *Existence of positive solutions for discrete fractional boundary value problems*, Adv. Dyn. Syst. Appl. **15** (2020), 79–97.
[17] M. Fečkan, J. Wang and H. Y. Zhao, *Maximal and minimal nondecreasing bounded solutions of iterative functional differential equations*, Appl. Math. Lett. **113** (2021), Article ID 106886, 8pp.
[18] R. Gao, C. Gu and X. Li, *Image zooming model based on fractional-order partial differential equation*, J. Discrete Math. Sci. Cryptogr. **20** (2017), 55–63.
[19] C. S. Goodrich, *Nonlocal systems of BVPs with asymptotically sublinear boundary conditions*, Appl. Anal. Discrete Math. **6** (2012), 174–193.
[20] C. S. Goodrich, *On nonlinear boundary conditions satisfying certain asymptotic behavior*, Nonlinear Anal., Theory Methods Appl. **76** (2013), 58–67.
[21] C. S. Goodrich and A. C. Peterson, *Discrete Fractional Calculus*, Springer, 2015.
[22] H. L. Gray and N. F. Zhang, *On a new definition of the fractional difference*, Math. Comput. **50** (1988), 513–529.
[23] D. Guo and V. Lakshmikantham, *Nonlinear Problems in Abstract Cones*, Academic Press, San Diego, 1988.
[24] C. Heil, *Introduction to Real Analysis*, Graduate Texts in Mathematics **280**, Springer, 2019.
[25] A. Ikram, *Lyapunov inequalities for nabla Caputo boundary value problems*, J. Differ. Equations Appl. **25** (2019), 757–775.
[26] R. Johnson, *Functional equations, approximations, and dynamic response of systems with variable time-delay*, IEEE Trans. Automatic Control **17** (1972), 398–401.
[27] J. M. Jonnalagadda, *On Two point Riemann–Liouville type nabla fractional boundary value problems*, Adv. Dyn. Syst. Appl. **13** (2018), 141–166.
[28] J. M. Jonnalagadda, *On a nabla fractional boundary value problem with general boundary conditions*, AIMS Math. **5** (2019), 204–215.
[29] M. Khuddush and K. R. Prasad, *Infinitely many positive solutions for an iterative system of conformable fractional order dynamic boundary value problems on time scales*, Turkish J. Math. **46** (2022), 338–359.
[30] A. A. Kilbas, H. M. Srivastava and J. J. Trujillo, *Theory and Applications of Fractional Differential Equations*, North-Holland Mathematics Studies, 204, Elsevier Science, Amsterdam, 2006.
[31] K. Nantomah, *Generalized Hölder's and Minkowski's inequalities for Jackson's q-integral and some applications to the incomplete q-gamma function*, Abstr. Appl. Anal. **2017** (2017), Article ID 9796873, 6 pp.
[32] K. R. Prasad, M. Khuddush and D. Leela, *Existence and Uniqueness of Positive Solutions for System of* (p, q, r)*-Laplacian Fractional Order Boundary Value Problems*, Adv. Theory Nonlinear Anal. Appl. **5** (2021), 138–157.
[33] K. R. Prasad, M. Khuddush and D. Leela, *Existence, uniqueness and Hyers–Ulam stability of a fractional order iterative two-point boundary value Problems*, Afr. Mat. **32** (2021), 1227–1237.
[34] G. Rahman, *Application of topological degree method in qualitative behaviour of fractional differential equations*, Filomat **34** (2020), 421–432.
[35] I. A. Rus, *On a fixed point theorem of Maia*, Stud. Univ. Babes-Bolyai, Math. **22** (1977), 40–42.
[36] J. Si, X. Wang and S. Cheng, *Nondecreasing and convex* C^2*-solutions of an iterative functional differential equation*, Aequationes Math. **60** (2000), 38–56.
[37] C. P. Stinson, S. S. Almuthaybiri and C. C. Tisdell, *A note regarding extensions of fixed point theorems involving two metrics via an analysis of iterated functions*, ANZIAM J. **61** (2020), C15–C30.
[38] D. Yang and W. Zhang, *Solutions of equivariance for iterative differential equations*, Appl. Math. Lett. **17** (2004), 759–765.
[39] Z. Yu, H. Jiang, C. Hu and J. Yu, *Necessary and sufficient conditions for consensus of fractional-order multiagent systems via sampled-data control*, IEEE Trans. Syst. Man Cybern. **47** (2017), 1892–1901.

[40] P. Zhang, *Analytic solutions for iterative functional differential equations*, Electron. J. Differ. Equ. **2012** (2012), Paper No. 180, 7 pp.
[41] F. Zheng, *New results for a class of boundary value problems involving impulsive fractional differential equations*, Filomat **34** (2020), 707–725.

Mahammad Khuddush, Department of Mathematics, Dr. Lankapalli Bullayya College, Visakhapatnam, 530013, India
e-mail: khuddush89@gmail.com

K. Rajendra Prasad, Department of Applied Mathematics, College of Science and Technology, Andhra University, Visakhapatnam, 530003, India
e-mail: rajendra92@rediffmail.com

Journal of Uncertain Systems
(2022) 2250013 (15 pages)
© World Scientific Publishing Company
DOI: 10.1142/S1752890922500131

World Scientific
www.worldscientific.com

imac21
2022-11-09 14:05:06

AQ: Please check throughout text for errors, figures and tables. Please check title, author names, affiliations and emails. Please check: Keywords, Codes, Corresponding author (if any).

Opinion Mining Using Normal Discriminant Piecewise Regressive (NDPR) Sentiment Classification Technique

K. Anuradha[*,§,‡], M. Vamsi Krishna[†,§] and Banitamani Mallik[*,¶]

[*]*Centurion University of Technology & Management*
R. Sitapur 761211, Odisha, India
[§]*Dr.Lankapalli Bullayya College of Engineering*
Resuvanipalam 530016,Visakhapatnam,India
[†]*Aditya Engineering College, Surampalem 533437*
Andhra Pradesh, India
[‡]*anukeshav76@gmail.com; anuradhaphd02@gmail.com*
[§]*vamsimangalam@gmail.com*
[¶]*banita.mallik@cutm.ac.in*

Received 17 January 2022
Revised 24 May 2022
Accepted 4 October 2022
Published

Sentiment analysis through opinion mining is determined through significant and growing interest for many industries including hotel, tourism, educations and so on. Sentiment analysis includes design of the system to search the user opinions in blog posts, comments, reviews or tweets regarding the product, policy or area. Many researchers carried out their research on opinion mining to identify the polarity of the statements. But the main problem during opinion mining is that the words chosen do not solve attribute relevancy and could not classify the positive and negative usage of uncertain terms. In order to address these problems, normal discriminant piecewise regressive (NDPR) sentiment classification technique is introduced. NDPR technique perform three processes, namely, pre-processing, feature extraction and classification to improve the accuracy level through forming classes (i.e., positive, neutral and negative) based on the extracted words from user review comments. Initially, NDPR technique performs the data pre-processing task for stemming and removing the stop words from review statements to reduce the file size that in turn improves the efficiency. After that, normal discriminant feature extraction process is carried out in NDPR technique to extract the opinion word from the review statements sent by reviewers. The related opinion words are systematized for their semantic equivalence of sentiment based on extracted word. This helps to reduce the time consumption to extract the opinions from reviewers. Finally, piecewise regressive sentiment classification (PRSC) process is carried out in NDPR technique to analyse the semantic opinion words for evaluating the sentiment class label. The sentiment class labels are categorized into positive, neutral and negative sentiments with the user review comments. This in turn helps to reduce the time consumption to extract the opinions from reviewers and to improve the

Page Proof

‡Corresponding author.

review detection accuracy. The performance evaluation of NDPR technique is carried out with standard benchmark datasets of consumer product and services reviews extracted. The parameters used in evaluation are number of customer review words, accuracy, time complexity (TC) and false positive rate. Experimental analysis shows that NDPR technique reduces the time to extract the opinions from reviewers and false positive rate.

Keywords: Sentiment analysis; NDPR; semantic opinion words; pre-processing; feature extraction; classification; stop words.

1. Introduction

Opinion mining is a developing research area in recent days. The designed methods are employed to identify the opinion of business product (i.e., positive, neutral or negative). An innovative MapReduce improved weighted ID3 decision tree classification approach was introduced in Ref. 1 for opinion mining. A multiple feature selector was employed to minimize the high feature dimensionality. But the accuracy level was not improved by designed approach. Bayesian-based framework termed Opinion Mine was introduced in Ref. 2 for opinion mining with Twitter Data. Tweets were collected through Twitter API. An imported Tweet was processed for making collection of untrained rules and random variables. However, the time consumption was not reduced by Bayesian-based framework.

A deep learning model was designed in Ref. 3 for fine-grained aspect-based opinion mining. Multi-head self-attention (MHSA) was employed to combine internal semantic text representation to model interaction with the sentiment features. A fuzzy system was employed in Ref. 4 for the instance selection to generate the minimum rules. Multi-objective Genetic Algorithm was introduced to the increase accuracy and to reduce the number of rules. Though the accuracy level was increased, the time complexity (TC) was not minimized.

A technology-based solution was provided in Ref. 5 for smart governance and interactive policy framing. The framework mined the user tweeting opinion about government policies and categorized into three polarities like positive neutral and negative. But the classification accuracy was not improved by technology-based solution. A neural network-based method was introduced in Ref. 6 for opinion mining from social web in healthcare domain. An opinion mining method was introduced for predicting the drug satisfaction level. But the complexity level was not reduced by neural network-based method.

A weighted aspect-based opinion mining using deep learning method was designed in Ref. 7 for recommender system (AODR) to extract product characteristics. A deep learning method used the weighted user opinions from the review text for improving the RS. However, the accuracy level was not increased by deep learning method. A Na¨ıve Bayes machine learning algorithm was introduced in Ref. 8 to perform the multi-level classification to identify the sentiments of the commenter's for various options. A Na¨ıve assumption was considered with the keywords related to particular option to minimize the computational requirements.

An opinion mining system was introduced in Ref. 9 for binary and fine-grained sentiment classification. Feature-based sentiment classification included the pre-processing task to remove the noise, feature extraction and tagging polarity. But the computational cost was not minimized by opinion mining system. Highly recommended web-based business sites was designed in Ref. 10 with collection strategy and swarm-based improvement system. A fuzzy c-means (FCM) grouping plan was used to collect the features. But the computational complexity was not reduced by FCM grouping plan.

The issues identified from the above literature are lesser accuracy, higher time consumption, higher computational cost, higher computational complexity, higher error rate (ER) and so on. The above problems are addressed through introducing a new technique termed NDPR technique.

- The main contribution of the NDPR technique is to perform pre-processing, feature extraction and classification for increasing accuracy level through forming classes (i.e., positive, neutral and negative) with help of extracted words from the user review comments.
- NDPR technique performed data pre-processing task for stemming and removing the stop words from the review statements to minimize the file size.
- Normal discriminant feature extraction process is carried out in NDPR technique to extract the opinion word from review statements sent by reviewers. The related opinion words are systematized for semantic equivalence of sentiment depending on extracted word.
- Piecewise regressive sentiment classification (PRSC) process in NDPR technique analyzes the semantic opinion words for evaluating the sentiment class label. The sentiment class labels are classified into positive, neutral and negative sentiments with the user review comments. This in turn helps to improve the performance of opinion mining.

This paper is arranged as follows. In Sec. 2, the existing opinion mining methods are reviewed. The detail description of the proposed NDPR technique is given in Sec. 3. The experimental evaluation and corresponding results of the various parameters are discussed in Sec. 4. Finally, the conclusion is presented in Sec. 5 to summarize our findings.

2. Related Works

Deep learning modified neural network (DLMNN) was introduced in Ref. 11 for sentiment analysis of online products review. An improved adaptive neuro-fuzzy inferences system (IANFIS) was introduced for online product prediction. The deep learning model with hybrid masking, review extraction and attention mechanism was designed in Ref. 12 to extract multi-dimensional product feature from e-commerce reviews and to determine the sentiment weights. But the TC was not reduced by DLMNN.

The feature mining in sentiment analysis was carried out in Ref. 13 with moment flattering in text analytics. Web content mining was employed for extraction from the web page filling. Frequent pattern mining from website data increased the website organization. But the feature extraction accuracy was not improved through sentiment analysis. A new pattern-based opinion mining method was designed in Ref. 14 for market trend prediction. The opinion mining was carried out with an event classification for trend prediction. But the computational cost was not minimized by designed method.

Reference 15 deals with social media (SM) technology and customer-centric management system for sustainable business growth of companies' social customer relationship management (SCRM). However, the computational complexity was not reduced by designed system. The positive or negative polarity extraction was carried out in Ref. 16 from SM text of sentiment analysis in natural language processing. The exponential development for business organizations and governments were employed to conduct their research in sentiment analysis. But the ER was not minimized through extraction.

A new detection approach was introduced in Ref. 17 to employ the aspect level sentiment detection aimed on item features. The designed system carried out pre-processing operation such as stemming, tokenization and stop-word removal to extract important information for its classification. However, the TC was not reduced by detection approach. The domain-dependent embedding model was introduced in Ref. 18 to attain the cross-domain aspect-based sentiment analysis in an end-to-end fashion. The designed model used the domain-dependent embedding's with multi-task learning plan to collect domain-invariant and domain-dependent knowledge. But the accuracy level was not improved by designed model.

The domain-specific seed list was introduced in Ref. 19 to categorize the tweets. Semantic and syntactic analysis on tweets was carried out to reduce the information loss during tweet classification. But the classification time was not reduced. A new pattern-based method was introduced in Ref. 20 for sentiment analysis with higher accuracy. The designed method was employed in Hadoop MapReduce framework for sentiment analysis with minimal time consumption. Though time consumption was reduced, the complexity level was not minimized by pattern-based method.

3. Methodology

An opinion mining is an essential one for the people to communicate or to express their opinions, feedbacks and attitudes toward entities products, services and their attributes. The key aim of opinion mining is to establish the attitude of writer regarding overall polarity of the document. Many researchers carried out their research on opinion mining in order to identify the polarity of the statements. But the accuracy was not improved and time consumption was not reduced by exiting opinion mining methods. In order to address these problems, normal discriminant piecewise regressive (NDPR) sentiment classification technique is introduced. The

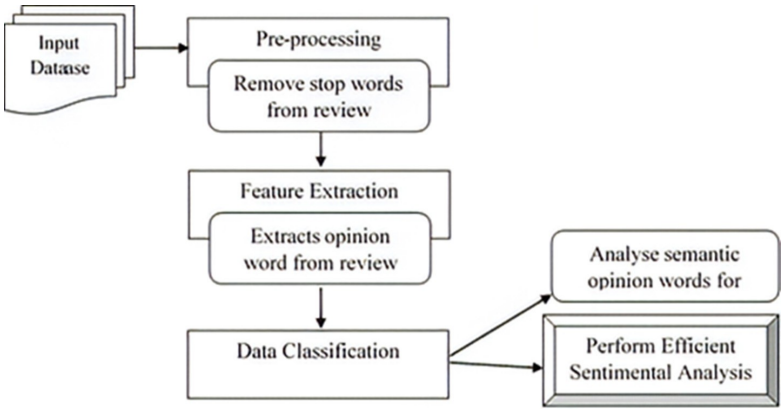


Fig. 1. Structural diagram of NDPR technique.

key objective of NDPR technique is to improve the accuracy of identifying the statement polarity with minimal time consumption. The structural diagram of NDPR technique is illustrated in Fig. 1.

Figure 1 illustrates the structural diagram of proposed NDPR technique for identifying the polarity of the review statements. Initially, the numbers of user reviews are collected from the input dataset "$ur_1, ur_2, ur_3, \ldots, ur_n$". After collecting the input data, the proposed NDPR technique uses normal discriminant feature extraction process to extract the opinion words from the user reviews. This in turn helps to reduce the file size of the review statements. After that, PRSC process is used in NDPR technique to perform the review statement classification with higher accuracy and lesser time consumption. By this way, an efficient sentiment analysis is carried out. The brief description of data pre-processing, feature extraction and classification is carried out in upcoming sections.

3.1. *Data pre-processing*

In NDPR technique, the data pre-processing task is an essential process for stemming and removing the stop words from review statements to minimize the file size that in turn improves the efficiency. Pre-processing cleans and organizes the text from review statements for an exact classification process. The review statements contain many words. The irrelevant word increases the dimensionality and makes the classification process more difficult one. Consequently, it increases the computational complexity of classification process. Pre-processing includes three different processes, namely, tokenization, stop words removal, stem words removal. Tokenization splits the raw text into different words termed as tokens. The generated tokens are employed for understanding the context. Stopword is a word used for linking the high discriminating power words while forming the sentence. The stop word does not have any meaning. Word stemming is a process used to extract root words through removing suffixes from word.

Page Proof

3.2. *Normal discriminant feature extraction*

In NDPR technique, we extract the opinion words from the user review statements. The key aim of feature extraction is to project entire dataset from high-dimensional space into low-dimensional space to avoid curse of dimensionality and reduce the complexity. Initially, normal discriminant describes two classes (i.e., relevant and irrelevant). After defining the two classes, the mean value of particular class is calculated. After that, the discriminant vector in normal discriminant feature extraction projects the words in the review statements into two different classes (i.e., opinion words and non-opinion words) depending on mean and variance value. The projection increases the variance between two classes and reduces the variance within the class. The mean of the classes are determined by

$$\text{Mean}_{\text{c}} = \frac{1}{N} \sum_{i=}^{n} wd_{i'} \tag{1}$$

where "Mean_{cl}" represents the mean of classes. "N^k" symbolizes the number of words 'wd_i' in kth class. After that, mean value of words in the class is determined as

$$\text{Mean}_{\text{W}} = \frac{1}{N} \sum_{i=}^{n} wd_{i'} \tag{2}$$

where "Mean_{wo}" represents the words mean value. "N " represents the number of words. Depending on their mean value, the scatter matrix gets formed. The scatter matrix is a product of mean of the two variables in NDPR technique. The matrix helps to find out whether the words are correlated within classes or not. The scatter matrix within the class is computed as

$$S_m(\text{within}) = \sum_{i=1} (wd_i - \text{Mean}_{\text{cl}}) * (wd_i - \text{Mean}_{\text{cl}})^T, \tag{3}$$

where "S_m(within)" denotes the scatter matrix within class, "wd_i" denotes words in the review statements, "Mean_{cl}" symbolizes the mean value of the classes. "T " represents the transpose matrix. In NDPR technique, Scatter matrix between the classes is determined as

$$S_m(\text{between}) = \sum_{i=1} N * (\text{Mean}_{\text{cl}} - \text{Mean}_{\text{wo}})(\text{Mean}_{\text{cl}} - \text{Mean}_{\text{wo}})^T, \tag{4}$$

where "S_m(between)" symbolizes the scatter matrix between the classes. "N " denotes the number of words. "Mean_{cl}" represent the mean value of classes. "Mean_{wo}" symbolizes the mean value of words. Depending on the two matrixes, the separation function is described as the ratio of variance between the classes to variance inside the class. It is denoted as

$$\text{SF} = \frac{\vartheta(\text{between})}{\vartheta(\text{within})} = \frac{\delta * S_m(\text{between}) * d}{\delta * S_m(\text{within}) * d'} \tag{5}$$

where "SF" represents the separation function. "ϑ(between)" symbolizes the variance between the classes, "ϑ(within)" denotes the variance within the class. "δ"

Page Proof

symbolizes the linear discriminant vector. "d" represents the optimal projection direction. The linear discriminant vector in NDPR technique projects the words into the classes depending on the optimal projection direction. Therefore, the projection vector in normalized discriminant analysis reduces the variance and increases the correlation within the class. As a result, opinion words and non-opinion words are separated. From that, the opinion words are considered in NDPR technique for performing the data classification task. The algorithmic process of normal discriminant feature extraction is given as

Input: Dataset
Output: Identify the opinion words
Step 1: Begin
Step 2: Collect user reviews with number of words
Step 3: Define two classes 'class$_1$, class$_2$'
Step 4: For every class
Step 5: Determine mean value Mean$_{cl}$
Step 6: Determine mean value Mean$_{wo}$
Step 7: Construct scatter matrix within and between classes S_m(within) and S_m(between)
Step 8: Define class separability function 'SF'
Step 9: Separate opinion words and remove non-opinion words
Step 10: End for
Step 11: End

As described in algorithm, normal discriminant feature extraction algorithm is described for performing the data classification. The normal discriminant vector is used for projecting the words as non-opinion words and opinion words. NDPR technique selects the opinion words and non-opinion words for data classification. The opinion words are employed for reducing the complexity involved in opinion mining and accuracy gets improved.

3.3. *PRSC*

PRSC process is carried out in NDPR technique to increase data classification for opinion mining. The opinion words are partitioned into intervals and separate line segment is assigned to every interval. PRSC is carried out on data through dividing the various independent variables (i.e., opinion words). When autonomous opinion words clustered into dissimilar set, PRSC is suitable to reveal diverse relationships between opinion words in the regions. The boundaries between segments are termed as the breakpoints. The PRSC process is illustrated in Fig. 2.

From Fig. 2, PRSC collects the opinion words as input and performs the piecewise regression analysis. Piecewise regression splits the domain into many "segments" and fits the separate line through each one. PRSC analysis is defined as

$$\text{PRSC} = \alpha 0 + \alpha 1\phi + \alpha 2(\phi - bp) + \varepsilon, \tag{6}$$

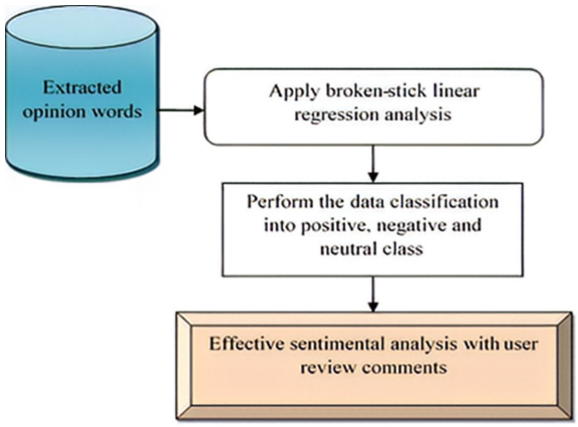


Fig. 2. PRSC.

where "bp" represents the breakpoint value. "ϕ" denotes the input opinion words. "$\alpha_0\alpha_1\alpha_2$" indicate the regression coefficients. "ε" refers the error vector and "PRSC" represents the predicted output. From that, PRSC identifies the class of opinion words with lesser time and higher accuracy. The algorithmic process of PRSC is given as

// Piecewise Regressive Sentiment Classification Algorithm
Input: Extracted opinion words
Output: Improves accuracy with lesser time consumption
Step 1: Begin
Step 2: For each extracted opinion words
Step 3: Apply Piecewise Regressive Sentiment Classification
Step4: Classify opinion words into three classes
Step5: End for
Step 6: End

Algorithm 2. PRSC.

Algorithm 2 explains the algorithmic process of PRSC. The extracted opinion words are considered as an input. After that, piecewise regression analysis is carried out for every opinion words to perform the sentiment classification. The opinions are categorized into three classes, namely, positive, neutral and negative class in more accurate manner. By this way, an efficient sentiment classification is carried out with minimal time consumption.

3.4. *Dataset preparation*

An experimental evaluation of NDPR technique is carried out using Java language. The tweets are collected from Sentiment140 dataset with 1.6 million tweets for

Page Proof

opinion mining through the classification. The URL of Sentiment140 dataset is https://www.kaggle.com/kazanova/sentiment140. This is the sentiment140 dataset. It contains 1,600,000 tweets extracted using the Twitter API. The tweets have been annotated (0 = negative, 4 = positive) and they can be used to detect sentiment. The dataset comprises six fields, namely, target, ids, date, flag, user and tweets. Target describes the polarity of the tweet (0 = negative, 2 = neutral, 4 = positive).

4. Experimental Evaluation and Result Discussion

An experimental evaluation of proposed NDPR technique and existing techniques, namely, MapReduce improved weighted ID3 decision tree classification approach[1] and Bayesian-based framework[2] is carried out using Java language. For conducting the experiments, the number of customer reviews is taken in the range 100–1000. Performance analysis of proposed NDPR technique is compared with the existing results with certain parameters listed as follows:

- Accuracy
- ER and
- TC

4.1. *Analysis on accuracy*

Accuracy is defined as the ratio of number of customer reviews that are correctly classified the polarity of the opinions to the total number of customer reviews considered as an input. Consequently, the accuracy is determined as

$$\text{Acc} = \left(\frac{\text{Number of customer reviews correctly classified polarity}}{\text{Number of customer reviews}} \right) * 100 \quad (7)$$

where accuracy level (Acc) is determined. The accuracy is measured in terms of percentage (%).

Table 1 describes the accuracy with respect to number of customer reviews varying from 100 to 1000. When the number of customer reviews gets increased, the accuracy gets increased or decreased, respectively. Let us consider that input number of customer reviews is 500. The accuracy achieved by NDPR technique is 93%. The accuracy attained by MapReduce improved weighted ID3 decision tree classification approach and Bayesian-based framework is 94% and 97%, respectively. The graphical representation of accuracy is illustrated in Fig. 3.

Figure 3 describes the accuracy versus number of customer reviews varying from 100 to 1000. The green color line denotes the accuracy of proposed NDPR technique. The blue line and red line symbolize the accuracy of MapReduce improved weighted ID3 decision tree classification approach and Bayesian-based framework. However, the accuracy of proposed NDPR technique is comparatively higher than that of the MapReduce improved weighted ID3 decision tree classification approach[1] and Bayesian-based framework.[2] This is due to application of normal discriminant feature extraction process and PRSC process. The feature extraction process extracts

Table 1. Tabulation of accuracy.

Number of customer reviews (number)	Accuracy (%)		
	MapReduce improved weighted ID3 decision tree classification approach	Bayesian-based framework	NDPR technique
100	85	88	92
200	88	91	93
300	88	92	95
400	89	92	94
500	93	94	97
600	90	94	96
700	89	92	95
800	90	91	98
900	91	92	95
1000	91	92	95

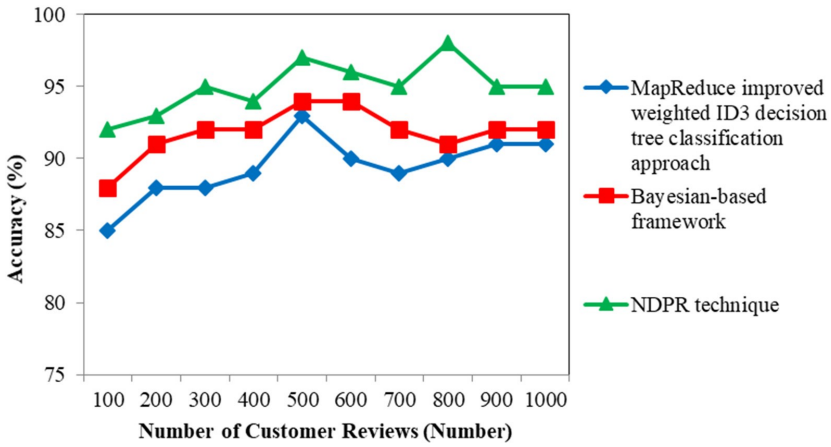


Fig. 3. (Color online) Measurement of accuracy.

the opinion word from review statements sent by reviewers. After that, PRSC process analyzes the semantic opinion words for determining the sentiment class label. The sentiment class labels are classified into positive, neutral and negative sentiments with the user review comments. Consequently, the proposed NDPR technique increases the accuracy of sentiment classification by 6% as compared to MapReduce improved weighted ID3 decision tree classification approach[1] and 3% when compared to Bayesian-based framework,[2] respectively.

4.2. *Analysis on TC*

TC is described as the product of number of customer reviews and amount of time utilized for classifying the customer reviews polarity of the opinion. The TC is

Table 2. Tabulation of TC.

Number of customer reviews (number)	TC (ms)		
	MapReduce improved weighted ID3 decision tree classification approach	Bayesian-based framework	NDPR technique
100	56	45	31
200	59	47	33
300	61	50	35
400	64	52	37
500	67	55	39
600	70	57	41
700	72	60	43
800	75	62	46
900	78	66	48
1000	80	68	50

determined as

$$\text{TC} = N * \text{Time consumed for classifying one customer review,} \tag{8}$$

where the time complexity (TC) is computed. "N" denotes the number of customer reviews. The TC is measured in terms of milliseconds (ms).

Table 2 explains the TC with respect to number of customer reviews changing from 100 to 1000. When the number of customer reviews gets increased, the TC also gets increased correspondingly. Let us consider that input number of customer reviews is 700. The TC attained by NDPR technique is 43 ms. The TC consumed by MapReduce improved weighted ID3 decision tree classification approach and Bayesian-based framework is 72 and 60 ms, respectively. The graphical representation of TC is illustrated in Fig. 4.

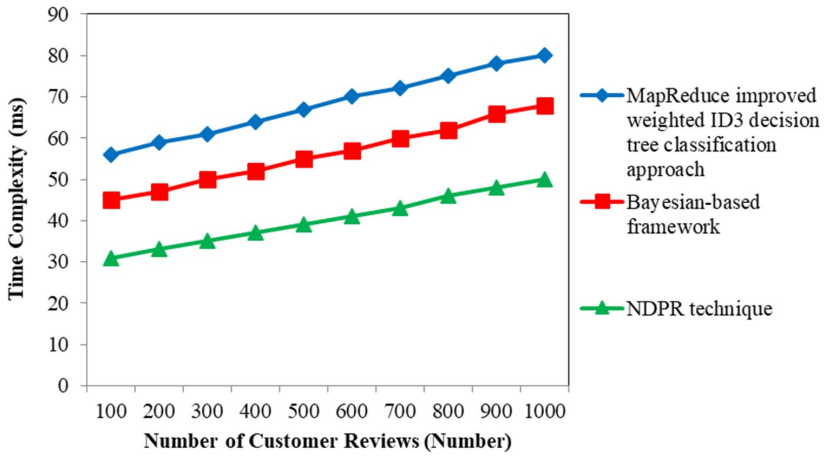


Fig. 4. (Color online) Measurement of TC.

Figure 4 illustrates the TC versus number of customer reviews varying from 100 to 1000. The green color line denotes the TC of proposed NDPR technique. The blue line and red line symbolize the TC of MapReduce improved weighted ID3 decision tree classification approach and Bayesian-based framework. However, the TC of the proposed NDPR technique is comparatively lesser than that of MapReduce improved weighted ID3 decision tree classification approach[1] and Bayesian-based framework.[2] This is due to application of normal discriminant feature extraction and PRSC process. The feature extraction process selects the opinion word from review statements sent by reviewers. The PRSC process examines the semantic opinion words for finding the sentiment class label. The sentiment class labels are categorized into positive, neutral and negative sentiments with user review comments. Consequently, the proposed NDPR technique reduces the TC of sentiment classification by 41% as compared to MapReduce improved weighted ID3 decision tree classification approach[1] and 28% when compared to Bayesian-based framework,[2] respectively.

4.3. *Analysis on ER*

ER is described as the ratio of number of customer reviews that are incorrectly classified the polarity of the opinions to the total number of customer reviewstaken as an input. Therefore, the ER is computed as

$$\mathrm{ER} = \left(\frac{\text{Number of customer reviews incorrectly classified polarity}}{\text{Number of customer reviews}} \right) * 100 \quad (9)$$

where error rate (ER) is computed. The ER is measured in terms of percentage (%).

Table 3 describes the ER with respect to number of customer reviews varying from 100 to 1000. When the number of customer reviews gets increased, the

Table 3. Tabulation of ER.

Number of customer reviews (number)	ER (%)		
	MapReduce improved ID3 decision tree weighted classification approach	Bayesian-based framework	NDPR technique
100			
15			
12	8		
200	12	9	7
300	12	8	5
400	11	8	6
500	7	6	3
600	10	6	4
700	11	8	5
800	10	9	2
900	9	8	5
1000	9	8	5

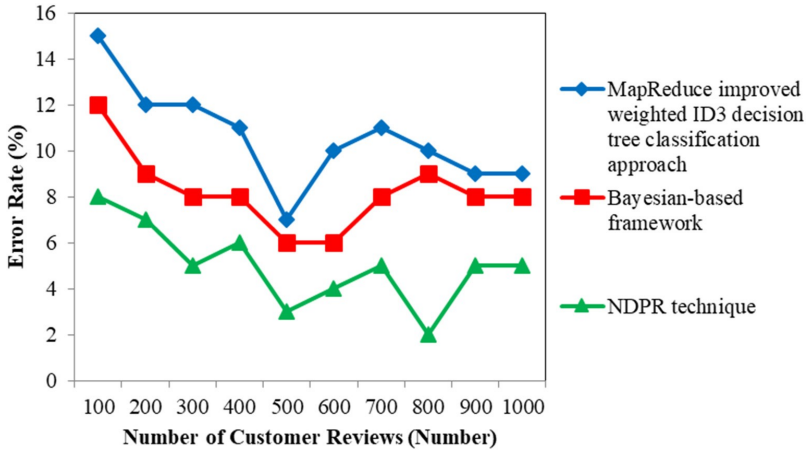


Fig. 5. (Color online) Measurement of ER.

ER also gets increased or reduced, respectively. Let us consider that input number of customer reviews is 300. The ER achieved by NDPR technique is 12%. The ER attained by MapReduce improved weighted ID3 decision tree classification approach and Bayesian-based framework is 8% and 5%, respectively. The graphical representation of ER is described in Fig. 5.

Figure 5 describes the ER versus number of customer reviews varying from 100 to 1000. The green color line denotes the ER of proposed NDPR technique. The blue line and red line symbolize the ER of MapReduce improved weighted ID3 decision tree classification approach and Bayesian-based framework. But the ER of proposed NDPR technique is comparatively lesser than that of MapReduce improved weighted ID3 decision tree classification approach[1] and Bayesian-based framework.[2] This is because of using normal discriminant feature extraction and PRSC process. The feature extraction process chooses the opinion word from review statements sent by reviewers. The PRSC process observes the semantic opinion words for identifying the sentiment class label. The sentiment class labels are classified into positive, neutral and negative sentiments with user review comments. Therefore, the proposed NDPR technique reduces the ER of sentiment classification by 53% as compared to MapReduce improved weighted ID3 decision tree classification approach[1] and 39% when compared to Bayesian-based framework,[2] respectively.

5. Conclusion

A new technique termed NDPR sentiment classification technique performed preprocessing, feature extraction and classification to increase the accuracy level through three classes depending on extracted words from user review comments. NDPR technique performed the data preprocessing task for removing stop words.

Normal discriminant feature extraction process extracts the opinion word from review statements sent by reviewers. This helps to minimize the time consumption to extract the opinions from reviewers. PRSC process analyzes the semantic opinion words for determining the sentiment class label. This in turn helps to minimize the time consumption to extract the opinions from reviewers. The efficiency of NDPR technique is evaluated with two exiting methods in terms of accuracy, ER and accuracy. The experimental results show that NDPR technique provides better performance with an enhancement of accuracy and reduced TC as well as ER when compared to state-of-the-art works.

References

1. F. Es-Sabery, K. Es-Sabery, J. Qadir, B. Sainz-De-Abajo, A. Hair, B. García-Zapirain and I. De La Torre-Diez, A MapReduce opinion mining for COVID-19-related tweets classification using enhanced ID3 decision tree classifier, *IEEE Access* **9** (2021) 58706–58739, doi:10.1109/ACCESS.2021.3073215.
2. S. Zervoudakis, E. Marakakis, H. Kondylakis and S. Goumas, OpinionMine: A Bayesian-based framework for opinion mining using Twitter data, *Mach. Learn. Appl.* **3** (2021) 1–16, doi:10.1016/j.mlwa.2020.100018.
3. A. R. Abas, I. El-Henawy, H. Mohamed and A. Abdellatif, Deep learning model for fine-grained aspect-based opinion mining, *IEEE Access*, **8** (2021) 128845–128855, doi:10.1109/ACCESS.2020.3008824.
4. T. Cerqueira, F. C. L. Bertoni and M. G. Pires, Instance genetic selection for fuzzy rule-based systems optimization to opinion classification, *IEEE Latin Am. Trans.* **18** (2020) 1215–1221, doi:10.1109/TLA.2020.9099762.
5. A. Sharma and H. Shekhar, Intelligent learning based opinion mining model for governmental decision making, *Procedia Comput. Sci.* **173** (2020) 216–224, doi10.1016/j.procs.2020.06.026.
6. V. Gopalakrishnan and C. Ramaswamy, Patient opinion mining to analyze drugs satisfaction using supervised learning, *Journal of Applied Research and Technol.* **15** (2017) 311–319, doi:10.1016/j.jart.2017.02.005.
7. A. Da'u, N. Salim, I. Rabiu and A. Osman, Weighted aspect-based opinion mining using deep learning for recommender system, *Expert Syst. Appl.* **140** (2020) 1–15, doi:10.1016/j.eswa.2019.112871.
8. A. U. R. Khan, M. Khan and M. B. Khan, Naïve multi-label classification of YouTube comments using comparative opinion mining, *Procedia Comput. Sci.* **82** (2016) 57–64, doi:10.1016/j.procs.2016.04.009.
9. M. K. Dalal and M. A. Zaveri, Opinion mining from online user reviews using fuzzy linguistic hedges, *Applied Computational Intelligence and Soft Comput.* **2014** (2014) 1–9, doi:10.1155/2014/735942.
10. P. Bellavista, D. Gupta, V. H. C. de Albuquerque, K. Shankar, A. Khanna, J. J. P. C. Rodrigues, P. R. Pinheiro and S. K. Lakshmanaprabu, Ranking analysis for online customer reviews of products using opinion mining with clustering, *Complexity* **2018** (2018) 1–15.
11. P. Sasikala and L. M. I. Sheela, Sentiment analysis of online product reviews using DLMNN and future prediction of online product using IANFIS, *J. Big Data Springer* **7**(33) (2020) 1–20.

Page Proof

12. Y. Liu, J. Lu, J. Yang and F. Mao, Sentiment analysis for e-commerce product reviews by deep learning model of Bert-BiGRU-Softmax, *Math. Biosci. Eng*. **17**(6) (2020) 7819–7837, doi:10.3934/mbe.2020398.
13. S. S. Gosavi, Opinion mining and web mining using sentiment analysis, *Int. J. Grid Distrib. Comput*. **14**(1) (2021) 1–15.
14. K.-F. Wong, Y. Xia, R. Xu, M. Wu and W. Li, Pattern-based opinion mining for stock market trend prediction, *Int. J. Comput. Process. Lang*. **21**(4) (2008) 347–361, doi:10.1142/S1793840608001949.
15. V.-D. Păvăloaia, E.-M. Teodor, D. Fotache and M. Danileţ, Opinion mining on social media data: Sentiment analysis of user preferences, *Sustainability*, **11**(16) (2019) 44–59, doi:10.3390/su11164459.
16. J. Singh, G. Singh and R. Singh, Optimization of sentiment analysis using machine learning classifiers, *Hum.-Centric Comput. Inf. Sci*. **7**(1) (2017) 1–15, doi:10.1186/s13673-017-0116-3.
17. N. Nandal, R. Tanwar and J. Pruthi, Machine learning based aspect level sentiment analysis for Amazon products, *Spat. Inf. Res*. **28**(5) (2020) 601–607, doi:10.1007/s41324-020-00320-2.
18. Y. Tian, L. Yang, Y. Sun and D. Liu, Cross-domain end-to-end aspect-based sentiment analysis with domain-dependent embeddings, *Complexity, Hindawi Publishing Corporation* **2021** (2021) 1–11.
19. R. Batool, F. A. Satti, J. Hussain, W. Ali Khan, A. M. Khan and B. Hayat, Tweets classification and sentiment analysis for personalized tweets recommendation, *Complexity Deep Neural Netw. Hindawi Publishing Coorporation* **2020** (2020) 1–9.
20. A. P. Rodrigues, N. N. Chiplunkar, R. Fernandes and M. Robnik-Sikonja, Aspect-based classification of product reviews using Hadoop framework, *Cogent Eng*. **7**(1) (2020) 1–14, doi:10.1080/23311916.2020.1810862.

ISSN No: 2348-4845
International Journal & Magazine of Engineering, Technology, Management and Research
A Peer Reviewed Open Access International Journal

Automated Smart Billing System Using RFID Technology

Seemanapalli Parvathi Pravallika, Palakula Gnana Prabha, Pediredla Kavitha, Gummadi Neelima
Department of Electronics and Communications
Guided by
Ms. Sabbi Surya Kala
Assistant Professor, Department of ECE
Dr. Lankapalli Bullayya College of Engineering for Women.

ABSTRACT: The embedded system is the one which has a computer-hardware with software embedded in it as one of its most important component. This makes our life better and simple. This smart billing system is one of the embedded systems. An automated smart shopping system is formed using the concept of RFID. Each of the shopping cart consists of an RFID reader, RF module, AVR Microcontroller, LCD display, and load cells and the products are embedded with the RFID tags. The RFID tag will have the details of the product to which it is attached. The tag is detected by the RFID reader and an automatic invoice gets generated near the cart or the trolley itself. This paper provides us how this billing system is made easy using the RFID. The main aim of this system is that the billing is made easy for the customers from waiting in the long queues in the supermarkets.

Keywords: RFID Reader, RFID Tags, RF module, AVR Microcontroller, Load cells.

1. INTRODUCTION

The concept of embedded systems has become common as it makes our work more efficient and quick, as the life of a common human being has become hectic and thus wants to make it as easy as possible. The embedded system is mainly based on a Microcontroller. These days most of the people aren't willing to spend their time at the shopping malls or supermarkets and hence are trying to purchase everything online along with the household products or groceries but there are people who still go the supermarkets and buy the products. Thus, this system makes it easier for them as the time taken to scan and bill the products is reduced a lot.

The Smart Billing System is based on the concept of Radio Frequency Identification (RFID). RFID technology uses radio waves in order to track or identify the products and objects which has a great potential in making great economic impacts in the industries. This is almost similar to the barcode system, but in this system the barcode must be within the line-of-sight to the scanner, whereas in the RFID system, when the object is in the reading range of the scanner i.e., the reader (in this system) the object gets detected.

These systems consists of transceivers, transponders, readers and the tags. RFID systems are also a type of automatic identification systems.

Cite this article as: Seemanapalli Parvathi Pravallika, Palakula Gnana Prabha, Pediredla Kavitha, Gummadi Neelima & Ms.Sabbi Suryakala, "Automated smart billing system using RFID technology.", International Journal & Magazine of Engineering, Technology, Management and Research (IJMETMR), ISSN 2348-4845, Volume 8 Issue 8, August 2021, Page 19-25.

ISSN No: 2348-4845
International Journal & Magazine of Engineering, Technology, Management and Research
A Peer Reviewed Open Access International Journal

The strengths of RFID also make it a natural fit for grocery stores. Items can be tagged and batch-read. This means the retailers knows exactly how many items are on shelves at all times with only one scan. This reduces waste and the labour costs associated with inventory and retagging.

The microcontroller used here is the AVR Microcontroller -- ATMega328. This is used to store the data regarding the price, the quantity, the total weight that are needed to generate the invoice. It is faster than the other types of microcontroller. Thus, using the above concepts the smart billing system i.e., the smart trolley is designed. Finally one can pay the total amount to the cashier either through cash or card and can get validated at the checkout points.

2. PRESENT TECHNOLOGY

The barcode technology is the existing technology and is used as means of identification. The barcode consists of white spaces and black lines which store the details of the product in a visual pattern. This is one-dimensional which is read by a scanner which can be a hand-held one.

The scanner sends out the laser which helps in detecting the details of the product to which it is attached. The scanner will read the pattern of the barcode and translates it such that our system understands it. These barcodes are widely used in the retail stores.

Barcodes help us to track, assist in accounting to generate invoices. These barcodes are sometimes not unique as two products can have a same barcode like retailer can have one barcode and the dealer can have another which can hamper the details of the product. This helps us to bring in the new technology, the RFID technology into existence.

RFID avoids the limitations of barcode scanning, which requires line-of-sight access to each barcode and can only be used to scan one item at a time. Instead, RFID tags do not require line-of-site, and multiple RFID tags can be detected and read remotely and simultaneously.

3. ABOUT THE PRODUCT

In this system, when the trolley gets initialized, the RFID reader starts to emit the radio waves continuously. When the customer starts dropping the products to which the RFID tags are embedded into the trolley and comes into the reading range of the reader, the tag gets detected and thus, the data that is related to that product gets displayed on the LCD. The price along with the count of the products gets added as the product is dropped and also gets deducted as the product is removed.

To remove a product, the process is same as for that of adding a product to the cart. The load cells used in this system help us to know whether there is a difference in the weight, which is between the total weight of the products scanned and dropped to the final weight of the products present in the trolley. A buzzer is used to indicate about the change in the weight. This process continues till the customer presses the final button.

4. HARDWARE COMPONENTS

The hardware components that are used to design the smart billing system – smart trolley are ATMega328 microcontroller, RFID reader, RFID tags, RF module, Load cells, and LCD display. The RFID tags are embedded to each

ISSN No: 2348-4845
International Journal & Magazine of Engineering, Technology, Management and Research
A Peer Reviewed Open Access International Journal

product and consists the data to which it is attached.

1) ATMega328:

The microprocessor used in this is ATMega328 also known as Arduino Nano. This is used to store the data that is related to the product and also acts an interface for the LCD display. This has an inbuilt SPI and I2C. It consists of 23 general purpose I/O ports out which 20 can be used as the other 3 are connected to two crystal oscillators and a timer, 6 ADC ports.



ARDUINO NANO



ATMega328

The specifications of this ATMega328 are

• It is a 28 pin microcontroller.

• It has a flash program memory of 32 kb.

• It has EEPROM data memory of 1kb and it has SRAM data memory of 2kb.

• It has 23 I/O pins and it has 2 timers: two 8 bit/ one 16 bit.

• Its communication protocol is USART.

2) RFID Reader:

The RFID reader used in this system is EM-18. It continuously emits radio frequency waves. The RFID reader consists of mainly three parts: signal generator, a receiver, and a microcontroller. The signal generator is used to generate the radio waves and transmits it using an antenna. The receiver is used in order to receive the feedback signal from the tag.





Fig: RFID Reader

3) RFID Tags:

RFID tags are usually embedded or attached to the products. These tags consists of a transponder and a rectifier. The transponder receives the radio waves from the reader and sends the feedback signal back to the reader, they rely on the radio waves from the reader. The rectifier is the place where the energy is stored across the capacitor, this energy is used as the power for the controller and memory.

ISSN No: 2348-4845
International Journal & Magazine of Engineering, Technology, Management and Research
A Peer Reviewed Open Access International Journal

There are three types of RFID tags. They are: Active, Passive, and Semi-Passive.

Active tags: They have their own power supply, transmit the signal to reader also they rely on own supply. Hence, the range is less.

Passive tags: They have no power supply on their own and thus, uses RFID reader as source of the energy. Hence, it is compact. It is of low cost.

Semi-passive: They have their own power supply but for transmission of data to the reader, they rely on the reader.

These tags are available in any shape or size, like, a keychain, label, or as a credit card.



Internal structure of RFID tag



RFID tags

4) Load cells:

A Load Cell is a type of transducer, specially a force transducer which converts one form into other such as tension, compression, pressure into electrical signal. These are mainly used for weighing purpose in an industrial process. Load cells are also used to test monitor, and run industrial machinery, medical devices, aircraft loads and many other applications.

Types:

1. Pneumatic
2. Hydraulic
3. Strain gauge
4. Capacitance

Specifications:

1. Non-linearity
2. Hysteresis
3. Operating temperature range
4. Combined error



Fig: Load cell

5) LCD Display:

A Liquid-Crystal Display is a flat panel display. LCDs are used to display preset words, digits, seven segments as in a digital clocks. The LCD is of size 16*2. Each block has its own Id. Pneumatic liquids or crystals are present in each block of the LCD. The LCD has HD44780 microprocessor in it.

Applications:

- LCD televisions
- Computer monitors
- Instrument panels
- Watches

ISSN No: 2348-4845
International Journal & Magazine of Engineering, Technology, Management and Research
A Peer Reviewed Open Access International Journal

• Digital cameras
• Calculators
• Mobile telephones

6) RF Module:

The RF module is a new generation multi-channel wireless module. It is a wireless transceiver which uses a half-duplex mode of communication. There are 100 channels, which helps us to change the transmission frequency according to the channel used.

Features:

• Maximum transmission power is 100mW.
• Baud rate is of 5000bps.
• Transmits up to 1000mts.

Applications:

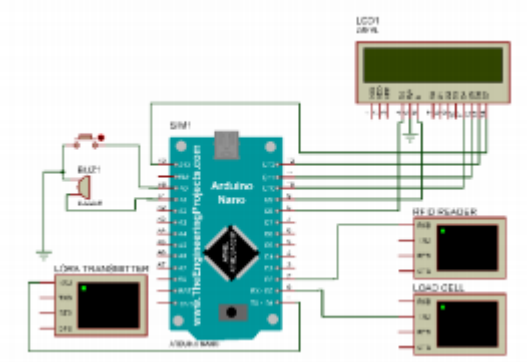
• Wireless sensor
• Robot wireless control
• PC wireless networking
• Automatic data acquisition.



Fig.: RF Module

5. DESIGN AND WORKING OF THE CART

The cart consists of a microcontroller which stores the data that is required to make it work. As this system is an embedded system, the software also plays a vital role. The microcontroller is connected to the RFID reader, LCD display, and RF module (LORA), Load cell and a buzzer.



The circuit diagram of the smart billing system is as shown above. The microcontroller comprises of a memory where the code is actually stored and the peripherals of it are connected to the other components of the smart billing system. The transmitter of the microcontroller is connected to receiver of the RF module, the transmitter of the load cell is connected to the receiver of the microcontroller. This helps us to make a communication path between these components.

When a product is dropped the RFID reader which continuously emits the radio waves will start detecting the product as they are embedded with the RFID tags. Once they are detected, the information is passed over the microcontroller which actually contains the name, price, weight etc., of the product and thus it gets displayed on the LCD. If there is any difference in weight between the scanned and unscanned products dropped into the cart, the buzzer helps us to know about this by turning on.

As the price gets added or deducted once the product is dropped or removed from the cart, the billing gets done at the cart itself. This helps us by reducing the time at the billing

ISSN No: 2348-4845
International Journal & Magazine of Engineering, Technology, Management and Research
A Peer Reviewed Open Access International Journal

counter from standing in the long queues and thus one can pay ones money at the counter.

6. ALGORITHM

Step 1: Start
Step 2: Initialize the system
Step 3: Swipe the RFID tag
Step 4: Check the RFID tag
Step 5: Read the related data from the memory
Step 6: Display data on the LCD
Step 7: Add product cost as the products are added
Step 8: Click the final button once the purchase is done
Step 9: Buzzer turns on when there is a mismatch of the weight
Step 10: Check the products and if needed re-insert them after scanning
Step 11: The total price gets displayed
Step 12: Stop

7. THE SMART CART – FINAL RESULT









ISSN No: 2348-4845
International Journal & Magazine of Engineering, Technology, Management and Research
A Peer Reviewed Open Access International Journal

8. CONCLUSION

Here, we have demonstrated a method for billing of products which is efficient, easier and faster. This smart trolley has a feature of calculating mechanically and displays the entire cost of all the products in the trolley. This makes simple for the customer to understand and also to pay amount during shopping which is displayed on LCD and also saves time without standing in the queue for hours.

In the supermarket the proposed model is easy to use, low cost and does not require any special training. This model keeps an account and uses the existing development and various types of radio frequency identification and detection technologies which are used for item recognition, billing and inventory update. As the whole system is becoming smart, the requirement of manpower will decrease. Theft in the mall will be controlled using this smart system.

Hence by using RFID based smart billing system, the shopping can be made easy for the customers as it is low cost and does not need any special training and also saves time.

9. FUTURE SCOPE

• In future we can look forward to implement in the shopping malls using a long range RFID reader with a range of 2 meters.
• Security can be improved by counting the number of items or placing weight sensors within the cart for tallying the weight and getting all the types of product names when cart is passed through a particular aisle using camera module.
• Multiple RFID tags can be read using a single RFID reader for more number of products which are added in the cart.
• Net banking can be included.
• Robotic ARM may be used for selecting and dropping of the product.

10. REFERENCES

[1] Dr. Suryaprasad J, Praveen Kumar B O, Roopa D & Arjun A K "A Novel Low-Cost Intelligent Shopping Cart", 2014 IEEE.
[2] Amine Karmouche, Yassine Salih-Alj, "Aisle-level Scanning for Pervasive RFID-based Shopping Applications", 2013 IEEE.
[3] Anon., 2017 Arduino-Wikipedia. [Online] https:en.wikipedia.org/wiki/Arduino
[4] RFID Technology. https://www.abr.com/what-is-rfid-how-does-rfid-work/
[5] Load Cell https://www.google.com/amp/s/instrumentationtools.com/load-cell-workingprinciple/amp

JETIR.ORG ISSN: 2349-5162 | ESTD Year : 2014 | Monthly Issue
JOURNAL OF EMERGING TECHNOLOGIES AND INNOVATIVE RESEARCH (JETIR)
An International Scholarly Open Access, Peer-reviewed, Refereed Journal

Design of Linear Antenna Array for Smart Antenna using Whale Optimization Algorithm

[1]Mr. Kandrapu Rajesh Kumar, [2]Lalem Sai Manisha, [3]Bharatula Yashwanti Vardhani, [4]Burramsetty Sri Lakshmi Yamini, [5]Khusabu Kumari
[2,3,4,5]Students, Dept. of ECE, Dr. Lankapalli Bullaya College of Engineering, Visakhapatnam, AP, India.
[1]Assistant Professor, Dept. of ECE, Dr. Lankapalli Bullaya College of Engineering, Visakhapatnam, AP, India.

ABSTRACT

The WOA is a new metaheuristic optimization algorithm and this technique is used for solving optimization problems. WOA has been designed to solve single-objective optimization problems. It mimics the hunting behavior of humpback whales. The inspiration results from the fact that a whale recognizes the location of a prey (i.e., optimal solution) by swimming around the prey within a shrinking circle and along a spiral-shaped path simultaneously. This algorithm includes three operators to simulate the search for prey, encircling prey, and bubble-net foraging behavior of humpback whales. An overview of WOA is described in this paper, rooted from the bubble-net hunting strategy, besides an overview of WOA applications that are used to solve optimization problems in various categories. The best solution has been determined to make something as functional and effective as possible through the optimization process by minimizing or maximizing the parameters involved in the problems. In this whale optimization algorithm, the parameters such as Amplitude, Position and Phase are used to determine the fitness function.

1. Introduction:

An antenna is defined as usually metallic device (as a rod or wire) for radiating or receiving radio waves. In other words, the antenna is the transitional structure between free-space and a guiding device. The guiding device or transmission line may take the form of a coaxial line or a hallow pipe(waveguide), and it is used to transport electromagnetic energy from the transmitting source to the antenna or from the antenna to the receiver. In the former case, we have a transmitting antenna and, in the latter, a receiving antenna.

An **antenna array** is a group of isotropic radiators such that the currents running through them are of different amplitudes and phases. These are radiators of electromagnetic frequency and energy. Antenna arrays are the solution to the problem defined as the limitations of operating a single antenna. An example of the problem is that although a dipole antenna allows for better control of direction than an isotropic (Omni-directional) antenna - as the length of the dipole increases, the control of direction decreases. Hence control by changing the length

of a single antenna is very limited. Greater flexibility and control can be obtained for directing the beam with an arrangement of multiple radiators.

The radiation pattern of a single element is relatively wide, and each element provides low values of directivity (gain). In many applications it is necessary to design antennas with high directive characteristics (very high gains) to meet the demand of long-distance communications. This can be accomplished by increasing the electrical size of antenna.

Enlarging the dimensions of single elements often leads to more directive characteristics. Another way to enlarge the dimensions of antenna, without necessarily increasing the size of the individual elements, is to form an assembly of radiating elements in an electrical and geometrical configuration. The new antenna, formed by multi-element, referred to as an array. In most cases, the elements of an array are identical.

2. Types of antenna arrays

There are a few different general types of antenna arrays.

2.1 Linear array - antenna elements arranged along a straight line. The array consists of N elements with a spacing of *d* between the elements. The output of each element is weighted by a factor of a_k and the results summed to form the signal out of the antenna.

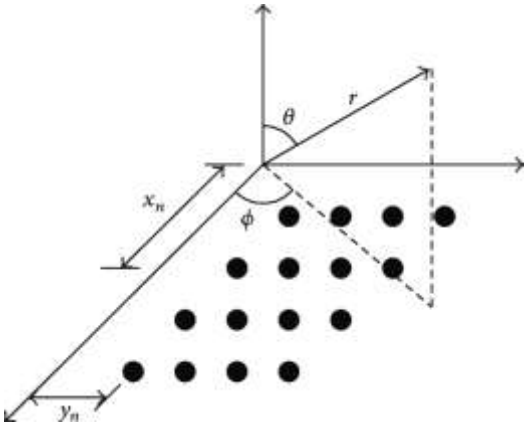
Application of Linear Array

1. Adaptive linear arrays are used extensively in wireless communication to reduce interference between desired users and interfering signals.
2. Many linear arrays spaced parallel on the common plane create a planar array antenna. These are used in mobile radar equipment.
3. The linear array is most often used to generate-a fan beam and is useful where broad coverage in one plane and narrow beam width in the orthogonal plane are desired.
4. Linear arrays can be made extremely compact and are therefore very attractive for shipboard applications.

2.2 Planar array - We now want to extend the results of linear arrays to planar arrays. In a planar array the antenna elements are located on some type of regular grid in a plane. Antenna elements arranged over some planar surface (example - rectangular array).

Applications

1. Radar
2. Smart antennas
3. Modem communication
4. Radio astronomy
5. Telemetry.



2.3 Circular array - antenna elements arranged around a circular ring. A circular array is high side-lobe geometry. If the distance of array elements is decreased to reduce the side lobes, the mutual coupling influence becomes more significant.

APPLICATION:

1. Span radio direction finding
2. Air and space navigation
3. Underground propagation
4. Radar
5. Sonar

3. Array Optimization

3.1 Linear antenna array optimization

In order to minimize the maximum SLL, the following fitness function is used:

Minimize $f_{itt} = \max\{20\ log|AF(\emptyset)|\}$

Subject to $\emptyset\ \epsilon\ [0, \emptyset_n]$ (3.1)

where $[0, \emptyset_n]$ is the side lobes region which depends on the number of elements. Here, it is chosen as $[0, 70^0]$ and $[0, 80^0]$ for 10 and 16 elements LAAs, respectively. Three optimization cases will be considered; optimizing elements amplitudes, optimizing elements positions, optimizing elements phases.

3.2 Circular antenna array (CAA) optimization

Here, the objective is to design a CAA with deep nulls in the directions φ*nu1* and φ*nu2* which define the first null beam width (FNBW) while minimizing the side lobes levels.

Thus, the following fitness function is used:

$$\text{Fitness} = (W1F1 + W2F2)/|AF_{max}|^2$$

$$\text{F1} = |AF(\emptyset_{nu1})|^2 + |AF(\emptyset_{nu2})|^2$$

$$\text{F2} = \max\{|AF(\emptyset_{ms1})|^2, |AF(\emptyset_{ms2})|^2\} \quad (3.2)$$

where the two angles {φ*nu1*, φ*nu2*} define the major lobe, i.e., the first null beam width (FNBW) = φ*nu2*-φ*nu1*=2φ*nu2*. φ*ms1* and φ*ms2* are the angles where the maximum side lobe level is attained during the optimization process in regions (from -180 to φ*nu1*) and (from φ*nu2* to 180), respectively. An increment of 1o is used in the optimization process

4. WHALE OPTIMIZATION ALGORITHM

4.1 Whale Optimization History

In order to solve Optimization problems in many fields swarm intelligence-based optimization algorithms have attracted much attention in recent years.

The whale Optimization algorithm (WOA) is a new type of swarm intelligence optimization algorithm proposed by Mir Jalili and Lewis in 2016 which is inspired by the unique predation behaviour of humpback whales. Whale optimization is a population-based method.

4.1 WHALE BEHAVIOUR

Whales are the biggest mammals on the earth. It is one of the larger rorqual species. One of the biggest baleen whales is humpback whales (Megaptera novaeangliae). Whales mostly live-in groups and they even can develop their own dialect.

It includes 3 operations to simulate:

(a) Search for prey, (b) Encircling prey and (c) Bubble-net feeding behaviour.

WOA is mainly used to solve the target problems of the antenna by imitating whales' predatory behaviour. bubble-net feeding is a unique behaviour that can be observed only in humpback whales.

In this work the spiral bubble-net feeding manoeuvre is mathematically modelled in order to perform optimization.

4.2 Whale Optimization Algorithm

The WOA is developed by the foraging behaviour of the humpback whales to search fishes near the surface via creating typical bubbles along a circle. In WOA the current best solution of the individual whale is the target prey. First, the best agent is defined and then the positions of other agents will be updated in the direction of the best agent. The mathematical representation of this behaviour is as follows [16]:

$$D = |C.* X'(t) - X(t)| \text{ (1)} \qquad (4.1)$$

Where t = current iteration

A, C = coefficient vectors

X' = position vector of the best solution obtained and is updated in each iteration.

X = position vector

$.*$ = element by element multiplication

The vectors A and C are determined as follows:

$$A = 2a.* r - a \qquad (4.2)$$

$$c = 2.* r \quad (4.3)$$

Where 'a' decreases linearly from 2 to 0 throughout the iterations and 'r' is a random vector in [0, 1]. The position vector X is updated by either shrinking encircling mechanism or by the spiral mechanism depending on the value of 'p', a random number in [0, 1]. When the value of 'p' is less than 0.5, the shrinking mechanism is adopted and the mathematical equation is expressed as

$$X(t+1) = X'(t) - A.* D \quad (4.4)$$

On the other hand, when 'p' is greater than or equal to 0.5 the spiral method is adopted using the equation

$$X(t+1) = D'.* e^{bl}.*cos\ cos(2\pi l) + X'(t) \quad (4.5)$$

Where $D' = |X'(t) - X(t)|$

b= a constant defining logarithmic spiral

l= random number in [-1 ,1]

The steps adopted by the WOA algorithm are as follow:

1. Initialize X_i , i=1, 2, …… n, as the whale population

2. Find the fitness value of an individual agent. Let X' be the best agent

3. In each iteration update a, A, C, l and p for each agent. If p is less than 0.5 and also $|A| < 1$, considering the equation (1) update the location of the present agent. Else if $|A| > 1$, get an agent randomly as $X_{rand}$and update the present agent's position by the equation

$$X(t+1) = X_{rand} - A.* D \quad (4.6)$$

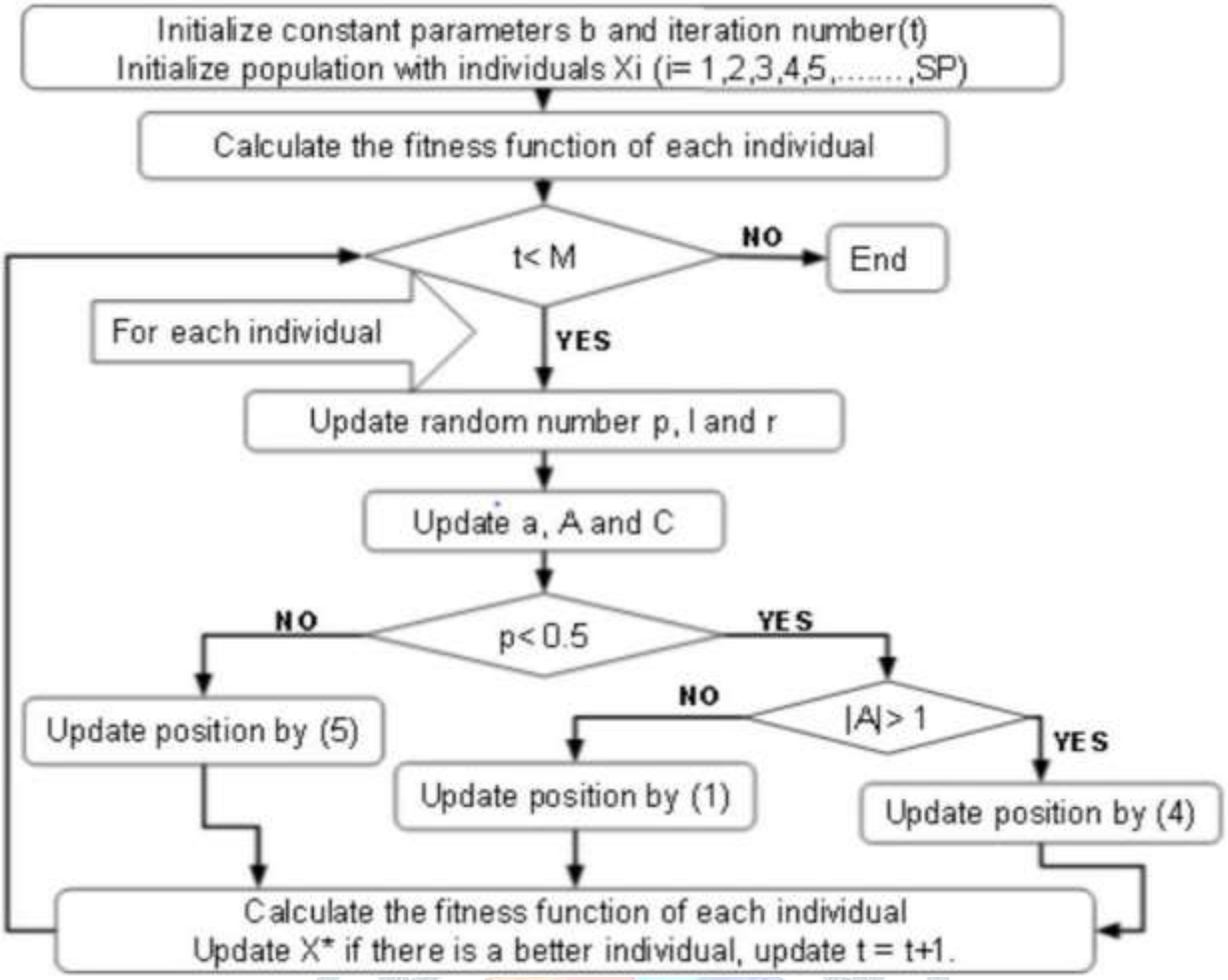
4. If p is greater than or equal to 0.5, then update the current position by equation (5)

5. Amend the agent if it goes beyond the search space. Calculate fitness of each agent.

6. If there arise a better solution, then update X'.

7. Go back to step 2.

4.3 WOA FLOW CHAT



4.4 WOA APPLICATIONS

1. It is used for getting the Radiation Pattern of an array.
2. It is used in Feature Selection.
3. It is used in Multi-objective Optimal Mobile Robot Path Planning.
4. It is used in Multi-objective Optimal Vehicle Fuel Consumption.
5. It is used in Skeletal Structures.
6. It is used in Image Segmentation.

However, since then this perspective has been expanded to include optimality.

5. RESULTS

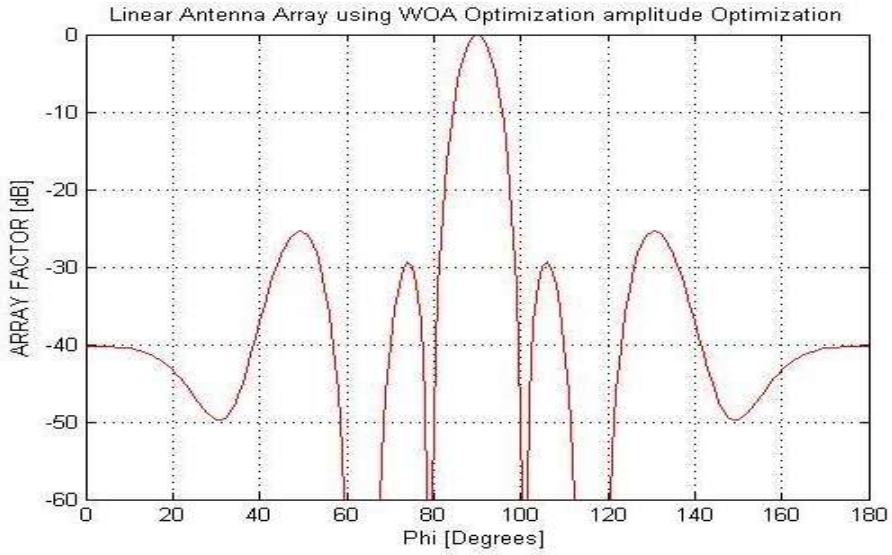
5.1.1 Optimizing elements amplitudes (I_n)

5.1.1(a) 12 elements LAA

Using the fitness function associated with the array factor for 12 elements, the linear array is optimized using the WOA method (population size=50, number of iterations=10). Table In shows the optimum amplitudes obtained using the WOA. The maximum sidelobe levels obtained using the WOA is –25.372 db. WOA results are slightly better than other methods.

N	1	2	3	4	5	6
In	0.8368	0.7268	0.4543	0.6065	0.4521	0.3953

Table 5.1. 1 (a) 12 elements LAA Optimizing elements amplitude



5.1.1 (a) 12 element LAA Optimizing elements amplitudes

5.1.1(b) 16 elements LAA

In this example, a 16-element LAA is optimized using the WOA method (population size=50, number of iterations=10). The best results are listed in Table II. Figure 4 shows the radiation pattern obtained by WOA. The maximum SLL obtained using WOA method is -29.160 db.

N	1	2	3	4	5	6	7	8
In	0.9746	0.2889	0.9936	0.2231	0.6776	0.1192	0.2071	0.2643

5.1.1(b) 16 elements LAA Optimizing elements amplitudes

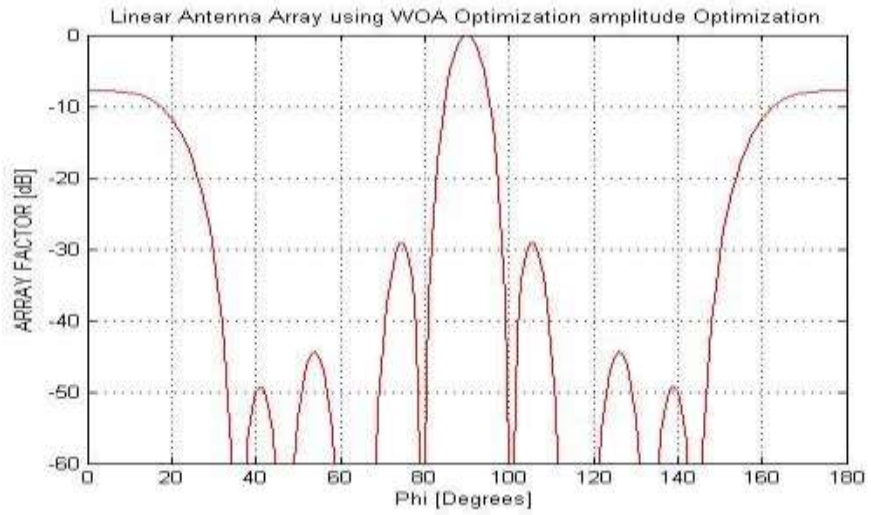


Figure 5.1.1(b) 16 elements LAA Optimizing elements amplitudes

5.1.2 Optimizing elements positions (x_n)

In order to optimize the element positions in the LAA by the WOA, the element amplitudes and the element phases are fixed as In =1 and φ_n=0 for $n=1 \ldots N$.

a) 18 ELEMENT LAA

The optimized positions obtained using the WOA (population size=50, number of iterations=10), while Figure 5 shows the obtained array factor. The maximum SLL obtained by WOA method is -35.746 dB.

N	1	2	3	4	5	6	7	8	9
Xn	0.0866	0.3496	0.3696	0.5075	0.8431	0.9318	1.2413	1.3580	1.5467

Table 5.1.2(a) 18 Element LAA Optimizing elements positions

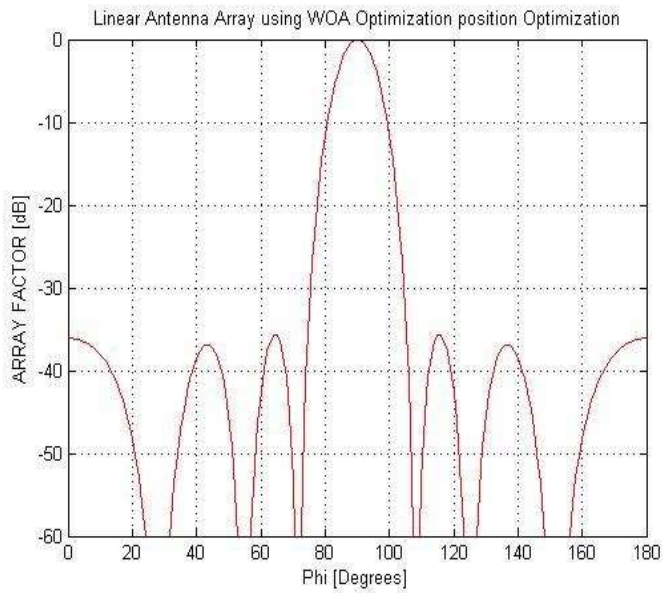


Figure 5.1.2 18 Element LAA Optimizing elements positions

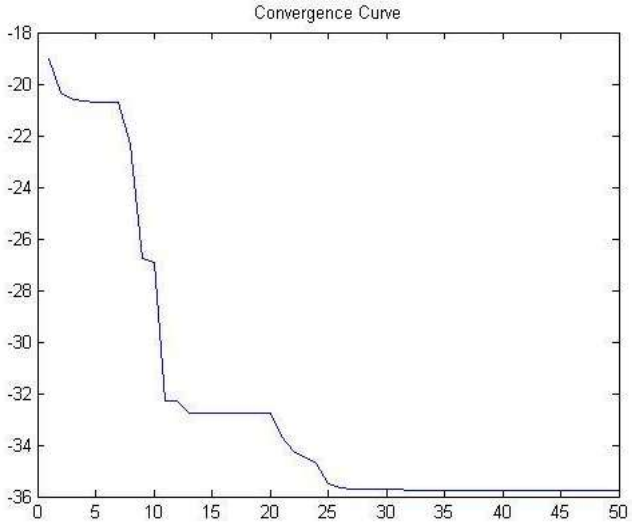


Figure 5.1.3 18 Element LAA Convergence Curve

b) 20 ELEMENT LAA

The optimized positions obtained using the WOA (population size=50, number of iterations=10),while Figure shows the obtained array factor. The maximum SLL obtained by WOA method is -36.951 dB.

N	1	2	3	4	5	6	7	8	9	10
Xn	0	0.1449	0.3085	0.4429	0.5473	0.7655	0.8133	0.9286	1.0388	1.3808

Table 5.1.2(a) 18 Element LAA Optimizing elements positions

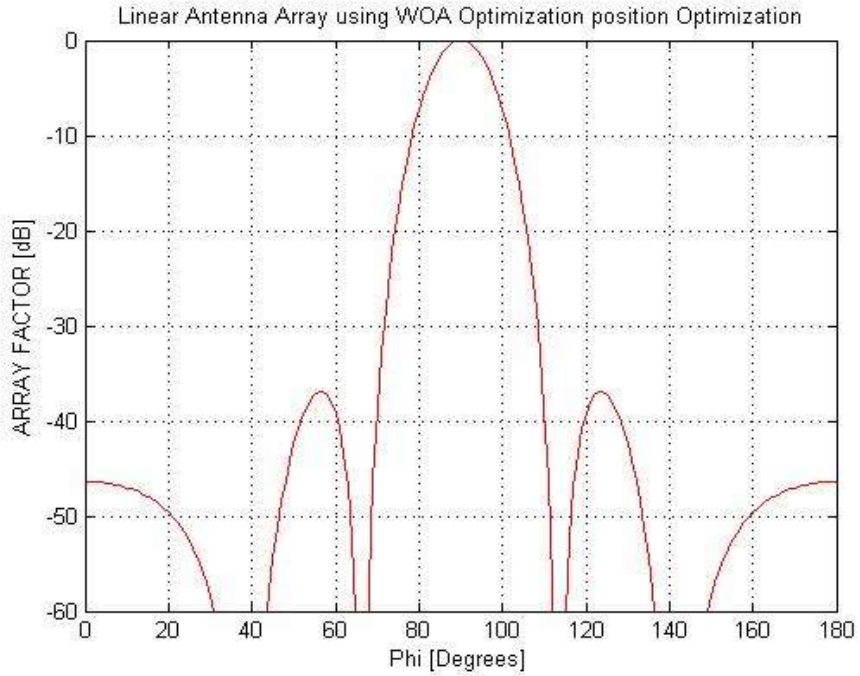


Figure 5.1.2 18 Element LAA Optimizing elements positions

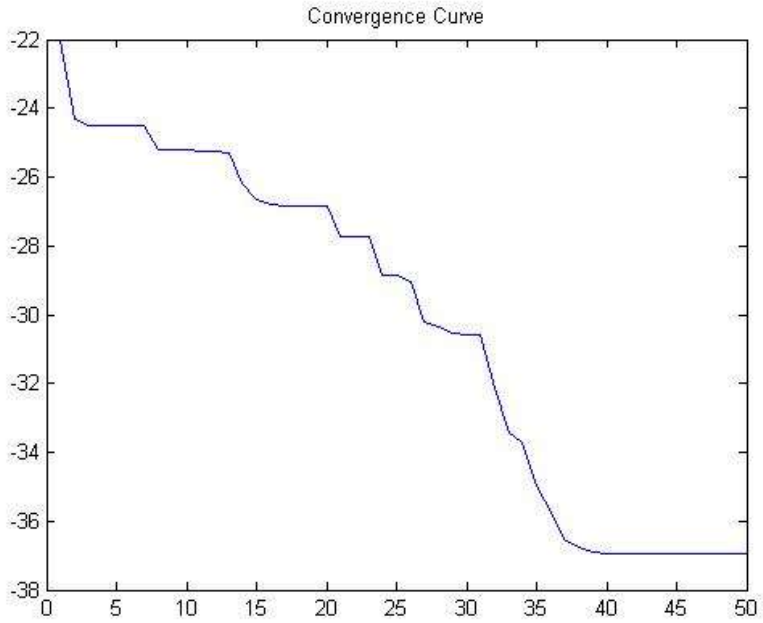


Figure 5.1.3 18 Element LAA Convergence Curve

5.1.3 Optimizing elements phases (φn)

Here, WOA method will be applied on a 26-element LAA to provide a beam-steering pattern with the main lobe in the direction of 45 degrees by optimizing the element's phases.

The phases of the element are assumed to be symmetric as φn =φ-n for *n=1, 2, …… N*, where φn is the phase of the *n* th element.

Table IV shows the optimum phases (in degrees) for 26 elements array using WOA method without nulls (population size=50, number of iterations=10) and beam-steering pattern with main lobe in the direction of 45 degrees by optimizing the element's phases.

5.1.3(a) 26 element LAA

The optimized positions obtained using the WOA (population size = 50, number of iterations = 10) where the number of elements is 26. The maximum SLL obtained by WOA method is -26.587 dB Figure 6 shows the radiation pattern obtained by WOA.

Method	Element wise phases
WOA	272.0521, 306.9103, 92.9872, 185.1558, 225.6845, 313.7484, 253.7998, 26.3113, 24.1070, 265.6433, 344.9554, 43.5846, 19.4335

5.1.3(a) 26 Element LAA Optimizing elements phases

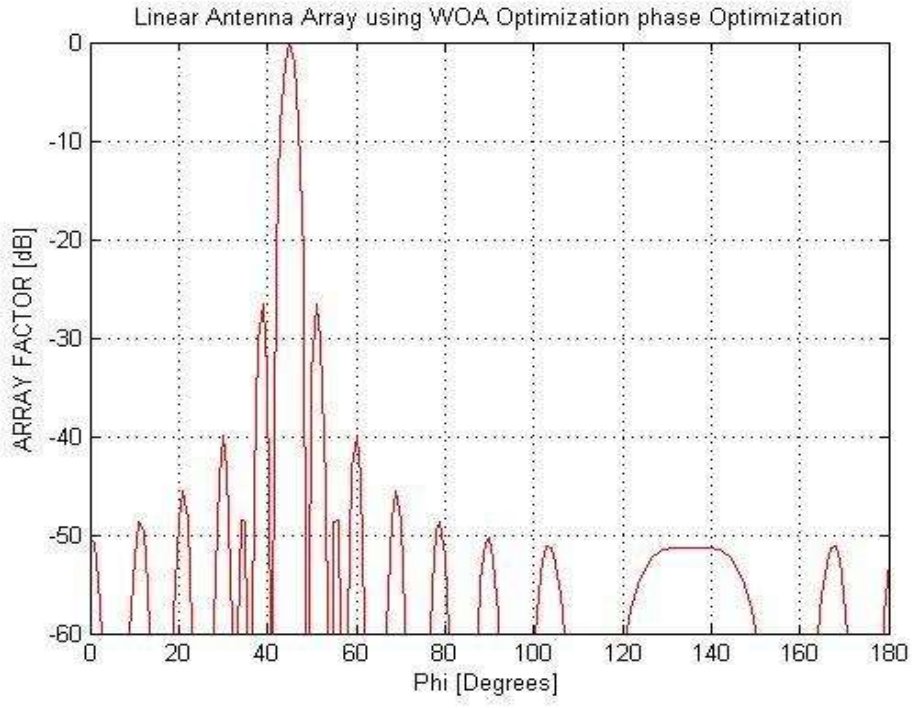


Figure 5.1.3(a) 26 Element LAA Optimizing elements phases

6. CONCLUSION

WOA is a new technique in electromagnetics optimization. It was applied on the optimization of antenna arrays. Three cases of linear array design have been considered; amplitudes optimization, positions optimization and phases optimization. WOA results have been very good algorithm and its results are as good as those obtained using other well-developed methods.

This optimization technique is very effective and put into practise for other array antenna of shapes like circular, elliptical, concentric circular etc

The Whale optimisation algorithm has given better results as compared to the other well-developed algorithms.

REFERENCES

[l] K.Rajesh Kumar, S. Aruna, K. Srinivasa Naik, Side Lobe Reduction of a Concentric Circular Antenna Array using Genetic Algorithim(GA) and Particle Swarm Optimization(PSO). IJEIT ISSN: 2277-3754 ISO 9001:2008.

[2] Vennapu. Krishna Tulasi, K. Rajesh Kumar, Dr. Vennapu. Lakshmana Rao Design of Linear and Circular Antenna Array for Side Lobe Reduction Using the Method Moth Flame Optimization Algorithm Visakkapatnam,2019 IJSEAS ISSN: 2395-3470.

[3] S. C. Swales, M. A. Beach, and D. J. Edwards, "Multi-Beam Adaptive Base- Station Antennas for Cellular Land Mobile Radio Systems," 39th IEEE Vehicular Technology Conference, Vol. 1, pp. 341-348, 1989.

[4] S. C. Swales, M. A. Beach, D. J. Edwards, and J. P. McGeehan, "The Performance enhancement of Multibeam Adaptive Base-Station Antennas for Cellular Land Mobile Radio Systems," IEEE Transactions on Vehicular Technology, Vol. 29, No. 1, pp. 56-67, February 1990.

[5] S. P. Stapleton and G. S. Quon, "A Cellular Base Station Phased Array Antenna System," 43rd IEEE Vehicular Technology Conference, pp. 93-96, 1993.

[6] G. V. Tsoulos, M. A. Beach, and S. C. Swales, "Application of Adaptive Antenna Technology to Third Generation Mixed Cell Radio Architectures," 44th IEEE Vehicular Technology Conference, Vol. 1, pp. 615-619, 1994.

[7] U. Forsse'n, J. Karlsson, B. Johannisson, M. Almgren, F. Lotse, and F. Kronestedt, "Adaptive Antenna Arrays for GSM900/DCS1800," 44th IEEE Vehicular Technology Conference, Vol. 1, pp. 605-609, 1994.

[8] T. Ohgane, "Spectral Efficiency Evaluation of Adaptive Array Base Station for Land Mobile Cellular Systems," 44th IEEE Vehicular Technology Conference, Vol. 3, pp. 1470-1474, 1994.

[9] W. C. Y. Lee, "Applying the Intelligent Cell Concept to PCS," IEEE Transactions on Vehicular Technology, Vol. 43, No. 3, pp. 672-679, August 1994.

[10] J. H. Winters, J. Salz, R. D. Gitlin, "Adaptive Antennas for Digital Mobile Radio," Proc. IEEE Long Island Section Adaptive Antenna Systems Symposium, pp. 81-86, Long Island, NY, Nov. 19, 1992.

[11] J. Kennedy and M. C. Sullivan, "Direction Finding and 'Smart Antennas' Using Software Radio Architectures," IEEE Communications Magazine, pp. 62-68, May 1995.

[12] R. Kohno, H. Imai, M. Hatori, and S. Pasupathy, "Combination of an Adaptive Array Antenna and a Canceller of Interference for Direct-Sequence Spread-Spectrum Multiple-Access System," IEEE JSAC, Vol. 8, No. 4, pp. 675-682, May 1990.

[13] S. Anderson, M. Millnert, M. Viberg, and B. Wahlberg, "An Adaptive Array for Mobile Communication Systems," IEEE Transactions on Vehicular Technology, Vol. 40, No. 1, pp. 230-236, February 1991.

[14] V. A. N. Barroso, M. J. Rendas, J. P. Gomes, "Impact of Array Processing Techniques on the Design of Mobile Communication Systems," Proc. 7th Mediterranean Electrotechnical Conf. - MELECON, Part 3/3, pp. 1291-1294, 1994.

[15] G. Xu, H. Liu, W. J. Vogel, H. P. Lin, S. S. Jeng, and G. W. Torrence, "Experimental Studies of Space-Division-Multiple-Access Schemes for Spectral Efficient Wireless Communications," IEEE International Communications Conference, Vol. 2, pp. 800-804, 1994.



Journal of Electrical Engineering & Technology (2021) 16:985–1002
https://doi.org/10.1007/s42835-020-00629-w

ORIGINAL ARTICLE

Electric Field Stress in a Three Phase Common Enclosure Gas Insulated Busduct with FGM Post Type Spacer and Reduction with Metal Inserts

Polamraju V. S. Sobhan[1] · Janaki Pakalapati[2] · Venkata Nagesh Kumar Gundavarapu[3] · Deepak Chowdary Duvvada[4] · Sravana Kumar Bali[5]

Received: 8 June 2020 / Revised: 3 November 2020 / Accepted: 3 December 2020 / Published online: 14 December 2020
© The Author(s) 2020

Abstract
The establishment of supporting insulators plays a vital role in the continuous operation of the three-phase Gas Insulated Busduct (GIB), which primarily depends on the distribution of electric field stress on the spacer surface. Shape control is a technique used along the spacer surface to achieve uniform field intensity, but this technique can also lead to very irregular shapes. The Triple Junction (TJ) is the region where the field stress has to be reduced. Over a period, high field stresses along the spacer surface will result in a surface flashover and thus de-energize the complete GIB, leading to enormous losses economically. In this paper, a Functionally Graded Material (FGM) spacer for a three-phase GIB has been designed with more number of gradings and further field stress at TJ is minimized by inserting and reshaping the metal inserts (MI) at the end of the enclosure. By doping them with different permittivity values, functionally graded materials are spatially distributed with multiple filler materials to achieve uniform stress on the electric field. Simulation is carried out with the FGM and epoxy (post type) Spacers for different voltages and FGM gradings. With MI, the stress is minimized and an enhanced uniform field allocation along the surface is obtained.

Keywords Functionally graded material (FGM) · Post type spacer · Electric field distributions · Dielectric materials · Insulators · Gas insulated substations · Triple junction · Enclosure · Electric field stress · Uniform field

List of symbols

$\vec{E}$	Field intensity
∇	Del
f	Scalar function
V	Potential
V_A, V_B and V_C	Voltage of conductor A, B and C
$\vec{D}$	Electric flux density
ρ_v	Charge density
ε	Permittivity of the insulating material
W	Energy stored

Abbreviations

GIB	Gas insulated busduct
FGM	Functionally graded material
TJ	Triple junction
MI	Metal insert
FEM	Finite element method
GL	Graded low
GH	Graded high
GU	Graded U-shape

✉ Venkata Nagesh Kumar Gundavarapu
gundavarapu_kumar@yahoo.com; drgvnk14@gmail.com

[1] Department of EEE, Vignan's Foundation for Science, Technology and Research, Guntur, Andhra Pradesh 522213, India

[2] Department of EEE, Lendi Institute of Engineering and Technology, Visakhapatnam, Andhra Pradesh 535005, India

[3] Department of EEE, JNTUA College of Engineering Pulivendula, Pulivendula, Andhra Pradesh 516390, India

[4] Department of EEE, Dr. L. Bullayya College of Engineering, Visakhapatnam, Andhra Pradesh 530013, India

[5] Department of EEE, GITAM University, Visakhapatnam, Andhra Pradesh 530045, India

1 Introduction

The Gas Insulated Busduct (GIB) is common because of its compactness, high reliability, low footprint, environmentally friendly and rapid growth in energy consumption and urbanization [1]. To meet the high electric demand, a three-phase GIB needs to emerge for practical implementation. For uninterruptible operations of GIB, the spacers'

performance has to be improved as it provides mechanical support to spacers. An appropriate design of spacers has to be chosen to overcome its failures due to several defects under various operating conditions. An appropriate method has to be implemented to identify the defects of insulators with impulse voltages to reduce the electric field intensity due to these failures [2–4]. Some reviewers [5, 6] has reviewed that the solid spacers provide the conductors and the enclosure with mechanical support. The distribution of electric fields in the spacer contributes to spacer failures. The existence of these solid insulators contributes to the inappropriate distribution of electrical fields distressing the complete GIB, in particular, because of unavoidable defects such as delamination, void, conductive particles etc.

In literature, several authors studied on the electric field intensity in GIB and its reduction in various insulators like a cone, disc type lost their dielectric strength due to insulator contamination. However, the above types of spacers have found to be more complicated. In addition to this, Zihao Guo et al. [7] have reviewed that the transmission capability of the gas-insulated transmission line (GIL) increases with the improvement of dielectric and mechanical strengths of GIL insulators. This happens due to uniform electric field distribution and the decrease of surface flashover strength. The surface charge accumulation in compressed SF_6 gas-insulated devices create major problems like surface flashover, dielectric failures during manufacturing, installation, and operation process [8–10]. Muneaki Kurimoto et al. [11] identified that the power equipment in GIB can be compact based on the field distribution around the spacer. Further, this is achieved by using the GU-FGM technique with an efficient method called ε-FGM at the junction of the electrode surface and solid dielectrics i.e. at TJ's to maintain the uniform field. In this context, Du et al. [12] has recognized different methods of grading the FGM spacers, like ε FGM, σ FGM, (ε /σ) FGM and frequency variation method for the design of cone type spacers. Ju et al. [13] studied that FGM was used as an insulator by varying the permittivity of FGM. The concentration of the Electric field can be decreased at the specific region by replacing the grounded round electrode with elliptical FGM spacer. Consequently, the electrical field near TJ of the enclosure end is reduced. Naoki Hayakawa et al. [14] recognized this new technique of FGM, uses permittivity distribution as a controlling factor for the field distribution in GIB spacers. As a result, it has given good results for the FGM at various special distributions both in fabrication and simulation approaches. However, this is implemented in the design of a single-phase gas-insulated busduct. Naoki Hayakawa et al. [15] have observed ε FGM as the efficient method for reducing the field stress over the length of the spacer. Zhaoyu Ran et al. [16] proposed a simplified design of an insulator with a surface graded functional material (SFGM) to suppress electric distortion at the triple junction of the superconducting gas-insulated transmission line(S-GIL) by using FEM. The focus on modelling of the proper spacer has made by Zhenlian et al. [17] and reviewed the performance of Electric parameters of unfilled epoxy insulators to improve it by using alumina filled epoxy composites in SF_6 gas-insulated systems.

In spite of this Lin Liu et al. [18] observed TJ as the weakest part in gas-insulated systems with complexity in the physical process affected by flashovers. In particular, Chakravorti et al. [19], has stated that with some efforts are needed to develop uniform field intensity at Triple Junctions (TJ's) which capable by incorporating metal insert. Several authors [20, 21] have considered a technique to minimize electrical field stress by incorporating the metal insert, which could reduce the electrical field successfully near the triple junction of the spacer. Estimations have been made on epoxy spacers, spacers with an imperfection at the TJ comes about unmistakably demonstrated that metal supplements moved the most extreme field to the mid hole locale. In addition, metal supplements have been found to provide good TJ protection, if the elevated stress remains below the allowable level.

Imai et al. [22, 23] developed a new technology with FGM for the design of insulation materials by tailoring two kinds of epoxy-based resins with different relative permittivities for cone type spacers. Du et al. [24, 25] has introduced a new concept of surface functionally graded material by depositing $BaTiO_3$ on the insulator surface to have a uniform field distribution. To improve HVDC gas-insulated lines, the fabrication technique under the deposition of ZnO films by a magnetron sputtering method is used. In another study, the investigation of numerical methods for the computation of the Electric field using Laplace's equation and Poisson's equation is flexible rather than an analytical approach by using one of the numerical methods like FEM. However, FGM technique the grading with epoxy spacer at different permittivity values is done by using FEM analysis [26–28].

Many researchers have worked on the above aspects for only single-phase Gas Insulated Substations. The FGM spacer is a modern technique, which is used by modulating the permittivity values to decrease the electric field strength. The FGM spacer is a modern technique, which is used by modulating the permittivity values to decrease the electric field strength. By using this grading technique with a proper range of permittivity, the field pressure can be decreased at the appropriate location. It is anticipated to extend these concepts of FGM spacer, computation of electric field in the design of three-phase GIB. By using FGM spacer, uniform electric field intensity can be achieved all over the spacer. The electric field intensity on the FGM spacer can be minimized by using Metal Inserts at Triple Junction.

In this paper, a detailed analysis has been done on a post/epoxy type spacer and FGM spacer in special

configurations like GL-FGM, GH-FGM, and GU-FGM in three-phase GIB. Simulation is done by constructing a three-phase GIB by assigning conductors and enclosures with appropriate charge conservation. After computing the designed model, the characteristics have been analyzed for electric field intensity at enclosure end at TJ of epoxy and FGM spacers. At the triple junction and conductor end, the electrical field strength produced by both the spacers is analyzed. The same procedure is applied for all ranges of permittivity for three conductors. The high electric field intensity is observed at TJ, a particular dimensioned MI is inserted at the enclosure end to reduce this effect.

2 Governing Equations of Three Phase GIB Using Fem Technique

The electrical field intensity of a three phase GIB is calculated by using Laplace's equation or poison's equation under boundary conditions applied to the common enclosure. The Laplace's equation is found to be simple and easy for proceeding with an analytical approach than Poisson's equation. Despite several numerical methods, FEM is identified as the most convenient method for simplifying complex problems. Here FEM is used to calculate the electrical field intensity over the spacer surface. The scalar electric potential is established for the electric field in electrostatic studies, for which Maxwell's first equation in differential form is reduced as

$$\nabla \times \vec{E} = 0 \tag{1}$$

From the properties of the field operators, we obtain

$$\nabla \times (\nabla f) = 0 \tag{2}$$

which establishes that the curl of the gradient of any scalar function (f) is identically null.

Thus, the electric field of Eq. (1) is a derivate of the gradient of a function called as electric potential function so that

$$\vec{E} = -grad(V) = -\nabla V \tag{3}$$

$$\text{Then} \quad \nabla \times (\nabla V) = 0 \tag{4}$$

$$\nabla \cdot \vec{D} = \rho_v \tag{5}$$

$$\vec{D} = \varepsilon \vec{E} \tag{6}$$

where $\varepsilon = \varepsilon_o \varepsilon_r$ is permittivity of the insulating material in Farad/ meter.

Equation (7) is obtained by substituting Eq. (6) in Eq. (5)

$$\nabla \cdot \vec{E} = \frac{-\rho_v}{\varepsilon} \tag{7}$$

$$\nabla \cdot (-\nabla V) = \frac{-\rho_v}{\varepsilon} \tag{8}$$

So the Eq. (8) can be cut down into Poisson's equation given by Eq. (9)

$$\nabla^2 V = \frac{-\rho_v}{\varepsilon} \tag{9}$$

At zero charge density, Eq. (9) can be cut down to Laplace's equation as represented in Eq. (10)

$$\nabla^2 V = 0 \tag{10}$$

3 Electric Field Computation

Finite Element Method is one of the boundary subdivision the method which usually have more reliable electric fields than domain subdivision methods (finite difference method and the binary element method). Galerkin's method is used as an optimization strategy to change the profile of the spacer. In order to render smooth operations of the post-type spacer is been streamlined by placing constraints on the column cross-sections of the spacer. Potential values can only be symmetric about the symmetry planes if the normal derivative of potential vanishes there. Thus the boundary-value problem to be solved consists of Fig. 1, subject to the boundary conditions for symmetry planes is given by

$$\frac{\partial V}{\partial n} = 0 \tag{11}$$

The well-known principle of minimum potential energy requires the potential V to distribute itself in the three-phase GIB in such a way as to minimize the energy stored. By using the Laplace Equation, in the steady-state electrostatics with a constant dielectric material, the electric energy stored is obtained by integrating it out over the whole two-dimensional problem region as shown in Eq. (12).

$$W = \frac{1}{2} \int_S \varepsilon (\nabla V \cdot \nabla V) dS \tag{12}$$

This minimum energy principle is mathematically equivalent to Laplace's equation, in the sense that a potential distribution and represented as

$$W = \frac{1}{2} \int_S \left(\varepsilon_x \frac{\partial^2 V}{\partial x^2} + \varepsilon_y \frac{\partial^2 V}{\partial y^2} \right) dxdy \tag{13}$$

By substituting Laplace's Equation in Eq. (12),

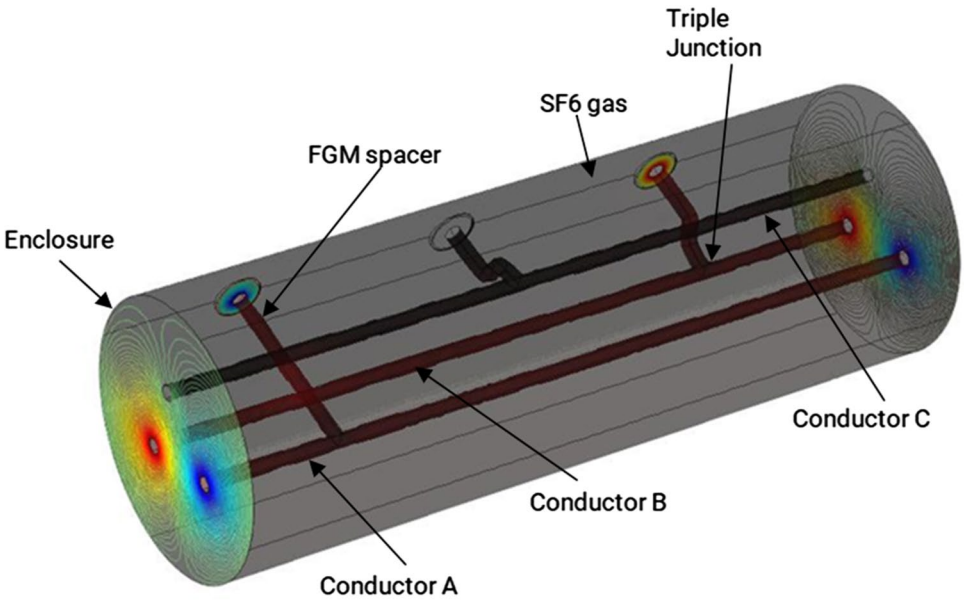


Fig. 1 Design model three phase GIB

$$dW = \frac{1}{2}\int_S \varepsilon\left(\nabla^2 V\right)dxdy = 0 \tag{14}$$

$$\text{Therefore} \quad dW = 0. \tag{15}$$

4 Post Type Functionally Graded Material Spacer

Post type spacers are one of the simplest insulators used in GIB when compared to other insulators like cone form, disc form spacers. This spacer is designed between the conductor end and the enclosure end, which is elevated perpendicularly. The distribution of the Electric field along the post type spacer is uniform under normal conditions and equal to the average field strength. The main drawback of the post type spacer is that it provides the shortest possible creeping distance in the event of a flashover between the live conductor and the outer enclosure as it with uniform permittivity. In the event of flashovers, the electric field distribution may be uneven due to high permittivity of spacer material than that of the surrounding gas. To reduce this electric field intensification along the interface surface, the relative permittivity of the spacer is redistributed across the spacer medium by using FGM technique. The FGM spacer with post type structure is designed with 20 equal gradings for all the three spacers as per lengths. The effect of FGM gradings is done by using GL, GH and GU for ranges of permittivity. The mathematical analysis of the Electric field has been calculated by using FEM as mentioned in the above section. The stepwise procedure for the simulation of the Post type FGM spacer is given below.

Step-1: The basic three-phase GIB model is designed with epoxy post type spacers on which the three conductors are mounted.

Step- 2: The three-post type spacers are graded into 20 equal gradings with dissimilar permittivity's as represented in Table 1 to generate uniform electrical field throughout the spacer length.

Step- 3: The above step 2 is repeated for different ranges of permittivity for Graded Low, Graded High and Graded U-shape FGM gradings.

In this paper, three distinct classes such as GL-FGM, GU-FGM and GU-FGM, are intended for the effectiveness of FGM. In GL- FGM the permittivity value is increasingly decreased from the end of the conductor to the end of the enclosure. Whereas the permittivity value in GH-FGM is gradually improved from the conductor to enclosure ends and in GU-FGM the permittivity value is gradually reduced from the end of the conductor to the middle of the FGM spacer and then gradually increased towards the end of the enclosure.

Table 1 Permittivity ranges of FGM post type spacer

Grading type	Permittivity ranges		
	Case I	Case II	Case III
GL-FGM	2.3 to 4.2	2.4 to 4.3	2.5 to 4.4
GH-FGM	2.5 to 4.4	2.4 to 4.3	2.3 to 4.2
GU-FGM	4.2 to 3.3 to 4.2	4.3 to 3.4 to 4.3	4.4 to 3.5 to 4.4

4.1 Graded Low-FGM (GL-FGM)

Permittivity at the conductor end is retained at high value and the enclosure end is steadily reduced as shown in Fig. 2. The permittivity range is taken to be a minimum value of 2.3 and a maximum value of 4.2. For three different cases with different ranges of permittivity, GL grading is preserved, as shown in Table 1. The equations pertaining to the case I, case II and case III of GL grading are $y = -0.1x + 4.3$, $y = -0.1x + 4.4$ and $y = -0.1x + 4.5$ respectively.

4.2 Graded High-FGM (GH-FGM)

Permittivity is retained at the conductor end at a low value and, as shown in Fig. 3, is steadily increased towards enclosure end. The range of permittivity shall be taken as a minimum value of 4.2 and a maximum value of 2.3. In three different cases, the GH rating is maintained with different allowability ranges as shown in Table 1. The equations pertaining to the case I, case II and case III of GH grading are, and respectively.

4.3 Graded U Shape-FGM

Permittivity is reduced as shown in Fig. 4 from high value to centre value and then the minimum value from the end of the conductor to the end of the enclosure. The permittivity range is taken from a high 4.2 to a 3.3 centre value and then increased to a 4.2. For three different cases, the GU grading is maintained by dissimilar permittivity ranges, as shown in Table 1. The equations pertaining to the case I, case II and case III of GH grading are $y = 0.009x^2 - 0.197x + 4.473y = 0.009x^2 - 0.197x + 4.573$ and $y = 0.009x^2 - 0.197x + 4.673$ respectively.

5 Results and Discussions

5.1 Model of Three- Phase GIB for Simulation

The simulation model for the three-phase gas-insulated busduct is taken with a radius of 225.5 mm of the enclosure with SF6 gas insulation and a relative permittivity of 1.0015. The three conductors are enclosed within a common enclosure each with 38.66 mm as the inner radius. The length of the spacer between the conductor A, B and C is considered to be 193.8 mm, 43 mm, and 193.8 mm respectively and 26 mm wide. The designed GIB is simulated by FEM analysis and its simulation model is as represented in Fig. 5 of which the spacer material is epoxy-alumina composite.

In the proposed model, all the conductors are placed at equidistant to each other and under balanced conditions inside the common enclosed GIB. Conductor A is applied with the root mean square voltage of V_A equal to 72.5 kV, 132 kV and 220 kV. The outer electrode is grounded to zero potential. The corresponding maximum voltage of three conductors to the considered root mean square voltage is shown in Table 2. Further, to create uniform electrical field intensity over the post type spacer, FGM technique is used for the above-mentioned dimensions of GIB.

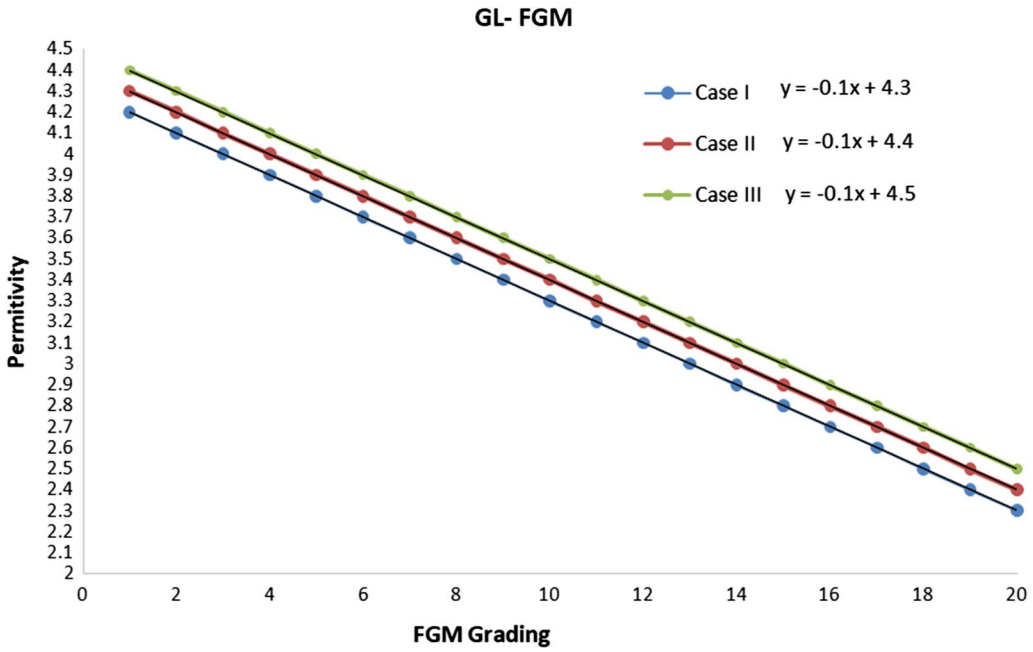


Fig. 2 Permittivity variation of graded low FGM

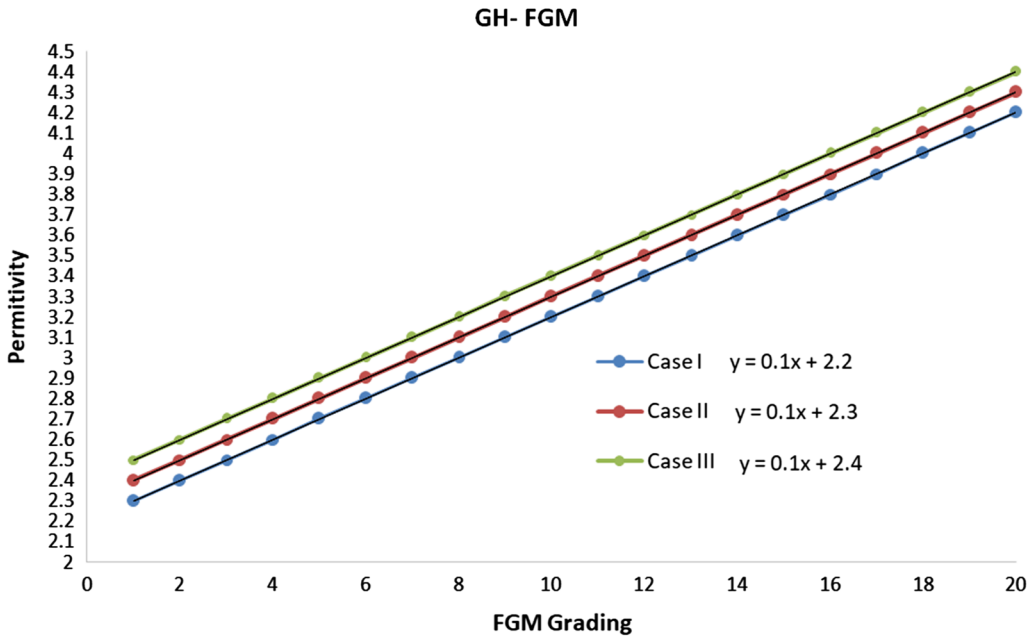


Fig. 3 Permittivity variation of graded high FGM

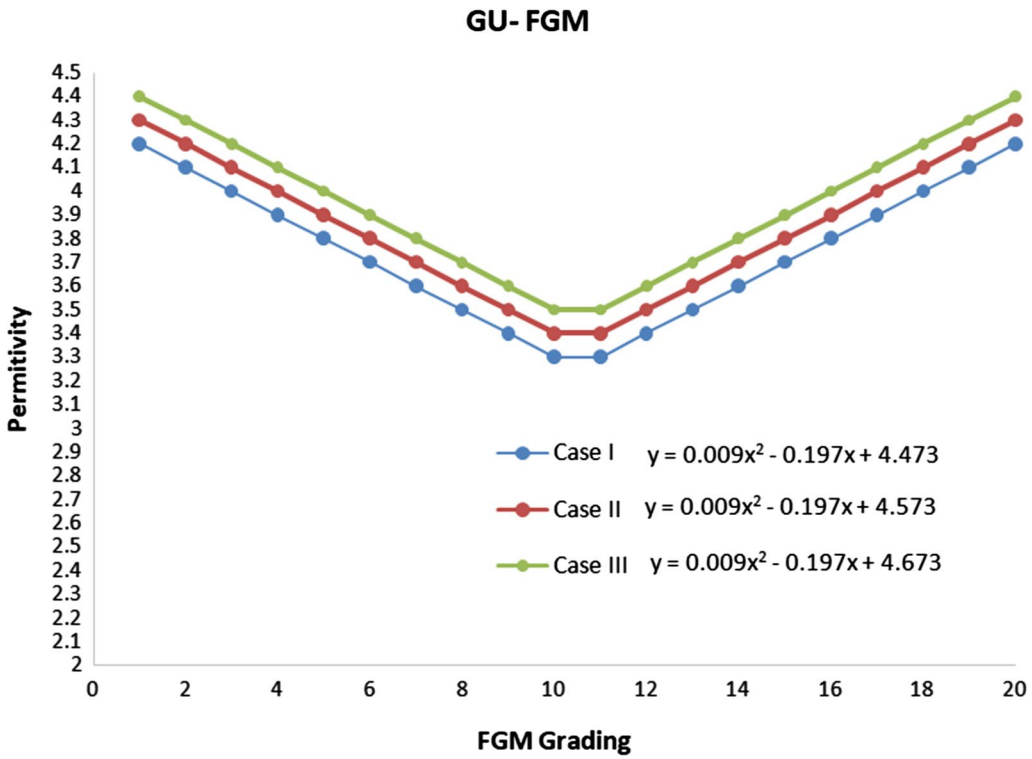


Fig. 4 Permittivity variation of graded U shape FGM

5.2 Epoxy/Plain Spacer

The designed epoxy type spacer under constant permittivity of 4.5 is simulated. The applied voltages are V_1, V_2 and V_3. The field intensity is noticed at both ends of the three conductors. TJ formed at the enclosure end must be reduced with its electric field in the proposed three-phase GIB.

It is observed from Table 3 that the electric field strength is high at TJ. Mainly it is noticed that conductor B gives high field intensity at enclosure end as it is located very nearer to the enclosure. It is also noticed that field intensity at the conductor A is maximum because of the maximum voltage at conductor A comparatively from the Table 1 maximum voltages if $V_1 = 72$ kV are observed as $V_A = 102.515$ kV, $V_B = -1.257$ kV and $V_C = -51.257$ kV respectively. Figure 6 represents the electrical field intensity of post type spacer without MI, which represents the magnitude of electrical field intensity is high at the enclosure end for the three conductors within in the range of 0.02 to 0.32 kV/cm at different applied voltages.

5.3 Epoxy Type Spacer with MI

The results of post/epoxy type spacer without metal insert have been obtained with high electrical field intensity at enclosure for three conductors A, conductor B, and conductor C. A recessed metal insert is designed with a two-dimensional combination of rectangular (18 mm × 4 mm) and ellipse (a-axis of 11 mm, b-axis of 3 mm) at the enclosure of the three conductors are arranged to minimize the field intensity at TJ for the three conductors to reduce electrical field intensity as shown in Fig. 7. From Tables 3 and 4, it is observed that the field intensity at TJ near the enclosure end is reduced at three conductors whereas no reduction is observed at the conductor ends as there is no impact of the MI at the HV conductors. It is also noticed

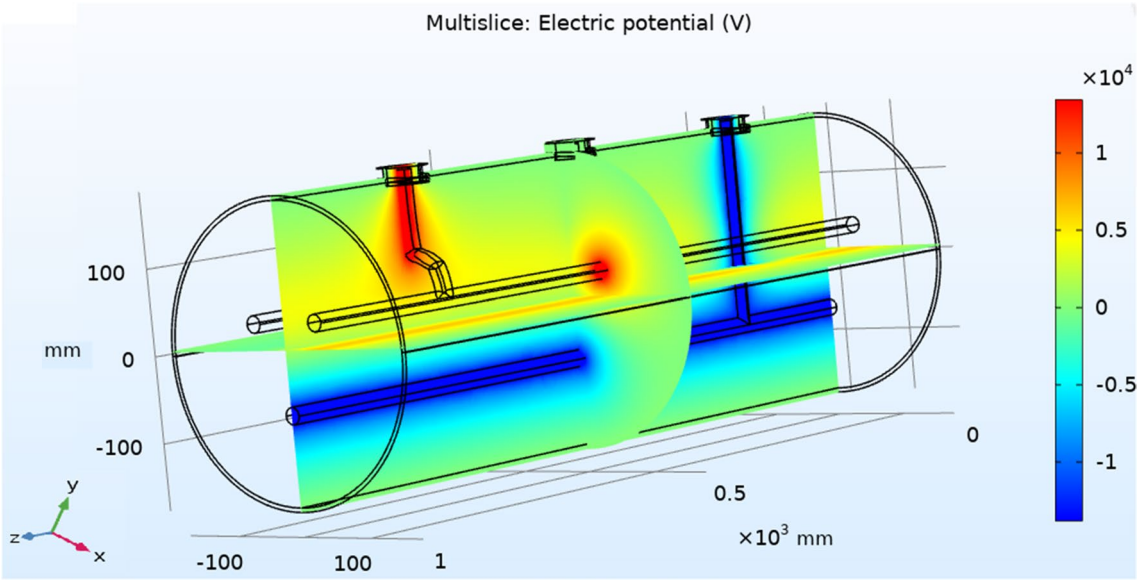


Fig. 5 Simulation model three phase GIB

Table 2 Maximum voltages of conductor A, B, C

Root Mean Square Voltage (kV)	Maximum V_A (kV)	Maximum V_B (kV)	Maximum V_C (kV)
$V_1 = 72.5$	102.515	– 51.258	– 51.258
$V_2 = 132$	186.65	– 93.324	– 93.324
$V_3 = 220$	311.08	– 155.54	– 155.54

Table 3 Electrical field intensity of plain post type spacer

Conductor	$V_1 = 72.5$ kV		$V_2 = 132$ kV		$V_3 = 220$ kV	
	$\mathbf{E}_{enclosure}$ (kV/cm)	$\mathbf{E}_{conductor}$ (kV/cm)	$\mathbf{E}_{enclosure}$ (kV/cm)	$\mathbf{E}_{conductor}$ (kV/cm)	$\mathbf{E}_{enclosure}$ (kV/cm)	$\mathbf{E}_{conductor}$ (kV/cm)
A	0.0084	0.1681	0.0153	0.30608	0.0255	0.51015
B	0.10645	0.14605	0.1938	0.2659	0.3231	0.4432
C	0.03485	0.1175	0.0635	0.21395	0.10585	0.3566

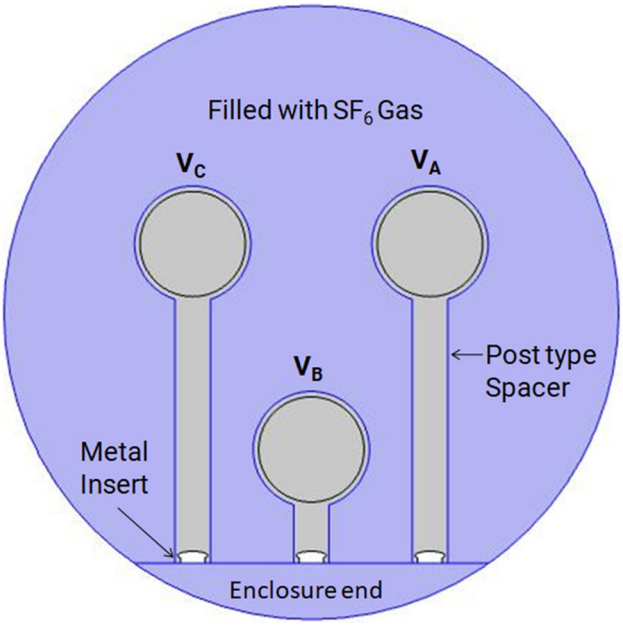


Fig. 6 Representation of post/epoxy type spacer along with MI

that the incorporated MI at the enclosure of conductor B has been minimized the developed electric field intensity largely when compared to supplementary conductors. It is observed that for conductor B, electric field intensity is reduced from 0.10645 to 0.007, which is reduced by a percentage of 93.42% at V_1. Similarly, at V_2 the field intensity is minimized from 0.1938 to 0.0127 with a percentage reduction of 93.44%. The field intensity is minimized from 0.323 to 0.0213 with a reduction of 93.40% at V_3. Reduction of the electric field has been shown in Fig. 6 after insertion of MI to epoxy post type spacer. From Fig. 8, the electrical field intensity is minimized drastically for all conductors within a range of 0.005 to 0.03 kV/cm for different applied voltages.

5.4 FGM Post Type Spacer Without MI

The above effects of the spacer style post/epoxy without and with metal insert resulted in the non-uniform distribution of the electric field over the spacer surface of all three conductors. A post-type FGM spacer is equipped with different FGM grades such as GL, GH, and GU-FGM with different permittivity's in different cases in order to create a consistent electrical field distribution. From Table 5, it is observed that GL-FGM grading is comparatively with the high electrical field strength at the TJ's ends of the enclosure for case I

Table 4 Electrical field intensity of post type spacer with metal insert

Conductor	$V_1 = 72.5$ kV		$V_2 = 132$ kV		$V_3 = 220$ kV	
	$\mathbf{E}_{\text{enclosure}}$ (kV/cm)	$\mathbf{E}_{\text{conductor}}$ (kV/cm)	$\mathbf{E}_{\text{enclosure}}$ (kV/cm)	$\mathbf{E}_{\text{conductor}}$ (kV/cm)	$\mathbf{E}_{\text{enclosure}}$ (kV/cm)	$\mathbf{E}_{\text{conductor}}$ (kV/cm)
A	0.0009	0.1693	0.0017	0.3085	0.0028	0.5137
B	0.0099	0.1461	0.0179	0.266	0.0299	0.4434
C	0.00285	0.1175	0.0051	0.214	0.00852	0.357

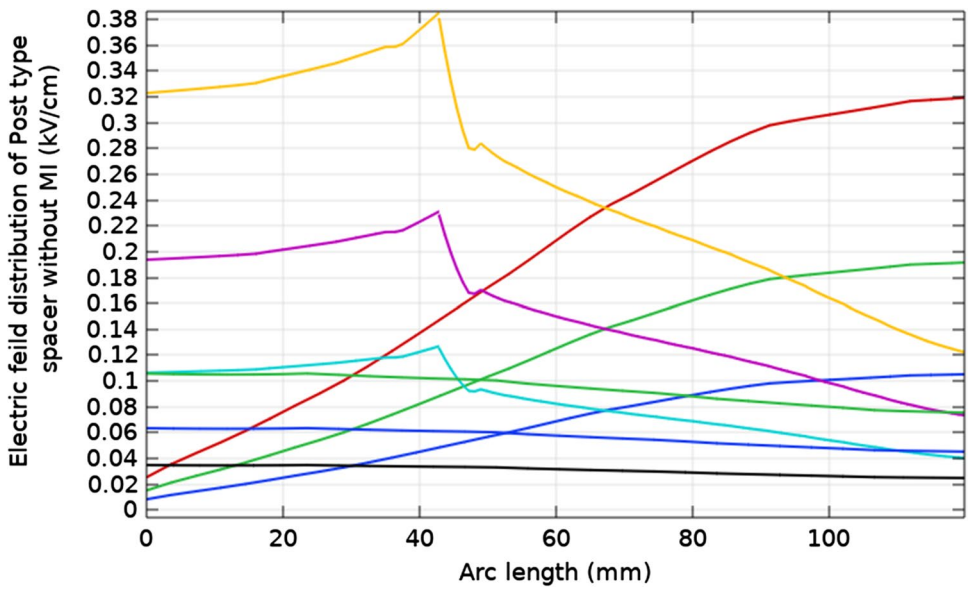


Fig. 7 Electrical field distribution of three conductors of post/epoxy type spacer at different applied voltages

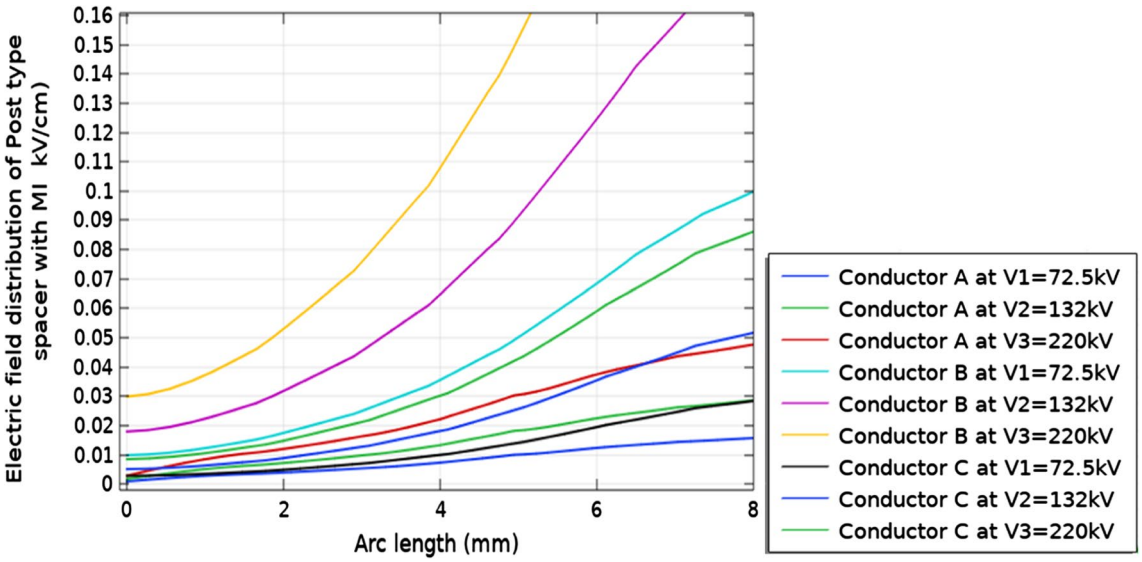


Fig. 8 Electrical Field distribution of three conductors of post/epoxy type spacer with MI at different applied voltages

Table 5 Electrical field intensity of FGM post type spacer without metal insert

Type	Conductor	Permittivity values	$V_1 = 72.5$ kV		$V_2 = 132$ kV		$V_3 = 220$ kV	
			$\mathbf{E}_{enclosure}$ (kV/cm)	$\mathbf{E}_{conductor}$ (kV/cm)	$\mathbf{E}_{enclosure}$ (kV/cm)	$\mathbf{E}_{conductor}$ (kV/cm)	$\mathbf{E}_{enclosure}$ (kV/cm)	$\mathbf{E}_{conductor}$ (kV/cm)
GL FGM	A	Case I	0.0104	0.1682	0.019	0.3062	0.0316	0.5105
		Case II	0.0108	0.1687	0.0197	0.3072	0.0329	0.512
		Case III	0.0113	0.1693	0.0205	0.3082	0.0342	0.5138
	B	Case I	0.1322	0.1445	0.2408	0.2631	0.4013	0.4386
		Case II	0.1327	0.1447	0.2417	0.2634	0.4028	0.439
		Case III	0.1333	0.1449	0.2426	0.2637	0.4044	0.4396
	C	Case I	0.0395	0.1178	0.0718	0.2146	0.1197	0.3576
		Case II	0.0396	0.1182	0.072	0.2153	0.12	0.3588
		Case III	0.0397	0.1186	0.0722	0.2161	0.1203	0.3601
GH FGM	A	Case I	0.0088	0.186	0.016	0.3385	0.0267	0.564
		Case II	0.009	0.1878	0.0165	0.3418	0.0274	0.57
		Case III	0.0093	0.1898	0.0169	0.3455	0.0282	0.576
	B	Case I	0.0843	0.1486	0.1534	0.2706	0.2557	0.4511
		Case II	0.0837	0.1491	0.1523	0.2715	0.2539	0.4524
		Case III	0.0831	0.1496	0.1512	0.2724	0.252	0.454
	C	Case I	0.0317	0.1331	0.0577	0.238	0.0962	0.3964
		Case II	0.03168	0.1318	0.0577	0.24	0.0961	0.4001
		Case III	0.0316	0.1306	0.0576	0.2425	0.096	0.404
GU FGM	A	Case I	0.0076	0.1681	0.0139	0.3062	0.0231	0.5102
		Case II	0.0079	0.1687	0.0144	0.3072	0.0239	0.512
		Case III	0.0081	0.1693	0.0149	0.3082	0.0248	0.5136
	B	Case I	0.0975	0.1449	0.1775	0.2637	0.2958	0.4396
		Case II	0.0972	0.1447	0.177	0.2635	0.295	0.4392
		Case III	0.0969	0.1446	0.1764	0.2632	0.294	0.4387
	C	Case I	0.03301	0.1179	0.06011	0.2146	0.10019	0.3578
		Case II	0.03302	0.1183	0.06015	0.2154	0.10025	0.359
		Case III	0.03304	0.1187	0.06018	0.2161	0.10032	0.3578

for conductor A and C and for case III for conductor B for all three applied voltages of V_1, V_2, and V_3. The electrical field intensity at conductor A is noticed high because of the maximum applied voltage to the conductor A comparatively as from Table 1. From Table 5, it is identified that the field stress is very high at TJ's for all three FGM gradings. For GL-FGM at 72.5 kV operating voltage of conductor A, the electrical field intensity is 0.0104 kV/cm in case I. Similarly, for case II the electrical field intensity is 0.0108 kV/cm and for case III it is 0.0113 kV/cm. However, for conductor B at $V_1 = 72.5$ kV, the electric field intensity is 0.1322 kV/cm in case I. Similarly, for case II the electrical field intensity is 0.1327 kV/cm and for case III it is 0.1333 kV/cm. Similarly, for conductor C at $V_1 = 72.5$ kV, the electrical field intensity is 0.0395 kV/cm in case I. Similarly, for case II the electric field intensity is 0.0396 kV/cm and for case III it is 0.0397 kV/cm. From Table 5, it is noticed that electric field intensity at the enclosure and conductor ends has been increased as the operating voltage increases. Similarly, for GH and GU-FGM gradings, the values of electric field intensity have observed from the table. The variation of electrical field intensity of three conductors of FGM post type spacer with respect to arc length is shown in Figs. 9, 10 and 11 respectively. From Fig. 9, the electrical field intensity is observed from 0.01 to 0.0316 kV/cm for V_1, V_2 and V_3 which is high at the enclosure end which may lead to

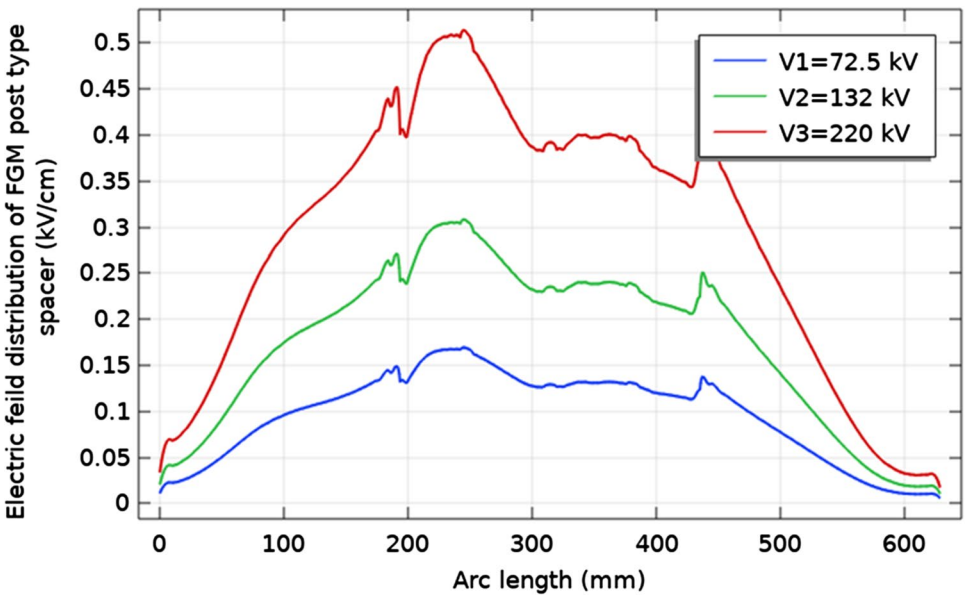


Fig. 9 Electrical field distribution of conductor A of post type FGM spacer at different applied voltages

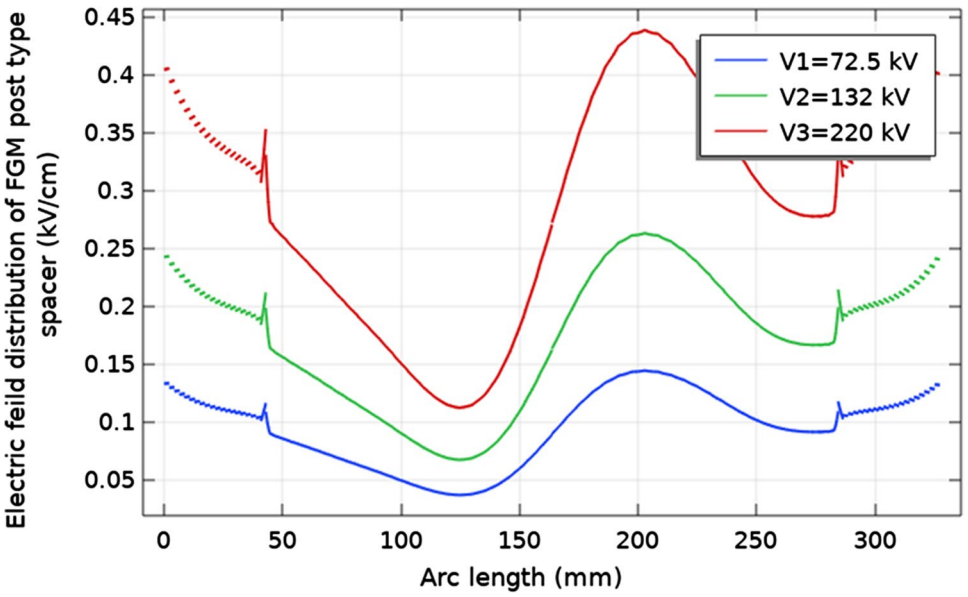


Fig. 10 Electrical field distribution of conductor B of post type FGM spacer at different applied voltages

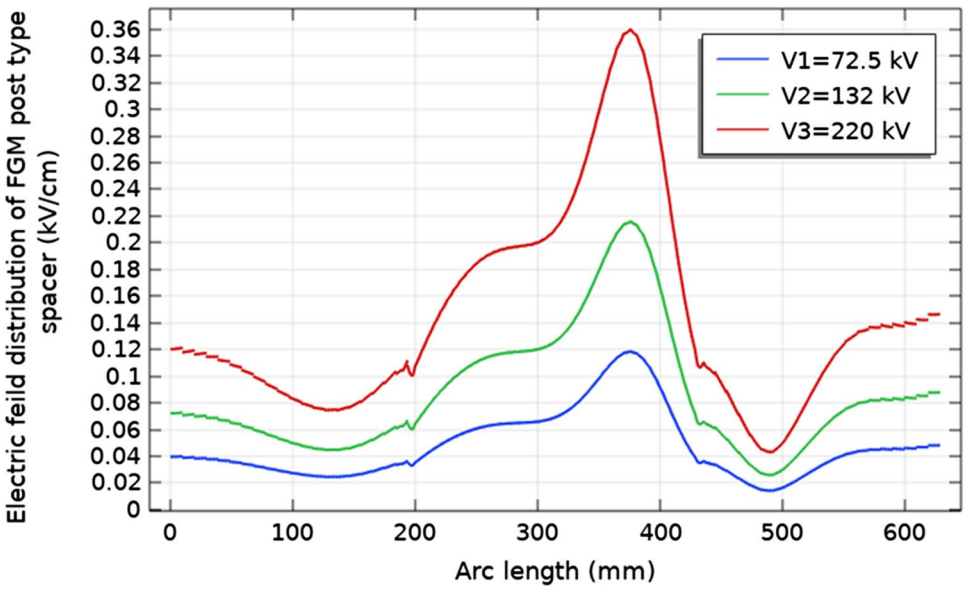


Fig. 11 Electrical field distribution of conductor C of post type FGM spacer at different applied voltages

failure of the spacer performance. Similarly, for conductor B as from Fig. 10, the field stress is in the range of 0.14 to 0.4 kV/cm at different applied voltages. Similarly, for conductor C the field stress is in the range of 0.04 to 0.12 kV/cm as shown in Fig. 11 at different applied voltages of V_1, V_2 and V_3.

5.5 FGM Post Type Spacer with Metal Insert

The results of the above post type FGM spacer without metal insert has resulted in the high electrical intensity at TJ's of all three conductors A, B and C. It's effect is minimized by designing a recessed metal MI with a two-dimensional combination of rectangular (18 mm × 4 mm) and ellipse (a-axis of 11 mm, b-axis of 3 mm) at the enclosure of post type FGM spacer as shown in Fig. 12. Table 6 represents the reduction of electrical field intensity with the insertion of MI, from this Table 6 the electrical field intensity at TJ is reduced for three conductors whereas there is no much reduction of electrical field intensity at the conductor ends as there is no impact of MI at this end for a three phase GIB. From Table 6 the maximum reduction is obtained in GU-FGM grading, hence further the analysis is done for conductor B of GH and GU-FGM gradings. For conductor B at the case I of GL grading, the electrical field intensity is reduced from 0.1322 to 0.0269 kV/cm, which is reduced by a percentage of 79.65% at V_1. At V_2, the field stress is minimized from 0.2408 to 0.049 kV/cm with a minimization of 79.65%. At V_3, the field stress is minimized from 0.4013 to 0.082 kV/cm with minimization of 79.57%. Similarly, at V_1 the percentage reduction of 79.13% and 78.62% is observed for case II and case III respectively. For conductor B at the case I of GH grading, the electrical field intensity

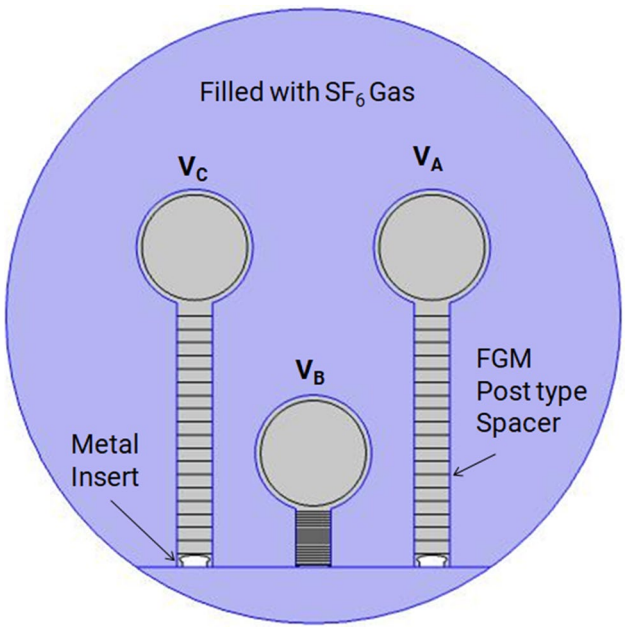


Fig. 12 Representation of post type FGM spacer with MI

is reduced from 0.0843 to 0.001295 kV/cm which is minimized by a percentage of 98.46% at V_1. At V_2 the field stress is reduced from 0.1534 to 0.02355 kV/cm with minimization of 84.65%. At V_3 the field stress is reduced from 0.2557 to 0.03925 kV/cm with minimization of 84.65%. Similarly, at V_1 the percentage minimization of 98.44% and 98.42% is observed for case II and case III respectively. For conductor B at the case I of GU-FGM grading, the electrical field intensity is minimized from 0.0975 to 0.001498 kV/cm, which is minimized by a percentage of 98.46% at V_1. At

Table 6 Electrical field intensity of post type FGM spacer with metal insert

Type	Conductor	Permittivity values	$V_1 = 72.5$ kV		$V_2 = 132$ kV		$V_3 = 220$ kV	
			$\mathbf{E}_{\text{enclosure}}$ (kV/cm)	$\mathbf{E}_{\text{conductor}}$ (kV/cm)	$\mathbf{E}_{\text{enclosure}}$ (kV/cm)	$\mathbf{E}_{\text{conductor}}$ (kV/cm)	$\mathbf{E}_{\text{enclosure}}$ (kV/cm)	$\mathbf{E}_{\text{conductor}}$ (kV/cm)
GL-FGM	A	Case I	0.0019	0.1682	0.0036	0.3062	0.006	0.5105
		Case II	0.0021	0.1687	0.0038	0.3072	0.0064	0.512
		Case III	0.0022	0.1693	0.004	0.3082	0.0067	0.514
	B	Case I	0.0269	0.145	0.049	0.264	0.082	0.4401
		Case II	0.0277	0.1449	0.05	0.2637	0.084	0.4396
		Case III	0.0285	0.1447	0.052	0.2635	0.0865	0.4391
	C	Case I	0.0049	0.1178	0.009	0.2146	0.015	0.3575
		Case II	0.0051	0.1182	0.0093	0.2152	0.0155	0.359
		Case III	0.0053	0.1186	0.0096	0.216	0.0161	0.36
GH-FGM	A	Case I	0.0011	0.187	0.00209	0.3405	0.00348	0.568
		Case II	0.00115	0.189	0.00215	0.344	0.00358	0.573
		Case III	0.00125	0.191	0.00222	0.3475	0.0037	0.5785
	B	Case I	0.001295	0.1489	0.02355	0.2719	0.03925	0.4518
		Case II	0.001302	0.1494	0.0237	0.2719	0.0395	0.4532
		Case III	0.00131	0.1499	0.02389	0.2729	0.0397	0.4548
	C	Case I	0.002602	0.1306	0.00479	0.238	0.00805	0.3965
		Case II	0.002606	0.1318	0.00488	0.24	0.0081	0.4
		Case III	0.002702	0.1311	0.00495	0.2425	0.0082	0.404
GU-FGM	A	Case I	0.00108	0.1681	0.00198	0.3062	0.00328	0.5105
		Case II	0.00112	0.1687	0.00208	0.3072	0.0034	0.512
		Case III	0.00118	0.1693	0.0021	0.3082	0.00352	0.5138
	B	Case I	0.001498	0.14475	0.0272	0.26355	0.00454	0.4392
		Case II	0.00151	0.14488	0.0275	0.26378	0.04588	0.4396
		Case III	0.001528	0.1452	0.0278	0.2644	0.0463	0.4401
	C	Case I	0.00275	0.1179	0.00498	0.2161	0.00832	0.3578
		Case II	0.00278	0.1183	0.00508	0.2154	0.00848	0.359
		Case III	0.00285	0.1187	0.00518	0.2146	0.00862	0.3602

V_2 the field stress is minimized from 0.1775 to 0.0272 kV/cm with minimization of 84.68%. At V_3 the field stress is reduced from 0.2958 to 0.00454 kV/cm with minimization of 98.47%. Similarly, at V_1 the percentage reduction of 98.45% and 98.42% is noticed for case II and case III respectively. From Figs. 9, 10 and 11, it is noticed that magnitude of electric field intensity at the enclosure is maximum for all the three conductors. This high electrical field intensity is further minimized by inserting MI's at the enclosure ends of all the three FGM post type spacer with MI are shown for three conductors in the corresponding Figs. 13, 14 and 15. By comparing Figs. 9 and 13, the electrical field intensity is reduced drastically at TJ of the enclosure end. Similarly, maximum minimization is obtained for conductors B and C as shown in Figs. 14 and 15 respectively.

Figure 16 represents the surface plots with height as a dimension for post type FGM spacer of a three phase GIB without MI and Fig. 17 represents the same in the presence of MI. In Fig. 16, the electric field lines are in congestion near the enclosure ends whereas after inserting MI, the congestion of these electric lines has been reduced which as observed from Fig. 17. The corresponding surface plot without its height dimension of Figs. 16, 17 is shown in Figs. 18 and 19 respectively. The contour plots of the FGM post form spacer without and with conductor B MI are shown in Figs. 20, 21 respectively, in order to provide a better understanding of the distribution of electrical field. From Fig. 21, the electric field intensity is reduced at the enclosure than that of Fig. 20. Similarly, the electrical field intensity of FGM post type spacer with MI can be noticed from mesh plot indicating less thickness of the mesh triangles in Fig. 22 when compared to mesh plot without MI as shown in Fig. 23.

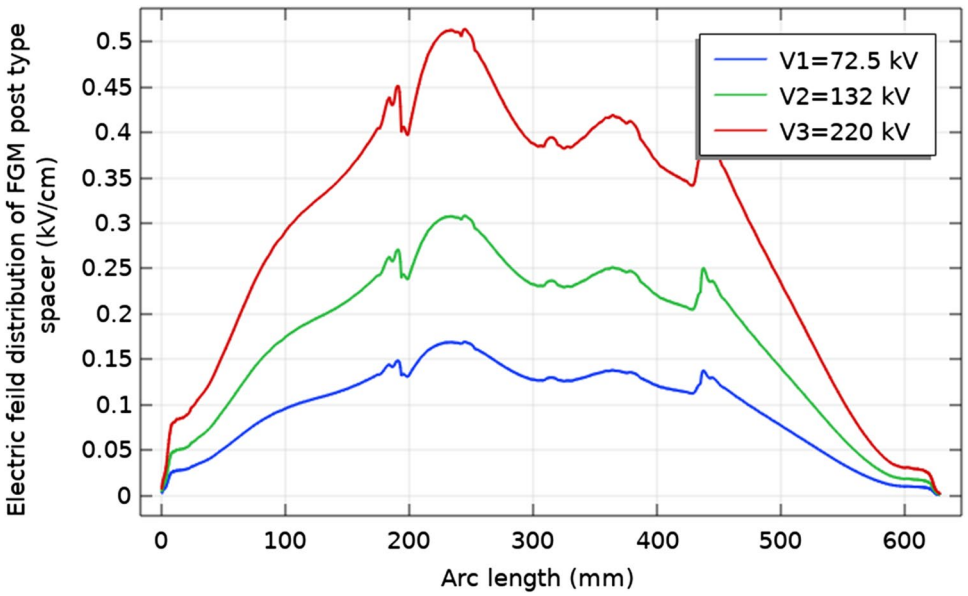


Fig. 13 Electrical field distribution of conductor A of post type FGM spacer with MI at different applied voltages

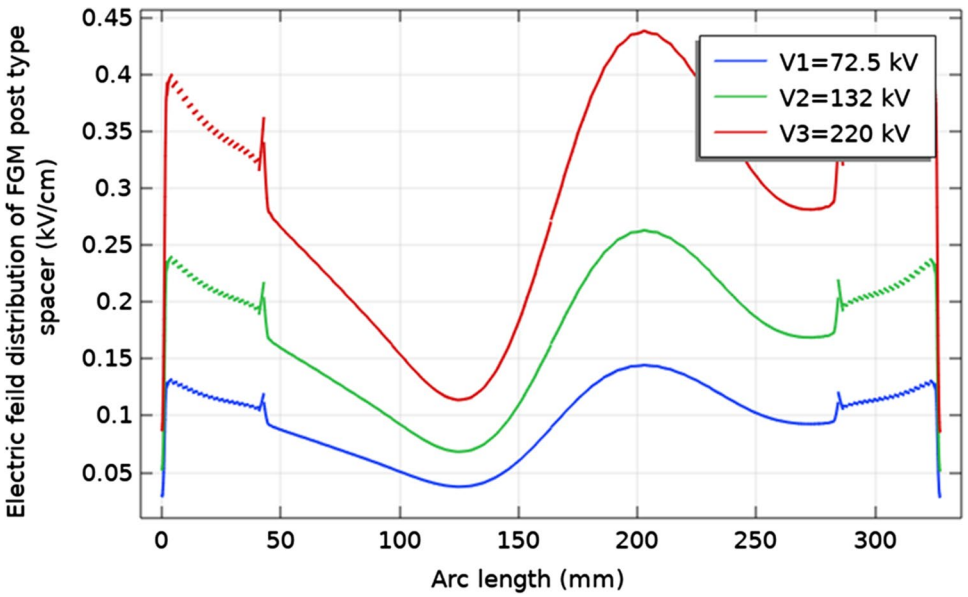


Fig. 14 Electrical field distribution of conductor B of post type FGM spacer with MI at different applied voltages

6 Conclusion

In this paper, the three-phase GIB with post/ epoxy type the spacer is simulated, using finite element method. The electric field distribution is obtained at both the enclosure and conductor ends of all the three post type spacers enclosed inside the GIB. By taking the highest electric field intensity of post type spacer into consideration, metal inserts have been inserted at the enclosure ends for all the three spacers. This highest electric field is reduced drastically for all conductors after inserting MI for different applied voltages. The main purpose of this paper is to introduce the FGM technique to the three-phase GIB to create a uniform electrical field intensity over the spacer at different applied voltages. Three different gradings like GL, GH, and GU-FGM are taken for the study of the effectiveness with specific dielectric permittivity ranges and from the results, the following conclusions were made:

- Comparatively the conductor ends has resulted in a high electric field intensity than the enclosure ends for all the three conductors.
- The obtained electrical field intensity is more at conductor end of conductor A than other two conductors at different applied voltages.

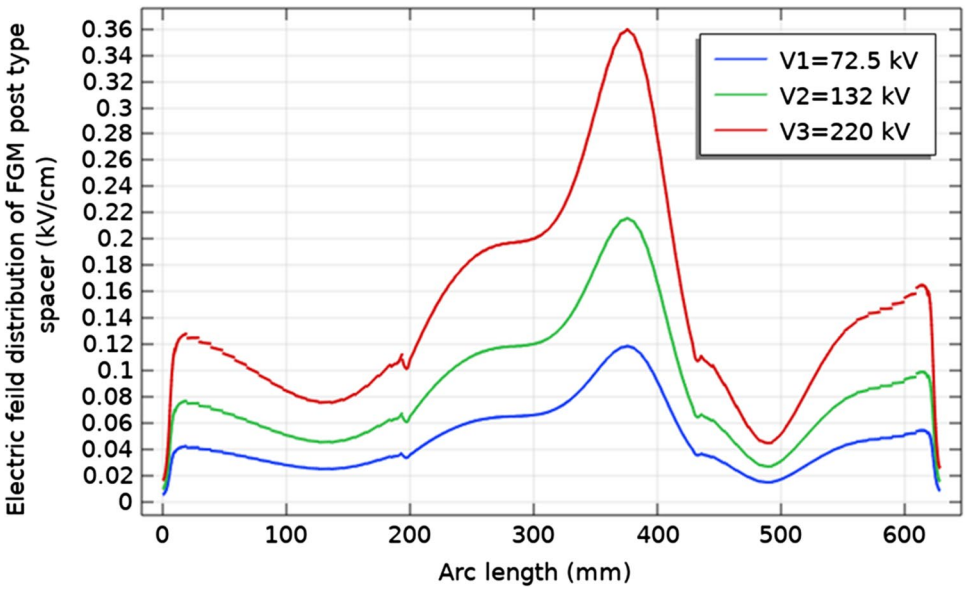


Fig. 15 Electrical field distribution of conductor C of post type FGM spacer with MI at different applied voltages

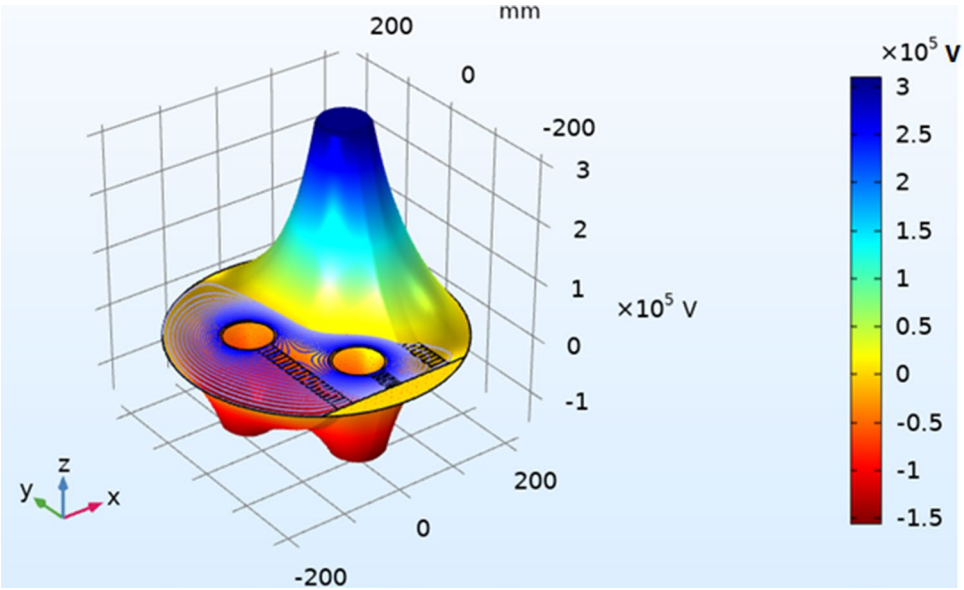


Fig. 16 FGM spacer surface plot with its height

- Due to the weakest link at enclosure end, the electric field distribution is to be concentrated at TJ and identified that it rises with the rise in operating voltage.
- It is noticed that electric field intensity is high at TJ for conductor B than other conductors for GL, GH and GU-FGM gradings.
- In the absence of metal inserts, metal inserts are used to minimize the electrical field strength and are limited to a value greater than their values.
- From the study of the three separate FGM gradings, GL-FGM has enhanced the reduction of the electrical field with the insertion of the metal inserts for a three-phase GIB to post form FGM spacer.

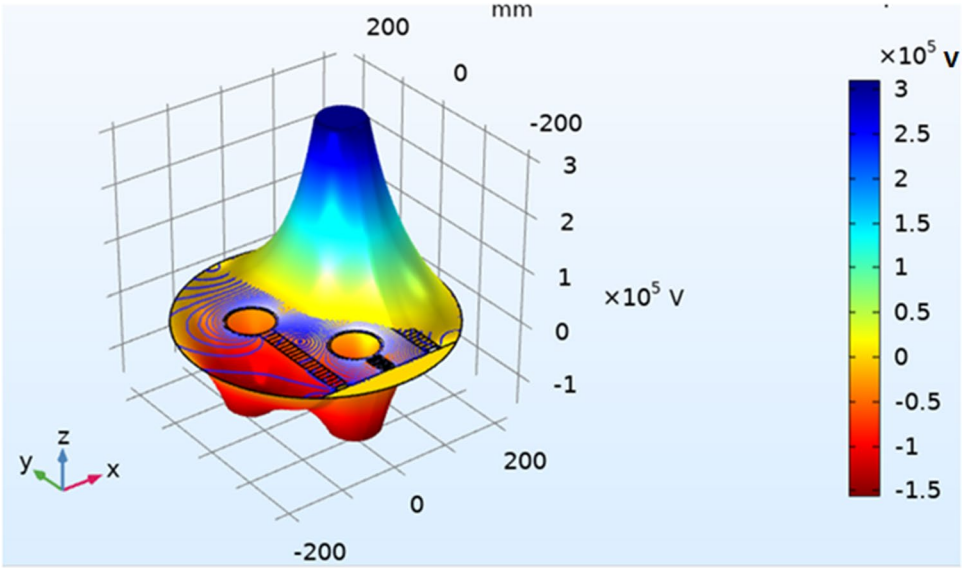


Fig. 17 FGM spacer surface plot with MI

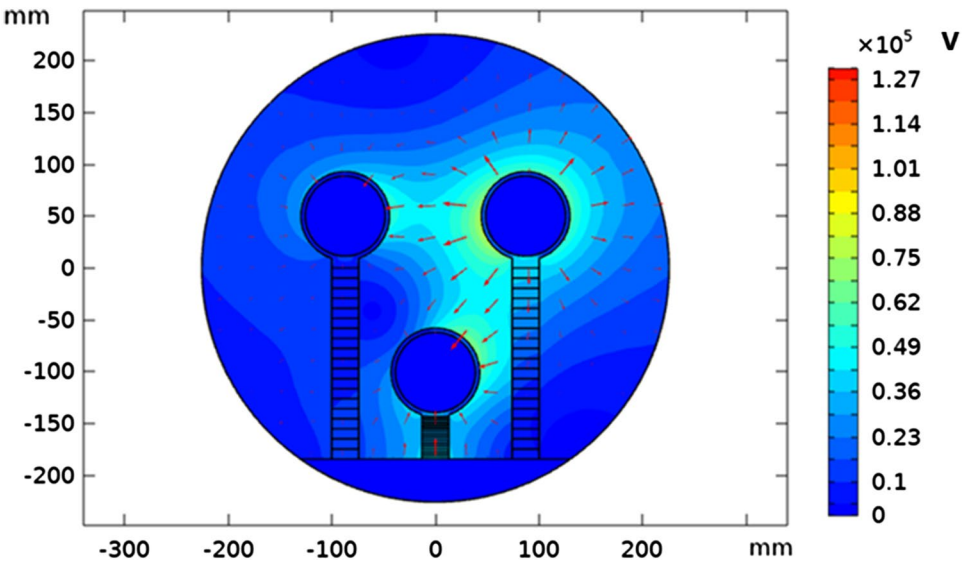


Fig. 18 Post FGM spacer surface plot

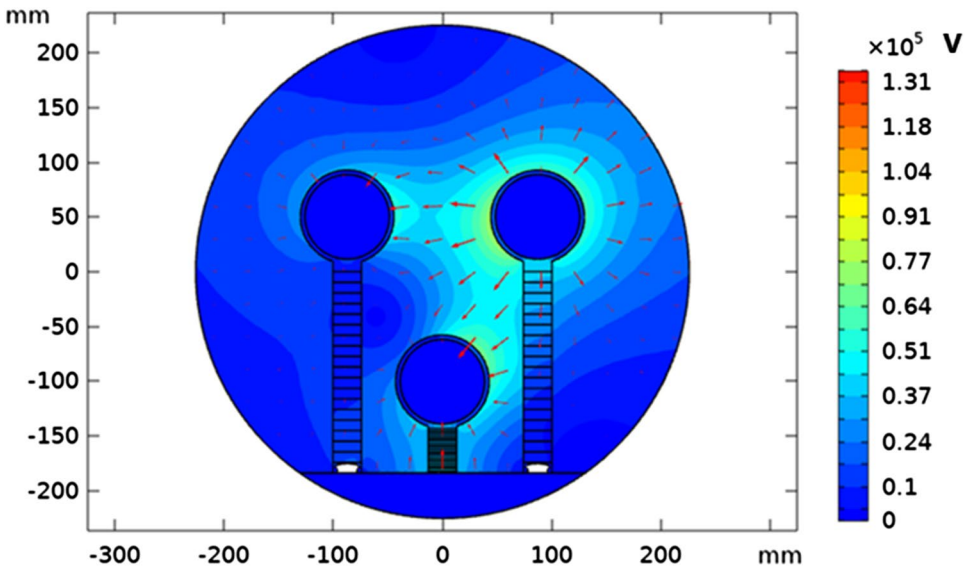


Fig. 19 Post FGM spacer surface plot with MI

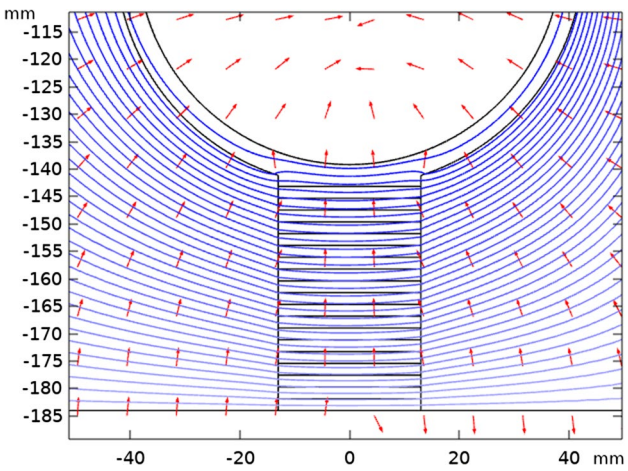


Fig. 20 Post FGM spacer contour plot

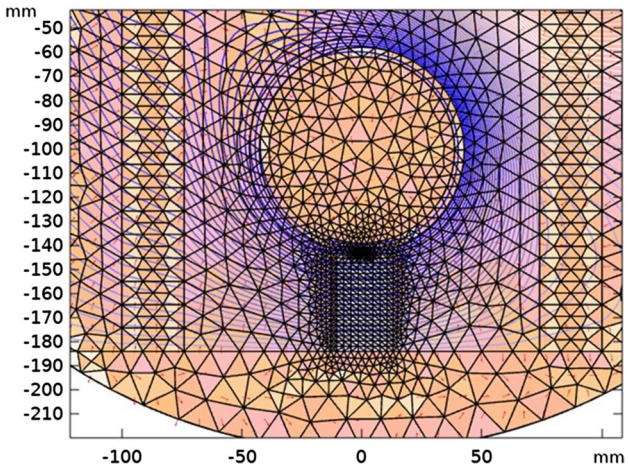


Fig. 22 Post FGM Spacer mesh plot without MI

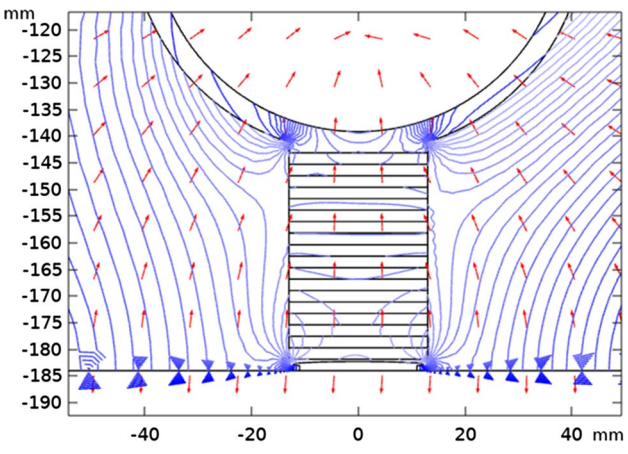


Fig. 21 Post FGM spacer contour plot with MI

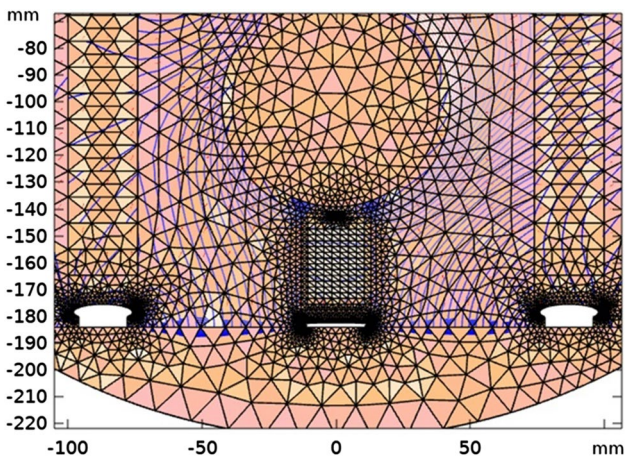


Fig. 23 Post FGM spacer mesh plot with MI

Open Access This article is licensed under a Creative Commons Attribution 4.0 International License, which permits use, sharing, adaptation, distribution and reproduction in any medium or format, as long as you give appropriate credit to the original author(s) and the source, provide a link to the Creative Commons licence, and indicate if changes were made. The images or other third party material in this article are included in the article's Creative Commons licence, unless indicated otherwise in a credit line to the material. If material is not included in the article's Creative Commons licence and your intended use is not permitted by statutory regulation or exceeds the permitted use, you will need to obtain permission directly from the copyright holder. To view a copy of this licence, visit http://creativecommons.org/licenses/by/4.0/.

References

1. He C, Zhang L, Li J, Zhang Q, Yao X (2019) Effect of AC and switching impulse superimposed voltage on PD characteristics in SF6 gas. IEEE Trans Dielectr Electr Insulat 26(5):1394–1402
2. Nakano Y, Kozako M, Hikita M, Tanaka T, Kobayashi M (2019) Estimation method of degraded vacuum in vacuum interrupter based on partial discharge measurement. IEEE Trans Dielectr Electr Insulat 26(5):1520–1526
3. Wen T, Zhang Q, Ma J, Wu Z, Shimomura N, Chen W (2019) A new method to evaluate the effectiveness of impulse voltage for detecting insulation defects in GIS equipment. IEEE Trans Dielectr Electr Insulat 26(4):1301–1307
4. Nagesh Kumar GV, Amarnath J, Singh BP, Srivastava KD (2007) Electric field effect on metallic particle contamination in a common enclosure gas insulated busduct. IEEE Trans Dielectr Electr Insulat 14(2):334–340
5. Arbutina D, Stankovic K, Perazic L, Pejovic M (2019) Influence of the shape, number, position and dimensions of conductive particles within inter-electrode gap on DC and pulse breakdown voltage value of SF6 and N2 mixture. Int J Electr Power Energy Syst 104:436–442
6. Talaat M, El-Zein A, Amin M (2018) Electric field simulation for uniform and FGM cone type spacer with adhering spherical conducting particle in GIS. IEEE Trans Dielectr Electr Insulat 25(1):339–351
7. Guo Z, Wu Z, Wang H, Tian H, Liu L, Peng Z, Li H, Wang Q (2019) Experimental and numerical study on formation of interface separation and interfacial dielectric strength of GIL insulator. IEEE Trans Dielectr Electr Insulat 26(6):1738–1746
8. Li C, Lin C, Zhang B, Li Q, Liu W, Hu J, He J (2018) Understanding surface charge accumulation and surface flashover on spacers in compressed gas insulation. IEEE Trans Dielectr Electr Insulat 25(4):1152–1166
9. Wu Z, Zhang Q, Ma J, Li X, Wen T (2018) Effectiveness of on-site dielectric test of GIS equipment. IEEE Trans Dielectr Electr Insulat 25(4):1454–1460
10. Liu X, Zhang L, Wen T, Zhang Q (2018) Influence of spike defect on the impulse breakdown characteristics of SF6 gas gap in GIS. IEEE Trans Dielectr Electr Insulat 25(4):1413–1420
11. Muneaki K, Katsumi K, Masahiro H (2010) Yoshikazu Hoshina, Masafumi Takei, Hitoshi Okubo, Application of functionally graded material for reducing electric field on electrode and spacer interface. IEEE Trans Dielectr Electr Insulat 17(1):256–263
12. Du BX, Liang HC, Li J (2019) Surface coating affecting charge distribution and flashover voltage of cone-type insulator under DC stress. IEEE Trans Dielectr Electr Insulat 26(3):706–713
13. Heung-Jin Ju, Ko K-C, Kim D-K (2013) Optimization of a grounded electrode shape in gas insulated switchgear with a reversely elliptical permittivity graded insulator. IEEE Trans Dielectr Electr Insulat 20(5):1749–1754
14. Hayakawa N, Ishiguro J, Kojima H, Kato K, Okubo H (2016) Fabrication and simulation of permittivity graded materials for electric field grading of gas insulated power apparatus. IEEE Trans Dielectr Electr Insulat 23(1):547–554
15. Hayakawa N, Miyaji Y, Kojima H, Kato K (2018) Simulation on discharge inception voltage improvement of GIS spacer with permittivity graded materials. IEEE Trans Dielectr Electr Insulat 25(4):1318–1323
16. Ran Z, Boxue Du, Li J, Liang H, Kong X, Jiang J, Wang M (2019) Electric field regulation of insulator interface by FGM with conductivity for superconducting-GIL. IEEE Trans Appl Supercond 29(2):1–5
17. An Z, Yang W, Xing Z, Chen W, Chen K, Gao W, Shen Z, Yang Y, Liu F, Liu X, Zhang Z (2020) Comparative study on direct fluorination and surface properties of alumina-filled and unfilled epoxy insulators. IEEE Trans Dielectr Electr Insulat 27(1):85–93
18. Liu L, Li X, Wen T, Zhang R, Wu Z, Zhao J, Zhang Q (2019) Investigation on surface electric field distribution features related to insulator flashover in SF6 gas. IEEE Trans Dielectr Electr Insulat 26(5):1588–1595
19. Chakravorti S (2004) A Lahiri, Electrode-spacer contour optimization by ANN aided genetic algorithm. IEEE Trans Dielectr Electr Insulat 11(6):964–975
20. Farish I, Bawy AI (1991) Effect of surface charge on impulse-flashover of insulators in SF6. IEEE Trans Electr Insulat 26(3):443–452
21. Deepak Chowdary D, Amarnath J (2011) Electric field analysis at the triple junction of a optimum profile disc type spacer in SF6 gas insulated system with abnormalities under DC voltages. In: IEEE Annual Report Conference, pp 215–218
22. Imai T, Hoshina Y, Kojima H, Hayakawa N (2019) Resin injection behavior in process of manufacturing insulation spacer with permittivity gradient using computational fluid dynamics. IEEE Trans Dielectr Electr Insulat 26(5):1669–1677
23. Imai T, Takeuchi M, Hoshina Y, Kojima H, Hayakawa N (2019) Comparison of permittivity gradient in resin injected and simulated cone-shaped spacers. IEEE Trans Dielectr Electr Insulat 26(5):1678–1685
24. Du BX, Wang ZH, Li J, Liang HC, Li ZH (2020) Epoxy insulator with surface graded-permittivity by magnetron sputtering for gas-insulated line. IEEE Trans Dielectr Electr Insulat 27(1):197–205
25. Du BX, Liang HC, Li J (2020) Novel spacer coated with functionally graded ZnO film for HVDC gas insulated line. IEEE Trans Dielectr Electr Insulat 27(1):231–239
26. Kurimoto M, Ozaki H, Sawada T, Funabashi T, Kato T, Suzuoki Y (2018) FEM simulation of local field enhancement close to lamination interface of permittivity-graded material. Electr Eng Jpn IEEJ Trans Electr Electron Eng 101(6):1–87
27. Straumann U, Stoller PC (2019) The impact of partly liquefied SF6 on the dielectric performance of SF6-insulated switchgear. IEEE Trans Dielectr Electr Insulat 26(1):137–145
28. Zhang JW, Gao FK, Cao DK, Putson C, Song C, Chen W, Zhang J (2018) Modeling of charge transport in insulating dielectric for gas-insulated transmission line based on multiple trap levels. IEEE Trans Dielectr Electr Insulat 25(4):1195–1201

Publisher's Note Springer Nature remains neutral with regard to jurisdictional claims in published maps and institutional affiliations.

Polamraju V. S. Sobhan received the B.Tech degree in Electrical and Electronics Engineering from SVHCE, Machilipatnam, and M.E degree from Andhra University, Visakhapatnam. He is presently working in the Department of EEE, VFSTR University, Guntur, India. His

research interests include Intelligent Controllers Design, Active Magnetic Bearings, and Bearingless drives, and Gas Insulated Substations.

Janaki Pakalapati was born in Visakhapatnam, A.P., India in 1984. She received her B.Tech degree in the Department of Electrical and Electronics Engineering from Raghu Engineering College, Visakhapatnam, India, and received her M.E. degree in Power Electronics Drives and Control in Department of Electrical and Electronics Engineering from the Andhra University College of Engineering, Visakhapatnam. She is working as Associate Professor in the Department of Electrical and Electronics Engineering at LENDI Institute of Engineering and Technology, Vizianagaram. Her main research area includes several abnormalities of spacers in Gas Insulated Substations.

Venkata Nagesh Kumar Gundavarapu received his B.E. degree from College of Engineering, Gandhi Institute of Technology and Management, Visakhapatnam, India and M.E. degree from the College of Engineering, Andhra University, Visakhapatnam. He received his doctoral degree from Jawaharlal Nehru Technological University, Hyderabad. He is presently working as Professor and Head in the Department of Electrical and Electronics Engineering, JNTUA College of Engineering Pulivendula. His research interests include gas-insulated substations, Evolutionary Computation, and FACTS devices. He has published research papers in reputed National and International Journals and Conferences.

Deepak Chowdary Duvvada was born in Srikakulam, Andhra Pradesh, India. He obtained his Bachelor of Engineering degree from GITAM College of Engineering, Visakhapatnam, Andhra Pradesh, India in the year 2000 and Master of Technology degree from JNT University, Hyderabad, Andhra Pradesh, India in the year 2007. He is presently working as Professor and Principal, Dr. L. Bullayya College of Engineering for Women, Visakhapatnam, India. His research areas include Gas Insulated Substations, High Voltage Engineering, and Custom power devices.

Sravana Kumar Bali working as Assistant Professor in EEE Dept., GITAM, Vizag, A.P, India. He received his Ph.D. from JNTU Kakinada. His area of interests are Power Systems, Contingency analysis, Algorithms and FACTS Devices and Gas Insulated Substations.

Journal of Alternative and Renewable Energy Sources

Volume-7, Issue-2 (May-August, 2021)

www.matjournals.com

https://doi.org/10.46610/JOARES.2021.v07i02.005

SPWM Fed Induction Motor Drive Performance Using SIMULINK

Anand Gondesi[1*], Ch. Ravi Kumar[1], Seerapu Varalakshmi[1], Singampalli Hema[1]
[1]Assistant Professor
Department of Electrical and Electronics Engineering, Dr. Lankapalli Bullayya College of Engineering, Visakhapatnam, Andhra Pradesh, India

*Corresponding Author: anandg@lbce.edu.in

ABSTRACT

In the former times, IC engines were used for transportation by most of the vehicles. But due to the depletion of fossil fuels day to day, the world is moving towards the Electric Vehicles (EVs) to overcome this problem. Electric Vehicles have higher efficiency and weight/power ratio. In general, DC motors were used in electric vehicles. The DC motors could not meet the requirements of customer needs because of its low speed range. In the recent studies, an AC Induction motor has several advantages over DC motors because of its robustness, high speed range, and efficiency and weight/power ratio. This paper presents the performance analysis of AC Induction motor when fed with the Single-Phase Inverter. The gate pulses are given by using Sinusoidal Pulse Width Modulation (SPWM) technique. The results are then compared with the performance of DC motor using MATLAB/SIMULINK.

Keywords-- Electric Vehicle [EV], Internal Combination [IC], Sinusoidal pulse width modulation [SPWM]

INTRODUCTION

An electric vehicle (EV) is a battery pack that stores the electrical energy to power the electric motor used for propulsion. They first came into existence in the mid-19th century. Till then, Internal Combustion(IC) engines were used for driving cars and trucks. With the emerging trends in the concept of Electric Vehicles [EVs] WHICH replaced fuel-based vehicles with IC engines. The machines used for supplying the mechanical energy are DC Motors, Induction Motors, etc. DC Motor is a classical motor and has been used for a longer time. The energy is being supplied through brushes via commutator to the armature. Due to the rubbing action, the brushes are subjected to wear and tear action which requires frequent maintenance because of a shorter life span. DC motors are suitable for low-power applications. With this drawback, AC Induction motors find its predominant application in the electric vehicle and it is mostly used in variable speed drive applications.

METHODOLOGY

This paper presents the performance analysis of AC induction motor when fed with single phase full bridge inverter incorporating with sinusoidal pulse width modulation (SPWM). The power supply is obtained from DC voltage source of 240V. For the conversion of DC to AC, we use power MOSFETS based single phase full bridge inverter with SPWM technique. MOSFET is voltage controlled device and requires only small input current. It is used for because of its high speed switching action which made it easy to drive and power loss is low. For triggering the power MOSFETS, The Sinusoidal Pulse Width Modulation technique is used.

SPWM

Pulse-width modulation (PWM) is a switching scheme used in inverter to modify the shape of the output voltage waveform. It is the most efficient method for controlling the output voltage. Besides, its classification, we are using Sinusoidal Pulse width modulation technique for triggering the gate. By SPWM technique, we can generate several pulses per half cycle whose width of the pulse is varied proportional to the amplitude of the sine wave. Sinusoidal signal which is called the reference signal when compared with triangular carrier wave of frequency, the gate pulses are generated. The modulation signal is a sinusoidal waveform which has the desired frequency of 50 or 60 Hz.

Page 29-38 © MAT Journals 2021. All Rights Reserved

www.matjournals.com https://doi.org/10.46610/JOARES.2021.v07i02.005

The Modulation index is defined as the ratio of amplitude of the reference signal and amplitude of the carrier signal. The output voltage has higher order harmonics for less than values of M. The order of the dominant harmonic can be raised and can be filtered out easily. The Fig. 1 and 2 represents the implementation of SPWM and output of the SPWM Gate Pulse Circuit.

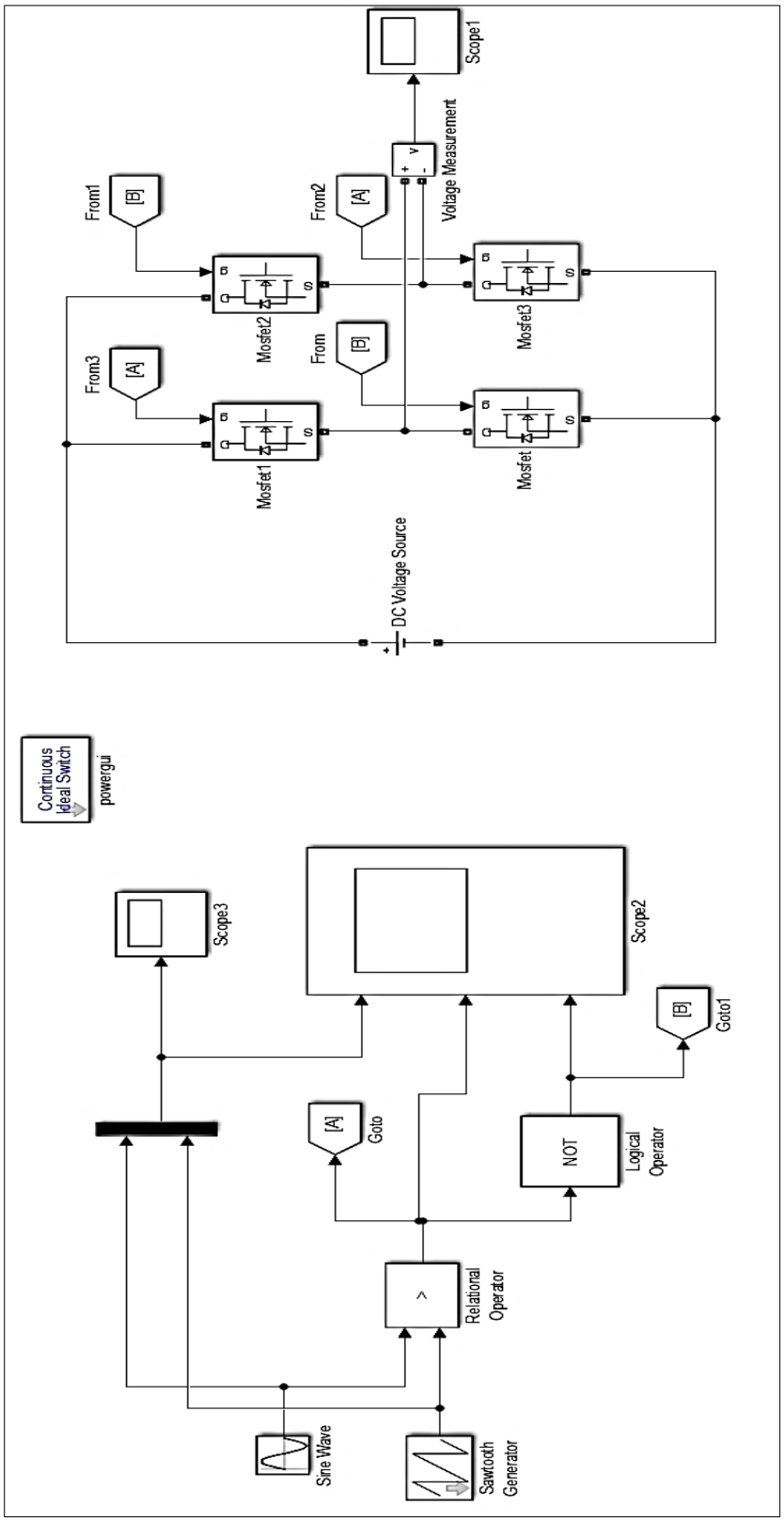


Figure 1: *SPWM implementation.*

Page 29-38 © MAT Journals 2021. All Rights Reserved

www.matjournals.com
https://doi.org/10.46610/JOARES.2021.v07i02.005

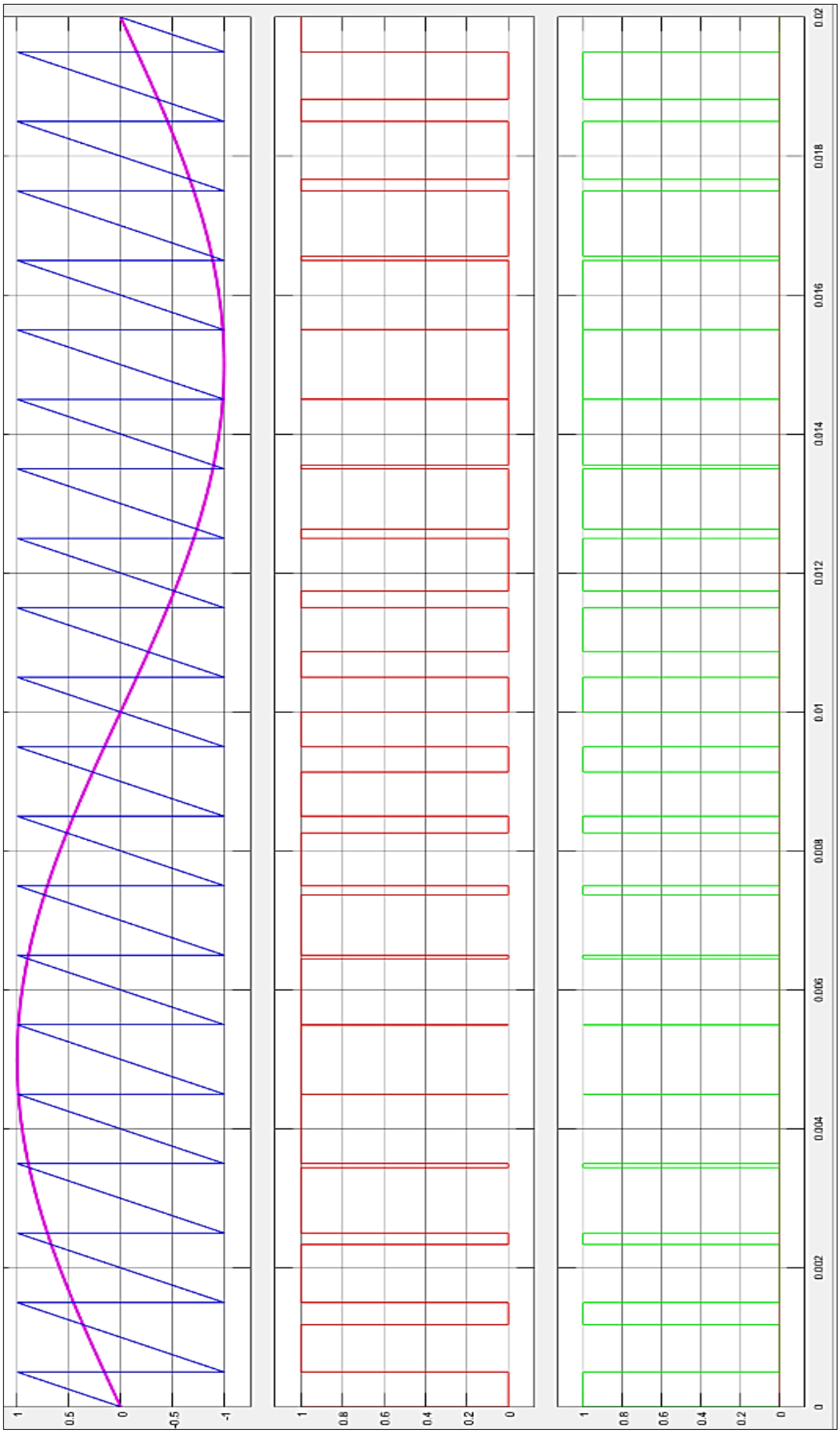


Figure 2: *Output of SPWM gate pulse circuit.*

Page 29-38 © MAT Journals 2021. All Rights Reserved

www.matjournals.com
https://doi.org/10.46610/JOARES.2021.v07i02.005

AC INDUCTION MOTOR

Motor is an electrical machine converts electrical energy into mechanical energy. Depending on the type of supply fed, the motors are classified into DC and AC motors. An AC Induction motor comes under the AC Motors classification. AC induction motor is simple in construction, cheaper in cost, less maintenance and highly efficient. It runs at a speed lower than the synchronuous speed therefore it is termed as Asynchronous motor. It has Stator and Rotor. Upon the staor, main winding is placed and on the rotor field winding is placed. The rotating magnetic field is produced according to Faraday's Laws of Electromagnetic Induction. Single phase induction machines are not self-starting, due to generation of pulsating torques when single phase ac supply is given. A starting winding or auxiliary winding is placed on the stator along with main winding provided with a centrifugal switch which disconnects when it reaches 70 to 80% of the speed.

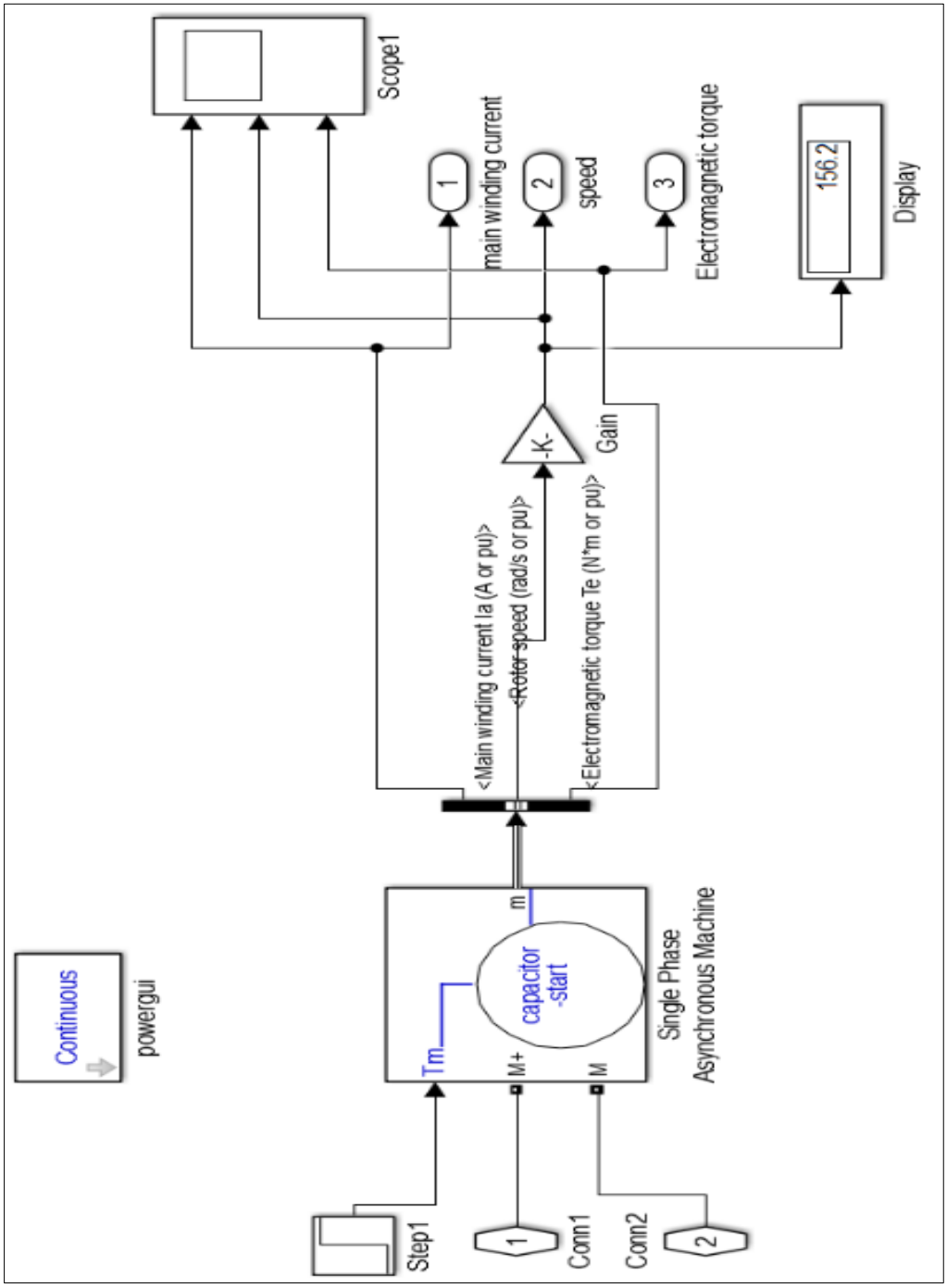


Figure 3: *Implementation of AC induction motor in Matlab/Simulink.*

Page 29-38 © MAT Journals 2021. All Rights Reserved

RESULTS

The DC motor is implemented in the MATLAB/Simulink and their performance characteristic is interpreted. The Fig. 4 represents the implementation of DC Motor in Matlab/Simulink and Fig. 5 represents the variations of armature currents, Speed and Torque of a DC Motor.

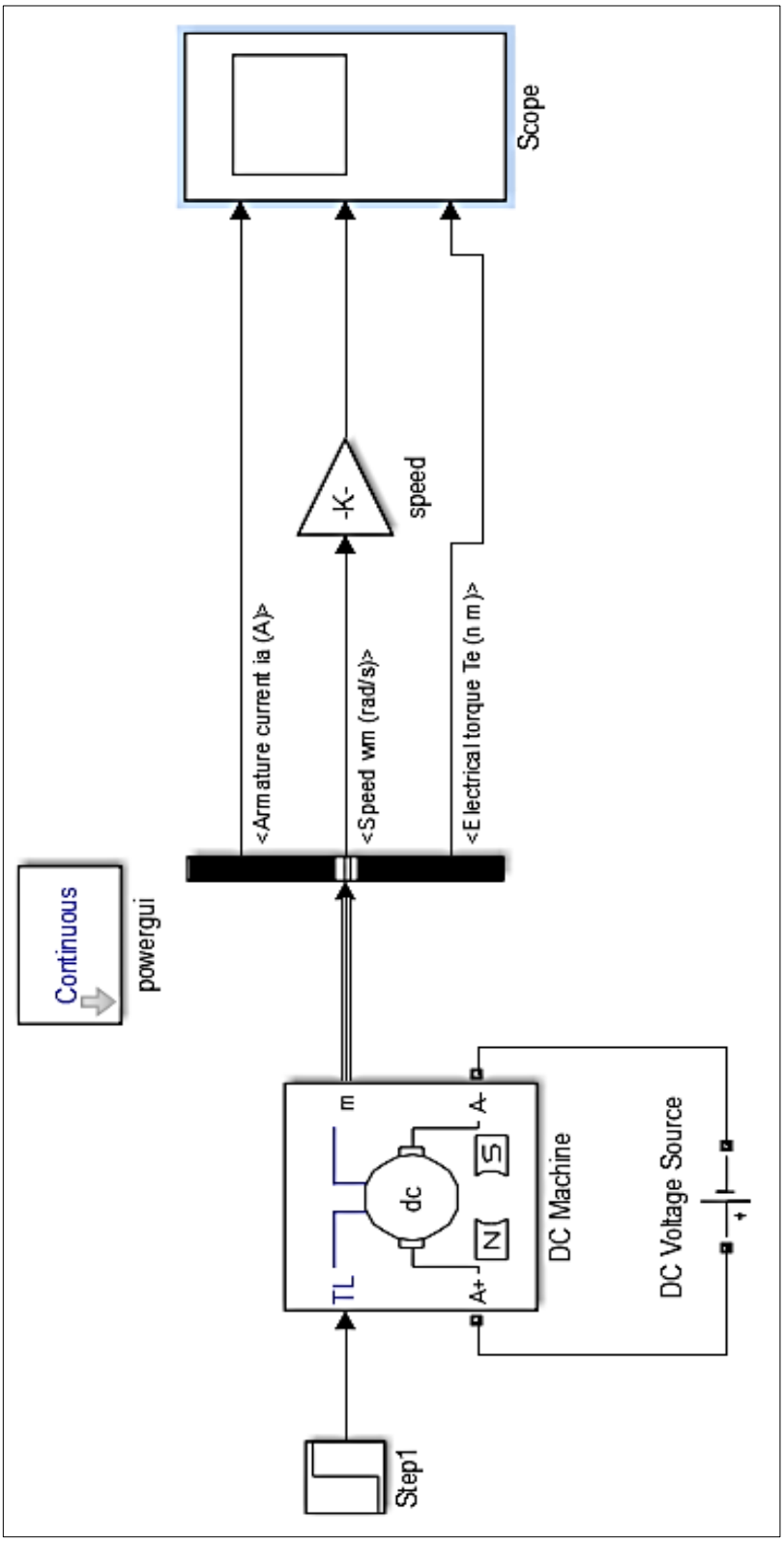


Figure 4: *Implementation of DC motor.*

Page 29-38 © MAT Journals 2021. All Rights Reserved

www.matjournals.com
https://doi.org/10.46610/JOARES.2021.v07i02.005

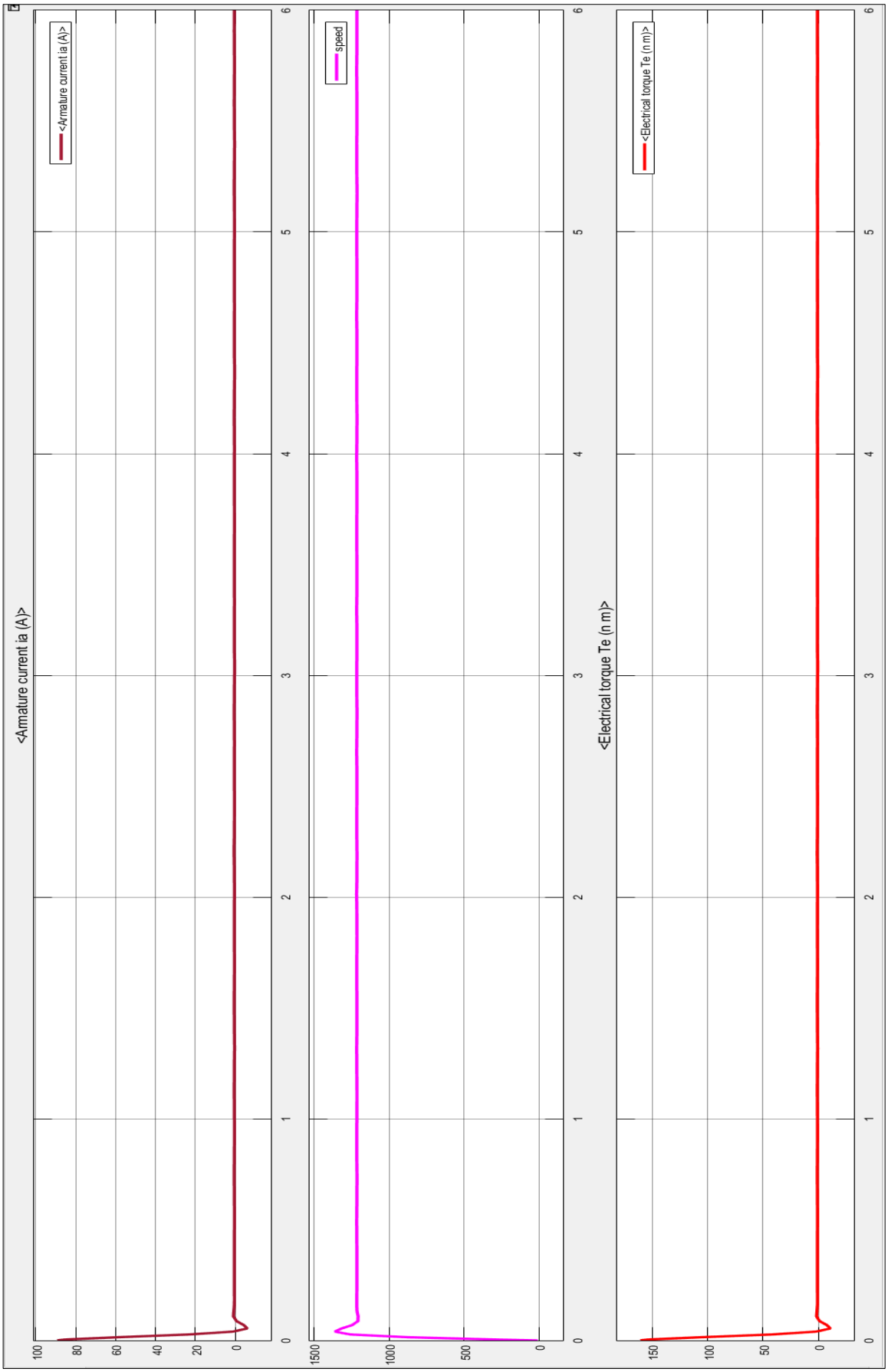


Figure 5: *Performance analysis of DC motor.*

Page 29-38 © MAT Journals 2021. All Rights Reserved

www.matjournals.com https://doi.org/10.46610/JOARES.2021.v07i02.005

The SPWM using MOSFET single phase full bridge inverter is simulated and the output voltage is measured as shown in Fig. 6. Quasi square wave is the output voltage of 230V magnitude is shown in Fig. 7. This output is then applied to the AC Induction Motor and the performance of the machine is analysed as shown in Fig. 8.

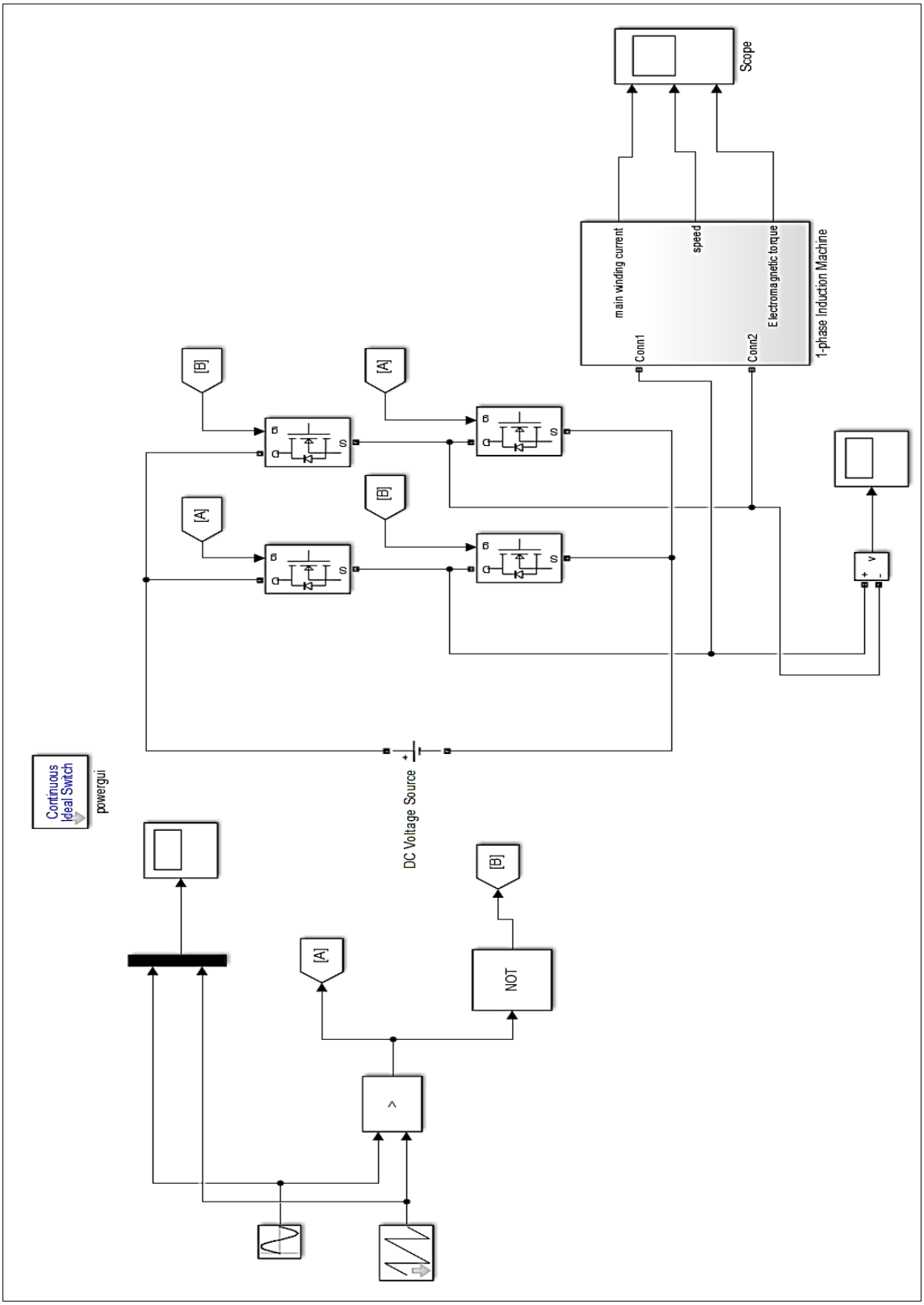


Figure 6: *Implementation of single phase full controlled bridge inverter with AC induction motor.*

Page 29-38 © MAT Journals 2021. All Rights Reserved

https://doi.org/10.46610/JOARES.2021.v07i02.005

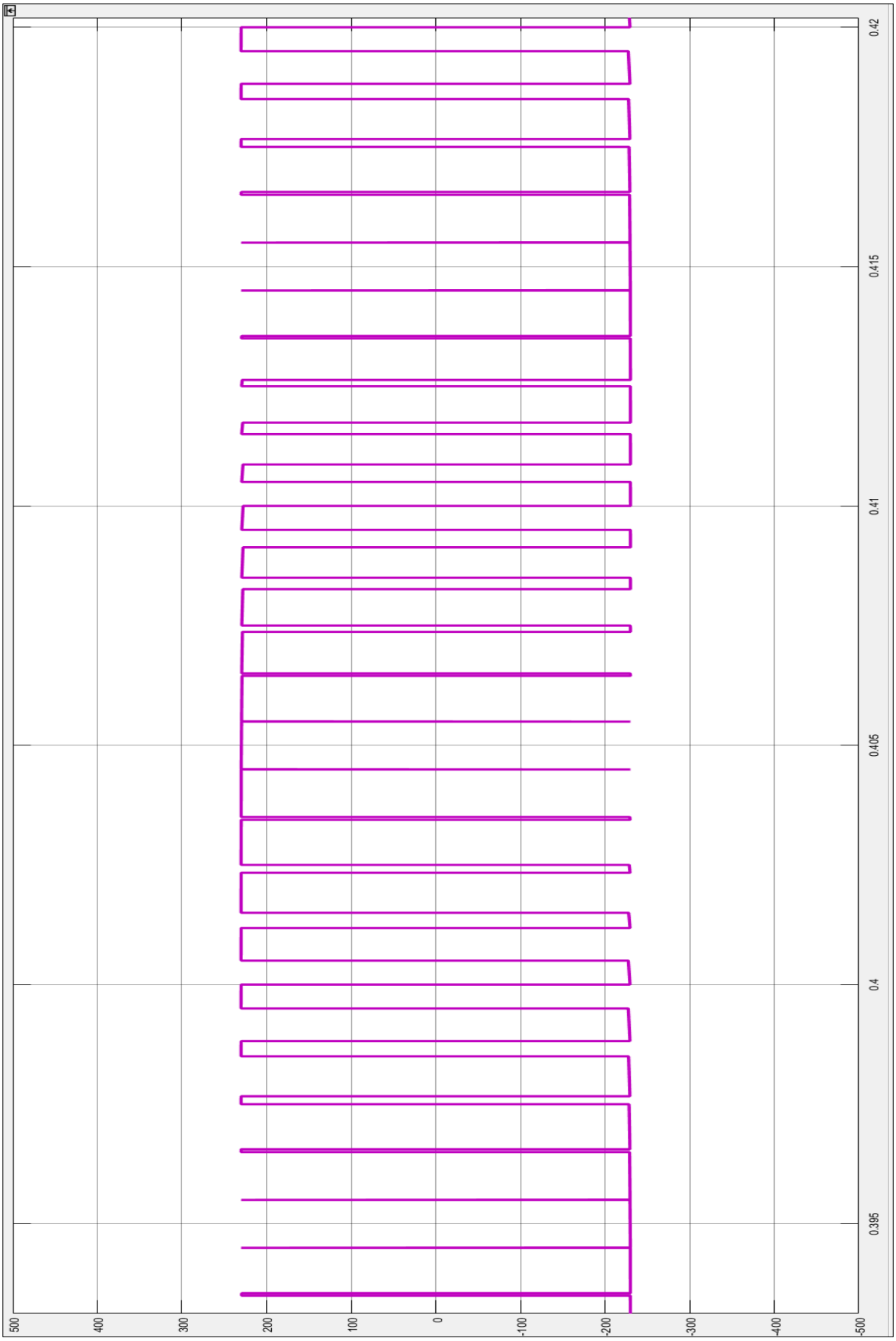


Figure 7: *AC output of bridge inverter.*

Page 29-38 © MAT Journals 2021. All Rights Reserved

www.matjournals.com
https://doi.org/10.46610/JOARES.2021.v07i02.005

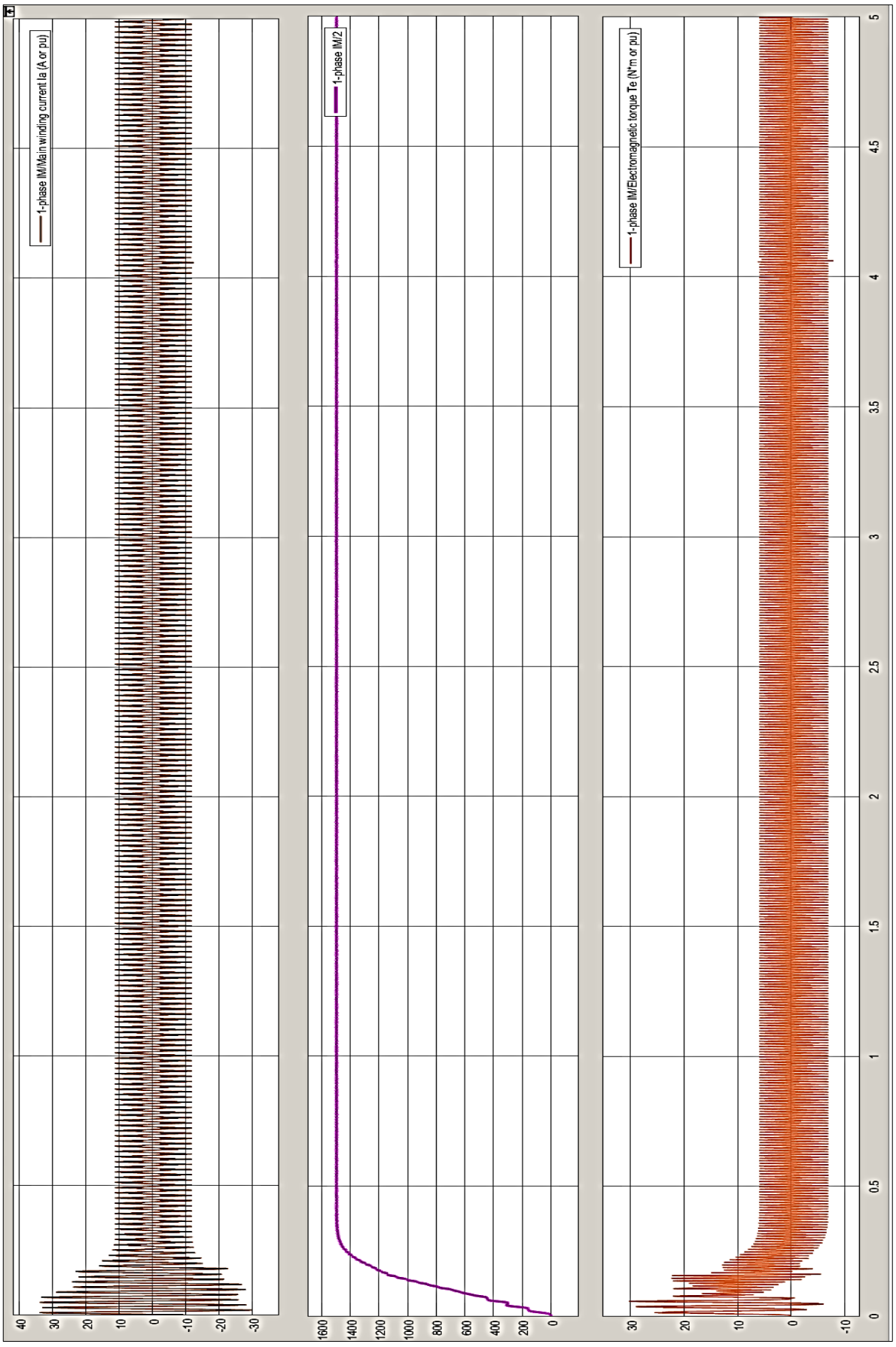


Figure 8: *Output of SPWM based Single phase induction motor.*

Page 29-38 © MAT Journals 2021. All Rights Reserved

www.matjournals.com
https://doi.org/10.46610/JOARES.2021.v07i02.005

CONCLUSION

The disadvantage of using DC Motor in Electric vehicle is its maintenance and high initial cost. The replacement of DC motor with AC induction motor has overwhelmed the drawbacks due to its low initial cost, less maintenance and robustness. Here, we have compared the operation of DC Motor with the SPWM based AC induction motor and observed its characteristic behaviour in terms of Torque, Speed, Armature Current. From the analysis, it is found that AC induction motor can also be used in the electric vehicle for its advantages.

REFERENCES

1. M. Al Rizwan Khan, R. Arun Bharathi, B. Gowtham, A. Elakya & A.S Akash Saravanan (2019). Smart Electric Vehicle. *5th International Conference on Advanced Computing & Communication Systems*, Coimbatore, India, Available at: https://ieeexplore.ieee.org/document/8728534.
2. Sundas Hannan, Sohaib Aslam & Muhammad Ghayur (2018). Design and Real-Time Implementation of SPWM based Inverter, Sundas Hannan, Sohaib Aslam, Muhammad Ghayur, Available at: https://ieeexplore.ieee.org/document/8338637.
3. Sachin Maheshri & Prabodh Khampariya (2014). Simulation of single phase SPWM (Unipolar) Inverter. *International Journal of Innovative Research in Advanced Engineering, 1(9),* 12-18, Available at: https://www.ijirae.com/volumes/vol1/issue9/OCEE10081(03).pdf.
4. Subhasis Nandi Hamid, A. Toliyat, IEEE Alexander G. Parlos (1997). Performance Analysis of a Single Phase Induction Motor under Eccentric Conditions. *IAS '97. Conference Record of the 1997 IEEE Industry Applications Conference Thirty-Second IAS Annual Meeting*, New Orleans, LA, USA, Available at: https://ieeexplore.ieee.org/document/643024.

Page 29-38 © MAT Journals 2021. All Rights Reserved

GIS BASED FLOOD HAZARD MAPPING: A CASE STUDY OF TANDAVA RIVER BASIN, ANDHRA PRADESH

Ms. S.Anita[1], Prof. Vazeer Mahammood[2], Er.Arunima Mahapatra[3], Ms. M Amareswari Reddy[4]

[1]*PG student, Department of Civil Engineering, Andhra University College of Engineering(A), Viskhapatnam-530003, Andhra Pradesh, India*

[2] *Professor, Department of Civil Engineering, Andhra University College of Engineering(A), Viskhapatnam-530003, Andhra Pradesh, India*

[3,4]*Assistant Professor, Department of Civil Engineering, Dr Lankapalli. Bullayya College of Engineering, Viskhapatnam-530013, Andhra Pradesh, India*

Email: arunimam@lbc.edu.in[3] amareswari@lbce.edu.in[4]

Abstract: **A flood occurs as water overflows and submerges normally dry land. Flooding is a natural phenomenon that occurs on the surface of the Earth. Although we cannot prevent floods, we can foresee flooding and protect lives, land, and other resources before it happens. The primary consideration of flood-prone areas for land use planning is the monitoring of flood hazard areas using Arc GIS. Most agricultural fields that are vulnerable to flooding are found in the villages next to the Tandava River. The study covers an area of 1283 km^2 in Visakhapatnam district, Andhra Pradesh aims to provide flood hazard risk zone maps for the Tandava River basin using a combination of Remote Sensing and Geographic Information System (GIS), based on a multi-criteria assessment. Using geospatial data, satellite imagery and GIS methods various landscape parameters and environmental factors, are taken into consideration to prepare the flood danger risk zone maps. The thematic map weightages are determined with the analytical hierarchy method (AHP). Weighted overlay analysis is applied and weightages are given to the various thematic maps such that a flood hazard risk zone map was generated for the study area. The hazard map was categorized into four flood hazards zones and their distributions are medium, moderate, mild, and extremely high danger zones. The results obtained were found to be helpful in better planning and flood disaster management.**

Key words: **Flood hazard map, Analytical Hierarchy Process (AHP), Geographic Information System (GIS), weighted overlay analysis**

I. INTRODUCTION

A hazard is a possible cause of risk. Substances, events, or circumstances should be declared dangers if their existence allows them to cause harm to health, life, property, or any other valuable concern, even if only potentially. Flooding is the most common and expensive natural hazard, causing more deaths than any other natural hazard and having the largest geographical distribution. Natural disasters such as earthquakes, tsunamis, landslides, tropical storms (hurricanes, cyclones, and typhoons), marine inundation, and floods affect large parts of the planet (Li., et al. 2012). Almost 85 percent of India's land area is exposed to a variety of natural hazards. India is one of the most flood-affected countries in the world, ranking second, and accounts for one-fifth of all flood-related deaths worldwide. Flood hazard danger zone maps are developed in ArcGIS software by combining thematic maps and satellite data. To build a flood hazard map, a weighted overlay mapping tool is used.

Nerantzis Kazakis et al. (2015) identified flood hazard areas in the study area by creating a multi-criteria database. This index has been used in Northern Greece's Rhodope-Evros area. The index was generated using an empirical hierarchy approach (AHP).Kamanchot Seejata et al. (2017) surveyed flood threat areas in Thailand's Lower Yom basin, Sukhothai province. The flood parameter weightages are determined using the analytical hierarchy method (AHP) and a flood hazard map for the study area is created. They compared the flood threat map generated with the observed flood extent from a secondary data source. Every year, approximately 40 million hectares of land in India are exposed to flooding, resulting in an estimated loss of 240 million USD, and approximately 22 states and one territory of India are vulnerable to flooding. The steel-framed railway bridge over the Tandava river near Tuni town in East Godavari was riddled with trash, tree stems, and rubble of all sorts in November 2012, according to India-times, as rainwater overran the bridge with great intensity. This big flood-affected eight districts in A.P. and claimed the lives

of 22 people. Hundreds of villages were inundated, road and rail traffic was halted, and tens of thousands of hectares of crops were destroyed.

II. STUDY AREA

The major study covers 1283 km2 and is located between latitudes 17°20' to 17°50' N and longitudes 82°20' to 82°40' E. It is included in the Survey of India toposheets 65 K/5, K/6, K/7, K/10, and K/11. While the majority of the sample area is in the Visakhapatnam district, the neighboring areas of East Godavari district are also included to see the total morphometry of the drainage basin. The Tandava river basin, located between the main river systems of Godavari and Mahanadi, is one of India's small and most significant watersheds. The river rises in the Eastern Ghats at an elevation of 1023 meters above mean sea level near the villages of Lingavaram and Mandhayam in Chintapalli Mandal, Visakhapatnam district. Tandava river originates in the Eastern Ghats and passes through much of the hilly terrain, undulating uplands, and plains until emptying into the Bay of Bengal at Pentakota. The flow chart of the methodology is shown in fig.1.

Materials and Methods

ArcGIS 10.5 and ILWIS 3.4 development tools were used to generate appropriate maps for the current analysis. The Equal Interval Method in ArcGIS 10.5 was used to create thematic maps of rainfall distribution, soil type, geology, geomorphology, land use and land cover, stream order, slope, and aspect maps by assigning weightages to each class. Weighted overlay analysis using the Spatial analyst tool was used to integrate the data layers in the GIS environment as shown in table 1.

Table 1
Database detail

Database type	Details of database	Source of database
Rainfall Data	Rain gauge station – Chintapalle, Payakaraopeta, Rajavommangi, Nathavaram	Climate Knowledge Portal
Toposheet	65 K/5, 65 K/6, 65 K/7, 65 K/10, 65 K/11	Survey of India
Thematic Maps	Soil	National Bureau of Soil Survey (NBSS).
	Geology	Bhukosh website
	Geomorphology	Bhukosh website
	LULC	Copernicus global land service

Analytical hierarchy process

The weight of each parameter is defined using the analytical hierarchy process (AHP) (Saaty, 1990). When a large number of interrelated objectives or criteria are involved, AHP provides us with a simple and structured technique for analyzing complex problems. After ranking these criteria as per the importance, their weights are defined. Consider the above table 2 as matrix A_1. The normalized values of the parameters obtained by:

$$\text{Slope} = (1*2*2*3*3*5*5*7)^{1/8} = 2.985$$

Here 8 represents the number of parameters. Similarly, the values of other parameters are also obtained. These values are normalized by dividing the value of each parameter with the total value of all parameters.

Consider the weightage values obtained in table 4 as matrix A_2. Now multiply the matrices A_1 and A_2 and name that matrix as A3. Summarize the values obtained in matrix A3. Divide matrix A_3 by A_2 and name that matrix as A_4. Take the average of the values obtained in matrix A_4. It represents the λ value.

$$A_3 = A_1 \times A_2$$
$$A_4 = A_3/A_2$$

Consistency check

After the creation of the AHP matrix, its consistency needs to be evaluated. The level of consistency is calculated using the following index.

$$CR = \frac{CI}{RI}$$

where, CR – consistency ratio, CI – consistency index and RI – random index

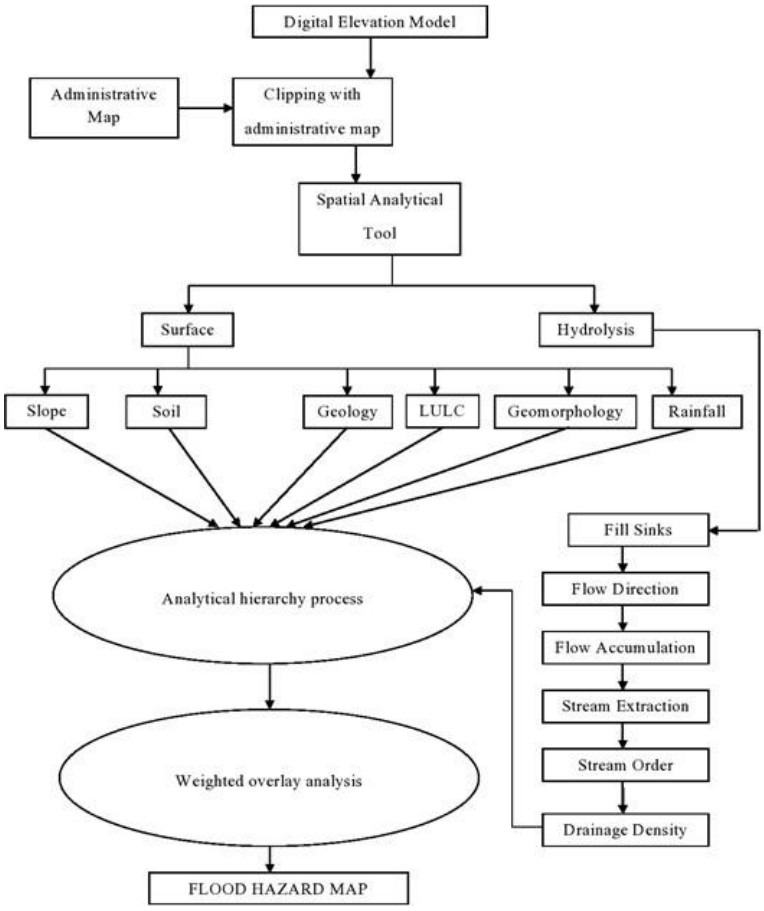


FIG 1
FLOW CHART OF METHODOLOGY

TABLE 2
PARAMETERS OF FLOOD HAZARD: AHP

Parameters	Slope	Drainage density	Rainfall	LULC	Elevation	Geology	Soil	Geomorphology
Slope	1	2	2	3	3	5	5	7
Drainage density	1/2	1	2	2	3	3	4	5
Rainfall	1/2	1/2	1	2	3	3	4	6
LULC	1/3	1/2	½	1	3	4	5	6
Elevation	1/3	1/3	1/3	1/3	1	2	2	3
Geology	1/5	1/3	1/3	1/4	1/2	1	2	5
Soil	1/5	1/4	1/4	1/5	1/2	1/2	1	5
Geomorphology	1/7	1/5	1/6	1/6	1/3	1/5	1/5	1

TABLE 3
CALCULATION OF MATRIX A_4

S.No	A_3	A_4
1	2.358	8.33
2	1.664	8.45
3	1.234	7.25
4	1.247	8.6
5	0.617	8.33
6	0.514	8.56
7	0.400	8.69
8	0.200	9.09

$\lambda = \text{Average of values of matrix A4} = 8.41$

In table 4 the values of RI are tabulated. These values are dependent on the number of parameters. In this study, the criteria are 8 and as a result the RI = 1.41.

TABLE 4
RANDOM INDEX USED TO COMPUTE CONSISTENCY RATIO

N	1	2	3	4	5	6	7	8	9
RI	0	0	0.58	0.90	1.12	1.24	1.32	1.41	1.45

$$\mathrm{CI} = \frac{\lambda - \mathrm{n}}{n-1} \qquad \mathrm{CI} = \frac{8.41-8}{8-1} = 0.058$$

$$\mathrm{CR} = \frac{\mathrm{CI}}{\mathrm{RI}} = \frac{0.058}{1.41} = 0.041 < 0.1$$

Since CR's value is lower than threshold (0.1) the weight's consistency is affirmed.

III. RESULTS AND DISCUSSIONS:

1. **Soil Influences**

Water holding capacity and infiltration in an area can be determined by soil type and texture. These soil characteristics of an area influence the flood susceptibility (Nyarko B.K., 2002). Water cannot infiltrate into impermeable soils like clay or shale, thereby increasing the surface runoff and flood risk in those areas. Ajin R.S. et al. has prepared soil map for Vamanapuram river basin, Kerala. In Tandava river basin there are three types of soils found i.e., Sandy-clay-loam, Loam, Sandy loam. The spatial distribution of soil in Tandava river basin is shown in fig 2.

2. **Slope**

The relief of the land can also have an impact. As the water can flow quickly down to the river as the overland flow, steep slopes reduce the amount of infiltration into the ground. More amount of water can also flow through the soil because of steep slopes, whereas high amount of water can be penetrated into soil and increase lag time in the case of gentle slopes. Thakuriah Gitika and Saikia Ranjan prepared slope map by taking SOI toposheet having 20 meter contour interval and slope angle of each pixel is generated from TIN for Krishnai watershed, Assam. Slope map of the study area is prepared using SOI toposheet having 20 meter contour interval within GIS environment. Tandava River Basin has been demarcated into five classes of slope i.e., level to nearly level $1^0 - 1.8^0$, gently sloping $1.8^0 - 2.6^0$, moderately sloping $2.6^0 - 3.4^0$, moderately steep sloping $3.4^0 - 4.2^0$ and steep sloping $4.2^0 - 5^0$.

3. **Land use and Land cover**

The land use and management of the area is one of the primary concerns because it is a factor through which not only the current use of the land, pattern and type of its use are reflected but also gives information about its use in relation to the living population and its relationship with the existing development. Type of vegetation plays a major role, with forests intercepting more rainfall than grasses. Because of this interception there is an increase in lag time and the risk of a flood is reduced. Generally, deforestation can increase soil erosion, reduce interception and increase flood risk. Afforestation i.e., where trees

are planted, can have the opposite effect. Suraji Bera prepared LULC map for the Subarnarekha river by using Landsat–7 ETM+ data help of ERDAS software. LULC in the study area include: built-up land, water bodies, deciduous broadleaf forest, shrub land, barren land, crop land, waste land etc.

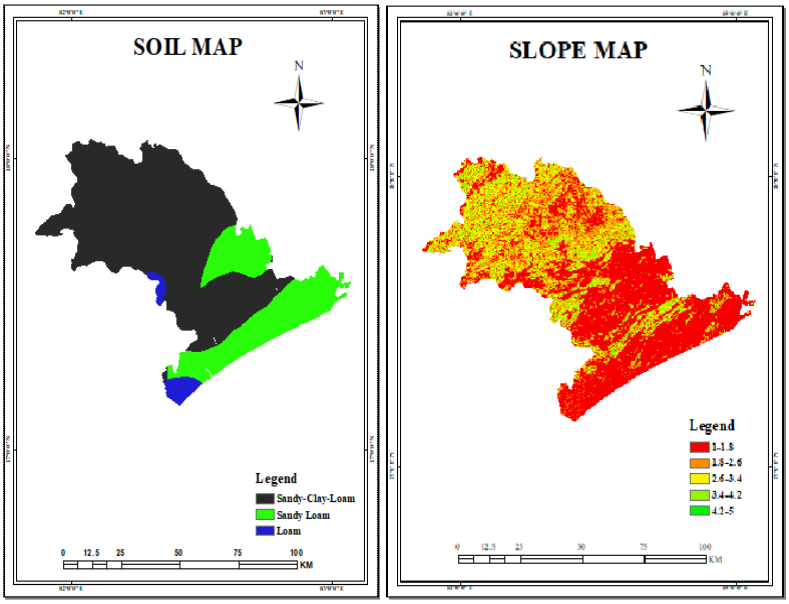


FIG 2 & 3
SOIL & SLOPE MAP

4. Rainfall Distribution:

Heavy rainfalls are one of the main reasons why floods occur. In association with the extreme rainfall, floods are the down slope runoff where the rain water cannot immediately step into the ground. The amount of runoff depends upon the amount of rain a region experience. Due to heavy rainfalls, the level of water in rivers or lakes rises. When the level of water rises above the river banks or dams, the water starts overflowing, this causes floods. The areas beside the rivers, lakes or dams are overflown by the rainwater thereby causing floods or deluge. There are four rain gauge stations in the catchment area. As shown in fig.4 & 5 the inverse distance weighted method used for preparing rainfall distribution map.

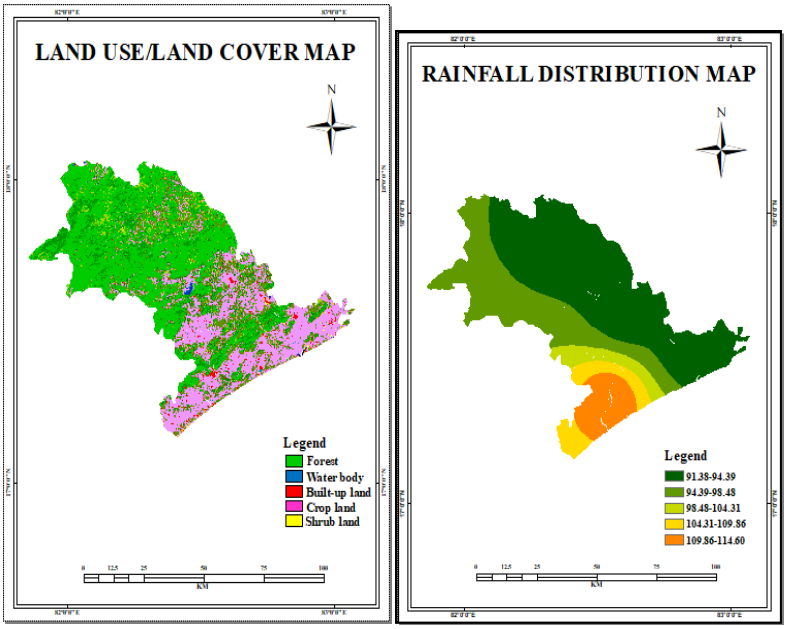


FIG 4 & 5
LAND USE & RAINFALL DISTRIBUTION MAP

For the present study the four rain gauge stations in the catchment area are taken into consideration and tabular in table 5.

TABLE 5

TABLE SHOWING THE RAINFALL DISTRIBUTION DETAILS

S.No.	Station Name	Average Annual Rainfall (mm) (2011-2015)
1	Chintapalle	95.01167
2	Narsipatnam	91.38667
3	Tuni	114.6033
4	Yelamanchili	92.40762

5. Geomorphology

Geomorphology is the study (fig6) of Earth's landforms created by mostly physical processes, including physical or chemical changes and those changes influenced by biological processes, including land use. In the aspect of preparation for flood hazards, geomorphology helps physical geographers in understanding Earths's physical changes that leads to major environmental disasters. The study area comprises of hills, valleys, dam and reservoir, old flood plain, younger coastal plain etc.

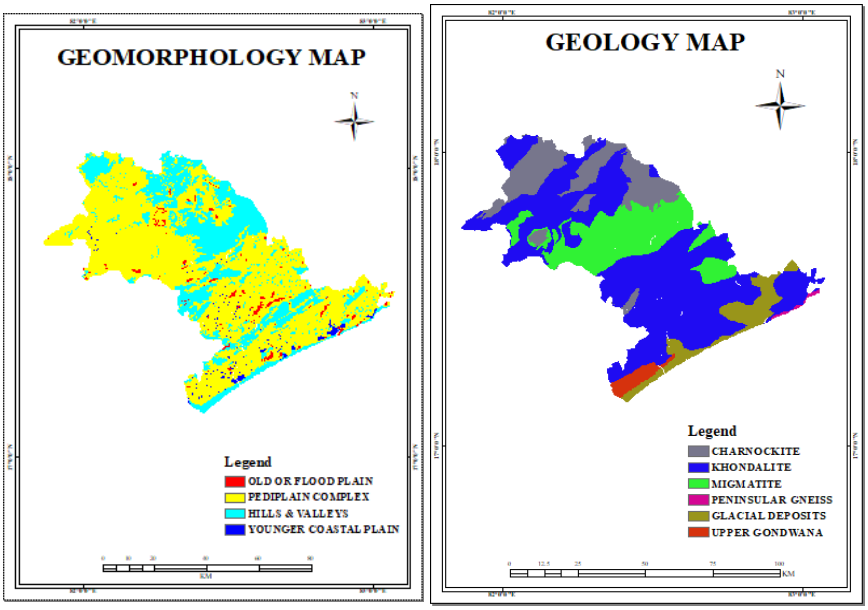


FIG 6 & 7

GEOMORPHOLOGY & GEOLOGY MAP

6. Geology

Water can flow through the cracks and layers of permeable rocks, whereas it cannot flow in the case of impermeable rocks. Valleys made of impermeable rocks are mostly prone to heavy floods as the rain water cannot flow through rocks, thereby increasing the amount of surface runoff. The study area comprises of Gneiss, fluvial and glacial sediments as shown in fig7. Gneiss is a metamorphic rock and water holding capacity for this rock is less compared to fluvial and glacial sediments. Most of the study area comprises of gneiss complex.

7. Drainage density

Drainage of rain water is an important environmental factor that controls the flood hazards (fig.8). Nature of the soil and other geotechnical properties indicates the drainage density of an area. Drainage density is the ratio of length to unit area of the basin. Areas having high drainage density indicate high flow accumulation path and those areas receive heavy floods.

8. Elevation

An elevation map is a representation of the Earth's relief that consists of an ordered array of elevations relieve to a datum, and referenced to a geographical coordinate system. Information that is helpful in hydrological modeling and other environmental applications can be obtained by elevation maps as shown in fig9. The topographic maps have been used to extract the contours at different interval. Elevation for each village polygon has been extracted by overlaying the village boundary layer using ArcGIS. Elevation plays a vital role in determining the severity of flood and bank erosion hazard.

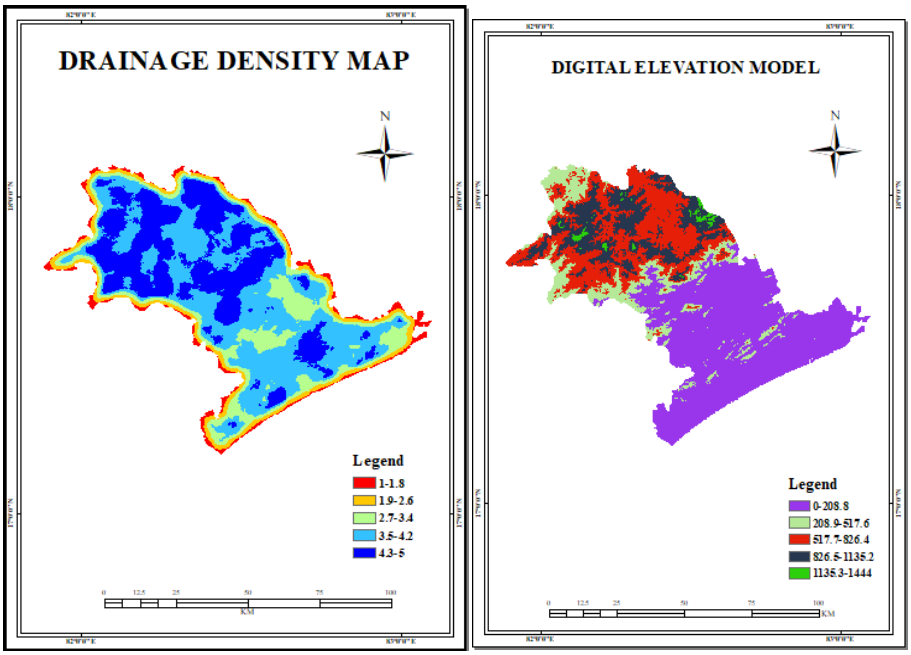


FIG 8 & 9

DRAINAGE DENSITY & DIGITAL ELEVATION MODEL

9. Flood Hazard Risk Zone

The net probability of occurrence of flooding in each flood hazard zone is estimated from the total sum of weight of each contributing factor considered. To obtain this total sum weight, all of contributing factor maps were overlaid. The total weightage as tabular in table 6 were find to the probability of a flood to occur in a flood zone are is the sum of weightages of all contributing factors. The decision maker is facilitated by ArcGIS software to identify a predefined set of criteria with the overlay analysis. The weighted overlay analysis tool of ArcGIS allows us to identify the flood hazard areas by compilation and overlaying of contributing factor maps. Finally, flood hazard map fig.10 is prepared in terms of low, moderate, high and very high and the percentage of each flood hazard risk zone is shown in table 7.

TABLE 6

WEIGHTAGES FOR FLOOD HAZARD RISK ZONES

S.No.	Thematic maps	Weightage
1	Slope	28.3%
2	Drainage density	19.7%
3	Rainfall	17%
4	Land use / Land cover	14.5%
5	Elevation	7.5%
6	Geology	6%
7	Soil	4.7%
8	Geomorphology	2.3%

TABLE 7

PERCENTAGES OF EACH FLOOD HAZARD RISK ZONES

S.No.	Hazard Zones	Area in km^2	Area in %
1	Low	78.65	6.13
2	Moderate	603.39	47.03
3	High	592.61	46.19
4	Very High	8.21	0.64

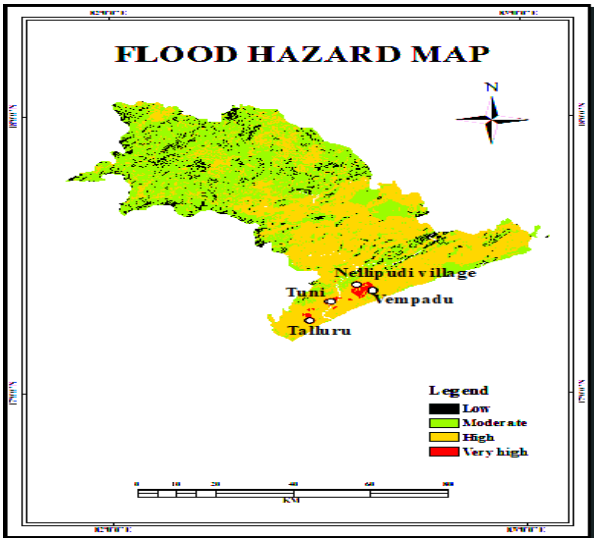


Fig 10
Flood Hazard Risk Zone Map

IV. CONCLUSIONS

It can be concluded that floods are natural phenomena which cannot be controlled. However, increased human activities towards urbanization in reducing the frequencies of flood occurrence and reflecting an adverse impact on the livelihood. Rainfall, slope, drainage density, elevation, land use and land cover, soil conditions are considered to be important factors contributing to flood hazard. The present study enhances a more cost effective and simple process of creating flood hazard maps using GIS. It will help in appropriate planning for hazard mitigation.

ACKNOWLEDGMENT

I would like to express my gratitude to Prof. Vazeer Mahammood, of civil engineering department Andhra university for his Constant support and encouragement at the Various stages of this work.

REFERENCES

1. Ajin. R.S., R.R. Krishnamurthy, M. Jayaprakash and Vinod. P.G. (2013): "Flood Hazard Assessment of Vamanapuram River Basin, Kerala, India: An approach using Remote Sensing and GIS techniques.
2. E.K. Furko Flood Hazard Mapping using ASTER Image data with GIS. International Journal of Geomatics and Geosciences, Volume 1, No. 4, 2011.
3. Floods in Tandava River Basin (http://timesofindia.indiatimes.com /city/hyderabad/No-let-up-in-rain-fury-in-AndhraPradesh).
4. G. Ashenafi Tolessa and P.Jagadeeswara Rao: A Geospatial based study on mapping of flood inundation zones in Tandava River Basin, Andhra Pradesh.
5. G. Ashenafi Tolessa: Surface water modelling for Tandava River Basin using SCS-CN model – Hydroinformatic Approach.
6. G. Ashenafi Tolessa, P. Jagadeeshwara Rao and N. Victor Babu: Morphometric Analysis of Tandava River Basin, Andhra Pradesh, India (2013).
7. H.Leenaers, and J.P. Okx. The use of Digital Elevation Models for Flood Hazard Mapping, Earth Surface Processes and Landforms, 14(6-7), pp 631-640, 1989.
8. Kamonchat Seejata et al., (2017). Assessment of flood hazard areas using analytical hierarchy process (AHP) over the Lower Yom basin, Sukhothai province, Northern Thailand.
9. Nerantzis Kazakis et al., (2015). Assessment of flood hazard areas at a regional scale using an index- based approach and analytical hierarchy process (AHP): Application in Rhodope-Evros region, Greece.
10. Pratik Dash and Jishnu Sar: Identification and validation of potential flood hazard area using GIS based multi-criteria analysis and satellite data derived water index (2020).
11. Rainfall data (https://climateknowledgeportal.worldbank.org/download-data).
12. Surajit Bera and Akash Bhandari (2013). Assessment of Flood Hazard Zone using Remote Sensing & GIS – A case study of Subarnarekha River Basin.

13. Thakuriah Gitika and Saikia Ranjan: GIS-based Flood Hazard Mapping: A case study in Krishnai River Basin, Assam, India.
14. Surjit Singh Saini, Kaushik. S.P., Itternational Journal of Geomatics and Geosciences, 2012, 3 (1): 42-54.
15. Vahdettin Demir, Ozgur Kisi: Flood hazard mapping by using GIS and hydraulic model – Mert River, Samsun, Turkey (2016).

International Journal of Advanced Technology and Engineering Exploration, Vol 8(81)
ISSN (Print): 2394-5443 ISSN (Online): 2394-7454
http://dx.doi.org/10.19101/IJATEE.2021.874272

Research Article

Development of real-time flood forecast model for vamsadhara river through hydrological approach

Arunima Mahapatra[1*], Vazeer Mahammood[2] and K H V Durga Rao[3]
Assistant Professor, Dr. Lankapalli Bullayya College of Engineering, Visakhapatnam, A.P, India[1]
Professor, Civil Engineering Department, Andhra University, Visakhapatnam, A.P, India[2]
Flood Forecasting & Hydrological Modeling Division, Water Resources Group, National Remote Sensing Centre (NRSC), Hyderabad, A.P, India[3]

Received: 21-June-2021; Revised: 20-August-2021; Accepted: 25-August-2021
©2021 Arunima Mahapatra et al. This is an open access article distributed under the Creative Commons Attribution (CC BY) License, which permits unrestricted use, distribution, and reproduction in any medium, provided the original work is properly cited.

Abstract
Hydrologic simulation of large river catchments, and the decision to choose a computerized model, is a complex job that necessitates a thorough knowledge of rainfall-runoff processes. While modeling involves proper estimation of direct surface runoff volume and peak discharge in a watershed. In the present study, a real-time flood forecasting model is developed using Hydrological Modelling System (HMS) to forecast floods and River Analysis System (RAS) to identify inundation areas in the Vamsadhara river basin located between Odisha and Andhra Pradesh in India. The flood prediction model is constructed using a simulation of spatial data. The approach includes a loss model to compute infiltration loss, a transform model to simulate runoff rate, and a Muskingum routing method to route flow in a river along with model calibration, and validation with field data. Topographic and hydrologic parameters for each of 17 sub-basins are computed using Land Use, Land Cover (LULC). Muskingum parameters are also calculated. The hydrological model has been calibrated using the precipitation and gauge discharge data of the 2006 flood event. For validation of the modeling process, flood events in 2010 and 2013 at two Gunupur and Kashinagar gauge stations were chosen. The simulated peak discharges obtained are sufficiently accurate with observed data at both the gauge stations. The Nash-Sutcliffe efficiency (NSE) obtained for the calibration period are 0.78 & 0.77, which shows that model performance is good and accepted for simulation of streamflow. Similarly, the model performance for validation period is 0.81 & 0.80 for 2010 flood event while for the 2013 flood event are 0.84 & 0.82 indicating very good model performance. Overall, the study revealed that the HMS model could be employed for the calculation of surface runoff and flood forecasting in similar areas and conditions existing nearby catchments. Flood inundation maps generated with HEC-GeoRAS and Hydrologic Engineering Center-River Analysis System (HEC-RAS) for 1D steady flow demonstrate the model's output. As a result, this would help in the effective monitoring of flood hazards and the sustainable management of watersheds.

Keywords
GIS, Flood forecast, DEM, Flood inundation map, HEC-HMS, HEC-GEORAS, HEC-RAS.

1. Introduction
River floods are usually caused by a combination of wind-driven flood surges, low barometric pressure, and massive waves colliding with high upstream river flows. These floods are known to be the most devastating natural hazards. In India, wide sectoral and regional variables impact country climate change adaptability [1]. According to Markus et al. [2] climate change effects in the catchment, this change in climate is the leading cause of floods, mostly due to deforestation, urbanization, etc.

Statistics suggest that floods account for almost 15% of all deaths from natural disasters and that the economic damages caused by floods have been seen to surpass billions of dollars worldwide, not just in developed countries in Asia but also in the countries of the European Union [3].

The occurrence of catastrophic weather conditions in recent years has proven the need of realistic flood models, which function as early warning systems in severe storm situations, reducing economic damage. An early warning system comprises both structural and non-structural measures. While structural incorporates the physical construction of embankments, canals, and so on, non-structural

*Author for correspondence

initiatives include flood forecasting models that reduce flood risks [4, 5]. Many countries have made modeling and forecasting such occurrences a top priority [6].

Hydrological Modelling System (HMS) developed by the United States Army Corps of Engineers (USACE) helps in simulating the hydrologic cycle of a dendritic watershed system [7]. This model is especially well adapted for simulating direct runoff, which incorporates (overland flow and interflow) and runoff volume, as well as routing to the outlet [8].

Infiltration loss (Loss model), Transform model, and Muskingum routing model are the three most important components in watershed management. The loss model is based on the Soil Conservation Service–Curve Number (SCS-CN). The transformation of rainfall to direct runoff is based on SCS-Unit Hydrograph (UH). The channel routing of river flow based on the Muskingum routing method. This method has been successively used for several hydrological case studies [9, 10, 11].

The Vamsadhara river basin flows east between Mahanadi and Godavari. Its catchment area is 10,830 km^2, of which 8015 km^2 is in Odisha and 2815 km^2 is in Andhra Pradesh (SANDRP) [12]). Almost every year, severe cyclones and heavy rain cause flooding in the Vamsadhara River affecting both Orissa and Andhra Pradesh. Both states experienced devastating floods in 2001, 2003, 2006, 2008, 2011, 2013 (Phallin) & 2019 (Fani). Rivers flowing downstream are primarily responsible for raising the risk of flooding and cause extreme flood events [13]. Andhra Pradesh lies downstream of the river basin, with districts like Guntur, Krishna, Srikakulam, and Vizianagaram is being extremely vulnerable.

Odisha's Rayagada, Ganjam, Kendrapada, and Jagatsinghpur districts are susceptible upstream. These flood disasters wiped out entire neighbourhoods or even towns, destroying a large portion of agricultural fields, and resulting in severe property and life loss. With the frequent occurrence of floods in Vamsadhara River, it's essential to develop and use event-based watershed model that explain precipitation–runoff processes, which have been a major focus of hydrological study and investigation for decades [14].

The most difficult aspect of analyzing the river basin is model selection, data availability, calculating the hydrological parameters of the watershed, and project budget. The decision to choose a model is a challenging and critical one for the success of the analysis is dependent on the accuracy of the results and the computer's processing speed. To date, however, no extensive hydrological investigations have been carried in most of the Vamsadhara River catchments. As a result, evaluating and predicting a flood risk has become a necessity to undertake a study on hydrologic simulations, and an effort is made to develop a suitable watershed model and classify flood-prone areas in the watershed.

The study's main objective is to produce flood hydrographs from real-time data at Gunupur and Kashinagar. Calibrate and validate the flood forecast model's peak discharges using Central Water Commission (CWC) data. A steady flow analysis of peak discharges was also done for selected flood events in 2006, 2010 and 2013.

2.Literature review

Remote sensing datasets from many satellites provide significant information not only for monitoring watersheds, but also for extracting input data, such as Land Use, Land Cover (LULC), Digital Elevation Model (DEM) etc. These geospatial data are utilized for land use mapping, ground water model, and flood risk assessment [15]. Geographic Information System (GIS) facilitates in the processing of Shuttle Radar Topography Mission (SRTM) DEM data used as input for rainfall runoff modeling in order to extract basin features for the Vamdsadhara River basin. Numerous researches have established that integrating GIS with Hydrologic Engineering Center (HEC)-GeoHMS enables the creation of a hydrological model [16, 17, 18]. Hydrological models provide a framework for forecasting and evaluating rainfall runoff processes.

The HMS components used in hydrological modeling systems range from lumped conceptual models to spatially distributed hydrological modeling techniques [8]. HEC-HMS is a lumped, event-based runoff model that may possibly simulate rainfall-runoff relationships within a basin [19, 20]. Event-based models are intended to simulate individual events, with a focus on infiltration and surface runoff, and they predict peak discharge and runoff volume. Many studies have demonstrated that event-based models outperform continuous models [21, 22].

The HMS is widely utilized in a variety of applications, like in the design of drainage systems quantifying the land-use effects on streamflow [23, 24]. Several studies have shown that hydrologic

models can be used efficiently for flood forecasting and simulating rainfall-runoff processes in various basins around the world [25–31]. Flood hydrographs obtained by HEC-HMS is used directly in various geographical areas to solve a high level of complexity, including large river basins, flood warning system, and natural watershed runoff [32].

A study on flood damage reduction indicates measuring the increased volume of runoff for proposed land-use changes in a watershed owing to floods [33–35].

Previous research has found that the HEC-HMS model can simulate direct runoff with a number of distinct combinations of loss methods, transform methods, and routing strategies [36].

Halwatura and Najim [37] applied the HMS model to the Attanagalu Oya river basin in Sri Lanka for simulation and validation. Finally, they concluded that Snyder's UH was the best transformation approach.

Azam et al. [38] obtained acceptable results using the modified SCS loss method and the Clarke Unit hydrograph to simulate peak runoff, whereas [39, 40] simulated runoff using the SCS-CN technique and the SCS UH method to estimate losses and direct runoff.

Vaishnava [41] examined several catchments of the Mahanadi basin, Seonath, and Jonk. The simulation findings of rainfall-runoff processes obtained for the Jonk catchment were preferable to those produced for the Seonath catchment.

The hydrologic model can further be utilized in floodplain studies which generate water surface profiles and flood inundation maps for flood-prone areas. [42–44] investigated steady flow analysis, i.e., river channel behavior, and found that the Hydrologic Engineering Center Analysis System (HEC-RAS) is an excellent tool for creating floodplain maps.

In [45, 46] investigated using both hydrologic and hydraulic modeling for estimating runoff from intense rainfall events, further flood risk and damages can be predicted and mitigated to some extent. Based on the review of the various literatures related to the application of HEC-HMS for hydrological modeling, it is concluded that this type of study provides a better response to analyzing future extreme conditions and serves as a tool for issuing early warnings during severe cyclonic rainfall in the basin. Large data needs, as well as a lack of clear guidance on the circumstances for their applicability, are a few key factors to consider while studying the river basin.

3.Methods

The HEC-HMS model is a physically and conceptually event-based model that is designed to simulate rainfall-runoff processes in a wide variety of geographic areas, from large river basin water supply and flood hydrology to small urban and natural watershed runoff [8]. *Figure 1* illustrates the overall methodology for accomplishing hydrologic and hydraulic modeling for the current study. Using real time daily rainfall data, discharge data in every reach of the river are determined for the selected flood events in the years 2006, 2010 and 2013 in HEC-HMS 4.2.1. Comparison between computed and observed flows is determined at the gauge station Gunupur and Kashinagar.

River geometry such as stream centerline, Bank lines, cross-section cutlines, levees are digitized in HEC-GeoRAS. Further stream centerline attributes and cross section cutline attributes are generated to export the HEC-GeoRAS file data to HEC-RAS 5.0.4. The steady flow analysis of the peak discharges obtained in the river is generated for the selected flood events using HEC-RAS 5.0.4. Further the water surface profiles obtained are imported in HEC-GeoRAS to generate flood inundation mapping. Section 3.3 contains a brief overview of methods.

3.1 Study area

Vamsadhara basin as depicted in (*Figure 2*) lies between the Mahanadi and Godavari river basins in the eastern part of India between 180 151 to 190 551 N latitudes and 830 201 to 840 201 East Longitudes. It has five principal tributaries viz. Chaldea, Phalphalia, Ganguda (Harbhangi), Sannanadhi, and Mahendrathanaya; all are on the left side of the river [47].

The basin is influenced by the south-west monsoon during these five months (June to October), receiving around 84.6 percent of rainfall and occasional cyclones as a result of the emergence of a low pressure in the Bay of Bengal. The average annual rainfall of magnitude is 1400mm. Two barrages are falling on the river are Neradi barrage and Gotta barrage. Since 1891 more the 11 no. of severe cyclones have occurred on this river basin (Source: Disaster Management Dept. A.P). The above categorization of river basins indicates that the Vamsadhara river basin with such a large catchment area needs a flood response time in

terms of weeks and reflects major seasonal meteorological conditions.

3.2 Input data

3.2.1 precipitation and river gauge discharge data

A basic prerequisite for any hydrological model, including the HEC-HMS model, is data on rainfall amount and timing. The National Remote Sensing Centre (NRSC) in Hyderabad provided gridded rainfall data with a resolution of 0.25×0.25 degrees for the years 2001 to 2013. The daily rainfall data have a spatial reference GCS_WGS_1984. To ensure the consistency of precipitation data, gridded raster data was converted into station rainfall using the zonal statistics mean method for 17 sub-basins that have been created within the catchment [48].

The Vamsadhara river basin is having two-level forecasts and one inflow forecast station i.e Kashinagar, Gunupur and Gotta (Source: Integrated Hydrological Data Handbook 2013) [49]. Gunupur and Kashinagar, located at a latitude and longitude of 180 42l N and 830 57l E, are the gauge stations considered for river discharge. The gauge discharge data are collected for the years 2006, 2010, and 2013 from CWC, Water Resources Department, Bhubaneswar, Odisha.

3.2.2 DEM and satellite data

The DEM with 30 m×30 m resolution is projected using Universal Transverse Mercator (UTM) zone 44; WGS 1984, and was acquired from SRTM from NRSC, Hyderabad. It takes as input, for preprocessing, basin processing, characteristics, and various hydrologic parameters in HEC-GeoHMS. Once the processing is completed mapping GeoHMS units to HMS units, background shapefile, and basin model file, meteorological model files are generated to export the file data from GeoHMS to HMS.

Bhuvan website provided Resourcesat-1, Linear Imaging Self Scanning Sensor (LISS-III) image of 3-02-2012 with a resolution of 23.5 m has been used to generate the river geometry and flood plains HEC-GeoRAS 10.2.

3.2.3 Soil and LULC data

The National Bureau of Soil Science & Land Use Planning (NBSS&LUP) provided the research region with soil data. Most of the soils in the river basin are identified as loamy, clayey, and clay soils which have low, medium, and high erosion properties respectively [50].

LULC chart was collected from NRSC, Hyderabad. It has been divided into eight classes of built-up/urban areas, cultivating land, current fallow, plantation, evergreen forest, deciduous forest wasteland, water bodies. LULC data are primarily required for the assigning of Curve Numbers (CN) to land areas for the computation of runoff and hydrological study.

3.2.4 Geology and slope data

The study area is part of the Achaeans' eastern ghats group, which is dominated by charnockites and kondalites on the left banks of the river basin and granite gneisses on the right bank [51]. The basin is narrow and undulated [52], with significant slope frequencies indicating rapid runoff in the northeast and the northwest region. The slope of the river basin has been grouped into five classes i.e., level, gentle, strong, moderate, and steep slopes [50].

3.3 Methodology

Runoff computations and execution phases in the HEC-HMS and HEC RAS model is shown in *Figure 3*.

3.3.1Rainfall-runoff model development

Basin Model: HEC-Geo HMS is used to create a basin model by DEM processing in ARC GIS 10.2 The processing includes DEM reconditioning, fill sinks, flow direction, stream definition, catchment delineation, drainage line delineation using 30m * 30 m resolution SRTM DEM. A total of 17 sub basins was generated for the present study. Delineation of the watershed into the appropriate number of subbasins is another critical job in modeling. According to Hromadka et al. [53] accuracy of the hydrological model increases, with the effect of watershed division. So to increase the model's overall accuracy, the catchment is divided into 17 sub-basins by different trials, and specified threshold values are used in the research area's watershed. The basin model with sub-basins and basin features created in the form of a background map file is imported to HEC-HMS from the data derived by HEC-GeoHMS for model simulation. In HEC-HMS 4.2.1 each model runs combined with a basin model, meteorological model control specification and time series data. The basin model consists of hydrologic elements (sub-basins, junctions, reach) and drainage network of the catchment. While in meteorological model defines daily rainfall given as input. To control specification starting date, time and ending date time is scheduled for simulation. Real time series data for all meteorological elements are fed with gauge discharge data for calibration and simulation of the developed model. *Figure 4* depicts the entire hydrological modeling with sub-basins, junctions, and reaches of the upper Vamsadhara river generated in HEC-HMS 4.2.1.

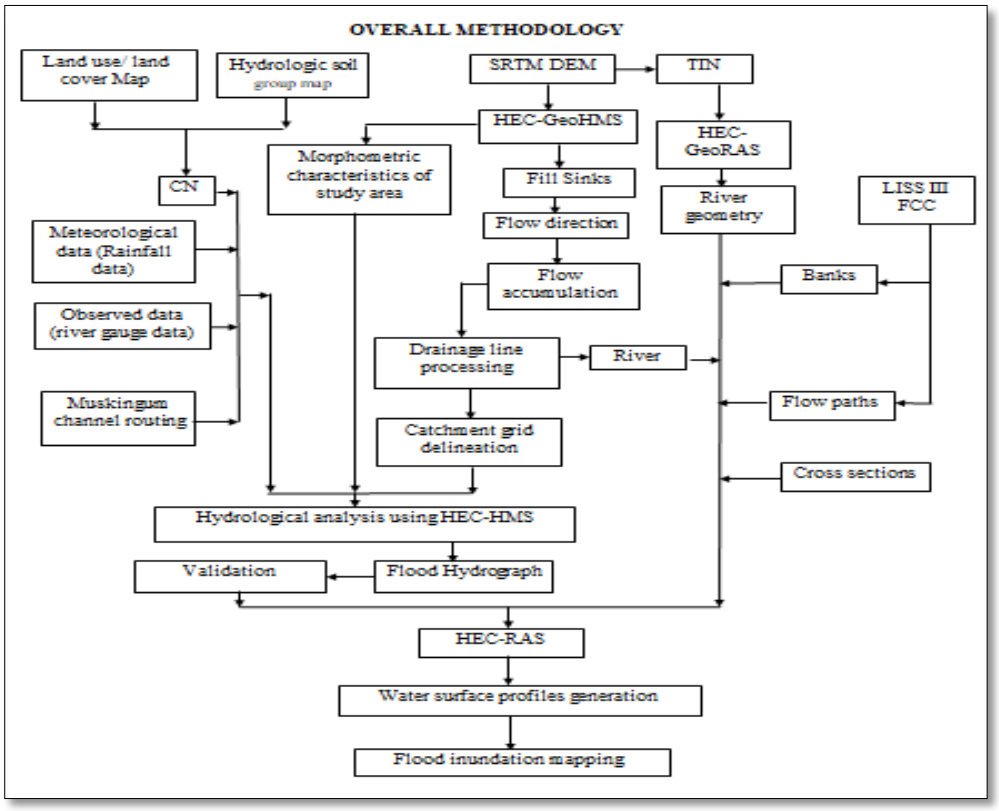


Figure 1 Methodology for modeling process

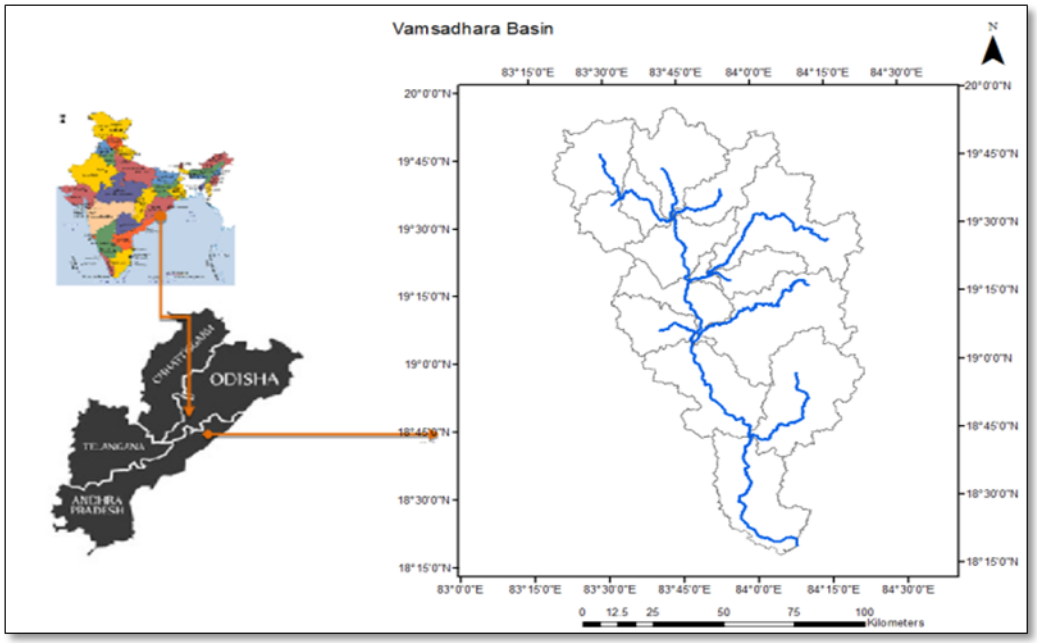


Figure 2 Vamsadhara basin: location map

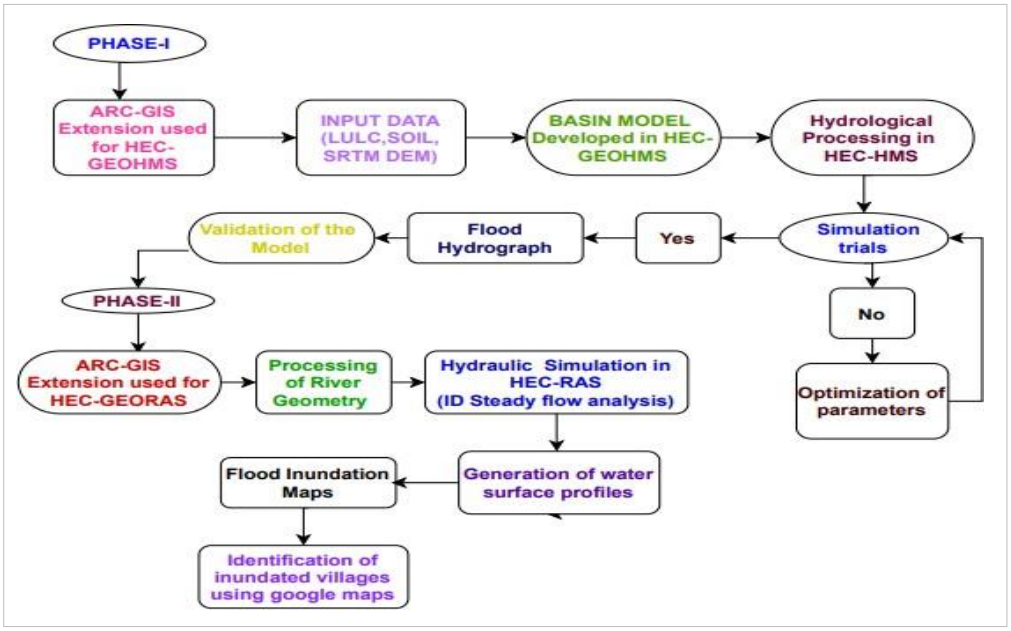


Figure 3 Block diagram showing execution phases in HEC-HMS & HEC-RAS

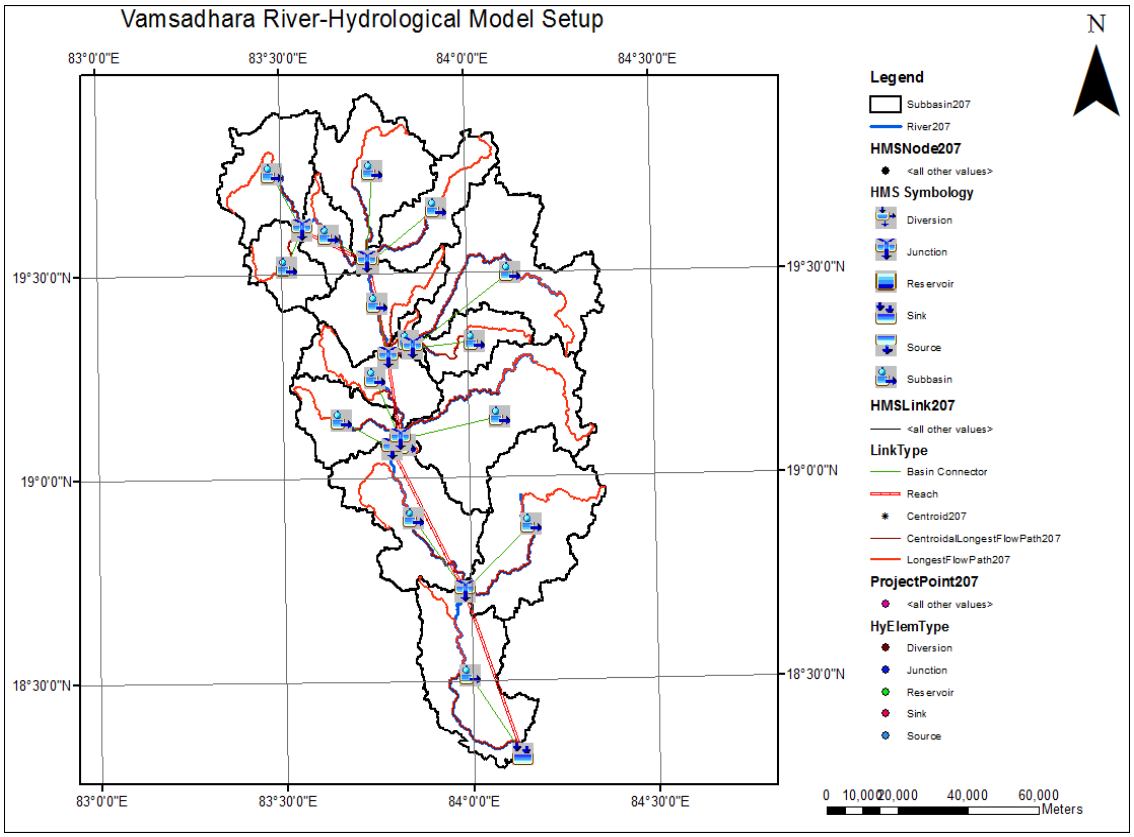


Figure 4 The hydrological modelling of Vamsadhara river

There are several approaches to calculate the hydrological parameters required to run a model before model simulation in HEC-HMS. Three methods were chosen for the study area to convert rainfall to run off, the SCS-Curve number as a loss model, SCS-Unit Hydrograph, as a transform model for simulating direct runoff, and a Muskingum routing model for channel routing. These approaches were chosen based data availability, adaptability for similar hydrologic conditions, and study applicability. The next section discusses these methods in further detail:

i) Loss model

The loss models in HEC-HMS determine runoff volume by computing the volume of water that is intercepted, infiltrated, stored, evaporated and subtracting it from the precipitation [8]. The SCS developed the SCS-CN loss model was selected in this study to calculate the quantity of runoff from inputs such as rainfall and watershed coefficients for each sub-basin. The watershed coefficient is called the CN. It ranges from 0 to 100. This approach was chosen because it is widely utilized in many applications and produces better results than the initial and the constant loss method [54].

McCuen [55] states that curve number is a simple conceptual method for computing direct runoff volume from a storm event, and is well supported by empirical data. It has been prepared by a combination of LULC and hydrological soil group data following the United States Department of Agriculture (USDA) standard table [56].

In [21, 57] emphasized the need of applying the loss model using SCS-CN for event based models.

ii) Transform model

The transform model, simulate the process of direct runoff of excess precipitation on a watershed. This excess precipitation is distributed uniformly spatially and is of constant intensity throughout a time interval [7]. A parametric UH model was proposed by the SCS 1972. The model is based on UH averages for a large number of watersheds calculated from gauged precipitation and runoff (HEC, 2000) [8]. SCS-UH was chosen because it is widely used and is more reliable in calculating runoff rate and produces better results than the Synder UH method [58]. Lag time is the only input for this method.

iii) Muskingum flood routing model

McCarthy [59] designed the Muskingum method, which is a common lumped flow routing approach. It was chosen for this study. The Muskingum routing technique utilizes a basic conservation of mass approach to traverse a stream reach [8].

Muskingum (K: travel time) & runoff coefficient (x) is the two parameters. This method has mostly been employed in the study of river engineering to compute hydrological routing parameters, since its introduction in 1930 [60], the Muskingum technique has been widely used. The data from the cross-section characteristics and flow conditions may be used to calculate travel time. Both of them are calibrated parameters, whereas x ranges from 0 to 0.5. Typical streams have values of x=0.2 to 0.3. The routing parameters K & x values for eight reaches were calculated for the basin models are presented in *Table 1*. Calibrated routing parameter K and x evaluated were shown in *Table 2*.

Table 2 summarizes the HEC-HMS Curve Number values for all sub-basins. As mentioned in section 3.2.3, LULC is classified into eight classes for the current study, and CN values calculated range from 34.098 to 91.084, as shown in *Table 3*, indicating that the land used is in fair to good hydrologic condition with low to moderate runoff potential (NRCS, 2007).

Table 1 Muskingum parameters are considered for the run 2006

S. No.	Reach	Travel time (K)	Runoff coefficient (x)
1	R40	0.05	0.2
2	R60	4.7	0.2
3	R90	4.46	0.2
4	R100	1.2	0.2
5	R110	3.95	0.2
6	R140	0.44	0.2
7	R150	7.2	0.2
8	R170	10.3	0.2

Table 2 Calibrated parameter values of Vamsadhara Basin

S. No	Sub-basin	Area (km2)	Curve number before simulation (CN)	Optimal values of (CN)	Muskingum Coefficient	
					x	*K (hr)*
1	W330	1016.6	45.35	38.582	0.196	7.235
2.	W320	1226.8	47.937	40.784	-	-
3.	W310	22.276	55.339	47.081	0.2	0.46
4.	W300	471.25	45.337	38.571	-	-
5.	W290	502.81	99	91.084	0.196	3.969
6.	W280	1312.0	37.063	34.889	-	-
7.	W270	80.339	53.95	49.636	0.2	2.7
8.	W260	369.31	48.059	44.216	-	-
9.	W250	609.22	41.691	38.357	0.196	5.0
10.	W240	0.5906	51	46.921	0.3	0.05
11.	W230	1289.5	37.063	34.098	-	-
12.	W220	363.88	46.305	42.602	-	-
13.	W210	584.01	41.072	37.789	-	-
14.	**W200**	288.90	45.736	42.080	0.196	7.0
15	W190	845.80	41.589	38.263	-	-
16.	W180	681.85	70.798	65.137	-	-
17.	**W340**	1011.0	76.682	76.682	0.2	10.3

Table 3 Comparison results of simulated and observed flow for Vamsadhara Basin at Gunupur

Period	Date	Simulated		Observed	
		Qs (m^3/sec)	Vs (MM)	Qs (m^3/sec)	Vs (MM)
Calibration	15th Aug'06 to 15th Nov'06	3598.9	323.49	3127.2	406.11
Validation	15th Aug'10 to 15th Nov'10	756.8	195.92	700	197.42
Validation	15th Aug'13 to 15th Nov'13	1308.8	220.62	1211.4	251.15

3.3.21D Steady flow in RAS

A river analysis system (HEC-RAS) is used for the current study to create water surface profiles. This system is capable of performing 1D steady flow analysis in natural or constructed channels and compute water surface profiles. This profile may be computed for various flow regimes such as subcritical, supercritical, and mixed flow regimes [61]. It may be computed from one cross-section to the next cross-section by solving the Energy equation with an iterative procedure called the standard step method. The Energy equation is written as follows:

$$Z_2 + Y_2 + \frac{\alpha_2 V_2^2}{2g} = Z_1 + Y_1 + \frac{\alpha_1 V_1^2}{2g} + h_e \quad (1)$$

(Courtesy: HEC-RAS 5.0.1)

$$h_e = LS_f + C\left|\frac{\alpha_2 V_2^2}{2g} - \frac{\alpha_1 V_1^2}{2g}\right| \quad (2)$$

$$\frac{L_{lob}Q_{lob} + L_{ch}Q_{ch} + L_{rob}Q_{rob}}{Q_{lob} + Q_{ch} + Q_{rob}} \quad (3)$$

3.4 Model performance

The accuracy of the model is calculated by evaluating its performance prior to and post calibration, and during validation, using the following criteria proposed by Moriasi et al. [62]. In this study, Nash-Sutcliffe Model Efficiency (NSE) and Coefficient of Determination (R^2) are utilized to evaluate the overall performance of the model.

The Nash-Sutcliffe Efficiency (E) criterion Nash and Sutcliffe [63] was recommended by an ASCE task committee in 1993. E is a positive integer in the range 0 to 1, with E equal to one being the optimum value. While values between zero and one are generally considered to be acceptable limits of performance, values less than or equal to zero implies that the observed discharge is a better indicator than the computed discharge, shows that the model performs insufficient.

$$NSE = 1 - \left[\frac{\sum_{i=1}^{M} (m_{obs,i} - m_{sim,i})^2}{\sum_{i=1}^{M} (m_{obs,} - m_{mean})^2}\right] \quad (4)$$

R^2 describes the ratio of variance and how the simulated data correlates with the observed values of data in the model.

$$RSR = \frac{\sqrt{\sum_{i=1}^{M} (m_{obs,i} - m_{sim,i})^2}}{\sqrt{\sum_{i=1}^{M} (m_{obs,i} - m_{mean})^2}} \quad (5)$$

4. Results

4.1 Simulation of the model

The hydraulic parameters that are primarily important for the model's good performance are calculated during the model's simulation of the flood event of 2006. Initial loss, CN, basin lag time, travel time (k), and runoff coefficient x are some of the most significant parameters in the model. The CN, k, initial loss, and lag time are identified as major sensitive parameters based on several parameter sensitivity investigations [54, 64]. Among the four sensitive ones, curve number and lag time can be computed in the ARC GIS 10.2 in GeoHEC-HMS component (USACE), and thus travel time (k) and initial loss become an emphasis for calibrating the model among the four sensitive ones. The initial loss is not taken into account in this study, and the remaining parameter, k, the flood travel time along the channel, is calibrated in the HEC-HMS system using the trial-and-error approach [65]. The hydrologic order from upstream of the basin to the outlet includes reaches R40, R60 & R90 i.e., Kutraguda to Gudari covering a distance of 60 km (CWC, Bhubaneswar), reaches R100, R110, R140 flows from Gudari to Gunupur covering a distance of 40 km (flood forecasting stations CWC, Bhubaneswar), while R150 flows from Gunupur to Kashinagar covers a distance of 37 km (gauge stations of the study area) and downstream of the basin is continued with R170 from Kashinagar to Gotta is 27.7 km. The Muskingum parameters K & x calculated for the run 2006 are shown the *Table 1*

4.2 Model calibration and validation

Parameters are finely tuned until the model's output is consistent with historical data, this tuning is nothing but adjusting of model parameter values which is known as calibration. By calibrating parameters and evaluating until the model hydrographs match and fit well between computed and observed flows. Cunderlik and Simonovic [66]. The hydrological developed model for this study is simulated, and the optimal parameter values evaluated are presented in *Table 2*. Calibration is performed using the optimal parameter values from *Table 2*, i.e., from 15th August to 15th November 2006 for 90 days utilizing daily rainfall data, gauge discharge data, and stage data.

The observed discharge data are taken as input at Gunupur and Kashinagar gauges which are located on J91 and J81 in the sub-basin. The computed hydrograph is compared to the observed hydrograph at Gunupur and Kashinagar gauge station. The observed data closely match with the output simulated hydrographs generated after the simulation run for the 2006 flood event. The results tabulated for model calibration are listed in *Table 3* for Gunupur and in *Table 4* for Kashinagar.

In *Table 3* the calculated peak discharge at Gunupur is 3598.9 m^3/sec is slightly higher than the observed peak, flood hydrographs exactly match with observed peak discharge as shown in *Figure 5(a)*. The total volume is underestimated and peak flow is overestimated than observed flow. Also, as shown in *Table 4* the calculated peak discharge at Kashinagar is 3883.9 m^3/sec is slightly higher than the observed peak with a discharge of 3830.3 m^3/sec, flood hydrographs exactly match with observed peak discharge as shown in *Figure 5(b)*.

Table 4 Comparison results of simulated and observed flow for Vamsadhara Basin at Kashinagar

Period	Date	Simulated		Observed	
		Qs (m^3/sec)	Vs (MM)	Qs (m^3/sec)	Vs (MM)
Calibration	15th Aug '06 to 15th Nov	3883.9	261.70	3830.3	347.86
Validation	15th Aug '10 to 15th Nov'10	856.9	197.39	750	186.39
Validation	15th Aug'13 to 15th Nov'13	2033.9	231.33	1998.9	238.91

The calibrated model parameters are then tested for another set of historic field observations i.e., for the flood event 2010 & 2013 for validation. In this process, if the calibrated parameters do not match with the historical data, the parameters must be refined using multiple trials.

The validation results computed are shown in *Table 3* and *Table 4*. From *Table 3* at Gunupur the computed peak discharge obtained is 756.8 m^3/sec & 1308.8 m^3/sec which are slightly higher than the observed peak for the flood events 2010 and 2013, flood hydrographs representing the following flood events are shown in Figure *6(a)* & *Figure 7(a)*. The total volume is nearly matched with the observed volume as shown in *Table 3*.

Similarly, from *Table 4* at Gunupur the computed peak discharge obtained is 856.9 m^3/sec & 2033.9 m^3/sec which are slightly higher than the observed peak for the flood events 2010 and 2013, flood hydrographs representatives for the following flood events are shown in *Figure 6(b)* and *Figure7(b)*. The total volume is nearly matched with the observed volume as shown in *Table 4*. The results calculated show that the model calibrated and validated illustrates a close agreement with computed and observed hydrographs in terms of timing of peak, peak flow, and volume of flow. The relative percent errors between the observed and simulated values obtained found to be below ±20% acceptance level [67].

4.3Processing of river geometry

ARC GIS 10.2 is used to analyze the DEM and produce a Triangulated Irregular Network (TIN). River Cross-Sections, Stream Centerlines, Stream Bank Lines, and Flow Lines, as well as other river geometry information, are generated and digitized using the TIN in the HEC-GeoRAS model. For Steady Flow Analysis, the geometry data collected from TIN are transferred to HEC-RAS. Manning's roughness coefficient is assigned to all river stations in the catchment after the cross-section is checked and the geometry is adjusted.

Manning's roughness coefficient (n) often ranges between 0.030 and 0.050 in thick forest areas. The analysis used a value of 0.035. The peak discharge in each reach of the river has been provided as flow data for profiles PF 2006, PF 2010, and PF 2013, which represent the discharges from selected flood events in 2006, 2010, and 2013. The water surface profiles for PF 2006, PF 2010, and PF 2013 are created using subcritical flow as the flow condition. HEC-RAS exports the produced water surface profiles to HEC-GeoRAS together with the modified geometry. Water surface profiles and flood inundation maps created in Arc GIS10.2 using RAS Mapping Tools are displayed in *Figure 11*. The villages flooded in Andhra Pradesh state in 2006 are depicted in *Figure 12*. The following *Table 5* and *Table 6* details the villages that were impacted by the 2006 and 2013 floods.

5.Discussions

As illustrated in *Figures 5* show graphs comparing observed and simulated flow at both Gunupur and Kashinagar gauge stations for the calibrated year of 2006. The observed flow recorded at gauge stations at the respective junctions (J91, J81) is represented by the black dotted lines The simulated outflow at the junction is represented by the blue solid line. The stage data for that junction is indicated by the yellow dotted line. *Figure 5(a)* shows that the calculated hydrograph overestimates peak discharge; the computed peak is 3598.9 m^3/sec, whereas the observed peak discharge is 3127.2 m^3/sec, a variance of approximately 400 m^3/sec; nevertheless, the graph at Gunupur matches the historical data well. *Figure 5(b)* clearly shows that the calculated hydrograph overestimates the peak discharge, with a computed peak discharge of 3883.9 m^3/sec compared to observed discharge 3830.3 m^3/sec, a percent variation of less than 1.4% that is acceptable.

The model was verified at both Gunupur and Kashinagar discharge stations during the flood's event of 2010 and 2013. *Figure 6* shows validation period hydrographs for 2010, whereas *Figure 7* shows validation period hydrographs for 2013. The calculated flow pattern resembles the observed flow pattern quite closely. From *Figure 6(a)* in 2010, the estimated peak discharge in Gunupur was 756.8 m^3/sec, whereas the observed flow was 700 m^3/sec, a variance of 50 cumecs that is negligible. Similarly, as shown in *Figure 6(b)*, the estimated peak discharge at Kashinagar gauge stations is 856 m^3/sec, with a range of 100 cumecs, which is acceptable.

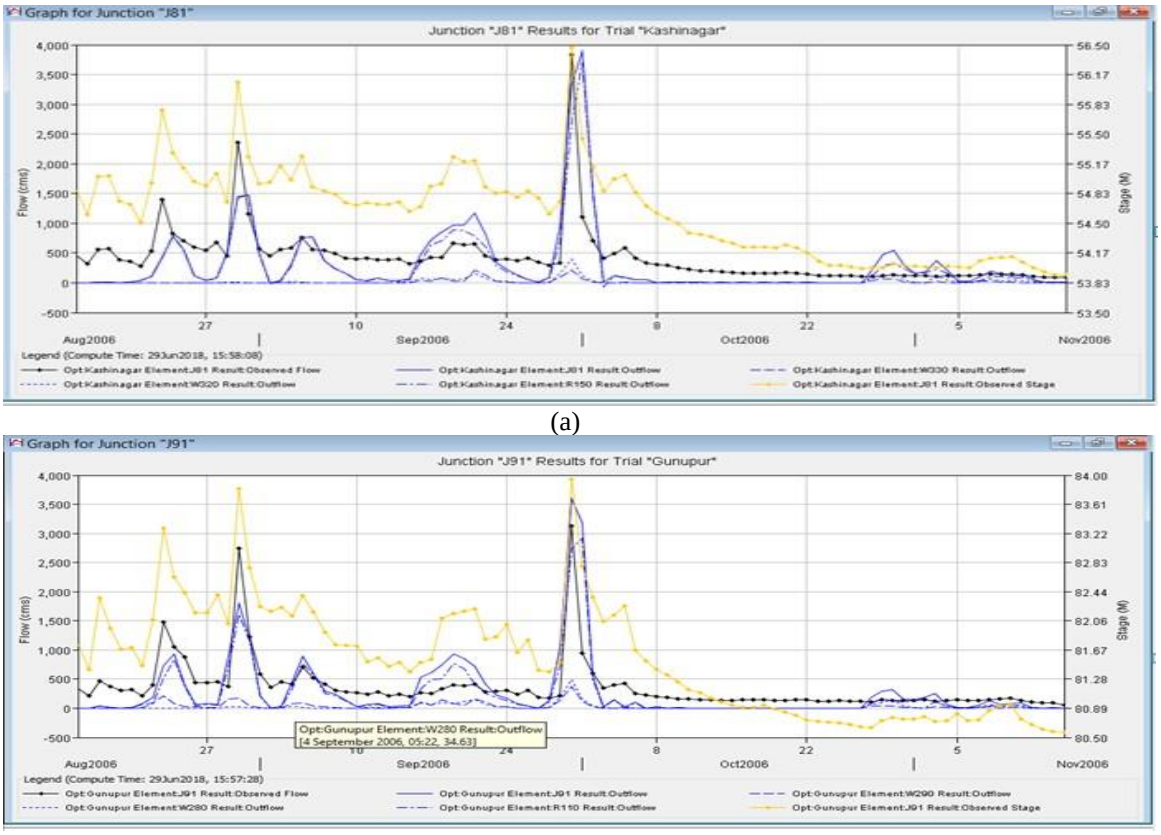
Figures 7(a) &7(b) shows the calculated flood discharges during the 2013 cyclonic storm at gauge stations Gunupur and Kashinagar are 1308.8 m^3/sec and 2033.9 m^3/sec, respectively, but the observed flows are 1211.4 m^3/sec and 1998.9 m^3/sec. The variation at the upstream gauge station, J91, is higher than that at the downstream junction, J81 that may be owing to the travel time 'K' taken from all upstream reaches. As this simulated hydrograph generated corresponds extremely well with the observed

hydrograph, the Muskingum parameters K and x computed may be considered accurate.

The model performance was further computed using NSE [NASH, SUTCLIFFE 1970], between simulated and observed flow given by the equation (1). *Figure 8* shows the scatter plot of the calibrated year, 2006 at J91 & J81 with an NSE value of 0.786 & 0.773 at Gunupur & Kashinagar gauge station. According to Moriasi et al. [62], E values obtained for calibrated model greater than 0.75 are considered to be good. R^2 calculated given by the equation (2). The range of R^2 lies from 0-1 where 0 is unacceptable i.e., lesser value indicates high error variance, but values greater than 0.5 are acceptable Van Liew [62]. The R^2 values obtained for the model are 0.703 & 0.707; Since R^2 values are greater than 0.5 are considered acceptable. *Figures 9, 10* shows the scatter plot for the validated years, 2010 & 2013, with an NSE value of 0.812 & 0.801 where as R^2 values are 0.729 & 0.758. NSE value is 0.843 & 0.823 along with R^2 value 0.707 & 0.731 for the flood event 2013. The overall performance rating of the model validated has been found to be satisfactory indicating very good model performance. *Figure 11* depicts the water surface profiles and flood inundation maps created in Arc GIS10.2 using RAS Mapping Tools. The villages flooded in Andhra Pradesh state in 2006 are depicted in *Figure 12*. Most of the villages are located in the downstream area of the sub-basin. The following *Table 5* and *Table 6* details the villages of Srikakulam district that were impacted by the 2006 and 2013 floods.

5.1Limitations

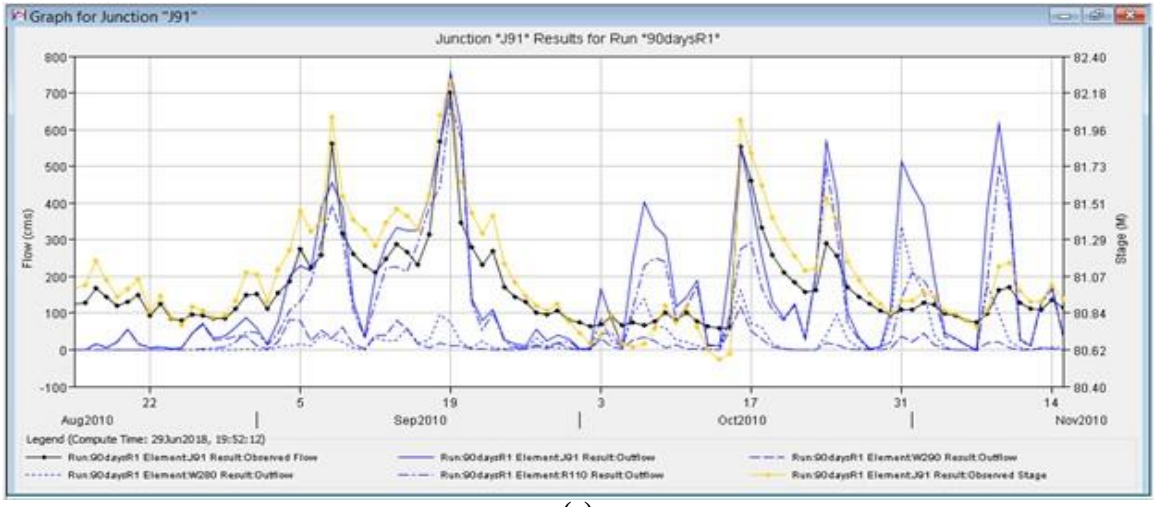
Although acquiring high resolution DEM as the input data is so expensive, used SRTM 30m data as input to our model to decrease project costs. 30m resolution is extremely low for achieving high accuracy results. Data such as rainfall and river cross-section data necessitate extensive fieldwork, which aid in enhancing the model's accuracy.



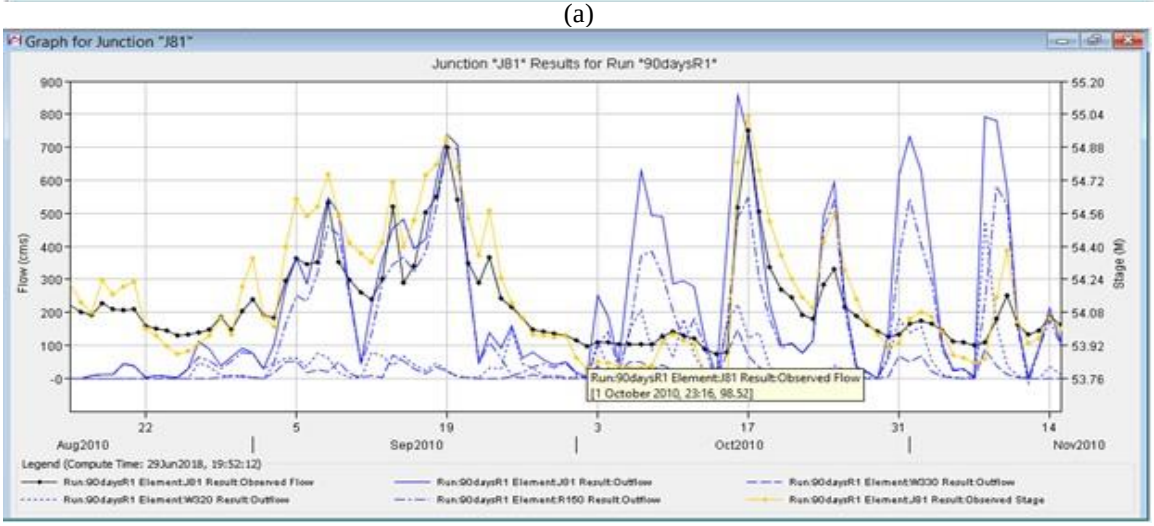
(a)

(b)

Figure 5 Observed & Simulated discharge of Vamsadhara River for the selected flood event 2006
(a) Aug-Nov 2006; Gunupur (b) Aug –Nov 2006; Kashinagar

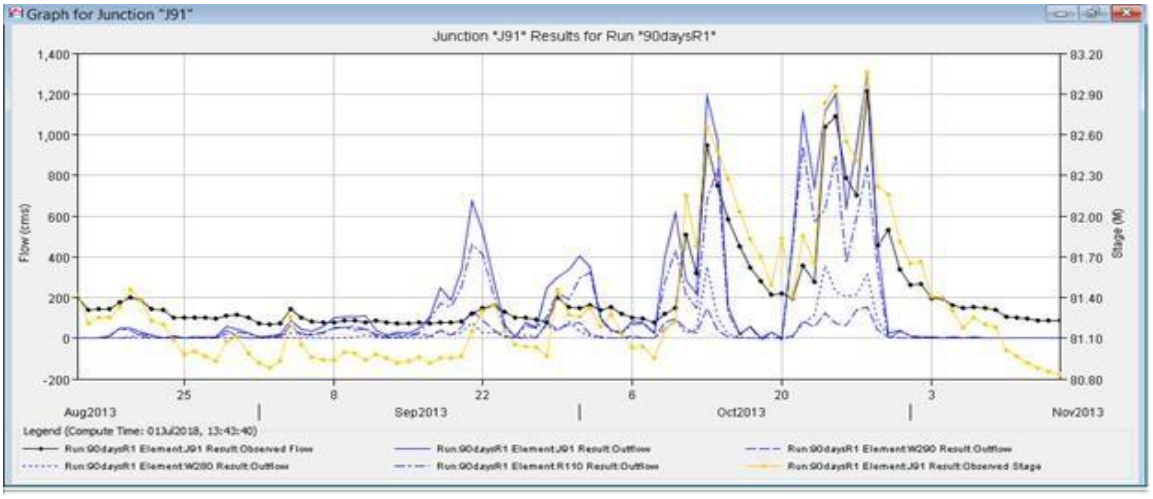


(a)

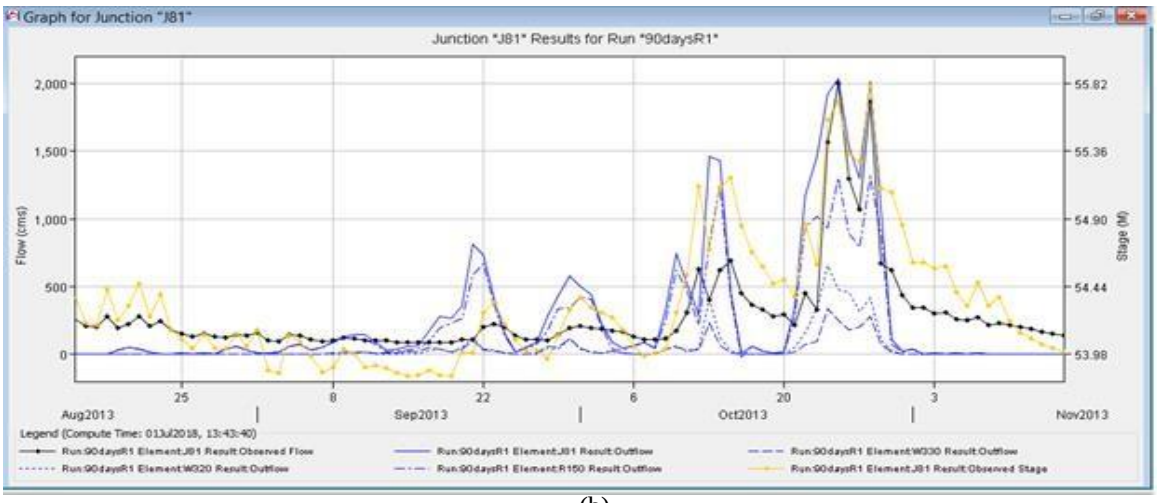


(b)

Figure 6 Observed & Simulated discharge of Vamsadhara River for the selected flood event 2010 (a) Aug-Nov 2010; Gunupur (b) Aug –Nov 2010; Kashinagar (2010)

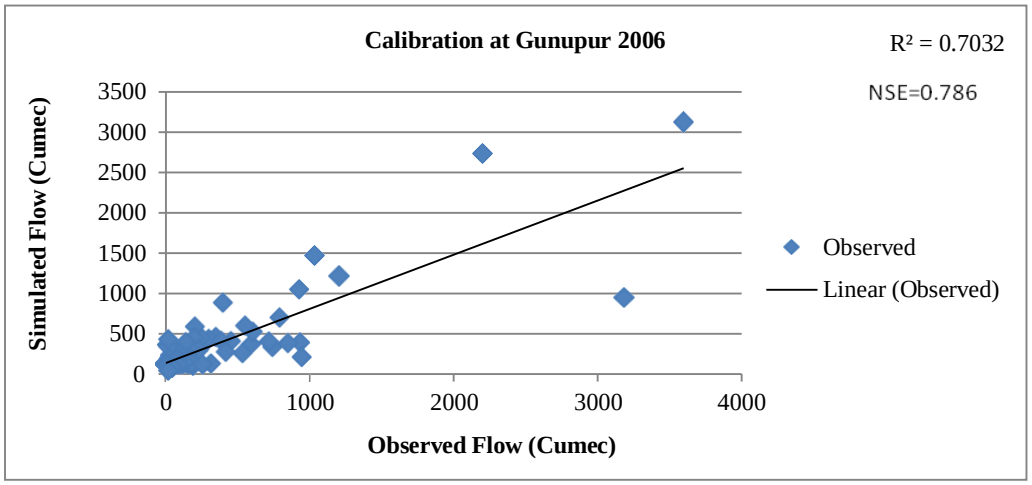


(a)

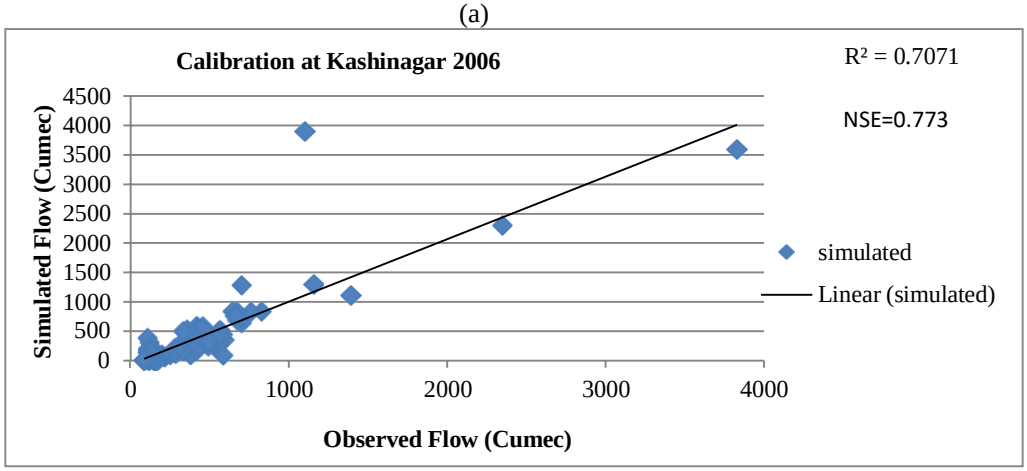


(b)

Figure 7 Observed & Simulated discharge of Vamsadhara River for the selected flood event 2010 (a) Aug-Nov 2013; Gunupur (b) Aug –Nov 2013; Kashinagar

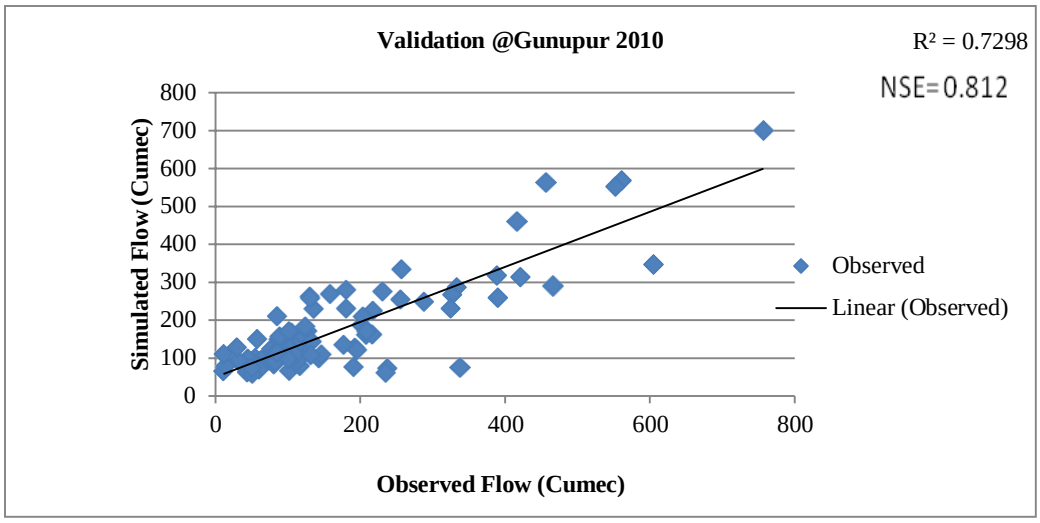


(a)

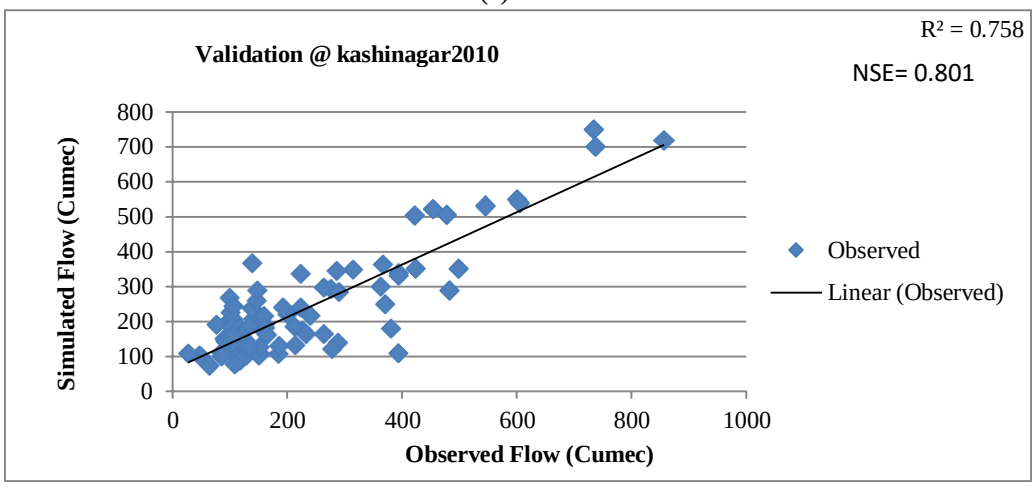


(b)

Figure 8 Scatter plot comparison between simulated & observed flow for calibrated year 2006 for Vamsadhara river (a) At Gunupur gauge station (b) At Kashinagar gauge station

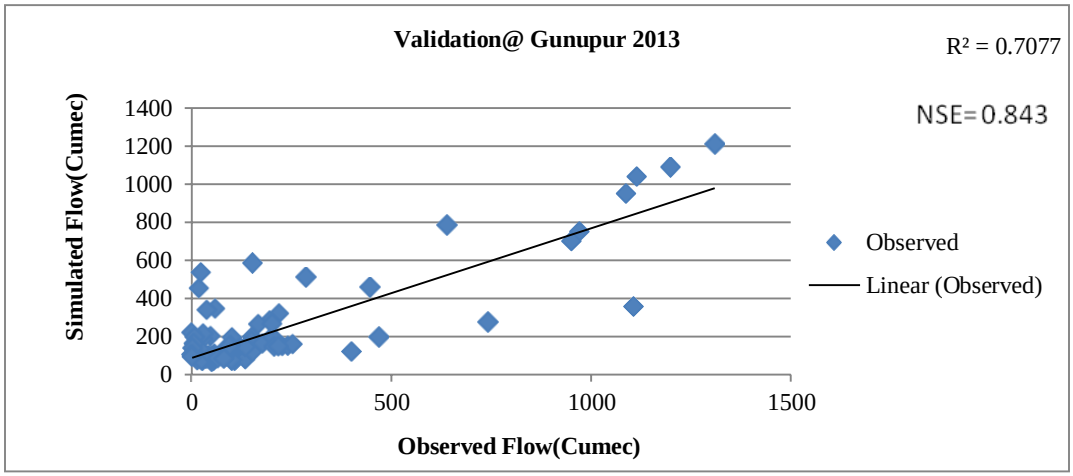


(a)

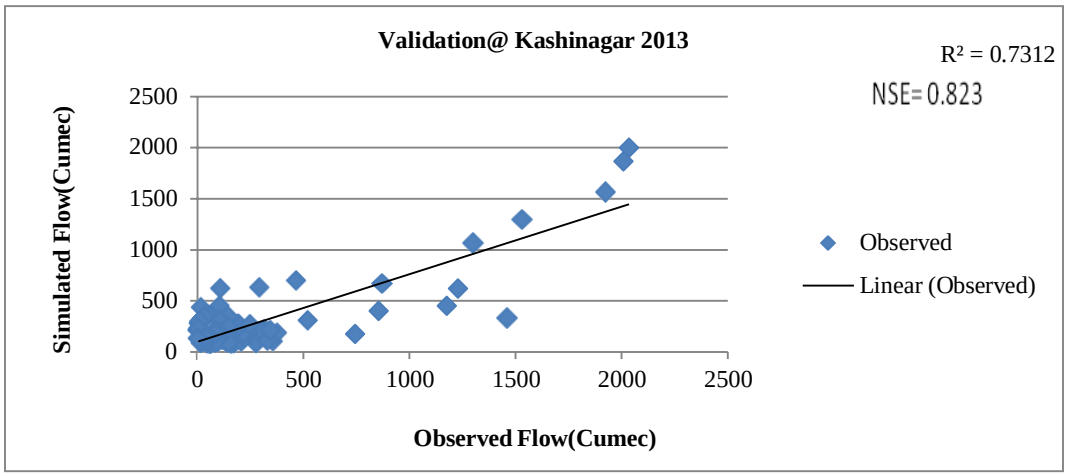


(b)

Figure 9 Scatter plot comparison between simulated & observed flow for calibrated year 2010 for Vamsadhara river (a) At Gunupur gauge station (b) At Kashinagar gauge station



(a)



(b)

Figure 10 Scatter plot comparison between simulated & observed flow for calibrated year 2013 for Vamsadhara river (a) At Gunupur gauge station (b) At Kashinagar gauge station

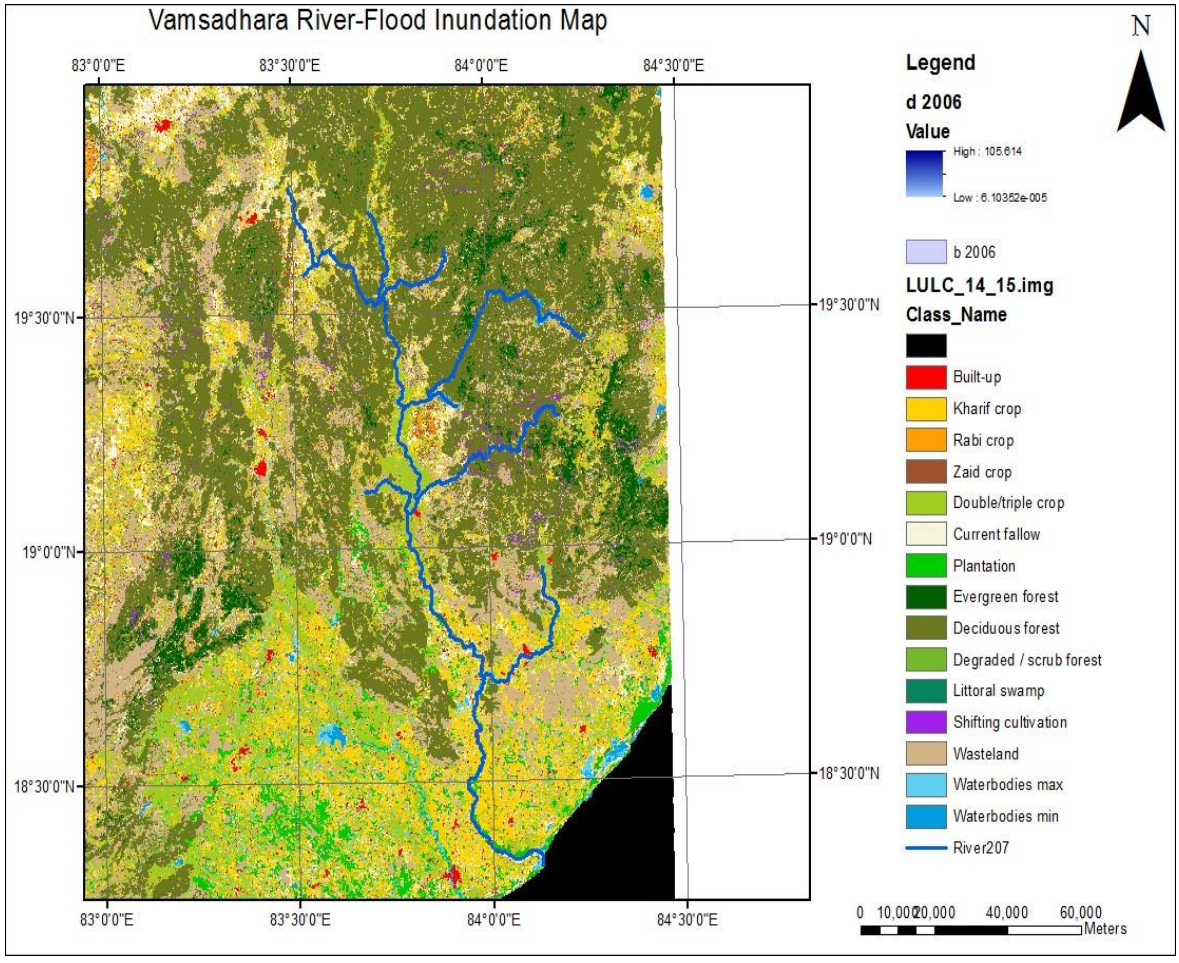


Figure 11 Flood inundation map during the cyclone, 2006

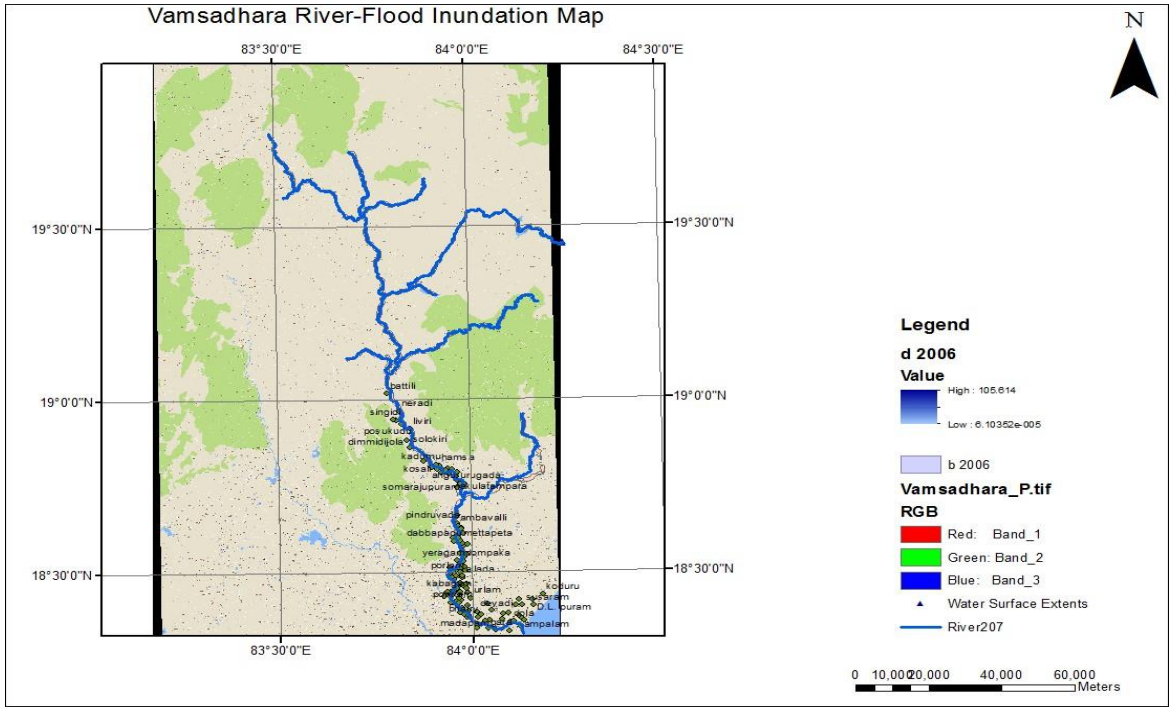


Figure 12 The villages inundated in AP state during the selected floods in Vamsadhara River are identified

Table 5 Villages inundated in Srikakulam district during the cyclone, 2006

Object Id	Name	Object Id	Name
1	Kajarada	26	Gollapeta
2	Batteru	27	Andhavaram
3	Ronanki	28	Ramakrishnapuram
4	Bhairy	29	Achyutapuram
5	Ponnam	30	Nagarikatakam
6	Buravalli	31	Mettapeta
7	Ambalavalasa	32	Srimukhalingam
8	Salihundam	33	Suravaram
9	Gara	34	Komanapalle
10	Posukudu	35	Yatapeta
11	Neradi	36	Mahalakshmipurm
12	Nivagam	37	Bhagirathipuram
13	Vasapa	38	Pindruvada
14	Hamsa	39	Ambavalli
15	Kadumu	40	Rellivalasa
16	Sirusuvada	41	Akkarapalle
17	Kuntibadhra	42	Ramachandrapuram
18	Somarajupuram	43	Chevakulapeta
19	Matala	44	Ponnampeta
20	Penugottivada	45	Lukulam
21	V.N. Puram	46	Kameshwaripeta
22	Akulatampara	47	Chennulavalasa
23	Vadavalasa	48	Butchipeta
24	Dabbapadu	49	Madapam
25	Telikipenta	50	Geddavanipeta

Table 6 Villages inundated in Srikakulam district during the cyclone Phailin, 2013

ID	Name	ID	Name	ID	Name
1	Kajarada	27	Yeragam	53	Ponnampeta
2	Batteru	28	PeddaSavalapuram	54	Lukulam
3	Ronanki	29	Dola	55	Kameshwaripeta
4	Bhairy	30	Pallipeta	56	Chennulavalasa
5	Ponnam	31	Linganayudupeta	57	Butchipeta
6	Buravalli	32	Udakalapeta	58	Madapam
7	Ambalavalasa	33	Dompaka	59	Geddavanipeta
8	Salihundam	34	Porlam	60	Muddadapeta
9	Gara	35	Gollapeta	61	Kabagam
10	Posukudu	36	Andhavaram	62	Venkatapuram
11	Neradi	37	Ramakrishnapuram	63	Ambajipeta
12	Nivagam	38	Achyutapuram	64	Gopalapenta
13	Vasapa	39	Nagarikatakam	65	Anguru
14	Hamsa	40	Mettapeta	66	Rugada
15	Kadumu	41	Srimukhalingam	67	Chodavaram
16	Sirusuvada	42	Suravaram	68	Allada
17	Kuntibadhra	43	Komanapalle	69	Ramadasupeta
18	Somarajupuram	44	Yatapeta	70	Gangammapeta
19	Matala	45	Mahalakshmipuram	71	Ampalam
20	Penugottivada	46	Bhagirathipuram	72	Nandigam
21	V.N. Puram	47	Pindruvada	73	Narasinghanaidupeta
22	Akulatampara	48	Ambavalli	74	Kottapalavalasa
23	Vadavalasa	49	Rellivalasa	75	Anandapuram
24	Dabbapadu	50	Akkarapalle	76	Kollavanipeta
25	Telikipenta	51	Ramachandrapuram		
26	Sivaramapuram	52	Chevakulapeta		

6. Conclusion

The study's primary aim is to develop a semi-distributed model for the Vamsadhara river basin. Further, the HEC-HMS model was calibrated and validated for two years using real-time historic flood events. In the study SCS loss method, SCS-UH, Muskingum routing methods were found to be very effective in calculating flood discharge in a sub-basin. The simulated peak discharge of the Vamsadhara catchment was slightly over predicted than the observed flow this variation in discharge values is due to differences in mean rainfall, geologic formation, slope, travel time, vegetation cover, and land use in the sub-basins. Model accuracy and performance still can further be improved by subdividing into more sub-basins [53].

Following are some of the specific conclusions from the analysis:

- Flood Hydrographs for flood events 2006, 2010 & 2013 showed that the model calibrated and validated illustrates a close agreement with the computed and observed flow in terms of timing of peak, peak flow, and volume of flow.
- Reasonable results were obtained for the semi distributed model with efficiency 78.6% for the calibration period (2006) and nearly 81.2%, 84.3 % for the validation period (2010 &2013).
- The model outputs i.e., the difference in total runoff volume resulted from the two flood events (validated) is within ±20% acceptance level for the modeling process Bingner et al. [68]
- The Muskingum parameters K and x calculated can be considered for accurate
- The Flood inundation maps generated from the present GIS modeling are also validated and the output maps generated are sufficiently accurate.

Though the structure of HEC-HMS is simple, it is a highly effective tool for flood forecasting. The above values obtained for the model are acceptable. This study also finds that, as it is a real-time hydrological model, it may be applied to other minor catchments in the Vamsadhara river basin as operational flood forecasting in monitoring floods and minimizing natural hazards to a certain extent.

Future scope

Future researchers may be able to expand their knowledge of flood modeling and develop the two-dimensional unsteady flow analysis.

Acknowledgment
We would like to convey our heartfelt appreciation to the Director of Flood Forecasting & Hydrological Modeling Division, Water Resources Group, National Remote Sensing Centre (NRSC), Hyderabad, for supplying us with the LULC, DEM, Satellite, and Rainfall grid data. We are also grateful to the CWC, Bhubaneswar, Odisha, for supplying us with the Vamsadhara River basin stage and gauge discharge data.

Conflicts of interest
The authors have no conflicts of interest to declare.

References
[1] Bhatt JR, Sharma SK. Impacts of climate change on India and climate change related activities. Tata McGraw-Hill Publishing Companay Ltd, New Delhi; 2002.
[2] Markus M, Angel JR, Yang L, Hejazi MI. Changing estimates of design precipitation in Northeastern Illinois: comparison between different sources and sensitivity analysis. Journal of Hydrology. 2007; 347(1-2):211-22.
[3] https://library.wmo.int/index.php?lvl=notice_display&id=5841#.YSx5nfozbIU. Accessed 26 October 2020.
[4] Matkan A, Shakiba A, Pourali H, Azari H. Flood early warning with integration of hydrologic and hydraulic models, RS and GIS (Case Study: Madarsoo Basin, Iran). World Applied Sciences Journal. 2009; 6(12):1698-704.
[5] Rao KH, Rao VV, Dadhwal VK, Behera G, Sharma JR. A distributed model for real-time flood forecasting in the Godavari Basin using space inputs. International Journal of Disaster Risk Science. 2011; 2(3):31-40.
[6] Morin E, Jacoby Y, Navon S, Bet-Halachmi E. Towards flash-flood prediction in the dry Dead Sea region utilizing radar rainfall information. Advances in Water Resources. 2009; 32(7):1066-76.
[7] https://www.hec.usace.army.mil/software/hec-hms/documentation/HEC-HMS_Users_Manual_4.2.pdf. Accessed 26 October 2020.
[8] Feldman AD. Hydrologic modeling system HEC-HMS. Technical Reference Manual. 2000.
[9] Majidi A, Shahedi K. Simulation of rainfall-runoff process using Green-Ampt method and HEC-HMS model (Case study: Abnama Watershed, Iran). International Journal of Hydraulic Engineering. 2012; 1(1):5-9.
[10] Choudhari K, Panigrahi B, Paul JC. Simulation of rainfall-runoff process using HEC-HMS model for Balijore Nala watershed, Odisha, India. International Journal of Geomatics and Geosciences. 2014; 5(2):253-65.
[11] Kabiri R. Simulation of runoff using modified SCS-CN method using GIS system, case study: klang watershed in Malaysia. Research Journal of Environmental Sciences. 2014; 8(4):178-92.
[12] https://sandrp.in/2017/05/23/rivers-profile-of-andhra-pradesh-and-telangana-states/. Accessed 26 October 2020.
[13] https://www.researchgate.net/publication/274703806_Inter_and_Transdisciplinary_Research_Methods_in_Rural_Transformation_Case_studies_in_Northern_Ethiopia. Accessed 26 October 2020.
[14] Jakeman AJ, Hornberger GM. How much complexity is warranted in a rainfall-runoff model? Water Resources Research. 1993; 29(8):2637-49.
[15] Sahour H, Mokhtari A, Ghahfarokh SS. Rainfall-runoff modeling using remotely sensed data and the hydrologic modeling system (HEC-HMS). Ecol. Environ. Conserv.2016; 22(4):163-73.
[16] Solaimani K. GIS-based multidate flood forecasting using hydraulic model. International Journal of Physical Sciences. 2011; 6(3):577-82.
[17] Shehata M, Mizunaga H. Geospatial analysis of surface hydrological parameters for Kyushu Island, Japan. Natural Hazards. 2019; 96(1):33-52.
[18] Abdelkarim A, Gaber AF, Alkadi II, Alogayell HM. Integrating remote sensing and hydrologic modeling to assess the impact of land-use changes on the increase of flood risk: a case study of the Riyadh–Dammam train track, Saudi Arabia. Sustainability. 2019; 11(21):6003.
[19] Sarminingsih A, Rezagama A. Simulation of Rainfall-runoff process using HEC-HMS model for garang watershed, semarang, Indonesia. In Journal of Physics: Conference Series 2019 (p. 012134). IOP Publishing.
[20] Othman N, Romali NS, Samat SR, Ahmad AM. Calibration and validation of hydrological model using HEC-HMS for Kuantan River Basin. In IOP conference series: materials science and engineering 2021 (p. 012028). IOP Publishing.
[21] De Silva MM, Weerakoon SB, Herath S. Modeling of event and continuous flow hydrographs with HEC–HMS: case study in the Kelani River Basin, Sri Lanka. Journal of Hydrologic Engineering. 2014; 19(4):800-6.
[22] Msaddek M, Kimbowa G, El Garouani A. Hydrological modeling of upper oumerrabia basin (Morocco), comparative study of the event-based and continuous-process HEC-HMS Model Methods. Computational Water, Energy, and Environmental Engineering. 2020; 9(4):159-84.
[23] McColl C, Aggett G. Land-use forecasting and hydrologic model integration for improved land-use decision support. Journal of Environmental Management. 2007; 84(4):494-512.
[24] Du J, Qian L, Rui H, Zuo T, Zheng D, Xu Y, Xu CY. Assessing the effects of urbanization on annual runoff and flood events using an integrated hydrological modeling system for Qinhuai River basin, China. Journal of Hydrology. 2012; 464:127-39.
[25] Knebl MR, Yang ZL, Hutchison K, Maidment DR. Regional scale flood modeling using NEXRAD rainfall, GIS, and HEC-HMS/RAS: a case study for the San Antonio River Basin Summer 2002 storm event. Journal of Environmental Management. 2005; 75(4):325-36.

[26] Li S, Qi R, Jia W. Calibration of the conceptual rainfall-run off model's parameters. In advances in water resources and hydraulic engineering 2009 (pp. 55-59). Springer, Berlin, Heidelberg.
[27] Khakbaz B, Imam B, Hsu K, Sorooshian S. From lumped to distributed via semi-distributed: Calibration strategies for semi-distributed hydrologic models. Journal of Hydrology. 2012; 418:61-77.
[28] Aghakouchak A, Habib E. Application of a conceptual hydrologic model in teaching hydrologic processes. International Journal of Engineering Education. 2010; 26(4):963-73.
[29] Oleyiblo JO, Li ZJ. Application of HEC-HMS for flood forecasting in Misai and Wan'an catchments in China. Water Science and Engineering. 2010; 3(1):14-22.
[30] Yener MK, Sorman AU, Sorman AA, Sensoy A, Gezgin T. Modeling studies with HEC-HMS and runoff scenarios in Yuvacik Basin, Turkiye. International Congress on River Basin Manage. 2007; 4(2007):621-34.
[31] Prabha JA, Tapas MR. Event-based rainfall-runoff modeling using HEC-HMS.
[32] Fleming M, Neary V. Continuous hydrologic modeling study with the hydrologic modeling system. Journal of Hydrologic Engineering. 2004; 9(3):175-83.
[33] Singh VP, Woolhiser DA. Mathematical modeling of watershed hydrology. Journal of Hydrologic Engineering. 2002; 7(4):270-92.
[34] Yusop Z, Chan CH, Katimon A. Runoff characteristics and application of HEC-HMS for modelling stormflow hydrograph in an oil palm catchment. Water Science and Technology. 2007; 56(8):41-8.
[35] Ali M, Khan SJ, Aslam I, Khan Z. Simulation of the impacts of land-use change on surface runoff of Lai Nullah Basin in Islamabad, Pakistan. Landscape and Urban Planning. 2011; 102(4):271-9.
[36] Zelelew DG, Langon S. Selection of appropriate loss methods in HEC-HMS model and determination of the derived values of the sensitive parameters for un-gauged catchments in Northern Ethiopia. International Journal of River Basin Management. 2020; 18(1):127-35.
[37] Halwatura D, Najim MM. Application of the HEC-HMS model for runoff simulation in a tropical catchment. Environmental Modelling & Software. 2013; 46:155-62.
[38] Azam M, San Kim H, Maeng SJ. Development of flood alert application in Mushim stream watershed Korea. International Journal of Disaster Risk Reduction. 2017; 21:11-26.
[39] Visweshwaran R. Application of the HEC-HMS model for runoff simulation in the Krishna basin. Master's thesis, National Institute of Technology Karnataka, Surathkal, India. 2017.
[40] Derdour A, Bouanani A, Babahamed K. Modelling rainfall runoff relations using HEC-HMS in a semi-arid region: case study in Ain Sefra watershed, Ksour Mountains (SW Algeria). Journal of Water and Land Development. 2018.
[41] Vaishnava S. Characteristics of hydrological modelling of mahanadi basin using the hec-hms software (Doctoral dissertation). Delhi Technological University. 2020.
[42] Goodell C, Warren C. Flood inundation mapping using HEC-RAS. Obras y Proyectos. 2006; 2:18-23.
[43] Forkuo EK. Flood hazard mapping using Aster image data with GIS. International journal of Geomatics and Geosciences. 2011; 1(4):932-50.
[44] Mehta DJ, Ramani MM, Joshi MM. Application of 1-D HEC-RAS model in design of channels. Methodology. 2013; 1(7):4-62.
[45] Abdessamed D, Abderrazak B. Coupling HEC-RAS and HEC-HMS in rainfall–runoff modeling and evaluating floodplain inundation maps in arid environments: case study of Ain Sefra city, Ksour Mountain. SW of Algeria. Environmental Earth Sciences. 2019; 78(19):1-7.
[46] Icyimpaye G, Abdelbaki C, Mourad KA. Hydrological and hydraulic model for flood forecasting in Rwanda. Modeling Earth Systems and Environment. 2021:1-1.
[47] RK R, Alka UP. Forecasting of runoff and sediment yield using artificial neural networks. Journal of Water Resource and Protection. 2009; 2009.
[48] Gann D. Rainfall Estimation raster conversion data preparation for hydrological modeling with SWAT mara basin (Kenya/Tanzania).
[49] http://cwc.gov.in/sites/default/files/Combined%20Final_HDD_09042012.pdf. Accessed 26 October 2020.
[50] Eadara A, Karanam H. Slope Studies of Vamsadhara River basin: a quantitative approach. Variations. International Journal of Engineering and Innovative Technology. 2013; 3(1):184-9.
[51] http://cgwb.gov.in/District_Profile/Orissa/Koraput.pdf . Accessed 26 October 2020.
[52] Agarwal A, Singh RD, Mishra SK, Bhunya PK. ANN-based sediment yield models for Vamsadhara river basin (India). Water Sa. 2005; 31(1):85-100.
[53] Hromadka TV, McCuen RH, Yen CC. Effect of watershed subdivision on prediction accuracy of hydrologic models. Hydrosoft. 1988; 1(1):19-28.
[54] Sardoii ER, Rostami N, Sigaroudi SK, Taheri S. Calibration of loss estimation methods in HEC-HMS for simulation of surface runoff (Case Study: Amirkabir Dam Watershed, Iran). Advances in Environmental Biology. 2012; 6(1):343-8.
[55] McCuen RH. Review of curve number hydrology: state of the practice by RH hawkins, TJ Ward, DE Woodward, and JA Van Mullem: ASCE, Reston, VA 20191-4400; ISBN 978-0-7844-1004-2.
[56] Cronshey R. Urban hydrology for small watersheds. US Department of Agriculture, Soil Conservation Service, Engineering Division; 1986.
[57] Patil VK, Saraf VR, Karad OV, Ghodke SB, Gore D, Dhekale SS. Simulation of rainfall runoff process using HEC-HMS model for Upper Godavari Basin Maharashtra, India. European Journal of Engineering and Technology Research. 2019; 4(4):102-7.
[58] Reddy NA, Seelam JK, Rao S, Nagaraj MK. Flood estimation at ungauged catchments of western

catchments of Karnataka, West coast of India. ISH Journal of Hydraulic Engineering. 2019; 25(3):325-35.
[59] McCarthy GT. The unit hydrograph and flood routing. In proceedings of Conference of North Atlantic Division, US Army Corps of Engineers 1938 (pp. 608-9).
[60] Tewolde MH, Smithers JC. Flood routing in ungauged catchments using Muskingum methods. Water Sa. 2006; 32(3):379-88.
[61] Brunner GW. HEC-RAS hydraulic reference manual. Davis: US Army Corps of Engineers, Hydrologic Engineering Center. 2001.
[62] Moriasi DN, Arnold JG, Van Liew MW, Bingner RL, Harmel RD, Veith TL. Model evaluation guidelines for systematic quantification of accuracy in watershed simulations. Transactions of the ASABE. 2007; 50(3):885-900.
[63] Nash JE, Sutcliffe JV. River flow forecasting through conceptual models part I—a discussion of principles. Journal of Hydrology. 1970; 10(3):282-90.
[64] Tahmasbinejad H, Feyzolahpour M, Mumipour M, Zakerhoseini F. Rainfall-runoff simulation and modeling of Karun River using HEC-RAS and HEC-HMS models, Izeh District, Iran. Journal of Applied Sciences. 2012; 12(18):1900-8.
[65] Lin M, Chen X, Chen Y, Yao H. Improving calibration of two key parameters in Hydrologic engineering center hydrologic modelling system, and analysing the influence of initial loss on flood peak flows. Water Science and Technology. 2013; 68(12):2718-24.
[66] Cunderlik J, Simonovic SP. Calibration, verification and sensitivity analysis of the HEC-HMS hydrologic model. Department of Civil and Environmental Engineering, The University of Western Ontario; 2004.
[67] Sabzevari T, Ardakanian R, Shamsaei A, Talebi A. Predicting the flood hydrographs of ungauged watersheds using the Hec-Hms model and the geographic information system (GIS)(Case Study: Kasilian Watershed). Water Engineering, 2009; 2(4): 1-11.
[68] Bingner RL, Murphree CE, Mutchler CK. Comparison of sediment yield models on watersheds in Mississippi. Transactions of the ASAE. 1989; 32(2):529-34.



Arunima Mahapatra is a research scholar at Andhra University working on her PhD part-time. In addition, she is currently working as Assistant Professor at Dr. Lankapalli Bullayya College of Engineering in Visakhapatnam. She received her B.E (Civil) from GITAM and her M.Tech (RS & GIS) from Andhra University. She has ten years of teaching experience. She has papers published in two international journals as well as three conference proceedings. She is a member of the Indian Society of Hydraulics (ISH) and the Indian Society of Geomatics (ISG).
Email: arunimamahapatra162@gmail.com



Dr. Vazeer Mahammood is a professor of Civil Engineering in Andhra University. Currently he is serving as Head of the Department in Geo-Engineering. He previously served as Assistant Principal of AUCOE during 2008-2010. He also rendered his services as a Deputy Director of the Regional Centre for Educational Development of Minorities for A.P state Government. He held the position of Associate director, A.U. Admissions, during 2013-2017. Since 2017 he has been assigned as Dean (Engineering Works). Currently he is playing an active role in a smart city development programme of Government of India for Visakhapatnam city as an independent director. He is a leading civil engineering consultant Government & Private agencies. He earned a B.Tech from Acharya Nagarjuna University, M.E (Hydraulics, Coastal & Harbour Engineering) from A.U, M.Tech (RS& GIS) from Centre for space science & Technology for Asia and the Pacific (Affiliated to United Nations), M.E (Structures) from A.U, and awarded PhD in 2005 from A.U. He has over 30 publications in national and international journals and conferences. Four students have successfully completed their PhDs under his supervision, and seven more are in various stages of completion. He has completed two UGC-funded major research projects and also completed a minor research project in collaboration with the NRSC, Hyderabad. He is a member of several professional organizations, including the Institute of Engineers, the Indian Society of Hydraulics, the Indian Society for Remote Sensing, and the Indian Society of Geomatics (ISG). His current research interests include the Coastal structures and the application of remote sensing and geographic information systems to the fields of 1) watershed management. 2) Lake and reservoir environmental studies 3) Modeling of hydrological systems.
Email: vazir81c158@gmail.com



Dr. K H V Durga Rao currently works as Group Head, Disaster Management Support Group of National Remote Sensing Centre (NRSC), Indian Space Research Organization. He is a scientist in NRSC & ISRO with an experience of more than 18 years. He had done his B.E (Civil) at Andhra University, M.Tech (IIT Kharagpur) and PhD Andhra University. He has over 29 publications in national and international journals and conferences. He does research in Hydrological modelling, flood early warning, spatial flood inundation modelling, Flood Vulnerability & Risk Assessment, and Disaster Risk Reduction.
Email: durgarao_khv@nrsc.gov.in

Appendix I

S.No	Abbreviation	Description
1	1D	One Dimensional
2	CWC	Central Water Commission
3	DEM	Digital Elevation Model
4	GCS-WGS84	Geographic Coordinates System-World Geodetic System84
5	GIS	Geographic Information System
6	HEC-HMS	Hydrologic Engineering Centre 's Hydrologic Modelling System
7	HEC-RAS	Hydrologic Engineering Centre 's River Analysis System
8	LISS-III	Linear Imaging Self Scanning Sensor
9	LULC	Land Use Land Cover
10	NBSS & LUP	The National Bureau of Soil Science & Land Use Planning
11	NRSC	National Remote Sensing Centre
12	NSE	Nash-Sutcliffe Model Efficiency
13	R^2	Coefficient of Determination
14	SCS-CN	The Soil Conservation Service-Curve Number
15	SCS-UH	The Soil Conservation Service- Unit Hydrograph
16	SANDRP	South Asia Network on Dams, Rivers and People
17	SRTM	Shuttle Radar Topography Mission
18	TIN	Triangular Irregular Networks
19	USDA	United States Department Of Agriculture
20	USACE	United States Army Corps of Engineers
21	UTM	Universal Transverse Mercator

Eco. Env. & Cons. 27 (November Suppl. Issue) : 2021; pp. (S267-S271)
Copyright@ EM International
ISSN 0971–765X

Determination of Guaiacol in presence of monovalent inorganic salt and its assessment in *Citrus sinensis* leaves and *Citrus limon* peels

N.V.S. Venugopal*[1], N. Swathi[2] and P. Padmavathi[2]

[1]Department of Chemistry, Institute of Science, GITAM University, Visakhapatnam, A.P, India
[2]Department of Chemistry, GITAM University, Visakhapatnam, A.P, India

(Received 6 March, 2021; Accepted 13 May, 2021)

ABSTRACT

Guaiacol (2-methoxy phenol) is a naturally occurring expectorant and biosynthesized by a variety of organisms. Guaiacol is also used medicinally as an expectorant, antiseptic, and local anaesthetic. In this study we reported a method for easy and rapid spectrophotometric determination of Guaiacol in presence of perbromate and periodate. The optimized method has been successfully applied for the determination of Guaiacol in orange (*Citrus sinensis*) leaves and lemon (*Citrus limon*) peels. The products obtained shows maximum absorbance at 515 nm in presence of potassium perioadate and 590 nm with potassium perbromate. Beer's law is obeyed in the linear dynamic range of 20-187.9 μg ml^{-1}. The correlation coefficient is 0.996 which indicates the linearity between the two variables. The molar absorptivity coefficient and sandal's sensitivity of the product are found to be 6.35x104L mol^{-1} cm^{-1} and 0.026 μg cm^{-2} respectively. Hence, the proposed method is fairly sensitive and reproducible.

Key words *: Guaiacol, Perbromate, Perioadate, Citrus sinensis leaves, Citrus limon peels*

Introduction

The most common biomass materials used for energy are plants, wood, and waste. In nature we found naturally occurring chemicals such as chemicals from plants, micro-organisms, animals, the earth and the sea. Wildfires and controlled burns generate smoke particulates that could be taken up by the berries and leaves of fruit plants. Bush fires are expected to become more frequent in the coming years with global warming. In order to minimize the financial loss associated with producing smoke pollution. Guaiacol (2-methoxy phenol) (GAL) is a naturally-occurring organic compound with the formula C6H4(OH)(OCH3). Due to its aroma, it is undesirable in some natural products. It has smoky and phenolic aroma.

Although it is biosynthesized by a variety of organisms, this aromatic oil is usually derived from guaiacum or wood creosote. It is also found in es-

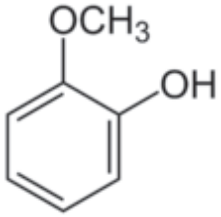


Fig. 1. Structure of Guaiacol

[2]Research Scholar

sential oils from celery seeds, tobacco leaves, orange leaves, and lemon peels. Guaiacol is also used medicinally as an expectorant, antiseptic, and local anaesthetic. Guaiacol is produced in the gut of desert locusts, *Schistocerca gregaria*, by the breakdown of plant material. This process is undertaken by the gut bacterium *Pantoea agglomerans* (*Enterobacter*). It is one of the main components of the pheromones that cause locust warming (Dillon Rod *et al*., 2000). Liquid guaiacol is colourless and it is soluble in alcohol. Guaiacol is less active antiseptic than phenol. Guaiacol can be sulphonated at 80 degree Celsius to yield a monosulphonic acid derivative which is converted to its potassium salt Almeida (Almeida *et al.,* 1999) reported the voltammetric determination of guaiacol by oxidation at a carbon paste electrode following a cathodic accumulation was first tried, with no success, because there was no accumulation of the compound. GUA are derived from phenolic compounds that are widely distributed in various plants and also be found in common foods (Kalayarasi *et al*., 2017). Reduced graphene oxide (RGO) nanosheets with high quality were chemically synthesized by hydrothermal reduction of a well-dispersed grapheme oxide (GO) suspension. The electrochemical behavior of guaiacol was studied on different carbon material surfaces (Yan Wu *et al.,* 2014). Waldemer Ternes investigated the formation of the oxidation products of guaiacol in brines and heated meat matrix: 6-nitrosoguaiacol, 4-nitroguaiacol and 6-nitroguaiacol. For this purpose we applied a newly developed HPLC-UV and LC–MS method (Sarah *et al.,* 2016). The methodology normally used in the determination of Guaiacol is gas chromatography with selective mass detection. Volta metric methods have also been proposed for the determination of phenolic compounds, based on their oxidation at the carbon paste electrode. Detection of *Alicyclobacillus acidoterrestris* was performed by determination of guaiacol in apple juice. Guaiacol produced by *A. acidoterrestris* was determined by using HPLC, UV-Vis spectrophotometer, and Minolta spectrophotometer (Bahceci *et al*., 2007).

Simple gas chromatography-tandem mass spectrometry (GC-MS/MS) method for quantification of guaiccol reported (Zhiqian Liu *et al*., 2020). GC-MS has been the predominant analytical technique in combination with various sample preparation protocols, including liquid-liquid extraction (LLE) from berry homogenate and wine (Wilkinson *et al.,* 2011), headspace solid-phase microextraction (HP-SPME) from beer (Pizarro *et al*., 2010), polymer stir bar sportive extraction from beer and wine (Zhou *et al*., 2015), and trimethylsilyl (TMS)-based derivatization following purification by solid-phase extraction (SPE) of berry homogenate and wine (Allen *et al*., 2013). The reported methods shows that guaiacol is determined through different methods whrein reagents and solvents are of less familiar and methods involving complicated procedures. The author reported the determination of Guaiacol with potassium ioadate and with bromate using aminobenzoic acid (ABA) as reagent

Materials and Methods

Preparation of reagents and solutions

All chemicals used were of analytical grade and were used as such. All laboratory reagents were freshly Prepared. 0.01 percent Guaiacol solution is prepared in methanol. 0.2 percent Aminobenzoic acid (ABA) solution is prepared in double distilled water 0.01M Potassium periodate and potassium per bromated solutions are prepared in distilled water.

Buffer solutions: Hydrochloric acid (1.0M) and sodium acetate (1.0M) are mixed to get the required pH (1.0-3.5), 0.2M sodium acetate and 0.2M acetic acid are mixed to get the required pH (4.0-6.0) and 0.01M Potassium dihydrogen phosphate and 0.01M disodium hydrogen phosphate are mixed to get the required pH (pH 7.0). The pH of the above buffer solutions are measured by a pH meter and finally adjusted suitably.

Apparatus

All spectrophotometric measurements were carried out using a UV-1800 Shidmazu and 752w UV - Vis grating with a silica glass cell of l cm thickness. All glassware are washed with a mixture of concentrated sulfuric acid and nitric acid (1:1) before use.

Procedures

With potassium periodate: 5.0 ml Guaiacol solution is taken in a volume of 15 ml buffer solution and it is mixed with 2 ml of potassium periodate and 1mL of ABA solution. The values of optical densities of the pink colored product obtained are measured at different wavelengths.

With potassium perbromate: 5.0 ml Guaiacol solution is taken in a volume of 15mL buffer solution

and it is mixed with 2 ml of potassium perbromate and 1mL of ABA solution. The value of optical densities of the yellow colored product obtained is measured at different wavelengths.

Results and Discussion

The present study was formulated to assess the Guaiacol content in the leaves of *Citrus sinensis* and *Citrus limon*. This aromatic oil is usually extracted from guaiacum and found in celery seeds, tobacco leaves, orange leaves, and lemon peels. The oxidation of Guaiacol in presence of strong oxidising agents like perbromate and periodate was studied as shown in Fig. 2.

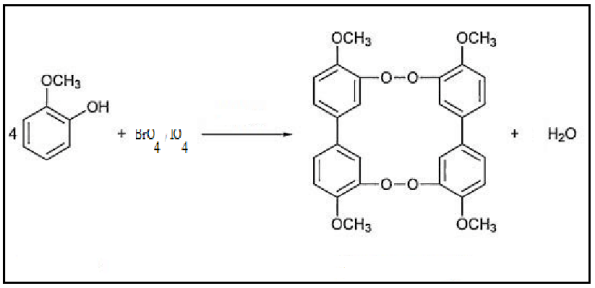


Fig. 2. Oxidation of Guaiacol

Absorption spectra

The absorption spectrum of the products obtained by the reaction between guaiacol and ABA in the presence of potassium perioate and potassium perbromate is shown in Figure 3. The reagent blank exhibited eligible absorbance despite having a wavelength in the same region from the absorption spectra, it is clear that the products obtained shows maximum absorbance at 515 nm in presence of potassium perioadate and 590 nm with potassium perbromate.

Applicability of Beer's law

Aliquots of 10ml solutions, each containing constant volumes of 3 ml of buffer (pH 5.0) 1.0 ml of ABA and periodate or perbromate and 1.0 mL of Guaiacol in the range from 0.02-10 ìg mL-1 are prepared. Absorbance measurements of these solutions are measured at 515 nm in presence of potassium perioadate and 590 nm with potassium perbromate. A graph plotted between the concentration of Guaiacol and its absorbance in presence of perbromate and periodate were given in Figs. 4 and 5. From the graph, it is observed that a linear plot passing

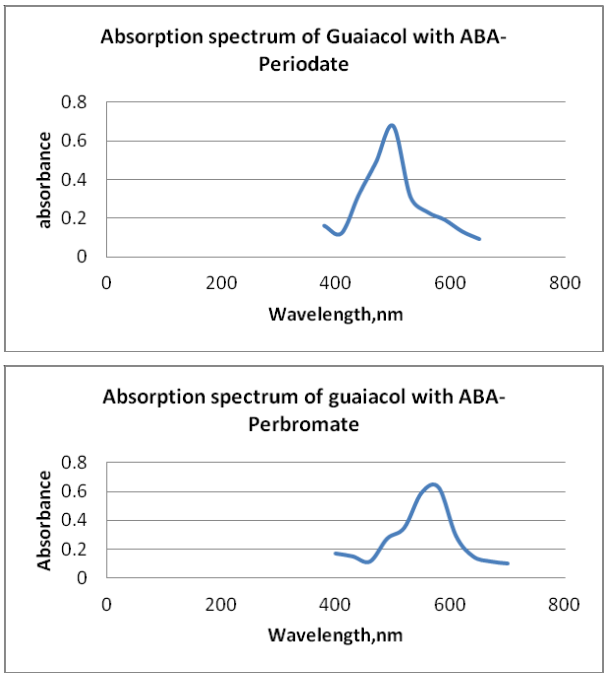


Fig. 3. Absorption spectra of GAL

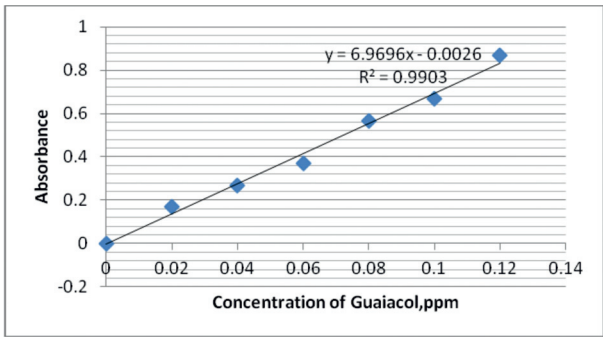


Fig. 4. Calibration graph of Guaiacol with ABA-periodate

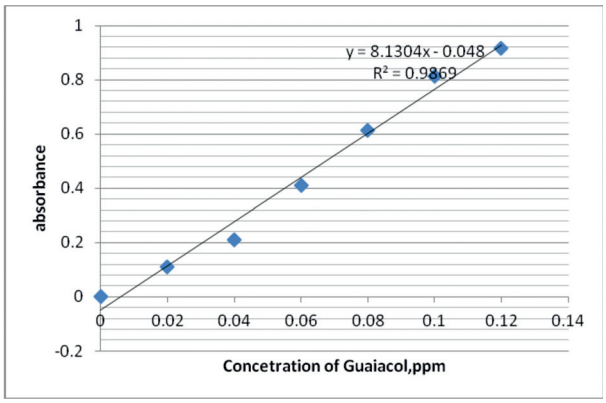


Fig. 5. Calibration of GAL with ABA-perbromate

through the origin obeys Beer's law in the range from 20-187.9 micro grams of Guaiacol. The correlation coefficient is 0.996 which indicates the linearity between the two variables. The molar absorptivity coefficient and sandal's sensitivity of the product are found to be 6.35 x 104L mol^{-1} cm^{-1} and 0.026 µg cm^{-2} respectively. The selected analytical paprameters in presence of periodate and perbromate are given in Table 1 and 2.

Suitable volume of aliquot was analyzed according to the proposed in presence of periodate and perbromate. The results are tabulated in Table 3.

Table 3. Quantitative determination of Guaiacol

Taken	Amount of Guaiacol, µg Found	
	Periodate	Perbromate
22.00	21.75	21.81
54.00	53.58	52.89
126.00	125.6	125.8
188.00	185.6	187.9

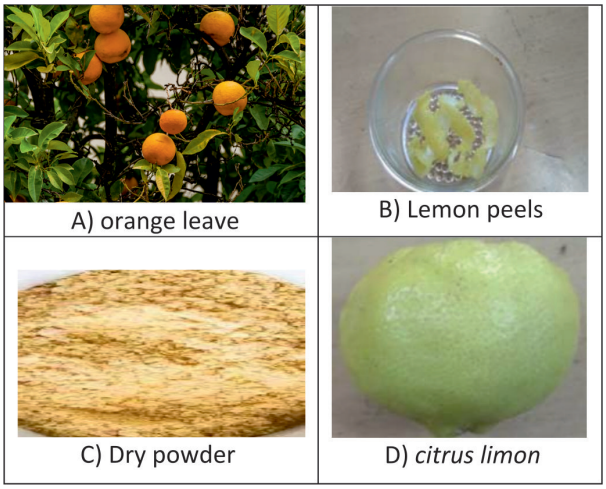


Fig. 6. Guaiacol in orangeleaves and lemon peels

Determination of Guaiacol in orange and lemon leaves

The *Citrus sinensi* leaves, *Citrus limon* peels used in this study were harvested from dierent regions of Visakhapatnam district, Andhra Pradesh, India. They were cleaned with running water, freed of dust and then shadow dried in the shade for 7 days and then transferred to an oven at forty degress celcius, *until* a stable weight. Twenty g of dried plant material each powder factory were extracted by absolute methanol at the ambient temperature (25 °C) for 24 h (200 ml, w/v: 1/10). The extracts were evaporated in the drying oven at 40 °C until the complete evaporation of methanol to obtain the crude extracts.

The prepared solutions are analyzed according to the optimized procedure. The obtained results are shown in the Table 4.

Conclusion

The determination of Guaiacol in presence of

Table 1. Selected analytical parameters obtained in presence of periodate

Parameter	Examined range	Selected value
Wavelength	380-750	515
pH	3.0-5.0	5.0
Temperature °C	-	25
Molar absorptivity L mol–1 cm–1 -	-	6.35 × 104
Sandal's sensitivity, µg cm-2	-	0.026
Detection limit/µg l–1 -	-	0.5
Regression coefficient	-	0.996

Table 2. Selected analytical parameters obtained in presence of perbromate

Parameter	Examined range	Selected value
Wavelength, nm	380-750	590
pH	3.0-5.0	5.0
Temperature °C	-	25
Molar absorptivity L mol–1 cm–1 -	-	6.85 × 104
Sandal's sensitivity, µg cm^{-2}	-	0.036
Detection limit /µg l–1 -	-	0.5
Regression coefficient	-	0.99

Table 4. Concentration of Guaiacol in presence of perioadate and perbromate in the leaves of *Citrus sinensis & Citrus limon*

Sample	*Citrus sinensis* (ppm)		*Citrus limon* (ppm)	
	Perioadate	Perbromate	Perioadate	Perbromate
1	0.610	0.592	0.037	0.029
2	0.307	0.309	0.043	0.036
3	0.160	0.154	0.0017	0.0011
4	0.093	0.085	0.224	0.116
5	0.110	0.107	0.0014	0.0009

perbromate and perioadate in orange and lemon leaves has been developed by using a sensitive and selective analytical reagent. The reported method offers advantages like sensitivity and quick colour development. The developed method found to be quantitative compared to other methods and applied to orange and lemon leaves.

Acknowledgements

We gratefully acknowledge the management of GITAM University and Department of Chemistry, GITAM institute of science for providing facilities and encouragement.

References

Allen, D., Bui, A.D., Cain, N., Rose, G. and Downey, M. 2013 Analysis of free and bound phenolics in wine and grapes by GC-MS after automated SPE. *Anal. Bioanal. Chem*. 405 : 9869- 9877. DOI: 10.1007/s00216-013-7405-0.

Bahçeci, K.S. and Acar, J. 2007 Determination of guaiacol produced by *Alicyclobacillus acidoterrestris* in apple juice by using HPLC and spectrophotometric methods, and mathematical modeling of guaiacol production. *Eur Food Res Technol*. 225 : 873–878. https://doi.org/10.1007/s00217-006-0495-6

Kalaiyarasi, J., Meenakshi, S., Pandian, K., Subash, C. and Gopinath, B. 2017. Simultaneous voltammetric determination of vanillin and guaiacol in food products on defect free graphene nanoflakes modified glassy carbon electrode. *Microchim Acta*. 184 : 2131–2140, DOI 10.1007/s00604-017-2161-z

Pizarro, C., Pérez-del-Notario, N. and González-Sáiz, J.M. 2010. Optimisation of a simple and reliable method based on headspace solid-phase microextraction for the determination of volatile phenols in beer. *J. Chromatogr*. A 1217 : 6013–6021. DOI: 10.1016/j.chroma.2010.07.021.

Sarah-Maria Bölicke and Waldemar Ternes, 2016 Isolation and identification of oxidation products of guaiacol from brines and heated meat matrix. *Meat Science.* 117 : 18-26. https://doi.org/10.1016/j.meatsci.2016.02.031

Wilkinson, K.L., Ristic, R., Pinchbeck, K.A., Fudge, A.L., Singh, D.P., Pitt, K.M., Downey, M.O., Baldock, G.A., Hayasaka, Y. and Parker, M. 2011. Comparison of methods for the analysis of smoke related phenols and their conjugates in grapes and wine. *Aust. J. Grape Wine Res*. 17 : S22–S28. https://doi.org/10.1111/j.1755-0238.2011.00147.x

Yan,Wu, Meng Huang, Nannan Song and Weibing Hu, 2014. Electrochemical detection of guaiacol in bamboo juice based on the enhancement effect of RGO nanosheets. *Anal. Methods.* 6 : 2729-2735. https://doi.org/10.1039/C4AY00195H

Zhiqian Liu, Vilnis Ezernieks, Priyanka Reddy, Aaron Elkins, Christian Krill, Kieran Murphy, Simone Rochfort and German Spangenberg, 2020. A Simple GC-MS/MS Method for Determination of Smoke Taint-Related Volatile Phenols in Grapes. *Metabolites*. 10 : 294; doi:10.3390/metabo10070294

Zhou, Q., Qian, Y. and Qian, M.C. 2015. Analysis of volatile phenols in alcoholic beverage by ethyleneglycol-polydimethylsiloxane based stir bar sorptive extraction and gas chromatography–mass spectrometry. *J. Chromatogr*. A 1390 : 22–27. DOI: 10.1016/j.chroma.2015.02.064.

FUZZY TRANPORTATION MODEL USING L-R FLAT TRAPEZOIDAL APPROXIMATIONS

[1]Ch.Uma Swetha, [2]N.Ravi Shankar,[3]B.Pardha Saradhi
[1]Dept. of Mathematics, Anil Neerukonda Institute of Technology &Sciences, Visakhapatnam
[2] Dept. of Mathematics, GIS, GITAM (Deemed to be University), Visakhapatnam
[3] Dept. of Engineering Mathematics,Dr.Lankapalli Bullayya college of Engineering, Visakhapatnam.

ABSTRACT
Transportation problem is applied for many differentcircumstances being scheduling,production, investment, plant location, inventory control, employment scheduling, and several methods. The aim of the fuzzy transportation problem is to resolve the transport schedule that minimizes the total fuzzy transportation cost while delightful the fuzzy supply and fuzzy demand limits. In view of this, a novel approach to optimize fuzzy transportation modelby using trapezoidal approximations of L-R flat fuzzy numbers is proposed. A few generalized and modern properties of the trapezoidal and triangular approximations of L-R flat fuzzy numbers forparameters in fuzzy transportation problem is suggested. Numerical example is illustrated for the novel fuzzy transportation model.
Keywords:L-R flat fuzzy numbers; Approximation of L-R flat fuzzy numbers; Fuzzy transportation problem; L-R type fuzzy ranking

1. INTRODUCTION

The transportation problem is an important application of Linear Programming Problem (LPP) models. The main view ofmentioned concept is obtaining the minimal transportation cost of a product for gratifying the demands at destination, using the available supply at origin. The transportation problem can be used in different type of positions, such as scheduling, production, investment, plant location & inventory control. The transportation models are explainedfrequently with the inference that the transportation costs, supply and demandsare stated accurately. However,for the transportation problem, the policy maker does not give correct data about the coefficientsin most of the situations.If the data has ambiguity which means that,the corresponding coefficientscan be developed by using fuzzy sets to determine the problem due to lack of precision and which approaches to fuzzy transportation problems.

Zadeh [1]developed the fuzzy set theory to discuss with the ambiguities. And in that uncertain information is transportation problem may be characterized by triangular and trapezoidal fuzzy numbers.Two examples are shown in trapezoidal approximation of fuzzy number to clarify such positions[2]. It developed the operator which gives some new properties.The concept of an approximation rangeof a fuzzy number was recommended [3]. Which fulfils two conditions and the opinion was correlated with an expected range of known fuzzy number.Two parameters, value and ambiguity were introduced to attain an authorized representation and to discuss with fuzzy numbers in policy – making problems[4]. The general arithmetic operations on real numbers areinvestigated using fuzzy fundamentals and these algorithms to be fitted for fuzzy settheory[5].Fuzzy numbers on intervals was defined andshown to be additive with respect to addition of fuzzy range while only inequalities are satisfied and defined that the theory of interval – valued mean fuzzy numbers [6]. In [6], how the problem to take measure- theoretical assumptions into the branch of possibility theory was discussed. In [7], two metrics in space of fuzzy numbers are introduced and they are used torank fuzzy numbers.Grzegorzewski [8] has explained the problem of an interval approximation of a fuzzy numbers and suggested to measure of distance between two different fuzzy numbers for a relevant new approximation period. The closest triangular approximation operator defending the expected range from the closest trapezoidal approximation operator preserving the expected interval is proposed [9]. The theory of trapezoidal approximations of a fuzzy numbers and the set of principles for nearest operators are developed[10], which are defending the expected interval. In [11], they revisiteddedicated to trapezoidal approximations of a fuzzy number and they shown a correct explanation for the approximation operator perpetuating the expected interval. This operator maintains several properties are showed in [10]. After corrections they suggested all these parameters are firmly connected with the expected interval invariance norms.[12] was introduced the concept of an expected interval and an expected value of a fuzzy numbers. The expected value of this number is explained as the middle of the expected period and the expected range is defined as the expected value of irregular set of fuzzy number. In [13], proposed a process to

determine the interrelated coefficient of fuzzy number by the virtue of an expected interval. Also the strength of the relationship between fuzzy numbers is computed. The ranking fuzzy numbers over the resemblance of its expected values are presented in [14]. These are certify that rationality and virtual qualities and also compared non normal fuzzy numbers. The basic of the kudo- Aumann integral of a set- valued mapping is defined and some properties of average level of a fuzzy set for some special cases are analyzed in [15].A few generalized and modern properties of the trapezoidal approximations of fuzzy numbers, some relations of distance betwixt a fuzzy number and its trapezoidal approximations are proved in [16].'Mehars Method' is an advanced method to deal with the problems on fuzzy sensitivity analysis with LR flat fuzzy numbers are discussed in [17], in which either few or all specifications are characterized from unregulated L-R flat fuzzy numbers, which are may or may not be explained by existing methods are presented in [17]. The fuzzy transportation problem is determined with a new procedure is given in [18], in which the cost, origin and destinations are described as non-negative L-R flat fuzzy numbers.

We focus on a particular type of L-R fuzzy numbers, where L and R represent left and right shaped functions. These are involves triangular fuzzy number, trapezoidal fuzzy number, Gaussian fuzzy number, Cauchy fuzzy number as special cases called regular L-R flat fuzzy numbers. In view of this paper constraints of existing works [10], [11] are referred. To get the better of these limitations we introduced a triangular and trapezoidal approximation of L-R flat fuzzy numbersforsolving transportation cost, origin and destinations, supply and demands of the product in which all the parameters are characterized with unrestricted L-R flat fuzzy numbers. For illustration of the proposed method a numerical example has been given.

This paper formulated as follows:Section2, discussed preliminaries like primary definitions and Yager's ranking approach for unrestricted L-R flat fuzzy numbers . Section3, discussed the properties of triangular and trapezoidal approximations of L-R flat fuzzy numbers are introduced in which all the variables are described with unrestricted L-R flat fuzzy numbers.Section4 discussed the Transportation model ,Section5 explained the proposed work ,Section 6 discussed the numerical example is determined., Section 7,explained the conclusions.

2. Preliminaries

In this segment, a few fundamentaldefinitions of LR- flat fuzzynumbers are given.

Definition2.1 [17]: Let $\tilde{P} = (m, n, \alpha, \beta)$ is L-R flat fuzzy number anditsmembership function is defined as

$$\mu_{\tilde{P}} = \begin{cases} L\left(\dfrac{m-x}{\alpha}\right) & x \le m \quad \alpha > 0 \\ 1 & m \le x \le n \\ R\left(\dfrac{x-n}{\beta}\right) & x \ge n \quad \beta > 0 \end{cases}$$

Let $P_\lambda = \{x \in \Re : \mu_P(x) \ge \lambda\}$ denote a $\alpha-$ cut of L-R flat fuzzy number and λ be a realnumber in the closed interval. Then α - cut of a fuzzy number is $P_\lambda = [P_L(\lambda)\ ,\ P_U(\lambda)]$, where $P_L(\lambda) = \inf\{x \in R :\ \mu_{\tilde{P}}(x) \ge \lambda\}$and $P_U(\lambda) = \sup\{x \in R :\ \mu_{\tilde{P}}(x) \ge \lambda\}$.

Definition2.2 [17]: If $m - \alpha \ge 0$, a L-R flat fuzzy number $\tilde{P} = (m, n, \alpha, \beta)$ is known as a non- negative.And alsoif $n + \beta \le 0$, $\tilde{P}$ is known as s a non – positive L-R flat fuzzy number.

Definition2.3 [17]:A L-R flat fuzzy number $\tilde{P} = (m, n, \alpha, \beta)$ and $\lambda \in \Re$ in the period[0, 1] then the crisp set is

$P_\lambda = \{x \in X :\ \mu_{\tilde{P}}(x) \ge \lambda\} = [m - \alpha L^{-1}(\lambda)\ ,\ n + \beta R^{-1}(\lambda)]$ is called α - cut of $\tilde{P}$.

Definition2.4[17]: Yager's ranking function is determined for L-R flat fuzzy number $\tilde{P} = (m, n, \alpha, \beta)$ from it's α - cut $P_\lambda = [m - \alpha L^{-1}(\lambda)\ ,\ n + \beta R^{-1}(\lambda)]$as stated by the following formula

$$\Re(\tilde{P}) = \int_0^1 \left(m - \alpha L^{-1}(\lambda)\right)\, d\lambda + \int_0^1 \left(n + \beta R^{-1}(\lambda)\right)\, d\lambda$$

i.e; $\Re(\tilde{P}) = m + n - \frac{2\alpha}{3} + \frac{\beta}{2}$

Let us suppose an expected interval $EI(\tilde{P})$ of an L-R flat fuzzy number $\tilde{P}$ is given by([6],[12])

$$EI(\tilde{P}) = \left[\int_0^1 P_L(\lambda)\, d\lambda \,,\, \int_0^1 P_U(\lambda)\, d\lambda\right] \quad (1)$$

Trapezoidal approximations of Fuzzy numbers were discussed in [11] and theyhaveexhibited to replace irrational fuzzy number by the Trapezoidal fuzzy number. Similarly we express thetrapezoidalL-R flat fuzzy number by linear parts and having the membership function is given below

$$\mu_{\tilde{P}} = \begin{cases} 0 & x \le m-\alpha \\ \dfrac{x-(m-\alpha)}{\alpha} & m-\alpha \le x < m \\ 1 & m \le x \le n \\ \dfrac{(n+\beta)-x}{\beta} & n < x < n+\beta \\ 0 & x \ge n+\beta \end{cases} \quad (2)$$

Since the trapezoidal L-R flat fuzzy number is fully describedby the real numbers (m, n, α, β) and they are denoted as $\tilde{P}(m, n, \alpha, \beta)$. A group of all trapezoidal L-R flat fuzzy number will be indicated as $(LR^T(\Re))$. From Eq. (1) and Eq.(2) an expected range of the trapezoidal L-R flat fuzzy number is presented as

$$EI(\tilde{Q}) = \left[\frac{2m-\alpha}{2}\,,\, \frac{2n+\beta}{2}\right] \quad (3)$$

For two arbitrary L-R flat fuzzy numbers $\tilde{P}$ and $\tilde{Q}$ with $\alpha-$cuts $\left[P_L(\lambda),\ P_U(\lambda)\right]$ and $\left[Q_L(\lambda),\ Q_U(\lambda)\right]$ respectively, then the distance between $\tilde{P}$ and $\tilde{Q}$.

$$d(\tilde{P},\tilde{Q}) = \sqrt{\int_0^1 \left(P_L(\lambda)-Q_L(\lambda)\right)^2 d\lambda + \int_0^1 \left(P_U(\lambda)-Q_U(\lambda)\right)^2 d\lambda} \quad (4)$$

3. Trapezoidal approximation:

In this part we introduce an approximate operator $T:(LR(\Re)) \to (LR^T(\Re))$ which develops trapezoidal L-R flat fuzzy number that is nearest to given actual L-R flat fuzzy number between the trapezoidal L-R flat fuzzy numbers are all having indistinguishableexpected interval by the actual thing [8]. Then this operator can be known as the nearest trapezoidal approximation operator perpetuating an expected interval.

Let us take $\tilde{P}$ as L-R flat fuzzy number and its $\alpha-$cut is $\left[P_L(\lambda),\ P_U(\lambda)\right]$. Given $\tilde{P}$ we seek to determine a trapezoidal L-R flat fuzzy number T ($\tilde{A}$) which is the closest to $\tilde{P}$ with respect to metric d from Eq.(4). Suppose $\left[T_L(\lambda),\ T_U(\lambda)\right]$ denote the $\alpha-$cutof $T(\tilde{P})$. Then we need to reduce

$$d\left(\tilde{P},T(\tilde{P})\right) = \sqrt{\int_0^1 \left(P_L(\lambda)-T_L(\lambda)\right)^2 d\lambda + \int_0^1 \left(P_U(\lambda)-T_U(\lambda)\right)^2 d\lambda} \quad (5)$$

Subject to $T_L(\lambda)$ and $T_U(\lambda)$. In spite of that, since a trapezoidal L-R flat fuzzy number is fully characterized by suchfour real numbers (m, n, α, β). Our proposal isminimizes to finding trapezoidal L-R flat fuzzy number is represented as $T(\tilde{P}) = T(m, n, \alpha, \beta)$.

It is assuming that the $\alpha-$cut of $T(\tilde{P})$ is equal to $\left[(m-\alpha)+\alpha\lambda\ ,\ (n+\beta)-\beta\lambda\right]$

Therefore (5) reduces to

(6)

$$d(\tilde{P},T(\tilde{P})) = \sqrt{\int_0^1 \left(P_L(\lambda)-((m-\alpha)+\alpha\lambda)\right)^2 d\lambda + \int_0^1 \left(P_U(\lambda)-((n+\beta)-\beta\lambda\right)^2 d\lambda}$$

And we will seek to reduce (6) with respect to m, n, α, β.

Yet, we need to solve a trapezoidal L-R flat fuzzy numberand which is not nearest to given L-R flat fuzzy number but it is perpetuates the expected interval of that L-R flat fuzzy number. We confirm this further necessity by the powerful role of the expected interval in several positions and applications([3], [6]-[8], [12]-[15]). Thus our issue is to identify such real numbers m, n, α, β that reduce (6) with respect to condition

(7) $$EI(T(\tilde{P})) = EI(\tilde{P})$$

From (1) and (3) we can write (7) as below

(8) $$\left[\frac{2m-\alpha}{2}\ ,\ \frac{2n+\beta}{2}\right] = \left[\int_0^1 P_L(\lambda)\ d\lambda\ ,\ \int_0^1 P_U(\lambda)\ d\lambda\right]$$

It is simply observable that one mayreduce $d(\tilde{P}, T(\tilde{P}))$ it satisfies to diminish the function $f(m,n,\alpha,\beta) = d^2(\tilde{P}, T(\tilde{P}))$ with respect to following conditions:

$$\frac{2m-\alpha}{2} - \int_0^1 P_L(\lambda)\ \ d\lambda\ = 0 \qquad (9)$$

$$\frac{2n+\beta}{2} - \int_0^1 P_U(\lambda)\ \ d\lambda\ = 0 \quad (10)$$

Moreover, For $m \le n$.

We havetodiminishing the function

(11) $$\phi(x) = \int_0^1 \left(P_L(\lambda) - ((m-\alpha) + \alpha\lambda)\right)^2\ d\lambda + \int_0^1 \left(P_U(\lambda) - ((n+\beta) - \beta\lambda)\right)^2\ d\lambda$$

Subject to

(12) $$\xi(x) = m - n \le 0$$

(13) $$\psi(x) = \left[2m - \alpha - 2\int_0^1 P_L(\lambda)\ d\lambda,\quad 2n + \beta - 2\int_0^1 P_U(\lambda)\ d\lambda\right]$$

Where $x \in R^4$.

FromKarush- Kuhn- Tucker theorem (KKT), if x^* is a provincialminimiser to the problem of reducing the function ϕ with respect to $\psi(x) = 0$, $\xi(x) \le 0$, then $\exists\ \lambda$ is Lagrange multiplier vector and μ is KKT multiplier such that,

$$D\phi(x^*) + \lambda D\psi(x^*) + \mu D\xi(x^*) = 0^T \quad (14)$$

$$\mu\xi(x^*) = 0 \quad (15)$$

$$\mu \ge 0 \quad (16)$$

In our case, after some calculations, we get

$$D\phi(x^*) = \begin{cases} 2m - \alpha - 2\int_0^1 P_L(\lambda)\ d\lambda \\ 2n + \beta - 2\int_0^1 P_U(\lambda)\ \ d\lambda \\ \frac{2\alpha}{3} - m + 2\int_0^1 P_L(\lambda)\ d\lambda - 2\int_0^1 \lambda P_L(\lambda)\ \ d\lambda \\ n + \frac{4\beta}{3} + 2\int_0^1 \lambda P_U(\lambda)\ \ d\lambda\ - 2\int_0^1 p_U(\lambda)\ \ d\lambda \end{cases} \qquad (17)$$

$$D\psi(x^*) = \begin{bmatrix} 2 & 0 & -1 & 0 \\ 0 & 2 & 0 & 1 \end{bmatrix} \quad (18)$$

$$D\xi(x^*) = \begin{bmatrix} 1 & -1 & 0 & 0 \end{bmatrix} (19)$$

Then, we will takethe following KKT conditions

$$2m - \alpha - 2\int_0^1 P_L(\lambda)\, d\lambda + 2\lambda_1 + \mu = 0 \quad (20)$$

$$2n + \beta - 2\int_0^1 P_U(\lambda)\, d\lambda + 2\lambda_2 - \mu = 0 (21)$$

$$\frac{2\alpha}{3} - m + 2\int_0^1 P_L(\lambda)\, d\lambda - 2\int_0^1 \lambda P_L(\lambda)\, d\lambda - \lambda_1 = 0 (22)$$

$$n + \frac{2\beta}{3} + 2\int_0^1 \lambda P_U(\lambda)\, d\lambda - 2\int_0^1 P_U(\lambda)\, d\lambda + \lambda_2 = 0 (23)$$

$$2m - \alpha - 2\int_0^1 P_L(\lambda)\, d\lambda = 0 (24)$$

$$2n + \beta - 2\int_0^1 P_U(\lambda)\, d\lambda = 0 (25)$$

$$\mu(m - n) = 0 \ , \ (26)$$

$$\mu \geq 0 (27)$$

To evaluate the values of m, n, α, β for satisfying the above equations and initially, we use $\mu > 0$, i.e; $m - n = 0$. So we deal with a linear system of equations.

$$2m - \alpha - 2\int_0^1 P_L(\lambda)\, d\lambda + 2\lambda_1 + \mu = 0 (28)$$

$$2n + \beta - 2\int_0^1 P_U(\lambda)\, d\lambda + 2\lambda_2 + \mu = 0 (29)$$

$$\frac{2\alpha}{3} - m + 2\int_0^1 P_L(\lambda)\, d\lambda - 2\int_0^1 \lambda P_L(\lambda)\, d\lambda - \lambda_1 = 0 (30)$$

$$n + \frac{2\beta}{3} + 2\int_0^1 \lambda P_U(\lambda)\, d\lambda - 2\int_0^1 P_U(\lambda)\, d\lambda + \lambda_2 = 0 (31)$$

$$2m - \alpha - 2\int_0^1 P_L(\lambda)\, d\lambda = 0 (32)$$

$$2n + \beta - 2\int_0^1 P_U(\lambda)\, d\lambda = 0 (33)$$

Finding the above linear equations, we get

$$m = n = -\int_0^1 P_L(\lambda)\, d\lambda + 3\int_0^1 \lambda P_L(\lambda)\, d\lambda - \int_0^1 P_U(\lambda)\, d\lambda + 3\int_0^1 \lambda P_U(\lambda)\, d\lambda \quad (34)$$

$$\alpha = -4\int_0^1 P_L(\lambda)\, d\lambda + 6\int_0^1 \lambda P_L(\lambda)\, d\lambda - 2\int_0^1 P_U(\lambda)\, d\lambda + 6\int_0^1 \lambda P_U(\lambda)\, d\lambda \quad (35)$$

$$\beta = 2\int_0^1 P_L(\lambda)\, d\lambda - 6\int_0^1 \lambda P_L(\lambda)\, d\lambda + 4\int_0^1 P_U(\lambda)\, d\lambda - 6\int_0^1 \lambda P_U(\lambda)\, d\lambda \quad (36)$$

$$\lambda_1 = -\int_0^1 \lambda P_L(\lambda)\, d\lambda + \frac{1}{3}\int_0^1 P_L(\lambda)\, d\lambda - \frac{-1}{3}\int_0^1 P_U(\lambda)\, d\lambda + \int_0^1 \lambda P_U(\lambda)\, d\lambda \quad (37)$$

$$\lambda_2 = \frac{-1}{3}\int_0^1 P_L(\lambda)\, d\lambda + \int_0^1 \lambda P_L(\lambda)\, d\lambda + \frac{1}{3}\int_0^1 P_U(\lambda)\, d\lambda - \int_0^1 \lambda P_U(\lambda)\, d\lambda \quad (38)$$

$$\mu = 2\int_0^1 \lambda P_L(\lambda)\, d\lambda - \frac{2}{3}\int_0^1 P_L(\lambda)\, d\lambda + \frac{2}{3}\int_0^1 P_U(\lambda)\, d\lambda - 2\int_0^1 \lambda P_U(\lambda)\, d\lambda \quad (39)$$

In any manner, by the assume that $\mu > 0$, then we get appropriate results for the KKT equationsiff

$$\left(\int_0^1 \lambda P_L(\lambda)\, d\lambda - \frac{1}{3}\int_0^1 P_L(\lambda)\, d\lambda\right) - \left(\int_0^1 \lambda P_U(\lambda)\, d\lambda - \frac{1}{3}\int_0^1 P_U(\lambda)\, d\lambda\right) > 0$$

$$\int_0^1 \lambda P_L(\lambda)\, d\lambda - \frac{1}{3}\int_0^1 P_L(\lambda)\, d\lambda > \int_0^1 \lambda P_U(\lambda)\, d\lambda - \frac{1}{3}\int_0^1 P_U(\lambda)\, d\lambda$$

$$\int_0^1 [P_L(\lambda) - P_U(\lambda)]\left(\lambda - \frac{1}{3}\right)\, d\lambda > 0 \quad (40)$$

And then we get a solution $x^* = (m, n, \alpha, \beta)$ is provided from (34)-(36)

We consider $\mu = 0$ in the second try. So we have to determine the below system of equations

$$2m - \alpha - 2\int_0^1 P_L(\lambda)\, d\lambda + 2\lambda_1 + \mu = 0 \quad (41)$$

$$2n + \beta - 2\int_0^1 P_U(\lambda)\, d\lambda + 2\lambda_2 - \mu = 0 \quad (42)$$

$$\frac{2\alpha}{3} - m + 2\int_0^1 P_L(\lambda)\, d\lambda - 2\int_0^1 \lambda P_L(\lambda)\, d\lambda - \lambda_1 = 0 \quad (43)$$

$$2m - \alpha - 2\int_0^1 P_L(\lambda)\, d\lambda = 0 \quad (44)$$

$$2n + \beta - 2\int_0^1 P_U(\lambda)\, d\lambda = 0 \quad (45)$$

Obtain the above equations, and then we have

$$m = 6\int_0^1 \lambda P_L(\lambda)\, d\lambda - 2\int_0^1 P_L(\lambda)\, d\lambda \quad (46)$$

$$n = -2\int_0^1 P_U(\lambda)\, d\lambda + 6\int_0^1 \lambda P_U(\lambda)\, d\lambda \quad (47)$$

$$\alpha = 12\int_0^1 \lambda P_L(\lambda)\, d\lambda - 6\int_0^1 P_L(\lambda)\, d\lambda \quad (48)$$

$$\beta = 6\int_0^1 P_U(\lambda)\, d\lambda - 12\int_0^1 \lambda P_U(\lambda)\, d\lambda \quad (49)$$

$\lambda_1 = 0$ (50)

$\lambda_2 = 0$ (51)

Hencewe get trapezoidal approximation of L-R flat fuzzy numbers.

For further calculations,

$$\int_0^1 P_L(\lambda)\ d\lambda = \frac{2m-\alpha}{2} \quad (52)$$

$$\int_0^1 \lambda P_L(\lambda)\ d\lambda = \frac{3m-\alpha}{6} \quad (53)$$

$$\int_0^1 P_U(\lambda)\ d\lambda = \frac{2n+\beta}{2} \quad (54)$$

$$\int_0^1 \lambda P_U(\lambda)\ d\lambda = \frac{3n+\beta}{6} \quad (55)$$

4. **Fuzzy Transportation Model**

The transportation model is considered that the decision maker has particular information about the specific values of cost, availability and demand of the commodity in regular transportation models. The parameters are all of the transportation problem may or may not be known accurately in real life situations due to wild components. For e.g: in general life applications the following position may appear: consider a commodity is to be shipped at a destination and skilled person have no idea about the cost then there exist ambiguity data about the shipping cost. In such cases for obtaining transportation problems, the costs are considered as L-R flat fuzzy numbers. In the fuzzy transportation model, the decision maker has confusion about the definite values of the shipping cost from ith source to jth destination but if it has correct data about the supply and demand of the commodity, then the mathematical expression of the transportation model is given by

$$\text{Min}\quad Z = \sum_{i=1}^{m}\sum_{j=1}^{n} c_{ij}\, t_{ij}$$

Subject to

$$\sum_{j=1}^{n} t_{ij} \le \alpha_i \qquad i = 1,2,3,....$$

$$\sum_{i=1}^{m} t_{ij} \ge \beta_j \qquad j = 1,2,3,....$$

$$t_{ij} \ge 0 \quad \forall\ i, j$$

Where α_i be the total availability of the commodity at source (i) and β_j be the total demand of the product at destination (j), c_{ij} be the unit rough shipping cost for a unit quantity from source(i) to destination (j) and $Z = c_{ij}\, t_{ij}$ s the total least fuzzy transportation cost.

If $\sum_{i=1}^{m}\alpha_i = \sum_{j=1}^{n}\beta_j$ is called balance fuzzy transportation problem and it is not equal fuzzy transportation problem.

5. Proposed Methodology:

There are several methods for finding Fuzzy transportation problem with L-R flat fuzzy numbers [17][18] etc. In which methods are finding initial basic feasible solution (IBFS) by using Mehar's method and linear programming with non-negative L-R flat fuzzy numbers.

In this part, a few new properties are introduced for solving IBFS and fuzzy optimal solution by using Yager's ranking function with unrestricted trapezoidal and triangular approximations of L-R flat fuzzy numbers. The process of proposed method is given below and also numerical example.

The steps are given below for finding IBFS and optimal solution:

Step1: Transform L-R flat fuzzy numbers to trapezoidal and triangular approximation of L-R flat fuzzy numbers.

Step2: Form the transportation table using Yager's ranking function with L-R flat fuzzy Numbers.

Step3: Finding initial basic feasible solution (IBFS) using **VAM**

The process for finding IBFS using VAM as follows:

Case1: Calculate the fuzzy penalty cost for every row and column by finding the negative mean of least cost and immediate next to the least cost of every row and column. i.e; the difference between least cost and next to least cost by every row and column is divided.

Case2: If least cost appears higher than one time in a row or column then select same shipping cost as lowest cost and next to lowest cost and penalty becomes zero.

Case3: Take the rows or columns with the largest penalty costs (i.e; select the least cost cell). If there is bind appears in largest penalty cost, then select that row or column where he cost is least.

Case4: Determine shipping costs for chosen rows or columns in step3 by assigning approximately feasible value to the feasible cell with the smallest shipping cost.

Case5: At present balanced all the rows and columns also delete the gratified row or column. And allocate zero if satisfied at the same time to persist rows and columns.

Case6: Continue this process step1 – 5 up to all demands have been reached.

Case7: Calculate the total transportation cost for the feasible allotments by using fuzzy transportation problem matrix.

Step4: Finding optimal solution by using modified distribution method. This method provides a least cost solution to the fuzzy transportation problem.

The process for finding optimal solution by MODI method as follows:

Case1: Determine IBFS of fuzzy transportation problem using VAM

Case2: Find the twin variables α_i and β_j for the very row and columns respectively. Write α_i ahead of every row and β_j at the ground of every column. Choose any α_i or β_j is to be zero trapezoidal or triangular L-R flat fuzzy number.

Case3: To find α_i and β_j, using the formula $\alpha_i + \beta_j = c_{ij}$ where c_{ij} is the cost amount for the assigned chamber.

Case4: Calculate the penalties using $P_{ij} = \alpha_i + \beta_j - c_{ij}$ for unassigned chambers. And write them in area of concerned chamber. It may appear some following rules

(i) If all the penalties $P_{ij} \geq 0$ then the optimality is reached. So find the optimal solution.

(ii) If at least one penalty P_{ij} is negative then optimality is not reached. So go to case5.

Case5: Select that P_{ij}, whose penalty is largest negative then developed the solution can be determined by entering a vacant chamber (i, j) into the solution mix. A vacant chamber having highest negative value of P_{ij} is selected for entering into the new transportation programme.

Case6: when P_{ij} is highest negative then make a loop and create the loop with chosen vacant chamber and highlight a plus sign (+) in their chamber. Mark a loop along the rows or columns to a vacant chamber, and highlight the corner with a minus sign (-). Repeat this process the row or column to an inhabited chamber. Then the corner with plus sign (+) or minus sign (-) is traced alternatively.

Case7: Choose the lowest value amongst the chambers with minus sign is denoted on the corners of the closed path. Assign this value to the chosen vacant chamber and add or subtract it to inhabited chambers are traced with plus sign and minus sign.

Case8: According to case5 determine a new developed solution by assigning units to the vacant chambers and compute the new total transportation cost.

Case9: Continue this process until $P_{ij} \geq 0$ for case1 to case8.

Case10: Solve the fuzzy optimal solution and optimal costs are t_{ij} and $\sum_{i=1}^{m}\sum_{j=1}^{n} c_{ij}\, t_{ij}$ respectively.

6. **Numerical Examples**

In this section, two examples are given to solve fuzzy transportation problem of the proposed method.

Example: 1

The table 1 represents LR- flat fuzzy numbers for Trapezoidal fuzzy transportation cost of the product between different sources and different destinations.

Table 1: Transportation costs

	D_1	D_2	D_3	Supply
S_1	4,9,3,10	2,5,1,4	5,8,3,10	5,7,4,2
S_2	9,12,1,14	5,8,2,4	9,13,2,15	7,8,3,2
S_3	12,20,1,7	5,10,5,5	5,8,1,3	5,8,1,3`
Demand	5,8,2,4	8,9,4,1	4,6,2,2	

Trapezoidal approximations of LR- flat fuzzy numbers for obtaining fuzzy transportation cost are represented in table 2.

Table 2:Trapezoidal Approximations of Transportation Costs

	D_1	D_2	D_3	Supply
S_1	4,9,3,10	2,5,1,4	5,8,3,10	5,7,4,2
S_2	9,12,1,14	5,8,2,4	9,13,2,15	7,8,3,2
S_3	12,20,1,7	5,10,5,5	5,8,1,3	5,8,1,3`
Demand	5,8,2,4	8,9,4,1	4,6,2,2	

$\Re(\tilde{A})$iscalculated for the fuzzy costs in table 2using the formula

$\mathfrak{R}(\tilde{A}) = \boldsymbol{m} + \boldsymbol{n} - \frac{2\alpha}{3} + \frac{\beta}{2}$.

Fuzzy transportation problem after implementing the ranking technique is presented in

Table 3

Table 3: Fuzzy transportation problem after fuzzy ranking

	D_1	D_2	D_3	Supply
S_1	16	8.3	16	10
S_2	27.3	13.7	28.2	14
S_3	34.8	20.8	13.8	14
Demand	14	15	10	

After applying fuzzy ranking function in Table 5, the optimal cost or the total minimum fuzzy transportation cost – 613.8 is obtained by using modified Vogel's approximation method.

Example: 2

From Table1, the triangular approximations of LR – flat fuzzy numbers are calculated and presented in Table-4

Table 4: Triangular approximations of Transportation costs

	D_1	D_2	D_3	Supply
S_1	6.5,8,15	3.5,4,7	6.5,6,13	6,6,4
S_2	10.5,4,17	6.5,5,7	11,6,19	7.5,4,3
S_3	16,9,15	7.5,10,10	7.5,4,6	7.5,4,6
Demand	6.5,5,7	8.5,5,2	5,4,4	

By applying ranking method $\Re(\tilde{A})$ is calculated for fuzzy costs in table 4 using the formula.

$$\Re(\tilde{A}) = m + n - \frac{2\alpha}{3} + \frac{\beta}{2}$$

Fuzzy transportation problem after implement the ranking technique is shown in table 5.

Table 5: Fuzzy Transportation problem after Fuzzy ranking

	D_1	D_2	D_3	Supply
S_1	10.2	7.8	15.5	10
S_2	26.8	13.2	29.5	14
S_3	33.5	13.3	15.3	16
Demand	13	15	9	

After applying fuzzy ranking function in Table 5,the optimal cost or thetotal minimum fuzzy transportation cost – 518.5 is obtained by using modified Vogel's approximation method.

7. Conclusion

In view of this paper, a new proposed method is to get the initial basic feasible solution and optimal solution of the fuzzy transportation problem. The transportation cost, supply and demands are taken as unrestrictedLR – flat fuzzy trapezoidal and triangular numbers, which are real and general in nature. The fuzzy transportation problem of trapezoidal and triangular approximations of LR– flat fuzzy numbers have been changed to crisp transportation problem by using Yager's ranking function. A numerical example is pageant that the proposed method gives the better results. The advantage of the proposed method is obtained thefuzzy optimal solution by unrestricted LR – flat fuzzy numbers. This method is simple to gain and apply for solving fuzzy transportation cost in the real life circumstances.

References:

[1].L.A.Zadeh.(1965), Fuzzy Systems, information and controls, 8 ,338-353.

[2]. T. Allahviranloo, M. AdabitabarFirozja(2005), Note on Trapezoidal approximations of fuzzy numbers, Fuzzy Sets and Systems, to appear. 153 ,115–135] .

[3]. S. Chanas(2001), On the interval approximation of a fuzzy number, Fuzzy Sets and Systems 122 353-356.

[4]. M. Delagado, M.A. Vila, W. Voxman, (1998) On a canonical representation of a fuzzy number, Fuzzy Sets and Systems 93 125-135.

[5]. D. Dubois, H. Prade(1978) , Operations on fuzzy numbers, Internat. J. Systems SCi. 9 613-626.

[6]. D. Dubois, H. Prade, (1987) The mean value of fuzzy number, Fuzzy Sets and Systems 24 ,279 – 300.

[7]. P. Grzegorzewski, (1998) Metrics and orders in space of fuzzy numbers, Fuzzy Sets and Systems 97 ,83 – 94.

[8]. P. Grzegorzewski, (2002) Nearest interval approximation of a fuzzy number, Fuzzy Sets and Systems 130 321 – 330.

[9]. chi-T. Yeh, (2008) Trapezoidal and triangular approximations preserving the expected interval, Fuzzy Sets and Systems 159, 1345 – 1353.

[10]. P. Grzegorzewski, E. Mrowka(2005), Trapezoidal approximation of a fuzzy numbers, Fuzzy Sets and Systems 153 ,115-135.
[11]. P. Grzegorzewski, E. Mrowka, (2007) Trapezoidal approximation of a fuzzy numbers – revisited, Fuzzy Sets and Systems 158 ,757 – 768.
[12]. S. Heilpern, (1992) The expected value of a fuzzy number, Fuzzy Sets and Systems 47 81 – 86.
[13]. W. Hung, J. Wu, (2001) A note on the correlation of fuzzy numbers by expected interval, Internat. J. Uncertainty Fuzziness and knowledge – Based Systems 9 ,517 – 523.
[14]. M. Jimenez, (1996) Ranking fuzzy numbers through the comparison of its expected intervals, Internat. J. Uncertainty Fuzziness and knowledge – Based Systems 4 ,379 – 388.
[15]. D. Ralescu, 2000 Average level of a fuzzy Set, in: proc. Eighth Internat. Conf. On Information Processing and Management of Uncertainty IPMU' 2000, Madrid, 3 – 7 July , pp.190 -194.
[16].Ch. T. Yeh(**2007**), A note on Trapezoidal approximations of fuzzy numbers, Fuzzy Sets and Systems, to appear**.** Volume 158, Issue 7**, 1 April 2007, Pages 757-768**

[17]. Neha Bhatia, Amit Kumar, Mehar's(2012) method for solving fuzzy sensitivity analysis problems with L-R fuzzy numbers. Applied Mathematical Modelling,36 4087 – 4095.
[18]. Ali Ebrahimnejad, (2016) New method for solving Fuzzy transportation problems with LR flat fuzzy numbers, Information Sciences 357 108 – 124.

Turkish Journal of Computer and Mathematics Education Vol.12 No.6 (2021), 5272-5286

Research Article

Hesitant Fuzzy Project Planning and Scheduling using Critical path Technique

B. Pardha saradhi[a] , H.Ramesh.[b],N.Ravi Shankar[c] , Rijwan Shaik[d]

[a] Dr. L.B .college of Engineering, Visakhapatnam, India.
[b]Rajiv Gandhi university of knowledge technologies, IIIT – Srikakulam,Visakhapatnam, India.
[c,d,]GITAM (Deemed to be University), Visakhapatnam, India.
Email:[a]dr.pardhasaradhibehara@gmail.com,[b]ramesh.hunumanthu@gmil.com.[c]drravi68@gmail.com,[d]rijwan2080@gmail.com4

Article History: Received: 10 November 2020; Revised 12 January 2021 Accepted: 27 January 2021; Published online: 5 April 2021

Abstract: Hesitant fuzzy set is extremely useful performance to express people's uncertainty. But there are delicate points in conventional hesitant fuzzy set, which articulated the membershipdegrees of an element to a given set only by some crisp numbers .Hesitant fuzzy set to Triangular Fuzzy Hesitant Fuzzy Set (THFS), in which the membership degreeof an element to a given set is expressed by several possible triangular fuzzy numbers. A new plan to determine the critical path in the project network using Triangular Hesitant Fuzzy set (THF).In this project network Each activity time is THFS.One of multicriteriadecision making Technique for Order of Preference by Similarity to Ideal Solution (TOPSIS) is used for the project network to identify the best path in the project.Finally a numerical exemplar is furnished to elucidate the critical path of the project network.

Keywords:

1. Introduction

Critical path method (CPM)` is one of the project network based method to evaluating the best project performance in the project network. The flourishing execution of CPM requires the accessibility of a apparent determined time duration for each activity. Nevertheless, in practical situations this very difficult to complete because number of activities are performing using vague data. So in advance the activity times of each activity is very difficult to know. As a result the unknowns or vagueness concerning the time duration of activities in network planning, has led to the improvement of fuzzy CPM. Interactive fuzzy subtraction on a ten point network was proposed by Nasution [21] ,Where In which each activity time represents a trapezoidal fuzzy numbers to determine newest allowable and slack for activities, Also discussed the $\alpha-$cut level of the slack fuzzy slack availability in critical path in the project network. Lin, etal [18],proposed the Critical path method in activity networks with Fuzzy activities duration times. In the project network membership grade project could be completed within the stipulated time was proposed by Liang et al. [19] as well as an algorithm to study critical path in a fuzzy environment. Tian et al. [27] delivered a method to find fuzzy critical path using probability theory and fuzzy-timing high level Petri nets. This way resource arrangement, time management and conflicts in shared work processes. Chen [4] discussed critical path in the project network in fuzzy environment. In this each activity time as a fuzzy number and also adapting the Yager's method of ranking. This method based on the principle of extension and linear programming formulation. A simple approach is developed to identify fuzzy critical path problem using Linear Programming and fuzzy number ranking method was proposed by app Chen et al.[5]. A Novel technique for finding earliest and latest events time of the project network using Linear Programming and Zadeh's principle of extension proposed by Zareei et al.[34]. Finding a critical path in the project network using lexicographic ordering method to rank the a trapezoidal fuzzy number. Mean while each activity in a project network is represented by a trapezoidal fuzzy number. Elizabeth et al. [10] presented Novel ranking methods to classify the fuzzy critical path in the project network using fuzzy membership function. Samayan[25], discussed the importance of hexagonal fuzzy numbers in Fuzzy critical path method based on ranking methods. Rajendran,C[22] discussed the comparison of Critical Path Problem under Fuzzy Environment with predictable process. Now the decision-making is the method of discovered the best alternative in a set of feasible alternatives. In this, several criteria's are taken into account called as multi-criteria decision making (MCDM) problems. MCDM refers to ordering the set of alternatives under usually conflicting criteria. These problems usually effect the delicacy of the tilted data being present, which makes the decision-making procedure complex. So in this decision-making often happens in fuzzy environment because the available date is vague. Therefore, in this state one of best method MCDM(Multi criteria decision making) to prioritizing the set of alternatives under usually inconsistent criteria. Now one of the MCDM method named as TOPSIS (Technique for Order Preference by Similarity to Ideal Solution) is presented. Initially Hwang and Yoon[13] presented TOPSIS method. This method discussed about the concept of ideal alternative, which is the optimum level for all considered attributes. Furthermore, the negative ideal is the one of the worst attribute value. In fuzzy environment extended TOPSIS method was proposed by Chen [6]. Linguistic terms are used for alternative's rating, weights criterion. Vertex method is adopting to Find the distance between triangular fuzzy numbers.

Yong [31],discussed place selection location in linguistic environment based on TOPSIS method. The product dispersal in a competitive automobile market and product adoption process in fuzzy TOPSIS and Agent-based diffusion model for an automobile market was discussed by Kim et al.[16].Ashrafzadeh et al.[2] presented a method for selecting the warehouse location under uncertain data in two steps .First identify the criteria and experts supply linguistic ratings to the promising alternatives against the preferred criteria. Fuzzy TOPSIS is used for choosing the best alternatives. An extension to fuzzy TOPSIS using distances of the alternatives method proposed by Dymova et al.[9].Also discussed generalization of particular aggregation modes method, local criteria aggregation in TOPSIS. Finally discussed critical path in the project network. Zammori et al[35] focused on complex critical path problems.The main aim is to determine time, cost,risk by using Fuzzy logic. TOPSIS and finally attain critical path in a project network .Amiri [1] proposed an algorithm, To establish the fuzzy critical path in the project network based on fuzzy TOPSIS. Also consisting of time, cost, risk and quality criteria and using linguistic triangular fuzzy numbers

Interval-valued intuitionistic hesitant fuzzy Choquet integral based TOPSIS method for multi-criteria group decision making was presented by Joshi, Deepa, [15] . Zyoud, [36] discussed A bibliometric-based survey on AHP and TOPSIS techniques. Kumar etal., [17] presented. "TOPSIS method based on the connection number of set pair analysis under interval-valued intuitionistic fuzzy set environment. Dos Santos[8] presented the Performance assessment of green suppliers using entropy-TOPSIS-F. Dorfeshan.Y etal. [7]],discussed a new group TOPSIS-COPRAS methodology with Pythagorean fuzzy sets taking into consideration weights of experts for project critical path problem.

A dual hesitant fuzzy set (DHFS) has been comprehensive form of HFS(Hesitant fuzzy set) and disagree with the effects of uncertainty in the collected data. Tyagi [29] derived The correlation coefficient between two DHFS. The shortcoming the HFS and DHFS is crisp numbers between 0 and 1 are used to represent the membership degree and non-membership degree of an element to a particular set. In addition, in quantitative atmosphere the fuzzy set theoretic tools were discussed. Suppose the decision in qualitative atmosphere, In this situation better to choose fuzzy linguistic Zadeh[33] to get more apparent result by Wu[30]. On the other hand, fuzzy sets, and fuzzy linguistic draw near to have a few limitations [20]. Rodriguez et al [23] observed that the decision maker apprehensive, the process of decision making be vague in providing a particular linguistic term to express their observation based on their ability in the anxious region. For example , in a decision making problem with high degree of uncertainty the decision makers desire to use linguistic terms such as “medium and “high” , “very high” to state their observation. To overcome such limitations he designed the concepts of hesitant fuzzy linguistic term sets(HFLTS).Modify the relative linguistic expressions into HFLTS and introduced an envelope of HFLTS by Rodriguez et al., [24]. But, these envelops of HFLTS are again intervals and these envelops of HFLTS convey the loss of original information. To conquer this problem Yu .D[32]introduced the idea of HTFS, wherein the membership degrees of an element to a given set are expressed as triangular fuzzy number TFN. TFN have been working to differentiate unusual linguistic terms used by decision maker for weight of attributes and to the linguistic terms used for the rating of the obtainable alternatives based on the given set of attributes. Since the HTFS has the dominance on both the TFN and HFS, it will be the most appropriate tool to symbolize the semantic of linguistic terms used in many real life situations of decision making. Garg, [12]. An advanced study on the similarity measures of intuitionistic fuzzy sets based on the set pair analysis theory and their application in decision making presented by Garg[11]. Kakati, Pankaj, et al.[14] presented "Interval neutrosophic hesitant fuzzy Einstein Choquet integral operator for multicriteria decision making. a novel methodology for time planning of resource-constrained software projects with hesitant fuzzy durations: a case study has been presented by Basar, Ayfer [3]. Now in this section- 2 recalls the prelimeners of Hesitant fuzzy sets , Triangular Hesitant Fuzzy set. section- 3 discussed the new distance measure using Triangular Hesitant Fuzzy set(THFS) ,section- 4 discussed the new fuzzy TOPSIS using using Triangular Hesitant Fuzzy set(THFS). section- 5 discussed proposed method for the critical path selection.A numarical exemplar is has been furnished for the proposed method.

2.Preliminaries

This segment deals with basic definations of Hesitant fuzzy sets, Triangular Hesitant Fuzzy set(THFS)

2.1. Hesitant fuzzy sets(HFS)

For a indication set X, Torra [28] defined a hesistant fuzzy set H on x in terms of function $h(x)$ when applied to $x \in X$ returns a subset of $[0,1]$

$H = \{\langle x, h(x) : x \in X \rangle\}$, Where $h(x)$ is a set of some different values in $[0,1]$,representing the possible membership degree of the element $x \in X$ to H and termed as hesitant fuzzy element(HFE)

2.2. Triangular Hesitant Fuzzy set[32]

This section deals with the concept of Triangular Fuzzy Hesitant Fuzzy set(THFS). The member ship degrees of an elements is to a set are represented by several possible triangular fuzzy numbers.Basic definitions of triangular fuzzy set,triangular fuzzy number and Triangular Fuzzy Hesitant Fuzzy sets are discussed.

Definition 1[26]

If R be the set of real numbers , Define a fuzzy number γ on R is a triangular fuzzy number such that the membership function $\mu_\gamma : R \to [0,1]$ defined by

$$\mu_\gamma(x) = \begin{cases} \dfrac{x-\tilde{\gamma}^L}{\tilde{\gamma}^M-\tilde{\gamma}^L}, & x \in \left[\tilde{\gamma}^L, \tilde{\gamma}^M\right] \\ \dfrac{x-\tilde{\gamma}^U}{\tilde{\gamma}^M-\tilde{\gamma}^U}, & x \in \left[\tilde{\gamma}^M, \tilde{\gamma}^U\right] \\ 0 & \text{otherwise} \end{cases}$$

Where $\tilde{\gamma}^L \le \tilde{\gamma}^M \le \tilde{\gamma}^U$ and $\tilde{\gamma}^L, \tilde{\gamma}^U$ are minimum and maximum values of $\tilde{\gamma}$ respectively and $\tilde{\gamma}^M$ is the model value. The triangle fuzzy number is represented as $\left(\tilde{\gamma}^L, \tilde{\gamma}^M, \tilde{\gamma}^U\right)$

The set $\left\{x / \tilde{\gamma}^L < x < \tilde{\gamma}^U\right\}$ is the support of $\tilde{\gamma}$ .If $\gamma^L = \gamma^M = \gamma^R$ then $\tilde{\gamma}$ reduces to a crisp number

Consider the triangular fuzzy numbers $\tilde{\gamma}_1 = \left(\tilde{\gamma}_1^L, \tilde{\gamma}_1^M, \tilde{\gamma}_1^U\right)$ and $\tilde{\gamma}_2 = \left(\tilde{\gamma}_2^L, \tilde{\gamma}_2^M, \tilde{\gamma}_2^U\right)$ *then*

$$\tilde{\gamma}_1 \oplus \tilde{\gamma}_2 = \left(\tilde{\gamma}_1^L, \tilde{\gamma}_1^M, \tilde{\gamma}_1^U\right) \oplus \left(\tilde{\gamma}_2^L, \tilde{\gamma}_2^M, \tilde{\gamma}_2^U\right) = \left(\tilde{\gamma}_1^L + \tilde{\gamma}_2^L, \tilde{\gamma}_1^M + \tilde{\gamma}_2^M, \tilde{\gamma}_1^U + \tilde{\gamma}_2^U\right)$$

$$\tilde{\gamma}_1 \otimes \tilde{\gamma}_2 = \left(\tilde{\gamma}_1^L, \tilde{\gamma}_1^M, \tilde{\gamma}_1^U\right) \otimes \left(\tilde{\gamma}_2^L, \tilde{\gamma}_2^M, \tilde{\gamma}_2^U\right) = \left(\tilde{\gamma}_1^L \tilde{\gamma}_2^L, \tilde{\gamma}_1^M \tilde{\gamma}_2^M, \tilde{\gamma}_1^U \tilde{\gamma}_2^U\right)$$

$$\tilde{\gamma}_1 = \tilde{\gamma}_2 \Leftrightarrow \tilde{\gamma}_1^L = \tilde{\gamma}_2^L, \tilde{\gamma}_1^M = \tilde{\gamma}_2^M, \tilde{\gamma}_1^U = \tilde{\gamma}_2^U$$

$$\tilde{\gamma}_1 \le \tilde{\gamma}_2 \Leftrightarrow \tilde{\gamma}_1^L \le \tilde{\gamma}_2^L, \tilde{\gamma}_1^M \le \tilde{\gamma}_2^M, \tilde{\gamma}_1^U \le \tilde{\gamma}_2^U$$

$$\lambda \square\ \tilde{\gamma}_1 = (\lambda, \lambda, \lambda)\left(\tilde{\gamma}_1^L, \tilde{\gamma}_1^M, \tilde{\gamma}_1^U\right) = \left(\lambda\tilde{\gamma}_1^L, \lambda\tilde{\gamma}_1^M, \lambda\tilde{\gamma}_1^U\right), \lambda > 0, \lambda \in R$$

$$\tilde{\gamma}_1^{-1} = \left(\tilde{\gamma}_1^L, \tilde{\gamma}_1^M, \tilde{\gamma}_1^U\right)^{-1} = \left(\frac{1}{\tilde{\gamma}_1^U}, \frac{1}{\tilde{\gamma}_1^M}, \frac{1}{\tilde{\gamma}_1^L},\right)$$

Definition 2[26]

Consider the triangular fuzzy number $\tilde{\gamma} = \left(\tilde{\gamma}_1^L, \tilde{\gamma}_1^M, \tilde{\gamma}_1^U\right)$ then the centriod of centroid[1] [502]is $\varsigma(\tilde{\gamma}) = \dfrac{\tilde{\gamma}_1^L + 7\tilde{\gamma}_1^M + \tilde{\gamma}_1^U}{9}$. *Assume that the* $\tilde{\gamma} = \left(\tilde{\gamma}_1^L, \tilde{\gamma}_1^M, \tilde{\gamma}_1^U\right)$ and $\tilde{\gamma}_2 = \left(\tilde{\gamma}_2^L, \tilde{\gamma}_2^M, \tilde{\gamma}_2^U\right)$ are two *triangular fuzzy numbersthen.Ranking of triangular fuzzy number* $\varsigma(\tilde{\gamma}_1) > \varsigma(\tilde{\gamma}_2)$ then $\tilde{\gamma}_1 > \tilde{\gamma}_2$, $\varsigma(\tilde{\gamma}_1) < \varsigma(\tilde{\gamma}_2)$ then $\tilde{\gamma}_1 < \tilde{\gamma}_2$, $\varsigma(\tilde{\gamma}_1) = \varsigma(\tilde{\gamma}_2)$ then $\tilde{\gamma}_1 = \tilde{\gamma}_2$. In such case, define the index associated with the ranking as $I_{\alpha,\beta}(\tilde{\gamma}) = \beta S_M(\tilde{\gamma}) + (1-\beta) I_\alpha(\tilde{\gamma})$ where $\beta \in [0,1]$. $S_M(\tilde{\gamma})$ is the mode associated with the fuzzy number which is equal to '$\tilde{\gamma}_1^M$' for a triangular fuzzy number $\tilde{\gamma} = \left(\tilde{\gamma}_1^L, \tilde{\gamma}_1^M, \tilde{\gamma}_1^U\right)$ and the average value of the area of stability for a triangular fuzzy number and we define the index associated with the ranking as

$I_{\alpha}\left(\tilde{\gamma}\right)=\alpha+\left(1-\alpha\right)\left(\frac{\tilde{\gamma}_1^L+7\tilde{\gamma}_1^M+\tilde{\gamma}_1^U}{9}\right)$ where $\alpha\in\left[0,1\right]$ is the index of optimism which represents the degree of optimism of a decision maker. The ranking is defined as

If $I_{\alpha,\beta}\left(\tilde{\gamma}_i\right)>I_{\alpha,\beta}\left(\tilde{\gamma}_j\right)\Rightarrow\tilde{\gamma}_i>\tilde{\gamma}_j$

If $I_{\alpha,\beta}\left(\tilde{\gamma}_i\right)<I_{\alpha,\beta}\left(\tilde{\gamma}_j\right)\Rightarrow\tilde{\gamma}_i<\tilde{\gamma}_j$

Definition 3[32].*Assume that the* X be a fixed set ,a Triangle fuzzy Hesitant Fuzzy set (THFS) $\tilde{F}$ *on* X *is a function* $\tilde{g}_E\left(x\right)$ *that takings several triangular fuzzy values represented as*

$$\tilde{F}=\left\{<x,\tilde{g}_{\tilde{F}}\left(x\right)>/x\in X\right\}$$

Here $\tilde{g}_{\tilde{F}}\left(x\right)$ contains numeroustriangular fuzzy number, the possible membership degrees of the elements $x\in X$. $\tilde{g}_{\tilde{F}}\left(x\right)$ is a Triangle fuzzy Hesitant Fuzzy set (THFS) and

$\tilde{g}_{\tilde{F}}\left(x_i\right)=\left\{\left(\tilde{\gamma}_1^L,\tilde{\gamma}_1^M,\tilde{\gamma}_1^U\right)/\tilde{\gamma}\in\tilde{g}_{\tilde{F}}\left(x_i\right)\right\}$ here $\tilde{\gamma}$ is the triangular fuzzy number. $\tilde{\gamma}^L,\tilde{\gamma}^U$ are minimum and maximum values of $\tilde{\gamma}$ respectively and $\tilde{\gamma}^M$ is the model value.

Triangular fuzzy hesistant fuzzy set is a very useful tool to express uncertainty .Let us consider the following case.

Case1: Three reviewers are decided to estimate the degrees that the members acceptability the criterionof honest.First time they had met each other and then evealuate under veage condition .The first reviewer believes the minimum possible of the members satisfies the criterion of honest is 0.1,the maximum possible is 0.5 and most possible is 0.3.Therefore evaluation about the candidate given by the first reviewer could be expressed by the triangular fuzzy number $\left(0.1,0.3,0.5\right)$.Similarly thr second reviewer and the third reviewer estimate and uttered by Triangular fuzzy number $\left(0.5,0.7,0.9\right)$ and $\left(0.4,0.9,1.0\right)$ respectively. If three reviewers have equal impact on this evaluation ,they can't be convinced by each other.In this case the complete evaluation about the members on honest can be expressed by a THFE $\left\{\left(0.1,0.3,0.5\right),\left(0.5,0.7,0.9\right),\left(0.4,0.9,1.0\right)\right\}$

Example- 1 . *Consider* $X=\left\{x_1,x_2\right\}$ *be a finite set,* $\tilde{g}_{\tilde{F}}\left(x_1\right)=\left\{\left(0.1,0.2,0.4\right)\left(0.2,0.5,0.6\right)\right\}$ and

$\tilde{g}_{\tilde{F}}\left(x_2\right)=\left\{\left(0.1,0.3,0.5\right)\left(0.4,0.6,0.8\right)\left(0.5,0.6,0.9\right)\right\}$ be the TFHFS of x_1,x_2 to the set $\tilde{F}$ and

$$\tilde{F}=\left\{<x_1,\left\{\left(0.1,0.2,0.4\right)\left(0.2,0.5,0.6\right)\right\}>,<x_2,\left\{\left(0.1,0.3,0.5\right)\left(0.4,0.6,0.8\right)\left(0.5,0.6,0.9\right)\right\}>\right\}$$

Definition 4[32]

Consider Triangular Hesitant Fuzzy sets(THFS), the sum of the HFS is presented as follows

$$\tilde{F}=\left\{\begin{array}{l}<x_1,\left\{\left(\delta_{11}^{L^1},\delta_{12}^{M^1},\delta_{13}^{U^1}\right)\left(\delta_{11}^{L^2},\delta_{12}^{M^2},\delta_{13}^{U^2}\right).....\left(\delta_{11}^{L^p},\delta_{12}^{M^p},\delta_{13}^{U^p}\right)\right\}>,\\<x_2,\left\{\left(\delta_{21}^{L^1},\delta_{22}^{M^1},\delta_{23}^{U^1}\right)\left(\delta_{21}^{L^2},\delta_{22}^{M^2},\delta_{23}^{U^2}\right).....\left(\delta_{21}^{L^q},\delta_{22}^{M^q},\delta_{23}^{U^q}\right)\right\}>,\\...\\<x_n,\left\{\left(\delta_{n1}^{L^1},\delta_{n2}^{M^1},\delta_{n3}^{U^1}\right)\left(\delta_{n1}^{L^2},\delta_{n2}^{M^2},\delta_{n3}^{U^2}\right).....\left(\delta_{n1}^{L^r},\delta_{n2}^{M^r},\delta_{n3}^{U^r}\right)\right\}\end{array}\right\}$$

Where $\tilde{g}_{\tilde{F}}(x_i)=\left\{\left(\delta_{i1}^{L^1},\delta_{i2}^{M^1},\delta_{i3}^{U^1}\right)\left(\delta_{i1}^{L^2},\delta_{i2}^{M^2},\delta_{i3}^{U^2}\right).....\left(\delta_{i1}^{L^\rho},\delta_{i2}^{M^\rho},\delta_{i3}^{U^\rho}\right)/\, i=1,2,3....,\rho\right\}$

$$\tilde{g}_{\tilde{F}}(x_i)=\left\{\min\left(\delta_{i1}^{L^1},\delta_{i1}^{L^2},...,\delta_{i1}^{L^\rho}\right),\text{mean}\left(\delta_{i2}^{M^1},\delta_{i2}^{M^2},...,\delta_{i2}^{M^\rho}\right),\max\left(\delta_{i3}^{U^1},\delta_{i3}^{U^2},...,\delta_{i3}^{U^\rho}\right)/\, i=1,2,3....,\rho\right\}$$

$$\tilde{g}_{\tilde{F}}(x_i)=\left\{\left(\nu_i^L,\nu_i^M,\nu_i^U\right)/\, i=1,2,3....,\rho\right\}\quad \text{Where}$$

$$\nu_i^L=\min\left(\delta_{i2}^{M^1},\delta_{i2}^{M^2},...,\delta_{i2}^{M^\rho}\right),\nu_i^M=\text{mean}\left(\delta_{i2}^{M^1},\delta_{i2}^{M^2},...,\delta_{i2}^{M^\rho}\right),\nu_i^U=\max\left(\delta_{i3}^{U^1},\delta_{i3}^{U^2},...,\delta_{i3}^{U^\rho}\right)$$

Suppose that $\tilde{g}_{\tilde{F}}(x_i),\tilde{g}_{\tilde{F}}(x_j)$ *are HFS in* $\tilde{F}$ *then*

$$\tilde{g}_{\tilde{F}}(x_i)\oplus\tilde{g}_{\tilde{F}}(x_j)=\left\{\left\{\left(\nu_i^L,\nu_i^M,\nu_i^U\right)/\, i=1,2,3....,\rho\right\}\right\}\oplus\left\{\left(\nu_j^L,\nu_j^M,\nu_j^U\right)/=1,2,3....,\rho'\right\}$$

$$\tilde{g}_{\tilde{F}}(x_i)\oplus\tilde{g}_{\tilde{F}}(x_j)=\left\{\left(\min\left\{\nu_i^L,\nu_j^L\right\},\text{mean}\left(\nu_i^M,\nu_j^M\right),\max\left\{\nu_i^U,\nu_j^U\right\}\right)\right\}$$

$$\tilde{g}_{\tilde{F}}(x_i)\oplus\tilde{g}_{\tilde{F}}(x_j)=\left\{\left(\Delta_1^L,\Delta_2^M,\Delta_3^U\right)\right\}\ \tilde{g}_1\otimes\tilde{g}_2=\left\{\left(\tilde{\gamma}_1^L\cdot\tilde{\gamma}_2^L,\tilde{\gamma}_1^M\cdot\tilde{\gamma}_2^M,\tilde{\gamma}_1^U.\tilde{\gamma}_2^U\right)/\,\tilde{\gamma}_1\in\tilde{g}_1,\tilde{\gamma}_2\in\tilde{g}_2\right\}$$

Also,

$$\tilde{g}^\lambda=\left\{\left(\left(\tilde{\gamma}_1^L\right)^\lambda,\left(\tilde{\gamma}_1^M\right)^\lambda\cdot\left(\tilde{\gamma}_1^U\right)^\lambda\right)/\,\tilde{\gamma}_1\in\tilde{g}\right\}$$

$$\lambda\tilde{g}=\left\{\left(1-\left(1-\tilde{\gamma}^L\right)^\lambda,1-\left(1-\tilde{\gamma}^M\right)^\lambda,1-\left(1-\tilde{\gamma}^U\right)^\lambda\right)/\,\tilde{\gamma}\in\tilde{g}\right\},\lambda>0$$

3.New Distance measure using Triangular Hesitant Fuzzy set(THFS)

In this segment a Novel distance measure with sutable illustration is introduced using THFS. *Consider a* Triangular Hesitant Fuzzy set and add by using following process, finally found the new distance measure with the assist of centroid of centroid point of Triangular fuzzy number.Now consider THFS

$$\tilde{F}=\begin{Bmatrix}<x_1,\left\{\left(\delta_{11}^{L^1},\delta_{12}^{M^1},\delta_{13}^{U^1}\right)\left(\delta_{11}^{L^2},\delta_{12}^{M^2},\delta_{13}^{U^2}\right).....\left(\delta_{11}^{L^p},\delta_{12}^{M^p},\delta_{13}^{U^p}\right)\right\}>,\\ <x_2,\left\{\left(\delta_{21}^{L^1},\delta_{22}^{M^1},\delta_{23}^{U^1}\right)\left(\delta_{21}^{L^2},\delta_{22}^{M^2},\delta_{23}^{U^2}\right).....\left(\delta_{21}^{L^q},\delta_{22}^{M^q},\delta_{23}^{U^q}\right)\right\}>,\\ ...\\ <x_n,\left\{\left(\delta_{n1}^{L^1},\delta_{n2}^{M^1},\delta_{n3}^{U^1}\right)\left(\delta_{n1}^{L^2},\delta_{n2}^{M^2},\delta_{n3}^{U^2}\right).....\left(\delta_{n1}^{L^r},\delta_{n2}^{M^r},\delta_{n3}^{U^r}\right)\right\}\end{Bmatrix}$$

Where $\tilde{g}_{\tilde{F}}(x_i)=\left\{\left(\delta_{i1}^{L^1},\delta_{i2}^{M^1},\delta_{i3}^{U^1}\right)\left(\delta_{i1}^{L^2},\delta_{i2}^{M^2},\delta_{i3}^{U^2}\right).....\left(\delta_{i1}^{L^\rho},\delta_{i2}^{M^\rho},\delta_{i3}^{U^\rho}\right)/\, i=1,2,3....,\rho\right\}$

$$\tilde{g}_{\tilde{F}}(x_i)=\left\{\min\left(\delta_{i1}^{L^1},\delta_{i1}^{L^2},...,\delta_{i1}^{L^\rho}\right),\text{mean}\left(\delta_{i2}^{M^1},\delta_{i2}^{M^2},...,\delta_{i2}^{M^\rho}\right),\max\left(\delta_{i3}^{U^1},\delta_{i3}^{U^2},...,\delta_{i3}^{U^\rho}\right)/\, i=1,2,3....,\rho\right\}$$

$$\tilde{g}_{\tilde{F}}(x_i)=\left\{\left(\nu_i^L,\nu_i^M,\nu_i^U\right)/\, i=1,2,3....,\rho\right\}\quad \text{Where}$$

$$\nu_i^L=\text{mean}\left(\delta_{i2}^{M^1},\delta_{i2}^{M^2},...,\delta_{i2}^{M^\rho}\right),\nu_i^M=\text{mean}\left(\delta_{i2}^{M^1},\delta_{i2}^{M^2},...,\delta_{i2}^{M^\rho}\right),\nu_i^U=\max\left(\delta_{i3}^{U^1},\delta_{i3}^{U^2},...,\delta_{i3}^{U^\rho}\right)$$

$$\tilde{g}_{\tilde{F}}(x_i)\oplus\tilde{g}_{\tilde{F}}(x_j)=\left\{\left\{\left(\nu_i^L,\nu_i^M,\nu_i^U\right)/\, i=1,2,3....,\rho\right\}\right\}\oplus\left\{\left(\nu_j^L,\nu_j^M,\nu_j^U\right)/=1,2,3....,\rho'\right\}$$

$$\tilde{g}_{\tilde{F}}(x_i)\oplus\tilde{g}_{\tilde{F}}(x_j)=\left\{\left(\min\left\{\nu_i^L,\nu_j^L\right\},\text{mean}\left(\nu_i^M,\nu_j^M\right),\max\left\{\nu_i^U,\nu_j^U\right\}\right)\right\}$$

$$\tilde{g}_{\tilde{F}}(x_i)\oplus\tilde{g}_{\tilde{F}}(x_j)=\left\{\left(\Delta_1^L,\Delta_2^M,\Delta_3^U\right)\right\}\quad ...\quad (1)$$

Where $\Delta_1^L = \min\left\{\nu_i^L, \nu_j^L\right\}$, $\Delta_3^U = \max\left\{\nu_i^U, \nu_j^U\right\}$, $\Delta_2^M = \text{mean}\left\{\nu_i^M, \nu_j^M\right\}$, $A = \left\{\left(\Delta_1^L, \Delta_2^M, \Delta_3^U\right)\right\}$ *the centroid of centroids points* $A = \left(\Delta_1^L, \Delta_2^M, \Delta_3^U\right)$ and $\in_{\tilde{A}} = \left(\frac{\Delta_1^{L^1} + 7\Delta_2^{M^1} + \Delta_3^{U^1}}{9}\right)$ *and left and right speards* $\in_{\tilde{A}} - \Delta_1^L, \Delta_3^U - \in_{\tilde{A}},$

The Distance measure using Triangular Hesitant Fuzzy set is

$$d\left(\tilde{g}_{\tilde{F}}(x_i), \tilde{g}_{\tilde{F}}(x_j)\right) = \max\left\{\left|\in_{\tilde{A}} - \Delta_1^L\right|, \left|\Delta_3^U - \in_{\tilde{A}}\right|\right\} \quad \ldots \quad (2)$$

Example- 2

Consider $X = \left\{x_1, x_2\right\}$ *be a finite set,* $\tilde{g}_{\tilde{F}}(x_1) = \left\{(0.1, 0.2, 0.4)(0.2, 0.5, 0.6)\right\}$ and

$\tilde{g}_{\tilde{F}}(x_2) = \left\{(0.1, 0.3, 0.5)(0.4, 0.6, 0.8)(0.5, 0.6, 0.9)\right\}$ be the THFS of x_1, x_2 to the set $\tilde{F}$ and

$$\tilde{F} = \left\{< x_1, \left\{(0.1, 0.2, 0.4)(0.2, 0.5, 0.6)\right\} >, < x_2, \left\{(0.1, 0.3, 0.5)(0.4, 0.6, 0.8)(0.5, 0.6, 0.9)\right\} >\right\}$$

$$\tilde{g}_{\tilde{F}}(x_1) = \left\{\left(\min(0.1, 0.2), \left(\frac{0.2 + 0.5}{2}\right), \max(0.4, 0.6)\right)\right\}$$

$$\tilde{g}_{\tilde{F}}(x_1) = \left\{(0.1, 0.35, 0.6)\right\}$$

$$\tilde{g}_{\tilde{F}}(x_2) = \left\{(0.1, 0.3, 0.5)(0.4, 0.6, 0.8)(0.5, 0.6, 0.9)\right\}$$

$$\tilde{g}_{\tilde{F}}(x_2) = \left\{\left(\min(0.1, 0.4, 0.5), \left(\frac{0.3 + 0.6 + 0.6}{3}\right), \max(0.5, 0.8, 0.9)\right)\right\}$$

$$\tilde{g}_{\tilde{F}}(x_2) = \left\{(0.1, 0.5, 0.9)\right\}$$

$$\tilde{g}_{\tilde{F}}(x_i) \oplus \tilde{g}_{\tilde{F}}(x_j) = \left\{\left(\min\left\{0.1, 0.1\right\}, 0.425, \max\left\{0.6, 0.9\right\}\right)\right\}$$

$$\tilde{g}_{\tilde{F}}(x_i) \oplus \tilde{g}_{\tilde{F}}(x_j) = \left\{(0.1, 0.425, 0.9)\right\}$$

$$\in_{\tilde{A}} = \frac{0.1 + 7(0.425) + 0.9}{9} = 0.442$$

$$d\left(\tilde{g}_{\tilde{F}}(x_i), \tilde{g}_{\tilde{F}}(x_j)\right) = \max\left\{\left|0.442 - 0.1\right|, \left|0.9 - 0.442\right|\right\} = \max\left\{0.342, 0.458\right\} = 0.458$$

4.*New Fuzzy TOPSIS using*Triangular Hesitant Fuzzy set(THFS)

The process of finding the best alternative in a set of feasible alternatives is called as decision-making. In this, the problems which are taken into account from several criteria are named as multi-criteria decision making (MCDM) problems. MCDM refers to prioritizing the set of alternatives under usually inconsistent criteria. These problems usually effect the preciseness of the skewed data being present, which makes the decision-making process complex. In other words, decision-making frequently happens in a fuzzy environment where the available information is uncertain. So, in such situations, one of the well known MCDM method is presented named as TOPSIS (Technique for Order Preference by Similarity to Ideal Solution). TOPSIS method was first presented by Hwang and Yoon[37]. This method depends on the concept of ideal alternative, which is the finest level for all considered attributes. A new TOPSIS Method is introduced on THFS.In this, the activity times are taken as THFS.The procedure of this method is presented as follows

Step-1

In this the feasible alternative are to be generated. Suppose that the number of alternatives and evaluation criteria are m, n *respectivelythen the* Decision matrix using THFS is

$$D = \begin{bmatrix} y_{11} & y_{12} & \cdots & y_{1n} \\ y_{21} & y_{22} & \cdots & y_{2n} \\ \cdots & \cdots & \cdots & \cdots \\ y_{m1} & y_{m2} & \cdots & y_{mn} \end{bmatrix}_{m\times n} \quad \textit{where}$$

$$y_{11} =< x_{11}, \left\{ \left(\delta_{11}^{L^1}, \delta_{11}^{M^1}, \delta_{11}^{U^1}\right)\left(\delta_{11}^{L^2}, \delta_{11}^{M^2}, \delta_{11}^{U^2}\right).....\left(\delta_{11}^{L^p}, \delta_{11}^{M^p}, \delta_{11}^{U^p}\right)\right\} >$$

$$y_{12} =< x_{12}, \left\{ \left(\delta_{12}^{L^1}, \delta_{12}^{M^1}, \delta_{12}^{U^1}\right)\left(\delta_{12}^{L^2}, \delta_{12}^{M^2}, \delta_{12}^{U^2}\right).....\left(\delta_{12}^{L^p}, \delta_{12}^{M^p}, \delta_{12}^{U^p}\right)\right\} > \ldots$$

$$y_{1n} =< x_{1n}, \left\{ \left(\delta_{1n}^{L^1}, \delta_{1n}^{M^1}, \delta_{1n}^{U^1}\right)\left(\delta_{1n}^{L^2}, \delta_{1n}^{M^2}, \delta_{1n}^{U^2}\right).....\left(\delta_{1n}^{L^p}, \delta_{1n}^{M^p}, \delta_{1n}^{U^p}\right)\right\} >$$

$$y_{m1} =< x_{m1}, \left\{ \left(\delta_{m1}^{L^1}, \delta_{m1}^{M^1}, \delta_{m1}^{U^1}\right)\left(\delta_{m1}^{L^2}, \delta_{m1}^{M^2}, \delta_{m1}^{U^2}\right).....\left(\delta_{m1}^{L^p}, \delta_{m1}^{M^p}, \delta_{m1}^{U^p}\right)\right\} >$$

$$y_{m2} =< x_{m2}, \left\{ \left(\delta_{m2}^{L^1}, \delta_{m2}^{M^1}, \delta_{m2}^{U^1}\right)\left(\delta_{m2}^{L^2}, \delta_{m2}^{M^2}, \delta_{m2}^{U^2}\right).....\left(\delta_{m2}^{L^p}, \delta_{m2}^{M^p}, \delta_{m2}^{U^p}\right)\right\} >$$

$$\ldots y_{mn} =< x_{mn}, \left\{ \left(\delta_{mn}^{L^1}, \delta_{mn}^{M^1}, \delta_{mn}^{U^1}\right)\left(\delta_{mn}^{L^2}, \delta_{mn}^{M^2}, \delta_{mn}^{U^2}\right).....\left(\delta_{mn}^{L^p}, \delta_{mn}^{M^p}, \delta_{mn}^{U^p}\right)\right\}$$

$$y_{ij} = \left(\min\left(\delta_{ij}^{L^1}, \delta_{ij}^{L^2} \ldots \delta_{ij}^{L^p}\right) = \varepsilon_{ij}^{L}, \varepsilon_{ij}^{M} = \text{mean}\left(\delta_{i2}^{M^1}, \delta_{i2}^{M^2}, ..., \delta_{i2}^{M^p}\right), \max\left(\delta_{ij}^{U^1}, \delta_{ij}^{U^2}, ..., \delta_{ij}^{U^p}\right) = \varepsilon_{ij}^{U}\right)$$

$$y_{ij} = \left\{\left(\varepsilon_{ij}^{L}, \varepsilon_{ij}^{M}, \varepsilon_{ij}^{U}\right)\right\} \quad i = 1, 2..., m, \; j = 1, 2..., n \quad \ldots \quad (3)$$

Step-2

It is clear that the alternatives are rated for dissimilarAttributesof dissimilar dimensions. To keep the rating y_{ij} ofeach alternative on a normalized scale, the procedure of

normalization is applied. The normalized matrix *N* can be obtainedas follows

$$N = \left[N_{ij} \right]_{m\times n} \ldots \quad (4)$$

where $N_{ij} = \left(\frac{\varepsilon_{ij}^{L}}{\rho}, \frac{\varepsilon_{ij}^{M}}{\rho}, \frac{\varepsilon_{ij}^{U}}{\rho} \right)$ where $\rho = \max\left\{\varepsilon_{11}^{U}, \varepsilon_{12}^{U}, ..., \varepsilon_{mn}^{U}\right\}, i, j = 1, 2, ..., n.$ The process of normalization which is presented above normalized THFS be supposed to

variety in the period [0, 1] is well preserved.:

Step-3

It has been observed that calculation withTHFS for a MCDM problem having large number of alternatives and attributes may result in computational monotony. To avoidthis computational complexity, in this process of decision making,first a weighted normalized matrix its entries will be obtained, by using the following equation

$$V = N \otimes w$$

*The Weighted Normalized*Decision matrix using THFS is as follows.

$$w=\left\{\begin{array}{l}
<x_{11},\left\{\left(w_{11}^{L^1},w_{11}^{M^1},w_{11}^{U^1}\right)\left(w_{11}^{L^2},w_{11}^{M^2},w_{11}^{U^2}\right).....\left(w_{11}^{L^p},w_{11}^{M^p},w_{11}^{U^p}\right)\right\}>,\\
<x_{12},\left\{\left(w_{12}^{L^1},w_{12}^{M^1},w_{12}^{U^1}\right)\left(w_{12}^{L^2},w_{12}^{M^2},w_{12}^{U^2}\right).....\left(w_{12}^{L^p},w_{12}^{M^p},w_{12}^{U^p}\right)\right\},...,\\
<x_{1n},\left\{\left(w_{1n}^{L^1},w_{1n}^{M^1}w_{1n}^{U^1}\right)\left(w_{1n}^{L^2},w_{1n}^{M^2},w_{1n}^{U^2}\right).....\left(w_{1n}^{L^p},w_{1n}^{M^p},w_{1n}^{U^p}\right)\right\}\\
\\
<x_{21},\left\{\left(w_{21}^{L^1},w_{21}^{M^1},w_{21}^{U^1}\right)\left(w_{21}^{L^2},w_{21}^{M^2},w_{21}^{U^2}\right).....\left(w_{21}^{L^p},w_{21}^{M^p},w_{21}^{U^p}\right)\right\},\\
<x_{22},\left\{\left(w_{22}^{L^1},w_{22}^{M^1},w_{22}^{U^1}\right)\left(w_{22}^{L^2},w_{22}^{M^2},w_{22}^{U^2}\right).....\left(w_{22}^{L^p},w_{22}^{M^p},w_{21}^{U^p}\right)\right\},...,\\
<x_{2n},\left\{\left(w_{2n}^{L^1},w_{2n}^{M^1},w_{2n}^{U^1}\right)\left(w_{2n}^{L^2},w_{2n}^{M^2},w_{2n}^{U^2}\right).....\left(w_{2n}^{L^p},w_{2n}^{M^p}w_{2n}^{U^p}\right)\right\}\\
...\\
<x_{m1},\left\{\left(w_{m1}^{L^1},w_{m1}^{M^1},w_{m1}^{U^1}\right)\left(w_{m1}^{L^2},w_{m1}^{M^2},w_{m1}^{U^2}\right).....\left(w_{m1}^{L^p},w_{m1}^{M^p},w_{m1}^{U^p}\right)\right\},\\
<x_{m2},\left\{\left(w_{m2}^{L^1},w_{m2}^{M^1},w_{m2}^{U^1}\right)\left(w_{m2}^{L^2},w_{m2}^{M^2},w_{m2}^{U^2}\right).....\left(w_{m2}^{L^p},w_{m2}^{M^p},w_{m2}^{U^p}\right)\right\},...,\\
<x_{mn},\left\{\left(w_{mn}^{L^1},w_{mn}^{M^1},w_{mn}^{U^1}\right)\left(w_{mn}^{L^2},w_{mn}^{M^2},w_{mn}^{U^2}\right).....\left(w_{mn}^{L^p},w_{mn}^{M^p},w_{mn}^{U^p}\right)\right\}
\end{array}\right\}$$

$$w=\begin{bmatrix} w_{11} & w_{12} & ... & w_{1n} \\ w_{21} & w_{22} & ... & w_{2n} \\ ... & ... & ... & ... \\ w_{m1} & w_{m2} & ... & w_{mn} \end{bmatrix}$$

where

$$w_{ij}=\left\{\left(\min\left(w_{ij}^{L^1},w_{ij}^{L^2}...w_{ij}^{L^p}\right)=w_{ij}^{L},w_{ij}^{M}=\text{mean}\left(w_{i2}^{M^1},w_{i2}^{M^2},...,w_{i2}^{M^p}\right),\max\left(w_{ij}^{U^1},w_{ij}^{U^2},...,w_{ij}^{U^p}\right)=w_{ij}^{U}\right)\right\}$$

$$w_{ij}=\left(w_{ij}^{L},w_{ij}^{M},w_{ij}^{U}\right) \quad \ldots \quad (5)$$

Step-4: Determine Fuzzy Positive and Negative Ideal solutions

According to the weighted normalized fuzzy decision matrix, normalized positive trapezoidal fuzzy number can be approximate by the elements $\tilde{v}_{ij}$. Then, the FPIS (Fuzzy Positive Ideal Solution) A^{+} FNIS (Fuzzy Negative Ideal Solution) A^{-} can be *defined as;*

$$A^{+}=\left\{\left(v_{ij1}^{+},v_{ij2}^{+},v_{ij3}^{+}\right)\right\}\ A^{-}=\left\{\left(v_{ij1}^{-},v_{ij2}^{-},v_{ij3}^{-}\right)\right\} \quad \ldots \quad (6)$$

Where $v_3^{+}=\max_i v_{ij3}$ and $v_1^{-}=\min_i v_{ij1}$ $i=1,2,....m,\ j=1,2,....n$. In the index, v_{ij1} and v_{ij3} are the first and third numbers in theTriangular Hesitant Fuzzy set, respectively.

Step-5: Distance of each alternative from Fuzzy positive Ideal solution and Fuzzy negative Ideal solutions using Triangular Hesitant Fuzzy set

The Distance measure using Triangular Hesitant Fuzzy set is

$$d\left(\tilde{g}_{\tilde{F}}\left(x_i\right),\tilde{g}_{\tilde{F}}\left(x_j\right)\right)=\max\left\{\left|\in_{\tilde{A}}-\Delta_1^L\right|,\left|\Delta_3^U-\in_{\tilde{A}}\right|\right\} \quad \ldots \quad (7)$$

Step-6

The closeness coefficient of each alternative is denoted by cc_i and isdefined as;

$$cc_i=\frac{d_i^-}{d_i^+ + d_i^-} \quad \ldots \quad (8)$$

Step-7: Best Alternative

*According to the*coefficient cc_i value, the larger closeness coefficient has a higher level ranking order. So the best alternative has the maximum closeness coefficient cc_i .

5. Proposed method for the critical path selection

A very methodical approach is put forth in this segment to deal with the critical path selection problem under a fuzzy environment. The importance weights of various criteria and the ratings of qualitative criteria are contemplated as Hesitant fuzzy sets in this paper. The times of each activity can be expressed in a Triangular Fuzzy Hesitant Fuzzy Set. The detailing of the proposed method is given hereunder.

A large project can be broken into several fragment which are called activities, determining the durations and precedence of these activities. The relationship of precedence among these activities is visualized in a network representation of the project so as to draw the precedence project network the arcs of which express the activities alongside determining all benchmarks which are important to choose a critical path under these criteria. A path intersecting a project network is one of the routes from the starting node to the ending node. Therefore, in this step, it is important to indicate all paths that start with the starting event and end with the ending event. These are our alternatives from which we need to choose one as a critical path. Also pick the most suitable Triangular Fuzzy Hesitant Fuzzy Set for quantitative criteria. The length of a path is the sum of spans of activities on the path. Hence add up the Triangular Fuzzy Hesitant Fuzzy Set to ascertain the value of the final evaluation of each criterion for paths. The duration of the project equals the length of the longest path in the network and a project is considered complete if the work along all paths is complete. Thus build up the fuzzy decision matrix in which all the alternatives are the paths which start with the starting event and end with the ending event. It is important to determine the critical path in the project network under different criterion in order to calculate the completion time of the project. Applying fuzzy TOPSIS method can be very handy with the ratings of both qualitative as well as quantitative criteria to designate a suitable alternative critical path under various criteria and the same is explained in section -5. The algorithm put forth to deal with the selection of critical path is summarized the following steps – draw the network of the precedence project (activity on arrows) – choose the befitting Triangular Fuzzy Hesitant Fuzzy set for the importance weight of the criteria – make a mention of all paths which start with the starting event and end with the ending event. Employ Triangular Fuzzy Hesitant Fuzzy Set to identify the fuzzy time under each criterion. Then sum up Triangular Fuzzy Hesitant Fuzzy Set to ascertain the value of the final evaluation of each criterion for paths – construct the fuzzy decision matrix in which all its alternatives are the parts that start with the starting event and end with the ending event. Then apply the fuzzy TOPSIS method that is proposed in Section 4. A numerical example is solved to exemplify the efficiency of the proposed method.

Numerical Example:

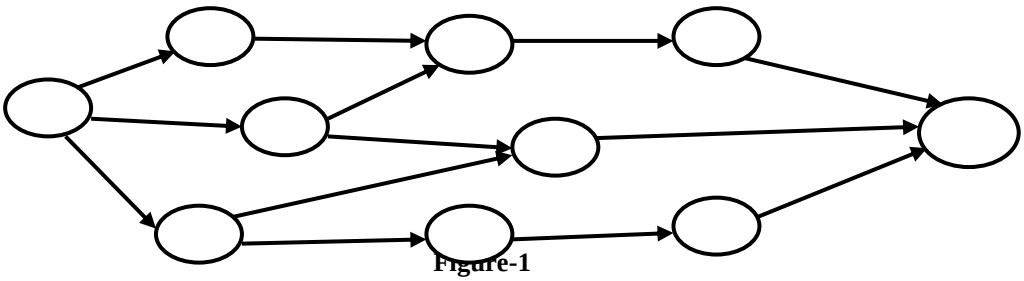


Figure-1

The proposed method is presently applied to solve the example the computational procedure of which is summarized hereunder;Draw the precedence project network as shown in the figure-1. The decision makers

estimate the time criteria of each activity of the project network in THFS which shows in table-1 as a decision matrix . Add up all activitie Times in each the path that start with the starting event and end with the ending event. The ratings of the activities by the decision makers under various criteria are described. So the normalized fuzzy decision matrix is built up as in table-3.Next the Weighed normalized fuzzy decision matrix is constructed as in table-4. Now collect the Triangle Hesitant Fuzzy set positive and negative ideal solution ideal solution . Then determine and FNIS so as to calculate the distance of each from Fuzzy positive ideal solution and Fuzzy negative ideal solution d- with respect to each criterion respectively as shown in tables 5 and 6. Calculate di+ and di – of the five possible paths and then calculate the closeness coefficient of each path as shown in table-6. As per the closeness coefficients of five paths, we get to know that the second path (1 – 3 – 6 – 10) is the critical path under the criteria of time. The problem is solved only with the time criterion.Further we can apply on cost ,risk and quality.

Decision Matrix

As per the times of each activity in the project network the following decision matrix is constructed and presented in the Table -1

(i,j)	***Activity times*** **(Triangular Hesitant Fuzzy set)**
$x_1 = (1,2)$	$< x_1, \{(0.1,0.3,0.4),(0.1,0.5,0.6)\} >$
$x_2 = (1,3)$	$< x_2, \{(0.1,0.4,0.5),(0.2,0.6,0.7),(0.8,0.9,0.9)\} >$
$x_3 = (1,4)$	$< x_3, \{(0.1,0.2,0.6),(0.2,0.6,0.7)\} >$
$x_4 = (2,5)$	$< x_4, \{(0.2,0.4,0.6)\} >$
$x_5 = (3,5)$	$< x_5, \{(0.1,0.7,0.9)\} >$
$x_6 = (4,6)$	$< x_6, \{(0.1,0.2,0.3),(0.4,0.5,0.6),(0.4,0.6,0.7)\} >$
$x_7 = (8,9)$	$< x_7, \{(0.2,0.3,0.3),(0.1,0.5,0.6)\} >$
$x_8 = (3,6)$	$< x_8, \{(0.2,0.2,0.4),(0.3,0.4,0.6)\} >$
$x_9 = (5,7)$	$< x_9, \{(0.1,0.3,0.4),(0.2,0.3,0.4)(0.5,0.6,0.9)\} >$
$x_{10} = (4,8)$	$< x_{10}, \{(0.6,0.7,0.75),(0.5,0.5,0.6),(0.3,0.5,0.7)\} >$
$x_{11} = (6,10)$	$< x_{11}, \{(0.7,0.8,0.8)\} >$
$x_{12} = (7,10)$	$< x_{12}, \{(0.4,0.5,0.6),(0.1,0.3,0.5)\} >$
$x_{13} = (9,10)$	$< x_{13}, \{(0.3,0.5,0.6),(0.3,0.4,0.6)\} >$

Table-1

Now, Add the times (which are in Triangular Hesitant Fuzzy set) *of each paths in the project network presented in Table -2*

Paths of the Network	***Activity times* (Triangular Hesitant Fuzzy set)**
$1-2-5-7-10$	$\{(0.1, 0.4, 0.9)\}$
$1-3-6-10$	$\{(0.1, 0.55, 0.9)\}$
$1-3-5-7-10$	$\{(0.1, 0.4625, 0.9)\}$
$1-4-6-10$	$\{(0.1, 0.51667, 0.9)\}$
$1-4-8-9-10$	$\{(0.1, 0.44375, 0.9)\}$

Table-2

Normalized decision Matrix

Applying step-2, to construct Normalized decision Matrix is presented in Table-3

Paths of the Network	***Normalized decision Matrix* (Triangular Hesitant Fuzzy set)**
$1-2-5-7-10$	$\{(0.111, 0.444, 1)\}$
$1-3-6-10$	$\{(0.111, 0.611, 1)\}$
$1-3-5-7-10$	$\{(0.111, 0.513, 1)\}$
$1-4-6-10$	$\{(0.111, 0.574, 0.88)\}$
$1-4-8-9-10$	$\{(0.1, 0.493, 0.833)\}$

Table-3

Weighted Normalized decision Matrix

Applying the procedure presented in step-3 to find the weighted normalized decision matrix

Paths of the Network	**(Triangular Hesitant Fuzzy set)**
$1-2-5-7-10$	$\{(0.111, 0.444, 0.99)\}$
$1-3-6-10$	$\{(0.11, 0.605, 1)\}$
$1-3-5-7-10$	$\{(0.111, 0.508, 0.99)\}$

$1-4-6-10$	$\{(0.111,0.568,0.88)\}$
$1-4-8-9-10$	$\{(0.1,0.488,0.825)\}$

Table-4

Fuzzy Positive Negative Ideal Solutions

Using Step-4,to identify Triangular Hesitant Fuzzy Set *Positive Negative Ideal Solutions presented in step-4* $A^- = \{(0.1,0.1,0.1)\}, A^+ = \{(1,1,1)\}$

Distance between Fuzzy Positive Ideal Solutions and

By means of step-5 to identify Distance between paths and A^+ with respect to each criterion presented in following table-5

Criteria Activity	**Time**
$d^+(A_1, A^+)$	0.61
$d^+(A_2, A^+)$	0.69
$d^+(A_3, A^+)$	0.64
$d^+(A_4, A^+)$	0.67
$d^+(A_5, A^+)$	0.63

Table-5

Distance between Fuzzy Negative Ideal Solutions and

By means of step-5 to identify distance between paths and A^- with respect to each criterion

Criteria Activity	**Time**
$d^-(A_1, A^-)$	0.17
$d^-(A_2, A^-)$	0.25
$d^-(A_3, A^-)$	0.20
$d^-(A_4, A^-)$	0.23
$d^-(A_5, A^-)$	0.19

Table-6

Closeness coefficient:

Using step-6 to caliculate the closeness cofficent of each alternative presented in the following .

Criteria Activity	d_i^+	d_i^-	$d_i^+ + d_i^-$	$cc_i = \frac{d_i^-}{d_i^- + d_i^+}$
1-2-5-7-10	0.61	0.17	0.78	0.217949
1-3-6-10	0.69	0.25	0.95	0.267196
1-3-5-7-10	0.64	0.20	0.85	0.240795
1-4-6-10	0.67	0.23	0.91	0.257798
1-4-8-9-10	0.63	0.19	0.83	0.23434

Table-7

Observe that the largest value of the closeness cofficent of each alternative gives the best path of ghe project network 1-3-6-10.

5.Conclusion:

In this paper TOPSIS method has been applied to fuzzy project network to determine the critical path using several criteria. Triangular Hesitant Fuzzy Set have been used as fuzzy activity times, to find critical path of the project network . A new Triangular Hesitant Fuzzy Set‘s distances measure has been proposed to select critical path in new TOPSIS method using Triangular Hesitant Fuzzy Set as activity times. A numerical example related to this problem has provided to explain the procedure of proposed TOPSIS method in determining critical path with different criteria.

References

1. Amiri, Maghsoud, and FarhanehGolozari. Application of fuzzy multi-attribute decision making in determining the critical path by using time, cost, risk, and quality criteria. The International Journal of Advanced Manufacturing Technology Vol.54, no. 1-4, 2011,pp. 393-401.
2. Ashrafzadeh, Maysam, FarimahMokhatabRafiei, NaserMollaverdiIsfahani, and Zahra Zare. Application of fuzzy TOPSIS method for the selection of warehouse location: A case study. Interdisciplinary Journal of Contemporary Research in Business 3, no. 9, 2012, pp. 655-671.
3. Basar, Ayfer. "a novel methodology for time planning of resource-constrained software projects with hesitant fuzzy durations: a case study." International Journal of Industrial Engineering 26.4 (2019).
4. Chen, Shih-Pin. Analysis of critical paths in a project network with fuzzy activity times. European Journal of Operational Research, Vol.183, no. 1 2007, pp.442-459.
5. Chen, Shih-Pin, and Yi-Ju Hsueh. A simple approach to fuzzy critical path analysis in project networks. Applied Mathematical Modeling, Vol.32, no. 7, 2008, pp.1289-1297.
6. Chen, C. T. Extension of the TOPSIS for group decision-making under fuzzy environment, Fuzzy Sets and Systems, Vol. 114, No. 1, 2000.
7. Dorfeshan, Y., and S. Meysam Mousavi. "A new group TOPSIS-COPRAS methodology with Pythagorean fuzzy sets considering weights of experts for project critical path problem." Journal of Intelligent & Fuzzy Systems Preprint (2019): 1-13.
8. Dos Santos, Bruno Miranda, LeoniPentiado Godoy, and Lucila MS Campos. "Performance evaluation of green suppliers using entropy-TOPSIS-F." Journal of cleaner production 207 (2019): 498-509.
9. Dymova, Ludmila, Pavel Sevastjanov, and Anna Tikhonenko. an approach to generalization of fuzzy TOPSIS method. Information Sciences Vol. 238, 2013, pp.149-162.
10. Elizabeth, S., and L. Sujatha. Fuzzy critical path problem for Project network. International Journal of Pure and Applied Mathematics Vol. 85, no. 2, 2013, pp.223-240.
11. Garg, Harish, and Kamal Kumar. "An advanced study on the similarity measures of intuitionistic fuzzy sets based on the set pair analysis theory and their application in decision making." Soft Computing 22.15 (2018): 4959-4970.

12. Garg, Harish, and Rishu Arora. "Distance and similarity measures for dual hesitant fuzzy soft sets and their applications in multicriteria decision making problem." International Journal for Uncertainty Quantification 7.3 (2017).
13. Hwang C. L. and Yoon K. Multiple Attribute Decision Making Methods and Applications, A State-of-the- Art Survey, Springer Verlag, New York. 1981,
14. Kakati, Pankaj, et al. "Interval neutrosophic hesitant fuzzy Einstein Choquet integral operator for multicriteria decision making." Artificial Intelligence Review (2019): 1-36.
15.]Joshi, Deepa, and Sanjay Kumar. "Interval-valued intuitionistic hesitant fuzzy Choquet integral based TOPSIS method for multi-criteria group decision making." European Journal of Operational Research 248.1 (2016): 183-191.
16. Kim, S., Lee, K., Cho, J. K. and Kim, C.O., Agent-based diffusion model for an automobile market with fuzzy TOPSIS- based product adoption process, Expert Systems with Applications, Vol. 38, no. 6, 2011, pp. 7270-7276.
17. Kumar, Kamal, and Harish Garg. "TOPSIS method based on the connection number of set pair analysis under interval-valued intuitionistic fuzzy set environment." Computational and Applied Mathematics 37.2 (2018): 1319-1329.
18. Lin, Feng-Tse. Critical path method in activity networks with Fuzzy activities duration times. In Systems, Man, and Cybernetics, IEEE International Conference on, Vol. 2, 2001,pp. 1155-1160.
19. Liang, Gin-Shuh, and Tzeu-Chen Han. Fuzzy critical path for project network. Information and Management Sciences , Vol.15, no. 4, 2004, pp.29-40.
20. Mendel J.M.,. Zadeh L.A, Yager R.R., J. Lawry, H. Hagras, and S.
21. Guadarrama, "What computing with words means to me," IEEE Comput.
22. Intell. Mag., vol. 5, no. 1, pp. 20–26, 2010.
23. Nasution, Sofjan H. Fuzzy critical path method. IEEE Transactions onSystems, Man, and Cybernetics, Vol. 24, no. 1, 1994, pp. 48-57.
24. Rajendran, C., and M. Ananthanarayanan. "Comparision of Critical Path Problem under Fuzzy Environment with Conventional Method." Journal of Computer and Mathematical Sciences 9.8 (2018): 969-976.
25. Rodrigues R. M., L. Martinez and F. Herrera, "Hesitant fuzzy linguistic term
26. sets for decision making," IEEE Trans. Fuzzy Systems, vol. 20, no. 1, pp.
27. 109-119, 2012.
28. Rodrigues R. M., L. Martinez and F. Herrera, "A group decision making
29. model dealing with comparative linguistic expressions based on hesitant fuzzy
30. linguistic term sets," Inf. Sci., vol 241, pp. 28-42, 2013.
31. Samayan, Narayanamoorthy, and MaheswariSengottaiyan. "Fuzzy critical path method based on ranking methods using hexagonal fuzzy numbers for decision making." Journal of Intelligent & Fuzzy Systems 32.1 , 2017,pp. 157-164.
32. Shankar, N. Ravi, B. PardhaSaradhi, and S. Suresh Babu. Fuzzy critical
33. path method based on a new approach of ranking fuzzy numbers using
34. centroid of centroids. International Journal of Fuzzy System Applications
35. (IJFSA) Vol.3, no. 2 ,2013,pp.16-31.
36. Tian, Feng, and Renhou Li. A fuzzy critical path method based scheduling approach for collaboration process. 10th International Conference on Computer Supported Cooperative Work in Design, IEEE, 2006, pp. 1-6.
37. Torra. V, "Hesitant fuzzy sets," Int. J. Intell. Syst., vol. 25, pp. 529–539,
38. Tyagi S. K, "Correlation coefficient of dual hesitant fuzzy sets and its
39. applications," Applied mathematical modelling, vol. 39, pp. 7082-7092,
40. 2015.
41. Wu .Dand J. M. Mendel, "Computing with words for hierarchical decision
42. making applied to evaluating a weapon system," IEEE Trans. Fuzzy Syst., vol.
43. 18, no. 3, pp. 441–460, 2010.
44. Yong, D. Plant location selection based on fuzzy TOPSIS, International Journal of Advanced Manufacturing Technologies, Vol. 28, no. 7-8,2006, pp. 323- 326.
45. Yu .D., "Triangular hesitant fuzzy set and its application to teaching quality

46. evaluation," Journal of Information & Computational Science, vol. 7, pp.
47. 1925-1934, 2013.
48. Zadeh L.A., "The concept of a linguistic variable and its applications to
49. approximate reasoning-Part III," Inf. Sci., vol 9, pp. 43-80, 1975.
50. mining. Berlin, Germany:Springer-Verlag, 2004.
51. Zareei, Abalfazl, FarzadZaerpour, MortezaBagherpour, Abbas Ali Noora, and AbdollahHadiVencheh. A new approach for solving fuzzy critical path problem using analysis of events. Expert Systems withApplications Vol.38, no.1 ,2011,pp. 87-93.
52. Zammori, Francesco A., Marcello Braglia, and Marco Frosolini. A fuzzymulti-criteria approach for critical path definition. International Journal of Project Management Vol. 27, no. 3, 2009,pp. 278-291.
53. Zyoud, Shaher H., and Daniela Fuchs-Hanusch. "A bibliometric-based survey on AHP and TOPSIS techniques." Expert systems with applications 78 (2017): 158-181.

Journal of Contemporary Issues in Business and Government Vol. 27, No. 2,2021
https://cibg.org.au/

P-ISSN: 2204-1990; E-ISSN: 1556-1571

DOI: 10.47750/cibg.2021.27.02.166

Legal Policies for Sustainable Security and Privacy in Big Data and Information sharing- *A managerial perspective*

K. Sowjanya Naidu
Department of Computer Science and Engineering, Dr. L. Bullayya College of Engg. (W), Visakhapatnam, India

Srinivasa L. Chakravarthy
Department of Computer Science and Engineering, GITAM University, Visakhapatnam, India

ABSTRACT

Information plays an important role as a resource in the development and success of an organization. It is useful in decision-making to achieve the goals of the organization in an optimized way. This has to be achieved without affecting the information security and privacy of the stakeholders. Organizational policies are addressing the above-stated requirements within the jurisdiction and domain of an organization. While accessing and sharing the information among the organizations, the interests of all the stakeholders across the organizations have to be considered. For this, the policies have to be implemented to safeguard the information of the individuals as well as the organization through regulations or laws.

Rapid strides in technology, availability of cheaper computing and networked application environments, high-speed networks, and the increase of data handiness made data sharing very easy across and within the organizations. Data sharing also involves application processing of transactions and analytics in a cloud environment. Sharing in a cloud environment increases the utility but also raises security and privacy issues. Technological changes and domain/legal issues go hand in hand, affecting each other and necessitate changes in laws and regulations. To make the processing of information using big-data and computing infrastructure to be more reliable and secure according to [1] have to be addressed in the design process by considering both technical and legal aspects.

Big data processing is not thoroughly vetted for security issues and is posing challenges to the research community. Laws and regulations have not been crystallized. Existing laws related to common issues are being adopted on an ad-hoc basis.With the growing number of breaches unfolding around the nation and the hacking of government websites, the need to create a safe system for all government agencies has never been more critical. This, at best, is a sub-optimal solution as the current laws and regulations may not be appropriate. This article discusses the prevailing issues related to big-data and the laws to protect them. In addition to that, an attempt

Journal of Contemporary Issues in Business and Government Vol. 27, No. 2,2021
https://cibg.org.au/

P-ISSN: 2204-1990; E-ISSN: 1556-1571

DOI: 10.47750/cibg.2021.27.02.166

is made to analyze several Country's privacy and security laws and regulation which addresses big data security challenges.

Keywords:Big Data Security Challenges, Security & Privacy, Legal Policies, Law Policies,

INTRODUCTION

In recent years, apart from the existing resources like capital, material, human, and machinery resources for the development of an enterprise organization, information also plays an important role. Information can be considered as an input for the product or services. Information is useful as a tool for decision making for the growth of an organization, is also used as a product, and also is taking a part in developments in the smart market growing. In the report [2], the authors present market growth predictions until 2023 on the smart manufacturing industry depicted in Figure 1. In the way of transformation from traditional to digital, termed as digital transformation, many smart emerging technologies such as Augmented & Virtual Reality, Connected Machine Vision, Collaborative Robotics, Self-Driving Vehicles, Drones/UAVs, Additive Manufacturing. The technology growth in the above specific areas impacts the development of industry and hence, the economic growth.

Apart from these advancements of various smart technologies mentioned above, there is another dimension in the advancements, called security and privacy. All these smart technologies and artificial agents communicate with each other and hence, sharing of information takes place between intelligent systems as well as with the environment. Communication between the agents located at severalplaces knockson the door of Bigdata, as it deals with cloud architectures and data sources. The information sharing between all these stakeholders who are the members of the system such as machines, humans, etc., causes a big threat of privacy and security which leads to communication security.

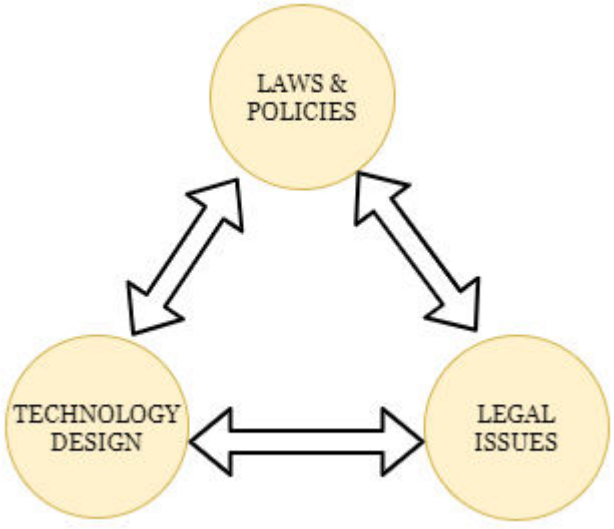


Fig1 : 3 fold design process for Legal laws and Policies

P-ISSN: 2204-1990; E-ISSN: 1556-1571

DOI: 10.47750/cibg.2021.27.02.166

Figure 1, shows the three fold design process for legal laws and policies.The technology may raise the legal issues which may provide a path to design of new laws and policies to control the technology consequences. Hence in the design process of computing infrastructure, the design team should integrate the technical aspect to meet the ideas of laws and polices makers or modifications may be included. At the expense of the security and privacy of the customers, the organizations are tending to capitalize. So, there is a need for policies regulations and laws to protect privacy and security in multi stake holder scenario. Private information, especially on the black market, is extremely valuable. The economic motivation to steal private information from malicious people is immense . The government departments and medical facilities have themost detailed information on people and this makes them leading targets for cyber criminals who are trying to profit from stealing this information.

Computer security deals with three fundamental areas namely confidentiality, integrity, and availability. Confidentiality is ensuring that the information is not accessed by unauthorized people. Integrity is assuring the information is not subjected to unauthorized alteration. Availability is the ability to access information in a reasonable time. Any effect on these areas will be affecting the quality of the information, decision making, and thus the overall business. The quantum of impact may be minor or it could be fatal. Because of this, information security is very crucial for the business. So, the organizations are attaching a lot of importance and investing in monitoring and ensuring information security.

The need for Big Data

Nowadays the responsibility of information gained from the available data is traversed beyond the other resources in the path of success of an organization. There is a need of sharing the data across the organizations for their development. In this aspect, organizations may utilize the data in four aspects:

1. Sharing between the organizations
2. From their own generated data
3. Purchase from other organizations
4. Accessing other sources.

All data is disparate and may fall into the categories of structured, semi-structured, and unstructured data. The data (e.g. user data, sensor data, and machine data), which is a great collection encapsulated with intelligence and insights and upon successive examination is termed as Big data [3], [4]. Upon appropriate analysis, big data provides business insight, opensthe latest markets, as well as gives rise to competitive advantages. Several aspects such as Emerging knowledge and social economies, limited information vs information abundance, business stability vs business flux, well-defined industry and industry transformation, global information flow and the emergence of social computing, global digital communities, real-time knowledge flows are the main mainsprings of the Big-Data.

Commodity hardware, technology innovations, growth of open source software, pervasive social networking, and persistent mobile devices combined determines big data. For the growth of the

P-ISSN: 2204-1990; E-ISSN: 1556-1571

DOI: 10.47750/cibg.2021.27.02.166

business, variation between real-time data gathering and analysis mission is critical with the advent of big data. The architectures, tools, infrastructure which support real-time analysis are different hence, gaining knowledge from this information should also be distinct. Information sources and content are escalated due to big data, also the pervasiveness of innovation is growing day by day. Due to the variety of sensors from which we expect progressing streams, and are more and more devices are engaged by a system makes data grow rapidly. With storage costs getting low, the cost associated with sparing and utilizing information turns into a non-complicated task [5], [6]. The data centers, servers, storage applications provide enormous log files and isolated data streams that able to be gathered, compiled, and analyzed.

Various security challenges in Big data architecture

Due to digital transformations, for industrial growth, the communication between intelligent agents (either machines or human beings) increased rapidly, hence, massive amounts of data are generated and collected by organizations and companies. They are using that huge collected big data for improving their markets. The data is getting doubled every year which in turn is more beneficial in the development of organizations.

Apart from the advantages of Big data for economic and market growth, the other side of the coin causes the magnification of security and privacy issues. In [7], the authors presented 17 V's and 1 C of Big-Data's characteristics, Volume, Vagueness, Variety, Velocity, Volatility, Veracity, Validity, Value, Verbosity, Variability, Venue, Vocabulary, Visualization, Virility, Versatility, Viscosity, Voluntariness and Complexity made security researchers concentrate more on the security and privacy aspects. The usage of cloud infrastructure on large scale with diversified software platforms that spread across large networks increases the scope of attacks on the system [1].

The present security mechanisms are limited to secure small-scale and static data. It is also difficult to add the security mechanisms to existing cloud infrastructure to reach the ultra-fast demands of security as it is the streaming source of data. In the report [1], the top ten security and privacy challenges and their classification is provided.

- Infrastructure Security.
    - Secure Distributed Processing of Data.
    - Security Best Actions for Non-Relational Data-Bases.
- Data Privacy
    - Data Analysis through Data Mining Preserving Data Privacy
    - Cryptographic Solutions for Data Security
    - Granular Access Control
- Data Management and Integrity
    - Secure Data Storage and Transaction Logs.
    - Granular Audits
    - Data Provenance

P-ISSN: 2204-1990; E-ISSN: 1556-1571

DOI: 10.47750/cibg.2021.27.02.166

- Reactive Security
    - End-to-End Filtering & Validation.
    - Supervising the Security Level in Real-Time.

Legal challenges & Regulations

Big data processing is not thoroughly vetted for security issues and is posing challenges to the research community. Laws and regulations have not been crystallized. Existing laws related to common issues are being adopted on an ad-hoc basis. This, at best, is a sub-optimal solution as the current laws and regulations may not be appropriate because of:

- Non-scalability of encryption for huge data sets
- Non-scalability techniques in real-time monitoring systems for smaller data
- Heterogeneity of devices that produce the data
- The abundance of diverse legal and regulatory policies leads to confusion

Organizations are tending to capitalize on this limitation at the expense of the security and privacy of the customers. Thus there is a need for designing laws and regulations apt for big data security. This article discusses the prevailing issues related to big-data and the laws to protect them. Considering the top ten big-data security and privacy issues recognized by Cloud Security Alliance (CSA) [1], an attempt is made to provide regulations and laws of various countries.

The technology may raise legal issues which may provide a path to the design of new laws and policies to control the technology consequences. So, in the design process of computing infrastructure, the design team should integrate the technical aspect to meet the ideas of laws and policymakers or modification s may be included. Figure 2, shows the three-fold design process for legal laws and policies. At the expense of the security and privacy of the customers, the organizations are tending to capitalize. So, there is a need for policies regulations, and laws to protect privacy and security in the multi-stakeholder scenario.

Global Applicability of the Policies: Policies are generally applicable within an organization. Laws are specific to a political nation and limited to boundaries of the nation whereas regulations are made and monitored by some of the influential non-political organizations and international regulatory bodies which are honored by all stakeholders. In certain ways, various countries may group to follow the regulations.

RELATED WORK

Three Phases of Big-Data

According to [8], however, the word Big Data has been using for three decades but it is not perfectly new and the essence has been using for data analysis to support their decision-making process. The three main phases of Big-data which mainly used for data analysis are provided as:

- Phase I (1970-2000): DBMS-based structure content and Data Warehousing were major core components. Querying, optimization, extraction, are key techniques used for

P-ISSN: 2204-1990; E-ISSN: 1556-1571

DOI: 10.47750/cibg.2021.27.02.166

analytical processing. In addition to this phase was adopted data mining and statistical analysis

- Phase II (2000-2010): Apart from the structured data, due to tremendous changes in internet and web development, there was an increase in semi-structured and unstructured data. In addition to the traditional structured data types, companies had to find innovative methods and storage strategies to deal with these new data types to analyze them effectively. The arrival and development of social media data have significantly exacerbated the need for tools, software, and analytical techniques to obtain useful information from this unstructured data.
- Phase III (2010- to date): Data transferred as wealth. Organizations having more focus on collecting data by adopting the advantage of emerging mobile services and usage. In addition to that growth in AI and IoT technologies, industry 4.0 is formed. New approaches like HCI, Mobile visualization, location-aware analysis, self-driving cars, etc are using concepts of Big-data.

Technology Evolution of Big-Data

- Batch processing (2003-2008): Huge collections of data are gathered, processed, and then results are produced for a batch. To handle fault-tolerance and scalability issues, DFS is used. To improve efficiency, Parallel programming models are used. Examples: HDFS, Apache Hadoop, MR, GFS.
- Ad-Hoc Processing(2005-2010): To overcome shortcomings of DFS which are appropriate for sequential data access, random read/write access is used. This issue is solved by NoSQL databases by considering column-based or key-value stores. In addition to that, it supports for storage of large unstructured datasets like graphs and documents. Examples: MongoDB, CouchDB, HBase,
- SQL (2008-2010): The data stores are accessed through very simple interfaces to query. The mechanisms of this approach and functionalities are as same as the traditional data warehousing mechanisms. Examples: Google Planner, HStore, Apache Hive/Pig, PrestoDB.
- Stream Processing(2010-2013): Before storing them data is continuously pushed to servers as streams for processing. Streaming data contains incoming patterns thatare unpredictable. Such data streams are processed with solutions that are fast, fault-tolerant, and highly available. Examples: Apache Kafka/Storm, Hadoop Streaming, Apache Drill, Google Big Query, Samza Apache Flume/Hbase, Google Dremel.
- Real-Time Analytical Processing(2010-2015): The live channels and machine-to-machine applications generated data streams which makes us take decisions automatically. These architectures help to apply real-times rules for the incoming events and existing events within a domain. Examples: Google Data flow, Amazon Kinesis, Apache Spark.
- Intelligent Systems (2014-to date): The data is rapidly generating wherever and whenever the GPS-equipped smart devices like mobile phones and intelligent machines like UAV

P-ISSN: 2204-1990; E-ISSN: 1556-1571

DOI: 10.47750/cibg.2021.27.02.166

are connected through high-speed internet. The communication between intelligent agents in the era of digital transformation generates streams of data.

Recent Impacts of Big Data on Industry 4.0

Two study technologies, Artificial Intelligence and Machine Learning transformun-widely big-data into an approachable stack. Several practical domains like dynamicpricing, video analytics, customer churn modeling, etc., in which the above saidtechnologies are employed to enable the business in algorithmic approach. The organizations which are spending revenue on AI & ML are expecting 39% of growth.According to [9], IDC estimates the spending revenue on AI & ML will hike by $ 57.6 billion in 2023.

As a prediction, next decade Quantum computing will take big data into its hands of data analytics and hence it will be a big stack holder in the future generation. Collecting the data at which it is being captured without storing it in central data locations, termed as Edge analytics, used for data analysis will also make an important role in big data and inturn in the Industrial growth. Ever-growing sensor information like video, text, voice changes almost all business models. Organizations wanted to do business according to customer's views and interests, hence trying to adopt big data and cloud architecture to run their operations most efficiently. According to IBM, by 2020, the Dark Data category captures about 93% of all data. Thus, big data in 2020 will be included in Dark Data.

Challenges:

Big Data provides a platform of opportunities in the development of the economic wealth of an organization, however, it is also carving new provinces and problems that are seeking special attention and upon failure, it can raise business threats not only in terms of reputation but also financially and legally. According to the literature review, the organizations who wants to make wealth with the help of Big Data must be addressing the concerns of:

- Data privacy: People may lose their rights to keep their data private, as big data generates data that contains a lot of information about our personal lives.
- Data security: Even if we decide to provide our information to someone for a purpose, we are unable to trust them whether they keep it safe.
- Data discrimination: We will try to discriminate against people based on data available about their lives, even though everything is known, may not be acceptable. For example, credit scoring is used to decide to provide lending money and insurance and it is heavily data-driven.
- Data quality: More raw data is being collected according to the trend with technology and it is very closer to the end-user. The prime hazard is the data in raw format is sensitive towards quality. The jeopardy increases when we try to reduce the gap between the end-user and raw data. Not more concern has been given on quality and contextual relevance.

The Economist Intelligence Unit, in their report 2015, mentioned the importance of security and privacy. Even top-notch organizations are also facing struggles with several technical facets of big data. These underpinned facets of data management still go deep in to facilitate more up-

P-ISSN: 2204-1990; E-ISSN: 1556-1571

DOI: 10.47750/cibg.2021.27.02.166

coming, the value-added facet of data management. The data management may be governance, compliance, and converting data into considerable perceptions. 29 % organizations financial performance ahead of peers ensuring security and Privacy and 25% organizations financial performance at par with peers ensuring security and privacy. 21% of an organization's financial performance are ahead of peers ensuring good data governance like integrity, security, usability, availability, and 19% of organizations' financial performance at par with peers ensuring good data governance like integrity, security, usability, and availability. 32% of organizations utilize cloud technologies for information security big data efforts. 28% Security challenges by an organization and 20% for good governance[10].

ASPECTS OF LAW IN BIG DATA

Problems in security pose a serious threat to the system, which is why it is crucial to process the gaps in the security. Big data is nothing naive to large organizations, however, it is gaining popularity among the small and medium firms as well due to the reduced cost of storing and easy management of data. Cloud-based storage also facilitates huge data storage. The maximum of the security issues are caused by the lack of effective measures provided by the firewalls and anti-virus software's of the systems which are developed to protect the information stored in the disk, but big data is much more when compared to that.

Hence, due to the increased storage of data, the data is posed with serious security and privacy threats. The concern with the highest priority to companies using Big data is providing security to cloud-based systems. If the cloud-based systems are targeted, the transfer of the data by malware can be done without raising any suspicion [11]. The legal issues in the big data scenario are not about just how to gather the data, but how you use it. Hence the data used in malicious ways may lead to legal issues for both the individual as well as firms. However, big data has serious limitations and dangers when applied in the legal context. These limitations can lead to generating unintended consequences in the legal system.

The breaches in Big data are putting forward a challenging task for law enforcement. The need for the setting up of the boundaries is an immediate task in emerging data markets. Some of the key areas on the list are:

- Digital Legal Pluralism means having multiple legal systems in any particular geographical area. The jurisdiction remains the same but has differentlegal systems.
- Balancing the citizens' rights and security digitally. Here the citizens' rights are meant to be the rights regarding the data and security is meant to how to deal with the rights of the individuals and the needs of the individuals.
- The need of the hour is the global digital legal culture. Digital legal culture meant the temporary outcomes of interactions to the challenges and response paradigm. The need to analyze the legal paradigms shapes the distinctive legal culture. Global digital legal culture meant the mix of digital laws all over the world.
- The National and International legal frameworks have to be enhanced which fits the new digital concepts and terminologies and allowing legal interoperability across different jurisdictions and cultures worldwide. Many of the countries are unaware of the digital

P-ISSN: 2204-1990; E-ISSN: 1556-1571

DOI: 10.47750/cibg.2021.27.02.166

trends and breaches taking place and are only following the old traditional laws which are being operated with the vulnerabilities. Hence the legal frameworks of national and international grounds have to be available in equal to all the data breaches taking place.

- Building social consciousness where privacy should be acknowledged as a social and collective responsibility of preserving the data.
- The legal and technological issues are some of the umbrella activities were identifying the knowledge about safety and security of the data and the metadata.
- The key point is the development of the measures to be taken from the technical point of view where the design of privacy and data protection should be developed. Encryption, Decryption, and other protocols should be developed with ethical and legal protection.
- Ethics also play an important role in the institutional system.

On par with the technological advancements and developments, Big data analytics have thoroughly changed the way how law enforcement and security agencies are examining information. Hence the legislation governing the functions should be focused on 20th-century trends instead of using the then existing laws for safeguarding personal data. The governments and law enforcement agencies are moving towards the modifications of laws to play a pivotal role in regulating the use and misuse of the data.

Big data is playing a minor role in many developing countries as of now but it is set to become increasingly popular in the coming years. It is estimated that Big data will play a major role in the coming years from now and will have a greater impact on government, public, private, and people's lives. Onthe other side of the coin, apart from the benefits which can be reaped from big data, there is also a downside when the data of the firms or individuals is at stake. Hence the governments are investing millions of rupees in big data Projects which are beneficial for using as well as safeguarding the data. Some of them are:

- The US reserved $ 200 Million for development and research on big data which can be used in all the spheres of government organizations.
- The UK spent 159 million on high-quality and network infrastructure, and 189 million to develop the UK's data infrastructure and support big data applications.
- In South Africa, the government invested 2 billion South African Rand in the Square Kilometer Array project which wheels around complex data sets.
- In France, research projects related to Big data were awarded 11.5 million.
- In Germany, the Ministry of Education and research invested 10 million in Big data research institutes.
- India launched “Digital India ” programme to transform india into a digitally empower society and knowledge economy to present huge potential to Big data analytics.

The governments are eager to start Big data projects by investing huge amounts of rupees. The governments apart from investing also should concentrate on formulating future-proof legal policies, as to how beneficial Big data is to the governments.There is always a risk from the

P-ISSN: 2204-1990; E-ISSN: 1556-1571

DOI: 10.47750/cibg.2021.27.02.166

whistleblowers who bring the confidential files out of their reasons. As Big data is taking a positive sphere, the negative sphere also arises. The confidential data kept by the big data mechanisms can be leaked by the whistleblowers who either for the public or personal interest expose the sensitive information or activity within the organization that is deemed illegal or unethical. There are also laws designed to protect the whistleblowers who for the benefit of society bring allegations to light in organizations, governments, or any agencies [12].

Need for Laws and Regulations

To the best of our knowledge, according to the literature survey, in most of the countries, the rules existing in the area of privacy and security in data protection are being applied to the Big Data processes. The Data Protection Agencies (DPA) in several countries play an important role in the protection and preserving of data of the individuals. Several Data Protection Agencies strongly recommend that the prevailing data protection principles must be enhanced to meet the requirements of bigdata processing and maintenance.

The UK DPA states that data protection rules apply to big data processes as well. Protecting the data poses a serious threat when the data is collected without consent or gathered from connected devices which are collected unconsciously from the individuals or firms. Big data dispose of the data for unknown and unusual purposes by which the limitation principle might be violated. The data which is used for big data processing might also violate the data minimization principle. The data minimization principle states that the data gathered and processed should not be availed withheld unless it is essential or it can be utilized for reasons which should be mentioned and meaningful [13], [14].

The French DPA proposed a new law called “The Digital Republic" with the help of the people by putting an online consultation to the public where they can suggest amendments ranging from net neutrality to open data. Despite this fact, steps are taking place for new dangers posed by big data and proposing new legislation that specifically addresses these issued. The DPA's opine that the new legislation can give support to face the issues raised of big data.

The question that now arises is that whether it is advisable to formulate new policiesfor Big data processes. The issues which have to address are:

- The current framework and its underlying principle could not be answerable to the new risks which big data poses.
- The current framework which is based on traditional approaches is restrictive to the private firms to adopt new technologies.
- The current framework could not be applied appropriately in the interpretation of big data.

Keeping the above points in consideration, the new regulatory scheme might provide a solution for the issues presented above. Since the data protection law is growing rapidly, a few gaps still exist. Some of the countries have not formulated any laws in the data protection area, and some countries have partial laws, and some laws are outdated as mentioned in the above points. The countries which are still formulating the laws should develop legislation that covers a wider range [15], [16].

P-ISSN: 2204-1990; E-ISSN: 1556-1571

DOI: 10.47750/cibg.2021.27.02.166

Laws policies in various countries

Driven by the rising concern about the possible vulnerability of networked societies and the number of cyber-domain disturbances, many countries have taken steps to better understand the vulnerabilities and threats to which their (information) infrastructure is subject, and have proposed measures to secure these assets in the form of guidelines and regulations. Below are some countries to advance towards the field of formulating laws in big data issues.

United Kingdom

UK implemented the Privacy and Electronic Communications Regulation (PECR) for E-privacy which led to the formulation of the General Data Protection Regulation (GDPR) and the act named Data Protection Act 2018 (DPA 2018). The GDPR applies to the processing of the personal data on personal interest, regardless of where the processing takes place under Article 3(1),GDPR [17], [13].

Even though the UK parted from the EU, the GDPR applies to everyone equally. Considering an example, if the controller who processes the purpose and means of data is in the UK or elsewhere in the EU, the GDPR applies the same. The GDPR included profiling which is taken as any form of processing of personal data that is used to estimate certain aspects of any person in the big data processing is dealt with under Article 4(4),GDPR [18].

Article 5(1) (a) of GDPR deals with the role of the controller of the data. The GDPR requires that the acceptance be given freely, unambiguous, informed, and specific of the subject whom he/she would give clear and affirmative action to be processed under Article 4(11), GDPR. Public authorities' legitimate interests are dealt with in Article 6(1)(f). All the other data protection principles are dealt with in Article 5, GDPR. The principle of data minimization is explained in Article 5(1) (c) [19].

United States of America

In the United States, unfortunately, there is no single law for data protection but a jumble of hundreds of laws to protect the personal information of US residents at both federal and state levels. In the USA, the laws are typically sector-specific i.e., the laws focus on a particular type of data. A few examples are quoted below [16], [19], [20].

- The Drivers Privacy Protection Act of 1994 governs the privacy and disclosure of personal information gathered by states Department of Motor Vehicles which includes SSN, Driver Identification Number, Name, Address, etc.
- Children's information is protected at the federal level under the Children's Online Privacy Protection Act which prohibits the collection of the data of any child under 13 years of age if needed so it requires parental consent.
- The Gramm Leach Bliley Act(GCBA) governs the protection of personal information in the hands of banks, insurance companies in the financial service industry.
- The Health Information Portability and Accountability Act (HIPPA) protects the information of the individuals regarding the health status and health care of the individuals.

P-ISSN: 2204-1990; E-ISSN: 1556-1571

DOI: 10.47750/cibg.2021.27.02.166

- The Telephone Consumer Protection Act (TCPA) deals with the calls, messages to the individuals and regulates the marketing calls to the people.

Hence, the laws in the US are sector-specific, there will not be a controller as specific and each sector takes care of the rights designed to the people.

Canada

Privacy in Canada is regulated through a mix of the constitutional, statutory and common law. The fundamental protection is provided by Section 8 of the Charter of Rights and Freedoms which explicitly states that Everyone has the right to be secure against unreasonable search". Some laws apply to the collection and disclosure of personal data by different organizations in both public and private sectors at all levels. Organizations in both sectors require laws to defend privacy-related lawsuits and torts. The Parliament of Canada is considering the recommendations to enact rules and guidelines related to data ownership and data sovereignty to put a stop to the non-consented collection, use, and disclosure of citizens' personal information [21], [22], [23], [19].

The Canadian Big data framework exists in different layers. Though there are 7 layers, we deal only with the first 3 layers which deal with the privacy of the data of the individual.

1. *Layer 1*:This layer involves core privacy legislation at federal and constitutional levels. Some of the important laws for the data protection imbibed in layer 1 are discussed below.
    a. The Personal Information Protection and Electronic Documents Act (PIPEDA)" was enacted in 2018. It applies to the personal information of the private sector and employee information of the public sector.
    b. The personal information held by the federal government institutions is covered by Federal Privacy Act.
    c. Canada's "Digital Charter" is the foundation for policies of the federal government for a people-centered data and digital economy.
2. *Layer 2:*This layer applies to and replaces the material parts of PIPEDA with some of the acts mentioned below.
    a. British Columbia's Personal Information Protection Act.
    b. Alberta's Personal Information Protection Act.
    c. Quebec's An Act for Protection of Personal Information in Private Sector.
3. *Layer 3*: This layer applies to the territories which cover both public and private activities and has a huge number of Acts imbibed in them.

India

India is one of the latest entrants in the field of data, protection, and security. The Information Technology Act (2000), amended by the Information Technology Act (2008) contains the provisions for the protection and security of electronic data [24].

P-ISSN: 2204-1990; E-ISSN: 1556-1571

DOI: 10.47750/cibg.2021.27.02.166

The Cyber Contraventions under sections 43(a) to (h) and cyber offenses under sections 63 to 74 from the Information Technology Act (2000). Under section 72A of the Information Technology Act, 2000 disclosure of information intentionally without the consent of the person is a breach in the lawful contract and is a punishableoffense with imprisonment for 3 years [25].

Section 65 of the Information Technology Act deals with the tampering of documents either knowingly or unknowingly shall be liable to the imprisonment of up to 3 years. In April 2011, the SPD rules under section 43A of the IT act as Information Technology (Reasonable Security Practices and Procedures and Sensitive Personal Data of Information Rules,2011).

The draft Legislation called the Privacy Bill was introduced in 2011 which recognized the individual's right to privacy of data. After many iterations, the bill was released over six years. The major leap took place with the Personal Data Protection Bill drafted by the Sri Krishna Committee and approved by the cabinet of the government of India. Several features are discussed and submitted by the Committee some of which are Data Judiciary, Data Processor, Territoriality, Exemption, Grounds for processing personal data, Transparency, Accountability, etc., [26], [27].

The personal data Protection Law is set to govern the collection, storage, and processing of data by private and public entities. Some other acts which deal with Data Protection are:

- The Copyright Act (1957): This Act protects the intellectual rights in different types of works including literary works which include databases, copying the computer database, distributing the database could amount to Copyright Infringement Act.
- The Indian Penal Code (1860): This is used to prevent the theft of the data.
- The Indian Constitution: Article 21 of the constitution protects an individual right to life and personal liberty. The Supreme Court of India in the nine-judge bench decision in Justice Puttuswamy Judgment held that the right to privacy is an intrinsic part of the fundamental right of life and personal liberty under Article 21.
- The 2013 National Cyber Security Strategy was designed to create healthy and resilient cyberspace for the people and businesses of India.The Ministry of Electronics and Information Technology said the policy is aimed at protecting cyberspace information and information infrastructure, building capacity to prevent and react to cyber-attacks, reducing vulnerabilities, and mitigating cyber incident harm through a combination of institutional frameworks, individuals, processes, technology, and cooperation.

The new data privacy authorities intend to safeguard the user's fundamental right to privacy from risks of unwanted exposure of people's sensitive data in this digital era. Data protection laws have impelled organizations to draw up stringent measures for protecting user's data from any kind of threat, data leakage, or cybersecurity breach. The end goal is to secure the digital citizens in all aspects from data breach and hence penal actions are needed in the majority of data protection enactment.

P-ISSN: 2204-1990; E-ISSN: 1556-1571

DOI: 10.47750/cibg.2021.27.02.166

CONCLUSION

Big data is useful in decision-making to achieve the goals of the organization in an optimized way. In the way of utilizing Big-Data, the information security and privacy of the stakeholders are at a sharp edge. Organizational policies are addressing the above-stated requirements within the jurisdiction and domain of an organization. For this, the policies have to be implemented as regulations or laws. Sharing in a cloud environment increases the utility but also raises security and privacy issues. The advent of Big data in this era is posing serious security issues.Technological changes and domain/legal issues go hand in hand, affecting each other and necessitate changes in laws and regulations. To make big data processing and computing infrastructure more secure accordingly have to be addressed in the design process by considering both technical and legal aspects.The authors presented laws and policies made in various countries and an acute analysis of each country.

Future direction: Big data processing is not thoroughly vetted for security issues and is posing challenges to the research community. Laws and regulations for safeguarding the data of the firms and individuals have not been crystallized. Existing laws related to common issues are being adopted on an ad-hoc basis. The laws and regulations which are existing now only provide a sub-optimal solution as the laws and regulations which are taken for Big data processing are inappropriate. The authors in this articleattempted to discuss the prevailing issues related to big-data and the laws to protect them. Considering many security and privacy issues, an attempt can be made to design a framework to deal with big data security challenges and comply with regulations and laws for many countries in the future which can be accepted globally.

Funding information if any:

This research received no specific grant from any funding agency in the public, commercial, or not-for-profit sectors.

REFERENCES

Report on Top 10 Big Data Security and Privacy Challenges. (Nov. 2012 (accessed April 2020)). https://www.securitymagazine.com/articles/84461-top-10-big-data-security-and-privacy-challenges-reportreleased

Industry 4.0 & Smart Manufacturing 2018-2023. (Nov. 2018 (accessed April 2020)). https://iot-analytics.com/product/industry-4-0-smart-manufacturing-market-report-2018-2023/

REPORT TO THE PRESIDENT BIG DATA AND PRIVACY: A TECHNOLOGICAL PERSPECTIVE. (May 2014 (accessed April 2020)). https://bigdatawg.nist.gov/pdf

Jain, P., Gyanchandani, M., Khare, N.: Big data privacy: a technological perspective and review. Journal of Big Data 3(1), 25 (2016)

Moura, J., Serr~ao, C.: Security and privacy issues of big data. In: Cloud Security: Concepts, Methodologies, Tools, and Applications, pp. 1598{1630. IGI Global, ??? (2019)

P-ISSN: 2204-1990; E-ISSN: 1556-1571

DOI: 10.47750/cibg.2021.27.02.166

Gholami, A., Laure, E.: Big data security and privacy issues in the cloud. International Journal of Network Security & Its Applications (IJNSA), Issue January (2016)

S, A.P., S, V.S., A, V.K.: The 17 v's of big data. International Research Journal of Engineering and Technology 4(9), 5 (2017)

Framework, E.B.D.: A Short History of Big Data. (May. 2019 (accessed April 2020)). https://www.bigdataframework.org/short-history-of-big-data/

FRAMINGHAM: New IDC Spending Guide. (Sept 2019, (accessed April, 2020)). https://www.idc.com/getdoc.jsp?containerId=prUS45481219

Limited, T.E.I.U.: Report on Big Data evolution: Forging New Corporate Capabilities for the Long Term. (2015 (accessed April, 2020)). https://www.manpowergroup.com/wps/wcm/connect.

Devins, C., Felin, T., Kau man, S., Koppl, R.: The law and big data. Cornell JL & Public Policy 27, 357 (2017)

Casanovas, P., De Koker, L., Mendelson, D., Watts, D.: Regulation of big data: Perspectives on strategy, policy, law, and privacy. Health and Technology 7(4), 335{349 (2017)

Kemp, R.: Big Data and Data Protection (GDPR and DPA 2018). ((accessed April, 2020)). https://tinyurl.com/y8ofws5g

Sumy, R., Natalie Donovan, S., May: AI and Data Protection: Balancing Tensions. (July. 2019 (accessed April 2020)). https://tinyurl.com/ydds7tjj

Mike Rebeiro, M.R.S.C. Malcolm Walton, Taylor, S.: Big Data and Competition Law: with Great Opportunities Come Great Risks. (June. 2019 (accessed April 2020)). https://tinyurl.com/y8jwxaut

Chabinsky, S.: USA: Data Protection 2019. (July. 2019 (accessed April 2020)). https://iclg.com/practice-areas/data-protection-laws-and-regulations/usa

Society, R.: Data management and use: Governance in the 21st-century British academy and royal society project (2017)

Group, R.S.W., et al.: Machine learning: the power and promise of computers that learn by example. Technical report, Technical report (2017)

Van der Sloot, B.: International and comparative legal study on big data (2016)

Myers, C.: Big Data, Privacy, and the Law: How Legal Regulations May A fact PR Research. (Jun 2018 (accessed April 2020)). https://instituteforpr.org/big-data-privacy-and-the-law-how-legal-regulations-may-aspect-pr-research/

Phull, C.: The Framework of Big Data Law in Canada, and Its Privacy Law Core. ((accessed April 2020)). https://www.smartblocklaw.com/blog/big-data-law-in-canada-ch2

Brown, S.: The Privacy, Data Protection, and Cybersecurity Law Review - Edition 6, Canada. (October 2019, (accessed April 2020)). https://thelawreviews.co.uk/edition/the-privacy-data-protection-and-cybersecurity-lawreview-edition-6/1210002/canada

P-ISSN: 2204-1990; E-ISSN: 1556-1571

DOI: 10.47750/cibg.2021.27.02.166

Big Data Guidelines. (May 2017, (accessed April, 2020)). https://www.ipc.on.ca/wp-content/uploads/2017/05/bigdata-guidelines.pdf

MeitY: DATA PROTECTION IN INDIA. (FEB 2018, (accessed April, 2020)). https://digitalindia.gov.in/writereaddata/les

Gupta, N.: Data Protection In India. (Oct 2018, (accessed April, 2020)).https://www.mondaq.com/india/privacy-protection/744160/data-protection-in-india

Subramaniam, H.: India:Data Protection 2019. (July 2019 (accessed April 2020)).https://iclg.com/practice-areas/data-protection-laws-and-regulations/india

Subhajit Basu, R.M.: BIG Data: A Challenge to Data Protection? ((accessed April, 2020)).https://www.indialawjournal.org/

Materials Today: Proceedings xxx (xxxx) xxx

Contents lists available at ScienceDirect

Materials Today: Proceedings

journal homepage: www.elsevier.com/locate/matpr

Particle Swarm Optimization for robot target tracking application

Santosh Sai Rayala [a,*], N. Ashok Kumar [b]

[a] Department of Electronics and Communication Engineering, Dr. Lankapalli Bullayya College of Engineering (Women), Visakhapatnam, Andhra Pradesh, India
[b] Department of Electronics and Communication Engineering, Raghu Engineering College(A), Visakhapatnam, Andhra Pradesh, India

ARTICLE INFO

Article history:
Received 22 May 2020
Accepted 26 May 2020
Available online xxxx

Keywords:
Estimation
Meta-heuristic
Particle swarm optimization
Tracking
Zero constant error

ABSTRACT

Tracking is a process of finding continuous path of a selected target. Tracking is important in various civil and defense applications. For tracking applications, various adaptive filters are being used such as Kalman Filter and it's variants. In this paper, a popular meta-heuristic algorithm, namely, Particle Swarm Optimization (PSO) algorithm is applied to track a target which is a robot and it is transmitting noisy data due to installation of cheap quality sensors onboard. These noisy observations are filtered by PSO algorithm in order to estimate true path of the robot. The simulated results are presented by using MATLAB software. From the results, it is observed that the PSO algorithm is very effective algorithm in estimating the target location continuously with almost zero estimation error. Thus, Particle Swarm Optimization algorithm is a suitable algorithm for robot tracking applications and it can also be used for nonlinear data processing in autonomous robot design applications.
© 2020 Elsevier Ltd. All rights reserved.
Selection and peer-review under responsibility of the scientific committee of the International Conference on Nanotechnology: Ideas, Innovation and Industries.

1. Introduction

Tracking of a target is an utmost requirement for civil and defense applications. Tracking depends on number of factors such as the propagation medium, types of targets etc. If the propagation medium is taken into consideration. The propagation medium is broadly classified as land, water, and air. In this paper, we are going to take land as the medium of propagation and the target is a robot. The simulated scenario is that the robot is roaming in a nonlinear path and it is equipped with a cheap quality sensor onboard. Thus, the robot is transmitting noisy data of its location at each instant. As it is roaming in a nonlinear path, the receiving data from the robot is highly unlikely. Hence, in order to estimate robot true location and path, the recorded noisy observation data is being used. utilized by Particle Swarm Optimization (PSO) algorithm. In this paper, Particle Swarm Optimization is applied to track the robot path by using the noisy data recorded from a from a remote location observer. From the results it is observed that the PSO algorithm is estimating the path of the robot with almost zero error. Hence, PSO is a better algorithm for robot tracking applications.

In Section 2, Particle Swarm Optimization algorithm is discussed in detail and in Section 3 simulation results are presented. Section 4 finishes with the conclusion.

2. Particle Swarm Optimization

PSO is a popular meta-heuristic optimization algorithm. It is famous swarm intelligence based algorithm [1–4]. It was first proposed by James Kennedy and Russell Eberhart in the year 1995 [5]. The algorithm is basically an inspiration from nature i.e., the exhibition of social behavior of bird flocking or fish schooling. This combines the self-experience with the social experience. In PSO a swarm means a collection of interacting organisms called particles. Particles moves around in the entire search space trying to find the best solution.

Each particle keeps track of two important parameters i.e., personal best and global best. Each particle's best solution is termed as personal best '*pbest*'. The best value of any particle is termed as global best '*gbest*'. Fig. 1 shows PSO algorithm estimation process and selection of '*gbest*' and '*pbest*' among a set of particles in the swarm.

Each particle in a search space have a movement towards a promising area to get the global optimum which is shown in Fig. 2.

Each particle modifies its position in space according to:

- Its current position
- its current velocity
- the distance between its current position and '*pbest*'
- the distance between its current position and '*gbest*'

* Corresponding author.
E-mail address: r.santoshsai@gmail.com (S. Sai Rayala).

https://doi.org/10.1016/j.matpr.2020.05.660
2214-7853/© 2020 Elsevier Ltd. All rights reserved.
Selection and peer-review under responsibility of the scientific committee of the International Conference on Nanotechnology: Ideas, Innovation and Industries.

Please cite this article as: S. Sai Rayala and N. Ashok Kumar, Particle Swarm Optimization for robot target tracking application, Materials Today: Proceedings, https://doi.org/10.1016/j.matpr.2020.05.660

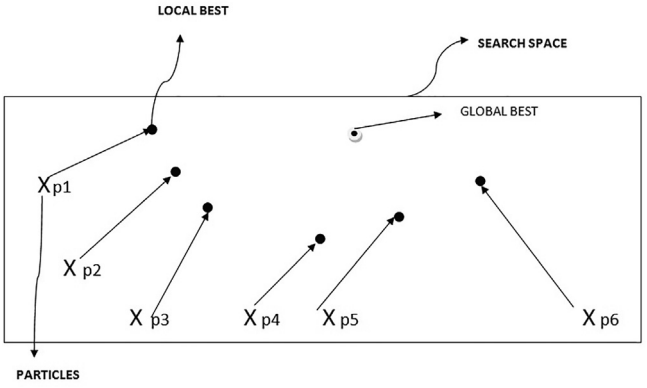


Fig. 1. PSO estimation process.

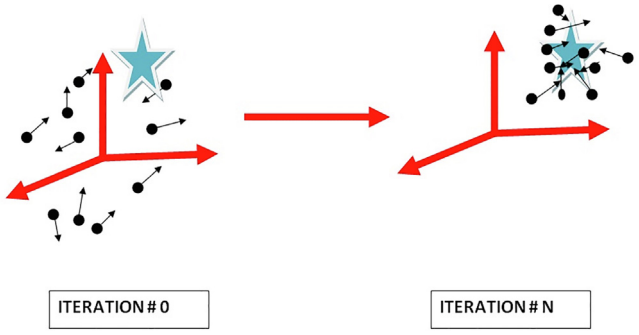


Fig. 2. Particles moving towards global best solution.

Each particle velocity and positions are updated in the swarm based on information available from the other particles. Mathematically particles velocity and position update equations are given by Eqs. (1) and (2). The position and velocity of a particle are updated at each time step until a termination condition is reached [6,7]. The search process is stopped automatically once the predetermined output or the maximum number of iterations are achieved. This is defined as the best solution or global best solution. Fig. 3 shows the velocity and acceleration of particle updated process.

Particle updated velocity:

$$v_i(t+1) = v_i(t) + c_1 * rand * (pBest(t) - -x_i(t)) + c_2 * rand * (gBest(t) - -x_i(t)) \quad (1)$$

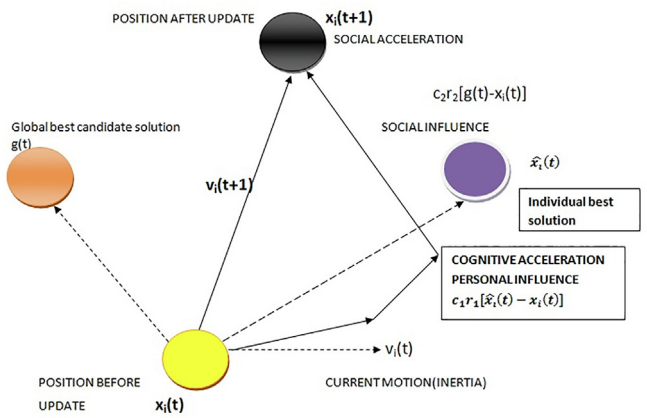


Fig. 3. Particles velocity and acceleration update process.

Particle updated position:

$$x_i(t+1) = x_i(t) + v_i(t+1) \quad (2)$$

where, $X_i(t)$ is particle position, $V_i(t)$ is particle velocity, '*pbest*' is personal best of the particle, '*gbest*' is global best of the particle, c_1 & c_2 are acceleration coefficients, and '*rand*' generates random numbers (usually between 0 and 1).

PSO algorithm flow chart is shown in Fig. 4 which describes the PSO algorithm processing steps [6–8].

In the following section implementation of PSO for the estimation of robot tracking from the noisy data is presented.

3. Results and discussion

Simulation results presented in this paper are simulated by using MATLAB software. The simulation scenario is that a robot

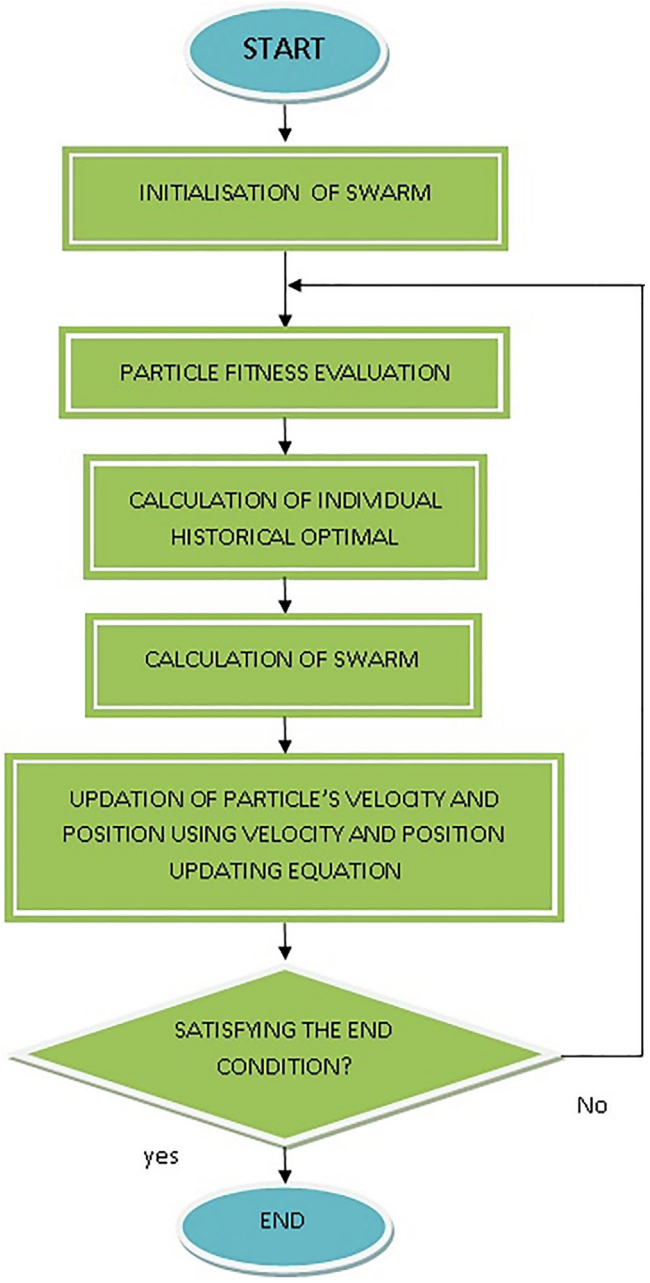


Fig. 4. PSO flow chart.

Please cite this article as: S. Sai Rayala and N. Ashok Kumar, Particle Swarm Optimization for robot target tracking application, Materials Today: Proceedings, https://doi.org/10.1016/j.matpr.2020.05.660

is equipped with cheap quality sensor and is transmitting noisy data instead of true data regarding its location in its path at each instant. Fig. 5 shows the true path and noisy path of the robot. True path will be remain as reference in order to check the performance of the PSO algorithm estimation results. For the implementation, noisy data is taken as input to the PSO algorithm in order to estimate the robot path.

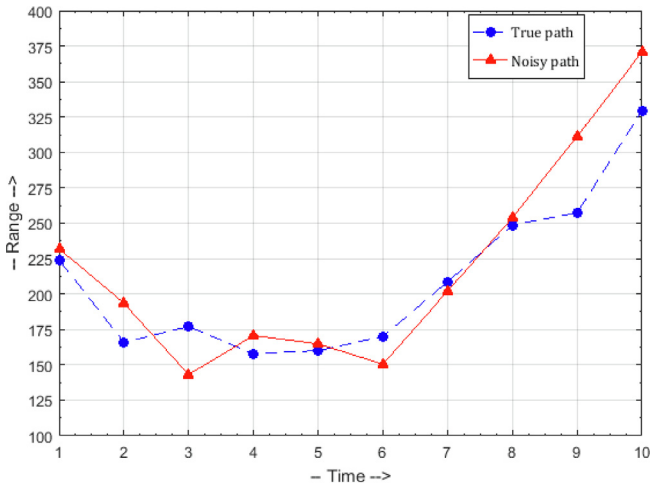


Fig. 5. Robot true path and noisy path.

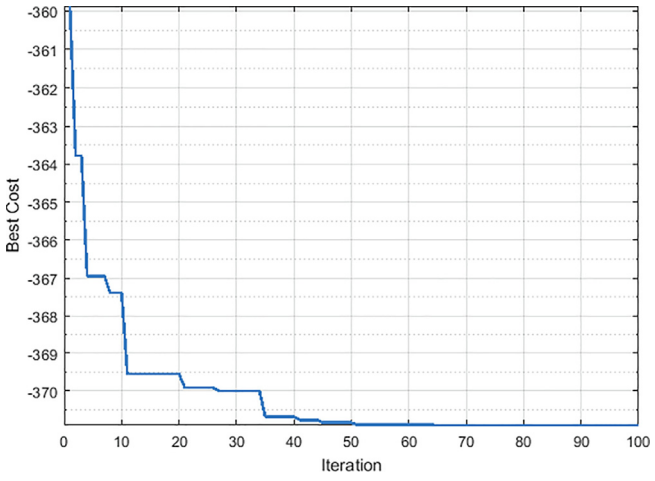


Fig. 6. PSO convergence plot.

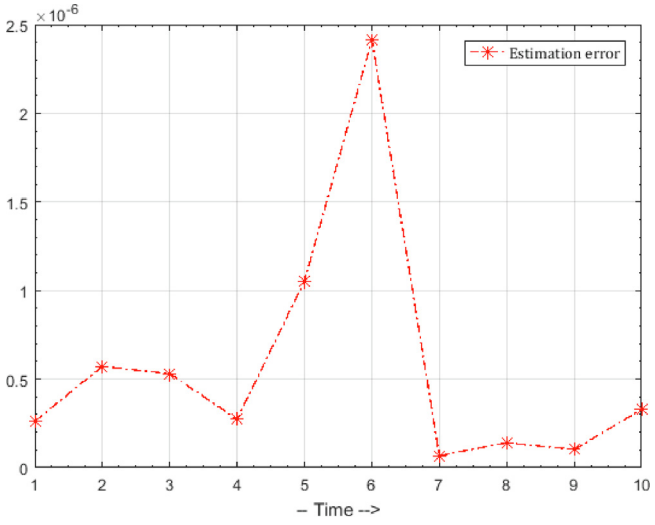


Fig. 7. Estimation error plot.

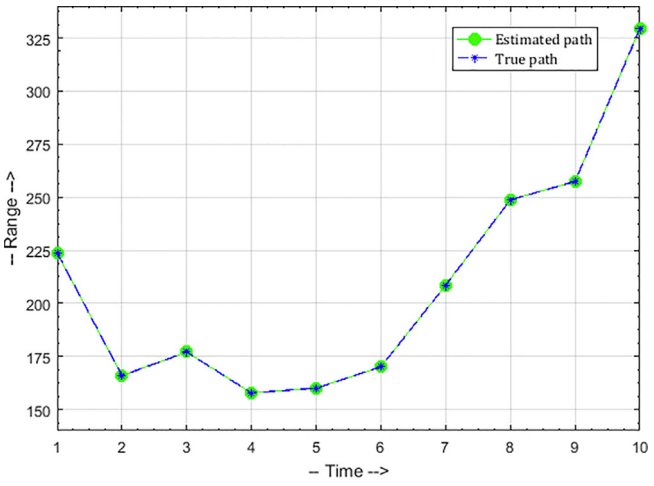


Fig. 8. Target path estimated results.

For the target path estimation, PSO algorithm parameters are initialized as following.

- Swarm Size (population) = 100
- Iterations = 100
- Inertia weight = 1
- Inertia weight damping ratio = 0.99
- Personal learning coefficient = 1.5
- Global learning coefficient = 2

Then, the PSO algorithm process the noisy data at each instant. The convergence of the algorithm can be observed by using cost function value (Best cost) versus iterations as shown in Fig. 6.

From the Fig. 6, it is observed that as the iterations increased from 0 to 100 the best cost got reduced to zero. It can be said that the error between true path and estimated path has been reduced drastically and almost zero.

In order to check the convergence of estimated results, estimation error has to be computed which is the difference between true path values and estimated path values. This is shown in Fig. 7. From Fig. 7, it is observed that the estimated error is almost zero at every instant. Hence, PSO algorithm accurately estimated the path of robot (target) efficiently. Fig. 8 shows the comparison between true path of the robot and estimated path using the PSO algorithm.

In Fig. 8, both estimated path and true path of the robot are same due to the zero estimation error as shown in Fig. 7. Therefore, both paths are coincided on the same line which is shown in Fig. 8 with different markers. Hence, PSO algorithm is an efficient algorithm for robot target tracking under nonlinear conditions.

4. Conclusion

The performance of Particle Swarm Optimization algorithm is presented in the estimation of a robot target which is roaming in a nonlinear path. The noisy data obtained from the cheap quality sensor of the robot is being used as the input to the PSO algorithm. PSO algorithm executed the estimation process with swarm size of 100 with 100 iterations; inertia weight and damping ratio are 1 and 0.99; Personal learning coefficient and global learning coefficients are 1.5 and 2, respectively. Estimation of the robot path is experimentally validated and has demonstrated the PSO algorithm

Please cite this article as: S. Sai Rayala and N. Ashok Kumar, Particle Swarm Optimization for robot target tracking application, Materials Today: Proceedings, https://doi.org/10.1016/j.matpr.2020.05.660

effectiveness in the estimation of the original path with almost zero error. The simulation results show that the Particle Swarm Optimization algorithm is a suitable algorithm for robot tracking applications. The PSO algorithm can also be used for nonlinear data processing in autonomous robot design applications.

Declaration of Competing Interest

The authors declare that they have no known competing financial interests or personal relationships that could have appeared to influence the work reported in this paper.

References

[1] A.P. Engelbrecht, Fundamentals of Computational Swarm Intelligence, Wiley, Hoboken, NJ, USA, 2005.
[2] J. Kennedy, R.C. Eberhart, Y. Shi, Swarm Intelligence, Academic Press, London, UK, 2001.
[3] X.S. Yang, A.H. Gandomi, S. Talatahari, A.H. Alavi, Metaheuristics in water, Geotech. Trans. Eng., Elsevier, Waltham, MA, USA, 2013.
[4] X.S. Yang, Z.H. Cui, R.B. Xiao, A.H. Gandomi, M. Karamanoglu, Swarm Intelligence and Bio-Inspired Computation: Theory and Applications, Elsevier, London, UK, 2013.
[5] J. Kennedy, R.C. Eberhart, Particle swarm optimization, in: Proceedings of the IEEE international conference on neural networks, Piscataway, NJ, USA, 1995, pp. 1942–1948.
[6] Xin-She Yang, Nature-Inspired Optimization Algorithms, 1st ed., Elsevier, 2014, pp. 99–110.
[7] J. Kennedy, R.C. Eberhart, Particle swarm optimization, in: Proceedings of IEEE international conference on neural networks, (4), 199, pp. 1942–1948.
[8] Daniel Bratton, Kennedy, Defining a standard for particle swarm optimization, in: proceedings IEEE swarm intelligence symposium (SIS 2007), Honolulu, HI, 2007, pp. 120–127.

Please cite this article as: S. Sai Rayala and N. Ashok Kumar, Particle Swarm Optimization for robot target tracking application, Materials Today: Proceedings, https://doi.org/10.1016/j.matpr.2020.05.660

International Journal of Scientific Engineering and Applied Science (IJSEAS) – Volume-6, Issue-9, September 2020
ISSN: 2395-3470
www.ijseas.com

Design of Linear and Circular Antenna Array for Side Lobe Reduction Using the Method Moth Flame Optimization Algorithm

Vennapu. Krishna Tulasi[1], K. Rajesh Kumar[2], Dr. Vennapu. Lakshmana Rao[3]

[1]. U.G Student, Dept. of ECE, Dr. L. B. College of Engg. (W), Visakhapatnam, India

[2.] Assistant Professor, Dept. of ECE, Dr. L. B. College of Engg. (W), Visakhapatnam, India

[3].Assistant Professor, Dept. of Meteorology and Oceanography, Andhra University, Visakhapatnam, India

ABSTRACT

A design problem of symmetrical linear antenna array (LAA) and a non-uniformly excited single ring circular antenna array (CAA) for minimized side lobe level (SLL) is presented in this paper .Moth Flame optimization (MFO) is considered one of the promising meta heuristic algorithms and successfully applied in various optimization problems .In this paper, MFO is applied to determine inter-element spacing and current excitation weights among the elements to reduce SLL and improve the half power beam width (HPBW) and improve first null beam width (FNBW). The simulation results of the designed LAA, CAA are compared with a fully populated array to illustrate the effectiveness of our proposed method.

KEYWORDS: linear antenna array, side lobe level, circular antenna array, moth flame optimization, half power beam width.

1. INTRODUCTION

A group of antenna elements which are excited to achieve a desired radiation pattern in a given direction is called Antenna array. They can provide capability of beam steering. Antenna arrays are widely used in sonar, radar, communication and high power transmission applications. The radiation pattern depends on the antenna array parameters like geometrical configuration of the array, inter-element spacing and the current excitation weights of each array element. Array antennas have a high gain and directivity compared to an individual radiating element. The goal in antenna array geometry synthesis is to determine the physical layout of the array that produces the radiation pattern that is close to the desired pattern (Ballanis CA.1997, Elliott RS.2003). The increasing pollution of electromagnetic environment prompts to design the antenna array with lower side lobe level (SLL) and narrower half power beam width (HPBW).

In this paper presents an accurate approach to design a symmetrical linear antenna array (LAA) and a non-uniformly excited single ring circular antenna array (CAA) to improve the far-field radiation characteristics. The LAA and CAA synthesis can be achieved either by optimizing the

inter-element spacing keeping a uniform current excitation weight and phase or optimizing the current and phase excitation weights while maintaining a uniform inter-element spacing.

The far-field radiation pattern is improved with SLL which is essential for the reduction of interference in the entire side lobe regions. The current excitation weights and the inter-element spacings are optimized in this paper by using MFO algorithm for the synthesis of LAA keeping the inter-spacing as d=λ/2 and phase excitation weights as zero for 10-element, 12-element, 18-element symmetrical LAA design. The current excitation weights and the inter-element spacing are optimized in this paper by using MFO algorithm for synthesis of non- uniform CAA for 10-element, 12-element, and 16-element non-uniform CAA design.

In this paper, the design constraints of narrower FNBW, lower SLL and narrower HPBW for symmetrical LAA and non-uniform CAA design have been considered by using MFO algorithm. The constraints are as follows: to improve the directivity of the radiation pattern by reducing the value of HPBW, to reduce side lobe levels, in the radiation pattern imposing nulls at all the peak of side lobes. The primary objective of this paper is to design non-uniform CAA and a symmetrical LAA with the lowest SLL value while maintaining a narrow HPBW by using MFO algorithm. MFO was initially proposed by S.Mirjalili. MFO is a meta-heuristic algorithm inspired by the behavior of moths converging towards the light. The current excitation amplitude weights of each array element and the inter-element spacing are optically calculated by using MFO, and the best results are presented.

2. DESIGN EQUATION

2.1 Linear antenna array (LCC)

Linear antenna array is array that consists of number of elements in a straight line. An isotropic array elements of even number, 2M is considered and positioned symmetrically along the z-axis (Khodier M, Al- Aqeel M.2009). The separation between the array elements is d=λ/2, M elements are placed on each side of the origin.

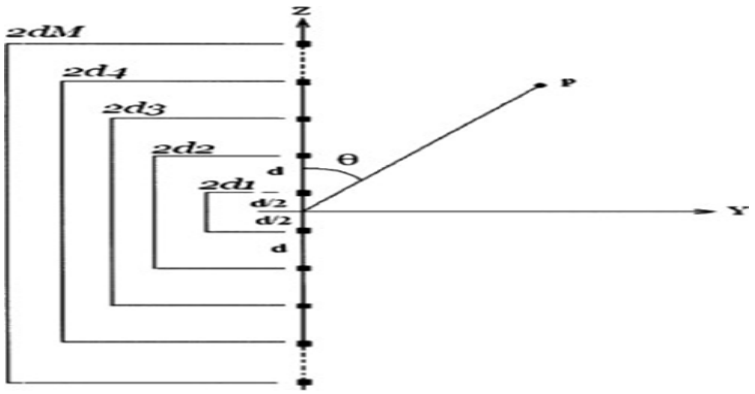


FIGURE 1: 2M-elements linear antenna array geometry along the Z axis

International Journal of Scientific Engineering and Applied Science (IJSEAS) – Volume-6, Issue-9, September 2020
ISSN: 2395-3470
www.ijseas.com

Assuming that the amplitude excitation is symmetrical about the origin and the array factor (AF) of the non-uniform amplitude broadside array is given by Equation (1).

$$(AF)_{2M}=2\sum_{n=1}^{M} I_n \cos[((2n-1)/2).k.d.\cos\theta+\Phi n] \quad (1)$$

Where In = current excitation amplitude weight of an nth element, 2 M = total number of elements in the array; k = propagation constant; φn = phase excitation weight of nth element and is considered to be zero for the design to keep the main beam fixed; d = spacing between the array elements, θ = angle of radiation of electromagnetic plane wave.

2.2 Circular antenna array (CAA)

A non uniform circular antenna array is an array that consists of single circle and number of elements on its surface with same centre, having different current excitation amplitude. Consider a non-uniformly spaced N elements CAA lying on the x-y plane, scanning at point PP in the far field and having radius "a" which is shown in Figure 2.

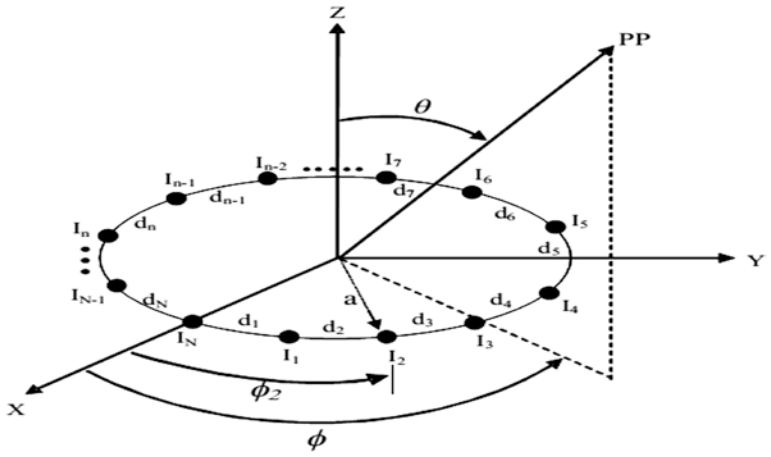


FIGURE 2 : The geometry of N-elements non-uniform CAA laid on the x-y plane for scanning at a point "PP" in the far field

In CAA, each element is assumed to be isotropic source and Array Factor (AF) of non-uniform CAA is given (Elliott RS.2003) by Equation (2).

$$AF(\theta, \Phi, I) = \sum_{n=1}^{N} I_n \exp(j[ka\sin\theta\cos(\Phi-\Phi_n)+\alpha_n]) \quad (2)$$

Where

$$ka = 2\prod a/\lambda = \sum_{i=1}^{N} d_i/\lambda = N \quad (3)$$

$$\Phi_n = 2\prod (n/N) \quad (4)$$

where I_n is the current excitation of n^{th} element of the array, $k = 2\pi/\lambda$; λ is the wavelength of operation; d_i is the inter- element spacing between the elements "i" and "$i+1$," θ is the elevation angle measured from positive z-axis, ϕ is the azimuth angle measured from the positive x-axis, and ϕ_n is the angular location of the n^{th} element along the x-y plane.α_n is the phase excitation of the n^{th} element. N is the total number of elements present in the CAA.

The AF value of Equation (2) attains maximum when

$$ka \sin\theta \cos(\Phi - \Phi_n) + \alpha_n = 2m\pi; \quad \text{where } m = 0, \pm1, \pm2, \ldots \pm n. \tag{5}$$

The principal maxima are defined by the direction (θ_0, φ_0)for which

$$\alpha_n = -ka \sin\theta \cos(\Phi - \Phi_n); \quad n=1,2,\ldots\ldots N. \tag{6}$$

To direct the peak of the main beam in the (θ_0, ϕ_0) direction, the following changes are assumed for the present design.

$$\theta = \prod/2, \Phi_0 = 0 \text{ and } \alpha_n = -ka\cos(\Phi - \Phi_n) \tag{7}$$

Thus, Equation (2) can be rewritten as

$$AF(\theta,\Phi,I) = \sum_{n=1}^{N} I_n \exp(jka[\cos(\Phi - \Phi_n) - \cos(\Phi_0 - \Phi_n)]) \tag{8}$$

3. COST FUNCTION FORMULATION

To achieve the design goal, a suitable Cost Function (CF) needs to be formulated for reducing the SLL and HPBW and it is given by equation (9).

$$CF = W_1 X \frac{|AF(\theta_{ms1}, I_n) + AF(\theta_{ms2}, I_n)|}{AF(\theta_0, I_n)} + W_2 X \frac{|\prod_{\theta=-\pi}^{\pi} AF(\theta_{SLL_{peaks}}, I_n)|}{|AF_{max}|} + W_3 X [HPBW_{computed} - HPBW(I_n=1)] \tag{9}$$

W_1, W_2, W_3 are the weighting factors whose values are selected as 18, 18, and 12, respectively, and θ_0 is the value of θ where the crest of the main lobe is attained; θ_{ms1}, θ_{ms2} are the angle of the maximum side lobe in the lower band and upper band respectively. HPBW is the angular separation between the 3-dB points on each side of the main beam. Thus, HPBW $_{Computed}$ and HPBW ($I_n = 1$) refer to the computed 3-dB beam width for the non-uniform excitation and uniform excitation cases, respectively. . These SLL peaks are represented as $AF(\theta_{SLL_Peaks}, I_n)$ within $\theta \in [-\pi:\theta_{ms1}, \theta_{ms2}:\pi]$, and $|AF_{max}|$ is the maximum value of AF. $\prod$ represents the product of all the values of $AF(\theta_{SLL_Peaks}, I_n)$. So, the

minimization of *CF* refers to the maximum reduction of SLL and reduction of HPBW as far as possible. MFO algorithm controls the current excitation weights and the inter-element spacing among the array elements to minimize the CF given in Equation (9).

4. MOTH FLAME OPTIMIZATION (MFO) ALGORITHM

Moth–flame optimization (MFO) algorithm was proposed by Mirjalili. It is under the population-based metaheuristic algorithms (Mirjalilli S.2015). As shown in flowchart MFO starts by generating moths randomly within the solution space, then calculating the fitness values (i.e., position) of each moth, and tagging the best position by flame. After that, updating the moths' positions depends on a spiral movement function to achieve better positions tagged by a flame, updating the new best individual positions, and repeating the previous processes (i.e., updating the moths' positions and generating new positions) until the termination criteria are met (Khalilpourazari S, Pasandideh SHR.2017).

The language used to explain the MFO follows from analogy of moth in flame. These key terms are

1. **Decision variable** :Moth's position in each dimension
2. **Solutions**: Moth's position
3. **Initial solutions**: Random positions of moths
4. **Current solutions**: Current positions of moths
5. **New solutions**: New positions of moths
6. **Best solutions:** Flame's position
7. **Fitness function:** Distance between moth and flame
8. **Process of generating new solution**: Flying in a spiral path toward a flame

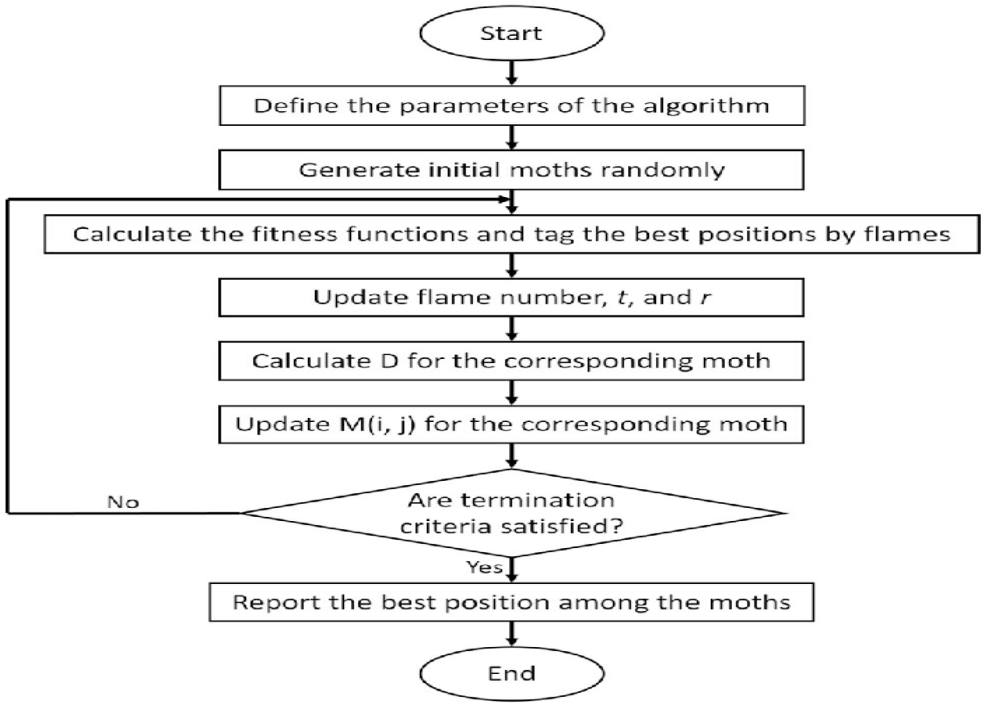


Figure 3: Flowchart of the MFO algorithm

The MFO algorithm has three main steps. These steps are shown below. Then, the pseudocode of the MFO as shown in Algorithm 1 and the summary of its parameters setting are illustrated in Table 2.

1. Generating the initial population of Moths: As mentioned, Mirjalili assumed that each moth can fly in 1-D, 2-D, 3-D, or hyperdimensional space. The set of moths can be expressed in equation 1. where n refers to the moths' number and d refers to the number of dimensions in the solution space

$$M = \begin{bmatrix} m_{1,1} & m_{1,2} & \cdots & \cdots & m_{1,d} \\ m_{2,1} & m_{2,2} & \cdots & \cdots & m_{2,d} \\ \vdots & \vdots & \vdots & \vdots & \vdots \\ m_{n,1} & m_{n,2} & \cdots & \ldots & m_{n,d} \end{bmatrix} \tag{10}$$

Also, the fitness values for all moths are memorized in an array as follows:

$$OM = \begin{bmatrix} OM_1 \\ OM_2 \\ \vdots \\ OM_n \end{bmatrix} \tag{11}$$

The rest elements in the MFO algorithm are flames. The following matrix shows the flames in the D-dimensional space followed by their fitness function vector:

$$F = \begin{bmatrix} F_{1,1} & F_{1,2} & \cdots & \cdots & F_{1,d} \\ F_{2,1} & F_{2,2} & \cdots & \cdots & F_{2,d} \\ \vdots & \vdots & \vdots & \vdots & \vdots \\ F_{n,1} & F_{n,2} & \cdots & \cdots & F_{n,d} \end{bmatrix} \quad (12)$$

$$OF = \begin{bmatrix} OF_1 \\ OF_2 \\ \vdots \\ OF_n \end{bmatrix} \quad (13)$$

It should be noted here that moths and flames are both solutions. The difference between them is the way we treat and update them in each iteration. The moths are actual search agents that move around the search space, whereas flames are the best position of moths that obtains so far. In other words, flames can be considered as flags or pins that are dropped by moths when searching the search space. Therefore, each moth searches around a flag (flame) and updates it in case of finding a better solution. With this mechanism, a moth never loses its best solution.

2. Updating the Moths' Positions: MFO employs three different functions to converge the global optimal of the optimization problems. These functions are defined as follows:

$$MFO = (I, P, T) \quad (14)$$

where I refers to the first random locations of the moths (I :Φ →{ M,OM}), P refers to motion of the moths in the search space(P : M→M), and T refers to finish the search process (T : M→true,false). The following equation represents I function, which is used for implementing the random distribution.

$$M(i,j)=(ub(i) – lb(j)) * rand() + lb(i) \quad (15)$$

where lb and ub indicate the lower and upper bounds of variables, respectively. As mentioned previously, the moths fly in the search space using the transverse orientation. There are three conditions that should abide when utilizing a logarithmic spiral subjected, as follows:

– Spiral's initial point should start from the moth.
– Spiral's final point should be the position of the flame.
– Fluctuation of the range of spiral should not exceed the search space.

Therefore, the logarithmic spiral for the MFO algorithm can be defined as follows:

$$S(M_i,F_j) = D_i \cdot e^{bt} \cdot \cos(2\prod t) + F_j \quad (16)$$

where D_i refers to the space between the i-th moth and the j-th flame (i.e., $D_i = |F_j - M_i|$), b indicates a fix to define the shape of the logarithmic spiral, and t indicates a random number between [-1, 1]. In MFO, the balancing between exploitation and exploration is guaranteed by the spiral motion of the moth near the flame in the search space. Also, to avoid falling in the traps of the local optima, the optimal solutions have been kept in each repetition, and the moths fly around the flames (i.e., each moth flies surrounding the nearest flame) using the OF and OM matrices.

3. Updating the number of flames: This section highlights enhancing the exploitation of the MFO algorithm (i.e., Updating the moths' positions in n various locations in the search space may decrease a chance of exploitation of the best promising solutions). Therefore, decreasing the number of flames helps to solve this issue based on the following equation:

PARAMETRS	MFO
Population size	10
T	50
B	1
T	[0,1]
R	[-1,-2]

flame no = round(N – l * (N – 1)/T) (17)

where N is the maximum number of flames, l is the current number of iterations, and T indicates the maximum number of iterations.

The P function is executed until the T function returns true. The main steps of MFO algorithm utilized for the LAA and CAA optimization problems are given as a flowchart in Figure 3.

5 RESULTS AND DISCUSSIONS

The method of parameter tuning for evolutionary algorithms is presented by Eiben and Smith (Eiben AE, Smit SK. 2011). The best control parameters of MFO are shown in table 1.

TABLE 1 MFO CONTROL PARAMETERS

5.1 Simulation results of LAA

Table 3 shows the initial values of SLL and HPBW for symmetrical LAAs having uniform excitation with λ/2 inter-element spacing. The current excitation amplitude weights obtained by using MFO algorithm for 16-element, 18-element, 20-element symmetrical LAA are shown in Table 4.

TABLE 2 The initial value of SLL, HPBW for uniformly excited and uniformly spaced linear antenna array

No. of elements	SLL(dB)	HPBW(deg)
12	-12.6133	13
16	-13.2483	9

TABLE 3 The current excitation amplitude weights (I_n) of symmetrical LAA using MFO algorithm

No. of elements	Current Excitation Weights	SLL(dB)	HPBW(deg)	FNBW(deg)
12	0.5317 0.4606 0.3974 1.0000 0.3820 0.3699	-27.9607	5	13
16	0.9695 0.9510 0.6974 0.6831 0.6775 0.6760 1.0000 0.6702	-33.9194	4	8

Table 3 shows that as the no of elements increased, SLL, HPBW, FNBW are decreased. The maximum SLL values achieved by using MFO algorithm for 12-elements and 16-elements symmetrical LAA are -25.4168 dB and -31.2912 dB, respectively. The HPBW of 12-elements and 16-elements symmetrical LAA achieved by using MFO algorithm are 5 and 4 degree, respectively.

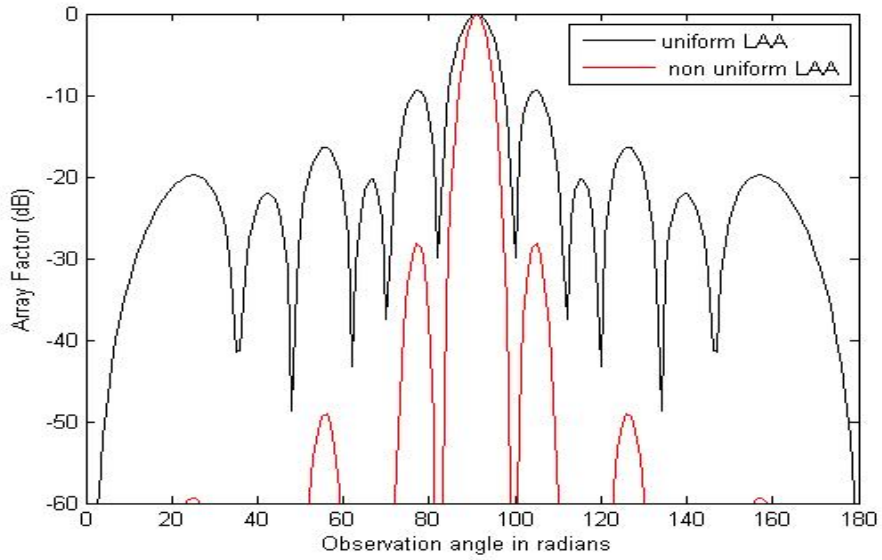


Fig 4: Radiation pattern of 12-element uniform and non-uniform LAA design.

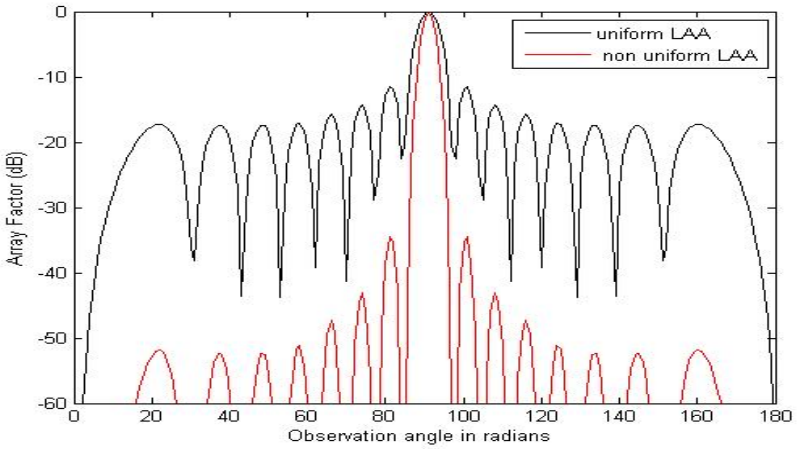


Fig 5: Radiation pattern of 16-element uniform and non-uniform LAA design.

5.2 Simulation results of non-uniform CAA

The current excitation weights and the inter-element spacing for 12-element, 14-element, 16-element non-uniform CAA design obtained by using MFO technique are shown in Table 7.Table 7 also contains SLL(dB) values, HPBW (deg) ,FNBW (deg) values are obtained by MFO algorithm when applied to optimize the 12-element, 14-element and 16-element CAA.

TABLE 4 The current excitation weights and inter element spacing of non uniform circular antenna arrays using MFO algorithm.

The results shows the SLL values of three different CAA structures of 12-element, 14-element and 16-element array are -21.14, -22.27, -23.56 dB, respectively.

No.of elements	Current Excitation Weights	Inter element Spacing	SLL (dB)	HPBW (deg)	FNBW (deg)
12	0.8612 0.7468 0.2581 0.5073 0.0031 0.1446 0.5194 0.4762 0.4963 0.1282 0.7163 0.7482	0.1750 1.9869 1.2144 0.8374 0.1522 1.3673 1.3903 0.8929 0.7153 0.1146 1.2714 1.0047	-21.14	4	10
14	0.5574 0.1696 0.2309 0.5749 0.4681 0.1518 0.1347 0.8429 0.3479 0.6760 0.2504 0.6426 0.0986 0.9525	1.4234 1.2735 1.5626 0.6440 0.9277 1.0742 0.9848 0.8372 0.2117 1.8010 0.5773 1.1537 1.0013 1.9585	-22.27	3	7
16	0.0649 0.7791 0.8397 0.8766 0.1061 0.5366 0.7821 0.0231 0.3380 0.9849 0.2616 0.8745 0.3882 0.3705 0.6788 0.8478	0.2621 0.3295 1.8647 0.5613 1.3470 0.2799 0.4790 0.7875 1.0031 0.8772 0.7267 1.5157 1.4665 1.4653 0.5299 1.4105	-23.56	2	4

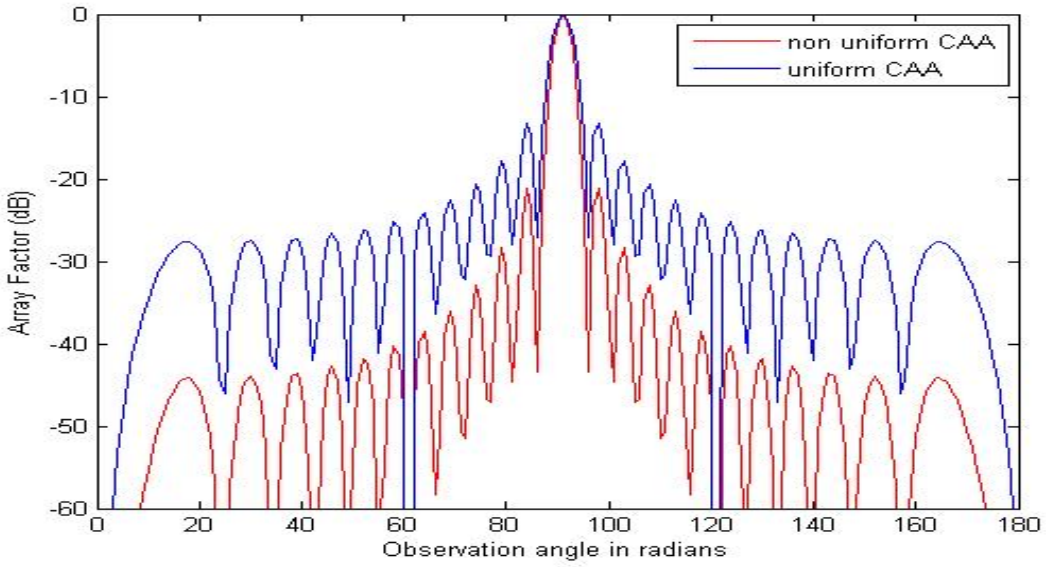


Fig 6 Radiation pattern of 12-element uniform and non uniform CAA design.

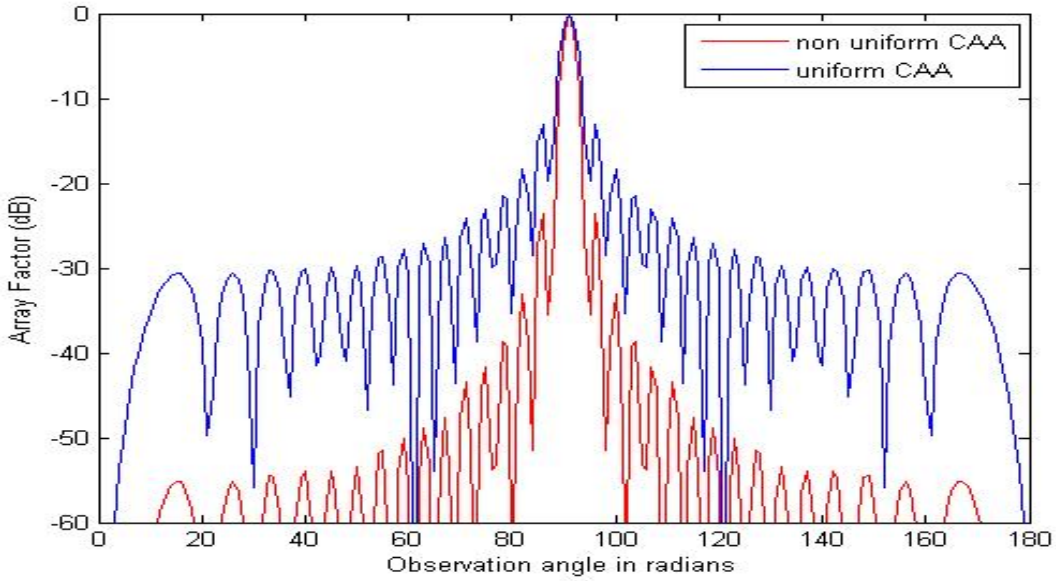


Fig 7: Radiation pattern of 14-element uniform and non-uniform CAA design.

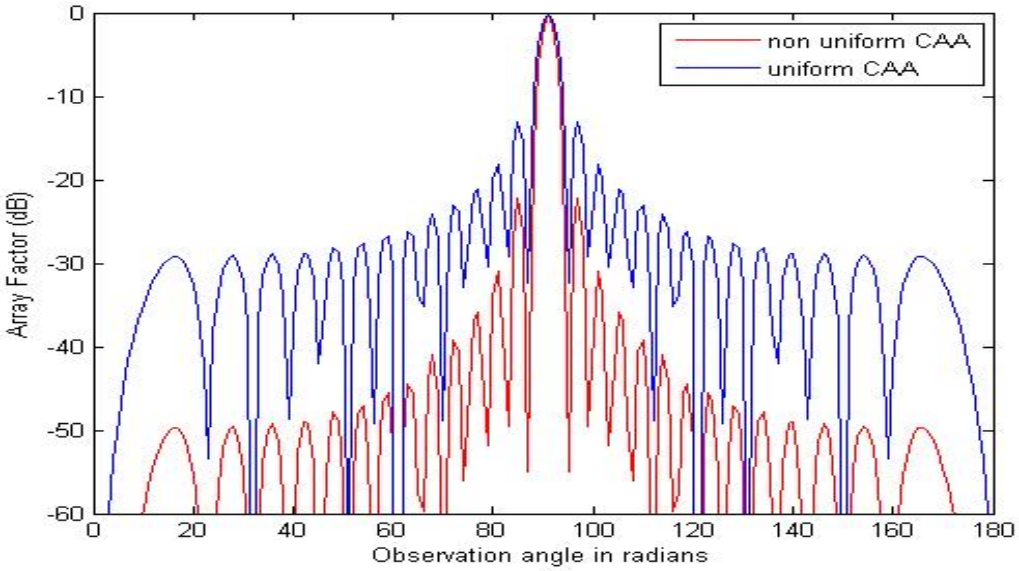


Fig 8: Radiation pattern of 16-element uniform and non-uniform CAA design.

6. CONCLUSIONS

This paper illustrates moth flame optimization for reduction of side lobe level(SLL) for symmetrical linear antenna array (LAA) and non-uniform single ring circular antenna array

(CAA) . By varying the number of elements, inter element spacing the reduced side lobe levels can be obtained. The results obtained by using MFO algorithm confirm an improved design in terms of suppressing the SLL and reducing HPBW and FNBW. The obtained results ensure that MFO algorithm has an excellent prospect to be used as an efficient optimizer for obtaining the optimal value of current excitation weights and the inter element spacing between the array elements for the synthesis and pattern modeling of a symmetrical linear antenna array and the non-uniform single ring circular antenna array.

ACKNOWLEDGMENT:

A special thanks to Prof. G. S.N. Raju (Vice Chancellor) for suggestions, constructive critiques and continued supports.

REFERENCES

1. Babayigit B, Senyigit E. Design optimization of circular antenna arrays using Taguchi method. *Neural Comput & Applic*. 2017; 28(6):1443-1452.
2. Ballanis CA. *Antenna Theory Analysis and Design*. 2nd ed. New York: John Willey and Son; 1997.
3. Dib N. Design of linear antenna arrays with low side lobes level using symbiotic organisms search. *Prog Electromagn Res B*. 2016; 68:55-71.
4. Dib N, Goudos S, Muhsen H. Application of Taguchi's optimization method and self-adaptive differential evolution to the synthesis of linear antenna arrays. *Prog Electromagn Res*. 2010; 102:159-180.
5. Eiben AE, Smit SK. Parameter tuning for configuring and analyzing evolutionary algorithms. *Swarm Evol Comput*. 2011;1(1):19-31.
6. Elliott RS. *Antenna Theory and Design*. New Jersey: IEEE Press; 2003), Revised edition.
7. Kennedy, J., Eberhart, R., Particle swarm optimization, IEEE International Conference on Neural Network, Perth,(1995) pp. 1942-848.
8. Khodier M, Al-Aqeel M. Linear and circular array optimization: a study using particle swarm intelligence. *Prog Electromagn Res B*. 2009;15:347-373
9. Khalilpourazari S, Pasandideh SHR. Multi-item EOQ model with nonlinear unit holding cost and partial back ordering: moth-flame opti- mization algorithm. *Jf Ind Prod Eng*. 2017; 34(1):42-51.
10. Mirjalili S. Moth-flame optimization algorithm: a novel nature-inspired heuristic paradigm. *Knowl-Based Syst*. 2015;89:228-249.
11. Panduro M, Mendez A, Dominguez R, Romero G. Design of non-uniform antenna arrays for side lobe reduction using the method of genetic algorithm. *AEU Int J Electron Commun*. 2006; 60(7):713-717.
12. Ram G, Mandal D, Kar R, Ghoshal SP. Circular and concentric circular antenna array synthesis using cat swarm optimization. *IETE Tech Rev*. 2015; 32(3):204-217.
13. Zhou A, Qu B-Y, Li H, Zhao S-Z, Suganthan PN, Zhang Q. Multiobjective evolutionary algorithms: a survey of state of the art. *Swarm Evol Comput*. 2011;1(1):32-49.
14. Zhao H, Zhao H, Guo S. Using GM (1,1) optimized by MFO with rolling mechanism to forecast the electricity consumption of Inner Mon- golia. *Appl Sci*. 2016;6(1):1-18.

International Journal of Advanced Science and Technology
Vol. 29, No. 5s, (2020), pp. 141-151

Reduction of PAPR and BER Using Hybrid Optimization GWOFA in OFDM Systems

[1]Reddi Sridevi, [2]Dr.T.Madhavi
[1]*Assistant Professor, Department of ECE, Dr. L.B College of Engineering, Visakhapatnam, India.*
[2]*Professor, Dept. of EECE, GIT, GITAM (Deemed to Be University), Visakhapatnam, India.*

Abstract
Orthogonal frequency division multiplexing (OFDM) system can assure a greater immunity to multipath fading under a wireless communication environment. But the major challenge is to address the issue of high peak to average power ratio (PAPR) in OFDM systems. Orthogonal frequency division multiplexing (OFDM) is an efficient multi-carrier modulation technique that underlies most of the current and probably future high-speed wireless communication systems. However, the OFDM waveform is characterized by a high peak-to-average power ratio (PAPR), especially when a large number of subcarriers are used. A high PAPR is a major waveform defect since it leads to non-linear distortion when passing through the transmitter's power amplifier. Most of the PAPR reduction techniques found in the literature reduce the PAPR mainly at the cost of either excessive computational complexity or degrading the transmission bit error rate (BER). In this paper, a new hybridization of optimization techniques is proposed. Combination of SLM with grey wolf and firefly algorithm (GWOFA) is proposed. The obtained results are compared with other techniques like SLM, GA, FA, GWO. The analytical and simulated results show that the proposed technique is capable of reducing the PAPR effectively with negligible effect on BER.

Keywords:
OFDM, Grey wolf optimization, Firefly Algorithm, PAPR, BER

1. Introduction

Orthogonal Frequency Division Multiplexing (OFDM) is a digital multi carrier (MC) modulation scheme, which uses a large number of closely spaced orthogonal sub-carriers [1]. The transmit signals in an orthogonal frequency division multiplexing (OFDM) system will have high peak values in the time domain since many subcarrier components are added via an inverse fast Fourier transform (IFFT) operation. The transmission data through the use of multicarrier modulation techniques like orthogonal frequency division multiplexing (OFDM) has been considered as a good choice for data transmission over single carrier systems. The OFDM technique has various advantages and now being used in a number of wireless communication systems. Meanwhile, the multiple-input multiple-output (MIMO) with OFDM system, has recently attracted a great deal of attention due to its various advantages such as high data rate, spectral efficiency, diversity in a fading environment, and robustness to channel fading [2].

Hence, a system with OFDM modulation and multiple transmit and multiple receive antennas (MIMOOFDM) is now becoming adopted by several applications such as digital audio broadcasting (DAB), Worldwide Interoperability for Microwave Access (WiMAX), the fourth generation of telecommunication systems (4G), digital video broadcasting (DVB), high speed WLAN standards, and many others application areas of MIMO-OFDM [3]. But besides these useful advantages, it still suffers from the high envelope fluctuations of the transmitted signal called the peak-toaverage power ratio (PAPR), which decreases the efficiency of high power amplifiers (HPA), improves the complexity of nonlinear elements, and causes out-of-band radiation with degradation of bit error rate (BER).

To deal with this problem, several solutions have been proposed to mitigate the high PAPR of OFDM [4] and MIMO-OFDM signals [5], as clipping [6], clipping and filtering [7], coding [8], tone injection [9], peak windowing [10], selected mapping [11], and partial transmit sequence (PTS) [12].

Selective mapping method is one of the promising PAPR reduction technique without any distortions in the signals. A new approach of PAPR reduction method is applying genetic optimization to

ISSN: 2005-4238 IJAST
Copyright ⓒ 2020 SERSC

the SLM . GA is applied to SLM-OFDM system, by which the random populations are considered whose fitness values are evaluated for looking the most appropriate section rotation elements and decreasing computational complexity[13].

A new technique for solving core problem of OFDM by reducing the PAPR. The technique proposed is Firefly optimization which is applied along with selective mapping technique in which rotation of phase factor for search was compared with initial OFDM, conventional SLM-OFDM and also compared with genetic algorithm based SLM[14]

Further, Grey wolf optimization technique is combined with SLM to reduce the PAPR, the grey wolf optimization the PAPR reduce to some extent. More studies need to be emerged to reduce the PAPR. There is much better reduction in PAPR value using grey wolf by which the problem of transmitting signal is minimised[15].

In [16], the performance and the traits of ODFM system is observed. A new PAPR reduction technique is implemented. The behaviour grasshopper is studied and SLM is combined with grasshopper optimization algorithm to achieve good rate of decrease in PAPR.

In this paper , hybridization of optimization technique is performed to reduce the PAPR and also verify the BER at the receiving end. The combination of grey wolf and firefly optimization is performed with selective mapping to obtain the best PAPR and Bit error rate.

2. OFDM System and SLM Approach

A. PAPR of OFDM Signal

The transmission of signal through the use of transceiver based on orthogonal frequency division multiplexing (OFDM) system is a typical technique which divides the effective spectrum channel to a number of orthogonal subchannels, and with equal bandwidth, each subchannel handles independently with its own data using individual subcarrier, and the OFDM signal is the sum of all independent subcarriers. In transmission systems with multicarrier signal, the input data of
binary sequences are mapped into symbols by a modulator (PSK, QPSK, QAM, etc.). Then, the N symbols
$X = [X_0, X_1, \ldots\ldots, X_{N-1}]^T$ are inserted into the IFFT block to modulate each subcarrier independently and to obtain the OFDM signal in time domain
$x = [x_0, x_1, \ldots\ldots, x_{N-1}]^T$
The complex envelope of OFDM signal in the discrete time domain with oversampled factor L (usually used L=4) can be mathematically written as

$$x[n] = \frac{1}{\sqrt{N}} \sum_{k=0}^{N-1} X_k e^{(j2\pi nk/LN)}, 0 \le n \le LN-1 \qquad (1)$$

where N is the number of subcarriers and X_k is the nth complex symbol carried and transmitted by the k_{th} subcarrier.

From equation (1), the signal in time domain generated by IFFT operation consists N number of independently modulated and orthogonal subcarriers with large peak values (PAPR) when added up at the output of IDFT block. The PAPR of the OFDM signal in discrete time is defined as the ratio between the maximum power and the average power of the complex OFDM signal, and it can be defined as

$$PAPR\{x[n]\} = \frac{\max\{|x[n]|^2\}}{E\{|x[n]|^2} , 0 \le n \le LN-1 \qquad (2)$$

where x[n] is given by (1) and E{ · } denotes the expected value (average power).

PAPR reduction techniques can be divided into two main categories [17]. The first is distortion-less techniques, which are applied prior to the IFFT stage. The second is signal distortion techniques, which are applied after the IFFT stage. Any PAPR technique presents a trade-off between a set of main performance parameters, namely: PAPR and BER.
The peak power occurs when modulated symbols are added with the same phase. It is easy to see from above that PAPR reduction may be achieved by decreasing the numerator, increasing the denominator, or both. The effectiveness of a PAPR reduction technique is measured by the complementary cumulative

Copyright ⓒ 2020 SERSC

distribution function (CCDF), which is the probability that PAPR exceeds some threshold, i.e.: CCDF = Probability (PAPR > $p0$) (3)
Where, $p0$ is the threshold.

B. SLM for OFDM

The selective mapping (SLM) scheme, which is one of the PAPR reduction methods, can be used in OFDM system for reducing PAPR. Fig. 1 shows the block diagram of SLM. In SLM scheme, the data block $X = [X_1, X_2, \dots\dots, X_N]$ is multiplied by the scrambling sequences,
$P^d = [P_1^d, P_2^d, \dots\dots, P_N^d], d = 1,2, \dots\dots, D$ to obtain the D sequences $X^d = [X_1^d, X_2^d, \dots\dots, X_N^d]$. These D sequences are used to generate the candidate sequences,
$x^d = [x_1^d, x_2^d, \dots\dots, x_N^d], d = 1,2, \dots\dots, D$ by the IFFT operation.

Therefore, the number of IFFT operation in this process is D. The signal with the lowest PAPR is selected from these candidate sequence and be the transmitted signal. In order for the receiver to recover the data block of the transmitted signal, the index of the selected phase should be sent as the side information to receiver.

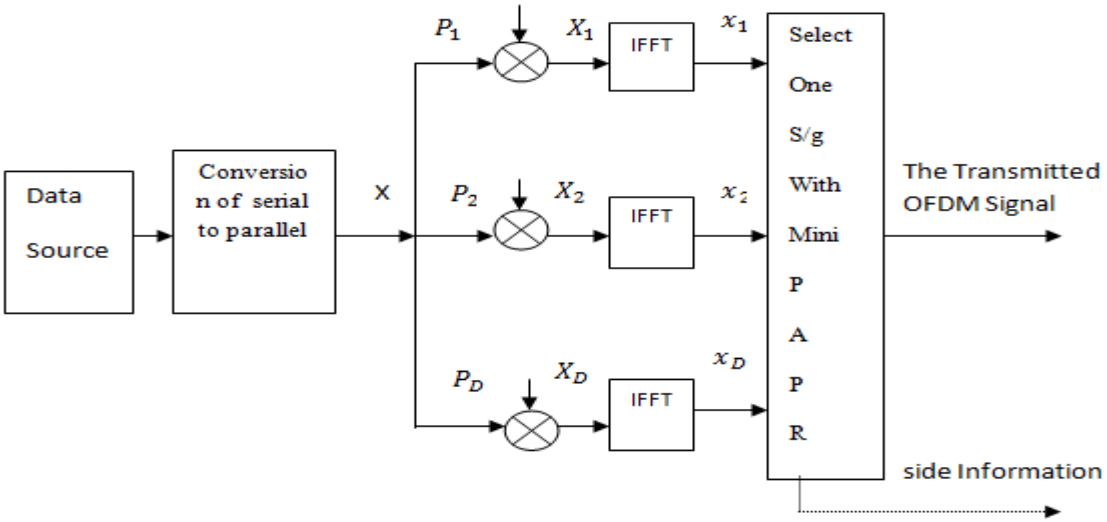


Fig 1. SLM System Model

3. Hybrid Optimization SLM-GWOFA

A. Firefly Optimization

Fireflies are unisex with the goal that each individual firefly will be pulled into different fireflies paying little mind to their opposite sex. The attractiveness and brightness are directly proportional to each other, and they both lessening as their separation increments. Along these lines for any two blazing fireflies, the less splendid one will attrack the more brilliant one. On the off chance that there is no more brilliant one than a specific firefly, it will move randomly. The brightness of a firefly is controlled by the scene of the goal work[18].

As a firefly's attractiveness is proportional to the light intensity seen by adjacent fireflies, can now define the variation of attractiveness β with the distance r by

$$\beta = \beta_0 e^{-\gamma r^2} \quad (4)$$

Where β_0 is attractiveness at r=0
The firefly i is attracted to another more brighter firefly j and move towards j and the sane is determined by

$$x_i^{t+1} = x_i^t + \beta_o e^{-\gamma r_{ij}^2}\left(x_j^t - x_i^t\right) + \alpha_t \epsilon_i^t \quad (5)$$

Copyright ⓒ 2020 SERSC

Where the second term $\beta_o e^{-\gamma r_{ij}^2}\left(x_j^t - x_i^t\right)$ is concern based on the attraction. The third term i.e $\boldsymbol{\alpha_t \epsilon_i^t}$ is randomization with $\boldsymbol{\alpha_t}$ being the randomization parameter, and $\boldsymbol{\epsilon_i^t}$ is a vector of random numbers drawn from a Gaussian distribution or uniform distribution at time *t*.

B. Grey Wolf Optimization

The Grey Wolf Optimizer(GWO) algorithm mimics the leadership hierarchy and hunting mechanism of grey wolves in nature. Four types of grey wolves such as alpha, beta, delta, and omega are employed for simulating the leadership hierarchy.

The Gray Wolf Optimizer(GWO) calculation copies the administration order and chasing mechanism of wolves. Four different of grey wolves need to be considered that are alpha, beta, delta, and omega are utilized for simulating the authority chain of command. There are three important steps in hunting- searching for prey, encircling prey and attacking the prey. These three are implemented to perform optimization technique. The three best agents are denoted as $P(\alpha), P(\beta)\ and\ P(\delta)$. The velocities are termed as Eq (6),(7),(8)

The equations can be shown as:

$$V_\alpha = |C.P_\alpha(t) - P(t)| \quad (6)$$

$$V_\beta = \left|C.P_\beta(t) - P(t)\right| \quad (7)$$

$$V_\delta = |C.P_\delta(t) - P(t)| \quad (8)$$

The position are updated as Eq (9), (10) (11):

$$P_1 = P_\alpha - B.V \quad (9)$$

$$P_2 = P_\beta - B.V \quad (10)$$

$$P_3 = P_\delta - B.V \quad (11)$$

Where B and C are the vector coefficients which are calculated as Eq 10 and Eq 11

$$B = 2b.r_1 - b \quad (12)$$

$$C = 2.r_2 \quad (13)$$

C. Hybridization GWOFA

The grey wolf optimization and Firefly optimization is combined to form a better search of agents to obtain the best position, to obtain the best PAPR value.

Here we consider the velocities of the grey wolf as,

$$R_\alpha = \frac{|C.P_\alpha(t) - P(t)|}{d_{max}} \quad (14)$$

$$R_\beta = \frac{|C.P_\beta(t) - P(t)|}{d_{max}} \quad (15)$$

$$R_\gamma = \frac{|C.P_\gamma(t) - P(t)|}{d_{max}} \quad (16)$$

where $d_{max} = (U_B - L_B) * \sqrt{Dim}$

Dim= Signal Length

Then the velocity is updated w.r t firefly and is given as,

$$V_\alpha = \beta_0 e^{-\gamma R_\alpha^m} \quad (17)$$

$$V_\beta = \beta_0 e^{-\gamma R_\beta^m} \quad (18)$$

$$V_\gamma = \beta_0 e^{-\gamma R_\gamma^m} \quad (19)$$

Here we consider $\beta_0 = 2, m = 2, \gamma = 1$

Now the positions are considered according to eq (9), (10), (11)

Algorithm for GWOFA-SLM

The GWOFA based SLM algorithm is given as:

Step1: Initialise input data $I_x = I_1 I_2 I_3 \dots\dots\dots\dots I_n$

Step2: Serial bit of data converted to parallel bits

Step3. Rotating the phase of bits and applying GWOFA for the bits

Step 4. Initialization of the search agents (wolf)

Search process w.r.t fireflies

Copyright ⓒ 2020 SERSC

Step5: Calculate the fitness function
Step6: Find the best position with respect to the velocities given as $V_\alpha, V_\beta \; and \; V_\delta$
Step7: Update the position
Step8: Calculate the fitness function
Step9: update the position of $V_\alpha, V_\beta \; and \; V_\delta$ w.r.t fireflies
Step10. Find the best and form a unique phases
Step11. Obtain the Min PAPR signal

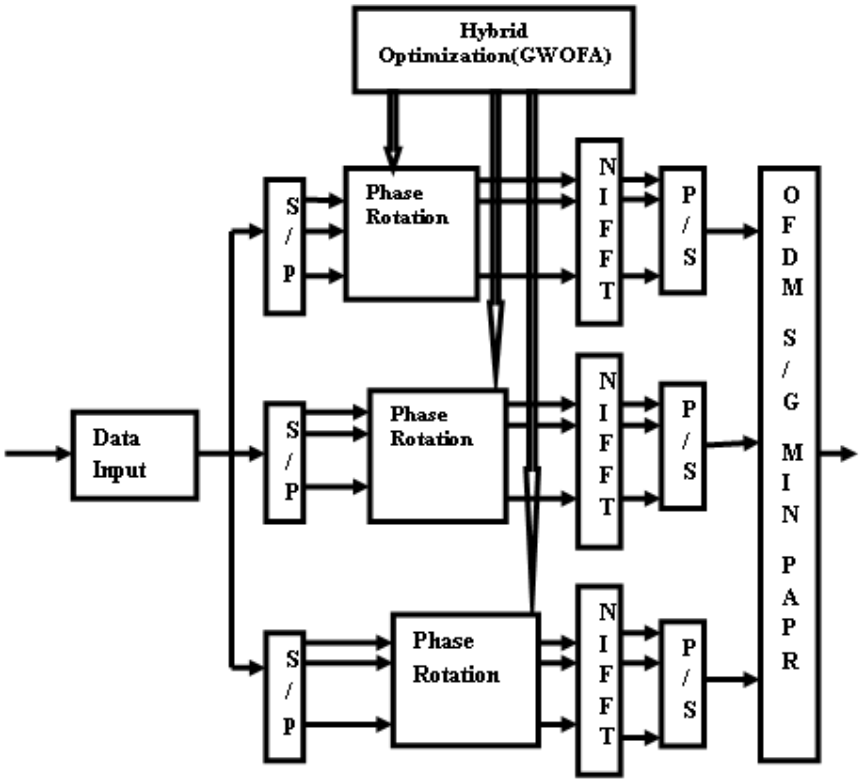


Fig 2. Proposed SLM GWOFA Model

4. Results and Discussion

In this section, we present simulated results for evaluating and comparing the performance of the proposed technique to other OFDM reduction techniques. Simulations are performed on a baseband model of the OFDM transmitter and receiver. PAPR performance is most commonly evaluated by the Complementary Cumulative Distribution Function (CCDF) metric, which is defined as the probability that the OFDM signal PAPR (ρ) exceeds a given threshold (ρ_0).

Copyright ⓒ 2020 SERSC

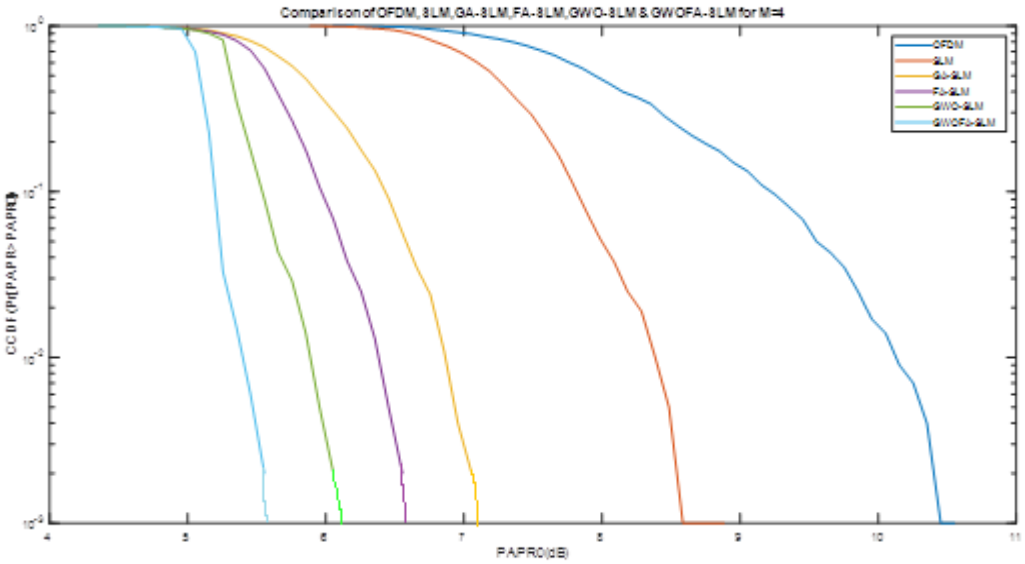


Fig 3. PAPR for M=4

Initially, we observe that the proposed technique achieves significant reduction of PAPR compared to the original waveform, where PAPR does not exceed 8.90 dB for SLM, 7.05 dB for GA-SLM, 6.62 dB for FA-SLM, 6.05 dB for GWO-SLM and 5.5 dB for GWOFA-SLM. These values agree with the analytic curves in Fig. 3.

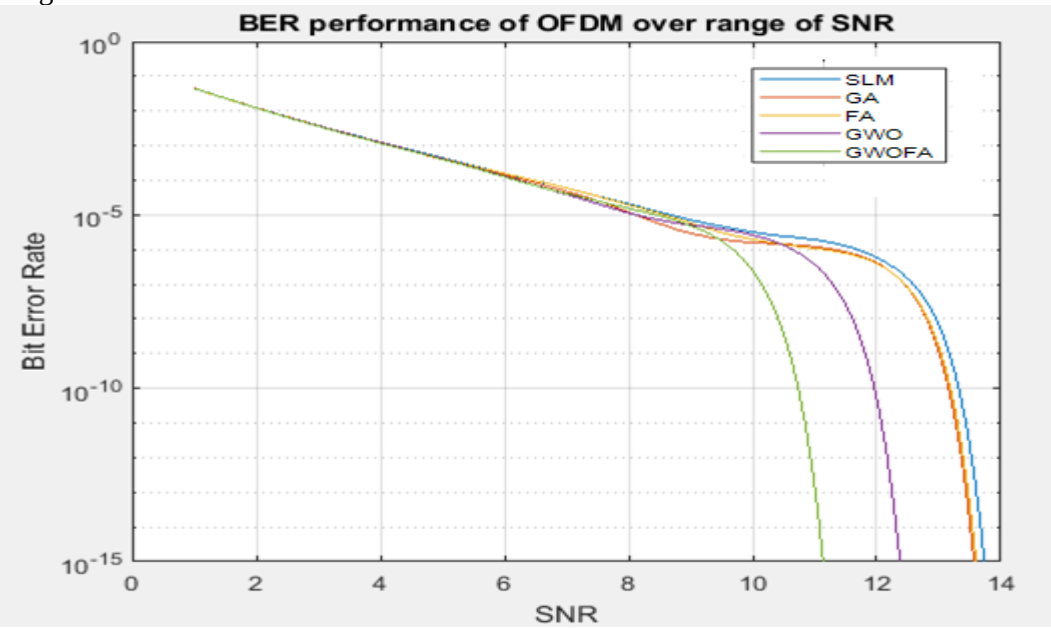


Fig 4. BER vs SNR for M=4

As compared to other techniques, the proposed technique outperforms all other examined techniques which has an obvious advantage in terms of PAPR reduction. However, the reduction in PAPR effects on receiving end is shown in BER performance as shown in fig 4.

Here we consider different values and 'M' and simulate the results, as shown below.

ISSN: 2005-4238 IJAST
Copyright ⓒ 2020 SERSC

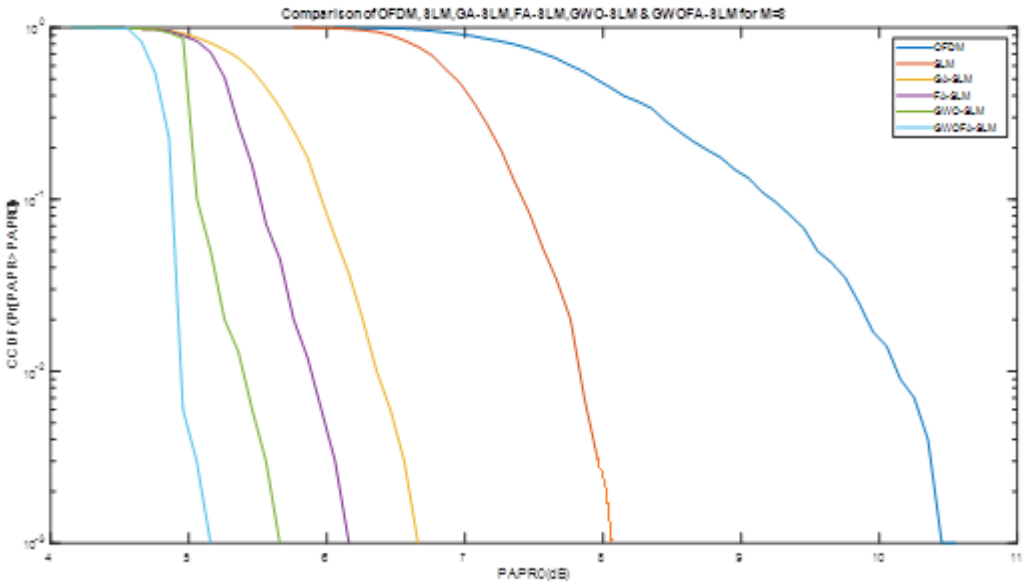


Fig 5. PAPR for M=8

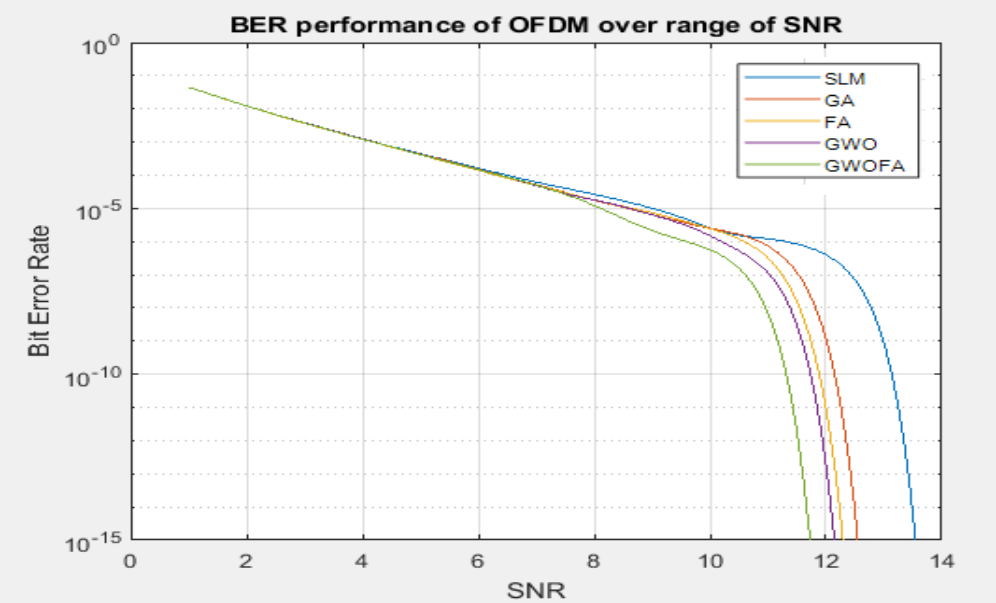


Fig 6. BER vs SNR for M=8

ISSN: 2005-4238 IJAST
Copyright ⓒ 2020 SERSC

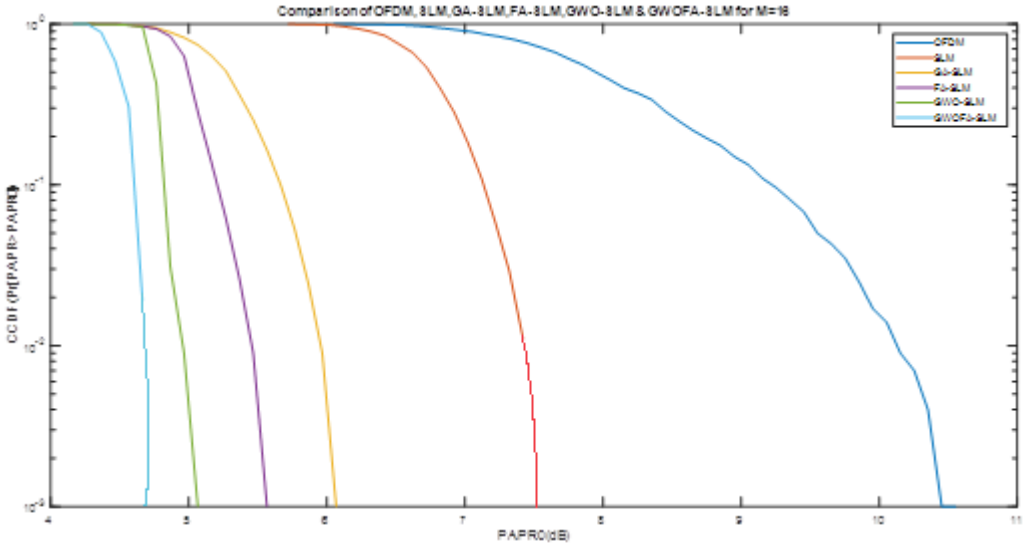


Fig 7. PAPR for M=16

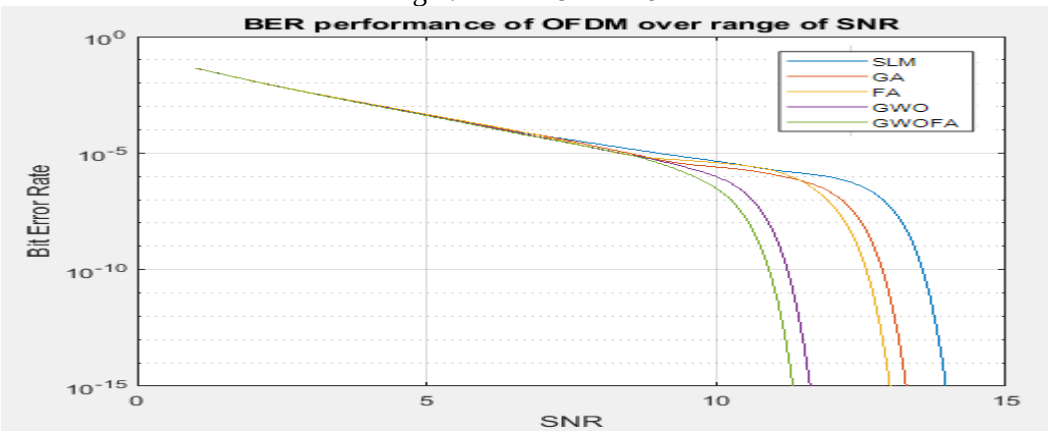


Fig 8. BER vs SNR for M=16

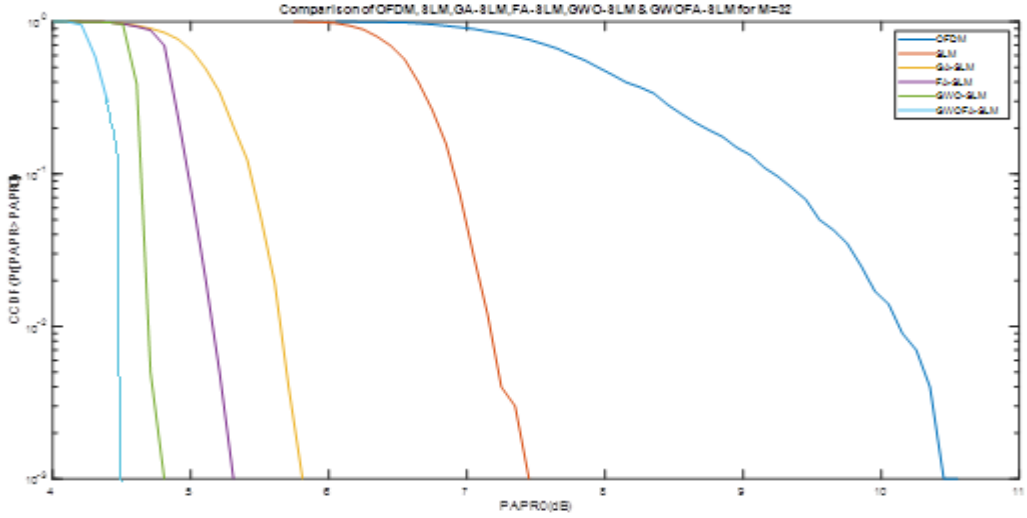


Fig 9. PAPR for M=32

Copyright ⓒ 2020 SERSC

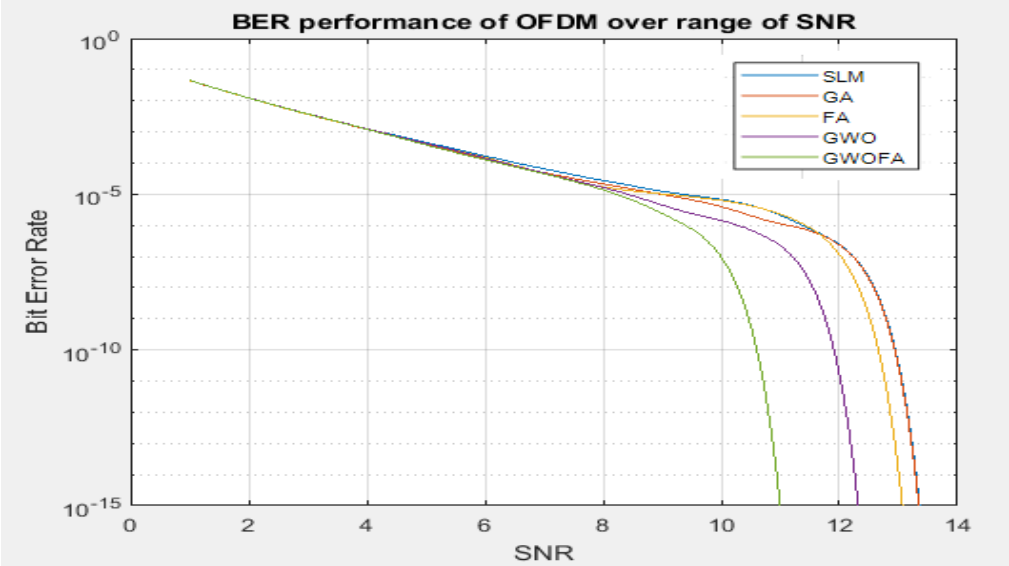


Fig 10. SNR vs BER for M=32

Here, from the above results, the PAPR reduction technique that maintains the effectiveness and simplicity of signal distortion techniques without degrading system BER. These gains are achieved in return for a slight (and controllable) reduction. However, we argue that although signal distortion techniques do not send side information, their degraded BER performance will probably entail applying channel coding in order to preserve the integrity of data. Hence, effectively, the data rate would be significantly reduced, in addition to the impact on computational complexity associated with the decoding process. On the other hand, we showed that the proposed technique is capable of achieving significant PAPR reduction, without BER degradation.

Table 1. Comparison of PAPR using various Techniques

Technique/M=	**4**	**8**	**16**	**32**
SLM	8.90dB	8.02dB	7.51dB	7.51dB
SLM-GA	7.05dB	6.65dB	6.07dB	5.81dB
SLM-FA	6.62dB	6.18dB	5.61dB	5.36dB
SLM-GWO	6.05dB	5.66dB	5.07dB	4.8dB
SLM-GWOFA	**5.5dB**	**5.16dB**	**4.67dB**	**4.4dB**

Table 2. Comparison BER w.r.t SNR of 11dB using various Techniques

Technique/M=	**4**	**8**	**16**	**32**
SLM	$10^{-5.6}$	$10^{-5.2}$	10^{-5}	$10^{-5.5}$
SLM-GA	$10^{-5.7}$	$10^{-5.5}$	$10^{-5.5}$	$10^{-5.5}$
SLM-FA	$10^{-5.8}$	10^{-6}	10^{-6}	$10^{-5.5}$
SLM-GWO	$10^{-5.9}$	$10^{-6.5}$	10^{-7}	$10^{-6.5}$
SLM-GWOFA	10^{-8}	$10^{-8.5}$	10^{-10}	10^{-15}

In table 2, we considered SNR as 11dB, the proposed technique SLM-GWOFA having zero bit error rate for SNR more than 11dB. The proposed techniques gives a promising value of PAPR, without degrading the BER.

5. Conclusion

Orthogonal frequency division multiplexing (OFDM) is known for its superiority and has become one of the standard choices for high speed data transmission over a wireless communication channel. OFDM technique is specially used for multicarrier data transmission but, the major challenge in OFDM system is

Copyright ⓒ 2020 SERSC

that a high peak to average power ratio (PAPR) will be resulted. In this paper, a new hybrid technique is proposed i.e GWOGA based SLM method is used for the reduction of PAPR in OFDM systems. It is clear evident from the simulation results, the proposed method meant for reducing PAPR of OFDM system offered an improved bit error rate (BER). It has been proved that the proposed technique performed well when compared to the existing PAPR reduction methods.

References

1. Y. Huo, X. Dong, andW. Xu, ``5G cellular user equipment: From theory to practical hardware design," *IEEE Access*, vol. 5, pp. 13992_14010, 2017.
2. Y. Wu and W. Y. Zou, "Orthogonal frequency division multiplexing: a multi-carrier modulation scheme," *IEEE Transactions on Consumer Electronics*, vol. 41, no. 3, pp. 392–399, 1995.
3. Y. S. Cho, J. Kim, W. Y. Yang, and C. G. Kang, *MIMO-OFDM Wireless Communications with MATLAB*, John Wiley & Sons, Hoboken, NJ, USA, 2010.
4. S. P. DelMarco, "A constrained optimization approach to compander design for OFDM PAPR reduction," *IEEE Transactions on Broadcasting*, vol. 64, no. 2, pp. 307–318, 2018.
5. L. Amhaimar, S. Ahyoud, and A. Asselman, "An efficient combined scheme of proposed PAPR reduction approach and digital predistortion in MIMO-OFDM systems," *International Journal on Communications Antenna and Propagation*, vol. 7, no. 5, 2017.
6. J. Wang, Y. Guo, and X. Zhou, "PTS-clipping method to reduce the PAPR in ROF-OFDM system," *IEEE Transactions on Consumer Electronics*, vol. 55, no. 2, pp. 356–359, 2009.
7. K. Anoh, C. Tanriover, B. Adebisi, and M. Hammoudeh, "A new approach to iterative clipping and filtering PAPR reduction scheme for OFDM systems," *IEEE Access*, vol. 6, pp. 17533–17544, 2018.
8. A. E. Jones, T. A. Wilkinson, and S. K. Barton, "Block coding scheme for reduction of peak to mean envelope power ratio of multicarrier transmission schemes," *Electronics Letters*, vol. 30, no. 25, pp. 2098-2099, 1994.
9. J.-C. Chen and C.-K. Wen, "PAPR reduction of OFDM signals using cross-entropy-based tone injection schemes," *IEEE Signal Processing Letters*, vol. 17, no. 8, pp. 727–730, 2010.
10. G. Chen, R. Ansari, and Y. Yao, "Improved peak windowing for PAPR reduction in OFDM," in *Proceedings of VTC Spring 2009-IEEE 69th Vehicular Technology Conference*, pp. 1–5, Barcelona, Spain, April 2009.
11. X. Cheng, D. Liu, S. Feng, H. Fang, and D. Liu, "An artificial bee colony-based SLM scheme for PAPR reduction in OFDM systems," in *Proceedings of 2017 2nd IEEE International Conference on Computational Intelligence and Applications (ICCIA)*, pp. 449–453, Beijing, China, September 2017.
12. H.-S. Joo, K.-H. Kim, J.-S. No, and D.-J. Shin, "New PTS schemes for PAPR reduction of OFDM signals without side information," *IEEE Transactions on Broadcasting*, vol. 63, no. 3, pp. 562–570, 2017.
13. Tarik Hadj Ali and A. Hamza, " A new SLM technique based on Genetic Algorithms for PAPR reduction in OFDM systems", IEEE DOI 10.1109/CICN.2016.113DOI
14. R Sridevi and Dr. T Madhavi, "SLM Technique based on Firefly Algorithm for Reduction of PAPR in OFDM Systems ", Jour of Adv Research in Dynamical & Control Systems, Vol. 11, 06-Special Issue, 2019.
15. R Sridevi and Dr. T Madhavi, " Reduction of PAPR in OFDM Signals Using Grey Wolf Optimization combined with SLM ", DSMLA 2019: Proceedings of the 1st International Conference on Data Science, Machine Learning and Applications.
16. Reddi Sridevi, Dr.T.Madhavi, Sreenivasulu Ummadisetty, " Performance Improvement of OFDM Systems by Reducing PAPR using SLM-Grasshopper Optimization", International Journal of Innovative Technology and Exploring Engineering (IJITEE), ISSN: 2278-3075, Volume-9, Issue-2S3, December 2019.

Copyright ⓒ 2020 SERSC

17. Y. Rahmatallah and S. Mohan, ``Peak-to-average power ratio reduction in OFDM systems: A survey and taxonomy," *IEEE Commun. Surveys Tuts.*, vol. 15, no. 4, pp. 1567_1592, 4th Quart., 2013.
18. Yang, X.S.: Firefly algorithms for multimodal optimization. In: Stochastic Algorithms: Foundations and Applications, SAGA 2009. Lecture Notes in Computer Sciences, vol. 5792, pp. 169–178 (2009)
19. Patil, V., Patil, H., Shah, K., Vasani, J., Shetty, P.Diastolic dysfunction in asymptomatic type 2 diabetes mellitus with normal systolic function(2011) Journal of Cardiovascular Disease Research, 2 (4), pp. 213-222.
DOI: 10.4103/0975-3583.89805
20. P. V. S. S sanjaymitra, g. N. K. Ganesh (2018) dissolution and solubility enhancement strategies: current and novel prospectives. Journal of Critical Reviews, 5 (3), 1-10. doi:10.22159/jcr.2018v5i3.23451s

ISSN: 2005-4238 IJAST
Copyright ⓒ 2020 SERSC

Optimization of PAPR in MB-OFDM UWB Signals Using SM-HOA Technique

[1]Reddi Sridevi, [2]Dr. T. Madhavi

[1] Assistant Professor, Department of ECE, Dr. L.B College of Engineering, Visakhapatnam, India.
[2]Professor, Dept. of ECE, GIT, GITAM (Deemed to Be University), Visakhapatnam, India.

Abstract

In wireless communication systems some require high data rate which can be greater than 100Mb/s which is a short range. Here ultra-wideband (UWB) systems can be used as it has high channel capacity. The spectrum available in UWB is used in orthogonal frequency division multiplexing systems with multi band (MB-OFDM) for various applications in communication. The major barrier in communication system is high peak average power ratio (PAPR) due to the disturbances caused in transmitting components which are nonlinear in nature. It is very much essential to reduce the PAPR to maximum extent in MB-OFDM UWB signals. In this paper, Hybrid optimization technique is considered by combining Grey-wolf and firefly algorithm for PAPR reduction. The noise reduction is performed for the UWB signals and results need to be analysed. In this paper the evaluation of proposed algorithm is shown by calculating the error rate per bit (BER) and PAPR. The obtained results are compared with other optimization techniques. Our results demonstrated hybridization of optimization technique is a promising technique for the transmission of MB-OFDM UWB signals compared to genetic algorithm, firefly optimization and grey wolf optimization-based MB-OFDM UWB signal transmission.

Keywords: *OFDM, UWB Signals, Firefly Algorithm, Grey wolf Optimization, PAPR, BER*

1. Introduction

In wireless communication systems short distance for transmission of data with high speed are given more importance in present scenario. The ultra-wide band (UWB) technology meets the requirement among the users [1]. In-order to use the entire bandwidth effectively which is available in UWB spectrum, OFDM systems is designed with multi-bands which is said to be MB-OFDM [2]. As the range of bandwidth increases, the number of sub-channels also increases this phenomenon leads to increase in peak average power ratio (PAPR). The major task is to reduce PAPR as the high PAPR limits the capacity of the channels which is occurred by High power amplifiers (HPA). The distortions present in OFDM systems are linear and nonlinear. Most of the signal interference problem in signals is caused by nonlinear distortions. The variations like increase or decrease in bit error rate depend on the interference which occurs in in-band and out-band. If the in-band interference increases the BER also increases and vice-versa. The inter-modulation and signal constellation are caused due to in-band interference and the spreading of spectral via channels is caused due to out-band interference. If there are no distortions in the transmitting signals, the PAPR can be reduced. The major interest in to come up with new techniques for reducing of PAPR, one of such technique is clipping and which is easy and simple to implement [3]. This is one of the initial techniques which is a nonlinear process. It helps in reducing the in-band and out-bands interferences. Performance of filtering processed by clipping helps in reduction of peaks that are reproduced, in [4] turbo codes are generated so that clipping effect can be reduced. Many techniques have been introduced for reduction of PAPR, in [5] a tunable predistorter based on Rapp's SSPA model is been

proposed. Further optimization techniques were introduced by which the process helps in obtaining the best solution for reducing the PAPR. In this paper, combination of two optimization techniques is performed for find optimal value of PAPR in MB-OFDM ultra-wideband signals and the results are matched with other optimization techniques such as, firefly algorithm [6], grey-wolf algorithm [7], Grasshopper algorithm [8]. The results are evaluated using MATLAB tool and the performance measures calculated are PAPR and BER. These factors show the efficiency level of the techniques which are used.

2. Multi Band UWB System

The use of ultra-wideband technology has been increased in wireless communication systems as it has short range, flow rate of data is high, consumes lower power and provides bandwidth which is required for the system [9]. Standard Institution like Federal Communication Commission (FCC) recognises UWB technology having a bandwidth range of greater than 500MHz or it provides minimum of twenty present of the center frequency on which the operations of the concern systems perform. Major range of applications are mobile communications, GPS systems, Satellite communications, United states Navy services (USNS) etc in which most of them uses high range of bandwidth which are not having license. The band width range above 7.5GHz are not having permission to use which is been stated by FCC. So, FCC controls the emission of power in UWB devices to reduce the threshold limit of noise that is considered by other technologies which use the same band range. One of the main advantages is cost function, which is free for UWB user, rather than being expensive using other technology for similar band range. In [10], it is given that -40dBm W/MHz or 10nW/MHz of spectrum is the max power that is been limited in UWB devices and is very less when compared with wireless local area networks with a limit of 10mW/MHz. Some of the standard working committee projection reveal that UWB in present trend have a mini speed requirement of 110Mbps with a distance to cover is 10m. The speed is very high when compared to current Bluetooth technology with a max speed limit of 1Mbps. The channel capacity as shown $ChannelCapacity=B.W*log2(1+SNR)$ [12] states that due to decrease in power, SNR goes down, so Bandwidth should be very large for high channel capacity which is the advantage of UWB which has a minimum B.W of 500MHz. The power and the range is given by Friss transmission equation as shown which states that the $Power\ received \propto 1/Range2$**.**

As the power function is not directly proportional to range, the ranges used for different coding techniques can be extended to larger distance. In current conditions the wireless USB uses UWB for transmitting data that assures a speed of 480Mbps. It is the future standard for Bluetooth as seen by Bluetooth Special Interest group IEEE 802.15.1

A. Single Band Technology

The difference of single band and multiband is shown in Fig1 and Fig 2. The transmission of single carrier with a limited bandwidth range is shown in below fig 1. In [12] the single carrier transmission proposal was used in Motorola and Path Cerva based DS-CDMA technology. In which the direct sequence transmission is performed.

B. Multi Band OFDM

Multiband is simply dividing the original given band into several sub-bands. The multiband concept in UWB is as shown in below fig 2.

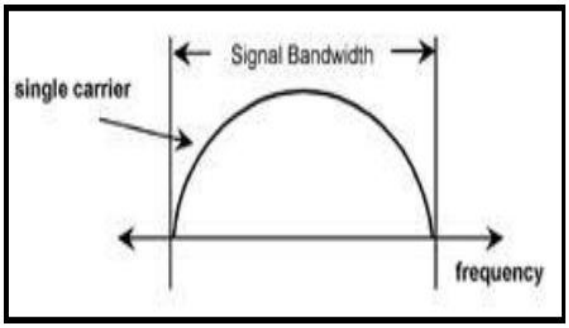


Fig: 1 Single Carrier Transmission

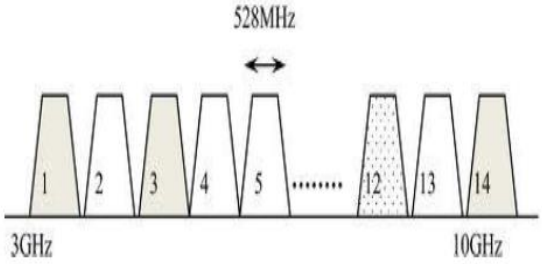


Fig:2 Multiband in UWB

The 7.5GHz of band is subdivided into smaller bands and each sub-band is of 528MHz wide according to FCC definition for UWB, minimum bandwidth requirement of 500MHz. It is of two types pulse-based transmission or OFDM based transmission.

3. UWB Signals in MB-OFDM

The equation which states the UWB signals in MB-OFDM can be shown as,

$$d_n = \frac{1}{N} \sum_{s1=0}^{N-1} D_{s1} \exp\left(\frac{j2\pi mn}{N}\right); n = 0,1,2, \ldots . N-1$$

where D_{s1} is the $s1^{th}$ symbol of QAM and for which the N values considered to be 128 [6]. The total length of the samples that are taken to be of L=165 in which the MB-OFDM symbol are designed with placements of the data blocks. To obtain the proposed length zero prefix position with 32 number of samples and the guard interval for every 5 samples. The design of MB-OFDM UWB signals is shown in below Fig 3.

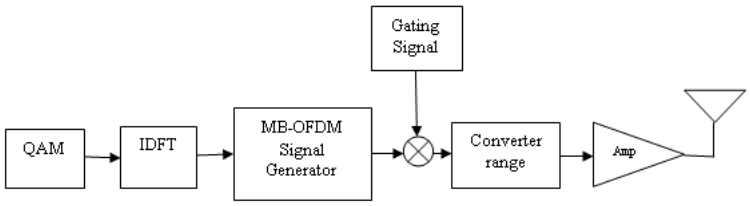


Fig 3. Transmitting side of MB-OFDM UWB signal [3].

The final k^{th} position of MB-OFDM symbol is given by

$$u_{k,l} = \begin{cases} 0 & 1 < l \leq 32 \\ d_{l-33} & 32 < l \leq 160 \\ 0 & 160 < l \leq 165 \end{cases}$$

Then the equation of Multi Band OFDM signal is given as

$$u(t) = \Re((\sum_{k=-\infty}^{\infty} \sum_{l=1}^{L} u_{k,l}\, h_{rect}(t - kT_{OFDM} - (l-1)\Delta t)\exp(-\mathrm{j}2\pi \mathrm{f_c t}))$$

In this a rectangular frequency response h_{rect} is a filter which is been bounded by $\pm 1/(2\Delta t)$, $T_{OFDM} = L\,\Delta t = 312.5$ nanoseconds is the MB-OFDM symbol period, $\Delta t = 1/(N\Delta f) \approx 1.9$ nanoseconds, and the complex number has real and imaginary parts, where the real part is denoted by $\Re$.

As said in [2] a specific time-frequency code is provided for MB-OFDM signals with a fourteen number of bands center frequencies for the signal hop's. Some of the gate functions are used for simulating the time-frequency code which is have a single range of frequency. These gate functions are multiplied as $g(t); T = bwT_{OFDM}$, $\tau = wT_{OFDM}$ where *b* represents the band number, the periodic signals in each band is **w.** The function for periodic gating is given as $g(t; T, \tau) = \sum_{k=-\infty}^{\infty} R(t - kT;\ \tau)$ where $R(t;\tau) = \begin{cases} 1 & 0 \leq t < \tau \\ 0 & otherwise \end{cases}$ and $T > \tau$

4. Proposed Hybridization for PAPR reduction

A. Firefly Optimization

Fireflies are unisex with the goal that each individual firefly will be pulled into different fireflies paying little mind to their opposite sex. The attractiveness and brightness are correlated to each other and are directly in proportional with each other, and they both lessening as their separation increments. Along these lines for any two blazing fireflies, the less splendid one will attract the more brilliant one. A specified firefly will be moving randomly which will be considered as a sharp fly for obtaining optimal result. The firefly brightness will be controlled based on the availability of flies.

The attractiveness concept in firefly is related with the intensity of light or brightness of the neighbour flies, the following is developed as the variation of attractiveness β with the distance *r* by

$$\beta = \beta_0 e^{-\gamma r^2} \qquad (4)$$

Where β_0 is attractiveness at r=0

The firefly *i* is attracted to another more brighter firefly j and move towards j and the sane is determined by

$$x_i^{t+1} = x_i^t + \beta_o e^{-\gamma r_{ij}^2}\left(x_j^t - x_i^t\right) + \alpha_t \epsilon_i^t \qquad (5)$$

Where the second term $\beta_o e^{-\gamma r_{ij}^2}\left(x_j^t - x_i^t\right)$ is concern based on the attraction. The third term i.e. $\boldsymbol{\alpha_t \epsilon_i^t}$ is randomization with $\boldsymbol{\alpha_t}$ being the randomization parameter, and $\boldsymbol{\epsilon_i^t}$ is a vector of random numbers drawn from a Gaussian distribution or uniform distribution at time *t*.

B. Grey Wolf Optimization

This optimization technique is based on the hunting nature of the wolf and the leadership way of behaving among the wolves which exist in nature. In this process initially four wolves are considered for obtaining the leadership qualities in search of prey. The names are termed as alpha, beta, delta, and omega respectively. The algorithm follows the administration skills and the general chasing concept of the grey wolves. In [9], the behaviour of wolves that are considered initially forms of chain of commands by its own individual level of authority. The hunting begins first by searching for the prey. Secondly the prey is been encircled, finally when the prey is stuck in within the boundary of wolves then prey gets attacked. After performing the three steps the final optimal solution is obtained. In this algorithm best agents need to identify and are denoted as $P(\alpha), P(\beta)\ and\ P(\delta)$. The velocities are termed as Eq. (6), Eq. (7), and Eq. (8)

The equations can be shown as:

$$V_\alpha = |C.P_\alpha(t) - P(t)| \quad (6)$$

$$V_\beta = \left|C.P_\beta(t) - P(t)\right| \quad (7)$$

$$V_\delta = |C.P_\delta(t) - P(t)| \quad (8)$$

The positions are updated as Eq. (9), Eq. (10), and Eq. (11):

$$P_1 = P_\alpha - B.V \quad (9)$$

$$P_2 = P_\beta - B.V \quad (10)$$

$$P_3 = P_\delta - B.V \quad (11)$$

Where B and C are the vector coefficients which are calculated as Eq. 10 and Eq. 11

$$B = 2b.r_1 - b \quad (12)$$

$$C = 2.r_2 \quad (13)$$

C. Hybridization of Optimization Techniques

The grey wolf optimization and Firefly optimization is combined to form a better search of agents to obtain the best position, to obtain the best PAPR value [11].

Here we consider the velocities of the grey wolf as,

$$R_\alpha = \frac{|C.P_\alpha(t) - P(t)|}{d_{max}} \quad (14)$$

$$R_\beta = \frac{|C.P_\beta(t) - P(t)|}{d_{max}} \quad (15)$$

$$R_\gamma = \frac{|C.P_\gamma(t) - P(t)|}{d_{max}} \quad (16)$$

where $d_{max} = (U_B - L_B) * \sqrt{Dim}$

Dim= Signal Length

Then the velocity is updated w.r.t. firefly and is given as,

$$V_\alpha = \beta_0 e^{-\gamma R_\alpha^m} \quad (17)$$

$$V_\beta = \beta_0 e^{-\gamma R_\beta^m} \quad (18)$$

$$V_\gamma = \beta_0 e^{-\gamma R_\gamma^m} \quad (19)$$

Here we consider $\beta_0 = 2, m = 2, \gamma = 1$. Now the positions are considered according to Eq. (9), Eq. (10), and Eq. (11).

Algorithm for SM-HOA

The SM-HOA algorithm given as,

Step1: Initialise input data $I_x = I_1 I_2 I_3 \ldots\ldots\ldots\ldots I_n$

Step2: Converting of SB of data to PB

Step3. The phase rotation process of bits is done, and hybrid optimization technique is applied

Step4. Consider the agents for search (wolves) and the process of search is based with respect to fireflies

Step5: Fitness function is evaluated

Step6: Find the best position with respect to the velocities given as $V_\alpha, V_\beta \; and \; V_\delta$

Step7: Update the position

Step8: Again, evaluate the fitness function after updating of positions

Step9: further update the position of $V_\alpha, V_\beta \; and \; V_\delta$ w.r.t. fireflies

Step10. Best solution needs to be identified

Step11. PAPR signal with minimum value is determined.

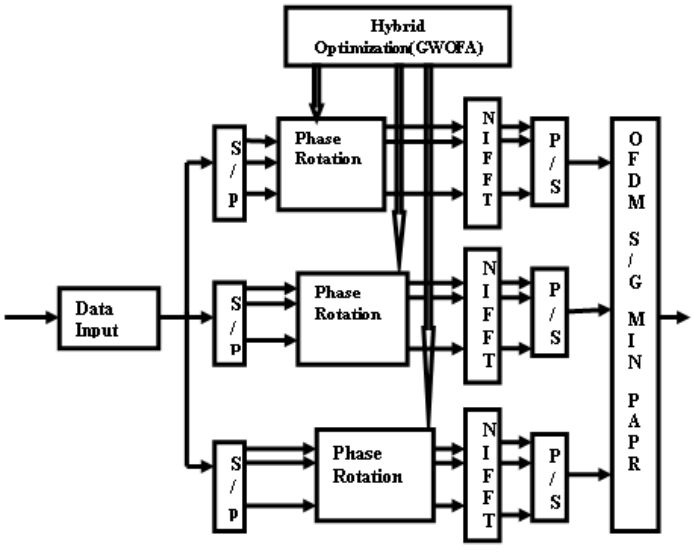


Fig 4. SM-HOA Model [11]

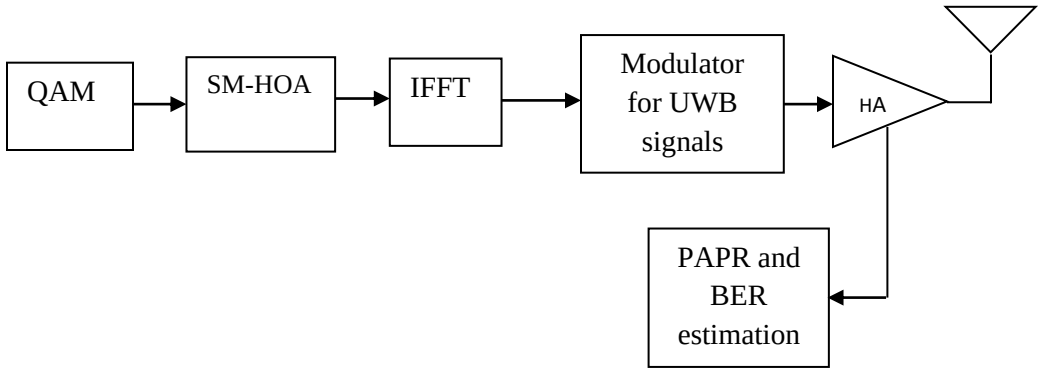


Fig 5. Proposed MB-OFDM-UWB hybrid system.

5. Results and Discussion

The results obtained using proposed technique is evaluated and shown in this section. Various techniques are been compared with the proposed hybrid optimization techniques. In this we consider multi band model for transmitting and receiving the information in OFDM system. CCDF metric is mostly used metric for evaluating the performance of PAPR. CCDF is the cumulative distribution function which judges the value of PAPR in OFDM signals for a given limit of threshold.

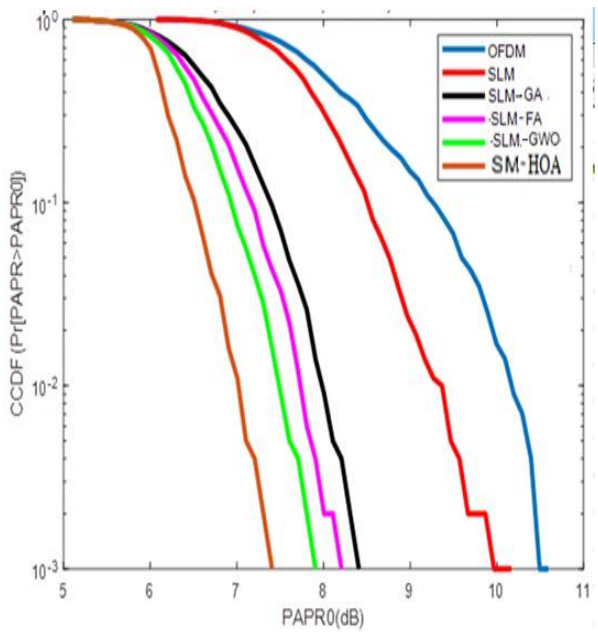


Fig 6. PAPR for M=2

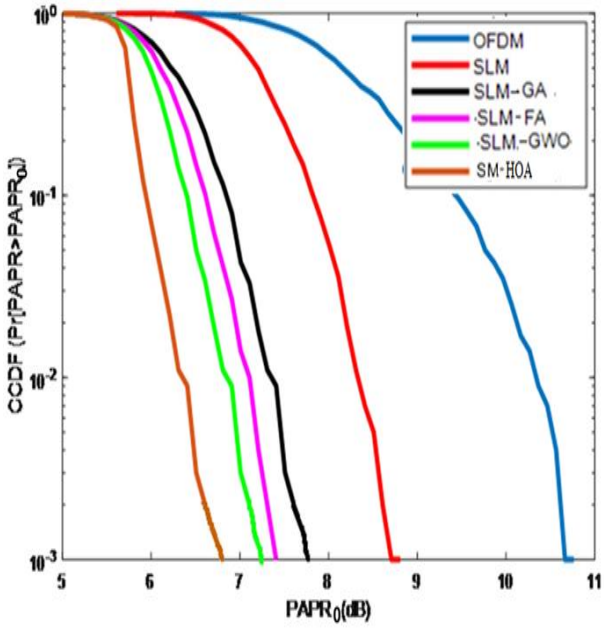


Fig 7. PAPR for M=4

The results shown prove that the proposed approach has good consideration for reducing the PAPR when compared with other approaches. The values of PAPR does not exceed 8.90 dB for SLM, 7.05 dB for SLM-GA, 6.62 dB for SLM-FA, 6.05 dB for SLM-GWO and 5.5 dB for SM-HOA. From fig 6 we can observe the values.

Here we consider different values and 'M' and simulate the results, as shown below.

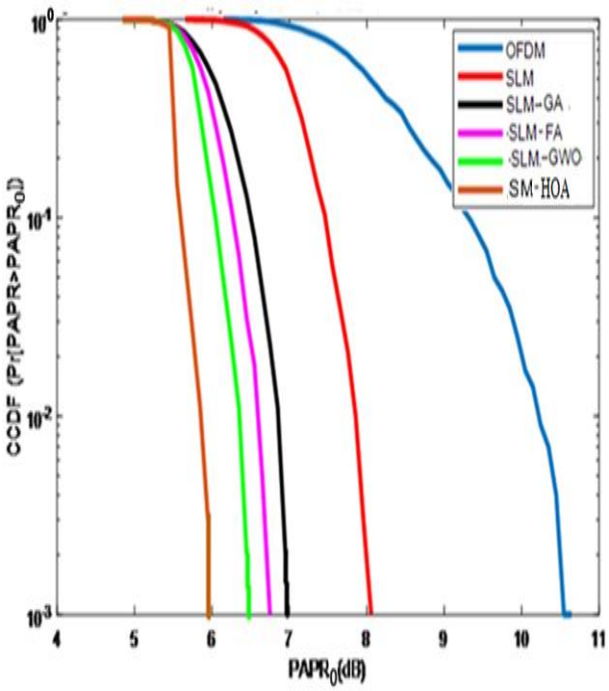


Fig 8. PAPR for M=8

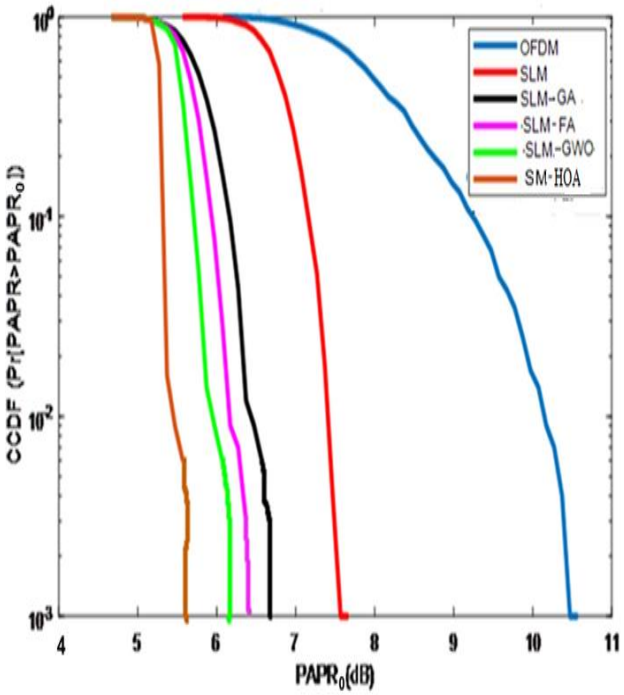


Fig 9. PAPR for M=16

For M=8 the results obtained using various techniques is shown in fig 8. As the size of M increases the PAPR gradually decreased, but the as the M size increases the system complexity will be increased.

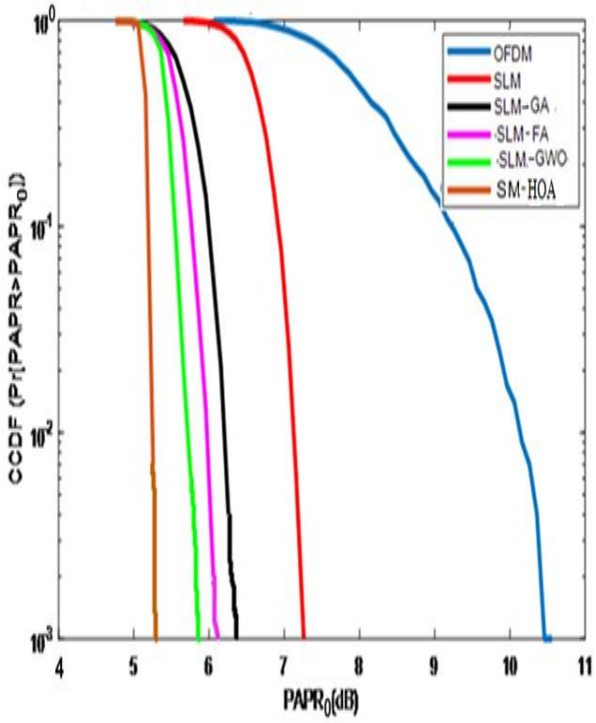


Fig 10. PAPR for M=32

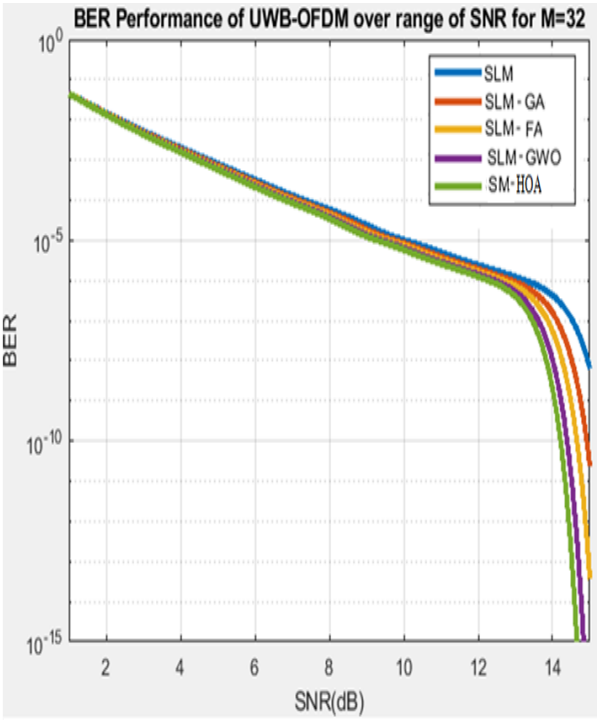


Fig 11. SNR vs BER for M=32

In this paper the analysis is done until M value is 32. Further the increase in value of M the steady PAPR value will be achieve. From our analysis it is observed that the PAPR is reduced using hybrid optimization technique in MB-OFDM UWB system.

Here, from the above results, the system BER and PAPR both are been balanced without disturbing the functionality of the MB-OFDM system. The proposed techniques maintain a cordial way of dealing the distortions in the signals. The gains and power achieved are in controllable stage. The side information is been restricted by applying channel coding. The data integrity is been preserved by which the rate of data flow will be reduced. The proposed technique has a good reduction in PAPR without degrading the Bit error rate which is shown in the above results.

Table 1. Comparison of PAPR using various techniques.

Technique/M=	**2**	**4**	**8**	**16**	**32**
SLM	10.13dB	8.78dB	8.14dB	7.75dB	7.28dB
SLM-GA	8.34dB	7.68dB	6.96dB	6.62dB	6.21dB
SLM-FA	8.14dB	7.49dB	6.80dB	6.40dB	6.05dB
SLM-GWO	7.84dB	7.17dB	6.46dB	6.12dB	5.70dB
SM-HOA	**7.34dB**	**6.67dB**	**5.96dB**	**5.62dB**	**5.20dB**

We considered SNR as 9dB, the proposed technique SM-HOA having zero-bit error rate for SNR more than 9dB. The proposed techniques give a promising value of PAPR, without degrading the BER. The BER obtained using proposed technique is low near all SNR values when compared with other techniques. Table 2 gives the values of SNR by considering 12dB for various 'M' values.

Table 2. BER vs SNR for 10dB using various techniques.

Technique/M=	**2**	**4**	**8**	**16**	**32**
SLM	10^{-6}	$10^{-6.2}$	$10^{-5.5}$	10^{-5}	$10^{-4.9}$
SLM-GA	10^{-7}	$10^{-6.3}$	$10^{-5.7}$	$10^{-5.5}$	$10^{-5.1}$
SLM-FA	10^{-8}	$10^{-6.5}$	$10^{-5.9}$	$10^{-5.8}$	$10^{-5.2}$
SLM-GWO	10^{-12}	10^{-7}	10^{-6}	$10^{-5.9}$	$10^{-5.3}$
SLM-GWOFA	10^{-15}	$10^{-7.5}$	$10^{-6.2}$	10^{-6}	$10^{-5.5}$

6. Conclusion

In wireless communication system short range transmission have given more importance for which UWB signals are consider. In this paper, MB-OFDM UWB signals are considered and the most common problem is high PAPR. To reduce the PAPR so many techniques have been implemented and four techniques, namely, SLM-GA, SLM-FA, SLM-GWO, SM-HOA are implemented and evaluated. The

proposed hybrid optimization is good in terms of PAPR and BER. Irrespective to the level of computational complexity and performance of BER, the proposed Hybrid optimization technique is said to be a promising technique for PAPR reduction in MB-OFDM UWB signals. Further hybridization of different optimization techniques can be applied for reducing the PAPR. Any of the best combination can provide low PAPR.

References

[1] FCC First report and order, revision of the Part 15 commission's rules regarding Ultra Wideband Transmission Systems, ET-Docket 98-153, April 22, 2002.

[2] MBOA-SIG "Multiband OFDM Physical Layer Proposal for IEEE 802.15 Task Group 3a," MBOA-SIG, Sep 14, 2004.

[3] K.Deergha Rao and T.S.N.Murthy, "Analysis of Effects of Clipping and Filtering on the Performance MB-OFDM UWB signals", IEEE International Conference on DSP-2007, Cardiff, U.K, July 2007.

[4] K.Deergha Rao and T.S.N.Murthy, "Effect of Filtering and Turbo Coding on the performance of Clipped MB-OFDM UWB signals", IEEE International Conference on (ICICS-2007), Singapore, Dec 2007.

[5] B. M. Lee and Rui J.P.de Figueiredo "A tunable predistorter for linearization of solid state power amplifier in mobile wireless OFDM", IEEE Emerging Technologies Workshop (ETW-05), 2005, Russia.

[6] R Sridevi and Dr. T Madhavi, "SLM Technique based on Firefly Algorithm for Reduction of PAPR in OFDM Systems ", Jour of Adv Research in Dynamical & Control Systems, Vol. 11, 06-Special Issue, 2019.

[7] R Sridevi and Dr. T Madhavi, " Reduction of PAPR in OFDM Signals Using Grey Wolf Optimization combined with SLM ", DSMLA 2019: Proceedings of the 1st International Conference on Data Science, Machine Learning and Applications.

[8] Reddi Sridevi, Dr. T. Madhavi, Sreenivasulu Ummadisetty, " Performance Improvement of OFDM Systems by Reducing PAPR using SLM-Grasshopper Optimization", International Journal of Innovative Technology and Exploring Engineering (IJITEE), ISSN: 2278-3075, Volume-9, Issue-2S3, December 2019.

[9] Ultra Wideband Systems Technologies and Application, by Robert Aiello and Anuj Batra.

[10] Ultra Wideband the next Generation Personal Area Network, by Mohit Lad, Patni.

[11] Reddi Sridevi, Dr.T.Madhavi." Reduction of PAPR and BER Using Hybrid Optimization GWOFA in OFDM Systems", International Journal of Advanced Science and Technology Vol. 29, No. 5s, (2020), pp. 141-151.

[12] M Cotton, R Archatz, J Wepman, and B Bedford, Interference Potential of Ultra Wideband Signals, NTIA Report TR 05-419.

International Journal for Modern Trends in Science and Technology, 6(9): 119-124, 2020
Copyright © 2020 International Journal for Modern Trends in Science and Technology
ISSN: 2455-3778 online
DOI: https://doi.org/10.46501/IJMTST060918
Available online at: http://www.ijmtst.com/vol6issue09.html

Design of Sliding Mode Observer Based Controller of Single-Phase Induction Motor

P. D.V. Seshasai[1] | Ch. V. N. Raja[2] | G. Anand[3]

[1]PG Scholar, Department of EEE, Anil Neerukonda Institute of Technology and Sciences (A), Visakhapatnam,
[2]Assistant Professor, Department of EEE, Anil Neerukonda Institute of Technology and Sciences (A), Visakhapatnam,
[3]Assistant Professor, Department of EEE, Dr L Bullayya college of Engineering for Women, Visakhapatnam

To Cite this Article
P. D.V. Seshasai, Ch. V. N. Raja and G. Anand, "Design of Sliding Mode Observer Based Controller of Single-Phase Induction Motor", *International Journal for Modern Trends in Science and Technology*, 6(9): 119-124, 2020.

Article Info
Received on 16-August-2020, Revised on 30-August-2020, Accepted on 06-September-2020, Published on 12-September-2020.

ABSTRACT

Single-phase induction motors are simple in construction, cheap in cost, reliable and easy to repair and maintain. Many controllers were designed to control the speed of a single-phase induction motor, but they are sensitive to plant parameter variations and disturbances. Speed control with very less transient response requires non-linear and robust control methods. Sliding mode control is one of the robust control techniques which is insensitive to disturbances. Here we propose a higher order sliding mode (SM) observer-based controller for a single-phase induction motor. The applied control depends on the dynamic model of the induction motor. The controller is structured by applying a blend of input linearization strategy and higher order sliding mode calculation with consistent estimation of rotor speed and stator currents, which limits the vulnerabilities continuously and lessen the chattering phenomenon in the control effort exertion utilizing a super twisting algorithm.

KEYWORDS:*Single phase induction motor (SPIM), sliding mode (SM) control, feedback linearization technique, super twisting algorithm.*

I. INTRODUCTION

Single-phase induction motors (SPIM) are generally manufactured in fractional kilowatt range and are generally utilized in numerous domestic applications like compressors, pumps, portable drills, hair dryers, refrigerators, washers, and other equipments, which need low-power motors. These motors are fundamentally powered directly from a viable establishment and are sometimes run in open loop configuration. Speed control of the motor with very less dynamic response requires non-linear and robust control methods. One such method is the sliding mode control.

In control systems, sliding mode control is a nonlinear control method that alters the dynamics of a nonlinear system by application of a discontinuous control signal that forces the systemto slide along a cross section of the system's normal behaviour.The advantage of sliding mode control is that it is less effected to plant and parameter variations. First order sliding mode (SMC-1) is the basic sliding mode control technique applied, but it has a disadvantage of chattering phenomenon. So, we are moving to higher order sliding mode i.e. second order sliding mode control to avoid the chattering phenomenon.

II. LITERATURE SURVEY

V.I. Utkin [1] and Ch. V.N. Raja [20] discussed about the design and analysis of variable structure control systems. C. Edwards, S.K. Spurgeon [2] discussed about thedevelopment of a robust control called sliding mode control methodology, a variable structure control and is characterised by a set of feedback control laws and a decision rule.V.I. Utkin [3] discussed the basic concepts, mathematics, and design aspects of variable-structure systems with sliding modes as a principle operation mode.V.I. Utkin et.al [4] proposed a novel sliding mode control method for mechanical systems with electric motors as actuators in such a way it is impervious to plant variations and uncertainties.A. Levant [5] introduced a new class of sliding modes and the concept of sliding mode order.

To estimate the speed, torque, flux, currents we have observers. Different types of observers have been proposed in the literature Z. Yan and V. I. Utkin [6] presented the review and synopsis of the main approaches used in the sliding mode observer design for electric machines. Y. Feng et.al [7] proposed a non-singular terminal sliding-mode observer for estimating the rotor flux of induction motors. W. Hammuoda et.al [8] proposed a second order sliding mode observer for induction motor. N. Zaidi et.al [9] implemented a second order sliding mode observer for a single-phase induction motor in real time using DSP.

J. Davila et.al [10] proposed the design of velocity observer for uncertain mechanical systems by modifying super-twisting second-order sliding-mode algorithm. R. Marino et.al [11] presented a new estimation algorithm which provides exponential estimation of rotor resistance for induction motor drives in physical operating conditions and may be used as an adaptive observer. T. Floquet et.al [12] proposed a new nonlinear sliding mode observer for induction motors.

A. Levant [13] demonstrated a robust homogeneousdifferentiator in the control structure which will make the design and investigation of new higher order sliding mode controllers easier with finite-time convergence. Z. Zhao et.al [14] presented a sensorless current-based output feedback sliding mode control for induction motors.A.G. Loukianov et.al [15] presented two sliding mode control algorithms for the (α,β) model of induction motors using block control linearization technique.

A. Loukianov [16] presented the problems involved in designing sliding mode manifold for uncertain nonlinear system. G. Bartolini et.al [17] proposed a control algorithm which does not require any observer and differential inequalities to evaluate the change of the sign of the derivative of the quantity accounting for the distance to the sliding manifold to abstain from chattering. A. Levant [18] proposed a universal finite-time-convergent controller to control the output of any uncertain SISO system. A. Estrada and L. Fridman [19] presented a new design algorithm based on the block control and quasi-continuous higher order sliding modes techniques. Ch.V.N. Raja and Narendra Kumar Dandu [20] proposed the design of induction machine and detuning of rotor parameters and their effects due to different values of constraints like air gap length (δ) and current density.Ch. V. N. Raja and K. Mohan [21] discussed about speed control technique of an induction motor using DTC strategy to improve the performance characteristics, the speed controller gains are tuned by means of Genetic Algorithm (GA).

III. PROPOSED SYSTEM

The block diagram of the proposed system is shown in Fig 1. consists of a PWM Inverter, single-phase induction motor, rotor speed and stator currents sliding mode observer, flux estimation, block control technique, sliding mode algorithm, rotor flux control. The PWM inverter is given gate pulses which triggers the induction motor and the sliding mode observer calculates the estimates of the rotor speed and stator currents. Then we design a sliding mode controller which involves design of a sliding manifold in conjunction with block control technique to ensure zero error dynamics.

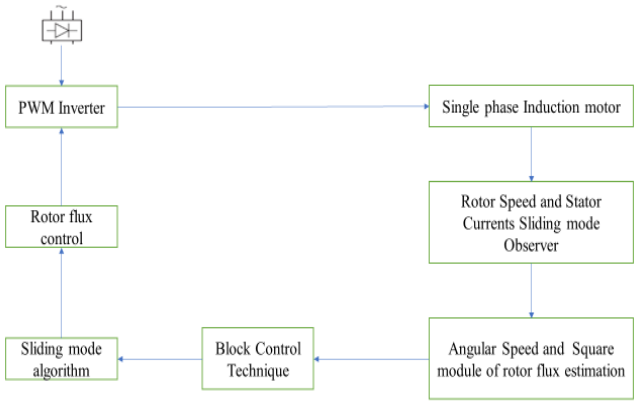


Fig.1 : Block diagram of proposed system

IV. MATHEMATICAL MODELLING

The dynamic model of the single-phase induction motor [21] is often considered as the transformed model of an unsymmetrical two phase (ab) machine into stationary fame ($a\beta$). The single-phase induction motor with stator currents and rotor flux is shown in Fig. 2 and the equations are given by

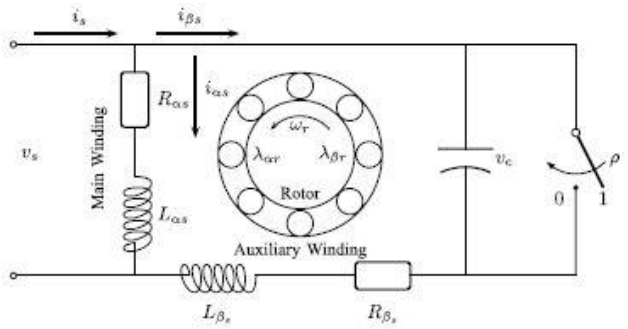


Fig. 2: Single phase induction motor

$$\frac{di_{\alpha s}}{dt} = -a_1 c_{10} i_{\alpha s} + a_1 a_{40} \lambda_{\alpha r} - a_1 a_3 n_p \omega_r \lambda_{\beta r} + a_1 v_{\alpha s} + \Delta_{\alpha s}$$

$$\frac{di_{\beta s}}{dt} = -a_2 c_{20} i_{\beta s} + a_2 a_{40} \lambda_{\beta r} + a_2 a_3 n_p \omega_r \lambda_{\alpha r} + a_2 v_{\beta s} + \Delta_{\beta s}$$

$$\frac{d\lambda_{\alpha r}}{dt} = -c_{30} \lambda_{\alpha r} + n_p \omega_r \lambda_{\beta r} + c_{40} i_{\alpha s} + \Delta_{\alpha r}$$

$$\frac{d\lambda_{\beta r}}{dt} = -n_p \omega_r \lambda_{\alpha r} - c_{30} \lambda_{\beta r} + c_{40} i_{\beta s} + \Delta_{\beta r}$$

$$\frac{d\omega_r}{dt} = p_1 p_2 (\lambda_{\beta r} i_{\alpha s} - \lambda_{\alpha r} i_{\beta s}) p_2 T_L \quad (1)$$

Considering the variations in rotor resistance of the form

$$R_r(t) = R_0(t) + \Delta R_r(t)$$

with $\Delta R_r(t)$an obscure but constrained function of time, prompting to a lot of dubious model parameters

$$c_1(t) = c_{10} + \Delta c_1(t)$$
$$c_2(t) = c_{20} + \Delta c_2(t)$$
$$c_3(t) = c_{30} + \Delta c_3(t)$$
$$c_4(t) = c_{40} + \Delta c_4(t)$$
$$a_4(t) = a_{40} + \Delta a_4(t)$$

where

$c_{10} = R_{\alpha s} + (L_m^2/L_r^2)R_0, c_{20} = R_{\beta s} + (L_m^2/L_r^2)R_0$

$c_{30} = (1/L_r)R_0$, $c_{40} = (L_m/L_r)R_0$, $a_{40} = (L_m/L_r^2)R_0$ are the boundary ostensible values.

The anomalies in the parameters are given by$\Delta c_1(t) = \Delta c_2(t) = (L_m^2/L_r^2)\ \Delta R_r(t), \Delta c_3(t) = (1/L_r)\ \Delta R_0(t)$,$\Delta c_4(t) = (L_m/L_r)\ \Delta R_0(t)$, $\Delta a_4(t) = (L_m/L_r^2)R_0(t)$.

While the model boundaries, which don't rely upon the variations in the resistance are given by $a_1 = L_r/(L_{\alpha s}L_r - L_m^2)$, $a_2 = L_r/(L_{\beta s}L_r - L_m^2)$, $a_3 = L_m/L_r$, $p_1 = (L_m/L_r)n_p$, and $p_2 = 1/J$.

The unidentified terms in (1) are given by

$$\Delta_{\alpha s} = \Delta a_4(t) a_1 \lambda_{\alpha r} - \Delta c_1(t) a_1 i_{\alpha s}$$
$$\Delta_{\beta s} = \Delta a_4(t) a_2 \lambda_{\beta r} - \Delta c_2(t) a_2 i_{\beta s}$$
$$\Delta_{\alpha r} = -\Delta c_3(t) \lambda_{\alpha r} + \Delta c_4(t) i_{\alpha s}$$
$$\Delta_{\beta r} = -\Delta c_3(t) \lambda_{\beta r} + \Delta c_4(t) i_{\beta s}$$

The capacitor dynamics are given by

$$\frac{dv_c}{dt} = \omega_0 X_c i_{\beta s}$$

where X_c is the capacitive reactance and $\omega_0 = 2\pi f$, and f is the fundamental frequency.

V. SLIDING MODE OBSERVER DESIGN

By using the rotor speed ω_r and stator currents a second order sliding mode observer is intended to assess the rotor flux.

By using the following transformation, let

$\lambda_{\alpha r}^* = \lambda_{\alpha r} - k_1 i_{\alpha s}$, $\lambda_{\beta r}^* = \lambda_{\beta r} - k_2 i_{\beta s}$ (2)

where k_1 , $k_2$are the transformation gains

Utilizing (2), (1) is represented using the transformed variables

$$\frac{di_{\alpha s}}{dt} = -q_{11} i_{\alpha s} - q_{12} n_p \omega_r i_{\beta s} - p_3 n_p \omega_r \lambda_{\beta r}^* + p_4 \lambda_{\alpha r}^* + a_1 v_{\alpha s} + \Delta_{\alpha s}$$

$$\frac{di_{\beta s}}{dt} = -q_{21} i_{\beta s} + q_{22} n_p \omega_r i_{\alpha s} + p_5 n_p \omega_r \lambda_{\alpha r}^* + p_6 \lambda_{\beta r}^* + a_2 v_{\beta s} + \Delta_{\beta s}$$

$$\frac{d\lambda_{\alpha r}^*}{dt} = -k_{11} \lambda_{\alpha r}^* + k_{12} n_p \omega_r \lambda_{\beta r}^* + \varsigma_{11} n_p \omega_r i_{\beta s} + \varsigma_{12} i_{\alpha s} - p_1 v_{\alpha s} - k_1 \Delta_{\alpha s} + \Delta_{\alpha r}$$

$$\frac{d\lambda_{\beta r}^*}{dt} = -k_{21} \lambda_{\beta r}^* - k_{22} n_p \omega_r \lambda_{\alpha r}^* - \varsigma_{21} n_p \omega_r i_{\alpha s} + \varsigma_{22} i_{\beta s} - p_2 v_{\beta s} - k_2 \Delta_{\beta s} + \Delta_{\beta r} \quad (3)$$

where $q_{11} = a_1c_{10} - k_1a_1a_{40}$, $p_{12} = k_2a_1a_3$, $q_{21} = a_2c_{20} - k_2a_2a_{40}$,$q_{22} = k_1a_2a_3$, $k_{11} = c_{30} + k_1a_1a_{40}$,$k_{12} = 1 + k_1a_1a_3$,$k_{21} = c_{30} + k_2a_2a_{40}$, $k_{22} = 1 + k_2a_2a_3$, $\varsigma_{11} = k_{12}k_2$,$\varsigma_{12} = c_{40} - k_{11}k_1 + k_1a_1c_{10}$, $\varsigma_{21} = k_{22}k_1$, $\varsigma_{12} = c_{40} - k_{21}k_2 + k_2a_2c_{20}$, $p_1 = k_1a_1$, $p_2 = k_2a_2$, $p_3 = a_1a_3$, $p_4 = a_1a_{40}$, $p_5 = a_2a_3$,$p_6 = a_2a_{40}$

With (3), a nonlinear observer is formulated which forms a secondorder sliding mode structure of the observer. Thus, we define$\hat{\lambda}^*_{\alpha r}$, $\hat{\lambda}^*_{\beta r}$, $\hat{i}_{\alpha s}$,$\hat{i}_{\beta s}$as the estimates of$\lambda^*_{\alpha r}$, $\lambda^*_{\beta r}$,$i_{\alpha s}$,$i_{\beta s}$respectively.

VI. SLIDING MODE CONTROLLER DESIGN

The principle objective here is to structure a sliding mode controller, which can adequately follow the anticipated speed ω_{ref} to the square of the rotor flux ϕ_{ref} reference signals by means of the constant basic control $v_s$and auxiliary control ρ as a spasmodic capacity. Here we design a finite-time sliding manifold to guarantee zero error dynamics.

A. *Design of Sliding Manifold*

The state variables y_1,$y_2$are defined as

$$y_1 = [\omega_r \ \ \phi]^T \ , \ y_2 = [i_{\alpha s} i_{\beta s}]^T \qquad (4)$$

where $\phi = |\varphi|^2 = \lambda^2_{\alpha r} + \lambda^2_{\beta r}$. At that point, utilising (4), (1) can be represented in the form of two nonlinear block structures with disturbances [19],

$$\frac{dy_1}{dt} = G_1(\phi) + M_1(\lambda_r)y_2 + P_1T_L + \Delta_r$$

$$\frac{dy_2}{dt} = G_2(\omega_r, \lambda_r, i_s) + M_2u + \Delta_s \qquad (5)$$

where

$\lambda_r = [\lambda_{\alpha r}\lambda_{\beta r}]^T$

$u = [v_{\alpha s}v_{\beta s}]^T$

$G_1(\phi) = [g_{11} \quad g_{12}]^T = [0 \quad -2c_{30}\phi]^T$

$P_1 = [-p_2 \quad 0]^T$

$G_2 = [g_{21} \quad g_{22}]^T$

$\Delta_r = [0 \quad 2\,\Delta_{\alpha r}\,\lambda_{\alpha r} + 2\,\Delta_{\beta r}\,\lambda_{\beta r}]^T$

$\Delta_s = [\Delta_{\alpha s} \quad \Delta_{\beta s}]^T$

$$M_1(\lambda_r) = \begin{bmatrix} p_1p_2\lambda_{\beta r} & -p_1p_2\lambda_{\alpha r} \\ 2c_{40}\lambda_{\alpha r} & 2c_{40}\lambda_{\beta r} \end{bmatrix}^T$$

$$M_2 = \begin{bmatrix} a_1 & 0 \\ 0 & a_2 \end{bmatrix}^T$$

with

$g_{21} = -c_{10}a_1i_{\alpha s} + a_1a_{40}\lambda_{\alpha r} - a_1a_3\omega_r\lambda_{\beta r}$

$g_{22} = -c_{20}a_2i_{\beta s} + a_2a_3\omega_r\lambda_{\alpha r} + a_2a_{40}\lambda_{\beta r}$

VII. SIMULATION RESULTS

The efficiency of the suggested controller is verified utilizing the simulation results and the real parameters of the system which are performed using the Euler integration method with a time step $t_s = 1\,ms$. The parameters of the induction motor are given in the Table I below:

TABLE I: Parameters of the single-phase induction motor

Phase voltage in rms [V]	220
Current in rms [A]	5.1
Frequency [Hz]	50
Power factor [pu]	0.81
Shaft speed [rpm]	1430
Magnetizing Inductance [H]	0.2350
Stator total inductivity [H]	0.2442
Rotor total inductivity [H]	0.2473
Stator resistance [ohms]	3.67
Rotor resistance [ohms]	2.32
Number of pole-pairs	2
Rotor moment of inertia [Nm^{-2}]	0.0069

The phase portrait of the above proposed scheme is shown below:

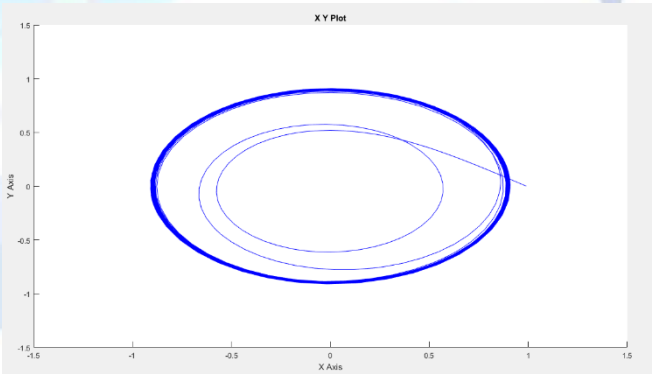


Figure 3 : Phase portrait

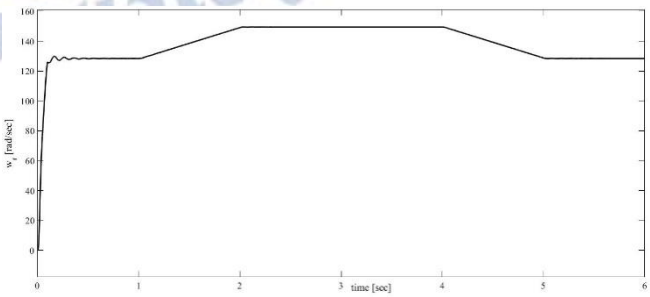


Fig.4 : Speed of the rotor in rpm

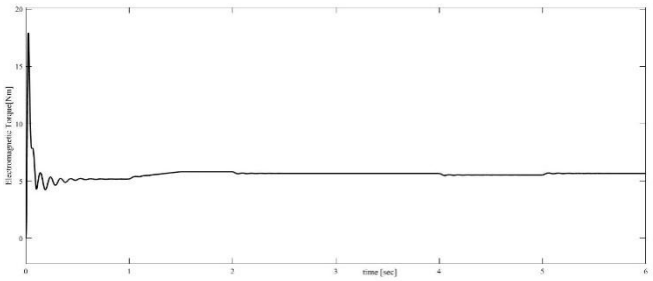


Fig.5 : Electromagnetic Torque in Nm

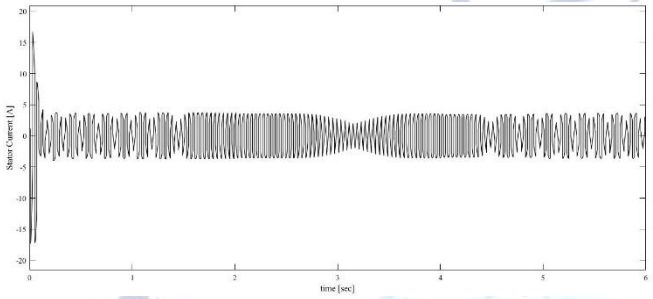


Fig.6 : Stator current in α axis

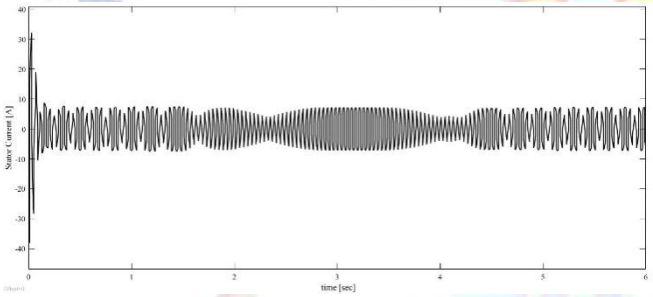


Fig.7 : Stator current in β axis

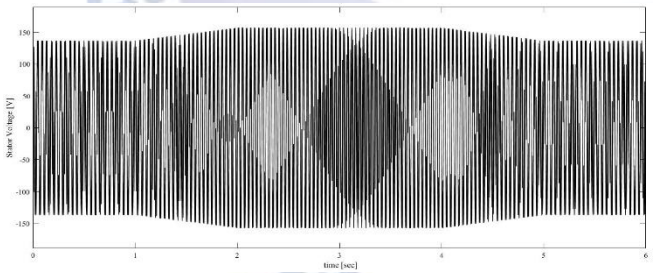


Fig.8 : Stator voltage in α axis

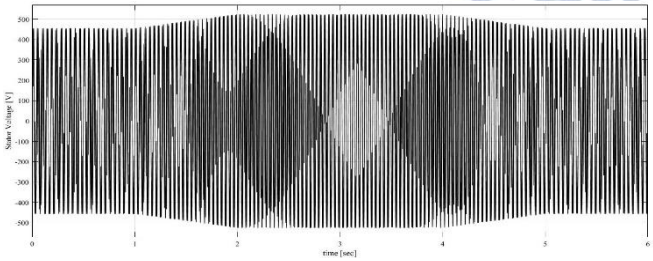


Fig.9 : Stator voltage in β axis

VIII. CONCLUSION

We propose a higher order sliding mode controller for a single-phase induction motor. The controller structure is based on the dynamic model of the motor. The simulation results obtained,exhibits the robustness property of the controller concerning the disturbances caused by the load torque and the rotor resistance variations. In addition, the proposed controller guarantees the constraints on stator currents.

In the near future, the proposed design method may be extended by usingintelligent controllers based on fuzzylogic and neural network to encompass flexibility and intelligence.

REFERENCES

[1] V. I. Utkin, "Variable Structure Systems with Sliding Modes", *IEEE Transactions on Automatic Control*, vol. 22, no. 2 , pp. 212-222, April 1977.

[2] C. Edwards and S.K. Spurgeon "Sliding mode control: Theory and Applications" *Taylor and Francis*, 1998.

[3] V. I. Utkin, "Sliding mode control design principles and applications to electric drives," *IEEE Trans. Ind. Electron.*, vol. 40, no. 1, pp. 23–36, Feb. 1993.

[4] V. I. Utkin, J.Guldner, and J.Shi, "Sliding mode control in electromechanical systems", *2nd ed. Taylor and Francis* , 2009.

[5] A. Levant, "Sliding order and sliding accuracy in sliding mode control," *Int. J. Control*, vol. 58, no. 6, pp. 1247–1263, 1993.

[6] Z. Yan and V. Utkin, "Sliding mode observers for electric machines—An overview," in *Proc. IEEE 28th IECON*, vol. 3. 2002, pp. 1842–1847.

[7] Y. Feng, M. Zhou and F. Han, "Terminal sliding-mode observer for rotor flux estimation of induction motors," *2017 12th IEEE Conference on Industrial Electronics and Applications (ICIEA)*, Siem Reap, 2017, pp. 803-806.

[8] W. Hammouda, T. Ladhari and F. M'sahli, "Second order sliding mode observer based on twisting algorithm for induction motor," 2015 16th International Conference on Sciences and Techniques of Automatic Control and Computer Engineering (STA), Monastir, 2015, pp. 763-767.

[9] N. Zaidi, H. Ben Azza, M. Jemli and A. Chaari, "DSP full implementation of second order sliding mode control to drive a SPIM," 2013 International Conference on Electrical Engineering and Software Applications, Hammamet, 2013, pp. 1-6.

[10] J. Davila, L. Fridman, and A. Levant, "Second-order sliding-mode observer for mechanical systems," *IEEE Trans. Autom. Control*, vol. 50, no. 11, pp. 1785–1789, Nov. 2005.

[11] R. Marino, S. Peresada, and P. Tomei, "Exponentially convergent rotor resistance estimation for induction motors," *IEEE Trans. Ind. Electron.*,vol. 42, no. 5, pp. 508–515, Oct. 1995.

[12] T. Floquet, J. P. Barbot, and W. Perruquetti, "A finite time observer for flux estimation in the induction machine," in *Proc. Int. Conf. Control Appl.*, vol. 2. 2002, pp. 1303–1308.

[13] A. Levant , "Homogeneity approach to high-order sliding mode design", *Automatica,* vol. 41, pp . 823-830, 2005.

[14] Z. Zhao, Z. Ruan, D. Meng, Y. Xue and C. Gu, "Sliding Mode Observer Based Sensorless Model Predictive Current Control for Induction Motor," 2019 IEEE 2nd International

Conference on Power and Energy Applications (ICPEA), Singapore, Singapore, 2019, pp. 84-88.
[15] A. G. Loukianov, J. M. Canedo, O. Serrano, V. I. Utkin, and S. Celikovsky, "Adaptive sliding mode block control of induction motors," in *Proc. IEEE Amer. Control Conf.*, vol. 1. Jun. 2001, pp. 149–154.
[16] A. Loukianov, "Robust block decomposition sliding mode control design," *Math. Problems Eng.*, vol. 8, nos. 4–5, pp. 349–365, 2002.
[17] G. Bartolini, A.Ferrara , and E.Usai, "Chattering Avoidance by Second-Order Sliding Mode Control", *IEEE Transactions on Automatic Control*, vol . 43, no. 2, pp. 241-246, February 1998.
[18] A. Levant, "Quasi-continuous high-order sliding-mode controllers," *IEEE Trans. Autom. Control*, vol. 50, no. 11, pp. 1812–1816, Nov. 2005.
[19] A. Estrada and L. Fridman, "Quasi-continuous HOSM control for systems with unmatched perturbations," *Automatica*, vol. 46, no. 11, pp. 1916–1919, 2010.
[20] Ch. V. N. Raja and Narendra Kumar Danda "Design and Analysis of Induction Machinebased on Internal Parameter," International Journal on Recent Technologies in Mechanical and Electrical Engineering (IJRMEE), Vol. 2, no 10, pp. 001-004, October 2015.
[21] Ch. V. N. Raja and K. Mohan, "Speed Control of an Inuction Motor Using GA Based Direct Torque Control," Innovative Systems Design and Engineering, Vol. 8, no. 2, pp. 34-44, 2017.

International Journal for Modern Trends in Science and Technology
IJMTST

Janaki Pakalapati, Venkata N. Kumar Gundavarapu*, Deepak Chowdary Duvvada and Sravana Kumar Bali

Study of electric field stress on the surface contour and at the triple junction in three phase GIS with FGM spacer under the depression defect

https://doi.org/10.1515/ijeeps-2020-0080
Received April 22, 2020; accepted August 30, 2020; published online September 10, 2020

Abstract: Now days, the establishment of spacers is in wide usage in three-phase Gas Insulated Busduct (GIB) for providing mechanical support and better insulation to the conductors. The region of the intersection of SF6 gas, enclosure end and the spacer is one of the weakest links in GIB, so the major concentration is done on minimization of electric field stress at this junction by using Functionally Graded Material (FGM) technique. The other incidents of insulation failures are due to several defects like depression, delamination etc. reduces the dielectric strength of the spacers. In this paper, an FGM post type spacer has been designed for a three-phase GIB under depression and further electric field stress at Triple Junction (TJ) is reduced by introducing a metal insert (MI) nearer to the TJ. Several filler materials are used as doping materials for obtaining different permittivity values using FGM technique to achieve uniform electric field stress. Simulation is carried out for the designed spacer at various operating voltages with different types of FGM gradings. The effect of depression with different dimensions and positions is analyzed before and after inserting MI to the FGM post type spacer in three-phase GIB.

Keywords: depression; electric field stress; FGM; gas insulated busduct; metal insert; spacer.

Nomenclature

Del	∇
Diameter of depression	D_d
Distance between conductors A, B, C	d_{AB}, d_{BC}, d_{CA}
Electric field intensity	$\vec{E}$
Electric Flux Density	$\vec{D}$
Electric potential	φ
Electric potential at conductor A, B, and C	φ_A;φ_B and φ_C
Energy stored	W
Maximum voltages of conductor A, B, and C	V_{Amax},V_{Bmax}, and V_{Cmax}
Operating Voltages of conductor A, B, and C	V_1; V_2, andV_3
Permittivity of the insulating material	ε
Radius of each conductor	R
RMS voltages of conductor A, B, and C	V_A(rms),V_B(rms), and V_C(rms)
Volume Charge Density	ρ_v
Volume charge density at conductors A, B, C	ρ_{AB}, ρ_{BC}, ρ_{CA}

Abbreviations

Boundary Element Method	BEM
Charge Simulation Method	CSM
Finite Difference Method	FDM
Finite Element Method	FEM
Functionally Graded Material	FGM
Gas Insulated Busduct	GIB
Graded Low Functionally Graded Material	GL-FGM
Graded High Functionally Graded Material	GH-FGM
Graded U Functionally Graded Material	GU-FGM
High Voltage	HV
Low Voltage	LV
Metal Insert	MI
Partial Discharge	PD
Three Dimensional	3D
Triple Junction	TJ
Two Dimensional	2D

1 Introduction

Presently, Gas Insulated Busduct (GIB) is in wide use, to meet the high electrical demand with low transmission losses and good efficiency. The GIB is more advantageous

***Corresponding author: Venkata N. Kumar Gundavarapu**, Department of EEE, JNTUA College of Engineering, Pulivendula, Andhra Pradesh, India, E-mail: gundavarapu_kumar@yahoo.com. https://orcid.org/0000-0002-9298-7708
Janaki Pakalapati, Department of EEE, Lendi Institute of Engineering and Technology, Vizianagaram, India
Deepak Chowdary Duvvada, Department of EEE, Dr L. Bullayya College of Engineering for Women, Visakhapatnam, India, E-mail: duvvada_27@yahoo.co.in. https://orcid.org/0000-0003-4716-9789
Sravana Kumar Bali, Department of EEE, GITAM University, Visakhapatnam, India, E-mail: sravanbali@gmail.com

Open Access. © 2020 Janaki Pakalapati et al., published by De Gruyter. This work is licensed under the Creative Commons Attribution 4.0 International License.

than air-insulated substations and they are based on the principle of enclosing all the conducting and energized parts inside a metallic enclosure with zero potential insulated with SF6 gas. Few authors [1, 2] has reviewed that most of the electrical-breakdown in the GIB is due to transient voltages which occurs during the switching operation of disconnectors or circuit breakers by weakening of the electric field inside the gas-insulated substations, affecting the performance of support insulators, transmission lines, cables, current transformers, voltage transformers, and high-voltage generators. Wenjia X. et al. [3] has identified new calculation methods for induced voltage and current for the hybrid transmission system in Gas Insulated Lines which occurs due to several switching operations of the switches under different conditions for hybrid transmission system. Talaat M. [4] described material spacer failures as the most challenges faced by GIB. Such spacers lose their power due to many defects such as void, delamination, etc. As a consequence of such faults, an effective approach must be implemented to minimize electrical field stress. This weakening of the electrical field across the spacer contributes to disruption to the whole GIB impacting the whole power system, resulting in a significant loss of resources. Few researchers [5–9] has observed that Gas Insulated Substation leads very fast transient overvoltage's and their associated transient currents during switching operations and analyzed parameters like arcing time, pre-arcing time, secondary discharges, trapped voltages, and level of contamination to design an appropriate switch to prevent induced current from fault-proof earthing switches. They also developed an analytical model to calculate ground resistance, step and touch potentials of the proposed GIS grounding system with proper concrete foundations and designed current sensors to measure the leakage current through the bushing insulation and surge arrester blocks.

In the literature, few researchers [10, 11] studied functional issues concerning the nature of cone type and disk type spacers. The analysis of electric field stress in GIB, where it was mainly observed that the efficiency of insulation ability over spacers can be enhanced by different techniques, such as shape regulation, the addition of shield electrodes, embedded electrodes, etc. However, these spacer design approaches have very limited influence over the distribution of electric field in the spacer and as a consequence, a new methodology called Functionally Graded Material (FGM) filled with specific permittivity materials has been described by few authors [12–14] in order to resolve the difficulties of the previous methods and to make them more economical. Some researchers [15–17] have stated that this is the latest technique of FGM design of spacer, has certain difficulties in processing, construction, and so on. However, they have come up with a remedy by producing an FGM spacer with three separate forms of gradings, such as increasing, decreasing, and U form of permitting ranges by utilizing centrifugal forces. Later Naoki Hayakawa et al. [18] identified that ε-FGM with spacial distribution is one of the effective methods for the reduction of the electric field in along the length of the spacer, despite several methods, Flexible Mixture Casting (FMC) the method is chosen for the fabrication of ε-FGM spacer. Muneaki K. et al. [19] reviewed that FEM analysis is a mathematical tool used in the design of FGM spacer by grading the plain epoxy spacer with different permittivity values for the reduction of the electric field stress in the GIS. Few authors [20, 21] have identified that electric field intensity is very high at Triple Junction (TJ) due to high electron emission and the reduction in the field stress has been achieved by inserting metal inserts (MI) at this junction of the enclosure end and the conductor end of the cone type spacer. C.M. Cooke et al. [22] investigated the surface flashover on post-type support spacer for GIL and proved that it can be reduced by placing MI, however, the concept of MI and its effect on electric field at TJ is carried out for cone type spacer in a single-phase GIS also the same can to be analyzed in three-phase GIB. Some of the researchers [23–25] have identified some defects like metal depression will be produced inevitably due to irregularities of GIS spacers during the installation and operation of GIS. These metal depressions along with suspended particles can cause distortion of the electric field over the spacer surface and hence high electric field stress inside GIS, which leads to Partial discharge and breakdown. Especially, with the increase of operating voltage, even a small defect leads to internal failures in compact GIS due to spacer failures. Several authors [26, 27] observed that the failures of the spacers are due to the presence of particles or defects like, Free particles on the inner surface of the enclosure, Depression on the high voltage (HV) conductor, Depression on the inner surface of the enclosure and narrow gaps between the spacer and the electrode as they develop high electric field stress at the contacts between the parts of the HV conductor and low voltage (LV) conductor. Though SF6 exhibits very high dielectric strength within the GIS the Electromagnetic wave is generated from the depression and short gap discharge in gas-insulated substation due to rise in partial discharge. It was observed by G. Ueta et al. [28] that the rise and fall times of a defect in the spacer is relatively longer than those of a defect in SF6 gas such as a metallic particle, metallic depression on the conductor, or floating electrode. Wensheng Gao et al. [29] have been identified that partial discharge occurs due to four types of

typical defects like floating metal, depression, particle on the spacer, and void in solid insulation and analyzed their effects at different sizes of each defect for observing the consistency frequency spectrum characteristics. Qikun Feng et al. [30] has studied the effect of metal depression on concave sides of the basin-type insulator in GIS at different heights and radii of metal depression and observed that at high voltage conductor the electric field stress is higher than that of grounded enclosure. Feng-Chang Gu et al. [31] has identified four GIS models with typical defects where the models include internal conductor of porcelain bushing at load side like Type 1: Conductor of porcelain bushing containing oil grease, Type 2: Gas tank containing metal particles, Type 3: Operation handle containing welding depression, Type 4: Metal ring with an abrasion defect. Tao Wen et al. [32] has evaluated the effectiveness of on-site GIS equipment with insulation defects, based on the insulation characteristics of a coaxial cylinder structure SF6 gas gap with a conductive depression under the impulses of different dimensions resulted with 50% breakdown voltage in the voltage-time curve. Ladani M. et al. [33] has reviewed a new method for the reduction of the electric field at the spacer surface and at the TJ by geometry shape optimization by using Finite Element Method (FEM) and Nelder–Mead algorithm by optimizing the shape and size of the MI and the spacer.

Many researchers have been worked on the reduction of electric field stress due to several defects on the spacers like cone type, disc type etc. in a single-phase gas-insulated busduct at the TJ's at HV and LV ends of the spacer by using several techniques like FGM rather than its shape control technique due to its complications. Whereas by considering dielectric failures of insulators as a challenge in a three-phase GIB the literature has been carried out on the defects like depression which on the solid materials. The main aim of this paper is to design a proper MI at the enclosure end for an FGM post type spacer for a three-phase GIB to study the electric field stress at the TJ's due to defects like depression and analyze for the reduction of electric field stress after inserting MI. The FGM of the spacer is a new technique which is used for minimizing the electric field stress in the GIS by modulating the permittivity values of the spacer. By using this grading technique with appropriate permittivity distribution the field stress at the required position can be minimized. In this paper, FGM grading is done by applying centrifugal forces in three different types of gradings like GL-FGM, GH-FGM, and GU-FGM. Depression is one of the defects of the spacers which affects the electric field stress drastically, on its surface and protrusion is caused mostly due to scratches on the spacer surface because of insufficient care during assembly of GIB. The permittivity-grading of materials can be done in two methods, i.e., by applying centrifugal forces and three dimensional (3D) printing by incorporating fillers of different diameters in order to obtain the permittivity distribution for uniform field distribution [34]. Here a centrifugal the approach is used for the grading of permittivity values as it is found to be the most efficient method.

In this paper, the electric field stress due to normal FGM gradings was introduced and a MI was placed at the enclosure end of the proposed FGM post type spacer, which essentially decreases the electrical field stress at the TJ and obtains a uniform field along the spacer surface. The recessed MI at conductor B offered an appropriate shielding to minimize electric field stress at TJ due to depression of various radii. However, this method of introducing MI has been minimized the complexity and the cost of replacement of spacer. Simulation shall be carried out by designing a three-phase GIB by giving proper charge to the conductors and the enclosure. The electrical field stress was analyzed at the end of the enclosure near the TJ of the FGM spacer. The electric field distribution produced by depression of the FGM post type spacer on the spacer surface and the TJ is determined. The electric field stress on the spacer surface, the conductor and at the TJ at the enclosure end are analyzed. The same procedure is applied to three different ranges of permittivity values, three types of FGM grading techniques for conductor B at the enclosure end. The recessed MI is incorporated into the FGM spacer at the end of conductor B to provide better electrical field stress at the critical/weak junction of the spacer in order to maintain uniform field stress by considering an appropriate shape and size of the MIs to analyze the results.

2 Mathematical modeling of three phase GIB

Many researchers have calculated the electrical field by using Laplace and Poisson equations applied to a particular assumed domain. The three phase GIB's are operating at HVs, so the analytical approach to Laplace's equation and Poisson 's equation is very difficult. So to overcome this complexity numerical methods are used for the calculation of electric field. These methods are classified into Finite Difference Method (FDM), FEM, Charge Simulation Method (CSM), and the Boundary Element Method (BEM). Despite advantages and disadvantages of the above methods, FEM is observed as more suitable for solving the complex problems. The FEM is used in this paper to determine the

electrical field stress on the surface of the spacer, which is an efficient method for solving electrical field problems. When considering the presence of depression in GIB, a two dimensional (2D) simulation model was created and the governing equations are described as below

$$\vec{E} = -\nabla \varphi \tag{1}$$

$$\nabla \bullet D = \rho_v \tag{2}$$

$$\vec{D} = \varepsilon \vec{E} \tag{3}$$

where D is the electric flux density, E is the electric field intensity, ρ_v is the charge density, ε is permittivity, φ is the electric potential. Then by substituting Equations (1) and (3) in Equation (2),

$$\nabla \bullet \varepsilon \vec{E} = \rho_v \tag{4}$$

then

$$\nabla \bullet \varepsilon(-\nabla \varphi) = \rho_v \tag{5}$$

The dielectrics under consideration are considered to be linear, isotropic and homogeneous, the 'ε' can be taken from derivatives, then Equation (5) can be simplified by Equation (6) in Poisson's equation.

$$\nabla^2 \varphi = \frac{-\rho_v}{\varepsilon} \tag{6}$$

The charge under consideration is distributed uniformly with zero volume charge density ρ_v, and hence Equation (6) can be simplified to Laplace's equation

$$\nabla^2 \varphi = 0 \tag{7}$$

Consider, φ_A, φ_B and φ_C are the voltage potentials of the three conductors A, B, C with respect to the zero potential end as shown in Figure 1. For a three phase balanced system, d_{AB}, d_{BC}, $d_{CA,}$ are distances between the three conductors with a radius of "r" mm and ρ_A, ρ_B, ρ_C are their line charge densities respectively.

$$\varphi = \varphi_A + \varphi_B + \varphi_C \tag{8}$$

$$\nabla^2 \varphi_A + \nabla^2 \varphi_B + \nabla^2 \varphi_C = 0 \tag{9}$$

$$\varphi_A = \frac{\rho_A}{6\pi\varepsilon_O}\left(\ln \frac{d_A d_B d_C}{r^3}\right) \tag{10}$$

$$\varphi_B = \frac{\rho_B}{6\pi\varepsilon_O}\left(\ln \frac{d_A d_B d_C}{r^3}\right) \tag{11}$$

$$\varphi_C = \frac{\rho_C}{6\pi\varepsilon_O}\left(\ln \frac{d_A d_B d_C}{r^3}\right) \tag{12}$$

Substituting Equations (10)–(12) in Equation (9).

$$\nabla^2 \varphi = \nabla^2\left([\rho_A + \rho_B + \rho_C]\ \ln \frac{d_A\, d_B\, d_C}{r^3}\right) = 0 \tag{13}$$

then Equation (13) can be simplified as,

$$\varphi = \left([\rho_A + \rho_B + \rho_C]\ \ln \frac{d_A d_B d_C}{r^3}\right) \tag{14}$$

From the concept of FEM analysis the electric field intensity for a 2D consideration for a three phase system is given by

$$\vec{E} = -\frac{\partial \varphi(x,y)}{\partial x}\vec{x} - \frac{\partial \varphi(x,y)}{\partial y}\vec{y} \tag{15}$$

$$\vec{E} = -\frac{\partial}{\partial x}\left(\ln \frac{d_A d_B d_C}{r^3}\ [\rho_A + \rho_B + \rho_C]\right)\vec{x} - \frac{\partial}{\partial y}\left(\ln \frac{d_A d_B d_C}{r^3}\ [\rho_A + \rho_B + \rho_C]\right)\vec{y} \tag{16}$$

But for a three-phase GIB, as all the conductors inside GIB are spaced at equidistant [25]. It is necessary to consider the symmetrical system, i.e., $d_{AB} = d_{BC} = d_{CA} = d$ and Equations (14) and (16) can then be written as,

$$\varphi = \left([\rho_A + \rho_B + \rho_C] \ln \frac{d}{r}\right) \tag{17}$$

$$\vec{E} = -\frac{1}{2\pi\varepsilon_O}\left\{\frac{\partial}{\partial x}\left(\ln \frac{d}{r}\ [\rho_{AB} + \rho_{BC} + \rho_{CA}]\right)\vec{x} + \frac{\partial}{\partial y}\left(\ln \frac{d}{r}\ [\rho_{AB} + \rho_{BC} + \rho_{CA}]\right)\vec{y}\right\} \tag{18}$$

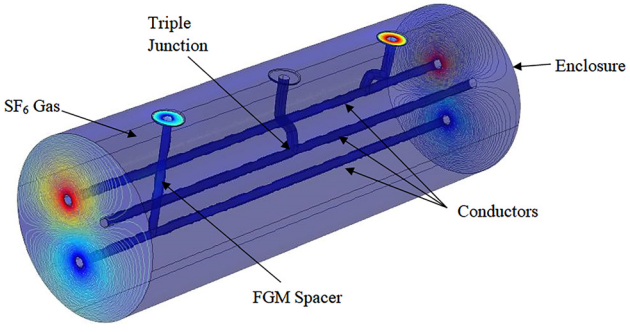


Figure 1: Representation of three-phase GIB with boundary conditions.

3 Electric field computation of three phase GIB by using finite element method

Finite Element Method has been commonly used to solve electrical field problems owing to its capacity to

understand the multiple constructions and dynamic forms of different domains electrodes. This approach relies on reducing the electrostatic energy function. Under steady state electrostatic fields within a dielectric material of constant dielectric strength , with the Cartesian coordinate system, and by using Laplace equation, the electrical energy "*W*" stored within the whole volume '*v*' of the region considered as given below with Equation (19).

$$W = \frac{1}{2} \iiint \varepsilon (\nabla^2 \varphi)\, dv \tag{19}$$

In 3D dimensions the electrostatic energy in terms of electrical potential is given as,

$$W = \frac{1}{2} \iiint \left(\varepsilon_x \frac{\partial^2 \varphi}{\partial x^2} + \varepsilon_y \frac{\partial^2 \varphi}{\partial y^2} + \varepsilon_z \frac{\partial^2 \varphi}{\partial z^2} \right) dv \tag{20}$$

where ε_x, ε_y, and ε_z are the x, y, and z-components of the dielectric constant in the Cartesian coordinates. Thus the entire region being considered is subdivided into triangular components. Therefore the electrostatic energy for a small area of the 2D domain ($dxdy$) is given by

$$W' = \frac{1}{2} \iint \left(\varepsilon_x \frac{\partial^2 \varphi}{\partial x^2} + \varepsilon_y \frac{\partial^2 \varphi}{\partial y^2} \right) dxdy \tag{21}$$

Since from Equations (7) and (19),

$$dW = \frac{1}{2} \iint \varepsilon (\nabla^2 \varphi)\, dxdy = 0 \tag{22}$$

Therefore

$$dW = 0 \tag{23}$$

4 Functionally graded material post type spacer

Figure 2 represents the FGM technique applied to the design of the post type spacer in the proposed three-phase GIB to develop uniform field distribution throughout the spacer length. In this paper, multiple grading methods for FGM post type spacers, have used ε-FGM with three separate grading forms such as GL-FGM, GH-FGM, and GU-FGM using centrifugal forces. The fabrication of GL-FGM Post type spacer is done by the following Algorithm.

Step-1. Consider the filler materials like Al_2O_3, TiO_2, and SiO_2 to combine with the Epoxy resin with hardener.

Step-2. Transfer the mixture of fillers and epoxy resin into a test cup.

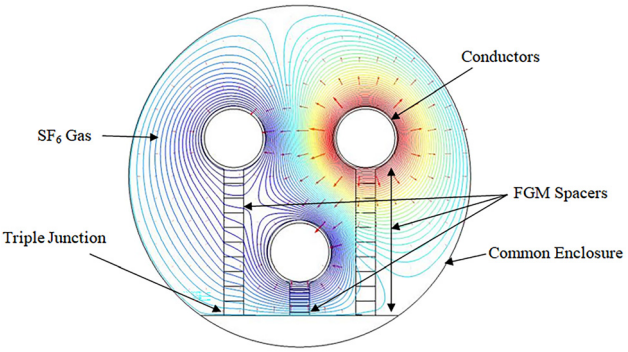


Figure 2: FGM post type spacer of common enclosure three phase GIB.

Step-3. Evaporate the above sample to be free from air bubbles by Degassing.

Step-4. Apply centrifugal forces to the sample with the help of the centrifugal separator.

Step-5. Repeat the above procedure for the fabrication of GH-FGM and GU-FGM with the corresponding fillers.

In this paper, the three different ranges of permittivity are considered as given below for the three types of grading. The different types of FGM grading i.e., GL-FGM, GH-FGM and GU-FGM are designed with the permittivity values of different cases are as shown in Table 1. For the above table the variation of permittivity values for different FGM gradings with respect to the three cases are as described , the permittivity is in the range of 3.95–3.5 in case 1, 4.05–3.6 in case 2 and 4.15–3.7 in case 3 from conductor end to enclosure end for GL-FGM grading. For GH-FGM grading, it is observed that the permittivity is in the range of 3.5–3.95 in case1, 3.6–4.05 in case 2 and 3.7–4.15 in case 3 from conductor end to enclosure end. Whereas for case 1 the filler concentration with high permittivity i.e., 3.95 at conductor end is considered, the filler permittivity is gradually decreased up to 3.5 and again increased in steps to 3.95 nearer to enclosure end. Similarly for case 2 and case 3 the permittivity is varied from 4.05 to 3.6 to 4.05 and 4.15 to 3.7 to 4.15 respectively as shown in Figure 3. The FGM spacer is designed with 10 equal height gradings for the three conductors of their respective lengths and widths. The grading is done with different ranges of permittivity in three different types of FGM technique. In the cases 1, 2, and 3 the permittivity ranges are chosen as 3.5–3.95, 3.6–4.05, and 3.7–4.15 respectively. The FGM spacer is analyzed for these three types of gradings GL-FGM, GH-FGM, GU-FGM gradings are achieved by adding centrifugal forces along with other materials to the mixture of

Table 1: Permittivity values of GL, GH, GU-FGM gradings.

Grading type	Permittivity ranges		
	Case 1	Case 2	Case 3
GL-FGM	3.95–3.5	4.05–3.6	4.15–3.7
GH-FGM	3.5–3.95	3.6–4.05	3.7–4.15
GU-FGM	3.95–3.5 to 3.95	4.05–3.6 to 4.05	4.15–3.7 to 4.15

epoxy content. For GL-FGM, permittivity is the function of the radius and the high permittivity at the end of the inner conductor shall be retained and slowly decreased by increasing the radius in the direction of the end of the enclosure. Likewise for GH-FGM grading high permittivity is at the end of the enclosure and for GU-FGM grading, permittivity distribution in U-shape.

5 Results and discussions

5.1 Simulation model of three phase GIB

The simple simulation model of a three-phase gas-insulated busduct with a radius of 225.5 mm of the typical enclosure busduct without depression. The three-phase GIB with a relative permittivity of 1.0015 is filled with SF6 gas. With a radius of 38.66 mm each, the three conductors A, B, and C are contained within the common enclosure and positioned at the corners of the equilateral triangle. The distance between the conductor A to that of the end of the enclosure is taken as 193.8 mm. Whereas the gap between the conductors B and C is taken as 43 and 193.8 mm respectively to that of the enclosure end and the width of each spacer is taken as 26 mm respectively. The three-phase GIB is simulated using the FEM concept. The proposed simulation model, positions of all three conductors A, B, and C within the common enclosed GIB are equidistant from each other. The conductor A is applied with the RMS voltages of V_A equal to 72.5, 132, and 220 kV and the voltages of the conductor's V_B and V_C are with a phase shift of –120° and +120° respectively. The outer electrode is grounded with zero voltage. Table 2 represents the corresponding maximum voltages of conductor A, B, C of the considered RMS voltages.

5.2 Effect of depression on FGM post type spacer

Depression is the most typical and frequently occurred defects on the spacer for its failure from the literature. Metal depressions are typically found on the spacers at the concave side and are often caused by scratches on the spacer surface due to inadequate care during assembly. Similar to the defects like metallic particles and delamination, depression occurs most commonly in GIB due to switching operations and lightning impulses. During high voltages, the shape of the depression tip can be either sharply angled and can also be modified to a round shape. Such two defects will affect the distribution of the electric field over the length of the spacer and thus the GIB operation. The rounded depression with several radii has been verified from the simulation of the designed FGM post type spacer for three-phase GIB as represented in Table 3. By

Table 2: Maximum values of RMS voltages of conductor A, B, C.

RMS voltage (kV)	$V_{A\ max}$ (kV)	$V_{B\ max}$ (kV)	$V_{C\ max}$ (kV)
$V_1 = 72.5$	102.515	–51.258	–51.258
$V_2 = 132$	186.65	–93.324	–93.324
$V_3 = 220$	311.08	–155.54	–155.54

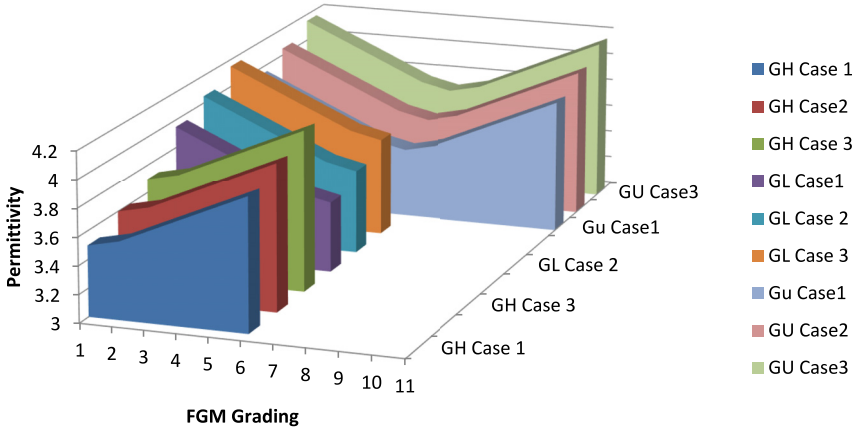


Figure 3: Permittivity values of GL, GH, GU-FGM gradings at different cases.

Table 3: Variation of electric field with different radii of depression.

Radius (mm)	Grading 1			Grading 2		
	72.5 kV	132 kV	220 kV	72.5 kV	132 kV	220 kV
2	0.055	0.1	0.173	0.102	0.1865	0.311
0.8	0.0631	0.115	0.1918	0.1095	0.199	0.332
0.6	0.082	0.1495	0.2487	0.11	0.201	0.335
0.2	0.1078	0.1963	0.3275	0.11105	0.2022	0.338

comparing all the values of depression from Table 3, the field is highly affected due to depression at the 2nd grading segment with D_d as the diameter of depression and radius 0.2 mm rather than the depression in 1st grading segment and the depression located at both the gradings at a time.

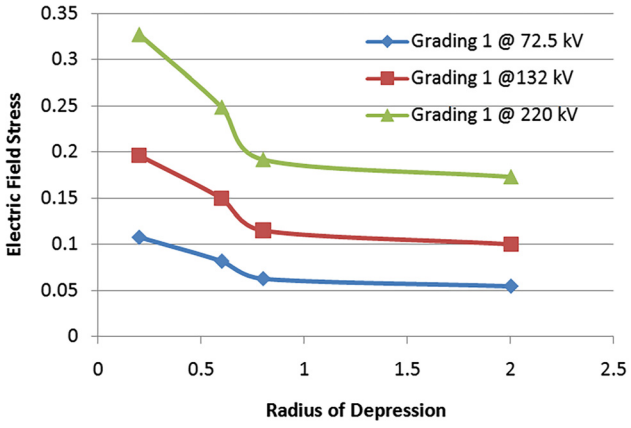


Figure 4: Variation of electric field stress at different radii of depression in grading-1.

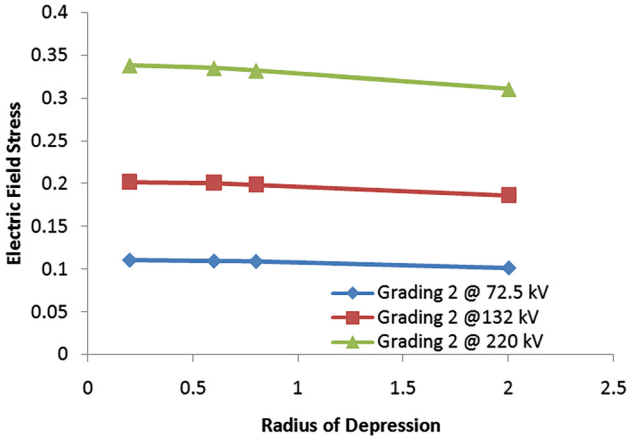


Figure 5: Variation of electric field stress at different radii of depression in grading-2.

Figure 4 shows that the electric field increases with an increase in the operating voltage from 72.5 to 220 kV and also increases as the radius decreases from 2 to 0.2 mm. This is evident from Figure 5 that the electrical field rises with an increase in the operating voltage from 72.5 to 220 kV and is held almost constant when the radius is decreased from 2 to 0.2 mm. Through comparing Figures 4 and 5 it is clear that at the respective voltages the high electric field stress is obtained at 0.2 mm in grading-2 as opposed to grading-1. The above study, therefore, considers depression with a radius of 0.2 mm in the 2nd FGM grading section for further analysis in the three-phase gas isolated busduct as shown in Figure 6. Due to the defect depression, the electric field distribution at the spacer surface can be measured using the contact angle produced by this defect at the TJ. Figure 6 shows the design diagrams

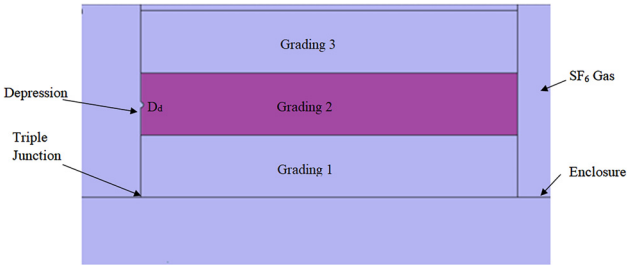


Figure 6: Representation of depression on conductor B.

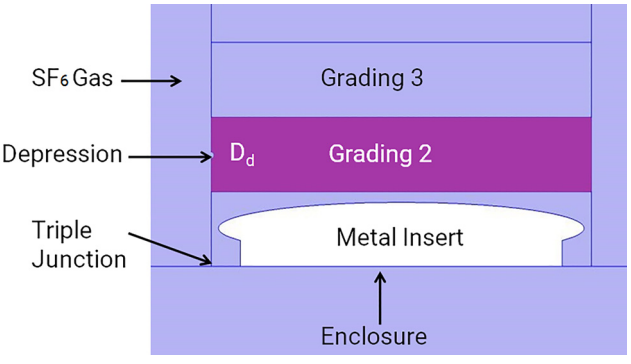


Figure 7: Design of FGM post type spacer with depression and MI.

for three-phase GIB with the FGM post-type spacer defect depression without MI. To reduce this effect of depression, a recessed MI (the combination of rectangle and ellipse in the 2D approach) with dimensions of the rectangle as (22×1.5 mm) along the ellipse of the axis length as 12.5 mm and a b-axis of 1.5 mm has been identified with a maximum reduction of an electric field being designed at the end of the enclosure. As shown in Figure 7, this particular MI was designed to be introduced at conductor B.

5.3 Analysis of FGM post type spacer

An FGM post type spacer is designed to create a uniform distribution of electric fields, as shown in Figure 2. The various types of FGM gradations i.e., GL-FGM, GH-FGM, and GU-FGM are constructed with different case permittivity values. Figure 3 represents the variance of permittivity values for different FGM gradations with respect to the three cases. From Table 4, it has been found that GL-FGM grading has high electric field stress at the ends of the enclosure at TJ, for case 1 for conductors A and C and for case 3 for conductor B for all three applied voltages of V_1, V_2, V_3 compared to other situations. It is observed that the electrical field stress at conductor A is high since the applied voltage is comparatively maximum at conductor A, for $V_1 = 72$ kV as applied RMS voltage then the maximum voltages at A, B, C is V_A = 102.515 kV, V_B = −51.257 kV, and V_C = −51.257 kV respectively. From Figure 8 it is observed that for all three conductors the magnitude of electric field stress at the enclosure end is high. Figures 8–10 show the distribution of the electric field for conductors A, B and C at V_1 = 72,5 kV, V_2 = 132 kV, and V_3 = 220 kV respectively over GL- FGM post type spacer. Though there is a uniform distribution over the spacer surface, it is found that the three conductors with peak

Table 4: Electric field stress of FGM post type spacer.

Type	Conductor	Permittivity values	V_1 = 72.5 kV		V_2 = 132 kV		V_3 = 220 kV	
			Electric field stress at enclosure in kV/cm	Electric field stress at conductor in kV/cm	Electric field stress at enclosure in kV/cm	Electric field stress at conductor in kV/cm	Electric field stress at enclosure in kV/cm	Electric field stress at conductor in kV/cm
GL-FGM	A	Case 1	0.00728	0.17245	0.01325	0.31397	0.0221	0.5233
		Case 2	0.00705	0.1718	0.01275	0.3128	0.0213	0.5214
		Case 3	0.00678	0.1714	0.01235	0.3121	0.0205	0.5205
	B	Case 1	0.1102	0.1453	0.2023	0.26458	0.3372	0.441
		Case 2	0.11118	0.1454	0.2024	0.2647	0.3373	0.4414
		Case 3	0.11121	0.1455	0.2025	0.2648	0.3375	0.4415
	C	Case 1	0.03595	0.1198	0.0655	0.2182	0.10915	0.3636
		Case 2	0.03593	0.1193	0.0654	0.2173	0.10898	0.3622
		Case 3	0.03585	0.1188	0.0653	0.2164	0.1088	0.3607
GH-FGM	A	Case 1	0.00705	0.1759	0.01285	0.3203	0.02143	0.53375
		Case 2	0.00685	0.1751	0.0124	0.3188	0.0208	0.5313
		Case 3	0.0066	0.1744	0.012	0.3175	0.02	0.529
	B	Case 1	0.1007	0.1456	0.1833	0.26512	0.3055	0.44188
		Case 2	0.1009	0.14562	0.1838	0.26515	0.3064	0.4419
		Case 3	0.1013	0.1457	0.1842	0.2652	0.307	0.442
	C	Case 1	0.0343	0.1222	0.06245	0.2225	0.1041	0.3709
		Case 2	0.03428	0.1215	0.0624	0.2214	0.104	0.3691
		Case 3	0.0342	0.121	0.06238	0.2204	0.1037	0.3675
GU-FGM	A	Case 1	0.007	0.1725	0.01278	0.3142	0.02128	0.5237
		Case 2	0.00687	0.172	0.0123	0.3135	0.0206	0.522
		Case 3	0.00655	0.1715	0.012	0.312	0.01998	0.52
	B	Case 1	0.1019	0.1445	0.1855	0.2635	0.3094	0.4395
		Case 2	0.102	0.145	0.1864	0.2638	0.31	0.4398
		Case 3	0.1024	0.14504	0.1862	0.264	0.3105	0.44
	C	Case 1	0.0345	0.12	0.0627	0.2198	0.1045	0.3635
		Case 2	0.0344	0.1193	0.0625	0.2173	0.1044	0.3621
		Case 3	0.03435	0.119	0.0622	0.2165	0.1042	0.361

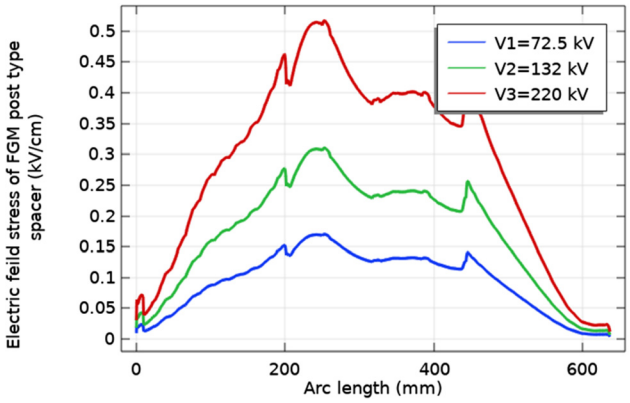


Figure 8: Electric field stress of FGM spacer of conductor A.

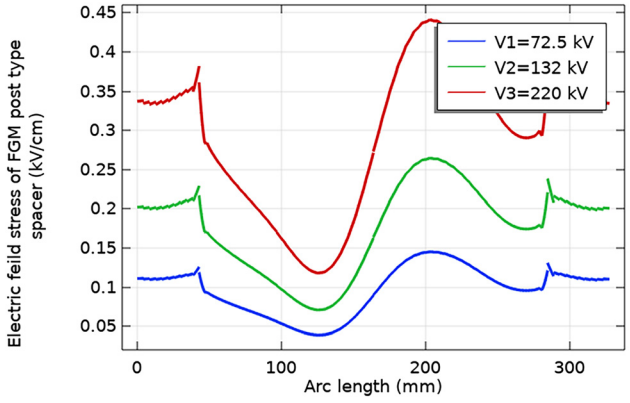


Figure 9: Electric field stress of FGM spacer of conductor B.

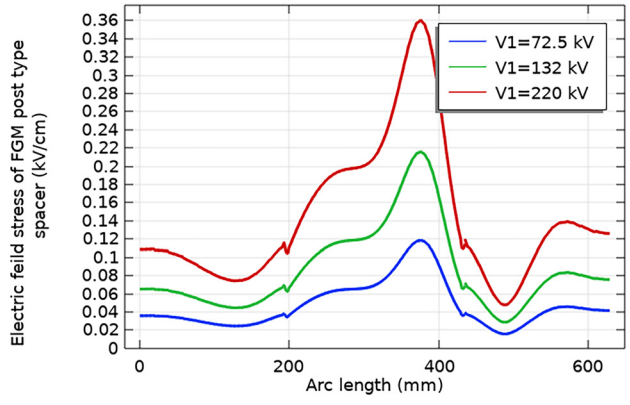


Figure 10: Electric field stress of FGM spacer of conductor C.

values in the plots have high electric field stress at the conductor ends. It is found that there is a spike with a sudden increase in the magnitude of electric field stress of conductor B as compared to the other two conductors at TJ. Figure 11 is the surface plot of the designed FGM spacers with height. Because of its high potential, the red-colored

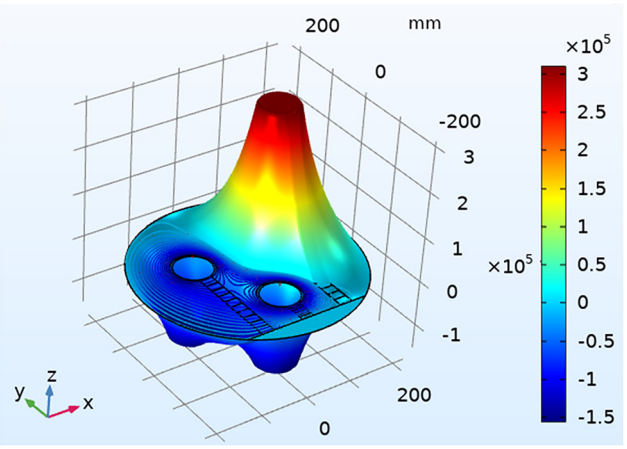


Figure 11: Surface plot with height of FGM type spacer.

rise in height represents high electric field stress at conductor A and the dark blue color indicates high electrical field stress that is observed at the ends of the enclosure.

5.4 Study of electric field stress FGM post type spacer with depression

The above designed FGM post type spacer with depression have been resulted with high electric field stress at TJ at the enclosure end of conductor B with 0.2 mm in grading 2 of the FGM spacer as shown in Figure 6. Accordingly, the simulation is carried for conductor B only and tabulated in Table 5. In order to develop a uniform distribution of electric fields over the spacer surface, an MI is incorporated in the conductor B enclosure as shown in Figure 7. It has been identified from Table 5 that case 3 of GL-FGM grading has high electric field stress at the ends of the enclosure at TJ for all three applied voltages of V_1, V_2, V_3 compared to other cases and gradations. For GL-FGM grading of case 3 of conductor B, the electric field stress is measured as 0.11115 kV/cm and the field stress after inserting MI it is measured as 0.0086 kV/cm which is reduced by 92.26% at V_1 = 72.5 kV, similarly at V_2 = 132 kV, the field stress is reduced from 0.20235 to 0.0157 kV/cm with a reduction of 92.24% and at V_3 = 220 kV, the field stress is reduced from 0.33725 to 0.02618 kV/cm with a reduction of 92.24%.

Figure 12 shows that the magnitude of electric field stress at the enclosure is high for all three operating voltages and also very high at the conductor end with the highest peak values and this high stress is further reduced by using MI at TJ's and the results obtained are shown in Figure 14. Figures 13 and 15 clearly show the zoomed

Table 5: Reduction of electric field stress due to depression with MI.

Type	Permittivity values	Electric field stress due to depression at TJ without MI in KV/cm			Electric field stress due to depression at TJ with MI in KV/cm			% Reduction of Electric field stress due to depression at TJ due to insertion of MI		
		$V_{B\ max}$ = −51.258 kV	$V_{B\ max}$ = −93.324 kV	$V_{B\ max}$ = −155.54 kV	$V_{B\ max}$ = −51.258 kV	$V_{B\ max}$ = −93.324 kV	$V_{B\ max}$ = −155.54 kV	$V_{B\ max}$ = −51.258 kV	$V_{B\ max}$ = −93.324 kV	$V_{B\ max}$ = −155.54 kV
GL-FGM	Case 1	0.111	0.2022	0.337	0.00905	0.01645	0.0275	91.85	91.86	91.84
	Case 2	0.1111	0.2023	0.33715	0.0088	0.016	0.0268	92.08	92.09	92.05
	Case 3	0.11115	0.20235	0.33725	0.0086	0.0157	0.02618	92.26	92.24	92.24
GH-FGM	Case 1	0.10062	0.1832	0.30535	0.00755	0.0137	0.0228	92.50	92.52	92.53
	Case 2	0.10088	0.18365	0.3061	0.0074	0.0134	0.02235	92.66	92.70	92.70
	Case 3	0.1011	0.1841	0.3068	0.00725	0.01315	0.022	92.83	92.86	92.83
GU-FGM	Case 1	0.1018	0.1854	0.309	0.0076	0.01385	0.0231	92.53	92.53	92.52
	Case 2	0.102	0.1857	0.3096	0.00745	0.01355	0.0226	92.70	92.70	92.70
	Case 3	0.10225	0.1861	0.31025	0.0073	0.0133	0.02215	92.86	92.85	92.86

electric field at the enclosure ends without and with MI. Figures 16 and 17 are the surface plots of the designed FGM spacers with depression at conductor B without and with MI's respectively and from Figure 16, the arrows with greater dimension is observed at depression in grading 2, TJ at enclosure end of the FGM post type spacer which is representing high electric field stress. This field stress is reduced at the location of depression as well as at TJ, after introducing MI at enclosure end as shown in Figure 17. It is apparent from Figure 18 that the electrical field at TJ is measured very high with more electric field lines and further reduced by using MI with comparatively fewer field lines at TJ as shown in Figure 19. The above Figures 20 and 21 represent conductor B's quiver plot for FGM post-type spacer with depression with high electric field stress and reduction of depression and MI in the electrical field stress. Likewise the electrical field stress in the designed FGM post type spacers can be seen from the mesh plot due to depression without and with MI. The mesh triangle's thickness indicates that the field is high because of its curved shape. Mesh plot's main purpose is to set the plot element quality, rather than a uniform color. Mesh plot uses various data sets for different plots and can be represented in a single plot group to achieve the most exciting results and the corresponding mesh plot of FGM post-type spacer with depression without and with MI is as shown in Figures 22 and 23.

6 Conclusion

In this paper, the effect of depression is analyzed which was developed due to aging, switching operations, and lightning impulses. This defect depression, affects the dielectric permittivity, insulation capacity and the electric field distribution of the FGM post type spacer. The 2D simulation model of FGM post type spacer for a three-phase GIB with GL-FGM, GH-FGM and GU-FGM gradings with different permittivity values are studied to analyze the effect of depression with several observations as listed below.

- The electric field stress at the conductor's ends is more than that of the enclosure end for all the three conductors as the conductors are with high potential compared to the potential of enclosure end.
- High electric field stress is observed at the TJ of enclosure end of conductor B rather than conductors A and C, hence the defect depression is introduced at this conductor.
- The electric field stress has been increased drastically at TJ if the depression is located at grading 2,

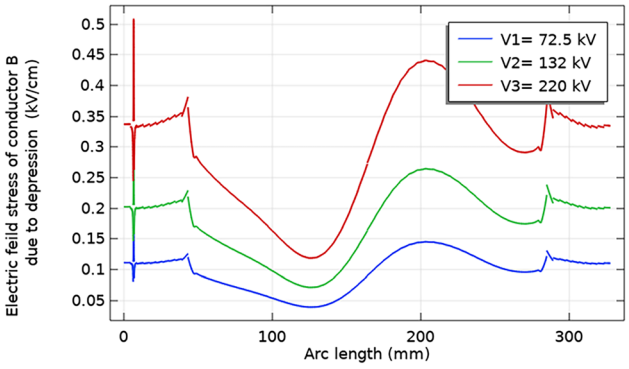


Figure 12: Effect of depression on FGM post type spacer.

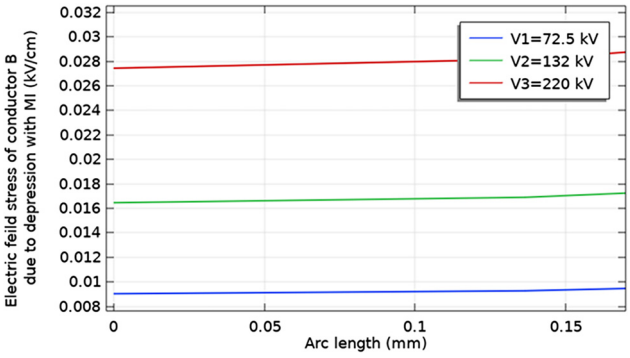


Figure 15: Electric field at enclosure end with MI.

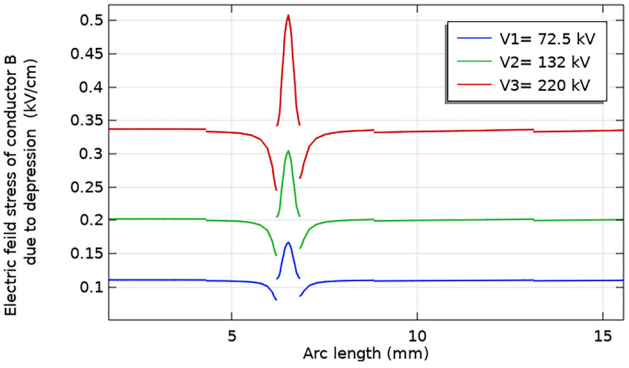


Figure 13: Electric field at enclosure end.

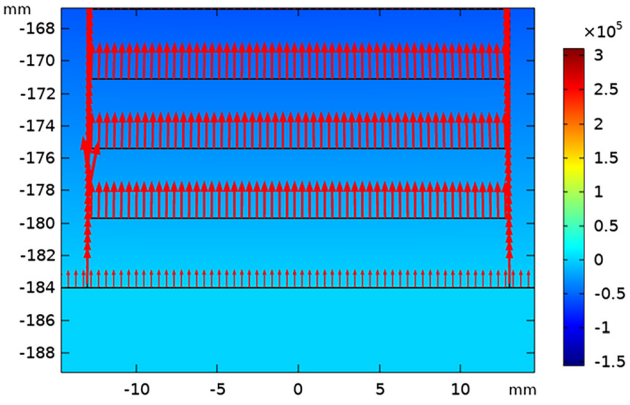


Figure 16: Surface Plot of FGM type spacer without MI.

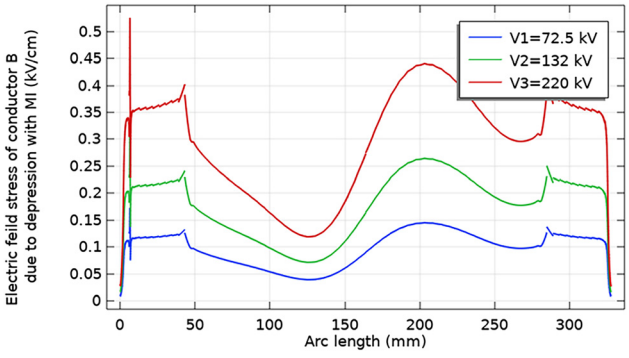


Figure 14: Reduction of electric field stress with MI.

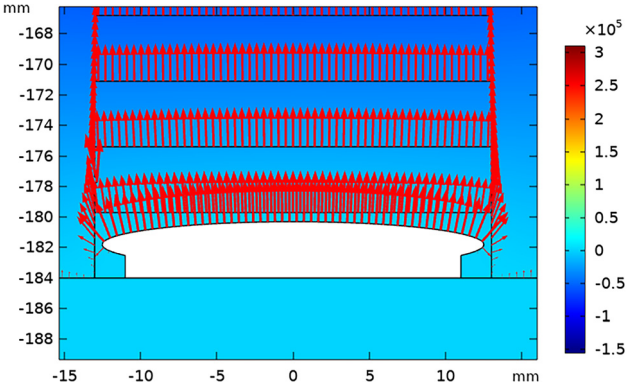


Figure 17: Surface Plot of FGM type spacer with MI.

which was also raised at 0.2 mm radius of the depression at different permittivity ranges of the spacer.

- The effect of depression on the electric field distribution increases as the relative permittivity of the spacer increases.
- For the above-mentioned location and the dimension of depression, it was observed that the highest electric field stress is obtained at case 3 of GL-FGM grading at the TJ of conductor B at all the operating voltages.
- The highest percentage reduction of electric field stress is observed in case 3 for GH-FGM and GU-FGM gradings.

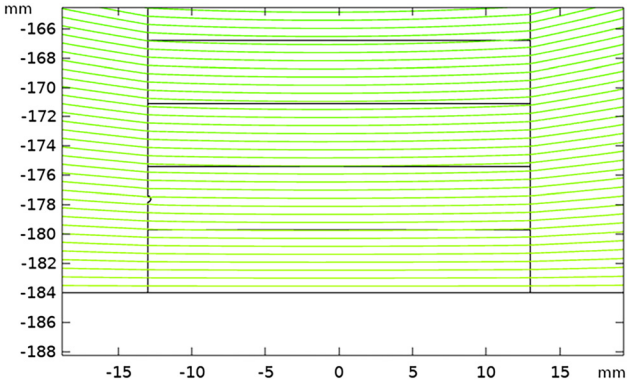


Figure 18: Contour plot of FGM post type spacer with depression.

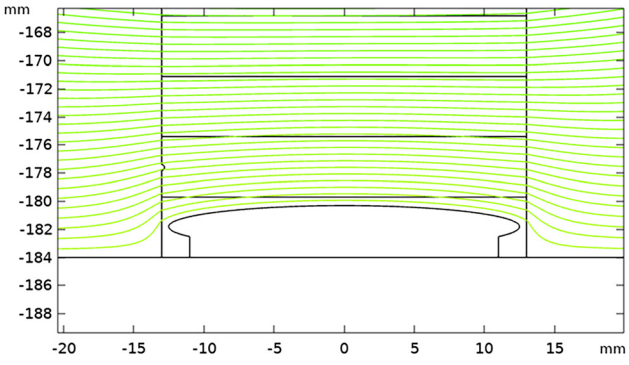


Figure 19: Contour plot of FGM post type spacer with depression and MI.

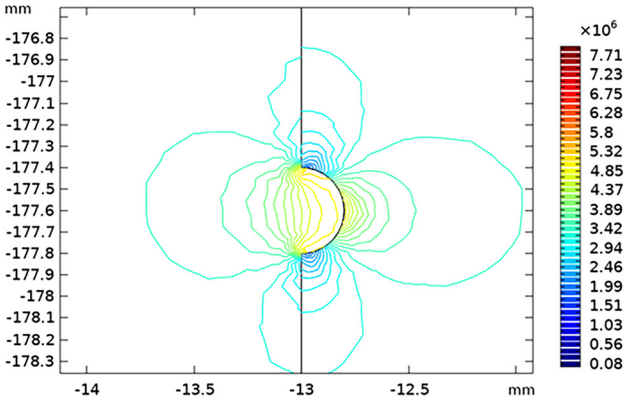


Figure 20: Quiver plot of FGM post type spacer with depression.

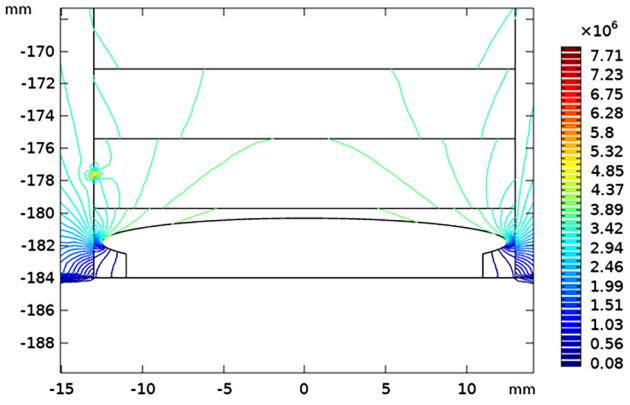


Figure 21: Quiver plot of FGM post type spacer with depression and MI.

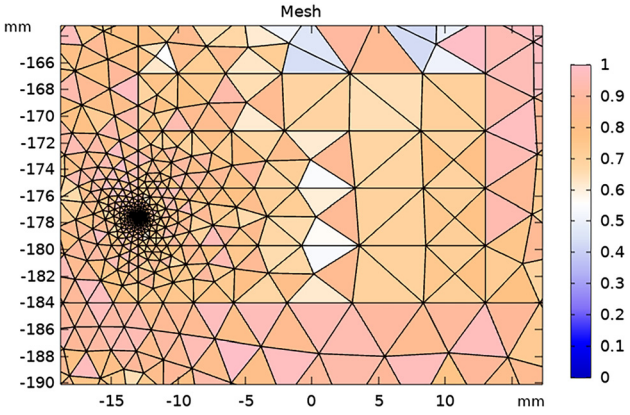


Figure 22: Mesh plot of FGM post type spacer with depression.

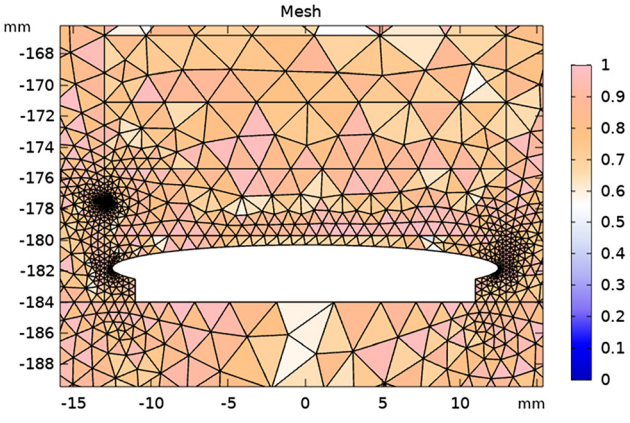


Figure 23: Mesh plot of FGM post type spacer with depression and MI.

So this new technique of FGM insulation will provide a better solution to the distribution of electric field in GIB and with the insertion of the MI at the TJ, the electric field stress can be reduced even under the effect of severe defect like depression on an FGM post type spacer in three-phase GIB.

Author contribution: All the authors have accepted responsibility for the entire content of this submitted manuscript and approved submission.
Research funding: None declared.
Conflict of interest statement: The authors declare no conflicts of interest regarding this article.

References

1. Cookson AH. Review of high voltage gas breakdown and insulators in compressed gases. IEE ProcPhys Sci Meas Instrum Manag Educ 1981;128:303–12.
2. Visakan S, Mandava MR, Mritunjay K, Sunitha K. Experimental study of fast transient currents in gas insulated substation. Int J Emerg Elec Power Syst 2019;20:1–13.
3. Wenjia X, Zutao X, Qiyan M. Research on induced voltage and current for hybrid transmission system composed of GIL and overhead line. Int J Emerg Elec Power Syst 2018;19:1–11.
4. Talaat M, El-Zein A, Amin M. Developed optimization technique used for the distribution of U-shaped permittivity for cone type spacer in GIS. Elec Power Syst Res 2018;163:754–66.
5. Rao MM, Joy Thomas M, Singh BP. Time-frequency spectrum analysis of very fast transient currents (VFTC) generated in a GIS. Int J Emerg Elec Power Syst 2007;8:1–18.
6. Rao MM, Paul M, Jain HS. Analytical and experimental studies on induced current switching by a fault-proof gas insulated earthing switch. Int J Emerg Elec Power Syst 2010;11:1–16.
7. Mohana Rao M. Evaluation of gas insulated disconnector switch for bus charging and bus transfer currents. Int J Emerg Elec Power Syst 2014;15:349–56.
8. Rao MM. A study on effect of concrete foundations on resistance and surface potentials of gas insulated substation grounding systems. Int J Emerg Elec Power Syst 2017;18:1–14.
9. Rao MM, Kumar M, Archana L. Development and experimental evaluation of leakage current measurement sensor for electrical power apparatus. Int J Emerg Elec Power Syst 2018;19:1–11.
10. Tsuboi H, Misaki T. Optimization of electrode and insulator contours by using Newton method. IEEE Trans Japan 1986;106A: 307–14.
11. Muneaki K, Katsumi K, Masahiro H, Hoshina Y, Takei M, Okubo H. Application of functionally graded materialfor reducing electric field on electrode and spacer interface. IEEE Trans Dielectr Electr Insul 2010;17:256–63.
12. Hayakawa N, Ishiguro J, Kojima H, Kato K, Okubo H. Fabrication and simulation of permittivity graded materials for electric field grading of gas insulated power apparatus. IEEE Trans Dielectr Electr Insul 2016;23:547–4.
13. Du BX, Liang HC, Li J, Zhang C. Temperature-dependent surface potential decay and flashover characteristics of epoxy/SiC composites. IEEE Trans Dielectr Electr Insul 2018;25:631–8.
14. Ran Z, Du B. Electric field regulation of insulator interface by FGM with conductivity for superconducting-GIL. IEEE Trans Appl Supercond 2019;29:1–5.
15. Hayakawa N, Shimomura J, Nakano T, Hanai M, Kato K, Okubo H. Fabrication technique of permittivity graded materials (FGM) for disk-type solid insulator. In: 2012 annual report conference on electrical insulation and dielectric phenomena, 14–7 Oct; 2012.
16. Matsuoka N, Fuchi Y, Kozako M, Hikita M. Effect of permittivity variation on surface flashover of GIS epoxy spacer model in SF6 gas. In: IEEE international conference on dielectrics; 2016, vol 2.
17. Tao J. Development and application of functionally gradient materials. In: International conference on industrial control and electronics engineering; 2012:1022–5 pp.
18. Hayakawa N, Miyaji Y, Kojima H. Simulation on discharge inception voltage improvement of GIS spacer with permittivity graded materials using flexible mixture casting method. IEEE Trans Dielectr Electr Insul 2018;25:1318–23.
19. Kurimoto M, Ozaki H, Sawada T, Funabashi Y, Kato T, Suzuoki Y. FEM simulation of local field enhancement close to lamination interface of permittivity-graded material, Electron Commun Jpn IEEJ Trans Electr Electron Eng 2018;101:1–87.
20. Chakravorti S, Lahiri A. Electrode-spacer contour optimisation by ANN aided genetic algorithm. IEEE Trans Dielectr Electr Insul 2004;11:964–75.
21. Adari J, Gadi VSKR, Gundavarapu VNK. Mitigation of field stress with metal inserts for cone type spacer in a gas insulated busduct under delamination. Eng Sci Technol Int J 2018;21:850–61.
22. Cooke CM, Velazquez R. The insulation of ultra-high-voltage in coaxial systems using compressed SF6gas. IEEE Trans Power Apparatus Syst 1977;96:1491–7.
23. Yao R, Hui M, Li J, Bai L, Wu Q. A new discharge pattern for the characterization and identification of insulation defects in GIS. Energies 2018;11:1–18.
24. Dai K, Liao Y. A novel system and experimental verification for locating partial discharge in gas insulated switchgears. Int J Emerg Elec Power Syst 2019;20:1–12.
25. Nagesh Kumar GV, Amarnath J, Singh BP, Srivastava KD. Electric field effect on metallic particle contamination in a common enclosure gas insulated busduct. IEEE Trans Dielectr Electr Insul 2007;14:334–40.
26. Nagesh Kumara GV, Amarnathb J, Singh BP, Srivastava KD. Particle initiated discharges in gas insulated substations by random movement of particles in electromagnetic fields. Int J Appl Electromagn Mech 2009;29:117–29.
27. Shibuya Y, Matsumoto S, Tanaka M. Electromagnetic waves from partial discharges and their detection using patch antenna. IEEE Trans Dielectr Electr Insul 2010;17:862–71.
28. Ueta G, Wada J, Okabe S, Miyashita M, Nishida C, Kamei M. Insulation performance of three types of micro-defects in inner epoxy insulators. IEEE Trans Dielectr Electr Insul 2012;19: 947–54.
29. Gao W, Ding D, Liu W, Huang X. Analysis of the intrinsic characteristics of the partial discharge induced by typical defects in GIS. IEEE Trans Dielectr Electr Insul 2013;20:782–90.
30. Feng Q, Dai Beijing N. Analysis and study on distribution of defect electric field on basin-type insulator in GIS. Guilin, China: ICAEER; 2018.
31. Gu F-C, Chen H-C, Chen B-Y. A fractional fourier transform-based approach for gas-insulated switchgear partial discharge recognition. J Electr Eng Technol 2019;14:2073–84.

32. Wen T, Zhang Q, Ma J, Wu Z, Shimomura N, Chen W. A new method to evaluate the effectiveness of impulse voltage for detecting insulation defects in GIS equipment. IEEE Trans Dielectr Electr Insul 2019;26:1301–7.
33. Ladani M, Preetha P. Reduction of electric field stress on the surface contour and at the triple junction in UHVAC GIS by spacer design optimization. Int J Emerg Elec Power Syst 2019; 20:1–12.
34. Li W-D, You X-Y, Mu H-B, Deng J-B, Zhang G-J. Numerical optimization and 3D-printing fabrication concept of high voltage FGM insulator. In: IEEE PES Asia-Pacific power and energy engineering conference; 2015. https://doi.org/10.1109/appeec.2015.7381007.

Available online at: http://www.ijmtst.com/vol6issue07.html

International Journal for Modern Trends in Science and Technology

ISSN: 2455-3778 :: Volume: 06, Issue No: 07, July 2020

Power System Contingency Analysis by using Voltage and Active Power Performance Index

Ummidi Sirisha[1] | M Sobha[2] | Arun Kumar Ch[2]

[1]PG Scholar, Dept. of E.E.E., Sanketika Vidya Parishad Engineering College, Visakhapatnam,
[2]Assistant Professor, Dept. of E.E.E., Sanketika Vidya Parishad Engineering College, Visakhapatnam,

To Cite this Article

Ummidi Sirisha, M Sobha and Arun Kumar Ch, "Power System Contingency Analysis by using Voltage and Active Power Performance Index", *International Journal for Modern Trends in Science and Technology*, Vol. 06, Issue 07, July 2020, pp.:52-60; https://doi.org/10.46501/IJMTST060708

Article Info

Received on 11-June-2020, Revised on 18-June-2020, Accepted on 21-June-2020, Published on 30-June-2020.

ABSTRACT

Now a days, power system protection is an important task for an operating engineer, which can be done by doing online security assessment. The contingency analysis technique is a prerequisite to predict the effects of various contingencies like failure of transformers, transmission lines, etc. To do contingency analysis first the operator has to know the parameters like voltage, power and voltage angle at each and every bus by doing load flow analysis on the system. Newton Raphson method is the best load flow method as it gives accurate results in less time. In this paper for each line outage contingency, load flow analysis has been done on the system and the active power and voltage performance indices have been calculated. These two performance indices will give the idea about the change in active power flow through the lines and voltages at the buses for a particular line outage. Summation of these two indices will give the performance index value through which ranking of severity will be given to the lines. Based on this, the ranking of most severe contingency has been done based on the values of performance indices. Simultaneously the value of bus voltages and active power flow before and after the most severe transmission line contingency has been analyzed. The effectiveness of the method has been tested on 5-Bus, 6-Bus, IEEE-14 Bus and IEEE-30 Bus test systems in MATLAB environment. This contingency analysis helps the operational engineer to know which line outage is dangerous to the system and what prior action is to be taken to minimize the effect of that particular line outage.

KEYWORDS:- *Contingency selection, Newton Raphson Method, Performance index, overload.*

Copyright © 2014-2020 International Journal for Modern Trends in Science and Technology
DOI: https://doi.org/10.46501/IJMTST060708

I. INTRODUCTION

Contingency is expressed as an unwanted event occurring in the power system for a short duration of time, which actually specify the loss or outage of one or more components of power system [1]. At the time of outage of any component or equipment in the power system, contingency analysis shows an indication, of what might be the position of power system [2]. It is fundamentally a software application run in power management system, simulating a speculative test on a list of notional cases, which would create power flow, voltage or reactive power violations in the sytem. These cases are recognized and ranked in order of their severity using contingency ranking approach [3]. Generally contingency analysis is separated into three parts, contingency creation, selection, and evaluation [4], but now a days the selection and the evaluation

both are doing in same section. Many work has been done on contingency selection mainly, whose aim is to reduce the indigenous long list of contingencies by selecting only the outages with severe limit violations [5]. This selection is seasoned by mainly two methods, i.e. contingency ranking and contingency screening. The screening methods are local solution based study, which primarily gives importance to the most dangerous cases for complete ac analysis, simultaneously the non-severe cases are deleted from the list [6]. Alternative method is ranking method, which uses performance index as a scalar value to narrate the effects of an outage on the whole system [7]. In this work, the effort has been given on contingency ranking. At starting the contingency list is formed, which contains those cases whose probability of getting outage is found to be high. The list, which is generally large, is translated into electrical network changes, mostly generator and/or line outages. Contingency evaluation using load flow is then carrying out on the following individual outages in decreasing order of severity. The activity will be remained up to the point where no post contingency violations are undergone.

II. CONTINGENCY ANALYSIS

A. Contingency Creation

It is the initial step of contingency analysis. It is made up of all set of viable contingencies that may happen in a power system. This process consists of making contingency lists.

B. Contingency Selection

It is the second step in contingency analysis; it is the process which includes finding of severe contingencies from all that may cause to violate bus voltages and power through lines. Here in this procedure contingency list is reduced by rejection of least severe contingency and taking into consideration of most severe outages. In this process the performance index has been used to find the most severe ones.

C. Contingency Evaluation

It is the third step and the most significant step as it includes necessary control and security actions which are required in order to reduce the effects of most severe contingencies in a power system.

III. UTILIZED LOAD FLOW METHOD

The Newton-Raphson method is the most useful method for load flow solutions because of its different advantages. It has dominant convergence characteristics compared to remaining load flow methods. And has less calculation. The Newton-Raphson method is benefit for large power system networks as because computer storage requirements are less and increases almost linearly with size of problem.

The following equations are used in N- R method to measure voltage, current, active power and reactive power at different buses.

The current injected at the bus m is

$$I_m = \sum_{l=1}^{n} Y_{ml} V_l \tag{1}$$

Where n is the number of buses in the system.

Y_{ml} is the admittance between lines m and l.

V_l is the voltage at bus I.

In polar form we can write equation 1 as

$$I_m = \sum_{l=1}^{n} |Y_{ml}||V_l| \angle(\theta_{ml} + \delta_l) \tag{2}$$

Where θ_{ml} is the admittance angle between lines m and l.

δ_l is the voltage angle of bus l.

We can write current in terms of active and reactive Power

$$I_m = \frac{P_m - jQ_m}{V_m^*} \tag{3}$$

Where P_m is the active power injected into the system from bus m.

Q_m is the reactive power injected into the system from bus m.

V_m is the voltage magnitude at bus m.

After substitution of I_m value in equation 3 we can get

$$P_m - jQ_m = |V_m| \angle -\delta_m \sum_{l=1}^{n} |Y_{ml}||V_l| \angle(\theta_{ml} + \delta_l) \tag{4}$$

By separating real and imaginary terms, we get

$$P_m = \sum_{l=1}^{n} |Y_{ml}||V_l||V_m| \mathrm{Cos}(\theta_{ml} - \delta_m + \delta_l) \tag{5}$$

$$Q_m = \sum_{l=1}^{n} |Y_{ml}||V_l||V_m| \mathrm{Sin}(\theta_{ml} - \delta_m + \delta_l) \tag{6}$$

By neglecting higher order terms if we expand equation 5 and 6 by using Taylor's series we will get

$$\begin{bmatrix}\Delta P_2^K \\ \vdots \\ \Delta P_n^K \\ \Delta Q_2^K \\ \vdots \\ \Delta Q_n^K\end{bmatrix} = \begin{bmatrix}\begin{pmatrix}\frac{\partial P_2^K}{\partial \delta_2^K} & \cdots & \frac{\partial P_2^K}{\partial \delta_n^K} \\ \vdots & \ddots & \vdots \\ \frac{\partial P_n^K}{\partial \delta_2^K} & \cdots & \frac{\partial P_n^K}{\partial \delta_n^K}\end{pmatrix} & \begin{pmatrix}\frac{\partial P_2^K}{\partial |V_2|^K} & \cdots & \frac{\partial P_2^K}{\partial |V_n|^K} \\ \vdots & \ddots & \vdots \\ \frac{\partial P_n^K}{\partial |V_2|^K} & \cdots & \frac{\partial P_n^K}{\partial |V_n|^K}\end{pmatrix} \\ \begin{pmatrix}\frac{\partial Q_2^K}{\partial \delta_2^K} & \cdots & \frac{\partial Q_2^K}{\partial \delta_n^K} \\ \vdots & \ddots & \vdots \\ \frac{\partial Q_n^K}{\partial \delta_2^K} & \cdots & \frac{\partial Q_n^K}{\partial \delta_n^K}\end{pmatrix} & \begin{pmatrix}\frac{\partial Q_2^K}{\partial |V_2|^K} & \cdots & \frac{\partial Q_2^K}{\partial |V_n|^K} \\ \vdots & \ddots & \vdots \\ \frac{\partial Q_n^K}{\partial |V_2|^K} & \cdots & \frac{\partial Q_n^K}{\partial |V_n|^K}\end{pmatrix}\end{bmatrix} \begin{bmatrix}\Delta \delta_2^K \\ \vdots \\ \Delta \delta_n^K \\ \Delta |V_2|^K \\ \vdots \\ \Delta |V_n|^K\end{bmatrix} \quad (7)$$

The jacobian matrix will give the linear relationship between small changes in the angle $\Delta\delta_i^K$ and change in bus voltage ΔV_i^K with small variations in real power and reactive power ΔP_i^K and ΔQ_i^K

$$\begin{pmatrix}\Delta P \\ \Delta Q\end{pmatrix} = \begin{pmatrix}J_1 & J_2 \\ J_3 & J_4\end{pmatrix}\begin{pmatrix}\Delta\delta \\ \Delta|V|\end{pmatrix} \quad (8)$$

The diagonal and off diagonal elements of J_1 are

$$\frac{\partial P_m}{\partial \delta_m} = \sum_{l\neq m}|V_m||V_l||Y_{lm}|\mathrm{Sin}\left(\theta_{ml} - \delta_m + \delta_l\right) \quad (9)$$

$$\frac{\partial P_m}{\partial \delta_m} = -|V_m||V_l||Y_{ml}|\mathrm{Sin}\left(\theta_{ml} - \delta_m + \delta_l\right), l \neq m \quad (10)$$

The power residuals ΔP_m^K, ΔQ_m^K can be written as

$$\Delta P_m^K = P_m^{sch} - P_m^K$$
$$\Delta Q_m^K = Q_m^{sch} - Q_m^K \quad (11)$$

Where P_m^{sch} is the scheduled active power at bus m.

Q_m^{sch} is the scheduled reactive power at bus m.

From the power residuals and jacobian matrix we can get the voltage magnitude $|V_m^K|$ and voltage angle δ_m^K.

The new values of voltages and angles are

$$|V_m^{(K+1)}| = |V_m^K| + \Delta|V_m^K| \quad (12)$$

$$\delta_m^{(K+1)} = \delta_m^K + \Delta\delta_m^K \quad (13)$$

IV. SYSTEM PERFORMANCE INDEX

The deviation of power system variables like bus voltages, power flows, from its rated value is measured by the system performance index. It is also used to evaluate the relative stability of a contingency [8].

1. Voltage performance index (PI_V)
2. Active power performance index (PI_{Mw})

A. Voltage Performance Index (PI_V):

The power system deficiency due to violation of bus voltages is described by the voltage performance index [2].

$$PI_v = \sum_{i=1}^{n}\left(\frac{W}{2z}\right)\left\{\frac{\left(|V_i| - |V_i^{sp}|\right)}{\Delta V_i^{\lim}}\right\}^{2z} \quad (14)$$

Where $|V_i|$ is the ith bus voltage magnitude.

$|V_i^{sp}|$ is the i[th] bus specified voltage magnitude.

$\Delta V_i^{\lim}$ is the voltage deviation limit which we can measure by taking average value of minimum and maximum allowable voltages at bus i.

z is exponent of the penalty function and value is (=1).

n is the number of buses in the given power system.

W is the real non negative weighting factor and value is (=1)

Here to calculate $\Delta V_i^{\lim}$ maximum voltage limit is 1.05 p.u and minimum voltage limit is 0.95 p.u since ±5% deviation in voltage is allowed. This voltage performance index will give the information about the change in voltage at each and every bus.

B. Active Power Performance Index (PI_{Mw}):

For identify the power over flows through the transmission lines the indices used is active power performance index [9].

$$PI_{MW} = \sum_{i=1}^{N_L}\left(\frac{W}{2z}\right)\left\{\frac{P_l}{P_l^{\max}}\right\}^{2z} \quad (15)$$

Where, P_l is the power flow (MW) through the line l.

$P_l^{\max}$ is the maximum capacity of power flow through the line l.

N_L is the number of the transmission lines of the power system

W is the real non-negative weighting facto and value is (=1)

z is exponent of penalty function and value is (=1)

$$P_l^{max} = \frac{V_i * V_j}{X} \quad (16)$$

Where V_i is the voltage at bus i.

V_j is the voltage at bus j.

X is the reactance of the line between bus i and bus j.

V. TEST CASES

To perform contingency analysis, IEEE standard 5 bus, 6 bus, 14 bus and30 bus systems are considered.

Test case 1: 5 BUS SYSTEM

TABLE 1.1: SYSTEM DATA

From Bus	To Bus	R (p.u.)	X (p.u.)	B/2 (p.u.)	Real Power Capacity(p.u.)
1	2	0.02	0.06	0.030	0.8
1	3	0.08	0.24	0.025	0.3
2	3	0.06	0.25	0.020	0.2
2	4	0.06	0.18	0.020	0.2
2	5	0.04	0.12	0.015	0.6
3	4	0.01	0.03	0.010	0.1
4	5	0.08	0.24	0.025	0.1

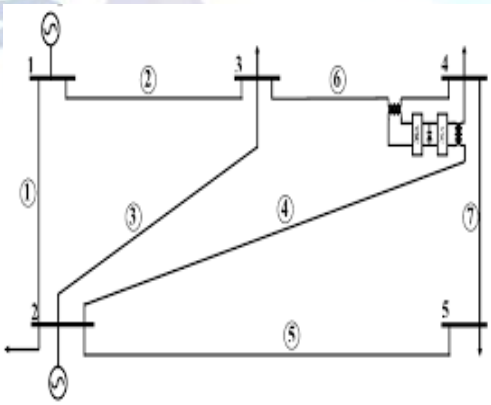


Fig. I: Five-bus Network

For analysis IEEE standard 5 bus system is considered. Bus 1 is slack bus, bus 2 is generator and 3,4, and 5 are load buses. Now for each line outage the load flow method has been carried out and the active power performance index and voltage performance index have been calculated using equations 14 and 15. The ranking has been given based on the Performance Index (P. I).

TABLE 1.2: RANKING OF THE LINES for 5-bus system

Tripped line	PI_V	PI_{MW}	PI	Rank
1-2	2.4587	0.1386	2.5973	3
1-3	3.2521	0.0276	3.2797	2
2-3	2.2540	0.0295	2.2834	6
2-4	2.3784	0.0293	2.4077	4
2-5	11.1376	0.0811	11.2186	1
3-4	2.2836	0.0235	2.3070	5
4-5	2.1436	0.0230	2.1666	7

TABLE 1.3: PRE CONTINGENCY AND POST CONTINGENCY STATE Bus VOLTAGES FOR THE LINE OUTAGE (2-5)

Bus No.	Pre-Contingency Voltage (p.u.)	Post-Contingency Voltage (p.u.)
1	1.0600	1.0600
2	1.0000	1.0000
3	0.9873	0.9602
4	0.9841	0.9503
5	0.9717	0.8579

TABLE 1.4: POST CONTINGENCY POWERFLOWS

From Bus	To Bus	When 2-5 line is tripped	Real Power Capacity (p.u.)
		Post-Contingency Power (p.u.)	
1	2	0.8147	0.8
1	3	0.5604	0.3
2	3	0.4517	0.2
2	4	0.5399	0.2
2	5	0	0.6
3	4	0.5215	0.1
4	5	0.6398	0.1

After the (2-5) line is tripped, all the transmission lines are overloaded as shown in the above table.

Test case 2: 6 BUS SYSTEM

TABLE 2.1: SYSTEM DATA

From Bus	To Bus	R (p.u.)	X (p.u.)	B/2 (p.u.)	Real Power Capacity (p.u.)
1	2	0.10	0.20	0.02	0.3
1	4	0.05	0.20	0.02	0.5
1	5	0.08	0.30	0.03	0.4
2	3	0.05	0.25	0.03	0.2
2	4	0.05	0.10	0.01	0.4

2	5	0.10	0.30	0.02	0.2
2	6	0.07	0.20	0.025	0.3
3	5	0.12	0.30	0.025	0.2
3	6	0.02	0.10	0.01	0.6
4	5	0.20	0.40	0.04	0.2
5	6	0.10	0.30	0.03	0.2

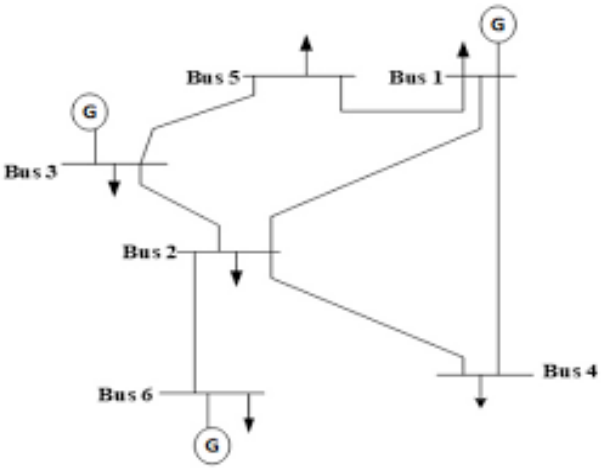


Fig.2: Six-bus Network

For analysis IEEE standard 6 bus system is considered. Bus 1 is slack bus, 2, 3 buses are generator and 4, 5, and 6 are load buses. Now for each line outage the load flow method has been carried out and the active power performance index and voltage performance index has been calculated using equations 14 and 15. The ranking has been given based on the Performance Index (P. I).

TABLE 2.2: RANKING OF THE LINES

Tripped line	PI_V	PI_{MW}	PI	Rank
1-2	4.0842	0.0455	4.1296	11
1-4	5.0979	0.0561	5.1539	3
1-5	4.7019	0.0511	4.7530	5
2-3	4.0974	0.0337	4.1311	10
2-4	8.9559	0.0500	9.0059	2
2-5	4.5972	0.0384	4.6356	6
2-6	4.2595	0.0396	4.2991	7
3-5	4.9139	0.0421	4.9560	4
3-6	9.6332	0.0811	9.7143	1
4-5	4.1636	0.0344	4.1980	9
5-6	4.2344	0.0335	4.2679	8

TABLE 2.3: PRE CONTINGENCY AND POST CONTINGENCY STATE Bus VOLTAGES FOR THE LINE OUTAGE (3-6)

Bus No.	Pre-Contingency Voltage (p.u.)	Post-Contingency Voltage (p.u.)
1	1.0500	1.0500
2	1.0500	1.0500
3	1.0700	1.0700
4	0.9894	0.9854
5	0.9854	0.9574
6	1.0044	0.8898

TABLE 2.4: POST CONTINGENCY POWERFLOWS

From Bus	To Bus	When 3-6 line is tripped: Post-Contingency Power (p.u.)	Real Power Capacity (p.u.)
1	2	0.3218	0.3
1	4	0.4602	0.5
1	5	0.3626	0.4
2	3	0.2132	0.2
2	4	0.3187	0.4
2	5	0.1500	0.2
2	6	0.5550	0.3
3	5	0.3847	0.2
3	6	0	0.6
4	5	0.0498	0.2
5	6	0.1990	0.2

Test case 3: 14 BUS SYSTEM

TABLE 3.1: SYSTEM DATA

From Bus	To Bus	R (p.u.)	X (p.u.)	B/2 (p.u.)	Real Power Capacity (p.u.)
1	2	0.01938	0.05917	0.02640	0.6
2	3	0.04699	0.19797	0.02190	0.7
2	4	0.05811	0.17632	0.01870	0.8
1	5	0.05403	0.22304	0.02460	0.5
2	5	0.05695	0.17388	0.01700	0.4
3	4	0.06701	0.17103	0.01730	0.3
4	5	0.01335	0.04211	0.0064	0.2
5	6	0.0	0.25202	0.0	0.5
4	7	0.0	0.20912	0.0	0.4
7	8	0.0	0.17615	0.0	0.2
4	9	0.0	0.55618	0.0	0.2
7	9	0.0	0.11001	0.0	0.2
9	10	0.03181	0.08450	0.0	0.2
6	11	0.09498	0.19890	0.0	0.3
6	12	0.12291	0.25581	0.0	0.2
6	13	0.06615	0.13027	0.0	0.2
9	14	0.12711	0.27038	0.0	0.2
10	11	0.8205	0.19207	0.0	0.2
12	13	0.22092	0.19988	0.0	0.2
13	14	0.17093	0.34802	0.0	0.2

Transformer	Between Buses	Tap Setting
1	4 – 7	0.978
2	4 – 9	0.969
3	5 – 6	0.932

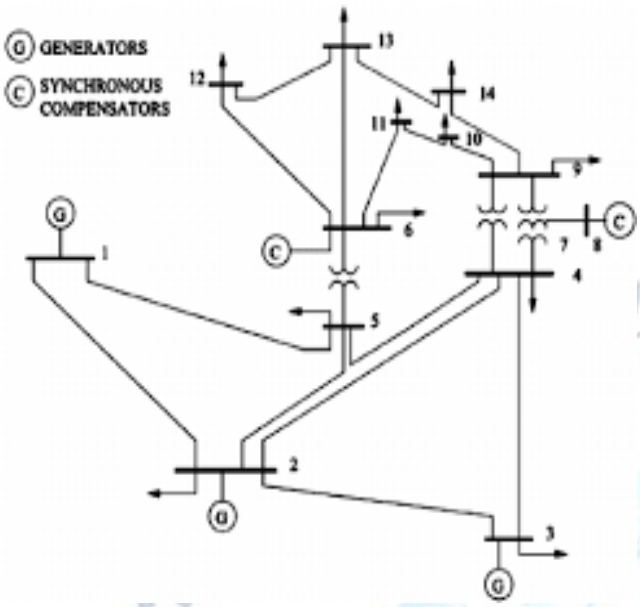


Fig. 3: Fouteen-bus Network

TABLE 3.2: RANKING OF THE LINES

Tripped line	PI_V	PI_{MW}	PI	Rank
1-2	13.8951	0.4008	14.2958	15
2-3	14.8189	0.2016	15.0204	10
2-4	14.4829	0.1589	14.6418	13
1-5	14.8244	0.1034	14.9278	11
2-5	14.8244	0.1034	14.9278	11
3-4	15.9340	0.0929	16.0269	2
4-5	14.3103	0.0953	14.4056	14
6-11	13.5478	0.0859	13.6338	17
6-12	14.1924	0.0849	14.2773	16
6-13	12.3364	0.1160	12.4524	20
7-8	12.6066	0.1014	12.7081	19
7-9	13.0923	0.0977	13.1900	18
9-10	15.0850	0.1025	15.1875	8
9-14	15.6176	0.1010	15.7186	4
10-11	15.3310	0.1046	15.4356	7
12-13	15.6541	0.0992	15.7533	3
13-14	14.9609	0.1023	15.0631	9
4-7	15.5247	0.1012	15.6259	5
4-9	15.2109	0.1079	15.3188	6
5-6	17.5626	0.1634	17.7260	1

TABLE 3.3: PRE CONTINGENCY AND POST CONTINGENCY STATE Bus VOLTAGES FOR THE LINE OUTAGE (5-6)

Bus No.	Pre-Contingency Voltage (p.u.)	Post-Contingency Voltage (p.u.)
1	1.0600	1.0600
2	1.0450	1.0450
3	1.0100	1.0100
4	1.0177	1.0181
5	1.0195	1.0272
6	1.0700	1.0700
7	1.0615	1.0656
8	1.0900	1.0900
9	1.0559	1.0682
10	1.0510	1.0614
11	1.0569	1.0623
12	1.0552	1.0543
13	1.0504	1.0525
14	1.0355	1.0422

TABLE 3.4: POST CONTINGENCY POWERFLOWS

From Bus	To Bus	When 5-6 line is tripped	Real Power Capacity (p.u.)
		Post-Contingency Power (p.u.)	
1	2	1.6147	0.6
2	3	0.7584	0.7
2	4	0.6166	0.8
1	5	0.7420	0.5
2	5	0.3771	0.4
3	4	0.2085	0.3
4	5	0.9963	0.2
5	6	0.0000	0.5
4	7	0.5613	0.4
7	8	0.0000	0.2
4	9	0.3191	0.2
7	9	0.5739	0.2
9	10	0.3349	0.2
6	11	0.1969	0.3
6	12	0.0455	0.2
6	13	0.0394	0.2
9	14	0.2733	0.2
10	11	0.2418	0.2
12	13	-0.0159	0.2
13	14	-0.1127	0.2

Test case 4: 30 BUS SYSTEM

TABLE 4.1: SYSTEM DATA

From Bus	To Bus	R (p.u.)	X (p.u.)	B/2 (p.u.)	Real Power Capacity (p.u.)
1	2	0.0192	0.0575	0.0528	1.0400
1	3	0.0452	0.1652	0.0408	1.0400
2	4	0.0570	0.1737	0.0368	0.5200
3	4	0.0132	0.0379	0.0084	1.0400
2	5	0.0472	0.1983	0.0418	1.0400
2	6	0.0581	0.1763	0.0374	0.5200
4	6	0.0119	0.0414	0.0090	0.7200
5	7	0.0460	0.1160	0.0204	0.5600
6	7	0.0267	0.0820	0.0170	1.0400
6	8	0.0120	0.0420	0.0090	0.2560
6	9	0.0	0.2080	0.0	0.5200

6	10	0.0	0.5560	0.0	0.2560
9	10	0.0	0.1100	0.0	0.5200
4	12	0.0	0.2560	0.0	0.5200
12	14	0.1231	0.2559	0.0	0.2560
12	15	0.0662	0.1304	0.0	0.2560
12	16	0.0945	0.1987	0.0	0.2560
14	15	0.2210	0.1997	0.0	0.1280
16	17	0.0524	0.1923	0.0	0.1280
15	18	0.1073	0.2185	0.0	0.1280
18	19	0.0639	0.1292	0.0	0.1280
19	20	0.0340	0.0680	0.0	0.2560
10	20	0.0936	0.2090	0.0	0.2560
10	17	0.0324	0.0845	0.0	0.2560
10	21	0.0348	0.0749	0.0	0.2560
10	22	0.0727	0.1499	0.0	0.2560
21	22	0.0116	0.0236	0.0	0.2560
15	23	0.1000	0.2020	0.0	0.1280
22	24	0.1150	0.1790	0.0	0.1280
23	24	0.1320	0.2700	0.0	0.1280
24	25	0.1885	0.3292	0.0	0.4800
25	27	0.1093	0.2087	0.0	0.1280
28	27	0.0	0.3960	0.0	0.5200
27	29	0.2198	0.4153	0.0	0.1280
27	30	0.3202	0.6027	0.0	0.1280
29	30	0.2399	0.4533	0.0	0.1280
8	28	0.0636	0.2000	0.4028	0.2560
6	28	0.0169	0.0599	0.0130	0.2560
9	11	0.0	0.2080	0.0	0.5200
12	13	0.0	0.1400	0.0	0.5200
25	26	0.2544	0.3800	0.0	0.1280

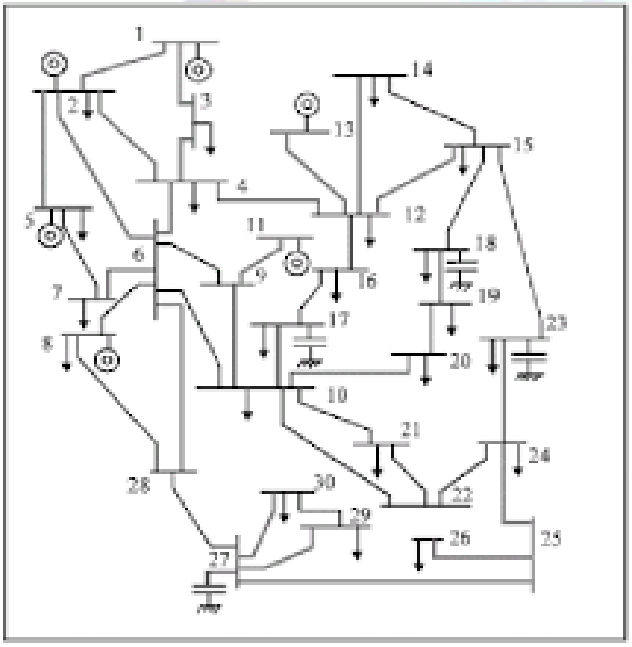


Fig. 4: Thirty-bus Network

TABLE 4.2: RANKING OF THE LINES

Tripped line	PI_V	PI_{MW}	PI	Rank
1-2	15.7079	0.1711	15.8791	33
1-3	15.5330	0.0479	15.5809	37
2-4	15.9123	0.0539	15.9661	31
3-4	16.4893	0.0606	16.5499	18
2-5	15.9673	0.0785	16.0458	30
2-6	15.9956	0.0529	16.0484	29
4-6	16.4688	0.0451	16.5139	19
5-7	16.2322	0.0418	16.2740	25
6-7	16.7208	0.0377	16.7585	16
6-8	16.0930	0.0470	16.1400	28
6-9	17.8893	0.0456	17.9348	5
6-10	15.1647	0.0433	15.2081	39
9-11	14.8014	0.0575	14.8589	41
9-10	14.9948	0.0524	15.0472	40
4-12	17.0075	0.0518	17.0593	9
12-13	17.7687	0.0690	17.8377	8
12-14	15.6947	0.0483	15.7430	35
12-15	16.3546	0.0514	16.4060	20
12-16	15.5754	0.0473	15.6227	36
14-15	16.2498	0.0445	16.2943	23
16-17	16.2244	0.0448	16.2692	26
15-18	15.9033	0.0448	15.9481	32
18-19	16.1722	0.0445	16.2167	27
19-20	16.6997	0.0469	16.7466	17
10-20	16.8525	0.0498	16.9022	15
10-17	15.7424	0.0468	15.7892	34
10-21	16.9585	0.0516	17.0101	12
10-22	16.3407	0.0485	16.3892	21
21-22	16.2294	0.0461	16.2755	24
15-23	17.8131	0.0487	17.8619	7
22-24	20.7223	0.0495	20.7718	4
23-24	17.0005	0.0476	17.0481	11
24-25	24.0833	0.0472	24.1305	1
25-26	15.2487	0.0422	15.2909	38
25-27	17.8429	0.0458	17.8887	6
27-28	17.0075	0.0518	17.0593	9
27-29	22.2469	0.0502	22.2971	2
27-30	21.9454	0.0502	21.9956	3
29-30	16.9006	0.0422	16.9428	14
8-28	16.3068	0.0600	16.3668	22
6-28	16.9376	0.0585	16.9961	13

TABLE 4.3: PRE CONTINGENCY AND POST CONTINGENCY STATE Bus VOLTAGES FOR THE LINE OUTAGE (24-25)

Bus No.	Pre-Contingency Voltage (p.u.)	Post-Contingency Voltage (p.u.)
1	1.0500	1.0500
2	1.0338	1.0338
3	1.0290	1.0291
4	1.0236	1.0237
5	1.0058	1.0058
6	1.0219	1.0216

7	1.0075	1.0074
8	1.0230	1.0230
9	1.0418	1.0443
10	1.0356	1.0409
11	1.0913	1.0913
12	1.0432	1.0457
13	1.0883	1.0883
14	1.0280	1.0317
15	1.0230	1.0280
16	1.0327	1.0364
17	1.0293	1.0341
18	1.0152	1.0203
19	1.0137	1.0189
20	1.0184	1.0236
21	1.0212	1.0284
22	1.0211	1.0289
23	1.0099	1.0196
24	1.0010	1.0169
25	0.9797	0.9412
26	0.9613	0.9220
27	0.9753	0.9506
28	1.0208	1.0177
29	0.9544	0.9290
30	0.9423	0.9166

TABLE 4.4: POST CONTINGENCY POWERFLOWS

From Bus	To Bus	When 24-25 line is tripped: Post-Contingency Power (p.u.)	Real Power Capacity (p.u.)
1	2	0.9077	1.0400
1	3	0.4786	1.0400
2	4	0.2920	0.5200
3	4	0.4452	1.0400
2	5	0.5814	1.0400
2	6	0.3785	0.5200
4	6	0.3877	0.7200
5	7	0.1300	0.5600
6	7	0.3623	1.0400
6	8	0.0093	0.2560
6	9	0.1522	0.5200
6	10	0.1204	0.2560
9	10	0.3292	0.5200
4	12	0.2698	0.5200
12	14	0.0776	0.2560
12	15	0.1777	0.2560
12	16	0.0682	0.2560
14	15	0.0148	0.1280
16	17	0.0328	0.1280
15	18	0.0568	0.1280
18	19	0.0244	0.1280
19	20	0.0706	0.2560
10	20	0.0937	0.2560
10	17	0.0575	0.2560
10	21	0.1645	0.2560
10	22	0.0805	0.2560
21	22	0.0117	0.2560
15	23	0.0517	0.1280
22	24	0.0682	0.1280
23	24	0.0194	0.1280
24	25	0	0.4800
25	27	0.0355	0.1280
28	27	0.1620	0.5200
27	29	0.0621	0.1280
27	30	0.0712	0.1280
29	30	0.0371	0.1280
8	28	0.0407	0.2560
6	28	0.1288	0.2560
9	11	0.1793	0.5200
12	13	0.1691	0.5200
25	26	0.0355	0.1280

VI. CONCLUSION

To give the contingency ranking, performance index has been used as a measuring tool. Newton Raphson power flow method is found most appropriate method in the approach of contingency selection, as it played a vital role in rejecting the large number of contingency cases and concentrated on the most severe contingency case. From the results, it is seen that the calculation of performance indices gives a good measure of the cases, which has the highest potential to form the system

parameters to go beyond their limits, calculation of PI are also obtained for the sake of increase in the accuracy of the sorting and ranking technique of the contingency analysis process.

VII. FUTURE SCOPE

From the above one can judge the state of power system if any equipment gets outage from the system. So by forecasting the effect of any outage, the operator come to know the prior action what should be done for the particular outage. Especially at this condition "FACT' devices will help to control the power flow and to maintain good voltage profile at each and every bus. TCSC will be used to control the power flow through the lines which is getting overloaded and ST ATCOM, SVC will be used to maintain good voltage profile by giving

reactive power or by taking reactive power from the bus. So we can extend this work by placing "FACT' devices in our system.

REFERENCES

[1] L.H. Fink and K. Carlsen, "Operating under stress and strain," IEEE Spectrum; (United States}. vol. 15, 1978.

[2] K.S. Swarup and G. Sudhakar, "Neural network approach to contingency screening and ranking in power systems," Neurocomputing, vol. 70, pp. 105-1 18, 2006.

[3] G. Ejebe and B. Wollenberg, "Automatic contingency selection," Power Apparatus and Systems. IEEE Transactions on, pp. 97-109, 1979.

[4] B. Stott, O. Alsac, and A. J. Monticelli, "Security analysis and optimization," Proceedings of the IEEE, vol. 75, pp. 1623-1644, 1987.

[5] A.J. Wood and B.F. Wollenberg, Power generation. operation. And control: John Wiley & Sons, 2012.

[6] J. Zaborszky, K.W. Whang, and K. Prasad, "Fast contingency evaluation using concentric relaxation," Power Apparatus and Systems. IEEE Transactions on, pp. 28-36, 1980.

[7] C.Y. Lee and N. Chen, "Distribution factors of reactive power flow in transmission line and transformer outage studies," Power Systems. IEEE Transactions on, vol. 7, pp. 194-200, 1992.

[8] F. Albuyeh, A. Bose, and B. Heath, "Reactive power considerations in automatic contingency selection," Power Apparatus and Systems. IEEE Transactions on, pp. 107-112, 1982.

[9] S. Naik, M. Khedkar, and S. Bhat, "Effect of line contingency on static voltage stability and maximum loadability in large multi bus power system," International Journal of Electrical Power & Energy Systems, vol. 67, pp. 448-452, 2015.

International Journal for Modern Trends in Science and Technology

International Journal of Engineering Innovations In Advanced Technology ISSN[O] :2582-1431
Volume-02,Issue-01

Design Of Functional Observer Based Load Frequency Controller For Inter-Connected Power System

Anand Gondesi
Department of EEE, Dr L Bullayya College of Engineering for Women, Visakhapatnam, India
Email: anandgondesi@gmail.com

R Vijaya Santhi and K R Sudha
Department of EE,A U College of Engineering, Andhra University, Visakhapatnam, India
Email: { santhikanth@gmail.com, arsudhaa@gmail.com }

Abstract— **This paper presents a novel peculiar functional observer based on quasi-decentralized load frequency control scheme for power systems. The quasi-decentralized functional observers are designed to implement any given state feedback controller based on functional observer theory. The designed functional observers are decoupled from each other to have a simpler structure when compared to the state observer based schemes. The proposed design method is based on the network topology and the proposed functional observer scheme is further applied to a complex nonlinear power system.**

Index Terms— **Functional Observer, Load Frequency Control, Luenberger observer.**

I. INTRODUCTION

With the growing complications on interconnected power systems, load frequency control (LFC) problem has modernized interest in recent years [1]–[4]. LFC is a scheme that keeps the frequency of a network within satisfactory limits regardless of the load variations by balancing the power consumption and production. Furthermore, it has competence to bring any deviations (i.e., tie-line power deviations) of the entire power exchange back to zero, amongst interconnected areas. In general, LFC is implemented on selected generation units. Each of the controllers generates a control signal to a prime-mover when the loads fluctuate to match the power supply and demand.Through an integral control action of the area control error (ACE), tie-line power deviations are also brought out to zero. Even though a number of solutions and schemes have been proposed and developed in the last decade, for LFC considering time delays in power systems see [1], [4] and [7], soft computing based LFC schemes which have attracted considerable attention are reported in [8]–[13]. Also linear control based LFC schemes are reported in [5] and [6], a sliding mode technique is presented in [3] and LFC based on a model reduction technique is presented in [2]. For other methods of LFC, see [14]–[16], and in [17] a survey of various control schemes can be found.

Literature of LFC is based on approximating all generators in a given area into a single generation unit. Furthermore, the power distribution network including various bus bars and transmission lines are all lumped into one single entity in the analysis and design of controllers. With growing complexity of power distribution, assumptions which loose the network topology may not be the correct representative of a complex power network. The present paper makes no such simplified assumptions thus presenting a quasi decentralized functional observer scheme to control the frequency and tie-line power of a multi-area interconnected power system. In one of the previous paper [18], two-area linear systems connected with a single tie-line model was considered and for the generation of control signals, the application of quasi-decentralized functional observer is considered. Based on this preliminary work in [18], this paper further develops the functional observer (FO) theory for the LFC of interconnected power networks of higher order. In the LFC signal generation process, only the estimate of the control signal is required. Also using a functional observer, it is more congruent to directly estimate the proper required signal than estimating all the individual states and then re-combining those individual state estimates to construct the desired control signal [22]. Actually we consider a quasi-decentralized functional observer to generate the control signal. The proposed quasi-decentralized functional observer based controllers have simpler structures. Furthermore, the functional observability requirement is less stringent than the state observability requirement see [19] and [20]. The rest of paper is organized as follows; Section II the power system dynamic modeling is presented. Section III focuses on functional observer algorithm and functional observer based LFC. A case study of a complex power system including a comparing study on functional and Luenberger observer is given in Section IV and followed by a conclusion in Section V.

II. Dynamic Modelling Of Two Area Inter-Connected System

The block diagram of a two area thermal power system for load frequency control [9]-[16] is shown in Fig.1.Consider the dynamic model of a linear two area LFC in state-space representation is given by

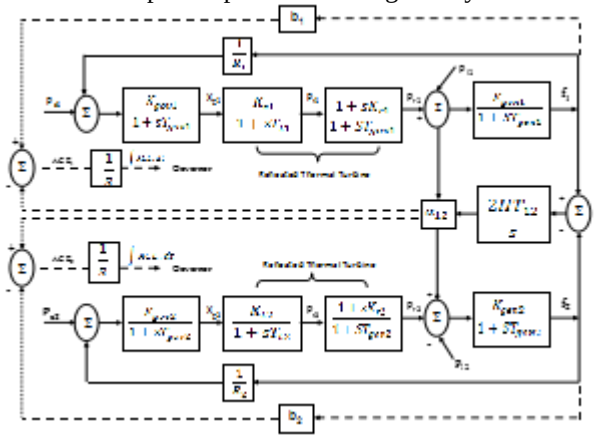


Figure.1.Block-diagram of two-area interconnected power system (TAIPS).

The state variable representation of the system is advantageous compared to the conventional transfer function representation. The state vector x(t) contains the information about the past behavior of the system and the future behavior which is governed by the ordinary differential equation (1). The properties of the system are determined by the constant matrices A, B and C. Thus the study of the system can be carried out in the field of matrix theory which has many notational and conceptual advantages.

In any control system, the input vector u(t) is chosen by proper control schemes such that the system behaves in an acceptable manner. As the state vector x(t) contains all the essential information about the system, the selection of u(t) is done using some combinations of x(t) and u(t) is obtained from the relation

$$u(t) = -K\,x(t) \qquad (3)$$

In a simplified manner, the power flow in the tie line can be considered as for Area 2 in a two area system consisting of reheat thermal turbines.

$P_{tie2}(t)= -P_{tie2}(t)$ from Fig. 1.

Let $x_i(t),u_i(t),d_i(t)$ and $y_i(t)$ (i=1,2) as state, control, load disturbance and output vectors

Where

$$x_1(t)= [P_{tie1}\ \ f_1\ \ P_{r1}\ \ P_{g1}\ \ X_{g1}\ ]^T \qquad (4)$$

$$x_2(t)= [f_2\ \ P_{r2}\ \ P_{g2}\ \ X_{g2}\ ]^T \qquad (5)$$

$$u_i(t)=P_{ci}(t),\ \ d_i(t)=P_{li}(t) \qquad (6)$$

$$y_i(t)=[P_{tiei}\ \ f_i\ \ X_g\ ]^T \qquad (7)$$

From this, the representation for the two area interconnected power system is determined for an eleventh-order, 2-input, 2-disturbance, where

$$\dot{x}(t) = Ax(t) + Bu(t) + D_d(t) \qquad (8)$$

From (7), the controlled feedback variables are provided by the integral of ACE's to ensure zero steady state values for tie line power and frequencies for the step change in load disturbances. Pole placement or optimal control by state feedback has been extensively covered in the literature [1]-[3].

III. FUNCTIONAL OBSEVER

A Functional observer uses recurring theme in state feedback control, i.e., only a linear function is enough rather than the complete state vector information. The primary aim of the literature is to produce observer with more stability and further reduced order noticing the affect on the performance due to the change in design.

The result to this problem is firstly presented by Luenberger. It states that A single linear state function of a linear system can be reconstructed by an observer with v-1 eigen values that may be chosen arbitrarily (where v is the observability index). For any completely observable system, v-1<n-m, it is often the case that the order v-1 of a linear functional observer is less than the order n-m of the reduced-order observer. As a consequence, observing a linear function of the states may result in a significant reduction in observer order compared to the entire state vector.

Fig. 2 shows a block diagram representation of the QDFO implementation for LFC of a two area interconnected power system. The flow of information from one area to another area is represented by the dotted lines. The two FO's are decoupled from each other. Thus, there is no transfer of data between them.

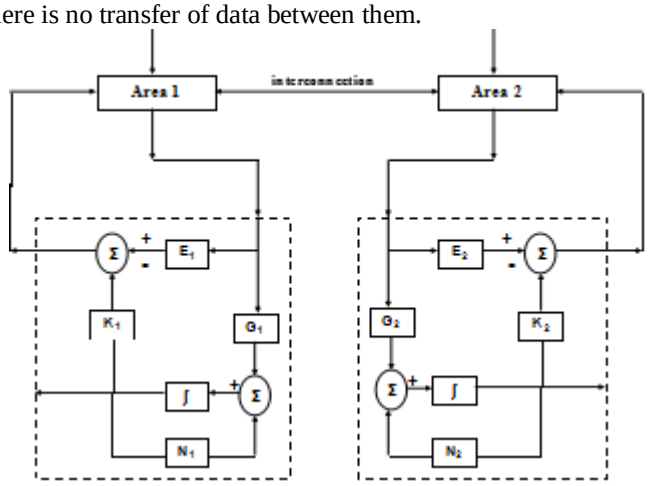


Figure. 2. Block diagram implementation of QDFO's for the two area interconnected power system.

A system involves many problems in decision making, monitoring, fault detection, and control which rely on the knowledge of state variables and time-varying parameters that cannot be measured directly. In such situations, the estimation of states and parameters in dynamic systems is a vital prerequisite. Hence observers that use the input and output signals can be employed to estimate the unknown states. Many estimation techniques are available for the construction of observers for linear models such as the Kalman filter and its variants. However there is no generalized procedure for the design of estimators for nonlinear systems as it involves high computational costs. One such model which facilitates the stability analysis and observer design for such

systems can be represented by a special type of a dynamic nonlinear model.[11].

special type of a dynamic nonlinear model.[11].

Consider a linear time-invariant system described by

$$\dot{x}(t) = Ax(t) + Bu(t) \quad (9)$$

$$y(t) = Cx(t) \quad (10)$$

$$z(t) = Lx(t) \quad (11)$$

A functional observer is a dynamical system that can track z(t) asymptotically and has the following structure,

$$\dot{w}(t) = Nw(t) + Jy(t) + Hu(t) \quad (12)$$

$$\hat{z}(t) = Gw(t) + Ey(t) \quad (13)$$

The system matrices *A, B* and *C* and observer matrices *N, J, H, D* and *E* are defined as follows:

$A \in R^{nxn}$ $N \in R^{qxq}$

$B \in R^{nxm}$ $J \in R^{qxp}$

$C \in R^{pxn}$ $H \in R^{qxm}$

$L \in R^{rxn}$ $D \in R^{rxp}$ $E \in R^{rxp}$

Theorem-1

The completely observable qth order functional observer of (12) and (13) will estimate Lx(t) if and only if the following conditions hold:

N is a stability matrix

$$JC = PA - NP \quad (14)$$

$$H = PB \quad (15)$$

$$L = DP + EC \quad (16)$$

Now we will define the observer error in estimating the states as

$$e(t) \triangleq w(t) - Px(t) \quad (17)$$

If we take the derivative and substituting the observer and system equations, we obtain

$$\dot{e}(t) = \dot{w}(t) + P\dot{x}(t) = Nw(t) + J\dot{C}x(t) + Hu(t) - PAx(t) - PBu(t) \quad (18)$$

Applying conditions (14) and (15) yields

$$\dot{e}(t) = Nw(t) + (PA - NP)x(t) + Bu(t) - PAx(t) - PBu(t)$$

$$= Nw(t) - NPx(t)$$

$$= Ne(t) \quad (19)$$

The differential equation solution is an exponential function of the form,

$$e(t) = e^{Nt} \quad (20)$$

On applying conditions, we get the result as,

$$\lim_{t \to \infty} e(t) = w(t) - Px(t) \quad (21)$$

on further simplification, we get

$$e_z(t) = \hat{z}(t) - Lx(t)$$

$$= Dw(t) - ECx(t) - Lx(t)$$

$$= D(w(t) - Px(t)) \quad (22)$$

As the above equation is expected to reach zero asymptotically, we can clearly say that A and N do not share a common eigen value and also ensuring P has unique solution. Now we can derive X and e by using above defined conditions

$$\dot{x}(t) = Ax(t) + Bu(t) = Ax(t) - B(Dw(t) + Ey(t))$$

$$= Ax(t) + BDw(t) + BECx(t)$$

$$= Ax(t) + BDw(t) + B(L - DP)x(t)$$

$$= (A + BL)x(t) + (BD)e(t) \quad (23)$$

$$\dot{e}(t) = Ne(t) \quad (24)$$

This results in a composite system similar to the full-state observer as

$$\begin{bmatrix} \dot{x}(t) \\ \dot{e}(t) \end{bmatrix} = \begin{bmatrix} A + BL & BD \\ 0 & N \end{bmatrix} \begin{bmatrix} x(t) \\ e(t) \end{bmatrix} \quad (25)$$

Aside from the variation in notation and the fact that the control law is Lx(t) instead of -Kx(t), they are similar to each other. If we consider the constraints, the functional state reconstruction almost revolves around constructing the least possible rth order observer provided all the observer matrices must satisfy the conditions without compromising other favorable aspects of observer, such as freedom of eigen value assignment and algorithm simplicity, so that it can be readily implemented in practice.

To satisfy the conditions of order estimation, we take the ranks into consideration.

$$rank \begin{bmatrix} LA \\ CA \\ C \\ L \end{bmatrix} = rank \begin{bmatrix} CA \\ C \\ L \end{bmatrix} \quad (26)$$

$$rank \begin{bmatrix} sL - LA \\ C \\ L \end{bmatrix} = rank \begin{bmatrix} CA \\ C \\ L \end{bmatrix} \quad s \in C, R(s) \quad (27)$$

Whether, condition is satisfied when the ranks on the LHS and RHS are equal. The author in [21] shows that this condition is equal to the delectability of the pair (F, G), where

$$F = LAL^{+} - LA(I - L^{+}L) \begin{bmatrix} CA(I - L^{+}L) \\ C(I - L^{+}L) \end{bmatrix}^{+} \begin{bmatrix} CAL^{+} \\ CL^{+} \end{bmatrix} \quad (28)$$

$$G = \left(I - \begin{bmatrix} CA(I - L^{+}L) \\ C(I - L^{+}L) \end{bmatrix} \begin{bmatrix} CA(I - L^{+}L) \\ C(I - L^{+}L) \end{bmatrix}^{+} \right) \begin{bmatrix} CAL^{+} \\ CL^{+} \end{bmatrix} \quad (29)$$

where L+ denotes the Moore-Penrose generalized inverse of matrix L. Furthermore, if matrices J,H and E satisfy Theorem 1, a Hurwitz matrix N is given by

$$N = F - ZG \quad (30)$$

where matrix Z is obtained by any pole placement method so that F -ZG is stable.

Matrices E and K are obtained according to

$$[E \quad K] = L\bar{A}\Sigma^{+} + Z(I - \Sigma\Sigma^{+}) \quad (31)$$

where $\bar{A} = A(I - L^{+}L)$, $\bar{C} = C(I - L^{+}L)$

and $\Sigma = \begin{bmatrix} C\bar{A} \\ \bar{C} \end{bmatrix}$

and matrix J is obtained according to

$$J = K + NE \quad (32)$$

Whilst matrix H is obtained according to

$$H = (L - EC)B \quad (33)$$

By using this algorithm we can easily compute all the required observer parameters which results in a functional observer of the form

$$\dot{w}(t) = Nw(t) + Jy(t) + Hu(t) \quad (34)$$

$$\hat{z}(t) = w(t) + Ey(t) \quad (35)$$

IV. RESULTS AND DISCUSSION

In order to verify the proposed technique, the results from the Matlab / Simulink are used for the increase in demand of the first area **Δ**PD1 and second area **Δ**PD2. In this condition, for which perturbation is applied to both the areas. In this case, a step change is applied to both the first area **Δ**PD1 and the second area **Δ**PD2. The frequency variation of the first area **Δ**f1 is shown in Figs. 3–8, using the method employed, the changes in frequency are quickly nullified to zero. Hence, QDFO are superior to Luenberger observer as it has the best performance in control and damping of frequency in all responses.

The performance for the above cases is shown tabulated at a particular operating condition and shown in Table 1. In this study, settling time, overshoot and undershoot are obatained for different operating points by calculation. The results from the simulation are shown for 10% band of step load change for the operating point of Appendix A. From the Table 1, it is found that the performance of the proposed QDFO is far superior to the Luenberger observer

Table 1: Δf_1 response performance in various control strategies

Operating point	Controller	Over shoot (P.U)	Under shoot (P.U)	Setting time (sec)
1	Full order Luenberger Observer	0.05211	-0.06554	5.213
	Quasi Decentralized Functional Observer	0.04539	-0.06088	5.111
2	Full order Luenberger Observer	0.09419	-0.09907	4.994
	Quasi Decentralized Functional Observer	0.06718	-0.0868	4.796
3	Full order Luenberger Observer	0.03961	-0.05186	6.369
	Quasi Decentralized Functional Observer	0.03681	-0.4921	6.251
4	Full order Luenberger Observer	0.09231	-0.09644	6.321
	Quasi Decentralized Functional Observer	0.06	-0.07916	5.051
5	Full order Luenberger Observer	0.0414	-0.05384	6.309
	Quasi Decentralized Functional Observer	0.03804	-0.05119	6.126
6	Full order Luenberger Observer	0.06955	-0.08092	5.154
	Quasi Decentralized Functional Observer	0.0551	-0.07296	5.088

In Fig.3 to Fig.8 are the comparison of Δf_1 (t) responses for various observers in terms of nominal values. The simulation results show that the proposed method QDFO is robust to change in the parameter of the system and has good performance as compared to Luenberger observer in all of the operating conditions.

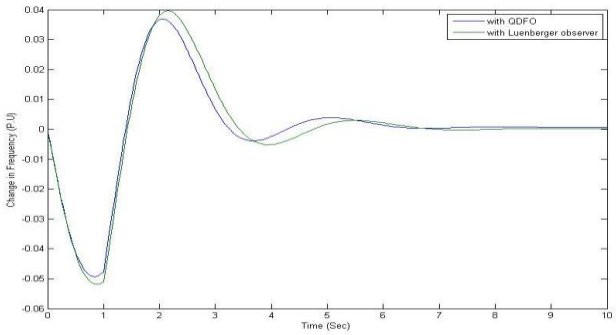


Figure. 3.Change in frequency with step increase in demand at operating point 1.

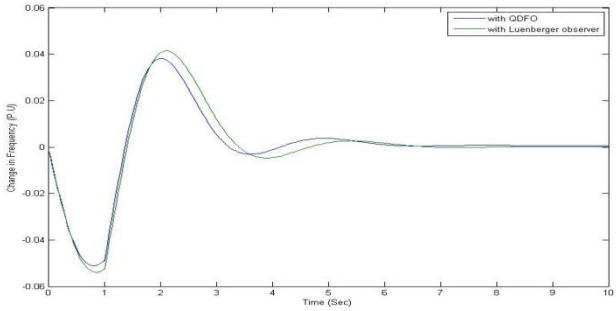


Figure.4. Change in frequency with step increase in demand at operating point 2.

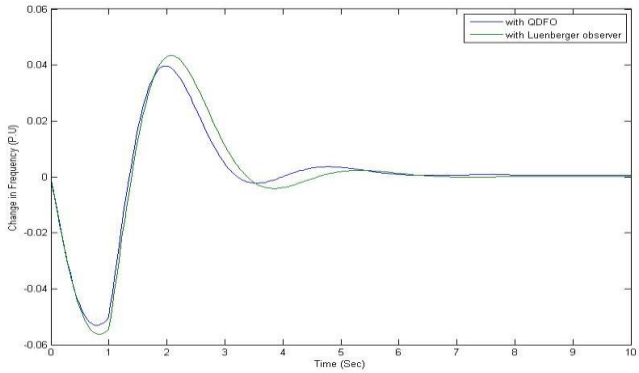


Figure. 5. Change in frequency with step increase in demand at operating point 3.

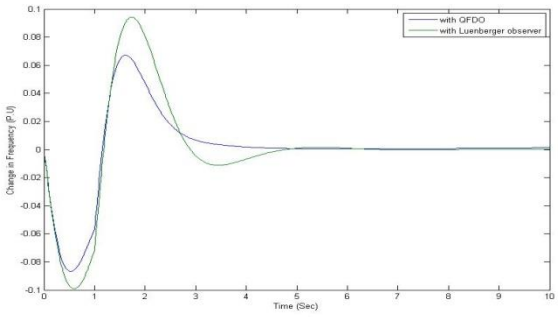


Figure. 6. Change in frequency with step increase in demand at operating point 4.

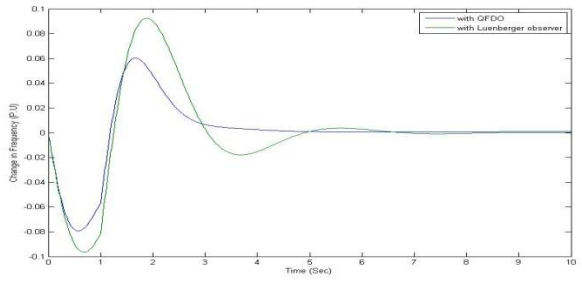


Figure. 7.Change in frequency with step increase in demand at operating point 5.

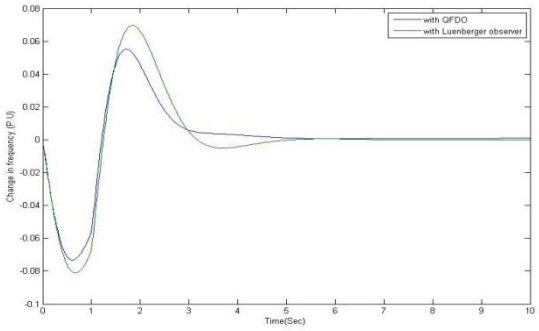


Figure. 8. Change in frequency with step increase in demand at operating point6.

V. CONCLUSIONS

In this paper, the solution of a load frequency control problem is obtained by using QDFO for a multi-area power system. The two area interconnected reheat thermal power system with system parameter uncertainty is chosen for the testing of the proposed observer. The results from the simulation shows that the designed observer guarantees the robust stability and performance. The proposed method is used to test the precise reference frequency tracking and disturbance attenuation under a wide range of parameter uncertainty and varying load conditions. To find the robustness of the proposed observer, it is compared with Luenberger observer in terms of settling time, maximum overshoot and undershoots under different operating conditions.

REFERENCES

[1] Jiang, L., and Yao, W., and Wu, Q., and Wen, J., and Cheng, S. (2012). Delay-dependent stability for load frequency control with constant and time-varying delays. *IEEE Trans. Power Syst*, 27(2), 932–941.

[2] Saxena, S., and Hote, Y.V. (2013). Load frequency control in power systems via internal model control scheme and model-order reduction. *IEEE Trans. Power Syst*, 28(3), 2749–2757.

[3] Mi, Y., and Fu, Y., and Wang, C., and Wang, P. (2013). Decentralized sliding mode load frequency control for multi-area power systems. *IEEE Trans. Power Syst*, 28(4), 4301–4309.

[4] Zhang, C.K., and Jiang, L., and Wu, Q., and He, Y., and Wu,M. (2013). Delay-dependent robust load frequency control for time delay power systems. *IEEE Trans. Power Syst.*, vol. 28(3) , 2192–2201.

[5] Tan, W. (2010). Unified tuning of pid load frequency controller for power systems via IMC. *IEEE Trans. Power Syst*., 25(1), 341–350.

[6] Aldeen, M., and Trinh, H. (1994). Load Frequency Control of interconnected power systems via constrained feedback control schemes. *Computers and Electrical Engineering*, 20(1), 71–88.

[7] Anderson, B., and Moore., J. (2007). *Optimal control: linear quadratic methods*. Dover Publications. Mineola.

[8] Mendel, J.M. Advances in type-2 fuzzy sets and systems. *Inform Science* 177(1), 84–110.

[9] Venkateswarlu, K., and Mahalanabis, A.K. (1987). Load frequency control using output feedback. *Journal of Institution of Engineers (India)*, 58(4), 200–203.

[10] Darouach, M., and Boutayeb, M. (1995). Design of observers for descriptor systems. *IEEE Transactions on Automatic Control*, 40(7), 1323-1327.

[11] Essabre, M., and Soulami, J., and Elyaagoubi, E. (2013). Design of State Observer for a Class of Non linear Singular Systems Described by Takagi-Sugeno Model. *Contemporary Engineering Sciences*, 6(3), 99-109.

[12] Michal, Polanský., and Cemal, Ardil.(2011). Robust Fuzzy Observer Design for Nonlinear Systems. *International Journal of Computer, Electrical, Automation, Control and Information Engineering*, 5(5), 539-543

[13] Ma, X.J., and Sun, Z.Q. (1998). Analysis and design of fuzzy controller and Fuzzy observer. *IEEE Trans. Fuzzy Systems*, 6(1), 41–51.

[14] Melin, P., and Castillo, O. (2003). A New Method for Adaptive Model based Control of Nonlinear Plants Using Type-2 Fuzzy Logic and Neural Network. *Proceedings of IEEE FUZZ conference*, St. Louis, USA, 420–425.

[15] Takagi, T., and Sugeno, M. (1985). Fuzzy identification of systems and its applications to modeling and control. *IEEE Transactions on Systems,Man and Cybernetics*,1(1), 116–132.

[16] Mathur, M.D. (2012). Fuzzy based HVDC regulation controller for load frequency control of multi-area system. *International journal of Computer Aided Engineering and Technology*, 4(1).72 – 79.

[17] Shayeghi, H., and Shayanfar, H., and Jalili, A. (2009). Load frequency control strategies: A state-of-the-art survey for the researcher. *Energy Convers. Manage*, 50(2) 344–353.

[18] Bennassar, A., and Abbou, A., and Akherraz, M., and Barara, M. (2016). Fuzzy logic based adaptation mechanism for adaptive luenberger observer sensorless direct torque control of induction motor. *Journal of engineering science and technology*, 11(1), 046 – 059.

[19] Fernando, T., and Trinh, H., and Jennings, L. (2010). Functional observability and the design of minimum order linear functional observers. *IEEE Trans.Autom. Control*, 55(5), 1268–1273..

[20] Jennings, L., and Fernando, T., and Trinh, H. (2011). Existence conditions for functional observability from an eigenspace perspective.*IEEE Trans. Autom. Control*, 56(12), 2957–2961.

[21] Darouach, M. (2000) “Existence and design of functional observers for linear systems. *IEEE Transactions on Automatic Control*, 45(5), 940-943.

[22] Al-samarraie, shibly.ahmed., and abbas, yasir.khudhair.(2013). Manifold based controller (mbc) design for linear systems. *Journal of engineering science and technology*, 8(6), 723 – 740.

USE OF BOTTOM ASH IN IMPROVING THE STRENGTH CHARACTERISTICS OF BLACK COTTON SOIL

1. Paidi Sridevi
Asst. Professor, Dept. Of Civil Engineering,
Dr. L. B. College of Engg. For Women, Visakhapatnam, AP

2. P. V. V. Satyanarayana
Professor, Dept. Of Civil Engineering,
Andhra University College of Engineering, Andhra University,
Visakhapatnam.

ABSTRACT:

Expansive soils cover about 20% of the total area in India. They are found in the states of Andhra Pradesh, Gujarat, Karnataka, Madhya Pradesh, Maharashtra and Tamil Nadu. Hot climate and poor drainage conditions are usually associated with the formation of these soils. Expansive soils are highly problematic because of their alternative swelling and shrinkage. The problem of expansive soils is causing failures in the structures like buildings, bridges, railway and highway embankments. In this work the use of bottom ash in stabilising the expansive soils is studied at varied proportions and extensive testing is done to determine the engineering properties. The strength properties of these soils are observed to be improved considerably when compared with their naturally existing state.

Key words: Expansive Soil, Bottom Ash, OMC, MDD, CBR, UCS

1.INTRODUCTION:

Expansive soils tend to be a worldwide problem that poses several challenges for civil engineers. They are considered as a prospective natural hazard that can cause excessive damage to structures, when not treated effectively. The overall loss due to extensive damage to highways running over expansive soil subgrades is estimated to be in billions of dollars in the world. To understand the severity and the characteristics, the soil is tested for Atterberg's limits, consistency indices, and swell characteristics. To arrest the failures in expansive soils, stabilization is one of the popular methods(1,2,3,4).

Bottom ash is a by-product of burning coal which is generated at the thermal power plants. Bottom ash particles are much coarser than fly ash particles. Bottom ash particles are coarser, angular material having porous surface texture, predominantly sand-sized. This material is composed of silica, alumina, and iron with small amounts of calcium, magnesium, and sulphate. Grain size typically ranges from fine sand to gravel in size. Bottom ash contains high carbon content and exhibits high shear strength and low compressibility. Bottom ash is an economic material because it has revealed to have not only good engineering property but also constructability benefits. Bottom ash can be utilized bulkily in geotechnical engineering applications such as constructions of embankments as a backfill material, as a sub-base material, etc.

In this study, strength characteristics of soil stabilized with bottom ash are studied. Geotechnical properties of clay such as compactioncharacteristics(Optimum Moisture Contents(OMC), Maximum Dry Density(MDD)), California Bearing Ratio(CBR), and Unconfined Compression Strength(UCS) are determined. The clay is classified as clay CH. Bottom ash is added to clay in varying proportions of0%,10%,20%,30%, 40%,50%,60%,70%,80%,90% ,100%.

Some of the earlier contributions in the area of black cotton soil and bottom ash are:**P.V.V.Satyanarayana et al(2013)** studied strength characteristics of expansive soil-flyash mixes at various moulding water contents and identified that expansive soil flyash mixes attained high strengths at their optimum moisture and plastic limits. **Gullu (2014)** discussed the use of bottom ash as a stabilizer. **Debra F. Pflughoeft-Hassett et al (2000)** studied the use of bottom ash and fly ash in rammed-earth construction. **Lech Balachowski, et al. (2013)** addressed in their paper the mechanical properties of bottom ash.

2. MATERIALS:

To study the geotechnical characterisation of the expansive soil, the sample of black cotton soil has beencollected locally and its engineering propertiesare determined. The stabilising material or bottom ashwas also collected and tested for its basic properties. The properties which are determined include compactioncharacteristics(OMC and MDD), CBR, andUCS, as per IS:2720(6).

3. TESTS AND RESULTS:

3.1Effect of bottom ash in improving compaction characteristics of black cotton soil:

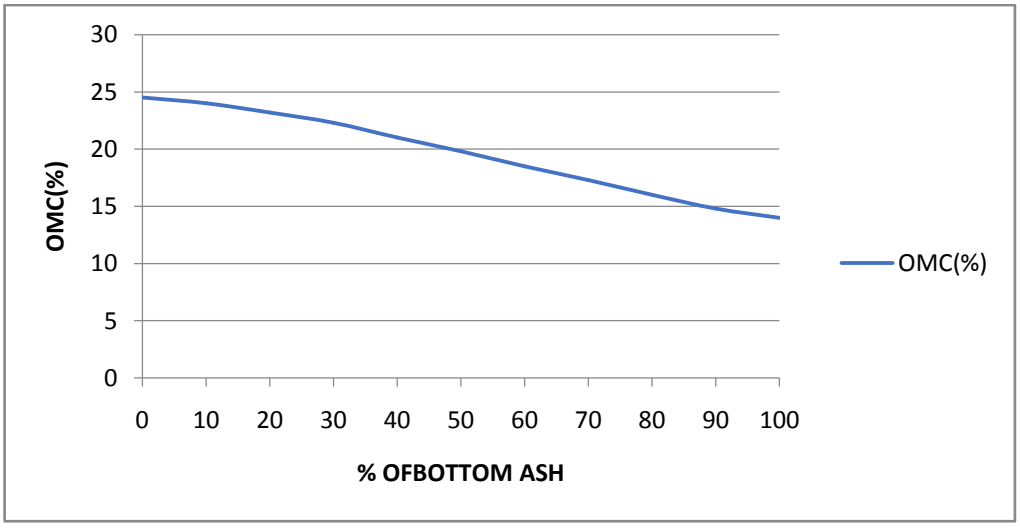
The compaction characteristics of the black cotton soil are determined by the addition of bottom ash at varied percentages. The tests are conducted in accordance with IS-2720-Part-7-1980. It is performed by compacting the black cotton soil to five layers, each of which is subjected to 25 number of blows with a rammer of 4.89 kg weight and height of fall of 450 mm. The observations are shown in Table 1.

Table 1: VARIATION OF OMC AND MDD OF BLACK COTTON SOIL WITH INCREASED PERCENTAGE OF BOTTOM ASH ADDED

% OF BOTTOM ASH ADDED	COMPACTION CHARATERSITICS	
	OMC(%)	MDD(g/cc)
0	24.5	1.60
10	24.0	1.58
20	23.2	1.55
30	22.3	1.50
40	21.0	1.44
50	19.8	1.38
60	18.5	1.34
70	17.3	1.28
80	16.0	1.20
90	14.8	1.15
100	14.0	1.10

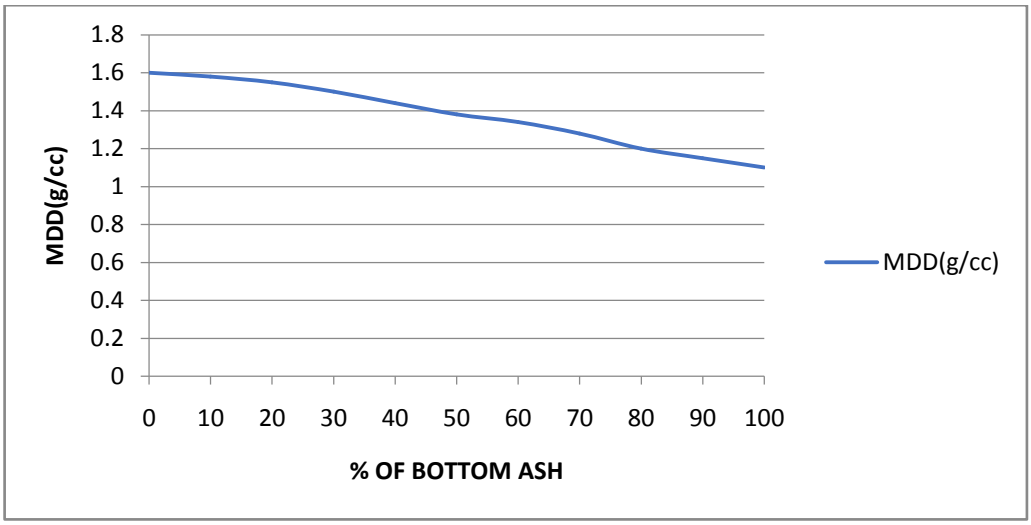
The figure1 shows the variation of OMC of the black cotton soil with increased percentages of bottom ash.

FIGURE 1: VARIATION OF OMC OF BLACK COTTON SOIL



The figure2 shows the variation of MDD of the black cotton soil with increased percentage of bottom ash.

FIGURE 2: VARIATION OF MDD OF BLACK COTTON SOIL



3.2Effect of bottom ash in improving CBR characteristics of black cotton soil:

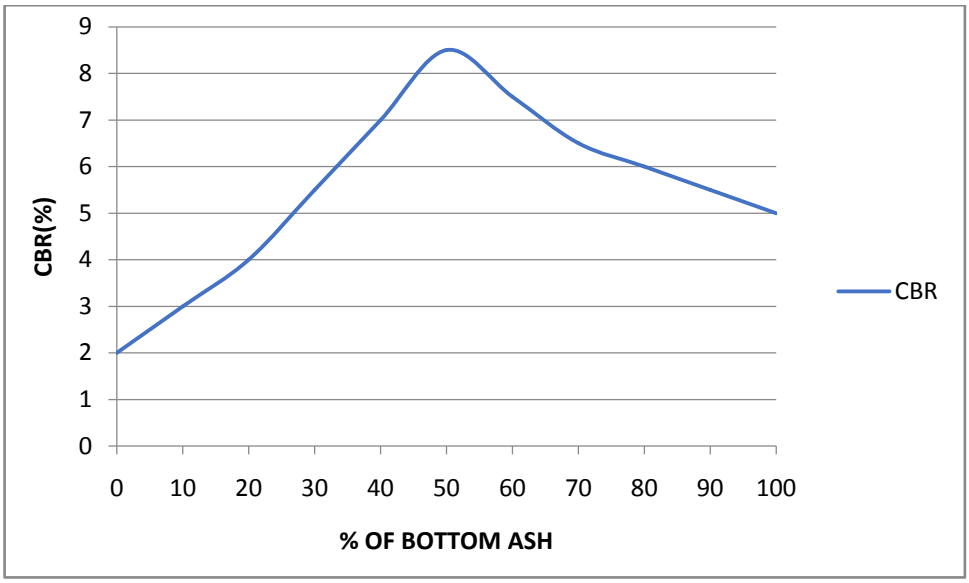
CBR characteristics of black cotton soil are determined by conducting the CBR test(IS-2720-Part-16-1986) on the soil with the addition of bottom ash at varied percentages and it is observed that at 50 % of bottom ash added, the CBR value is found out to be optimum. Table 2 shows the observations of CBR tests.

TABLE 2: VARIATION OF THE CBR VALUES WITH INCREASING PERCENTAGES OF BOTTOM ASH

% OF BOTTOM ASH ADDED	CBR (%)
0	2.0
10	3.0
20	4.0
30	5.5
40	7.0
50	8.5
60	7.5
70	6.5
80	6.0
90	5.5
100	5.0

The variation is also shown as a graph in figure3.

FIGURE 3: VARIATION OF CBR VALUE WITH INCREASING PERCENTAGE OF BOTTOM ASH



3.3Effect of bottom ash in improving UCS values of black cotton soil:

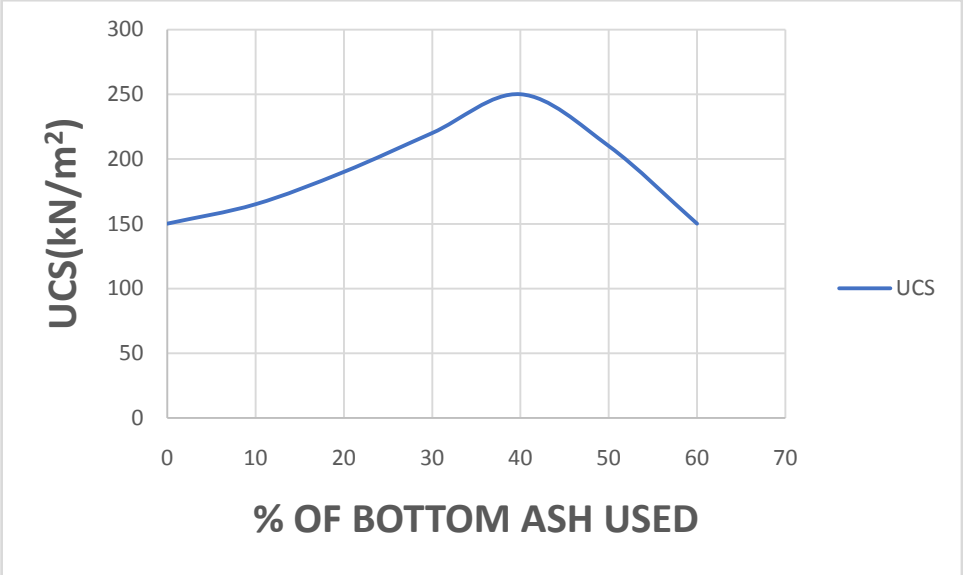
UCS characteristics of black cotton soil are determined by conducting the UCS test(IS-2720-Part-10-1991) on the soil with the addition of bottom ash at varied percentages and it is observed that at 40 % of bottom ash added, the UCS value is found out to be optimum.Table 3 shows the observations of UCS tests.

TABLE 3: VARIATION OF THE UCS VALUES WITH INCREASING PERCENTAGES OF BOTTOM ASH

% OF BOTTOM ASH ADDED	UCS (kN/m^2)
0	150
10	165
20	190
30	220
40	250
50	210
60	150
70	-
80	-
90	-
100	-

The variation is also shown as a graph in figure4.

FIGURE 4: VARIATION OF UCS VALUES WITH INCREASING PERCENTAGE OF BOTTOM ASH



4. CONCLUSIONS:

Based on the observed experimental results the following identifications are made:

- Compactioncharacteristics: the value of OMC & MDD decrease with increase in percentage of bottom ash.
- The CBR values increase with increase in percentage of bottom ash up to 50%, beyond that the strength decreases.
- The UCS values first increase with increase in percentage of bottom ash in black cotton soil till it reaches the peak at 40% of bottom ash added. Upon further increase in percentage of bottom ash causes the UCS values to decrease.

REFERENCES:

1. P.V.V.Satyanarayana, S.Hemanth Kumar, P.Praveen, B.V.Suresh Kumar“A Study on Strength Characteristics of ExpansiveSoil-Flyash Mixes at Various Moulding WaterContents” ISSN: 2277-3878, Volume-2, Issue-5, November 2013.
2. Debra F. Pflughoeft-Hassett et al (2000), "Use of bottom ash and fly ash in rammed-earth construction". Final report, Energy & Environmental Research Center, University of North Dakota, Grand Forks, ND 58202-9018.
3. Lech Balachowski, et al. (2013), "Mechanical properties of bottom ash", Gdansk University of Technology, Department of Geotechnics, Geology and Maritime Engineering 80-233 Gdansk, Poland.
4. Joseph E. Bowles(2001), “Engineering properties of soils and their measurement” TMH.
5. Hamza Gullu“Factorial experimental approach for effective dosage rate of stabilizer: Application for fine-grained soil treated with bottom ash” Soils and FoundationsVolume 54, Issue 3, June 2014, Pages 462-477.
6. IS 2720: Part 16; 1987 Methods of Test for soil part 16: Laboratory determination of CBR.

7. Ogunro, V.O.; Inyang, H.I.; Hooper, F.; Young, D.; Oturkar, A. (2004) Gradation control of bottom ash aggregate in superpave bituminous mixes. Journal of Materials in Civil Engineering 16 [6], 604–613. http://dx.doi.org/10.1061/(ASCE)0899-1561(2004)16:6(604).
8. Guruprasad Jadhav, Gavhane Dinesh &BehereBabaso "An Experimental study on stabilization of expansive soil using admixtures" IJSTM-2016.

Solid State Technology
Volume: 63 Issue: 1s
Publication Year: 2020

Impact of Niobium on Lithium - Titanate Anode Materials of Lithium-ion Batteries

K. Surendra[1], B. Vikram Babu[2], M. Sushma Reddi[3], G. Chandana[4], A. Rama Krishna[5], D. Deenabandhu[6], A.D.P. Rao[7]

[1,7]Department of Nuclear Physics, Andhra University, Visakhapatnam, 530003, India
[2,4,6]Department of Physics, Andhra University, Visakhapatnam, 530003, India
[3]Department of Physics, Dr. B. R. Ambedkar University, Srikakulam, 532410, India
[5]Department of ECE, Aditya College of Engineering and Technology, Kakinada, 533005, India
e-mail: vikramphdau@gmail.com[2]

***Abstract*—**Effect of the Nb5+ substitution at the expense of Ti on the lithium titanate (LTO) anode materials of lithium ion materials has been carried out having the chemical composition Li4Ti5-xNbxO12 (x=0, 0.0125, 0.025). These materials are synthesized by solid state reaction method, which calcinated for 20 hours at 800 °C. A systematic presentation of the results relating to the structural, morphological, vibrational bonding nature and impedance of the anode materials are investigated through TG/DTG, X-ray diffraction (XRD), SEM with EDS and FT-IR techniques. The observed diffraction peaks show agreement with the ordered LTO cubic spinel structure belonging to the Fd-3m space group. The synthesized compounds are quite large up to around 1 μm in diameter and the grain size had a wide distribution range. EDS is used to identify the elements. All the vibrational bands are shifted as a function of doping concentration (x). The FTIR spectra show that the oxide lattice structure comprises of MO6 tetrahedra and octahedra

Keywords- *Lithium Titanate, Anode Materials, XRD, SEM, FTIR*

I. INTRODUCTION

Investigations on batteries have been gaining scientific community attention for raising power storage systems. Lithium ion batteries (LIBs) are occupied higher prioritized position among energy storage available technologies. These materials unique advantageous features namely higher capacity, higher energy density and rate capability relative to other batteries. The structure of a battery includes a cathode, anode, electrolyte and the separator. Anode is the source of Li-ions and cathode acts as a sink for the Li-ions [1-3].

Graphite and its related materials have safety related problems of dendritic Li growth due to its lower lithiation potential (close to 0 V Vs Li^+/Li). The conventional graphite based anode materials show 10% volume change that also considered as too higher for battery applications. Spinel $Li_4Ti_5O_{12}$ (LTO) has many advantages over conventional graphite. Earlier studies [4-6] shown that Sn-, Sb- and Si- etc substituted materials, different transition metal oxides and spinel LTO are some of the suitable anode materials.

Spinel LTO anode material is one of the good alternatives to graphite to be an anode material for LIBs [7] by having extremely flat charge/discharge relations / curves at ~ 1.5 V, good cycling stability and zero strain volume insertion nature [8−10]. Mostly, LTO materials are mainly prepared by solid state reactions that involve mechanical mixing of oxides and carbonates, heating at higher temperature (700−1000 ℃) and

sol-gel preparation techniques [4, 11]. Three Li^+ ions per formula unit of LTO can be reversibly inserted and extracted. Consequently the theoretical capacity of LTO materials found to show175 $mAh.g^{-1}$ [12-15].

Besides the above mentioned features of the LTO anode material; electrically it is an insulator having lower electrical conductivity (10^{-13} $S.cm^{-1}$) resulting as main obstacle exhibiting its limit. To overcome this disadvantage (lower conductivity of LTO anode material), transition metals such as Mg, Ca, Cr, La, Cu, Zn, V, Ru, Sn and Nb may be used as dopant(s) at the expense of Li and Ti ions or sites. In the present work nniobium is chosen as doping element because it does not affect or change the lattice of lithium and titanium ($Li_4Ti_{5-x}Nb_xO_{12}$) by using solid-state reaction [15-19]. It does not vary the lattice constants and the phase of the LTO as well. Hence it is proposed to develop or prepare new materials by using a cation-substituted compound; namely $Li_4Ti_{5-x}Nb_xO_{12}$; where $x = 0.00, 0.0125$ and 0.025, the charge compensation is maintained by Li deficiency [19-22].

II. Preparation of Samples

Anode materials relating to the above mentioned composition have been prepared with the solid state reaction method by following stoichiometric ratios of starting materials such as lithium carbonate (Li_2CO_3), titanium dioxide (TiO_2) and niobium oxide (Nb_2O_5) having 99.9% obtained from the Merck company. An excess amount of Li_2CO_3 (5%) was used to compensate the loss of the metal that take place during the heating process. Initially the raw materials were thoroughly mixed by using agate and mortar; further methanol added to obtain homogeneity of the materials and grinded for 6 h. These materials were annealed in air for 20 hours at 800°C by using a muffle box furnace to dry the compounds and make them free from unwanted gases. After cooling down the materials to room temperature, those were again crushed in the mortar for 1 h to get the fine powder. The powdered samples were mixed with a binder such as polyvinyl alcohol (PVA). Further these powdered materials were pressed with a pressure of 5 tons /5 minutes to form pellets in the shape of circular discs. At 900 °C temperature, these pellets were sintered for 20 hours in air at 5°C/minute heating and cooling rate.

III. Experimental Procedures

Measurements were carried out by using Mettler Toledo TG/DTG 851^e instrument in the range 30 °C - 1000°C in the N_2 gas environment at 10°C/minute rate of heating. The PAN analytical X-pert pro diffractometer containing diffraction angle range from 10º to 90º with the successive increments of 0.02º was used to collect the powder XRD spectra of the materials. The Scherrer's equation is applied to the obtained data of the XRD pattern to evaluate the crystallite sizes of the concerned samples. The SEM with EDS images were taken from the sintered pellets. SEM and EDS related data taken from JEOL JSM-6610LV is used to observe the elemental analysis and morphology of the prepared samples. Shimadzu IR-Prestige21 spectrometer is utilized to obtain the FT-IR spectra by using KBr pellet method in the range of wave number 400 and 3000 cm^{-1}.

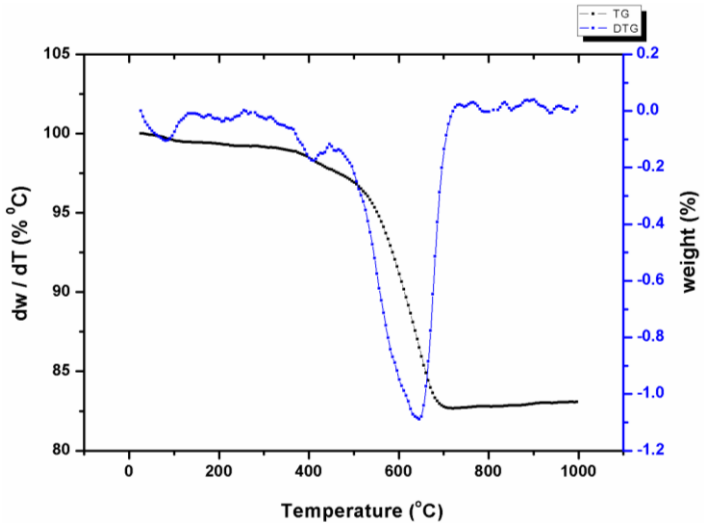
IV. Results and Discussion

4.1 Thermal Studies

Measurement of the materials thermal parameters as a function of temperature has been performed. The curves concerned to the results obtained due to thermal behavior of the present materials having chemical composition $Li_4Ti_{5-x}Nb_xO_{12}$ ($x = 0, 0.0125$ and 0.025) heated at 10 ºC /min in the flowing nitrogen atmosphere are shown in Fig 1(a-c). From the TG/DTG plots, it is observed that no significant weight loss occurs from 30 ºC to 400 ºC. All the four plots of TG/DTG show the first weight loss in the region 400 ºC to

520 ºC is approximately (1.6%). This loss can be attributed to the moisture content absorbed on the surfaces and some inserted water molecules during grinding on the addition of methanol to the materials. Further these compounds fond to exhibit significant weight loss (~ 16%) between the temperatures 520 ºC and 700 ºC.

The above mentioned maximum weight loss in the region 500 ºC and 700 ºC relating to Niobium substituted precursors indicate decomposition of the precursors namely lithium carbonate, titanium dioxide and Nb_2O_5 and the reaction among decomposed materials. This can be corroborated with the observed sharp peak around 600 ºC by the DTG curves of all the materials. All the TG plots show a small weight loss above 700 ºC indicating the formation of spinel phases around 900 ºC.



(a) x=0

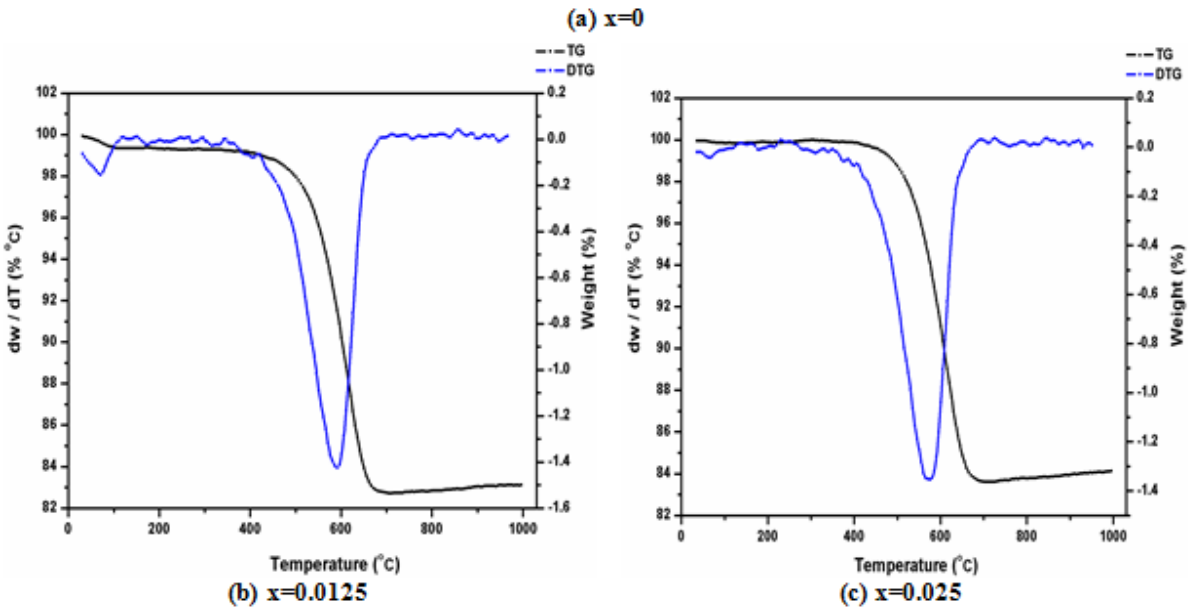


Fig 1(a-c): TG/DTG graphs of $Li_4Ti_{5-x}Nb_xO_{12}$ (x =0, 0.0125 and 0.025) materials.

The obtained thermal results of the base or un-substituted LTO material show good agreement with the earlier reported values [21]. The obtained transitions at higher temperature indicate the consolidation and crystallization of the anode materials. All the TG profiles show more flattening at higher temperatures

resulting the stable $Li_4Ti_{5-x}Nb_xO_{12}$ series of spinel crystalline phases formed around 850 ºC authenticating the undertaken preparation conditions and temperatures. As shown by the TG curves in the Fig 1; no mass loss is observed in the temperature region 700 °C to 1000 °C, it can be attributed to the formation of spinel crystalline structures of $Li_4Ti_{5-x}Nb_xO_{12}$ series [4, 21, 23, 24]. All the TG profiles found to show more flattening at high temperatures.

4.2 X-RAY POWDER DIFFRACTION STUDIES

The observed XRD pattern (Fig 2) of the anode materials under taken in the present studies facilitate understand the relation between crystallographic properties and their variation as a function of Niobium (Nb) concentration (x). All the diffraction peaks are sharp and narrow indicating highly crystalline nature of the materials. From the Fig 2, it can be observed that all the diffraction peaks of doped materials are similar to those of LTO base material. All the fingerprint peaks (111), (2 2 0), (3 1 1), (2 2 2), (4 0 0), (3 3 1), (3 3 3), (4 4 0), (5 3 1), (5 3 3), (6 2 2), (4 4 4), (5 5 1) and (7 3 1) indexed *hkl* values are legibly identifiable.

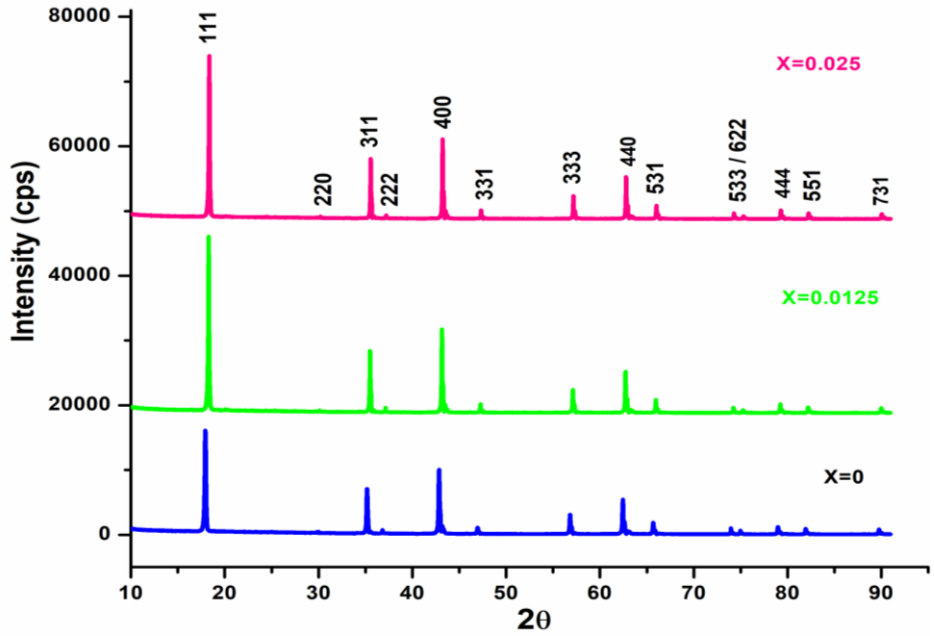


Fig 2: XRD patterns for Li4Ti5-xNbxO12 (x = 0, 0.0125 and 0.025) compounds.

The observed XRD patterns comprised of the above quoted peaks only confirming the formation of single phase and no additional phase is observed. These diffraction patterns are in accordance with an ordered cubic spinel structure belonging to the Fd-3m space group symmetry having consistency with the JCPDS Card # 49-0207 [4, 15,19, 23-25]. This indicates that partial substitution of Nb at the expense of Ti found to show no change in the basic arrangement of LTO particles. This reveals that both Ti^{4+} and Li^{+} ions; which belong to the octahedral sites can be substituted by Nb^{5+} ions. The computation of XRD data clearly indicates the increase of lattice constant as a function of Nb concentration (x = 0.0125 and 0.025) relative to the basic or un-substituted compound (x = 0.00). This can be attributed to the ionic radius of the Ti^{4+} (0.67 Å) being smaller than that of the Nb^{5+} ionic radius (0.69 Å) [20, 26, 27].

Values of the present materials crystallite sizes are evaluated by using Debye Scherrer formula that given below [15]. In association with the UnitCell software (1997) to understand

$$L = \frac{k\lambda}{\beta \cos\theta} \qquad \text{----------} \qquad (1)$$

the impact of the Nb substitution in the LTO anode material; structural parameter (lattice parameters and unit cell volumes) values evaluated and are displayed in the table 1.

4.3 SEM WITH EDS STUDIES

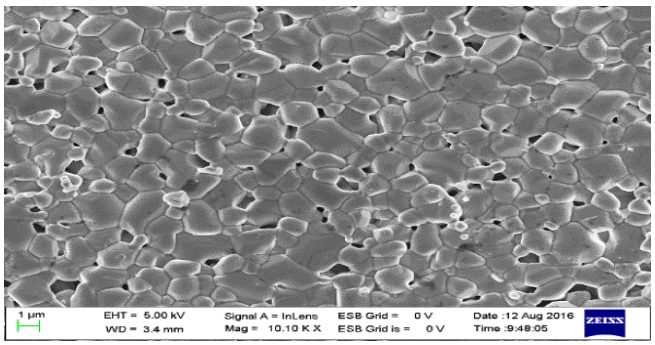
Scanning Electron Microscope (SEM) uses electron beam to characterize the morphological structure and texture of the prepared or synthesized materials. The typical SEM micro graphs (images) and energy dispersive X-ray spectra (EDX) with different magnifications and grain sizes of spinel structured $Li_4Ti_{5-x}Nb_xO_{12}$ compositions are shown in Fig 3(a-c) to estimate the impact of niobium on micro structural properties of anode materials of lithium ion batteries.

Table 1: Lattice constants, Unit cell volumes, Crystallite sizes and average Grain sizes of synthesized

$Li_4Ti_{5-x}Nb_xO_{12}$ (x = 0, 0.0125 and 0.025) compounds.

Samples	Lattice Constant a (Å)	Unit Cell Volume $(Å)^3$	$I_{(111)}/I_{(400)}$	Crystallite Size from (111) (nm)	Average Grain Size (µm)
$Li_4Ti_5O_{12}$	8.3625	584.8013	1.66	48.02	0.96
$Li_4Ti_{4.9875}Nb_{0.0125}O_{12}$	8.3735	587.1121	1.06	58.12	1.02
$Li_4Ti_{4.975}Nb_{0.025}O_{12}$	8.3780	588.0592	1.05	57.10	1.04

It is observed that the present materials show uniform grain size distribution, which indicates the good crystallinity nature exhibiting compaitability with the XRD pattern. Moreover, the prepared compounds showing the porous structure facilitating high penetration of the electrolyte through the anode materials. Smaller grains are observed as surrounded by larger ones. The variation of morphological structures and increase of grain size with the rise of Nb concentration has been observed. The average value of grain sizes is computed and it found to be within the range of 1 µm (0.9 -1.1 µm) for all the materials; which is stable with their crystalline form that detected by XRD as shown in the table 1.



(a) x=0

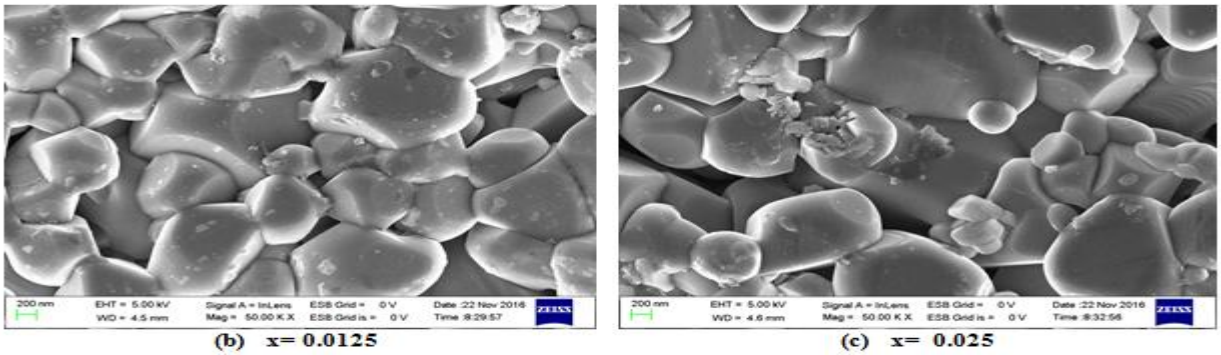
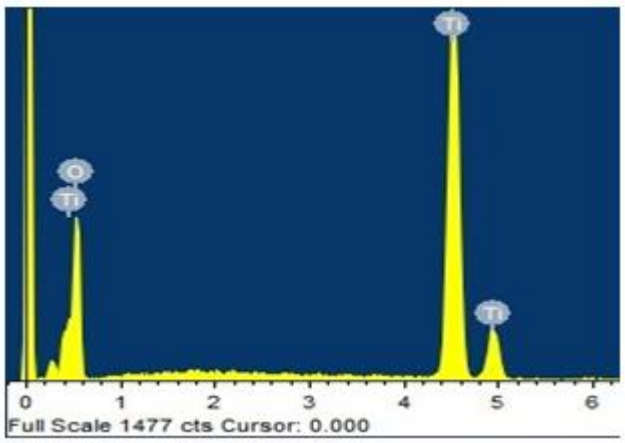


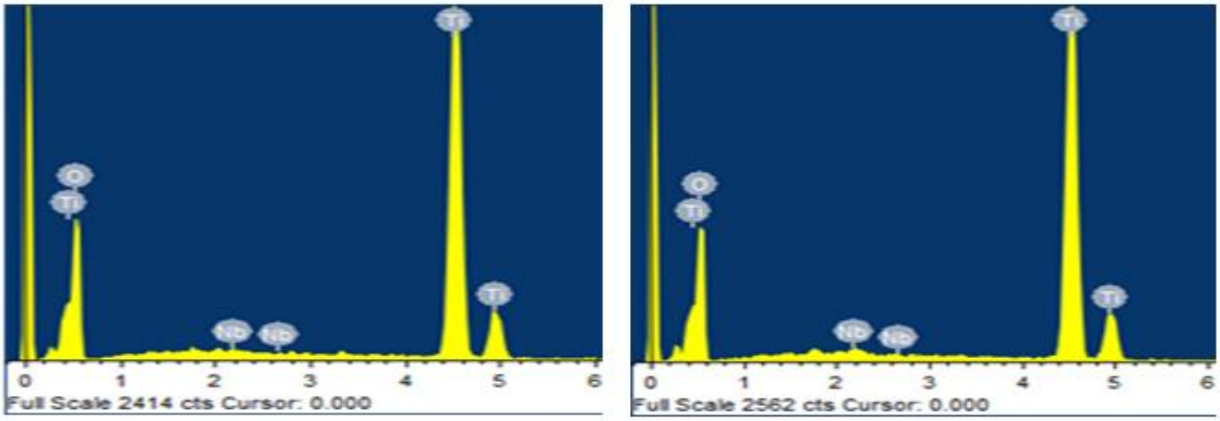
Fig 3(a-c): SEM micrographs for $Li_4Ti_{5-x}Nb_xO_{12}$ (x =0.00, 0.0125 and 0.025) compounds.

The uniform grain sizes of the Nb substituted LTO materials may contribute to improve the electrochemical activity and also enhance the charge/discharge efficiency of the LIBs [15, 19-21].

The energy dispersive X-ray spectroscopy (EDX) is highly useful to estimate the stoichiometry of the materials and to analyze the elemental composition. However, this technique cannot identify the elements having atomic number less than four; therefore, Li element cannot be detected by this method. The energy dispersive spectra and quantitative results of $Li_4Ti_{5-x}Nb_xO_{12}$ materials are shown in Fig 4(a-c) and 5(a-c) respectively. It is observed that EDS shows the appropriate concentrations of the elements. EDS spectra shown in Fig 4(a-c) confirmed the presence of Ti, Nb and O elements except Li in the $Li_4Ti_{5-x}Nb_xO_{12}$ anode materials. The EDS histogram spectra and quantitative results of $Li_4Ti_{5-x}Nb_xO_{12}$ (x =0, 0.0125, 0.025) shown in Fig 5(a-c) are facilitating to verify the concentration of each element present in a compound to compare with the concentration of corresponding element taken for the preparation of each composition of the LIBs.



(a) x=0

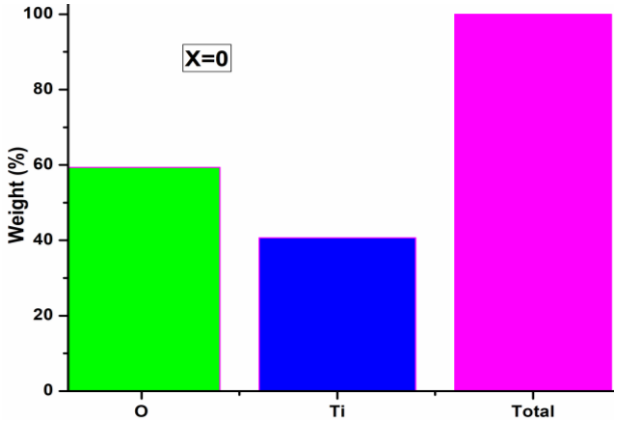


(b) x= 0.0125 **(c) x= 0.025**

Fig 4(a-c): EDS Spectra of Li4Ti5-xNbxO12 (x =0, 0.0125 and 0.025) compounds.

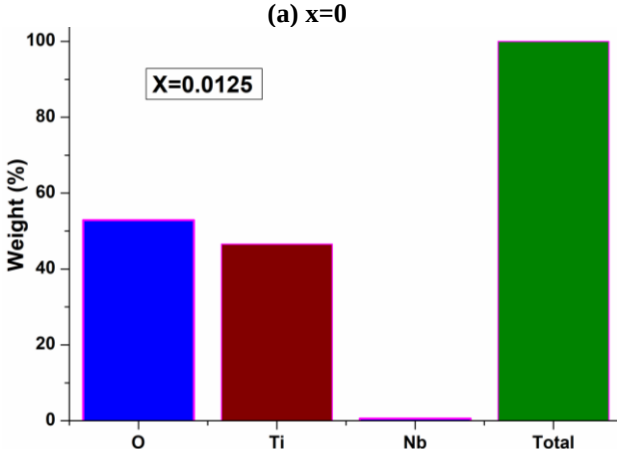
4.5 FT-IR STUDIES

The typical FTIR spectra of all the present materials are shown in Fig 6. These are useful for identification and to determine whether the functional groups are present or absent in the materials. The IR spectra of materials scanned at frequencies ranging from 400 - 3000 cm^{-1} are revealed in the Fig 6. The enlargement of FTIR bands might have caused due to the cation mixing in the crystal structures. $Li_4Ti_{5-x}Nb_xO_{12}$ materials are divided into LiO_6 and TiO_6 bands and clearly seen them in the wave numbers region 400-900 cm^{-1} [15, 16]. The FT-IR spectra of $Li_4Ti_{5-x}Nb_xO_{12}$ materials are not recorded below 400 cm^{-1} to observe the vibrations of LiO_6 because of the limitations related to instruments. Irregular layers of MO_6 (M= Li, Ti and Nb) separated in triangle manner by sharing octahedral positions present in the spinel structure formation of $Li_4Ti_{5-x}Nb_xO_{12}$ materials. The Wyckoff sites 8*a* and 16c consist of Nb and Ti cations and Li-ions respectively.



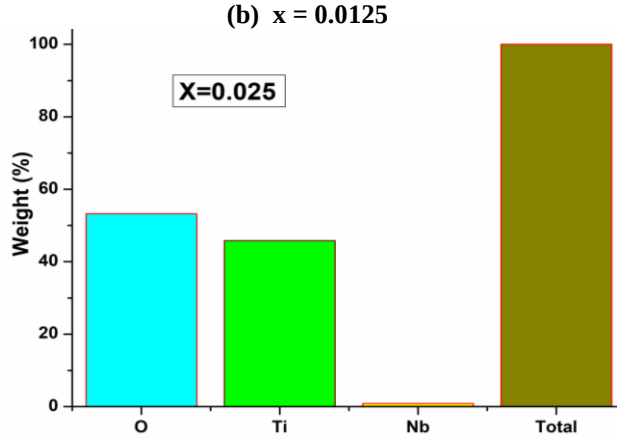
(a) x=0

Composition	x= 0	
Element	Weight %	Atomic %
O	48.62	80.26
Ti	51.38	19.74
Total	100	100



(b) x = 0.0125

Composition	x = 0.0125	
Element	Weight %	Atomic %
Ti	46.55	23.56
Nb	0.57	0.17
O	52.88	76.27
Total	100	100



(c) x=0.025

Composition	x = 0.025	
Element	Weight %	Atomic %
Ti	45.84	20.57
Nb	0.89	0.21
O	53.27	79.22
Total	100	100

Fig 5(a-c): EDS Histogram Spectra and composition of elements of

$Li_4Ti_{5-x}Nb_xO_{12}$ (x =0, 0.0125 and 0.025) compounds.

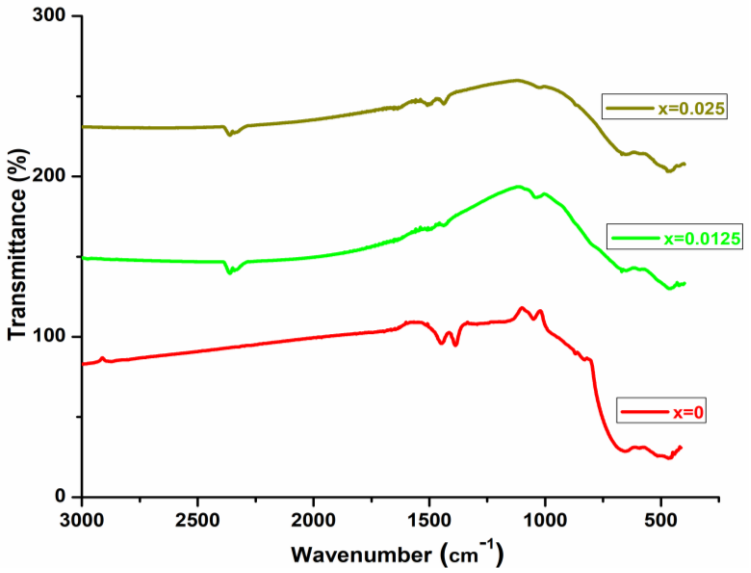


Fig 6: FT-IR spectra for $Li_4Ti_{5-x}Nb_xO_{12}$ (x =0, 0.0125 and 0.025) compounds.

Nearly four prominent bands are presented in the FTIR spectra of the present materials. The identification details of the major peaks in these spectra are summarized in the table 2. The comparison of the spectra due to different compositions of the materials showed that most of the peaks are nearly identical. The FT-IR patterns are characterized by the appearance of a small variation at a wave number around 462.5 cm^{-1}. This wave number found to move in the direction of higher wave number side besides the increase of peaks width with the rise of Nb concentration.

Table 2: Infrared wavenumber and band assignments in Li4Ti5-xNbxO12 (x =0, 0.0125 and 0.025)

S. No	Infrared wavenumber (cm^{-1})			
	x = 0	x = 0.0125	x = 0.025	Assignment
1	462.5	462.8	463.1	(Li-O)
2	672.5	673.1	674.5	(Ti-O)
3	848 (Ti-O)	848.8	851.4	(Nb-O)
4	1050 (Li-Ti-O)	1051	1052.6	(Li-Nb-O)

The observed absorption band may be understood due to Li-O stretching mode. In other words, the bands are observed around 462.5 cm^{-1} and these attributed to the asymmetric stretching vibrations of MO_6 presented in the octahedral sites. The presence of extra absorption peaks around 672 cm^{-1} and 848 is indicative of the Nb-Ti-O bending modes. $Li_4Ti_{5-x}Nb_xO_{12}$ materials represent a strong absorption peak at ~ 672 cm^{-1}; which is a specific peak for the cubic spinel structure and confirms that TiO_6 octahedra stretching modes are formed [28-31].

V. CONCLUSIONS

Spinel structured anode materials $Li_4Ti_{5-x}Nb_xO_{12}$ (x = 0, 0.0125 and 0.025) of lithium ion batteries are well prepared by ceramic route at 850° C for 20 hours. These materials structural, morphological and vibrational characterizations are carried out with the variety of techniques namely TG/DTG, XRD, SEM, EDS and FT-

IR. TG/DTG studies revealed the temperature dependence of the materials' properties. XRD analysis shows that the doping of Nb at the expense of Ti is more favorable as it not collapsed due to the lattice structure of LTO. Insertion of transition metals also prevents the lattice structure but slightly affects the lattice parameters within the concentration range studied. SEM analysis revealed that all the materials exhibit uniform morphology with sphere like particles. This kind of morphology is more significant to achieve high capacity. FTIR analysis confirms that the Nb dopant exactly occupy the corresponding sites of the Ti in the host lattice. These microstructural studies are very important and vital for carrying out further investigations of electrical and electrochemical properties.

REFERENCES

[1] M. M. Thackeray, J. Electrochem. Soc., 142 (1995) 2558-2563.

[2] T. Placke, R. Kloepsch, S. Duhnen, M. Winter, J. Solid State Electrochem. 21 (2017) 1939-1964.

[3] H.E. Katz, A.J. Lovinger, J.G. Laquindanum, Chem. Mater. 10 (1998) 457.

[4] W. Zhi-guo, P. Wen-jie, W. Zhi-xing, LI Xin-hai, G. Hua-jun, WU Ling, Trans. Nonferrous Met. Soc. China 20 (2010) s271−s274.

[5] M. Tarascon, M. Armand, Nature, 414 (2001) 359-367.

[6] X. Sun, P. V. Radovanovic, B. Cui, New J. Chem. 39 (2015) 38-63.

[7] G. Izquierdo, A.R. West, Mat Res Bull, 15(11) (1980) 1655−1660.

[8] C. Ouyang, Z. Zhong, M. Lei, Electrochemistry Communications, 9(5) (2007) 1107−1112.

[9] Z. Wen, X. Yang, S. Huang, J. Power Sources, 174(2) (2007) 1041−1045.

[10] K. Kataokaa, Y.Takahashia, N. Kijimaa, J. Akimotoa, K. Ohshima, J. Phys Chem Solids, 2008, 69(5/6): 1454−1456.

[11] K. Hsiao, S. Liao, J. Chen, Electrochimica Acta, 53(24) (2008) 7242−7247.

[12] T. Ohzuku, A. Ueda, N. Yamamoto, J. Electrochem. Soc. 142 (1995) 1431-1435.

[13] X. Sun, P. V. Radovanovic, B. Cuia, New J. Chem. 39 (2015) 38-63.

[14] J. Christensen, V. Srinivasan, J. Newman, J. Electrochem Soc, 153(3) (2006) 560−565.

[15] B. Vikram Babu, K.V. Babu, G.T. Aregai, L.S. Devi, B. M. Latha, M. S. Reddi, K. Samatha, V. Veeraiah, Results in Physics, 9 (2018) 284-289.

[16] B. Vikram Babu, M. Sushma Reddi, B. V. Rao, G. Chandana, A. R. Krishna, M.V.K. Mehar, L. Usha Kumari, K. Samatha, V. Veeraiah, Test Engineering and Management 83 (2020) 9175-9180.

[17] G. Yang, S.J. Park, Scientific Reports, 9 (2019) 4774.

[18] H.F. Xiang, X. Zhang, Q.Y. Jin, C.P. Zhang, C.H. Chen, X.W. Ge, J. Power Sources, 183 (2008) 355-360.

[19] XY.B. Tian, H. Xiang, L. Zhang, H.H. Wang, J. Solid State Electrochem., 16 (2012) 205-211.

[20] J. Wolfenstine, J.L. Allen, J. Power Sources, 180 (2008) 582-585.

[21] T.F. Yi, Y. Xie, J. Shu, Z.H. Wang, C.B. Yue, R.S. Zhu H.B. Qiao, J. Electrochem. Soc., 158 (2011) A266-A274.

[22] Q. Zhang, Xi Li, Int. J. Electrochem. Sci., 8 (2013) 6449-6456.

[23] K. Zaghib, M. Simoneau, M. Armand, M. Gauthier, J. Electrochem. Soc., 145 (1998) 3135-3140.

[24] M. Ganesan, M. V. T. Dhananjeyan, K. B. Sarangapani, N. G. Renganathan, J. Electroceramics, 18 (2007) 329-337.

[25] E. Ferg, R. J. Gummow, A.de Kock, M. M. Thackeray, J. Electrochem. Soc., 141(11) (1994) L147-L150.

[26] R.D. Shannon, Acta Cryst A., 32 (1976) 751-767.

[27] A.Y. Shenouda, K.R. Murali, J. Power Sources, 176 (2008) 332-339.

[28] B. X. Lu, X. Mou, J. Wu, D. Zhang, L. Zhang, F. Huang, F. Xu, S. Huang, Adv. Funct. Mater., 20 (2010) 509-515.

[29] L. G. Devi, B. N. Murthy, Catal. Lett., 125 (2008) 320-330.

[30] R. Nakamura, A. Imanishi, K. Murakoshi, Y. Nakato, J. Am. Chem. Soc., 125 (2003) 7443-7450.

[31] V. S. Braga, J. A. Dias, S. C. L. Dias, J. L. de Macedo, Chem. Mater., 17 (2005) 690-695.

INTERNATIONAL JOURNAL OF MULTIDISCIPLINARY EDUCATIONAL RESEARCH
ISSN:2277-7881; IMPACT FACTOR :6.514(2020); IC VALUE:5.16; ISI VALUE:2.286
Peer Reviewed and UGC Approved:VOLUME:9, ISSUE:2(3), FEBRUARY:2020

SELF-REALIZATION TO SEARCH FOR IDENTITY A STUDY ON SELECT NOVELS OF MAYA ANGELOU

Dr Rada Devi Vadapalli
Associate Professor of English
Dr Lankapalli Bullayya College of Engineering for Women
Visakhapatnam, A.P, India

Abstract
Maya Angelou shared her mission for human distinction, recognizing her own battle with the general circumstances of the Black Americans, which take up part in connection to the Black Americans, as well as in connection to the general thought of America. Her collections of memoirs praise the extravagance and imperativeness of Southern Black life that endure even with neediness and racial bias. At first, her festival of the Southern Black life is uncovered through the representation of the creator's life as a dark child in Arkansas of the 1930s in I Know Why the Caged Bird Sings. The second portrayed a young lady attempting to make a presence endeavoring to accomplish a promising life and love in America amid post-World War II in Gather Together in My Name. Her journey for character, slow acknowledgment and acknowledgment of black excellence and self-acknowledgment of black womanhood and parenthood are likewise essentially depicted in her writings. Truth be told, she is one of the principal African American women who freely depicted her private life. These characteristics roused to examine her initial two exemplary autobiographies.

Keywords: Racism, Sexism, Self-realization, Identity.

Though the society exhibit a celestial and radiant status to women, the position of womenismarginal in any general public, particularly for black women in American culture. The fair sex has been subjected to various sorts of maltreatment in her everyday life in the male decreed society: physical, financial, emotional and psychological. Just a couple of women put a conclusion to their lives, however the vast majority of them surmounted their horrible circumstances all through their household fields and made due from various individual hardships.

They demonstrated that they were not any more second rate, yet sufficiently incredible in various circles of life. A couple of women approached to verbalize their powerful position in the public arena, what they truly are and their differed encounters in their everyday life through the artistic articulation. Maya Angelou's is a fine case of such.

Scanned by PDF Scanner

Objective of the Study

The general goal of the investigation is to explore the encounters of unappreciated women with reference to Maya Angelou's I Know Why the Caged Bird Sings and Gather Together in My Name. In accordance with the general goal, the examination has the accompanying particular destinations- To get into the idea of African-American resistance writing and to analyze the tyranny on African American women.

Significance of the Study

The select novels would give more extensive oppurtunity to understand the uncertainties of African-American writing, Negro resistance and women's activist composition. It is additionally trusted that it would help raise awareness about Black women personal history and women's activist feedback on it. The investigation will start readers to find out about Black female involvement in America.

Methodology

The study is descriptive in nature, for takes a gander at encounters of neglected women in Angelou's novels. In addition, since the research is mainly concerned with the textual analysis of the novel, subjective research strategy was observed to be the most appropriate approach for the present investigation. The research used both primary source and secondary sources. The essential research strategy was made through direct examination and investigation of the content.

Literature review

Despite the fact that the underlying compositions of African American works were on slave narratives and spirituals as songs, prose writings, collection of memoirs as a classification was relied on the self-disclosure and articulation of the writer by staying into the inward considerations and mysteries of the author. African Americans record their lives through personal works which has not just tested supremacist convictions and racially oppressed foundations like bondage, yet additionally presented ideal models of their solid assurance and encounter.

"Thematically and structurally, the tradition of the African American novel is dominated by the struggle for freedom from all forms of oppression and by the personal odyssey to realize the full potential of one's complex bicultural identity as an African American". (Bernard W. Bell, 2006)

Despite the fact that they were basically worried about their individual assessments, convictions, sentiments, considerations and encounters in their personal histories, they represented the black community on the whole. Collections of memoirs of black women were stories of freedom, cases of uniqueness, and depiction of racial oppressor supremacist patriarchy. Their works were the fortunes of selfhood, battle, talk bent, immense experience, twofold awareness, boundless torment and conceiving opportunity. In consequent decades, stories by African American women expressed the specific

Scanned by PDF Scanner

issues confronted by black women in a general public overwhelmed by males and also whites.

"The problem of twentieth century is the problem of color line," W.E.B.Du Bois wrote in "The Souls of Black Folk." African Americans were free from bondage after the Civil War, however the color line kept them isolated and underestimated. In spite of the fact that the white populace had an origination of "the Negro" as a gathering, it appeared to have no origination of it as a person. Ralph Ellison's "Invisible Man "is a sparkling case of this topic. His book is a cerebral record of a black man who, notwithstanding extensive endeavors to beat the color line, gets himself distanced from both blacks and whites.

Zora Neale Hurston in her autobiography -Dust Tracks on a Road described the history of the land-fights between White Americans and Native Americans with African Americans caught in between. Unlike many black authors nurtured during the Harlem Renaissance period, Hurston rarely portrayed blacks as victims of the oppression and racist attitudes held by white society and instead represented blacks as autonomous beings. Throughout The Color Purple, Walker portrayed female friendships as a means for women to summon the courage to tell stories. In turn, she revealed that these stories allow women to resist oppression and dominance. Further, she added that relationships among women form a refuge, providing reciprocal love in a world filled with male violence. In all her major novels Toni Morrison had dwelt upon the theme of violence, oppression and sacrifice. In Morrison's novels violence was exhibited in various forms. Apart from narrating the problems of racism, gender bias, Angelou proved her mettle by surmounting the encounters and by proving herself as unique. By this, she stood as a role model for all the African American women.

Angelou wants to break all the obstacles and shackles of the society which is beset by the narrow domestic walls of sex, caste, and racism. Like great Noble Laureate Rabindranath Nath Tagore, she also wants to take a fresh breath of air in an environment equal both for men and women. Angelou envisages the barrier free world like Rabindranath Tagore (Usha Jaina and Nobert Solomon,2014).Angelou is aware that there have to be changes, but she does not want to achieve them using violence. She sees no solution in violence and probably she believes that words can be more powerful than physical means. Her writing is a peaceful way of fighting (Kathrin Gerbe, 2004). Though, the writing techniques and style of Toni Morrison and Maya Angelou are different, the novels perfectly reflect the lives of black people (Fatimah Aslam Bahauddin, 2016)

Angelou's work in not limited however to the Black – White issue, instead it is expansive in its focus on such universal issues as romantic love, lust, friendship, betrayal and loyalty. Ultimately her work is about survival – the survival of not

Scanned by PDF Scanner

only the Afro-American, but also the survival of the human race (S.Farhad, 2016). Racial discrimination, sexual abuse and oppression was delineated in her first autobiographic novel I Know Why the Caged Bird Sings (Saptarini, 2008). The main subjects in her verse, plays, and screen plays were her self-portraying books. Her central mission was to inspire basic self-reflection. She knew that her intense and vexed past drove her to taste the sugar of her present triumphant position as the prestigious Renaissance woman called Maya Angelou. Indeed, her creativity made her appreciate the statures of her life and achievement went about as a main impetus to the readers to grasp themselves better.

Maya Angelou shared her mission for human distinction, recognizing her own battle with the general circumstances of the Black Americans, which take up part in connection to the Black Americans, as well as in connection to the general thought of America. Her collections of memoirs praise the extravagance and imperativeness of Southern Black life that endure even with neediness and racial bias. At first, her festival of the Southern Black life is uncovered through the representation of the creator's life as a dark child in Arkansas of the 1930s in I Know Why the Caged Bird Sings. The second portrayed a young lady attempting to make a presence endeavoring to accomplish a promising life and love in America amid post-World War II in Gather Together in My Name. Her journey for character, slow acknowledgment and acknowledgment of black excellence and self-acknowledgment of black womanhood and parenthood are likewise essentially depicted in her writings. Truth be told, she is one of the principal African American women who freely depicted her private life. These characteristics roused to examine her initial two exemplary autobiographies.

I Know Why the Caged Bird Sings is the first of five volumes of Maya Angelou's personal history, which cover the years from the mid 1930's, up until around 1970.Dolly Aimee McPherson as-I Know Why the Caged Bird Sings is a carefully conceived record of her initiation into her world and her discovery of her inner identity.

This volume starts with Maya's adolescence and closures with her bringing forth an infant kid. The preface and early sections are to a great extent basic, giving the setting of the black culture, building up the primary characters, and presenting the subjects. The core of the book talks about how diverse occurrences throughout Angelou's life influenced her and her battles towards self-comprehension and freedom. Maya's assault, ensuing muteness, her communication with Mrs. Flowers, deriding pro-white trash girls, her visit to the dental practitioner, Maya's month living in a Junkyard, her battle to end up plainly a San Francisco Bus conductor, question about her sex. Her graduation, and tolerating parenthood were the vital occasions as they formed her identity and cast her to the light of comprehension about existence.

Scanned by PDF Scanner

Gather Together in My Name is the progressive novel of Maya Angelou's first novel, I Know Why the Caged Bird Sings. In Gather Together in My Name, Maya Angelou records her odyssey with her recently conceived infant, who came out of an impulsive testing of her sexual identity.

Her narratives the battles to achieve a promising life convey both the excellence and the weight of parenthood and womanhood. In this adventure she went into unsuccessful connections and turned out disappointed. The men with whom she created connections notwithstanding her sibling, Bailey and her neighborhood, L. C. Smith and Troubadour Martin whom she saw at her manager's restaurant in Oakland, misused her physically, fiscally and mentally. In this volume Maya functioned as an artist, a cook, a Madam, a server, and quickly as a whore. In spite of the fact that she was strong willed and sharp disapproved, she was not able keep her life far from her vulnerabilities. Readers sense an unfortunate decrease in her key quality from time to time. The novel delineates how a large portion of the African American women in the urban setting were caught into the world of drugs and prostitution.

Self-realization to Search for Identity

All through her two years life's adventure, she experienced many obstacles and disappointments. She profoundly ached for a safe life, however the fantasy never worked out. Her constancy, certainty and human concerns made plan to grow her vision forever. In spite of the fact that she was tricked by Curly, R. L. Poole and L.D. Tolbrook, she never pointed the finger at them; rather she attempted to find her own defects and understand the circumstance better. She never floated away from her universe of imagination as winning a perfect man's hand that must yield profound extinguish for both physical and otherworldly love, and finishing a secured life. At one phase of life, she learnt that material comfort alone couldn't bring satisfaction, yet it could make danger and disorder to life. Her delicacy, sensuality, innocence and honesty drove her to the flawed field with respect to disappointments throughout her life. Though she longed for better living first with Curly, next with R. L. Poole and after that with L.D. Tolbrook and Troubadour Martin individually resulted in vain. Assembling every one of these occasions together were her life's unforgotten encounters. Her various occupations reflected the regrettable circumstances and obliged ways of life of African American women in the so called promised land,, United States of America. Her story spoke to the heartbreaking existences of youthful young black women.

Maya Angelou's initial two self-portraying works, I Know Why the Caged Bird Sings and Gather Together in My Name made a one of a kind place in black autobiographical custom, by their capacity through sagaciously designed shape to quantify both the vulnerabilities and the natural greatness of black people and social conventions. The collections of memoirs uncover the creator's solid

Scanned by PDF Scanner

craving for a definitive presence, and tolerating the biting substances in existence with brave heartedness. The determination of Maya Angelou made her a recognized identity over the span of her different encounters. She faulted neither the general public nor the family foundation for her anguish and basic circumstances, though numerous authors disregarded this perspective and anticipated it contrarily.

Through the autobiography of Maya Angelou shared her journey for human uniqueness, recognizing her own battle with the general states of the Black Americans, which made her assume a delegate part in connection to Black Americans, as well as in connection to the general thought of America. Her self-portrayals commend the wealth and imperativeness of Southern Black life and the feeling of group that continues even with neediness and racial bias.

Maya Angelou's serial collection of memoirs recovered her own subjective encounters. All through her work, she described the personal, social, cultural, and historical influences which shaped her life and personality. She investigated herself and individual identity and her association with the family, the community and the world.

Angelou saw her work as an open door for her readers to look into her reality and pondered their own particular universes, a state of self-reflection that would connect with one to watch oneself and simultaneously to watch humankind. She pursued her own particular upset and turned into a worldview to her readers to survive and rise above a socially developed philosophy intended to control self-comprehension and financial versatility. It is no doubt that because of Angelou's efforts, the African American woman has gained wider respectability and greater reception. Her vividness and veracity have moved the impetus to the blacks to struggle for equality. She has richly recorded the African American feminine experience from the early days of the Civil Rights Movement to the present day. In her lectures, Angelou brought to public attention the countless and important contributions that African Americans have made to American culture and literature.

According to Angelou, the African American Woman epitomizes the strong-will to survive without losing empathy and compassion. She herself, promoted the archetypal black female representative for black female inclusiveness. With her autobiographical novels she had shown a path for the women to balance the circumstances and life. Her books continue to be studied in American Studies and Women's Studies classes.

A study of Maya Angelou's autobiographical works reveals that Maya Angelou's main objective is not only to narrate her story of triumph at the personal level but also to voice the trail and tribulations of African American women in the backdrop of racial and gender discrimination even in the advanced west. In her endeavor, she succeeded to document the social history of

Scanned by PDF Scanner

her fellow women and social economic conditions of the west. She exhibited in her novels the importance of self-awareness, hope, strong will as the tools of women to prove their mettle.

References

- Angelou, Maya. I Know Why the Caged Bird Sings. New York: Random House, 1969.
- Angelou, Maya. Gather Together in My Name. New York: Random House, 1974.
- Abrams, M.H. Ed. 17 A Glossary of Literary Terms, New Delhi: Harcourt College Publishers Papers Ltd., 2001.
- Baisnée, Valérie. Gendered Resistance: The Autobiographies of Simone de Beauvoir, Maya Angelou, Jenet Frame and Marguerite Duras. Amsterdam-Atlanta GA, 1997.
- Braxton, Joanne M. ed. Maya Angelou's I Know Why the Caged Bird Sings: A Casebook. New York: Oxford University Press, 1999.
- Bernard W. Bell, Women and literature: the dual tradition of African American fiction, Oxford University Press's Academic Insights for the Thinking World, 2006.
- Chapman, Abraham. ed. Black Voices: An Anthology of African American Literature. US: Signet Classic, 2001.
- Elliot, Jeffrey M. ed. Conversations with Maya Angelou. US: University Press of Mississippi, 1998.
- Franklin, Hope J. From Slavery to Freedom: A History of Negro Americans. 3rd ed., rev. New Delhi: Amerind, 1967.
- Fatimah Aslam, Comparison Between The Novel Beloved By Toni Morrison And I Know Why The Caged Birds Sings By Maya Angelou, International Journal of English Language, English Literature and Humanities, Vol-IV,Issue-VII, July, 2016.
- Farhad.S, Research Journal of English Language and Literature, Vol.4.Issue 4. 2016
- Hoffman, Daniel. ed. Harvard Guide to Contemporary American Writing. Delhi: Oxford, 1981.
- Lupton, Mary Jane. Maya Angelou: A Critical Companion. US: Greenwood Publishers, 1998.
- Lupton, Mary Jane. "Singing the Black Mother: Maya Angelou and Autobiographical Continuity" Black American Literature Forum 24.2 (Summer 1990) 257-276.
- McPherson, Dolly A. Order Out of Chaos. New York: Peter Lang, 1990.

Scanned by PDF Scanner

- Maxine, Sample. Gender, Identity, and the Liminal Self. North- South Linkages and connection in continental and Diaspora African Literatures. (2005), 213-225.
- Nelson, Emmanuel S. Ed. African American Autobiographies: A Sourcebook. US: Greenwood Press, 2002
- Ramprasad, Arnold. Introduction. The Collected Works of Langston Hughes: The Poems, 1921-1940. vol. 1. US: University of Missouri Press, 2001.
- Shuman, R. Baird, Lyrical Language in Maya Angelou's Autobiographies. New York: Cavendish, 2002.
- Saptarini, Racial Discrimination in Maya Angelou's I Know Why The Caged Bird Sings: A Marxist Approach, 2008
- Stevenson, Robert Louis ed., Memories and Portraits-Memoirs of Himself-Selection from His Notebook. US: Read Books, 2006.
- Usha Jain and Nobert Solomon, Ego Resistance, Oppression and Resilience of Self Esteem in "I Know Why the Caged Bird Sings" By Maya Angelou, International Journal of Multidisciplinary and Current Research, Vol.2 March-April-2014.
- Walker, Pierre. "Racial Protest, Identity, Words, and Form in Maya Angelou's I Know Why the Caged Bird Sings" College Literature 22.3 (October 1995): 91-108
- Washington, Mary Helen. Invented Lives: Narratives of Black Women 1860-1960 . New York: Anchor Press,1987.
- Washington, Robert E. The ideologies of African American literature: from the Harlem Renaissance to the Black Nationalist revolt: A Sociology of Literature Perspective. Ed: illustrated. Chicago: Rowman& Littlefield, 2001.
- Williams, Yolanda. ed. Encyclopedia of African American Women Writers. vol. 2. US: Green Wood Press, 2007.

Scanned by PDF Scanner

"Collaborative Teaching and Learning in ESL Classroom"

***Dr RadhaDevi Vadapalli**, Associate Professor of English, Dr Lankapalli Bullayya College of Engineering for Women, Visakhapatnam, Andhra Pradesh., India

ABSTRACT

It's clear that globalization is making English language especially important not just for the students in the universities, but in areas such as law, electronics, aviation, computers, medicine, shipping, tourism and entertainment. At the college level, as English remains a major medium of instruction, the students are paying additional attention to learn and excel. Various strategies like TBLT, CLT, and CALL etc. were implemented to equip the students with better communication skills. The factors like lack of motivation, fear, and anxiety are the challenges still need to be addressed. The study was conducted among 120 girl students to equip writing and speaking skills. The results obtained revealed peer interaction, peer correction, student centered teaching yielded better results than the former methods implemented in the ESL classroom.

KEY WORDS- Affective factors, Peer involvement, ESL Classroom, Student Centeredness

Introduction

It is a known fact that the importance of English language is growing day by day as it is the international language of media and arts. It is the most widely used language globally in the fields of politics, business, science and cultural exchange. With an outstanding proficiency, one could seek for even more rewarding and high-end jobs. The factors like international commerce, financial and technological is demanding fluency to communicate in English with the people across the globe. It's clear that globalization is making English language especially important not just for the students in the universities, but in areas such as law, electronics, aviation, computers, medicine, shipping, tourism and entertainment.

At the college level, as English remains a major medium of instruction, the students are paying additional attention to learn and excel. Either to comprehend the latest scientific discoveries which are documented in English or to access any authentic academic material available in the internet, the mere competence on English language is insufficient. Thus, the primary aim of an English teacher is to develop language proficiency among the students. Language proficiency is commonly defined as a person's ability to speak or perform in an acquired language using all the four language skills like listening, speaking, reading, and writing.

Among all the skills of English language- Listening, Speaking, Reading and Writing, Speaking and Writing are considered as important skills for the students of undergraduate as they have to face the Campus Recruitment Interviews.

Along with the factors like past learning experience, socio- economic conditions, cultural background the teachers also face the challenges the factors like lack of motivation and confidence, fear. Most of the students express their difficulty to convey their thoughts due to two major reasons- either they have studied in a regional medium school or lack of support from parents and peers.

Objective

The study contributes in improving teaching and learning English language speaking and writing skills. It reveals challenges and opportunities in teaching and learning English language to overcome the affective factors like fear, anxiety and lack of confidence.

Literature Review

To develop communication skills among the L2 students, David Nunan emphasized, “the students must have conversations in the target language in the classroom.” (Nunan, 1991).Underwood stated that listening to be given more importance while learning a second language. (Underwood, 1989).C. Wallace proposed,” Reading helps the students to comprehend and to learn language skills.” (Wallace, 2001).Harmer stated that the factors like shyness and fear would inhibit the students to express themselves in the target language. (Harmer, 2007). William and Burden suggested that the success or failure of the student to learn the target language would only depends on the strategies that were implemented by the teacher (Williams and Burden, 2004). Later studies shifted their importance to student teacher interaction in the classroom. It is teacher-student interaction that makes students aware of their own ideas and gives them the opportunity to rehearse the use of a language that is appropriate for dealing with nature in a scientific manner (Carvalho 2013).

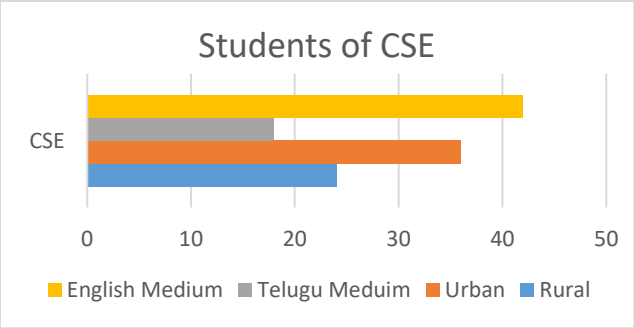
Communicative classes focus on communication rather than on grammar, although grammar is an essential element in the communicative classroom. The functional use of language in different social situations or contexts is emphasized and classroom activities relate language form and function as well as meaning (Larsen-Freeman, 2003).Nunan (2004) suggests for, "experiential learning" or "learning by doing" which can also be termed as Task-based Language Teaching (TBLT), fundamentally a branch of open language educating, student centeredness. Moreover, TBLT goes far in separating the progressions of the customary classroom in light of the fact that the very demonstration of endeavoring to finish an open errand includes arranging and utilizing techniques with respect to the student

.

This communicative task by Nunan (2004) was defined as a piece of classroom work that involves L2 students in comprehending, working, constructing, or interacting in the target language. Fluency-oriented activities would not only reflect the natural use of language but also motivates the learner to focus on the language related activities (Richards, 2004). Poudel stated that the quantity of student participation and interaction would be more in student centered teaching. Ashman and Gillies (2003) stated," peer mediation actively involves students in the learning process through a student who helps other students by giving them an effective way to complete difficult tasks." Through this way, students would be able to overcome their speaking problems more easily. If the traditional classroom is shifted from teacher centered to student centered then the teacher as a facilitator could curb even factors of students fear, anxiety and to gain proficiency.

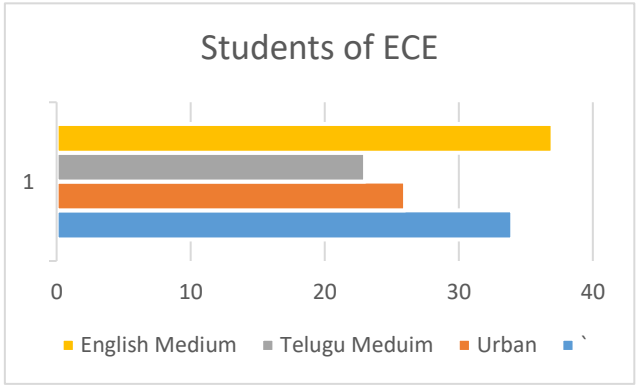
Methodology

The study was conducted among 120 girl students who were studying II year engineering. Among which 60 students are from Computer Science and 60 students are from Electronics and Communication.



In the branch of ECE, 34 students are from rural background and 23 students have completed their education up to their intermediate/SSC in Telugu medium.26 students are from urban and 37 students have studied in English medium

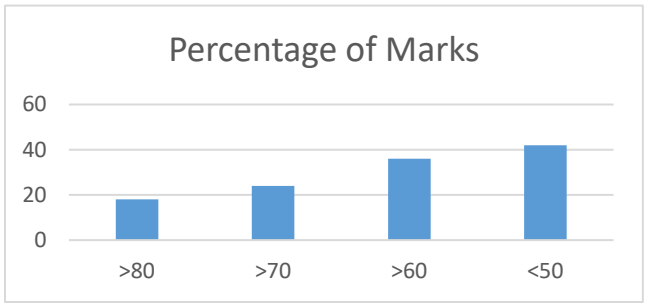
In the branch of CSE, 24 students are from rural background and 36 students have completed their education up to their intermediate/SSC in Telugu medium.18 students are from urban and 42 students have studied in English medium.



All these students have completed their Ist year Engineering course where the medium of instruction is in English Language and they have to pass English Language exam to get promoted to IInd year. The syllabus of that paper is on autobiographies of celebrities, science fiction, cultural aspect, moral values and ethics. The student reads either the abridged versions of the same syllabus or gather material available in the internet. Though, the student passes the examination, he fails to apply the knowledge he/she has gained during the conversations.

Thus, we divided them into 4 groups with 30 students in each group. We made it mandatory that each group to attend 2 sessions in a week and each session is of 2 hours. Among these 30 students we formed sub groups in which each sub group contains only 6 students. In every sub group, a student teacher, was appointed as group leader who has moderate proficiency. While forming the sub groups, a mixture of rural and urban students, slow and fast learners were purposefully designed to encourage peer interaction. Two ELT teachers were allotted to facilitate throughout the study.

Initially, diagnostic test was conducted to test the student competencies. The test was conducted both on oral and written. In the oral test both accuracy and fluency were given equal importance. In the written test, the students were tested on sentence structure, grammar, coherence, usage of vocabulary etc.



The test was conducted for a total of 100 marks. Equal weightage is given for speaking and writing. After obtaining the results, only 39 students could cross 70% and above and 81 students could achieve below 70%.Further there were 41 students who could only pass the examination. A bridge course was conducted basing on the performance separately for slow learner and fast learners. The bridge course covered all the topic that were useful to focus on form and meaning. Further, the basic skills of writing like clarity, coherence, candidness, courtesy, topic sentence, connectives were taught. The course was conducted for 60 hours in an interactive way.

After conducting the bridge course, the students were divided into sub groups and they were given tasks to perform both in written and spoken. The speaking tasks were on the topics- describing place, festival, role model, family initially. Later, they were asked to participate in group discussions, debates. In the same way, the students were asked to write narrative, descriptive, argumentative, comparative essays to develop their writing skills.

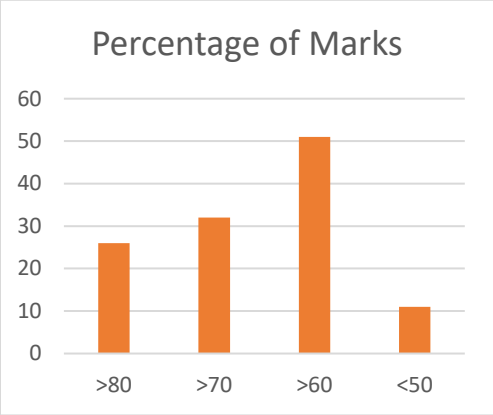
Here, the peer involvement was given more importance. Freedom was given for the peers of a group and the group leader to check their written copies before submitting the final copy to the teacher. Similarly, during the speaking activities, all the group members were instructed to identify and share within a group.

Analysis and Results

Besides the bridge course of 60 hours extensive teaching, the study was conducted for 96 hours. Continuous assessments were taken to change the topics for writing and speaking. Various topics

were given to use adjectives, adverbs, conditionals while framing the sentence structure. In the final assessment 58 students could achieve more than 70%. The students who could get more than 60% were 51. Only 11 students could not get the expected results.

Student feedback was taken every week and they were counselled when demotivated. After observing the results, one could identify that peer involvement would bring faster results. The students resolved their problems in an amicable manner. Here, the teacher was not only a facilitator but also had performed many duties. The teachers served as motivators, conflict managers, time and team managers etc. After taking the complete feedback from the students, the success was due to peer involvement. As their peer only gives the feedback, the student had reduced fear and anxiety. Further, before submitting, the written copy, peer students helped each other. Though, there were errors initially, the teachers also helped all the groups. In some groups, the students were able to develop self -correction before submitting to their group leader. The students could also use complex sentences, phrases and clauses effectively during their oral and written presentations.



Future Scope

If the strategy is implemented for vocabulary development, the students opting to write competitive exams will be benefitted. Further, it would be more useful for reading comprehension exercises, sentence equivalent tasks. If the tasks are conducted in the seminar hall, the students will have a conducive atmosphere to perform enthusiastically and actively.

REFERENCES

Ashman, A. (Ed.), Gillies, R. (Ed.). (2003). Cooperative Learning. London: Routledge.

Brown, G., Bull, J. and Pendlebury, M. (1997) Assessing Student Learning in Higher Education. Routledge, London

Bloom, B. S. (1984). Taxonomy of educational objectives. Boston, MA: Allyn & Bacon.

Benson, P. (2001). *Teaching and researching autonomy in language learning*, London: Longman.

Carvalho, A. (2013). Students' perceptions of fairness in peer assessment: evidence from a problem-based learning course. Teaching in Higher Education.

Gardner, H. (1993). *Multiple intelligences: The theory and practice*. New York: Basic Books.

Harmer, Jeremy. (2007). How to Teach English. China: Pearson Education Limited.

Larsen-Freeman, D. (2003). Teaching language: from grammar to grammaring. Boston: Heinle& Heinle.

Marion Williams, Robert Burden (2004) Learners' perceptions of their successes and failures in foreign language learning, The Language Learning Journal.

Nunan, D. (1991). Language Teaching Methodology: A Textbook for Teacher. Upper Saddle River, NJ: Prentice Hall.

Nunan, D. (2004). Task-based language teaching: A comprehensively revised edition of designing tasks for communicative classroom. Cambridge: Cambridge University Press.

Nunan, D. (1992). Collaborative language learning and teaching. Cambridge: Cambridge University Press

Underwood, M. (1989). Teaching Listening. New York: Longman.

Wallace, C. (2001). Reading. In R. Carter, & D. Nunan (Eds.), The Cambridge guide to teaching English to speakers of other languages , Cambridge: Cambridge University Press

Eco. Env. & Cons. 26 (November Suppl. Issue) : 2020; pp. (S345-S350)
Copyright@ EM International
ISSN 0971–765X

Trace element contamination in fruits and vegetables grown in low nutrient availability soil environment by using inductively coupled plasma mass spectrometry

N. Swathi [1], P. Padmavathi[1] and N.V.S. Venugopal[2*]

Department of Chemistry, GITAM University, Visakhapatnam, A.P, India

(Received 13 April, 2020; Accepted 1 June, 2020)

ABSTRACT

The major concern of the people in the world is food safety and food quality. The significant aspect of food quality and food safety in general is the state of trace element contamination in fruits and vegetables. In this communication the concentration of different elements were determined by using Inductively coupled plasma mass spectrometry (ICP-MS). The various vegetables such as Brinjol (*Solanum melongena*), carrot (*Daucuscarota* subsp. sativus), Tamoto (*Solanum lycopersicum)* cucumber (*Cucumis sativus*) etc and fruits like orange (*Citrus X sinensis*), grape (*Vitis*), apple (*Malus domestica*) and kiwi (*Apteryx)* were grown in low nutrient available soil environment and procured from varied agricultural farms. At low concentration toxic metals can be very harmful when ingested over a long time period. About twenty seven elements were recorded in various fruits and vegetables by using ICP-MS. after microwave digestion, employing only nitric acid in this step. Trace element determination is important for the prevention of different diseases occurred due to the excessive presence in fruits and vegetables.

Key words*: Trace elements, Absorption spectrometry, Fruits, Vegetables*

Introduction

Vegetables are part of daily diets in many households forming an important source of vitamins and minerals required for human health. They are made up of chiefly cellulose, hemi-cellulose and pectin substances that give them their texture and firmness (Abdulla, 1990). Consumers demands for better quality vegetables are increasing. The perceptions of what is regarded as 'better quality' are however subjective. Some consumers consider undamaged, dark green and big leaves as characteristics of good quality leafy vegetables.

However, the external morphology of vegetables cannot guarantee safety from contamination.

Heavy metals ranks high amongst the chief contaminants of leafy vegetables (Ward, 1995; Rajeshkumar Sarma, 2004; Jeffieries, 2009; Sobukala, 2007; Mapanda, 2007). The intake of heavy metals can lead to altering of humans and animals healthiness state. Thus, the carcinogenic effects generated by continuous consumption of fruits and vegetables loaded with heavy metals such as Cadmium, Lead or even Copper and Zinc are known. There are already published works related to the incidence of gastrointestinal cancer (Tricopoulas, 1997; Turkdogan, 2002) and cancer of the pancreas, urinary bladder or prostate (Waalkes, 1994). Heavy metal contamination of the food items is one of the most important aspects of food quality. Heavy metal contamination of vegetables cannot be under-

([1]Research scholar)

estimated as these foodstuffs are important components of human diet. Vegetables are rich sources of vitamins, minerals, and fibers, and also have beneficial anti oxidative effects. However, intake of heavy metal-contaminated vegetables may pose a risk to the human health. Rapid and unorganized urban and industrial developments have contributed to the elevated levels of heavy metals in the urban environment of developing countries. The aim of this study is to measure the levels of metal ions found in selected fruits and vegetables using Inductively coupled plasma-mass spectrometry (ICP-MS) technique. It is used to determine various elements in fruits and vegetables. This technique offer multi element capabilities. Numerous studies have quantified levels of toxic metal ions in common foodstuffs and in some cases these results have been extended by statistical analyses to generate 'target hazard quotients' (THQ) for a limited number of foodstuffs relating to individual and combinations of metals (Chien, 2002; Wang, 2005; Liu, 2006; Chien, 2006; Zheng, 2007).

Rapid and unorganized urban and industrial developments have contributed to the elevated levels of heavy metals in the urban environment of developing countries. Heavy metals are found everywhere in nature, and cannot be degraded or destroyed. While some metals like selenium, copper and zinc are essential to our diet at trace levels, but any metal in our food is toxic at high levels. The most notorious heavy metal contaminants are mercury, lead, and cadmium. They tend to be dangerous because they bioaccumulation in animal tissues over time. Heavy metal contamination usually originates from polluted water supplies. Fish are most susceptible to heavy metal contamination. The most widely used analytical methods for determination of heavy metals in food are graphite furnace atomic absorption spectrometry (GFAAS) and Inductively Coupled Plasma (ICP).

Various researchers deal with determination of metals in fruits and vegetables at trace, ultra-trace levels using spectrometric, electrometric techniques and inductively coupled plasma mass spectrometer (ICP-MS). ICP technique has become more popular since the early 1990s. Although the use of AAS (flame, graphite furnace, hydride generation and cold vapour) has declined during the same period, it is still the most widely used technique (Rose, 2001).

Materials and Method

All samples of the fruits and vegetables were procured from varied agricultural farms. All the samples, divided in skin and pulp, were oven-dried at 75°C until constant weight and ground to a fine powder by a Fritsch pulverisette 6 with an agate pocket. All precautions taken to prevent element contamination.

Sample Preparation

Vegetables, fruit, crop and plant samples were thoroughly washed to remove all adhered soil particles. Samples were cut into small pieces, air-dried for 2 days and finally dried at 100 ± 1°C in a hot-air oven for 3 h. The samples were ground in warm condition and passed through 1 mm sieve. Digestion of these samples (2 g each) was carried out using 10 ml nitric acid, according to the procedure used for soil samples. Well-mixed milk samples of 250 ml each were taken in 500 ml glass beakers and digested in 24 ml of aqua regia on a sand bath for 3 days. After evaporation to a lesser volume, the samples were filtered and diluted to 50 mL with distilled water.

Acid digestion

Digestion procedures are regularly carried out with either open vessels using acid, acid mixture or basic reagents on hot plates or open- and closed-vessel microwave ovens. The decomposition in open system is hard, time consuming and prone to systematic error sources, i.e. contamination or analyte losses. In case of using microwave radiation, the high cost of instrumentation and dilution of the sample can be considered as disadvantages in the microwave assisted digestion system. Although the amount of sample in vessels is limited due to the generation of gaseous reaction products that can increase of pressure, the use of closed high-pressure vessels is appropriate for efficient sample digestion. On the other hand, in the use of open-focused microwave ovens, the advantages are decreasing the risk to the operator, possible introduction of reagents, During procedure, opportunity to digest larger amounts of sample and low cooling time (Sant'Ana, 2007).

Dry ashing

In general, ashing methods may provide lower analyte recovery and exhibit poorer accuracy com-

pared to acid digestion methods. Although dry ashing procedures are effective, they are time consuming and can often result in loss of analyte species that could occur during the preparation of the sample.

Multi element Analysis

The different conditions of ICP-MS are shown in Table 1

Table 1. ICP-MS Instrumental (PerkinElmer) Conditions

Nebulizer	Quartz Concentric
Spray chamber	Quartz Cyclonic
RF power	1500 W
Integration time	1000 ms (per analyte)
Replicates	3
Cell gas mode	Helium

Results and Discussion

Soil pollution and contamination is indeed a serious problem. Vegetables and fruits are part of daily diets in many households forming an important source of vitamins and minerals required for human health. They are grown in different varieties of soil environments. Before preceding the assessment of trace element contamination in vegetables and fruits, it is customary to know the quality of precious resource soil applied for growth. Poor soil always reduces nutrient mineralization, microbial biomass and activity. Soil health has direct relation with the type of food nutrition they capitulate. The soil map of study area is shown in Fig. 1.

Soil analysis

Soil samples were collected in different sites without undergoing any industrial exposure in and around Visakhapatnam district, Andhra Pradesh, India. Soil samples were dried two days and grind by using mortar and pestle. Filtered through stainless steel sieve (0.2-2 mm). Parameters such as temperature, Electrical conductivity (EC), pH, soil moisture, organic carbon, NPK were determined by using standard procedures and the status is shown in Table 2.



Fig. 1. Soil map of study area

About twenty seven elements were recorded in various fruits and vegetables by using ICP-MS after microwave digestion, employing only nitric acid in this step. Potassium was not found in many fruit and vegetables. The method has been validated by using both an oil reference material and recovery experiments over different fruits and vegetable samples, obtaining satisfactory results in all cases. The mean (±SD) concentrations were calculated for each trace metal in all kind of fruits and vegetables. Based on the average concentration and the average consumption of edible vegetables, estimates of the amount of each trace metal consumed were calcu-

Table 2. Preliminary properties

Parameter	Sample1	Sample1	Sample1	Sample1
Temperature ^{0}C	26	26.8	26.5	27.1
pH	6.8	7.9	6.85	7.1
Electrical conductivity(S/m)	220	217	238	241
Organic carbon/Kg	2.2	2.95	2.43	3.1
Moisture (%)	1.8	2.4	5.2	3.7
N kg/Ha	142.2	167.5	141.8	179
P kg/Ha	28	31	26	29.5
K kg/Ha	302	341	298	352

Table 3. Trace elements in vegetables determined by Inductively coupled plasma-mass spectrometry

Analyte	Cell gas mode; Helium		Concentration; microgram per litre	
	BRINJOL µg L^{-1}	CARROT µg L^{-1}	TOMATO µg L^{-1}	CUCUMBER µg L^{-1}
Na	162957.924	418336.559	58197.041	S
Mg	167728.203	149077.305	89505.283	1077778.53
Al	1192.118	71478.474	2970.597	13130.186
Si	122800.202	62684.303	11601.634	171372.718
K	S	S	S	687421.06
Ca	218589.478	359213.563	68265.649	1325244.174
V	249.694	692.642	220.257	476.922
Cr	111.900	267.612	117.245	462.883
Mn	1143.617	3831.361	721.555	1923.889
Fe	3074.207	42076.326	3049.325	11653.478
Ni	399.438	361.889	267.907	951.185
Co	11.162	89.108	11.298	46.967
Cu	797.314	879.350	390.685	2276.666
Zn	2916.913	1620.642	1363.559	5707.169
As	104.312	281.066	133.543	843.105
Se	7.343	-4.441	3.841	-11.907
Rb	383.620	2124.950	2198.879	5350.073
Sr	1184.871	2414.766	614.699	15976.091
Mo	18.784	20.555	18.072	314.418
Ag	8.786	10.035	12.494	20.070
Cd	2.997	1.125	4.891	8.599
Sb	1.490	1.861	1.518	3.048
Ba	959.165	4724.498	477.951	3856.353
Tl	0.027	0.655	0.035	0.046
Pb	56.596	69.086	76.439	108.391
U	1.708	2.378	0.718	2.540

S - Beyond detection (Over saturated)

Table 4. Trace elements in fruits determined by Inductively coupled plasma-mass spectrometry

ANALYTE	Cell gas mode; Helium		Concentration ; microgram per litre	
	ORANGE µg L^{-1}	GRAPES µg L^{-1}	APPLE µg L^{-1}	KIWI µg L^{-1}
Na	311099.157	14858.646	145442.216	137251.951
Mg	309052.734	19953.586	70932.983	96694.948
Al	1393.29	1678.014	2578.263	3996.808
Si	105708.537	8639.017	80865.670	112768.234
K	S	S	S	S
Ca	1636550.440	32239.319	101444.128	250210.138
V	286.726	302.120	265.712	256.342
Cr	73.782	102.225	134.135	96.781
Mn	1060.928	425.685	245.302	391.169
Fe	6433.767	1926.157	2183.239	2624.397
Ni	273.257	1144.834	160.968	257.314
Co	11.654	5.598	38.069	13.066
Cu	313.782	171.380	127.746	663.476
Zn	1698.208	731.695	1411.135	1900.260
As	1503.823	143.570	167.119	260.239
Se	28.414	3.862	4.416	0.845

Table 4. *Continued ...*

ANALYTE	Cell gas mode; Helium		Concentration ; microgram per litre	
	ORANGE	GRAPES	APPLE	KIWI
	µg L^{-1}	µg L^{-1}	µg L^{-1}	µg L^{-1}
Rb	352.278	484.866	157.193	524.060
Sr	23418.949	222.025	799.751	1801.222
Mo	12.537	7.767	14.468	11.058
Ag	11.535	13.191	5.561	11.605
Cd	1.099	1.127	0.989	1.279
Sb	2.048	1.052	1.369	1.919
Ba	8890.318	170.539	756.155	2026.063
Tl	0.233	0.060	0.043	0.055
Pb	56.631	79.055	69.929	67.894
U	1.820	0.674	1.435	1.587

S - Beyond detection (Over saturated)

lated. The results of trace elements in vegetables and fruits were given in Table 3 and 4.

Conclusion

The intake of heavy metals can lead to altering of humans and animals healthiness state. The aim of this study was to determine the concentrations of trace metals in selected edible fruits and vegetables. ICP-MS has excellent analytical features such as simultaneous multielement capability, extremely high sensitivity, and wide linear dynamic range for most metal elements. Therefore the method has been validated by using both an oil reference material and recovery experiments over different fruits and vegetable samples, obtaining satisfactory results in all cases.

Acknowledgements

We are deliberately thankful to the department of chemistry, Institute of science, GITAM University for their immense support and huge encouragement.

References

Abdulla, M. and Chmielnicka, 1990. New aspects on the distribution and metabolism of essential trace elements after dietary exposure to toxic metals. *Biol. Trace Element Res.* 23 : 25-53.

Chien, L.C., Hung, T.C., Choang, K.Y., Yeh, C. Y., Meng, P.J., Shieh, M.J. and Han, B. C. 2002. Daily intake of TBT, Cu, Zn, Cd and As for fishermen in Taiwan. *Sci Total Envi.* 285 : 177-185.

Chien, L.W., Han, B.C., Hsu, C.S., Jiang, C. B., You, H. J., Shieh, M.J. and Yeh, C.Y. 2006. Analysis of the health risk of exposure to breast milk mercury in infants in Taiwan. *Chemosphere.* 64 : 79-85.

Jefferies, J. and Martin, I. 2009. Updated technical background to the CLEA model. Science Report, Environment Agency, SC050021/SR Environment Agency, 1-169.

Liu, C.W., Liang, C.P., Huang, F.M. and Hsueh, Y. M. 2006. Assessing the human health risks from exposure of inorganic arsenic through oyster consumption in Taiwan. *Sci Total Environ.* 361 : 57-66.

Mapanda, F., Mangwayana, E.N., Nyamangara, J., Giller, K.E. 2005. Uptake of Heavy Metals by Vegetables Irrigated Using Wastewater and the Subsequent Risks in Harare, Zimbabwe. *Agric. Ecosys. Envi.* 107: 151-165.

Rajesh Kumar Sharma, Madhoolika Agrawal and Marshall, 2004, Effects of waste water irrigation on heavy metal accumulation in soil and plants. F. M., Paper presented at a National Seminar, Bangalore University, Bangalore, Abst. no. 7, p. 8.

Rose, M., Knaggs, M., Owen, L. and Baxter, M. 2001. A Review of Analytical Methods for Lead, Cadmium, Mercury, Arsenic and Tin Determination Used in Proficiency Testing. *Journal of Analytical Atomic Spectrometry.* 16 : 1101-1106.

Sant'Ana, F. W., Santelli, R. E., Cassella, A. R. and Cassella R. J. 2007. Optimization of An Open-ocused Microwave Oven Digestion Procedure for Determination of metals in Diesel Oil by Inductively Coupled Plasma Optical Emission Spectrometry. *Journal of Hazardous Materials.* 149 : 67-74.

Sobukola, O.P. and Dairo, O.U. 2007. Food, Modeling drying kinetics of fever leaves (*Ocimum viride*) in a convective hot air dryer. *Niger. Food. J. J.* 25 (1) : 145-153.

Tricopoulas, D. and De Vita, V.T. 1997. (Ed) *Cancer: Principles and Practice of Oncology.* Lippincott Company,

Philadelphia, pp: 231-258.
Turkdogan, M.K., Kilicel, F. and Kara, K. 2002. Tuncer I. *Environmental Toxicology and Pharmacology.* 13 : 175-179.
Waalkes, M.P. and Rehm, S. 1994. Cadmium and prostate cancer. *J. Toxicol. Environ. Health.* 43 : 251-269.
Wang, X., Sato, T., Xing, B. and Tao, S. 2005. Health risks of heavy metals to the general public in Tianjin, China via consumption of vegetables and fish. *Sci Total Envi.* 350 : 28-37.
Ward, N.I. 1995. Environmental analytical chemistry. *Journal of Trace Elements*, Blackie Academic and Professional, UK, pp. 320–328.
Zheng, N., Wang, Q.C., Zhang, X.W., Zheng, D.M., Zhang, Z.S. and Zhang, S.Q. 2007. Population health risk due to dietary intake of heavy metals in the industrial area of Huludao city, *China. Sci Total Environ*. 387 : 96-104.

American Journal of Analytical Chemistry, 2020, 11, 197-204
https://www.scirp.org/journal/ajac
ISSN Online: 2156-8278
ISSN Print: 2156-8251

Synthesis and Characterization of Nano-Acetamiprid—New Plant Safeguard Nanomaterial

P. Padmavathi, N. Vasundhara, Swathi Kovvuri, N. V. S. Venugopal*

Department of Chemistry, Institute of Science, GITAM University, Visakhapatnam, India
Email: *venu7000@gmail.com

How to cite this paper: Padmavathi, P., Vasundhara, N., Kovvuri, S. and Venugopal, N.V.S. (2020) Synthesis and Characterization of Nano-Acetamiprid—New Plant Safeguard Nanomaterial. *American Journal of Analytical Chemistry*, **11**, 197-204.
https://doi.org/10.4236/ajac.2020.115015

Received: March 30, 2020
Accepted: April 25, 2020
Published: April 28, 2020

Copyright © 2020 by author(s) and Scientific Research Publishing Inc.
This work is licensed under the Creative Commons Attribution International License (CC BY 4.0).
http://creativecommons.org/licenses/by/4.0/
Open Access

Abstract

In present days many types of materials are used to reduce the environmental pollution in the world which includes nanomaterials. Nanopesticides increase the efficacy, durability and reduction in the amount of active constituent. The potential applications of nanotechnology in pesticides are quick decomposition in soil or plant, targeted delivery, apparent solubility and controlled release. In this communication the author reported a neonicatonoid insecticide called as Nano-acetamiprid and it is widely used to control fungal infections in different crops like cotton, leafy vegetables, citrus fruits, pome etc. The author reported a facile method *i.e.* a new Nano-acetamiprid for plant disease control and its subsequent characterization of encapsulated complex using polycaprolactone as an encapsulated agent. Nano-acetamiprid encapsulated particles were characterized by dynamic light scattering (DLS), ultraviolet spectroscopy and scanning electron microscopy (SEM). To ascertain the formation and the stability of nanoencapsulated acetamiprid pesticide, the maximum absorption spectra formulated at 421 nm and unformulated pesticide at 520 nm were observed. The size distribution was noted at 40 - 50 nm. The bioactivity study was conducted against various *Aspergillus niger*. The performance of nano particles was many fold times effective when compared to the original parental particles. The bio-assay of Nano-acetamiprid shows better results when compared to the normal commercial acetamiprid.

Keywords

Acetamiprid, Nano Encapsulation, Polycaprolactone, Antifungal Studies

1. Introduction

Acetamiprid is a neonicotinoid with a chloropyridinyl group and it is used to

protect plants against sucking aphid insects. It is also applied on plants ranging from leafy vegetables and fruit trees to ornamental plants. Acetamiprid is a carboxamidine that is acetamidine in which the amino hydrogens are substituted by a (6-chloropyridin-3-yl) methyl and a methyl group while the hydrogen attached to the imino nitrogen is replaced by a cyano group. Acetamiprid is an organic compound with the chemical formula $C_{10}H_{11}ClN_4$. (molar mass 222.67 g/mol). It is an odorless neonicotinoid insecticide produced. It has a role as a neonicotinoid insecticide, an environmental contaminant and a xenobiotic. It is a monochloropyridine, a nitrile and a carboxamidine. It derives from a 2-chloropyridine. Acetamiprid has a high potential for bioaccumulation and is highly toxic to birds and moderately toxic to aquatic organisms. Excessive use of the pesticide could pose a threat to human life.

Researchers concentrated on recent development of nanotechnology [1]. New colorimetric sensors based on the aggregation of metallic nanoparticles are emerging [2] [3] [4] [5]. Among all the materials explored, gold nanoparticles (AuNPs) have received more consideration owing to their intrinsic characteristics such as easy preparation, biocompatibility, stability, and high extinction coefficients [6]. Various substances have been detected by the gold nanoparticles based colorimetric method [7]-[12]. Encapsulation process has wide applications such as foods, cosmetics, paints, paper, textiles etc. To remove harmful effects on the non-target organisms, encapsulation of the active ingredient with other materials such as a polymer can allow sensitive ingredients to be physically enveloped into a protective matrix in order to protect core materials from adverse reactions due to factors like air or light. Rapid growth has been found in the field of nanotechnology over the past few years and it has successfully ventured into different fields of science. Nanoformulations of pesticides based on polymers have been exploited for the encapsulation of most of the insecticides. The first polymer contained formulation was developed in the year 1970 for control release of biocides. Techniques like electrochemical synthesis, chemical vapour deposition, sol-gel synthesis, microwave assisted synthesis, ultrasonication, "precipitation method etc", were reported for the synthesis of nanoparticles [13] [14] [15]. How nanoparticles can act and control of pests is less studied. In certain cases pesticide nanoparticles present possibilities for controlling pest effectively [16] [17]. Few studies reported on polymer nanocomposites like polyethylene glycol due to its properties and multifunctional structures of each segment [18] [19].

Hence the nano size of pesticide particles could reduce the threat to the living organisms. In this communication we reported a non-hazardous polycaprolactone as a capping agent to prepare the nano formulation of acetamiprid pesticide. Ever since nanopesticides emerge as a developing field in agriculture for best yields, better penetration towards the target molecule, low concentration of pesticide moleculs. Increased surface area of nano shaped particles allows us to use the less quantity of traditional pesticides in the agricultural land.

2. Materials and Methods

2.1. Reagents

Polycaprolactone was procured from E. Merck, India. All other chemicals used were of analytical grade. Water used throughout the process was double-distilled water.

Acetamiprid was generously gifted by S. N. Agro traders, Visakhapatanam, India. Glassware used in this experimental work was properlyacid washed.

2.2. Preparation of Nano-Acetamiprid

Commercially available acetamiprid is finely grounded with the help of mortar and pestle. The soluble form of the finely powdered acetamiprid was mixed in ultra sonicate bath for 40 minutes with the twice the polycaprolactone solvent. The formulation was subjected to continuous mixing followed by stirring for 5 - 6 hours and then the excess solvent was removed by using Rota-evaporator.

2.3. Instrumentation

Particle size distribution was obtained by Dynamic light scattering (DLS) Horiba, nanopartica, Japan, s2100. UV-V is measurements were obtained by using Shimadzu UV-1650 PC Spectrophotometer through a quartz cell with 10 mm optical path and this was used to characterize and identify the organic molecule. Surface topology was determined through scanning electron microscopy (Zeiss Evol8).

3. Results and Discussion

The pressing concern of the world at present is the excessive use of agrochemicals and it leads to risks for human health and many environmental problems. So many observations foresee that nanoscience and nanotechnology allow the development of agricultural fields with high technology contains nanoproducts and that leads precise management and less utilization of pesticides. Nanopesticides are the best alternative to the traditional pesticides.

Nano-acetamiprid is highly active at lower level concentration and reduces toxicity in agricultural fields. The polycaprolactone enhances the stability and it slowly releases the active ingredient to the target. The mode of action of Nano-acetamiprid is shown in Figure 1.

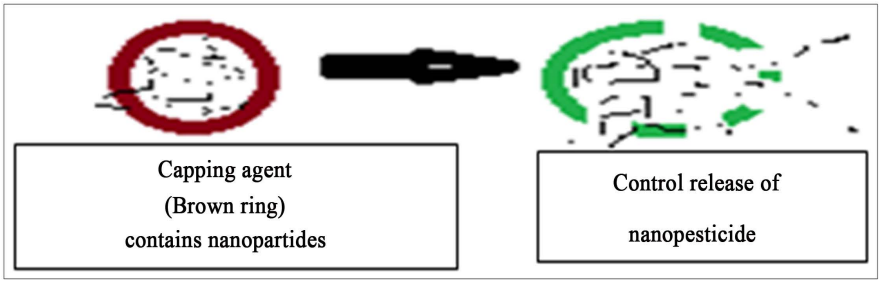


Figure 1. Mode of action of Nano-acetamiprid.

Nano-acetamaprid reduces toxicity in agricultural fields and it is highly active at lower level concentration. In general better efficacy, better control of application and less use of chemicals is the benefits of nanopesticides. Our study provides a novel nanoformulation of acetamiprid pesticide by Polycaprolactone as capping agent. The polycaprolactone enhances the stability and it slowly releases the active ingredient to the target. The structure of acetamiprid and polycaprolactone (capping agent) are shown in Figure 2 and Figure 3.

3.1. DLS Analysis

The diameter of the nano-encapsulated acetamiprid was obtained by pade laplace dispersion. It mainly depends on Rayleigh scattering, oscillations, Brownian movement and fluorescence exponential decay. In this method a time dependent signal was transformed into the hydro colloidal solution and it results in the exponential decay of the particles. The transformed laplace signal is defined as an infinite integral over time. Through this transformed signal number of components in the encapsulated solution can be easily obtained. It can be clearly depicted in the following pade laplace dispersion graph. Dynamic light scattering (DLS) measures the scattering intensity based on Rayleigh scattering. One milli litre of nano-encapsulated acetamiprid was suspended in 5 ml of water. The resultant hydro dispersed suspension was analyzed with DLS at 25˚C - 40˚C. The particle size distribution was appeared around 40 - 50 nm. The particle size distribution is shown in Figure 4.

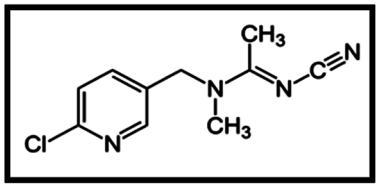


Figure 2. Structure of acetamiprid.

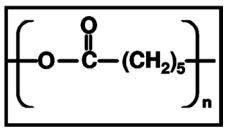


Figure 3. Structure of polycaprolactone (capping agent).

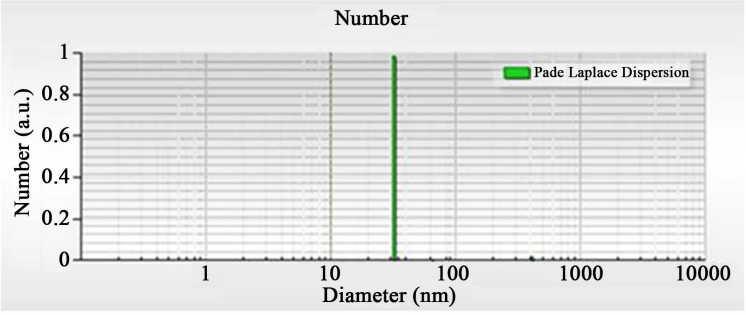


Figure 4. Nano-acetamiprid size distribution.

3.2. UV-Vis Spectral Study

To ascertain the formation and the stability of nanoencapsulated acetamiprid pesticide, UV-Vis spectra is necessary. 19 The maximum absorption spectra formulated at 421 nm and unformulated pesticide at 520 nm were shown in **Figure 5**.

3.3. SEM Analysis

The surface topology, size of Nano-acetamiprid was obtained by scanning electron microscope at 500× - 35 k× magnification. A drop of encapsulation complex is taken on the stub and it was air dried then subjected to sputtering using sputter coater. The SEM image reveals the homogeneity in shape and it is regular among different scan a regions. SEM image which was depicted in **Figure 6** shows a number of Nano-acetamiprid particles in the clusters.

3.4. Application of Nano Acetaprid on *Aspergillus bacillus*

The antifungal activity of encapsulated acetamiprid was examined in petridish assay by disc diffusion method. The fungal isolates were cultured on potato dextrose agar (PDA) medium which induce the conidia production incubated at 37˚C for 10 days. Sterile de-ionized water was used as control. The antifungal activity of encapsulated acetamiprid was examined in petridish assay by disc diffusion method [20]. The fungal isolates were cultured on potato dextrose (PDA) medium which induce the conidia for 10 days. Sterile ionized water was used as control. The sample ppm, 40 ppm and 20 ppm, diluted 100-fold with de-ionized water. On to the PDA mediums filter paper discs dipped in different ppm were inserted and the petridishes were incubated at 37˚C for 2 - 4 days respectively. The size of the zone was determined by measuring the diameter of the zone in mm. Nano encapsulated acetamiprid shows best results when compared with commercial acetamiprid which can be clearly depicted below. The various inhibitory zones of Nano-acetamiprid samples are shown in **Figure 7**.

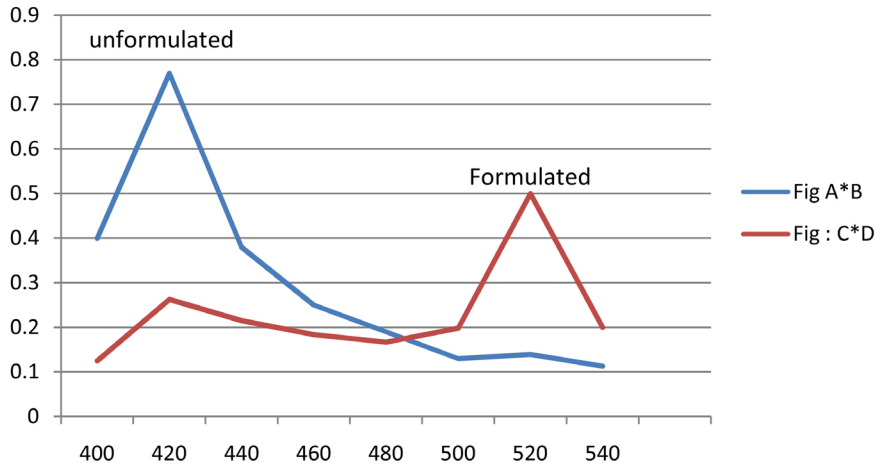


Figure 5. Maximum absorption of formulated and unformulated acetamiprid.

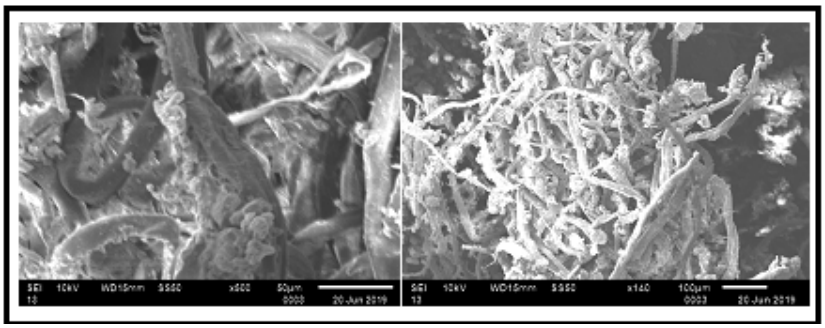
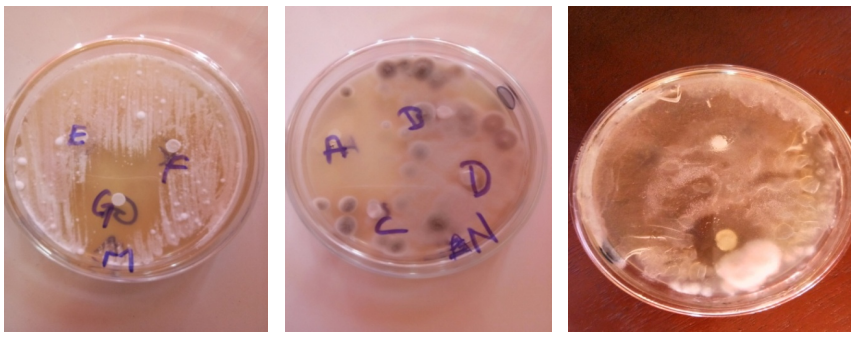


Figure 6. SEM images of Nano-acetamiprid.



(a) (b) (c)

Figure 7. Inhibitory zones ((a), (b), and (c)) of *Aspergillus niger*. (a) Nano-acetamiprid on agar plates; (b) Formation of clear zone; (c) Nano-acetamiprid inhibitory zone at 50 ppm.

4. Conclusion

Nanoscience has greatly contributed to major achievements in various fields. The biodegradable additive polycaprolactone is used to minimize the size of pesticide molecules. A better alternative to conventional pesticide is nanopesticide. Nano-acetamiprid was formulated by using polycaprolactone as capping agent. The properties of characterization of different techniques support the encapsulation, characterization and stability of Nano-acetamiprid pesticide. The nano encapsulated acetamiprid was found to have more antifungal activity. The result suggests that the synthesized nano-carbendazim pesticide undergo interaction with bacterial cell and thereby exhibit strong action. The formation of clear zone with restricted bacterial growth around the cavity is shown in the figure. The valuable information has paved way to further development and practical application of polymeric nano insecticides with huge potential.

Acknowledgements

We are deliberately thankful to the department of chemistry, Institute of science, GITAM University for their immense support and huge encouragement.

Conflicts of Interest

The authors declare no conflicts of interest regarding the publication of this re-

search paper.

References

[1] Liu, S.Q., Yuan, L., Yue, X.L., Zhang, Z.Z. and Tang, Z.Y. (2008) Recent Advances in Nanosensors for Organophosphate Pesticide Detection. *Advanced Powder Technology*, **19**, 419-441. https://doi.org/10.1016/S0921-8831(08)60910-3

[2] Liu, J.W. and Lu, Y. (2006) Colorimetric Sensing of Adenosine and Cocaine Based on a General Sensor Design Involving Aptamers and Nanoparticles. *Angewandte Chemie International Edition*, **45**, 90-94. https://doi.org/10.1002/anie.200502589

[3] Wu, W.Y., Bian, Z.P., Wang, W. and Zhu, J. (2010) Gold Nanoparticle Composite Film-Based Silver Enhanced Colorimetric Detection of Cardiac Troponin. *Sensors and Actuators B: Chemical*, **147**, 298-303. https://doi.org/10.1016/j.snb.2010.03.027

[4] Zhang, Y.M., Lin, Q., Wei, T.B., Wang, D.D., Yao, H. and Wang, Y.L. (2009) Simple Colorimetric Sensors with High Selectivity for Acetate and Chloride in Aqueous Solution. *Sensors and Actuators B: Chemical*, **137**, 447-455. https://doi.org/10.1016/j.snb.2009.01.015

[5] Zhang, S.H., Wang, J., Han, L., Li, C.G., Wang, W. and Yuan, Z. (2010) Colorimetric Detection of Bis-Phosphorylated Peptides Using Zinc (II) Dipicolylamine-Appended Gold Nanoparticles. *Sensors and Actuators B: Chemical*, **147**, 687-690. https://doi.org/10.1016/j.snb.2010.03.071

[6] Rosi, N. and Mirkin, C.A. (2005) Nanostructures in Biodiagnostics. *Chemical Reviews*, **105**, 1547-1562. https://doi.org/10.1021/cr030067f

[7] Ai, K.I., Liu, Y.L. and Lu, L.H. (2009) Hydrogen-Bonding Recognition Induced Color Change of Gold Nanoparticles for Visual Detection of Melamine in Raw Milk and Infant Formula. *Journal of the American Chemical Society*, **131**, 9496-9497. https://doi.org/10.1021/ja9037017

[8] Han, C.P., Zeng, L.L., Li, H.B. and Xie, G.Y. (2009) Colorimetric Detection of Pollutant Aromatic Amines Isomers with p-Sulfonatocalix Arene-Modified Gold Nanoparticles. *Sensors and Actuators B: Chemical*, **137**, 704-709. https://doi.org/10.1016/j.snb.2008.12.038

[9] Zhao, W., Brook, M.A. and Li, Y.F. (2008) Design of Gold Nanoparticle Based Colorimetric Biosensing Assays. *ChemBioChem*, **9**, 2363-2371. https://doi.org/10.1002/cbic.200800282

[10] Zhao, W., Chiuman, J.C.F., Lam, S.A., McManus, W., Chen, Y.G., Cui, R., Pelton, M.A., Brook, A. and Li, Y.F. (2008) DNA Aptamer Folding on Gold Nanoparticles: From Colloid Chemistry to Biosensors. *Journal of the American Chemical Society*, **130**, 3610-3618. https://doi.org/10.1021/ja710241b

[11] Zhao, W., Chiuman, W., Brook, M.A. and Li, Y.F. (2007) Simple and Rapid Colorimetric Biosensors Based on DNA Aptamer and Noncrosslinking Gold Nanoparticle Aggregation. *ChemBioChem*, **8**, 727-731. https://doi.org/10.1002/cbic.200700014

[12] Zhang, Y.F., Li, B.X. and Chen, X.L. (2010) Simple and Sensitive Detection of Dopamine in the Presence of High Concentration of Ascorbic Acid Using Gold Nanoparticles as Colorimetric Probes. *Microchimica Acta*, **168**, 107-113. https://doi.org/10.1007/s00604-009-0269-5

[13] Horwat, D.I., Zakharov, J.L., Endrino, *et al*. (2011) Chemistry, Phase Formation, and Catalytic Activity of Thin Palladium-Containing Oxide Films Synthesized by Plasma-Assisted Physical Vapor Deposition. *Surface and Coatings Technology*, **205**,

S171-S177. https://doi.org/10.1016/j.surfcoat.2010.12.021

[14] Chandraboss, V.L., Senthilvelan, S., Natanapatham, L.M., Murugavelu, B., Loganathan, B. and Karthikeyan, J. (2013) Photocatalytic Effect of Ag and Ag/Pt Doped Silicate Non Crystalline Material on Methyl Violet—Experimental and Theoretical Studies. *Journal of Non-Crystalline Solids*, **368**, 23-28. https://doi.org/10.1016/j.jnoncrysol.2013.02.027

[15] Karthikeyan, B. and Loganathan, B. (2013) Rapid Green Synthetic Protocol for Novel Trimetallic Nanoparticles. *Journal of Nanoparticles*, **2013**, Article ID: 168916. https://doi.org/10.1155/2013/168916

[16] Karunaratne, V., Kottegoda, N. and Alwis, A.J. (2012) *National Science Foundation*, **40**, 3-8. https://doi.org/10.4038/jnsfsr.v40i1.4165

[17] Khot, L.R., Sankaran, S.H., Maja, E.W., *et al.* (2012) Applications of Nanomaterials in Agricultural Production and Crop Protection: A Review. *Crop Protection*, **35**, 64-70. https://doi.org/10.1016/j.cropro.2012.01.007

[18] Ajayan, P.M. (1999) Nano Tubes from Carbon. *Chemical Reviews*, **99**, 1787-1799. https://doi.org/10.1021/cr970102g

[19] Choudary, S.R., Pradhan, S. and Goswami, A. (2012) A Preparation and Characterisation of Acephate Nanocomplex. *Nanoscience Methods*, **1**, 9-15. https://doi.org/10.1080/17458080.2010.533443

[20] Barry, A.L. and Brown, S.D. (1996) Fluconazole Disk Diffusion Procedure for Determining Susceptibility of Candida Species. *Journal of Clinical Microbiology*, **34**, 2154-2157. https://doi.org/10.1128/JCM.34.9.2154-2157.1996

ISSN 2347 - 3983
Volume 8. No. 3, March 2020
International Journal of Emerging Trends in Engineering Research
Available Online at http://www.warse.org/IJETER/static/pdf/file/ijeter35832020.pdf
https://doi.org/10.30534/ijeter/2020/35832020

Q-HeteLearn: A Progressive Learning approach for Classifying Meta-Paths in Heterogeneous Information Networks

Sadhana Kodali [1], Madhavi Dabbiru [2], B Thirumala Rao [3]
[1,]PhD Scholar, Department of Computer Science and Engineering, Koneru Lakshmaiah Education Foundation, Vaddeswaram, AP, India.
[2]Professor, Department of Computer Science Engineering, Dr.L.Bullayya College of Engineering for Women, Visakhapatnam, Andhra Pradesh, India.
[3,] Professor, Department of Computer Science and Engineering, Koneru Lakshmaiah Education Foundation, Vaddeswaram, AP, India.

ABSTRACT

Reinforcement learning is a machine learning paradigm which has a number of applications in gaming, stock prediction, robot navigation etc. The reinforcement learning can be applied to complex real-world tasks which have adjustable problem spaces. In this paper a novel approach called Q-HeteLearn a Progressive Learning method is introduced to classify the objects by traversing the meta-paths in the Heterogeneous Information Networks. The proposed approach showed best results when compared to a traditional learning strategy called the Q-Learning and also the comparative study showed a better result with Deep Q-Learning. The concept of Q-HeteLearn which is a Progressive Learning technique is introduced to improve the swift traversal of the objects in the meta-paths and to classify them.

Keywords: Reinforcement learning, , Q-Learning, Heterogeneous Information Networks.

1.INTRODUCTION

The objects in the real world are heterogeneous and often associated by a semi-structured semantic relationship which we call as heterogeneous information network [1] examples include biological networks, bibliographic networks ,social networks ,highway networks[2]etc. By observing these semantically connected links between objects, we can get consequential meta-paths[3]that help us take significant decisions. Traversing these gigantic networks[4,5] and learning the relationships between them using traditional approaches is very time taking and involves a lot of effort. Breaking down these gigantic interconnected objects to semi-structured information networks can be possible by classifying the interconnecting objects which are responsible to form the meta-path is the main aim of this paper. The authors implemented the Q-HeteLearn which is a progressive learning approach that has faster computation performance when compared with one of the traditional reinforcement learning algorithm called Q-Learning. The proposed approach is also compared with Deep Q-Learning. This paper is organized as follows: In section 2 the literature survey is provided, section 3 the proposed methodology is discussed, section 4 gives the experimentation results and concluded in section 5.

2. LITERATURE SURVEY

The Q-Learning [6]algorithm is one of the reinforcement learning technique and a model free learning strategy. Q-Learning is a policy based approach which tells an agent the next action to be taken at the corresponding circumstances. Q-Learning has many applications one of which includes the addressing of autonomous mobile robot navigation problem[7],in which the authors projected an improved Q-Learning algorithm for the navigation of a robot using a non-repeated state-action trajectory. The agents learned from reinforcement which has absolute value. The co-operative Q-Learning exhibited better performance than traditional Q-leaning in the context of a segmented world. In the traditional Q-Learning approach the Qvalues are infinitely updated for few steps. The condition to terminate is to check the difference in the Qvalues obtained from the successive iterations. The drawback of this approach is the time complexity. The other case of Q-Learning is named as extended Q-Learning [8], the best action state is stored. The limitation of storing the best action state may not permit another updated state.In [9] the authors used an approach to address the reinforcement learning for continuous actions. The authors in [10] used a disease prediction attack for asthma using Q-Learning. But the model constructed in the above technique made use of historical. In [11] the authors used the Q-Learning approach to model the energy consumption by integrating Q-Learning with radio networks which showed an improved levels of energy consumption. Q-Learning is also applied for home energy management using fuzzy reasoning in [12]. The Q-HeteLearn Progressive Learning approach is experimented on an image dataset to classify the images.

3. METHODOLOGY

The proposed approach is appropriate for stochastic transition problems like growth of bacteria, fluctuating electric current and so on. On the other hand, in a practical application the function approximation may vary and another overhead exists with the speed of learning. In the traditional Q-Learning algorithm, The major task is to accomplish the goal state where in for every action(change from current state to new state)there is a reward and it helps in attainment of the goal state. At this point if the system is capable to progress in the accurate direction (closer to the goal state),then a certain weight is to be associated along with the feedback component. If the Q-System is unsuccessful to arrive at the goal state then a negative signal should be communicated so as to make the Q-System change its progression path. The weight can be a probability component d may vary with the closeness to the goal state. Thus, the progression factor helps in accelerating the Q-algorithm in reaching its goal state swiftly. In the Q-HeteLearn approach a progression factor is defined by the symbol Ғ.

Ғ=diff (Qgoal, Q)*P (A, W) (1)

In the equation (1) Qgoal is the expected goal state and Q is the current state. The progression factor Ғ gives δ difference. P (A, W) is the probability of our taking action $a_i$in state s_{cur} to choose another near state s_{next}

$$P(Ai, w) = \frac{\exp(wi)}{\sum_j exp(wj)} (2)$$

Where exp is the expected weightage to the change of state from s_{cur} to s_{next}.The equation in (2) indicates weighted probability P (A_i, w) is the number of ways to achieve the desired outcome divided by the number of total possible outcomes. The performance of the algorithm is enhanced if this δ meets the threshold range Ғ. When the diff(Qgoal,Q) is calculated if it doesn't fall in the threshold range Ғ,which indicates that the current state Q is isolated from the goal state and it can be bypassed as there is nothing much to be trained from this state. According to the Q-HeteLearn Progressive Learning approach the threshold value is computed to reach the goal state. Traversing all the states may not accomplish to reach the goal state. To drop off the time complexity the progression factor is computed at every state and checked with the threshold. If the value is in the range of the threshold value, the state can be considered to be closer to the goal state. The PTable for the target state is set initially taking a query image and converting this query image to an array. The Pgoal state for this image is computed. The images in the folder are compared with this goal state and the similar images are identified.

Q-HeteLearn :Progressive Learning approach

Step:1Initialization:
I=Read the target image;
Convert Ito an array.
Pgoal initialised to No of zeros equal to the shape of the target image.
diff initialised to No of zeros equal to the shape of the target image.
Step 2:
Repeat for every image{
Repeat for I.shape()
{
Pgoal[i][j] = I[i][j] + α*(rw + γ*(I2[i][j]) - I[i][j])
Compute the difference for the target image and every image in the folder cv2.subtract(I,Pgoal)
Estimate the progression factor:
Ғ=diff(Pgoal,I)*P(A_i,w)
If Ғ<=Ғ
Update Ptable
continue
else
skip state and goto next;
}
}

Figure 1: Q-HeteLearn approach.

The Figure 1 represents an algorithm which explains the proposed methodology.

4. EXPERIMENTATION

A stochastic process changes over time and so is the plant growth and the size, colour of the leaf changes with time, climate and various other conditions. If the leaf is observed as a set of numbers represented in a two-dimensional array, then the array of a healthy leaf indicates different set of points while the diseased leaf indicates a different number in the given array. When we observe a spotted leaf and compare it with the goal state, where the goal state is that of a healthy leaf, the action taken should be different recommendations of pest control to reduce the plant disease. The dataset to do the experimentation is obtained from [13]. This is an image repository of different plants and their corresponding diseases. The plant village image dataset contains 20639 images. The foremost step to this approach is the data pre-processing step. Pre-process the images by comparing them using cv2.subtract() method then set a threshold value Ғ ,If the threshold value constraint is not set then it is a completely different image. The experimentation is carried on an Intel core 2 duo processor with 4GB Memory. The code for implementing the Progressive Learning algorithm is written using python.

The Table 1 and graph in Figure 2 give explanation about the time taken for execution of the number of images corresponding to Q-Learning and Q-HeteLearn Progressive Learning approach. From the graph it can be observed that the time taken to execute in the Q-HeteLearn approach is comparatively less. The Q-Learning approach takes more time as the number of images increases considerably. From the 997 images 396 images are used for test and residual 601 images are considered for training.

Table 1: Runtimes of Q-Learning and Q-HeteLearn Progressive Learning.

No of Images in the folder	**Q-Learning Execution time**	**Q-HeteLearn Execution time**
16	2:75secs	2:56secs
35	4:32secs	2:75secs
45	5:46secs	2:97secs
59	7:26secs	3.46secs

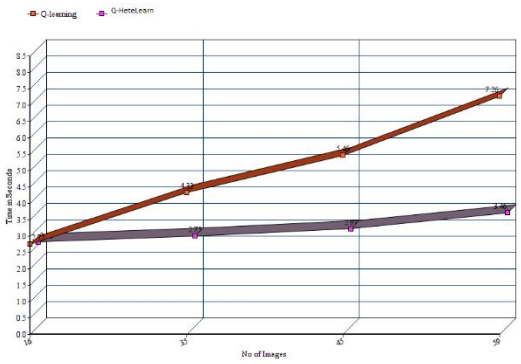


Figure 2: Graph used to represent the runtime of Q-Learning and Q-HeteLearn.

Table 2: Runtime results

Number of Images	**Q-Learning**	**Q-HeteLearn**
997	5.46mins	28 Sec

From Table 2 we can examine that the time to execute is less than a minute in case of 997 images which contain different classes. The target image matches only with a few images and this algorithm quickly prunes the images that do not match the threshold value.

4.1 Comparison with Deep Q-Learning:

Q-Learning has certain limitations that it works better for smaller environments with discrete, finite state and action spaces. But a meta-path expands as new objects add to it and new relationships exist. Therefore, the Deep Q-Learning strategy is also used to compare Q-HeteLearn. The Deep Q-Learning makes use of the neural network which approximates the values which are unstable and diverging. Adjusting the weights in the neural networks include back propagation.In Deep Q-Learning a small update to Q has significant change in the policy. These variable changes are updated and managed by experience replay and iterative updates which increases the time complexity when compared to Q-HeteLearn which took minimal time to learn about the meta-paths. We compare Deep Q-Learning with Q-HeteLearn by already available results in [14] the input of Deep Q-Learning is the pixels and game scores. The input of Q-HeteLearn is an image which is converted to an array of pixels. The state and actions are obtained by playing a game 30 times for 5 minutes with an □=0.05. The value of γ=0.99 is set for Deep Q-Learning and γ=0.9 for Q-HeteLearn. The Deep Q-Learning uses the deep neural networks to categorize the objects from raw sensory data whereas the Q-HeteLearn traverses the meta-paths and applies a progression factor to categorize objects.

5. CONCLUSION

In this paper a Progressive reinforcement learning approach called the Q-HeteLearn is devised for classification of meta-paths in heterogeneous information networks .This approach uses a progression factor for Q-Learning for improving the execution time. The Q-HeteLearn shows a better performance with regard to runtime when compared with the traditional Q-Learning as well as the latest algorithm deep Q-Learning.As a part of the future work, the deep learning techniques will be used to propose recommendations in heterogeneous information networks without clipping the rewards and by optimizing the P table.

REFERENCES

1. Chuan Shi,Yitong Li,Jiawei Zhang,Yizhou Sun, PhilipSYu,**A survey of heterogeneous information network analysis** IEEE transactions on Knowledge and Data Engineering", Volume 29,Issue 1,Jan 1 2017. https://doi.org/10.1109/TKDE.2016.2598561
2. Srivastava, Rupesh & Greff, Klaus & Schmidhuber, Jürgen. (2015). **Highway Networks.**
3. Yizhou Sun,Jiawei Han,Xifeng Yan,Philip S. Yu ,Tianyi Wu, **PathSim: Meta Path-Based Top-K Similarity Search in Heterogeneous Information Networks** Proceedings of the VLDB endowmwent,Vol 4 ,No 11,September 2011.
4. B.Tirapathi Reddy, M.V.P Chandra Sekhara Rao **Filter Based Data Deduplication in Cloud Storage using Dynamic Perfect Hash Functions** International Journal of Simulation Systems, Science & Technology, and ISSN: 1473-804x online, 1473-8031print. DOI 10.5013/IJSSST.a.19.04.08. 2018

5. B.Tirapathi Reddy, Dr.M.V.P. Chandra Sekhara Rao, **Performance evaluation of various data deduplication schemes in cloud storage**, IJPAM,Sep-2016,Vol. 116, Issue No.5,175-180.
6. Christopher J.C.H.Watkins **Technical Note Q-Learning** Machine Learning, 8,279-292(1992). https://doi.org/10.1023/A:1022676722315
7. Jawad Muhammad, Ihsan ÖmürBucak **An improved Q-Learning algorithm for an autonomous mobile robot navigation problem** International Conference on Technological Advances in Electrical, Electronics and Computer Engineering, May 2013.
8. V.Borkar **Q-Learning for Risk-Sensitive control Mathematics of Operations Research**27(2),294-311,2002. https://doi.org/10.1287/moor.27.2.294.324
9. Jose del R Millan,Daniele posenato,Eric Dedieu **Continuous-Action Q-Learning**, Machine Learning Volume 49 Issue pp-247-265,November 2002.
10. Q. Do, S. Tran and A. Doig, **Reinforcement Learning Framework to Identify Cause of Diseases - Predicting Asthma Attack Case** *2019 IEEE International Conference on Big Data (Big Data)*, Los Angeles, CA, USA, 2019, pp. 4829-4838
11. Mohammed saleh, Bendella, Badr Benmammr, Francine Krief **Using cognitive radio to deliver Green Communication** International Journal of Knowledge Engineering and Data Mining,Vol 6,Issue 4. February 2020.
12. Fayiz alfaver, M Danal,Y Sun **Demand Response Strategy Based on Reinforcement Learning and Fuzzy Reasoning for Home Energy Management** IEEE Access February 2020. https://doi.org/10.1109/ACCESS.2020.2974286
13. https://github.com/spMohanty/PlantVillage-Dataset
14. Volodymyr Mnih, Koray Kavukcuoglu , David Silver et.al **Human-level control through deep reinforcement learning** NATURE ,VOL 518,26 February 2015. https://doi.org/10.1038/nature14236

Biosc.Biotech.Res.Comm. Special Issue Vol 13 No (6) 2020 Pp-63-70

BBRC
Bioscience Biotechnology Research Communications

Efficient Road Side Framework Placement using VANET for Reducing Network Delays

G.Vamsi Krishna[1], R.Shankar[2], N.Vadivelan[3] and M.Nalini[4]

[1]*Assistant Professor, Dr.Lankapalli Bullayya Engineering College for Women.*
[2]*Professor, Dept. of Electronics and Communications Engineering, Teegala Krishna Reddy Engineering College, Hyderabad India*
[3]*Professor, Dept. Computer Science and Engineering, Teegala Krishna Reddy Engineering College, Hyderabad, India*
[4]*Assistant Professor, Dept. Computer Science and Engineering, Saveetha School of Engineering, Chennai, India*

ABSTRACT

The Road Side Unit (RSU) is a transmitter, it is facilitate along with route to us for communication between network surface and vehicles. The RSU is one of the components of VANET (vehicular ad hoc network). In this research paper mainly focused on problem of placement of RSU on road side like highway and also avoids the network delay along with efficient network. For this problem the proposed ERSF (Efficient Road Side Framework) avoid the network delays with help of number linear conceptual model along with optimization network delay and under consideration of network. The ERSF framework has been tested that performance using metrics of Generating Traffic Mobility Patterns (GTMP) by VanetMobiSim. The experimental results comparisons has been shows standard distribution and cost effective reduction is 23% and the network delay is 9% respectively and these results are gives clear definition of efficiency of ERSF solutions.

KEY WORDS: GTMP, RSU, ERSF, VANETMOBISIM, NETWORK DELAYS, ROAD SIDE UNIT.

INTRODUCTION

Now a day the emerging network technology for Ad-Hoc Network is Vehicular Ad Hoc Network (VANET), that is allows the methods of ITS (Intelligent Transportation System) techniques for making an efficient networking systems for between network surface and vehicles in road infrastructure through Vehicular Ad Hoc Network. The VANET facilitate vehicles interactive with every other network in read unit and get efficient internet on the moving state.

The VANET is a part of Mobile Ad-hoc Networks; these VANET and MANET is self organized, independent and focused for the sharing manner along with self organized authentication Ranjan Senapati B et al., (2020) With help of Dedicated Short Range Communication (DSRC) the VANET has gives wireless link for communication for roaming vehicles Babu Ram and Neelendra Badal (2019) along with the standard of IEEE 802.11a Malhi et al., (2019). In VANET changes sequence is very problem in traffic network, Because of high portability the topology. Besides, long range interaction, the serious issues is inaccessibility of RSU within certain regions which brings about separation and undesirable network late.

ARTICLE INFORMATION

*Corresponding Author: vamsikrishna527@gmail.com
Received 19h June 2020 Accepted after revision 3rd August 2020
Print ISSN: 0974-6455 Online ISSN: 2321-4007 CODEN: BBRCBA

Thomson Reuters ISI Web of Science Clarivate Analytics USA and Crossref Indexed Journal

Clarivate Analytics
crossref

NAAS Journal Score 2020 (4.31) SJIF: 2020 (7.728)
A Society of Science and Nature Publication, Bhopal India 2020. All rights reserved.
Online Contents Available at: http//www.bbrc.in/

The limit and effectiveness of VANET is unequivocally relies on situation of RSU with the path. One of the very much planned RSU position system can enormously improve the limit along with effectiveness of the system, and simultaneously lessens usage cost. In the RSU designation technique must be contrived with the end goal that it can gather all the traffic information and disperse it progressively over the whole system. The wide scope for VANET has lot of applications going from diversion to street authentications Lin et al., (2017). Wellbeing applications intensely depend on close to constant transmission of crisis information sharing A. Arora et al., (2019). For that kinds of uses need for solid activity communication of between vehicle-to-framework and vehicle-to-vehicle.

The principle reason for existing is to stay away from incidents, stay alive of humans and give obstruction less condition to crisis reaction group. On interstates, VANET should be had transmit ready information sharing utilizing RSU is to facilitate speed up the crisis reaction if there should be an occurrence of an episode. A perfect time for helping for medical facility during accident happening time period is called golden time S. S. Shah et al., (2019), at the point when a mishap occurs, ready messages ought to be engendered to the respect specialists inside portion of the best time Salah, Ket al., (2017). That is manifest limiting transmission late is the way to give crisis reaction with in time. The ERSF manages along with fitting of RSUs on road side. Every vehicle able get to RSUs in various approaches; direct communicate conveyance, happens when the vehicle come in to the RSU transmission scope, and handing-off of multi-bounce, it is happens when the vehicle is exit of the RSU transmission boundary. The proposed ERSF approach performed defining by whole Number Linear Conceptual Model (NLCM) model.

The goal of this technique is to reduce the framework of delay, at the same time as regarding the all out spending plan accessible for the sending. Because of building up the technique has taken both vehicle-to-RSU and vehicle-to-vehicle swapping. Distributions of Vehicle along with versatility designs are produced by utilizing VanetMobiSim Zhang, Z et al., (2011), simulations. During the ERSF is approved in NS2 by arrange reproductions acted. This research paper has been organized as the following phases. Related work and problem statements were placed in phase two. The system models in phase three. In phase four had optimal position placement of RSU. The results of simulations are represented in section five. The results and discussion and conclusion are placed were phases six and seven respectively. The vast majority Shaik, S et al., (2013) of the exploration work finished on RSU situation has concentrated on boosting framework execution regarding throughput or by [10, 13 and 15] and large framework limit.

Not many authors have thought about the issue of limiting idleness. The most part cantered [9] around limiting handover inertness and related system. The analysts [17] considered the issue of how to moderate the effect of multichannel hand-off clash and keep up high data engendering speed and proposed a hand-off conflict calculation. The displayed and dissected Liu [7] along with Hu, Y., et al. (2017) the postponement of broadcasting an alarm sharing VANET. The issue of limiting [16] transmission late by ideally putting RSU was considered. In any case, the proposed arrangement was centered on limiting deferrals in urban conditions.

2.Related Work: The issue of the minimization situation for had tended to by a few research authors. The author Liu et al investigated the absolute literacy of broadcasting cautions in VANET and road [7]. The authors likewise built up a connection between the minimum number for the RSUs along with the separation secured by vehicles or cars. Nonetheless, the authors didn't produce any RSU sending methodology. Another author has Ahmed and Bouk has taken the RSU position issue and contrived a plan that limits handover length from starts RSU to destination RSU. The model ascertains a variable called Inclusion/Administration situation, were is utilized to decide the while time which an endorser station can get administration from the objective RSU. Limiting handover postponement can be gainful in decreasing system late; however it can't give any bound on the general system inertness.

After that, another one author Cheng has been produced a geometry-based meagre inclusion [10] convention for RSU installation is utilized which taken numerous qualities, for example, the geometry of street systems, traffic examples, and asset confinements. For traditional information, the convention can find the most reasonable inclusion regions. Hereditary and eager has both calculations are utilized to determine the inclusion issue. Be that as it may, that plan doesn't address the issue of limiting network late.

the proposed Zhang, Y et al., (2015). an RSU produced by Chi et al. situation methodology dependent on the traffic stream. The plan limits the quantity of RSU belongs putting RSUs at highways convergences and spots with most elevated vehicle recurrence. The thought is to group street crossing points and discover capacity RSU placed by utilizing Markov bunching calculation. Then again, T. J. Wu gave a similar to Chi et al report that demonstrated that the scheme that is not efficient Bariah, L et al., (2015). The authors have proposed the practical methodology of RSU arrangement that plans to amplify the framework limit. The plan gives great throughput however the system delay accomplished by it is not minimum cost.

The author displayed the most extreme inclusion with time edge issues Abdelhamid, S et al., (2015) by utilizing a hereditary calculation for taking care of the issue. A total of four certifiable informational indexes were tried and contrasted and an avaricious methodology. Another proposed Bhoi, et al., (2018) Aslam has been delivered two diverse advancement techniques for the sending of a predetermined number of RSUs along with urban territory. A method is called the Inflatable Development

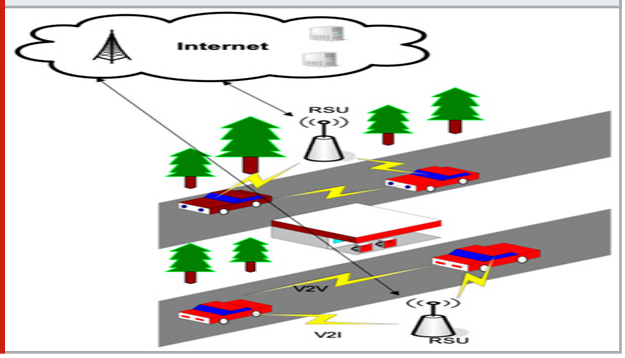
Heuristic technique, the remaining is a diagnostic BIP strategy. The BIP uses branch along with headed methodology for finding an ideal scientific arrangement, while the strategy utilizes swell extension relationships get finding an ideal or close to the ideal arrangement. The two strategies were utilized to tackle the enhancement issue of limiting the normal detailing average.

The new method conspires indicated BEH technique performs superior to BIP strategy as far as computational expense and adaptability. The master represented by Patil et al., (2015) a novel Voronoi arrange based calculation for a powerful portion of RSU's that shapes a Voronoi network as far as the measure of deferral brought about by information bouch has been RSU above So also, the calculation for picturing by Jalooli et al., (2018) the exhibition of message proliferation in VANET, represented Security-Based Separated RSU Position calculation through which message spread postponement can be limited in urban zones.

The calculation for changing by Ruinet al., (2014) for proposed an effect of a multichannel condition called Achievement Likelihood-based Transfer Conflict procedure. The property of stochastic to vehicular conveyance and constant area data of vehicles by by SPRCA were investigated. To investigate the SPRCA performance with stochastic geometry-based approach and determine their properties. No methodology for limiting system delay was proposed by the creators. The nature of administration by Hu, Y., et al. (2017) in VANET the defer limits and start to finish excess were considered as the critical measurements.

3.The Proposed ERSF Approach: The ability and effectiveness for VANET is unequivocally based on the position of RSU with rout. A perfect organized framework RSU position method able to perform upgraded the ability and effectiveness of the network in road side unit, during as well as the minimized installation cost also. The ERSF is handling along with installation positioning of RSU on road side unit surface boundary.

Figure 1: Architecture of Efficient Road Side Framework



Around able to all things considered a RSU put in a fragment. This ERSF strategy to the effective organization of RSU is as per the following:

- Vehicle versatility designs are created under various situations by utilizing VanetMobiSim to imitate practical vehicular condition.
- A Number Liner Conceptual model is planned that limits the general inactivity of the traffic network and decreases RSU sending cost also.
- The ERSF has been improvement model is unravelled to get delay RSU situation.
- The proposed model is then approved by recreations performed on the streamlined model in NS2 test system.
- Results comparison of experimental is done between the proposed ERSF situation and WKUDS.

Table 1

$A_l^k = 1$:	The vehicles are in. fragment l for facilitating by the ERSF in section k. During, suppose $A_l^k = 0$ there no vehicle in fragment l for facilitating by the ERSF in fragment k
St:	There is not an ERSF in fragment l Sl €{0,1}.
Ft:	The mean late up on the connectivity through direct access to an ERSF located in segment l.
F k_1n-:	The mean late belongs with connection since a vehicle inside fragment k to an ERSF inside fragment k through various bouncing in towards the back. Suppose it is in k > l.
F k_1n+ :	The mean late belongs with connection since a vehicle inside fragment k to an ERSF inside fragment k through various bouncing in towards the back. Suppose it is in k < l.
L_{th}:	A integer is representative an positive of capacity of hop count for various level hop segments.
ERSF R:	Consumption minimization cost for one ERSF.
ERSF T:	Total budget for ERSF installation.

The underlying advance of this research paper has been producing a vehicular portability design by utilizing VanetMobiSim simulation. This is a sensible vehicular Harri, J et al., (2014). development follow generator that be utilized for mimicking huge scope transmission traffic networks. In the simulator VanetMobiSim has various situations were produced by picking a road map with 10, 30, 40, 60 and 70 vehicles, separately. The highway comprises of different paths, upstairs road be to vehicular

development for right to left, and though on the lower street traffic is moving from left to right.

The high way like road surface is divided into five fragments; every segmental separation is group equivalent to the communication scope of an ERSF. Each car are roaming with speed between 65 to 125 kilometres by hour. Irregular Outing Originator is utilized for arbitrary age of vehicular models. Subsequent to creating portability design VanetMobiSim gives a yield record that can be utilized as a contribution for simulation NS2. Issue definition is talked about in detail in the following phase.

4. Problem Statement: In this phase, ERSF arrangement issue is planned as a Number Linear Conceptual design. The goal of this issue is to devise a base inertness cost effective ERSF arrangement plot, for example the model decides what number of ERSF s to convey and where to put them so the general system delays be limited at the base conceivable sending cost. Let take that every vehicle able get to the ERSF in 2 distinct manners on a road, for example straight interaction and multi bounce transferring. The accompanying choice factors are characterized to encourage Number Linear Conceptual model detailing:

This problem statement is elaborated as follows:

$$Min\left(\sum_{l=1}^{k} S_l F_l + \sum_{m=1}^{l-1} A_l^k F_l^{k\,m^{-1}} + \sum_{k=l+1}^{k} A_l^k F_l^{k\,m^{+1}}\right)$$

Where:

$$Si \in \{0, 1\}, \in \{1, 2, 3\ldots, Y\} \quad \text{(I)}$$

$$A_i^k = 0 \text{if} | k\text{-}1 | > ERSF_{th} \text{ else } A_i^k = \in \{0, 1\} \quad \text{(II)}$$

$$\sum_{l=0}^{k} A_l^k \leq 1, k \in \{1, 2, 3\ldots, Y\} \quad \text{(III)}$$

$$Si = 1, if \prod_{k}^{\square}(1 - Y_l^k) = 0, \in \{1, 2, 3\ldots, Y\} \quad \text{(IV)}$$

$$\sum_{l=1}^{k} S_l ERSF_k \leq ERSF_T \quad \text{(V)}$$

The main goal is to limit the whole of deferrals coming about because of both direct associations and multi jump associations. The main term $(\sum_{l=1}^{k} S_l F_l)$ represents the general postponements because of direct associations as it were. The Equation II and III of the goal speak to the absolute postponements in reverse multi bounce associations and forward multi jump associations, individually. Prototype I demonstrates that at most one ERSF is able sent in a fragment. Prototype II authorizes the jump check limit (for example ERSFth) refer to vehicle to vehicle correspondence.

That needs to guarantee palatable execution in multi bounce handing off associations. As indicated by Prototype III, every multi jump association can be served by all things considered one ERSF at a given moment. Prototype IV demonstrates that there must be a ERSF sent in section 'k' if any were vehicles in some other fragment will be served by the ERSF in that portion. Nonetheless, that is doesn't confine the situation of ERSF in some other section for which the condition isn't valid. Prototype V determines the absolute spending plan for this ERSF organization.

5. Maximization Data Rate Achievement: The maximization data rate achievement is solved by Shannon Capacity Theorem for connection path, here data rate is (R) and bandwidth is (BW):

$$R=BW \log2 (1+SECR) \quad \text{(VI)}$$

Were, the SGR be Signal Error Clearance Ratio (SECR) for the receiver.

Here the ESRF have two situations to regard: strait connection data transfer and multi hop data transfer. The strait connection data transfer, one vehicle is in connection area circle of a ESRF, and consequently an immediate correspondence connection able be set up between vehicle and ESRF. Because of the Public Area Method with irrelevant background commotion, the sign force at the collector is following by

$$T_e = \frac{G_t}{H^2} \quad \text{(VII)}$$

Where Gt and H2 are data transfer power and the data transfer power receiver, and the H is the strait connection length for both data transmitter and data transfer receiver. Suppose, In the event that there is a vehicle in the obstruction scope of the beneficiary, the quality of clamour signal at the recipient because of the single impedance source can be given as follows:

$$T'_e = \frac{G'_t}{H'^2} \quad \text{(VIII)}$$

Where T'_t and T'_e are the transmitter intensity of obstruction source and the impedance signal force at the collector separately, and H' is the most brief separation between the meddling vehicle and the recipient. In the event that there are V meddling vehicles inside the impedance scope of the collector, the all out obstruction experienced by the recipient is the joined impact of all the impedance data. Most pessimistic scenario, every one of these signs will join usefully at the beneficiary and the complete obstruction able it is shown as follows:

$$T'_{total} = \sum_{k=1}^{V} \cdot \frac{G'_{ti}}{H'^2_i} \quad \text{(IX)}$$

After that the SECR at the destination able to be refer by

$$SECR = \frac{G_r}{G'_{total}}$$

$$SECR = \frac{G_t}{H^2} \chi \sum_{k=1}^{V} \frac{G'^2_t}{H'^{\square}_{ti}} \quad \text{(X)}$$

The maximization data rate achievement able to defined by the combination of equations XI and X:

$$\tau = X\, log_2 \left(1 + \frac{G_t}{H^2}\, x\, \sum_{k=1}^{V} \frac{H_i'^2}{G_{ti}'}\right) \quad \text{(XI)}$$

The fruitful correspondence connects, it was vital that SECR is more prominent than limit esteem (C). Let's see ß(y) will the likelihood closeness capacity of the vehicle area distribution and Ø be the obstruction scopes of the collector, at that point the likelihood of precisely one vehicle in the impedance go is shows by

$$G_{\emptyset} = \int_{\emptyset}^{\cdot\cdot\cdot} ß(y)\,dx \quad \text{(XII)}$$

After that mean integer of vehicles inside the Ø is shown by

$$D_{\emptyset} = DA_{\emptyset} \quad \text{(XIII)}$$

Where, D is the complete integer of vehicles the framework. Let Øy,u will the likelihood of a fruitful transmission [20] between the transmitter y and the beneficiary u, at that point Øy,u can be controlled by the accompanying scientific connection. For a multi jump hand-off, the exchange rate relies on fruitful foundation of the association. Along these lines, s relies on the likelihood of fruitful broadcast. The normal estimation of s can be controlled by joining equation XII.

6. Mean Value of Dissemination Delay: The mean value achievable late is easy to compute for example it can send any integer of SECRs to such an extent that every dynamic vehicle has an immediate connection with a SECR. Right now, joins are immediate and there is no multi bounce association, and along these lines the all out system spread deferral is the base. It is for V associations it very well may be given by the accompanying condition:

$$F_{min} = \sum_{j=1}^{V} T_i G_i \quad \text{(IX)}$$

Be that as it may, this hopeful situation isn't constantly conceivable. The normal engendering deferral of a multi bounce interface relies on the normal integer of transfers and the normal separation between nearby handing off vehicles or motors. Allows first taking the instance of a one hop connect. Right now, proliferation delay relies just on the normal separation between imparting vehicles in nearby portions. Between vehicles dividing on a highway able to be which demonstrated by an exponential dispersion with average proliferation separation between two vehicles equivalent to 1/ ¥. In ERSF have expected the transmission scope of a vehicle (D) will equivalent to the fragment distance. From D is a lot littler than the sign engendering speed (S), subsequently the average separation between vehicles x and y in neighboring fragmentation can be overall assuming to fragmentation length 1/¥ = D. The engendering delay can be communicated via the following mathematical formation.

$$S = \frac{D}{S}\, x_{a,b(\propto)} \quad \text{(X)}$$

Where the x_(a,b) is represented probability for achieved communication.

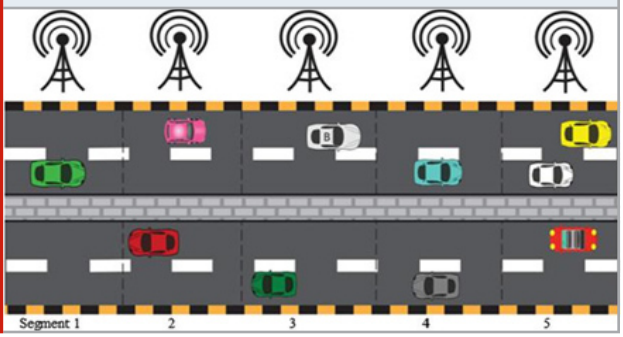
The intrigue is to decide the normal number of bounces in a transfer procedure. The Vehicles sequence moving Wang, X. (2014) a free homogenous state of process along with sequence f vehicle force { along the highway. The assuming number of bounces (A(b)) has given for circulation able to be explore by the accompanying with mathematical equations.

$$A(b) = \sum_{m=0}^{I-J-K} \left(1 - \left\langle \right\rangle\right)^{m} [1 + A(m)] \forall 0 \le I \le J \le K - 1 \; and \; A(D) = 0 \quad \text{(XI)}$$

Where D is the communication range of concern vehicle and S is the length between vehicles and communication unit. Along these lines, the total proliferation delay for multi bounce connection can be found by consolidating mathematical equations X and XI.

7. Simulation Experiments: To validate the results of the proposed ERSF methodology through simulation process, here take the some highway map like one appeared in figure 1, where the highway comprises of different roads and the elements of path are 1500 meters of length by 200 meters of widths. The highway is segregated by five parts. The 200 meters length is segregated by equal meters for each part of ERSF. Different re-enactment situations were made along with vehicle conveyance of 10 to 60 vehicles are sequence moving along the interstate with the speed in the scope of 60–120 km for every hour on a read like highway. The cars are moving in two distinct ways: right to left and left to right. Has been utilized the simulation to create mobility design to represents the exact sharing on the road side surface.

Figure 2: Five ERSF placed on the segmented parts



The vehicle quantity does not consistently for sharing; along with populace congested is not good for equal distributions. The normal transmission late among vehicle and ERSF is taken via NS2 because of being the way that a vehicle able to create both roads and multi bounce associations. The communication scope of every ERSF and vehicle to be 350 meter along with

the obstruction run is 600 meters; it was yield about five parts. Every vehicle able to connect near ERSF of a related for with the closest ERSF for this either towards or backwards ways. The significant re-enactment metrics are appeared in the following table. Because of every one of the reproduction situation, here performed fifty runs with SECR, equal sharing and model plans, and the normal outcomes are accounted for here. For illustrate

Table1. Metrics of simulations

Parameter	Value
Road Side Area	1500 meters length, 200 meters width
Number of Cars	10, 20, 30, 40, 50, 60, 70
Speed	60–120 km/h
Count of SCER	1, 2, 3, 4, 5
Direction	Right to Left and Left to Right
SCER transmission scope	350 m
SCER interference scope	600 m
vehicle transmission scope	350 m
Vehicle interference scope	600 m
Type	Wireless channel
Network interface type	Wireless
Time for simulation	510 sec.

Figure 3: Two ERSF placed with reference of SECR and DSF

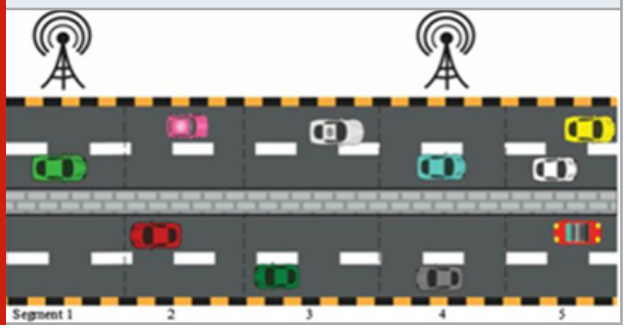
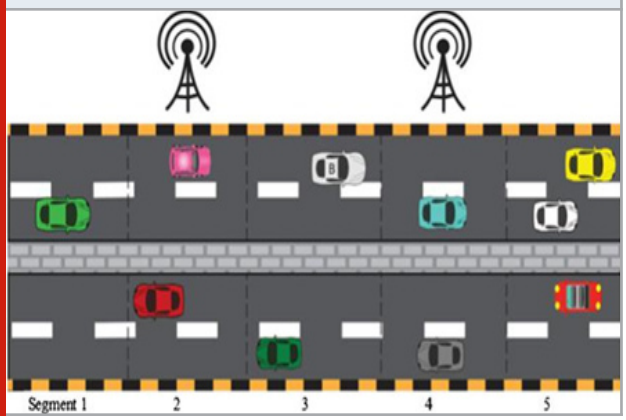


Figure 4: Two ERSF placed with reference of equal sharing.



RESULTS AND DISCUSSION

The proposed ERSF solutions are comparing with CES and UD, along with assess the mean value of network delay and validate the average delay for every installation methodology. Maximize network limitation is main objective of CSE. The budget minimization is controlled belongs to cumulative of RSU. In figures four and five are demonstrate for the results of DMP1 refers scheme with DMP and RSU, in the same manner DMP2 is refers with DMP and used two RSU. The figure six and seven also represented the similar figure four and five for the DMP 10 has been taken 10 vehicles measurement.

Figure 5: Different quantity of communication of delay of Average

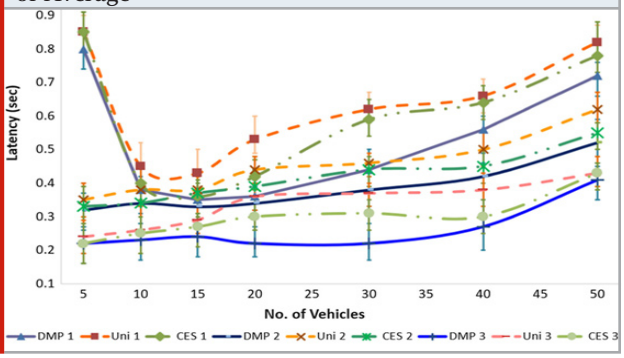


Figure 6: Various quantity communication of average throughput

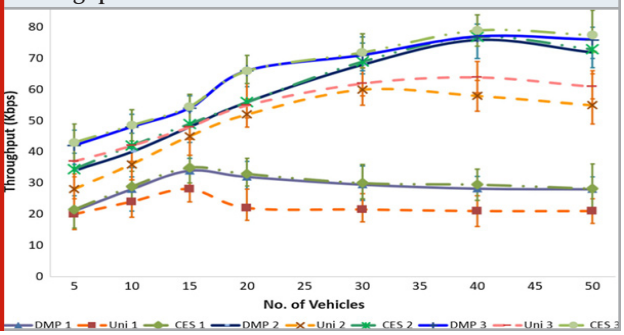


Figure 7: Various quantities ERSF of average delay

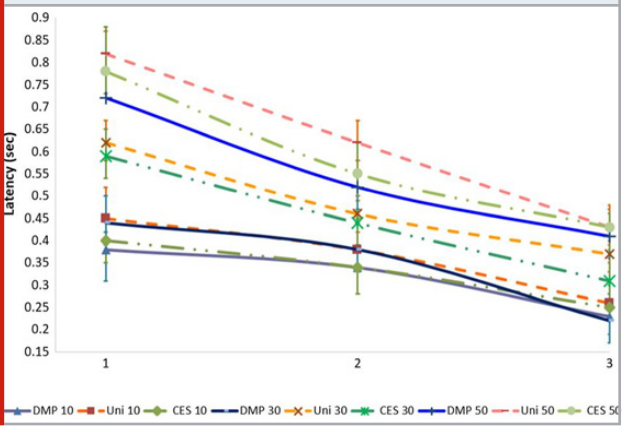
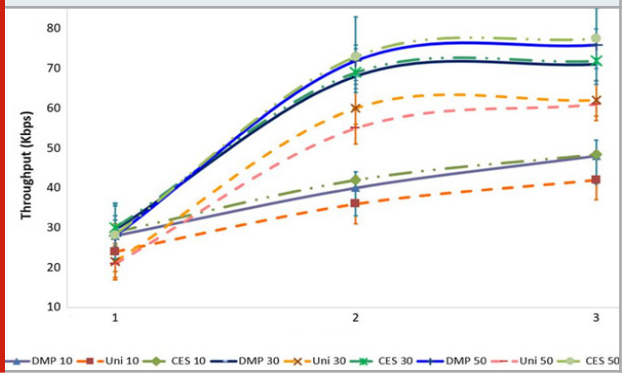


Figure 8: Various quantities ERSF of average throughput



The DMP was fitted in ERSF fragments neighbour surface of hue vehicle quantity. The figure 5 demonstrated about the ERSF has been taken average of delay and population of various traffics of CES. It was clearly shown the ERSF has produced efficient performance in the all kind of aspects using metrics. The throughput average metrics results are represented clearly in figure 6 plot. The proposed ERSF is yielding the 20 % of reduction average and 9% of uniform placement delay and CES also. The delay is the high latency because it should not take the mobility topology was gathering ERSF.

The ERSF has fragments where vehicles remain the maximum, during DMP will in general send proposed framework in portions with most elevated vehicle deluge. In this way, DMP gives connection chances to maximum vehicles per segment time along these lines it can accomplish the most minimal deferral for all aspects. The plot of the picture demonstrates the average of latency for methods of the number for the proposed method segment for situations of start with 5 and end with 70 for each step have increased 5 vehicles it has been represented by Figure 7.

The average latency is high for 1 ERSF along with 5 vehicles or car, for that 1 ERSF for the strait to connection and not many vehicles to set up multi bounce connections, every vehicle needs to hold up a significant measure of at the time it can set up an association and send its information packets are has been sent. The circumstance improves by expanding the quantity of proposed and the quantity of cars, these metrics increment the chance to set up either immediate or multi jump associations.

The relating average of the throughput is demonstrated by figure 8. True to form, the base throughput is acquired for the instance of 1 proposed and 5 car. The presentation improves extensively with an expanding number of ERSF. It is clear, DMP beats Uniform Circulation in everyone has 33% of improvement. In any case, the throughput gave by the existing is on normal 2% all the more for throughput gave by the DMP system. The average from Uniform dispersion doesn't take vehicle versatility designs while conveying proposed. In this manner, ERSF permits vehicles to communicate high information because of a more prominent association lifetime along these lines, it can give efficient throughput.

CONCLUSION

In this research paper has been represented about case of ERSF exploitation methodology to the VANET taken for the highway or road side, which is every vehicle able to get access with ERSF in various paths: strait connection and multi jumping. The two RSU equal sharing models are has been compared namely Uniform Distribution (UD) and another one is Delay Minimization Problem (DMP). The NS2 experimental results are demonstrated efficient performance comparably existing systems. The DMP scheme recommends to the efficient ERSF sending system by carry in shows the complete minimized budget have an extent that the average delay of the system is limited. These able to exceptionally helpful in the opportune delivery of aware if there should be an occurrence of an episode, and furthermore gives upgrades in the total throughput of the system.

REFERENCES

Ranjan Senapati B., Mohan Khilar P. (2020) Optimization of Performance Parameter for Vehicular Ad-hoc NETwork (VANET) Using Swarm Intelligence. In: Rout M., Rout J., Das H. (eds) Nature Inspired Computing for Data Science. Studies in Computational Intelligence, vol 871.

Babu Ram & Neelendra Badal (2019) Latency estimation based routing (LEBR) protocol in vehicular adhoc networks (VANETs), Journal of Discrete Mathematical Sciences and Cryptography, 22:8, 1517-1531, DOI: 10.1080/09720529.2019.1700923.

Malhi, A.K., Batra, S. & Pannu, H.S. An Efficient Privacy Preserving Authentication Scheme for Vehicular Communications. Wireless Pers Commun 106, 487–503 (2019). https://doi.org/10.1007/s11277-019-06175-7.

Lin, Y.-W., Chen, Y.-S., & Lee, S.-L. (2017). Routing protocols in vehicular ad hoc networks: A survey and future perspectives. Journal of Information Science and Engineering, vol.26.no.3,pp.913–932.

A. Arora, A. Mehra and K. K. Mishra, "Vehicle to Vehicle (V2V) VANET based analysis on waiting time and performance in LTE network," 2019 3rd International Conference on Trends in Electronics and Informatics (ICOEI), Tirunelveli, India, pp. 482-489.

S. S. Shah, M. Ali, A. W. Malik, M. A. Khan and S. D. Ravana, "vFog: A Vehicle-Assisted Computing Framework for Delay-Sensitive Applications in Smart Cities," in IEEE Access, vol. 7, pp. 34900-34909, 2019.

Maratha, B. P., Sheltami, T. R., & Salah, K. (2017). Performance study of MANET routing protocols in VANET. Arabian Journal of Science and Engineering, vol.42,no.8 pp.3115–3126.

Zhang, Z., Boukerche, A., & Pazzi, R. (2011). A novel multi-hop clustering scheme for vehicular ad-hoc networks. In Proceedings of the 9th ACM international symposium on mobility management and wireless access pp. 19–26.

Ahmed, S. H., Hussain, S., & Kim, D. (2015). Target RSU selection with low scanning latency in WiMAX-enabled vehic-ular networks. Mobile Networks and Applications, vol.20, no.2, pp.239–250.

Liu, H., Yang, L., & Zhang, Y. (2015). Improved AODV routing protocol based on restricted broadcasting by communication zones in large-scale VANET. Arabian Journal of Science and Engineering, vol.40,no.3, pp.857–872.

Shaik, S., Venkata Ratnam, D., & Bhandari, B. N. (2018). An efficient cross layer routing protocol for safety message dissemination in VANETs with reduced routing cost and delay using IEEE 802.11P. Wireless Personal Communications, vol.100,no.4, pp.1765–1774.

Bariah, L., Shehada, D., Salahat, E., Yeun, C.Y.(2015), Recent advances in VANET security: a survey. In: 2015 IEEE 82nd Vehicular Technology Conference (VTC2015-Fall), pp. 1–7.

Abdelhamid, S., H. Hassanein, and G. Takahara. 2015. Vehicle as a resource (vaar). IEEE Network no.29, pp.12–17.

Bhoi, S.K., D. Puthal, P.M. Khilar, J.J. Rodrigues, S.K. Panda, and L.T. Yang. 2018. Adaptive routing protocol for urban vehicular networks to support sellers and buyers on wheels. Computer Networks no.142, pp.168–178.

Younes, M.B., and A. Boukerche. 2013. Efficient traffic congestion detection protocol for next generation vanets. In 2013 IEEE international conference on communications (ICC), pp. 3764–3768. IEEE.

Nayak, J., B. Naik, A. Jena, R.K. Barik, and H. Das. 2018. Nature inspired optimizations in cloud computing: Applications and challenges. In Cloud computing for optimization: Foundations, applications, and challenges, pp. 1–26. Springer.

Kaiwartya, O., and S. Kumar. 2014. Geocasting in vehicular adhoc networks using particle swarm optimization. In Proceedings of the international conference on information systems and design of communication, pp. 62–66. ACM.

Hu, Y., Li, H., Chang, Z. and Han, Z., 2017. End-to-end backlog and delay bound analysis for multi-hop vehicular ad hoc networks. IEEE Transactions on Wireless Communications, no.16, vol.10, pp.6808-6821.

Härri, J., Filali, F., Bonnet, C., & Fiore, M. (2006). VanetMobiSim: generating realistic mobility patterns for VANETs. In Proceedings of the 3rd international workshop on Vehicular ad hoc networks, pp. 96-97.

Wang, X. (2014). Modeling the process of information relay through inter-vehicle communication. Transportation Research Part B: Methodological, no.41, pp.684–700.

SLM Technique based on Firefly Algorithm for Reduction of PAPR in OFDM Systems

Reddi Sridevi, Assistant Professor, Department of ECE, Dr.L.B College of Engineering, AP, India.

E-mail: himasri_sss@yahoo.com

Dr.T. Madhavi, Professor, Department of ECE, GITAM Deemed to be University, AP, India.

Abstract--- In communications OFDM method has been broadly received in numerous remote correspondence frameworks because of its high capacity rate of transmission of information and heartiness to the multipath blurring channel. The Peak to average power ratio (PAPR) problem is been addressed from many years and to decrease PAPR in OFDM systems had been primary problem in the transmitter end. One of the promising PAPR decrease strategies is the Selective Mapping strategy (SLM) with some enhancement systems which can accomplish better PAPR execution without flag bending. The current streamlining strategies, for example, Genetic Algorithm system, swarm optimization technique etc have been proposed in the writing to enhance PAPR. In this paper, a new effective PAPR reduction technique is introduced i.e SLM based on Firefly Algorithm (FA) is proposed and compared with the existing algorithms. It is observed that the proposed SLM with FA technique achieves better performance over the existing techniques.

Keywords--- OFDM, Selective Mapping, Genetic Algorithm, Firefly Algorithm.

I. Introduction

The entire OFDM systems are termed to be wireless communications. As it represents the transfer of information over a distance without the use of electrical conductors or "wires". The distance may be more or less but the need of wireless communication in present scenario is more and more increasing. The problems in the transmitting and receiving end are been considered and many researchers are still evaluating new techniques to reduce the concern noticed problem in OFDM system. Many problem like LOS, ISI, PAPR etc are been araising and new techniques are been implemented to reduce.

It is generally expected that future portable correspondence frameworks will apply multicarrier OFDM transmission due to the way that it takes into account high data transfer capacity productivity. Moreover, multicarrier transmission guarantees high adaptability in transmission asset task, which is extremely alluring for future rich collection of expected administrations including different information transmission rates and QoS prerequisites.

Nonetheless, in spite of numerous points of interest of OFDM, there are a few downsides of it also. Among them, a high estimation of Peak-to-Average Power Ratio (PAPR) is the one, which draws consideration of numerous researchers [1]. For this situation some momentary power yield may increment significantly what's more, turned out to be far higher than the mean energy of framework. To transmit signals with such high PAPR, it requires control speakers with high power scope. These sorts of speakers are extremely costly and have low proficiency cost [2]. On the off chance that the pinnacle control is too high, it could be out of the extent of the direct power intensifier. These offers ascend to nonlinear bending which changes the superposition of the flag range bringing about execution debasement. Assuming no measure is taken to lessen the high PAPR, MIMO-OFDM framework could confront genuine confinement for viable applications [3-4]. PAPR can be portrayed by its corresponding aggregate circulation work (CCDF) [5].

This paper organised as follows: Section 2 provides information station OFDM communication system and PAPR. Section 3, gives an overview of SLM and its level of Complexity. Section 4, describes the new technique i.e Firefly algorithm combined with SLM, followed by results in section 5 and conclusion.

II. OFDM System and PAPR

The basic transmitting and receiving model of OFDM is presented in fig 1. This model consists of a transmitting path, a channel which can be rician fading or rayleigh fading and a receiving path.

Received: 04 June 2019/Accepted: 18 June 2019

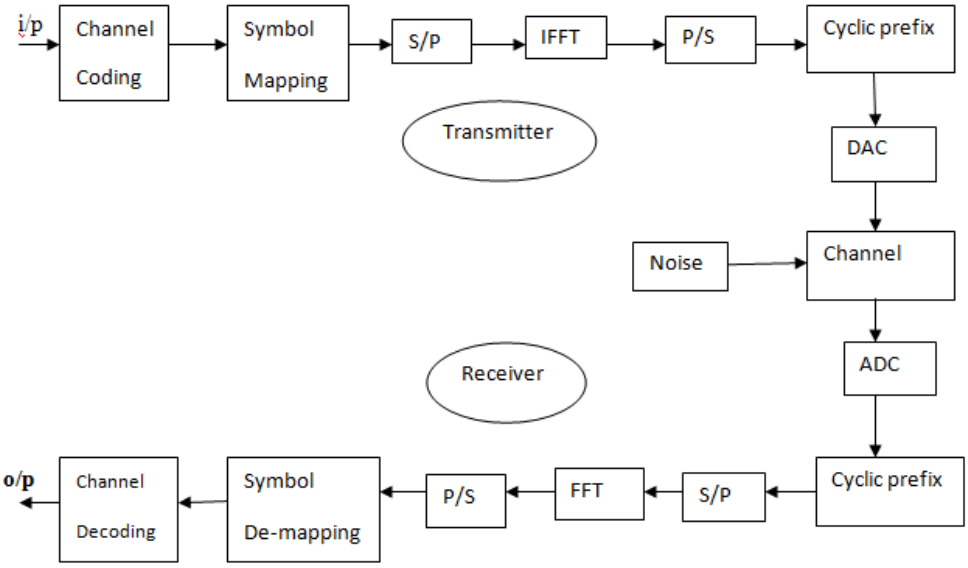


Fig. 1: Model of OFDM Communication System

The model of OFDM communication system block with transmitter and receiver end is shown in Figure. 1 and works as follows: the input serial bits are given as $i_o, i_1, i_2 \ldots i_n$ and given stream of bits are encoded such that i_n = 0 or 1; for n = 0,1,2,… .. A serial to parallel converter is used to perform N numbers of parallel streams which are represented as the number of subcarriers that are used in communication system.

IFFT operation is performed to convert number of subcarriers into multiple power of two. Analog to digital converter is placed, where the analog form is converted to digital form. The number of bits available for each subcarrier is termed as L = $\log_2 M$ where M is the constellation size used by the mapper and depends on the modulation scheme being used.

The IFFT sequence is given by [6]:

$$s(q) = \frac{1}{\sqrt{N}} \sum_{k=0}^{N-1} d_k e^{j2\pi kq/N}; k, q = 0,1 \ldots\ldots N-1 \quad (1)$$

Where $s(q)$ are samples for the resultant baseband signal. The output of the IFFT block is the result of summation of various complex sinusoids with varying amplitudes and phases. At some sample points of these sinusoidal signals, constructive summations may occur, resulting in high peaks in the signal.

When the signal transmitted with high number of peaks with the help of power amplifier which is termed to be non-linear, the distortion occurs within the transmitted signal at the output of the amplifier is termed to be inter symbol interference (ISI) and out-of-band radiation[7]. These peaks are obtained at the output of IFFT block. The power factor measured for these peaks is Peak to Average Power Ratio (PAPR) which is mathematically expressed as:

$$PAPR = \frac{\max\{P(q)\}}{P_{avg}} \quad (2)$$

Here, $P(q)$ represents the instantaneous power and P_{avg} represents the average power of the OFDM signal.

III. Selected Mapping (SLM) Method For PAPR Reduction

In SLM technique as shown in Figure 2, from a single OFDM system, the input sequence which is given as 'D' having a length of N, number of sequences generated represent the same information using some rotation factors and the sequence with lowest PAPR is transmitted.

If the number of generated new sequences is U, called the SLM length, then all these sequences are the result of multiplying the incoming original OFDM sequence D by U different rotation factors. These factors are given in vector form as [8],

$$B^{(i)} = b_0^{(i)}, b_1^{(i)}, \ldots\ldots\ldots\ldots b_{N-1}^{(i)} \quad (3)$$

Received: 04 June 2019/Accepted: 18 June 2019

where i = 1 to U and represents the indices of these factors and B represents the represent the rotation factor in vector form. After multiplying these factors by the original OFDM sequence D, we get:

$$X^{(i)} = d_0 b_0^{(i)}, d_1\ b_1^{(i)}, \ldots\ldots\ldots\ldots d_{N-1} b_{N-1}^{(i)} \quad (4)$$

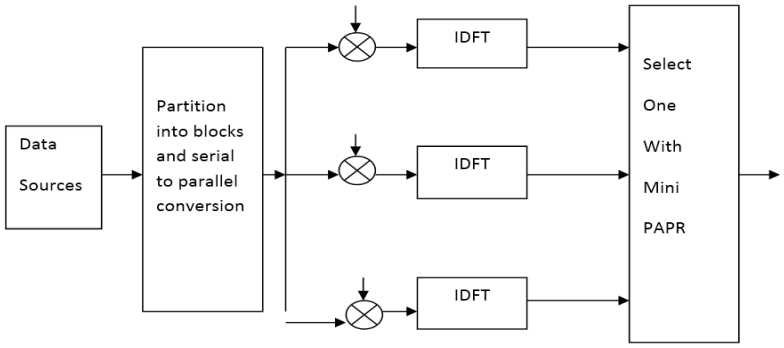


Figure 2: SLM Block at the End of transmitter [1]

In this phases are considered and they rotate accordingly based on the inputs generated. They multiply a complex number with the rotating factor and find the one more number. The selection process will be continued till mini PAPR is achieved. The calculations are performed at each phase [10]. Hence,

$$b_n^i = e^{-j\theta_n^i}\ where\ \theta_n^{(i)} \epsilon [0, 2\pi] \quad (5)$$

where θ is the angle of rotation. The rotation vectors are used as side information which are transmitted for signal recovery. The efficiency of SLM approach depends on the amount of scrambling done by these rotation factors on the original OFDM sequence and the length of SLM U. Based on the number of iterations or sequences the performance of SLM can be evaluated, by increasing the sequence the system complexity may increase but the major problem which is considered in transmitting end i.e PAPR can be reduce to some extent. The complexity of implementing SLM is termed to be moderate. Some works have been preferred to reduce the level of complexity in SLM. The complexity of SLM can be termed as

$$Complexity = UNLog_2 N \quad (6)$$

IV. FA- SLM OFDM

Firefly Algorithm (FA) was first developed by Xin-She Yang in late 2007 and 2008 at Cambridge University [12, 13], which was based on the flashing patterns and behaviour of fireflies. Evolution of firefly algorithm in recent years became more significant and many research works are been performed based on Firefly Algorithm. The results obtained using this optimization techniques termed to be accurate and several papers were published.

Fireflies are unisex with the goal that each individual firefly will be pulled into different fireflies paying little mind to their opposite sex. The attractiveness and brightness are directly proportional to each other, and they both lessening as their separation increments. Along these lines for any two blazing fireflies, the less splendid one will attrack the more brilliant one. On the off chance that there is no more brilliant one than a specific firefly, it will move randomly. The brightness of a firefly is controlled by the scene of the goal work[13].

As a firefly's attractiveness is proportional to the light intensity seen by adjacent fireflies, can now define the variation of attractiveness β with the distance r by

$$\boldsymbol{\beta = \beta_0 e^{-\gamma r^2}} \quad (7)$$

Where β_0 is attractiveness at r=0

The firefly i is attracted to another more brighter firefly j and move towards j and the sane is determined by

$$\boldsymbol{x_i^{t+1} = x_i^t + \beta_o e^{-\gamma r_{ij}^2}\left(x_j^t - x_i^t\right) + \alpha_t \epsilon_i^t} \quad (8)$$

Where the second term $\boldsymbol{\beta_o e^{-\gamma r_{ij}^2}\left(x_j^t - x_i^t\right)}$ is concern based on the attraction. The third term i.e $\boldsymbol{\alpha_t \epsilon_i^t}$ is randomization with $\boldsymbol{\alpha_t}$ being the randomization parameter, and $\boldsymbol{\epsilon_i^t}$ is a vector of random numbers drawn from a Gaussian distribution or uniform distribution at time t.

Received: 04 June 2019/Accepted: 18 June 2019

If $\boldsymbol{\beta_0}$ = 0, it becomes a regular pattern for determining the optimised value. On the other hand, if γ = 0, FA in generally termed to be particle swarm optimisation [12].

The complexity of firefly algorithm has inner loop and outer loop and the complexity of FA algorithm is given as *O(nt* log*(n))*. This is obtained based on inner loop population size n and number of iteration t [14]. If the value of n is more the ranking of fireflies which are brighter will be obtained more easily.

The progression of firefly close to the ideal arrangement ought to be set little. Also, the progression of firefly far from the ideal arrangement ought to be set substantial. Fireflies between the over two are utilized to adjust the worldwide inquiry and neighbourhood look. Accordingly, the progression of firefly ought to likewise be worried about its authentic data and current circumstance. Based on the comments mentioned above and many experiments, the step of each firefly is calculated by (9) and (10), respectively

$$h_i(t) = \frac{1}{\sqrt{\left(f_{pi}(t-1) - f_{pi}(t-2)\right)^2 + 1}} \tag{9}$$

$$\propto_i (t+1) = 1 - \frac{1}{\sqrt{\left(f_{best}(t) - f_i(t)\right)^2 + h_i(t)^2 + 1}} \tag{10}$$

Algorithm

The firefly algorithm is implemented in this paper and the process is stated below:

Step 1. Initialization

Step 2. The population of fireflies are gives as, $\{x_1, x_2, \ldots\ldots, x_n\}$.

Step 3. Calculate brightness value using cost function for assigned firefly

Step 4. Fireflies intensity are given as $\{I_1, I_2, \ldots\ldots, I_n\}$.

Step 5. Update the step of each firefly.

Step 6. Ranking of fireflies and finding current best

Step 7. Moving of each firefly *i* towards other brighter fireflies.

Step 8. Update the solution set.

Step 9. Stop when result obtained; otherwise go to Step 2.

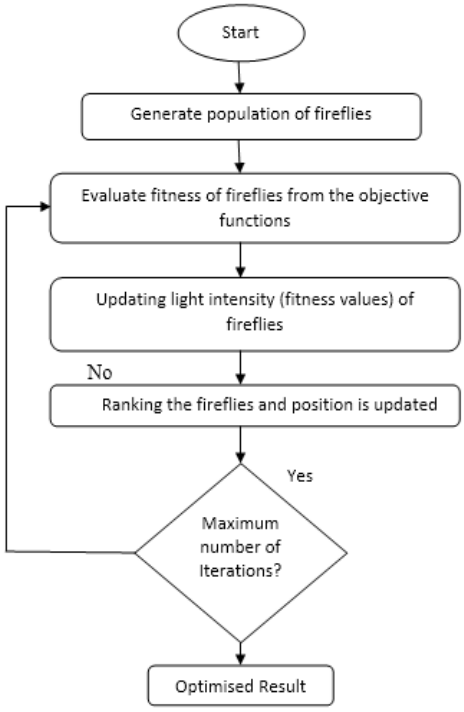


Fig. 3: Flow of the Proposed Technique

Received: 04 June 2019/Accepted: 18 June 2019

V. Results

In-order to perform the analysis of PAPR reduction, over 2000 OFDM symbols were chosen randomly. The comparison of various techniques like SLM, GA-SLM and FA-SLM are shown in below results. The comparisons results are shown in terms of CCDF.

In this project, cumulative distribution function parameter is use to mark the report of PAPR. Typically, the Complementary CDF (CCDF) is utilized, which encourages us to quantify the PAPR of a specific information square and the likelihood of surpassing the given edge. The CCDF-PAPR of the information is wanted for this situation to think about yields of different decrease procedures.

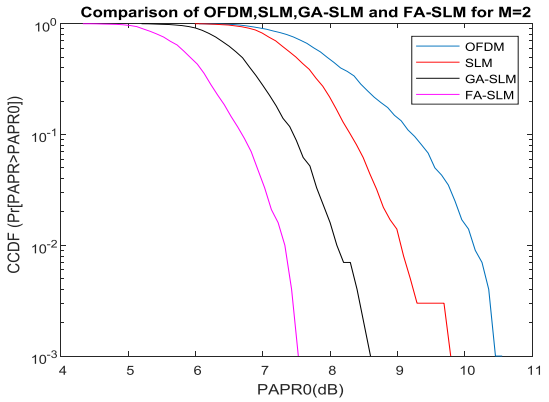


Fig. 4: CCDF vs. PAPR for *M*=2

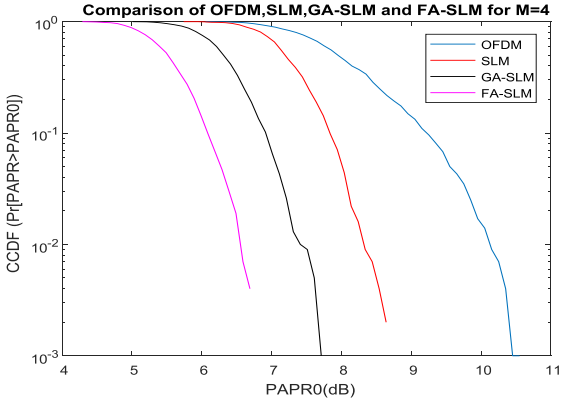


Fig. 5: CCDF vs. PAPR for M=4

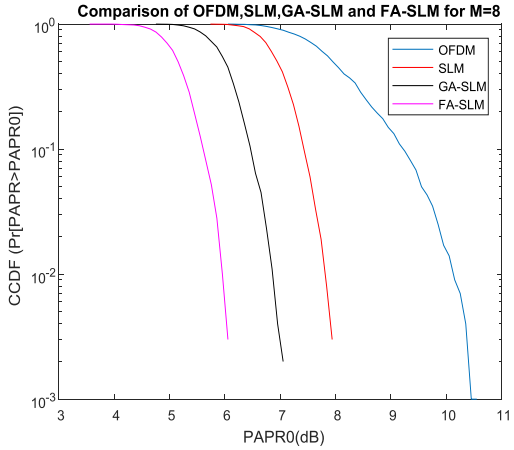


Fig. 6: CCDF vs. PAPR for M=8

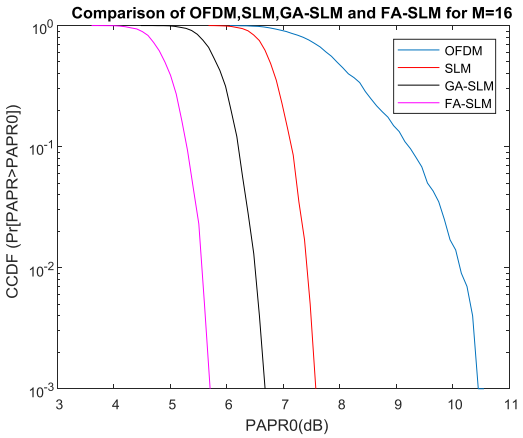


Fig. 7: CCDF vs. PAPR for *M*=16

The PAPR reduction for original OFDM signal is not significantly improved by increasing the value of *M*. For greater values of M the PAPR remains constant in original OFDM, hence it is observed that the computational complexity increases but there is no much change in PAPR.

Hence the PAPR reductions techniques are proposed. The experimental results shown in Fig 8 prove that as the *M* value increases the FA-SLM technique obtained less PAPR compared to conventional SLM and GA based SLM. The difference of PAPR value achieved using proposed system is 1dB compared to other techniques.

Table 1: Comparison of Results using Different Techniques

Method PAPR	M=2	M=4	M=8	M=16	M=32
OFDM	10.5dB	10.4dB	10.3dB	10.3dB	10.3dB
SLM	9.8dB	8.9dB	8dB	7.7dB	7.3dB
GA-SLM	8.8dB	7.9dB	7.1dB	6.8dB	6.3dB
FA-SLM	7.6dB	6.9dB	6.1dB	5.8dB	5.4dB

ISSN 1943-023X

Received: 04 June 2019/Accepted: 18 June 2019

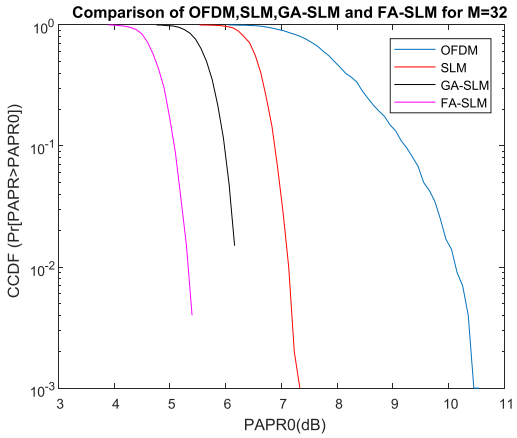


Fig. 8: CCDF vs. PAPR for M=32

VI. Conclusion

This paper effectively presented a new technique for solving core problem of OFDM by reducing the PAPR. The technique proposed is Firefly optimization which is applied along with selective mapping technique in which rotation of phase factor for searching was compared with base OFDM, conventional SLM-OFDM and also compared with genetic algorithm based SLM. The experimental results are shown using matlab tool. According to the result shown the proposed system performance is good and achieves low computational complexity. The PAPR obtained using FA-SLM is 7.6db and is further reduce by increasing the number of phase sequences.

References

[1] Tarik Hadj Ali and A. Hamza, "A new SLM technique based on Genetic Algorithms for PAPR reduction in OFDM systems", IEEE DOI 10.1109/CICN.2016.,Volume 10, 2016

[2] Krzysztof Wesołowski, “On the PAPR Minimization Using Selected Mapping Algorithm in Pilot-Assisted OFDM Systems” Pozna´n University of Technology Chair of Wireless Communications Pozna´n, Poland.

[3] Y. Wu and W. Y. Zou, “Orthogonal frequency division multiplexing: A multi-carrier modulation scheme,” IEEE Trans. Consumer Electronics, vol. 41, no. 3, pp. 392–399, Aug. 1995.

[4] University of Alberta, “Home page - High capacity digital communications laboratory,”2007.Available: http://www.ece.ualberta. ca/~ HCDC/mimohistory.html.

[5] Shinsuke Hara, Ramjee, “Principle and history of MCM/OFDM,” in Multicarrier techniques for 4G mobile communication, Artech House.

[6] Suverna Sengar, Partha Pratim Bhattacharya,” Performance Improvement In OFDM system By PAPR Reduction,” Signal & Image Processing : An International Journal (SIPIJ) Vol.3, No.2, April 2012 Department of Electronics and Communication Engineering, Faculty of Engineering and Technology, Mody Institute of Technology & Science (Deemed University), Lakshmangarh, Dist – Sikar, Rajasthan, Pin – 332311, INDIA.

[7] Jayalath, A.D.S., Tellambura C., “SLM and PTS peak-power reduction of OFDM signals without side information”, IEEE Transactions on Wireless Communications, vol. 4, no. 5, pp. 2006 – 2013, 2005.

[8] C. Tellambura, “Use of m-sequences for OFDM peak-to-average power ratio reduction", IEE Elec. Lett, vol.33, no.15, pp. 1300-1301, 1997.

[9] Chin-Liang Wang, Sheng-Ju Ku., “Novel conversion matrices for simplifying the IFFT computation of an SLM-based PAPR reduction scheme for OFDM systems”, IEEE Transaction on Communication, vol. 57, no. 7, pp. 1903 – 1907, 2009.

[10] Chin-Liang Wang, Yuan Ouyang, “Low-complexity selected mapping schemes for peak to- average power ratio reduction in OFDM systems”, IEEE Trans. on Signal Processing, vol. 53, no. 12, pp. 4652 – 4660, 2005.

[11] Y. Wang, W. Chen, and C. Tellambura, “Genetic algorithm based nearly optimal peak reduction tone set selection for adaptive amplitude clipping PAPR reduction,” IEEE Trans. on Broadcast., vol. 58, no. 3, pp. 462- 471, Sept. 2012.

[12] Yang, X.S.: Nature-Inspired Metaheuristic Algorithms. Luniver Press, UK (2008)

Received: 04 June 2019/Accepted: 18 June 2019

[13] Yang, X.S.: Firefly algorithms for multimodal optimization. In: Stochastic Algorithms: Foundations and Applications, SAGA 2009. Lecture Notes in Computer Sciences, vol. 5792, pp. 169–178 (2009)
[14] Fister, I., Fister Jr., I., Yang, X.S., Brest, J.: A comprehensive review of firefly algorithms. Swarm Evol. Comput. 6 (in press) (2013). http://dx.doi.org/10.1016/j.swevo.2013.06.001
[15] Richard van Nee, Ramjee Prasad. OFDM for wireless multimedia Communications. Artech house, 2000.

Received: 04 June 2019/Accepted: 18 June 2019

International Journal of Innovative Technology and Exploring Engineering (IJITEE)
ISSN: 2278-3075, Volume-X, Issue-X, July 2019

PERFORMANCE IMPROVEMENT OF OFDM SYSTEMS BY REDUCING PAPR USING SLM-GRASSHOPPER OPTIMIZATION

[1]Reddi Sridevi, [2]Dr.T.Madhavi, [3]Sreenivasulu Ummadisetty
[1] Assistant Professor, Department of ECE, Dr.L.B College of Engineering, Visakhapatnam, India. himasri_sss@yahoo.com
[2]Professor, Dept. of EECE, GIT, GITAM (Deemed to Be University), Visakhapatnam, India. madhavi.tatineni@gitam.edu
[3]Assistant Professor, Dept. of EECE, GIT, GITAM (Deemed to Be University), Visakhapatnam, India. sreenuaswarth@gmail.com

Abstract: ***Orthogonal Frequency Division Multiplexing (OFDM) is an emerging technology which is been most commonly used for transmission of data in wireless based systems. The OFDM technique is capable of achieving more speed i.e it has higher data rate transmission which is reliable and efficient. Peak power is the major drawback while transmitting the signal which is termed as PAPR. The signals achieves high peak value while transmitting due to the presence of large subcarriers which are independent in nature. The amplitude of the signal need to be reduced. Many PAPR reductions schemes have been presented in past and the reduction is done to some extents. In this paper , a new optimisation technique i.e grasshopper optimization (GOA) is proposed. The optimization technique is combined with one of the efficient PAPR reduction technique i.e selective mapping technique. The combination of SLM-Grasshopper help in reducing the PAPR as low as possible and is also compared with other techniques like SLM-GA, SLM-FA and SLM-GWO. The experimental results are performed using matlab.***

Keywords: ODFM, PAPR, SLM, Grasshopper Algorithm

I. INTRODUCTION

Orthogonal frequency division multiplexing (OFDM) is a system which have multiple subcarriers and modulation method which looks to be an captivating candidate for fourth generation (4G) wi-fi verbal exchange systems. The system have good level of spectral form which is efficient in nature, immune to the multipath delay, the interference present while transmitting the data is low. The system is immune to frequency selective fading and the efficiency level fo power is efficient. As OFDM have many merits it is chosen as excessive records charge communication systems such as Digital Video Broadcasting (DVB) and based cellular worldwide makes use for microwave get entry to the wi-max systems. However OFDM device has a major level of problem that is increase in PAPR.

In OFDM device output is superposition of a couple of sub-carriers. Contingent upon some of the spot energy output may amplify appreciably and emerge as a ways higher than the power that is utilised of the system. High PAPR signals need to be transmitted in some cases which should have a minimum requirement of electricity amplifier with high level scope of the power[1]. The degradation of performance of OFDM is due to the quick distortions in the non linear form which adjustments the spectrum signals postions[2]. If no measure is taken to decrease the excessive PAPR, MIMO-OFDM systems ought to face serious restriction for practical functions [3][4].

Complementary cumulative distribution characteristic (CCDF) is used to describe PAPR. The researchers have been developed and proposed probabilistic method positive schemes. These include clipping, coding and sign scrambling techniques. Partial transmit sequence (PTS) and Selected Mapping (SLM) are the two popular schemes under the heading of signal scrambling techniques. Some of

Retrieval Number: paper_id//2019©BEIESP

DOI: 10.35940/ijitee.xxxxx.xxxxxx

Published By:
Blue Eyes Intelligence Engineering
& Sciences Publication

the methods that are used to reduce the PAPR are determined and summarized in [5], it is nevertheless indeed wanted to provide some of the stratagies that are used to reduce the PAPR has a comprehensive evaluation, such as electricity saving, and to evaluate some typical methods of PAPR discount via theoretical evaluation and simulation effects thoroughly.

Selective mapping method is one of the promising PAPR reduction technique without any distortions in the signals. A new approach of PAPR reduction method is applying genetic optimization to the SLM . GA is applied to SLM-OFDM system, by which the random populations are considered whose fitness values are evaluated for looking the most appropriate section rotation elements and decreasing computational complexity[6].

A new technique for solving core problem of OFDM by reducing the PAPR. The technique proposed is Firefly optimization which is applied along with selective mapping technique in which rotation of phase factor for search was compared with initial OFDM, conventional SLM-OFDM and also compared with genetic algorithm based SLM[7]

Further, Grey wolf optimization technique is combined with SLM to reduce the PAPR, the grey wolf optimization the PAPR reduce to some extent. More studies need to be emerged to reduce the PAPR. There is much better reduction in PAPR value using grey wolf by which the problem of transmitting signal is minimised[8].

In this paper, the performance and the traits of ODFM system is observed. A new PAPR reduction technique is implemented. The behaviour grasshopper is studied. Finally SLM is combined with grasshopper optimization algorithm to achieve good rate of decrease in PAPR.

II. OFDM AND PAPR

In OFDM system the signal which is transferred from source to destination is made of subcarriers which are modulated with the aid of constellations mapping. The modulation techniques like QAM and PSK are used for performing the function of mapping and are process is been completed. For an OFDM device with N sub-carriers, the high-speed binary serial enter circulate is denoted as $\{q_i\}$. After conversion of signal from serial to parallel (S/P) and process of mapping, a new parallel sign sequence is obtained and given as,

$\{a_0, a_1, a_2, \dots\dots, a_i, \dots\dots\dots, a_{N-1}\}$ is obtained, a_i is termed as sign value of discrete signal[6]. Each element of parallel signal sequence is supplied to N orthogonal sub-carriers is given as,

$\{e^{j2\pi f_0 t}, e^{j2\pi f_1 t}, \dots\dots\dots, e^{j2\pi f_{N-1} t}\}$ for modulation, respectively. The signals which are modulated are added together to form an OFDM symbol. The system structure of OFDM is been simplified with the use of discrete Fourier transform. The transmitted OFDM signals can be written as

$$x(t) = \frac{1}{\sqrt{N}} \sum_{k=0}^{N-1} X_k \, e^{j2\pi f_k t} \;, 0 \le t \le NT \qquad (1)$$

Probability Density Function (PDF) for a signals with large value of N is given by [5].

$$P_r\{x(t)\} = \frac{1}{\sqrt{2\pi\sigma}} \; e^{-\frac{[x(t)]^2}{2\sigma^2}} \qquad (2)$$

where σ is the variance of x(t)

PAPR

The signal is considered as x(t), for a given x(t) the PAPR is calculated and is defined as maximum power obtained during the transmitting of signal to its average range of power[3].

$$PAPR[x(t)] = \frac{P_{PEAK}}{P_{AVERAGE}} = 10\, log_{10} \frac{\max\,[|X(n)|^2]}{E[|X(n)|^2]} \qquad (3)$$

where P_{PEAK} - peak power at output,

$P_{AVERAGE}$ - average output power, the expected value can be termed as E[·], By performing the IFFT operation on the signals which are modulated to obtain the signal and which is a need that to be transmitted signals in OFDM with symbols X_k is given as x_n [11]. x_n is expressed as:

$$x_n = \frac{1}{\sqrt{N}} \sum_{K=0}^{N-1} X_k \, W_N^{nk} \qquad (4)$$

when compared with normal single carrier systems, the output achieved from an OFDM system has high fluctuations in a regular manner. Due to which the system requires an power amplifier, converters etc. If the condition is not satisfied an undesirable inference will be encountered and the signal moves into non linear region at the transmitter side, which is called as distortion due to inter modulation which have high radiations. In OFDM system reducing of PAPR is an incredible process.

III. SELECTED MAPPING (SLM)

The approach of SLM is shown in Figure 1, from a single OFDM system, the sequence is presented as D and the length of the sequence is denoted as N. Based

on the number of sequences generated , the element rotation will be defined. Here , the consideration of sequence and rotation is equal. So the signal which is transmitted has lowest PAPR. The generation of new sequence is performed and is termed to be M, which is called as length of SLM. The sequences which are obtained are the result of multiplying the incoming authentic sequence of OFDM 'A' with the aid of M exclusive rotation factors. The vector shapes are provided for the elements [9],

$$B^{(i)} = b_0^{(i)}, b_1^{(i)}, \dots\dots\dots\dots b_{N-1}^{(i)} \quad (5)$$

where i represents the indices of these factors with i=1 to M and representation B is known as rotation factor in the form of vector. The original OFDM sequence D is multiplied with rotation factor and we get:

$$X^{(i)} = a_0 b_0^{(i)}, a_1\, b_1^{(i)}, \dots\dots\dots\dots a_{N-1} b_{N-1}^{(i)} \quad (6)$$

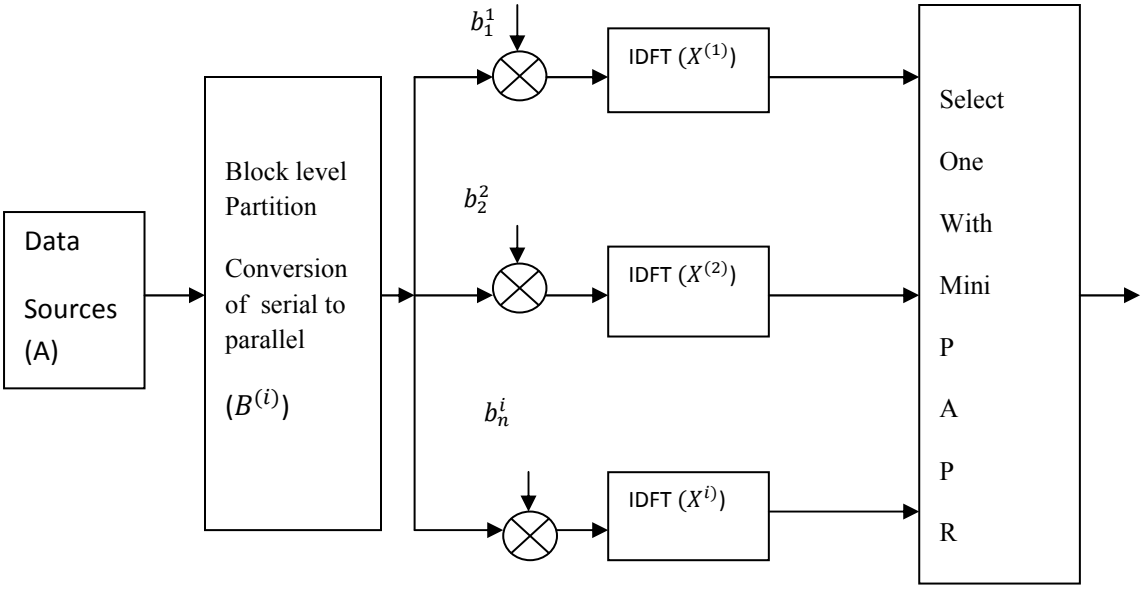


Figure 1. SLM block at the end of transmitter [7]

In this phases are viewed and they rotate for this reason based totally on the inputs generated. They multiply a complicated number with the rotating factor and find the one more number. The decision process will be endured until mini PAPR is achieved. The calculations are performed at every section [5]. Hence,

$$b_n^i = e^{-j\theta_n^i} \; where \; \theta_n^{(i)} \epsilon [0, 2\pi] \quad (7)$$

where θ is the phase rotation. These vectors are used to recover the signal that are used as facet records which are been transmitted. The amount of scrambling performed resembles the effectiveness and efficiency SLM. The scrambling is done with help of rotation factors on the unique sequence of OFDM and the length of SLM sequence. Here the length of the SLM is viewed as U and the level of complexity is calculated. The overall performance of SLM is evaluated based on the quantity of iterations or sequences and by the way of increasing the sequence the system complexity may additionally expand but the most important hassle which is considered in transmitting give up i.e PAPR can be minimize to some extent. The complexity of imposing SLM is termed to be moderate. Some works have been preferred to limit the stage of complexity in SLM. The complexity of SLM can be termed as

$$Complexity = UNLog_2 N \quad (8)$$

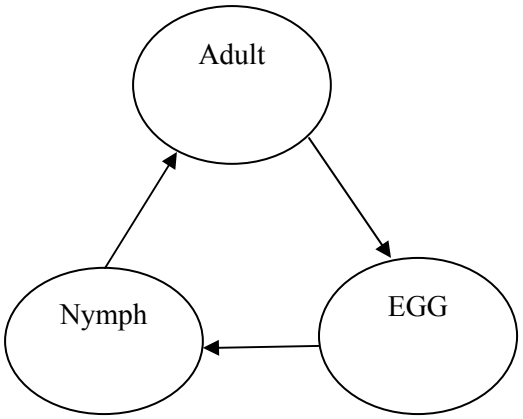
IV. SLM-GRASSHOPPER OPTIMIZATION

It is one of the famous optimization technique proposed by mirjalili and inspired by swarm optimization model. The existence of grasshoppers life process is shown in Figure. 2 . Although grasshoppers are generally considered for my part in nature, they be a part of in one of the biggest swarm among all the insects [12] . The grasshoppers has a unique feature in nymph and adulthood is its swarming behaviour [13] . As nymph is the starting

stage of grasshoppers life cycle , even it is observed that Millions of them move and sour. In their path, they devour nearly all vegetation. Later, at the end of adult stage the grasshoppers develop a swarm in air. The way how grasshoppers migrate over massive routes covering long distances. One of the major trait of the swarm is its larval condition in which it has slow movement with small steps. The larger distance and the movement which is very much abrupt is the indispensable characteristic of the swarm in stage of adulthood. Food source in search of is every other vital attribute of the swarming of grasshoppers. The search process is performed using two types of tendencies which are separated logically and are termed as: exploration and exploitation. In case of exploration, the search sellers are motivated to go abruptly, in the course of exploitation local crossing is observed . The target seeking functions are carried out in two function by the mean
of natural behaviour of grasshopper.



(a) original grasshopper



(b) grasshopper life process

Figure 2. Grasshopper and process of its life

The model representation for simulation of the behaviour of grasshopper that are swarming are given as[14]

$$X_i = S_i + G_i + A_i \quad (9)$$

position of i^{th} grasshopper is X_i, the interaction of grasshoppers socially is S_i , the i^{th} grasshopper gravitational force is G_i, and the direction of wind which the grasshoppers moves is A_i. The random behaviour of grasshoppers with various conditions is written as $X_i = r_1 S_i + r_2 G_i + r_3 A_i$ where $r_1, r_2 and\ r_3$ are random numbers in [0,1].

$$S_i = \sum_{\substack{j=1 \\ J\neq 1}}^{N} s(d_{ij})\widehat{d_{ij}} \quad (10)$$

The distance between i^{th} grasshopper and j^{th} grasshopper is given as d_{ij} and is calculated as, $d_{ij} = |x_j - x_i|$ and $\widehat{d_{ij}} = \frac{x_j - x_i}{d_{ij}}$, s is termed as social force which defines the strength of grasshopper socially.

A conceptual mannequin of the interactions between grasshoppers and the relief area the use of the characteristic s. It may additionally be stated that, in simplified form, this social interplay used to be the motivating pressure in some until now locust swarming models [15] . The house of grasshoppers is divided into three zones by function S. The zone are named as comfort zone, repulsion zone and enhancement zone. if the distance between the two grasshoppers is above 10 then the value is set to zero. When the value is set to zero the grasshopper is not able to follow the study forces that are described above. The distance between the grasshopper are calculate for every update of the positions.

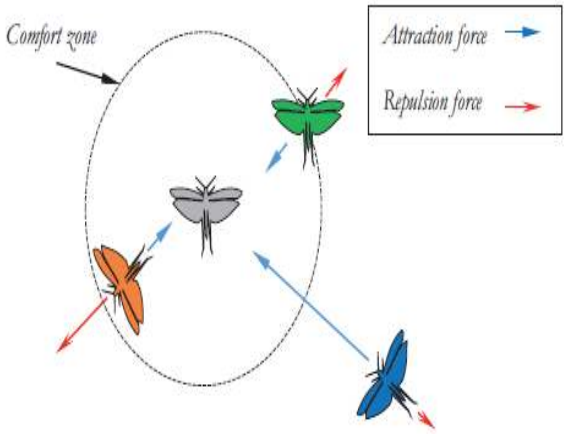


Figure 3. Zones and behaviour of grasshoppers

The component G is given as,

$$G_i = -g\widehat{e_g} \quad (11)$$

here g is termed as constant of gravitation and the unit vector is $\widehat{e_g}$ which acts moving towards the centroid position of the earth .

The component A is given as,

$$A_i = u\widehat{e_w} \quad (12)$$

The expanded equation by including all the components is given by

$$X_i = \sum_{\substack{j=1 \\ J\neq 1}}^{N} S(|x_j - x_i|)\frac{x_j - x_i}{d_{ij}} - g\widehat{e_g} + u\widehat{e_w} \quad (13)$$

The grasshoppers are very quick in reaching the comfort zone , so that the opimization problem cannot be solved accurately. Inorder to solve the optimizations problem the modified version of the equation 13 is given as

$$X_i^d = c\left(\sum_{\substack{j=1 \\ j\neq 1}}^{N} c\,\frac{ub_d - lb_d}{2} s\left(|x_j^d - x_i^d|\right)\frac{x_j - x_i}{d_{ij}}\right) + \widehat{T_d} \quad (14)$$

.

The role of grasshopper relies on the sting position, target position and eventually the position of all grasshoppers that is shown in eq (14). Note that the primary side of this equation considers the locality of the up to date grasshopper with appreciate to different grasshoppers. The grasshoppers quality is taken into account to stipulate the search sellers spherical region. In GOA, the search is performed position vectors of every search agent. supported the present position, the search agents operate is updated and more updates to next position supported international best, and therefore the role of all totally different search agents. The state involves all the search dealers in shaping the position of the search agent that is extremely distinctive feature to provide optimized results.

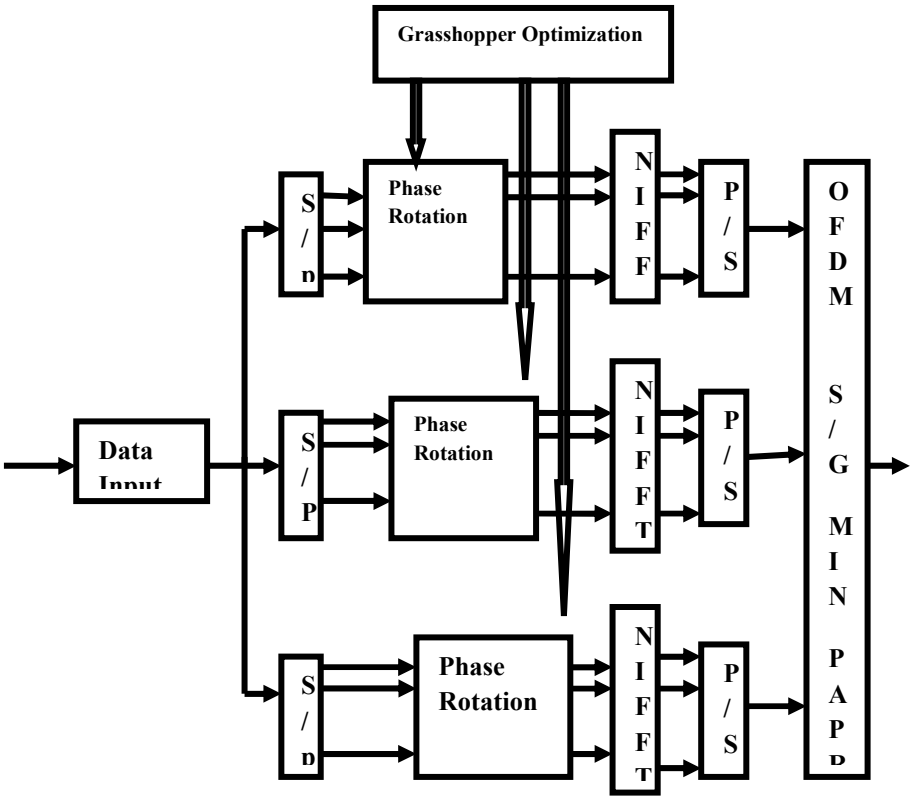


Figure 4. Proposed SLM-Grasshopper Model

Algorithm:

The grasshopper optimization based SLM algorithm is given as:

Step1: Initialise input data $I_x = I_1 I_2 I_3 \ldots\ldots\ldots\ldots I_n$

Step2: Serial bit of data converted to parallel bits

Step3. Rotating the phase of bits and applying Grasshopper optimization for the bits
Step 4. Initialization of the search agents nymph and adult grasshopper
Step5: Calculate the fitness function
Step6: Find the best grasshopper among nymph and adult
Step7: Update the position of nymph w r t Social interaction, gravitation force and wind advection
Step8: Calculate the distances between nymph and adult grasshopper
Step9: update the position and calculate the fitness value of nymph and adult
Step10. Find the best value and form a unique phases
Step11. Obtain the Min PAPR signal

V. RESULTS AND DISCUSSION

The results obtained are shown in below Figures. From Figure 4, more reduction in PAPR is observed for SLM-Grasshopper method than the techniques which are used o compared. Hence the OFDM is a bit free form power factor issue by the proposed method and also better compared to other techniques like SLM, GA-SLM, FA-SLM, GWO-SLM. The results shows the variation in PAPR with respect to the CCDF for different phase sequences like 4, 8, 16 and 32.

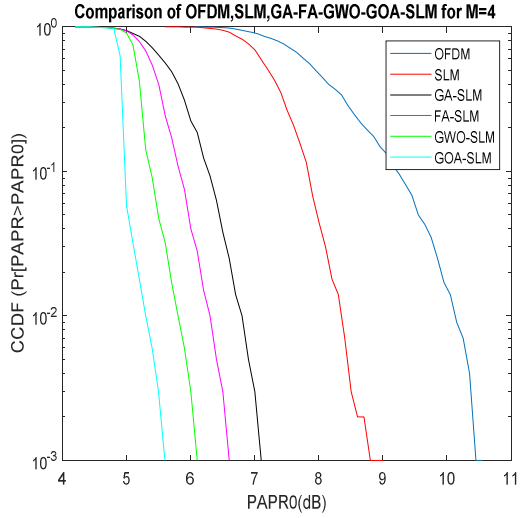


Figure 5. PAPR vs CCDF for M=4

Here the phase sequences is denoted with M. As the M value increases the PAPR get reduced and remains stable after reaching certain point. From the experimental results it is shown that the PAPR is no further reduced for M value above 32. There is no use in increasing the phase value as the system level of complexity increases with increase in number of phases. By considering M= 4 to M=32 , 0.5dB decrease is observed in each case.

For M=8,

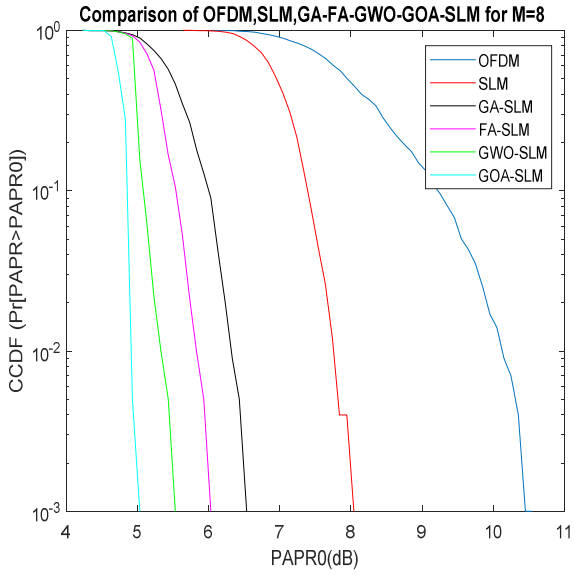


Figure 6. PAPR vs CCDF for M=8

As shown in Figure 7, for 16 phases by estimating the global value the best optimal value for PAPR found by GOA is : 4.6371

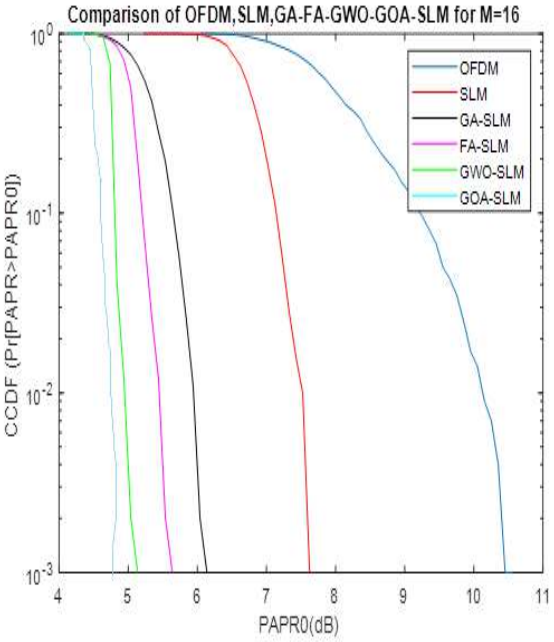


Figure 7. PAPR vs CCDF for M=16

As the number of number of phases increases the PAPR reduces and some breakeven point the PAPR value remains constant. The PAPR optimal value obtained for M=32 while performing with GOA is 4.4 which is shown in Figure 8.

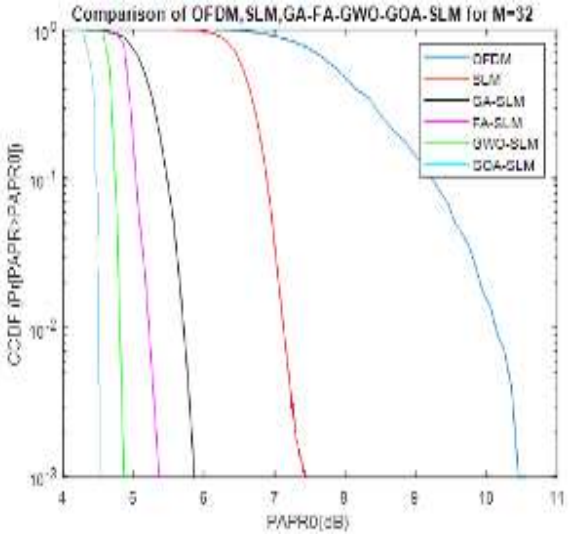


Figure 8. PAPR vs CCDF for M=32

VI. CONCLUSION

In terms of spectrum efficiency and the performance of channel OFDM is a technique which is greater pinching in wi-fi communications. The only primary disadvantage need to think about is its PAPR. It achieves greater PAPR when the number of subcarriers increases. One of the useful scrambling approach i.e SLM and most efficient optimization technique i.e grasshopper algorithm together mixed to decrease PAPR to increase the entire performance of OFDM communication system. The decrease in PAPR is proven with amplify in phase sequence M. The overall performance of proposed approach is in contrast with many present strategies and proved to be best. The experimental outcomes shows that SLM-Grasshopper algorithm outperforms and the sizable adjustments in PAPR is observed.

REFERENCES

[1] Y.Wu and W. Y. Zou, "Orthogonal frequency division multiplexing: A multi-carrier modulation scheme," IEEE Trans. Consumer Electronics, vol. 41, no. 3, pp. 392–399, Aug. 1995.

[2] U1niversity of Alberta, "Home page - High capacity digital communications laboratory," 2007. Available: http://www.ece.ualberta.ca/~HCDC/mimohistory.html.

[3] Shinsuke Hara, Ramjee, "Principle and history of MCM/OFDM," in Multicarrier techniques for 4G mobile communication, Artech House.

[4] E. Telatar, "Capacity of multi-antenna Gaussian channels," European Transactions on Telecommunications, vol. 10, no 3, Dec 1999.

[5] Foschini G J, Gans M J, "On limits of wireless communication in a fading environment when using multiple antennas," Wireless Personal Communication, vol. 6.

[6] Tarik Hadj Ali and A. Hamza, " A new SLM technique based on Genetic Algorithms for PAPR reduction in OFDM systems", IEEE DOI 10.1109/CICN.2016.113DOI

[7] R Sridevi and Dr. T Madhavi, "SLM Technique based on Firefly Algorithm for Reduction of PAPR in OFDM Systems ", Jour of Adv Research in Dynamical & Control Systems, Vol. 11, 06-Special Issue, 2019.

[8] R Sridevi and Dr. T Madhavi, " Reduction of PAPR in OFDM Signals Using Grey Wolf Optimization combined with SLM ", DSMLA 2019: Proceedings of the 1st International Conference on Data Science, Machine Learning and Applications.

[9] Suverna Sengar, Partha Pratim Bhattacharya," Performance Improvement In OFDM system By PAPR Reduction," Signal & Image Processing : An International Journal (SIPIJ) Vol.3, No.2, April 2012 Department of Electronics and Communication Engineering, Faculty of Engineering and Technology, Mody Institute of Technology & Science (Deemed University),Lakshmangarh, Dist – Sikar, Rajasthan, Pin – 332311, INDIA.

[10] Chin-Liang Wang, Yuan Ouyang, "Low-complexity selected mapping schemes for peakto-average power ratio reduction in OFDM systems", IEEE Trans. on Signal Processing, vol. 53, no. 12, pp. 4652 – 4660, 2005.

[11] Peled A, Ruiz A, "Frequency domain data transmission using reduced computational complexity algorithms," Acoustics, Speech, and Signal Processing, IEEE International Conference.

[12] Simpson SJ , McCaffery A , HAeGELE BF . A behavioural analysis of phase change in the desert locust. Biol Rev 1999;74:461–80 .

[13] Rogers SM , Matheson T , Despland E , Dodgson T , Burrows M , Simpson SJ . Mechanosensory-induced behavioural gregarization in the desert locust Schis- tocerca gregaria. J Exp Biol 2003;206:3991–4002 .
[14] Topaz CM , BernoffAJ , Logan S , Toolson W . A model for rolling swarms of lo- custs. Eur Phys J Special Top 2008;157:93–109 .
[15] Lewis A . Low Cost: a spatial social network algorithm for multi-objective optimisation. In :Evolutionary computation, 2009. CEC'09. IEEE congress on; 2009. p. 2866–70.



SRIDEVI.R received the B.Tech degree in Electronics and Communications Engineering from Rajasthan Vidyapeeth, Udaipur, India in 2007.M.Tech degree from Andhra University, Visakhapatnam, India in 2011.She is currently working as Assistant Professor, Dept of ECE, Dr.Lankapalli Bullayya Engineering College for Women, Visakhapatnam, AP, India. Her Research interest include Wireless Communications, cellular/Mobile communications and Embedded systems



Dr. T. Madhavi is currently working as Professor in the Department of EECE, GITAM, Visakhapatnam, India. She received her M.Tech in Radar and Microwave Engineering in 2004 and Ph.D in 2013 from Andhra University, India. She has over 25 years of experience in Industry and Teaching. She has published several papers in Reputed Journals like IET, Springer, etc. Her main research interest includes modeling and performance analysis of wireless communications systems, Cellular/mobile communications and Wireless Sensor Networks



SREENIVASULU.UMMADISETTY received the B.Tech degree in Electronics Instrumentation and Control Engineering from S.V .University, Tirupati,A.P., India in 2007, M.Tech degree from NIT Rourkela, Orissa, India in 2010. He is currently working as Assistant Professor, Dept. of EECE, GIT,GITAM University, Visakhapatnam, AP, India. His Research interests include Bio medical Signal Processing, Radar Signal Processing, soft computing applications.

Retrieval Number: paper_id//2019©BEIESP

DOI: 10.35940/ijitee.xxxxx.xxxxxx

Published By:
Blue Eyes Intelligence Engineering
& Sciences Publication

ANALYSIS OF INDIAN NATURAL CHROMITE ORE AND ROCKS BY NUCLEAR ANALYTICAL TECHNIQUE

R.Venkateswara Rao
Senior Assistant Professor, Department of Physics,
Lendi Institute of Engineering & Technology, Jonnada, Vizianagaram, A.P, India
K. Srinivasa Rao
Assistant Professor, Department of Physics, ANITS, Sangivalasa, Visakhapatnam A.P, India
S. Siva Jyothi
Assistant Professor, Department of Physics,
Dr. L.B. College of Engineering for women, Visakhapatnam, A.P., India
C.Kasipathi
Professor, Department of Geology, Andhra University, Visakhapatnam, A.P, India

Received: Jul. 2019 Accepted: Aug. 2019 Published: Sep. 2019

Abstract: A number of Indian chromitites have been studied by using complementary and non-destructive PIXE technique. Thirteen elements including Co, Ni, Cu, Zn, Ga, Zr, Mo, Nb and Pb were established in these chromitites, which may be useful to interpret the various geochemical conditions and the probable cause of their inceptions in chromitite matrix. PIXE technique is a powerful method for fast determination of variable multi elemental analyses. The advantage of this technique is that one can obtain all major and minor elements present at once in pure concentration. The chemical constituents of chromite ores and ultrabasic rocks of Boula, Keonjhar district of Orissa State, India, a part of the Eastern Ghats terrain, were analyzed by using PIXE technique. The present work, thus, establishes the usefulness and versatility of the PIXE technique for research in geo-scientific methodology.

Keywords: PIXE, Nuclear Analytical Technique, Peninsular India, Chromite Ores.

1. Introduction: Multi-elemental analysis of geological samples is of great importance in geological research and mineral prospecting. In geological research, the classification of ore and rock samples is done by studying the presence of elements such as Si, Ti, Al, Fe, Mn, Mg, Ca, Na, K and P. Similar information on trace elements will also be obtained using the analytical techniques. A trace element in the present study is defined as an element which is present in a sample with concentrations less than 1000 ppm. Owing to their low concentrations, it is difficult to get information on trace elements unless a suitable technique is adapted. Many methods are employed to characterize the geological areas in according with potentially interesting findings. Traditional geological survey reveals the areas of potential interest. Areas, thus selected, are investigated in greater detail by drilling. Since, the cost of

final drilling is very high, it is essential to extract as much initial information as possible. Small samples at regular depth levels from the drilled core are collected and accurate elemental analysis is performed on these samples. It is therefore important to adapt useful analytical techniques to get more reliable information. A brief description of the various available analytical techniques which are adapted in geo research is given below to get information about the elemental concentrations.

The essential information on the elemental composition of the geological material can be deduced from the use of several analytical methods such as Atomic Absorption Spectrometry (AAS), Instrumental Neutron Activation Analysis (INAA), X-ray Fluorescence (XRF), Inductively Coupled Plasma Mass Spectroscopy (ICP-MS) and Particle Induced X-ray Emission (PIXE) etc [1-4]. Some of these methods are destructive for the reason that the samples cannot be used for further studies; some of the techniques give information on one element only or they require sample preparation before analysis. In contrast, PIXE has some distinctive features of being nondestructive, quick and rapid measurements, allowing multi elemental determination and requiring little or no sample preparation.

PIXE is a non-destructive technique for rapid analysis of a wide range of trace elements with ppm sensitivity. Due to its high sensitivity, it is used in the fields of geology and geophysics for investigating trace elements in geological specimens [5-7]. Use of protons offers a good sensitivity even at lower atomic numbers due to the fact that Bremsstrahlung background caused by protons is very low compared to electron excitation. PIXE technique has rapidly gained acceptance as a valuable analytical tool because of the ever-increasing need for elemental analysis of very small amounts of sample, as in the case of geological materials. In the present work, we estimated the concentrations of trace elements in the Indian Peninsular chromite ores and ultra basic rocks by using PIXE technique.

Chromium (Cr) is a grey, hard metal most commonly found in the trivalent state in nature. Hexavalent (chromium (VI)) compounds are also found in small quantities. Chromite ($FeOCr_2O_3$) is the only ore containing a significant amount of chromium. The ore has not been found in the pure form; its highest grade contains about 55% chromic oxide. Chromium levels in soil vary according to area and the degree of contamination from anthropogenic chromium sources. Tests on soils have shown chromium concentrations ranging from 1 to 1000 mg/kg, with an average concentration ranging from 14 to about 70 mg/kg. Chromium (VI) in soil can be rapidly reduced to chromium (III) by organic matter. As chromium is almost ubiquitous in nature, chromium in the air may originate from wind erosion of shale's, clay and many other kinds of soil. In countries where chromite is mined, production processes may constitute a major source of airborne chromium. In Europe, endpoint production of chromium compounds is probably the most important source of chromium in air.

The largest producers of chromium ore are South Africa (44%), India (18%), Kazakhstan (16%), Zimbabwe (5%), Finland (4%), Iran (4%) and Brazil (2%) with several other countries

producing the rest, which is less than 10% of the world production [8]. In India, Chromite deposits are found in association with basic and ultrabasic rocks like dunite, pyroxenite, amphibolite and their altered masses. The Peninsular Indian chromites contribute to the entire Indian Chromium production and are distributed in the States of Orissa, Karnataka, Andhra Pradesh and Tamil Nadu. Geologically, the chromite formations are restricted to the Eastern Ghats, Iron Ore Series and Green Schist's of the Peninsular India. The present area of investigation, Boula is a part of the Eastern Ghats terrains, where chromium enriched chromite is associated with pyroxenites.

The industrial development in the world mostly depends on the utility of chromium metal as an important component with Fe and Mn. Chromium is the chief mineral in the production of Chromium metal which is the primary component in the manufacture of stainless steels, and high tech machinery. It is useful in metallurgical refractory and chemical industries based on certain specification of ore. Chromite mineralogy is very interesting area of study, because of the isomorphous mixtures of spinal group. In view of its importance the estimation of the amount of chromium present in Chromite ore and the rock samples along with the minor and trace elements is of greater importance. This forms the backdrop of this research paper.

2. Materials and Methods:

2.1. Sample collection and Preparation:

2.1.1. Study Area: The chromite ore and rock samples have been procured from various chromite mines of Boula in Keonjhar District of Orissa of Eastern India. Boula area is mostly a hilly county made up of chains of low ridges and their foot hills with the northeastern spurs and separated by broad rivers like Salandhi, which flow in the South-Eastern direction. The highest elevation is Δ1343, Phyljora Huli. Apart from the River Salandhi and Bintkholi stream, all the other rivulets remain dry for most part of the year.

2.1.2. Ore Samples: About 200g of chromite ore is crushed into granules in a stainless steel mortar with hard strokes. The strongly magnetic material has been separated as magnetite. Observing the granular shape, size and color under the microscope, the chromium grains are separated. Heavy liquids like tetrabromo ethane used for more clear separation of gangue form the ore mass. The granules are washed with water, decanted and dried at room temperature and powdered to -230 microns. Then the powder is ground in an agate mortar for about 45 minutes each to a mesh size of -400 microns.

2.1.3. Rock Samples: About 200g of fresh rock sample was taken and washed thoroughly under water flow and dried in an oven. The sample was crushed into small chips through -170 microns of mesh. The powder thus obtained was subjected to coning and quartering till the powder was finally ground in an agate mortar for easy digestion. This powder was used in the following analytical work.

Contamination during sample preparation is a serious source of error in geochemical analysis. It usually occurs during grinding and crushing and may create cross contamination. In the

present work, the cross contamination is eliminated by careful cleaning and by pre-contaminating the apparatus with the sample to be crushed or ground. Contamination during grinding process is eliminated by carrying out the grinding in agate. The cleaned, processed and separated ore and rock samples were then made into pellets by the following procedure. Small amounts (~150 mg) of ore and rock from each sample were crushed, finely powdered and thoroughly mixed with the binding material (such as boric acid etc) in the ratio 1:1 by weight. 150 mg of high purity (99.9997%) graphite powder was mixed with the samples in order to monitor the beam current. These solid mixtures were thoroughly ground, homogenized and pressed into pellets. A hydraulic press was used to compress the resulting mixture into a pellet of 13 mm diameter and about 1.5mm thickness. The pellets were then used as targets. The prepared targets were placed over the target ladder. The collimated beam was made to fall on the samples and the emitted respective characteristic X-rays were collected using Si (Li) detector which is maintained at liquid nitrogen temperature.

2.2. The details of PIXE Experiment: The present PIXE experiment was performed using a 3 MV Pelletron accelerator at the Institute of Physics, Bhubaneswar in Orissa of India. This accelerator has been regularly used for carrying out material analysis using the PIXE technique [9-10]. A 3 MeV proton beam was used to excite the samples. The samples were suspended on an aluminium sample holder. Then the target holder was loaded into the PIXE chamber and the irradiation was carried out in vacuum conditions. A collimated proton beam of 4 mm diameter was made to fall on the target. The beam current was kept at 20 nA. The targets on the aluminium holder were positioned in the scattering chamber at an angle of 45° with respect to the proton beam. With respect to that beam, an energy dispersive Si (Li) detector (with 160 KeV FWHM resolutions at 5.9 KeV) recorded the characteristic X-ray spectra at 90°. For each sample, the total charge collected and the average beam current were noted. The spectra were gathered for a sufficiently long time in order to obtain good statistics. Spectra were recorded by using a Canberra series MCA. In the present study, PIXE technique was adapted to analyze the chromite ore and rock samples belonging to Boula in Keonjhar district of Orissa, India. The concentrations of different elements were estimated in each sample using GUPIX software package. The estimated concentration of chromite and other trace elements is furnished in tables 1, 2 and3.

2.3 Data Analysis: The collected data were analyzed with the GUPIX software package [11-12]. The relationship between characteristic X-ray yield Y (Z) for an element of atomic number Z and its concentration C_z in a given target matrix is

$$Y(Z) = HY_1(Z)\, C_z Q \epsilon_z t_z,$$

Where Y1 (Z) is the computed Yield from the database per steradian per unit concentration and per unit integrated beam charge; Q the beam charge; ϵ_z the intrinsic efficiency of the Si (Li) X-ray detector; and t_z the transmission of the X-rays through any absorber placed between the detector and the specimen. The instrumental constant H is the product of the geometric solid angle of the X-ray detector and any systematic normalization factor present in the charge integration system. The instrumental constant H was measured using 3 MeV protons and a wide range of pure single-element standards emitting both K and L X-rays in the energy region 3–26 KeV. Thus the X-ray yield (Y) is converted to elemental concentration via a defined

standardization technique involving H value, the theoretical yield, detection efficiency and filter transmission values.

3. Results and Discussion: The chromite ore and ultrabasic rock samples collected from different parts of Boula were irradiated with the 3MeV proton beam obtained from tandem type Pelletron accelerator at IOP, Bhubaneswar, India. From the emitted characteristic x-rays, elemental concentrations in the samples were calculated. The estimated major elemental concentrations are provided in table 1 and the concentration values are specified in percentage. The measured minor and trace elemental concentrations of chromite ore and ultrabasic rocks are presented in table 2 and table 3 respectively along with their standard deviation. The elemental concentrations in table 2 and table 3 are given in μg/g (ppm) except for the elements Ti, V, Mn, Co and Ni and their concentration is specified in terms of percentage. In the above mentioned tables, the experimental errors in each of the measured concentrations are also given along with the concentrations. Errors in PIXE results are based on number of counts and on the least-square fitting of the peak areas, which include the uncertainties in the background subtraction. It can be seen from tables numbered 1, 2 and 3 that the results are consistent within the permissible errors.

The range of concentration of Ti was found in these samples between 0.013% and 0.96%, whereas Mn is between 0.0078% and 0.36% (tables 2 and 3).On the other hand, the range of concentration for the element Ni is quite large, which is in between 0.41% and 2.56%. Further–more, the concentrations of trace elements (tables 2 and 3) show interesting behavior with large variation except for the elements Cu and Pb, which are present in some 10's of ppm (range:14-73ppm and 12-78ppm respectively)in these samples.

In the literature [13-14], it is reported that the average values of nickel (Ni) in igneous rocks of the Proterozoic period are above 200 ppm. It is found that the concentration of nickel (Ni) in our samples shows the higher values than the previous researcher literature values for the rocks of igneous origin. It indicates that our samples are of igneous origin belonging to the Proterozoic period. Another important geochemical parameter is that the concentration of zirconium (Zr) can be used as an effective indicator of the province considered as less prone to weathering, and is believed to be neither affected by transportation during weathering nor by any other specific later geochemical event of less significance [3]. Furthermore, it is immobile, highly stable and rarely decomposes in nature. So the concentration of Zr in ores may represent the constituent of source rock or solution from which it is generated. In these samples, the content of Zr is rather high with a significantly large variation, leading to the situation that there may be many geological events responsible for their natural and the consequent formations.

Table.1: Major elements determined (values are in percentage) in chromitites by PIXE.

S.No	CR1	CR2	CR3	CR4	CR5	CR6	CR7	CR8	CR9	CR10
Chromium	19.96	14.95	23.88	16.51	12.78	13.72	17.92	31.88	15.90	18.32
Iron	8.45	12.32	10.42	21.38	14.36	19.28	24.45	15.35	6.40	11.31

Note: CR1 to CR10 represent chromitite samples from Boula (FACOR) mines of Keonjhar District, Orissa from south to north of the mining district.

Table .2: Distribution of minor and trace elemental concentrations in chromite ores–by PIXE method (values are in ppm) & (* = concentrations are in percentage)

S.No.	Ti*	V*	Mn*	Ni*	Cu	Zn	Ga	Zr	Nb	Mo	Pb
CR1	0.96	0.45	0.36	0.41	46 ± 3.86	919 ± 39.51	778 ± 32.67	48 ± 3.79	38 ± 3.11	16 ± 1.40	73 ± 5.69
CR2	0.95	0.32	0.32	1.53	18 ± 1.51	940 ± 40.42	724 ± 30.40	34 ± 2.68	10 ± 0.82	11 ± 0.96	48 ± 3.74
CR3	0.88	0.42	0.24	0.62	34 ± 2.85	382 ± 16.42	516 ± 21.67	41 ± 3.23	6 ± 0.49	08 ± 0.70	21 ± 1.63
CR4	0.51	0.38	0.18	1.43	28 ± 2.35	906 ± 38.95	638 ± 26.79	26 ± 2.05	18 ± 1.47	12 ± 1.05	33 ± 2.57
CR5	0.78	0.36	0.21	0.96	31 ± 2.60	328 ± 14.10	580 ± 24.36	18 ± 1.42	22 ± 1.80	07 ± 0.61	70 ± 5.46
CR6	0.72	0.28	0.26	0.52	22 ± 1.84	248 ± 10.66	732 ± 30.74	16 ± 1.26	28 ± 2.29	05 ± 0.52	54 ± 4.21
CR7	0.92	0.45	0.33	0.56	40 ± 3.36	882 ± 37.92	542 ± 22.68	8 ± 0.63	9 ± 1.38	09 ± 0.79	18 ± 1.40
CR8	0.88	0.35	0.31	0.63	37 ± 3.10	661 ± 28.42	328 ± 13.77	30 ± 2.37	14 ± 1.14	08 ± 0.70	46 ± 3.58
CR9	0.90	0.40	0.22	0.48	25 ± 2.10	761 ± 32.72	676 ± 28.39	19 ± 1.50	11 ± 0.9	08 ± 0.70	51 ± 3.97
CR10	0.32	0.31	0.13	1.76	15 ± 1.26	309 ± 13.28	346 ± 14.53	21 ± 1.65	17 ± 1.39	09 ± 0.79	14 ± 1.09

Table 3: Distribution of minor and trace elements in ultrabasic rocks–by PIXE method

S.No.	Ti*	V*	Mn*	Co*	Ni*	Cu	Zn	Ga	Zr
CR1	0.18	0.080	0.27	0.01518	1.79	69.3 ± 3.95	77.8 ± 5.83	40.7 ± 2.8	240 ± 16.56
CR2	0.34	0.024	0.014	0.0088	1.53	34 ± 1.93	41 ± 3.07	21 ± 1.44	18 ± 1.24
CR3	0.41	0.029	0.018	0.0096	0.86	40 ± 2.28	24 ± 1.80	28 ± 1.93	32 ± 2.20
CR4	0.017	0.004	0.031	0.0036	1.43	27 ± 1.53	15 ± 1.12	11 ± 0.7	16 ± 1.60
CR5	0.30	0.030	0.01612	0.0132	1.96	73 ± 4.16	28 ± 2.10	30 ± 2.07	22 ± 1.51
CR6	0.14	0.014	0.0986	0.0086	0.52	28 ± 1.59	14 ± 1.05	24 ± 1.65	11 ± 0.75
CR7	0.013	0.0014	0.0094	0.0025	2.56	16 ± 0.92	24 ± 1.80	8 ± 0.55	9 ± 0.62
CR8	0.48	0.0229	0.10	0.0071	0.63	31 ± 1.77	8 ± 0.60	18 ± 1.24	14 ± 0.92
CR9	0.011	0.0026	0.015	0.0122	2.04	19 ± 1.08	6 ± 0.45	10 ± 0.6	19 ± 1.31
CR10	0.44	0.0014	0.0078	0.0092	1.76	12 ± 0.68	10 ± 0.75	6 ± 0.41	4 ± 0.27

(* = concentrations are in percentage & Values are in ppm)

We would further like to bring the attention of the readers towards the fact that a significant number of geologists consider chromite deposits as the product of magmatic differentiation of basalt melts [15] which are segregated at the beginning of the process, due to fractional crystallization of dry magmas or at the end of the process segregated from residual melt enriched with volatiles that reduces the crystallization temperature of chromites. Hence, in order to understand the probability of this differentiation process that may lead to association of various trace metals with major elements, a series of inter-elemental correlation has been attempted from the results of the concentrations of various elements and only the outstanding and the extra ordinary correlations have been plotted and considered for further understanding and discussion. It is observed that there are excellent correlations and some similar behavior pattern between Fe-Co (Fig.1) and Cr-Ni (Fig.3) and there is no specific relation between Fe-Ni (Fig.2) and Cr-Co (Fig.4), in other words in terms of geology the elements of iron and chromium follow the sympathetic relation with cobalt and nickel where as iron and chromium elements follow the antipathetic relation with nickel and cobalt respectively. It may be possible that there is a simultaneous precipitation in case of former two groups of elements and simultaneous differentiation in the latter groups of elements with that of the source solution.

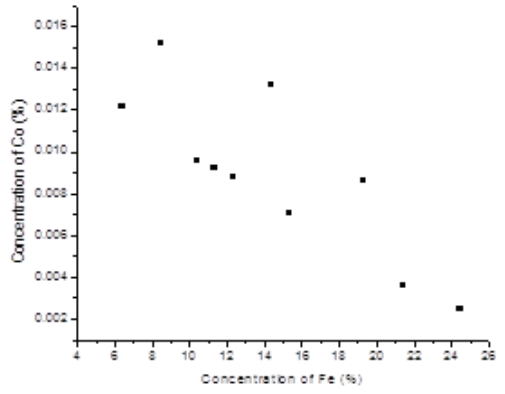


Fig.1: Variation of Co with respect to Fe

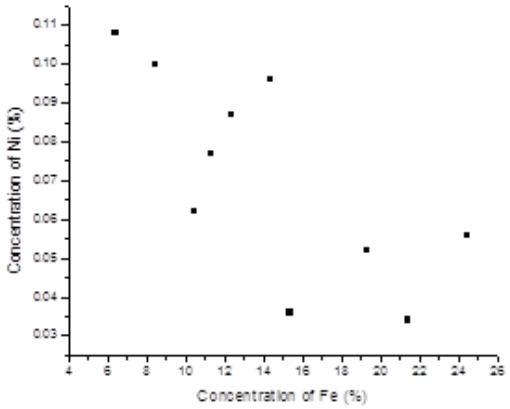


Fig.2: Variation of Ni with respect to Fe

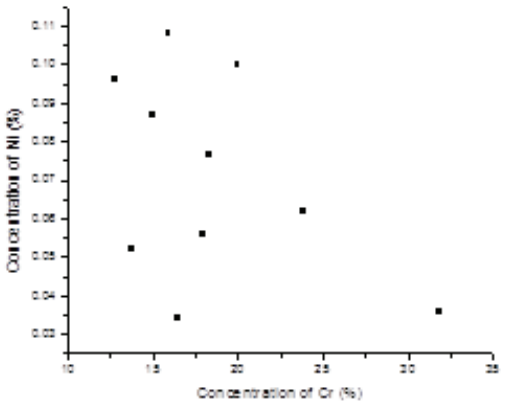


Fig 3: Variation of Ni with respect to Cr

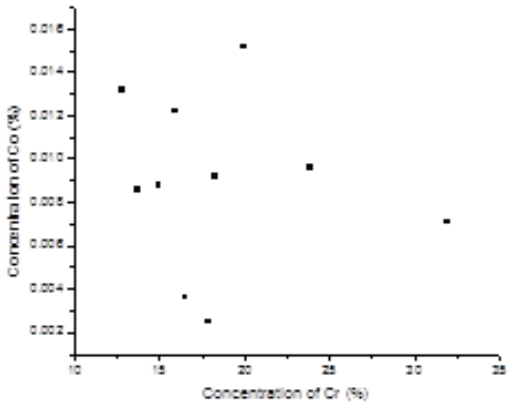


Fig.4: Variation of Co with respect to Cr

To compare the elemental concentration profile between chromite ore and rock samples, the ranges and the mean elemental concentrations have been determined from each set of these samples. The mean minor and trace elemental concentrations of the chromite ore and rock samples are summarized in Fig.5. The minor element concentrations were found to be very similar between the chromite ore and rock samples, except for Zn and Ga. The concentrations of Zn and Ga are comparatively high in Chromite ore samples than the Rock samples whereas Co is low in chromite ore samples. It is clear from Table2 and Fig.5, the concentration of elements Mo, Nb and Pb are observed only in Chromite ore samples, which are not observed in the host rocks, viz. pyroxenite, dunite and gabbro. Although the exact cause and mechanism for the presence and absence of these elements in the specific types of chromite ore and rock samples is not established yet, it may be possible that the variation of different factors such as energy, pressure, temperature and gravity etc during the precipitation process or the formation of these chromite ore and rock samples are responsible for aforementioned findings. So, these elements play very important role in order to identify various types of ore and rock samples.

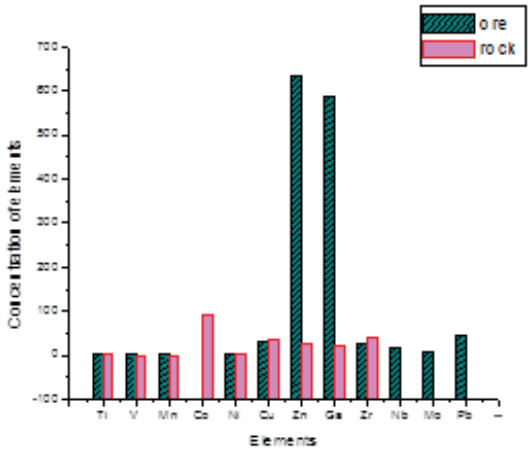


Fig.5: Mean Minor and Trace Elemental Concentration in Chromite Ore and Rock Samples

Conclusions: Thus, a selected number of Indian Peninsular chromitites have been studied by using complimentary and non-destructive PIXE technique. Thirteen elements including Co, Ni, Cu, Zn, Ga, Zr, Mo, Nb and Pb were established in these chromitites, which may be useful to interpret the various geochemical conditions and the probable cause of their inceptions in chromitite matrix. It was found that Ti, Mn and Ni are present in substantial amount with respect to other trace elements. It is interesting to observe that the concentration of nickel indicates the origin of these chromitites in Proterozoic period. Moreover, it is worth mentioning here that the amount of zirconium indicates the effect of many geological events on this specific geological belt. The study advocates the use of PIXE in quantifying trace elements in high-grade ores. However, as the present work is preliminary one, detailed further investigation may lead towards better understanding of the role of trace elements in Proterozoic period.

The accelerator-based nuclear technique of PIXE analyses was used for characterization of some natural chromitites. These minerals are mainly used for scientific and technological applications. Several major, minor and trace elements and their concentrations were determined from these samples. The chromitites are identified by means of their elemental concentrations. Therefore, the PIXE technique helps in determining the chemistry and mineralogy of the chromitites, as it is a non-destructive type of the analyses and it aids in full characterization. Hence the present study advocates the use of PIXE technique, for the characterization of geological materials, especially where a large number of elements are of specific interest.

References:

1. Benjamin, T.M., Duffy, C.J., Maggiore, C.J., Rogers, P.S.Z., Woolum, D.S., Burnett, D.S, Murrell, M.T., 1984. Microprobe analyses of rare earth element fractionation in meteoritic minerals. Nucl. Instr. Meth. B, 3, 677-680.
2. Johansson, S.A.E., Campbell, J.L., 1988. PIXE - A Novel Technique for Elemental Analysis. John Wiley & Sons, New York.
3. Nayak, P.K., Das, D., Vijayan, V., Singh, P., Chkravortty, V., 2004. PIXE and EDXRF studies on banded iron formations from eastern India. Nucl. Instrum. Methods. B, 215,251- 261.
4. Tenorio, D., Almazán-Torres, M. G., Monroy-Guzmán, F., Rodríguez-García, N. L.,LuisC. Longoria., 2005. Characterization of ceramics from the archaeological site of San Miguel Ixtapan, Mexico State, Mexico, using NAA, SEM, XRD and PIXE techniques. Journal of Radio analytical and Nuclear Chemistry, Vol. 266, No.3,471– 480.
5. Mohanty, A.K., Das, S.K., Vijayan, V., Senagupta, D., Saha, S.K., 2003. Geochemical studies of monazite sands of chhatrapur beach deposit of Orissa, India by PIXE and EDXRF method. Nucl. Instrum. Methods B, 211, 145-154.
6. Nayak, P.K., Vijayan, V., 2006. Complementary PIGE, PIXE, EDXRF and γ-ray spectroscopic investigation on natural chromites. Nucl. Instrum. Methods. B,245, 505-510.
7. Kasipathi, C., Venkateswarlu, P., Bharani, A., Venkateswara Rao, R., and Rautray, T.R.,2009. Advanced instrumental analytical technique in the characterization of heavy minerals-A case study of east coast beach deposits, Andhra Pradesh, India. National. Symp on Advances in Atomic Mineral Science in India during the 50 year period: 1959-2009; 26th to 28th Aug.2009, Hyderabad, India. Abst. Vol. p, 76.
8. Papp, John F. "Mineral Yearbook 2002: Chromium". United States Geological Survey. Retrieved 2009-02-16.
9. Sekar, K., Satyam, P.V., Kuri, G., Mahapatra, D.P., Dev, B.N., 1993. Nucl. Instr. and Meth. B 73, 63.
10. Vijayan, V., Ramamurty, V.S., Behera, S.N., 1995. Particle induced X-ray emission (PIXE) analysis of coal fly ash. Int. J. PIXE 5, 211-219.
11. Maxwell, J.A., Campbell, J.L., Teesdale, W.J., 1995. The Guelph PIXE software package II. Nucl. Instrum. Methods B, 95, 407.

12. Campbell, J.L., Hopman, T.L., Maxwell, J.A., Nejedly, Z., 2000. Nucl. Instr. And Meth. B, 70,193.
13. Pascoe, E.H.,1950. A Manual of the Geology of India and Burma, Vol. 1, Government of India Press, p. 483.
14. Rossler, H. J., Lange, H., 1972. Geochemical Tables, Elsevier publication, Amesterdam.
15. Padmavathi,M.V.L., and Kasipathi,C., 1992. Chromites-Pyroxenites and associated PGE of Tekuru, Easternghats, India. Abst, 29th Int. Geol. Con., Kyoto, P725.

***

NUCLEAR ANALYTICAL TECHNIQUE-PIXE, A SUITABLE METHOD FOR ELEMENTAL ANALYSIS OF CONVENTIONAL TO ADVANCED MATERIALS - AN OVERVIEW

K.SrinivasaRao
Assistant Professor, Department of Physics,
College of Engineering, ANITS, Sangivalasa, Visakhapatnam, A.P., India
R.Venkateswara Rao
Senior Assistant Professor, Department of Physics,
Lendi Institute of Engineering & Technology, Jonnada, Vizianagaram, A.P, India
S.SivaJyothi
Assistant Professor, Department of Physics,
Dr. L.B. College of Engineering for women, Visakhapatnam, A.P., India
P.Easwaraji
Assistant Professor, Department of Physics,
GMR Institute of Technology, Rajam, A.P., India.

Received: Jul. 2019 Accepted: Aug. 2019 Published: Sep. 2019

Abstract: Particle induced X-ray emission (PIXE) technique has been used for a variety of analytical problems with MeV accelerator. In general, the sample has to be kept inside a high vacuum chamber for analysis by PIXE. To overcome the difficulties arising for analysis of large archaeological and incompatible biological specimens, there is a need to take the beam outside the chamber and the technique is known as external PIXE technique. The paper presents some of the preliminary experimental results along with various aspects on which studies could be extended.

Keywords: PIXE, Nuclear Analytical Techniques, External PIXE, Biological Specimens.

1. Introduction: A brief description of the various available analytical techniques that are adopted to characterize various materials, for getting the information about the elemental concentrations, all major, minor and trace, is presented. Various analytical techniques are available for characterization of materials and the determination of elemental composition in conventional samples to advanced materials. Widely used methods are INAA, XRF, ICP-MS, EMPA, AAS and PIXE. Some of these methods are destructive, therefore the samples cannot be used for further studies; some of the techniques give information on one element only or require sample preparation before the analysis. In comparison, PIXE has some distinctive

features of being non destructive and quick, allowing multi elemental determination and requiring little or no sample preparation.

PIXE is a unique technique for performing non-destructive analysis using characteristic X- rays induced by a proton beam of few MeV directed towards the surface of the specimen. This technique has been successfully used for analysis in various fields, including environmental, biological, archeological, biomedical, archeometrical, geological and also in the field of nanotechnology. Since PIXE is one of the most promising methods of multi elemental analysis introduced in recent years. Many applications and examples which show that PIXE method can be used for geological applications have been described.

PIXE is a relatively simple, yet powerful analytical technique that can be used to identify and quantify trace elements in a sample. It is a nuclear analytical technique for rapid analysis of a wide range of trace elements with ppm sensitivity. Due to its high sensitivity, it is used in the fields of geology and geophysics for investigating trace elements in minerals of geological specimens. Use of protons offers a good sensitivity even at lower atomic numbers due to the fact that bremsstralung caused by protons is low compared to the electron excitation. PIXE technique has rapidly gained acceptance as a valuable analytical tool because of the ever-increasing need for the elemental analysis of very small amounts of sample, as in the case of geological materials such as gemstones, precious minerals etc.

Proton induced x-ray emission (PIXE) is a unique technique for performing non-destructive analysis using measurements of characteristic x-rays induced by a millimetre of proton beam (MeV energy scale) directed onto the surface of specimen[1]. This technique has successfully been used for analysis of various types including environmental [2], biological [3], archaeological [4] and geological [5] materials for almost three decades. The reasons that the PIXE technique is a method of choice for analysis of samples are its well-known features like: multi elemental capabilities, small sample mass requirement, high sensitivity, dynamic range, and simple sample or virtually no need for sample preparation. While dealing with specific archaeological (manuscripts etc), biological (fishes, teeth etc.) and geological materials (big rocks etc.), the vacuum PIXE technique is destructive due to the requirement for either sub-sample or a part for compatible that destroy the original material at the sample preparation stage itself. Elements of anthropogenic origin like sulphur, potassium, lead, bromine, etc. are present in environmental samples mainly as micron to sub-micron fractions. They often adhere on the larger particles of natural origin (silicates, carbonates, sea spray, etc.) and form a thin film over these particles. This technique has several other advantages apart from easy sample handling and positioning in air. Objects of large size and complex structure and shape can be analysed in-situ without the need of sampling, a fact particularly valuable for art objects. Also, it is possible to study materials containing volatile compounds, which could otherwise not stand vacuum. The risk of damage due to heating is considerably reduced because of efficient cooling by the air or the helium flow. However, charging of insulating materials is totally avoided without the need of a thin conducting coating required when

operating under vacuum [7-9]. Indeed charging effects can produce potentials up to several tens of keV, accelerate accordingly secondary electrons with a subsequent extension of the bremsstralung background to higher energy. The detection limit would then be marked increased [11]. The PIXE technique of ion beam analysis is first used in 1992 at Ion Beam Laboratory, Institute of Physics (IOP), Bhubaneswar. Since then, PIXE analysis of various environmental, geological [10] and biological [6] samples including fly ash, pond ash, plant soil, water, iron & chromium ores, human & animal tissue, blood, kidney stone, gallstone, hair, etc. has been analysed at IOP and were reported from time to time. The PIXE technique employs 3 MV Tandem pelletron accelerator and samples are kept in vacuum and irradiated. This paper describes the recent development of PIXE set-up at Institute of Physics and some of the preliminary experiments that were carried out [12].

2. Experimental Facility: The proton beam energy of 3 MeV obtained from the 3 MV tandem type pelletron accelerator collimated by a graphite collimator to a beam of 3 mm diameter and beam was extracted using a Kapton foil at exit point of the chamber (8 microns thickness). The Kapton^{TM} foil is used as exit window due to its special characteristics like low beam-induced background emission, minimal energy loss and radiation damage resistance [3, 13-16]. The beam was allowed to travel about 3 cm in air and about 2.4 MeV proton beam was used to irradiate the targets and the external PIXE set-up as shown in Fig.1. The targets were kept in air over a sample stand (capacity: 5kg) making an angle 45° to the beam direction. The samples are irradiated with maximum beam current of 20 nA that exits through 8 μm thick Kapton^{TM} window designed to withstand the atmospheric pressure. A Si(Li) detector (active area 30 mm^2) of CANBERRA with a full-width at half maximum (FWHM) of 165 eV at 5.9 keV (active area 30mm^2, beryllium window thickness 8 μm, placed at 90° with respect to the beam direction) was used to detect characteristic X-rays emitted from the targets. A 25 μm thick aluminised Mylar absorber (with 6% hole) was kept in front of the detector to attenuate the bremsstrahlung background and dominant low energy X-ray peaks. Spectra were recorded by using a CANBERRA S-100 multi channel analyser, which was calibrated with ^{241}Am X-ray source.

3. Performance and Applications of the PIXE Set-Up: PIXE technique has been successfully used for analysis in various fields, such as environment, biology, biomedicine, geology and nanotechnology. But here in this paper we discussed very few applications of this technique in Environment, biomedicine and geology.

3.1 Environment: Nowadays, many laboratories are involved in environmental research using the PIXE technique. The characterization of fly ash, which is an environmental material of importance, mostly due to its potential for utilization by plants and animals, was studied extensively in IOP, Bhubaneswar, laboratory using this technique. Fly ash is associated with various useful constituents such as Ca, Mg, Mn, Fe, Cu, Zn, Ba, S and P, along with appreciable amounts of toxic elements like Cr, Pb, Hg, Ni, V, As and Ba. The concentration of trace elements in ash is extremely variable and depends on the composition of the parent coal,

conditions during coal combustion, efficiency of emission control devices, etc. Figure 1 is a fly ash spectrum taken with the external PIXE set-up. The study indicates that the PIXE technique with external proton beam could effectively be used for characterization of fly ash with good sample turnover time. Aerosols are another frequently studied environmental material using vacuum PIXE technique. But this technique causes the loss of volatile elements like mercury. Another practical obstacle being the beam current used for aerosol samples in conventional PIXE is usually less, but could be increased by about four times in the case of external PIXE.

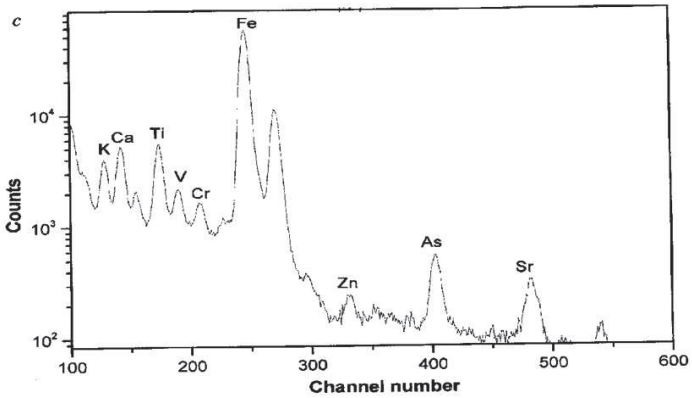


Figure 1: External PIXE Spectrum of Fly Ash, An Environmental Sample.

3.2 Geology: In geochemical explorations, PIXE has been widely used by several workers, which includes pioneering works of CSIRO (Australia) and Schonland research (South Africa) groups on various materials, including diamond. But due to the requirement of large number of samples to be irradiated in order to achieve better statistics, the conventional PIXE technique requires more sample turnover time. Another aspect, which should not be ignored, is the characterization of particular spots of a geological material followed by identification through ore microscopy. Vijayan and his group has reported the use of PIXE and other X-ray techniques on geological materials in finding out the trace elemental ratios, which were used in interpreting the environment of a depositional basin. It is felt that the problem of analyzing big samples could be overcome successfully by the external PIXE technique. Figure 2 is an external PIXE spectrum of soapstone taken using the present set-up at IOP, Bhubaneswar, with no sample preparation procedure. Among other elements, Fe is found to be present dominantly in this sample. We are planning to use the external PIXE set-up to analyze different spots and inclusions observed in geological materials, followed by cross-sectional cutting in order to investigate the distribution of trace elements.

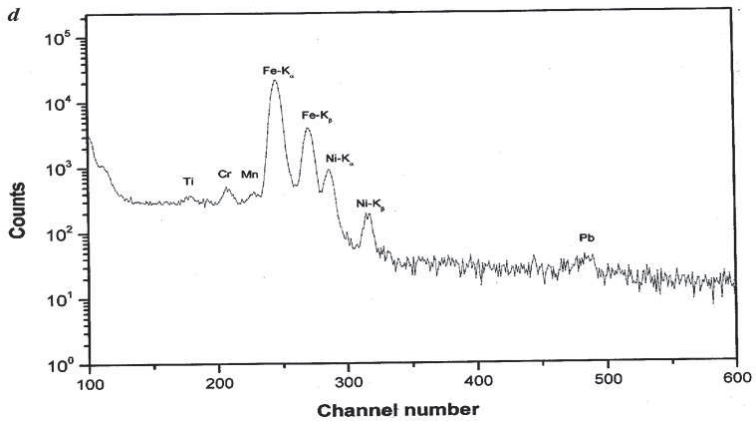


Figure 2: The spectrum of Soapstone studied using External PIXE

A selected number of Eastern Ghats moonstone gems have been studied by our group using complementary and non-destructive PIXE (Proton Induced X-ray Emission) technique. Thirteen elements including V, Co, Ni, Zn, Ga, Ba and Pb were established in these moonstones, which may be useful to interpret the various geochemical conditions and the probable cause of their inceptions in moonstone gemstones matrix. The chemical constituents of moonstones from parts of the Eastern Ghats geological formations of Andhra Pradesh, India and their gemological studies were carried out.

3.3 Biology & Biomedicine:

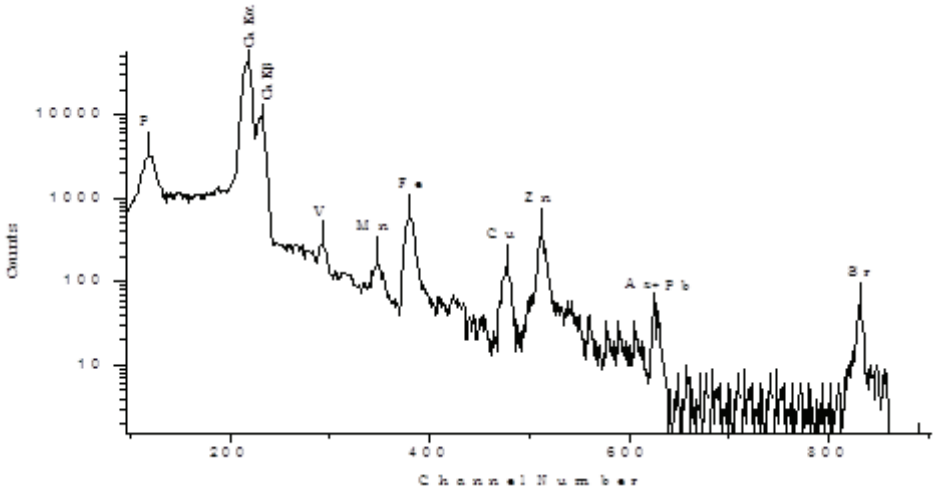


Figure 3: The External PIXE Spectrum of the Dental Cementum Part of a Tooth

The current study is an attempt for the specific detection of trace elemental role on different parts of human teeth and their result on caries regions. In the present study, 12 elements together with trace namely P, V, Ca, Fe, Cu, Mn, Sr, Zn, Ba, As, Pb and Ni were determined. Among the detected elements, Calcium and Phosphorous were found to be the major elements whereas all other elements were found at trace level It is examined that the respective concentrations of Phosphorous, Calcium, Iron, Zinc and Lead elements in enamel are high in quantity than those in cementum and dentine. From the nondestructive elemental analysis on

various parts of the teeth, it was clear that the elemental profile in the carious part of the teeth are badly affected compared with other portions of teeth. The excess and deficiency of these identified elements may also cause the dental carries.

Conclusion: A brief description of the various available analytical techniques that are adopted in georesearch and mineral industry, for getting the information about the elemental concentrations, all major, minor and trace, is presented. Widely used methods are Instrumental Neutron Activation Analysis (INAA), X-ray Fluorescence (XRF), Inductively Coupled Plasma Mass Spectroscopy (ICP-MS), Electron Micro Probe Analysis (EMPA), Atomic Absorption Spectrometry (AAS) and Particle Induced X-ray Emission (PIXE). Some of these methods are destructive, therefore the samples cannot be used for further studies; some of the techniques give information on one element only or require sample preparation before the analysis. In comparison, PIXE has some distinctive features of being non destructive and quick, allowing multi elemental determination and requiring little or no sample preparation.
PIXE is a relatively simple, yet powerful analytical technique that can be used to identify and quantify trace elements in a sample. It is a nuclear analytical technique for rapid analysis of a wide range of trace elements with ppm sensitivity. Due to its high sensitivity, it is used in the fields of geology and geophysics for investigating trace elements in minerals of geological specimens. Use of protons offers a good sensitivity even at lower atomic numbers due to the fact that bremsstralung caused by protons is low compared to the electron excitation. PIXE technique has rapidly gained acceptance as a valuable analytical tool because of the ever-increasing need for the elemental analysis of very small amounts of sample, as in the case of geological materials such as gemstones, precious minerals etc. In the present work we reviewed the various mineral deposits and geological applications of PIXE technique in and around Andhra Pradesh, India. The present study, thus establishes usefulness and versatility of the PIXE technique for research in Geo-scientific methodology.

Acknowledgements: Authors are grateful to the staff members of Ion beam laboratory for their help during the course of the present work. The authors are the College Administration of ANITS & Lendi Institute of Engineering & Technology, Dr.L.B college of Engineering for women and GMRIT for granting necessary permissions and time to undertake this sophisticated work.

References:

1. P. Prati, P. Putti, A. Zucchiatti, F. Lucarelli, P.A. Mando, Nucl. Insr. Meth. B, 1999, 150, 428
2. S.F. Bongiovanni, P. Prati, A. Zucchiatti, F. Lucarelli, P.A. Mando, V. Ariola, C. Bertone, Nucl. Insr. Meth. B, 2000, 161-163 786
3. C. Neelmeijer, I. Brissaud, T. Calligaro, G. Demortier, A. Hautojarvi, M. Mader, L. Martinot, M. Schreiner, T. Tuurnala, G. Weber, , X-Ray spectrometry, 2000, 29, 101-110
4. I. Orlic, S. Zhou, F. Watt, Nucl. Insr. Meth. B 158 (1999) 505

5. Z. Nejedly, J. Kral, J. Voltr, R. Krejci, E. Swietlicki, J. Cerny, P. Kubik, J. Swejda, Nucl. Insr. Meth. B, 1998, 136-138, 981
6. T. Calligaro, J. C. Dran, E. Ioannidou, B. Moignard, L. Pichon, J. Salomon, Int. conf. 1999, IBA 14, ECAART6,
7. M. Kohno, K. Yosida, K. Moritani, K. Norizawa, M. Naito, K. Enami, J. Takada, Int. Journ. PIXE, 2000, pp493, 10
8. H.K. Bandhu, S. Puri, M.L. Garg, B. Singh, J.S. Shahi, D. Mehta, E. Swietlicki, D.K. Dhawan, P.C. Mangal, N. Singh, Nucl. Insr. Meth. B, 2000, 160, 126
9. P.A. Mando, Nucl. Insr. Meth. B, 1994, 85, 815
10. A.K. Rath, G.S. Acharya, V. Vijayan, J. Medical Physics, 1993, 18, 1
11. V.Vijayan, N.Padhy and V.S.Ramamurthy, Ind. Jr. of Physics, 1996, 70A (2) 237
12. V. Vijayan, S. N. Behera, V. S. Ramamurthy, Sanjiv Puri, J. S. Shahi, Nirmal Singh, X-Ray spectrometry, 1997, Vol. 26, pp 65-68
13. R.K.Datta, M.Sudarshan, S.N.Bhattacharyya, V.Vijayan, S.Ghosh, V. Chakravortty and S.N.Chintalapudi, Jr. of Radioanal. and Nucl. Chem.,1997, 221 (1-2), 193.
14. M. Hajivaliei, M.L.Garg, D.K.Handa, K.L.Govil, T.Kakavand, V.Vijayan, K.P.Singh and I.M.Govil, Nucl. Inst. and Methods in Physics Research B 150 (1999) 645.
15. V.J. Kennedy, A. Augusthy, K.M. Varier, P. Magudapathy, S.Panchapakesan, V. Vijayan, K.G.M. Nair, Nucl. Insr. Meth. B, 1999, 150, 277.
16. M.Ashok, S.Narayana Kalkura, V. Vijayan, K.G.M.Nair P.Ramasamy, J. Medical Physics, 2000 25 (4), 205.
17. P.K. Nayak, D. Das, S.N. Chintalapudi, P. Singh, S. Acharya, V. Vijayan, V. Chakravortty, J. Radioanal. Nucl. Chem., 2002, 254 (2)

***

A Cuisine Based Recommender System Using k-NN And Mapreduce Approach

Sadhana Kodali, Madhavi Dabbiru, B Thirumala Rao

Abstract*: *In the present days, life can be made smarter, including the food we eat by taking an option from the restaurant recommender systems. In this paper the authors proposed a restaurant recommender system based on the search of user cuisine. The top-k restaurants are identified along with the ratings of the restaurants recommended. The recommendations are retrieved based on the preference of the user cuisines which is an important category which inherently defines the other features and these features are considered to provide a good service which is the novelty of this paper. Providing recommendations based on user cuisines is the complexity of the problem. The well known k-Nearest Neighbor algorithm is implemented with the MapReduce paradigm which can quickly process huge amounts of data. Its performance is tested on benchmarked data set and the results are found to be successful.

Index Terms*: *Restaurant Recommender System, Nearest Neighbor approach, MapReduce, Cuisine based search.

I. INTRODUCTION

In this world of competition it is essential to be healthy and choose proper food to eat by making use of the improved resources that we have around us. The various search engines provide a set of restaurants that are suitable to us but they do not focus on food specific search. In this paper we propose a restaurant recommender system where the user can get the restaurants based on his taste and he can also have a list of restaurants that provide the food including the ratings of the restaurants which provide a better option for the user to choose. We classify the restaurants based on user specific food by making use of the well known kNN algorithm. This also helps to a group of users who have the same food habits to get good recommendations based on the similarity. This may be helpful to have good, happy and tasty get together where all the group of people have the same savour. With the use of internet and promotion in websites many restaurants data are available which has a great need of good restaurant recommendation system that filters and promotes good suggestion for tasty food. The proposed approach is an application of Machine learning based classification to classify the restaurant.

Revised Manuscript Received on May 10, 2019

Sadhana Kodali, Ph.D Scholar,Department of CSE, Koneru Lakshmaiah Education Foundation,Vaddeswaram, Guntur Dt, AndhraPradesh, India.
Madhavi Dabbiru , Professor&Head , Department of Computer Science Engineering, Dr.L.Bullayya College of Engineering for Women,Visakhapatnam, AndhraPradesh, India.
Thirumala Rao B, Professor,Department of CSE, Koneru Lakshmaiah Education Foundation,Vaddeswaram, Guntur Dt, AndhraPradesh, India.

The food- restaurant-customer form a kind of semantic network where multiple paths can be used to traverse different semantic relationships like: identifying food of same or different type, customers of same age, taste, restaurants of same or different ratings which are nothing but various Meta paths in the Information Network. Information Networks can be classified as Homogeneous Information Networks where objects interact with similar kind of links and Heterogeneous Information Networks[1] where different kind of objects communicate with various semantically interconnecting links. A heterogeneous network can contain a homogeneous network within it. If the homogeneous network formed between food and person is considered the meaningful relationship established is “Person eats Food”. From Figure 1 we can observe that a person may be male, female or children. Food can be of any kind burgers,pizzas,fries etc.But the meaningful interaction among person and food is “eats” which is a link between these objects.



Fig 1: Homogeneous Network formed between person and food.

Figure 2 depicts a heterogeneous network formed between customer-food-restaurant. Different semantic Meta-paths can be formed between the objects shown in figure-2 Example Meta-path:
Customer—visits—restaurant—has a type of—food

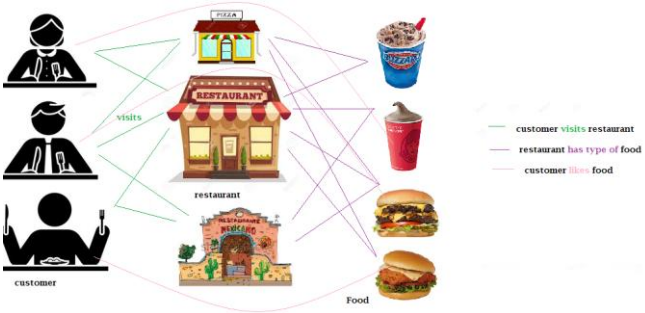


Fig-2: customer-restaurant-Food Network

Published By:
Blue Eyes Intelligence Engineering
& Sciences Publication

In order to predict the semantic relationship between the objects in the Information Networks, it is significant to compute the similarity between the objects. Many Similarity algorithms are proposed to compute the similarity between objects present in Information Networks.

With the increase of data automation and the World Wide Web we have heterogeneous Information Networks identified in every field like social media, medical databases data, paper-author network etc. Also with heap of information flow in the network a number of traditional Data Mining techniques like clustering, classification, link prediction etc. are suitable and can be applied on the data present in the Information network. In the past few years Heterogeneous Information Networks has a wide spread applications like finding friends on social networks, link prediction, recommendation of products, food and friends. Apart from applying the Data Mining techniques, similarity measure can also be used to compute the similarity between the objects present in the Information Network. Similarity measure is a statistical measure used in DataMining to compute the likeliness between the objects which communicate with each other. The key factor in the recommender systems is to compute the similarity to compare two items that are closer to each other. In this paper the authors proposed restaurant recommender system based on the user cuisine and also provide the related restaurants which are suitable to the cuisine of the customer, the price of the food in a sorted order and also the distance from the current location of the customer. The paper is organized as follows: In Section 2 the related work is discussed, Section 3 focuses on the Methodology adopted, Section 4 showcase experimental results, Section 5 concludes with future scope and research perspective.

II. Related Work

Recommender systems are more prominent with the increase in usage of web and work on the machine learning principle of learning about the Neighbors for better solution. Recommender systems are classified as collaborative filtering models which are also called as Neighborhood models [2], the second approach is content based filtering also called as knowledge based models and the combination of the former and the later is the hybrid model. With the growing data it is a good option to make use of the MapReduce paradigm for processing the data parallelly. In [3] the authors proposed the user based collaborative filtering recommender algorithm using Hadoop MapReduce. On the similar lines content based recommender systems is proposed in [4].The methodology proposed in [5] is a novel approach of using Bhattacharya coefficient for collaborative filtering in sparse data. Chenyang Li and Kejing He [6] proposed an item based collaborative filtering using MapReduce. Though there are many MapReduce based recommenders proposed, applying kNN with MapReduce is a new idea for identifying the nearest Neighbors of the nominal attributes. In [7] Moon-hee Park et al proposed a restaurant recommender systems based on decision made by group of people in mobile environment using Bayesian Networks to model the preference of the users.

Similarity measure is used to measure the likeness between the objects and their interaction. Many similarity algorithms are proposed to analyze the Information Networks. The similarity algorithms are useful for the prediction of links in the heterogeneous information networks and also to detect duplicate web documents. SimRank [8] is a similarity measure proposed based on random surfers' model. It is mainly used for ranking the web documents. PRank [9] is another similarity algorithm which uses unified framework for computing the similarity. PathSim [10] is a similarity measure which uses a commuting matrix. HeteSim [11] makes use of transition probability matrix.

III. Methodology

In this section we discuss about various terminologies like the Meta-Paths which are formed between the heterogeneous objects. Next we also discuss the algorithm for calculating the similarity between the heterogeneous objects using PathSim measure. A Meta-path is a semantic path that exists between the objects. For example for this food chain network which can be treated as a heterogeneous network we consider three different kinds of objects like user, restaurant and cuisine. Though these are of different kind, now they communicate with each other by the following relationships: uservisitsrestaurant, restaurantofferscuisine, cuisineliked byuser

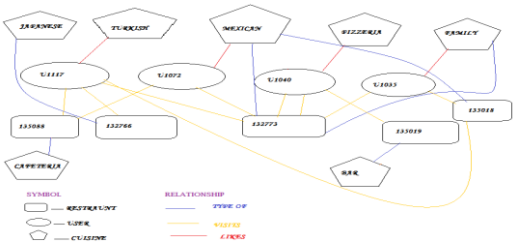


Fig-3: Meta-Path between user-restaurant-cuisine

We have considered the food data set and tried to retrieve the similarity scores for each user, the places they visit and the food they eat. There are many approaches to calculate the similarity but we have chosen the PathSim similarity score as it exhibits properties like [i] symmetric property [ii]self maximum property [iii] Balance of visibility. The PathSim is a meta-path based approach to compute the similarity. According to PathSim, an adjacency matrix must be constructed between these objects to find how one object is similar to another. Instead of an adjacency matrix we build a commuting matrix which is proposed in [12].But any Information Network is huge of its kind as there are number of objects that interact with each other.

When we need to deal with huge datasets which forms the BigData we can make use of the MapReduce strategy which takes the <key,value> pairs as input and produces the output as <key,value> pairs. HDFS (Hadoop Distributed File System) works with Map Reduce to divide the data for parallel processing. The Input files are split into input format, Splits the files into tasks, provides a place for RecordReader Object. The input format defines the list of tasks that forms the Map phase. The Record Reader loads the data and converts into <Key, Value> pairs. The Mappers with the <key, Value> pairs sends these to the reducers. The process of moving the Map output to the Reducers is known as Shuffling. Partitions are the inputs to the Reduce task. Partitioners in Reduce phase identify which are the key value pairs that are stored and reduced. An instance of reducer is created for each Reduce task to create an output format. The Output format governs the way objects are written to the files in HDFS. The Figure 4 represents the Map Reduce procedure.

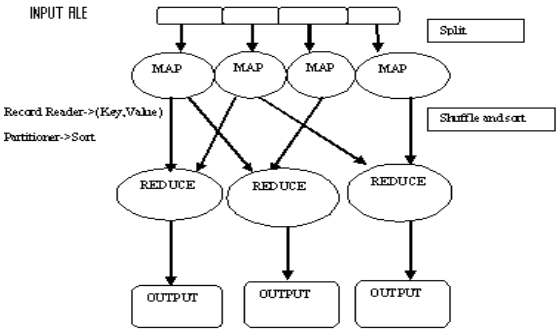


Fig4 Map Reduce Phases

To proceed with, the overall ratings file is given as an input to get the unique location id as the key which is visited by the set of users as value. By considering each row a new Meta-path can be constructed by using the matrix. From the first line of the MapReduce output, it is understood that there are four users (U1067,U1082,U1087,U1050) who visit the place id 132560.By traversing all the other places visited by these four users we get an commuting matrix between the users and places is depicted in figure-4.

User-id Place-id	U1067	U1082	U1087	U1050
132560	1	1	1	1
132584	1			1
132630	1	1		
132733	1	1		
135104	1			
132663		1	1	
132732		1		
132740			1	1
132594				1
132608				1
132609				1
132068				1

Fig 5: Adjacency Matrix for user and place.

Figure 5 depicts the commuting matrix between the user-id and the restaurant-id. A '1' represents the user visits the place and an empty gap represents that he did not visit the place. From this commuting matrix we can compute the similarity between two users using the formula

$$S(x:y)=2(P_{x->y} : P_{x->y}\mathcal{E}P) / | (P_{x->x} : P_{x->x}\mathcal{E}P)+ |(P_{y->y} : P_{y->y}\mathcal{E}P)| \quad ..Eqn(1)$$

This can be computed as follows for the above example:

Similarity (U1067, U1082) =A/B =0.666

A = 2[(1X1)+(1X0)+(1X1)+(1X1)+(1X0)+(0X1)+(0X1)]

B = [(1+1+1+1+1) + (1+1+1+1+1)]

Similarity (U1067, U1087) =0.25

Similarity (U1067, U1050) =0.166

Similarity (U1082, U1087) =0.25

Similarity (U1087, U1050) =0.4

Similarity (U1082, U1050) =0.0571

In the same way we can also compute the similarity between the restaurant and the cuisine it provides. After doing this we get a Meta-Path between the user-restaurant-cuisine. The figure 6 depicts the commuting matrix formed between the restaurant id and the cuisine offered in the restaurant.

Type-of-food place-id	Mexican	Regional	pizzeria	Fast-food
132630	1			
132560		1		
132732	1			
132733			1	
132663	1			
132594	1			
132740	1			
132608	1			
132609				1

Fig 6: Commuting Matrix between cuisine and restaurant-id.

Once we obtain the commuting matrix we can calculate the similarity between the heterogeneous objects using the Algorithm-1 as follows:

Algorithm to find the similarity of Meta-paths between the heterogeneous objects

Step 1:Input X
Step 2: Construct the commuting matrix.
Step 3: for all
Apply the PathSim similarity measure using Eqn 1.
$S(x:y)=2(P_{x->y} : P_{x->y}\mathcal{E}P) / | (P_{x->x} : P_{x->x}\mathcal{E}P)+ |(P_{y->y} : P_{y->y}\mathcal{E}P)|$

Algorithm-1: To compute the similarity between the heterogeneous objects.

The Figure-7 represents the Input file X on which the first MapReduce task is run to get the list of unique restaurant ids, the file will also provide you the list of user ids and the ratings given by them.

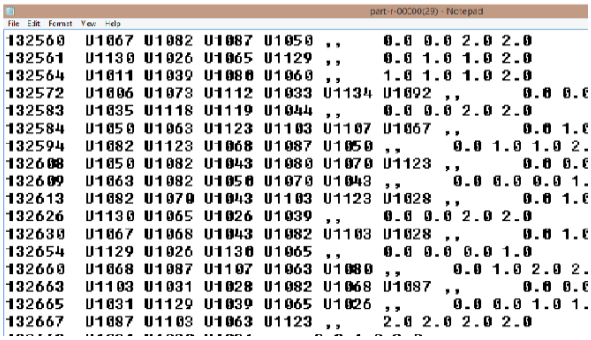


Fig-7: Snapshot of Input File obtained after running the MapReduce

The algorithm to write the first phase of MapReduce before data pre-processing is as follows:

MapReduce paradigm is a parallel approach for processing huge data in the distributed platform. We use Hadoop Distributed File System for the storage of the dataset and implement the MapReduce which takes the <key,value > pair as input and gives the <key,value> pair as output.

Every record id in the document is given as a key and each line is given as input value. After the MapReduce task is completed we get the place id as key and the list of users and their corresponding ratings as value.

Algorithm: MapReduce to retrieve the list of restaurant ids and userids who visit the restaurant.

Step 1:Input Ratings_final.csv file
L is the LongWritable address of each line, Line of text which contains userid and restaurant id.
Step 2: The Map() function
for all(L,Line of Text)
split(",") and tokenize each restaurant id assign it to data[0]
each user_id assign it to data[1]

Step 3: context.write(data[0]+data[1],ratings)
Step 4:end for.
Step 5:The Reduce() function
Step 6:for all<list of values>
Step 7:Use Comparator to sort the ratings
Step 8:end for
Step 9:context.write(<key,Value>);

Algorithm-2: To prepare the input file from raw dataset.

The main aim of the authors is to classify the restaurants using the well known algorithm kNN with the MapReduce flavour. Using the kNN we identify the nearest Neighbor to classify the restaurants based on which cuisine most of its users are likely to eat in that restaurant.

k-NN algorithm is a distance based classification algorithm which assigns a class label of an unknown case to its nearest Neighbor. Distance metrics like Euclidean, cosine and Manhattan distances can be used for each Neighbor if it is a continuous attribute. The Euclidean distance is used in the case of continuous variables but with nominal variables we use the Hamming Distance. The cuisine op distance can be stated as dist (hamming) =$|obj_i\text{-}obj_j|$.-Eqn2.
As an example if the user U1067 prefers Mexican dish and U1082 also prefers Mexican then the Hamming Distance between U1067 and U1082 is zero. Else if U1082 prefers Chinese to Mexican it is one. The Algorithm 3 as mentioned below does the classification.

Algorithm: MapReduce to classify the list of restaurant ids and based on user cuisine.

Step 1:Pre-processed Input file X
Step 2: The Map() function
for all(L,Line of Text)
split(",") and tokenize each restraunt id as Text s[0];
each user_id as Text s[1];
Assign the user_id to a HashMap
Calculate the Hamming Distance by using if map.containsKey();
While(itr.hasnext())
int val=map.get(ky);
int max=0;
String str="";
If(val>max)
max=val;
Str=ky;
Step 3: context.write(s[0],str)
Step 4:end for.
Step 5:The Reduce() function
Step 6:for all<list of values>
Step 7:context.write(<key,Value>);

Algorithm-3: To classify the restaurants.

IV. EXPERIMENTAL RESULTS

The experiment is conducted on a single node with 8 GB RAM, 500GB HDD, intel core i3 processor with a speed of 2.86 GHz. The average runtime of all the records in the file turned to be 3.59Milli-seconds. Hadoop is installed in pseudo distributed mode. The input is stored onto HDFS as input file. The input file consists of the restaurant id as the first field with a tab separated space and the user-ids and the cuisine they are interested in using comma separated values.

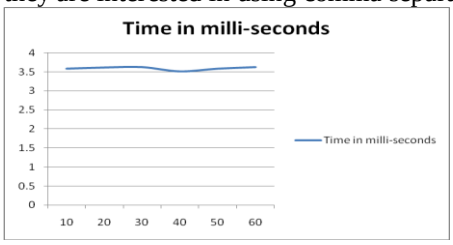


Fig- 8: Graph showing no. of records and run time

4.1 Description of data Set

The data set is taken from the UCI Machine Learning repository from the DataFolder with the URL https://archive.ics.uci.edu/ml/datasets/Restaurant//consume data.The raw data set contains 1161 instances. The first column gives the user_id the second column provides the restaurant_id and three kinds of ratings are provided column three specifies the overall rating column five and six provide the food and service rating respectively. The cuisines offered by the restaurants are 59 but of which we classify the restaurant on the maximum savour of the users who visit the restaurant.



Fig-9: Famous cuisines offered by the number of restaurants

The figure-9 represents the graph in which we can understand that the Mexican is the most famous cuisine offered by 239 restaurants and the classification results also agree with this fact.

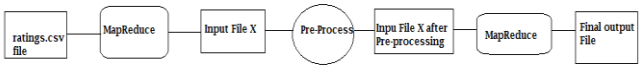


Fig-10: Steps applied to experiment

From the figure-10 the procedure adopted to get the restaurants classified is depicted. The Data pre-processing is done by identifying which user_id will order which cuisine and replaced with that particular cuisine. The empty values are eliminated and the data cleaning is done. The refined and processed file is given as input to the second phase of MapReduce.

The Restaurant Recommender application is developed by the authors and we can view user interface shown in figure 11.

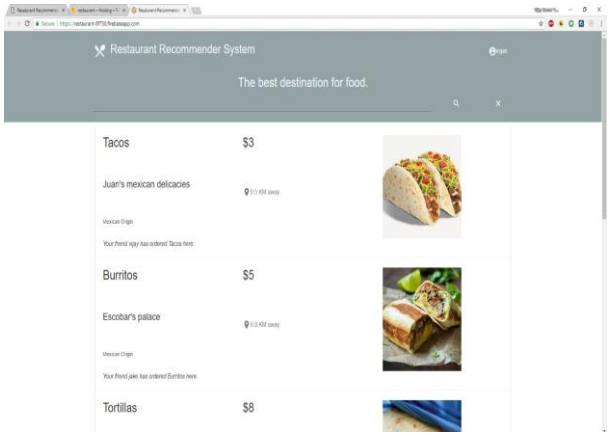


Fig- 11: User Interface of Restaurant recommender system

The predicted top-k recommendations given by the Recommender system are evaluated and shown in figure 11. The classification accuracy is calculated using the formula given below.

Accuracy = (No of correctly predicted Records)

Total No of Records.

Predicted Top-k	Accuracy
Top-3	100%
Top-4	95.38%
Top-5	76.15%

Fig10: Accuracy table

V. CONCLUSION

The restaurant recommender system based on cuisine search is developed based on kNN based MapReduce approach. This can be useful to individual users. The methodology proposed may be useful to any person who visits an unknown place and can be helpful to identify the best restaurants of his or her choice. The use of MapReduce in our paper is a novel idea because huge records can be processed with few milli-seconds. The choice of k-NN makes use of the machine learning concept to identify the nearest Neighbors. In the future, the paper can be extended to group users.

REFERENCES

1. Chuan Shi, Yitong Li, Jiawei Zhang, Yizhou Sun, and Philip S. Yu, "A Survey of Heterogeneous Information Network Analysis", IEEE Transactions on Knowledge and Data Engineering , Volume: 29, Issue: 1, Jan. 2017.
2. C.C. Aggarwal, *Recommender Systems: The Textbook*, Springer International Publishing Switzerland 2016.
3. Zhi-Dan Zhao, Ming-Sheng Shang, "User-based Collaborative-Filtering Recommendation Algorithms on Hadoop" Third International Conference on Knowledge Discovery and Data Mining 2010.
4. Anjali Gautam and Punam Bedi, "Developing content-based recommender system using Hadoop Map Reduce", Journal of Intelligent & Fuzzy Systems 32 (2017) 2997–3008, 2017.
5. Bidyut Kr. Patra, Raimo Launonen, Ville Ollikainen, Sukumar Nandi, "A new similarity measure using Bhattacharyya coefficient for collaborative filtering in sparse data", KNOSYS 3090, 12 March 2015.
6. Chenyang Li Kejing He "CBMR: An optimized MapReduce for item-based collaborative filtering recommendation algorithm with empirical analysis", Concurrency and computation Practice and experience Volume 29, Issue10 25 May 2017.
7. Moon-Hee Park, Han-Saem Park, and Sung-Bae Cho "Restaurant Recommendation for Group of People in Mobile Environments Using Probabilistic Multi-criteria Decision Making", APCHI 2008, LNCS 5068, pp. 114–122, 2008.
8. Glen Jeh, Jennifer Widom,"SimRank: A measure of Structural-Context similarity" in KDD, pp. 538–543, 2002.
9. Peixiang Zhao, Jiawei Han, Yizhou Sun," P-Rank: a Comprehensive Structural Similarity Measure over Information Networks". CIKM'09, Hong Kong, China. November 2–6, 2009.
10. Yizhou Sun, Jiawei Han, Xifeng Yan, Philip S. Yu, Tianyi Wu, "PathSim: Meta path Based TopK Similarity Search in Heterogeneous Information Networks" *Proceedings of the VLDB Endowment,* Vol. 4, No. 11 2011.
11. C. Shi, X. Kong, Y. Huang, S. Y. Philip, and B. Wu, "HeteSim:A general framework for relevance measure in heterogeneous networks" , IEEE Transactions on Knowledge & Data Engineering, vol. 26, no. 10, pp. 2479–2492, 2014.
12. Sadhana Kodali, Madhavi Dabbiru, Kamalakar Meduri,"Constraint based approach for minging Heterogeneous Information Networks", 6th IEEE IACC 2016, 27th -28th February 2016.

A Survey Paper on Sentiment Analysis : Approches, Methods & Challenges

Dr.K.Anuradha[1], Dr.M.Vamsi Krishna[2], Dr.Banitamani Mallik[3],Prof.B.P.Mishra[4]

1. Research Scholar, Centurion University of Technology & Management, Odisha and Assistant Professor, Dr. L. B. College of Engineering for women, Visakhapatnam.
2. Principal, Chaitanya Institute of Science & Technology, Kakinada
3. Associate Professor, Centurion University of Technology & Management , Odisha
4. Director, (R&D), GITA, Bhuvaneswar, Odisha

1. *Abstract*

Sentiment Analysis is the domain of understanding these emotions with software, and it's a must-understand for developers and business leaders in a modern workplace. As with many other fields, advances in Deep Learning have brought Sentiment Analysis into the foreground of cutting-edge algorithms. Today we use natural language processing, statistics, and text analysis to extract, and identify the sentiment of text into positive, negative, or neutral categories. In this paper, an attempt is made to give an overview of different methods available for sentiment analysis, along with different approaches, challenges in sentiment analysis

Keywords: Sentiment Analysis, Data Mining, SVM, Deep Learning Algorithms

2. *Introduction*

Sentiment Analysis or Opinion Mining is a type of contextual mining for text, which identifies and extracts subjective information in source material, and also helps a business to understand the social sentiment of their brand, product or service while monitoring online comments or feedback. However, analysis of social media streams is usually restricted to just basic sentiment analysis and count based metrics. This is just scratching the surface and missing out on those high value insights that are waiting to be discovered. So what should a brand do to capture that low hanging fruit?

With the recent advances in deep learning, the ability of algorithms to analyze text has improved considerably. Creative use of advanced artificial intelligence techniques can be an effective tool for doing in-depth research. We believe it is important to classify incoming customer conversation about a brand based on what are the key aspects pertaining to that brand and what are the reactions and intentions concerning these aspects.

The online medium has become a significant way for people to express their opinion and with social media; there is an abundance of opinion information available. There are more than a hundred websites such as Facebook, Twitter, LinkedIn and Youtube offering a range of services for users who depend on the networks for sharing their interests, photos, videos and blogs. However, the main purpose of online social networks is sharing information. According to the ranking from ebizMBA in January2019, top 10 social networking sites are shown in below table [4].

Table 1

S.NO	WEBSITE	NO OF USERS
1	facebook	1,500,000,000
2	YouTube	1,499,000,000
3	Twitter	3 400,000,000
4	Instagram	275,000,000
5	LinkedIn	250,000,000
6	Reddit	125,000,000
7	VK	120,000,000
8	Tumblr	110,000,000
9	Pinterest	105,000,000
10	Google Plus	100,000,000

3. ***Sentiment Analysis***: This is one of the most common text classification tool which analyses an incoming message and tell whether the underlying sentiment is positive, negative our neutral.

Sentiment Analysis can be used to determine sentiment on a variety of level. It will score the entire document as positive or negative, and it will also score the reaction of individual words or phrases in

the document. Sentiment analysis can track a particular topic, many companies use it to track or observe their products, services or status in general. For Example, if someone is attacking your brand on social media, sentiment analysis will score the post as enormously score negative, and you can create alerts for posts with hyper negative sentiment scores. [3]

Intent Analysis: This analysis steps up the game by analyzing the user's intention behind a message and identifying whether it relates an opinion, news, marketing, complaint, suggestion, appreciation or query.Intent analysis basically detects what people want to do with a text rather than what people say with that text. Look at the following examples:

- "Your customer support is a disaster. I've been on hold for 20 minutes".
- "I would like to know how to replace the cartridge".
- "Can you help me fill out this form?"

A human being has no problems detecting the complaint in the first text, the question in the second text, and the request in the third text. However, machines can have some problems to identify those. Sometimes, the intended action can be inferred from the text, but sometimes, inferring it requires some contextual knowledge.

Contextual Semantic Search(CSS): This is one of the interesting approaches. To derive actionable insights, it is important to understand what aspect of the brand a user is discussing about. For example: Amazon would want to segregate messages that are related to: late deliveries, billing issues, promotion related queries, product reviews etc. On the other hand, Starbucks would want to classify messages based on whether they relate to staff behavior, new coffee flavors, hygiene feedback, online orders, store name and location etc.

We introduce an intelligent smart search algorithm called Contextual Semantic Search (a.k.a. CSS). The way CSS works is that it takes thousands of messages and a concept (like Price) as input and filters all the messages that closely match with the given concept. The graphic shown below demonstrates how CSS represents a major improvement over existing methods used by the industry.

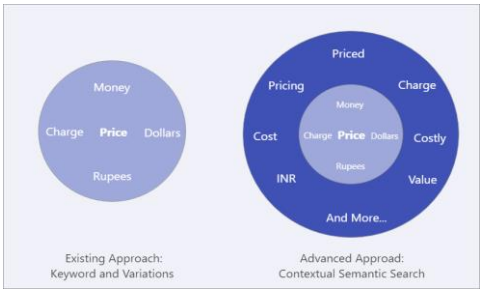


Figure 1. Existing approach vs Contextual Semantic Search

A conventional approach for filtering all Price related messages is to do a keyword search on Price and other closely related words like (pricing, charge, $, paid). This method however is not very effective as it is almost impossible to think of all the relevant keywords and their variants that represent a particular concept. CSS on the other hand just takes the name of the concept (Price) as input and filters all the contextually similar even where the obvious variants of the concept keyword are not mentioned.

For the curious people, we would like to give a glimpse of how this works. An AI technique is used to convert every word into a specific point in the hyperspace and the distance between these points is used to identify messages where the context is similar to the concept we are exploring. A visualization of how this looks under the hood can be seen below:

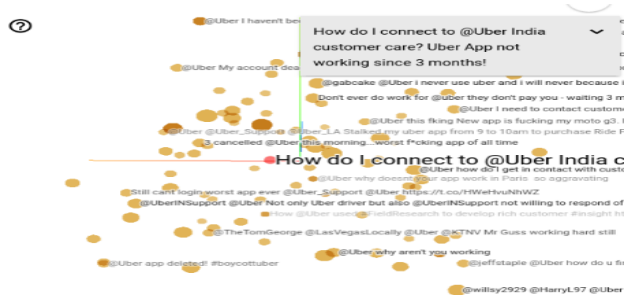


Figure 2. Visualizing contextually related Tweets

4. Scope of sentiment analysis

Sentiment analysis can be applied at different levels of scope by breaking the document into its basic grammatical level. Now some sentiment-bearing phrases such as "Worst-service" are identified using specially designed algorithm. Eachsentiment-bearing phrase is given a score based on a logarithmic scale between -10 and 10. Finally, the scores are summed up tocalculate the overall sentiment of the document or sentence. The scores of the document range between -2 and 2. Most of the researchers have mainly classified the study of sentiment analysis into three basic levels of granularity. [2]

- Document level sentiment analysis obtains the sentiment of a complete document or paragraph. The major hindrance in this level is that the useful insights are hidden so that the clients cannot extract useful information. [1]

- Sentence level sentiment analysis obtains the sentiment of a single sentence .Here, the sentences related to factual information are separated from the sentences related to subjective views and opinions. [5] Then the opinionated sentences are expressed as either positive or negative opinion, which is called sentiment classification. In this we have three-classification problem, that is, to classify a sentence as positive, negative or neutral.
- Sub-sentence level sentiment analysis obtains the sentiment of sub-expressions within a sentence. This can be broadly specified as the fine graining when compared to both the earlier approaches i.e. Document Level and Sentence level. The main goal of this level is to target the features of entities which are called as targets. [6] The aspect level analysis involves few steps which are aspect extraction, entity extraction, and aspect sentiment classification. For example, from the sentence, "At Novotel the food quality is good, but the service is worst", entity extraction should identify "Novotel" as the entity and aspect extraction must identify the "food quality" and "the service" as the two aspects. Aspect classification should classify the sentiment expressed on the "food quality" and "the service" as "positive" and "negative".

5. *Overview of Text Mining and Analytics*

Since an enormous amount of data has emerged over the years at a staggering rate, there is a need to incorporate some sort of analytics to gain meaningful insights from the raw and unstructured data in the form of text, images, and videos. Text mining is one of the approaches that are the predecessors to text analytics. Text mining uses natural language processing, knowledge management, data mining, and machine learning techniques to process text documents [8]. Text analytics, while similar to text mining in terms of method, usually deal with a bigger amount of data to extract and generate useful non-trivial information and knowledge [9].

Text mining/analytics are originally conducted for two purposes. The first purpose is to analyze people's sentiment on an issue or phenomenon. Hence, sentiment analysis goes through a huge amount of textual data to identify people's attitudes, thoughts, judgments, and emotions on an issue [10], [11]. The second purpose is to assess people's opinion on a product, person, event, organization, or topic from a user or group of user perspectives. Similar to sentiment analysis, opinion mining is a natural language processing task that employs an algorithmic technique to recognize opinionated content and categorize it into positive, negative, or neutral polarity [12]. Nonetheless, the application of text mining/analytics has been extended to other areas of human computer applications, and the applications are growing with the growth in big data analytics.

6. *Overview of Opinion Mining and Sentiment Analysis*

An opinion refers to a person's or group's sentiment or views, emotions, and attitudes about a product, service, occasion, or other topic present in the environment. Like sentiment analysis, opinion mining is also grounded on the algorithmic technique [12]. Covering a huge variety of pubic opinions, [13] have argued that opinion can be classified into three main types: regular opinions, which refer to a single entity only; comparative opinions, which compare or contrast more than one entity; and suggestive opinions, which suggest a single or multiple entities. The regular opinion is mainly used to identify a positive or negative outlook of a particular product [14]. On the other hand, comparative opinions help in elucidating the association among multiple entities and are mainly used for competitive intelligence [14]. However, there is a dearth of literature concerning the identification of comparative sentences that is being used for the comparison of multiple entities. Recently, suggestive review has been introduced in the field of opinion mining [15]. The extraction of these types of opinions from text can be utilized for various application areas in the field of business, engineering, medical science, and e-learning. It can be offered to various online communities for their assistance as well [13].

Similarly, private statements of individuals are called sentiments, which comprise thoughts, opinions, attitudes, views, judgments, and feelings. These are commonly gathered by conventional scientific methods [10], [11]. [16] Pronounced the feelings that are expressed in language by using subjective expression. The sentiments can be analyzed through the machine learning technique, which can be further classified into supervised and unsupervised, using a lexicon-based approach, using a keyword, and using a concept-based technique [17]. Recently, research on sentiment analysis has focused on multiple modalities such as in speech and video as opposed to earlier work that focused on unimodality related to text [18], [19]. Sentiment analysis tackles many NLP

subtasks, including aspect extraction [20], subjectivity detection [21], named entity recognition, and sarcasm detection [22].

In most cases, the main objective of sentiment analysis is to unearth people's opinions to gain meaningful insight about products or services. Its aim is to exhibit useful information to both customers and manufacturers. It is established that both manufacturer and customers look upon summarized opinions instead of detailed reviews. Hence the opinions that are categorized on positive, negative, or neutral sentiments are useful for both parties in making the right call [23]. Despite the large number of studies on opinion mining and sentiment analysis techniques, the impact they have on people has been less explored. There has been great emphasis on the techniques used and less on how people can benefit from the findings. Hence, this study aims to investigate the human element in opinion mining and sentiment analysis research. To achieve this aim, we will systematically review the relevant literatures that have employed both approaches.

The study offers several contributions. The first and foremost significance of this study is to refocus the study of opinion mining and sentiment analysis to both technical and non-technical challenges. Secondly, it places emphasis on the areas of opportunity by looking at the trends of application coverage that would offer some potential areas for research. Thirdly, the paper presents information on different datasets that were used in opinion mining and sentiment analysis studies that future researchers could use in their research.

7. *Review of Opinion Mining and Sentiment analysis*

Literature reviews are rooted in medical science, which has been categorized as a critical approach mainly applied where evidence is important [24]. They involve a stringent process of finding, selecting, and examining secondary data [25], [26]. The synthesis of evidence from the current literature can create new knowledge in the current studies, which is as significant as conducting new research [27].

Rousseau et al. [28] maintained an argument that systematic reviews are different from tradition reviews in that systematic literature reviews are comprehensive in nature, use transparent and unbiased analysis, and apply certain criteria for interpretation of the findings that provided in the previous literature. In addition, systematic literature reviews mainly focus on objectivity and reproducibility of results [26]. The process of review starts with framing the questions and conducting a systematic and step-by-step process and applying a replicable method to answer these questions [26]. Thus, the evidence generated from the rigorous approach of identifying, selecting, and analyzing the data can have a significant impact on the body of knowledge collected, but the supreme concern of this practice is synthesizing the results produced through this systematic process [25], [26].

The methodology used in the study is a five-step process shown in Figure 3, as proposed by [25]. It is systematic in nature, clear and reproducible, and involves identifying, examining, synthesizing, deducing, and reporting the evidence from the existing sentiment analysis and opinion mining literature.

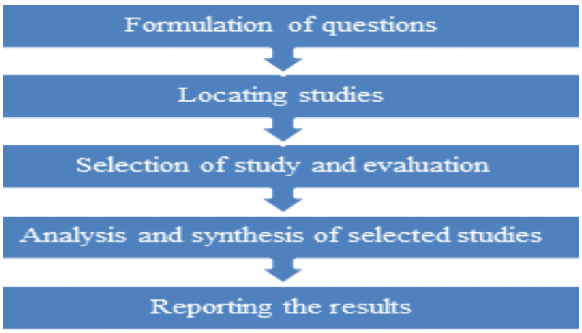


Figure 3. Research methodology of systematic literature review

A. *Question Formulation*

A deep and insightful literature review should start with the development of a clear understanding about your objectives [27]. Therefore, to ascertain this, we clearly formulated and considered research questions to evade doubts in our study [28]. The purpose of the paper is to discuss the methodological and application side of opinion mining and sentiment analysis and explore whether the intervention of opinion mining and sentiment analysis would be applicable to humans or in an organization as a whole. Hence the purpose of our systematic review is to answer two research questions:

1. What are the trends of opinion mining and sentiment analysis publication from 2000–2018?
2. Which are the areas in which opinion mining and sentiment analysis have been applied?
3. What are the sources of data in the areas in which opinion mining and sentiment analysis have been applied?

B. *Locating Studies*

The objective of identifying an appropriate journal articles is to develop a list of all related articles to our research questions. We have selected Web of Science as a core database. The study has only focused on peer-reviewed articles that were written in English and published in the Web of Science Journal category. The study did not consider articles in other categories like conference proceeding papers, book chapters, review papers, and theses.

Since the study is based on opinion mining and sentiment analysis, we used different strings to identify relevant papers. The researcher employed different techniques for searching, including separate keywords for "sentiment analysis" and "opinion mining", combining two keywords at the same time through simple operators and Boolean logic. For example, we used the string "opinion mining" and "sentiment analysis" for exploring the papers containing the exact phrases "opinion mining" and "sentiment analysis."

C. Study Selection and Evaluation

In order to ensure and maintain the quality of the paper, we have constrained our selection of articles to only peer-reviewed journals. Peer-reviewed journals have strict quality control and have gone through systematic, rigorous processes and have stringent requirements for publication, which leads to better research output [27]. The process began with scanning of selected articles from the Web of Science database. The timeline we set was from the years 2000 to 2018. The initial criterion of selection was based on choosing the keywords "opinion mining" and "sentiment analysis."

We have further followed the criteria suggested by [29] for the inclusion and exclusion of the articles from the selected list. Basically, we have developed the inclusion criterion as follows:

- Published in peer-reviewed journals
- Within the database of the last 17 years (2001 to 2018).
- In the English language
- Containing at least one keyword

The exclusion criteria are as follows:

- Have very narrow horizon or context
- Do not explicitly focus on application side (human or organizational level) of opinion mining and sentiment analysis

Our search resulted in an initial list of 274 articles for sentiment analysis and 91 articles for opinion mining. Thus, the preliminary results provided a total of 365 articles that were written on opinion mining and sentiment analysis.

The next step involved reading the abstracts to evaluate whether it was relevant to our research topic. Initially a single person read it, but to warrant its rigor, an independent person to improve its objectivity and validity read the same number of articles. Scholarly outputs that did not align with our developed research questions or that seemed irrelevant and non-substantive were excluded. The articles that were included exhibited good fit with the objective of the study. Thus, a total of 99 articles were shortlisted based on the initial evaluation.

In the next step, two authors reviewed the pre-selected articles separately. The total number of peer-reviewed journal papers selected for critical reviews after rigorous assessment were 58, published over a period of 17 years. The selected papers were then examined in detail and synthesized to answer the research questions.

8. Methods for Sentiment Analysis

In this section we discuss the general process for sentiment analysis. A common process of sentiment analysis loop starts with goal setting for employing the sentiment analysis. This depends on the application of sentiment analysis, and then big data is extracted either from a single or multiple sources. The next step is the application of specific sentiment analysis methods in order to mine this huge data and get insight into the company in making final decisions regarding their products.

A. *Keyword-Based Classification*

This method classifies text based on the presence of positive or negative polarity words such as happy, joyful, delighted, miserable, sad, terrified, and uninterested [30]. The main drawback of keyword-based classification is the inability to steadfastly classify the negated words and polarity, as this approach depends on surface features [30]. Another drawback is that this approach is based on the obvious presence of positive or negative polarity. However, occasionally, a post may covey sentiment or opinion through underlying meaning rather that obvious polarity words [30].

B. *Lexicon-Based Classification*

Lexicon-based approaches construct lists of words manually labeled as having positive and negative polarity, and a polarity score for each word is created. This constructed lexicon is used to calculate the overall sentiment score of a given post or text. The

notable advantage of the lexicon-based method is that these methods do not need training data (as the supervised machine-learning method does). The lexicon-based method is widely used in conventional text like reviews, forums, and blogs [31], [32]. However, they are less likely to be used for big data extracted from social media websites [32]. The key reason is the unstructured format and nature of social media websites (the data contains textual peculiarities, informal and dynamic nature of language, new slang, abbreviations, and new expressions) [32]. Even though this approach outperforms the keyword-based classification, it still has drawbacks. Since it works at the word level, negated posts and posts with other meanings trick the lexicon polarity score measurement [30]. Second, lexical dictionary and polarity scores are usually biased toward the text of a specific type, dictated by the linguistic corpora source [30]. Therefore, it is challenging to construct a more generalized model regardless of the application domain.

C. ***Machine Learning-Based Approach***

Machine learning research has become a significant task in numerous application areas. Machine learning reaches throughout recent years have magnificently created algorithms for handling volumes of data to unravel real-world issues. Machine learning algorithms are grouped into supervised learning and unsupervised learning algorithms. Supervised learning algorithms will help users train and learn from the training example, which is then tested and evaluated using the test data. The main drawback of supervised machine learning algorithms is the obligation to create a training example. The training example must be comprehensive enough to make the algorithm effective and reliable enough to classify the instance in test data. Another type of machine learning is a unsupervised learning algorithm. The working principle of this algorithm is to identify the hidden associations in unlabeled data. The unsupervised learning methods are based on calculating similarity differences between data. For example, it calculates k-means in which similarity between data is computed based on proximity measures, such as Euclidean distance.

The constructing machine learning-based method involves the following important steps.

1) ***Features Extraction***

As shown in Figure 4, feature extraction is an important part of building an effective machine learning method in which the textual posts (P1,P2,P3,…,Pn) are transformed into valuable word features (wf1,wf2,wf3,…wfn) by using various feature engineering approaches. Feature extracting is one the most important steps of constructing effective classifiers [33]–[34][35][36]. The accomplishment or failure of the sentiment classification model is intensely dependent on the features quality. If the extracted features relate well with the sentiment polarity and can provide discrimination power between positive and negative, then classification will be more precise. In contrast, if the extracted features do not relate well with the sentiment polarity and the similar features exist in both positive and negative posts, then the classification task will be more challenging and less precise. The most commonly used features are the first automatic generated features of Bag of Words (BoW), Bag of Phrases (BoP), n - gram, and Bag of Concepts (BoC). The second group of features is based on lexical features such as opinion words, sentiment words, and negation words. The third group of features is varied based on the data source; for example, the data from social media normally adds features such as the number of hashtags and social media-related features such as abbreviations and emojis.

2) ***Machine Learning Algorithms***

This subsection briefly describes the most commonly used machine learning algorithms in literature for sentiment analysis.

a: ***Artificial Neural Network (ANN)***

The Artificial Neural Network (ANN) is a mathematical modeling approach that is stimulated by the operative processes of the human mind [37]. It is based on the artificial adaptive system, which has some form of distributive architecture [38]. The system in ANN encompasses closely-knit adaptive processing elements called artificial neurons or nodes which are proficient in carrying out enormous analogous and parallel computations for the purpose of information processing and knowledge representation [38].

These systems can also adapt to their internal structure in relation to a functional purpose. There are several types of artificial neural networks, which have been used for different problems. Generally, their application is appropriate for a problem, which is nonlinear in nature [39]. The nature of the problem can be carrying out pattern recognition, modeling memory, and envisaging the development of a

dynamic system [38]. In most cases, these network types perform data modeling which is driven in a supervised or unsupervised fashion. The supervised learning technique is provided with both input and output. Then the network uses this input to generate output, and hence it is compared to desired outputs. On the other hand, in unsupervised training, only input is being provided and the network is used to find natural grouping with a dataset independent of external constraints. That is, the system itself must have the capability to decide which features to incorporate in order to group the input data.

b: ***Random Forest***

Random Forests is a classification and regression method based on the ensemble of a proliferation of decision trees [40]. Recently, attention has been given to ensemble learning, a method which can create several classifiers and produce aggregate results [41]. The two commonly known and used methods for the classification of trees are boosting as proposed by [42] and bagging as proposed by [43]. The latter proposed the general operating mechanism of the Random Forest (RF), which augments the additional layer of randomness to bagging. In RF, each tree is a standard Classification or Regression Tree (CART) that uses the so-called splitting criteria like Decrease of Gini Impurity (DGI). Moreover, it picks the splitting predictor from a randomly chosen subset of predictors. Each tree is fabricated by using a bootstrap sample of the data, and the prediction of all trees are ultimately accumulated by means of majority voting [40].

c: ***Support Vector Machine***

Support vector machines are considered to be universal learners. Generically they learn linear threshold functions. However, with the use of a suitable kernel function plug in, they can be used to learn in different applications in the form of radical basic function and sigmoid neural networks and be trained on polynomial classifiers [44]. SVMs were initially intended for binary classification, but research has extended it into a multiclass classification. There are two commonly used approaches for multiclass SVMs. The first deals with fabricating and conjoining the number of binary classifiers, and the second one directly involves keeping all data in one optimization construction [45].

d: ***Genetic Algorithm***

The idea of developing the Genetic Algorithm was initiated and developed by John Holland. He proposed this idea in the year 1975 in his book “Adaptation in natural and artificial systems”. Since then, the Genetic Algorithm (GA) has been increasingly recognized as a popular evolutionary computational research technique [46]. It has gained popularity over the years as an optimization tool in a variety of research domains, including computer science, operational research, engineering, management, and social sciences [47]. A major reason behind the realization of this technique is its diversified applicability, efficiency of operations, and applicability on global scenario [48].

Genetic Algorithms are search and optimization techniques in a multifaceted search space. They are inspired by the concept of genetics and natural selection. Some essential and principal ideas are adopted from the field of genetics and then used artificially to create a kind of algorithm, which is flexible, robust, and efficient in nature [49]. Moreover, it characterizes the emergent technique, which is to be used to understand different relationships in the course of the development of data, in which the data can come in the form of binary strings, formula, program, query, grammar, and images [47].

e: ***Naïve Bayes***

The Naïve Bayes (NB) classifier has long been used in most applications of supervised machine learning. It is considered a tool for the retrieval of data [50]. It is based on a simple theorem of probability for making a probabilistic model of data. The mechanics of the NB algorithm are applied to numeric data [51]. It is simple, easy to understand, and quick for classification. It normally entails a minimal data set for training and then is used to predict the parameters needed for classification purposes.

f: ***Decision Tree***

The decision tree (DT) classifier has been widely used for prediction and classification of tasks. The rules in creating the decision tree are easy to understand. The classifiers built through the decision tree are given in hierarchical representation. The tree is composed of decision nodes, event nodes, edge, and path [52]. A variety of classifiers are used in a variety of applications. Some of the DT classifiers are ID3, C4.5, and C5.0, but a common problem that has been found in the DT classifier is the ability to incorporate all types of variations in data, including noise when

trees get bigger and deeper. This problem is commonly known as overfitting. In addition, the structure of the tree is distorted with the addition of data. To avoid this problem, the random forest technique is recommended in which many trees are formed and trained by dividing the training sets, and outcomes are generated through aggregation of all trees.

g: ***K-Nearest Neighbour***

The K–nearest neighbor algorithm performs classification based on instance learning. It works through a non-parametric procedure of storing all inputs and instances and classifies new inputs by means of similarity measures like Euclidean distance [46], [47].

h: ***Ensemble Voted Classifier***

An ensemble of classifiers is the collection of many classifiers in which their decisions are aggregated by means of weighted an unweighted voting mechanism to predict the outcome. The classification in the ensemble voted classifier is based on a voting mechanism in which classification of new instances is done by considering the majority vote of the prediction [43], [48]–[49][50].

9. Validation Metrics

To validate the proposed machine learning/ Deep learning models, one has to measure the performance by standard metrics. The standard metrics for performance is derived from the special matrix called confusion matrix. Confusion matrix gives the True positives, False Positives, True Negatives and False Negatives as elements.

True Positive (TP): Number of predictions as Positives, as they are Positive in ground truth

False Positive (FP): Number of predictions as Positives, as they are not positive in ground truth

True Negative (TN): Number of predictions as Negatives, as they are Negative in ground truth

False Negative (FN): Number of predictions as Negatives, as they are not negative in ground truth

True Positive (TN)	False Positive (FP)
False Negative (FN)	True Negative (TN)

Table 2. Confusion Matrix

Accuracy (ACC) is calculated as the number of all correct predictions divided by the total number of the dataset. The best accuracy is 1.0, whereas the worst is 0.0.

Sensitivity (Recall or True positive rate) Sensitivity(SN) is calculated as the number of correct positive predictions divided by the total number of positives. It is also called recall (REC) or true positive rate (TPR). The best sensitivity is 1.0, whereas the worst is 0.0.

Specificity (SP) is calculated as the number of correct negative predictions divided by the total number of negatives. It is also called true negative rate (TNR). The best specificity is 1.0, whereas the worst is 0.0

Precision (PREC) is calculated as the number of correct positive predictions divided by the total number of positive predictions. It is also called positive predictive value (PPV). The best precision is 1.0, whereas the worst is 0.0.

Negative positive rate (NPR) is calculated as the number of incorrect positive predictions divided by the total number of negatives. The best false positive rate is 0.0 whereas the worst is 1.0. It can also be calculated as 1 – specificity.

The false positive rate usually refers to the probability of falsely rejecting the null hypothesis for a particular test.

The false discovery rate (FDR) is a method of conceptualizing the rate of errors in null hypothesis testing when conducting multiple comparisons.

False omission rate (FOR) is a statistical method used in multiple hypothesis testing to correct for multiple comparisons and it is the complement of the negative predictive value. It measures the proportion of false negatives which are incorrectly rejected.

Mathew's correlation coefficient and F-score can be useful, but they are less frequently used than the other basic measures. F-score is a harmonic mean of precision and recall.

Matthews correlation coefficient (MCC) is a correlation coefficient calculated using all four values in the confusion matrix.

10.***Challenges to Sentiment Analysis***

Sentiment Analysis runs into a similar set of problems as emotion recognition does – before deciding what the sentiment of a given sentence is, we need to figure out what "sentiment" is in the first place. Is it categorical, and sentiment can be split into clear buckets like happy, sad, angry, or bored? Or is it dimensional, and sentiment needs to be evaluated on some sort of bi-directional spectrum?[7]

In addition to the definition problem, there are multiple layers of meaning in any human generated sentence. People express opinions in complex ways; rhetorical devices like sarcasm, irony, and implied meaning can mislead sentiment analysis. The only way to really understand these devices are through context: knowing how a paragraph is started can strongly impact the sentiment of later internal sentences.

Most of the current thinking in sentiment analysis happens in a categorical framework: sentiment is analyzed as belonging to a certain bucket, to a certain degree. For example, a given sentence may be 45% happy, 23% sad, 89% excited, and 55% hopeful. These numbers don't add up to 100 – they're individual indications of how "X" a sentence's sentiment is.

To address the context issue, a lot of research surrounding sentiment analysis has focused on feature engineering. Creating inputs to a model that recognize context, tone, and previous indications of sentiment can help increase accuracy and get a better overall sense of what the author is trying to say. For an interesting example, check out this paper in Knowledge-Based Systems that explores a framework for this kind of context focus.

Finally, one more challenge in sentiment analysis is deciding how to train the model you'd like to use. There are a number of pre-trained models available for use in popular Data Science languages. For example, TextBlob offers a simple API for sentiment analysis in Python, while the Syuzhet package in R implements some of research from the NLP Group at Stanford.

These modules can help you get off the ground quickly, but for the best long term results you're going to want to train your own models. Getting access to labeled training data for sentiment analysis can be difficult, but it's key to building models that work for your specific use case. You may execute a workflow where you gather your proprietary data (e.x. customer service conversations) and use a service like CrowdFlower to label and prepare it.

10. Conclusion and future scope

Sentiment Analysis works to analyze the emotion of the people, which is written in the form of text. Further different algorithms and different data mining techniques are to be applied to get accurate emotions. In order to get accuracy, we try to use deep learning algorithm so as to get more accuracy and optimum solutions.

11. References

[1]. B. Pang, et al., "Thumbs up?: sentiment classification using machine learning techniques," in Proceedings of the ACL-02 conference on Empirical methods in natural language processing-Volume 10, 2002, pp. 79-86.

[2]Turney, Peter D. "Thumbs up or thumbs down?: semantic orientation applied to unsupervised classification of reviews." Proceedings of the 40th annual meeting on association for computational linguistics.Association for Computational Linguistics, 2002.

[3]Rajini Singh, RajdeepKaur, Sentiment analysis on social media and online review.

[4] http://www.ebizmba.com/articles/social-networking-websites

[5] S.-M. Kim and E. Hovy, "Determining the sentiment of opinions," in Proceedings of the 20th international conference on Computational Linguistics, 2004, p. 1367.

[6] T. Wilson, et al., "Recognizing contextual polarity in phrase-level sentiment analysis," in Proceedings of the conference on human language technology and empirical methods in natural language processing, 2005, pp. 347-354.

[7] ShahidShayaa, et al, "Sentiment analysis of Big Data: Methods Applications and Challenges", IEEE Access ,Vol – 6 Issue 2018, Pg: 37807 – 37827

[8] F. R. Lucini et al., "Text mining approach to predict hospital admissions using early medical records from the emergency department", Int. J. Med. Inf., vol. 100, pp. 1-8, Apr. 2017.

[9] Z. Khan, T. Vorley, "Big data text analytics: An enabler of knowledge management", J. Knowl. Manage., vol. 21, no. 1, pp. 18-34, 2017.

[10] T. T. Thet, J.-C. Na, C. S. G. Khoo, "Aspect-based sentiment analysis of movie reviews on discussion boards", J. Inf. Sci., vol. 36, no. 6, pp. 823-848, 2010.

[11]H. Yu,V.Hatzivassiloglou, "Towards answering opinion questions: Separating facts from opinions and identifying the polarity of opinion sentences", Proc. Conf. Empirical Methods Natural Lang. Process., pp. 129-136, 2003.

[12] R. Piryani, D. Madhavi, V. K. Singh, "Analytical mapping of opinion mining and sentiment analysis research during 2000–2015", Inf. Process. Manage., vol. 53, no. 1, pp. 122-150, 2017.

[13] A. Qazi, A. Tamjidyamcholo, R. G. Raj, G. Hardaker, C. Standing, "Assessing consumers' satisfaction and expectations through online opinions: Expectation and disconfirmation approach", Comput. Hum. Behav., vol. 75, pp. 450-460, Oct. 2017.

[14] N. Jindal, B. Liu, "Identifying comparative sentences in text documents", Proc. 29th Annu. Int. ACM SIGIR Conf. Res. Develop. Inf. Retr., pp. 244-251, 2006.
[15] A. Qazi, R. G. Raj, M. Tahir, E. Cambria, K. B. S. Syed, "Enhancing business intelligence by means of suggestive reviews", Sci. World J., vol. 2014, Jun. 2014.
[16] M. Quigley, Encyclopedia of Information Ethics and Security, Hershey, PA, USA:IGI Global, 2007.
[17] E. Cambria, "Affective computing and sentiment analysis", IEEE Intell.Syst., vol. 31, no. 2, pp. 102-107, Mar./Apr. 2016.
[18] S. Poria, E. Cambria, N. Howard, G.-B. Huang, A. Hussain, "Fusing audio visual and textual clues for sentiment analysis from multimodal content", Neurocomputing, vol. 174, pp. 50-59, Jan. 2016.
[19] S. Poria, I. Chaturvedi, E. Cambria, A. Hussain, "Convolutional MKL based multimodal emotion recognition and sentiment analysis", Proc. IEEE 16th Int. Conf. Data Mining (ICDM), pp. 439-448, Dec. 2016.
[20] S. Poria, E. Cambria, A. Gelbukh, "Aspect extraction for opinion mining with a deep convolutional neural network", Knowl.-Based Syst., vol. 108, pp. 42-49, Sep. 2016.
[21] I. Chaturvedi, E. Cambria, S. Poria, R. Bajpai, "Bayesian deep convolution belief networks for subjectivity detection", Proc. IEEE 16th Int. Conf. Data Mining Workshops (ICDMW), pp. 916-923, Dec. 2016.
[22] S. Poria, E. Cambria, D. Hazarika, P. Vij, A deeper look into sarcastic tweets using deep convolutional neural networks, 2016, [online] Available: https://arxiv.org/abs/1610.08815.
[23] E. Cambria, B. White, "Jumping NLP curves: A review of natural language processing research", IEEE Comput. Intell. Mag., vol. 9, no. 2, pp. 48-57, May 2014.
[24] A. Zaslavsky, C. Perera, D. Georgakopoulos, Sensing as a service and big data, 2013, [online] Available: https://arxiv.org/abs/1301.0159.
[25] D. Denyer, D. Tranfield, "Producing a systematic review" in The Sage Handbook of Organizational Research Methods, Thousand Oaks, CA, USA:Sage, 2009.
[26] D. Tranfield, D. Denyer, P. Smart, "Towards a methodology for developing evidence-informed management knowledge by means of systematic review", Brit. J. Manage., vol. 14, no. 3, pp. 207-222, 2003.
[27] R. J. Light, D. B. Pillemer, Summing Up: The Science of Reviewing Research, Cambridge, MA, USA:Harvard Univ. Press, 1984.
[28] D. M. Rousseau, J. Manning, D. Denyer, "11 evidence in management and organizational science: Assembling the field's full weight of scientific knowledge through syntheses", Acad. Manage. Ann., vol. 2, no. 1, pp. 475-515, 2008.
[29] S. L. Newbert, "Empirical research on the resource-based view of the firm: An assessment and suggestions for future research", Strategic Manage. J., vol. 28, no. 2, pp. 121-146, 2007.
[30] E. Cambria, B. Schuller, Y. Xia, C. Havasi, "New avenues in opinion mining and sentiment analysis", IEEE Intell. Syst., vol. 28, no. 2, pp. 15-21, Mar. 2013.
[31] M. Taboada, J. Brooke, M. Tofiloski, K. Voll, M. Stede, "Lexicon-based methods for sentiment analysis", Comput.Linguistics, vol. 37, no. 2, pp. 267-307, 2011.
[32] A. Giachanou, F. Crestani, "Like it or not: A survey of Twitter sentiment analysis methods", ACM Comput. Surv., vol. 49, no. 2, pp. 28, 2016.
[33] C. C. Aggarwal, C. Zhai, "A survey of text classification algorithms" in Mining Text Data, Boston, MA, USA:Springer, pp. 163-222, 2012.
[34] P. Domingos, "A few useful things to know about machine learning", Commun.ACM, vol. 55, no. 10, pp. 78-87, 2012.
[35] I. H. Witten, E. Frank, M. A. Hall, C. J. Pal, Data Mining: Practical Machine Learning Tools and Techniques, San Mateo, CA, USA:Morgan Kaufmann, 2016.
[36] D. H. Wolpert, W. G. Macready, "No free lunch theorems for search", 1995.
[37] W. S. McCulloch, W. Pitts, "A logical calculus of the ideas immanent in nervous activity", Bull. Math. Biophys., vol. 5, no. 4, pp. 115-133, 1943.
[38] C. A. L. Bailer-Jones, R. Gupta, H. P. Singh, "An introduction to artificial neural networks" in Automated Data Analysis in Astronomy, New Delhi, India:Narosa Publishing House, vol. 52, pp. 18, Sep. 2001.
[39] E. Grossi, M. Buscema, "Introduction to artificial neural networks", Eur. J. Gastroenterol.Hepatol., vol. 19, pp. 1046-1054, Dec. 2007.
[40] A.-L. Boulesteix, S. Janitza, J. Kruppa, I. König, "Overview of random forest methodology and practical guidance with emphasis on computational biology and bioinformatics", Wiley Interdiscipl. Rev. Data Mining Knowl.Discovery, vol. 2, no. 6, pp. 493-507, 2012.
[41] A. Liaw, M. Wiener, "Classification and regression by randomforest", R News, vol. 2, no. 3, pp. 18-22, 2002.
[42] R. E. Schapire, Y. Freund, P. Bartlett, W. S. Lee, "Boosting the margin: A new explanation for the effectiveness of voting methods", Ann. Stat., vol. 26, no. 5, pp. 1651-1686, 1998.

[43] L. Breiman, "Bagging predictors", Mach. Learn., vol. 24, no. 2, pp. 123-140, 1996.
[44] T. Joachims, "Text categorization with support vector machines: Learning with many relevant features", Proc. Eur. Conf. Mach. Learn., vol. 98, pp. 137-142, 1998.
[45] C.-W. Hsu, C.-J. Lin, "A comparison of methods for multiclass support vector machines", IEEE Trans. Neural Netw., vol. 13, no. 2, pp. 415-425, Mar. 2002.
[46] S. N. Sivanandam, S. N. Deepa, "Genetic algorithms" in Introduction to Genetic Algorithms, New York, NY, USA:Springer-Verlag, 2007.
[47] M. Mitchell, "An introduction to genetic algorithms", Sadhana, vol. 24, no. 4, pp. 293-315, Aug. 1999.
[48] D. E. Goldberg, Genetic Algorithms in Search Optimization and Machine Learning, Reading, MA, USA:Addison-Wesley, 1989.
[49] A. Kumar, R. M. Pathak, Y. P. Gupta, "Genetic algorithm based approach for file allocation on distributed systems", Comput. Oper. Res., vol. 22, no. 1, pp. 41-54, 1995.
[50] D. D. Lewis, "Naive (Bayes) at forty: The independence assumption in information retrieval", Proc. Eur. Conf. Mach. Learn., pp. 4-15, 1998.
[51] M. Sahami, S. Dumais, D. Heckerman, E. Horvitz, "A Bayesian approach to filtering junk e-mail", Proc. Learn. Text Categorization Papers Workshop, vol. 62, pp. 98-105, 1998.
[52] J. R. Quinlan, "Induction of decision trees", Mach. Learn., vol. 1, no. 1, pp. 81-106, 1986.

Three Node Tandem Communication Network Model with Duane Arrival Process having Phase Type Service

Kalavala Asish Vardhan
Department of CS&SE
Andhra University
Visakhapatnam
India

K. Srinivasa Rao
Department of Statistics
Andhra University
Visakhapatnam
India

P. Srinivasa Rao
Department of CS&SE
Andhra University
Visakhapatnam
India

ABSTRACT
This paper introduces a three node Tandem communication network model in which the arrival process follows a Duane process such that the inter arrival times follow Weibull distribution. In this model it is assumed that intermediator departures after transmission from first and second nodes are allowed it is further assumed that the inter transmission times in each node follow Poisson process and the transmission strategy is Dynamic bandwidth allocation. The network behavior is analyzed by deriving expressions for average number of packets in each Queue. The mean delays in transmission, the throughput of the nodes, the Utilization of the transmitters and the variability of the content of buffers. Through Sensitivity analysis it is observed that the arrival process has significant influence on network performance measures. The strategy of allowing inter mediatory departures reduce conjunction in buffers and mean delay of transmission of packets. This model also includes some of the earlier models as particular cases for specific limiting for specific values of the parameter. This model is useful for design and monitoring self-Similarity networks.

Keywords
Duane Arrival process, Communication network model, Sensitivity analysis, DBA

1. INTRODUCTION
William Cock and Charles Wheatstone [1] have pioneered the mathematical theory of communication. Thereafter in 1948 a tremendous revolution in communication network modeling is brought by Barden and Barttain. Later AT&T Bell labs, USA network group at MIT, IEEE communication society and other reputed organizations have put considerable efforts for invoking and designing efficient communication systems. (IEEE Communication Society, 2002). Conducting laboratory experiments under variable load conditions is highly complex and time consuming. Hence for efficient design and evaluation of communication networks, the network models are developed and analyzed with various assumptions on constituent processes of the model like arrival process, service process, flow control mechanisms, allocations, routing, etc. To improve Quality of Service, packet switching gives better utilization over circuit or message switching and yields relatively shorter delay in statistical multiplexing in communication network can reduce the delay in packet switching. Many of communication networks which support teleprocessing applications are mixed with dynamic engineering skills and statistical multiplexing [2], [3], [4]. To reduce the congestion in buffers the dynamic bandwidth allocation is evolved as an alternative and efficient control strategy over bit dropping or flow control strategies [5], [7], [8, 9]. In DBA, a large portion of the unutilized bandwidth is utilized by changing the transmission rate of packets depending on the content of the buffer connected to it. Much work has been reported recently regarding communication network model with dynamic bandwidth [10]. In all these papers, the authors assumed that the arrival rate of packets is constant and follows a Poisson process.

But in many communication systems the assumption regarding Poisson process are seldom satisfied due to the time dependent nature of arrivals. Therefore, many phenomenon encountered in communication systems which reveal time dependent behavior of arrival process due to the factors like work load fluctuations, initiating, failures, congestion and flow control, overload peaks, reconfigurations, adaptive routing and others. So to have an efficient performance evaluation entities problem of communication systems like adaptive isolated routing and load balancing, evaluating alternative buffer of changed sharing schemes and effects and to study the effects of flow and control strategies it is needed to develop communication network models with time dependent arrivals. In addition to this [10] have showed that the packet arrival process of heavy tail distribution inter arrivals form a non homogeneous process and the mean packet arrival rate is not constant but it is time varying. This is also supported by the studies [18], who demonstrated the TCP connection arrival process is bursty and time dependent. Recently, much emphasis is given for modeling the arrival process of the communication networks using, Non-homogeneous Poisson Process with the assumption that the arrival rate is linearly dependent on time [9] [10], [11, 12]. In all these papers they assumed that the burstness of the traffic is either linearly increasing or decreasing depending on time, but in LAN, WAN, and MAN the traffic structure is quite different from the, arrival rates being linearly dependent function of time. This is also supported by [18] who have, modeled the packet arrivals as Log Normal distributions, since, the associated network traffic inter arrivals are distributed with heavy tail distributions. Feldmann [18] demonstrated that the Transport Control Protocol (TCP) connection arrival bursty and are characterized by heavy tail distributions such as Weibull distributions. Fisher et al [19], has analyzed a singer server queuing model with Weibull inter arrivals using simulations studied. Araik Tamazian and Mikhail Bogachev [17] have used Weibull distributions for inter arrival times in analyzing the performance of World Wide Web (WWW) servers. In these studies, they consider that the server is single and the queues are independent. But in LAN, WAN and MAN the output of one queue is an input to the other queue, and queues are not independent. No work has been reported in literature regarding Tandem communication network models with Weibull inter arrival times which model the LAN, WAN, MAN and other self-similarity network traffic with time dependent bursts, more close to the reality. This motivated to develop and analyze a two node tandem communication network model with Weibull inter arrival times having dynamic band width

allocation with modified phase type transmission. The Weibull distribution includes exponential distribution and several other skewed distributions as particular cases. Using the differential calculus, the explicit expressions for the network performance parameters such as mean number of packets in each buffer, mean delay in transmission, the throughput of the nodes, and the variability of the buffer content are derived. Through numerical analysis the performance of the communication network is evaluated with respect to the changes in input parameters. A comparative study of the proposed model with that of exponential inter arrival times is also carried.

2. COMMUNICATION NETWORK MODEL AND TRANSIENT SOLUTION

In this section, a communication network model having three nodes in tandem is studied. The arrivals to the buffer connected at node one is assumed to follow a Duane process with mean arrival rate as a function of time t. It is of the form $\lambda(t) = abtb\text{-}1$. The transmission process from node one to node two follows a Poisson process with parameter $\mu 1$. It is also assumed that the packets arrive to the second buffer directly from outside of the network in a Poisson process with mean arrival rate ϵ. After getting transmitted from node one the packets are forwarded to the second buffer for transmission with probability θ or get terminated with probability π i.e., the packets arrived at second buffer contains the packets received from first node and directly from outside. After getting transmitted from second node the packet are forwarded to the third buffer for transmission with probability π or get terminated with probability $(1- \pi)$. The transmission process of node two and three also follow Poisson process with parameters $\mu 2$ and $\mu 3$ respectively. The transmission rate of each packet is adjusted just before transmission depending on the content of the buffer connected to the transmitter. The packets are transmitted through the transmitters by the first in first out discipline. The schematic diagram representing the communication network model is shown in Figure 1.

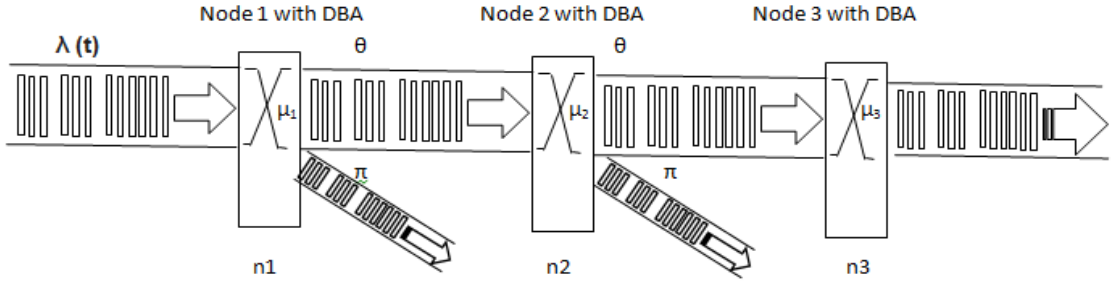


Figure 1: Schematic diagram of the CNM model with three stage arrival

Let P n_1,n_2,n_3 (t) be the probability that there are n_1 packets in the first buffer and n_2 packets in the second buffer and n_3 packets in the third buffer at the time t. with this structure, the difference –differential equations of the communication network are :

3. PERFORMANCE MEASURES OF THE NETWORK

The mean number of packets in the first buffer is

$$L_1(t) = E[N_1] = \sum_{n_1=0}^{\infty} n_1 P_{n_1}(t) = \left[ab\left[\left[e^{-\mu_1 t}\int_0^t e^{-\mu_1 v} v^{b-1} dv - \frac{e^{-\mu_1 t}}{\mu_1}\right]\right]\right]$$

The utilization of the first buffer is

$$U_1(t) = 1 - P_0(t)$$

$$= \left[1 - \exp\left[-ab\left[e^{-\mu_1 t}\int_0^t e^{-\mu_1 v} v^{b-1} dv - \frac{e^{-\mu_1 t}}{\mu_1}\right]\right]\right]$$

For computing the variability of the number of packets in first buffer is

$$E(N_1^2 - N_1) = ab\left[e^{-\mu_1 t}\int_0^t e^{-\mu_1 v} v^{b-1} dv - \frac{e^{-\mu_1 t}}{\mu_1}\right]^2$$

Therefore, the variance of the number of packets in the first buffer is

$$Var(N_1) = ab\left[e^{-\mu_1 t}\int_0^t e^{-\mu_1 v} v^{b-1} dv - \frac{e^{-\mu_1 t}}{\mu_1}\right]$$

In this section, the performance measures of the communication network under transient conditions are derived and analyzed. Expanding $P(s_1, s_2, s_3; t)$ given equation (16) and collecting the constant terms, the probability that the network is empty achieved as follows,

The throughput of the first transmitter is

$$Thp_1(t) = \mu_1\left(1 - P_0(t)\right) = \mu_1\left[1 - \exp\left[-ab\left[e^{-\mu_1 t}\int_0^t e^{-\mu_1 v} v^{b-1} dv - \frac{e^{-\mu_1 t}}{\mu_1}\right]\right]\right]$$

The mean delay in the first buffer size is

$$W_1(t) = \frac{L_1(t)}{Thp_1(t)}$$

Similarly, by substituting $s_1=1$, and $s_3=1$, $s_1=1$, and $s_2=1$, the probability generating function of the second buffer and third buffer size distributions are achieved and values are tabulated as follows,

4. PERFORMANCE EVALUATION OF THE NETWORK

In this section, the performance of the developed communication network is discussed through a numerical illustration. Different values of the parameters are considered for bandwidth allocation and arrival of packets. After interacting with the technical staff an internet providing station, is considered the packet arrival rate parameter "a" varies from 11 $x10^4$ packets/sec to $14x10^4$ packets/sec, and 'b' varies from 1.25 to 2.5 with an average packet size of 52 bytes. After transmitting from node l, the forward

transmission rate 'μ_1' varies from $11x10^4$ packets/sec to $14x10^4$ packets/sec. The rate of transmission rate 'μ_2' varies from $26x10^4$ packets/sec to $29x10^4$ packets/sec. The rate of transmission rate 'μ_3' varies from $28x10^4$ packets/sec to $31x10^4$ packets/sec. In all these nodes, dynamic bandwidth allocation strategy is considered i.e., the transmission rate of each packet depends on the number of packets in the buffer connected to it at that instant.

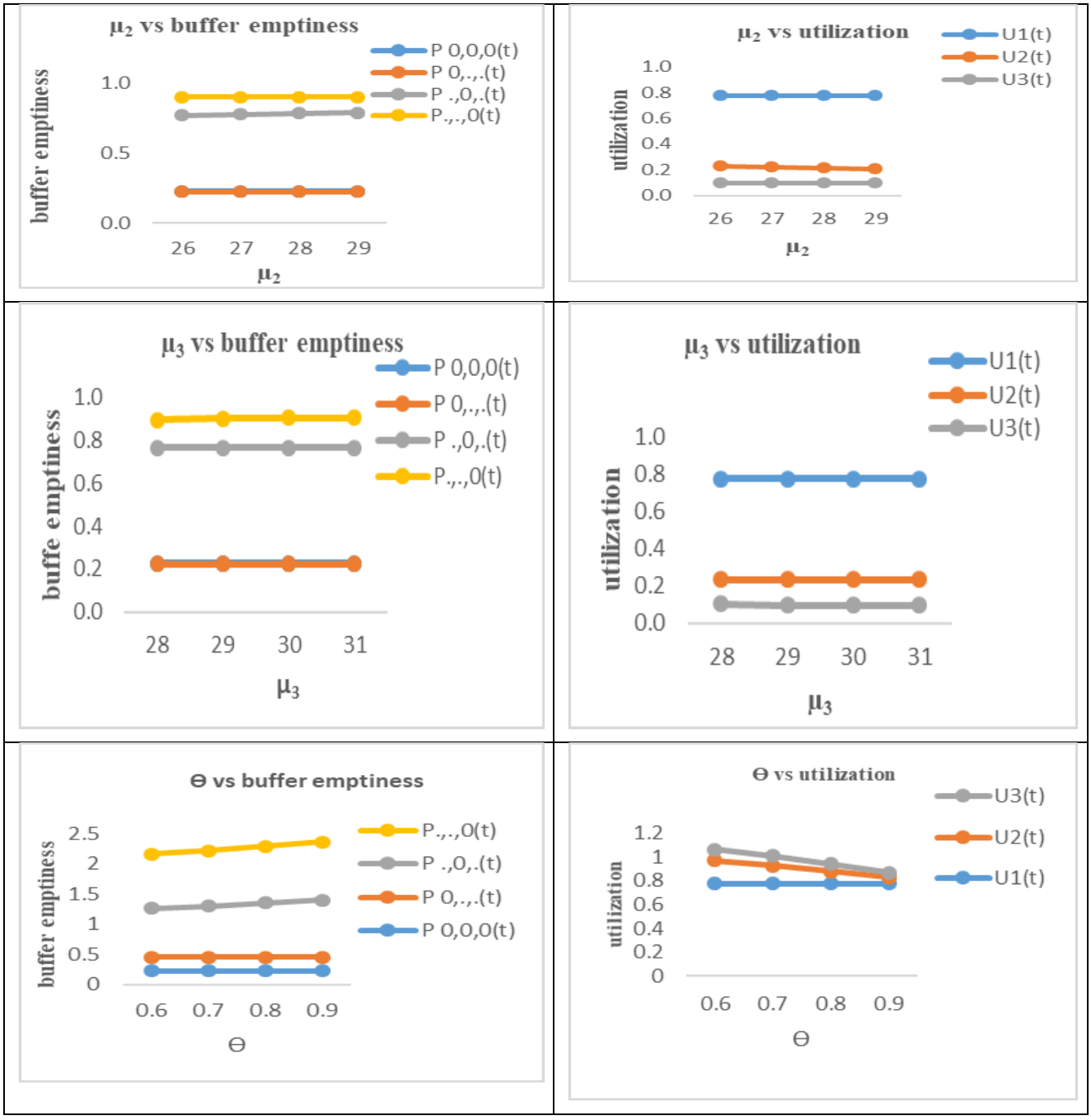
Since performance characteristics of communication network are highly sensitive with respect to time, the transient behavior of the model is studied through computing the performance measures with the set of values for the model parameters as t = 0.8,0.9,1.0,1.1 seconds, a = 11,12,13,14 (with multiplication to $10x10^4$ packets/sec) b=1.25,1.5,2,2.5 μ_1=11,12,13,14($10x10^4$packets/sec), μ_2=26,27,28,29

(10x104packets/sec), μ3 =28,29,30,31(10x104 packets/sec), π = 0.4,0.3,0.2,0.1, θ = 0.6,0.7,0.8,0.9.

The probability of the network emptiness and buffer emptiness are computed for different values of t, a, b, μ_1, μ_2, μ_3, π, θ and presented in Table 1. The probability of network emptiness and different buffers emptiness with various parameters are represented graphically in Figure 2. From the Table 1 it is observed that the probability of emptiness in the entire communication network and in three buffers are highly sensitive with respect to changes in time. As time 't' varies from 0.8 seconds to 1.1 seconds, the probability of emptiness in the network reduces from 0.2261 to 0.0496 when other parameters are fixed at (10,3,10,25,30,0.5,0.5) for (a, b, μ_1, μ_2, μ_3, π, θ). Similarly, the probability for emptiness in three buffers vary from 0.2234 to 0.0483, 0.7649 to 0.5713and 0.9036 to 0.8042 for node l, node2 and node 3 respectively. The decrease in the node l is more rapid when compared to node 2, node 3. The influence of mean arrival rate of packets on the system emptiness is also studied. As the arrival rate parameters 'a' varies from $11x10^4$ packets/sec to 14 x 10^4 packets/sec, the probability of emptiness of the network decreases from 0.1946 to 0.1242 when other parameters are fixed at (0.8,3,10,25,30,0.5,0.5) for (t, b, μ_1, μ_2, μ_3, π, θ). The same phenomenon is observed with respect to three nodes. This decrease is more in first node and moderate in second and third nodes.

Table 1: Values of network and buffer emptiness probability and utilization of the communication network with DBA*=seconds, $= multiples of 1000 packets/seconds.

t*	a$	b	$\mu_1$$	$\mu_2$$	$\mu_3$$	π	θ	$P_{0,0,0}(t)$	$P_{0,.,.}(t)$	$P_{.,0,.}(t)$	$P_{.,.,0}(t)$	$U_1(t)$	$U_2(t)$	$U_3(t)$
0.8	10	3	10	25	30	0.5	0.5	0.2261	0.2234	0.7649	0.9036	0.7766	0.2351	0.0962
0.9	10	3	10	25	30	0.5	0.5	0.1447	0.1423	0.7023	0.8735	0.8577	0.2977	0.1264
1.0	10	3	10	25	30	0.5	0.5	0.0872	0.0854	0.6372	0.8403	0.9146	0.3628	0.1597
1.1	10	3	10	25	30	0.5	0.5	0.0496	0.0483	0.5713	0.8042	0.9517	0.4287	0.1957
0.8	**11**	3	10	25	30	0.5	0.5	0.1946	0.1923	0.7447	0.8945	0.8077	0.2553	0.1053
0.8	**12**	3	10	25	30	0.5	0.5	0.1676	0.1655	0.725	0.8855	0.8345	0.275	0.1143
0.8	**13**	3	10	25	30	0.5	0.5	0.1442	0.1425	0.7058	0.8765	0.8575	0.2942	0.1232
0.8	**14**	3	10	25	30	0.5	0.5	0.1242	0.1226	0.6872	0.8677	0.8774	0.3128	0.1320
0.8	10	**1.25**	10	25	30	0.5	0.5	0.3281	0.3199	0.799	0.9119	0.6801	0.201	0.0881
0.8	10	**1.5**	10	25	30	0.5	0.5	0.293	0.2864	0.7846	0.9062	0.7136	0.2154	0.0937
0.8	10	**2**	10	25	30	0.5	0.5	0.2513	0.2467	0.7681	0.9008	0.7533	0.2319	0.0991
0.8	10	**2.5**	10	25	30	0.5	0.5	0.2322	0.2287	0.7629	0.9006	0.7713	0.2371	0.0992
0.8	10	3	**11**	25	30	0.5	0.5	0.2514	0.2482	0.7601	0.9014	0.7518	0.2399	0.0985
0.8	10	3	**12**	25	30	0.5	0.5	0.2757	0.2722	0.756	0.8995	0.7278	0.244	0.1004
0.8	10	3	**13**	25	30	0.5	0.5	0.2991	0.2952	0.7524	0.8979	0.7048	0.2476	0.1021
0.8	10	3	**14**	25	30	0.5	0.5	0.3214	0.3172	0.7494	0.8965	0.6828	0.2506	0.1035
0.8	10	3	10	**26**	30	0.5	0.5	0.2261	0.2234	0.772	0.9032	0.7766	0.228	0.0966
0.8	10	3	10	**27**	30	0.5	0.5	0.226	0.2234	0.7787	0.9028	0.7766	0.2213	0.097
0.8	10	3	10	**28**	30	0.5	0.5	0.2259	0.2234	0.7849	0.9025	0.7766	0.2151	0.0974
0.8	10	3	10	**29**	30	0.5	0.5	0.2259	0.2234	0.7909	0.9021	0.7766	0.2091	0.0977
0.8	10	3	10	25	**28**	0.5	0.5	0.2262	0.2234	0.7649	0.8978	0.7766	0.2351	0.102
0.8	10	3	10	25	**29**	0.5	0.5	0.2261	0.2234	0.7649	0.9036	0.7766	0.2351	0.0962
0.8	10	3	10	25	**30**	0.5	0.5	0.2261	0.2234	0.7649	0.9063	0.7766	0.2351	0.0935
0.8	10	3	10	25	**31**	0.5	0.5	0.2261	0.2234	0.7649	0.9063	0.7766	0.2351	0.0935
0.8	10	3	10	25	30	**0.4**	**0.6**	0.2257	0.2234	0.807	0.9073	0.7766	0.193	0.0925
0.8	10	3	10	25	30	**0.3**	**0.7**	0.2252	0.2234	0.8515	0.9184	0.7766	0.1485	0.0815
0.8	10	3	10	25	30	**0.2**	**0.8**	0.2246	0.2234	0.8984	0.9372	0.7766	0.1016	0.0627
0.8	10	3	10	25	30	**0.1**	**0.9**	0.224	0.2234	0.9478	0.9642	0.7766	0.0522	0.0358



When the arrival rate parameter 'b' varies from 1.25 to 2.5, the probability of emptiness of the network decreases from 0.3281 to 0.2322 when the other parameters remain fixed. The same phenomenon is observed for three nodes. The decrease is faster in node 1 and moderate in the next two nodes.

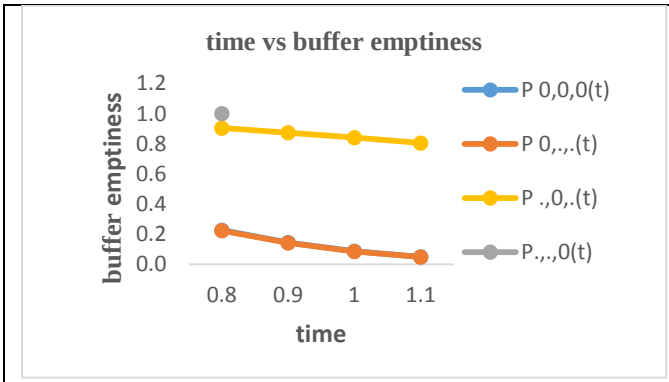
When the transmission rate 'μ_1' of node 1 varies from 11 x10^4 packets/sec to 14 x 10^4 packets/sec the probability of emptiness in the network increase from 0.2514 to 0.3214 when the other parameters remain fixed. Similarly, the transmission rate 'μ_2' of node2 varies from 26 x 10^4 packets/sec to 29 x 10^4 packets/sec. The probability of emptiness of the network increases from 0.2261 to 0.2259 when the other parameters remain fixed. Similarly, the transmission rate 'μ_3' of node3 varies from 28 x 10^4 packets/sec to 31 x 10^4 packets/sec. The probability of emptiness in the network increases from 0.2262 to 0.2261 when the other parameters remain fixed. The same phenomenon is observed with respect to the emptiness of the three buffers.

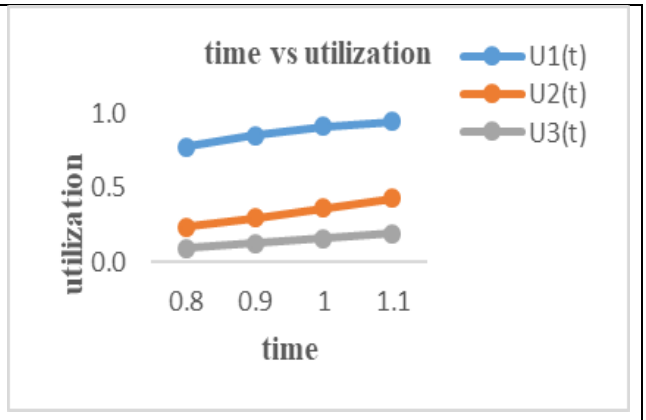
When arrival rate Parameter 'θ' increases from 0.6 to 0.9, the probability of emptiness in the network decreases from 0.2257 to 0.224 when other parameter is remaining fixed. The utilization of transmitters of node 1, node 2 and node 3 for different parameters are computed and presented in Table 1 and the relationship with performance measures is shown in Figure 2. As time't' and arrival rate parameter 'a' increase the utilization of transmitters are increasing for fixed values of the other parameters. It is also observing that the as the arrival rate parameter 'a' increases the utilization of transmitters in three nodes are increasing for fixed values of the other parameters. As the transmission rate 'μ_1' increases, the utilization of the first node decreases. Similarly, as the

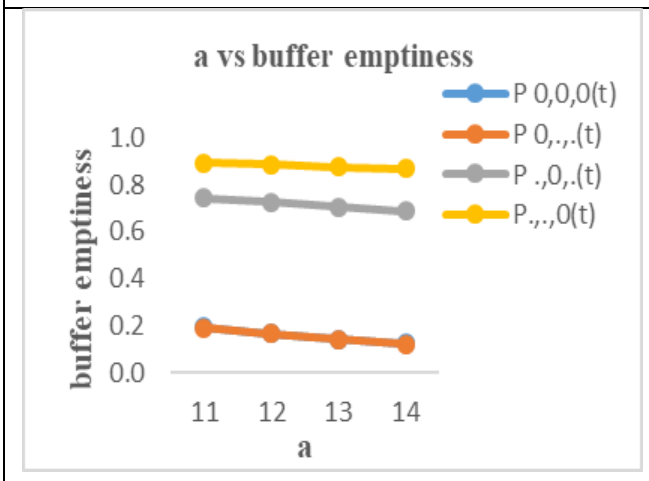
transmission rate 'μ_2' increases the utilization of the second node decreases when the other parameters remain fixed.

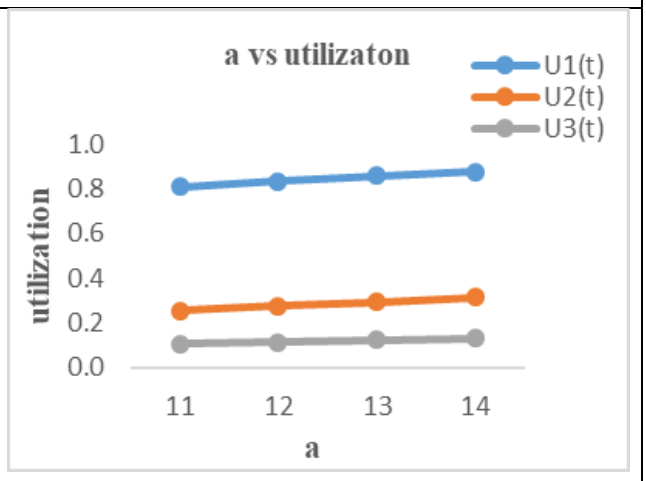
Similarly, as the transmission rate 'μ_3' increases the utilization of in third node decreases when the other parameters remain fixed.

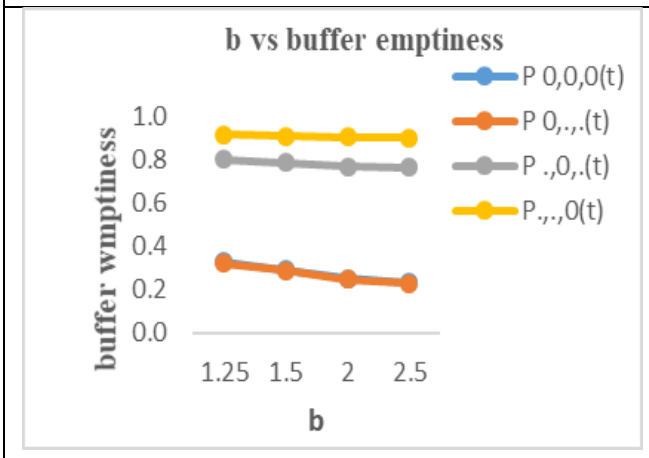
The mean number of packets in the buffer and in the network, mean delays in transmission of both nodes are computed for different values are t, a, b, μ_1, μ_2, μ_3, π, θ and presented at Table 2. The relationship between the parameters and the performance measures are shown in the Figure 3.











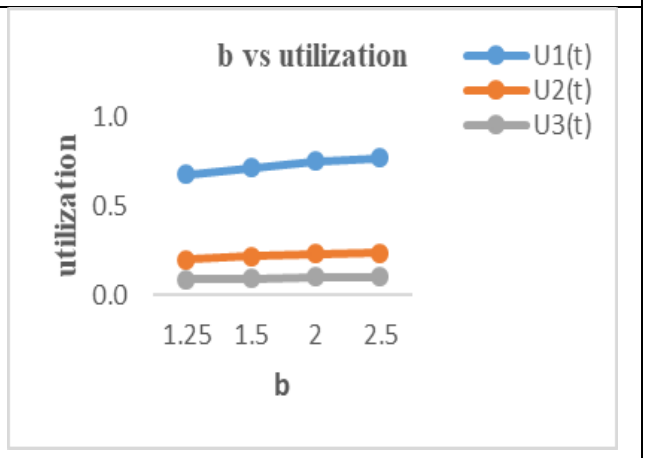


Table 2: Values of mean number of packets and mean delay of the communication network with DBA *=seconds, $= multiples of 1000 packets/seconds

t*	a$	b	μ1$	μ2$	μ3$	π	θ	$L_1(t)$	$L_2(t)$	$L_3(t)$	$L_n(t)$	$W_1(t)$	$W_2(t)$	$W_3(t)$
0.8	10	3	10	25	30	0.5	0.5	1.4990	0.2680	0.1011	1.8681	0.1930	0.0456	0.0350
0.9	10	3	10	25	30	0.5	0.5	1.9496	0.3534	0.1351	2.4381	0.2273	0.0475	0.0356
1.0	10	3	10	25	30	0.5	0.5	2.4599	0.4507	0.1740	3.0845	0.2690	0.0497	0.0363
1.1	10	3	10	25	30	0.5	0.5	3.0299	0.5599	0.2178	3.8077	0.3184	0.0522	0.0371
0.8	**11**	3	10	25	30	0.5	0.5	1.6489	0.2948	0.1113	2.0549	0.2041	0.0462	0.0352
0.8	**12**	3	10	25	30	0.5	0.5	1.7988	0.3216	0.1214	2.2417	0.2156	0.0468	0.0354
0.8	**13**	3	10	25	30	0.5	0.5	1.9487	0.3484	0.1315	2.4285	0.2272	0.0474	0.0356
0.8	**14**	3	10	25	30	0.5	0.5	2.0986	0.3752	0.1416	2.6153	0.2392	0.0480	0.0357
0.8	10	**1.25**	10	25	30	0.5	0.5	1.1399	0.2244	0.0922	1.4565	0.1676	0.0447	0.0349
0.8	10	**1.5**	10	25	30	0.5	0.5	1.2504	0.2425	0.0983	1.5913	0.1752	0.045	0.035
0.8	10	**2**	10	25	30	0.5	0.5	1.3994	0.2638	0.1043	1.7675	0.1858	0.0455	0.0351
0.8	10	**2.5**	10	25	30	0.5	0.5	1.4753	0.2707	0.1045	1.8505	0.1913	0.0457	0.0351
0.8	10	3	**11**	25	30	0.5	0.5	1.3934	0.2744	0.1037	1.7715	0.1685	0.0457	0.0351
0.8	10	3	**12**	25	30	0.5	0.5	1.3012	0.2798	0.1058	1.6868	0.149	0.0459	0.0351
0.8	10	3	**13**	25	30	0.5	0.5	1.2201	0.2844	0.1077	1.6122	0.1332	0.046	0.0352
0.8	10	3	**14**	25	30	0.5	0.5	1.1484	0.2885	0.1093	1.5461	0.1201	0.046	0.0352
0.8	10	3	10	**26**	30	0.5	0.5	1.499	0.2588	0.1016	1.8594	0.193	0.0437	0.0351
0.8	10	3	10	**27**	30	0.5	0.5	1.499	0.2502	0.102	1.8512	0.193	0.0419	0.0351
0.8	10	3	10	**28**	30	0.5	0.5	1.499	0.2422	0.1024	1.8435	0.193	0.0402	0.0351
0.8	10	3	10	**29**	30	0.5	0.5	1.499	0.2346	0.1028	1.8364	0.193	0.0387	0.0351
0.8	10	3	10	25	**28**	0.5	0.5	1.499	0.268	0.1076	1.8746	0.193	0.0456	0.0377
0.8	10	3	10	25	**29**	0.5	0.5	1.499	0.268	0.1011	1.8681	0.193	0.0456	0.035
0.8	10	3	10	25	**30**	0.5	0.5	1.499	0.268	0.0982	1.8651	0.193	0.0456	0.0339
0.8	10	3	10	25	**31**	0.5	0.5	1.499	0.268	0.0982	1.8651	0.193	0.0456	0.0339
0.8	10	3	10	25	30	**0.4**	**0.6**	1.499	0.2144	0.0971	1.8105	0.193	0.0444	0.035
0.8	10	3	10	25	30	**0.3**	**0.7**	1.499	0.1608	0.085	1.7447	0.193	0.0433	0.0348
0.8	10	3	10	25	30	**0.2**	**0.8**	1.499	0.1072	0.0647	1.6709	0.193	0.0422	0.0344
0.8	10	3	10	25	30	**0.1**	**0.9**	1.499	0.0536	0.0364	1.589	0.193	0.0411	0.0339

It is observed that when time t=0.8 seconds the mean number of packets in the first buffer is 14990 packets after one seconds it is rapidly increases to 24599 packets, and at 1.1 seconds it becomes 30299 packets and there after its stabilizes. The mean number of packets in the second and third buffers in the network are increasing from 2680 packets to 5599 packets, from 1011 to 2178 packets when other parameters are fixed when the arrival rate parameter 'a' varies from 11 $x10^4$ packets/sec to 14 $x10^4$ packets/sec, the mean number of packets in the first, second and third buffers in the network are increasing from 16489 to 20986 packets, 2948 packets to 3752 packets 1113 packets to 1416 packets respectively. The parameter 'b' varies from 1.25 to 2.5 the mean number of packets in the first, second and third buffer in the network are increasing from 11399 packets to 14753 packets, 2244 packets to 2707packets, 0922 packets to 1402 packets respectively, when other parameters remain fixed.

The transmission parameter 'μ_1' varies from 11 x 10^4 packets/sec to 14 x 10^4 packets/sec, the mean number of packets in the first, second and third buffers are increasing from 13934 packets to 11484 packets, from

2744 packets to 2885 packets, from 1037 packets to 1093 packets respectively, when other parameters remain fixed.

Similarly, the transmission rate 'μ_2' varies from 26 x 10^4 packets/sec to 29 x 10^4 packets/sec, the mean number of packets in the first buffer remains at 14990 packets and the mean number of packets in the second and third buffers are

increasing from 2588 packets to 2346 packets, and 1016 packets to 1028 packets respectively when other parameters are remaining fixed. Similarly, the transmission parameter 'μ_3' varies from 28 x 10^4 packets/sec to 31 x 10^4 packets/sec, the mean number of packets in the first and second buffers remain constant at 14990 packets and 268 packets respectively. and third buffer decreases from 1076 to 0982 when other parameters remain fixe

It is observed that as time 't' and the arrival parameters 'a''b' are increasing the mean delay in buffers are increasing for fixed values of the other parameters. It

is also observed that as parameter 'θ' varies the mean delay in buffers are decreasing for fixed values of the other parameters.

The parameters π and, θ varies the mean delay in first buffer remain constant and in the second and third buffers its values are decreasing for fixed values of the other parameters. The variance of the number of packets in each buffer and in the network, throughput of each node are computed for different values of t, a, b, μ_1, μ_2,μ_3,π,θ are presented in Table 3. It is observed as time 't' increases, the throughput of first, second and third nodes are increasing from 77664 packets to 95168 packets, 58769 to 107184 packets and 28859 packets to 58725 packets respectively.

As the arrival parameter 'a' varies from 11 x10^4 packets/sec to 14 x 10^4 packets/sec, the throughput of the first, second and third nodes are increasing from 80773 packets to 87737 packets, from 63825 to 78207 packets and from 31587 packets to 39609 packets. As the arrival parameter 'b' varies from 1.25 x10^4 packets/sec to 2.5 x 10^4 packets/sec, the throughput of the first, second and third nodes are increasing from 68015 packets to 77129 packets, from 50250 to 59284 packets and from 26419 packets to 29773packets.

When the transmission parameter "**μ_1**" varies from 11 x10^4 packets/sec to 14 x 10^4 packets/sec, the throughput of the first, second and third nodes are increasing from 82695 packets to 95598 packets, from 59986 to 62650 packets and from 29547 packets to 31054 packets when other parameters remain fixed. The transmission parameter "**μ_2**" varies from 26x10^4 packets/sec to 29 x 10^4 packets/sec, the throughput of the first node remain constant at 77664 packets, for the second and third nodes its values are increasing from packets to 59282packets top 60645 packets, and from 2893 packets to 29306 packets respectively when other parameters are remaining fixed. Similarly, the transmission parameter "**μ_3**" varies from 28 x10^4 packets/sec to 31 x 10^4 packets/sec, the throughput of the first and second nodes remain constant at 77664 packets and 58769 packets respectively and for third node it increases from 28565 packets to 28993 packets, respectively when other parameters are fixed. The graphical representation for the table 2 and table 3 are also calculated in thesimilarfashion.

Table 3: Effect of Various Parameters on Throughput and Variance under Transient State for Communication Network Model *=seconds, $= multiples of 1000 packets/seconds

t*	a$	b	μ1$	μ2$	μ3$	π	θ	Var(N_1)	Var(N_2)	Var(N_3)	Thp$_1$(t)	Thp$_2$(t)	Thp$_3$(t)
0.8	10	3	10	25	30	0.5	0.5	1.4990	0.2680	0.1011	7.7664	5.8769	2.8859
0.9	10	3	10	25	30	0.5	0.5	1.9496	0.3534	0.1351	8.5767	7.4425	3.7914
1.0	10	3	10	25	30	0.5	0.5	2.4599	0.4507	0.1740	9.1455	9.0700	4.7909
1.1	10	3	10	25	30	0.5	0.5	3.0299	0.5599	0.2178	9.5168	10.7184	5.8725
0.8	**11**	3	10	25	30	0.5	0.5	1.6489	0.2948	0.1113	8.0773	6.3825	3.1587
0.8	**12**	3	10	25	30	0.5	0.5	1.7988	0.3216	0.1214	8.3450	6.8748	3.4288
0.8	**13**	3	10	25	30	0.5	0.5	1.9487	0.3484	0.1315	8.5754	7.3541	3.6962
0.8	**14**	3	10	25	30	0.5	0.5	2.0986	0.3752	0.1416	8.7737	7.8207	3.9609
0.8	10	**1.25**	10	25	30	0.5	0.5	1.1399	0.2244	0.0922	6.8015	5.025	2.6419
0.8	10	**1.5**	10	25	30	0.5	0.5	1.2504	0.2425	0.0983	7.1362	5.3839	2.8096
0.8	10	**2**	10	25	30	0.5	0.5	1.3994	0.2638	0.1043	7.5325	5.7968	2.9719
0.8	10	**2.5**	10	25	30	0.5	0.5	1.4753	0.2707	0.1045	7.7129	5.9284	2.9773
0.8	10	3	**11**	25	30	0.5	0.5	1.3934	0.2744	0.1037	8.2695	5.9986	2.9547
0.8	10	3	**12**	25	30	0.5	0.5	1.3012	0.2798	0.1058	8.7336	6.1011	3.0126
0.8	10	3	**13**	25	30	0.5	0.5	1.2201	0.2844	0.1077	9.1625	6.1889	3.0623
0.8	10	3	**14**	25	30	0.5	0.5	1.1484	0.2885	0.1093	9.5598	6.265	3.1054
0.8	10	3	10	**26**	30	0.5	0.5	1.499	0.2588	0.1016	7.7664	5.9282	2.8983
0.8	10	3	10	**27**	30	0.5	0.5	1.499	0.2502	0.102	7.7664	5.9764	2.9098
0.8	10	3	10	**28**	30	0.5	0.5	1.499	0.2422	0.1024	7.7664	6.0218	2.9206
0.8	10	3	10	**29**	30	0.5	0.5	1.499	0.2346	0.1028	7.7664	6.0645	2.9306

0.8	10	3	10	25	**28**	0.5	0.5	1.499	0.268	0.1076	7.7664	5.8769	2.8565
0.8	10	3	10	25	**29**	0.5	0.5	1.499	0.268	0.1011	7.7664	5.8769	2.8859
0.8	10	3	10	25	**30**	0.5	0.5	1.499	0.268	0.0982	7.7664	5.8769	2.8993
0.8	10	3	10	25	**31**	0.5	0.5	1.499	0.268	0.0982	7.7664	5.8769	2.8993
0.8	10	3	10	25	30	**0.4**	**0.6**	1.499	0.2144	0.0971	7.7664	4.824	2.7759
0.8	10	3	10	25	30	**0.3**	**0.7**	1.499	0.1608	0.085	7.7664	3.7132	2.4435
0.8	10	3	10	25	30	**0.2**	**0.8**	1.499	0.1072	0.0647	7.7664	2.5412	1.8804
0.8	10	3	10	25	30	**0.1**	**0.9**	1.499	0.0536	0.0364	7.7664	1.3046	1.0727

If the variance of the number of packets in each buffer increases, then the burstness of the buffer will be high. Hence, the parameters are to be adjusted in such a way that the variance of the content of each buffer is become small. The coefficients of variation of the number of packets in each buffer is computed. To understand the consistency of the traffic flow. Its help us to control the smooth flow of packets in buffers. From this analysis it is observe that the dynamic bandwidth allocation strategy has significant influence on all performance measures of the network. It is further observed that the performance measures are highly sensitive towards smaller values of time. Hence, it is optimal to consider dynamic bandwidth allocation under and Duane arrival process and evaluate the performance under transient conditions. It is also to be observed that the congestion in buffer and delays in transmission got reduced to a minimum level by adopting dynamic bandwidth allocation. This phenomenon has a vital bearing on quantity of transmission.

As time t increases, the percentage variation of performance measures between the models are increasing. For the proposed models with non-homogenous Poisson arrivals having dynamic bandwidth allocation has more utilization compared to that of the model with Poisson arrivals under dynamic bandwidth allocation. From this analysis it is observed that the assumption of non-homogenous arrivals has a significant influence on all the performance measures of the network.

5. COMPARATIVE STUDY

The comparative study between the proposed communication network model with that of homogenous Poisson arrivals is presented in this section, the computed performance measure of both models are presented in the Table 5 for different values of t=0.8 ,0.9,1.0, 1.1.

Table 4: Comparative study of models with homogeneous and Non-homogeneous Duane Arrivals

Time	Parameters	Poisson	Proposed model	Difference	Variance
0.8	$L_1(t)$	0.9993	1.499	0.4997	33.33555704
	$L_2(t)$	0.1998	0.268	0.0682	25.44776119
	$L_3(t)$	0.0832	0.1011	0.0179	17.70524233
	$U_1(t)$	0.6319	0.7766	0.1447	18.63250064
	$U_2(t)$	0.1811	0.2351	0.054	22.96894938
	$U_3(t)$	0.0798	0.0962	0.0164	17.04781705
	$Thp_1(t)$	6.3187	7.7664	1.4477	18.64055418
	$Thp_2(t$	4.5272	5.8769	1.3497	22.96618966
	$Thp_3(t)$	2.3948	2.8859	0.4911	17.01722166
	$W_1(t)$	0.1582	0.193	0.0348	18.03108808
	$W_2(t)$	0.0441	0.0456	0.0015	3.289473684
	$W_3(t)$	0.0347	0.035	0.0003	0.857142857
0.9	$L_1(t)$	0.9998	1.9496	0.9498	48.71769
	$L_2(t)$	0.1999	0.3534	0.1535	43.4352
	$L_3(t)$	0.0833	0.1351	0.0518	38.34197
	$U_1(t)$	0.632	0.8577	0.2257	26.31456
	$U_2(t)$	0.1812	0.2977	0.1165	39.13336
	$U_3(t)$	0.0799	0.1264	0.0465	36.78797
	$Thp_1(t)$	6.3203	8.5767	2.2564	26.30849

	Thp_2(t	4.53	7.4425	2.9125	39.13336
	Thp_3(t)	2.3972	3.7914	1.3942	36.7727
	W_1(t)	0.1582	0.2273	0.0691	30.40035
	W_2(t)	0.0441	0.0475	0.0034	7.157895
	W_3(t)	0.0347	0.0356	0.0009	2.52809
1	L_1(t)	0.9999	2.4599	1.46	59.35200618
	L_2(t)	0.2	0.4507	0.2507	55.62458398
	L_3(t)	0.0833	0.174	0.0907	52.12643678
	U_1(t)	0.6321	0.9146	0.2825	30.88781981
	U_2(t)	0.1812	0.3628	0.1816	50.05512679
	U_3(t)	0.0799	0.1597	0.0798	49.9686913
	Thp_1(t)	6.3209	9.1455	2.8246	30.88513477
	Thp_2(t	4.5311	9.07	4.5389	50.0429989
	Thp_3(t)	2.3981	4.7909	2.3928	49.9446868
	W_1(t)	0.1582	0.269	0.1108	41.18959108
	W_2(t)	0.0441	0.0497	0.0056	11.26760563
	W_3(t)	0.0347	0.0363	0.0016	4.407713499
1.1	L1(t)	1	3.0299	2.0299	66.99561042
	L2(t)	0.2	0.5599	0.3599	64.2793356
	L3(t)	0.0833	0.2178	0.1345	61.75390266
	U1(t)	0.6321	0.9517	0.3196	33.58201114
	U2(t)	0.1813	0.4287	0.2474	57.70935386
	U3(t)	0.0799	0.1957	0.1158	59.17220235
	Thp1(t)	6.3211	9.5168	3.1957	33.57956456
	Thp2(t	4.5315	10.7184	6.1869	57.72223466
	Thp3(t)	2.3985	5.8725	3.474	59.15708812
	W1(t)	0.1582	0.3184	0.1602	50.31407035
	W2(t)	0.0441	0.0522	0.0081	15.51724138
	W3(t)	0.0347	0.0371	0.0024	6.469002695

6. CONCLUSION

In this paper, a new and novel three nodes tandem communication network model with Duane arrival process having dynamic bandwidth allocation with phase type transmission was introduced. The arrival of packets in a network traffic is characterized through Weibull inter arrival time distribution which better represents the self-similarity network traffic having time dependent burstness. The Duane process is a generalization of Poisson process. Here it is, assumed that the three nodes are connected in tandem and the transmission processes follow Poisson. The transmission rate at every instant of packet transmission is adjusted depending on the content of the buffer connected to it. The explicit expressions for the performance measures of the communication network such as mean content of the buffers mean delays in transmission, the throughput of the nodes, utilization of the buffers are derived. The sensitivity of the model revealed that the inter arrival rate parameters has significant influence on predicting the performance measures of the network more accurately. A comparative study of the proposed network with that of inter exponential transmission times shown that the proposed model outperforms the existing communication network model in scheduling self-similarity networks such as LAN, WAN and MAN. It is, also possible to derive the optimal operating policies of the networks with suitable cost consideration which will be taken elsewhere.

7. REFERENCES

[1] William cook and Charles Wheatstone (1939), IEEE communication society (2002).

[2] Gaujal. B, Hyon.E (2002) optimal routing policies in deterministic queues in tandem, proceedings of south international work shop on discrete event systems, pp:251-257.

[3] Parthasarathy.P.R. R and Selvaraju.N (2001) Transient analysis of a queue where potential customers are discouraged by queue length. Mathematical problem in engineering, Vol. 7, pp:433-454

[4] Srinivasa Rao., Vasantha. M.R, Vijaya Kumar. C.V.R.S (2002) on an independent communication network, opsearch vol.37, No.2, pp: 134-143.

[5] Sriram. K (1993) methodologies for bandwidth allocation transmission scheduling and congestion avoidance in broadband ATM networks, Computer network, ISDN system, J.26, pp:43-59

[6] Suresh Varma. P, Srinivasa Rao K, P. Srinivasa Rao (2007) a communication with load dependent transmission, International journal of mathematical sciences, vol.12, No.2, pp:1-15

[7] Padmavathi, G., Srinivasa Rao, K and Reddy, K.V.V.S (2009), "Performance Evaluation of parallel and series communication network with dynamic band width allocation CIIT" International, Journal of Networking and Communication, Vol.1, No.7, pp:410-42.

[8] Nageswara Rao, K., Srinivasa Rao, K. and Srinivasa Rao, P. (2010), "A tandem communication network with dynamic band width allocation and modified phase type transmission having bulk arrivals, International Journal of Computer Sciences, Issues, Vol. 7, No.2, pp:18-26.

[9] Kuda nageswarararao, K. Srinivasa Rao and P. Srinivasa Rao (2011) – "transient analysis of a tandem communication network with dynamic bandwidth allocation having two stage direct bulk arrivals, international journal of computer applications, vol.13, no.7, pp.14-22. Rakesh Singhai, Shiva Dutt Joshi and Rajendra K. P. Bhatt, (2007), "A Novel Discrete Distribution and Process to Model Self-SimilarTraffic, "9th IEEE international conference on telecommunications – Con TEL 2007, Zagreb, Croatia, pp 167-1

[10] Kuda nageswarararao, K. Srinivasa Rao and P. Srinivasa Rao (2011) – "transient analysis of a tandem communication network with dynamic bandwidth allocation having two stage direct bulk arrivals, international journal of computer applications, vol.13, no.7, pp.14-22.

[11] Kuda Nageswarararao Rao, K. Srinivasa Rao and P. Srinivasa Rao (2011) – performance evaluation of a communication network with dynamic bandwidth allocation and bulk arrivals, performance evaluation, vol.16, no.8.

[12] Padmavathi, G., Srinivasa Rao, K and Reddy, K.V.V.S (2009), "Performance Evaluation of parallel and series communication network with dynamic band width allocation CIIT" International, Journal of Networking and Communication, Vol.1, No.7, pp:410-42.

[13] P.Abry, R. Baraniuk, P. Flandrin, R. Riedi, D. Veitch, (2002), "Multi-scale Nature of Network Traffic," IEEE Signal Processing Magazine, pp. 28-27.

[14] Cappe O, E. Moulines, J. C. Pesquet, A. Petropulu, X. Yang (2002), "Long-Range Dependence and Heavy-Tail Modeling for Teletraffic Data," IEEE signal Processing Magazine, pp.14-27.

[15] W.Leland, M. Taqqu, W. Willinger, and D. Wilson,(1994) "On the self-similar nature of Ethernet traffic(extended version)," IEEE/ACM Trans. Networking, vol. 2, pp

[16] Crovella (1997) ME and Bestarros A (1997) self-similarity in worldwide traffic, evidence and possible cases, IEEE / ACM transaction networking, vol.5, No.6, pp:835-846

[17] A. Feldmann, (2000), "characteristics of TCP connection Arrivals" chapter 15, Self-Similar Network traffic and Performance evolution, edited by K.Park, W. Willinger, John Wiley& Sons Inc.

[18] M. J. Fisher, D. Gross, D. Masi and J. F. Shortle, (2001), "Analyzing the Waiting Time Process in Internet Queuing Systems with the Transform Approximation Method," The Telecommunications Review,12, pp 21-32

Design of a Novel Sliding Mode Functional Observer based Load Frequency Controller for Inter Connected Power System

Anand Gondesi, Department of EEE, Dr.L.B. College of Engineering (W), Visakhpatnam, India.

E-mail:anandgondesi@gmail.com

R. Vjaya Santhi, Department of EE, A.U. College of Engineering(W), Andhra University, Visakhpatnam, India.

E-mail:santhikanth@gmail.com

K. Rama Sudha, Department of EE, A.U. College of Engineering(W), Andhra University, Visakhpatnam, India.

E-mail:arsudhaa@gmail.com

Abstract--- The prime objective of this research paper is to present an innovative Sliding Mode Functional Observer controller for stability of Power System. When the states of the system are not quantifiable for State-Feedback Control, a new operational observer has been designed to estimate the control input directly to substitute the system states. The observer gains can be obtained numerically and the stability can be assured concurrently. The Sliding Type Functional Observer is also capable of reducing the order of the observer. The above mentioned approaches are tested for Load Frequency Control (LFC) problems of highly interconnected system. As the controllers in state estimation process require tie-line powers, the quasi decentralized technique is employed for the LFC problem. As these controllers consider the entire topology of the system they differ from the other traditional controllers. The superiority of Sliding Mode Functional Observer (SMFO) is demonstrated clearly with respect to Proportional Integral based Functional Observer (PIFO) and Functional Observer (FO).

Keywords--- Load Frequency Control, Sliding Mode Functional Observer, Functional Observers, Quasi-Decentralized Functional Observers, State Feedback Controller, Leunberger Observer, Interconnected Power Systems.

I. Introduction

Due to growing complication in interconnected power systems, the LFC scheme plays a very important role using a Proportional Integral Control Strategy [1]–[4].The control action is generated as an important function of Area Control Error (ACE). LFC is a scheme that keeps the frequency of a network within satisfactory limits regardless of load variations by balancing the power consumption and production. Furthermore, it has competence to bring any deviations (i.e., tie-line power deviations) of the entire power exchange back to zero, amongst interconnected areas. In general, LFC is implemented on selected generation units. Literatures [1] - [3] developed different controllers to a prime –movers for reduce load fluctuation effects and also to meet required power demand. Integral controller [4], proposed to reduce area control error and power deviation in tie-line. Soft computing techniques also proposed [8]-[13] for LFC to minimize power deviation in tie-line. In [2] developed model order reduction technique to reduce the order of LFC and also designed Internal model controller (IMC) controller for reject disturbances for original LFC system. For other methods of LFC, see [14]–[16], and also in [17] suggested various control methods.

During the last decade, several attempts were made for a better control strategy suggested to achieve improved dynamic system performance and wider stability margins based on modern optimal control theory in which the control strategies are mostly based on linear state regulator theory. Threquise require either state reconstruction or full state vector feedback using a Luenberger observer for the control realization. However, it is seldom in practice that all these state variables are accessible for the measurement whereas state reconstruction using an observer may become prohibitive due to cost and complexity considerations. Therefore, to circumvent these problems, LFC designs were proposed in literature using quasi-decentralized functional observer. Although, these strategies depends on the quantifiable output variables alone as currently used in practice, they need feedback of output variables from other areas through telecommunication links requiring additional hardware and high implementation cost. Moreover, with the present growth in number of interconnected areas, centralized controller design may result in complexity in implementation. Hence, it is desirable to propose a quasi-decentralized control strategy which is

Received: 20 June 2018/Accepted: 15 July 2018

compatible with the existing LFC schemes and which depends for its realization of control signal in a particular area on the output variables pertaining to that area only.

Keeping the above considerations in view, a decentralized LFC design is illustrated in the present paper. In the paper [18], the application of a QFO is considered. Based on this preliminary work in [18], this paper further develops the Functional Observer (FO) theory for LFC of interconnected power networks of higher order. In the signal generation process of LFC, the estimate of the control signal alone is required. Upon using a functional observer, it is more congruent to estimate the required signal directly. All the states are estimated individually and re-combined to build the desired control signal. Actually a control signal is generated by considering QFO.

Sliding mode functional observer estimates the state vector linear function without estimating all individual states while ensuring sliding on a manifold where a function of output prediction error is zero. Such state vector functional estimates are very useful in the design of feedback control system as the control signal is linear combination of all the states, and utilization of a linear functional observer based on sliding mode is possible to estimate the feedback control signal directly. Although the sliding mode theory for State observers are well established for the linear systems [1]- [6], the linear sliding mode functional observers concept has not been reported for LFC. Here, sliding mode to functional observer concept is introduced for LFC. A key feature in this Utkin observer is the basic introduction of the switching function to achieve a sliding mode along with stable error dynamics [1]. Similarly, the sliding mode functional observer also makes use of a switching function in its design and invariably inherits the insensitivity benefits to the variations in parameter and noise rejection as of the Utkin observer. Furthermore, sliding mode functional observers will have lower order which is one of the characteristic of the functional observers [7] - [13]. In this paper, special circumstances of the proposed observer are shown.

II. Dynamic Modeling of Interconnected System

The block diagram of a thermal power system (two area) for the load frequency control [9]-[16] is as shown in *Fig.1.*

Consider a dynamic model of the linear two area LFC in state-space representation is as follows:

$$\dot{x}(t) = Ax(t) + Bu(t) \quad (1)$$

$$y(t) = Cx(t) \quad (2)$$

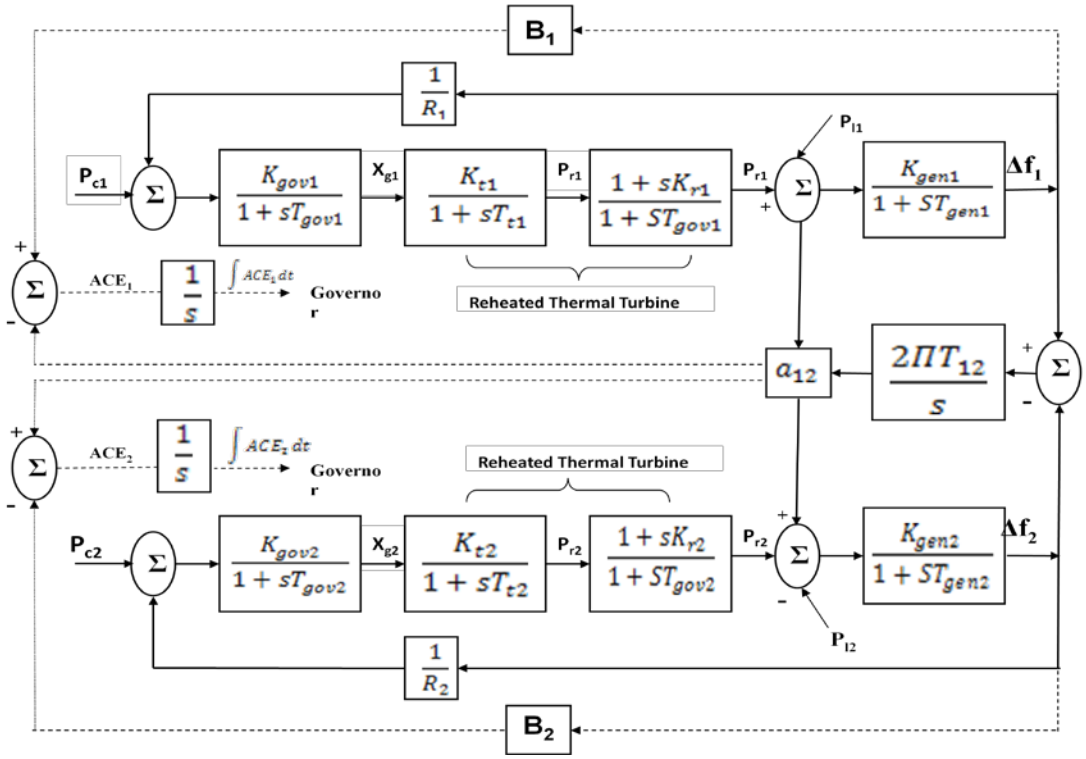


Fig. 1: Block-Diagram of Two-Area Interconnected Power System (TAIPS)

Received: 20 June 2018/Accepted: 15 July 2018

Where $x(t) \in R^n$, $u(t) \in R^m$ and $y(t) \in R^p$ are state vector, the control input vector and the measurement output vector, respectively. Matrices A$\in R^{n\times n}$, B$\in R^{n\times m}$ and C$\in R^{p\times n}$ are known constants.

The state variable representation is advantageous compared to the conventional transfer function representation. State vector, x(t) contains the information about the past behavior of system and the future behavior governed by an ordinary differential equation (1). The properties of this system are determined by the constant matrices A, B and C. Thus, this study can be carried out in the field of matrix theory which has many notational and conceptual advantages.

In any control system, the input vector u(t) is chosen by proper control schemes such that the system behaves in an acceptable manner. As the state vector x(t) contains all the essential information about the system, the selection of u(t) is done using some combinations of x(t) and u(t) is obtained from the relation

$$u(t) = -K\,x(t) \tag{3}$$

Where K $\in R^{m\times n}$ is a constant matrix.

In a simplified manner, the tie line power flow can be taken as Area 2 in a two area system consisting of reheats thermal turbines. From Fig. 1.

$$P_{tie2}(t) = -P_{tie2}(t)$$

Let $x_i(t), u_i(t), d_i(t)$ and $y_i(t)$ (i=1,2) as state, control, load disturbance and the output vectors.

Where

$$x_1(t) = [P_{tie1}\ \ f_1\ \ P_{r1}\ \ P_{g1}\ \ X_{g1}\ \int ACE_1\,dt\ ]^T \tag{4}$$
$$x_2(t) = [f_2\ \ P_{r2}\ \ P_{g2}\ \ X_{g2}\ \int ACE_2\,dt\ ]^T \tag{5}$$
$$u_i(t) = P_{ci}(t),\ \ d_i(t) = P_{li}(t) \tag{6}$$
$$y_i(t) = [P_{tiei}\ \ f_i\ \ X_g\ \int ACE_2\,dt]^T \tag{7}$$

From this, the representation for the two area interconnected system is determined for an eleventh-order, 2-input, 2-disturbance, where

$$\dot{x}(t) = Ax(t) + Bu(t) + D_d(t) \tag{8}$$

From equation (7), the controlled feedback variables of ACE's are provided with integral of to ensure steady state values for tie-line power and frequencies is zero for load disturbances which is in step change. Pole placement or optimal control by state feedback has been broadly shrouded in the literature [1]-[3].

III. Sliding Mode Functional Observer

A Functional observer uses repeating theme in state feedback control, i.e., only linear function is enough rather than the complete state vector information [5]-[9]. The essential point of the literature is to deliver observer with more stability and further reduced order noticing the affect on the performance because of the change in design.

The result to this problem is presented by Luenberger in earlier days. It states that single linear system state function can be reconstructed by an observer with v-1 eigen values that may be chosen arbitrarily (where v is the observability index). For any completely observable system, v-1< n-m, it is regularly the case that order v-1 of a linear functional observer is less than the order n-m of the reduced-order observer. As a corollary, observing linear function of states may result in a significant of reducted order of observer compared with entire state vector.

Fig. 2 shows a block diagram of QDFO implementation for LFC of TIPS. The flow of information is represented by the dotted lines from one area to another area. The two FO's are decoupled from each other. Thus, transfer of data between them not possible.

A system is involved in many problems like decision making, monitoring, fault detection, and control which rely on the knowledge of state variables and time-varying parameters that cannot be quantifiable directly. In such situations, the state estimation and the parameters in dynamic systems is a vital prerequisite. Hence the observer is employed to estimate the unknown states by using the input and output signals. Various estimation techniques are presented for the construction of observers for linear models such as the Kalman filter. However there is no comprehensive procedure for a design of estimators for non-linear system as it involves high computational costs. One such model which facilitates the stability analysis and observer design for such systems can be represented by a special type of a dynamic nonlinear model[11].

Received: 20 June 2018/Accepted: 15 July 2018

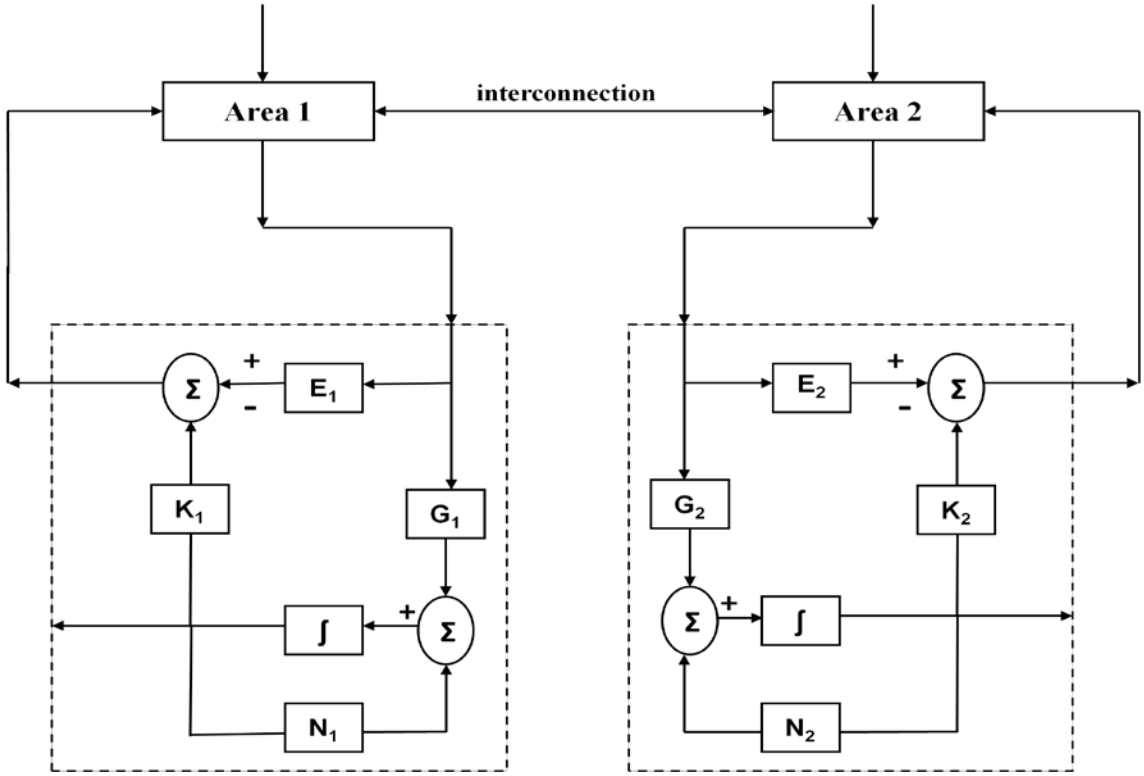


Figure 2: Block Diagram Implementation of QDFO's for the TIPS

Consider a linear time-invariant system described by

$$\dot{x}(t) = Ax(t) + Bu(t) \quad (9)$$

$$y(t) = Cx(t) \quad (10)$$

$$z(t) = Lx(t) \quad (11)$$

Where $x(t) \in R^n$, $u(t) \in R^m$ and $y(t) \in R^p$ the state input and the output vectors, respectively. $z(t) \in R^r$, is a vector to be estimated. $A \in R^{nxn}$, $B \in R^{nxm}$, $C \in R^{pxn}$ and L $\in R^{rxn}$ are known constant matrices. A dynamical system is functional observer that can track $z(t)$ asymptotically and has the following structure,

$$\dot{w}(t) = Nw(t) + Jy(t) + Hu(t) + \Gamma sgn(Me(t)) \quad (12)$$

$$\hat{z}(t) = Gw(t) + Ey(t) \quad (13)$$

$$e(t) = z(t) - \hat{z}(t) \quad (14)$$

Where $w(t) \in R^r$, $M \in R^{\bar{r}\times r}$, $\Gamma \in R^{r\times\bar{r}}$, $sgn(.)$ is the sign function and also the sliding surface is given by

$$Me(t) = 0 \quad (15)$$

In the view of the dimension of matrix M, the error vector e(t) can be written as

$$e(t) = \begin{bmatrix} e_y(t) \\ e_1(t) \end{bmatrix} \quad (16)$$

Where $e_y(t) \in R^{\bar{r}}$, and $e_1(t) \in R^{r-\bar{r}}$

The problem to be solved in this paper is to design a sliding mode linear functional observer of the form (12)-(14) where N, J,H, E,M and Γ are to be determined such that e(t) slide along the surface Me(t) = 0 and $e_1(t) \rightarrow 0$ as $t\rightarrow\infty$.

To define the sliding surface for the functional observer let us first partition matrix *L* as follows

$$L = \begin{bmatrix} L_1 \\ L_2 \end{bmatrix} \quad (17)$$

Where L1 belong to the row space of C. Since L1 belong to the row space of C, there always exist a full row rank matrix $G \in R^{\bar{r}\times p}, \bar{r} \leq r$ such that

$$L_1 = GC \quad (18)$$

Received: 20 June 2018/Accepted: 15 July 2018

If $M \in R^{\bar{r}\times r}$, is chose such that

$$M = [I_{\bar{r}} \quad 0_{\bar{r}\times(r-\bar{r})}] \tag{19}$$

and *G* according to (18), then the sliding surface (15) is

$$Me(t) = e_y(t) = Gy(t) - M\hat{z}(t) = 0 \tag{20}$$

Using (9)-(14) and (20) the error dynamics of the observer can be written as follows

$$\dot{e}(t) = Ne(t) + (PA - NP - JC)x(t) + (PB - H)u(t) + \Gamma sgn(e_y(t)) \tag{21}$$

where $P = L - EC$. Considering the partitioning of $e(t)$ in (16), matrix N can be partitioned as follows

$$N = \begin{bmatrix} N_{11} & N_{12} \\ N_{21} & N_{22} \end{bmatrix} \tag{22}$$

If we now choose $\Gamma = \begin{bmatrix} \Gamma_1 \\ 0_{(r-\bar{r})\times\bar{r}} \end{bmatrix}$ $\Gamma_1 \epsilon R^{\bar{r}\times\bar{r}}$ then the error dynamics (21) can be rewritten as

$$\begin{bmatrix} \dot{e}_y(t) \\ \dot{e}_1(t) \end{bmatrix} = \begin{bmatrix} N_{11} & N_{12} \\ N_{21} & N_{22} \end{bmatrix} \begin{bmatrix} e_y(t) \\ e_1(t) \end{bmatrix} + (PA - NP - JC)x(t) + (PB - H)u(t) + \begin{bmatrix} \Gamma sgn(e_y(t)) \\ 0 \end{bmatrix} \tag{23}$$

The existence conditions of the observer (12)-(14) are given in the following Theorem.

The system matrices *A, B* and *C* and observer matrices *N, J, H, D* and *E* are defined as follows:

$$A \in R^{nxn} \qquad N \in R^{q\text{x}q}$$
$$B \in R^{nxm} \qquad J \in R^{qxp}$$
$$C \in R^{pxn} \qquad H \in R^{qxm}$$
$$L \in R^{rxn} \qquad D \in R^{rxp} \qquad E \in R^{rxp}$$

Theorem-1

Theorem: $e1(t) \to 0$ as $t \to \infty$ and also $e(t)$ slide along the surface $Me(t) = 0$, $t \geq ts$ where $t_s \leq \left(\frac{\|G_y(0) - M\hat{z}(0)\|}{\eta}\right)$, $\eta > 0$ for any $x(0)$, $\hat{z}(0)$, and $u(t)$ if the following conditions are satisfied:

$$N_{22} \text{ Hurwitz} \tag{24}$$
$$JC = PA\text{-}NP \tag{25}$$
$$H = PB \tag{26}$$
$$e_y^T(t)\dot{e}_y(t) < -\eta\|e_y(t)\| \tag{27}$$

Proof : If conditions (25) and (26) are satisfied then the error dynamics (23) of the observer is given by

$$\dot{e}_y(t) = N_{11}e_y(t) + N_{12}e_1(t) + \Gamma_1 sng(e_y(t)) \tag{28a}$$
$$\dot{e}_1(t) = N_{21}e_y(t) + N_{22}e_1(t) \tag{28b}$$

If (27) is satisfied then an ideal sliding motion will take place on the surface

$$S = \{e_1(t), e_y(t) : e_y(t) = 0\} \tag{29}$$

It follows that after some finite time t_s, for all subsequent time, $\dot{e}_y(t) = 0$ [6]. The dynamics of $e_1(t)$ then reduces to

$$\dot{e}_1(t) = N_{22}e_1(t) \tag{30}$$

If (24) is satisfied then $e_1(t) \to 0$ as $t \to \infty$.Considering the partitioning of $e(t)$ in (8), matrices *P, J* and *E* can be partitioned as$P = \begin{bmatrix} P_1 \\ P_2 \end{bmatrix}$, $J = \begin{bmatrix} J_1 \\ J_2 \end{bmatrix}$ and $E = \begin{bmatrix} E_1 \\ E_2 \end{bmatrix}$. Using the definition of $P = L - EC$, the partitioned matrices P_1 and P_2 can be written as

$$P_1 = L_1 - E_1C \tag{31a}$$
$$P_2 = L_2 - E_2C \tag{31b}$$

Furthermore, equation (25) can be rewritten as

$$P_1A - N_{11}P_1 - N_{12}P_2 - J_1C = 0 \tag{32a}$$
$$P_2A - N_{21}P_2 - N_{22}P_2 - J_2C = 0 \tag{32b}$$

Let L^+ denote the Moore-Penrose generalized inverse of *L*. Equation (32a) is equivalent to

$$(P_1A - N_{11}P_1 - N_{12}P_2 - J_1C)[L^+I - L^+L] = 0 \tag{33}$$

because $[L^+ I - L^+L]$ is a full row rank matrix. Let us now partition L^+as follows

Received: 20 June 2018/Accepted: 15 July 2018

$$L^+ = [M_1 \quad M_2] \tag{34}$$

Where $M_1 \epsilon R^{n\times \bar{r}}$ and $M_2 \epsilon R^{n\times(r-\bar{r})}$ Using (31a), (31b) and (32), equation (33) leads to

$$N_{11} = L_1 A M_1 - [E_1 \quad K_1]\begin{bmatrix} CAM_1 \\ CM_1 \end{bmatrix} \tag{35a}$$

$$N_{12} = L_1 A M_2 - [E_1 \quad K_1]\begin{bmatrix} CAM_2 \\ CM_2 \end{bmatrix} \tag{35b}$$

$$[E_1 \quad K_1]\Sigma = L_1 \bar{A} \tag{35c}$$

$$K_1 = J_1 - N_{11}E_1 - N_{12}E_2 \tag{36}$$

$$\Sigma = \begin{bmatrix} C\bar{A} \\ \bar{C} \end{bmatrix} \tag{37}$$

$$\bar{A} = A(I - L^+L) \tag{38}$$

$$\bar{C} = C(I - L^+L) \tag{39}$$

Adopting the same procedure as in [13], it can be shown that equation (35c) can always be solved for E_1 and K_1 because $L_1\bar{A}(I - \Sigma^+\Sigma) = 0$ (i.e. $rank\begin{bmatrix} L_1\bar{A} \\ \Sigma \end{bmatrix} = rank[\Sigma]$) and the general solution is given by

$$[E_1 \quad K_1] = L_1\bar{A}\Sigma^+ + Z_1(I - \Sigma\Sigma^+) \tag{40}$$

where Z_1 is any arbitrary matrix of appropriate dimension. Using (40) in (35a) and (35b), the following can be written

$$N_{11} = F_{11} - Z_1 G_1 \tag{41a}$$

$$N_{12} = F_{12} - Z_1 G_2 \tag{41b}$$

Where

$$F_{11} = L_1 A M_1 - L_1\bar{A}\Sigma^+\begin{bmatrix} CAM_1 \\ CM_1 \end{bmatrix} \tag{42a}$$

$$F_{12} = L_1 A M_2 - L_1\bar{A}\Sigma^+\begin{bmatrix} CAM_2 \\ CM_2 \end{bmatrix} \tag{42b}$$

$$G_1 = (I - \Sigma\Sigma^+)\begin{bmatrix} CAM_1 \\ CM_1 \end{bmatrix} \tag{42c}$$

$$G_2 = (I - \Sigma\Sigma^+)\begin{bmatrix} CAM_2 \\ CM_2 \end{bmatrix} \tag{42d}$$

As with (32a), we can adopt the same procedure starting from equation (32b). Equation (32b) is equivalent to

$$(P_2 A - N_{21}P_1 - N_{22}P_2 - J_2 C)[L^+\mathrm{I} - \mathrm{L}^+L] = 0 \tag{43}$$

Because $[L^+\mathrm{I} - \mathrm{L}^+L]$ is a full row rank matrix. Using (31a), (31b) and (34), equation (43) leads to

$$N_{21} = L_2 A M_1 - [E_2 \quad K_2]\begin{bmatrix} CAM_1 \\ CM_1 \end{bmatrix} \tag{44a}$$

$$N_{22} = L_2 A M_2 - [E_2 \quad K_2]\begin{bmatrix} CAM_2 \\ CM_2 \end{bmatrix} \tag{44b}$$

$$[E_2 \quad K_2]\Sigma = L_2\bar{A} \tag{44c}$$

Where

$$K_2 = J_2 - N_{21}E_1 - N_{22}E_2 \tag{45}$$

In [13], it is shown that equations (44c) can be solved for E_2 and K_2 if and only if

$$rank\begin{bmatrix} L_2 A \\ CA \\ C \\ L_2 \end{bmatrix} = rank\begin{bmatrix} CA \\ C \\ L_2 \end{bmatrix} \tag{46}$$

and the general solution is given by

$$[E_2 \quad K_2] = L_2\bar{A}\Sigma^+ + Z_2(I - \Sigma\Sigma^+) \tag{47}$$

where Z_2 is any arbitrary matrix of appropriate dimension. Using (47) in (44a) and (44b), the following can be written

$$N_{21} = F_{21} - Z_2 G_1 \tag{48a}$$

$$N_{22} = F_{22} - Z_2 G_2 \tag{48b}$$

Where

Received: 20 June 2018/Accepted: 15 July 2018

$$F_{21} = L_2AM_1 - L_2\bar{A}\Sigma^{+}\begin{bmatrix}CAM_1\\ CM_1\end{bmatrix} \quad (49a)$$

$$F_{22} = L_2AM_2 - L_2\bar{A}\Sigma^{+}\begin{bmatrix}CAM_2\\ CM_2\end{bmatrix} \quad (49b)$$

The matrix N_{22} can be made Hurwitz if and only if the pair (F_{22},G_2) is detectable. In the following we present the design algorithm for the sliding mode functional observer.

Design Algorithm

1) Partition L according to $L = \begin{bmatrix}L_1\\ L_2\end{bmatrix} = \begin{bmatrix}GC\\ L_2\end{bmatrix}$
2) Check if condition (26) is satisfied, if yes continue, otherwise a sliding mode functional observer doesn't exist.
3) Compute $F22$ using (41b), $G2$ using (34d) and check if the pair ($F22$,$G2$) is detectable. If yes continue, otherwise $N22$ cannot be made Hurwitz and consequently as table sliding mode functional observer doesn't exist.
4) Using (40b) and any pole placement method obtain $Z2$ to make $N22$ Hurwitz.
5) Use (41a) to compute $F21$, compute $G1$ using (34c) and then use (40a) to compute $N21$.
6) Choose any $Z1$ and use (33a) and (33b) to compute $N11$ and $N12$ respectively.
7) Use (32) and (39) to compute $E1$, $K1$, $E2$ and $K2$.
8) Use (28) and (37) to compute $J1$ and $J2$ respectively.
9) Compute $P1$ and $P2$ using (23a) and (23b) respectively.
10) Compute H according to (18).
11) Use any standard sliding mode technique [6], [14] to obtain Γ1 to make the error dynamics of (20a) table.

The structure of the sliding mode observer proposed in this paper is more general than the Utkin observer [1], if we choose the specific case when $L = In$ then the observer proposed in this paper reduces to the Utkin observer as detailed below. if

$$L = I_n \quad (50)$$

Then from (11) $z(t) = x(t)$ and $\hat{z}(t) = \hat{x}(t)$ where $\hat{x}(t)$is an estimate of $x(t)$. From (17) it follows that

$$L_1 = [I_p \quad 0_{p\times(n-p)}] \quad (51)$$

$$L_2 = [0_{(n-p)\times p} \quad I_{(n-p)}] \quad (52)$$

And from (19)

$$M = [I_p \quad 0_{p\times(n-p)}] \quad (53)$$

Using (18), (51) and (53), the sliding surface (20) can be written as

$$Me(t) = Gy(t) - M\hat{z}(t) = Gy(t) - GC\hat{z}(t) = G(y(t) - C\hat{x}(t)) = 0 \quad (54)$$

Since G in this case is a non-singular square matrix, the sliding surface can be rewritten as

$$Me(t) = y(t) - C\hat{x}(t) = 0 \quad (55)$$

Which is in fact the sliding surface for the Utkin observer. Furthermore, if $L = I_n$ then the following can be deduced:

$$M_1 = L_1,\ M_2 = L_2, F_{11} = A_{11}, F_{12} = A_{12}, F_{21} = A_{21}, F_{22} = A_{22}, G_1 = \begin{bmatrix}A_{11}\\ I_p\end{bmatrix}, G_2 = \begin{bmatrix}I_{(N-P)}\\ A_{12}\end{bmatrix}.$$

The observer matrix N then reduces to $N_{11} = A_{11} - Z_1G_1$, $N_{12} = A_{12} - Z_1G_2$, $N_{21} = A_{21} - Z_2G_1$ and $N_{22} = A_{22} - Z_2G_2$. Since Z_1 is any arbitrary matrix it can be chosen as $Z_1 = 0$. Furthermore, $Z2$ can be chosen as $z_2 = [0 \quad z_{22}]$.

Matrix N can then be written as

$$N = \begin{bmatrix}A_{11} & A_{12}\\ A_{21} & A_{22} - Z_{22}A_{12}\end{bmatrix} \quad (56)$$

The other observer parameters J,E and H reduces to

$$J = \begin{bmatrix}0 & 0\\ 0 & Z_{22}\end{bmatrix} \quad (57)$$

$$E = 0 \quad (58)$$

$$H = B \quad (59)$$

Clearly the observer structure proposed this paper reduces to the Utkin observer when $L = I_n$.

Received: 20 June 2018/Accepted: 15 July 2018

IV. Results and Discussion

The simulation is carried out with the optimum gain settings. Matlab/Simulink software is use to simulate the power to obtain dynamic system responses for 10% load perturbation (LP) is applied in both first area $\mathbf{\Delta}PD_1$ and the second area $\mathbf{\Delta}PD_2$ for the increase in demand. The frequency deviation responses of the control area $\mathbf{\Delta}f_1$, control area $\mathbf{\Delta}f_2$ and the Tie-line power of Area1-2 are shown in Figure 3 to Figure 11 respectively. It is observed that the proposed scheme gives improved dynamic responses having comparatively smaller peak overshoot and quicker settling time with steady state error zero as compared to PIQDFO and Functional observer. The quantitative comparison is made in Figure 12 and Figure 13 where percentage reduction in the peak overshoot of $\mathbf{\Delta}f_1$, $\mathbf{\Delta}f_2$ and the tie-line power and settling time of $\mathbf{\Delta}f_1$, $\mathbf{\Delta}f_2$ and the tie-line power are shown with different operating points. It is evident that for 10% SLP, peak overshoot and undershoots are gradually decreased and settling time remains approximately same with steady state error Zero. From Figure 3 to Figure 13 it is found that the performance of the Desined SMQDFO is far superior to the PIQDFO and Functional observer.

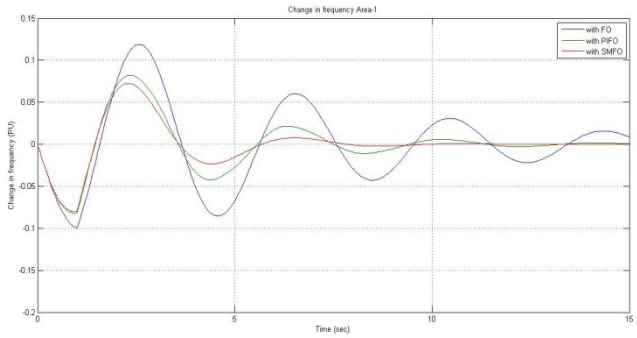


Figure 3: Change in Frequency Deviation Response of Control Area 1 at Operating Point 1

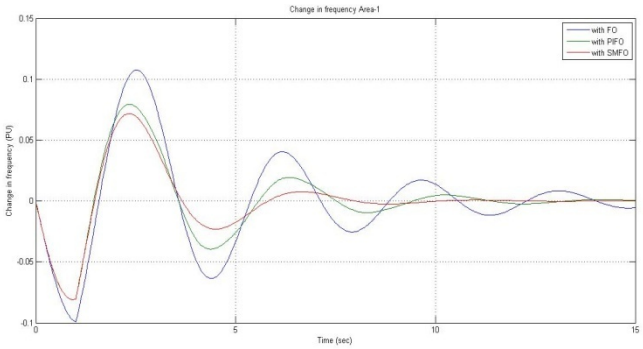


Figure 4: Change in Frequency Deviation Response of Control Area 1 at Operating Point 2

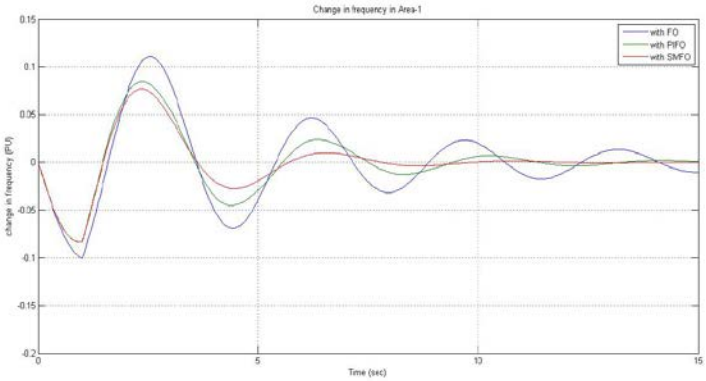


Figure 5: Change in Frequency Deviation Response of Control Area 1 at Operating Point 3

Received: 20 June 2018/Accepted: 15 July 2018

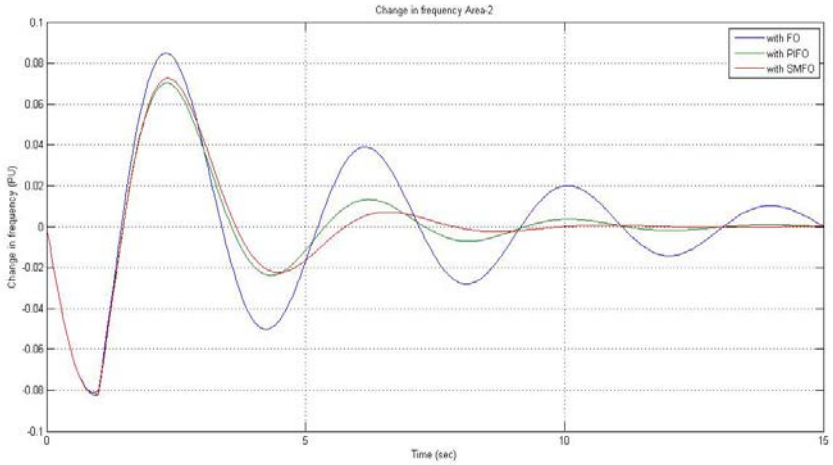


Figure 6: Change in Frequency Deviation Response of Control Area 2 at Operating Point 1

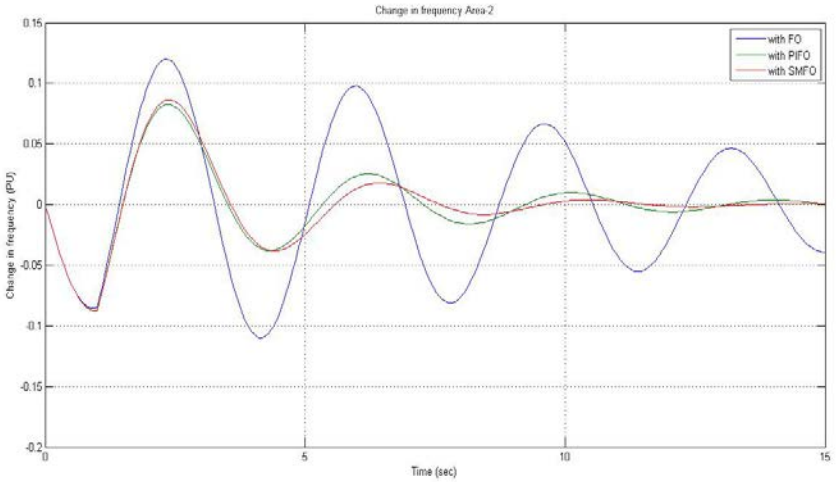


Figure 7: Change in Frequency Deviation Response of Control Area 2 at Operating Point 2

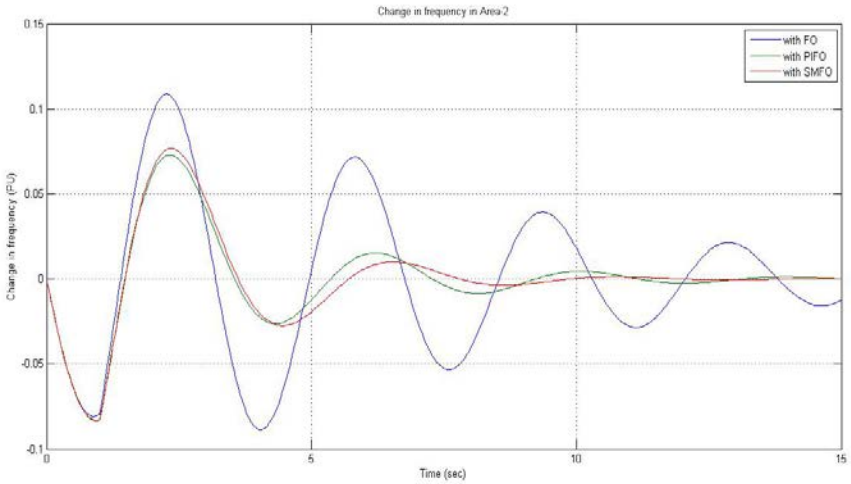


Figure 8: Change in Frequency Deviation Response of Control Area 2 at Operating Point 3

Received: 20 June 2018/Accepted: 15 July 2018

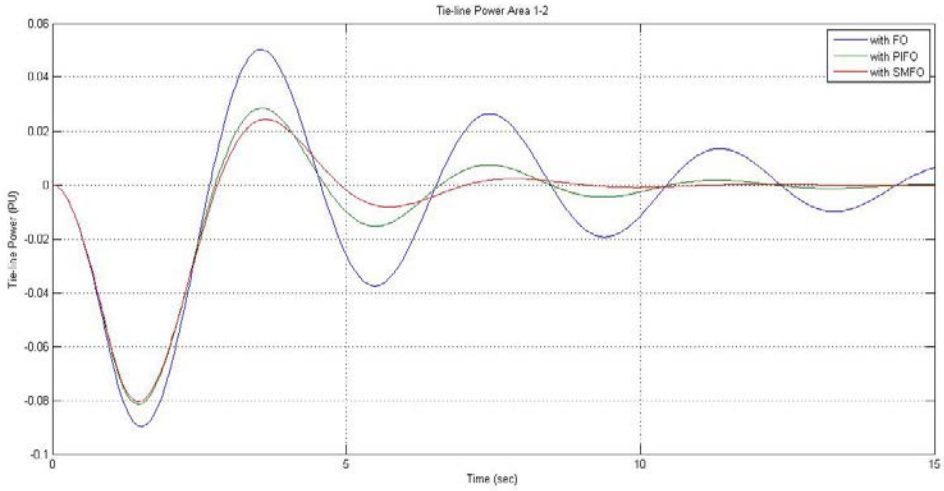


Figure 9: Tie-Line Power Response of Area 1-2 at Operating Point 1

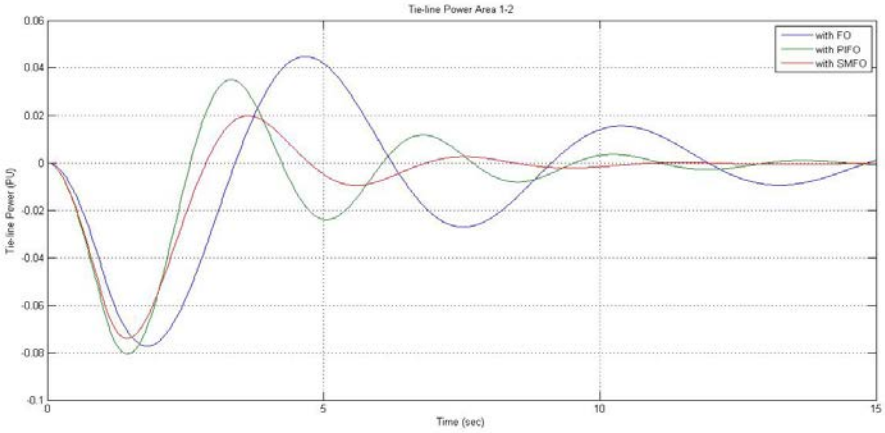


Figure 10: Tie-Line Power Response of Area 1-2 at Operating Point 2

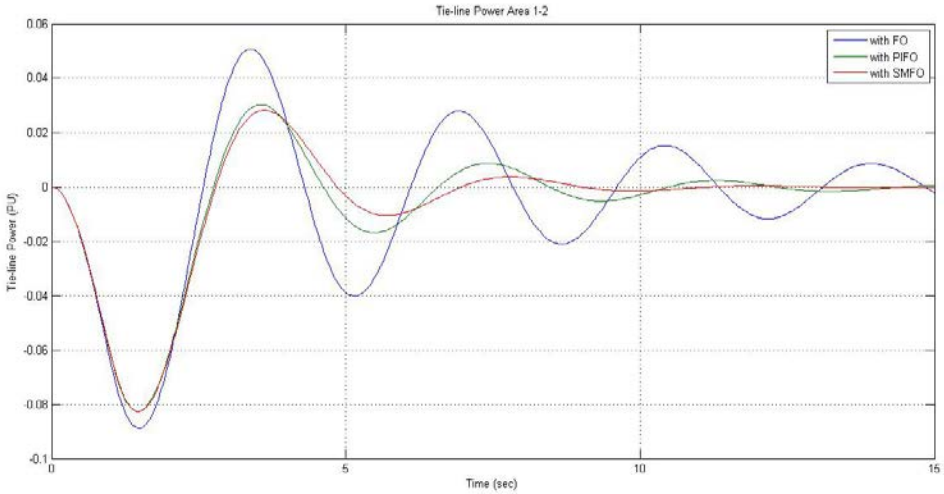


Figure 11: Tie-Line Power Response of Area 1-2 at Operating Point 3

Received: 20 June 2018/Accepted: 15 July 2018

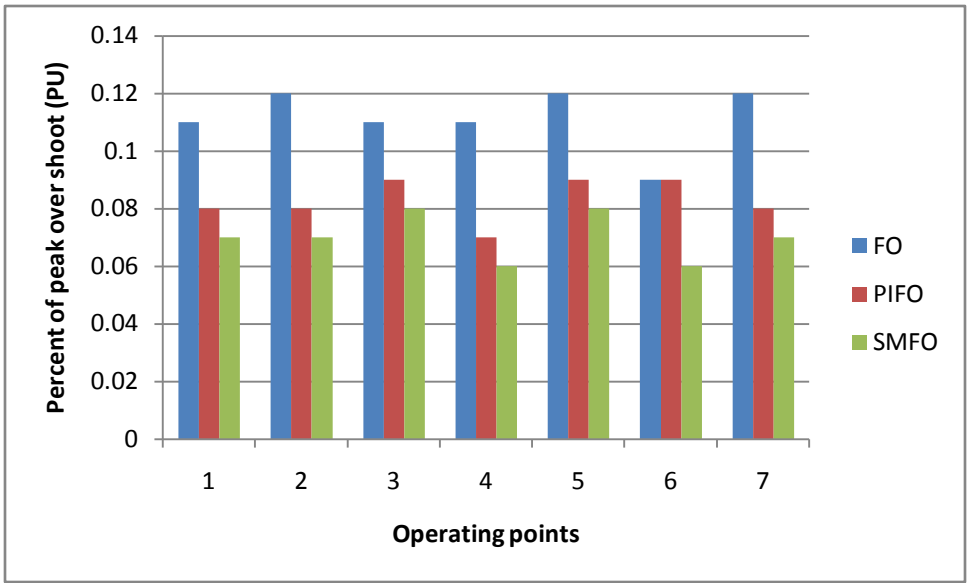


Figure 12: Response at Different Operating Conductions of Percent of Peak Over Shoot

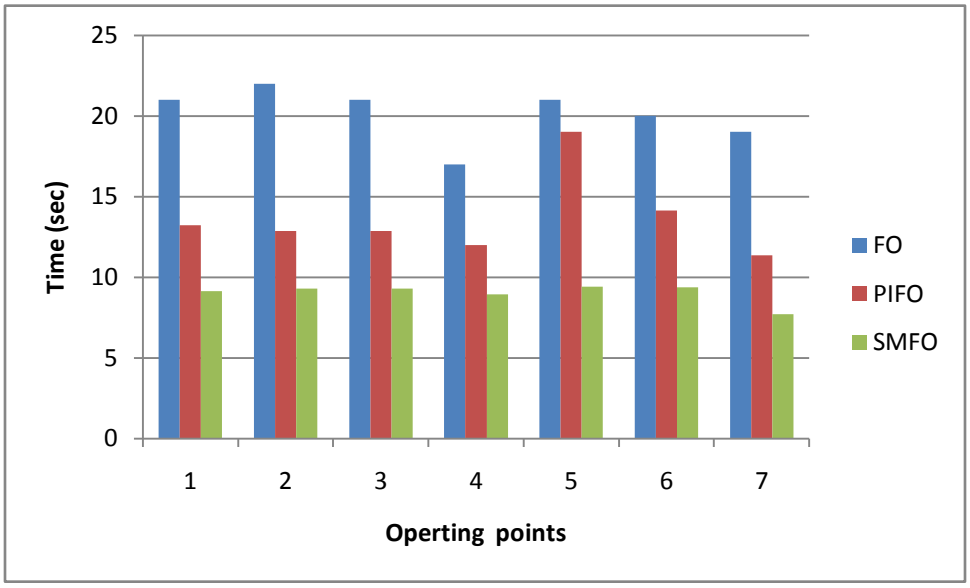


Figure 13: Response at Different Operating Conductions of Settiling Time

V. Conclusions

In this paper, the solution for load frequency control problem is obtained by using SMQDFO for a multi-area power system. The two TIPS with system parameter uncertainty are chosen for the testing the proposed observer. Simulation results show the proposed observer guarantees the robust stability and performance. The proposed method is used to test the precise reference frequency tracking and disturbance attenuation under a wide range of parameter uncertainty and varying load conditions. The robustness of the proposed observer is obtained by comparing with QDFO and Functional observer in terms of settling time, maximum overshoot and undershoots under different operating conditions.

Appendix

f=60hz; $P_{r1}=P_{r2}=1000$MW; $K_{p1}=K_{p2}=120$HZ/pu; MW $T_{p1}=T_{p2}=20.0$s; $K_{r1}=K_{r2}=0.5$; $T_{r1}=T_{r2}=10.0$s; $T_{g1}=T_{g2}=0.08$s; $T_{t1}=T_{t2}=0.3$s; $R_1=R_2=2.4$ HZ/ pu MW; $B_1=B_2=0.425$ pu MW/HZ

ISSN 1943-023X

Received: 20 June 2018/Accepted: 15 July 2018

References

[1] Jun Liu, M.Sami Fadali, Rujing Zhou "Performance constrained stabilization of uncertain systems: application to load-frequency control" Science Direct Publication: Computers & Electrical Engineering , Volume 25, Issue 2, Pages 135-152,March 1999

[2] S. Saxena and Y. V. Hote, "Load frequency control in power systems via internal model control scheme and model-order reduction," IEEE Trans. Power Syst., vol. 28, no. 3, pp. 2749–2757, Aug. 2013.

[3] Y. Mi, Y. Fu, C. Wang, and P. Wang, "Decentralized sliding mode load frequency control for multi-area power systems," IEEE Trans. Power Syst., vol. 28, no. 4, pp. 4301–4309, Nov. 2013.

[4] C.-K. Zhang, L. Jiang, Q. Wu, Y. He, and M. Wu, "Delay-dependent robust load frequency control for time delay power systems," IEEE Trans. Power Syst., vol. 28, no. 3, pp. 2192–2201, Aug. 2013.

[5] W. Tan, "Unified tuning of PID load frequency controller for power systems via IMC," IEEE Trans. Power Syst., vol. 25, no. 1, pp. 341–350, Feb. 2010.

[6] M. Aldeen, H. Trinh, "Load Frequency Control of Interconnected Power Systems via Constrained Feedback Control Schemes", Computers and Electrical Engineering 20, 71–88, 1994.

[7] B. Anderson, J. Moore, "Optimal Control: Linear Quadratic Methods", Dover Publications, Mineola, 2007.

[8] Mendel JM, "Advances in Type-2 Fuzzy Sets and Systems", Inform Science 177, 84–110, 2007.

[9] M Aldeen, H Trinh "Load-frequency control of interconnected power systems via constrained feedback control schemes ", Science Direct Publication: Computers & Electrical Engineering Volume 20, Issue 1, January 1994, Pages 71-88

[10] M. Darouach and M. Boutayeb, Design of observers for descriptor systems, IEEE Transactions on Automatic Control, vol. 40, pp. 1323-1327, 1995.

[11] Li Zhixiong, Guo Zhiwei, Hu Chongqing, Li Aihua "On-line indicated torque estimation for internal combustion engines using discrete observer" Science Direct Publication: Computers & Electrical Engineering, Volume 60, Pages 100-115, May 2017.

[12] Michal Polanský, and Cemal Ardil" Robust Fuzzy Observer Design for Nonlinear Systems" International Journal of Computer, Electrical, Automation, Control and Information Engineering Vol:5, No:5, 2011

[13] X. J. Ma, Z. Q. Sun, "Analysis and design of fuzzy controller and Fuzzy observer" IEEE Trans. Fuzzy Systems. 1998, vol. 6, no. 1, p. 41–51.

[14] Melin P, Castillo O, "A New Method for Adaptive Model based Control of Nonlinear Plants Using Type-2 Fuzzy Logic and Neural Networks", Proceedings of IEEE FUZZ conference, St. Louis, USA, p. 420–25, 2003.

[15] T.Takagi, M. Sugeno, "Fuzzy identification of systems and its applications to modeling and control" IEEE Transactions on Systems, Man and Cybernetics. 1985, vol. 1, no. 1, p. 116–132

[16] H.D. Mathur, "Fuzzy based HVDC regulation controller for load frequency control of multi-area system" International journal of Computer Aided Engineering and Technology Vol.4, No.1 pp.72 – 79, 2012.

[17] H. Shayeghi, H. Shayanfar, and A. Jalili, "Load frequency control strategies: A state-of-the-art survey for the researcher," Energy Convers. Manage., vol. 50, no. 2, pp. 344–353, 2009.

[18] H. Trinh, T. Fernando, H. H. Iu, and K. P. Wong, "Quasi-decentralized functional observers for the LFC of interconnected power systems," IEEE Trans. Power Syst., vol. 28, no. 3, pp. 3513–3514, Aug. 2013.

[19] V.I. Utkin, A Method of Separation of Motion for Designing a State Identifier, Problems of Control of multivariable Systems, Nauka, Moscow,1983.

[20] S.V. Drakunov, Sliding-Mode Observers Based on Equivalent Control Method, Proceedings of the 31st IEEE Conference on Decision and Control, Tucson, Arizona, December 16-18, 1992, pp. 2368- 2369.

[21] S.V. Draknnov, D.B. Izosimov, A.G. Lukyanov, V.A. Utkin and V.I.Utkin, The Block Control Principle, Part II, Automation and Remote Control ,Vol 51, No. 6, 1990, pp. 737-746.

[22] B.L. Walcott and S.H. Zak, Observation of Dynamical Systems in the Presence of Bounded Non linearires-Uncertaities, Proceedings of 25thConference on Decision and Control, pp. 961-966, 1986.

[23] B.L. Walcott, M.J. Codess and S.H. Zak, Comparative Study of Nonlinear State Observation Techniques, Int.J. Control, Vol 45, No. 6, pp.2109-2132, 1987.

[24] S. Sutha, P. Lakshmi, S. Sankaranarayanan "Fractional-Order Sliding Mode Controller Design for a Modified Quadruple Tank Process via Multi-Level Switching" Science Direct Publication: Computers & Electrical Engineering, Volume 45, Pages 10-21, July 2015

[25] D. G. Luenberger, Observers for multivariable systems, IEEE Trans. Automat. Contr., vol. 11, pp. 190-197, 1966.

Received: 20 June 2018/Accepted: 15 July 2018

[26] D. G. Luenberger, An introduction to observers, IEEE Trans. Automat.Contr., vol. 16, pp. 596-602, 1971.
[27] K. Furuta and S. Kawaji, ”Linear functional observer with possible minimal dimension,” IEEE Trans. Automat. Contr., vol. 22, pp. 977-980,1977.
[28] H. R. Sirisena, ”Minimal-order observer for linear functions of the state vector,” Int. J. Contr., vol. 29, pp. 235-254, 1979.
[29] Bao-Lin Zhang, Ai-Ming Feng, Juan Li, “Observer-based optimal fault-tolerant control for offshore platforms”, Science Direct Publication: Computers & Electrical Engineering, Volume 40, Issue 7, Pages 2204-2215 October 2014
[30] M. Aldeen and H. Trinh, ”A reduced-order linear functional observer for linear systems,” IEE Proceedings, Part D, Control Theory and Applications, vol. 146, pp. 399-405, 1999.
[31] M. Darouach, Existence and design of functional observers for linear systems, IEEE Trans. Automat. Contr., Vol. 45, pp. 940-943, 2000.[14] B. Bandyopadhyay and S. Janardhanan, Discrete-time Sliding Mode Control: A Multirate Output Feedback Approach, Springer, Germany,2006.
[32] T. Fernando, H. Trinh, and L. Jennings, “Functional observability and the design of minimum order linear functional observers,” IEEE Trans. Autom. Control, vol. 55, pp. 1268–1273, 2010.
[33] L. Jennings, T. Fernando, and H. Trinh, “Existence conditions for functional observability from an eigen space perspective,” IEEE Trans. Autom. Control, vol. 56, pp. 2957–2961, 2011
[34] M. Darouach, Existence and design of functional observers for linear systems," IEEE Transactions on Automatic Control, vol. 45, pp. 940-943, May 2000.

Received: 20 June 2018/Accepted: 15 July 2018

ResearchGate

See discussions, stats, and author profiles for this publication at: https://www.researchgate.net/publication/325117179

A Survey of Data Mining Techniques on Information Networks

Article *in* International Journal of Engineering & Technology · March 2018

DOI: 10.14419/ijet.v7i2.6.11267

CITATIONS
0

READS
47

3 authors, including:



Madhavi Dabbiru
Andhra University
7 PUBLICATIONS **19** CITATIONS
SEE PROFILE



Dr. B.Thirumala Rao
K L University
43 PUBLICATIONS **649** CITATIONS
SEE PROFILE

Some of the authors of this publication are also working on these related projects:

Medical Image Classification Through Deep Learning View project

All content following this page was uploaded by Madhavi Dabbiru on 23 December 2019.

The user has requested enhancement of the downloaded file.

International Journal of Engineering & Technology, 7 (2.6) (2018) 293-300

International Journal of Engineering & Technology

Website: www.sciencepubco.com/index.php/IJET

Research Paper

A Survey of Data Mining Techniques on Information Networks

Sadhana Kodali[1]*, Madhavi Dabbiru[2], B Thirumala Rao[3]

[1]PhD scholar,Department of CSE,Koneru Lakshmaiah Education foundation,Vaddeswaram,Guntur Dt,Andhra Pradesh,India.
[2] Professor,Dept of CSE,Dr L Bullayya College of Engineering for Women,Visakhapatnam,Andhra Pradesh,India.drlbcse@gmail.com
[3] Professor,Department of CSE,Koneru Lakshmaiah Education foundation,Vaddeswaram,Guntur Dt,Andhra Pradesh,India.
**Corresponding author E-mail:sadhanalendicse@gmail.com*

Abstract

An Information Network is the network formed by the interconnectivity of the objects formed due to the interaction between them. In our day-to-day life we can find these information networks like the social media network, the network formed by the interaction of web objects etc. This paper presents a survey of various Data Mining techniques that can be applicable to information networks. The Data Mining techniques of both homogeneous and heterogeneous information networks are discussed in detail and a comparative study on each problem category is showcased.

Keywords: *InformationNetworks,DataMining Techniques, Homogeneous Information Networks,HeterogeneousInformation Networks*

1. Introduction

When different objects interact and communicate with each other it forms an information network. The examples include the social networks where different people interact with each other, an author-paper network where the communication is between the authors and conferences related via a paper, the DNA structure in a biological network etc. The object relationships in the database form an information network that may be categorized as homogeneous (formed between objects of same type) or heterogeneous (formed between objects of different types which may also be distributed at various locations).An information network is the set of objects that are related to each other and these objects can communicate and interact with each other. There may exist a set of objects of different types and a set of relationships. Therefore an information network is an object from the set of objects that can communicate with another object in a different set in the form of a directed graph. The edge is the relationship that exists between these objects. An information network is categorized as homogeneous if the objects belong to the same set and the relationship belongs to the same type of relationship. Otherwise the information network is said to be heterogeneous which means that there may be more than one type of objects or the objects may communicate with more than one type of relationship. A homogeneous network can be derived from a heterogeneous network by excluding the diversified object features. The link mining techniques are based on homogeneous network analysis and can also be extended to heterogeneous networks. If a network has only multiple interactions among the same type of objects it is called a multi relational network and can be treated as a special case of heterogeneous network. The multi-relational network is equivalent to a multi dimensional network. A network can be composite if the relationships exhibited between the objects depend on the context in a sub-network. And the example of a social media network and genetically structured biological networks are treated as complex networks. The heterogeneous networks can be formed from objects that can be derived from and are not restricted to only structured, semi-structured data but also to unstructured data. A combined path from one object to another with interlinking relationships is called as the meta-path between the objects. A meta-path from one object to another is symmetric if the path is equal to its inverse. The information network adheres to a template called the network schema. The meta-path is a semantic and a significant feature of the heterogeneous information network. The network schema is a mapping from the source object to the target object using a directed link.

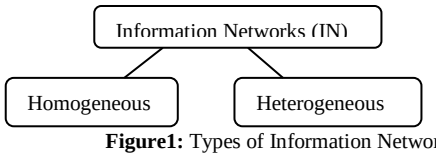


Figure1: Types of Information Networks.

The Figure1 shows the classification of the Information Networks and the Figure 2 depicts the type of Data-Mining techniques like similarity, clustering, classification and it can also be extended for recommender systems.

Copyright © 2018 Authors. This is an open access article distributed under the Creative Commons Attribution License, which permits unrestricted use, distribution, and reproduction in any medium, provided the original work is properly cited.

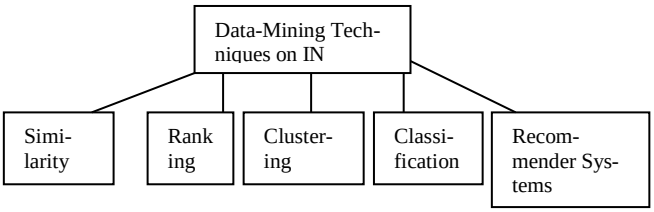


Figure2: Knowledge extraction techniques on Information Networks.

The various algorithms corresponding to each technique are discussed and compared in the preceding sections. The rest of the paper is organized as: Section 2 discusses the Similarity measures Section 3 focuses on Ranking, Section 4 gives an insight to clustering ,Section 5 a briefing about classification, Section 6 about Recommender Systems , followed by conclusions.

2.Similarity Measure

Similarity measure estimates the similarity or the likeliness between the objects. Similarity measure has its applications in web-search, clustering and product recommendation [1].Similarity measures can be of two types: Feature based similarity and web based similarity. In the feature based similarity the objects similarity are measured with cosine similarity, Euclidean distance, Jaccard coefficient. If the similarity is measured with the help of link structures in the graph it is called web based similarity. Similarity measure plays a vital role in product search and web search**.**

The SimRank algorithm [2] states that two objects are similar if they are related to similar objects. The SimRank works on a graph-theoretic model. The basic directed graph theory is considered where the nodes represent the objects and the directed edge refers to the web page link or reference. If the object is similar to itself the similarity score to it is given as one. In the graph, there may be nodes with singleton similarity or zero similarity which can be excluded. Similarity can be extended to any two types of objects. SimRank equations are applicable to homogeneous objects as well as heterogeneous objects. The SimRank algorithm considers an ordered pair of a graph G called the node pair graph G^2.The pairs in G^2 represent similarity of nodes and if they refer to the same object they are said to be similar. If the example of Web pages is considered, the graph G is given as (V, E) where V is the set of nodes in the domain and E is the relationship between the nodes. Here each node is an object which is homogeneous in nature. The user-item example is considered as a bipartite graph where the nodes in V represent the users-items and the directed edge indicates the purchase between them. The in-degree and out-degree for every node in the set v are considered and the computed similarity is between 0 and 1.To compute the similarity a naive method is used to compute the SimRank score between *a* and *b* for every iteration *k.* The score is 0 if a≠b, else if *a* and *b* are equal it is 1.When the neighbourhood of G^2 node pairs is observed the nodes with nearby neighbourhood have more similarity than the nodes which are far away and have little overlap. Within a given radius *r* the node pairs are considered and the remaining are pruned. To have a clear perception about the computation of similarity scores a Random surfers model [3] is observed where it starts from two directions namely node *a* and node *b*. A random walk is applied backwards towards a meeting point and the number of steps that lead toward the meeting point is called the Expected Meeting Distance (EMD). In a directed graph which forms a cycle the EMD between the random surfers is always ∞ and this is called a lock step. The EMD is said to be 1 if the random surfers meet. Another new technique to compute the structural similarity is proposed by the authors in [4] called the P-Rank algorithm where P stands for *Penetrating*. The P-Rank algorithm states that two objects in an information network are similar if they exhibit relationship between similar entities. The similarity score computed is similar to SimRank except that it is based on a damping factor C and it depends on the factor for balancing the in-link and the out-link which is denoted as λ. If the P-Rank score computed between two nodes *a* and *b* is the same as that from *b* to *a* in a given iteration then it exhibits similarity. If the similarity score computed for an iteration k and its next iteration k+1 lies between 0 and 1 it exhibits monotonicity. P-Rank similarity score has the property of existence in which the similarity score unite at a fixed point. The P-Rank score displays the property of uniqueness if the damping factor C≠1.The other forms of P-Rank are *Co-citation, Coupling and Amsler*. In the Co-citation measure [5] on iteration 1, the damping factor C=1 and λ =1.In the Coupling [6] technique which is an another form of P-Rank on iteration 1, damping factor is 1 and λ =0. Amsler [7] is a one step form of P-Rank which works with iteration k=1, C=1, λ =1/2.As the number of iterations increase and becomes ∞ using λ =1 P-Rank exhibits the property of SimRank. As the number of iterations increase and becomes ∞ using λ =1, the P-Rank works as reverse-SimRank also known as rvs-SimRank [4] which is a more practical measure than the SimRank. The computation of P-Rank is preceded by computing the similarity score for two nodes at each iteration and it is stored in a data structure like sparse matrix and hash tables. The time complexity O (n^2) and space complexity O (n^4) of P-Rank and SimRank are the same. The time and space complexities can be reduced in homogeneous networks using radius based pruning and in heterogeneous networks category based pruning.

To make the similarity search faster and to identify the similarity between the peer objects in an information network the authors in [8] proposed an algorithm called as PathSim. PathSim measures the similarity between the objects based on semantic similarity of the objects. The other similarity measures are applicable to densely visible objects. PathSim proposes a framework based on meta-path based similarity. To compute the similarity measures we need to be compute Path count, random walk, and pair-wise random walk. Path count is the number of occurrences between node *x* and node *y*. Random walk is a probability of traversing a path from node x to node y. Pair-wise Random Walk is the probability of conjunction between two path occurrences. A commuting matrix needs to be formed for a network for which a network schema is defined. Figure 4 shows a meta-path symptoms-disease-patient and Figure 3a indicates the adjacency matrix for Symptom-Disease and Figure 3b depicts an adjacency matrix for Disease-Treatment. The commuting matrix is the product of the adjacency matrices that are formed for the meta-path. This matrix is the adjacency matrix formed between two different types of object sets.

With the PathSim similarity measure a top-k similarity measure is proposed where the objects in a given set are of the same type and are sorted. The similarity measure is computed based on symmetric meta-path based calculation. The efficiency of this measure is increased by applying co-clustering pruning technique. To apply this pruning the set of query dependent objects called target clusters and the set of objects for which the features to compute the similarity measure is called as the feature cluster.

The target cluster is partitioned into co-clusters (objects with similar features) by partitioning and these are observed to have any likely objects, if the co-clusters don't have any likely objects they are pruned which is shown in the Figure 5. The PathSim uses a pair wise random walk and is called as a two random walker model. Another approach SimFusion [9] was proposed to integrate different relationships of objects in a heterogeneous network. SimFusion is based on the Unified Relationship Matrix which is an adjacency matrix formed between two different set of objects which are said to have inter-object relationship. The essence of SimFusion is similar to that of SimRank but with less time complexity. The assumption considered in the SimFusion algorithm is called similarity reinforcement which means the similarity between two data objects is supported by the same type of data objects which are related and also by the different types of relationships between the objects.

	Dis-	Dis-	Dis-		Dis-
Symptom1				....	1
Symptom2	1	1		...	
Symptom3		1	1	....	
.....					
Symp-tomN					

Figure 3a: adjacency matrix symptom-disease

	Treatment1	Treatment2	TreatmentN
Disease 1	1	1	
.....	1		1
Disease N			

Figure 3b: adjacency matrix for disease-treatment.



Figure 4a: meta-pathsymptom-disease-treatment

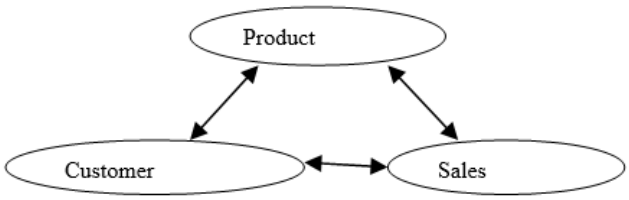


Figure 4b: Meta-path Product-sales-customer

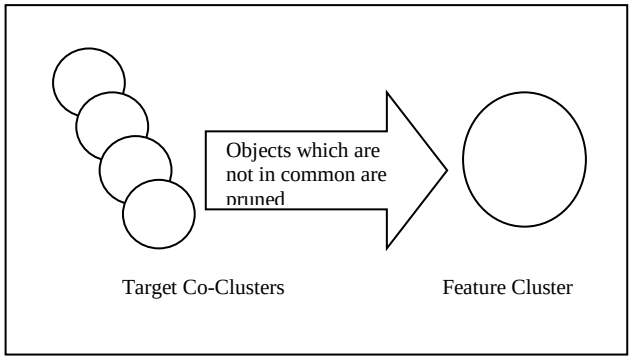


Figure 5: extracting feature cluster from target co-clusters.

The target cluster is partitioned into co-clusters (objects with similar features) by partitioning and these are observed to have any likely objects, if the co-clusters don't have any likely objects they are pruned which is shown in the Figure 5. The PathSim uses a pair wise random walk and is called as a two random walker model. Another approach SimFusion [9] was proposed to integrate different relationships of objects in a heterogeneous network. SimFusion is based on the Unified Relationship Matrix which is an adjacency matrix formed between two different set of objects which are said to have inter-object relationship. The essence of SimFusion is similar to that of SimRank but with less time complexity. The assumption considered in the SimFusion algorithm is called similarity reinforcement which means the similarity between two data objects is supported by the same type of data objects which are related and also by the different types of relationships between the objects.

The novel framework HeteSim is proposed in [10] to identify the object relevance using three metrics called the uniform measure, path constrained measure and a semi-metric measure. HeteSim algorithm is a framework to identify the similarity measure in heterogeneous objects. HeteSim is a path based relevance measure. HeteSim has the following properties: A relation can be decomposed to unique relationships. The significance of relationship between objects in two different sets is based on a relevance path. HeteSim generally exhibits symmetric property not only for paths which are symmetric but also for asymmetric paths. HeteSim exhibits the path maximum property for two objects whose value is 1 if they have similar structure based on the given path. HeteSim is related to SimRank. The only difference between SimRank and HeteSim is that SimRank adds the meeting probability of the objects after all possible steps but HeteSim just computes the meeting probability in the relevance path. In [11] the paper authors proposed an approach for mining meta-paths in heterogeneous information networks using the HeteSim algorithm for the given data to identify the Meta paths then the MapReduce [12] is applied to form the clusters and to get the summarized result. The algorithm proceeds by constructing a constraint based matrix to which HeteSim algorithm can be applied and the MapReduce is applied to the resultant clusters.

HN-similarity is proposed in [13] which is cost-effective and considers the heterogeneous neighbourhood of objects which is a network formed by the structural similarity between nodes. The similarity between objects is computed by an influence dependent function named as HN-Sim. The similarity between two nodes v1 and v2 is a function of weighted factor λ and a product of homogeneous similarity and heterogeneous similarity computed for v1, v2.The similarity function acts in three modes when λ=0 the similarity function computes only heterogeneous neighbourhood. If λ=1 the HN-Sim works just like a homogeneous similarity function and if λ value lies between 1 and 0 it exhibits both homogeneous similarity and heterogeneous similarity.
The Table 1 shows the similarity measures and the models or approaches used by the similarity measures. Also the usage for each of the measures is discussed in the table.

Table 1: Similarity measures and their usage

Name	Model	Time and Space Complexity	Usage
SimRank	Uses random surfers model which is a graph theoretic model based on expected meeting distance. Considers only In-links in the graph	$O(n^3)$-Time $O(n^2)$-Space	1.Used in web document ranking especially in the search engine. 2.Used for document corpora clustering
Prank	Graph based model which uses iterative computing and converges to a fixed point. Considers both the in-link and out-link of the node in a graph.	$O(k(d1^2+d2^2)n^2)$ Average Time $O(n^4)$-worst case Time $O(n^2)$-Space	It is a unified framework for structured similarity computation.
PathSim	A commuting Matrix is used.Meta-path is based on sequence of relations of different objects.	O(n*d)-Time O(n)-Space	For online concatenation and combination of a path to give a top k result for a query.
HeteSim	Uses a transition probability matrix.	O(l*d*n*2)-time O(n2)-Space	1.Automatic object profiling. 2.Expert finding

3. Ranking

Ranking is used to compute the importance of an object. Ranking techniques can be classified into two types: homogeneous ranking techniques and heterogeneous ranking techniques. The popularity of an object is computed based on the ranking functions. HITS-Hyperlink Induced Topic Search [14] identifies the pages that are authoritative for a given query which contain information relevant to the given search query. The HITS classifies second category of pages called hubs contains link towards the authoritative pages. The pages are assigned two kinds of weights authority weight ai and hub weight hi. It is a ranking algorithm that analyses the link among the web pages and rates them. This algorithm is a kind of link prediction by observing the sub-graph which is formed from a base set of web pages that are linked from it and to the pages that link to it. It has structural link among mostly homogeneous kind of entities. It is a ranking algorithm for web pages. Another ranking algorithm to rank the websites was proposed in [15] known as PageRank and is used in Google Search. PageRank is also a link analysis algorithm among the entities which are hyperlinked set of documents. The PageRank is also an algorithm for homogeneous objects. Page Rank assigns global ranking to the web pages. Similarly one more link structure algorithm was proposed by R Lempel and S Moran Stochastic approach for Link Structure Analysis, SALSA [16], which combines the features of PageRank and HITS. In SALSA a result set R is considered from which a neighbourhood graph is considered. For each vertex in the neighbourhood graph an authority and a hub score is computed. A markov chain model is used to perform a random walk in which the sub-graph will visit the authorities which have high probability. To improve the context based searching the topic-sensitive PageRank was proposed in [17].The topic-sensitive PageRank algorithm is a combination of both the page rank and HITS algorithms. This algorithm has two steps: PageRank score vector is captured for each predefined topic statically. The probability that a query of every topic is resolved dynamically. The final ranking is the weighted blend of the rankings for every topic.

Personalized PageRank [18] aims at computing biased PageRank score to a customized question vector q, which is referred to as preference vector. The preference vector is unique in relation to topic sensitive page rank where the query vectors have predefined topics which are fixed. The query vectors are subjective in Personalized PageRank. The Personalized PageRank starts a random walk from source s to target t and a teleport probability of α these steps are carried out iteratively and either the process stops with a probability α else will continue and it is given as πs(t) whose value is calculated and named as P.P is nothing but the walk from source s to target t until it reaches a threshold estimate δ. TrustRank [19] is a kind of Link analysis technique which separates the useful web pages from spam. Many web spam pages are made just with the goal of deceiving web indexes. These pages, mainly made for business reasons, utilize different procedures to accomplish fake rankings on the web search tools' outcome pages. While human specialists can without much of a stretch distinguish spam, a manual survey of the Internet is not feasible. One famous technique for enhancing rankings is to build the apparent significance of an archive through complex connecting plans. Google's PageRank and other pursuit positioning calculations have been subjected to such control.
TrustRank looks to battle spam by filtering the web based on unwavering quality. The strategy calls for choosing a little arrangement of seed pages to be assessed by a specialist. Once the legitimate seed pages are physically identified, a slighter augmenting outward from the seed set searches out comparably solid and dependable pages.

Here we discuss about the heterogeneous ranking algorithms. Sorting the objects from a given order from a database is called as Object Ranking [20]. Object Ranking is very much useful for surveys, retrieval of the information and decision making. The Object Ranking method is Cohen's method which is a greedy algorithm that sequentially chooses the most-preceding object. Other Ranking methods are for Object ranking are the Rank Boost algorithm [21], Support Vector Machine based algorithms like Order SVM [22] and Herbrich's method [23]. After one of the application of above methods to the objects a regression method called Expected Rank Regression is applied to obtain the expected ranks of the objects. Pop-Rank [24] is an extension to the Page Rank model with the addition of a Popularity Propagation Factor for each link that points to an object which uses different types of propagation factors to each structural link with different types of relationships. Pop Rank model is used in a paper search engine called as Libra. A random object finder model which keeps clicking on successive Web page links, Web page to object links, and object relationship links at random. The search strategy Pop Rank is based on Simulated Annealing for Factor Assignment, the algorithm adapts the simulated annealing algorithm to automatically assign popularity propagation factors. The neighbours are observed to get a best combination of Popularity Propagation factor. To make the search strategy better a sub-graph with k-diameter is chosen which forms k concentric circles and all these circles contain the objects that are less than k-links away from the main object inclusive of all the links from these objects. The distance between the ranking results and the ranking given by domain experts is the final computed cost. PopRank gives a global score for every object. The Co-ranking method [25] is a ranking framework on heterogeneous networks by using two random walks on GA a Social Network of Authors, GD a network containing connecting documents. It is a method based on Page Rank and the mutual reinforcement principle. Co Rank has three drawbacks .Firstly it does not consider the venue information. Secondly it is good for an older paper with good citation. Thirdly the Self Citation is given equal priority to the other citations. The Co Rank considers the un-weighted undirected graph which is used to indicate the set of heterogeneous objects. The bidirectional edges between them are

the relationships between the objects. For example in an author document graph If the given graph is subdivided into three sub-graphs like one sub-graph ssconsists of the other sub-graph the nodes that represent authors and the edges that represent the social ties between them. That contains nodes which represent the set of documents and the links between them .The last sub-graph consists of the nodes which contain the set of authors and documents and the edges contain the relationship between these nodes. On the three sub-graphs identified, the random walk is applied for each path. The random walk on the graph is the Markov chain which is represented by a stochastic matrix which contains non-negative entities and the sum of each row is 1. The co-ranking is done by coupling two intra-class random walks. However the Co-rank algorithm has some drawbacks such as lack of venue information, the citations of previous papers are more and they are not given more weightage ,the priority for self citation should be less when considered with other papers. To prevail over the above said drawbacks a heterogeneous ranking framework has been proposed by the Tri-Rank Algorithm [26] three bipartite graphs are considered. Here they have considered a heterogeneous connectivity of objects which are all papers, authors and venues. The intra-relationships within the graph are denoted using a bidirectional edge the inter-relationships between the bipartite graphs is called uni-directional relationships. Tri-Rank can be observed as the extension of co-rank and it follows certain rules. The first rule specifies that the score of the current paper is mostly affected by the score of the papers cited. The second one emphasizes on the rank of the author and the venue. The third depend on the score of the venue and on the rank of the author. The score of the author is also based upon the rank of the co-authors and also on those who cite the author. The fourth rule states that score is also influenced by the scores of the paper published and also depends on the venues attended by the author. The fifth rule is inclined by the scores of the other venues that cite this venue. Lastly the score of the paper depends on the average score of the papers at the venues and the average of the score of authors who attended it. The Tri-Rank framework proceeds in four steps .On the first iteration the PageRank is applied on the graph of papers. Now as the scores of the papers are restructured, using these scores of the authors and venues are reorganized and the scores of the author network are normalized by applying one iteration PageRank. As a next step the venue's score is updated and normalized with one iteration PageRank. The scores of the papers are updated and normalized and this procedure iterates. Table 2 shows the ranking algorithms their time complexities and applications.

Table 2: Ranking techniques their time complexities and applications.

Algorithm Name	Model Used	Time and Space Complexity	Usage
SALSA	Stochastic approach with less computing between hubs and authorities by isolating Tightly Knit community	Time-O(k*E) Space – O(k*E)	Query search
Personalized Page Rank	Make use of Scalable Hyper-link score .The graph is stored in a social store. All jumps are made to the seed node.	$\Theta(n)$	Personalized recommendations
Trust Rank	Seed set is computed using inverted page Rank. Trust Rank scores are calculated by trust damping and trust splitting.	O(p)	For the separation of spam pages from useful pages.
Object Rank	Object Rank is computed using Index based table. The authority transfer data graph is DAG on which object rank is computed.	$O(n^2)$-Cohens Approach O(n log n) – Rank-Boost,Order SVM	To rank Objects
TriRank	A tripartite graph is used where each edge carries a weight and a global minimum function is applied	$O(L_u)$	Used for recommender purpose

4. Clustering

Clustering forms groups of objects which are similar according to a closeness rule that objects within the same cluster are more similar to each other and objects of two different clusters are less similar to each other. Clustering can be done on objects which are homogeneous in nature and also can be extended to objects which are heterogeneous in nature. The basic data-mining techniques like the K-Means, K-medians are good examples for homogeneous clustering. Clustering can also be done on heterogeneous objects. Clustering on heterogeneous objects is quite different and complex when compared with homogeneous techniques. Clustering on heterogeneous web objects is performed using compression technique by considering a clustering structure C {c1, c2,.., cm} of a data set 'x' and the defined partition set for the data P as {p1,p2,…,ps}. A pair of points are defined on these data sets using the points from SS which is a cluster which belong to the same cluster and the same partition which is indicated as 'a'. A pair of points are said to be from a set of points named as SD if the cluster belong to the equivalent structure. The dissimilar groups of partitions are indicated as 'b', the pair of points from the set DS if the points belong to different cluster C but of the same group given as 'c', a pair of points are said to be from DD if they are from different cluster and belong to diverse group and named as'd'. The sum of the four points is said to be M. Using the
four points a, b, c, d and the value M indices are defined as follows: The rank index is defined as (a+d)/M this value should lie between 1 and 0. If the value is close to 1 then C and P have high similitude. The Jaccard coefficient is calculated whose value lies between 0 and 1 which is used to estimate the similitude between C and P. Similarly the Fowles –Mallow measure is calculated whose value close to 1 indicates the similitude between C and P. In order to classify the network as heterogeneous in nature the objects must be at least of two different categories which are said to be bi-typed. The RankClus is proposed in [27] which perform clustering and then ranking on a given set of data objects so that the objects after clustering can be ranked within a cluster and this could give a better analysis about that cluster. The RankClus algorithm runs on a bi typed information network. The ranking functions considered to rank the objects in an information network are simple ranking and authority ranking. The example heterogeneous information network considered here is author-conference network in which authors who publish more papers are ranked high in-spite of the value of the conferences. The next approach is the authority ranking which proceeds with certain rules that the set of ranks that are highly ranked will publish in highly ranked conference. The second rule is that the conferences which are very popular draw the papers from authors which are highly ranked. The next rule tells that if an author may be co-authored with highly ranked authors then his popularity increases. The algorithm proceeds with assigning a conditional rank to each object depends on that cluster. The conditional ranks within the clusters are not similar to each other. A conditional rank can be used as an important attribute to observe the cluster. The mixture model components are calculated using the EM algorithm [28] and the cluster is adjusted. The drawbacks of the RankClus algorithm is that it has less number of object types and if we observe the bi-typed networks the clusters formed have only homogeneous objects. To overcome these drawbacks the NetClus [29] algorithm is proposed by Sun et al with a star schema. In the initial step of the algorithm net clusters are formed. The probabilistic generative model is used where the probability of an object is calculated based on the probability of visiting that object in the entire heterogeneous networks and the probability of that object corresponding to all other objects. The probability of two different objects may not be the same and is independent of each other. If the target object belongs to a different cluster the posterior probabilities are calculated. Once the clusters are formed the ranking techniques adopted to rank the cluster are simple ranking and authority ranking.

Table 3: Clustering techniques their time complexities and applications

Algorithm Name	Model Used	Time and Space Complexity	Usage
RankClus	A mixture model is used and objects are adjusted to the clusters. Conditional rank for each cluster is calculated.	$O(t(t_1\|E\|+t_2(K\|E\|+K+mK)+mK^2))$	Ranking databases
NetClus	Ranking on a star schema network using authority ranking .	$O(k.\eta_p.\xi_p)$	Trajectory aware services, Facility Location queries
MedRank[30]	Ranks Heterogeneous Objects in medical information. Authority ranking formula is used.	$O(l\|E'\|)$	For Ranking heterogeneous objects in medical databases.

5. Classification

Classification is a way of specifying categorical groups and giving them labels. The basic classification techniques like the decision tree induction can be quoted a good example for classification of data objects which are homogeneous in nature. Classification can also be extended to data objects which are heterogeneous which are discussed in this section. ComClus [31] is defined on hybrid networks which include the homogeneous as well as the heterogeneous objects. This approach is a graph based classification and is applicable for heterogeneous networks. The nodes are of distinct types and are heterogeneous in nature they belong to various classification labels. The NetClus is proposed with a star schema and the ComClus is a star schema with a self loop. ComClus uses a probability model to represent a generative probability. The generative probability model and the expert's model are used to combine the relationships from heterogeneous and homogeneous relations. The algorithm proceeds by randomly partitioning the given network G. For each subnet in the graph the homogeneous probability, conditional probability, the heterogeneous probability and the mixed probability are calculated on centre node. For every centre node the posterior probabilities are calculated and these are used for ranking the nodes. The Graffiti [32] works as follows: Firstly the contents of the nodes which indicate the description is identified. If there is an edge among the same type of node it is called as the S-edge. If there exits an edge among different type of nodes it is called the X-edge. A random walk procedure is applied on the graph to provide a convergence solution and also it gives a unique solution. The algorithm proceeds with taking initial graph nodes with labels as input, then it identifies the nodes which have similar neighbours by identifying the reciprocal influence of each node and it must be higher to form the S-edge. The RankClass [33] algorithm gives the ranking of an object among a class of objects. The RankClass proceeds with the following steps: 1) A class of labelled data is considered and it initializes the ranking distribution function. The type of network structure considered is also identified and is initialized. 2) In each class the network structures are adjusted. This resembles the similarity of boosting technique and the ranking distribution is done based on the graph based ranking model.3) Steps 1 and 2 are iteratively repeated and the posterior probability is calculated until the object is assigned a class label. It is a transductive classification [34] strategy. This is a new graph based classification approach in identifying the link structures in heterogeneous networks where the information is processed from labelled data to unlabelled data. The confidence of two objects of an estimated class label k should be same.

6. Recommender Systems

Recommender systems utilize the knowledge discovery techniques and statistical methods to predict recommendations and have its prominence in e-commerce applications. The recommendation algorithms are designed based on collaborative filtering model or cluster model. The other models are search based models which identifies similar items. The working of the collaborative filtering uses a database where the customer is matched with the entities or other customers who have similar interests in purchasing items and the other products which are purchased by the neighbours are recommended to the customer. The two main challenges of the recommender systems are 1) scalability which is a great factor that has influence on its neighbours for high dimensional data when trying to apply recommender algorithms for huge, dynamic and realistic datasets2) the veracity derived from the recommender systems should not be false. This factor also affects the quality of the recommender systems. The most prominent data mining technique to apply for the recommender systems is the association rule mining technique which applies the support and the confidence thresholds to suggest the entity recommendations in a given transaction. Collaborative filtering is the most effective way for suggesting the recommendations among the neighbours. The recommendation for any customer depends on the opinions of the group of other customers. In [35] collaborative filtering is designed in three subtasks 1)representation 2)formation of the neighbourhood 3)recommendation generation. In the representation step a cross product matrix is used with the number of row a is based on products and the number of columns b represent the transactions. The corresponding value in the matrix is one if the user purchases that product otherwise zero. The second step which includes forming of similar neighbours using the measure of similarity. The similarity is measured using the correlation technique or the cosine similarity. The final step is to generate recommendation using most-frequent item based recommendation where the count of most frequent items purchased are calculated ,sorted and the most frequent products are given for recommendation or the next approach for generating recommendation is Association rule based recommendation where only few neighbours are considered for generating association rules. As a limited set is considered for recommendations there may be a drawback of inadequate products for recommendation and the reduction in dimensions may not be considered as a best approach for recommendations. The most primitive application of the collaborative filtering is used in the Tapestry which is an experimental mail system.

The basic algorithms used in collaborative filtering are K-NearestNeighbor or the K-means algorithm which may not be useful for dense data and may not be apt for recommendations. The other approach for recommender systems is cluster model which suggests the recommendations treating it as a classification problem. The method implemented to form clusters is called as *repeated clustering*. One method is to cluster a set of entities based on the relationships with the set of second category of entities. Later in the second step the set of second category of entities are clustered using K-Means using the influence of the first category of entities. The clustered formed are re-clustered based on the number of first category of entities influencing the second category and vice-versa. A *"soft clustering"* method is also used which is based on K-Means clustering method in which a set of objects are assigned to a class based on the degree which is equivalent to the similarity measure calculated.

The other category of recommendation system algorithms include search based models which identify the solution for proposing a

recommendation as a search for interconnected items. But this search based model is not so effective for recommendation systems. The most popularly used recommendation system for Amazon.com uses item-to-item collaborative filtering approach. In this approach the items purchased by the user are matched with the rated items and these two lists are observed to combine and form a recommendation list. A similar items table is built by observing the most affinity of the customer to purchase an item. A product-to –product matrix is also built but the inefficiency is that it does not have similar customers. By using an iterative algorithm similarity is computed between two items. In [36] Xiao Yu, Jiawei Han et al proposed an entity recommendation approach based on meta-path where user feed-backs are diffused across the meta-path. The diffusion scores corresponding to each user versus item is called as the diffused user preference matrix. If we traverse across the matrix we can identify the set of users and their preferences which also give the diffusion scores to propose the recommendations considering and applying the facts of the global model. Not only global recommendations but also personalized recommendations can be built using user implicit feedback. The users are clustered using K means algorithm with cosine similarity based on their preferences also matrix factorization techniques are used when clusters are formed. On these clusters formed the Bayesian ranking based optimization or stochastic gradient descent [37] method is used to learn the personalized entity recommendation. The figure 6 shows how recommender systems use the meta-paths and the diffusion matrix to suggest the recommendations.

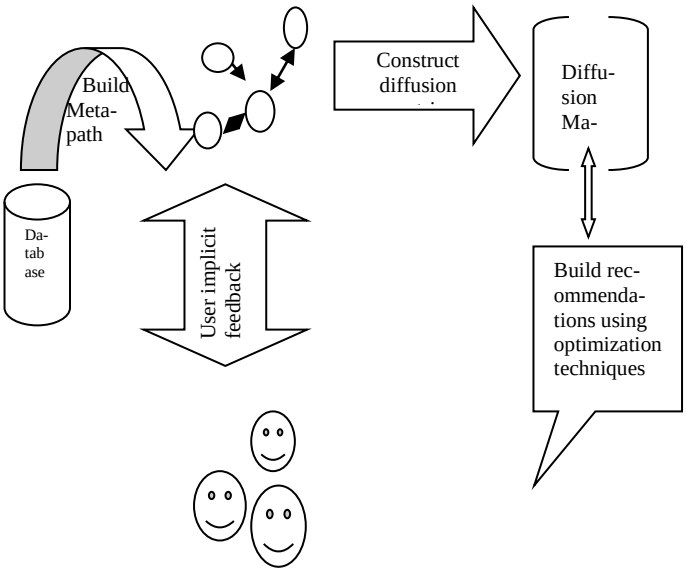


Figure 6: Recommender Systems based on Meta-path.

7. Conclusion

In this paper the authors discussed various Data Mining techniques for addressing information mining of homogeneous as well as heterogeneous information networks. Mining techniques based on similarity, ranking, clustering, classification are discussed in detail. The prominence of the recommender systems is increasing in the present day purchases, suggestions for product recommendations, venue recommendation, hotels and restaurant recommendations etc. The recommender systems are also discussed for both homogeneous and heterogeneous networks. Application and usage of the techniques are also tabulated. There is a lot of scope for research in any of the above discussed techniques by identifying the semantics and the structural behaviour of the objects interacting with each other. The research areas like image retrieval based on texture is a very challenging area of research where we need the information networks to identify the texture, another area of research based on similarity includes identification of patterns in continuous data which is an information network based on text documents. Shape based similarity and classification is also an interesting area of research. The readers can visualize various areas of research as different perspectives of usage areas are presented here.

References

[1] Chuan Shi, Yitong Li, Jiawei Zhang, Yizhou Sun, Philip S. Yu," A Survey of Heterogeneous Information Network Analysis", in Journal Latex class Files, Vol 14,no 8,August 2017.

[2]Glen Jeh, Jennifer Widom,"SimRank: A measure of Structural-Context similarity" in KDD, pp. 538–543, 2002.

[3] A. Blum, T.-H. H. Chan, and M. R. Rwebangira. A random-surfer web-graph model. In ANALCO '06: Proceedings of the eighth Workshop on Algorithm Engineering and Experiments and the third Workshop on Analytic Algorithmic and Combinatorics, pages 238- 246, Philadelphia, PA, USA, 2006. Society for Industrial and Applied Mathematics.

[4] Peixiang Zhao, Jiawei Han, Yizhou Sun," P-Rank: a Comprehensive Structural Similarity Measure over Information Networks".CIKM'09, Hong Kong, China. November 2–6, 2009

[5] H. G. Small. Co-citation in the scientific literature: A new measure of the relationship between two documents. Journal of the American Society for Information Science, Science, 24(4):265-269, 1973.

[6] M. M. Kessler. Bibliographic coupling between scientific papers. American Documentation, 14:10-25, 1963.

[7] R. Amsler. Application of citation-based automatic classification. Technical report, The University of Texas at Austin Linguistics Research Center, December 1972.

[8] Yizhou Sun, Jiawei Han, Xifeng Yan, Philip S. Yu, Tianyi Wu, "PathSim: Meta path Based TopK Similarity Search in Heterogeneous Information Networks" *Proceedings of the VLDB Endowment*, Vol. 4, No. 11 2011.

[9] Wensi Xi, Benyu Zhang, Edward A. Fox, SimFusion: A Unified Similarity Measurement Algorithm for Multi-Type Interrelated Web Objects, in the www conference May10-14, 2005.

[10] C. Shi, X. Kong, Y. Huang, S. Y. Philip, and B. Wu, "HeteSim:A general framework for relevance measure in heterogeneous networks," IEEE Transactions on Knowledge & Data Engineering, vol. 26, no. 10, pp. 2479–2492, 2014.

[11] Sadhana Kodali,Madhavi Dabbiru,Kamalakar Meduri,"Constraint based approach for minging Heterogeneous Information Networks" 6th IEEE IACC 2016 ,27th -28th February 2016.

[12] Jeffrey Dean and Sanjay Ghemawat ," MapReduce: Simplified Data Processing on Large Clusters" ,OSDI 2004 11th March.

[13] Jiazhen Nian, Shanshan Wang, and Yan Zhang,"HN-Sim: A Structural Similarity Measure over Object-Behavior Networks", Part I, LNAI 8346, pp. 48–59 ,ADMA-2013.

[14]J. M. Kleinberg, "Authoritative sources in a hyperlinked environment," in SODA, pp. 668–677. 1999.

[15] L. Page, S. Brin, R. Motwani, and T. Winograd, "The Page Rank citation ranking: Bringing order to the web." Technical report, Stanford University Database Group, 1998.

[16] R. LEMPEL and S. MORAN, SALSA: The Stochastic Approach for Link Structure Analysis, ACM Transactions on Information Systems, Vol. 19, No. 2, April 2001.

[17] Taher H. Haveliwala, Topic Sensitive Page Rank WWW May 7–11, Honolulu, Hawaii, USA, 2002.

[18] G.Jeh and J. Widom, "Scaling personalized web search," in WWW, pp 271–279, 2003.

[19] Gyongyi Z, Garcia-Molina H, Pedersen J Combating web spam with TrustRank. In: Proceedings of the Thirtieth international conference on Very large data bases - Volume 30, VLDB Endowment, VLDB '04, pp 576-587, 2004.

[20] Balmin A, Hristidis V, Papakonstantinou ObjectRank: authority-based keyword search in databases. In: Proceedings of the Thirtieth international conference on Very large data bases - Volume 30, VLDB Endowment, VLDB, pp 564-575, 2004.

[21] Yoav Freund, Raj Iyer, Robert E. Schapire, Yoram Singer, An Efficient Boosting Algorithm for Combining Preferences, Journal of Machine Learning Research 4 pp.933-969,2003.

[22] Kazawa, H., Hirao, T.Maeda,: Order SVM: a kernel method for order learning based on generalized order statistics. Systems and Computers in Japan pp 35–43, 2005.

[23] Herbrich, R., Graepel, T., Bollmann-Sdorra, P Obermayer, K.: Learning preference relations for information retrieval. In: ICML-98 Workshop: Text Categorization and Machine Learning.pp 80–84, 1998.
[24] Nie Z, Zhang Y, Wen JR, Ma WY (2005) Object-level ranking: bringing order to web objects. In: Proceedings of the 14th international conference on World Wide Web, WWW '05, pp 567-574,2005.
[25] Hai-jiang He, A Co-Ranking Algorithm for Learning Listwise Ranking Functions from Unlabeled Data, journal of computers, vol. 6, no. 11, november 2011.
[26]Zhirun Liu,Heyan Huang,Xiaochi Wei,Xianling Mao, Tri-Rank: An Authority Ranking Framework in Heterogeneous Academic Networks by Mutual Reinforce,26 th IEEE International Conference on tools with Artificial Intelligence,2014.
[27] Y. Sun, J. Han, P. Zhao, Z. Yin, H. Cheng, and T. Wu, "RankClus:Integrating clustering with ranking for heterogeneous information network analysis," in EDBT,pp. 565–576, 2009
[28] A. P. Dempster; N. M. Laird; D. B. Rubin, Maximum Likelihood from Incomplete Data via the EM Algorithm, Journal of the Royal Statistical Society. Series B (Methodological), Vol. 39, No. 1. , pp. 1-38, 1977.
[29] Y. Sun, Y. Yu, and J. Han, "Ranking-based clustering of heterogeneous information networks with star network schema," in KDD, pp. 797–806, 2009.
[30] Ling Chen,XueLi,Jiawei Han "MedRank: Discovering Influential Medical Treatments from Literature by Information Network Analysis" Twenty-Fourth Australasian Database Conference (ADC2013), Adelaide, Australia,2013.
[31]R. Wang, C. Shi, P. S. Yu, and B. Wu, "Integrating clustering and ranking on hybrid heterogeneous information network," in PAKDD, pp. 583–594, 2013.
[32] R. Angelova, G. Kasneci, and G. Weikum, "Graffiti: Graph-based classification in heterogeneous networks," in WWW, pp.139–170, 2012.
[33] M. Ji, J. Han, and M. Danilevsky, "Ranking-based classification of heterogeneous information networks," in KDD pp. 1298–1306, 2011.
[34] C. Luo, R. Guan, Z. Wang, and C. Lin, "HetPathMine: A novel transductive classification algorithm on heterogeneous information networks," Advances in Information Retrieval, vol. 8416, pp. 210–221, 2014.
[35]L. Ungar and D. Foster, "Clustering Methods for Collaborative Filtering," Proc. Workshop on Recommendation Systems, AAAI Press, 1998.
[36] Xiao Yu, Jiawei Han et al."Personalized Entity Recommendation: A Heterogeneous Information Network Approach"WSDM'14, , New York, New York, USA, February 24–28, 2014.
[37] R. H. Byrd, P. Lu, J. Nocedal, and C. Zhu. "A limited memory algorithm for bound constrained optimization." SIAM Journal on Scientific Computing, 16(5):1190–1208, 1995.

View publication stats

International Journal of Pure and Applied Mathematics
Volume 120 No. 6 2018, 7305-7320
ISSN: 1314-3395 (on-line version)
url: http://www.acadpubl.eu/hub/
Special Issue

http://www.acadpubl.eu/hub/

DIAGNOSIS CHILDRENS WITH DYSLEXIA USING MACHINE LEARNING TECHNIQUE

[1]DR. A. V. Prathap kumar, Professor,
Teegala Krishna Reddy Engineering college,
dravprathapkumar@gmail.com
[2]Dr. G. Vamsi Krishna, Assistant Professor,
Dr.lankapalli Bullayya engineering college
vamsikrishna527@gmail.com
[3]Dr. K . Satish kumar, Associate Professor,
Teegala Krishna Reddy Engineering college
satish7433@gmail.com

June 14, 2018

Abstract

Worldwide, around 10% of the population has dyslexia, a specific learning disorder. Most of previous eye tracking experiments with people with and without dyslexia have found dierences between populations suggesting that eye movements reflect the diculties of individuals with dyslexia. In this paper, we present the first statistical model to predict readers with and without dyslexia using eye tracking measures. The model is trained and evaluated in a 10-fold cross experiment with a dataset composed of 1,135 readings of people with and without dyslexia that were recorded with an eye tracker. Our model, based on a Support Vector Machine binary classifier, reaches 80.18% accuracy using the most informative features. To the best of our knowledge, this is the first time that eye tracking measures are used to predict automatically readers with

dyslexia using machine learning.
Categories and Subject Descriptors
K.4.2 [Computers and Society]: Social IssuesAssistive technologies for persons with disabilities; I.2.1 [Artificial Intelligence]: Applications and Expert SystemsMedicine and science.

***Keywords*:**Dyslexia, eye tracking, eye movements, diagnosis, detection, prediction, machine learning, support vector machine.

1 INTRODUCTION

Dyslexia is the most common neurological learning disability [24]. It affects from 10 to 17.5% of the population in the U.S.A. [23] and from 8.6 to 11% in Spain [6, 25] and has a considerable presence in web text [1]. Competitive reading and writing is required in our education system; therefore school failure is associated with dyslexia, even if dyslexia is not related to overall intelligence [24].Permission to make digital or hard copies of all or part of this work for personal or classroom use is granted without fee provided that copies are not made or distributed for profit or commercial advantage and that copies bear this notice and the full citation on the first page. Copyrights for components of this work owned by others than ACM must be honored. Abstracting with credit is permitted. To copy otherwise, or republish, Dyslexia detection is crucial. When diagnosed, dyslexia can be treated avoiding its consequences such as high rates of academic failure. At the same time, diagnosing dyslexia is not a trivial task; it is expensive and it normally requires an expert. Also, dyslexia manifestations vary depending on the language. In fact, dyslexia is called a hidden disability due to the diculty of its diagnosis in languages with shallow orthographies [72], as Spanish.Previous eye tracking studies with people with dyslexia from psychology research have concluded that the eye movements of people with dyslexia are not the cause but the reflection of the diculties they have while reading [21, 45, 49]. Although there are number of studies that presents how eye tracking measures show individual dierences [12, 37, 40], most of the studies agree in finding significant dierences among readers with and without

dyslexia.Human-computer interaction studies that use eye tracking with people with dyslexia have normally focused in finding the most accessible text presentations [55, 57]. Again, differences between people with and without dyslexia were found.

Even if eye tracking measures have already been used to predict where people tend to look [26] or to improve the interface design of search engines [17], among others; we believe this is the first eort to automatically detect dyslexia using eye tracking measures.In this paper we present a statistical model to classify readers with and without dyslexia using a Support Vec tor Machine binary classifier. We trained the model with a dataset composed of 1,135 readings of Spanish speakers with and without dyslexia from 11 to 54 years old recorded with an eye tracker. The contribution of this paper is: a statistical model to classify Spanish readers with and without dyslexia that achieves 80.18% accuracy in a 10-fold cross validation experiment.1

Next section focuses on dyslexia and its detection. Section 3 explains related work that have shown dierences between populations using eye tracking. We present the dataset used in Section 4 and show the experiments with our statistical model in Section 5. We discussed the results in Section 6. Finally, we draw conclusions and future work in Section 7.

2 DYSLEXIA DETECTION

Dyslexia is defined as a specific learning disability with neurological origin. It is characterized by diculties with accurate and/or fluent word recognition and by poor spelling and decoding abilities. These diculties typically result as a deficit in the phonological component of language that is often unexpected in relation to other cognitive abilities. Secondary consequences may include problems in reading comprehension and reduced reading experience that can impede growth of vocabulary and background knowledge [24, 30].

Dyslexia detection is crucial since academic failure is associated with dyslexia when it is not detected and treated accordingly [14]. Diagnosing dyslexia and early detection of risk of dyslexia have been addressed from dierent fields, especially in psychology and neuroimaging.

In psychology, traditional paper based diagnosed of dyslexia such as TALE [70] for Spanish or Diagnostischer Rechtschreibtest [18] for German, analyze both reading and writing skills. Diagnoses of dyslexia are confirmed when the reading and the spelling performance of the child is significantly under the level expected due to her or his age and general intelligence.2

More recently, Lyytinen et al. [32] created the computer game Literate, later called GraphoGame [31],3 which was developed to identify children at risk of having dyslexia before school age in Finland. Its exercises are aimed towards the connection of graphemes (letters) and phonemes (sounds). They conducted two user studies with 12 and 41 children between 6 and 7 years old with very promising results. Although these exercises were conceived as preventive training, children who used Literate improved their accuracy in grapheme-phoneme connections, reading words, and naming phonemes after playing for less than 4 hours.

On the other hand, neuroimaging with children with dyslexia has revealed relationships between brain responses at infancy and later reading performance. Molfese [36] reported that there are brain responses (event-related brain potentials) to speech sounds within 36 hours of birth that can be used to discriminate children who would become readers with dyslexia with 8 years old. The accuracy of this prediction is 81%.

3 EYE MOVEMENTS AND DYSLEXIA

Related work on diagnose and early detection of risk of dyslexia is very extensive and comes from dierent fields such as cognitive neuroscience, psychology or biology. In this related work we only focus on how eye tracking measures have been studied in relationship with dyslexia. These studies come from psychology and human-computer interaction research.

3.1 Psychology Research

Rayner [50] presents a review of the studies from the mid 70s to the 90s that have used eye movements to investigate cognitive processes. He demonstrates that eye movement measures can be used to infer moment-to-moment cognitive processes in reading. For instance, shorter fixations are associated with better readability while longer fixations can indicate that processing loads are greater. As a matter of fact, non impaired readers present longer fixations at low-frequency words than at high-frequency words [22, 27, 46, 51, 54, 59].

The eye movements of readers with dyslexia are dierent from regular readers. People with dyslexia as well as beginner readers, make longer fixations, more fixations, shorter saccades4 and more regressions than readers without dyslexia [11, 35, 50].

During the 80's-90's it was discussed to which extent eye movements are the cause of reading problems. If eye movements were a causative factor, then dyslexia could easily be diagnosed with a simple eye movement test. There have been some studies concerning whether eye movements are the cause of dyslexia: erratic eye movements [41, 42, 43], instability during fixation [11], and selective attentional deficit [13, 15, 44]. However, the results presented in those experiments could not be later replicated by others (see [3, 5, 38, 39, 65, 66] for erratic eye movements; Raymond et al. [47] for instability during fixation; and [16, 28, 52, 53, 64] for selective attentional deficit). At the same time, Tinker [67, 68] and Rayner [48, 50] studies show how eye movements are generally not a cause of the reading disability but were a reflection of other underlying problems. More concretely, there are three studies that are consistent with the conclusion that eye movements reflect the diculties that individuals with dyslexia have while reading and that are not the cause of the reading problem.

First, Hyona and Olson [21] found that readers with dyslexia show the typical word frequency eect in which low-frequency words are fixated longer (fixation duration, number of fixations, and regressions) than high-frequency words.

Second, Pirozzolo and Rayner [45] and Olson et al. [39] found that when people with dyslexia were given a text appropriate for their reading level, their eye movements (fixations, saccades, and

regressions) were much like those of regular readers at that particular age level.

Third, Rayner [49] showed that regular children's eye movements (fixation durations, saccade lengths, and the size of the perceptual span) shared the characteristics of readers with dyslexia when they were given a text that was too dicult for them.

Taking into account all these studies the evidence suggests that the vast majority of people with dyslexia have a language processing deficit and, that their eye movements simply reflect their diculty processing language [50].

Later literature on eye tracking and dyslexia have focused on the eect of other factors, such as regular orthography [20], orthographic neighbors [33], or letter length and phoneme length [34].

3.2 Human-Computer Interaction

In her PhD thesis, Rello [55], performed twelve eye tracking experiments and eleven sub experiments to explore the impact of text presentation and text content on the readability and comprehension of people with dyslexia.

The text presentation parameters tested were typeface, font size, colors, character spacing, line spacing, paragraph spacing, dierent grey scales for text, and column width [61]. representations [60], verbal paraphrases, graphical schemes, keywords, and dierent strategies of lexical simplification [58]. Each experiment had between 23 to 48 participants with dyslexia plus a control group. In all the experiments, except from one where the participants had to read texts with orthographic errors [56] there were found significant dierences between participants with and without dyslexia regarding eye tracking measures.

3.3 What is missing?

Previous literature on eye movements and dyslexia have found pattens, correlations, individual dierences, and significant dierences between populations. However, to the best of our knowledge, none of them have applied machine learning to classify people with and without dyslexia, that is, to detect readers with dyslexia.

What is missing is the connection of two points that were not previously joined: eye tracking measures and machine learning techniques to predict readers with dyslexia automatically.

4 DATASET

We used a dataset derived from an eye tracking experiment with 97 subjects with normal or corrected-to-normal vision; 48 of then with diagnosed dyslexia. The participants with dyslexia (22 female, 26 male) presented a confirmed diagnosis of dyslexia. Their ages ranged from 11 to 50 (x = 20.96, s = 9.98). Except from 3 participants, all of the participants were attending school or high school (26 participants), or they were studying or had already finished university degrees (19 participants). The group of participants without dyslexia was composed of 49 people (28 female, 21 male). Their ages ranged from 11 to 54 (x = 29.30, s = 9.03). Except from 5 participants, the rest were either attending or had finished school or high school (17 participants) or university (27 participants).

This dataset was derived from a within-subject design experiment. Each participant read 12 dierent texts with 12 dierent typefaces. The texts and the fonts were counterbalanced to avoid sequence eects. Therefore, the data with respect to text-font combinations was evenly distributed.

The twelve fonts were: Arial, Arial Italic, Times and Times Italic the most common fonts used on screen and printed texts, respectively [8]; OpenDyslexic and OpenDyslexic Italic designed specifically for people with dyslexia5; Verdana, recommended by the British Dyslexia Association [4]; Courier the most common example of monospaced font [8]; Helvetica and Myriad broadly used in graphic design and typeface of choice of Microsoft and Apple, respectively ; Garamond for its strong legibility for printed materials [8] and CMU widely used in scientific publishing, as is the default of the typesetting program TeX, as well as a free typeface supporting many languages [29].

The readings of each text were recorded using eye tracking, the user preferences towards the fonts were gathered using questionnaires with five-point Likert scales. Comprehension

questions were presented at the end of each text as a control variable.

The text used in the experiments met comparability requirements. They were extracted from the same book, Impostores ('Impostors'),6 by Lucas Sanchez [62]. They all had the same genre and same style; the same number of words (60 words); similar word length, with an average length ranging from 4.92 to 5.87 letters; absence of numerical expressions, acronyms, and foreign words, because people with dyslexia especially encounter problems with such words [9]. An example of a text read by the participants is given in the Appendix.

The text presentation was also controlled, except from the typeface. All the texts were left-justified, using a 14 points font size, and the column width did not exceeded 70 characters/column, as recommended by the British Dyslexia Association [4]. The color used was the most frequently used in the Web for text: black text on white background.

The equipment used was the eye tracker Tobii 1750 [69], which has a 17-inch TFT monitor with a resolution of 1,024768 pixels. The time measurements of the eye tracker have a precision of 0.02 seconds. Hence, all time values are presented in the dataset with an accuracy of two decimals. The eye tracker was calibrated individually for each participant and the light focus was always in the same position. The distance between the participant and the eye tracker was constant (approximately 60 cm. or 24 in.) and controlled by using a fixed chair.

For more details about the experimental design on how these readings were collected, please refer to [55].

Therefore, our dataset is composed of readings marked as D if the participant has dyslexia and N if not, there are 12 readings per participant, that is 1,164 readings; 29 of these readings were not properly recorded with not a number values. Hence, we removed those readings from the dataset having a final dataset containing 1,135 readings. From the dataset we extracted the following features:

Age of the participant: ranging from 11 to 54 years old.

Typeface: One of the 12 typefaces used for the text.

Italic: This is a binary feature with two values, italic when the text had an italic type and roman when the text had a roman

type.
Serif: This is a binary feature with two values, sans serif when the font of the text had an typeface with out serif -Arial, Helvetica, Myriad, and Verdana, and serif when the text had typefaces with serif CMU,
Garamond, and Times.
Typeface designed for dyslexia: A binary feature that shows when the font in the text had a typeface specifically designed for people with dyslexia.
Typeface preference of the participant: Value given to a typeface by the participant using a five-point Likert scale.
Number of visits: Total number of visits to the area of interest.
Mean of visit: Duration of each individual visit within the area of interest (the text).
Sum of visits (in the following, reading time): Sum of all the visits. This is equivalent to the reading time of the whole text.
Mean of fixation: When reading a text, the eye does not move contiguously over text, but alternates saccades and visual fixations, that is, jumps in short steps and rests over pieces of text. It denotes how long the eye rests still on a single spot of the text.
Number of fixations: Total number of fixations while reading a text per visit.
Sum of fixations: Sum of all fixations.
Some of the features have numeric (real or integer) values, so we established some ranges for each of them to discretize the data. For instance, the age of the participants is divided in 3 dierent groups: (1) younger than 14 years old, (2) from 14 to 19 years old, and (3) from 20 to 54 years old.

5 EXPERIMENTS

In order to find out whether it is feasible to detect readings of users with dyslexia, we set up a machine learning experiment. Machine learning is the scientific discipline that studies algorithms that can learn from data and make predictions. The output of a machine learning algorithm is called a model which is capable of making predictions given unseen data (normally for evaluation).

We carried out an experiment with a binary classifier of LIBSVM [7] in the polynomial Support Vector Machine (SVM) set-up. An SVM is a method for supervised learning that analyzes data and recognize patterns for classification. Given a set of training examples, each marked as belonging to a category, an SVM training algorithm builds a model that assigns new examples into the categories. It represents the examples as points in space and classifies them according to hyperplanes. When there is an input for the classifier it tries to assign a hyperplane to the input and then this is the classification output. Our SVM is trained on datasets as the one described in Section 4, and it is able to perform predictions on new readings.

We performed a 10-fold cross validation experiment by dividing the data in 10 dierent roughly equal subsets (10% of the data in each subset). Then we trained a statistical model on the rest of the data (90%) and tested on the corresponding fold by iterating 10 times, at the end we had all the data tested independently. We randomized the data and we did stratified sampling to ensure a similar distribution of data in all folds. We also kept all readings by the same user in the same fold, meaning that we had, in each fold, a similar number of readings marked as participants with and without dyslexia, and that a user does not serve for training a model that will predict readings of the same user. The idea is to see how the results of the statistical analysis will generalize on an independent dataset, in our case: new readings. We used 10-fold cross validation because it is normally recommended for smaller datasets when a single train-development test split might not be informative enough [2].

Table 1 shows the accuracy of the SVM models for each of the folds. This result suggests that the model is able to predict readings of users with dyslexia quite accurately with a final result of 80.18% by using the most informative

features (reading time, mean of fixations and age of the participants),7 meaning that the statistical models are able to make a correct prediction in 910 of the 1,135 readings. The features that we found useful for classification were: (1) reading time, (2) mean of fixations, and (3) age of the participant. Some features that were useful standing alone, such as (1) number of visits or (2) number of fixations were not useful when they are

Dataset	Accuracy
Fold-1	83.62 % (97/116)
Fold-2	96.26 % (103/107)
Fold-3	69.90 % (72/103)
Fold-4	89.74 % (105/117)
Fold-5	86.48 % (96/111)
Fold-6	73.15 % (79/108)
Fold-7	61.21 % (71/116)
Fold-8	82.41 % (89/108)
Fold-9	85.47 % (100/117)
Fold-10	74.24% (98/132)
All	80.18% (910/1,135)

Table 1: Accuracy of the classifiers in the 10-fold cross validation experiment.

used jointly with the features listed above, due to redundancy as they express very similar information. Other features, such as typeface, italic or serif do not aect at all in the predictions, which is also expected, and good news, because they are independent from the participant. This means that we are able of detecting users with dyslexia without taking into account the typeface.

6 DISCUSSION

First, it is worth noting that the age of the participants range from 11 to 54 years old, and the users with dyslexia tend to improve their reading skills with age. In order to test whether this was aecting the final result we run the same experiment (with the same folds), as in Section 5, by removing the age of the participant as a feature. Table 2 shows the results of the SVM models without considering the age of the participants. The final result is 76.38 of final accuracy (losing 3.8 points). This indicates that the age of the users shows clearer dierences in their reading performance. Nonetheless, in the dataset, the age average of the participants with dyslexia is 20.96, with a standard deviation of 9.98 while the age average of the participants without dyslexia is 29.20 with a standard deviation of 9.03 [55]. If the ages of both groups were perfectly matched, we could expect

to have more homogenous results between folds. Nonetheless, we had more participants without dyslexia without higher education (5) than participants with dyslexia (3) [55].

Fleshing out a bit more the results, we also observe that some folds achieved higher results than others, being 96.26% the highest and 61.21% the lowest, even though we performed stratified sampling we encountered this outcome. This means that some of the readings are dicult to predict. For instance, a participant with dyslexia who is 50

Dataset	Accuracy
Fold-1	83.62% (97/116)
Fold-2	85.98% (92/107)
Fold-3	65.05% (67/103)
Fold-4	84.62% (99/117)
Fold-5	74.77% (83/111)
Fold-6	72.22% (78/108)
Fold-7	56.03% (65/116)
Fold-8	82.41% (89/108)
Fold-9	85.47% (100/117)
Fold-10	73.48% (97/132)
All	76.39% (867/1,135)

Table 2: Accuracy of the classifiers in the 10-fold cross validation experiment without considering the age of the participant as a feature.

years old and might have already overcome most of its reading issues, would be ideally classified as a participant with dyslexia, however our model fails and classifies it as a participant without dyslexia. We believe that the main problem is the size of the dataset, since having more input data would lead our model to generalize better in those cases. Therefore, in order to improve our results, we plan to increase the dataset by carrying out more eye tracking experiments. Moreover, the age of the participants is also playing a role in this issue, since we have participants that range from 11 to 54 years old, we also believe that having dierent datasets depending on the age of the participants will also lead to a proper classification of the readings, since our model is general and a first attempt trying to predict dyslexia based on eye tracking measures.

As we mention above, the features related with the typeface were not useful for classification. Even that previous work has shown that typeface have a significant impact on the readability of people with and without dyslexia, this fact does not have an impact to dierentiate their readings. The fonts that improve the readability of people without dyslexia are also beneficial for the readability of people with dyslexia [55]. This can explain why typeface is not an informative feature for classification, similarly of the font related features, such as, serif, italic, and fonts designed for people with dyslexia.

Even if the results of this experiment are only valid for Spanish language, previous literature on eye tracking has found significant dierences on eye movements for languages with deeper orthographies such as English [21], German [20] or Bulgarian [19] as well as it was reported for Spanish [35]. Therefore we believe that dyslexia prediction in other languages using eye tracking measures is feasible, especially in languages with shallow orthographies where reading speed is a strong indicator for diagnosing dyslexia, such as Spanish [63] or Italian [71].

7 CONCLUSIONS AND FUTURE WORK

The eye movements of readers with dyslexia are dierent from regular readers. People with dyslexia have longer reading times, make longer fixations, and make more fixations than readers without dyslexia. In this paper we have shown how these characteristics can be used to train a machine learning model. We have presented a method that predicts readings of people with dyslexia with 80.18% of accuracy. To the best of our knowledge, this is the first attempt to build a statistical model to predict automatically readers with dyslexia using eye tracking measures. The model uses common eye tracking features such as reading time, mean of fixation, as well as the age of the participant. However, note that these are only seminal results on this topic and that the dataset was intended for other purposes.

Dyslexia is called a hidden disability because it is hard to diagnose. Diagnosing dyslexia is crucial to address this condition

but estimations of dyslexia are much higher than the actual diagnosed population. Our model is just the first attempt on predicting dyslexia by using a machine learning approach with eye tracking measures. However, we believe it has a great potential impact.

This study suggests that eye tracking measures have the potential to be used to diagnose dyslexia in the future. Eye trackers are becoming more and more aordable and reading a text in silence is less intrusive than being exposed to the tests needed in current diagnoses. Moreover, there are other human-computer interaction measures that were found to be related to eye tracking measures, such as mouse tracking, that are yet to be explored. Their potential applications go from diagnosing to user modelling via their interaction with the computer.

For future work we plan to enlarge the dataset by carrying out more eye tracking experiments in dierent languages. Then, we also plan to try with other kind of classifiers, such as perceptron learning, recursive neural networks, or conditional random fields. Currently, we are exploring other human-computer interaction measures to detect dyslexia in collaboration with schools.

Acknowledgments

This paper was partially developed under a grant from the Department of Education, NIDRR grant number H133A130057.

References

[1] R. Baeza-Yates and L. Rello. Estimating dyslexia in the Web. In Proc. W4A '11), Hyderabad, India, 2011. ACM Press.

[2] M. Ballesteros and J. Nivre. Maltoptimizer: A system for maltparser optimization. In Proceedings of the Eight International Conference on Language Resources and Evaluation (LREC'12). European Language Resources Association (ELRA), may 2012.

[3] J. L. Black, D. W. K. Collins, J. N. De Roach, and S. Zubrick. A detailed study of sequential saccadic eye movements for

normal-and poor-reading children.Perceptual and motor skills, 59(2):423434, 1984.

[4] British Dyslexia Association. Dyslexia style guide, January 2012. http://www.bdadyslexia.org.uk/.

[5] B. Brown, G. Haegerstrom-Portnoy, C. Yingling, J. Herron, D. Galin, and M. Marcus. Tracking eye movements are normal in dyslexic children. American journal of optometry and physiological optics, 60(5):376, 1983.

Authors Details



Dr. A.V.Prathap Kumar is working as a professor in ECE and Dean of academics in TKR Engineering College. He published many National and International journals and he received Best teacher award. He conducted many workshop sand international conferences. Under his Guidance 6 Research Scholars doing in different areas. He worked as a R&D Head in K.L. University. And also he worked as Principal in Various Colleges affiliated to JNTUA. He also act as IEEE , Conference Judge. He is life member of ISTE.

International Journal of Pure and Applied Mathematics
Volume 118 No. 24 2018
ISSN: 1314-3395 (on-line version)
url: http://www.acadpubl.eu/hub/
Special Issue

http://www.acadpubl.eu/hub/

IoT Using by Machine learning techniques

DR. A. V. Prathap kumar,
Dr. G. Vamsi Krishna,
Dr. K . Satish kumar
Professor , Assistant Professor,Associate Professor
Teegala Krishna Reddy Engineering college
Dr.lankapalli Bullayya engineering college
dravprathapkumar@gmail.com,
vamsikrishna527@gmail.com,
satish7433@gmail.com,

May 29, 2018

Abstract

Machine learning is a part of computer science that developed from the study of pattern recognition and computational learning concept in artificial intelligence. Machine learning determines the study and construction of algorithms that can absorb from and make guesses on data. The Internet of Things (IoT) is the network of physical objects or "things" rooted with electronics, software, sensors, and network connectivity, which allows these objects to collect and exchange data. Collections of devices will act as systems that can be enhanced in new ways, and systems of systems will share data and perform as annetwork of data and devices. Machine learning - a term that describes numerous methods to evolving meaning from data - will have to be part of the calculation, but so will outdatedprofessional and data investigation techniques as organizations prepare for the Internet of Things (IoT). This paper will

provide an overview of challenges and openings presented by this new model.

***Key Words*:**Internet of Things, Cloud computing, Machine learning, Smart Environments

1 Introduction

The term Internet of Things was first coined by Kevin Ashton in 1999 in the context of supply chain management [1]. However, in the past decade, the definition has been more inclusive covering wide range of applications like healthcare, utilities, transport, etc[2]. Although the definition of Things has changed as technology evolved, the main goal of making a computer sense information without the aid of human intervention remains the same. A radical evolution of the current Internet into a Network of interconnected objectsthat not only harvests information from the environment(sensing) and interacts with the physical world (actuation/command/control), but also uses existing Internet standards to provide services for information transfer, analytics, applications, and communications. Fueled by the prevalence of devices enabled by open wireless technology such as Bluetooth, radio frequency identification (RFID), Wi-Fi, and telephonic data services as well as embedded sensor and actuator nodes, IoT has stepped out of its infancy and is on the verge of transforming the current static Internet into a fully integrated Future Internet [3].

The goal of machine learning is to program computers to use example data or past experience to solve a given problem. Many successful applications of machine learning exist already, including systems that analyze past sales data to predict customer behavior, optimize robot behavior so that a task can be completed using minimum resources, and extract knowledge from bioinformatics data [4]. In order to present a unified treatment of machine learning problems and solutions, it discusses many methods from different fields, including statistics, pattern recognition, neural networks, artificial intelligence, signal processing, control, and data mining. All learning algorithms are explained so that the student can easily move from the equations in the book to a computer program.

2 UNDERSTANDING ANAL YTICS AND MACHINE LEARNING

Data and functionality can be accessed from any location and through multiple devices. Specialized devices provide context in which the user accesses the data.A fitness bracelet can access data about the users physical health via an iPhone or laptop in the specific context of exercise. In this case, the fitness bracelet acts as an IoT sensor as well as provides a means for accessing and consuming data. The device also subsumes other devices (such as a pedometer) through software functionality. The data provided by the device can offer additional insights about the consumers usage and preferences, which can be leveraged when updating functionality and developing new features. If aggregated across a population of users and combined with other datasets, new insights can shed light on epidemiological data, activity levels across populations, lifestyles, and demographic data. This information has value to marketers, healthcare providers, insurance companies, and government agencies.

Machine learning algorithms can be used to make predictions based on these data patterns. For example, in a Mayo Clinic study, activity data was correlated with recovery rates for cardiac patients[5]. The same machine learning and predictive algorithms are the basis for a number of connected intelligent consumer devices. Nest thermostats are an example of a device that leverages data patterns to predict the preferred temperature in a specific room at a certain time of day. Other consumer devices

include those that learn from voice patterns (such as Echo, a personal-assistanttype device from Amazon [6] to those that learn from much more complex behavior and activity patterns (such as Jaguars Land Rover monitoring system, which "relies on a complicated software which enables the car to study, predict, check, and remind the cars occupants to help the driver auto-delegate his tasks and make him concentrate more on his driving [7].

Optimization algorithms use machine learning mechanisms to leverage data from both sensors and intelligent devices that interact under dynamic conditions. These variable conditions cant be precisely predicted beyond certain parameters. The algorithms will need to sense, respond, and adapt. For example, as cars take on more responsibilities from the driver, they will be interacting with

more environmental sources of data (sensors, lights, other cars, and so on). Classes of applications in industrial automation, logistics and transportation, power grid and energy systems, traffic management, security systems, and other "systems of systems" will let machines communicate directly with other machines. Furthermore, such applications will help machines interpret dataflows based on algorithms that can evolve and adapt, so the machines can achieve the desired end states given certain operational parameters.

3 UNDERSTANDING IOT CAPABILITIES

When products are intelligent and connected to the Internet, they become variable and have the ability to change as the users needs change. Now, physical objects become vehicles or containers for softwaredriven functionality. These levels of capability require increasingly sophisticated data analytics approaches - from collecting and applying data to allowing algorithms themselves to apply data and learn while doing so.

So, the first level of capability - monitoring - becomes a real-time mechanism to better understand field performance and user needs and offer new capabilities. This means that the boundaries of an organizations traditional products and services are blurred and extended. Consider field equipment that was traditionally maintained by a contract field service firm, not by the manufacturer. With intelligence and monitoring, equipment can inform the manufacturer of needed service ahead of a breakdown. Routine maintenance can become part of the manufacturers offering, with complex repairs still being handled by a specialist contractor if the margins and logistics make sense for the organization. This disintermediation can extend to distribution chains as well. Equipment can automatically call for a replenishment of supplies, removing distribution costs and inventory from the supply chain[8].

Consider the role of humans in running a system or machine, where most of the functions are automated. Humans guide the operation and look for edge conditions, anomalies, and exceptions that werent anticipated (or cost-effective) during the system design. Then, they use their judgment to make a change, correction, or

adjustment. The human doesnt need to be with the equipment and might not need to be monitoring in real time (depending on the process). Monitoring is simply taking in the data and processing it (something must be done with the data at some point). Control is applying that data in real (or near real) time to the operation of the equipment or device. The strategic decision that organizations need to make is whether and when to make more control capabilities part of the product offering and whether to offer that as a service or to allow the customer to have that capability.

The third level of capability - optimization - can extend to the performance of an individual object, a fleet of objects, or an ecosystem of objects across multiple manufacturers and technologies. The strategic decision about whether to extend offerings to this realm hinges on the level of knowledge and sophistication around the value chain and the boundaries of the processes. A truck manufacturer, for example, would be poorly positioned to optimize complex mining equipment but would benefit from optimizing its fleet of trucks (and potentially a fleet of other manufacturers trucks) if the industry dynamics made business sense.There are four types of IoT capabilities [4]: monitoring - sensors provide data about the operating environment and product usage and performance; control - product functions can be controlled and personalized; optimization - feedback loops from monitoring and control allow for improved efficiency, better performance, preventative maintenance, and diagnostics and repair; and autonomy - monitoring, control, and optimization allow for independent operation, coordination with other systems, interaction with the environment, personalization, replenishment, and self-diagnosis and repair.

Extending optimization to independent operation requires an extension of capabilities to allow for less constrained interaction with the environment and with other systems. Autonomy requires greater intelligence around algorithms that can deal with unplanned situations - those situations for which programmers and system engineers didnt explicitly design. Autonomous operations require incorporating adaptable machine learning approaches for dealing with novel situations into the core algorithms used for monitoring, control, and optimization.

4 CHALLENGES FACING A SECURE INTERNET OF THINGS

While the full scope of security concerns is broad, Freescale sees four key challenges impacting the evolution to a secure IoT [9]:

1. Emergence of consumer IoT solutions introduced by startup companies, for which security may not be a focus.

2. A lack of system security standards for end nodes, where performance and low power requirements make security integration difficult.

3. Increasing complexity of end node security as the car itself becomes an end node. The more than 100 ECUs in the average car are now adding wireless connectivity, opening up new vulnerabilities to data privacy and driver safety.

4. New challenges of securing data with evolution of Software Defined Networking. The physical separation of the control and data plane in virtualized environments requires secure data over multiple miles versus inches in traditional networks. Other challenges exist in securing multiple channels for every communication versus one in traditional networks.

5 THE IMPORTANCE O F M ACHINE LEARNING IN T HE I NTERNET THINGS

Some of the most exciting work being done to reap value from the Internet of Things (IoT) involves taking data insights to the next level using machine learning (ML). A good IoT solution gives you an extraordinarily useful view of your organizations data; a great one allows you to build algorithms that can predict whats nextthe next equipment breakdown based on historic failure data; the next tune-up needed based on lifespan data from component sensors; the best time to turn on the heat based on last years data and next weeks weather report [10]. When you put enormous compute against enormous data and you bring machine learning to bear along with it, and the Internet of Things feeding data into the cloud and streaming analytics running on live data. It is a very short time,

to see a completely different picture of analytics.Some of the most exciting work being done to reap value from the Internet of Things (IoT) involves taking data insights to the next level using machine learning (ML). A good IoT solution gives you an extraordinarily useful view of your organizations data; a great one allows you to build algorithms that can predict whats nextthe next equipment breakdown based on historic failure data; the next tune-up needed based on lifespan data from component sensors; the best time to turn on the heat based on last years data and next weeks weather report.

Machines are good at mechanical and physical processes, but still not that great at automating decision-making especially in very complex environments. The challenges associated with employment and wealth distribution in an environment of seemingly ever-increasing automation, but the panelists admitted they couldnt predict exactly how this trend might play out[11].The ML marketplace as a place where data scientists can publish their innovative ideas as web services, all panelists issued a call to action to the audience to be ever more data-driven in their work and build their ML skills, as there are many possibilities ahead of us to make products and services more intelligent.Next, the opinions on whether there is a danger to using ML systems as "black boxes" inside systems such as drones, cars, etc. without fully understanding what's inside.ML as being any different than any software algorithm collection, and there is a lot of software to ask the same question about. There must be systems in place

to ensure reliability that mistakes can be made, and that experience and decision-making responsibilities have to be assigned appropriately. "People are teaching ML incorrectly. They teach what the need to learn statistical hygiene is inside the black box, but before that.There should be a test set, and no cheat, there should be confidence intervals, and need to worry about outliers. Learn statistical hygiene to avoid disasters"[12].

6 CONCLUSIONS

Analysts expect that new Internet of Things (IoT) products and services will grow exponentially in next years. IoT-A relies on se-

mantic types (Semantic Web, semantic clustering) to discover IoT resources and their vibrantrelationshipboard. IoT as a global set-up for the data society, enabling advanced services by interconnecting (physical and virtual) things based on, current and developing, interoperable information and communication technologies. To note that, in this view, the Machine to Machine (M2M) communication capabilities are seen as an essential enabler of the IoT, but represent only a subset of the whole set of abilities of IoT. Finally, the motivation for all is that through the collaboration and the integration of multiple data sources, it can be reached more powerful solutions, better data-analysis, more precise data-driven modeling, position awareness, and in absolute better solutions.

References

[1] K. Ashton That Internet of Things thing RFiD Journal (2009)

[2] H. Sundmaeker, P. Guillemin, P. Friess, S. Woelffl, Vision and challenges for realising the Internet of Things, Cluster of European Research Projects on the Internet of Things CERP

[3] J. Buckley (Ed.), The Internet of Things: From RFID to the Next-Generation Pervasive Networked Systems, Auerbach Publications, New York (2006)

[4] EthemAlpaydin, Introduction to Machine Learning, Publication MIT Press 2009.

[5] D.J. Cook et al., "Functional Recovery in the Elderly After Major Surgery: Assessment of Mobility Recovery Using Wireless Technology", Annals of Thoracic Surgery, vol. 96, no. 3, 2013, pp. 10571061;

[6] D. Etherington, "Amazon Echo Is A $199 Connected Speaker Packing an Always-On Siri- Style Assistant", Tech Crunch, 6 Nov. 2014;

[7] M. Mendoza, "Jaguar Land Rover Develops Self-Learning, Intelligent Car", Tech Times, 17 July 2014;

[8] M.E. Porter and J.E. Heppelmann, "How Smart Connected Devices are Transforming Competition", Harvard Business Rev., Nov. 2014, pp. 7086.

[9] http://www.freescale.com /applications /intern et-of-things-iot: IOT-INTERNET-OF- THINGS? cid=ps_en_57hj4x1k & gclid=CN7_v8i qq8kCFdeJaAodGIwB1Q

[10] https://blogs.microsoft.com/iot/2014/12/09/ machine-learning-adding-impact-to-iot/

[11] http://blogs.technet.com/b/machinelearning/ archive/2014/12/09/ machine-learning-hype-or- reality-microsoft-ml-experts-weigh-in.aspx

[12] Barnaghi, P., Wang, W., Henson, C., and Taylor, K., Semantics for the Internet of Things: Early Progress and Back to the Future, International Journal on Semantic Web and Information Systems, vol. 8, No. 1, 2012.

Author details



Dr. A.V.Prathap Kumar is working as a professor in ECE and Dean of academics in TKR Engineering College. He published many National and International journals and he received Best teacher award. He conducted many workshop sand international conferences. Under his Guidance 6 Research Scholars doing in different areas. He worked as a R&D Head in K.L. University. And also he worked as Principal in Various Colleges affiliated to JNTUA. He also act as IEEE , Conference Judge. He is life member of ISTE.

ACADEMIA
Accelerating the world's research.

Implementation of Smart Home Automation with Enhanced Security

International Journal of Scientific Research in Science, Engineering and Technology IJSRSET

Related papers

Download a PDF Pack of the best related papers



MOBILE PHONE BASED ELEGANT SECURITY SYSTEM WITH ANDROID APPLICATION
Swati Bembde

Web Based Home Automation and Security
International Journal of Scientific Research in Science, Engineering and Technology IJSRSET

A Review on ZIGBEE Smart Energy Implementation for Energy Efficient Building.
ijesrt journal

© 2018 IJSRSET | Volume 4 | Issue 4 | Print ISSN: 2395-1990 | Online ISSN : 2394-4099
Themed Section : Engineering and Technology

Implementation of Smart Home Automation with Enhanced Security

M. Ummay Hagera*[1], K. Lokesh Krishna[2], K. Anuradha[3]
*[1]ECE Department, SVCET, Chittoor, Andhra Pradesh, India
[2]Department of ECE, S. V. College of Engineering, Tirupati, Andhra Pradesh, India
[3]Department of CSE, L.B.C.E.W., Visakhapatnam, Andhra Pradesh, India

ABSTRACT

With the surge in usage of power and human population, there is a vital need to conserve electricity in every way possible. The lack of ability to access and control the appliances from remote locations is one of the major reasons for power loss. To overcome this automatic techniques are employed in every aspect of day to day activities. Automation refers to the ability to program and plan a list of events for the devices on the network. The programming may include time-related commands, such as having your lights turn on or off at specific times each day. It can also include non-scheduled events, such as turning on all the lights in your home when your security system alarm is triggered. This paper describes the design and prototype implementation of new home automation system with enhanced security that uses Wi-Fi technology as a network arrangement connecting its parts. The proposed implementation consists of a hardware interface segment, which includes fingerprint sensor, temperature sensor, motion sensor, and camera and provides appropriate interface to sensors and actuators of home automation system. Unlike most of the home automation systems available in the present scenario, the proposed system is accessible that one server can handle many hardware interface modules as long as it exists on Wi-Fi network communication coverage. The proposed system supports a widespread variety of home automation devices like power management components, and security components.

Keywords: Wireless, sensor, simulation, hardware, Wi-Fi, network coverage and actuator.

I. INTRODUCTION

As advanced technologies are evolving day by day, information or raw data plays a very major role in every aspect of communication. In fact it is everything in today's real life. Particularly when this data is liable to affect their life in close way, then data has to be properly monitored and executed. People are left from their home for work or for any other reasons and there is always insecure of what's happening in their home and equipment related to home appliances whether they are operating or turned On/Off and several other things associated to their house. Home automation is the alternative to solve these problems and provides the user with live monitoring and controlling of the entire home with electronic hardware.

Today people are considering at various ways and means to improve their life-style using the newest technologies that are available. Any new capacity or home appliance that promises to improve their life-style is grabbed by the customers. The more and more such facilities and appliances are added, it becomes inevitable to have easy and convenient methods and means to control and operate these appliances. Conventional wall switches are located in different parts of a house and thus necessitates manual

operations like to switch on or off these switches to control various appliances. It gets virtually unmanageable to keep track of various appliances that are running and also to monitor their performances. Also installing a home security system is very costly and a difficult task. The advantages of home security system are that it protects from unauthorized intruders entering into the house, it helps monitor and save power usage for the house and it helps to control various aspects of the house from a simple smartphone.

Home automation has been around for the past decade in terms of lighting the house and simple house hold appliances control, and only in recent time's technology caught up the idea of the interconnected world, permitting full control of the home from anywhere, to become an actuality [1]-[3]. With home automation, any device in the house can be made to react i.e. when it should react, and why it should react. The schedule of the event is prepared and the rest is automated and based on the personal preferences it provides convenience, control, money savings, and an overall smarter home will be built.

In general Smart home technology commonly refers to any suite of devices, appliances, or systems that connect into a common network and that can be independently and remotely controlled. When a home technology like this works together in one system, it can also be mentioned more loosely as a "connected home". As an example, in an individual home various devices such as thermostat, lights, audio speakers, TVs, security cameras, locks, appliances, and more are all connected into a shared system, which can be controlled from a smart phone or through a mobile touch screen device. Smart home automation allows tapping into high-tech functionality and luxury that had not been possible in the past. As technological developments continue to grow, so will be the potential for consumer home automation to make life easier and more enjoyable [5].

A "smart home" typically is a domestic atmosphere that has been partially automated. Home automation includes centralized control for lighting, HVAC (heating, ventilation and air conditioning), appliance management, and others. The main objective of home automation is to boost the comfort, reduce the energy consumption and increase security in domestic scenarios. Generally, houses are furnished with independent control panels to regulate all of the systems and appliances present in the house. Furthermore, these control panels are often not associated each other. The main purpose of a smart home is to consolidate the control of all the devices into a single control unit, which can be programmed to do specific tasks suitable for the house owner and the home of importance. Also other parameters such as reduction of consumption of resources such as power, gas, etc. play a very major role. Due to the very high pricing on energy, resource conservation has become a part of a person's day-to-day life [6]-[7]. If a person has the possibility to control his home automation remotely he can reduce the consumption of energy and thus reduce his own expenses.

Furthermore, environmental sustainability has gained significance in the recent years. If a person is away from home there is no need for the air conditioner or ventilation to operate. The same principle applies to illuminations, heating and other appliances. Some smart homes systems suspend the operation of house hold appliances until they are operated again as per their wish. Furthermore, there are several different technologies for implementing such smart homes. Some standards utilize complex communication protocols and control wiring; others rely on embedded signals in the existing power circuit of the house. A portion relies on radio frequency signals, and others become hybrids by combining several methods. All of the controlling tasks are done through a microcontroller, such as 8051, PIC, ARM and Arduino, which enables the communication and upon receiving some commands controls the different systems in the house. Finally, the commands to

control the appliances in the house are sent by a central control unit such as a computer, remote control or smartphone.

This paper proposes a novel design and implementation for the smart home automation using the wireless sensor network and the biometric technologies. Also the proposed system employs the biometric technology in the authentication for home entrance which enhances home security as well as easiness of home entering process.

This paper is organized as follows. Section II presents the design and implementation of the proposed system using LPC2148 ARM7TDMI microcontroller. Section III explains the working of the system and shows flowchart. The hardware prototype implementations are presented in Section IV. Finally, conclusions are drawn in Section V.

II. DESIGN AND IMPLEMENTATION OF THE SMART HOME AUTOMATION SYSTEM

The proposed smart home automation system has the ability to control and monitor the following physical parameters in house environment. They are temperature and humidity, motion detection, fire and smoke, detection, door status, light level and video monitoring. Also the implemented home automation system can be used to switch on/off the following electrical appliance Lights on/off/dim, HVAC on/off, Door lock, Window shutdown and on/off different appliances. The main challenges faced during the implementation of Home automation systems are poor manageability, high cost of ownership, inflexibility, and difficulty in achieving good level of security.

The proposed working model of the smart home automation system is as shown in the figure1. The system consists of different sensors for measurement of physical parameters such as temperature, gas, motion, and video. The threshold levels for all the sensors are set as T_1, T_2, T_3 and T_4 etc. The microcontroller used in the proposed work is LPC2148 ARM7TDMI microcontroller. These microcontrollers are ideal for applications where miniaturization is a key requirement, such as access control and point-of-sale. The program is written such that if the sensor parameters are greater than the predetermined threshold levels, then the corresponding alarm circuits are activated. Once this happens, the home appliances are switched ON/OFF based on the physical parameter monitored. The proposed smart home automation system is shown in figure 1.

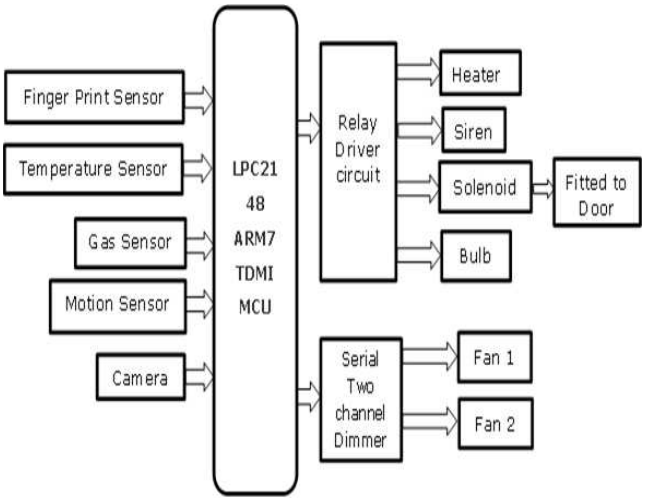


Figure 1. Implementation of the proposed smart home automation system

III. FLOWCHART

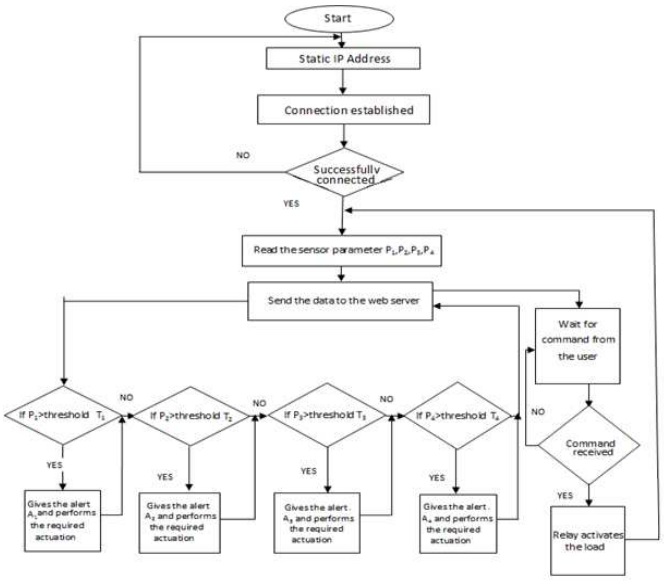


Figure 2. Flow chart of the entire process

The flowchart of the proposed smart home automation with enhanced security is shown in figure 2. If the temperature exceeds the threshold level T_1=35ºC, then the air conditioned machine will turn on automatically and will turn off when the temperature returns to normal conditions. Likewise when there is a leakage of cylinder gas in the house, an alarm is raised giving the alert sound. This alerts the nearby people, so that they can switch off the cylinder. Using the passive infra-red sensor and light dependent sensor, and based on the movement of the individuals, the lights are turned on/off automatically by detecting the individual inside the house. The threshold values T_2, T_3, and T_4 are set according to the individual room requirements. The individuals can also monitor the electric appliances through the internet via web server technologies. If electric lights or any other electrical appliances are left unoperated, then it can be sensed by the corresponding sensors and can be turned off remotely by entering the IP address of the web server.

IV. HARDWARE IMPLEMENTATION

In this proposed work, is LPC2148 ARM7TDMI is used as the main microcontroller. All the sensors such as temperature, PIR, fingerprint and gas sensor are interfaced to LPC2148 ARM7TDMI which is located in the home of interest. Camera is also interfaced to the LPC2148 ARM7TDMI to capture the live events occurring inside the home. Figure 3, shows the hardware prototype of the smart home automation system and figure 4, shows the on/off controlling of the electric bulb.

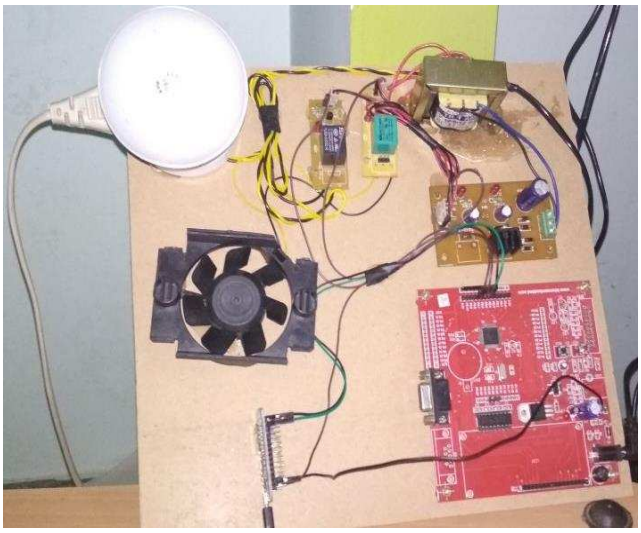


Figure 3. Prototype of the smart home automation system



Figure 4. controlling of electric bulb

The controlling of fan is shown in figure 5.



Figure 5. controlling of fan

V. CONCLUSION

Smart home automation is an emergent, active market and a very popular research field where lot of changes and new ideas are possible. It is becoming more popular due to the latest developments in electronic hardware which have significantly reduced the cost and improved the capabilities. This is due to the fact that advanced technologies around us evolve and the access to desired information is easier than ever before. In this paper a highly secured, low cost, remotely controlled, easily accessible smart home is designed and implemented. The proposed system is a novel implementation and uses Wi-Fi technology for controlling the various sensors in home. A prototype of the entire system is carried out and remote monitoring/controlling of the smart home is effectively implemented practically and satisfied results have been achieved. In future, more improvements can be carried out in monitoring and controlling part. Also more sensors and devices can be connected and monitored on. Furthermore, camera module can be adjusted to operate in different modes. Lastly, the selection of home automation system depends on the situation and requirements.

VI. REFERENCES

[1]. Matthias Gauger,Daniel Minder,Arno Wacker, Andreas Lachenmann,"Prototyping Sensor-Actuator Networks for Home Automation", REALWSN'08, April 1, 2008, Glasgow, United Kingdom.

[2]. Greichen, J.J., "Value based home automation or today's market," IEEE Transactions on Consumer Electronics, vol.38, no.3, pp.34-38, Aug.1992

[3]. C.-L.Hsu, S.-Y.Yang, and W.-B.Wu, "Implementing Speech-Recognition Microprocessor into Intelligent Control-System of Home- Appliance," 2008 IEEE Asia-Pacific Services Computing Conference, pp.881-885, (Dec.2008)

[4]. Ahmed ElShafee, Karim Alaa Hamed," Design and Implementation of a WiFi Based Home Automation System", International Journal of Computer, Electrical, Automation, Control and Information Engineering Vol: 6, No: 8, 2012.

[5]. K.L.Krishna, O.Silver, W.F.Malende and K.Anuradha, "Internet of Things application for implementation of smart agriculture system," 2017 International Conference on I-SMAC (IoT in Social, Mobile, Analytics and Cloud) (I-SMAC), Palladam, 2017, pp.54-59.

[6]. Ardam H.and Coskun I., "A remote controller for home and office appliances by telephone", IEEE Transactions on Consumer Electronics, vol.44, no.4,pp.1291-1297, 1998.

[7]. YunCui, Myoungjin,Kim, YiGu, Jong-jinJung, and HankuLee, "Home Appliance Management System for Monitoring Digitized Devices Using Cloud Computing Technology in Ubiquitous Sensor Network Environment",Hindawi Publishing Corporation International Journal of Distributed Sensor Networks Volume 2014.

[8]. Alfakhri M.Murshed, K.Lokesh Krishna, Hussam Alqubati, Noordin Ali, "Implementation of Enhanced Finger Print based Door Locking System", International Journal of Scientific Research in Computer Science, Engineering and Information Technology (IJSRCSEIT), ISSN : 2456-3307, Volume 3 Issue 3, pp.275-279, March-April 2018.

[9]. Khusvinder Gill, Shuang-Hua Yang, Fang Yao, and Xin Lu.A ZigBee-Based Home Automation System.IEEE Transactions on Consumer Electronics, 55(2):422-430, May 2009.

ACADEMIA
Accelerating the world's research.

Implementation of High Speed Double Tail Comparator

International Journal of Scientific Research in Science and Technology IJSRST

Related papers

Download a PDF Pack of the best related papers



Low Power and Low Voltage Double Tail Dynamic Latch Comparator using 180nm Technology
IJAERS Journal

DESIGN OF LOW POWER HIGH SPEED CASCADED DOUBLE TAIL COMPARATOR.pdf
Dr. N. Muthu kumaran

A Double-Tail Comparator with Reduced Delay and Low Power Dissipation
IJSTE - International Journal of Science Technology and Engineering

© 2018 IJSRST | Volume 4 | Issue 5 | Print ISSN: 2395-6011 | Online ISSN: 2395-602X
Themed Section: Science and Technology

Implementation of High Speed Double Tail Comparator

U.S.Harshanga Kalingage*[1], K. Lokesh Krishna[2], K. Anuradha[3]
*[1]ECE Department, SVCET, Chittoor, Andhra Pradesh, India
[2]Department of ECE, S.V.College of Engineering, Tirupati, Andhra Pradesh, India
[3]Department of CSE, L.B.C.E.W., Visakhapatnam, Andhra Pradesh, India

ABSTRACT

In recent years, with the advance of wireless communication systems, microelectronics and sensor technologies, wireless sensor networks (WSNs) are becoming a hot-spot for scientific research and industrial applications. High speed and low power comparators are very much essential in the design of a very good analog to digital converter. In this paper a novel high speed, low offset voltage and low power double tail comparator is designed and simulated. The proposed design does not use any preamplifier stages before the latch stage, which accounts for the direct reduction of power dissipation and silicon area. For power optimization, the MOSFETs of the input differential pair comparator are designed to operate in sub-threshold region rather than in saturation region. The designed double tail comparator consumes 366μW when operated from a 1.8V power supply. The operating speed of the design is 100MHz and exhibits a propagation delay of 600μs. The simulated propagation delay is found to be 600μs and the entire design of the proposed double tail comparator circuit is carried out in 180nm CMOS technology and verified using the cadence-spectre simulator.

Keywords: high speed, positive feedback, analog to digital converter (ADC), digital to analog converter (DAC), threshold, and offset voltage.

I. INTRODUCTION

Comparators play very crucial part in the design of several mixed signal systems. They are widely used in many applications such as high speed Analog to Digital Converter (ADC), Digital to Analog Converters (DAC) and higher order filters. ADCs have become a major component in driving the semiconductor industry over the past decade. Increased integration of various functional blocks within an integrated circuit single chip makes ADCs more conventional and they are able to offer very high speed along with low power consumption. The operating speed of a comparator circuit can be changed by changing the various parameters of a transistor. Though, it is not straightforward approach to scale down transistor dimensions, as it requires high channel doping, gate-induced drain leakage, and band to band tunneling across the junction. The difficulty of short channel effects in transistors also needs to be properly controlled. Furthermore, the design of analog circuits becomes more complex and reliability also concerns, when supply voltages (V_{DD}) need to be decreased according to the nano and micro dimensions of the transistors. Comparator's plays a key role on the overall performance of the ADC. Currently in most applications, there is a need for high speed and high resolution ADCs, in which an high speed and highly accurate comparator circuit is desirable. With only a few external components, it can perform a wide variety of analog signal processing tasks. Comparators are among the utmost widely used electronic circuits today, being used in a vast group of consumer, industrial, and scientific devices.

With the rapid improvements of computer aided design (CAD) tools, advancements of semiconductor

modeling, miniaturization in transistor scaling, and the developments in fabrication processes, the integrated circuit market is growing rapidly. Nowadays, Complementary Metal-Oxide Semiconductor (CMOS) technology has become dominant over Bipolar (BJT) technology for analog circuit design in a mixed-signal system due to the industry trend of applying standard process technologies to implement both analog circuits and digital circuits on the same chip. While many digital circuits can be implemented in smaller device lengths with a lower power supply voltage, most existing analog circuitry requires minimum voltage to operate or even a redesign to accomplish the same design. With transistor length being scaled down to a few tens of nanometers, analog circuits are becoming increasingly more difficult to design. Scaling down of CMOS feature sizes results in higher unity gain frequency (fT) which means the transistors operate faster than before. However, this is achieved at the cost of a reduction in transistor's open loop gain (AOL). Also due to scaling power supply voltage can be reduced. So because of this the weight and size of the battery reduces and enables longer battery life time. Hence for the same reason, low-powered circuits reduce thermal dissipation.

This paper is organized as follows. Section II presents the theoretical explanation of double tail comparator. Section III explains the working and design of the proposed comparator circuit. The simulated results and performance summary of the proposed double tail comparator circuit are presented in Section IV. Finally, conclusions are drawn in Section V.

II. COMPARATOR CIRCUIT

A comparator is a circuit that compares an analog signal with another analog signal or reference voltage and generates a binary signal. The output signal generated is based on the comparison of the two inputs. The schematic diagram of the proposed double tail comparator is shown in figure 1.The comparator is one of the most commonly used circuits for converting a given input analog signal to output digital signal. In the analog to digital conversion process, it is necessary to first sample the input. This sampled signal is then applied to a combination of comparators to determine the digital equivalent of the input analog signal. The important parameters considered in the design of a comparator circuit are speed, input capacitance, kickback noise, offset voltage, power dissipation and input common mode range.

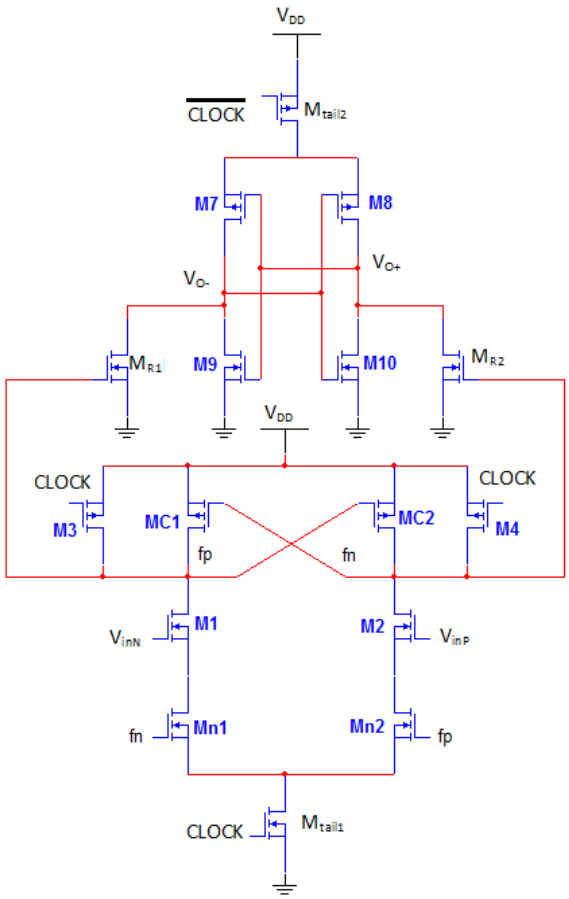


Figure 1. Schematic diagram of double tail comparator

In general, voltage comparator circuits are categorized into three types. They are open-loop comparators (operational amplifiers without compensation), Preamplifier based latch comparators (open loop comparator combined with dynamic regenerative latch) and fully dynamic latched comparator. The preamplifier based comparator consists of three stages

namely input amplifier stage, a latch stage and an output buffer stage. The preamplifier stage consists a differential amplifier with active loads. The preamp stage amplifies the input signal to improve the comparator sensitivity. It increases the minimum input signal with which the comparator can make a decision and isolates the input of the comparator from switching noise (often called kickback noise) coming from the positive feedback stage. It also can reduce the input referred latch offset voltage

III. OPERATION

The double tail comparator design is based on the double tail architecture. The idea of this comparator is to increase $\Delta V_n/f_p$ in order to increase the latch regeneration speed. To achieve this constraint, the two control transistors M_{C1} and M_{C2} are added to the first stage in parallel to (M_3-M_4) transistors however in a cross-coupled manner.

The operation of the modified double tail comparator is as follows. During reset phase (CLK = 0, M_{tail1} and M_{tail2} are off, avoiding static power), M_3 and M_4 pulls both f_n and f_p nodes to V_{DD}, hence transistor M_{c1} and M_{c2} are cut off. Intermediate stage transistors, M_{R1} and M_{R2}, reset both latch outputs to ground.

During decision-making phase (i.e. when CLOCK = V_{DD}, M_{tail1}, and M_{tail2} are on), transistors M_3 and M_4 are switched off. Likewise, at the beginning of this phase, the control transistors are still off (since f_n and f_p are about power supply voltage V_{DD}). Thus, f_n and f_p start to drop with not the same rates according to the input voltages. Suppose $V_{inP} > V_{inN}$, thus f_n drops faster than f_p, (since M_2 provides more current than M_1). As long as f_n continues decreasing, the corresponding PMOS control transistor (M_{C1} in this case) starts to switch on, pulling f_p node back to the power supply voltage V_{DD}; so another control transistor (M_{C2}) switches off, allowing f_n to be discharged completely.

In other words, unlike conventional double-tail dynamic comparator, in which $\Delta V_n/f_p$ is just a function of input transistor transconductance and input voltage difference, in the existing double tail structure as soon as the comparator detects that for instance node f_n discharges faster, a PMOS transistor (M_{C1}) turns on, pulling the other node f_p back to the V_{DD}. Therefore by the time passing, the difference between f_n and f_p ($\Delta V_n/f_p$) increases in an exponential manner, leading to the reduction of latch regeneration time.

IV. SIMULATION RESULTS

The proposed double tail comparator circuit has been verified and simulated using the spectre simulator from cadence. The cadence virtuoso in an 180nm CMOS process parameter is utilized in this design. The transient analysis behavior of the double tail comparator is demonstrated in Figure 2.

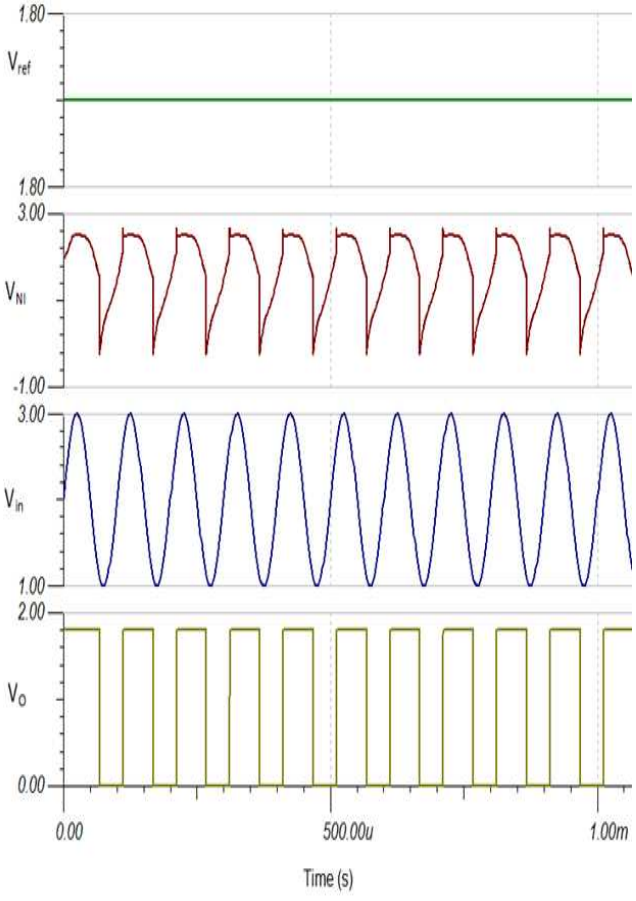


Figure 2. Transient analysis of the comparator

Table 1 shows the summary of the designed double tail comparator circuit.

Table 1. Summary of the double tail comparator circuit

Clock frequency	100MHz
Power supply	1.8V
Offset voltage	2.5mV
Technology	180nm CMOS
Propagation delay	600µs
Input Signal Frequency	upto 1GHz
Power dissipation	366µW

The total magnitude and phase response of the proposed double tail comparator circuit is shown in figure 3.

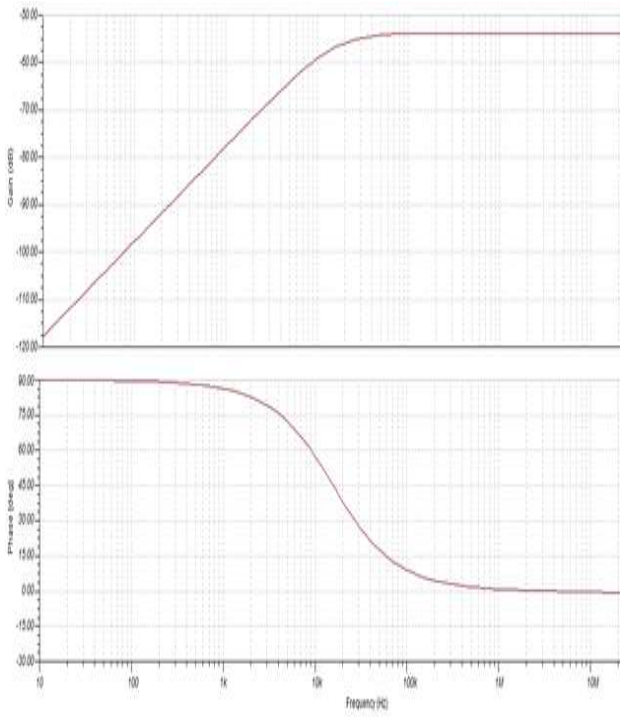


Figure 3. Magnitude and Phase response analysis of the comparator

The total output noise response of the proposed double tail comparator circuit is shown in figure 4.

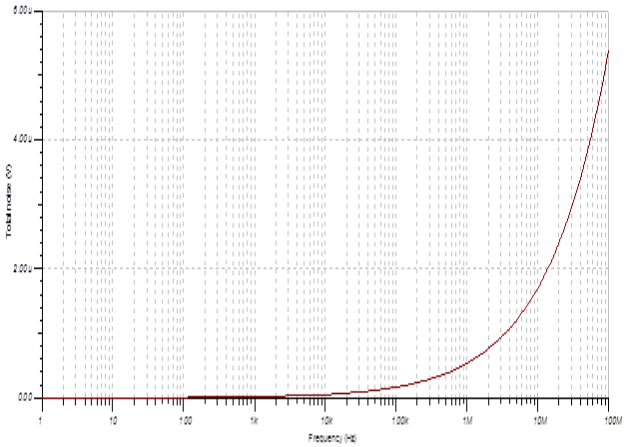


Figure 4. Total output noise response analysis of the comparator

V. CONCLUSION

In this work, a high speed CMOS double tail comparator circuit architecture for flash type ADC or pipelined ADC is designed and implemented. High speed and low power are very important parameters that need to be considered in the design of double tail comparator circuit. For reducing the power dissipation in the circuit, the transistors present in the input differential section of the comparator are operated in sub-threshold region rather than in the saturation region. The double tail comparator is designed and simulated using cadence-spectre in 180nm CMOS technology. Simulation results show that the designed double tail comparator circuit can work under as high clock frequency as 100MHz and its maximum offset voltage is about 2.5mV. The circuit exhibits a propagation delay of 600µs when operated at a power supply of 1.8V.

VI. REFERENCES

[1]. Pedro M. Figueiredo, Joao C. Vital, "Kickback noise reduction techniques for CMOS latched comparators", Circuits and Systems II: Express

Briefs IEEE Transactions on, vol. 53, no. 7, pp. 541-545, 2006.

[2]. Junjie Lu, Jeremy Holleman, "A low-power high-precision comparator with time-domain bulk-tuned offset cancellation", Circuits and Systems I: Regular Papers IEEE Transactions on, vol. 60, no. 5, pp. 1158-1167, 2013.

[3]. J. C. Jensen, and L. E. Larson, "A 16-GHz ultra-high-speed Si-SiGe HBT comparator," IEEE Journal of Solid-State Circuits, vol. 38, no. 9, pp. 1584-1589, September 2003.

[4]. K. Deepika, K. Lokesh Krishna, Dr. K. Anuradha, "A Low Power High Speed Double-Tail Comparator in 90nm CMOS Technology", International Journal of Computer Science Trends & Technology (IJCST), Volume 3 Issue 2, ISSN: 2347-8578, pp: 203- 207, Mar-Apr 2015.

[5]. B. Razavi, Principles of Data Conversion System Design. New York: IEEE Press, 1995.

[6]. C. R. Grace, P. J. Hurst, S. H. Lewis, "A 12-bit 80-MSample/s pipelined ADC with bootstrapped digital calibration", Solid-State Circuits IEEE J., vol. 40, no. 5, pp. 1038-1046, 2005.

[7]. S. Babayan-Mashhadi, R. Lotfi, "Analysis and Design of a Low-Voltage Low-Power Double-Tail Comparator", Very Large Scale Integr. Syst. IEEE Trans., vol. 22, no. 2, pp. 343-352, 2014.

[8]. K. L. Krishna, T. Ramashri and D. Reena, "A 1V second order delta sigma ADC in 130nm CMOS," International Conference on Information Communication and Embedded Systems (ICICES2014), Chennai, 2014, pp. 1-5.

[9]. N. B. Romli, M. Mamun, M. A. S. Bhuiyan, H. Husain, "Design of a low power dissipation and low input voltage range level shifter in CEDEC 0.18-μm CMOS process", World Applied Sciences Journal, vol. 19, pp. 1140-1148, 2012.